



# AEROSPACE STRUCTURES

ERIC RAYMOND JOHNSON

**Aerospace Structures** is a 600+ page text and reference book for junior, senior, and graduate-level aerospace engineering students. The text begins with a discussion of the aerodynamic and inertia loads acting on aircraft in symmetric flight. A linear theory for the statics and dynamic response of thin-walled straight bars with closed and open cross-sections is presented. Isotropic and fiber-reinforced polymer (FRP) composite materials including temperature effects are modeled with Hooke's law. Methods of analyses are by differential equations, Castigliano's theorems, the direct stiffness method, the finite element method, and Lagrange's equations. There are numerous examples for the response of axial bars, beams, coplanar trusses, coplanar frames, and coplanar curved bars. Failure initiation by the von Mises yield criterion, buckling, wing divergence, fracture, and by Puck's criterion for FRP composites are presented in the examples.

# **Aerospace Structures**

**Eric Raymond Johnson**

DOI: <https://doi.org/10.21061/AerospaceStructures>

Kevin T. Crofton Department of Aerospace and Ocean Engineering at Virginia Tech

IN ASSOCIATION WITH

  
**VIRGINIA TECH**<sup>TM</sup>  
PUBLISHING  


Blacksburg, VA



Unless otherwise noted, this textbook is licensed with a Creative Commons Attribution NonCommercial-ShareAlike 4.0 license: <https://creativecommons.org/licenses/by-nc-sa/4.0>. You are free to copy, share, adapt, remix, transform, and build upon the material for any not primarily commercial purpose, as long as you follow the terms of the license: <https://creativecommons.org/licenses/by-nc-sa/4.0/legalcode>.

This work is published by the Kevin T. Crofton Department of Aerospace and Ocean Engineering in association with Virginia Tech Publishing, a division of the University Libraries at Virginia Tech.

Virginia Tech Publishing. 560 Drillfield Drive, Blacksburg, VA 24061, USA. [publishing@vt.edu](mailto:publishing@vt.edu).

Kevin T. Crofton Department of Aerospace and Ocean Engineering, Randolph Hall, RM 215, Virginia Tech 460 Old Turner Street, Blacksburg, VA 24061, USA.

Suggested citation: Johnson, Eric R. (2022) Aerospace Structures. Blacksburg: Virginia Tech Kevin T. Crofton Department of Aerospace and Ocean Engineering. <https://doi.org/10.21061/AerospaceStructures>. Licensed with CC BY NC-SA 4.0. <https://creativecommons.org/licenses/by-nc-sa/4.0>.

Peer Review: This book has undergone single-blind peer review by seven external subject matter experts.

Publication of this book was made possible in part through funding from VIVA (the Virtual Library of Virginia), the Open Education Initiative at the University Libraries at Virginia Tech, and Virginia Tech Publishing.

Accessibility Statement: Virginia Tech Publishing is committed to making its publications accessible in accordance with the Americans with Disabilities Act of 1990. The ePub version of this book is accessible. The LaTeX source files also include alternative text for all images and figures.

#### Publication Cataloging Information

Johnson, Eric R., author

Aerospace Structures / Eric R. Johnson

Pages cm

ISBN 978-1-949373-44-8 (print)

ISBN 978-1-949373-46-2 (PDF)

ISBN 978-1-949373-45-5 (LaTeX)

ISBN 978-1-949373-65-3 (ePub)

DOI: <https://doi.org/10.21061/AerospaceStructures>

Airframes -- Mathematical models.

Failure analysis (Engineering) -- Mathematical models.

Structural analysis (Engineering) -- Mathematical models.

1. Title

TL671.6.J64 2022

629.134

Cover design (licensed CC BY 4.0): Kindred Grey

Cover image: Adapted from (c) Tom Cleary. Unsplash license <https://unsplash.com/license>. Retrieved from <https://unsplash.com/photos/MFZYwRJnKAo>.

#### About the author

Eric Raymond Johnson is emeritus professor of aerospace and ocean engineering at Virginia Tech. He earned his doctoral degree in applied mechanics from the University of Michigan in 1976, and from 1976 to 2003 was a member of the engineering faculty at Virginia Tech. Dr. Johnson's research area is composite structures. Research activities include the mechanics of the response and failure of advanced composite material structures with applications to flight and land vehicles, buckling and post-buckling of plates and shells, progressive failure analysis for the prediction of energy absorption in laminated composites and in bonded joints, and fracture mechanics. He has sixty-four publications in structural mechanics, and has been awarded research funding from government agencies and industries. He is a senior member of the American Institute of Aeronautics and Astro-nautics and a member of the American Society of Mechanical Engineers.

# Features of This Open Textbook

## Additional Resources

The following resources are freely available at <http://hdl.handle.net/10919/102306>.

Downloadable PDF

Errata and error reporting form

Print edition ordering details

Links to collaborator portal and listserv

LaTeX source files

If you are an instructor reviewing, adopting, or adapting this textbook, please help us understand your use by completing this form: <http://bit.ly/interest-aerospace-structures>



You are free to copy, share, adapt, remix, transform, and build upon the material for any not primarily commercial purpose, as long as you follow the terms of the license: <https://creativecommons.org/licenses/by-nc-sa/4.0>.



**You must** Attribute - You must give appropriate credit, provide a link to the license, and indicate if changes were made. You may do so in any reasonable manner, but not in any way that the licensor endorse you or your use.

Suggested citation for an adapted work: Adapted by \_\_[your name]\_\_ from © Eric R Johnson, Aerospace Structures, <https://doi.org/10.21061/AerospaceStructures>, CC B NC SA 4.0, <https://creativecommons.org/licenses/by-nc-sa/4.0>.



**You must** ShareAlike - If you remix, transform, or build on the material, you must distribute your contributions under the same license as the original.



**You may not:**

Noncommercial - You may not use the material for uses that are primarily intended for or directed toward commercial advantage or monetary compensation.

**You may not:**

Add any additional restrictions - You may not apply legal terms or technological measures that legally restrict others from doing anything the license permits.

If adopting or building upon, you are encouraged to:

- Register your use at <http://bit.ly/interest-aerospace-structures>
- Incorporate only your own original work or works with a CC BY, CC BY NC, or CC BY NC SA license.
- Attribute all added content.
- Have your work peer reviewed.
- Include a transformation statement that describes changes, additions, accessibility features, and any subsequent peer review.
- If incorporating text or figures under an informed fair use analysis, mark them as such and cite them.
- Share your contributions in the collaborator portal

### Suggestions for creating and adapting

Create and share learning tools and study aids.

Translate. Modify the sequence or structure.

Add or modify problems and examples.

Transform or build upon in other formats.

### Adaptation resources

LaTeX source files are available or

Adapt on your own at <https://libretext.org>

### Submit suggestions and comments

Submit suggestions (anonymous): <http://bit.ly/feedback-aerospace-structures>

Email: [publishing@vt.edu](mailto:publishing@vt.edu)

# Table of Contents

CHAPTER 1	Function of flight vehicle structural members . . . . .	1
1.1	Space truss/frame	1
1.2	Monocoque and semimonocoque constructions	2
1.3	Rocket structure	4
1.4	References	5
CHAPTER 2	Aircraft loads . . . . .	7
2.1	Aircraft design process	7
2.2	Inertia loads	7
2.2.1	Coordinate systems and Newton's laws of motion	8
2.2.2	Principle of D'Alembert	10
2.2.3	Relative velocity and acceleration	11
2.2.4	Uniform linear and angular accelerations	12
2.3	Load factors	12
2.4	The V-n diagram	13
2.4.1	Airplane design requirements	14
2.4.2	Regulations	14
2.4.3	Specified data	14
2.4.4	Basic maneuver V-n diagram	14
2.4.5	Aerodynamic data	15
2.4.6	Maneuver V-n diagram including aerodynamic stall	19
2.5	Design gust load factors	21
2.5.1	Gust alleviation factor	22
2.5.2	Gust load factor	22
2.5.3	NACA discrete gust conditions	22
2.5.4	Design V-n diagram	23
2.6	Design V-n diagram example	24
2.7	References	26
2.8	Practice exercises	27
CHAPTER 3	Elements of a thin-walled bar theory . . . . .	31
3.1	Open cross section	31
3.2	Contour geometry	33
3.3	Displacements	35
3.4	Strains	37
3.5	Stresses, stress resultants and bar resultants	38
3.6	External loads and equilibrium of an element of the bar	40
3.6.1	Differential equilibrium equations	41
3.7	Hooke's law	44
3.7.1	Effect of thermal expansion	44
3.7.2	Material law for extension and bending	45
3.8	Shear flow due to the transverse shear forces	49
3.8.1	Open cross-sectional contour	51
3.8.2	Location of the shear center for an open cross section	53
3.8.3	Notes concerning the shear center	57

3.9 Torsion of an open section with a straight contour	57
3.9.1 Torsion of built-up open sections	63
3.10 Inclusion of stringers in the analysis of the cross section	64
3.10.1 Effect of stringers on the shear flow distribution	65
3.11 Closed cross-sectional contour	67
3.11.1 Twist per unit longitudinal length	68
3.11.2 Location of the shear center and the final expression for the shear flow	69
3.12 References	75
 CHAPTER 4 Some aspects of the structural analysis. . . . .	 77
4.1 Review of the thin-wall bar theory	78
4.1.1 Extension and bending	78
4.1.2 Shear stresses in open and closed sections	80
4.1.3 Hooke's law for transverse shear and torsion	82
4.2 Yield criteria	83
4.3 Structural analyses for extension and flexure	84
4.3.1 Bending moment diagrams	84
4.3.2 Buoyancy force distribution on ships	89
4.3.3 Properties of plane areas	91
4.3.4 Neutral axis of the cross section	95
4.4 Structural analyses for transverse shear and torsion	102
4.4.1 Resultant of uniform shear flow	110
4.4.2 Torsion of a hybrid section	112
4.5 References	125
4.6 Practice exercises	125
 CHAPTER 5 Work and energy methods. . . . .	 129
5.1 Hooke's law and its corollaries	129
5.1.1 Work of the external loads	130
5.1.2 Maxwell's reciprocal theorem	131
5.2 Extensions of Hooke's law to include a couple and rotation	133
5.2.1 Generalized forces and displacements	134
5.2.2 Stiffness influence coefficients	134
5.3 Strain energy density functions	135
5.3.1 Strain energy density in uniaxial normal strain	135
5.3.2 Complementary energy density in uniaxial normal stress	138
5.3.3 Strain energy density in shear	139
5.4 Strain energy for extension and bending of a thin-walled bar	140
5.5 Strain energy for shear and torsion of a thin-walled bar	141
5.5.1 Open cross-sectional contour	142
5.5.2 Closed cross-sectional contour	142
5.5.3 Material law for transverse shear and torsion	143
5.6 Total strain energy expressions for a thin-walled bar	145
5.7 Castigliano's first theorem	146
5.8 Castigliano's second theorem	149

<b>CHAPTER 6</b>	<b>Applications of Castigliano's Theorems . . . . .</b>	<b>153</b>
6.1	Coplanar trusses	153
6.1.1	Castigliano's first theorem	153
6.1.2	Castigliano's second theorem for a statically determinate truss	158
6.2	Beam structures	160
6.2.1	Castigliano's second theorem	162
6.3	Coplanar Frames	171
6.4	Castigliano's second theorem and statically indeterminate structures	173
6.4.1	Function of a Turnbuckle	178
6.5	References	182
6.6	Practice exercises	182
<b>CHAPTER 7</b>	<b>Arches, rings and fuselage frames . . . . .</b>	<b>189</b>
7.1	Coplanar curved bars	189
7.1.1	Displacements and strain	191
7.1.2	Normal stress, stress resultants, and strain energy	193
7.2	Strain-displacement and Hooke's law for thin curved bars	199
7.3	Differential equilibrium equations of a curved bar	204
7.4	Loads on fuselage frames	208
7.5	References	219
7.6	Practice exercises	220
<b>CHAPTER 8</b>	<b>Laminated bars of fiber-reinforced polymer composites .</b>	<b>223</b>
8.1	Fibrous composites	223
8.1.1	Material law in principal directions	224
8.1.2	Compliance matrix in bar coordinate directions	225
8.1.3	Plane stress	229
8.1.4	Nomenclature of composite materials	231
8.1.5	Laminated wall	232
8.1.6	Balanced and specially orthotropic laminates	234
8.2	Composite thin-walled bar with a closed cross-sectional contour	235
8.2.1	Anisotropic Hooke's law for the cross section	237
8.2.2	Expressions for the shear flow and normal stress resultant	239
8.2.3	Complementary work and energy	240
8.2.4	Cross-sectional compliance matrix	243
8.3	Open cross-sectional contour	252
8.4	Uniform torsion of an FRP bar with a rectangular cross section	252
8.4.1	Displacements	253
8.4.2	Equilibrium	256
8.4.3	Static equivalence	257
8.4.4	Principle of complementary virtual work	259
8.5	References	269
<b>CHAPTER 9</b>	<b>Failure initiation in FRP composites. . . . .</b>	<b>271</b>
9.1	Strength of a composite ply	271
9.1.1	Puck's failure criterion	272
9.1.2	Matrix failure criteria for a plane stress state	279
9.2	Stresses in the principal material directions	282
9.3	References	288



## CHAPTER 10 Structural stability of discrete conservative systems . . . 289

10.1 Model A: stable symmetric bifurcation buckling	289
10.1.1 Equilibrium method	290
10.1.2 Kinetic method	291
10.1.3 Energy method	293
10.1.4 Eccentric load	296
10.1.5 Initial angle	297
10.2 Model B: unstable symmetric bifurcation	298
10.2.1 Initial angle imperfection	300
10.3 Model C: asymmetric bifurcation	302
10.4 Discussion of models A, B, and C	304
10.5 Model D: snap-through instability	305
10.6 Model E: a two-degree-of freedom system	307
10.7 References	312
10.8 Practice exercises	312

## CHAPTER 11 Buckling of columns and plates . . . . . 315

11.1 Perfect columns	315
11.1.1 Pre-buckling equilibrium	318
11.1.2 Buckling	318
11.1.3 Buckling equations for negligible strain at the bifurcation point	324
11.2 Initial post-buckling of the pinned-pinned column	324
11.2.1 Summary of the nonlinear equations	325
11.2.2 The perturbation expansion.	325
11.2.3 Relations between the expansion functions for the rotations and lateral displacement	326
11.2.4 Perturbation expansion of the load P	326
11.2.5 Solutions for the rotation and lateral displacement functions	328
11.2.6 Solutions for the axial displacement functions	330
11.2.7 Summary	330
11.3 In-plane buckling of trusses	333
11.4 Geometrically imperfect column	336
11.4.1 Southwell plot	338
11.5 Column design curve	339
11.5.1 Inelastic buckling	340
11.6 Bending of thin plates	343
11.7 Compression buckling of thin rectangular plates	346
11.7.1 Simply supported rectangular plate	348
11.8 Buckling of flat rectangular plates under shear loads	352
11.9 Buckling of flat rectangular plates under combined compression and shear	355
11.10 References	358
11.11 Practice exercises	359

## **CHAPTER 12 Introduction to aeroelasticity . . . . . 361**

- 12.1 The Collar diagram of aeroelastic forces **361**
- 12.2 Divergence analysis of a rigid wing segment **363**
  - 12.2.1 Responses of the rigid wing segment and the imperfect column **365**
  - 12.2.2 Divergence experiments **366**
- 12.3 Straight, uniform, unswept, high aspect ratio, cantilever wing in steady incompressible flow **367**
  - 12.3.1 Aerodynamic strip theory **368**
  - 12.3.2 Differential equation of torsional divergence **369**
- 12.4 Effect of wing sweep on divergence **371**
- 12.5 References **372**
- 12.6 Practice exercises **372**

## **CHAPTER 13 Fracture of cracked members . . . . . 375**

- 13.1 Comet disasters of 1954 **375**
- 13.2 Cracks as stress raisers **377**
- 13.3 LEFM stress field in the vicinity of the crack tip for mode I **378**
- 13.4 LEFM stress field in the vicinity of the crack tip for mode II **385**
- 13.5 Energy criterion for crack growth **387**
  - 13.5.1 Griffith criterion **387**
- 13.6 Relation between K and G **390**
  - 13.6.1 Mixed mode fracture **391**
- 13.7 Interlaminar failure in composites: delamination **392**
  - 13.7.1 Mixed mode fracture **396**
- 13.8 References **398**
- 13.9 Practice exercises **399**

## **CHAPTER 14 Design of a landing strut and wing spar . . . . . 403**

- 14.1 Landing strut **403**
  - 14.1.1 Strut deflection **403**
  - 14.1.2 Strut design exercise **407**
- 14.2 Wing spar design **407**
  - 14.2.1 Evaluation of stresses at root cross section **409**
  - 14.2.2 Trial design of the monocoque box beam spar **412**
  - 14.2.3 Design exercise A **412**
- 14.3 Additional limit states for buckling and fracture **413**
  - 14.3.1 Buckling margin of safety **413**
  - 14.3.2 Fracture margin of safety **414**
  - 14.3.3 Design exercise B **415**
- 14.4 References **416**

<b>CHAPTER 15</b>	<b>Direct stiffness method . . . . .</b>	<b>417</b>
15.1	Physical interpretation of influence coefficients	417
15.2	Unrestrained structural stiffness matrix	423
15.3	Assembly of unrestrained structural stiffness matrices	425
15.4	Prescribed nodal displacements and forces	427
15.5	Solution for the unknown nodal variables	429
15.6	Stress matrix	431
15.7	Summary of the direct stiffness method	432
15.8	Reference	435
15.9	Practice exercises	435
<b>CHAPTER 16</b>	<b>Applications of the direct stiffness method. . . . .</b>	<b>437</b>
16.1	Coplanar trusses	437
16.1.1	Assembly algorithm	443
16.1.2	Self-strained truss	450
16.2	Structures containing beam members	456
16.2.1	Boundary value problem (16.28). Generalized displacements at the boundaries	458
16.2.2	Boundary value problem (16.27). Fixed-end actions	462
16.2.3	Results of the combined superposition solutions for the beam	463
16.3	Coplanar frame structures	473
16.3.1	Transformation of Cartesian coordinates	475
16.3.2	Frame stiffness matrix in global coordinate directions	478
16.3.3	Frame stress matrix	479
16.4	Practice exercises	483
<b>CHAPTER 17</b>	<b>Finite element method. . . . .</b>	<b>489</b>
17.1	Elastic bar subject to axial loads	489
17.2	Finite elements in one dimension	494
17.2.1	Results from 4, 8, and 16 finite element solutions to example 17.1	502
17.2.2	Convergence requirements	503
17.2.3	Apparent loadings from the 8- and 16-element solutions of example 17.1	503
17.2.4	Adaptive mesh refinement beginning with the 8-element solution to example 17.1	504
17.3	A beam element including transverse shear deformation	506
17.3.1	Element displacement functions and strains	508
17.3.2	Principle of virtual work for a typical element	511
17.3.3	Static condensation	514
17.3.4	Bending moment and shear force	515
17.3.5	Requirements of the interpolation functions.	516
17.3.6	Gaussian integration	526
17.4	Euler-Bernoulli beam element	530
17.4.1	Element displacement functions and strains	531
17.5	References	534

## CHAPTER 18 Introduction to flexible body dynamics . . . . . 535

18.1 Description of Atlas I	535
18.2 Rigid body load factor	537
18.3 Steps in flexible body dynamics	538
18.4 Eigenvalue problems for real symmetric matrices	543
18.5 Hamilton's principle and Lagrange's equations	547
18.5.1 Lagrange's equations	549
18.6 The dynamic response of an elastic thin-walled bar	551
18.7 Finite element model for the dynamics of an axial bar	556
18.7.1 Truss element	561
18.8 Dynamic bending of a bar with two axes of symmetry	565
18.8.1 Finite element	566
18.8.2 Method of dynamic condensation	569
18.9 Vibrations of a coplanar frame	575
18.10 References	584
18.11 Practice exercises	585

Additional materials listed below are not included in this print volume. They are freely available at <https://doi.org/10.21061/AerospaceStructures>.

## APPENDIX A Linear elasticity of solid bodies

A.1 Geometry of deformation	
A.1.1 Physical interpretation of strain components	
A.1.2 Engineering strain	
A.1.3 Linear strain-displacement relations	
A.1.4 Transformation of the strains between two Cartesian coordinate systems	
A.2 Stress	
A.2.1 Equilibrium differential equations	
A.2.2 Transformation of stresses between two Cartesian coordinate systems	
A.2.3 Cartesian tensors	
A.3 Linear elastic material law	
A.3.1 First law of thermodynamics	
A.3.2 Material symmetry	
A.4 Summary and the boundary value problems of elasticity	
A.5 References	

# Introduction

## About this book

In this textbook analytical methods are developed for the response and failure of the primary structural components of aircraft. Newton's laws of motion, Hooke's law, and the first law of thermodynamics are the basis to model the thermoelastic response of thin-walled, straight bars and coplanar curved bars. Analytical methods include energy principles to develop Castigliano's theorems and to develop the cross-sectional material law for transverse shear and torsion. Stiffened shells typical of aircraft structures are analyzed with the thin-walled bar theory. Externally prescribed loads are due to accelerated flight and the thermal environment. Velocity-load factor ( $V$ - $n$ ) diagrams for maneuvers and gusts are described to evaluate flight loads.

Initiation of failure is predicted by one of the following criteria: von Mises yield criterion for ductile metals; the critical load to cause buckling (failure by excessive displacements); fracture criteria for the critical stress to cause crack propagation; and Puck's criterion for the brittle failure modes in fiber-reinforced polymer composites (FRP).

The subject of structural stability of discrete conservative systems introduces the methods of stability analysis, classification of bifurcation buckling problems, the concept of imperfection sensitivity, and snap-through at a limit point. Static instability of an elastic column from pre-buckling equilibrium, buckling, and through initial post-buckling is presented in detail. Buckling of flat rectangular plates subject to compression and shear is presented in a qualitative way using the classic charts from the National Advisory Committee for Aeronautics (NACA). The analysis for the static instability of a wing in steady incompressible flow, or divergence, is part of the discussion of aeroelastic phenomena.

- Results from linear elastic fracture mechanics (LEFM) are introduced to illustrate the relation between crack size and the stress to cause crack propagation. Airplane damage-tolerant design is based on LEFM such that subcritical length cracks do not grow to critical length between inspection intervals.
- The incentive to study optimal design is illustrated by the example of an aluminum wing spar. The objective is to achieve minimum weight by a search for two design variables. Constraints on yielding, buckling, and fracture are evaluated with the thin-walled bar theory.
- The analyses are developed for closed and open section bars made from fiber-reinforced polymer composites. The cross-sectional compliance matrix for bars with a closed cross-sectional contour and an open cross-sectional contour include shear-extension coupling. The first ply failure envelope for a graphite epoxy circular tube subject to an axial force and torque is determined by Puck's intralaminar criterion. Interlaminar failure, or delamination, is modeled with fracture mechanics, and the method is illustrated by analyses of standard fracture test specimens.
- Numerical methods for static analysis begin with the direct stiffness method, which originated to model skeletal structures consisting of bars connected by joints. Applications include coplanar trusses, beams, and coplanar frames. The finite element method is developed from the integral formulation of the ordinary differential equations of an axial bar and a beam.
- Analyses for the linear elastic, dynamic response of axial bars, coplanar trusses, beams, and coplanar frames are presented using the finite element method and the mode-separation method. Hamilton's principle and Lagrange's equations are developed for discrete mechanical systems.
- Numerous examples to illustrate the application of the structural analysis are presented in each chapter using either U.S. customary units, or SI units.

I acknowledge the technical discussions with Professors William Hallauer, Raphael Haftka, Rakesh Kapania, Raymond Plaut, and Mayuresh Patil whose contributions to the subject matter of this course have been used in the preparation of the text. I accept responsibility for any errors in the text, and would appreciate if the reader would inform me of comments and corrections via email ([erjohns4@vt.edu](mailto:erjohns4@vt.edu)). Thanks to Professor Anita Walz, open education librarian at Virginia Tech, and her staff for all the work necessary to publish this text as an open educational resource. Also, thanks to Mr. Joseph Brooks and Ms. Varakini Sanmugadas who assisted in the preparation of the text.

Eric R. Johnson  
Warm Springs, Virginia

## Audience

This text is evolved from lecture notes by the author for junior and senior students in the aerospace engineering curriculum at Virginia Tech. The subjects covered in the book presume some knowledge of statics, dynamics of rigid bodies, mechanics of deformable bodies, and mechanical vibrations. Several practice exercises in the text require programming, and typically the students use *Mathematica*<sup>1</sup> or MATLAB<sup>2</sup> software to complete them. Examples in the text were programmed in *Mathematica*.

A first semester sequence for junior students includes chapters 1 through 6. Note that chapter 3 on thin-wall bar theory may be too mathematical for some students, but can be used as a reference for the applications of the theory provided in chapter 4. The important topic of work and energy is covered in chapter 5, and chapter 6 is devoted to the application of Castigliano's theorems to trusses, beams, and frames.

A second semester sequence for junior students includes topics selected by the instructor from chapter 7 on curved bars, and chapters 10 through 16. The influence of imperfection sensitivity on the buckling load of discrete systems is presented in chapter 10, followed by buckling of columns and plates in chapter 11. Article 11.2 is optional. Analysis for wing divergence is presented in the introduction to aeroelasticity in chapter 12. The methods of linear elastic fracture mechanics to predict critical loads for crack propagation is discussed in chapter 13. Design of a landing strut, and the optimal design of a spar subject to constraints on yielding, buckling and fracture are presented in chapter 14. Chapters 15 and 16 detail the direct stiffness method for trusses, beams and frames.

Topics appropriate for senior students are in chapters 8, 9, 17, and 18, and initial post-buckling in article 11.2. The response of closed and open section bars fabricated from a fiber-reinforced polymer composite (FRP) is presented in chapter 8, and failure initiation of FRP bars is presented in chapter 9. The finite element method applied to the extension and bending of bars is presented in chapter 17, which includes transverse shear deformations. The topic of adaptive mesh refinement in article 17.2.4 is optional. Articles 18.1 to 18.4 cover the dynamic response of lumped mass models, eigenvalue problems, and Lagrange's equations. The remainder of chapter 18 utilizes the finite element method for the dynamic response of beams, trusses, and frames.

## Peer reviewers

Joseph Brooks, Doctoral Student and Graduate Assistant, Virginia Tech  
Christine Gilbert, Assistant Professor, Virginia Tech  
Mayuresh Patil, Associate Professor, Virginia Tech / Professor of Practice, Georgia Tech  
Varankini Sangmudas, Doctoral Candidate and Graduate Teaching Assistant, Virginia Tech  
Gary Seidel, Associate Professor, Virginia Tech  
Namiko Yamamoto, Assistant Professor, Penn State  
Anonymous, Professor, University of Virginia

## Contributors

Co-investigators: Mayuresh Patil, Rakesh Kapania  
Managing editor and co-investigator: Anita Walz  
Alt text writer: Joseph Brooks  
Alt text assistant: Claire Colvin  
Cover design and selected graphics: Kindred Grey

---

1. *Mathematica* is a registered trademark of Wolfram Research, Inc., Champaign, IL 61820, USA.  
2. MathWorks, Inc., 3 Apple Hill Drive, Natick, Massachusetts 01760, USA.

# *Function of flight vehicle structural members*

---

The purpose of this chapter is to present a brief description of aircraft structural members and their function.

A structure may be defined as any assemblage of materials that is intended to sustain loads. It is important to recognize that structures are made from materials, and that the history of structures follows the development of materials and the development of tools to fabricate the materials. Ashby (1992) details a systematic approach to material selection in mechanical design, and the manufacturing processes required produce the functional shape of a design. The evolution of the airframe, for example, is tied closely to the introduction of materials and cost-effective means for their fabrication. Early aircraft were constructed of wire-braced wood frames with fabric covers. Currently, advanced composite materials are very attractive for weight-sensitive structures, like aircraft, because of their high stiffness-to-weight and strength-to-weight ratios. There is an interesting and rich history of the evolution of aircraft structures, but for the sake of brevity it is not presented here. Instead, the interested reader is referred to the textbook by Curtis (1997). Curtis details the history of fixed-wing aircraft structures from 1903 to modern aircraft.

In this text analytical methods are developed for the response and failure of the primary structural components of aircraft. The primary structure of a flight vehicle consists of the components that are necessary to sustain design ultimate flight and ground loads. Failure of the primary structure causes catastrophic collapse and loss of control. For aircraft the primary structure consists of the wings, fuselage, tail, and landing gear. Forms of construction are space trusses/frames, monocoque and semimonocoque.

## *1.1 Space truss/frame*

A truss structure fuselage is often used in lightweight aircraft. See figure 1.1. It consists of wood or steel tubes with a fabric covering providing aerodynamic shape. Members in a space truss are subject to axial forces, and members of a space frame are subject to axial forces, shear forces, and bending moments. The fabric covering does not add much to the overall stiffness of the structure.

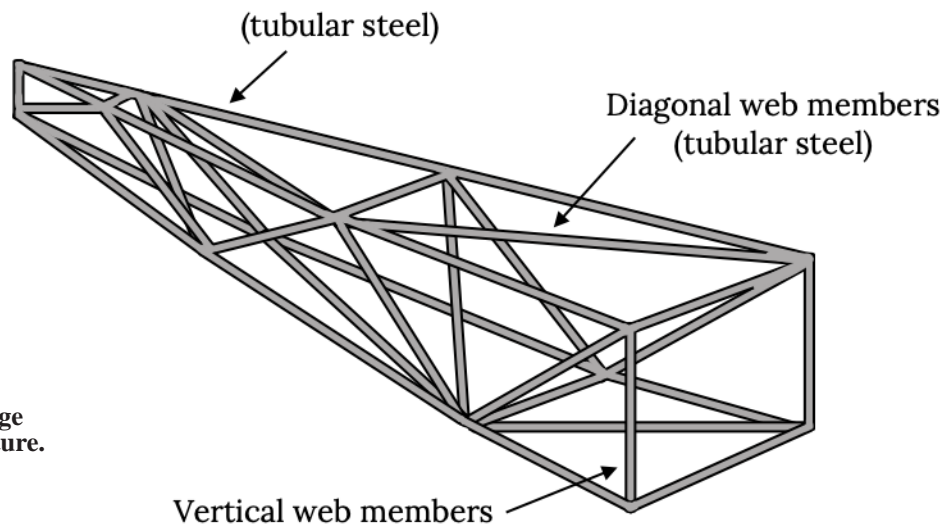


**Fig. 1.1** A fuselage space frame structure.

## 1.2 Monocoque and semimonocoque constructions

Most flight vehicle structures are thin shells with the cover skin providing the aerodynamic shape. Monocoque refers to a shell without supporting stiffening members, whose origin is from the twentieth-century Greek word “mono” meaning alone, plus the French “coque” meaning shell. See figure 1.2 The wall of a monocoque structure has to be strong enough to resist bending and compressive and torsional loads without buckling. The challenge in monocoque design is maintaining strength within allowable weight limits. Another difficulty with monocoque structure is how to design it to accommodate concentrated loads such as engine mountings and wing-fuselage interface, which may require the incorporation of formers (frames) and bulkheads. For large cross-sectional dimensions the skin of a monocoque structure must be relatively thick. A more efficient type of construc-

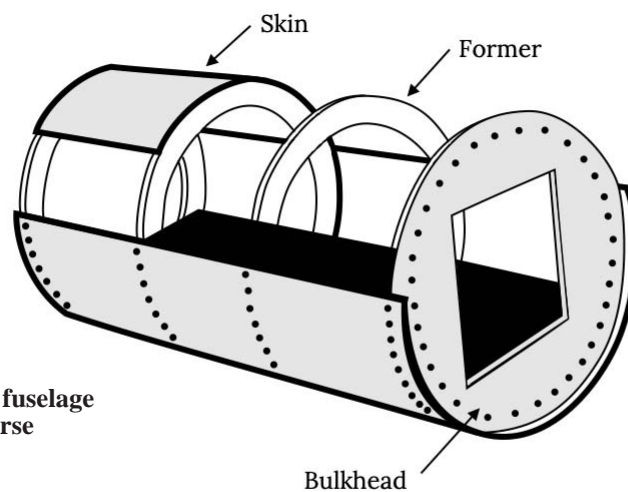


**Fig. 1.2** Monocoque fuselage structure with transverse stiffeners.

tion is one which contains stiffening members that permit a thinner skin. Also, stiffening members can be used to



diffuse concentrated loads into the skin. A stiffened thin-walled shell is called semimonocoque. A semimonocoque body structure and wing structure are shown in figure 1.3. Both the body structure figure 1.3(a) and the wing structure in figure 1.3(b) have longitudinal stiffening members and transverse stiffening members supporting thin skins.

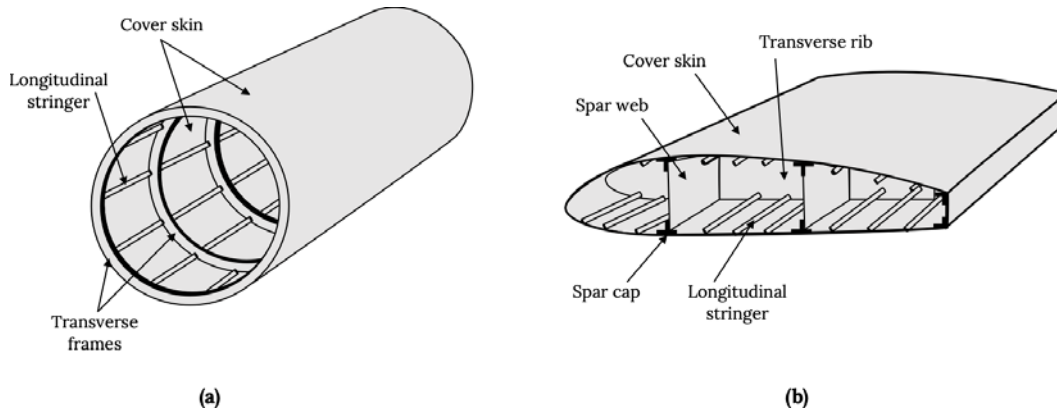


**Fig. 1.3 (a) Semimonocoque body structure. (b) Semimonocoque wing structure.**

Longitudinal members are called longitudinals, stringers, or stiffeners. Longerons are longitudinal members having a large cross section. Longitudinal members act with the skin to resist applied bending and axial loads. Transverse members in a body structure are known as frames, rings, and if they cover most of the cross section they are called bulkheads. Pressure bulkheads cover the entire cross section. Frame members maintain cross-sectional shape and are used to distribute concentrated loads to the skin.

In a wing the longitudinal member is called a spar, and it consists of the spar web and spar cap. The spar cap act with the skin to resist axial and bending loads applied to the wing. The skin and the spar web develop shear stresses to resist torsion and transverse shear due to bending. Transverse members in a wing are called ribs, and they act to maintain the airfoil shape. Ribs act with the skin and longitudinals in resisting circumferential loads due to pressurization.

Longitudinal and transverse members also function to divide the skin into smaller panels to increase the buckling strength. (See Example 11.5 on page 354.)

Additional components of a wing are shown in figure 1.4. The internal wing structure consists of spars, ribs, and stringers. The external wing structure is the skin. Ribs are also used in ailerons, elevators (flaps), fins, and stabilizers. In a fixed-wing aircraft, the spar is the main structural member connected to the fuselage at its root and running spanwise to the tip of the wing. It bends in transmitting the lift due to flight loads acting on the wing. The flight loads acting on a wing not only cause bending, but a significant amount of torsion/ twisting of the wing as well. The skin and shear webs form closed cells in a wing, and torsion is resisted by shear stresses developed in the wall of these cells.

A semimonocoque fuselage structure for a transport aircraft is shown in figure 1.5. The skin is stiffened by longitudinal stringers, spaced six to ten inches apart, which function to increase the buckling strength of the skin and resist fuselage bending loads. Transverse frames maintain the shape of the fuselage and are typically spaced twenty inches apart (Young, 2011).

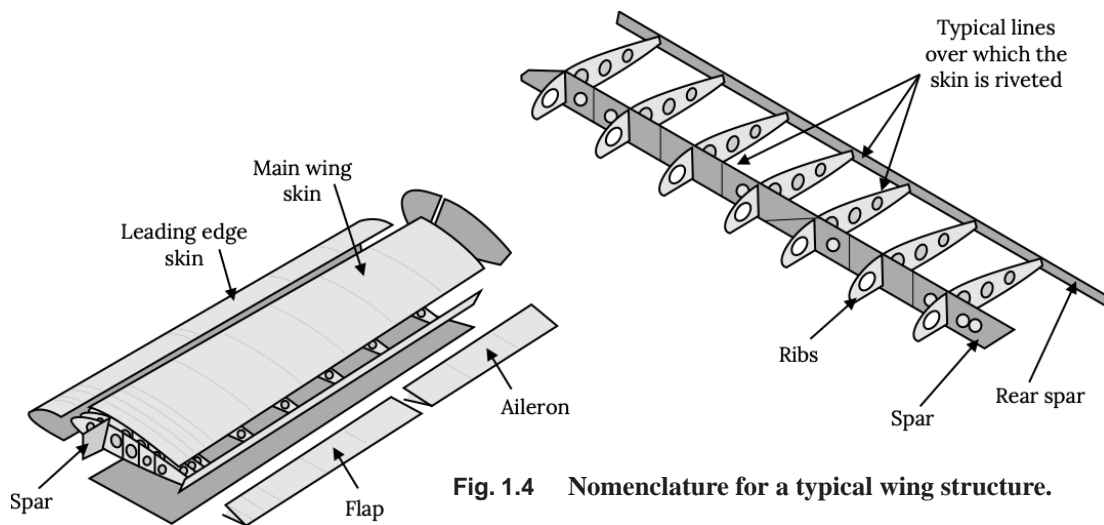


**Fig. 1.4** Nomenclature for a typical wing structure.

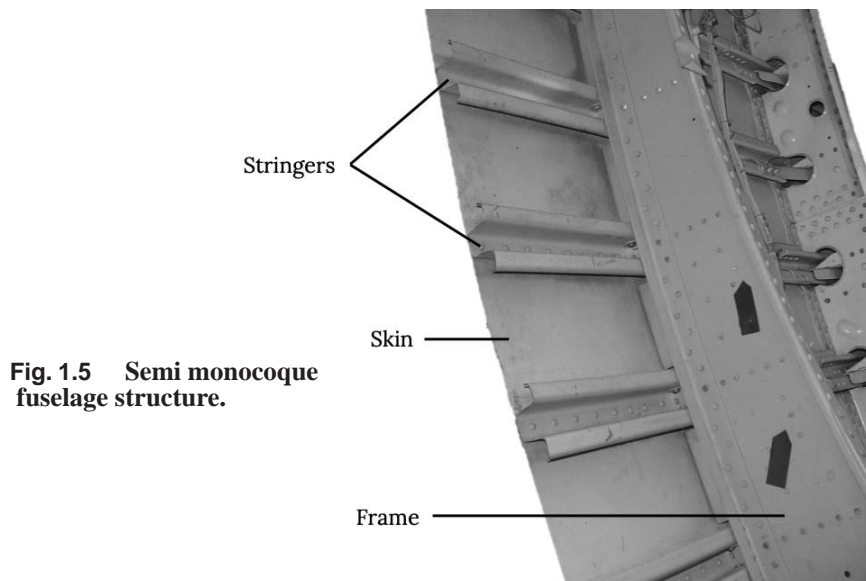


**Fig. 1.5** Semi monocoque fuselage structure.

### 1.3 Rocket structure

A full-scale rocket consists of a launch vehicle and payload. There are four major systems in a full-scale rocket: the structural system, the payload system, the guidance system, and the propulsion system. The structural system includes the cylindrical body, the fairings, and any control fins. The payload is the entire spacecraft such as a satellite, experiment, or whatever else is being lifted into space. When a spacecraft is to be launched by an expendable booster, a booster adapter, or a launch-vehicle adapter, structurally links the spacecraft to the launch vehicle. The payload and its structure is protected by a fairing. Also, refer to the configuration of the Atlas I launch vehicle shown in figure 18.1 on page 534. Atlas I consists of an expendable booster and an expendable second stage.

The cylindrical body of the launch vehicle, or frame, has a thin skin to reduce weight. Engine thrust is the dominate load that causes compression in the rocket parts. The buckling resistance of the thin skins is increased under compression loading by a grid of internal stiffening members attached to the skins similar to those shown in figure 1.3(a). The buckling loads for axially compressed cylindrical shells in experiments are significantly less than the buckling load determined from an analysis of the perfect structure. Imperfection in the shell geometry is main the reason for the discrepancy between theory and experiment Refer to the discussion at the end of article 10.2.1 on page 298. The buckling knockdown factor (KDF) has been introduced to reduce the buckling load predicted by the analysis of the prefect structure to aid in the structural design (Hilburger, 2018).

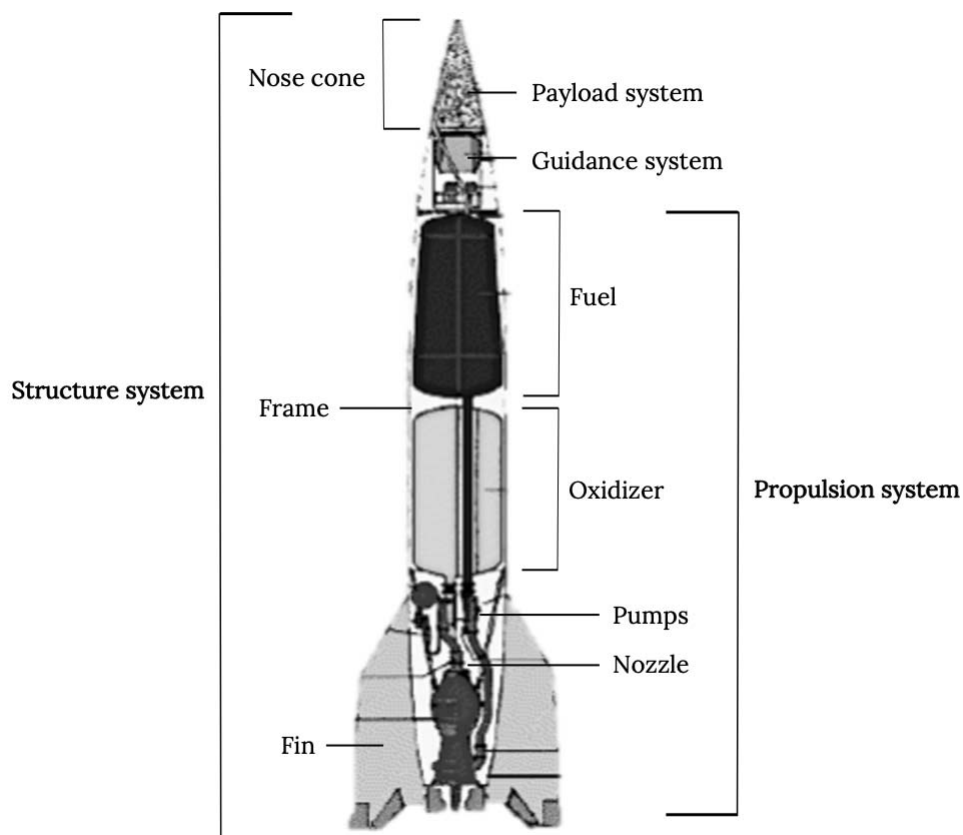


Fig. 1.6 Rocket systems and components.

## 1.4 References

- Ashby, M. F., *Materials Selection in Mechanical Design*. Oxford: Pergamon Press, 1992.
- Curtis, Howard D., *Fundamentals of Aircraft Structural Analysis*. Jefferson City, MO: Richard D. Irwin, a Times Mirror Higher Education Group, Inc. Company, 1997, pp. 1-34.
- Hilburger, M. W., “*On the Development of Shell Buckling Knockdown Factors for Stiffened Metallic Launch Vehicle Cylinders.*” Presented at the 2018 AIAA/ASCE/AHS/ASC Structures, Structural Dynamics, and Materials Conference, Kissimmee FL, AIAA 2018-1990. Washington, DC: American Institute of Aeronautics and Astronautics, 2018.

Young, Richard, “*Fuselage Design 101: Basic Terms and Concepts.*” Presented at the NTSB Airplane Structural Integrity Forum, Washington, D. C., September 21, 2011.

---

Consider an airplane moving through calm air. Particles of air affected by the airplane are accelerated and the reaction of the accelerated particles is felt over the surfaces of the airplane as a distribution of pressures. The pressure distribution acting on the surfaces of the airplane can be resolved into the total lift and drag forces. In addition to the aerodynamic forces of lift and drag, there are so-called inertia loads resulting from the acceleration of the airplane. Other loading conditions such as landing loads, ground-handling loads, horizontal and vertical tail loads, and monocoque body loads are discussed in detail by Lomax (1996).

Load analysis is important in aircraft design, and a design cannot proceed without information on loads. The aircraft loads analysis presented in this chapter is used in preliminary design, which is defined in the next section. In this chapter we define load factors, discuss the aerodynamic data required for structural analysis, develop the basic maneuver V-n diagram, and discuss gust load factors used in design.

## *2.1 Aircraft design process*

Phases of the aircraft design may be divided into a concept formulation, a concept design, a preliminary design, and a detail design. Concept formulation is where the basic requirements for new aircraft are developed. Requirements are developed by a combination of market and customer surveys, and statistical analyses. Concept design begins with the basic requirements and sizes the aircraft. Only the most simple analysis methods and historical data are used. In preliminary design the sized conceptual baseline aircraft is further developed. Increased level of analysis is used to define the aerodynamics, performance, weight, propulsion, acoustic and cost parameters of the design. Detailed design is where the various parts of the aircraft are designed for fabrication. Part and assembly drawings are developed for manufacturing.

## *2.2 Inertia loads*

The maximum load on any part of the airplane structure occurs when it accelerates. In preliminary design, inertia force calculations are usually based on rigid body dynamics of the airplane. Once these loads are determined they

are imposed on the airplane, and the structural design proceeds by assuming the airplane is flexible (i.e., a deformable body). Determining inertia loads for a deformable body is more complex, and may be warranted later in the structural design process.

### 2.2.1 Coordinate systems and Newton's laws of motion

The right-handed Cartesian coordinate system  $OXYZ$  is fixed to the Earth, origin at point  $O$ , and it is assumed that this is an inertial system. That is, Newton's laws of motion are valid in the Earth axis system. The unit base vectors in the  $OXYZ$  system are denoted by  $(\hat{i}, \hat{j}, \hat{k})$ . The right-handed Cartesian coordinate system  $Gxyz$  is fixed in the body of the aircraft, with its origin at the center of gravity, which is labeled  $G$ . The unit base vectors in the  $Gxyz$  system are denoted by  $(\hat{i}, \hat{j}, \hat{k})$ . Consider planar motion of the aircraft – that is, symmetrical maneuvers of the aircraft, and where the aircraft is symmetrical about its vertical fore and aft plane. Body axis  $Gx$  is directed forward, axis  $Gy$  is directed toward the starboard wing, and body axis  $Gz$  is in the normal direction. For symmetrical maneuvers there is no roll or yaw of the airplane, so symmetrical maneuvers imply  $\hat{j} = \hat{J}$  for all time  $t$ . Let  $\vec{R}_G$  denote the position vector of the center of gravity  $G$  with respect to fixed point  $O$ . The flight path is a plane curve in the  $X-Z$  plane with the arc-length along the curve denoted by  $s$ . The unit tangent vector to the flight path at  $s$  is denoted by  $\hat{t}$ , the unit normal vector at  $s$  by  $\hat{n}$ , and the angle between the flight path and the unit tangent vector, or the  $x$ -axis, by  $\theta$ . Note that  $\hat{t} = \hat{i}$ . Angle  $\theta$  represents the clockwise rotation of the aircraft in pitch. See figure 2.1.

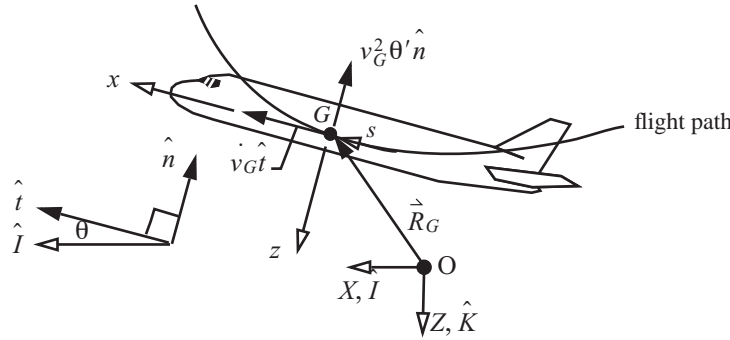


**Fig. 2.1** Acceleration of the center of gravity tangent and normal to the flight path.

The unit tangent vector and its derivative along the path are

$$\hat{t} = \frac{d\vec{R}_G}{ds}, \text{ and } \frac{d\hat{t}}{ds} = \frac{d\theta}{ds} \hat{n}. \quad (2.1)$$

Let  $\theta' = d\theta/ds$ . The change in slope of the flight path with respect to arc-length  $\theta'$  defines the curvature of the path, and the radius of curvature is  $R = 1/\theta'$ . The velocity of the center of gravity  $G$  along the flight path is

$$\vec{v}_G = \frac{d\vec{R}_G}{dt} = \frac{d\vec{R}_G}{ds} \frac{ds}{dt} = \hat{t} v_G, \quad (2.2)$$

where the speed of the center of gravity of the aircraft along the flight path is  $v_G = ds/dt$ . The acceleration of

the center of gravity is

$$\vec{a}_G = \frac{d\vec{v}_G}{dt} = \frac{d}{dt}(v_G \hat{t}) = \dot{v}_G \hat{t} + v_G \frac{d\hat{t}}{ds} \frac{ds}{dt} = \dot{v}_G \hat{t} + v_G^2 \theta' \hat{n}. \quad (2.3)$$

where  $\dot{v}_G = dv_G/dt$  is the acceleration component tangent to the path. The acceleration component normal to the path  $v_G^2 \theta' = v_G^2/R$ , or centripetal acceleration, is directed toward the concave side of the path.

A free body diagram of the aircraft at time  $t$  and its time rate of change of momenta are shown in figure 2.2.

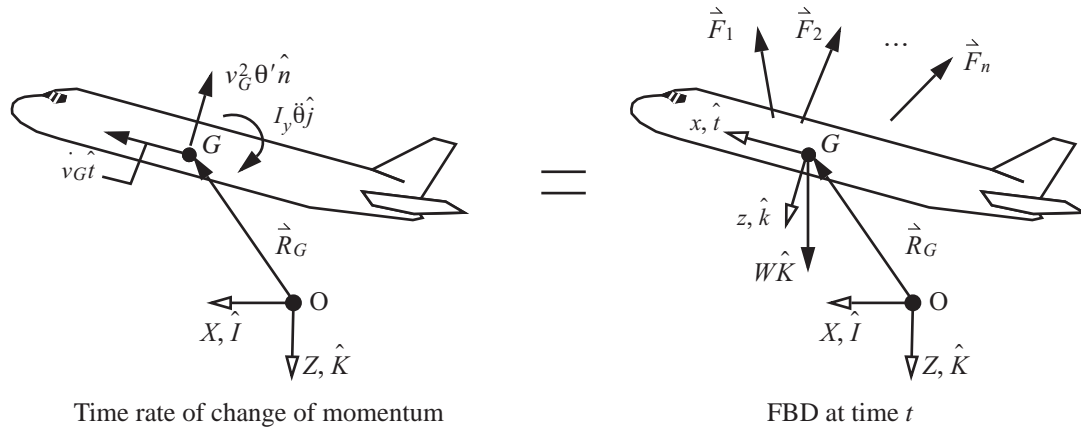


**Fig. 2.2** Free body and rate of momenta diagrams for symmetrical motion of an aircraft at time  $t$ .

Derivatives with respect to time of the pitch angle are written as

$$\frac{d\theta}{dt} = \dot{\theta}, \text{ and } \frac{d^2\theta}{dt^2} = \ddot{\theta}. \quad (2.4)$$

The mass of the aircraft is denoted by  $m$ , the moment of inertia about the center of gravity by  $I_y$ , the local acceleration due to gravity by  $g$ , and the weight of the aircraft by  $W$  where  $W = mg$ . Equations for Newton's second law at time  $t$  are

$$\vec{F} = m(\dot{v}_G \hat{t} + v_G^2 \theta' \hat{n}) \quad \vec{M}_G = I_y \ddot{\theta} \hat{j} \quad \vec{M}_O = \vec{R}_G \times m(\dot{v}_G \hat{t} + v_G^2 \theta' \hat{n}) + I_y \ddot{\theta} \hat{j}, \quad (2.5)$$

where the resultant force is denoted by  $\vec{F}$ , the moment about the center of gravity by  $\vec{M}_G$ , and the moment about the fixed point by  $\vec{M}_O$ . These force and moment vectors are determined from

$$\vec{F} = \sum_{m=1}^n \vec{F}_m \quad \vec{M}_G = \sum_{m=1}^n \vec{r}_{m/G} \times \vec{F}_m \quad \vec{M}_O = \vec{M}_G + \vec{R}_G \times \vec{F}, \quad (2.6)$$

where  $\vec{r}_{m/G}$  is the position vector of the point of application of force  $\vec{F}_m$  with respect to the center of gravity.

### 2.2.2 Principle of D'Alembert

D'Alembert in 1743 proposed a principle that would reduce a problem in dynamics to an equivalent one in statics by introducing so-called *inertial forces*. The inertial force acting at the airplane's center of gravity is defined as  $-m\vec{a}_G$ , and the inertial moment about the center of gravity is defined as  $-I_y\ddot{\theta}\hat{j}$ . These inertial forces are drawn on the free body diagram of the airplane in addition to all the applied forces. *D'Alembert's principle states that the applied forces together with the inertial forces form a system in equilibrium.* Thus we write Newton's second law as

$$\vec{F} + (-m\dot{v}_G\hat{t} - mv_G^2\theta'\hat{n}) = 0 \quad \vec{M}_G + (-I_y\ddot{\theta}\hat{j}) = 0. \quad (2.7)$$

The free body diagram is modified accordingly as shown in figure 2.3. In the free body diagram the inertial forces and moment are indicated by dashed lines. From the free body diagram we proceed as in statics to write the conditions of (dynamic) equilibrium.

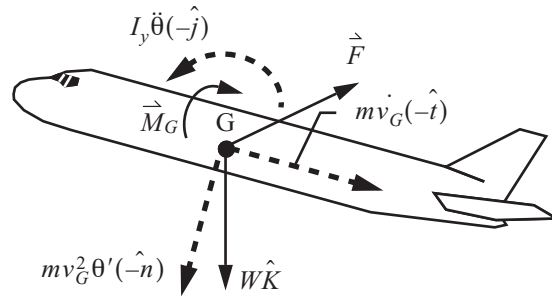


Fig. 2.3 Aircraft free body diagram at time  $t$  including the inertial forces and the inertial moment.

The curvature of the flight path  $\theta'$  can change sign. As shown in figure 2.4, the curvature is positive for a pull-up maneuver from a dive, and the curvature is negative for a push-down maneuver from a climb. Consequently, the inertia force normal to the flight path is directed toward the convex side of the path.

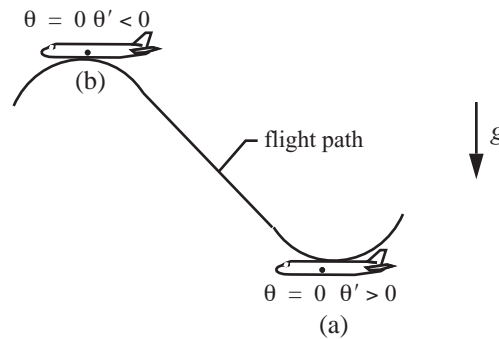


Fig. 2.4 Sign of the curvature for (a) pull-up from a dive, and (b) push-down from a climb.



### 2.2.3 Relative velocity and acceleration

Often it is necessary to determine the inertial forces at locations within the airplane not coincident with the center of gravity. For these computations we need the relative velocity and acceleration formulas from rigid body dynamics. Consider two points  $A$  and  $G$  fixed in the body. The position of point  $A$  relative to  $G$  is taken as  $x_{A/G}\hat{i}$ , as shown in figure 2.5.

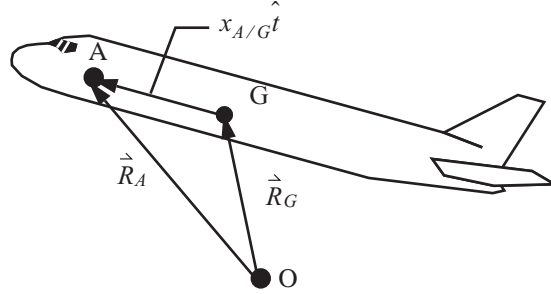


Fig. 2.5 Relative position of two points fixed in a rigid body.

The position vectors of points  $A$  and  $G$  are related by

$$\vec{R}_A = \vec{R}_G + x_{A/G}\hat{i}. \quad (2.8)$$

The velocity vectors of points  $A$  and  $G$  are then

$$\vec{v}_A = \vec{v}_G + \frac{d}{dt}(x_{A/G}\hat{i}). \quad (2.9)$$

Since vector  $x_{A/G}\hat{i}$  is embedded in the rigid body for all time, its rate of change is determined from its cross product with the vector of the time rate of change of pitch rotation. That is,

$$\frac{d}{dt}(x_{A/G}\hat{i}) = \dot{\theta}\hat{j} \times x_{A/G}\hat{i} = x_{A/G}\dot{\theta}\hat{n}. \quad (2.10)$$

Hence,

$$\vec{v}_A = \vec{v}_G + x_{A/G}\dot{\theta}\hat{n}. \quad (2.11)$$

The time rate of change of this velocity expression (2.11) relates the acceleration of  $A$  relative to  $G$  by

$$\vec{a}_A = \vec{a}_G + \frac{d}{dt}[x_{A/G}\dot{\theta}\hat{n}] = \vec{a}_A + x_{A/G}\ddot{\theta}\hat{n} + \dot{\theta}\frac{d}{dt}[x_{A/G}\hat{n}] = \vec{a}_G + x_{A/G}\ddot{\theta}\hat{n} + \dot{\theta}[\dot{\theta}\hat{j} \times x_{A/G}\hat{n}]. \quad (2.12)$$

Perform the vector cross product in eq. (2.12) to find

$$\vec{a}_A = \vec{a}_G + x_{A/G}\ddot{\theta}\hat{n} - \dot{\theta}^2 x_{A/G}\hat{t}. \quad (2.13)$$

### 2.2.4 Uniform linear and angular accelerations

In some inertial load problems it is reasonable to assume that the acceleration of a particle and/or the angular acceleration of a rigid body are constant over a time interval. Let  $s$  denote the distance of a particle along a straight line,  $v$  its speed along the line, and  $a$  its constant acceleration. Then, we have the following formulas

$$v = at + v_0 \quad s = \frac{1}{2}at^2 + v_0t + s_0 \quad 2a(s - s_0) = v^2 - v_0^2, \quad (2.14)$$

where  $s = s_0$  and  $v = v_0$  at time  $t = 0$ . Similarly if the angular acceleration  $\ddot{\theta}$  is constant over some time interval, then

$$\dot{\theta} = \ddot{\theta}t + \dot{\theta}_0 \quad \theta = \frac{1}{2}\ddot{\theta}t^2 + \dot{\theta}_0t + \theta_0 \quad 2\ddot{\theta}(\theta - \theta_0) = \dot{\theta}^2 - \dot{\theta}_0^2, \quad (2.15)$$

where  $\dot{\theta} = \dot{\theta}_0$  and  $\theta = \theta_0$  at time  $t = 0$ .

## 2.3 Load factors

It is convenient to combine the inertial forces and gravity forces in the analysis of aircraft structural components. Consider an airplane in general plane motion as depicted in figure 2.6.

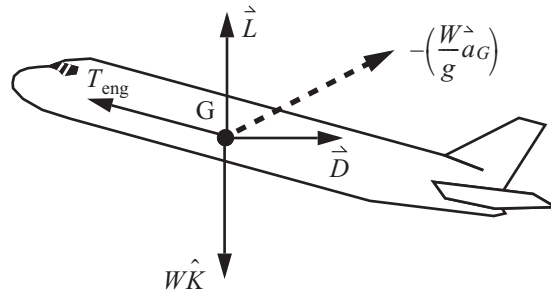


**Fig. 2.6** Inertial force, weight, and other forces acting on an airplane in general plane motion.

The actions shown in figure 2.6 represent:  $\vec{L}$  = lift force (wing and tail),  $\vec{D}$  = drag force,  $\vec{T}_{\text{eng}}$  = thrust force,  $-\frac{W}{g}\vec{a}_G$  = inertia force, and  $\vec{a}_G$  = acceleration of the center of gravity given by eq. (2.3). We are not considering the moment of momentum equation for now. However,  $\ddot{\theta} \neq 0$  in general. For the configuration shown in figure 2.6 dynamic equilibrium is

$$\vec{L} + \vec{D} + \vec{T}_{\text{eng}} + W\hat{K} - \frac{W}{g}\vec{a}_G = 0. \quad (2.16)$$

Let the total applied force on the airplane excluding weight be noted by  $\sum \vec{F}$ . The total applied force, in general, may include other effects than those shown in the sketch above (e.g., wheel reactions on landing.) Then dynamic equilibrium is written as

$$\sum \vec{F} - \underbrace{\left[ -W\hat{K} + \frac{W}{g}\dot{a}_G \right]}_{\text{combined weight and inertia force}} = 0 \quad (2.17)$$

As shown in figure 2.7, the projection of the gravity unit vector on the tangent and normal directions is  $\hat{K} = \sin\theta(-\hat{t}) + \cos\theta(-\hat{n})$ . Similarly, we define the projections of the resultant forces in the tangent and normal directions as

$$\sum \vec{F} \cdot \hat{t} = (\sum F)_x \quad \sum \vec{F} \cdot \hat{n} = (\sum F)_n. \quad (2.18)$$

Dynamic equilibrium (2.17) separated into tangent and normal directions is

$$\left[ (\sum F)_x - W \left( \sin\theta + \frac{\dot{v}_G}{g} \right) \right] \hat{t} + \left[ (\sum F)_n - W \left( \cos\theta + \frac{v_G^2 \theta'}{g} \right) \right] \hat{n} = 0. \quad (2.19)$$

Rewrite dynamic equilibrium (2.19) in the form

$$[(\sum F)_x - n_x W] \hat{t} + [(\sum F)_n - n_z W] \hat{n} = 0, \quad (2.20)$$

where the load factors in the tangent and normal directions are defined by

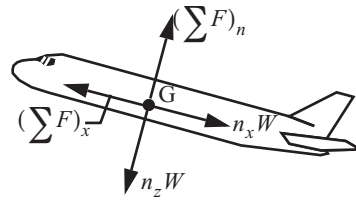
$$n_x = \left( \sin\theta + \frac{\dot{v}_G}{g} \right) \quad n_z = \left( \cos\theta + \frac{v_G^2 \theta'}{g} \right). \quad (2.21)$$

Also, eq. (2.20) shows that the load factors can be determined from

$$n_x = (\sum F)_x / W \quad n_z = (\sum F)_n / W. \quad (2.22)$$

Note that the load factor is a dimensionless number, and it can be negative, zero, or positive. The free body diagram for dynamic equilibrium of the airplane employing load factors is shown in figure 2.8.

**Fig. 2.8** Inertial forces and gravity forces represented by load factors for dynamic equilibrium of the airplane.



## 2.4 The V-n diagram

First, some definitions:

**Limit load** – the maximum load that an aircraft may be expected to encounter at any time in service

**Limit load factor** –  $n$  associated with limit load  $nW = LL$

**Ultimate load** – force necessary to rupture

**Ultimate load factor** –  $n$  associated with ultimate load  $nW = UL$

**Factor of safety** – ultimate load/limit load  $> 1$ ; usually 1.5

### 2.4.1 Airplane design requirements

1. All parts of the airplane are designed so they are not stressed beyond the yield point at the limit load factor.
2. The airplane structure must carry the ultimate loads for at least 3 seconds without collapsing, even though the members may acquire permanent deformation.

### 2.4.2 Regulations

Limit load factors are specified by regulations, which depend on the type of aircraft (e.g., transport, aerobatic, etc.). Criteria for civil aerospace vehicles in the United States.

Code of Federal Regulations

Title 14, Aeronautics and Space

Parts 1 – 59

Federal Aviation Administration (Department of Transportation is the regulatory agency.)

Military requirements in the United States. issued in **MIL–Specs** covering specific topics of structural design of US Air Force, Navy, and Marine aircraft.

### 2.4.3 Specified data

Specified maximum positive load factor;  $n_{\max} > 1$ .

Specified maximum negative load factor;  $n_{\min} < 0$ .

Specified design airspeeds:

$V_C$  = maximum level flight cruise speed

$V_D$  = maximum dive speed  $\sim 1.2$  to  $1.5 V_C$

### 2.4.4 Basic maneuver V-n diagram

This is predicated on pilot-controlled, symmetrical maneuvers in flight through calm air (i.e., no gust). Assumptions made for analytical purposes are that the pitching acceleration is assumed zero or negligible, the airspeed is constant during the maneuver, and there is no rolling or yawing of the aircraft, although rolling or yawing maneuvers may be considered in design as well. For no pitching acceleration the pitch rate  $\dot{\theta}$  is constant with respect to time. Use the chain rule to write the pitch rate as

$$\dot{\theta} = \frac{d\theta}{dt} = \frac{d\theta}{ds} \frac{ds}{dt} = \theta' v_G. \quad (2.23)$$

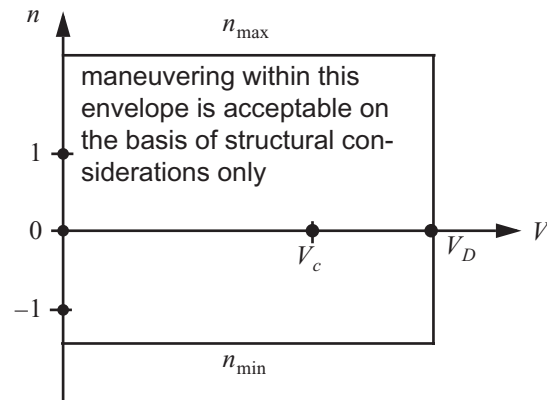
Hence, in a steady state maneuver  $\theta' v_G$  is constant with respect to time. The load factors (2.21) for a steady state maneuver are

$$n_x = \sin \theta \quad n_z = \left( \cos \theta + \frac{v_G^2 \theta'}{g} \right). \quad (2.24)$$

A pull-up from a dive, and a push-down from a climb are examples of steady state symmetrical maneuvers and

are depicted in figure 2.4. Also, a level flight, coordinated turn is considered a symmetrical maneuver even though the airplane does have a lateral acceleration in the turn. (Refer to practice exercise 2.) In general, the steady state symmetrical maneuvers will produce the maximum design wing loads. See figure 2.9.

**Fig. 2.9** Maneuver V-n diagram based on structural considerations only.



### 2.4.5 Aerodynamic data

When a two-dimensional airfoil is subject to a relative wind there is a net pressure distribution over the airfoil that depends on the angle of attack, which is denoted by  $\alpha$ . The angle of attack is the angle between the relative wind and the chord of the airfoil. The chord is the width of the airfoil and its length is denoted by  $c$ . The resultant action of the pressure distribution is a force  $R$  and no moment at the center of pressure, which is labeled C.P. in figure 2.10(a). The center of pressure location varies with the angle of attack. The resultant action of the pressure distribution is a force and a moment at any other location. The standard reference point for aerodynamic data is the aerodynamic center, which is labeled A.C. in figure 2.10(b). The aerodynamic center is the point where the pitching moment is independent of the angle of attack. For most subsonic wing sections the A.C. is around 25 percent of the chord. The net force of the pressure distribution is resolved at the aerodynamic center into a lift force perpendicular to the relative wind and a drag force parallel to the relative wind and the pitching moment.

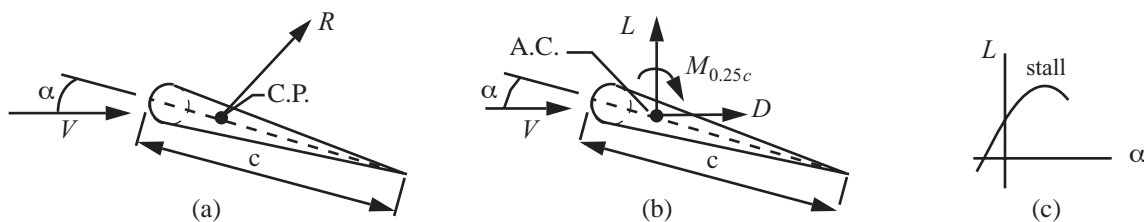


**Fig. 2.10** Characteristics of a two-dimensional airfoil: (a) center of pressure, (b) aerodynamic center, (c) stall.

The lift increases as the angle of attack increases. At some point, however, the flow can no longer stay attached to the upper surface and detaches. This results in a decrease in lift, which is called **aerodynamic stall** as shown in figure 2.10(c). The sharpness of the decrease in lift is dependent on the type of airfoil.

Airplanes are three-dimensional vehicles with three-dimensional aerodynamic surfaces, so the aerodynamic loads are spread over these surfaces. This distribution in the spanwise direction of the wing results in a force and moment at the root of the wing. The spanwise distribution of the airload is a function of the wing planform shape, the airfoil sections, and the geometric twist. The basic aerodynamic reference for three-dimensional wings is the

**mean aerodynamic chord (MAC).** The thickness, chord length, and angle of attack of the MAC airfoil section is used as a reference for all aerodynamic data. For a rectangular wing planform, the MAC is equal to the wing chord, and for a trapezoidal planform of the semiwing the MAC is equal to the chord at the centroid of the trapezoid.

**Methods of data acquisition.** Basic methods to calculate aerodynamic data for aircraft design and analysis are preliminary design estimates, wind tunnel testing, numerical fluid analysis, and aircraft flight test. The wind tunnel test is the major source for aerodynamic data in the preliminary design phase, and it involves construction of a scale model of the aircraft. The model is instrumented with pressure and force transducers. Data required for the structural analysis are the lift, drag, and pitching moment curves for the complete airplane with the horizontal tail removed through the range of angles of attack from the negative stalling angle to the positive angle. Data for the combination of the wing and fuselage, or the wing, fuselage, and nacelles, are more difficult to calculate accurately from the published data, because of the uncertain effects of the aerodynamic interference of the various components.

The lift force  $L$  is normal to the relative velocity (flight path), the drag force  $D$  is parallel to the relative velocity, and the pitching moment  $M_{0.25}$  is nose-up positive at the mean aerodynamic chord as shown in figure 2.11(a). The angle  $\theta$  is measured from the flight path to the  $x$ -axis and is equal to the difference between the angle of attack  $\alpha$  and the angle of wing incidence  $i$ .

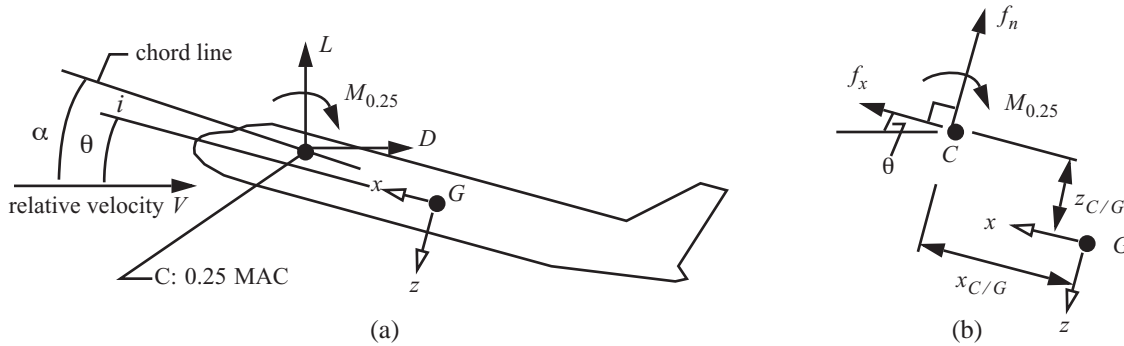


**Fig. 2.11 (a) Lift force, drag force, and pitching moment at the MAC. (b) Lift and drag resolved along the body  $x$ - and  $z$ -axes at MAC.**

The lift force, drag force, and pitching moment for the tail-off are expressed in terms of the dynamic pressure  $q$ , wing reference area  $S$ , and dimensionless aerodynamic coefficients  $C_L$ ,  $C_D$ , and  $C_{M0.25}$ . The dynamic pressure is

$$q = \frac{1}{2} \rho V^2, \quad (2.25)$$

where the air density at altitude is denoted by  $\rho$ . The aerodynamic actions are expressed as

$$L = C_L q S \quad D = C_D q S \quad M_{0.25} = C_{M0.25} q S \bar{c}, \quad (2.26)$$

where the mean aerodynamic chord is denoted by  $\bar{c}$ .

The aerodynamic actions  $L$ ,  $D$ , and  $M_{0.25}$  at the mean aerodynamic chord are statically equivalent to the aerodynamic actions  $f_n$ ,  $f_x$ , and  $M_y$  at the center of gravity. The lift and drag forces are resolved into components normal  $f_n$  and parallel  $f_x$  to the flight path by

$$f_n = L \cos \theta + D \sin \theta, \text{ and } f_x = L \sin \theta - D \cos \theta. \quad (2.27)$$

The moment at the center of gravity is determined from figure 2.11(b):

$$M_y = M_{0.25} + x_{C/G} f_n - z_{C/G} f_x. \quad (2.28)$$

The forces acting on the airplane are shown in figure 2.12, in which the tail force  $L_t$  acts perpendicular to the flight path at the center of pressure of the horizontal tail.

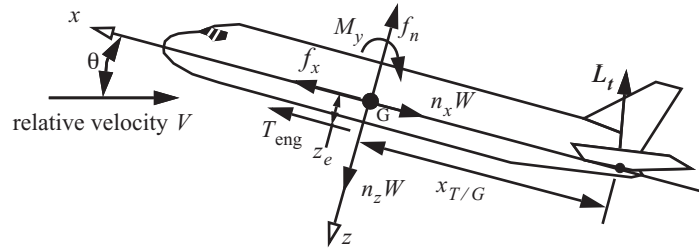


**Fig. 2.12** Forces acting on the airplane during steady state symmetrical maneuvers. No pitching acceleration.

The dynamic equilibrium equations for no acceleration in pitch are

$$f_x + T_{\text{eng}} - n_x W + L_t \sin \theta = 0, \quad (2.29)$$

$$f_n - n_z W + L_t \cos \theta = 0, \text{ and} \quad (2.30)$$

$$M_y + z_e T_{\text{eng}} - x_{T/G} L_t \cos \theta = 0. \quad (2.31)$$

Substitute the moment at the center of gravity (2.28) into eq. (2.31) to get

$$M_{0.25} + x_{C/G} f_n - z_{C/G} f_x + z_e T_{\text{eng}} - x_{T/G} L_t \cos \theta = 0. \quad (2.32)$$

Introduce aerodynamic coefficients  $C_n$ ,  $C_x$  and  $C_t$  by the relations

$$f_n = C_n q S, f_x = C_x q S, \text{ and } L_t = C_t q S. \quad (2.33)$$

Substituting  $f_n$  and  $f_x$  from the definitions (2.33) into eq. (2.27) determines the coefficients  $C_n$  and  $C_x$  as

$$C_n = C_L \cos \theta + C_D \sin \theta, \text{ and } C_x = C_L \sin \theta - C_D \cos \theta. \quad (2.34)$$

The balancing tail force coefficient  $C_t$  is to be determined from the equations of dynamic equilibrium. From the relations (2.33) and (2.34), the equilibrium equations (2.29) and (2.30) are written as

$$n_x W = (C_x + C_t \sin \theta) q S + T_{\text{eng}}, \text{ and} \quad (2.35)$$

$$n_z W = (C_n + C_t \cos \theta) q S. \quad (2.36)$$

Let  $n_z W = C_N q S$ , where the airplane normal coefficient is denoted by  $C_N$ . From eq. (2.36) the normal coefficient is

$$C_N = C_n + C_t \cos \theta. \quad (2.37)$$

In terms of the aerodynamic relations introduced, the moment about the center of gravity (2.32) is

$$C_{M0.25} q S \bar{c} + x_{C/G} C_n q S - z_{C/G} C_x q S + z_e T_{eng} - x_{T/G} C_t q S \cos \theta = 0. \quad (2.38)$$

Rearrange eq. (2.38) to

$$(C_{M0.25} \bar{c} + x_{C/G} C_n - z_{C/G} C_x - x_{T/G} C_t \cos \theta) q S + z_e T_{eng} = 0. \quad (2.39)$$

Consider the case of power-off so that  $T_{eng} = 0$ , and solve for  $C_t \cos \theta$  to get

$$C_t \cos \theta = (\bar{c}/x_{T/G}) C_{M0.25} + (x_{C/G}/x_{T/G}) C_n - (z_{C/G}/x_{T/G}) C_x. \quad (2.40)$$

If the term on the right side containing longitudinal coefficient  $C_x$  is assumed small with respect to the other terms and neglected, then the resulting expression for coefficient  $C_t$  is consistent with the traditional equation for the balancing tail load (Lomax, p. 9). Substitute  $C_t \cos \theta$  from eq. (2.40) into eq. (2.37) to get the expression for the normal coefficient determined from the aerodynamic coefficients with the tail off:

$$C_N = (\bar{c}/x_{T/G}) C_{M0.25} + (x_{C/G}/x_{T/G}) C_n - (z_{C/G}/x_{T/G}) C_x. \quad (2.41)$$

The total normal force is denoted by  $L_z$ . From eq. (2.30)  $L_z = f_n + L_t \cos \theta = n_z W$ , and  $n_z W = C_N q S$ . Hence,

$$L_z = n_z W = C_N q S = \left( \frac{1}{2} \rho V^2 \right) S C_N. \quad (2.42)$$

From wind tunnel data for complete airplane the aerodynamic coefficient of lift along the  $z$  axis is plotted against the angle of attack as depicted in figure 2.13. Generally, the magnitudes of the maximum and minimum values of the normal aerodynamic coefficient corresponding to stall and inverted stall, respectively, satisfy

$$|(C_N)_{\min}| < |(C_N)_{\max}|.$$

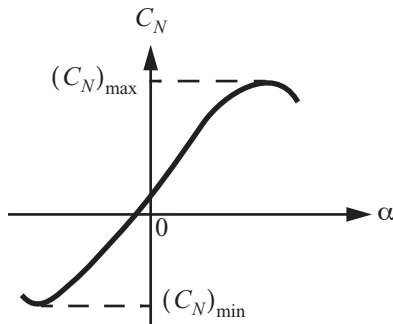


**Fig. 2.13** Normal force coefficient as a function of the angle of attack.

Substitute  $C_x$  from eq. (2.34) into eq. (2.35) to find the longitudinal load factor as

$$n_x W = [(C_L + C_t) \sin \theta - C_D \cos \theta] q S + T_{eng}. \quad (2.43)$$

At a given airspeed



$$\begin{aligned}
 (L_z)_{\max} &= \left(\frac{1}{2}\rho V^2\right) S(C_N)_{\max} = n_{z\max} W && \text{pull-up from dive} \\
 (L_z)_{\min} &= \left(\frac{1}{2}\rho V^2\right) S(C_N)_{\min} = n_{z\min} W && \text{push-down from climb.}
 \end{aligned} \tag{2.44}$$

Hence,

$$n_{z\max} = (C_N)_{\max} \frac{(\rho V^2/2)}{(W/S)} \quad n_{z\min} = (C_N)_{\min} \frac{(\rho V^2/2)}{(W/S)}, \tag{2.45}$$

which are quadratic functions of  $V$ .

#### 2.4.6 Maneuver V-n diagram including aerodynamic stall

The maneuver V-n diagram including aerodynamic stall is shown in figure 2.14.

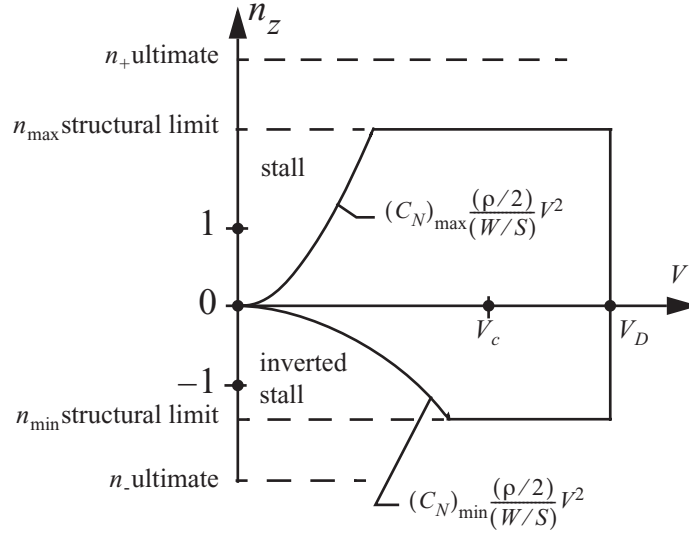


**Fig. 2.14** Maneuver V-n diagram including aerodynamic stall and specified data.

Note:

1.  $C_N$  varies with compressibility, and varies with the C.G. location as shown in eq. (2.41). Generally we must consider different altitudes and weight configurations.
2. For flight in incompressible air, the dynamic pressure  $q = \frac{1}{2}\rho V^2$ , where  $V$  is the airspeed and  $\rho$  is the air density, both at altitude. Define **equivalent airspeed**  $V_{\text{EAS}}$  at sea level by

$$q = \frac{1}{2}\rho V^2 = \frac{1}{2}\rho_{\text{s.l.}} V_{\text{EAS}}^2. \tag{2.46}$$

Then the equivalent airspeed is given by  $V_{\text{EAS}} = \sqrt{\frac{\rho}{\rho_{\text{s.l.}}}} V$ . Use  $V_{\text{EAS}}$  on V-n diagram to cover all altitudes. Some

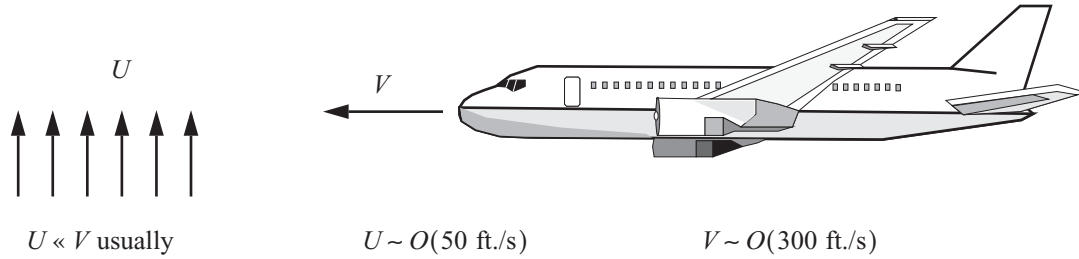
	Structural limits	
Category	$n_{\max}$	$n_{\min}$
U.S. civil transports (Boeing)	2.5	-1.0
U.S. military heavy bomber	3.0	-1.0
U.S. military subsonic attack	8.0	-3.0
U.K. civil aerobatic	6.0	-3.0
U.K. sailplane, aerobatic	7.0	-5.0

Figure 2.15 is a graph of the flight maneuvering envelope per FAR 25.333. The vertical axis represents the load factor  $n_z$ , ranging from -1 to 3. The horizontal axis represents the equivalent air speed, with key points  $V_{s1}$ ,  $V_F$ ,  $V_C$ , and  $V_D$  marked. The envelope is defined by two main curves: a solid line for 'Flaps up' and a dashed line for 'Flaps down'. The 'Flaps up' curve starts at the origin (0,0), rises to a point A at  $(V_F, 2.5)$ , then levels off at  $n_z = 2.5$  until  $V_D$ . The 'Flaps down' curve starts at the origin (0,0), rises to a point I at  $(V_{s1}, 2)$ , then levels off at  $n_z = 2$  until  $V_F$ . The 'Flaps up' curve also has a lower branch starting at the origin (0,0), reaching a minimum at point H at  $(V_{s1}, -1)$ , then levels off at  $n_z = -1$  until  $V_C$ , and finally rises to point E at  $(V_D, 0)$ . The 'Flaps down' curve also has a lower branch starting at the origin (0,0), reaching a minimum at point F at  $(V_C, -1)$ , then rises to point D at  $(V_D, 0)$ . A dashed line at  $n_z = 1$  intersects the envelope at  $V_{s1}$ ,  $V_F$ , and  $V_C$ . A solid line at  $n_z = 0$  intersects the envelope at  $V_{s1}$ ,  $V_F$ ,  $V_C$ , and  $V_D$ . A solid dot is located at  $(V_C, 1)$ .

**Fig. 2.15** Flight maneuvering envelope per FAR 25.333.

## 2.5 Design gust load factors

Turbulent conditions of varying intensity occur in air through which an airplane flies. For example, atmospheric phenomena that create turbulence are thermals (convection), mountain waves (terrain effects), wind shears, and jet streams. Assume steady level flight from still air,  $n = 1$ , into an ideal sharp-edged gust as shown in figure 2.16.



**Fig. 2.16** Steady level flight into a sharp-edged gust.

The change in the angle of attack due to the idealized sharp-edged gust is depicted in figure 2.17.

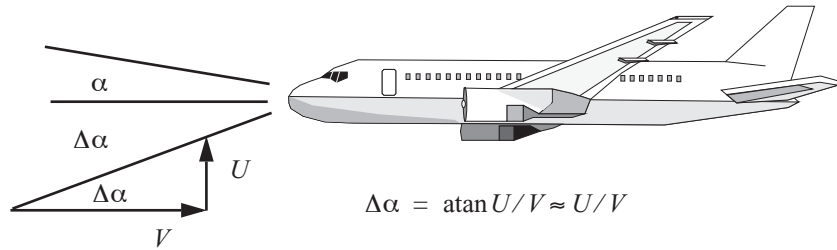


**Fig. 2.17** Equivalent relative wind.

The lift curve slope between stall points is  $m = (dC_N)/(d\alpha)$ . Therefore, the change in the aerodynamic coefficient is

$$\Delta C_N = m(\Delta\alpha), \quad (2.47)$$

and the change in lift is

$$\Delta \text{Lift} = \left(\frac{1}{2}\rho V^2\right) S m(\Delta\alpha) = \frac{1}{2}\rho V S m U. \quad (2.48)$$

Now the change in the load factor due to the gust is

$$\Delta n = \frac{\Delta \text{Lift}}{W} = \left[\frac{(\rho m)/2}{(W/S)}\right] UV, \quad (2.49)$$

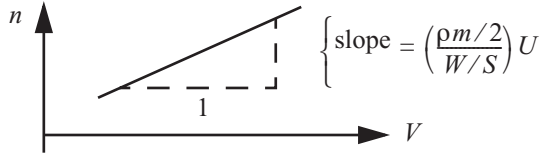


**Fig. 2.18** The linear change in the load factor

where  $W/S$  is the wing loading in  $\text{lb./ft.}^2$ . The change in the load factor  $\Delta n$  varies linearly with airspeed  $V$  as depicted in figure 2.18.

### 2.5.1 Gust alleviation factor

A more realistic, semiempirical treatment of gust effects, based on experience and analysis, is to replace the sharp-edged gust speed  $U$  by  $K_g U$ , where  $K_g$  is the gust alleviation factor. In reality there is no such thing as a sharp-edged gust so we account empirically for gust build-up and airplane response. For transport airplanes, NACA specified

$$K_g = \frac{0.88\mu_g}{5.3 + \mu_g} < 0.88, \quad (2.50)$$

where  $\mu_g$  is the airplane mass ratio defined by

$$\mu_g \equiv \frac{W/S}{(\bar{\rho} c g m)/2}, \quad (2.51)$$

and where  $\bar{c}$  is the mean aerodynamic chord;  $\bar{c} = S/b$ , and  $b$  is the wing span. See figure 2.19.

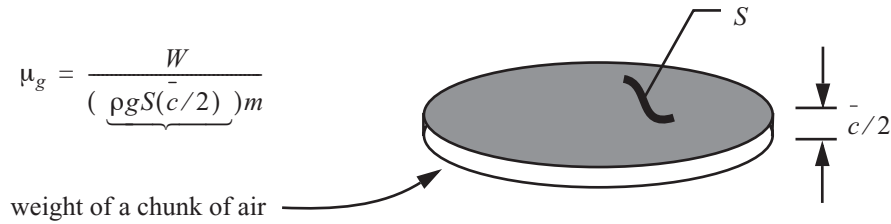


**Fig. 2.19** Depiction of the airplane mass ratio.

### 2.5.2 Gust load factor

For steady level flight, the gust load factor is

$$n = 1 + \left( \frac{\rho m/2}{W/S} \right) K_g U V. \quad (2.52)$$

Note that a lightly loaded airplane is more susceptible than when heavily loaded. This is because the increment in lift is independent of the weight. A heavily loaded airplane has more inertia with which to smooth out gusts than a lightly loaded airplane, all other things being equal.

### 2.5.3 NACA discrete gust conditions

Discrete gusts refer to sudden changes, or alleviated sharp-edged gusts, as opposed to continuous turbulence aircraft gust analysis. In continuous turbulence gusts are represented as a stationary Gaussian random process lead-

ing to specification of a power spectral density (Hoblit, 1988). For civil transport airplanes 0–20,000 ft., three discrete gusts are specified:

1. Rough air gust:  $U = 66$  ft/s at  $V = V_B$  a speed related to the stall speed.
2. High speed gust:  $U = 50$  ft/s at cruise speed  $V_C$ .
3. Dive speed gust:  $U = 25$  ft/s at dive speed  $V_D$ .

The gust V-n diagram is shown in figure 2.20, and it is almost symmetrical with  $n = 1$  line since gusts are as likely to act down as up.

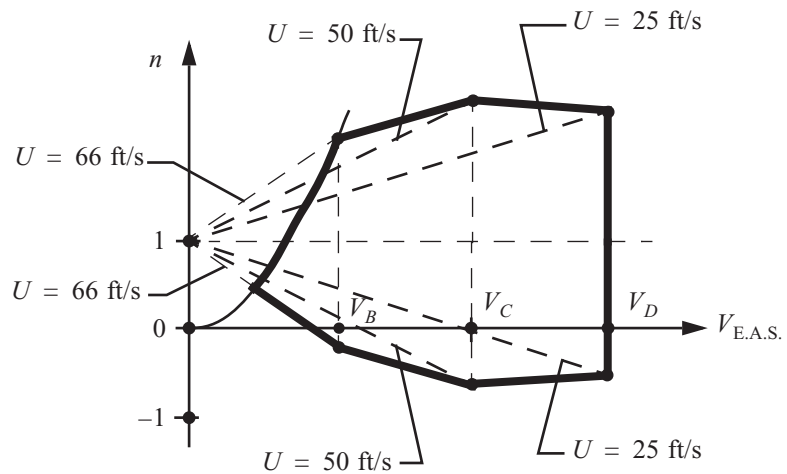


Fig. 2.20 Gust V-n diagram.

#### 2.5.4 Design V-n diagram

The extreme load factors of both maneuver and gust diagrams must be met. Superimpose the two and take the outer boundaries as shown in figure 2.21. Generally, large airplanes are designed primarily by gust load factors. Small military and aerobatic airplanes are designed by maneuver load factors.

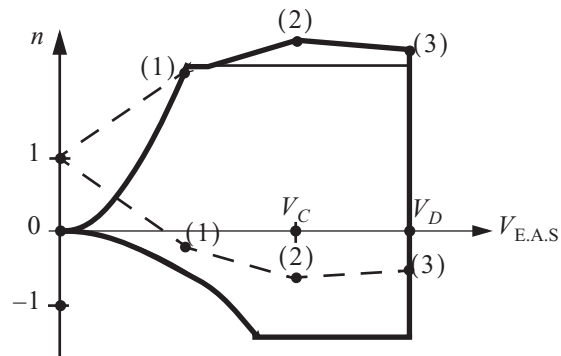


Fig. 2.21 Design V-n diagram.

## 2.6 Design V-n diagram example

This example is typical of a small aerobatic or perhaps military airplane, with specified data given figure 2.22.

$$W = 10,000 \text{ lb.}$$

$$S = 100 \text{ ft}^2$$

$$b = 25 \text{ ft.}$$

$$\bar{c} = S/b = 4 \text{ ft.}$$

$$V_C = 500 \text{ mph} \quad V_D = 650 \text{ mph} \quad (C_N)_{\max} = 2.07$$

$$(C_N)_{\min} = -1.2 \quad m = dC_N/d\alpha = 4.37 \text{ per radian}$$

$$\text{str. limit load factors} \quad n_{\max} = 7.5 \quad n_{\min} = -3$$

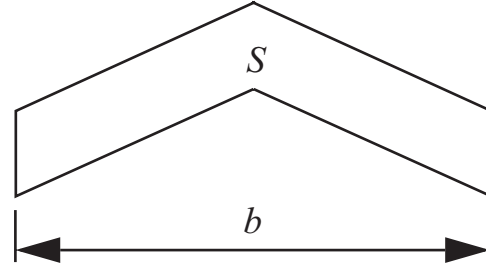


**Fig. 2.22** Data for the small aerobatic or military airplane.

**Problem statement:** Determine the design V-n diagram at sea level using the NACA formulas for gust loads.

First, draw the maneuver V-n diagram. The stall boundary is given by

$$n_{\text{stall}} = (C_N)_{\max} \frac{\rho_{\text{s.l.}}/2}{W/S} V^2. \quad (\text{a})$$

The density of air at sea level is

$$\rho_{\text{s.l.}} = 0.002378 \frac{\text{slugs}}{\text{ft.}^3}, \text{ where } 1 \text{ lb.} = (1 \text{ slug})(1 \text{ ft./s}^2). \quad (\text{b})$$

The wing loading is

$$W/S = (10,000 \text{ lb.})/(100 \text{ ft.}^2) = 100 \text{ lb./ft.}^2. \quad (\text{c})$$

Substitute eqs. (b) and (c) into eq. (a) to get

$$n_{\text{stall}} = (2.07) \frac{\left(0.002378 \frac{\text{lb.s}^2}{\text{ft.}^4} / 2\right)}{100 \text{ lb./ft.}^2} V^2, \text{ or} \quad (\text{d})$$

$$n_{\text{stall}} = 2.46 \times 10^{-5} V^2 \quad V \text{ in ft./s.} \quad (\text{e})$$

The inverted stall boundary is

$$n_{\text{istall}} = (C_N)_{\min} \frac{\rho_{\text{s.l.}}/2}{W/S} V^2 = \frac{-1.2(0.002378/2)}{100} V^2, \text{ or} \quad (\text{f})$$

$$n_{\text{istall}} = -1.43 \times 10^{-5} V^2 \quad V \text{ in ft./s.} \quad (\text{g})$$

The airspeeds at stall and structural limit factors are

$$2.46 \times 10^{-5} V_T^2 = 7.5 \quad V_T = 552 \text{ ft./s} \left( \frac{60 \text{ mph}}{88 \text{ ft./s}} \right) = 376 \text{ mph, and} \quad (\text{h})$$

$$-1.43 \times 10^{-5} (V'_T)^2 = -3.0 \quad V'_T = 459 \text{ ft./s} = 313 \text{ mph.} \quad (\text{i})$$

The maneuver V-n diagram is shown in figure 2.23.

Second, draw the gust V-n diagram using NACA formulas. Find the value of the gust alleviation factor as given in eq. (2.50). The airplane mass ratio is

$$\mu_g = \frac{W/S}{(\rho c g m)/2} = \frac{100 \text{ lb./ft}^2}{(0.002378 \text{ lb s}^2/\text{ft}^4)(4 \text{ ft.})(32.2 \text{ ft/s}^2)(4.37)/2}, \text{ where} \quad (\text{j})$$

$$\mu_g = 149 \quad \text{dimensionless.}$$

Hence, the gust alleviation factor is  $K_g = 0.85$ . The change in the load factor due to the gust is

$$\Delta n_{\text{gust}} = \left( \frac{\rho m/2}{W/S} \right) K_g UV = \frac{0.002378(4.37)/2}{100} (0.85) UV, \text{ or} \quad (\text{k})$$

$$\Delta n_{\text{gust}} = 4.42 \times 10^{-5} UV \quad U, V \text{ in ft./s.} \quad (\text{l})$$

For gust (1)  $U = 66 \text{ ft/s}$  at  $V = V_B$ . To find the airplane speed  $V_B$  on the stall boundary we set the load factor in eq. (2.52) equal to its relationship to the airplane speed on the stall boundary; i.e.,

$$\underbrace{2.46 \times 10^{-5} V_B^2}_{\text{stall}} = 1 + \underbrace{4.42 \times 10^{-5} (66)}_{2.91 \times 10^{-3}} V_B \quad (\text{m})$$

Solve eq. (m) for speed  $V_B$  as follows:

$$V_B = \frac{2.91 \times 10^{-3} \pm \sqrt{(2.91 \times 10^{-3})^2 + 4(2.46 \times 10^{-5})(1)}}{2(2.46 \times 10^{-5})}, \quad (\text{n})$$

$$V_B = \frac{2.91 \times 10^{-3} \pm 1.03 \times 10^{-2}}{2(2.46 \times 10^{-5})} \quad \text{choose +.} \quad (\text{o})$$

Hence,  $V_B = 269 \text{ ft/s} = 184 \text{ mph}$ , and the change in load factor for gust (1) is

$$\Delta n_1 = 4.42 \times 10^{-5} (66)(269) = 0.78. \quad (\text{p})$$

For gust (2)  $U = 50 \text{ ft/s}$  at  $V_C = 500 \text{ mph}$ . Hence, the change in load factor is

$$\Delta n_2 = 4.42 \times 10^{-5} (50) \left[ 500 \text{ mph} \left( \frac{88 \text{ ft/s}}{60 \text{ mph}} \right) \right] = 1.62. \quad (\text{q})$$

For gust (3)  $U = 25$  ft/s at 650 mph, and the change in load factor is

$$\Delta n_3 = 4.42 \times 10^{-5} (25) \left[ 650 \text{ mph} \left( \frac{88 \text{ ft/s}}{60 \text{ mph}} \right) \right] = 1.05 . \quad (r)$$

Thus, the six points on the gust V-n diagram are

$$\begin{aligned} 1 \pm \Delta n_1 &= 1.78, 0.22 & V_B &= 184 \text{ mph} \\ 1 \pm \Delta n_2 &= 2.62, -0.62 & V_C &= 500 \text{ mph} \\ 1 \pm \Delta n_3 &= 2.05, -0.05 & V_D &= 650 \text{ mph} \end{aligned} \quad (s)$$

A sketch of the gust V-n diagram is shown in figure 2.23. Here the design V-n diagram is the maneuver V-n diagram since the gust V-n diagram is contained inside the maneuver V-n diagram.

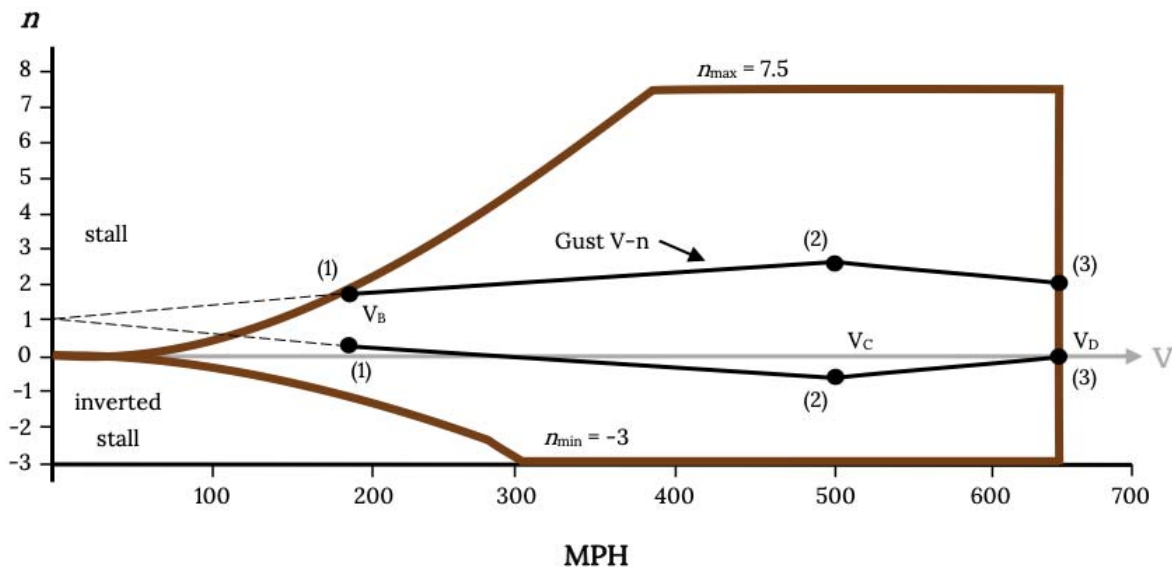


Fig. 2.23 Maneuver and gust V-n diagrams for the example of a small aerobatic or military airplane.

## 2.7 References

- Hoblitt, F.M., *Gust Loads on Aircraft: Concepts and Applications*. Reston, VA: American Institute of Aeronautics and Astronautics, Inc., 1988.
- Lomax, T. L., *Structural Loads Analysis for Commercial Transport Aircraft: Theory and Practice*. Reston, VA: American Institute of Aeronautics and Astronautics, Inc., 1996.
- Megson, T.H.G., *Aircraft Structures for Engineering Students*, 3d ed., New York: John Wiley & Sons Inc.; Lon-



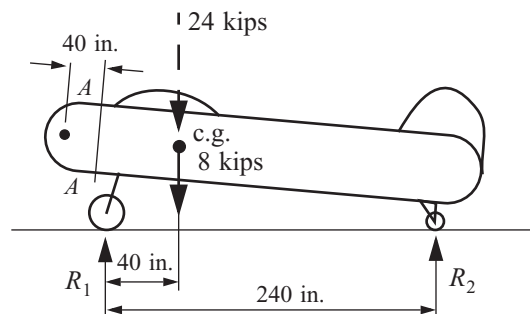
don: Arnold, a member of the Hodder Headline Group, 1999.

Peery, D. J., 2011, *Aircraft Structures*. Dover Publications, Inc., 2011. (Unabridged republication of the work originally published in 1950 by the McGraw-Hill Book Company, New York.) Chapter 3.

## 2.8 Practice exercises

1. An airplane weighting 8,000 lb. has an upward acceleration of  $3g$  when landing. If the dimensions are as shown in figure 2.24, what are the wheel reactions  $R_1$  and  $R_2$ ? What is the time required to decelerate the airplane from a vertical velocity of 12 ft./s? What is the shear and bending moment on a vertical section A–A, if the weight forward of this section is 2,000 lb. and has a center of gravity 40 in. from this cross section. (Peery, 2011, p. 54).

Fig. 2.24 Exercise 1.

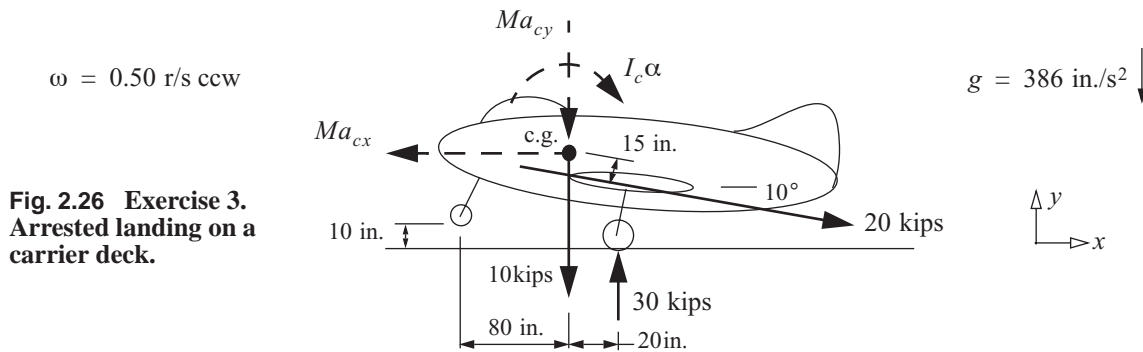


2. An 8,000 lb. airplane is making a horizontal turn with a radius of 1,000 ft. and with no change in altitude. See figure 2.25. Find the angle of bank and the load factor for a speed of (a) 200 mph., (b) 300 mph, and (c) 400 mph. Find the loads on the wing and tail if the dimensions are as shown (Peery, 2011, p. 72).

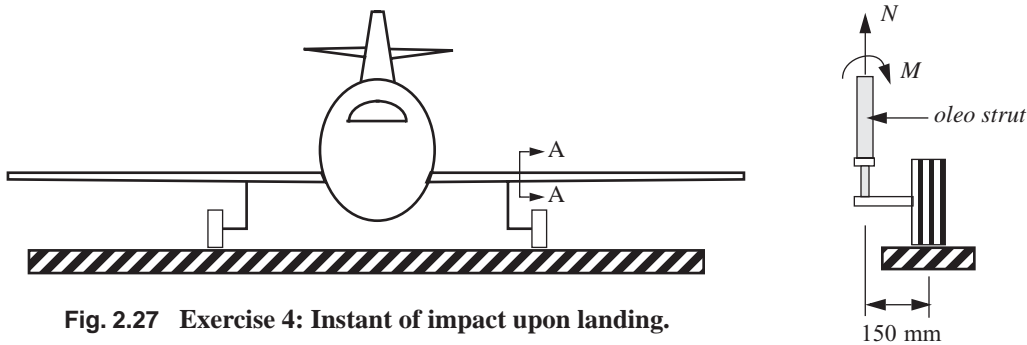


Fig. 2.25 Exercise 2. Level flight coordinated turn.

3. The airplane shown in figure 2.26 is making an arrested landing on a carrier deck. At the position shown, the angular velocity is 0.5 rad/s counterclockwise and the vertical velocity of the center of gravity is 12 ft./s. The radius of gyration for the mass of the airplane about the center of gravity is 60 in. Find the load factors  $n_x$  and  $n_y$ , parallel and perpendicular to the deck, for a point at the center of gravity, a point 200 in. aft of the center of gravity, and a point 100 in. forward of the center of gravity. Find the vertical velocity with which the nose wheel strikes the deck. Assume no change in the dimensions or loads, and the downward acceleration of the nose wheel is constant in the 10 in. of vertical travel (Peery, 2011, p. 72).



4. The aircraft shown below weighs 135 kN and has landed such that at the instant of impact the ground reaction on each main undercarriage wheel is 200 kN and its vertical velocity is 3.5 m/s. (Adapted from Megson,



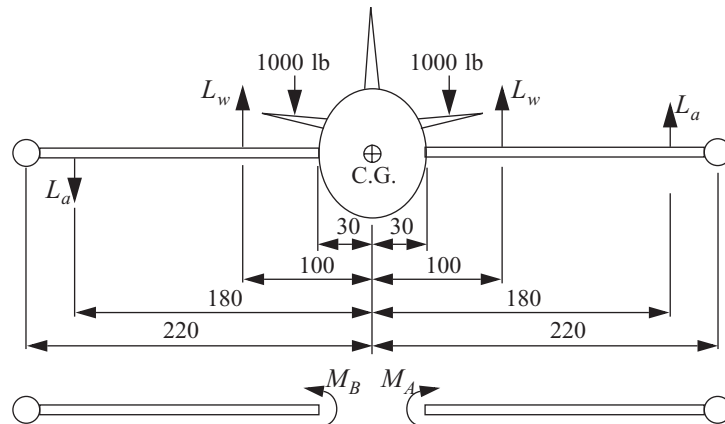
1999, P.8.1, p. 272.)

Each undercarriage wheel weighs 2.25 kN and is attached to an oleo strut.

- What is an oleo strut? What is its purpose? Describe its components and how it functions.
  - Calculate the axial load  $N$  and bending moment  $M$  in the strut, assuming the strut is vertical.
  - Determine the shortening of the strut when the vertical velocity of the aircraft is zero.
  - Calculate the shear force and bending moment in the wing section A-A if the wing outboard of section A-A weighs 6.6 kN and has a center of gravity 3.05 m from A-A.
5. An airplane has a **total** weight of 40,000 lb. and **total rolling** moment of inertia about the C.G. of 1,000,000 lb.-s<sup>2</sup>-in. Each wing-tip store weighs 2,000 lb. In steady level flight, each wing's resultant lift is  $L_w = 21,000$  lb. (The tail carries stabilizing a negative lift of 2,000 lb.) In a sudden evasive roll maneuver from steady level flight, each aileron introduces a lift increment  $L_a = \pm 3,000$  lb. Assuming the airplane to be rigid and, neglecting wing weight, calculate the total root bending moment for each wing (i.e.,  $M_A$  and  $M_B$ ). Neglect the moment of inertia of each wing-tip store about its own C.G.
6. Use the data given in table 2.2 and the NACA gust formulas to develop the design V-n diagram for the Boeing 727 aircraft at sea level. The airspeed should be in knots. One knot equals one nautical mile per hour, and

**Fig. 2.28 Exercise 5:**  
Evasive roll maneuver  
from steady level flight.

All dimensions in  
inches.



approximate one nautical mile as 6,080 ft.<sup>1</sup> Clearly label the plot. Also calculate the level flight stall speed  $V_{S1}$ .

**Table 2.2 Exercise 6**

$S$	1560 ft. <sup>2</sup>
$b$	108 ft.
$W$	170,000 lb.
$(dC_{za})/(d\alpha)$	5.0 per radian
$C_{zamax}$	0.951
$C_{zamin}$	-0.400
$n_{max}$	2.5 (structural)
$n_{min}$	-1.0 (structural)
$V_C$	350 knots
$V_D$	440 knots

7. Shown below is the maneuver V-n diagram at sea level for an aircraft of wing span 27.5 m, mean aerodynamic chord 3.05 m, and total weight 196,000 N. The aerodynamic center is 0.915 m forward of the center of gravity and the center of lift for the tail unit is 16.7 m aft of the C.G. The pitching moment coefficient is

$$C_{M0.25} = -0.0638(\text{nose-up positive}).$$

1. A nautical mile is based on the circumference of the planet Earth. If you were to cut the Earth in half at the equator, you could pick up one of the halves and look at the equator as a circle. You could divide that circle into 360 degrees. You could then divide a degree into 60 minutes. A minute of arc on the planet Earth is 1 nautical mile. This unit of measurement is used by all nations for air and sea travel. A nautical mile is 1,852 meters, or 1.852 kilometers. In the English measurement system, a nautical mile is 1.1508 miles, or 6,076 feet. [<http://www.howstuff-works.com>]

Both the pitching moment coefficient and the position of the aerodynamic center are specified for the complete aircraft less the tail unit.

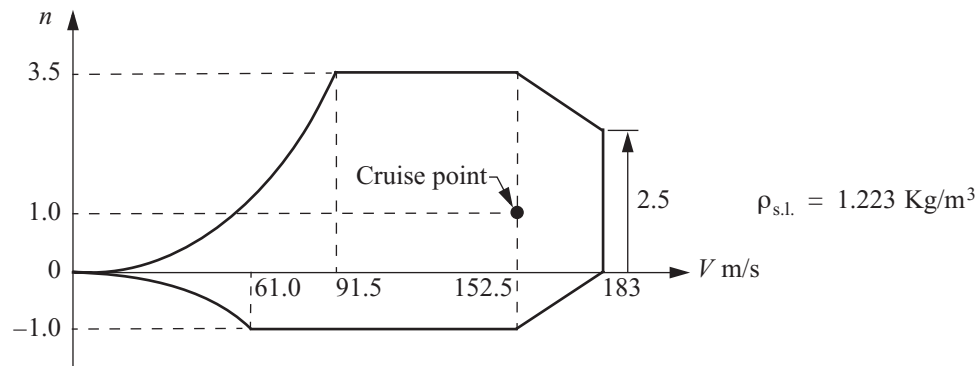


**Fig. 2.29 Exercise 7: Maneuver V-n diagram at sea level (U.K. regulations).**

For steady level flight at sea level the fuselage bending moment at the C.G. was recorded by test equipment to be 600,000 N m. Calculate the maximum value of this bending moment for the given flight envelope, or V-n diagram. For this purpose it may be assumed that the aerodynamic loadings on the fuselage structure itself can be neglected; i.e., the only loads on the fuselage aft of the C.G. are those due to tail lift and the inertia of the fuselage.

# Elements of a thin-walled bar theory

Essential aspects of a linear elastic theory for straight, uniform, thin-walled bars is presented. It is assumed that the material is homogeneous and isotropic. Bars with an open cross section are presented first, followed by bars with a closed cross section. The thin-walled bar theory presented in this chapter allows for free warping of the cross section out of its plane under torsion and transverse shear. Constrained warping theory is not discussed, but it is presented in texts by Gjelsvik (1981), Oden and Ripperger (1981), Vasiliev (1993), and Vasiliev and Morozov (2013). Bars fabricated by laminating fibrous composite materials are discussed in article 8.1.

## 3.1 Open cross section

A bar with an open cross section is shown in figure 3.1(a). There are two branches in the cross section. A vertical straight branch of length  $a$  with wall thickness  $t$ , and a semicircular branch of radius  $a$  with wall thickness  $t$ .

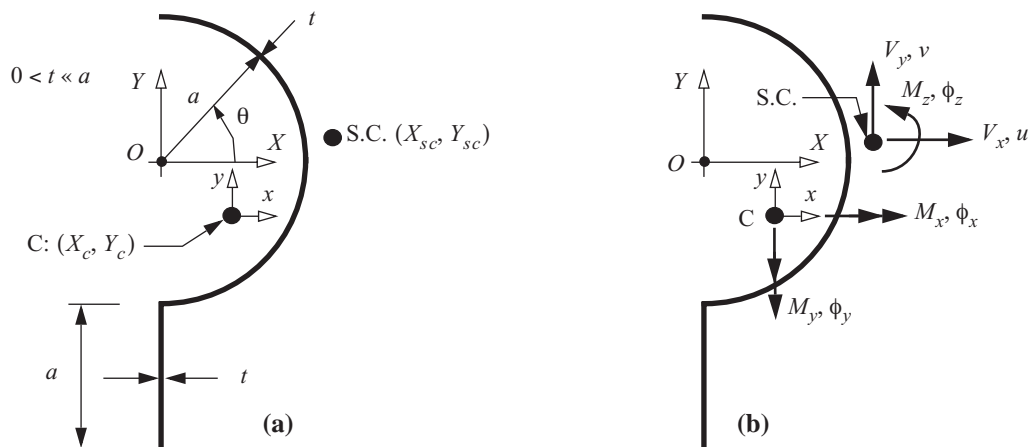


**Fig. 3.1** Thin-walled open cross section: (a) geometry and coordinate systems and (b) internal actions.

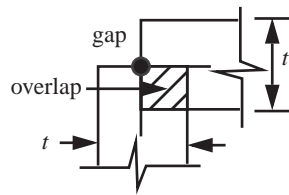


**Fig. 3.2 Idealized junction.**

The geometry of the bar's cross section is defined by the locus of points along the center line of the wall, which is called the **contour**, and the thickness  $t$  of the wall. The contour consists of piece-wise continuous lines or curves in the plane of the cross section whose subdivisions are called branches. Points between branches occur at junctions or sharp corners. Let the arc-length along the contour be denoted by  $s$ , and the thickness can be a function of  $s$ . That is  $t = t(s) > 0$ , as long as it is small with respect to the length of a branch and to its radius of curvature (e.g.,  $0 < t \ll a$  for the section shown in figure 3.1(a)). At junctions between branches overlaps and gaps of cross-sectional areas can occur as shown in figure 3.2, but its effect on the geometrical properties of the section are small under the thin-walled assumption. A step change in thickness along a contour is accommodated by defining a junction at the location of the step.

The bar is referenced to two, right-handed Cartesian coordinate systems labeled  $(X, Y, Z)$  and  $(x, y, z)$ . The positive directions of the  $Z$ -axis and the  $z$ -axis are out of the plane of the cross section shown in the figure with  $Z = z$ , where  $z \in [0, L]$  and  $L$  is the axial length of the bar. The cross section shown figure 3.1(a) is called a positive  $z$ -face since the normal to the cross section points outward (positive  $z$ -direction) from the material contained behind the cross section. The origin of the  $(X, Y)$  system in the cross section is taken at the center of the semicircular branch for convenience, and is labeled point  $O$ . The  $(x, y)$  system is parallel to the  $(X, Y)$  system, and the origin of the  $(x, y)$  system is at the centroid, which is labeled point  $C$ . The shear center in the cross section is labeled as point  $S.C.$

The internal resultants acting on the cross section of the bar are  $N, V_x, V_y, M_x, M_y$ , and  $M_z$ , and these resultants are functions of the axial coordinate  $z$ . Refer to figure 3.1(b). The axial normal force is labeled  $N$ , and is defined positive in tension acting at the centroid. Note that  $N$  is not shown in figure 3.1(b). The axial displacement corresponding to  $N$  is denoted by  $w(z)$ . The transverse shear forces  $V_x$  and  $V_y$  are defined positive in positive  $x$ - and  $y$ -directions on a positive  $z$ -face, respectively, and act at the shear center. The displacements corresponding to  $V_x$  and  $V_y$  are denoted by  $u(z)$  and  $v(z)$ , respectively. The bending moment  $M_x(z)$  and its corresponding rotation  $\phi_x(z)$  are referenced to the centroid, and are defined positive in the positive  $x$ -direction by the right-hand screw rule. (Put your right thumb along the positive  $x$ -axis and your fingers curl in the direction of the positive moment and corresponding rotation.) The bending moment  $M_y(z)$  and its corresponding rotation  $\phi_y(z)$  are referenced to the centroid and are defined positive in the negative  $y$ -direction by the right-hand screw rule. Note that positive bending moments cause tension of the axial fibers in the first quadrant of the  $x$ - $y$  coordinate system. The torque is denoted by  $M_z(z)$ , and its corresponding rotation  $\phi_z(z)$  are defined at the shear center and are positive counterclockwise on the positive  $z$ -face.

**Centroid C.** The centroid decouples the extension and bending responses of the bar in the material law. Refer to eq. (3.80) on page 47. The procedure to locate the centroid is presented in example 3.1 on page 47 for an open cross-sectional contour, and in part (a) of example 3.4 on page 71 for a closed cross-sectional contour.

**Shear center S.C.** The shear center is a point in the cross section through which the plane of the loading must pass for the bar to bend and not twist in torsion. That is, the resultant of the shear forces in the cross section must act through the shear center to prevent torsion. Using energy methods in article 5.5.3 it is shown that the shear center decouples the transverse shear and torsion responses of the bar in the material law. Refer to eq. (5.76) on page 144. The procedure to locate the shear center is presented in example 3.3 on page 54 for an open cross-sectional contour, and in part (c) of example 3.4 on page 71 for a closed cross-sectional contour.

### 3.2 Contour geometry

The contour in the cross section is defined in parametric form by its coordinates  $x(s)$  and  $y(s)$  where  $s$  denotes the arc-length of the contour as shown in figure 3.3(a). The position vector from point  $C$  to a point  $s$  on the contour is

$$\vec{r}(s) = x(s)\hat{i} + y(s)\hat{j}, \quad (3.1)$$

where the Cartesian unit vectors are denoted  $\hat{i}, \hat{j}, \hat{k}$  along the positive  $x$ -,  $y$ -, and  $z$ -directions, respectively. The Cartesian coordinates are a right-handed system, or  $\hat{i} \times \hat{j} = \hat{k}$ , and the arc-length  $s$  is taken positive counter-clockwise along the contour. The differential arc-length on the contour is given by

$$ds^2 = d\vec{r} \cdot d\vec{r} = dx^2 + dy^2, \quad \text{which implies} \quad \left(\frac{dx}{ds}\right)^2 + \left(\frac{dy}{ds}\right)^2 = 1. \quad (3.2)$$

Unit vectors tangent and normal to the contour are denoted by  $\hat{t}(s)$  and  $\hat{n}(s)$ , respectively. Let the angle between the positive  $x$ -direction and the unit normal  $\hat{n}$  be denoted by  $\theta(s)$ . From the differential geometry along the contour shown in figure 3.3, the trigonometric functions of the angle  $\theta(s)$  are given by

$$\frac{dx}{ds} = -\sin\theta \quad \frac{dy}{ds} = \cos\theta. \quad (3.3)$$

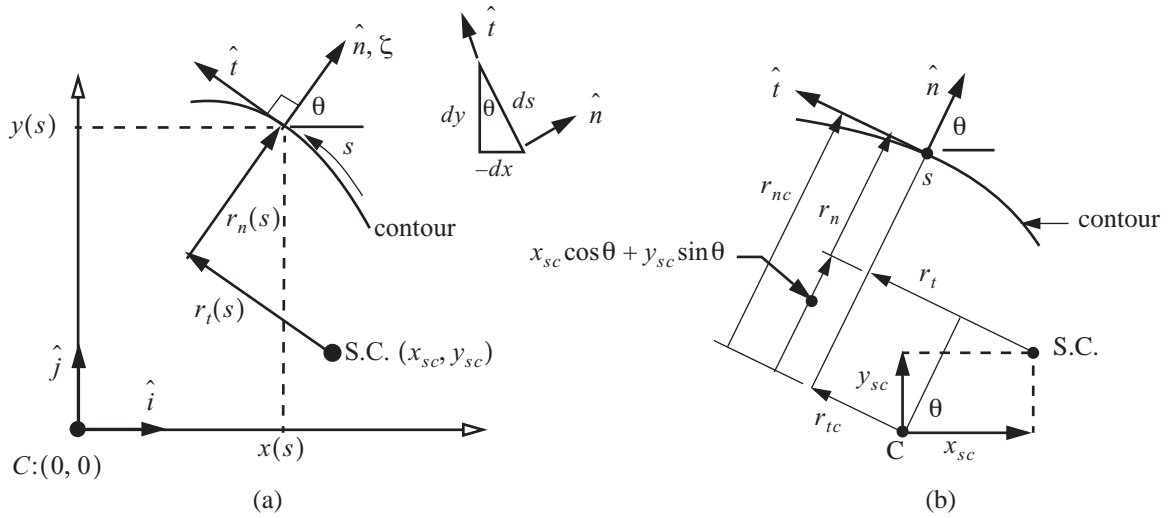


**Fig. 3.3** (a) Analytic geometry of the contour. (b) Tangential and normal coordinates with respect to the shear center and centroid.

The unit tangent vector to the contour is

$$\hat{t} = \frac{d\vec{r}}{ds} = \left(\frac{dx}{ds}\right)\hat{i} + \left(\frac{dy}{ds}\right)\hat{j} = (-\sin\theta)\hat{i} + (\cos\theta)\hat{j}. \quad (3.4)$$

The unit normal to the contour is given by the cross product  $\hat{n} = \hat{t} \times \hat{k}$ , which yields

$$\hat{n} = (\cos\theta)\hat{i} + (\sin\theta)\hat{j} = \left(\frac{dy}{ds}\right)\hat{i} - \left(\frac{dx}{ds}\right)\hat{j}. \quad (3.5)$$

The derivatives of the unit tangent and normal vectors along the contour are obtained by differentiating eq. (3.4) and eq. (3.5) with respect to arc-length  $s$ . The results are expressed as

$$\frac{d\hat{t}}{ds} = \frac{-\hat{n}}{R_s} \quad \frac{d\hat{n}}{ds} = \frac{\hat{t}}{R_s} \quad \frac{1}{R_s} = \frac{d\theta}{ds}, \quad (3.6)$$

where  $d\theta/ds$  is the curvature of the contour at  $s$ , and  $R_s$  is the radius of curvature at  $s$ . For subsequent computations the direction cosines between the two Cartesian and contour unit vectors are listed in table 3.1.

**Table 3.1 Direction cosines**

	$\hat{i}$	$\hat{j}$	$\hat{k}$
$\hat{n}$	$\cos\theta$	$\sin\theta$	0
$\hat{t}$	$-\sin\theta$	$\cos\theta$	0
$\hat{k}$	0	0	1

The position vector  $\vec{r}(s)$  is also expressed as a function of the tangential coordinate  $r_t(s)$  and normal coordinate  $r_n(s)$  by

$$\vec{r}(s) = x_{sc}\hat{i} + y_{sc}\hat{j} + r_t(s)\hat{t}(s) + r_n(s)\hat{n}(s), \quad (3.7)$$

where the coordinates of the shear center with respect to the centroid are denoted by  $x_{sc}$  and  $y_{sc}$ . Equating the two expressions (3.1) and (3.7) for the position vector and using the direction cosine table 3.1, the following relations between the contour coordinates result:

$$\begin{aligned} r_t(s) &= -[x(s) - x_{sc}]\sin\theta(s) + [y(s) - y_{sc}]\cos\theta(s) \\ r_n(s) &= [x(s) - x_{sc}]\cos\theta(s) + [y(s) - y_{sc}]\sin\theta(s) \end{aligned} \quad (3.8)$$

$$x(s) - x_{sc} = -r_t(s)\sin\theta(s) + r_n(s)\cos\theta(s) \quad y(s) - y_{sc} = r_t(s)\cos\theta(s) + r_n(s)\sin\theta(s). \quad (3.9)$$

Replace the trigonometric functions in eq. (3.8) by derivatives of the contour coordinates using eq. (3.3). Then expand eq. (3.8) and write it as

$$r_t = r_{tc} - x_{sc}\frac{dx}{ds} - y_{sc}\frac{dy}{ds} \quad r_n = r_{nc} - x_{sc}\frac{dy}{ds} + y_{sc}\frac{dx}{ds}, \quad (3.10)$$

where

$$r_{tc} = x(s)\frac{dx}{ds} + y(s)\frac{dy}{ds} \quad r_{nc} = x(s)\frac{dy}{ds} - y(s)\frac{dx}{ds}. \quad (3.11)$$

In eq. (3.11), the tangent and normal coordinates to a generic point on the contour relative to the centroid are denoted by  $r_{tc}(s)$  and  $r_{nc}(s)$ , respectively. The relationship expressed by eq. (3.10) is shown in figure 3.3(b).



The derivative of the position vector with respect to the arc length coordinate  $s$  is the unit tangent vector in eq. (3.4). Take the derivative of  $\vec{r}(s)$  with respect to  $s$  using eq. (3.7) to get

$$\frac{d\vec{r}}{ds} = \hat{t} = \left(\frac{dr_t}{ds} + \frac{r_n}{R_s}\right)\hat{t} + \left(\frac{dr_n}{ds} - \frac{r_t}{R_s}\right)\hat{n}. \quad (3.12)$$

Since  $d\vec{r}/ds = \hat{t}$ , it follows that coordinates  $r_t(s)$  and  $r_n(s)$ , and the radius of curvature  $R_s$  are related by

$$\frac{dr_t}{ds} + \frac{r_n}{R_s} = 1 \quad \frac{dr_n}{ds} - \frac{r_t}{R_s} = 0. \quad (3.13)$$

### 3.3 Displacements

Consider a material point in the wall of the cross section located by coordinates  $(s, \zeta)$ , where  $\zeta$  denotes the thickness coordinate. Coordinate  $\zeta = 0$  on the contour and  $-t/2 \leq \zeta \leq t/2$ . Denote the position vector  $\vec{R}$  to point  $(s, \zeta)$  relative to the shear center by

$$\vec{R}(s, \zeta) = r_t \hat{t} + (r_n + \zeta) \hat{n}. \quad (3.14)$$

**It is assumed that the cross section displaces, and then undergoes an infinitesimal rotation as a rigid disk.** Let  $\vec{u}_{sc}(z)$  denote the displacement vector of the shear center of the cross section, and let  $\vec{u}(s, z, \zeta)$  denote the displacement vector of the particle at point  $(s, z, \zeta)$ . The position vector  $\vec{R}$  in the cross section is displaced and rotated in the rigid disk to  $\vec{R}^{(*)}$ . Since  $\vec{R}^{(*)}$  is embedded in the rigid disk, the magnitudes of vector  $\vec{R}^{(*)}$  and vector  $\vec{R}$  are the same; i.e.,  $\vec{R}^{(*)} \cdot \vec{R}^{(*)} = \vec{R} \cdot \vec{R}$ . As shown in figure 3.4 the displacement  $\vec{u}(s, z, \zeta)$  related to displacement  $\vec{u}_{sc}(z)$  and the change in direction of vector  $\vec{R}$  by

$$\vec{u}(s, z, \zeta) = \vec{u}_{sc}(z) + \vec{R}^{(*)} - \vec{R}. \quad (3.15)$$

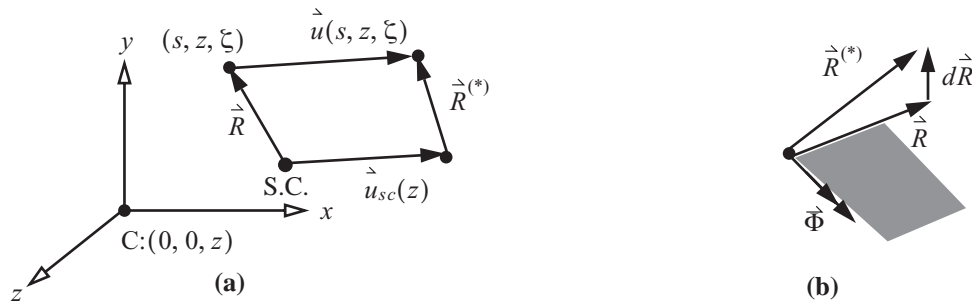


**Fig. 3.4** (a) Displacement vectors of the shear center and a generic particle in the bar. (b) Change in direction of position vector  $\vec{R}$  due to an infinitesimal rotation  $\vec{\Phi}$ .  $d\vec{R}$  is normal to the plane of  $\vec{R}$  and  $\vec{\Phi}$ .

Let  $\vec{\Phi}$  denote the infinitesimal rotation vector of the cross section embedded in the rigid disk. The change in

direction of  $\vec{R}$  is denoted as  $d\vec{R}$  and is determined by the vector cross product (Goldstein, p.128):

$$\vec{R}^{(*)} - \vec{R} = d\vec{R} = \vec{\Phi} \times \vec{R}. \quad (3.16)$$

Substitute eq. (3.16) for  $\vec{R}^{(*)} - \vec{R}$  in eq. (3.15) to get

$$\vec{u}(s, z, \zeta) = \vec{u}_{sc}(z) + \vec{\Phi} \times \vec{R}. \quad (3.17)$$

The vectors  $\vec{u}_{sc}(z)$ ,  $\vec{u}(s, z, \zeta)$ , and  $\vec{\Phi}(z)$  are written in the Cartesian basis or contour coordinate basis as follows:

$$\begin{aligned} \vec{u}_{sc}(z) &= u(z)\hat{i} + v(z)\hat{j} + w_{sc}(z)\hat{k} \\ \vec{u}(s, z, \zeta) &= u_s(s, z, \zeta)\hat{t} + u_z(s, z, \zeta)\hat{k} + u_\zeta(s, z, \zeta)\hat{n}, \\ \vec{\Phi}(z) &= \phi_x(z)\hat{i} - \phi_y(z)\hat{j} + \phi_z(z)\hat{k} \end{aligned} \quad (3.18)$$

where  $w_{sc}(z)$  is the axial displacement of the shear center. The components of the displacement vector  $\vec{u}(s, z, \zeta)$  in terms of the displacement vector  $\vec{u}_{sc}(z)$  of the shear center and the contribution from the rotation is given by the following scalar products:

$$\begin{aligned} u_s(s, z, \zeta) &= \vec{u}(s, z, \zeta) \cdot \hat{t} = \vec{u}_{sc}(z) \cdot \hat{t} + \vec{\Phi} \times (r_t\hat{t} + (r_n + \zeta)\hat{n}) \cdot \hat{t} \\ u_z(s, z, \zeta) &= \vec{u}(s, z, \zeta) \cdot \hat{k} = \vec{u}_{sc}(z) \cdot \hat{k} + \vec{\Phi} \times (r_t\hat{t} + (r_n + \zeta)\hat{n}) \cdot \hat{k} \\ u_\zeta(s, z, \zeta) &= \vec{u}(s, z, \zeta) \cdot \hat{n} = \vec{u}_{sc}(z) \cdot \hat{n} + \vec{\Phi} \times (r_t\hat{t} + (r_n + \zeta)\hat{n}) \cdot \hat{n} \end{aligned} \quad (3.19)$$

Performing the scalar products in eq. (3.19) with the aid of (3.9) and (3.18) and table 3.1, we find that the displacement components of a particle in the cross section with respect to the shear center are

$$u_s(s, z, \zeta) = -u(z)\sin\theta(s) + v(z)\cos\theta(s) + [r_n(s) + \zeta]\phi_z(z), \quad (3.20)$$

$$u_z(s, z, \zeta) = w_{sc}(z) + [y(s) - y_{sc}]\phi_x(z) + [x(s) - x_{sc}]\phi_y(z) + \zeta[\phi_x(z)\sin\theta(s) + \phi_y(z)\cos\theta(s)], \quad (3.21)$$

$$u_\zeta(s, z, \zeta) = u(z)\cos\theta(s) + v(z)\sin\theta(s) - r_t(s)\phi_z(z). \quad (3.22)$$

Let  $\vec{u}_c(z)$  denote the displacement of the centroid, with the component form given by

$$\vec{u}_c(z) = u_c(z)\hat{i} + v_c(z)\hat{j} + w(z)\hat{k}. \quad (3.23)$$

where  $u_c(z)$  and  $v_c(z)$  denote the  $x$ -direction and  $y$ -direction displacements of the centroid. From figure 3.5 the displacement of the shear center relative to the displacement of the centroid is

$$\vec{u}_{sc}(z) = \vec{u}_c(z) + \vec{R}_{sc}^* - \vec{R}_{sc} = \vec{u}_c(z) + d\vec{R}_{sc} = \vec{u}_c(z) + \vec{\Phi} \times \vec{R}_{sc}. \quad (3.24)$$

where it is noted that position vector  $\vec{R}_{sc}$  is embedded in the rigid disk containing the cross section which undergoes the infinitesimal rotation  $\vec{\Phi}(z)$ .

Position vector  $\vec{R}_{sc} = x_{sc}\hat{i} + y_{sc}\hat{j}$ , and the rotation vector is given in eq. (3.18). From the forgoing vector relations, the displacement components of the shear center relative to the centroid are

$$\begin{aligned} u(z) &= u_c(z) - y_{sc}\phi_z(z) \\ v(z) &= v_c(z) + x_{sc}\phi_z(z) \\ w_{sc}(z) &= w(z) + x_{sc}\phi_y(z) + y_{sc}\phi_x(z) \end{aligned} \quad (3.25)$$

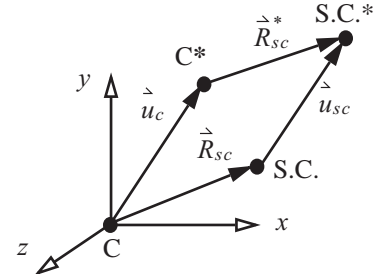


Fig. 3.5 Displacements of the centroid and shear center.

Substitute the expression for axial displacement  $w_{sc}(z)$  from eq. (3.25) into eq. (3.21) to get

$$u_z(s, z, \zeta) = w(z) + y(s)\phi_x(z) + x(s)\phi_y(z) + \zeta[\phi_x(z)\sin\theta(s) + \phi_y(z)\cos\theta(s)]. \quad (3.26)$$

### 3.4 Strains

Consider three mutually perpendicular, infinitesimal line elements  $dS$ ,  $dz$ , and  $d\zeta$  in the undeformed body, where the arc-length of the line element parallel to the contour is related to the arc-length of the contour by  $dS = (1 + \zeta/R_s)ds$ . Let  $\epsilon_{ss}$  denote the normal strain for line element  $dS$ ,  $\epsilon_{zz}$  the normal strain for  $dz$ , and  $\epsilon_{\zeta\zeta}$  the normal strain for line element  $d\zeta$ . For infinitesimal deformations, these normal strains are related to displacements  $u_s$ ,  $u_z$ , and  $u_\zeta$  by

$$\epsilon_{ss} = \left( \frac{\partial u_s}{\partial s} + \frac{u_\zeta}{R_s} \right) / \left( 1 + \frac{\zeta}{R_s} \right) \quad \epsilon_{zz} = \frac{\partial u_z}{\partial z} \quad \epsilon_{\zeta\zeta} = \frac{\partial u_\zeta}{\partial \zeta}. \quad (3.27)$$

Let  $\gamma_{zs}$  denote the engineering shear strain between line elements  $dS$  and  $dz$ ,  $\gamma_{s\zeta}$  the engineering shear strain between  $dS$  and  $d\zeta$ , and  $\gamma_{z\zeta}$  the engineering shear strain between line elements  $dz$  and  $d\zeta$ . For infinitesimal deformations, the shear strain-displacement relations are

$$\gamma_{zs} = \frac{\partial u_s}{\partial z} + \frac{1}{(1 + \zeta/R_s)} \frac{\partial u_z}{\partial s} \quad \gamma_{s\zeta} = \frac{\partial u_s}{\partial \zeta} + \frac{1}{(1 + \zeta/R_s)} \left( \frac{\partial u_\zeta}{\partial s} - \frac{u_s}{R_s} \right) \quad \gamma_{z\zeta} = \frac{\partial u_z}{\partial \zeta} + \frac{\partial u_\zeta}{\partial z}. \quad (3.28)$$

Substitute the displacements from eqs. (3.20), (3.22), and (3.26) into the strain-displacement relations for  $\epsilon_{ss}$ ,  $\epsilon_{\zeta\zeta}$  and  $\gamma_{s\zeta}$ , to find

$$\epsilon_{ss} = \frac{\left( \frac{dr_n}{ds} - \frac{r_t}{R_s} \right)}{1 + \zeta/R_s} \phi_z = 0 \quad \epsilon_{\zeta\zeta} = 0 \quad \gamma_{s\zeta} = \left[ 1 - \frac{\left( \frac{dr_t}{ds} + \frac{r_n}{R_s} + \frac{\zeta}{R_s} \right)}{1 + \frac{\zeta}{R_s}} \right] \phi_z = 0. \quad (3.29)$$

Strains  $\epsilon_{ss} = \gamma_{s\zeta} = 0$  result from the relations between the coordinates  $r_n$  and  $r_t$  given by eq. (3.13). More-

over, the vanishing of the strains in eq. (3.29) is a consequence of the assumption that the cross section is undeformable in its own plane. Substitute the axial displacement from eq. (3.26) into the axial normal strain-displacement in eq. (3.27) to get

$$\varepsilon_{zz} = \frac{dw}{dz} + y(s)\frac{d\phi_x}{dz} + x(s)\frac{d\phi_y}{dz} + \zeta \left[ \frac{d\phi_x}{dz} \sin\theta(s) + \frac{d\phi_y}{dz} \cos\theta(s) \right]. \quad (3.30)$$

Substitute the displacements from eqs. (3.20), (3.22), and (3.26) into the last two shear strain-displacement equations to find

$$\gamma_{zs} = -\psi_x \sin\theta + \psi_y \cos\theta + (r_n(s) + \zeta) \frac{d\phi_z}{dz} \quad \gamma_{z\zeta} = \psi_x \cos\theta + \psi_y \sin\theta - r_t \frac{d\phi_z}{dz}. \quad (3.31)$$

In previous expressions for the shear strains new quantities  $\psi_x$  and  $\psi_y$  are introduced. These new quantities represent shear strains averaged over the cross section of the bar and are defined by

$$\psi_x(z) = \frac{du}{dz} + \phi_y(z) \quad \psi_y(z) = \frac{dv}{dz} + \phi_x(z). \quad (3.32)$$

See figure 3.6 for a graphical representation of these averaged transverse shear strains.

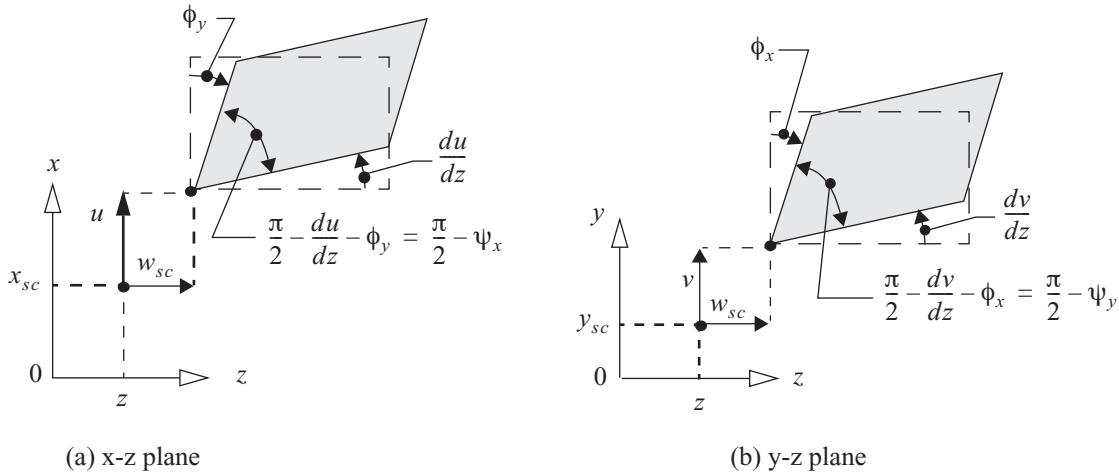


**Fig. 3.6** Transverse shear strains of the bar with respect to the shear center: (a) projection in the x-z plane, (b) projection in the y-z plane.

### 3.5 Stresses, stress resultants and bar resultants

Let  $\sigma_{zz}$  denote the stress normal to the cross section,  $\sigma_{zs}$  denote the shear stress acting tangent to the contour of the cross section, and let  $\sigma_{z\zeta}$  denote the shear stress normal to the contour acting on the cross section. These stress components act on an infinitesimal area of the cross section denoted by  $dA = (1 + \zeta/R_s)dsd\zeta$ . These stress components are shown in figure 3.7(a).

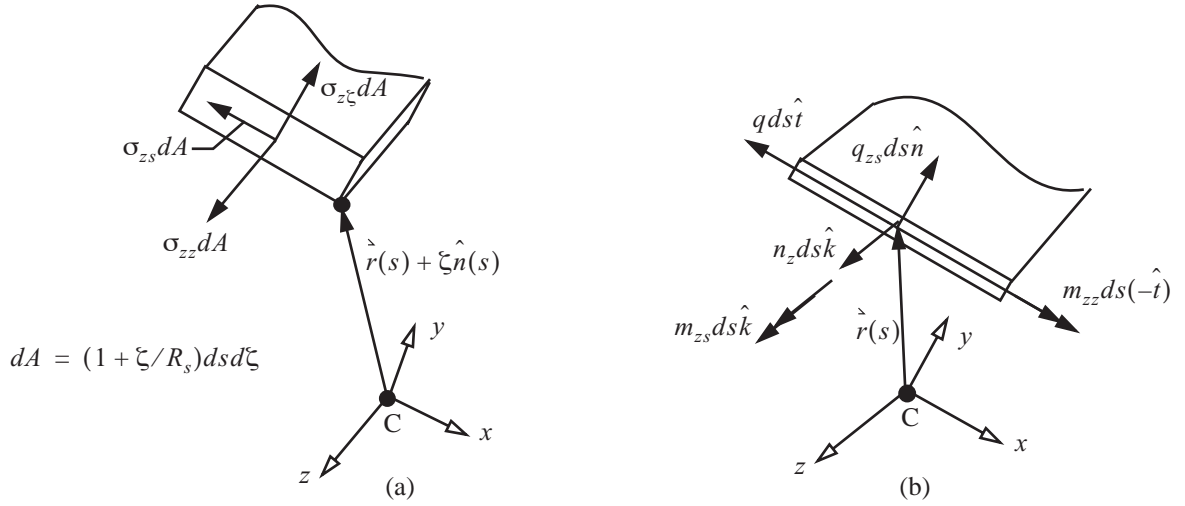


**Fig. 3.7** (a) Stress components acting on differential area  $dA$  of the cross section. (b) stress resultants acting at the contour of length  $ds$ .

Consider the work done on a cross section at a fixed value of  $z$  by the stresses acting through incremental displacements. The incremental displacement corresponding to  $\sigma_{zz}$  is  $\delta u_z$ , incremental displacement corresponding to  $\sigma_{zs}$  is  $\delta u_s$ , and the incremental displacement corresponding to  $\sigma_{z\zeta}$  is  $\delta u_\zeta$ . Let  $\delta W_z$  denote the incremental work, which is given by the integral

$$\delta W_z = \int_c \left[ \int_{-t/2}^{t/2} (\sigma_{zz} \delta u_z + \sigma_{zs} \delta u_s + \sigma_{z\zeta} \delta u_\zeta) (1 + \zeta/R_s) d\zeta \right] ds. \quad (3.33)$$

The incremental displacements are determined from eqs. (3.20), (3.22), and (3.26), and are

$$\begin{aligned} \delta u_z(s, z, \zeta) &= \delta w(z) + y(s) \delta \phi_x(z) + x(s) \delta \phi_y(z) + \zeta [\delta \phi_x(z) \sin \theta(s) + \delta \phi_y(z) \cos \theta(s)] \\ \delta u_s(s, z, \zeta) &= -\delta u(z) \sin \theta(s) + \delta v(z) \cos \theta(s) + [r_n(s) + \zeta] \delta \phi_z(z) \\ \delta u_\zeta(s, z, \zeta) &= \delta u(z) \cos \theta(s) + \delta v(z) \sin \theta(s) - r_t(s) \delta \phi_z(z) \end{aligned} \quad (3.34)$$

where  $\delta u(z)$ ,  $\delta v(z)$ , and  $\delta w(z)$  denote the incremental displacements of the cross section,  $\delta \phi_x(z)$ ,  $\delta \phi_y(z)$ , and  $\delta \phi_z(z)$  denote the incremental rotations of the cross section. Substitute the incremental displacements from eq. (3.34) into the expression (3.33) for the incremental work, followed by integration through the thickness of the wall. The result of this process is written as

2. The notation  $\delta u_z$  denotes a continuous function of infinitesimal magnitude added to the displacement function  $u_z$ , which vanishes at prescribed values of  $u_z$ . That is,  $u_z + \delta u_z$  is a new displacement function. Function  $\delta u_z$  is interpreted as a change in displacement at fixed values of independent coordinates  $s$ ,  $z$ , and  $\zeta$ , where the independent variables identify a material point. In differential calculus  $du_z$  is the infinitesimal change in the displacement function with respect to changes in the independent variables without changing the function itself.

$$\delta W_z = \int_c [(-q \sin \theta + q_z \cos \theta) \delta u + (q \cos \theta + q_z \sin \theta) \delta v + n_z \delta w + (y n_z + m_{zz} \sin \theta) \delta \phi_x + (x n_z + m_{zz} \cos \theta) \delta \phi_y + (r_n q + m_{zs} - r_t q_z) \delta \phi_z] ds. \quad (3.35)$$

The integration through the thickness leads to the definition of stress resultants acting at the contour. The normal stress resultant is denoted by  $n_z$ , shear flow resultant by  $q$ , transverse stress resultant by  $q_z$ , bending moment resultant by  $m_z$ , and twisting moment resultant by  $m_{zs}$ . These stress resultants are given by the following integrals through the thickness:

$$(n_z, m_z) = \int_{-t/2}^{t/2} (1, \zeta) \sigma_{zz} (1 + \zeta/R_s) d\zeta, \quad (3.36)$$

and

$$(q, m_{zs}) = \int_{-t/2}^{t/2} (1, \zeta) \sigma_{zs} (1 + \zeta/R_s) d\zeta \quad q_z = \int_{-t/2}^{t/2} \sigma_z \zeta (1 + \zeta/R_s) d\zeta. \quad (3.37)$$

See figure 3.7(b).

The integral over the contour of the incremental work in (3.35) is written as

$$\delta W_z = V_x \delta u + V_y \delta v + N \delta w + M_x \delta \phi_x + M_y \delta \phi_y + M_z \delta \phi_z. \quad (3.38)$$

Integration over the contour defines the bar resultants in terms of the stress resultants as

$$N = \int_c n_z ds \quad M_x = \int_c (y n_z + m_{zz} \sin \theta) ds \quad M_y = \int_c (x n_z + m_{zz} \cos \theta) ds, \text{ and} \quad (3.39)$$

$$V_x = \int_c (-q \sin \theta + q_z \cos \theta) ds \quad V_y = \int_c (q \cos \theta + q_z \sin \theta) ds \quad M_z = \int_c (r_n q + m_{zs} - r_t q_z) ds. \quad (3.40)$$

### 3.6 External loads and equilibrium of an element of the bar

The prescribed external traction components acting on the bar are denoted by functions  $p_n(s, z)$ ,  $p_s(s, z)$  and  $p_z(s, z)$ , which are defined per unit area of the middle surface where  $\zeta = 0$ . The dimensional units of these traction components are  $F/L^2$ . See figure 3.8. At a typical cross section these tractions are resolved into distributed line loads  $f_x$ ,  $f_y$  and  $f_z$  having dimensional units  $F/L$ . The line loads are determined from the following vector relation:

$$\vec{f}(z) = f_x \hat{i} + f_y \hat{j} + f_z \hat{k} = \int_c (p_n \hat{n} + p_s \hat{t} + p_z \hat{k}) ds. \quad (3.41)$$

Using the direction cosines in table 3.1, these line load intensities are related to the specified tractions by

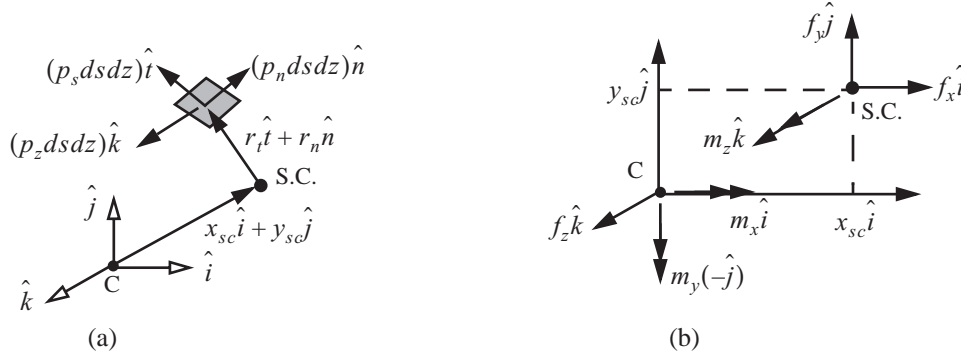


**Fig. 3.8** (a) External tractions prescribed on the reference surface. (b) Statically equivalent external line load intensities.

$$f_x(z) = \int_c (p_n \cos \theta - p_s \sin \theta) ds \quad f_y(z) = \int_c (p_n \sin \theta + p_s \cos \theta) ds \quad f_z(z) = \int_c p_z ds. \quad (3.42)$$

At a typical cross section these traction components result in an external torque per unit axial length with respect to the centroid denoted by  $\vec{m}_z|_C$ , with dimensional units  $(F-L)L$ . The external moment per unit axial length with respect to centroid is determined from the following vector cross product relation:

$$\vec{m}_C = \int_c [(x_{sc}\hat{i} + y_{sc}\hat{j}) + (r_n\hat{n} + r_t\hat{t})] \times [p_n\hat{n} + p_s\hat{t} + p_z\hat{k}] ds. \quad (3.43)$$

Perform the cross products to find the moment per unit axial length about the centroid from the prescribed traction to get

$$\vec{m}_C = m_x\hat{i} - m_y\hat{j} + [x_{sc}f_y(z) - y_{sc}f_x(z) + m_z(z)]\hat{k}, \quad (3.44)$$

where

$$m_x = \int_c y(s)p_z(s, z) ds \quad m_y = \int_c x(s)p_z(s, z) ds \quad m_z = \int_c [r_n(s)p_s(s, z) - r_t(s)p_n(s, z)] ds, \quad (3.45)$$

Equation (3.38) is applicable at each end of the bar where  $z = 0$  and  $z = L$ . Hence,  $[N, w]$ ,  $[V_x, u]$ ,  $[V_y, v]$ ,  $[M_x, \phi_x]$ ,  $[M_y, \phi_y]$ , and  $[M_z, \phi_z]$  are corresponding variables. We can prescribe a “force” variable or its corresponding “displacement” variable as external “loads” acting on the end cross sections, but not both the “force” and the “displacement” simultaneously.

### 3.6.1 Differential equilibrium equations

Let the internal forces acting on the cross section at  $z$  be denoted by the vector  $\vec{F}(z)$ , and let the internal moments acting on the cross section resolved at the centroid be denoted by the vector  $\vec{M}(z)$ . These vectors of internal actions are

$$\vec{F}(z) = V_x\hat{i} + V_y\hat{j} + N\hat{k}, \text{ and} \quad (3.46)$$

$$\vec{M}(z) = M_x \hat{i} - M_y \hat{j} + M_z \hat{k}. \quad (3.47)$$

Consider the forces and moments acting on a bar element defined by  $z$  and  $z + \Delta z$ ,  $\Delta z > 0$ , as shown in figure 3.9.

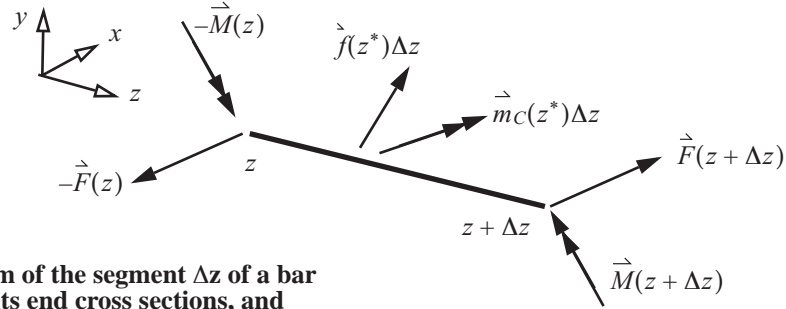


**Fig. 3.9** A free body diagram of the segment  $\Delta z$  of a bar subject to internal actions at its end cross sections, and subject to prescribed external actions along its length.

The vector equations of equilibrium are

$$\vec{F}(z + \Delta z) - \vec{F}(z) + \vec{f}(z^*)\Delta z = 0 \quad \vec{M}(z + \Delta z) - \vec{M}(z) + \Delta z \hat{k} \times \vec{F}(z + \Delta z) + (z^* - z)\hat{k} \times \vec{f}(z^*)\Delta z + \vec{m}_C(z^*)\Delta z = 0, \quad (3.48)$$

where  $z < z^* < z + \Delta z$ . For a continuous force vector and moment vector with respect to coordinate  $z$ , eq. (3.48) can be written as

$$\left. \frac{d\vec{F}}{dz} \right|_z \Delta z + \vec{f}(z^*)\Delta z = 0 \quad \left. \frac{d\vec{M}}{dz} \right|_z \Delta z + \Delta z \hat{k} \times \vec{F}(z + \Delta z) + (z^* - z)\hat{k} \times \vec{f}(z^*)\Delta z + \vec{m}_C(z^*)\Delta z = 0. \quad (3.49)$$

Divide the latter equations by  $\Delta z$  and take the limit as  $\Delta z \rightarrow 0$  and note that  $z^* \rightarrow z$  in the limit. The differential equations of equilibrium obtained from the limiting procedure are

$$\frac{d\vec{F}}{dz} + \vec{f}(z) = 0 \quad \frac{d\vec{M}}{dz} + \hat{k} \times \vec{F}(z) + \vec{m}_C(z) = 0. \quad (3.50)$$

Expand the differential equation (3.50) in terms of components to get

$$\left( \frac{dV_x}{dz} + f_x \right) \hat{i} + \left( \frac{dV_y}{dz} + f_y \right) \hat{j} + \left( \frac{dN}{dz} + f_z \right) \hat{k} = 0\hat{i} + 0\hat{j} + 0\hat{k}, \text{ and} \quad (3.51)$$

$$\left( \frac{dM_x}{dz} - V_y + m_x \right) \hat{i} + \left( -\frac{dM_y}{dz} + V_x - m_y \right) \hat{j} + \left( \frac{dM_z}{dz} + m_z + x_{sc}f_y - y_{sc}f_x \right) \hat{k} = 0\hat{i} + 0\hat{j} + 0\hat{k}. \quad (3.52)$$

**Axial equilibrium.** From  $\hat{k}$ -component of eq. (3.51) the differential equilibrium equation is

$$\frac{dN}{dz} + f_z(z) = 0 \quad N = N(z) \quad 0 < z < L. \quad (3.53)$$

At the end points  $z = 0$  and  $z = L$ , prescribe either axial force  $N$  or the corresponding displacement  $w$ , but not both.

**Bending in the  $y$ - $z$  plane.** From the  $\hat{j}$  component of eq. (3.51) the differential equation for the shear force is



$$\frac{dV_y}{dz} + f_y(z) = 0 \quad V_y = V_y(z) \quad 0 < z < L. \quad (3.54)$$

At the end points  $z = 0$  and  $z = L$ , prescribe either shear force  $V_y$  or the corresponding displacement  $v$ , but not both. From the  $\hat{i}$ -component of eq. (3.52) the differential equation for the bending moment is

$$\frac{dM_x}{dz} - V_y + m_x(z) = 0 \quad M_x = M_x(z) \quad 0 < z < L. \quad (3.55)$$

At the end points  $z = 0$  and  $z = L$ , prescribe either bending moment  $M_x$  or the corresponding rotation  $\phi_x$ , but not both.

**Bending in the  $x$ - $z$  plane.** From the  $\hat{i}$ -component of eq. (3.51) the differential equation for the shear force is

$$\frac{dV_x}{dz} + f_x(z) = 0 \quad V_x = V_x(z) \quad 0 < z < L. \quad (3.56)$$

At the end points  $z = 0$  and  $z = L$ , prescribe either shear force  $V_x$  or the corresponding displacement  $u$ , but not both. From the  $\hat{j}$ -component of eq. (3.52) the differential equation for the bending moment is

$$\frac{dM_y}{dz} - V_x + m_y(z) = 0 \quad M_y = M_y(z) \quad 0 < z < L. \quad (3.57)$$

At the end points  $z = 0$  and  $z = L$ , prescribe either bending moment  $M_y$  or the corresponding rotation  $\phi_y$ , but not both.

**Torsion.** From the  $\hat{k}$ -component of eq. (3.52) the differential equation for torsion about the shear center axis is

$$\frac{dM_{zC}}{dz} + x_{sc}f_y - y_{sc}f_x + m_z = 0. \quad (3.58)$$

The torque at the centroid is related to the torque and the shear forces acting at the shear center by static equivalence. (Refer to Fig. 3.23 on page 69.) That is,

$$M_{zC} = M_z + x_{sc}V_y - y_{sc}V_x. \quad (3.59)$$

Substitute eq. (3.59) for  $M_{zC}$  into eq. (3.58) to get

$$\frac{dM_z}{dz} + x_{sc}\left(\frac{dV_y}{dz} + f_y\right) - y_{sc}\left(\frac{dV_x}{dz} + f_x\right) + m_z = 0. \quad (3.60)$$

Impose equilibrium eqs. (3.54) and (3.56) in eq. (3.60) to get

$$\frac{dM_z}{dz} + m_z = 0 \quad M_z = M_z(z) \quad 0 < z < L. \quad (3.61)$$

At the end points  $z = 0$  and  $z = L$ , prescribe either torque  $M_z$  or the corresponding rotation  $\phi_z$ , but not both.

### 3.7 Hooke's law

For a linear elastic, isotropic material, there are two independent material constants: the modulus of elasticity  $E$  and Poisson's ratio  $\nu$ . (Refer to eq. (A.146) in the appendix.) Hooke's law for the normal strains is

$$\begin{bmatrix} \epsilon_{ss} \\ \epsilon_{zz} \\ \epsilon_{\zeta\zeta} \end{bmatrix} = \begin{bmatrix} 1/E & -\nu/E & -\nu/E \\ -\nu/E & 1/E & -\nu/E \\ -\nu/E & -\nu/E & 1/E \end{bmatrix} \begin{bmatrix} \sigma_{ss} \\ \sigma_{zz} \\ \sigma_{\zeta\zeta} \end{bmatrix}, \quad (3.62)$$

where  $\sigma_{ss}$  denotes the normal stress acting on the  $s$ -face, and where  $\sigma_{\zeta\zeta}$  denotes the normal stress on the  $\zeta$ -face acting on an infinitesimal element  $ds$ -by- $dz$ -by- $d\zeta$ . The thickness normal stress  $\sigma_{\zeta\zeta}$  is assumed to be very small with respect to the axial normal stress  $\sigma_{zz}$ , and hence is neglected in Hooke's law. From the kinematic assumption, eq. (3.29), the normal strain  $\epsilon_{\zeta\zeta} = 0$ . Setting  $\epsilon_{\zeta\zeta} = \sigma_{\zeta\zeta} = 0$  in the third row of eq. (3.62), leads to  $\sigma_{ss} + \sigma_{zz} = 0$ , which is a very unlikely result. Thus, we neglect this third equation in Hooke's law. Furthermore, in most thin-walled beam theories (e.g., see Gjelsvik, 1981, p. 16), the normal stress  $\sigma_{ss}$  is assumed to be small with respect to the axial normal stress  $\sigma_{zz}$  and is neglected in Hooke's law. Setting  $\sigma_{ss} = \sigma_{\zeta\zeta} = 0$  leads to

$$\sigma_{zz} = E\epsilon_{zz}. \quad (3.63)$$

Consequently, the first row of matrix eq. (3.62) leads to  $\epsilon_{ss} = -\nu\sigma_{zz}/E$ . However, the kinematic assumption, eq. (3.29), resulted in  $\epsilon_{ss} = 0$ . If we set  $\epsilon_{ss} = 0$  in the first row of eq. (3.62), solve it for  $\sigma_{ss}$ , followed by substitution into the second row of eq. (3.62), we get

$$\sigma_{zz} = \frac{E}{1-\nu^2}\epsilon_{zz}. \quad (3.64)$$

It is recognized that Hooke's law in the elasticity sense of eq. (3.62) is violated under the assumptions of the thin-walled beam theory under consideration. In the following developments of the theory, eq. (3.63) is assumed as the material law governing the axial normal stress and axial normal strain, which is a common assumption in classical beam theory.

#### 3.7.1 Effect of thermal expansion

Consider structures subject not only to external forces, but also subject to heating. Aerospace examples include high-speed flight vehicles and orbiting space structures. Aerothermal loads consisting of pressure, skin friction or shearing stresses, and aerodynamic heating, are exerted on the external surfaces of high-speed flight vehicles. Conduction and radiant heat transfer result in significant thermally induced forces acting on orbiting space structures. These aerospace examples are discussed in detail by Thornton (1996), who provides an historical account, and methods of analysis, of thermal structures for aerospace applications.

It is assumed that a change in temperature (thermal state) causes a change in deformation and stress (mechanical state) in the structure, but a change in deformation does not cause a change in temperature. For example, under adiabatic conditions strain can cause a change in temperature. However, in many structural applications the change in temperature under adiabatic straining is negligible and can be ignored (Fung, 1965, p. 390). Thornton (1996, p.51) defines the change in thermal energy state causing a change in mechanical state, but not the reverse, as one-way thermal-mechanical coupling. Thus, heat conduction and thermoelasticity separate into two separate problems. In this text it is assumed that the heat conduction problem has been solved so that the

temperature distribution in the structure is known. The **thermoelastic problem** is to determine the mechanical state in an elastic structure for the specified temperature distribution and the specified external loads.

For a uniaxial stress state the generalized Hooke's law including temperature is

$$\epsilon_{zz} = (\sigma_{zz} + \beta \Delta T)/E \quad \text{or} \quad \sigma_{zz} = E\epsilon_{zz} - \beta \Delta T, \quad (3.65)$$

where  $\beta = E\alpha$ , and  $\alpha$  is the coefficient of thermal expansion. The change in temperature is denoted by  $\Delta T = T - T_0$ , and  $T_0$  is the spatially uniform temperature in the reference state. The reference state is stress free when the external loads acting on the bar are removed and the spatially uniform temperature  $T = T_0$ . Assume a linear distribution of the change in temperature in the thickness, which we write as

$$\Delta T(s, z, \zeta) = \Delta T(s, z) + \zeta DT(s, z), \quad (3.66)$$

where

$$\Delta T(s, z) = \Delta T(s, z, 0) \quad \text{and} \quad DT(s, z) = \left. \frac{\partial \Delta T}{\partial \zeta} \right|_{\zeta=0}. \quad (3.67)$$

### 3.7.2 Material law for extension and bending

Substitute the expression (3.30) for the axial strain, and substitute eq. (3.66) for the change in temperature, into Hooke's law (3.65) to get the following expression for normal stress.

$$\sigma_{zz} = E \left[ \frac{dw}{dz} + y(s) \frac{d\phi_x}{dz} + x(s) \frac{d\phi_y}{dz} - \alpha \Delta T(s, z) \right] + \zeta E \left[ \frac{d\phi_x}{dz} \sin \theta(s) + \frac{d\phi_y}{dz} \cos \theta(s) - \alpha DT(s, z) \right]. \quad (3.68)$$

**In the thin-wall bar theory we neglect the distribution of the normal stress and normal strain across the thickness of the wall.** Therefore, the normal strain and stress is assumed uniform in the thickness coordinate, and are given by

$$\epsilon_{zz} = \frac{dw}{dz} + y(s) \frac{d\phi_x}{dz} + x(s) \frac{d\phi_y}{dz}, \quad \text{and} \quad (3.69)$$

$$\sigma_{zz} = E \left[ \frac{dw}{dz} + y(s) \frac{d\phi_x}{dz} + x(s) \frac{d\phi_y}{dz} - \alpha \Delta T(s, z) \right]. \quad (3.70)$$

In other words, the local bending of the wall represented by the bending moment resultant  $m_{zz}$  in (3.36) is neglected with respect to the membrane stiffness of the wall represented by the normal stress resultant  $n_z$ . In addition, for a thin, curved wall we neglect the term  $\zeta/R_s$  in the factor  $(1 + \zeta/R_s)$  appearing in the integrand of eq. (3.36)<sup>3</sup>. The definition of the normal stress resultant reduces to

$$n_z = \int_{-t/2}^{t/2} \sigma_{zz} d\zeta. \quad (3.71)$$

Substitute eq. (3.70) for the normal stress into the normal stress resultant (3.71) to get

3. Note that  $|\zeta/R_s| \leq |t/(2R_s)|$ . A contour that is a straight line has  $1/R_s = 0$ . A thin, curved wall is one in which

$R_s > 10t$ . Hence,  $0 \leq |t/(2R_s)| < 0.05$  for most practical contour geometries.

$$n_z = Et \left[ \frac{dw}{dz} + y(s) \frac{d\phi_x}{dz} + x(s) \frac{d\phi_y}{dz} - \alpha \Delta T(s, z) \right]. \quad (3.72)$$

The constitutive equation for the axial normal force  $N$  is obtained by substituting eq. (3.72) for the normal stress resultant in the expression (3.39). The result is

$$N = EA \frac{dw}{dz} + EQ_x \frac{d\phi_x}{dz} + EQ_y \frac{d\phi_y}{dz} - N_T, \quad (3.73)$$

where  $A$  denotes the cross-sectional area,  $Q_x$  the first area moment about the  $x$ -axis,  $Q_y$  the first area moment about the  $y$ -axis, and  $N_T(z)$  the thermal axial force. These geometrical measures of the cross section are given by the formulas

$$A = \int_c t ds \quad Q_x = \int_c y t ds = 0 \quad Q_y = \int_c x t ds = 0. \quad (3.74)$$

The first area moments  $Q_x$  and  $Q_y$  are equal to zero because the origin of the  $x$ - $y$  coordinate system is located at the centroid. The thermal axial force is given by the expression

$$N_T(z) = \int_c \beta \Delta T(s, z) t(s) ds. \quad (3.75)$$

The constitutive equations for the bending moments  $M_x$  and  $M_y$  are obtained by substituting eq. (3.72) for  $n_z$  into the definitions of the bending moments in eq. (3.39), with the contribution of  $m_z$  neglected. The result is

$$M_x = EQ_x \frac{dw}{dz} + EI_{xx} \frac{d\phi_x}{dz} + EI_{xy} \frac{d\phi_y}{dz} - M_{xT} \quad M_y = EQ_y \frac{dw}{dz} + EI_{xy} \frac{d\phi_x}{dz} + EI_{yy} \frac{d\phi_y}{dz} - M_{yT}, \quad (3.76)$$

where  $I_{xx}$ ,  $I_{yy}$ , and  $I_{xy}$  denote the second area moments of the cross section with respect to the centroidal  $x$ - $y$  coordinate system. The second area moments are given by the formulas

$$I_{xx} = \int_c y^2 t ds \quad I_{yy} = \int_c x^2 t ds \quad I_{xy} = \int_c xy t ds. \quad (3.77)$$

The thermal bending moments in eq. (3.76) are given by the expressions

$$M_{xT}(z) = \int_c \beta \Delta T(s, z) y(s) t(s) ds \quad M_{yT}(z) = \int_c \beta \Delta T(s, z) x(s) t(s) ds. \quad (3.78)$$

Since the origin of the  $x$ - $y$  system is taken at the centroid of the cross section, the first area moments are zero by the definition of the centroid. For  $Q_x = Q_y = 0$ , eqs. (3.73) and (3.76) reduce to

$$\begin{bmatrix} N + N_T \\ M_x + M_{xT} \\ M_y + M_{yT} \end{bmatrix} = E \begin{bmatrix} A & 0 & 0 \\ 0 & I_{xx} & I_{xy} \\ 0 & I_{xy} & I_{yy} \end{bmatrix} \begin{bmatrix} dw/dz \\ d\phi_x/dz \\ d\phi_y/dz \end{bmatrix}. \quad (3.79)$$

**Locating the origin of the cross-sectional Cartesian system at the centroid decouples the extensional and bending responses in the material law (3.79) for the bar.** Solve eq. (3.79) for the derivatives of the displace-

ment  $w$  and the rotations  $\phi_x$  and  $\phi_y$ , and write it as

$$\begin{bmatrix} dw/dz \\ d\phi_x/dz \\ d\phi_y/dz \end{bmatrix} = \frac{1}{E} \begin{bmatrix} 1/A & 0 & 0 \\ 0 & k/I_{xx} & (-kn_x)/I_{yy} \\ 0 & (-kn_y)/I_{xx} & k/I_{yy} \end{bmatrix} \begin{bmatrix} N + N_T \\ M_x + M_{xT} \\ M_y + M_{yT} \end{bmatrix}. \quad (3.80)$$

Following Vasiliev (1993, p. 205), the new terms in eq. (3.80) are defined by

$$n_x = I_{xy}/I_{xx} \quad n_y = I_{xy}/I_{yy} \quad k = \frac{1}{1 - n_x n_y}. \quad (3.81)$$

Substitute the derivatives of the displacement and rotations from eq. (3.80) into the expressions for the strain (3.69) and stress (3.70) to get

$$\varepsilon_{zz} = \frac{N + N_T}{EA} + k \frac{(M_x + M_{xT})^-}{EI_{xx}} y(s) + k \frac{(M_y + M_{yT})^-}{EI_{yy}} x(s), \text{ and} \quad (3.82)$$

$$\sigma_{zz} = \frac{N + N_T}{A} + k \frac{(M_x + M_{xT})^-}{I_{xx}} y(s) + k \frac{(M_y + M_{yT})^-}{I_{yy}} x(s) - \beta \Delta T(s, z). \quad (3.83)$$

In the previous equation coordinate functions  $\bar{x}(s)$  and  $\bar{y}(s)$  are defined by

$$\bar{x}(s) = x(s) - n_x y(s) \quad \bar{y}(s) = y(s) - n_y x(s). \quad (3.84)$$

### Example 3.1 Centroidal coordinates and second area moments for the open section shown in figure 3.1

Let  $s_1$  denote the contour coordinate in the straight branch 1 with  $s_1 = 0$  at its lower end and  $s_1 = a$  at its upper end where it meets at the junction with the semicircular branch 2. Let  $s_2 = a(\pi/2 + \theta)$  denote the contour coordinate in branch 2 with  $\theta = -\pi/2$  at its lower end where it meets at the junction with branch 1 and  $\theta = \pi/2$  at its upper end. The Cartesian coordinates with respect to point  $O$  for each branch are

$$X_1(s_1) = 0 \quad Y_1(s_1) = -2a + s_1 \quad 0 \leq s_1 \leq a, \text{ and} \quad (a)$$

$$X_2(\theta) = a \cos \theta \quad Y_2(\theta) = a \sin \theta \quad -\pi/2 \leq \theta \leq \pi/2. \quad (b)$$

Let  $S$  denote the total arc-length of the contour and let  $A$  denote the area of the cross section. Then  $S$  and  $A$  are given by

$$S = \int_0^a (1) ds_1 + \int_{-\pi/2}^{\pi/2} (1) a d\theta = a + a\pi \quad A = \int_0^a (t) ds_1 + \int_{-\pi/2}^{\pi/2} (t) a d\theta = at + a\pi t. \quad (c)$$

The first area moment of the cross-sectional area about the  $X$ -axis is denoted by  $Q_X$ , and the first area moment of the cross-sectional area about the  $Y$ -axis is denoted by  $Q_Y$ . These first area moments are determined from the integrals

$$Q_X = \int_0^a [Y_1(s_1)] t ds_1 + \int_{-\pi/2}^{\pi/2} [Y_2(\theta)] t a d\theta = -(3/2)a^2 t, \text{ and} \quad (\text{d})$$

$$Q_Y = \int_0^a [X_1(s_1)] t ds_1 + \int_{-\pi/2}^{\pi/2} [X_2(\theta)] t a d\theta = 2a^2 t. \quad (\text{e})$$

The relationship between the Cartesian coordinates with origin at point  $O$  and the parallel coordinates with the origin at the point  $C$  (centroid) are

$$X(s) = x(s) + X_c \quad Y(s) = y(s) + Y_c. \quad (\text{f})$$

The definition of the centroid is that the value of the first area moments about the  $x$ -axis and  $y$ -axis are zero. Substitute eq. (f) into the definitions of the first area moments about the centroidal axes (3.74) to get

$$Q_x = \int_c [y(s)] t ds = \int_c [Y(s)] t ds - Y_c \int_c t ds = Q_X - Y_c A = 0, \text{ and} \quad (\text{g})$$

$$Q_y = \int_c [x(s)] t ds = \int_c [X(s)] t ds - X_c \int_c t ds = Q_Y - X_c A = 0. \quad (\text{h})$$

Hence the coordinates of the centroid relative to point  $O$  are given by

$$X_c = Q_Y/A = \frac{2a}{1+\pi} = 0.482906a \quad Y_c = Q_X/A = \frac{-3a}{2(1+\pi)} = -0.36218a. \quad (\text{i})$$

The contour coordinates with respect the centroid are determined from eqs. (a), (b) and (f). The results are

$$x_1(s_1) = -0.482906a \quad y_1(s_1) = -1.63782a + s_1 \quad 0 \leq s_1 \leq a \quad (\text{j})$$

$$x_2(\theta) = -0.482906a + a \cos \theta \quad y_2(\theta) = 0.36218a + a \sin \theta \quad -\pi/2 \leq \theta \leq \pi/2. \quad (\text{k})$$

The expressions for second area moments about the  $x$ - $y$  system with origin at the centroid are given in eq. (3.77). Substitute the eqs. (j) and (k) for the contour coordinates into the definitions of the second area moments, followed by integration to get following results:

$$I_{xx} = \int_c y^2 t ds = \int_0^a y_1^2 t ds_1 + \int_{-\pi/2}^{\pi/2} y_2^2 t a d\theta = 3.36086a^3 t, \quad (\text{l})$$

$$I_{yy} = \int_c x^2 t ds = \int_0^a x_1^2 t ds_1 + \int_{-\pi/2}^{\pi/2} x_2^2 t a d\theta = 0.604984a^3 t, \text{ and} \quad (\text{m})$$

$$I_{xy} = \int_c xy t ds = \int_0^a x_1 y_1 t ds_1 + \int_{-\pi/2}^{\pi/2} x_2 y_2 t a d\theta = 0.724359a^3 t. \quad (\text{n})$$

### 3.8 Shear flow due to the transverse shear forces

The shear flow  $q$  is defined in eq. (3.37) as the definite integral of the shear stress component tangent to the contour  $\sigma_{zs}$  across the thickness of the wall. In this article the shear flow is determined from axial equilibrium.<sup>4</sup> A free body diagram for axial equilibrium of a differential element with area  $\Delta s$ -by- $\Delta z$  of the middle surface is shown in figure 3.10. It is assumed that there is no prescribed surface traction acting on the middle surface of the

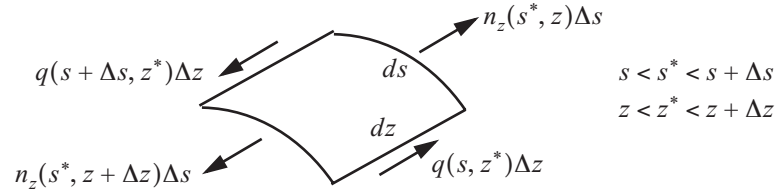


**Fig. 3.10** Free body diagram for axial equilibrium of a differential element of the middle surface

wall in the axial direction. Refer to figure 3.8(a) on page 41. For prescribed traction component  $p_z(s, z) = 0$ , it follows from eq. (3.42) that the axial force per unit length  $f_z = 0$ , and from eqs. (3.45) that the bending moments per unit axial length  $m_x = m_y = 0$ .

Summation of the forces in the  $z$ -direction yields

$$[n_z(s^*, z + \Delta z) - n_z(s^*, z)]\Delta s + [q(s + \Delta s, z^*) - q(s, z^*)]\Delta z = 0. \quad (3.85)$$

Division by  $\Delta s \Delta z$  followed by taking the limit as  $\Delta s \rightarrow 0$  and  $\Delta z \rightarrow 0$  yields the partial differential equation

$$\frac{\partial n_z}{\partial z} + \frac{\partial q}{\partial s} = 0. \quad (3.86)$$

The normal stress resultant  $n_z$  is given by eq. (3.72) and it is based on the kinematic assumption for the displacements made in article 3.3, infinitesimal deformation, and Hooke's law. The expression for the normal stress resultant is written as  $n_z = t(s)[E\varepsilon_{zz} - \beta\Delta T]$ . Substitute eq. (3.82) for the normal strain to get

$$n_z = t(s) \left[ \frac{N + N_T}{A} + k \frac{(M_x + M_{xT})^-}{I_{xx}} y(s) + k \frac{(M_y + M_{yT})^-}{I_{yy}} x(s) - \beta\Delta T \right]. \quad (3.87)$$

Take the partial derivative of the normal stress resultant (3.87) with respect to  $z$ . In the process of taking the derivative we eliminate the derivative of the axial force using equilibrium eq. (3.53), and we eliminate the derivative of the bending moments using equilibrium eqs. (3.55), and (3.57). The final result for the derivative of the normal stress resultant with respect to  $z$  is

$$\frac{\partial n_z}{\partial z} = \frac{t(s)}{A} \frac{dN_T}{dz} - \beta \frac{\partial \Delta T}{\partial z} t(s) + \frac{k}{I_{xx}} [V_y + V_{yT}] \bar{y}(s) t(s) + \frac{k}{I_{yy}} [V_x + V_{xT}] \bar{x}(s) t(s). \quad (3.88)$$

4. The alternative is to derive the shear flow from Hooke's law in shear with the shear strain  $\gamma_{zs}$  given in eq. (3.31). This alternative derivation is not used in the theory of thin-walled bars under consideration.

Assume differentiation with respect to  $z$  can be interchanged with the definite integrals with respect to  $s$  (Leibniz's rule). Then, the new terms in eq. (3.88) are given by the equations

$$\frac{dN_T}{dz} = \int_c \beta \frac{\partial \Delta T}{\partial z} t(s) ds \quad V_{xT} = \frac{dM_{yT}}{dz} = \int_c \beta \frac{\partial \Delta T}{\partial z} x(s) t(s) ds \quad V_{yT} = \frac{dM_{xT}}{dz} = \int_c \beta \frac{\partial \Delta T}{\partial z} y(s) t(s) ds. \quad (3.89)$$

The functions  $V_{xT}(z)$  and  $V_{yT}(z)$  are defined as thermal shear forces. Integrate the differential equation (3.86) with respect to the contour coordinate from  $s = 0$  to  $s = s$  to get

$$\int_0^s \frac{\partial n_z}{\partial z} ds + q(s, z) - q(0, z) = 0. \quad (3.90)$$

Solve the latter equation for the shear flow to write

$$q(s, z) = q_0(z) - \int_0^s \frac{\partial n_z}{\partial z} ds, \quad (3.91)$$

where  $q_0(z) = q(0, z)$ . Note that the origin of the contour coordinate where  $s = 0$  is arbitrary at this point. Now the result for the integral with respect to the contour coordinate of the derivative of the normal stress resultant is written as

$$\int_0^s \frac{\partial n_z}{\partial z} ds = \frac{k}{I_{xx}} V_y(z) \bar{Q}_x(s) + \frac{k}{I_{yy}} V_x(z) \bar{Q}_y(s) + q_T(s, z). \quad (3.92)$$

In eq. (3.92) the functions  $\bar{Q}_x(s)$  and  $\bar{Q}_y(s)$  are called distribution functions. They are defined with respect to coordinate functions  $\bar{x}(s)$  and  $\bar{y}(s)$  for the segment of the contour from  $s = 0$  to  $s$ , and are given by

$$\bar{Q}_x(s) = \int_0^s [\bar{y}(s) t(s)] ds = Q_x(s) - n_y Q_y(s) \quad \bar{Q}_y(s) = \int_0^s [\bar{x}(s) t(s)] ds = Q_y(s) - n_x Q_x(s). \quad (3.93)$$

In eq. (3.93) the distribution functions with respect to the centroidal coordinates  $x(s)$  and  $y(s)$  are defined by

$$Q_x(s) = \int_0^s y(s) t(s) ds \quad Q_y(s) = \int_0^s x(s) t(s) ds. \quad (3.94)$$

The function  $q_T(s, z)$  in eq. (3.92) is the shear flow from the temperature gradient in the axial coordinate  $z$ . It is defined by

$$q_T(s, z) = \frac{A(s)}{A} \int_c \beta \frac{\partial \Delta T}{\partial z} t(s) ds - \int_0^s \beta \frac{\partial \Delta T}{\partial z} t(s) ds + \frac{k}{I_{xx}} \left( \int_c \beta \frac{\partial \Delta T}{\partial z} y(s) t(s) ds \right) \bar{Q}_x(s) + \frac{k}{I_{yy}} \left( \int_c \beta \frac{\partial \Delta T}{\partial z} x(s) t(s) ds \right) \bar{Q}_y(s), \quad (3.95)$$

where the area of the contour segment is

$$A(s) = \int_0^s t(s) ds. \quad (3.96)$$



The shear flow from the change in temperature vanishes for two practical cases: (1) The temperature is spatially uniform in the axial coordinate  $z$  so that  $\Delta T(s)$  and  $\frac{\partial \Delta T}{\partial z} = 0$ , and (2) the change in temperature and material coefficient  $\beta$  are spatially uniform over the cross section so  $\Delta T = \Delta T(z)$ .

Substitute the result for the integral in eq. (3.92) into eq. (3.91), we write the formula for the shear flow due to the transverse shear forces as

$$q(s, z) = q_0(z) - \frac{k}{I_{yy}} V_x \overline{Q}_y(s) - \frac{k}{I_{xx}} V_y \overline{Q}_x(s) - q_T(s, z) \quad (3.97)$$

### 3.8.1 Open cross-sectional contour

From eq. (3.97) the shear flow at the contour origin is  $q(0, z) = q_0(z)$ . For most open cross sections, there is a longitudinal edge of the bar that is free of external tractions. If the contour origin is taken at the location of the free longitudinal edge, then  $q(0, z) = q_0(z) = 0$ . The shear flow for an open cross section with the contour origin located at the longitudinal free edge and  $q_T = 0$  is given by

$$q(s, z) = -\frac{k}{I_{yy}} V_x \overline{Q}_y(s) - \frac{k}{I_{xx}} V_y \overline{Q}_x(s) \quad (3.98)$$

#### Example 3.2 Shear flow distribution in the open cross section shown in figure 3.1

Take the change in temperature  $\Delta T(s, z) = 0$ ,  $0 \leq s \leq S$ , and  $0 \leq z \leq L$ . Hence,  $q_T = 0$  for the shear flow expression given by eq. (3.98). Second area moments were computed in example 3.1 page 47 with the results listed in eqs. (l) to (n). Cross-sectional properties that depend on the second area moments, eq. (3.81), are

$$n_x = \frac{I_{xy}}{I_{xx}} = \frac{0.724359a^3t}{3.36086a^3t} = 0.215528 \quad n_y = \frac{I_{xy}}{I_{yy}} = \frac{0.724359a^3t}{0.604984a^3t} = 1.19732 \quad k = 1.34781 \quad (a)$$

The first area moments of the segment of branch 1 from  $s_1 = 0$  to  $s_1 \in [0, a]$  with respect the centroidal coordinates are

$$Q_{x1} = \int_0^{s_1} y_1(s_1) t ds_1 \quad Q_{y1} = \int_0^{s_1} x_1(s_1) t ds_1 \quad (b)$$

From eq. (j) of example 3.1  $x_1(s_1) = -0.482906a$  and  $y_1(s_1) = -1.63782a + s_1$ . Performing the integrals in the first area moments we get

$$Q_{x1} = \frac{t(-a - 4a\pi + s_1 + \pi s_1)s_1}{2(1 + \pi)} = -1.63782ats_1 + 0.50ts_1^2 \quad Q_{y1} = \frac{-2at}{1 + \pi} s_1 = -0.482906ats_1 \quad (c)$$

The distribution functions of the segment with respect to the  $\bar{x}$ - $\bar{y}$  system are given by eq. (3.93), which for branch 1 results in

$$\bar{Q}_{x1} = -1.63782ats_1 + 0.50ts_1^2 - (1.19732)(-0.482906ats_1) = -1.05963ats_1 + 0.5ts_1^2, \quad (d)$$

$$\bar{Q}_{y1} = (-0.482906ats_1) - (0.215528)(-1.63782ats_1 + 0.50ts_1^2) = -0.12991ats_1 - 0.107764ts_1^2. \quad (e)$$

At  $s_1 = 0$ , the longitudinal free edge condition requires  $q_0 = 0$ . The shear flow in branch 1 can now be computed from eq. (3.98). The result is

$$q_1(s_1) = \left[ 0.289419\left(\frac{s_1}{a}\right) + 0.240081\left(\frac{s_1}{a}\right)^2 \right] \frac{V_x}{a} + \left[ 0.424944\left(\frac{s_1}{a}\right) - 0.200516\left(\frac{s_1}{a}\right)^2 \right] \frac{V_y}{a} \quad 0 \leq s_1 \leq a. \quad (f)$$

The first area moments of the cross-sectional area consisting of branch 1 and a segment of branch 2 are given by

$$Q_{x2}(\theta) = Q_{x1}(a) + \int_{-\pi/2}^{\theta} y_2(\theta) t a d\theta \quad Q_{y2}(\theta) = Q_{y1}(a) + \int_{-\pi/2}^{\theta} x_2(\theta) t a d\theta. \quad (g)$$

where from eq. (c) we find

$$Q_{x1}(a) = (-1.13782)a^2t \quad Q_{y1}(a) = (-0.482906)a^2t. \quad (h)$$

From eq. (k) of example 3.1  $x_2(\theta) = -0.482906a + a \cos \theta$  and  $y_2(\theta) = 0.36218a + a \sin \theta$ . Evaluating the integrals in the first area moments for branch 2 we get

$$\int_{-\pi/2}^{\theta} y_2(\theta) t a d\theta = (0.56891 + 0.36218\theta - \cos \theta)a^2t \quad \int_{-\pi/2}^{\theta} x_2(\theta) t a d\theta = (0.241453 - 0.482906\theta + \sin \theta)a^2t.$$

Thus, the first area moments of the cross-sectional area consisting of branch 1 and a segment of branch 2 are

$$Q_{x2} = ((-1.13782) + 0.56891 + 0.36218\theta - \cos \theta)a^2t = (-0.56891 + 0.36218\theta - \cos \theta)a^2t$$

$$Q_{y2} = ((-0.482906) + 0.241453 - 0.482906\theta + \sin \theta)a^2t = (-0.241453 - 0.482906\theta + \sin \theta)a^2t. \quad (i)$$

Note that at  $\theta = \pi/2$  both  $Q_{x2} = Q_{y2} = 0$ , since the origin of the  $x$ - $y$  system is at centroid of the cross section (i.e., the first area moments of the entire cross-sectional area about the centroidal coordinate system vanish).

The first area moment  $\bar{Q}_x$  given in eq. (3.93) for the cross-sectional area consisting of branch 1 plus a segment of branch 2 is computed as

$$\bar{Q}_{x2} = (-0.56891 + 0.36218\theta - \cos \theta)a^2t - (1.19732)((-0.241453 - 0.482906\theta + \sin \theta)a^2t).$$

Combining terms we get

$$\bar{Q}_{x2} = (-0.279814 + 0.940372\theta - \cos \theta - 1.19732 \sin \theta)a^2t. \quad (j)$$

The first area moment  $\bar{Q}_y$  given in eq. (3.93) for the cross-sectional area consisting of branch 1 plus a segment of branch 2 is computed as

$$\bar{Q}_{y2} = (-0.241453 - 0.482906\theta + \sin \theta)a^2t - (0.215528)((-0.56891 + 0.36218\theta - \cos \theta)a^2t). \quad (k)$$

Combining terms we get

$$\bar{Q}_{y2} = (-0.118837 - 0.560966\theta + 0.215528\cos\theta + \sin\theta)a^2t. \quad (l)$$

The shear flow in branch 2 can now be computed from eq. (3.98), which yields

$$q_2(\theta) = [0.26475 + 1.24974\theta - 0.480162\cos\theta - 2.22784\sin\theta]\frac{V_x}{a} + [0.112214 - 0.377118\theta + 0.401031\cos\theta + 0.480162\sin\theta]\frac{V_y}{a}. \quad (m)$$

Note that  $q_2(\pi/2) = 0$ , which is consistent with the vanishing of the shear flow at the top free edge. Shear flow distributions are plotted normal to the contour in figure 3.11. ■

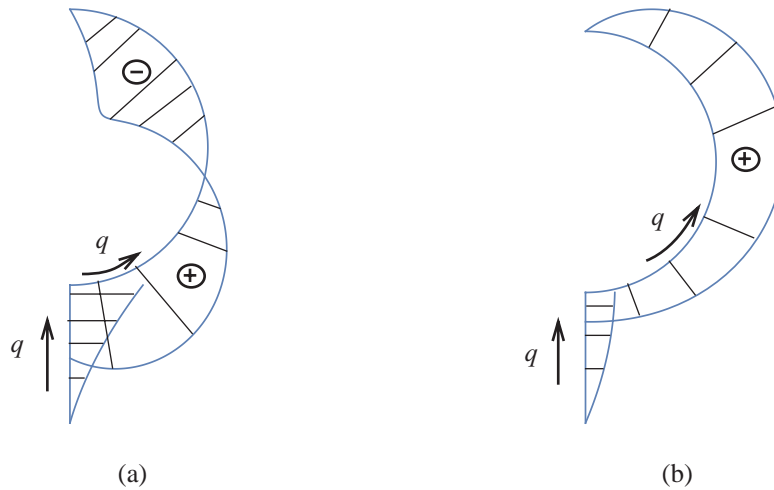


**Fig. 3.11** Shear flow distributions for the open section in figure 3.1.  
(a)  $V_x > 0$  &  $V_y = 0$ . (b)  $V_x = 0$  &  $V_y > 0$ .

### 3.8.2 Location of the shear center for an open cross section

The shear flow given by eq. (3.98) is determined by transverse shear forces  $V_x$  and  $V_y$ , and is independent of the torque  $M_z$ . For transverse bending the shear flow  $q$  is the dominate term in the expression (3.40) for the torque. Hence, the contribution of the twisting moment resultant  $m_{zs}$  and the transverse stress resultant  $q_z$  are neglected in eq. (3.40) with respect to the shear flow.<sup>5</sup> The torque with respect to the shear center resulting from the shear flow is then

$$M_z = \int_c r_n q ds = \int_c r_n(s) \left[ -\frac{k}{I_{yy}} V_x \bar{Q}_y(s) - \frac{k}{I_{xx}} V_y \bar{Q}_x(s) \right] ds. \quad (3.99)$$

Expanding eq. (3.99), we get

5. Note that  $m_{zs}$  and  $q_z$  are the main contributors to  $M_z$  under pure torsion of an open section as is discussed in article 3.9.

$$M_z = - \left[ \left( \frac{k}{I_{yy}} \right) \int_c r_n(s) \bar{Q}_y(s) ds \right] V_x - \left[ \left( \frac{k}{I_{xx}} \right) \int_c r_n(s) \bar{Q}_x(s) ds \right] V_y. \quad (3.100)$$

The contribution of the shear forces acting at the shear center to the torque in eq. (3.100) must vanish by the definition of the shear center. Thus,

$$- \left( \frac{k}{I_{yy}} \right) \left[ \int_c r_n(s) \bar{Q}_y(s) ds \right] V_x - \left( \frac{k}{I_{xx}} \right) \left[ \int_c r_n(s) \bar{Q}_x(s) ds \right] V_y = 0 \quad \forall V_x \text{ \& } V_y. \quad (3.101)$$

Equation (3.101) can only be satisfied if

$$\int_c r_n(s) \bar{Q}_y(s) ds = 0 \quad \int_c r_n(s) \bar{Q}_x(s) ds = 0. \quad (3.102)$$

To locate the shear center relative to the centroid, substitute the expression for the normal coordinate  $r_n(s)$  from eq. (3.10) into the preceding geometric properties of the shear center to get

$$\int_c r_n(s) \bar{Q}_y(s) ds = \int_c r_{nc}(s) \bar{Q}_y(s) ds - x_{sc} \int_c \bar{Q}_y(s) \frac{dy}{ds} ds + y_{sc} \int_c \bar{Q}_y(s) \frac{dx}{ds} ds = 0, \text{ and} \quad (3.103)$$

$$\int_c r_n(s) \bar{Q}_x(s) ds = \int_c r_{nc}(s) \bar{Q}_x(s) ds - x_{sc} \int_c \bar{Q}_x(s) \frac{dy}{ds} ds + y_{sc} \int_c \bar{Q}_x(s) \frac{dx}{ds} ds = 0. \quad (3.104)$$

With the aid of eqs. (3.93), (3.84), (3.81), and (3.77), integrate by parts the following terms in eqs. (3.103) and (3.104) to find

$$\int_c \bar{Q}_y(s) \left( \frac{dx}{ds} \right) ds = \frac{-I_{yy}}{k} \quad \int_c \bar{Q}_x(s) \left( \frac{dx}{ds} \right) ds = 0 \quad \int_c \bar{Q}_y(s) \left( \frac{dy}{ds} \right) ds = 0 \quad \int_c \bar{Q}_x(s) \left( \frac{dy}{ds} \right) ds = \frac{-I_{xx}}{k}. \quad (3.105)$$

Substitute the results from eq. (3.105) into eqs. (3.103) and (3.104), and then solve for the coordinates of the shear center relative to the centroid as

$$\boxed{x_{sc} = - \left( \frac{k}{I_{xx}} \right) \left[ \int_c r_{nc}(s) \bar{Q}_x(s) ds \right] \quad y_{sc} = \frac{k}{I_{yy}} \left[ \int_c r_{nc}(s) \bar{Q}_y(s) ds \right]}. \quad (3.106)$$

Note that normal coordinate  $r_{nc}(s)$  is computed from the second of eq. (3.11) once the contour coordinates with respect to the centroid are established.

### Example 3.3 Shear center of the open section shown in figure 3.1

**Method 1.** For the open section consisting of two branches, the coordinates of the shear center relative to the centroid from eq. (3.106) are given by

$$x_{sc} = (-k/I_{xx}) \left( \int_0^a r_{nc1} \bar{Q}_{x1} ds_1 + \int_{-\pi/2}^{\pi/2} r_{nc2} \bar{Q}_{x2} a d\theta \right) \quad y_{sc} = (k/I_{yy}) \left( \int_0^a r_{nc1} \bar{Q}_{y1} ds_1 + \int_{-\pi/2}^{\pi/2} r_{nc2} \bar{Q}_{y2} a d\theta \right).$$

Some of the terms in these formulas are listed as eqs. **(l)** and **(m)** in example 3.1 page 47, and eqs. **(d)**, **(c)**, **(j)**, and **(l)** in example 3.2 on page 51. We list these terms for convenience as follows:

$$\begin{aligned}
 k &= 1.34781 & I_{xx} &= 3.36086a^3t & I_{yy} &= 0.604984a^3t, \\
 \bar{Q}_{x1} &= -1.05963ats_1 + 0.5ts_1^2 & \bar{Q}_{y1} &= -0.12991ats_1 - 0.107764ts_1^2, \text{ and} \\
 \bar{Q}_{x2} &= (-0.279814 + 0.940372\theta - \cos\theta - 1.19732\sin\theta)a^2t \\
 \bar{Q}_{y2} &= (-0.118837 - 0.560966\theta + 0.215528\cos\theta + \sin\theta)a^2t
 \end{aligned}$$

From eq. (3.11) the coordinates normal to the contour relative to the centroid are given by

$$r_{nc1} = x_1\left(\frac{dy_1}{ds_1}\right) - y_1\left(\frac{dx_1}{ds_1}\right) \quad r_{nc2} = \frac{x_2}{a}\left(\frac{dy_2}{d\theta}\right) - \frac{y_2}{a}\left(\frac{dx_2}{d\theta}\right).$$

The Cartesian coordinates of the contour for each branch are given by eqs. (j) and (k) in example 3.1, which are repeated below:

$$\begin{aligned}
 x_1(s_1) &= -0.482906a & y_1(s_1) &= -1.63782a + s_1 & 0 \leq s_1 \leq a \\
 x_2(\theta) &= -0.482906a + a\cos\theta & y_2(\theta) &= 0.36218a + a\sin\theta & -\pi/2 \leq \theta \leq \pi/2
 \end{aligned}$$

The results for the coordinates normal to the contour are

$$r_{nc1} = -0.482906a \quad r_{nc2} = a(1 - 0.482906\cos\theta + 0.36218\sin\theta).$$

The shear center coordinates are determined from the following integrals

$$\begin{aligned}
 x_{sc} &= \left(\frac{-1.34781}{3.36086a^3t}\right) \left[ \int_0^a (-0.482906a)(-1.05963ats_1 + 0.5ts_1^2)ds_1 + \right. \\
 &\quad \left. \int_{-\pi/2}^{\pi/2} [a(1 - 0.482906\cos\theta + 0.36218\sin\theta)][(-0.279814 + 0.940372\theta - \cos\theta - 1.19732\sin\theta)a^2t]ad\theta \right] \\
 y_{sc} &= \left(\frac{1.34781}{0.604984a^3t}\right) \left[ \int_0^a (-0.482906a)(-0.12991ats_1 - 0.107764ts_1^2)ds_1 + \right. \\
 &\quad \left. \int_{-\pi/2}^{\pi/2} [a(1 - 0.482906\cos\theta + 0.36218\sin\theta)][(-0.118837 - 0.560966\theta + 0.215528\cos\theta + \sin\theta)a^2t]ad\theta \right].
 \end{aligned}$$

The preceding integrals were evaluated in *Mathematica* to get

$$x_{sc} = 0.67169a \quad y_{sc} = 0.490767a. \quad (\mathbf{a})$$

**Method 2.** The shear flow distributions were determined in example 3.2 on page 51 with the results given by eq. (f) for branch 1 and by eq. (m) for branch 2. These shear flows are illustrated in the left-hand sketch in figure 3.12. It is convenient to determine the resultant of the shear flow distribution at point *O* first. As shown in figure 3.12 the components of the resultant force are  $F_X$  and  $F_Y$ , and the torque is  $M_{z0}$ . Under transverse bending the contributions of the transverse shear resultant  $q_z$  and twisting moment resultant  $m_{zs}$  are negligible with respect to the shear flow  $q$  in the expressions for the shear forces and the torque<sup>6</sup> in eq. (3.40). Hence, the force components and the torque are given by the following integrals of the shear flow over the contour.

$$F_X = \int_{-\pi/2}^{\pi/2} q_2(\theta)(-\sin\theta)a d\theta \quad F_Y = \int_0^a q_1(s_1)ds_1 + \int_{-\pi/2}^{\pi/2} q_2(\theta)(\cos\theta)a d\theta \quad M_{z0} = \int_{-\pi/2}^{\pi/2} a[q_2(\theta)a d\theta]. \quad (\text{b})$$

The line of action of the shear flow in branch 1 is parallel to the  $Y$ -direction and so does not contribute to the force component  $F_X$  in eq. (b). From example 3.2 substitute eq. (d) for  $q_1$  and eq. (h) for  $q_2$  into eq. (b) above, then perform the integrations, to find  $F_X = V_x$  and  $F_Y = V_y$ . It is expected that the force components would be equal to their respective transverse shear components, since the shear flows were determined from equilibrium conditions with respect to the transverse shear forces in article 3.8. Only the shear flow in branch 2 contributes to the torque about point  $O$ , since the line of action of the shear flow in branch 1 passes through point  $O$ . The moment arm to the differential force  $q_2 a d\theta$  in branch 2 about point  $O$  is simply the radius  $a$ . From example 3.2 substitute eq. (h) for  $q_2$  in the expression for the torque in eq. (b) above, and perform the integration to get

$$M_{z0} = -0.128587aV_x + 1.15459aV_y. \quad (\text{c})$$

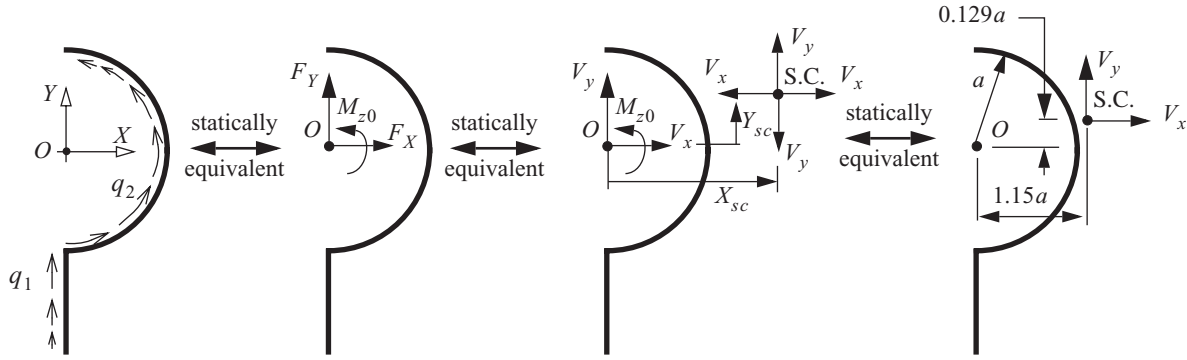


**Fig. 3.12 Resultant of the shear flow distribution**

Now add and subtract the shear forces  $V_x$  and  $V_y$  at the shear center (S.C.) in order to preserve force equivalence as is shown in figure 3.12. The upward force  $V_y$  at point  $O$  and the downward force  $V_y$  at S.C. form a clockwise couple  $X_{sc}V_y$  and no net vertical force. Similarly, force  $V_x$  at point  $O$  and the equal and opposite force  $V_x$  at the S.C. form a counterclockwise couple  $Y_{sc}V_x$  and no net horizontal force. The total counterclockwise torque in the cross section must vanish by the definition of the S.C.; i.e.,  $M_{z0} - X_{sc}V_y + Y_{sc}V_x = 0$ . Substitute eq.(c) for  $M_{z0}$  in the total torque to get

$$(-0.128587a + Y_{sc})V_x + (1.15459a - X_{sc})V_y = 0 \quad \forall(V_x, V_y). \quad (\text{d})$$

Therefore, the location of the shear center relative to point  $O$  is given by

$$X_{sc} = 1.15459a \quad Y_{sc} = 0.128587a. \quad (\text{e})$$

The coordinates of the shear center relative to the centroid are given by  $x_{sc} = X_{sc} - X_c$  and  $y_{sc} = Y_{sc} - Y_c$ ,

6. Under pure torsion the transverse shear resultant and the twisting moment resultant are the major contributors to the torque as discussed in article 3.9.

where the coordinates of the centroid relative to point  $O$  is given by eq. (i) in example 3.1 on page 47. Thus,

$$x_{sc} = 1.15459a - 0.48290a = 0.67169a \quad y_{sc} = 0.128587a - (-0.36218a) = 0.490767a, \quad (f)$$

which is the same result obtained in eq. (a) by method 1. ■

### 3.8.3 Notes concerning the shear center

- The resultant of the shear flow distribution over the contour is a force with components  $V_x$  and  $V_y$  acting through the shear center such that there is no torque acting at the shear center. If the cross section is subject to a torque, this torque cannot be balanced by the shear flow which, according to eq. (3.98), is uniquely determined by the shear forces  $V_x$  and  $V_y$ .
- The location of the shear center in the cross section is determined by the pattern of the shear flow distribution and not on the magnitude of the transverse shear forces.
- Transverse shear forces  $V_x$  and  $V_y$  act in the plane of loading to equilibrate the externally applied lateral load intensities  $f_x(z)$  and  $f_y(z)$ . (Refer to equilibrium equations (3.54) and (3.56).) Thus, the line of action of the external lateral loads must pass through the shear center to bend the bar without twisting it in torsion.
- The shear center is located on an axis of symmetry of the cross section if there is one. If there are two axes of symmetry in the cross section the shear center and the centroid lie on the intersection of the symmetry axes.
- For an open cross section with straight branches and one junction the shear center is at the junction, since the torque from the shear flows at the junction vanishes. See figure 3.13.

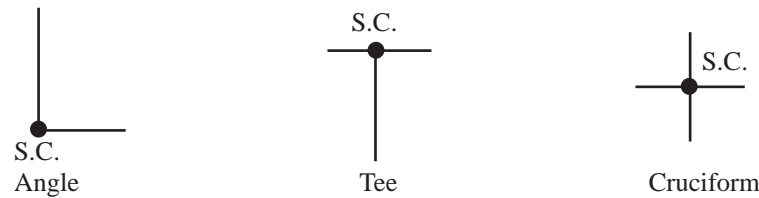


Fig. 3.13 Shear center locations for open sections with straight branches and one junction.

## 3.9 Torsion of an open section with a straight contour

Although we have located the shear center for the open cross-sectional contour, a material law for the torque acting at the shear center remains to be determined. Torsion of an open section bar is an important problem in engineering, but it is not a simple problem in elasticity. Saint-Venant (1855) guided by the solution of the bar with a circular cross section, made a brilliant guess and showed that an exact solution to a well-defined problem can be obtained. Here, we consider a simplified approach following the presentation given by Vasiliev (1993).

Consider a prismatic bar with a rectangular cross section subject to equal and opposite torques acting on the end cross sections at  $z = 0$  and  $z = L$ . The lateral surfaces of the bar are traction free so  $f_x = f_y = 0$  in eq. (3.31) and  $m_z(z) = 0$  in eq. (3.44) on page 41 for  $0 \leq z \leq L$ . Equilibrium equations (3.53) to (3.57) are identically satisfied when  $N = V_x = V_y = M_x = M_y = 0$  for  $0 \leq z \leq L$ , and torsional equilibrium (3.58) is satisfied for a

torque  $M_z$  independent of axial coordinate  $z$ . Also, there is no change in temperature from the reference state  $\Delta T = 0$ . For a Hookean material the twist per unit length  $d\phi_z/dz$  is proportional to the torque, and so it is also a constant with respect to the  $z$ -coordinate.

The contour of a rectangular cross section is a straight horizontal line of length  $b$  as shown in figure 3.14. The angle  $\theta = 90^\circ$  in figure 3.3 for all values of  $s$ , and the geometric relations given by eqs. (3.3) to (3.6) and (3.8) specialize to

$$x = -s \quad y = 0 \quad \hat{t} = -\hat{i} \quad \hat{n} = \hat{j} \quad r_t = s \quad r_n = 0 \quad d\theta/ds = 1/R_s = 0.$$

The cross-sectional coordinates are  $(s, \zeta)$  with  $s \in [-b/2, b/2]$  and  $\zeta \in [-t/2, t/2]$ , and the origin is the location of the centroid and also of the shear center.

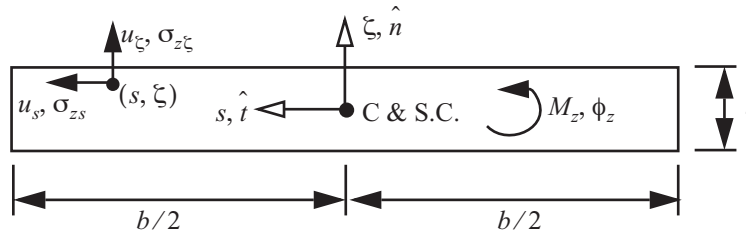


Fig. 3.14 A bar with rectangular cross section subject to uniform torsion

**Displacements and strains.** Saint-Venant assumed that as the bar twists the cross section is displaced normal to the  $s$ - $\zeta$  plane (i.e., it warps) but its projection on the  $s$ - $\zeta$  plane rotates as a rigid body. To prevent rigid body displacement, the displacement components of the centroid are set equal to zero. Then, the in-plane displacements given by eqs. (3.20) and (3.22) reduce to

$$u_\zeta(s, z, \zeta) = -s\phi_z(z) \quad u_s(s, z, \zeta) = \zeta\phi_z(z). \quad (3.107)$$

The out-of-plane displacement given by eq. (3.26) is

$$u_z(s, z, \zeta) = -s\phi_y(z) + \zeta[\phi_x(z)]. \quad (3.108)$$

However, this out-of-plane displacement is changed to account for the warping of the cross section in uniform torsion. **It is assumed that the rotation about the  $x$ -axis, or the negative  $s$ -axis, is independent of the  $z$ -coordinate but is an unknown function of the  $s$ -coordinate.** Consequently, the out-of-plane displacement in eq. (3.108) is changed to

$$u_z(s, z, \zeta) = \zeta\phi_x(s) - s\phi_y(z). \quad (3.109)$$

The only non-zero strains determined from the displacements (3.107) and (3.109) are shear strains  $\gamma_{zs}$  and  $\gamma_{z\zeta}$ . From the strain-displacement relations given by eq. (3.28) these shear strain-displacement relations are

$$\gamma_{zs} = \left( \frac{d\phi_z}{dz} + \frac{d\phi_x}{ds} \right) \zeta - \phi_y \quad \gamma_{z\zeta} = \phi_x - s \frac{d\phi_z}{dz}. \quad (3.110)$$

Hooke's laws for the shear stresses are  $\sigma_{zs} = G\gamma_{zs}$  and  $\sigma_{z\zeta} = G\gamma_{z\zeta}$ .



**Stress resultants and equilibrium** The stress resultants associated with these non-zero shear strains (3.110) are determined from Hooke's law, and the definition of stress resultants  $q$ ,  $m_{zs}$ , and  $q_z$  in eq. (3.37). The expressions for the stress resultants are

$$(q, m_{zs}) = \int_{-t/2}^{t/2} (1, \xi) \sigma_{zs} d\xi = G \int_{-t/2}^{t/2} (1, \xi) \left[ \left( \frac{d\phi_z}{dz} + \frac{d\phi_x}{ds} \right) \xi - \phi_y \right] d\xi \quad q_z = \int_{-t/2}^{t/2} \sigma_{z\xi} d\xi = G \int_{-t/2}^{t/2} \left( \phi_x - s \frac{d\phi_z}{dz} \right) d\xi. \quad (3.111)$$

Performing the integrations through the thickness in eq. (3.111) we find the stress resultants are given by

$$q = -Gt\phi_y \quad m_{zs} = \frac{Gt^3}{12} \left( \frac{d\phi_z}{dz} + \frac{d\phi_x}{ds} \right) \quad q_z = Gt \left( \phi_x - s \frac{d\phi_z}{dz} \right). \quad (3.112)$$

Since  $V_x = V_y = q_T = 0$ , the shear flow from eq. (3.97) reduces to  $q(s, z) = q_0(z)$ . That is, the shear flow is spatially uniform in the  $s$ -coordinate. Furthermore, the longitudinal edges at  $s = \pm b/2$  are free of tractions, which means the shear flow vanishes. Hence,  $q = 0$  for  $-b/2 \leq s \leq b/2$ . It follows from the first equation in (3.112) that rotation  $\phi_y = 0$ .

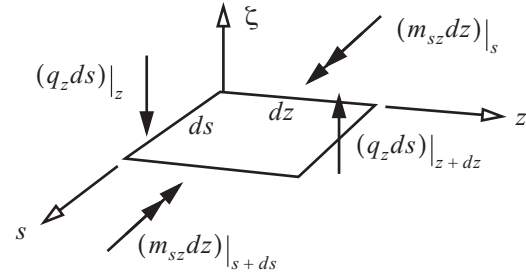


Fig. 3.15 FBD for moments about the  $s$ -axis

The twisting moment resultant  $m_{sz}$  and the transverse shear resultant  $q_z$  are related by moment equilibrium about the  $s$ -axis for a differential element  $ds$  by  $dz$  cut from the wall. From the free body diagram for differential element of the wall shown in figure 3.15 moment equilibrium gives

$$\frac{dz}{2} (q_z ds)|_{z+dz} + \frac{dz}{2} (q_z ds)|_z - [(m_{sz} dz)|_{s+ds} - (m_{sz} dz)|_s] = 0. \quad (3.113)$$

Division of eq. (3.113) by area element  $ds$  by  $dz$ , followed by the limit as  $ds \rightarrow 0$  and  $dz \rightarrow 0$  yields the moment equilibrium differential equation

$$q_z - \frac{dm_{sz}}{ds} = 0. \quad (3.114)$$

**Governing boundary value problem.** Substitute  $m_{zs}$  from eq. (3.112) into the differential equation (3.114), followed by substitution of  $q_z$  from eq. (3.112) into (3.114). After these substitutions and re-arrangement, the result is

$$\frac{d^2 \phi_x}{ds^2} - \frac{12}{t^2} \phi_x = - \left( \frac{12 d\phi_z}{t^2 dz} \right) s \quad \phi_x = \phi_x(s) \quad -b/2 < s < b/2. \quad (3.115)$$

The longitudinal edges at  $s = \pm b/2$  are free of tractions, which additionally means the twisting moment  $m_{sz}$  vanishes at  $s = \pm b/2$ . From eq. (3.112) the vanishing of the twisting moment at the end points leads to the boundary conditions

$$\frac{d\phi_z}{dz} + \frac{d\phi_x}{ds} = 0 \quad \text{at } s = \pm b/2. \quad (3.116)$$

The solution to differential equation (3.115) subject to boundary conditions (3.116) is

$$\phi_x(s) = \left[ s - \frac{2 \sinh ks}{k \cosh \lambda} \right] \frac{d\phi_z}{dz}, \quad (3.117)$$

where

$$k = \frac{2\sqrt{3}}{t} \quad \lambda = \frac{kb}{2} = \sqrt{3} \left( \frac{b}{t} \right). \quad (3.118)$$

Substitute the solution for  $\phi_x(s)$  from (3.117) into the expressions for the twisting moment  $m_{zs}$  and transverse shear  $q_z$  listed in (3.112) to find

$$m_{zs} = \frac{Gt^3}{6} \left( 1 - \frac{\cosh ks}{\cosh \lambda} \right) \left( \frac{d\phi_z}{dz} \right) \quad q_z = -2Gt \frac{\sinh ks}{k \cosh \lambda} \left( \frac{d\phi_z}{dz} \right). \quad (3.119)$$

From the third expression in eq. (3.40) the torque about the z-axis, counterclockwise positive, is given by

$$M_z = \int_{-b/2}^{b/2} (m_{zs} - sq_z) ds. \quad (3.120)$$

Substituting the results for  $m_{zs}$  and  $q_z$  from eq. (3.119) into the expression for the torque we write the result as

$$M_z = GJ \left( \frac{d\phi_z}{dz} \right), \quad (3.121)$$

where the torsion constant  $J$  is given by the integral

$$J = \int_{-b/2}^{b/2} \left[ \frac{t^3}{6} \left( 1 - \frac{\cosh(ks)}{\cosh \lambda} \right) + 2ts \left( \frac{\sinh(ks)}{k \cosh \lambda} \right) \right] ds.$$

After performing the integration, the result for the torsion constant is

$$J = \frac{bt^3}{3} \left( 1 - \frac{\tanh \lambda}{\lambda} \right). \quad (3.122)$$

For a thin, elongated rectangular cross section the value of the ratio of  $b/t \gg 1$ , which from the expression for  $\lambda$  in eq. (3.118) implies  $\lambda \gg 1$ . In the limiting case of  $\lambda \rightarrow \infty$  we find

$$J = \frac{bt^3}{3} \quad \text{as} \quad \lambda \rightarrow \infty. \quad (3.123)$$

In the simplified theory of thin-walled open section bars, the torsion constant in each open branch is given by eq. (3.123).

The distribution of the twisting moment resultant  $m_{zs}$  over the length of the contour for  $b/t = 20$  is shown in figure 3.16. As shown in the plot the distribution of  $m_{zs}$  is symmetric with respect to the contour coordinate, attains a uniform magnitude over the majority of the contour, and decreases rapidly to zero near the boundaries of the contour where  $s = \pm b/2$ . The distribution of the transverse shear resultant  $q_z$  over the contour is shown in figure 3.17. The distribution of  $q_z$  is antisymmetric with respect to the contour coordinate, it is essentially equal to zero over the majority of the contour, and its maximum magnitude occurs in the narrow boundaries of the contour at  $s = \pm b/2$ .

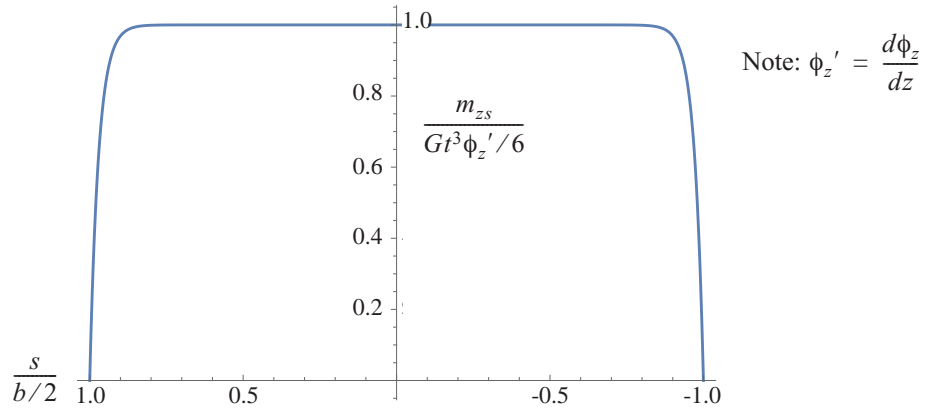


**Fig. 3.16** Distribution of the twisting moment resultant over the contour for  $b/t = 20$ .

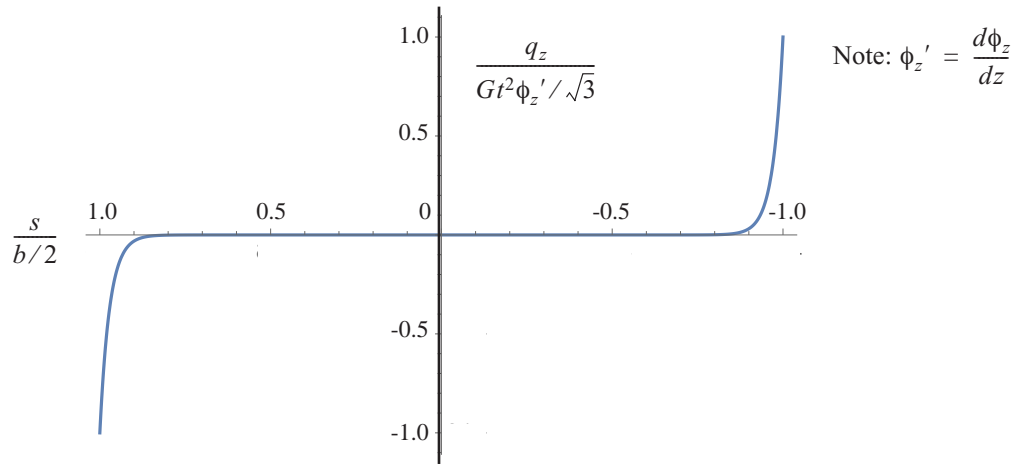


**Fig. 3.17** Distribution of the shear stress resultant over the contour for  $b/t = 20$ .

From Hooke's law and eq. (3.110), the shear stress component tangent to the contour is

$$\sigma_{zs} = G\gamma_{zs} = G\left(\frac{d\phi_z}{dz} + \frac{d\phi_x}{ds}\right)\xi.$$

Substitute the solution for  $\phi_x$  from eq. (3.117) into the previous equation to get

$$\sigma_{zs}(s, \zeta) = 2G \left( \frac{d\phi_z}{dz} \right) \left( 1 - \frac{\cosh(ks)}{\cosh \lambda} \right) \zeta. \quad (3.124)$$

Note that this shear stress vanishes on the contour where  $\zeta = 0$  and attains its maximum magnitude along the top and bottom edges where  $\zeta = \pm t/2$ . Shear stress  $\sigma_{zs}$  is the dominate shear stress in the rectangular cross section subject to uniform torsion, since through-the-thickness shear stress  $\sigma_{z\zeta} = q_z/t$  is essentially zero over most of the contour. For large values of  $b/t$ , we neglect the shear stress  $\sigma_{z\zeta}$  with respect to  $\sigma_{zs}$ , and we use the following approximation

$$\sigma_{zs} = 2G \left( \frac{d\phi_z}{dz} \right) \zeta \quad b/t \gg 1. \quad (3.125)$$

**Warping of the cross section.** Substitute eq. (3.117) for  $\phi_x(s)$  in eq. (3.109), and recall that  $\phi_y = 0$ , to find that the warping displacement  $u_z(s, \zeta)$  is given by

$$u_z(s, \zeta) = \zeta \left[ s - \frac{t}{\sqrt{3}} \frac{\sinh ks}{\cosh \lambda} \right] \left( \frac{d\phi_z}{dz} \right). \quad (3.126)$$

A contour plot of the warping displacement divided by  $u_z(b/2, t/2)$  for  $b/t = 4$  and  $\frac{d\phi_z}{dz} > 0$  is shown in figure 3.18, where

$$u_z(b/2, t/2) = 0.7113 t^2 \left( \frac{d\phi_z}{dz} \right) \quad b/t = 4.$$

Along the  $s$ -axis and the  $\zeta$ -axis the warping displacement is zero, and it attains maximum magnitude near the corners of the rectangular cross section. For a positive unit twist,  $u_z > 0$  if the product  $s\zeta > 0$ , and  $u_z < 0$  if the product  $s\zeta < 0$ .

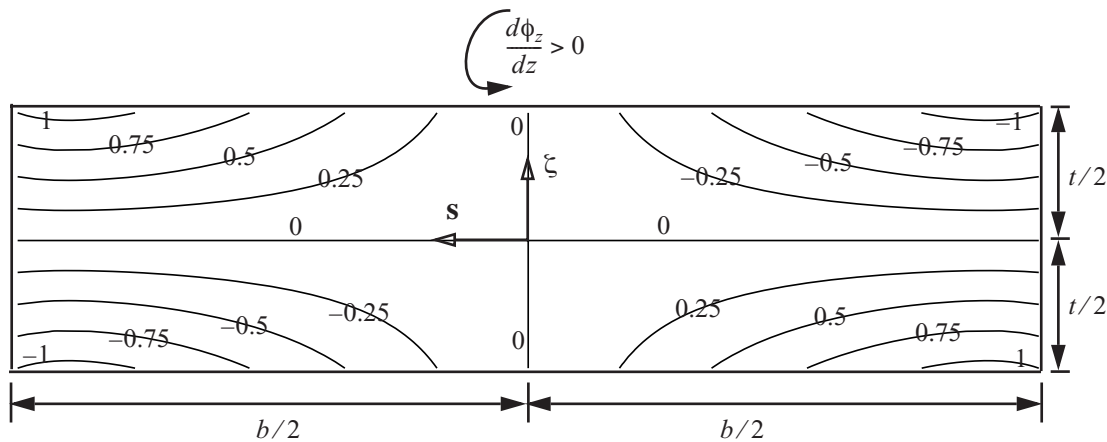


**Fig. 3.18** Contour plot of the normalized warping displacement in torsion for  $b/t = 4$ .

For a thin rectangular cross section a good approximation to the warping function is

$$u_z \approx u_{za} = s\zeta \quad b/t \gg 1. \quad (3.127)$$

To show eq. (3.127) is a good approximation, let

$$I_e = \left( \int_{-t/2-b/2}^{t/2} \int_{-b/2}^{b/2} [u_z(s, \zeta)]^2 ds d\zeta \right)^{1/2} \quad \text{and} \quad I_a = \left( \int_{-t/2-b/2}^{t/2} \int_{-b/2}^{b/2} [u_{za}(s, \zeta)]^2 ds d\zeta \right)^{1/2}.$$

Define the percentage error between the approximate warping function and the exact one by

error =  $(I_a - I_e)100/I_e$ . For  $b/t = 20$  the error is 0.482 percent, and for  $b/t = 40$  the error is 0.123 percent.

### 3.9.1 Torsion of built-up open sections

For large values of the ratio of  $b/t$ , the analysis of thin-walled rectangular section of article 3.9 results in the following formulas given by eqs (3.121), (3.123), and (3.125):

$$M_z = GJ \left( \frac{d\phi_z}{dz} \right) \quad J = \frac{bt^3}{3} \quad \sigma_{zs} = 2G \left( \frac{d\phi_z}{dz} \right) \zeta. \quad (3.128)$$

The maximum magnitude of the shear stress  $\sigma_{zs}$  occurs at  $\zeta = \pm t/2$ . Then from the previous equations for large values of the ratio of  $b/t$  this maximum shear stress can be expressed as

$$\sigma_{zs}|_{\max} = \frac{3M_z}{bt^2}. \quad (3.129)$$

Now consider torsion of open section bars of more complex shape as are shown in figure 3.19. Understand-

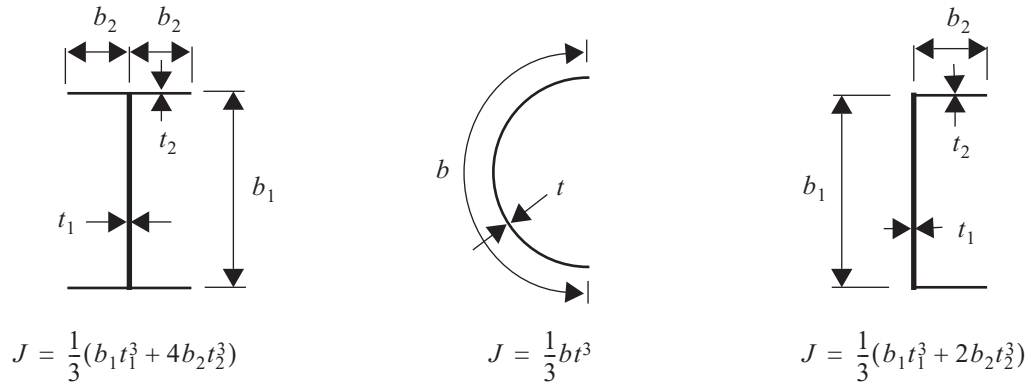


Fig. 3.19 Some thin-walled open sections and their torsion constants

ing the torsional response of these bars with complex, open cross-sectional shapes is facilitated by an analogy to the response of an initially flat membrane supported on its edges over an opening, where the edges of the opening are in the same shape as the cross section. The membrane is stretched under a uniform tension, and then subject to an internal pressure to cause the membrane to deflect. The deflected shape of this pressurized membrane is analogous to the torsion problem in that level contours on the surface of the deflected membrane coincide with the lines of action of the shear stresses, and that the slope of the membrane normal to the level contour is proportional to the magnitude to the shear stress. Also, the volume between the  $x$ - $y$  plane and the deflected surface of

the membrane is proportional to the total torque carried by the section. The following text excerpted from Oden and Ripperger (1981, p. 46) summarizes this analogy.

*This analogy was first discovered by Ludwig Prandtl in 1903 and is known as **Prandtl's membrane analogy**. Prandtl took full advantage of the analogy and devised clever experiments with membranes. By measuring the volumes under membranes formed by a soap film subject to a known pressure, he was able to evaluate torsional constants. By obtaining the contour lines of the membranes he determined stress distributions.*

Torsional constants and the maximum shearing stress can be found for complex cross sections by using the results for the thin-walled rectangular section. The membrane analogy shows that the torsional load carrying capacity of the complex open section is nearly the same as the narrow rectangular section, because the volumes under the membranes are nearly the same if we neglect the small error introduced at the corners or junctions. In this way, the membrane analogy implies that the complex open cross section has about the same torsional load carrying capacity as a thin-walled rectangular section with a length equal to the total arc length of the contour of the complex section.

Since each branch of the open section is equivalent to a narrow rectangular section with the same developed length and thickness, we can sum the torques carried by each branch in the following way

$$M_z = \sum_{\text{branches}} M_{zi} = \sum_{\text{branches}} GJ_i \left( \frac{d\phi_z}{dz} \right) = GJ \left( \frac{d\phi_z}{dz} \right), \quad (3.130)$$

where the torsion constant for the entire cross section is

$$J = \sum_{\text{branches}} J_i = \sum_{\text{branches}} \frac{1}{3} b_i t_i^3. \quad (3.131)$$

Note that the twist per unit length is the same for all branches in the open section, because the cross section is assumed to be rigid in its own plane. The use of eq. (3.131) for several open sections is shown in figure 3.19.

Starting from eq. (3.129), the maximum shear stress in the  $i^{\text{th}}$  branch of the section is given by

$$(\sigma_{zs}|_{\max})_i = \frac{3M_{zi}}{b_i t_i^2} = \frac{3GJ_i d\phi_z}{b_i t_i^2 dz} = \frac{3G}{b_i t_i^2} \left( \frac{1}{3} b_i t_i^3 \right) \left( \frac{M_z}{GJ} \right) = \frac{M_z t_i}{J}. \quad (3.132)$$

That is, the maximum shear stress in the  $i^{\text{th}}$  branch of the open section is the total torque divided by the torsion constant for the entire section times the thickness of the  $i^{\text{th}}$  branch. Note that the largest shear stress magnitude in a built-up open section occurs in the thickest branch.

### 3.10 Inclusion of stringers in the analysis of the cross section

A stringer is a longitudinal flange element connecting thin skins or webs in aerospace structures, and the cross-sectional area of the flange is denoted by  $A_f$ . Over the cross-sectional area of the flange it is assumed that

- the longitudinal normal stress  $\sigma_{zz}$  is uniformly distributed, and
- the shear stresses  $\sigma_{zs} = \sigma_{z\zeta} = 0$ .

That is, the stringer is a longitudinal bar element that does not resist shear. It is modeled as a point on the contour

with coordinates  $[x_f(s_f), y_f(s_f)]$  relative to the centroid, where the contour coordinate of the stringer is denoted by  $s_f$ . Thus, the stringer is mathematically represented as a point on the contour having the attribute of area. See figure 3.20.

The area and first area moments given by eq. (3.74) are modified to account for the cross section with stringers as

$$A = \int_c t(s) ds + \sum_{\text{stringers}} A_f \quad Q_x = \int_c y(s)t(s) ds + \sum_{\text{stringers}} y_f A_f \quad Q_y = \int_c x(s)t(s) ds + \sum_{\text{stringers}} x_f A_f. \quad (3.133)$$

Note that first area moments about the centroid are required to satisfy  $Q_x = Q_y = 0$ . The second area moments about the centroid in eq. (3.77) are modified to

$$I_{xx} = \int_c y^2 t ds + \sum_{\text{stringers}} y_f^2 A_f \quad I_{yy} = \int_c x^2 t ds + \sum_{\text{stringers}} x_f^2 A_f \quad I_{xy} = \int_c xy t ds + \sum_{\text{stringers}} x_f y_f A_f. \quad (3.134)$$

The material law for extension and bending (3.79) on page 46 remains valid with the geometric properties specified by eqs. (3.133) and (3.134). The thermal axial force  $N_T$  is given by eq. (3.75) on page 46, and the thermal bending moments  $M_{xT}$  and  $M_{yT}$  are given by eq. (3.78).

### 3.10.1 Effect of stringers on the shear flow distribution

The shear flow exiting the stringer location is denoted by  $q^{(+)}$ , the shear flow entering the stringer location by  $q^{(-)}$ , and the increase in the axial force in the stringer by  $\Delta N_f$ . See figure 3.20. Sum the forces in the  $z$ -direction of the free body diagram shown in figure 3.20 to get

$$q(s_f^{+})\Delta z - q(s_f^{-})\Delta z + \Delta N_f = 0.$$

Divide this equilibrium equation by the incremental length  $\Delta z$ , then let  $\Delta z \rightarrow 0$  to get in the limit

$$q(s_f^{+}) - q(s_f^{-}) + \frac{dN_f}{dz} = 0. \quad (3.135)$$

Combine eqs. (3.95) and (3.97) to write the shear flow as

$$q(s) = q_0 - \frac{k}{I_{yy}}(V_x + V_{xT})\bar{Q}_y(s) - \frac{k}{I_{xx}}(V_y + V_{yT})\bar{Q}_x(s) - \frac{A(s)}{A} \frac{dN_T}{dz} + \int_0^s \beta \frac{\partial \Delta T}{\partial z} t(s) ds. \quad (3.136)$$

Equation (3.89) was used to identify the derivative of the thermal force in the previous result. Then the jump in the shear flow across the stringer is

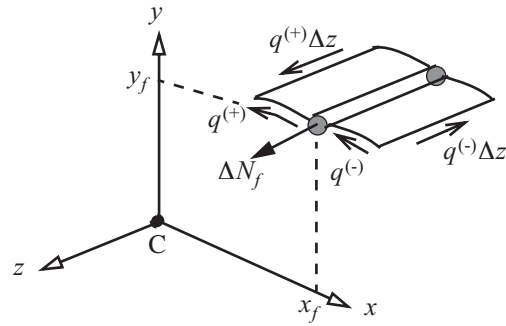


Fig. 3.20 Free body diagram of the stringer

$$q(s_f^{(+)}) - q(s_f^{(-)}) = - \left\{ \frac{k}{I_{yy}} (V_x + V_{xT}) [\bar{Q}_y(s_f^{(+)}) - \bar{Q}_y(s_f^{(-)})] \right\} - \left\{ \frac{k}{I_{xx}} (V_y + V_{yT}) [\bar{Q}_x(s_f^{(+)}) - \bar{Q}_x(s_f^{(-)})] \right\} \\ - \frac{[A(s_f^{(+)}) - A(s_f^{(-)})]}{A} \frac{dN_T}{dz} + \left( \int_{s_f^{(-)}}^{s_f^{(+)}} \beta \frac{\partial \Delta T}{\partial z} t(s) ds \right). \quad (3.137)$$

Note that

$$A(s_f^{(+)}) - A(s_f^{(-)}) = A_f \quad \text{and} \quad \int_{s_f^{(-)}}^{s_f^{(+)}} \beta \frac{\partial \Delta T}{\partial z} t(s) ds = A_f \beta \frac{\partial \Delta T}{\partial z} \Big|_{s_f}. \quad (3.138)$$

Under the assumption made to model the stringer  $N_f = \sigma_{zz} A_f$ . The axial normal stress in the stringer is given in eq. (3.83) on page 47. Thus,  $\frac{dN_f}{dz} = A_f \frac{d\sigma_{zz}}{dz}$ . Derivatives of the axial force and bending moments with respect to  $z$  appearing in  $d\sigma_{zz}/dz$  were replaced by equilibrium differential equations (3.53), (3.55), and (3.57), respectively. The result for the derivative of the normal force in the stringer is

$$\frac{dN_f}{dz} = \frac{k}{I_{yy}} (V_x + V_{xT}) A_f \bar{x}_f + \frac{k}{I_{xx}} (V_y + V_{yT}) A_f \bar{y}_f + \frac{A_f dN_T}{A dz} - A_f \beta \frac{\partial \Delta T}{\partial z} \Big|_{s_f}. \quad (3.139)$$

Substitute eqs. (3.137) and (3.139) into (3.135) to find

$$- \left\{ \frac{k}{I_{yy}} (V_x + V_{xT}) [\bar{Q}_y(s_f^{(+)}) - \bar{Q}_y(s_f^{(-)}) - A_f \bar{x}_f] \right\} - \left\{ \frac{k}{I_{xx}} (V_y + V_{yT}) [\bar{Q}_x(s_f^{(+)}) - \bar{Q}_x(s_f^{(-)}) - A_f \bar{y}_f] \right\} \\ - \frac{A_f dN_T}{A dz} + \frac{A_f dN_T}{A dz} + A_f \beta \frac{\partial \Delta T}{\partial z} \Big|_{s_f} - A_f \beta \frac{\partial \Delta T}{\partial z} \Big|_{s_f} = 0. \quad (3.140)$$

Equation (3.140) simplifies to

$$- \left\{ \frac{k}{I_{yy}} (V_x + V_{xT}) [\bar{Q}_y(s_f^{(+)}) - \bar{Q}_y(s_f^{(-)}) - A_f \bar{x}_f] \right\} - \left\{ \frac{k}{I_{xx}} (V_y + V_{yT}) [\bar{Q}_x(s_f^{(+)}) - \bar{Q}_x(s_f^{(-)}) - A_f \bar{y}_f] \right\} = 0. \quad (3.141)$$

Equation (3.141) is valid for every choice of the shear actions  $(V_x + V_{xT})$  and  $(V_y + V_{yT})$ . Then to satisfy eq. (3.141), the coefficients of the shear actions must vanish, which leads to

$$\bar{Q}_y(s_f^{(+)}) - \bar{Q}_y(s_f^{(-)}) - A_f \bar{x}_f = 0 \quad \bar{Q}_x(s_f^{(+)}) - \bar{Q}_x(s_f^{(-)}) - A_f \bar{y}_f = 0. \quad (3.142)$$

Relations (3.84) and (3.93) evaluated at  $s = s_f$  are repeated in the following relations:

$$\bar{x}_f = x_f - n_x y_f \quad \bar{y}_f = y_f - n_y x_f \quad \bar{Q}_x(s_f^-) = Q_x(s_f^-) - n_y Q_y(s_f^-) \quad \bar{Q}_y(s_f^-) = Q_y(s_f^-) - n_x Q_x(s_f^-). \quad (3.143)$$

After substituting the relations (3.143) into eq. (3.142) we get

$$Q_y(s_f^{(+)}) - Q_y(s_f^{(-)}) - A_f x_f = 0 \quad Q_x(s_f^{(+)}) - Q_x(s_f^{(-)}) - A_f y_f = 0. \quad (3.144)$$

Equation (3.144) shows that the jump in the shear flows exiting and entering the stringer (3.135) is equivalent to



a jump in value of the first area moments across the stringer area.

### 3.11 Closed cross-sectional contour

Consider a single-cell, closed cross-sectional contour as shown in figure 3.21. The shear flow acting tangent to the contour is given by eq. (3.97) on page 51, where we assume the shear flow from the prescribed change in temperature vanishes. (Refer to the discussion in the paragraph preceding eq. (3.97).) Then the shear flow is given by

$$q(s, z) = q_0(z) - \frac{k}{I_{yy}} V_x \overline{Q}_y(s) - \frac{k}{I_{xx}} V_y \overline{Q}_x(s). \quad (3.145)$$

The shear flow is statically equivalent to the shear forces and the torque acting on the cross section. The static

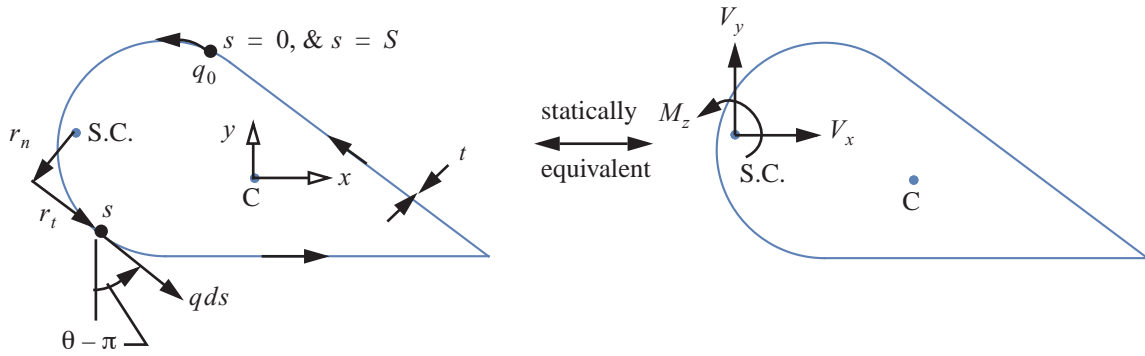


**Fig. 3.21** Static equivalence of the shear flow acting along a closed contour to shear forces and torque.

equivalence with respect to the shear center given by eq. (3.40) on page 40 reduces to

$$V_x = \oint (-q \sin \theta) ds \quad V_y = \oint (q \cos \theta) ds \quad M_z = \oint (r_n q) ds. \quad (3.146)$$

(It is assumed that the transverse shear resultant  $q_z$  and the twisting moment resultant  $m_{zs}$  are small with respect to the shear flow, and therefore are neglected in eq. (3.40).) The shear flow formula (3.145) is the sum of the open section shear flow, eq. (3.98), plus a shear flow  $q_0$  that is the spatially uniform around the contour. If (3.145) is substituted for the shear flow in the two expressions for the shear forces in (3.146), it can be shown<sup>7</sup> that we get identities  $V_x = V_x$  and  $V_y = V_y$ . That is, the shear flow (3.145) is statically equivalent to the shear forces  $V_x$  and  $V_y$ , independent of  $q_0$ . If we substitute the shear flow (3.145) into the expression for the torque in eq. (3.146), then the shear flow  $q_0$  can be determined from the torque acting at the shear center. However, the location of the shear center is not known.

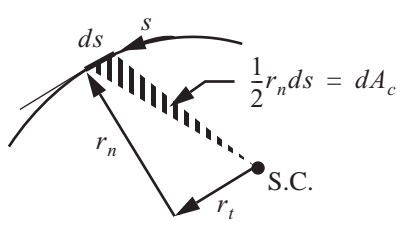
Since the location of the centroid is determined before the location of the shear center, consider the torque from the shear flow resolved at the centroid. That is  $M_{zC} = \oint r_{nC}(s) q(s) ds$ . The coordinate normal to the con-

7. Employ eq. (3.3) and integrate by parts using the results from eq. (3.105).

tor relative to the centroid  $r_{nc}(s)$  is determined by the second equation in eq. (3.11) on page 34. Substitute the shear flow (3.145) into the expression for the torque at the centroid to get

$$M_{zC} = \oint r_{nc} \left( q_0 - \frac{k}{I_{yy}} V_x \bar{Q}_y - \frac{k}{I_{xx}} V_y \bar{Q}_x \right) ds = q_0 \oint r_{nc} ds - \frac{k}{I_{yy}} V_x \oint r_{nc} \bar{Q}_y ds - \frac{k}{I_{xx}} V_y \oint r_{nc} \bar{Q}_x ds. \quad (3.147)$$

Let the area enclosed by the contour be denoted by  $A_c$ . As shown in figure 3.22, the enclosed area is given by



$$A_c = \frac{1}{2} \oint r_n ds = \frac{1}{2} \oint r_{nc} ds. \quad (3.148)$$

The two expressions given above for the enclosed area is a consequence of the relation (3.10) between the normal coordinates  $r_n$  and  $r_{nc}$  when integrated around the closed contour. Solve eq. (3.147) for  $q_0$  to find

**Fig. 3.22 Enclosed area element.**

$$q_0 = \frac{M_{zC}}{2A_c} + \frac{k}{2A_c I_{yy}} V_x \oint r_{nc} \bar{Q}_y ds + \frac{k}{2A_c I_{xx}} V_y \oint r_{nc} \bar{Q}_x ds. \quad (3.149)$$

Substitute the result for  $q_0$  from eq. (3.149) the into eq. (3.145) and denote the resulting expression for this shear flow as  $q_C$ : the shear flow with respect to the centroid. The result for  $q_C$  is written as

$$q_C(s, z) = \frac{M_{zC}(z)}{2A_c} - F_{xc}(s) V_x(z) - F_{yc}(s) V_y(z), \quad (3.150)$$

where the shear flow distribution functions relative to the centroid are defined by

$$F_{xc}(s) = \frac{k}{I_{yy}} \left[ \bar{Q}_y(s) - \frac{1}{(2A_c)} \oint r_{nc}(s) \bar{Q}_y(s) ds \right] \quad F_{yc}(s) = \frac{k}{I_{xx}} \left[ \bar{Q}_x(s) - \frac{1}{(2A_c)} \oint r_{nc}(s) \bar{Q}_x(s) ds \right]. \quad (3.151)$$

We have used all the conditions of static equivalence to determine the shear flow, with respect to the centroid. Thus, it is a statically indeterminate problem to find the expression for shear flow relative to the shear center, as well as the location of the shear center in the cross section. The additional relation we need is a constitutive relation between the twist per unit length  $d\phi_z/dz$  and the shear flow  $q$ .

### 3.11.1 Twist per unit longitudinal length

The shear strain  $\gamma_{zs}$  evaluated at the contour from eq. (3.31) on page 38 is

$$\gamma_{zs}(s, z) = \psi_x(z) \frac{dx}{ds} + \psi_y(z) \frac{dy}{ds} + r_n(s) \frac{d\phi_z}{dz} \quad \text{at} \quad \xi = 0, \quad (3.152)$$

where eq. (3.3) was used to write the trigonometric functions in terms of the derivatives of the contour coordinate functions. Integrate the shear strain (3.152) around the closed contour to get

$$\oint \gamma_{zs} ds = \underbrace{\psi_x(z) \oint \frac{dx}{ds} ds}_{=0} + \underbrace{\psi_y(z) \oint \frac{dy}{ds} ds}_{=0} + \underbrace{\oint r_n ds}_{=2A_c} \frac{d\phi_z}{dz}. \quad (3.153)$$

Continuity of the contour and the eq. (3.148) for the enclosed area results in

$$\frac{d\phi_z}{dz} = \frac{1}{2A} \oint \gamma_{zs} ds.$$

Hooke's law relates the shear strain to the shear stress by  $\gamma_{zs} = \sigma_{zs}/G$ , where  $G$  is the shear modulus of the material. In torsion of a closed cross-sectional contour the shear stress is assumed uniform through the thickness of the wall. Hence, the shear stress is determined by the shear flow divided by the thickness of the wall, or  $\sigma_{zs} = q/t$ . Substitute  $\gamma_{zs} = q/(Gt)$  into the equation for the twist per unit length to get.

$$\boxed{\frac{d\phi_z}{dz} = \frac{1}{2A} \oint \left( \frac{q}{Gt} \right) ds.} \quad (3.154)$$

### 3.11.2 Location of the shear center and the final expression for the shear flow

Substitute eq. (3.150) for the shear flow in eq. (3.154) to find

$$\frac{d\phi_z}{dz} = \frac{M_{zC}}{4A^2} \oint \frac{ds}{Gt} - \frac{V_x}{2A} \oint \frac{F_{xc}}{Gt} ds - \frac{V_y}{2A} \oint \frac{F_{yc}}{Gt} ds. \quad (3.155)$$

The torque  $M_{zC}$  and shear forces  $V_x$  and  $V_y$  are resolved at the centroid. We can find a statically equivalent torque and force system resolved at the shear center: Simply add and subtract the shear forces at the shear center which does not change static equivalence as shown in figure 3.23(a). The upward force  $V_y$  at point C and the downward

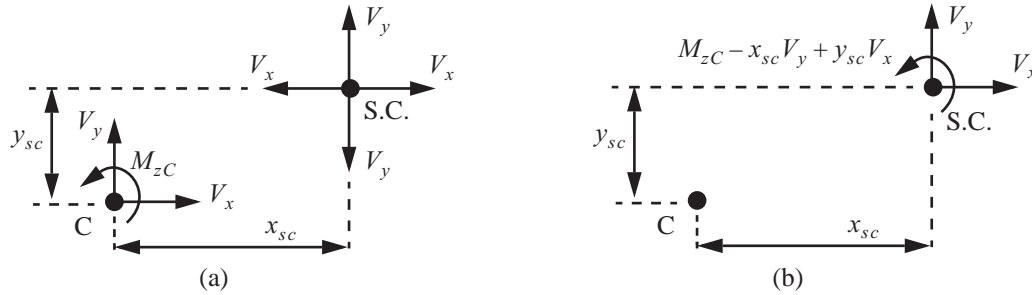


**Fig. 3.23 The method to move the shear forces from the centroid to the shear center while maintaining static equivalence.**

force  $V_y$  at S.C. form a clockwise couple  $x_{sc}V_y$  and no net vertical force. Similarly, rightward force  $V_x$  at point C and the leftward force  $V_x$  at the S.C. form a counterclockwise couple  $y_{sc}V_x$  and no net horizontal force. The total counterclockwise torque in the cross section is  $M_{zC} - x_{sc}V_y + y_{sc}V_x$ . Formulating these couples leave forces  $V_x$  and  $V_y$  at the shear center as shown in part (b) of figure 3.23 and a counterclockwise torque. Thus, the torque at the shear center must be

$$M_z = M_{zC} - x_{sc}V_y + y_{sc}V_x. \quad (3.156)$$

Solve eq. (3.156) for the torque at the centroid and substitute the result for  $M_{zC}$  into eq. (3.155) to get

$$\frac{d\phi_z}{dz} = \frac{M_z}{4A^2} \oint \frac{ds}{Gt} - \left[ \frac{y_{sc}}{4A^2} \oint \frac{ds}{Gt} + \frac{1}{2A} \oint \frac{F_{xc}}{Gt} ds \right] V_x + \left[ \frac{x_{sc}}{4A^2} \oint \frac{ds}{Gt} - \frac{1}{2A} \oint \frac{F_{yc}}{Gt} ds \right] V_y. \quad (3.157)$$

At the shear center the twist per unit length depends on the torque resolved at the shear center and not on the shear forces. In other words, the shear forces acting at the shear center do not contribute to torsion. This require-

ment means the coefficients of the shear forces in eq. (3.157) must vanish. Equating these coefficients to zero determines the coordinates of the shear center relative to the centroid as

$$x_{sc} = \left[ \frac{2A_c}{\oint \frac{ds}{Gt}} \oint \left( \frac{F_{yc}(s)}{Gt} \right) ds \right] \quad y_{sc} = - \left[ \frac{2A_c}{\oint \frac{ds}{Gt}} \oint \left( \frac{F_{xc}(s)}{Gt} \right) ds \right]. \quad (3.158)$$

Equation (3.157) reduces to the form

$$\frac{d\phi_z}{dz} = \frac{M_z}{(GJ)_{\text{eff}}}, \quad (3.159)$$

where the effective torsional stiffness is

$$(GJ)_{\text{eff}} = \frac{4A_c^2}{\oint \frac{ds}{Gt}}. \quad (3.160)$$

If the shear modulus is uniform around the contour, then

$$\frac{d\phi_z}{dz} = \frac{M_z}{GJ} \text{ and the torsion constant is } J = \frac{4A_c^2}{\oint \frac{ds}{t}}. \quad (3.161)$$

Substitute the solution for the torque at the centroid from eq. (3.156) into the expression for the shear flow in eq. (3.150). In the process, we drop the “C” subscript on  $q_C$  to indicate that we are formulating the shear flow relative to the shear center. The result is

$$q = \frac{M_z + x_{sc}V_y - y_{sc}V_x}{2A_c} - F_{xc}(s)V_x(z) - F_{yc}(s)V_y(z). \quad (3.162)$$

Equation (3.162) is written in the form

$$q(s, z) = \frac{M_z(z)}{2A_c} - F_x(s)V_x(z) - F_y(s)V_y(z), \quad (3.163)$$

where the shear flow distribution functions relative to the shear center are defined by

$$F_x(s) = \frac{y_{sc}}{2A_c} + F_{xc}(s) \quad F_y(s) = -\left(\frac{x_{sc}}{2A_c}\right) + F_{yc}(s). \quad (3.164)$$

In **pure torsion** only torque  $M_z$  acts on the section, and the shear terms in eq. (3.163) vanish. Then in pure torsion the shear flow is spatially uniform around the contour and leads to

$$q = \frac{M_z}{2A_c} \quad \text{or} \quad M_z = 2A_c q. \quad (3.165)$$

Equation (3.165) is called **Bredt’s formula**, or the Bredt-Batho formula, and it relates the torque to the uniform shear flow in a single-cell section subject to torsion only.

### Example 3.4 A single-cell cross section stiffened by axial stringers

A uniform bar of length  $L$  with a closed, cross-sectional contour is stiffened by four axial stringers. The configuration and the associated nomenclature is shown in figure 3.24(a), where the  $X$ -axis is an axis of symmetry. The areas of the stringer flanges are denoted by  $A_{f1}$  and  $A_{f2}$ , and the wall thickness  $t$  is uniform along the entire contour. As shown in figure 3.24(b), the contour is divided into four branches. Branch 1 is a semicircle segment of radius  $a$  between the lower stringer  $A_{f1}$  and the upper stringer  $A_{f1}$  of length  $a\pi$ , branch 2 is the horizontal segment between upper stringer  $A_{f1}$  and upper stringer  $A_{f2}$  of length  $b$ , branch 3 is the vertical segment between the upper stringer  $A_{f2}$  and the lower stringer  $A_{f2}$  of length  $2a$ , and branch 4 is the horizontal segment between lower stringer  $A_{f2}$  and lower stringer  $A_{f1}$  of length  $b$ . Dimensional data are

$$a = 6 \text{ in.} \quad b = 7 \text{ in.} \quad t = 0.03 \text{ in.} \quad A_{f1} = 0.30 \text{ in.}^2 \quad \text{and} \quad A_{f2} = 0.70 \text{ in.}^2$$

The numerical results presented in the solution of this example were performed in *Mathematica*.

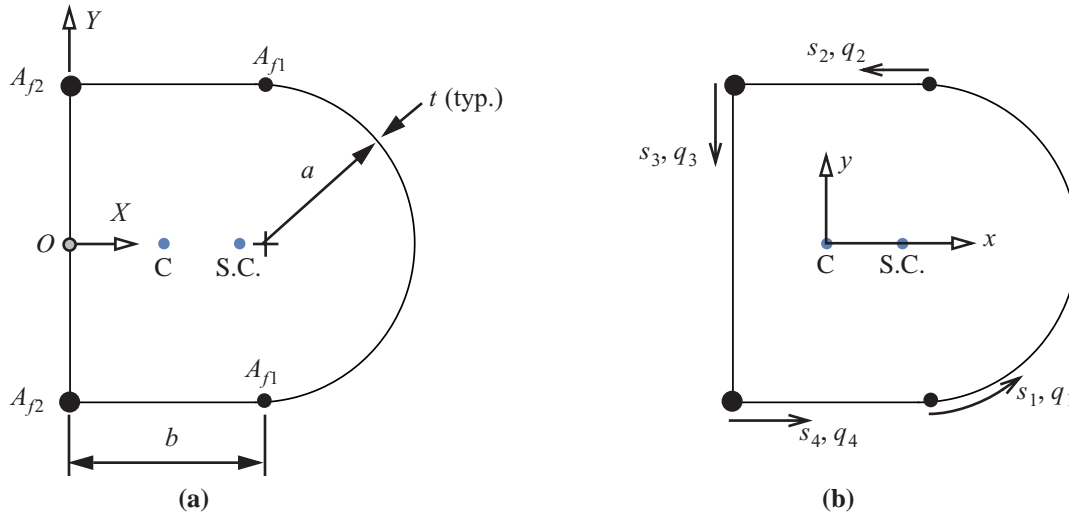


**Fig. 3.24** Single-cell cross section. (a) Geometry. (b) Branch coordinates and associated shear flows.

- Determine the location of the centroid (C) and the second area moments  $I_{xx}$  and  $I_{yy}$ .
- Determine the shear flow distribution functions  $F_{xc}(s)$  and  $F_{yc}(s)$  with respect to the centroid.
- Determine the location of the shear center (S.C.) relative to the centroid.

**Solution to part (a).** Take the origin of the  $X$ - $Y$  system at point  $O$ , the center of the vertical web. The parametric equations of the contour in each branch are listed in table 3.2,

**Table 3.2** Parametric equations of the contour in example 3.4

Branch	$X_i =$	$Y_i =$	Range
$i = 1$	$b + a \sin(s_1/a)$	$-a \cos(s_1/a)$	$0 \leq s_1 \leq a\pi$
$i = 2$	$b - s_2$	$a$	$0 \leq s_2 \leq b$

**Table 3.2 Parametric equations of the contour in example 3.4**

Branch	$X_i =$	$Y_i =$	Range
i = 3	0	$a - s_3$	$0 \leq s_3 \leq 2a$
i = 4	$s_4$	$-a$	$0 \leq s_4 \leq b$

The area  $A$  of the cross section is given by

$$A = \sum_{i=1}^4 \int_0^{(s_i)_{\max}} t ds_i + 2A_{f1} + 2A_{f2} = 3.34549 \text{ in.}^2. \quad (\text{a})$$

Since the cross section is symmetric about the  $X$ -axis, the centroid is located on this axis of symmetry. To locate the centroid we only need to compute the first area moment about the  $Y$ -axis. The first area moment  $Q_Y$  is given by

$$Q_Y = \sum_{i=1}^4 \int_0^{(s_i)_{\max}} X_i(s_i) t ds_i + X_1(0)A_{f1} + X_2(0)A_{f1} + X_3(0)A_{f2} + X_4(0)A_{f2} = 11.7884 \text{ in.}^3. \quad (\text{b})$$

The centroid coordinate is  $X_c = Q_Y/A = 3.52367 \text{ in.}$ , and by symmetry  $Y_c = 0$ . The Cartesian coordinates  $x$  and  $y$  with origin at the centroid are related to coordinates  $X$  and  $Y$  by

$$x_i(s_i) = X_i(s_i) - X_c \text{ and } y_i(s_i) = Y_i(s_i) - Y_c = Y_i(s_i), \quad i = 1, 2, 3, 4. \quad (\text{c})$$

From eq. (3.77) the second area moment about the  $x$ - and  $y$ -axes are given by

$$I_{xx} = \sum_{i=1}^4 \int_0^{(s_i)_{\max}} y_i^2(s_i) t ds_i + y_1^2(0)A_{f1} + y_2^2(0)A_{f1} + y_3^2(0)A_{f2} + y_4^2(0)A_{f2} = 101.619 \text{ in.}^4, \text{ and} \quad (\text{d})$$

$$I_{yy} = \sum_{i=1}^4 \int_0^{(s_i)_{\max}} x_i^2(s_i) t ds_i + x_1^2(0)A_{f1} + x_2^2(0)A_{f1} + x_3^2(0)A_{f2} + x_4^2(0)A_{f2} = 62.8491 \text{ in.}^4. \quad (\text{e})$$

The product area moment  $I_{xy} = 0$  since the  $x$ -axis is an axis of symmetry of the cross-sectional area.

**Solution to part (b).** The first area moments about the  $x$ -axis for segments of each branch including stringers are

$$Q_{x1}(s_1) = y_1(0)A_{f1} + \int_0^{s_1} y_1(s_1) t ds_1 = -1.8[1 + \sin(s_1/6)] \quad 0 \leq s_1 \leq 6\pi, \quad (\text{f})$$

$$Q_{x2}(s_2) = Q_{x1}(6\pi) + y_2(0)A_{f1} + \int_0^{s_2} y_2(s_2) t ds_2 = 0.18s_2 \quad 0 \leq s_2 \leq 7\text{in.}, \quad (\text{g})$$

$$Q_{x3}(s_3) = Q_{x2}(7) + y_3(0)A_{f2} + \int_0^{s_3} y_3(s_3)tds_3 = 5.46 + 0.18s_3 - 0.015s_3^2 \quad 0 \leq s_3 \leq 12 \text{ in.}, \quad (\text{h})$$

$$Q_{x4}(s_4) = Q_{x3}(12) + y_4(0)A_{f2} + \int_0^{s_4} y_4(s_4)tds_4 = 1.26 - 0.18s_4 \quad 0 \leq s_4 \leq 7 \text{ in.} \quad (\text{i})$$

As a check on the computation we evaluate  $Q_{x4}(7)$  to find  $Q_{x4}(7) = -2.2 \times 10^{-16} \sim 0$ . The value of  $Q_{x4}(7)$  equals the first area moment about the  $x$ -axis through the centroid of the entire cross section, which vanishes by the definition of the centroid. The first area moments about the  $y$ -axis for segments of each branch including stringers are

$$Q_{y1}(s_1) = x_1(0)A_{f1} + \int_0^{s_1} x_1(s_1)tds_1 = 2.1229 + 0.10429s_1 - 1.08 \cos(s_1/6) \quad 0 \leq s_1 \leq 6\pi, \quad (\text{j})$$

$$Q_{y2}(s_2) = Q_{y1}(6\pi) + x_2(0)A_{f1} + \int_0^{s_2} x_2(s_2)tds_2 = 6.21161 + 0.10429s_2 - 0.015s_2^2 \quad 0 \leq s_2 \leq 7 \text{ in.}, \quad (\text{k})$$

$$Q_{y3}(s_3) = Q_{y2}(7) + x_3(0)A_{f2} + \int_0^{s_3} x_3(s_3)tds_3 = 3.74007 - 0.10571s_3 \quad 0 \leq s_3 \leq 12 \text{ in.}, \quad (\text{l})$$

$$Q_{y4}(s_4) = Q_{y3}(12) + x_4(0)A_{f2} + \int_0^{s_4} x_4(s_4)tds_4 = 0.00497169 - 0.10571s_4 + 0.015s_4^2 \quad 0 \leq s_4 \leq 7 \text{ in.} \quad (\text{d})$$

We evaluate  $Q_{y4}(7)$  to find  $Q_{y4}(7) = -1.6 \times 10^{-15} \sim 0$ , which is as expected for a correct computation of the first area moment functions  $Q_{yi}(s_i)$ ,  $i = 1, 2, 3, 4$ . From eq. (3.11) on page 34, the results for the normal coordinate functions with respect to the centroid for each branch are

$$r_{nc1} = 6 + 3.347633 \sin(s_1/6) \quad r_{nc2} = 6 \quad r_{nc3} = 3.52367 = X_c \quad r_{nc4} = 6. \quad (\text{m})$$

The area enclosed by the contour is

$$A_c = \frac{1}{2} \sum_{i=1}^4 \int_0^{(s_i)_{\max}} r_{nci} ds_i = 140.549 \text{ in.}^2. \quad (\text{n})$$

Since the product area moment  $I_{xy} = 0$ , eq. (3.81) gives  $n_x = 0$ ,  $n_y = 0$ , and  $k = 1$ . Moreover, from eq. (3.93) we find  $\bar{Q}_x(s) = Q_x(s)$  and  $\bar{Q}_y(s) = Q_y(s)$ . Thus, the expressions for the shear flow distribution functions  $F_{xc}(s)$  and  $F_{yc}(s)$  in eq. (3.151) simplify. For each branch the shear flow distribution functions are given by

$$F_{xci}(s_i) = \left[ Q_{yi}(s_i) - \left( \frac{1}{2A_c} \right) \sum_{i=1}^4 \oint [r_{nci}(s_i)] Q_{yi}(s_i) ds_i \right] \frac{1}{I_{yy}}, \text{ and} \quad (\text{o})$$

$$F_{yci}(s_i) = \left[ Q_{xi}(s_i) - \left( \frac{1}{2A_c} \right) \sum_{i=1}^4 \oint r_{nci}(s_i) \right] Q_{xi}(s_i) ds_i \left] \frac{1}{I_{xx}} \right. \quad (\text{p})$$

Evaluation of the following terms in the previous equations are

$$\left( \frac{1}{2A_c} \right) \sum_{i=1}^4 \oint r_{nci}(s_i) Q_{yi}(s_i) ds_i = 3.10581 \text{ in.}^3 \quad \left( \frac{1}{2A_c} \right) \sum_{i=1}^4 \oint r_{nci}(s_i) Q_{xi}(s_i) ds_i = -0.330117 \text{ in.}^3. \quad (\text{q})$$

The results for shear flow distribution functions  $F_{xci}(s_i)$  are

$$F_{xc1}(s_1) = -0.0156392 + 0.00165937s_1 - 0.017184 \cos(s_1/6) \quad 0 \leq s_1 \leq 6\pi, \quad (\text{r})$$

$$F_{xc2}(s_2) = 0.494169 + 0.00165937s_2 - 0.000238667s_2^2 \quad 0 \leq s_2 \leq 7 \text{ in.}, \quad (\text{s})$$

$$F_{xc3}(s_3) = 0.0100918 - 0.00168197s_3 \quad 0 \leq s_3 \leq 12 \text{ in.}, \text{ and} \quad (\text{t})$$

$$F_{xc4}(s_4) = -0.0493378 - 0.00168197s_4 + 0.000238667s_4^2 \quad 0 \leq s_4 \leq 7 \text{ in.} \quad (\text{u})$$

The results for shear flow distribution functions  $F_{yci}(s_i)$  are

$$F_{yc1}(s_1) = -0.0144647 - 0.010628 \sin(s_1/6) \quad 0 \leq s_1 \leq 6\pi, \quad (\text{v})$$

$$F_{yc2}(s_2) = 0.00324859 + 0.00177133s_2 \quad 0 \leq s_2 \leq 7 \text{ in.}, \quad (\text{w})$$

$$F_{yc3}(s_3) = 0.0569788 + 0.00177133s_3 - 0.000147611s_3^2 \quad 0 \leq s_3 \leq 12 \text{ in.}, \text{ and} \quad (\text{x})$$

$$F_{yc4}(s_4) = 0.0156479 - 0.00177133s_4 \quad 0 \leq s_4 \leq 7 \text{ in.} \quad (\text{y})$$

The dimensional unit of each shear flow distribution function is  $\text{in.}^{-1}$

**Solution to part c.** The  $x$ -coordinate of the shear center is given by eq. (3.158). First evaluate the following integral that appears in the denominator of (3.158):

$$\oint \frac{ds}{Gt} = \frac{1}{Gt} \sum_{i=1}^4 (s_i)_{\max} = \frac{1,494.99}{G}. \quad (\text{z})$$

From (3.158) the coordinates of the shear center with respect to the centroid are

$$x_{sc} = \frac{2A_c}{\oint \frac{ds}{Gt}} \sum_{i=1}^4 \int_0^{(s_i)_{\max}} \frac{F_{yci}(s_i)}{Gt} ds_i = 2.8727 \text{ in.}, \text{ and } y_{sc} = - \left[ \frac{2A_c}{\oint \frac{ds}{Gt}} \sum_{i=1}^4 \int_0^{(s_i)_{\max}} \frac{F_{xci}(s_i)}{Gt} ds_i \right] = -1.3 \times 10^{-15} \text{ in.} \sim 0. \quad (\text{aa})$$

This result for  $y_{sc}$  is expected since the shear center lies on an axis of symmetry, and the  $x$ -axis is the axis of symmetry for the cross section. From eq. (3.164) the shear flow distribution functions with respect to the shear center are  $F_{xi}(s_i) = F_{xci}(s_i)$ .

We record below for later use the remaining shear flow distribution functions with respect to the shear center, which are determined from eq. (3.164).

$$F_{y1}(s_1) = -0.0246843 - 0.010628 \sin(s_1/6) \quad 0 \leq s_1 \leq 6\pi \quad (\text{ab})$$



$$F_{y2}(s_2) = -0.00697102 + 0.00177133s_2 \quad 0 \leq s_2 \leq 7 \text{ in.} \quad (\text{ac})$$

$$F_{y3}(s_3) = 0.0467592 + 0.00177133s_3 - 0.000147611s_3^2 \quad 0 \leq s_3 \leq 12 \text{ in.} \quad (\text{ad})$$

$$F_{y4}(s_4) = 0.00542827 - 0.00177133s_4 \quad 0 \leq s_4 \leq 7 \text{ in.} \quad (\text{ae})$$

### 3.12 References

Fung, Y. C. *Foundations of Solid Mechanics*. Englewood Cliffs, NJ: Prentice-Hall, Inc., 1965, p. 390.

Gjelsvik, Atle. *The Theory of Thin Walled Bars*. New York: John Wiley & Sons, 1981.

Goldstein, H. *Classical Mechanics*. Reading MA: Addison Wesley Publishing Inc., 1950, p.128.

Oden, J. T., and E. A. Ripperger, E. A. *Mechanics of Elastic Structures*, 2d ed. New York: Hemisphere Publishing Corporation, New York, 1981, p.46.

Thornton, Earl, A. *Thermal Structures for Aerospace Applications*. Reston VA: American Institute of Aeronautics and Astronautics, Inc., 1996, Chapters 1 and 2, and p. 51.

Vasiliev, Valery, V. *Mechanics of Composite Structures*. Edited by Robert M. Jones, DC: Taylor & Francis, 1993, p. 205.

Vasiliev, Valery V., and Evgeny V. Morozov. *Advanced Mechanics of Composite Materials and Structural Elements*, 3d ed., Waltham, MA: Elsevier, 2013, Chapter 10.



## *Some aspects of the structural analysis*

---

The thin-wall bar theory presented in chapter 3 accounts for the deformations due to extension, bending, transverse shear, and torsion/twist. The inclusion of transverse shear strains is usually referred to as a Timoshenko bar theory. A summary of some of the equations from the theory is presented in article 4.1

The von Mises criterion for yielding of a ductile metal under a combined stress state is reviewed in article 4.2. The permissible limits of the loads that prevent permanent deformation of the bar are determined by implementing the yield criterion.

In article 4.3 we present examples to determine the axial displacement, axial normal strain, and axial normal stress, which include the following topics:

- shear force and bending moment diagrams for distributed loads acting on a wing and a ship,
- the composite area technique to compute properties of plane areas,
- for a bar with a zee cross section, we determine the neutral axis of the cross section for the section subject to bending, the normal stress distribution, and the displacements due to pure bending and transverse bending.

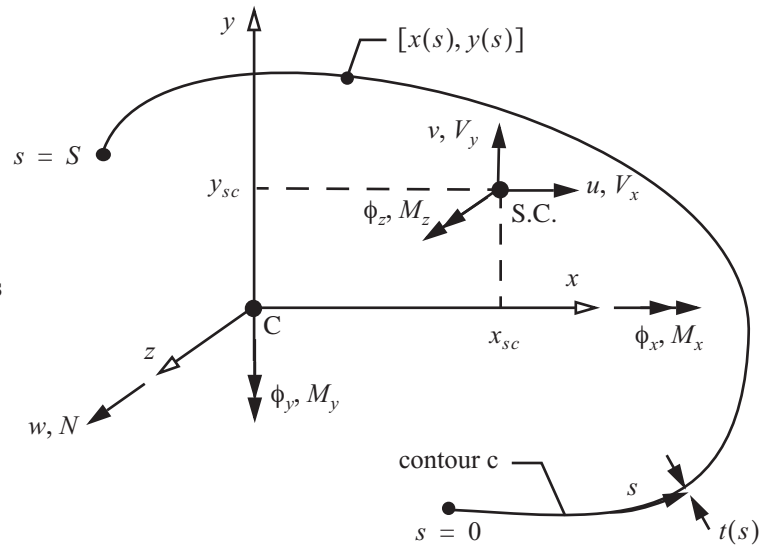
In article 4.4 the shear stresses are determined for several examples, including:

- an open cross-sectional contour and a closed cross-sectional contour subject to a transverse shear force and a torque,
- comparison of an open section and equivalent closed section subject to torsion,
- resultant of a uniform shear flow and Bredt's formula,
- torsion of cross sections composed of two and three cells, and
- transverse bending of a bar with a two-cell cross section.

## 4.1 Review of the thin-wall bar theory

A straight bar is referenced to the Cartesian coordinate system  $x$ - $y$ - $z$ , with the  $z$ -axis coinciding with the longitudinal axis of the bar. In the  $x$ - $y$  plane the cross section is described by the contour and the thickness of the wall normal to the contour. The contour is a piece-wise continuous curve in the  $x$ - $y$  plane whose subdivisions are called branches, and the tangent to the contour is continuous within a branch. The origin of the  $x$ - $y$  system in the cross section is at the centroid, which is the point labeled C in figure 4.1. In the bar theory the dependent variables acting at the centroid the cross section of the bar are  $[w(z), N(z)]$ ,  $[\phi_x(z), M_x(z)]$ , and  $[\phi_y(z), M_y(z)]$ . The axial displacement of the centroid is denoted by  $w$  and its corresponding axial force is denoted by  $N$ , the rotation of the cross section about the  $x$ -axis is denoted by  $\phi_x$  and its corresponding bending moment is denoted by  $M_x$ , and the rotation about the negative  $y$ -axis is denoted by  $\phi_y$  and its corresponding bending moment is denoted by  $M_y$ . The shear center of the cross section is labeled S.C. in figure 4.1, and the dependent variables acting at the shear center are  $[u(z), V_x(z)]$ ,  $[v(z), V_y(z)]$ , and  $[\phi_z(z), M_z(z)]$ . The  $x$ -direction displacement of the shear center is denoted by  $u$  and its corresponding force by  $V_x$ , the  $y$ -direction displacement of the shear center is denoted by  $v$  and its corresponding force by  $V_y$ , and the twist of the cross section is denoted by  $\phi_z$  and its associated torque by  $M_z$ .

**Fig. 4.1** Coordinate systems in the bar theory, and the dependent variables referenced to the centroid and the shear center of the cross section.



### 4.1.1 Extension and bending

Hooke's law for extension and bending of the bar is defined relative to the centroid. From eq. (3.80) on page 47 the compliance form of Hooke's law is

$$\begin{bmatrix} dw/dz \\ d\phi_x/dz \\ d\phi_y/dz \end{bmatrix} = \frac{1}{E} \begin{bmatrix} 1/A & 0 & 0 \\ 0 & k/I_{xx} & (-kn_x)/I_{yy} \\ 0 & (-kn_y)/I_{xx} & k/I_{yy} \end{bmatrix} \begin{bmatrix} N + N_T \\ M_x + M_{xT} \\ M_y + M_{yT} \end{bmatrix}. \quad (4.1)$$

Geometric properties of the cross section are its area  $A$ , its first area moments  $Q_x$  and  $Q_y$ , and its second area

moments  $I_{xx}$ ,  $I_{yy}$ , and  $I_{xy}$ . In eq. (4.1) the modulus of elasticity of the material is denoted by  $E$ . The locus of points on the contour is expressed parametrically by the equations  $x(s)$  and  $y(s)$ , where the arc-length of the contour is denoted by  $s$ . Let  $t(s)$  denote the thickness of the contour. See Fig. 4.1. The area and first area moments are given by

$$A = \int_c t(s) ds \quad Q_x = \int_c y(s)t(s) ds = 0 \quad Q_y = \int_c x(s)t(s) ds = 0. \quad (4.2)$$

First area moments  $Q_x$  and  $Q_y$  vanish since origin of the  $x$ - $y$ -axes is located at the centroid of the cross section. Hence, the definition of the centroid allows decoupling of the extension and bending responses of the bar. That is, the axial strain  $dw/dz$  is independent of the bending moments  $M_x$  and  $M_y$ , and bending rotation gradients  $d\phi_x/dz$ , and  $d\phi_y/dz$  are independent of axial force  $N$ . The second area moments are given by,

$$I_{xx} = \int_c y^2(s)t(s) ds \quad I_{yy} = \int_c x^2(s)t(s) ds \quad I_{xy} = \int_c x(s)y(s)t(s) ds. \quad (4.3)$$

The dimensionless parameters are defined by

$$n_x = I_{xy}/I_{xx} \quad n_y = I_{xy}/I_{yy} \quad k = \frac{1}{1 - n_x n_y}. \quad (4.4)$$

The thermal loads  $N_T$ ,  $M_{xT}$ , and  $M_{yT}$  appearing in eq. (4.1) are from the prescribed change in temperature from the reference state. Refer to eqs. (3.75), and (3.78) on page 46.

The axial normal stress  $\sigma_{zz}$  and the shear stress tangent to the contour  $\sigma_{zs}$  are shown in figure 4.2. The axial

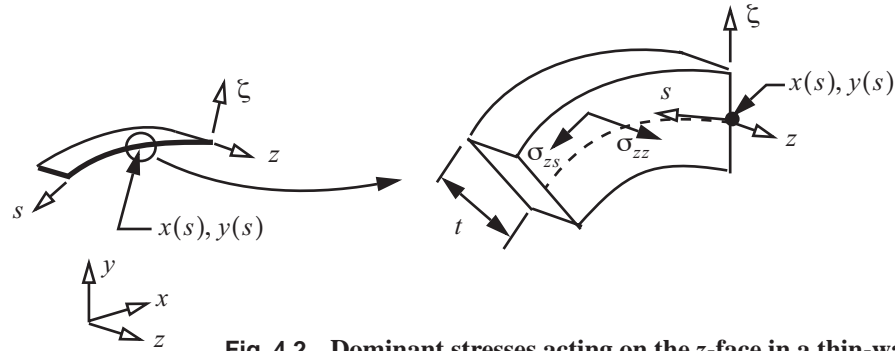


**Fig. 4.2** Dominant stresses acting on the  $z$ -face in a thin-walled bar.

normal strain  $\epsilon_{zz}$  and the axial normal stress  $\sigma_{zz}$  are given by eqs. (3.82) and (3.83) on page 47, respectively. These results are repeated below as eqs. (4.5) and (4.6), respectively.

$$\epsilon_{zz} = \frac{N + N_T}{EA} + k \frac{(M_x + M_{xT})^-}{EI_{xx}} y(s) + k \frac{(M_y + M_{yT})^-}{EI_{yy}} x(s), \text{ and} \quad (4.5)$$

$$\sigma_{zz} = \frac{N + N_T}{A} + k \frac{(M_x + M_{xT})^-}{I_{xx}} y(s) + k \frac{(M_y + M_{yT})^-}{I_{yy}} x(s) - \beta \Delta T(s, z). \quad (4.6)$$

In eq. (4.6)  $\beta = E\alpha$ , where  $\alpha$  is the linear coefficient of thermal expansion of the material. The cross-sectional

coordinates of the contour  $\bar{x}(s)$  and  $\bar{y}(s)$  appearing in eq. (4.6) are defined by

$$\bar{x}(s) = x(s) - n_x y(s) \quad \bar{y}(s) = y(s) - n_y x(s). \quad (4.7)$$

#### 4.1.2 Shear stresses in open and closed sections

The location of the shear center and the equation for the shear stress depend on whether the cross-sectional contour is open or closed.

**Open cross-sectional contour** The coordinates of the shear center with respect to the centroid for an open cross-sectional contour are given by

$$x_{sc} = -\left(\frac{k}{I_{xx}}\right) \left[ \int_c r_{nc}(s) \bar{Q}_x(s) ds \right] \quad y_{sc} = \frac{k}{I_{yy}} \left[ \int_c r_{nc}(s) \bar{Q}_y(s) ds \right]. \quad (4.8)$$

In eq. (4.8) the functions denoted by  $\bar{Q}_x(s)$  and  $\bar{Q}_y(s)$  are called distribution functions. The equations for the distribution functions are

$$\bar{Q}_x(s) = \int_0^s [\bar{y}(s) t(s)] ds \quad \bar{Q}_y(s) = \int_0^s [\bar{x}(s) t(s)] ds. \quad (4.9)$$

In eq. (4.8) the coordinate normal to the contour with respect to the centroid is denoted by  $r_{nc}(s)$ . Coordinate  $r_{nc}(s)$  is shown in figure 3.3(b) on page 33, which is given by

$$r_{nc}(s) = x(s) \frac{dy}{ds} - y(s) \frac{dx}{ds}. \quad (4.10)$$

Also shown in figure 3.3(b) is the coordinate normal to the contour with respect to the shear center which is denoted by  $r_n(s)$ . It is given by

$$r_n(s) = r_{nc}(s) - x_{sc} \frac{dy}{ds} + y_{sc} \frac{dx}{ds}. \quad (4.11)$$

The shear stress  $\sigma_{zs}$  for an open cross-sectional contour consists of the sum of two terms, and it is given by

$$\sigma_{zs} = \frac{q(s, z)}{t(s)} + 2 \frac{M_z(z)}{J} \zeta \quad -t/2 \leq \zeta \leq t/2. \quad (4.12)$$

where the shear flow is denoted by  $q(s, z)$ , the torsion constant by  $J$ , and the thickness coordinate by  $\zeta$ . The shear flow for an open section is related to the distribution functions and the shear forces by

$$q(s, z) = -\frac{k}{I_{yy}} \bar{Q}(s) V_x(z) - \frac{k}{I_{xx}} \bar{Q}_x(s) V_y(z). \quad (4.13)$$

The first term on the right-hand side of eq. (4.12) is the shear stress component that varies with the contour coordinate  $s$ , but it is independent of the thickness coordinate  $\zeta$ . The second term on the right-hand side of eq. (4.12) is a linear function of the thickness coordinate  $\zeta$ , but it is independent of the contour coordinate  $s$  in a branch of the cross section where the torsion constant is spatially uniform. The torsion constant is derived in article 3.9 on page 57 and in article 3.9.1. For thin-wall bars it is given by

$$J = \sum_{branches} \frac{1}{3} b_i t_i^3, \quad (4.14)$$

where  $b_i$  is the arc-length of the  $i$ -th branch and  $t_i$  is the thickness of the  $i$ -th branch.

**Closed cross-sectional contour.** We begin with the shear flow given by eq. (3.145) on page 67, which is repeated below as eq. (4.15).

$$q(s, z) = q_0(z) - \frac{k}{I_{yy}} V_x \bar{Q}_y(s) - \frac{k}{I_{xx}} V_y \bar{Q}_x(s). \quad (4.15)$$

The shear flow  $q_0(z)$  is spatially uniform around the contour, and it is determined from

$$M_{zc} = \oint r_{nc}(s) q(s) ds, \quad (4.16)$$

where the torque with respect to the centroid is denoted by  $M_{zc}$ . Substitute eq. (4.15) for the shear flow into eq. (4.16) and solve for  $q_0(z)$ . The shear flow with respect to the centroid is expressed as

$$q_C(s, z) = \frac{M_{zc}(z)}{2A_c} - F_{xc}(s) V_x(z) - F_{yc}(s) V_y(z), \quad (4.17)$$

where  $A_c$  is the area enclosed by the contour, and functions  $F_{xc}(s)$  and  $F_{yc}(s)$  account for the distribution of the shear flow due to the transverse shear forces. It is tacitly implied that the torque  $M_{zc}$  and shear forces  $V_x$  and  $V_y$  are resolved at the centroid in the derivation of the shear flow given by eq. (4.17). Then the area enclosed by the contour is given by

$$A_c = \frac{1}{2} \oint r_{nc}(s) ds. \quad (4.18)$$

The shear flow distribution functions relative to the centroid appearing in eq. (4.17) are defined by

$$F_{xc}(s) = \frac{k}{I_{yy}} \left[ \bar{Q}_y(s) - \frac{1}{(2A_c)} \oint r_{nc}(s) \bar{Q}_y(s) ds \right] \quad F_{yc}(s) = \frac{k}{I_{xx}} \left[ \bar{Q}_x(s) - \frac{1}{(2A_c)} \oint r_{nc}(s) \bar{Q}_x(s) ds \right]. \quad (4.19)$$

The twist per unit longitudinal length due to torsion for a closed cell is derived in article 3.11.1 on page 68. It is an important equation and is given by

$$\frac{d\phi_z}{dz} = \frac{1}{2A_c} \oint \left( \frac{q}{Gt} \right) ds, \quad (4.20)$$

where the shear modulus of the material is denoted by  $G$ . From figure 3.23 on page 69, the torque at the shear center is related to the torque at the centroid and the shear forces acting at the shear center by

$$M_z = M_{zc} - x_{sc} V_y + y_{sc} V_x. \quad (4.21)$$

Substitute the shear flow from eq. (4.17), and substitute the torque at the centroid from eq. (4.21), into eq. (4.20) to find

$$\frac{d\phi_z}{dz} = \frac{M_z}{4A_c^2} \oint \frac{ds}{Gt} - \left[ \frac{y_{sc}}{4A_c^2} \oint \frac{ds}{Gt} + \frac{1}{2A_c} \oint \frac{F_{xc}}{Gt} ds \right] V_x + \left[ \frac{x_{sc}}{4A_c^2} \oint \frac{ds}{Gt} - \frac{1}{2A_c} \oint \frac{F_{yc}}{Gt} ds \right] V_y. \quad (4.22)$$

At the shear center the twist per unit length depends on the torque resolved at the shear center and not on the

shear forces. In other words, the shear forces acting at the shear center do not contribute to torsion. This requirement means the coefficients of the shear forces in eq. (4.22) must vanish. Hence, the location of the shear center with respect to the centroid is

$$x_{sc} = \left[ \frac{2A_c}{\oint \frac{ds}{Gt}} \oint \left( \frac{F_{yc}(s)}{Gt} \right) ds \right] \quad y_{sc} = - \left[ \frac{2A_c}{\oint \frac{ds}{Gt}} \oint \left( \frac{F_{xc}(s)}{Gt} \right) ds \right]. \quad (4.23)$$

It follows from eq. (4.22) that the twist per unit length is related to the torque by

$$\frac{d\phi_z}{dz} = \frac{M_z}{(GJ)_{\text{eff}}},$$

where the effective torsional stiffness is given by

$$(GJ)_{\text{eff}} = \frac{4A_c^2}{\oint \frac{ds}{Gt}}. \quad (4.24)$$

The shear flow defined with respect to the shear center is obtained as follows: Substitute eq. (4.21) for the torque acting at the centroid into the shear flow eq. (4.17) to get the result

$$q(s, z) = \frac{M_z(z)}{2A_c} - F_x(s)V_x(z) - F_y(s)V_y(z), \quad (4.25)$$

where the shear flow distribution functions relative to the shear center are defined by

$$F_x(s) = \frac{y_{sc}}{2A_c} + F_{xc}(s) \quad F_y(s) = - \left( \frac{x_{sc}}{2A_c} \right) + F_{yc}(s). \quad (4.26)$$

The shear stress for a closed cross-sectional contour is given by  $\sigma_{zs} = q(s, z)/t(s)$ . Note that the shear stress is uniform through the thickness of the wall but is a function of the contour coordinate.

### 4.1.3 Hooke's law for transverse shear and torsion

Hooke's law for transverse shear and torsion is defined relative to the shear center. From eq. (5.76) on page 144 the compliance form of Hooke's law is

$$\begin{bmatrix} \psi_x \\ \psi_y \\ \frac{d\phi_z}{dz} \end{bmatrix} = \begin{bmatrix} c_{xx} & c_{xy} & 0 \\ c_{yx} & c_{yy} & 0 \\ 0 & 0 & 1/(GJ) \end{bmatrix} \begin{bmatrix} V_x \\ V_y \\ M_z \end{bmatrix}, \quad (4.27)$$

where  $\psi_x(z)$  and  $\psi_y(z)$  denote the averaged shear strains. These shear strains are depicted in figure 3.6 on page 38 and are given by

$$\psi_x(z) = \frac{du}{dz} + \phi_y(z) \quad \psi_y(z) = \frac{dv}{dz} + \phi_x(z). \quad (4.28)$$

In eq. (4.27) the compliance coefficients are denoted by  $(c_{xx}, c_{yy}, c_{xy})$ . From eq. (5.62) on page 142 the compliance coefficients for an open cross section are



$$c_{xx} = \left(\frac{k}{I_{yy}}\right)^2 \int_c \frac{[\bar{Q}_y(s)]^2}{Gt} ds \quad c_{xy} = c_{yx} = \frac{k^2}{I_{xx}I_{yy}} \int_c \frac{[\bar{Q}_x(s)\bar{Q}_y(s)]}{Gt} ds \quad c_{yy} = \left(\frac{k}{I_{xx}}\right)^2 \int_c \frac{[\bar{Q}_x(s)]^2}{Gt} ds. \quad (4.29)$$

For a closed cross-sectional contour the compliance coefficients are given by eq. (5.66) on page 143, which are

$$c_{xx} = \oint \frac{F_x^2(s)}{Gt} ds \quad c_{yy} = \oint \frac{F_y^2(s)}{Gt} ds \quad c_{xy} = c_{yx} = \oint \frac{F_x(s)F_y(s)}{Gt} ds. \quad (4.30)$$

The shear flow functions defined relative to the shear center result in a decoupling of the transverse shear and torsional responses of the bar as shown in eq. (4.27). That is, the shear strains are independent of the torque, and the twist per unit length is independent of the shear forces. For an open section the torsion constant is given by eq. (4.14) and for a single-cell, closed section  $GJ$  is given by eq. (4.24).

## 4.2 Yield criteria

From “Airplane design requirements” on page 14: All parts of the airplane are designed so they are not stressed beyond the yield point at the limit load factor. That is, there shall be no permanent deformation of the structure on removal of the loads. We first consider yielding of the material in uniaxial tension, and then discuss yield criteria for combined stress states.

The yield point, or yield strength, of a material is determined from material characterization tests performed on standard specimens under simple loading situations as specified by the American Society of Testing Methods (ASTM). The standard governing the tensile test of ductile metals is ASTM E8--Standard Test Methods for Tension Testing of Metallic Materials. A plot of the normal stress with respect to the normal strain from typical tensile test of an aluminum alloy is depicted in figure 4.3. There is an initial linear elastic region whose slope is the modulus of elasticity  $E$ . Following the linear portion, the slope of the stress-strain curve continuously decreases until a relative maximum engineering stress occurs deep into the response regime where plastic deformation is dominant. For such material behavior we define an *offset yield stress*. A straight line is drawn parallel to the linear elastic portion of the stress-strain curve starting from a strain  $\epsilon_{zz} = \epsilon_{0.2} = 0.002$  on the strain axis. The stress at the intersection of this straight line with the stress-strain curve is defined to be the yield strength  $\sigma_{\text{yield}}$  of the material. Note that the strain of 0.002, or 0.2 percent (percent strain is defined as  $100\epsilon_{zz}$ ), is plastic strain, since unloading the specimen from the point  $(\epsilon_{\text{yield}}, \sigma_{\text{yield}})$  on the stress strain-curve would follow the straight dashed line in figure 4.3 and the strain of 0.002 would not be recovered. However, a permanent strain of 0.2 percent is not considered detrimental for most structural components, and the 0.2 percent offset yield strength has the advantage of being a precisely defined quantity. The offset yield stress is generally the most satisfactory means of defining the yielding event for engineering materials. Metals usually break in tension by the shear stresses acting on planes at  $45^\circ$  with respect to the tension axis.

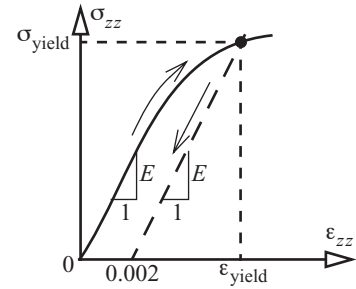


**Fig. 4.3 0.2 percent offset yield strength**

Aircraft structural components modeled as thin-walled bars are not only subject to tension, but also compression, bending, and torsion, or a combination of these. Consequently, the material is subject to a combined state of stress. For straight bars with thin-walled cross sections, the dominant stress components are shown in figure 4.2. These stress components acting on the cross section are directly related to the axial normal force, bending moments, transverse shear forces, and the torque as detailed in article 4.1.

The maximum shear stress criterion and the von Mises criterion were developed to predict yielding for combined stress states in ductile metals (Dowling, 1993). We use von Mises criterion since it compares favorably to test results (Dowling, p. 252) and it is easy to program. The von Mises criterion is based on the shear stress acting on octahedral planes, and it is alternatively called the octahedral shear stress yield criterion. The formula for the von Mises effective stress in thin-walled bar theory is

$$\sigma_{\text{Mises}} = \sqrt{\sigma_z^2 + 3\sigma_{zs}^2}. \quad (4.31)$$

If  $\sigma_{\text{Mises}} < \sigma_{\text{yield}}$ , then there is no yielding of a ductile metal under a combined stress state, where  $\sigma_{\text{yield}}$  is determined in the uniaxial tension test. At the initiation of yielding  $\sigma_{\text{Mises}} = \sigma_{\text{yield}}$ .

Criteria for failure initiation in modes other than yielding are also formulated in terms of stresses. Examples of stressed-based criteria for failure initiation in fiber-reinforced polymer composites are presented in chapter 9, and the criteria for the initiation crack propagation are presented in chapter 13.

### 4.3 Structural analyses for extension and flexure

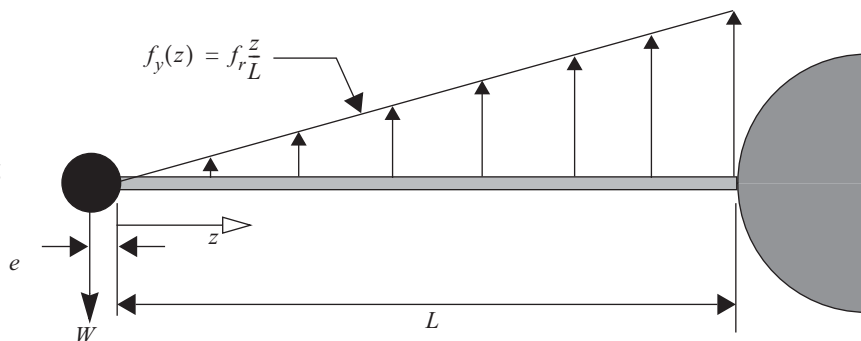
#### 4.3.1 Bending moment diagrams

To determine the axial normal stress distribution in bars subject to lateral loading, we have to first find the distribution of the bending moment. Analyses are presented for a cantilever wing and barge in still water. Airplanes and ships can be regarded as vehicles moving in different mediums, the air or water. In this regard, the study of buoyancy distribution acting on ship structures is instructive in determining the distribution of the bending moment in the hull.

##### Example 4.1 Cantilever wing with tip tank

Consider the cantilever wing with tip tank as shown in figure 4.4. Given the weight of the tip tank and its contents  $W$ , the distance  $e$  of the weight  $W$  from the wing tip, the wing span  $L$ , and the value of the distributed load intensity  $f_r$  at the wing root, determine the shear force and bending moment along the span.

**Fig. 4.4** Cantilever wing with tip tank.



**Solution.** The differential equilibrium for the shear force is given by eq. (3.54) on page 43. Integration of this differential equation from  $z = 0$  to  $z$  results in

$$V_y(z) = V_y(0) - \int_0^z f_r(u/L) du, \text{ which evaluates as } V_y(z) = V_y(0) - f_r \left( \frac{z^2}{2L} \right). \quad (\text{a})$$

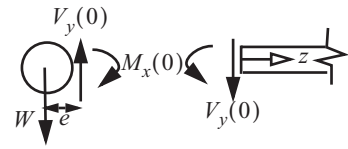
The differential equation for the bending moment is given by eq. (3.55), where in this example the distributed moment per unit length  $m_x = 0$ . Integrating this differential equation from  $z = 0$  to  $z$  results in

$$M_x(z) = M_x(0) + \int_0^z V_y(u) du, \text{ which evaluates as } M_x(z) = M_x(0) + V_y(0)z - f_r \left( \frac{z^3}{6L} \right). \quad (\text{b})$$

At the wing tip, equilibrium of the tip tank as shown in figure 4.5 leads to

$$V_y(0) = W \quad M_x(0) = eW. \quad (\text{c})$$

**Fig. 4.5** Free body diagram of tip tank.



Hence, the shear force and bending moment are

$$V_y(z) = W - f_r \left( \frac{z^2}{2L} \right) \quad M_x(z) = eW + Wz + f_r \left( \frac{z^3}{6L} \right) \quad 0 \leq z \leq L. \quad (\text{d})$$

Take  $L = 144$  in.,  $e = 6$  in.,  $W = 500$  lb., and  $f_r = 70$  lb./in. Numerical evaluation gives

$$V_y(z) = 500 - (35z^2)/144 \quad M_x(z) = 3,000 + 500z - (35z^3)/432. \quad (\text{e})$$

The shear force and bending moment distributions with respect to the normalized coordinate  $z/L$  are plotted in figure 4.6

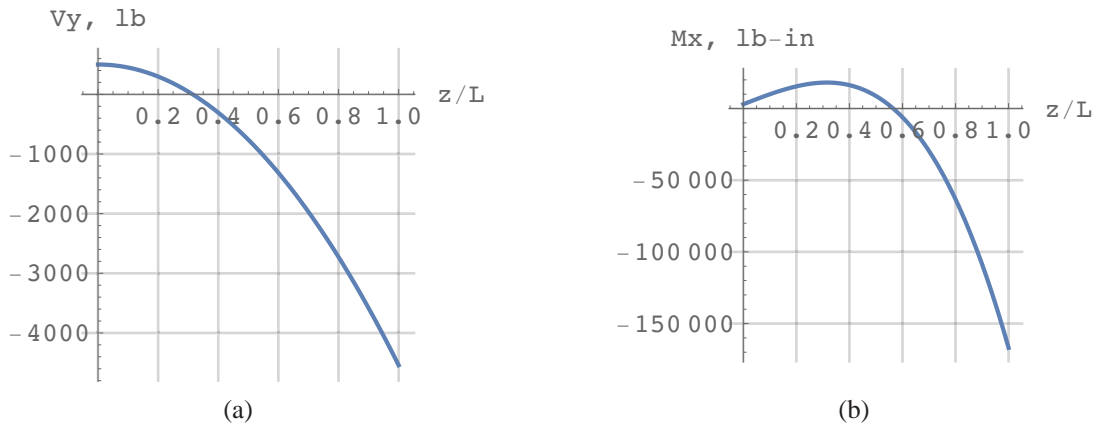


**Fig. 4.6** (a) Shear force diagram, and (b) Bending moment diagram for example 4.1.

The shear force equals zero at  $z/L = 0.315$ , which corresponds to  $z = 45.3557$  in. At  $z = 45.3557$  in. the bending moment exhibits a horizontal slope. Thus, the bending moment is a relative maximum at  $z = 45.3557$  in. with a value of 18,118.6 lb.-in. The largest magnitudes of the shear force and bending moment occur at the wing root where,  $V_y(L) = -4,540$  lb. and  $M_x(L) = -166,920$  lb.-in. ■

### Example 4.2 Uniform barge with symmetric load

Consider a barge at rest in still water with a uniform immersed cross section, and subjected to the symmetrical loads shown in figure 4.7. There is a distributed load acting on the barge due to buoyancy forces produced by

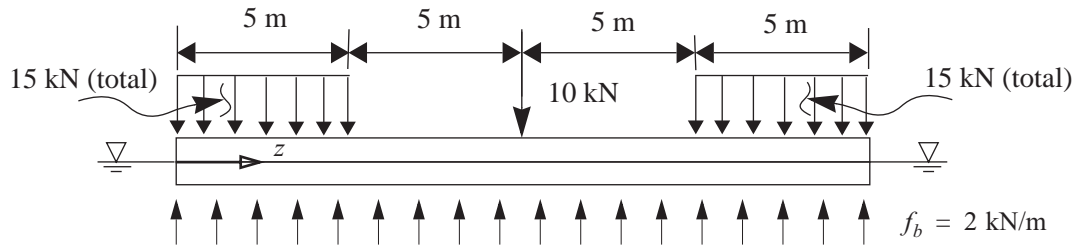


Fig. 4.7 Uniform section barge in still water with symmetric load.

displacing the water. Let  $f_b$  represent the distributed load intensity due to buoyancy, and  $f_b$  is a constant along the barge because the immersed cross section is uniform and the water is still. This is an example of a structure with no boundary supports, and is typical of aerospace and ocean vehicle structures.

- Plot the shear force and bending moment diagrams for the barge,
- Determine the maximum axial normal stress.

**Solution to part (a).** Vertical equilibrium of the entire barge requires that the buoyant upthrust equals 40 kN, so that  $f_b = 2 \text{ kN/m}$ . The total distributed load intensity is the difference between  $f_b$  and the magnitude of the downward acting applied loading intensity. The point force of 10 kN acting at  $z = 10 \text{ m}$  is shown schematically in the  $f_y(z)$ -diagram as a downward pointing arrow. Actually,  $f_y \rightarrow -\infty$  as  $z \rightarrow 10 \text{ m}$ , because a point force is a finite load acting over zero length. Point forces are idealizations to actual loads and introduce discontinuities in the mathematical descriptions of some of the dependent variables.

A semigraphical method is used to sketch the shear force and bending moment diagrams. In this approach we first sketch the distributive load  $f_y(z)$  (F/L), then the shear force  $V_y(z)$ , and finally the bending moment  $M_x(z)$ . The differential equilibrium equations governing the shear force and the bending moment are eqs. (3.54) and (3.55) on page 43. These equations are repeated in eq. (a) below.

$$\frac{dV_y}{dz} + f_y(z) = 0 \quad \frac{dM_x}{dz} - V_y + m_x(z) = 0. \quad (\text{a})$$

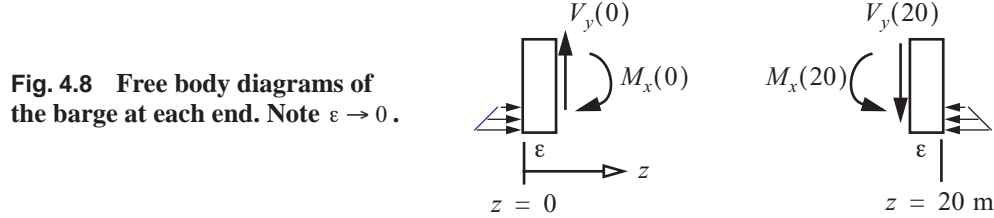
The prescribed external moment intensity  $m_x = 0$  (F-L/L) in this example. From eq. (a) we note that the slope of shear diagram at  $z$  is the negative of the distributed load intensity at  $z$ , and that the slope of the moment diagram at  $z$  is the shear force at  $z$ . Integrate eq (a) with respect to  $z$  from  $z = z_1$  to  $z = z_2$  to get

$$V_y(z_2) - V_y(z_1) = -\int_{z_1}^{z_2} f_y(z) dz, \text{ and } M_x(z_2) - M_x(z_1) = \int_{z_1}^{z_2} V_y(z) dz. \quad (\text{b})$$

Equation (b) is interpreted in a graphical sense to mean that the difference in the shear force between  $z_2$  and  $z_1$  is the negative of the area under the distributed loading diagram from  $z_1$  to  $z_2$ , and the difference in the bending

moment between  $z_2$  and  $z_1$  is the area under the shear force diagram from  $z_1$  to  $z_2$ . These are not geometrical areas. The area between the  $f_y(z)$  curve and the  $z$ -axis has units of force, and may be positive, zero, or negative.

Free body diagrams of the barge at each end are shown in figure 4.8. The water pressure varies linearly with

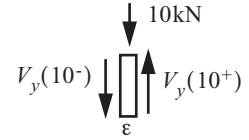


the depth of the immersed cross section and acts in  $z$ -direction. We assume the moment about the  $x$ -axis caused by the water pressure is small and can be neglected. As the infinitesimal distance  $\varepsilon \rightarrow 0$ , the distributed loading acting at each end vanishes. In the limit we get the equilibrium conditions

$$V_y(0) = 0 \quad M_x(0) = 0, \text{ and } V_y(20) = 0 \quad M_x(20) = 0. \quad (\text{c})$$

From eq. (c) the shear force diagram begins at zero, and the slope  $dV_y/dz$  at  $z=0$  is equal to 1 kN/m. The slope is constant between  $0 < z < 5$  m, thus  $V_y(z)$  is a straight line in this range of  $z$ . The difference in the shear force between  $z=5$  m and  $z=0$  is equal to the negative of the area under the  $f_y(z)$  curve, which is 5 kN. Thus

**Fig. 4.9 Jump in the shear force.**

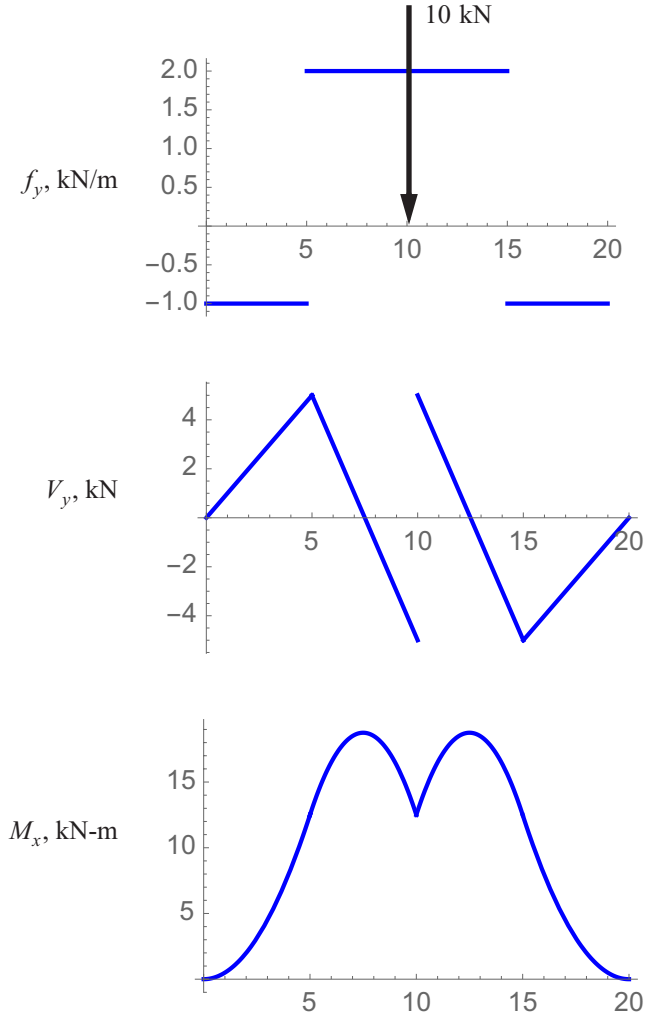


$V_y(5) = 5$  kN since  $V_y(0) = 0$ . At  $z = 5^+$  m the loading intensity jumps to +2 kN/m. The slope of the shear force jumps from 1 kN/m to -2 kN/m at  $z = 5$  m, but the shear force is itself continuous. The difference  $V_y(10) - V_y(5)$  is equal to the negative of the area between the  $f_y(z)$ -curve and the  $z$ -axis between  $z = 5$  m and  $z = 10$  m. Thus  $V_y(10) - V_y(5) = -10$  kN, so  $V_y(10) = -5$  kN. Note the shear force is zero at  $z = 7.5$  m. At  $z = 10$  m the point force of 10 kN acts. As shown in figure 4.9, vertical equilibrium at  $z = 10$  m yields a jump in the shear force  $V_y(10^+) - V_y(10^-) = 10$  kN, so that  $V_y(10^+) = 5$  kN. The slope of the shear at  $z = 10$  m is +2 kN/m, and remains constant until  $z = 15$  m. The difference  $V_y(15) - V_y(10^+) = -10$  kN, so that  $V_y(15) = -5$  kN. Finally, the slope changes to +1 kN/m at  $z = 15^+$  m and remains constant in the range  $15 < z < 20$ . The difference  $V_y(20) - V_y(15) = 5$  kN, so that  $V_y(20) = 0$ . The shear force equal to zero at  $z = 20$  m is expected from the result in eq. (c). The shear force diagram is drawn below the loading intensity diagram in figure 4.10.

From eq. (c) the bending moment at  $z = 0$  equals zero, and its slope  $z = 0$  is equal to zero since the shear force is zero at  $z = 0$ . The slope  $dM_x/dz$  of the moment diagram increases linearly from zero at  $z = 0$  to the 5 kN, which is the value of the shear force at  $z = 5$  m. The difference  $M_x(5) - M_x(0)$  is equal to the area under shear diagram from  $z = 0$  to  $z = 5$  m. Hence,  $M_x(5) - M_x(0) = 12.5$  kNm, and  $M_x(5) = 12.5$  kNm since  $M_x(0) = 0$ . From  $z = 5$  to  $z = 7.5$  the slope of the moment decreases from 5 kN to zero. At  $z = 7.5$ ,  $M_x$  is a local maximum with a magnitude of 18.75 kNm. The slope of  $M_x(z)$  for  $7.5 < z < 10$  is negative, decreasing linearly from zero to -5 kN. The difference  $M_x(10) - M_x(7.5) = -6.25$  kNm, so that  $M_x(10) = 12.5$  kNm. The slope of  $M_x(z)$  at  $z = 10$  m jumps from a -5 kN to +5 kN as shown in figure 4.10, but the moment itself is continuous. That is, the bending moment exhibits a cusp at  $z = 10$  m. The bending moment diagram in the range  $10 < z < 20$  is completed in a manner similar to the description of its construction in the range  $0 < z < 10$ . In this example the shear force diagram is anti-

symmetric about  $z = 10$  m and the bending moment is symmetric about  $z = 10$  m. This follows from the symmetrical loading on the barge.

**Fig. 4.10** The distributed loading, shear force, and bending moment diagrams for the barge in still water.



**Solution part (b).** Let us assume an open cross section of the barge is as shown in figure 4.11. The thickness of the three branches is 5 mm, and the section is symmetric about the  $y$ -axis so the product area moment  $I_{xy} = 0$ .

From (4.4) the cross-sectional coefficients  $n_x = n_y = 0$ ,  $k = 1$ , and  $\bar{y} = y$ . At  $z = 7.5$  m the shear force is equal to zero and the bending moment has a maximum value of 18.75 kNm. Hence, the shear stress  $\sigma_{zs} = 0$  and the axial normal stress (4.6) is given by

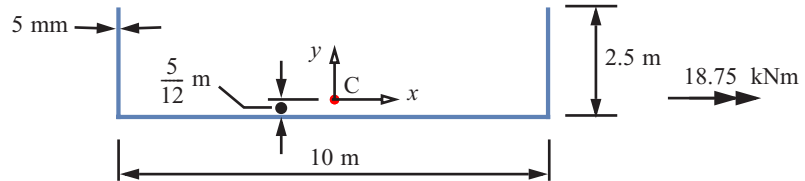
$$\sigma_{zz} = \frac{M_x}{I_{xx}} y \quad -\frac{5}{12} \text{ m} \leq y \leq \frac{25}{12} \text{ m}, \quad (\text{d})$$

where the second area moment about the  $x$ -axis  $I_{xx} = (5/128) \text{ m}^4$ . The maximum magnitude of the normal

stress occurs at  $y = (25/12)\text{m}$ , and it is a tensile stress with the value of

$$\sigma_{zz}|_{\max} = \frac{18.75 \text{ kNm}(25/12 \text{ m})}{(5/128)\text{m}^4} = 1,000 \times 10^3 (\text{N/m}^2) = 1.0 \text{ MPa}. \quad \blacksquare \quad (\text{e})$$

**Fig. 4.11** Cross section of the barge in example 4.2.



### 4.3.2 Buoyancy force distribution on ships

The simple uniform buoyancy distribution acting on the barge in example 4.2 is an exception to the buoyancy distributions found in practice. It is true that equilibrium requires the total buoyant upthrust to equal the weight of the ship and its contents. However, the distribution of the buoyancy and weight along the length of the ship is not necessarily the same. The difference in the magnitudes of the buoyancy and weight distribution intensities is the applied load intensity  $f_y(z)$ . In ship design three conditions are recognized to compute  $f_y(z)$  for the same ship. These conditions are called

- the still water condition,
- the sagging condition, and
- the hogging condition.

A more detailed account of these conditions on the longitudinal bending of the ship is given by Muckle (1967) and Zubaly (1996), and here we only summarize the basic ideas.

A ship in still water is shown in figure 4.12, and a section A-A between  $z$  and  $z + dz$  is also shown.

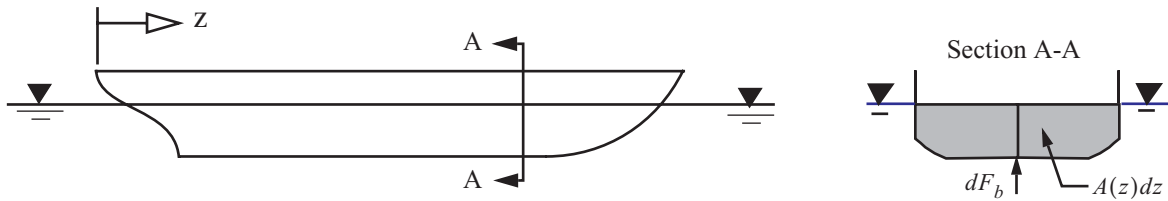


**Fig. 4.12** A ship in still water.

Archimedes's principle asserts that the buoyant upthrust is equal to the weight of the fluid displaced. Let  $A(z)$  denote the submerged cross section at  $z$ , and let  $\gamma$  denote the specific weight (force per volume) of the fluid. The differential buoyancy force  $dF_b$  acting on the ship over a differential length  $dz$  is

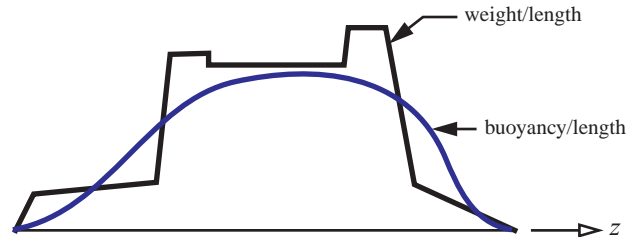
$$dF_b = \gamma A(z) dz. \quad (4.32)$$

Consequently, the buoyant upthrust per unit ship length, which we designate  $f_b$ , is equal to  $\gamma A(z)$ ; i.e.,

$$f_b = \frac{dF_b}{dz} = \gamma A(z). \quad (4.33)$$

A curve of  $f_b$  for a ship as well as the weight per unit length is shown in figure 4.13. Overall equilibrium

**Fig. 4.13 Conceptual longitudinal weight and buoyancy distributions acting on a ship.**



requires the area under these curves to have the same magnitude. If the submerged cross section is uniform in  $z$ , as is the case for the barge in example 4.2, the distribution of the buoyancy per unit length  $f_b$  is a constant.

At sea a ship is subject to waves, and this alters the buoyancy distribution. For longitudinal bending of the ship two extreme static conditions are assumed: sagging and hogging. In each condition, the length of the wave is assumed to be the length of the ship. This is an “accepted” assumption for the worst buoyancy distribution causing the most severe bending of the ship.

The sagging condition is shown in figure 4.14(a). The wave crests are at the bow and stern, and the wave trough is amidships. A schematic of the buoyancy per unit length is shown below the ship in figure 4.14(a). The immersed cross section is the largest at or near the wave crests, and is least near the trough. The intensity of the buoyancy distribution reflects this. In this condition the deck sags and is in compression while the bottom is in tension. The worst location to concentrate the cargo in the ship is amidships, as this will result in the largest bending moment.

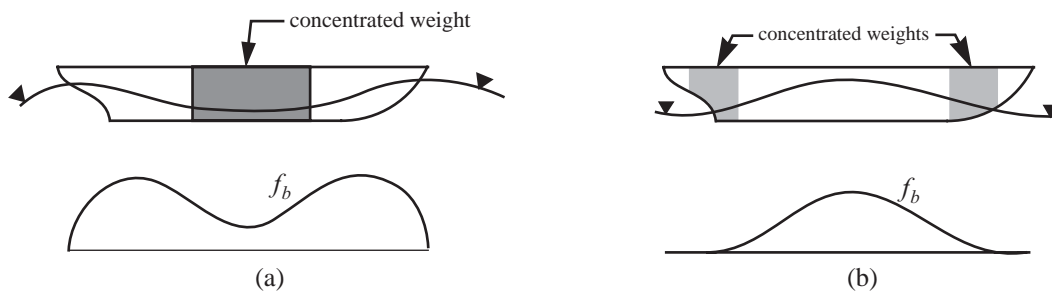


**Fig. 4.14 Longitudinal bending conditions for a ship. (a) Sagging. (b) Hogging.**

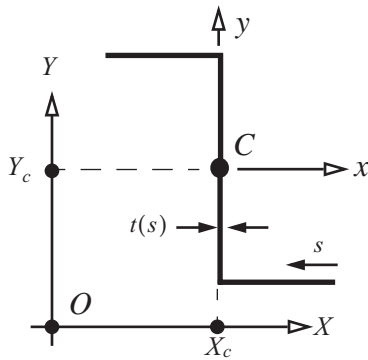
The hogging condition is depicted in figure 4.14(b). Here the wave troughs are at bow and stern, and the crest is amidships. The immersed cross section is greatest near amidships and is least near bow and stern. The distribution of the buoyancy per unit length  $f_b$ , shown in figure 4.14(b), reflects this situation. In hogging the deck is in tension and the bottom is in compression. The worst possible locations to concentrate cargo is fore and aft, as this will produce the greatest bending moment in the ship.



### 4.3.3 Properties of plane areas

First and second area moments of the cross-sectional area need to be determined before evaluating eq. (4.6) for the normal stress. Analytical procedures were used in Example 3.1 on page 47 to compute first and second area moments for a thin-walled bar. Frequently, the composite area technique in conjunction with the parallel axis theorem are used to determine these geometric properties.

**Parallel axis theorem.** Consider two parallel axes systems in the cross section. The origin of the Cartesian axes  $x$  and  $y$  coincide with the centroid of the cross-sectional area, which is labeled  $C$  in figure 4.15. The second Cartesian system  $X$  and  $Y$  has its origin at an arbitrary point  $O$ , the  $X$ -axis is parallel to the  $x$ -axis, and the  $Y$ -axis is parallel to the  $y$ -axis. The location of the centroid in the  $X$  and  $Y$  system is denoted by coordinate values  $(X_c, Y_c)$ . Usually the  $X$  and  $Y$  system is selected as something convenient to start with, and the first and second area moments with respect to the  $X$  and  $Y$  system are computed or looked up in tables. Then the  $(X_c, Y_c)$  coordinates of the centroid are computed and the parallel axis theorem is used to find the second area moments in the  $x$  and  $y$  system.



For a thin-walled bar the area element is  $dA = t(s)ds$ , in which  $s$  denotes the arc-length along the contour  $c$ , and  $t(s)$  denotes the thickness of the wall. In general, the thickness may vary smoothly with arc-length, but its magnitude must remain small with respect to the overall dimensions of the cross section. An abrupt change in thickness is modeled by a step change in thickness at a junction. The area of the cross section is given by

$$A = \int_c t(s)ds. \quad (4.34)$$

In the  $X$  and  $Y$  system, the first area moments are defined as

**Fig. 4.15** Parallel Cartesian axes systems.

$$Q_X = \int_c Y t ds \quad Q_Y = \int_c X t ds. \quad (4.35)$$

The relationship between the two parallel coordinate systems is determined from the location of a generic point  $s$  on the contour in each system. This relationship is

$$X(s) = X_c + x(s) \quad Y(s) = Y_c + y(s). \quad (4.36)$$

If eq. (4.36) is substituted into eq. (4.35), we get

$$Q_X = Y_c A + Q_x \quad Q_Y = X_c A + Q_y. \quad (4.37)$$

where

$$Q_x = \int_c y(s) t(s) ds \quad Q_y = \int_c x(s) t(s) ds. \quad (4.38)$$

Since the origin of the  $x$  and  $y$  system is at the centroid, the first moments  $Q_x$  and  $Q_y$  are zero by definition. Setting  $Q_x = 0$  and  $Q_y = 0$  in eq. (4.37), we can solve to find the location of the centroid as

$$X_C = \frac{Q_Y}{A} \quad Y_C = \frac{Q_X}{A}. \quad (4.39)$$

In the  $X$  and  $Y$  coordinate system the second area moments are defined by

$$I_{XX} = \int_c Y^2 tds \quad I_{YY} = \int_c X^2 tds \quad I_{XY} = \int_c XY tds. \quad (4.40)$$

Second area moments are often called moments of inertia in analogy to moments of inertia of mass elements used in rigid body dynamics. The fact that eq. (4.40) is second moments of area elements and not mass elements should be kept in mind even if the terminology “moments of inertia” is used in the context of beam bending. Now substitute eq. (4.36) for the  $X$  and  $Y$  coordinates into eq. (4.40) to get

$$I_{XX} = Y_C^2 A + 2Y_C Q_X + I_{xx} \quad I_{YY} = X_C^2 A + 2X_C Q_Y + I_{yy} \quad I_{XY} = X_C Y_C A + X_C Q_Y + Y_C Q_X + I_{xy}, \quad (4.41)$$

where the second area moments with respect to the centroid are given by

$$I_{xx} = \int_c y^2 tds \quad I_{yy} = \int_c x^2 tds \quad I_{xy} = \int_c xy tds. \quad (4.42)$$

Since the origin of the  $x$  and  $y$  coordinates is at the centroid  $Q_x = Q_y = 0$ , and eq. (4.41) reduces to

$$I_{XX} = Y_C^2 A + I_{xx} \quad I_{YY} = X_C^2 A + I_{yy} \quad I_{XY} = X_C Y_C A + I_{xy}. \quad (4.43)$$

Equation (4.41) is the generalized parallel axis theorem, but in problem solving we usually use eq. (4.39) to locate the centroid and then the parallel axis theorem reduces to the use of eq. (4.43). Note that eq. (4.42) shows that  $I_{xx}$  and  $I_{yy}$  for real areas are always positive in value with dimensional units of  $L^4$ . The product area moment  $I_{xy}$  can be positive, zero, or negative in value. The product area moment  $I_{xy}$  is zero if either the  $x$ -axis or  $y$ -axis is an axis of symmetry of the cross section.

**Radii of gyration.** Define radii of gyration by

$$r_{xx} = \sqrt{I_{xx}/A} \quad r_{yy} = \sqrt{I_{yy}/A}. \quad (4.44)$$

The radii of gyration (4.44) have dimensional units of length. However, the radii of gyration do not locate a physically significant point in the cross section. For example,  $r_{XX} \neq Y_C + r_{xx}$ , where  $r_{XX}$  is the radius of gyration with respect to the  $X$ -axis. (Using the parallel axis theorem, the relation between the radius of gyration about the  $X$ -axis to the  $x$ -axis is  $r_{XX}^2 = Y_C^2 + r_{xx}^2$ .)

**Composite area technique.** The composite area technique for computing the centroid and second area moments is a method applicable to cross-sectional areas that can be subdivided into simple geometric shapes whose properties are known. An entire area  $A$  is subdivided into  $N$  sub-areas  $A_i$ ,  $i = 1, 2, \dots, N$  as shown in figure 4.16(a). Known properties of the  $i$ -th sub-area are its centroid denoted by  $C_i$ , and  $A_i$ ,  $(I_{xx})_i$ ,  $(I_{yy})_i$ ,  $(I_{xy})_i$ . Sub-area coordinate axes are denoted by  $(x_i, y_i)$  with origin at  $C_i$ . Reference axes are denoted by  $(X, Y)$  with origin at point O. The  $x_i$ -axis is parallel to the  $X$ -axis, and the  $y_i$ -axis is parallel to the  $Y$ -axis. Coordinates  $(X_i, Y_i)$  in the reference system locate the centroid  $C_i$  of the  $i$ -th sub-area.

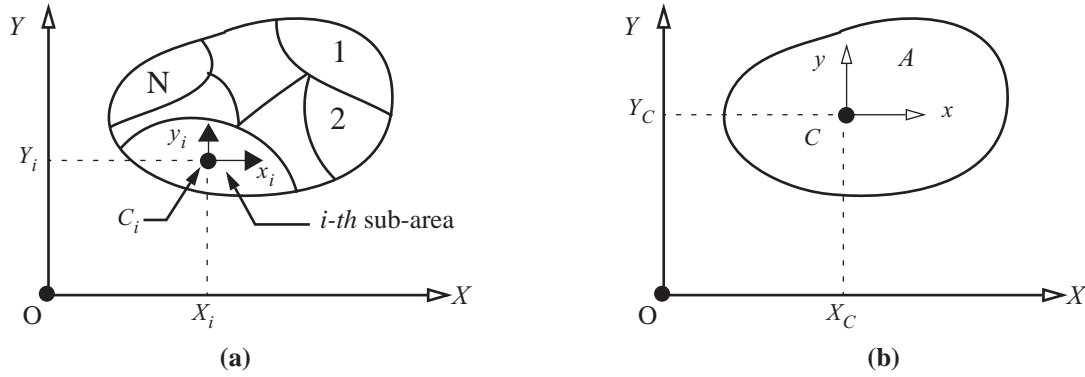


**Fig. 4.16 (a) Division of area A into sub-areas. (b) Assembled properties of area A.**

The pertinent equations for the assembled area properties are

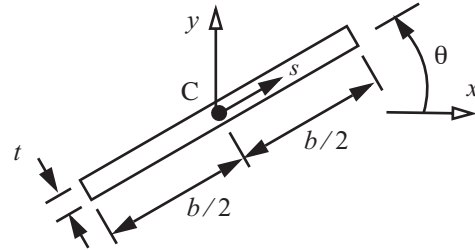
$$A = \sum_{i=1,2,\dots}^N A_i \quad AY_C = \sum_{i=1,2,\dots}^N Y_i A_i \quad AX_C = \sum_{i=1,2,\dots}^N X_i A_i, \text{ and} \quad (4.45)$$

$$I_{XX} = \sum_{i=1,2,\dots}^N (I_{xx} + Y_i^2 A_i) \quad I_{YY} = \sum_{i=1,2,\dots}^N (I_{yy} + X_i^2 A_i) \quad I_{XY} = \sum_{i=1,2,\dots}^N (I_{xy} + X_i Y_i A_i). \quad (4.46)$$

The coordinates  $(X_C, Y_C)$  of the centroid C for the entire area shown in figure 4.16(b) are computed from the last two expressions in eq. (4.45). The origin of the parallel coordinate system  $x-y$  is located at the centroid C as shown in figure 4.16(b). The parallel axis theorem (4.43) is used to find the second area moments about centroidal system  $x-y$  after the second area moments in the reference system are determined from eq. (4.46).

For branches that can be represented by a thin-walled rectangular area, we can obtain simple formulas for the second area moments. Consider a thin rectangular area, where  $0 < t \ll b$ . The contour is a straight line inclined at an angle  $\theta$  as is shown in figure 4.17. The contour coordinate is denoted by  $s$ , and the area element is  $dA = t ds$ . The  $x$  and  $y$  coordinates of the point  $s$  on the contour are given by  $x = s \cos \theta$  and  $y = s \sin \theta$ .

**Fig. 4.17 Thin rectangular area inclined at an angle  $\theta$ .**



Hence, the second area moments are computed from

$$\begin{aligned}
 I_{xx} &= \int_{-b/2}^{b/2} (s \sin \theta)^2 t ds = \frac{b^3 t}{12} \sin^2 \theta \\
 I_{yy} &= \int_{-b/2}^{b/2} (s \cos \theta)^2 t ds = \frac{b^3 t}{12} \cos^2 \theta \\
 I_{xy} &= \int_{-b/2}^{b/2} (s \sin \theta)(s \cos \theta) t ds = \frac{b^3 t}{12} \sin \theta \cos \theta
 \end{aligned} \quad (4.47)$$

### Example 4.3 Thin-walled zee section properties by the composite area technique

Determine the centroid and the second area moments for the thin-walled zee section shown in figure 4.18. The section is subdivided into three rectangular branches. One branch corresponds to the web and two branches cor-

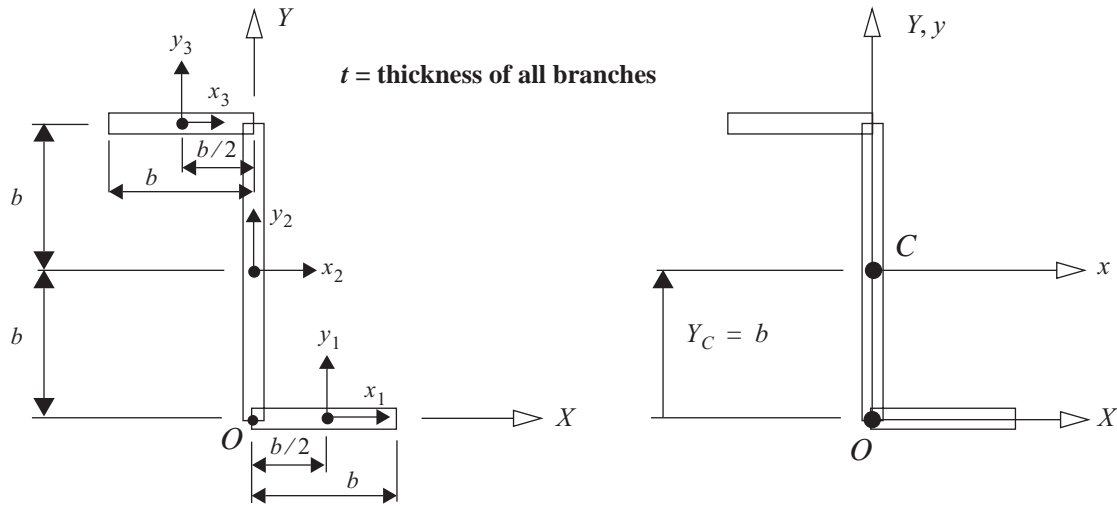


Fig. 4.18 Zee section approximated by three rectangular branches.

respond to the flanges.

**Solution.** First we find the centroid. Equation (4.45) is represented in table 4.1 shown below.

Table 4.1 Areas and first area moments for the zee section

$i$	$A_i$	$X_i$	$Y_i$	$X_i A_i$	$Y_i A_i$
1	$bt$	$b/2$	0	$b^2 t/2$	0
2	$2bt$	0	$b$	0	$2b^2 t$
3	$bt$	$-b/2$	$2b$	$-b^2 t/2$	$2b^2 t$
Sum	$4bt$			0	$4b^2 t$

Summation of the appropriate columns gives

$$A = 4bt \quad X_c A = 0 \quad Y_c A = 4b^2t, \quad (\text{a})$$

so that the centroid has coordinates  $X_c = 0$  and  $Y_c = b$ .

The second area moments are computed for the reference coordinate system  $(X, Y)$  using table 4.2 shown below. Note that for the local coordinate systems originating at the centroid in each branch we can identify the angle  $\theta$  in eq. (4.47) as  $\theta_1 = 0^\circ$ ,  $\theta_2 = 90^\circ$ , and  $\theta_3 = 0^\circ$ . These values of the angle  $\theta$  in each branch are used to compute the local second area moments in each rectangular branch via eq. (4.47).

**Table 4.2 Second area moments for each branch of the zee section**

$i$	$Y_i^2 A_i$	$(I_{xx})_i$	$X_i^2 A_i$	$(I_{yy})_i$	$X_i Y_i A_i$	$(I_{xy})_i$
1	0	0	$b^3t/4$	$b^3t/12$	0	0
2	$(b^2)2bt$	$(2b)^3t/12$	0	0	0	0
3	$(2b)^2bt$	0	$b^3t/4$	$b^3t/12$	$-b^3t$	0
Sum	$6b^3t$	$2b^3t/3$	$b^3t/2$	$b^3t/6$	$-b^3t$	0

From the summation of the columns, the second area moments in the  $(X, Y)$  system via eq. (4.46) are

$$\begin{aligned} I_{XX} &= 6b^3t + 2b^3t/3 = (20b^3t)/3 \\ I_{YY} &= (b^3t)/2 + (b^3t)/6 = (2b^3t)/3. \\ I_{XY} &= -b^3t \end{aligned} \quad (\text{b})$$

Now we use the parallel axis theorem to transfer these moments to the  $x$ - $y$  system. Equation (4.43) gives

$$I_{xx} = I_{XX} - Y_c^2 A = \frac{20}{3}b^3t - b^2(4bt) = \frac{8}{3}b^3t \quad (\text{c})$$

$$I_{yy} = I_{YY} - X_c^2 A = \frac{2}{3}b^3t - (0)(4bt) = \frac{2}{3}b^3t \quad (\text{d})$$

$$I_{xy} = I_{XY} - X_c Y_c A = -b^3t - (0)(b)(4bt) = -b^3t. \quad (\text{e})$$

#### 4.3.4 Neutral axis of the cross section

For the case of a vanishing axial normal force  $N$ , and neglecting temperature effects, the axial normal stress (4.6) reduces to

$$\sigma_{zz} = \frac{kM_x}{I_{xx}}y + \frac{kM_y}{I_{yy}}x = \frac{kM_x}{I_{xx}}(y - n_y x) + \frac{kM_y}{I_{yy}}(x - n_x y) = k\left(\frac{-n_y M_x}{I_{xx}} + \frac{M_y}{I_{yy}}\right)x + k\left(\frac{M_x}{I_{xx}} - \frac{n_x M_y}{I_{yy}}\right)y. \quad (\text{4.48})$$

At the centroid where  $x = y = 0$  the axial normal stress vanishes. Set the axial normal stress equal to zero to get

$$\left(\frac{-n_y M_x}{I_{xx}} + \frac{M_y}{I_{yy}}\right)x + \left(\frac{M_x}{I_{xx}} - \frac{n_x M_y}{I_{yy}}\right)y = 0. \quad (4.49)$$

Equation (4.49) defines a straight line in the cross section that is called the neutral axis. Substitute the definitions of  $n_x$  and  $n_y$  from eq. (4.4) into eq. (4.49), and then solve for  $y$  in terms of  $x$ . Let these coordinates be denoted as  $(x_{NA}, y_{NA})$ . After some algebra we find

$$y_{NA} = -\left(\frac{-I_{xy}M_x + I_{xx}M_y}{I_{yy}M_x - I_{xy}M_y}\right)x_{NA} = -(\tan\beta)x_{NA}, \quad (4.50)$$

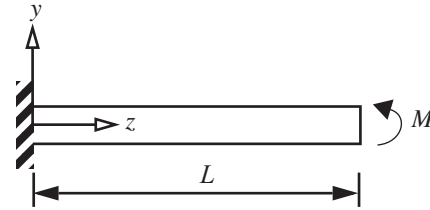
where

$$\tan\beta = \frac{-I_{xy}M_x + I_{xx}M_y}{I_{yy}M_x - I_{xy}M_y}. \quad (4.51)$$

#### Example 4.4 Normal stress distribution in a cantilever beam subject to pure bending.

The cantilever beam shown in figure 4.19 is subject to a bending moment  $M$  at its tip. The cross section is the thin-walled zee shown in figure 4.18. The second area moments about the centroidal axes are given by eqs. (c) to (e) in example 4.3. Determine the neutral axis in the cross section and the distribution of the bending normal stress.

**Fig. 4.19** Pure bending of a cantilever beam with a zee cross section.



**Solution.** First, note that the components of the prescribed bending moment are  $M_x = -M$  and  $M_y = 0$ . Thus, the cantilever beam is subject to loading in the  $y$ - $z$  plane. The equation of the neutral axis is  $y_{NA} = -(\tan\beta)x_{NA}$ , where eq. (4.51) is

$$\tan\beta = \frac{(-I_{xy})(-M)}{I_{yy}(-M)} = \frac{-(-b^3t)}{\frac{2}{3}b^3t} = \frac{3}{2}. \quad (a)$$

The angle  $\beta = 56.31^\circ$ .

To compute the distribution of the normal stress (4.6) in the cross section, we begin by evaluating section coefficients (4.4):

$$n_x = I_{xy}/I_{xx} = -3/8 \quad n_y = I_{xy}/I_{yy} = -3/2 \quad k = \frac{1}{1 - n_x n_y} = 16/7. \quad (b)$$

The coordinates in each branch of the cross section defined by eq. (4.7) are

$$\bar{x}_i(s) = x_i(s) - n_x y_i(s) \quad \bar{y}_i(s) = y_i(s) - n_y x_i(s) \quad i = 1, 2, 3. \quad (c)$$

The normal stress (4.6) in  $i$ -th branch is given by

$$(\sigma_{zz})_i = \left[ \frac{k(-M)}{I_{xx}} \right] y_i(s) = \left[ \frac{k(-M)}{I_{xx}} \right] (y_i - n_y x_i) = \frac{6}{7b^3 t} (-M) \left( y_i + \frac{3}{2} x_i \right). \quad (d)$$

Coordinates in branch 1 are  $(x_1, y_1) = (x_1, -b)$ , in branch 2  $(x_2, y_2) = (0, y_2)$ , and in branch 3  $(x_3, y_3) = (x_3, b)$ . The normal stress in each branch is a linear function of the contour coordinate. The results are

$$(\sigma_{zz})_1 = \frac{6}{7b^3 t} (-M) \left( -b + \frac{3}{2} x_1 \right) \quad 0 \leq x_1 \leq b, \quad (e)$$

$$(\sigma_{zz})_2 = \frac{6}{7b^3 t} (-M) (y_2 - n_y x_2) = \frac{6}{7b^3 t} (-M) y_2 \quad -b \leq y_2 \leq b, \text{ and} \quad (f)$$

$$(\sigma_{zz})_3 = \frac{6}{7b^3 t} (-M) (y_3 - n_y x_3) = \frac{6}{7b^3 t} (-M) \left( b + \frac{3}{2} x_3 \right) \quad -b \leq x_3 \leq 0. \quad (g)$$

The neutral axis and the bending normal stress distribution are shown in figure 4.20. ■

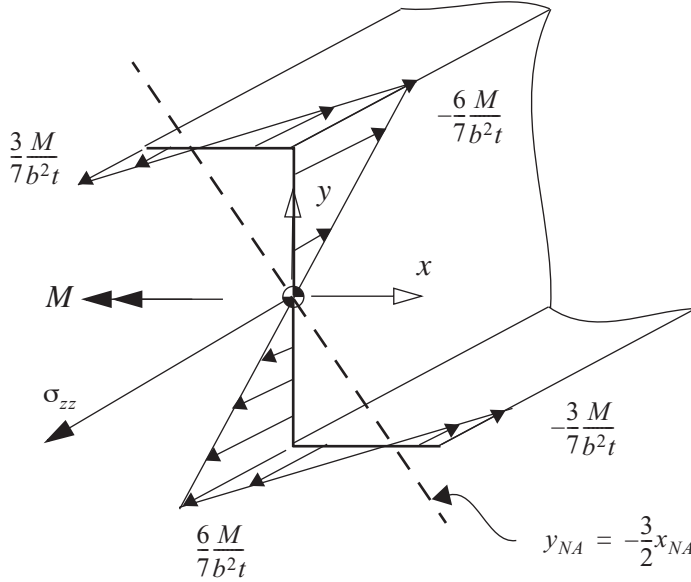


**Fig. 4.20** Bending normal stress distribution along the contour of the zee section.

#### Example 4.5 Displacements of the cantilever beam of example 4.4

Determine the lateral displacement functions  $u(z)$  and  $v(z)$ ,  $0 \leq z \leq L$ , for the zee section beam of example 4.4.

**Solution.** First note that this is a statically determinate beam subject to pure bending. The equilibrium equations are satisfied for  $M_x = -M$  and  $M_y = 0$  for all  $z \in (0, L)$ , where  $M$  denotes the specified end moment. To find the lateral displacements  $u(z)$  and  $v(z)$ ,  $0 \leq z \leq L$ , we begin with matrix eq. (4.1), which for this example reduces to

$$\begin{bmatrix} dw/dz \\ d\phi_x/dz \\ d\phi_y/dz \end{bmatrix} = \frac{1}{E} \begin{bmatrix} 1/A & 0 & 0 \\ 0 & k/I_{xx} & (-kn_x)/I_{yy} \\ 0 & (-kn_y)/I_{xx} & k/I_{yy} \end{bmatrix} \begin{bmatrix} 0 \\ -M \\ 0 \end{bmatrix}. \quad (\text{a})$$

For this pure bending case the derivatives of the rotations are given by

$$\frac{d\phi_x}{dz} = \frac{k(-M)}{EI_{xx}} = \frac{16/7}{(8/3)Eb^3t}(-M) = -\frac{6}{7}\left(\frac{M}{Eb^3t}\right), \text{ and} \quad (\text{b})$$

$$\frac{d\phi_y}{dz} = -\frac{kn_y}{EI_{xx}}(-M) = -\frac{(16/7)(-3/2)}{(8/3)Eb^3t}(-M) = -\frac{9}{14}\left(\frac{M}{Eb^3t}\right). \quad (\text{c})$$

Integrate eqs. (b) and (c) from  $z = 0$  to  $z$  to get

$$\phi_x(z) - \phi_x(0) = \int_0^z \left[ -\frac{6}{7}\left(\frac{M}{Eb^3t}\right) \right] dz = \left[ -\frac{6}{7}\left(\frac{M}{Eb^3t}\right) \right] z, \text{ and} \quad (\text{d})$$

$$\phi_y(z) - \phi_y(0) = \int_0^z \left[ -\frac{9}{14}\left(\frac{M}{Eb^3t}\right) \right] dz = \left[ -\frac{9}{14}\left(\frac{M}{Eb^3t}\right) \right] z. \quad (\text{e})$$

At  $z = 0$  the beam is clamped to the rigid wall so that the rotations of the cross section at the wall are  $\phi_x(0) = \phi_y(0) = 0$ . The results for the rotations are

$$\phi_x(z) = -\frac{6}{7}\left(\frac{M}{Eb^3t}\right)z \quad \phi_y(z) = -\frac{9}{14}\left(\frac{M}{Eb^3t}\right)z. \quad (\text{f})$$

The cantilever beam is subject to pure bending and by equilibrium the transverse shear forces  $V_x = V_y = 0$ , for  $0 \leq z \leq L$ . Hooke's law (4.27) then yields that the transverse shear strains  $\psi_x = \psi_y = 0$ , for  $0 \leq z \leq L$ . Vanishing of the transverse shear strains in eq. (4.28) leads to

$$\psi_x = \frac{du}{dz} + \phi_y = 0 \quad \psi_y = \frac{dv}{dz} + \phi_x = 0. \quad (\text{g})$$

From eqs. (f) and (g) the derivatives of the displacements are given by

$$\frac{du}{dz} = -\phi_y = \frac{9}{14}\left(\frac{M}{Eb^3t}\right)z \quad \frac{dv}{dz} = -\phi_x = \frac{6}{7}\left(\frac{M}{Eb^3t}\right)z. \quad (\text{h})$$

Integrate eq. (h) from  $z = 0$  to  $z$  to get

$$u(z) - u(0) = \frac{9}{14}\left(\frac{M}{Eb^3t}\right)\frac{z^2}{2} \quad v(z) - v(0) = \frac{6}{7}\left(\frac{M}{Eb^3t}\right)\frac{z^2}{2}. \quad (\text{i})$$

At the clamped end the beam displacements equal zero. Thus, the displacements are

$$u(z) = \frac{9}{14}\left(\frac{M}{Eb^3t}\right)\frac{z^2}{2} \quad v(z) = \frac{6}{7}\left(\frac{M}{Eb^3t}\right)\frac{z^2}{2}. \quad (\text{j})$$



The view of the lateral displacements of the beam at  $z = L$  are shown in figure 4.21. As a result of  $I_{xy} \neq 0$  the beam displaces both vertically and horizontally for a load that is applied in  $y$ - $z$  plane.

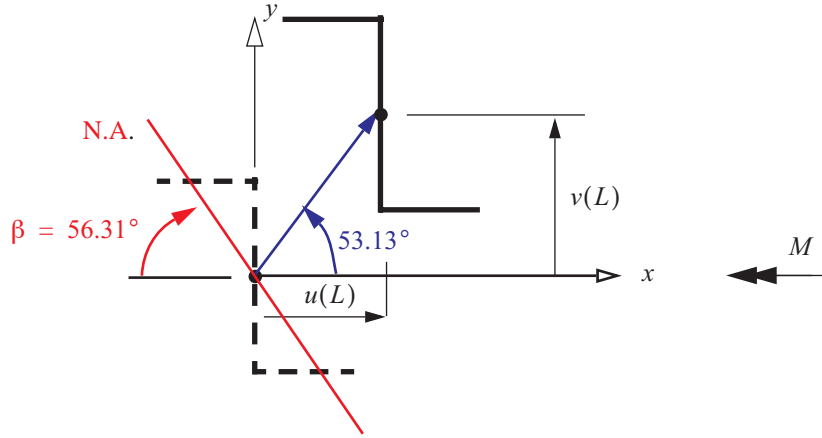


Fig. 4.21 Displacement of the centroid at the tip of the cantilever beam subject to pure bending.

#### Example 4.6 Transverse bending of a cantilever beam

Consider a uniform cantilever beam from example 4.4 subject to a vertical force  $F$  acting through the shear center at its free end as shown in figure 4.22. There is no change in temperature from the stress-free state. The cross section is the thin-walled zee shown in figure 4.18. Determine the displacements of the cantilever.

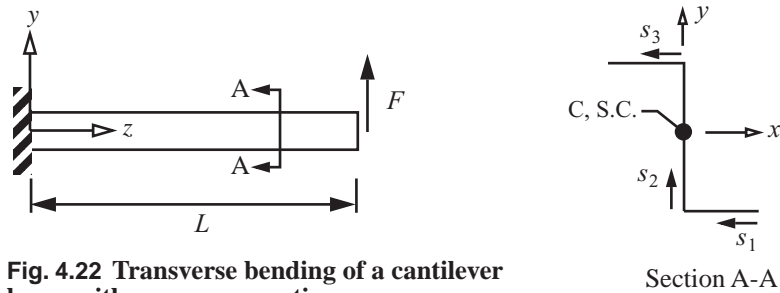


Fig. 4.22 Transverse bending of a cantilever beam with a zee cross section.

**Solution.** The cantilever is statically determinate, and from equilibrium the shear force and bending moment are

$$V_y = F \quad M_x = -(L-z)F \quad 0 \leq z \leq L. \quad (\text{a})$$

From Hooke's law (4.1) we find the derivatives of the rotations are

$$\frac{d\phi_x}{dz} = \frac{kM_x}{EI_{xx}} = \frac{-k}{EI_{xx}}(L-z)F \quad \frac{d\phi_y}{dz} = -\frac{kn_y M_x}{EI_{xx}} = \frac{kn_y}{EI_{xx}}(L-z)F. \quad (\text{b})$$

Integrate the rotations in eq. (b) with respect to coordinate  $z$  and impose  $\phi_x(0) = \phi_y(0) = 0$  at the clamped end of the cantilever to get

$$\phi_x = \frac{-3z(2L-z)}{7Eb^3t}F \quad \phi_y = \frac{-9z(2L-z)}{14b^3tE}F. \quad (\text{c})$$

From eq. (4.27) the shear strains of the cantilever beam are

$$\psi_x = c_{xy}F \quad \psi_y = c_{yy}F. \quad (\text{d})$$

The compliance coefficients (4.29) for this example are

$$c_{xy} = \frac{k^2}{I_{xx}I_{yy}} \left[ \int_0^b \bar{Q}_{x1} \bar{Q}_{y1} ds_1 + \int_0^{2b} \bar{Q}_{x2} \bar{Q}_{y2} ds_2 + \int_0^b \bar{Q}_{x3} \bar{Q}_{y3} ds_3 \right] \frac{1}{Gt}, \text{ and} \quad (\text{e})$$

$$c_{yy} = \left( \frac{k}{I_{xx}} \right)^2 \left[ \int_0^b \bar{Q}_{x1}^2 ds_1 + \int_0^{2b} \bar{Q}_{x2}^2 ds_2 + \int_0^b \bar{Q}_{x3}^2 ds_3 \right] \frac{1}{Gt}. \quad (\text{f})$$

To evaluate the compliance coefficients in eq. (d) we need the parametric equations of the contour of the cross section with respect to centroidal coordinates. The equations are listed in table 4.3.

**Table 4.3 Contour coordinate functions**

Branch	$x_i(s_i)$	$y_i(s_i)$	
i = 1	$b - s_1$	$-b$	$0 \leq s_1 \leq b$
i = 2	0	$-b + s_2$	$0 \leq s_2 \leq 2b$
i = 3	$-s_3$	$b$	$0 \leq s_3 \leq b$

We need to determine the distribution functions  $\bar{Q}_{xi}(s_i)$  and  $\bar{Q}_{yi}(s_i)$ ,  $i = 1, 2, 3$ , beginning with the contour origin from the general expression in eq. (4.9). The contour origin is in branch 1 where  $s_1 = 0$  at its intersection with the traction-free longitudinal edge. As we move along the contour each branch is cut at a generic value of its contour coordinate. The area of the contour preceding the cut determines the range of integration for the distribution function as shown in figure 4.23. Using the parametric equations in table 4.3 the results for branch one are

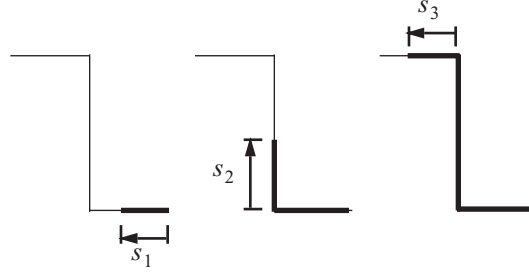
$$\bar{Q}_{x1}(s_1) = \int_0^{s_1} [y_1(s_1) - n_y x_1(s_1)] t ds_1 = \frac{1}{4}(2b - 3s_1)s_1 t, \text{ and } \bar{Q}_{y1}(s_1) = \int_0^{s_1} [x_1(s_1) - n_x y_1(s_1)] t ds_1 = \frac{1}{8}(5b - 4s_1)s_1 t. \quad (\text{g})$$

For a cut in branch 2, the integration includes all of branch 1 and the integration of the segment in branch 2. The distribution functions for the cut in branch 2 are

$$\bar{Q}_{x2}(s_2) = \bar{Q}_{x1}(b) + \int_0^{s_2} [y_2(s_2) - n_y x_2(s_2)] t ds_2 = -\frac{1}{4}(b^2 + 4bs_2 - 2s_2^2)t, \text{ and} \quad (\text{h})$$

$$\bar{Q}_{y2}(s_2) = \bar{Q}_{y1}(b) + \int_0^{s_2} [x_2(s_2) - n_x y_2(s_2)] t ds_2 = \frac{1}{16}(2b^2 - 6bs_2 + 3s_2^2)t, \text{ where } 0 \leq s_2 \leq 2b. \quad (\text{i})$$

**Fig. 4.23** Range of integration along the contour to compute the distribution functions.



For a cut in branch 3, the integration includes all of branch 1, all of branch 2, and the integration of the segment in branch 3. The distribution functions for the cut in branch 3 are

$$\bar{Q}_{x3}(s_3) = \bar{Q}_{x2}(2b) + \int_0^{s_3} [y_3(s_3) - n_y x_3(s_3)] t ds_3 = -\frac{1}{4}(b^2 - 4bs_3 + 3s_3^2)t, \text{ and} \quad (j)$$

$$\bar{Q}_{y3}(s_3) = \bar{Q}_{y2}(2b) + \int_0^{s_3} [x_3(s_3) - n_x y_3(s_3)] t ds_3 = \frac{1}{8}(b^2 + 3bs_3 - 4s_3^2)t, \text{ where } 0 \leq s_3 \leq b. \quad (k)$$

Substitute the distribution functions in eqs. (g) to (k) into the compliance coefficients of eqs. (e) and (f), followed by integration, to find

$$c_{xy} = \frac{9}{196bGt} \quad c_{yy} = \frac{267}{490bGt}. \quad (l)$$

From the definition of the shear strains (4.28), we get the following integrals for the displacements that satisfy the boundary conditions  $u(0) = v(0) = 0$ :

$$u(z) = \int_0^z (\psi_x - \phi_y) dz \quad v(z) = \int_0^z (\psi_y - \phi_x) dz. \quad (m)$$

Substitute the compliance coefficients from eq. (i) into Hooke's law (d), followed by substituting the result for shear strains into eq. (m). Then substitute eq. (c) for the rotations into eq. (m). Perform the integration with respect to  $z$  to get:

$$u(z) = \frac{9Fz}{196bGt} + \frac{9LFz^2}{14b^3tE} - \frac{3Fz^3}{14b^3tE} \quad v(z) = \frac{267Fz}{480btG} + \frac{3LFz^2}{7b^3tE} - \frac{Fz^3}{7b^3tE}. \quad (n)$$

The vertical displacement at point of application of the force  $F$  is

$$v(L) = \left( \frac{2L^3}{7b^3tE} + \frac{267L}{490btG} \right) F = \left( \frac{3L^3F}{7b^3tE} \right) \left[ 1 + \frac{267b^2E}{140L^2G} \right], \quad (o)$$

where the last result was obtained by factoring out the first term on the right-hand side. For aluminum alloys  $E/G \approx 2.5$ , eq. (o) can be manipulated to the form

$$v(L) = \frac{16L^3F}{21EI_{xx}} \underbrace{\left[ 1 + \frac{4.77}{(L/b)^2} \right]}_{= g(L/b)} \quad . \quad (\text{p})$$

The function  $g(L/b)$  is evaluated for several ratios of  $L/b$ , and the results are listed in table 4.4. The function  $g(L/b) \rightarrow 1$  for values of  $L/b > 10$ , which implies the displacement  $v(L) \rightarrow \frac{16L^3F}{21EI_{xx}}$  for  $L/b > 10$ .

**Table 4.4 Ratio of the transverse shear displacement to the bending displacement**

$L/b$	$g(L/b)$
1	5.77
2	2.19
5	1.19
10	1.05
15	1.02

This result means the contribution of the displacement due to transverse shear deformation is negligible with respect to the component due to bending for beams that are long with respect to their cross-sectional dimensions. To neglect the influence of transverse shear means we can set shear strains  $\psi_x = 0$  and  $\psi_y = 0$ . Setting the shear strains equal to zero in Hooke's law for transverse shear in (4.27) means the shear forces equal zero. However, the shear forces are necessary for beam equilibrium. Hence, we omit Hooke's law for transverse shear in a theory where the shear strains are assumed equal to zero. The beam theory neglecting transverse shear strains is called the **Euler-Bernoulli** beam theory. ■

#### 4.4 Structural analyses for transverse shear and torsion

The shear stress  $\sigma_{zs}$  is directly proportional to the transverse shear force components  $V_x$  and  $V_y$ , and the torque  $M_z$  for a straight bar and for infinitesimal deformations of a Hookean material. Procedures to calculate  $\sigma_{zs}$  are different for an open contour and for a closed contour. The stress analysis for an open cross-sectional contour is presented in example 4.7, and the stress analysis for a closed cross-sectional contour is presented in example 4.8.

##### Example 4.7 Shear stress analysis for an open cross-sectional contour

The open contour shown in figure 4.24 consists of a semicircular branch of radius  $a$ . For simplicity the origin of the  $X$ - $Y$  system is at the center of the semicircle which is labeled point O in figure 4.24. The  $X$ -axis is an axis of symmetry, and the centroid C and shear center S.C. lie on this axis. To find the shear center we take the shear force  $V_x = 0$ . The shear force  $V_y$  and the torque  $M_z$  act at the shear center. If  $M_z = 0$ , then the shear force  $V_y$  causes a displacement  $v$  in bending of the bar, and  $\phi_z = 0$ . If  $V_y = 0$ , then the torque  $M_z$  causes a rotation  $\phi_z$  twisting the bar, and  $v = 0$  at the shear center.

Determine

- the location of the centroid,
- the shear flow due  $V_y$ ,
- the location of the shear center, and
- the shear stress  $\sigma_{zs}$  in terms of  $V_y$  and  $M_z$ .

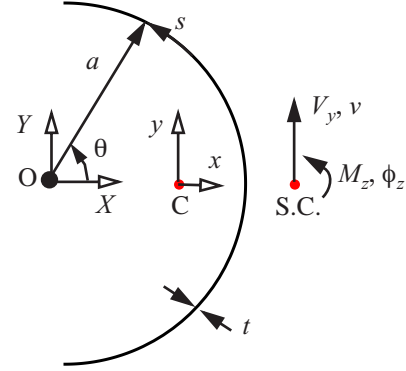


Fig. 4.24 Semicircular, open section.

**Solution to part (a).** The parametric equations of the semicircular contour are

$$X(\theta) = a \cos \theta \quad Y(\theta) = a \sin \theta \quad s = a\theta \quad -\pi/2 \leq \theta \leq \pi/2. \quad (\text{a})$$

We compute the area  $A$ , the first area moment about the  $Y$ -axis  $Q_Y$ , and the location of the centroid as follows.

$$A = \int_{-\pi/2}^{\pi/2} t a d\theta = a\pi t \quad Q_Y = \int_{-\pi/2}^{\pi/2} X(\theta) t a d\theta = 2a^2 t \quad X_C = Q_Y/A = 2a/\pi. \quad (\text{b})$$

The coordinates relative to the centroid, and the second area moment about the  $x$ -axis through the centroid are

$$x(\theta) = X(\theta) - X_C = a \cos \theta - 2a/\pi \quad y(\theta) = Y(\theta) \quad I_{xx} = \int_{-\pi/2}^{\pi/2} y^2(\theta) t a d\theta = a^3 \pi t / 2. \quad (\text{c})$$

**Solution to part (b).** The distribution function for the shear flow with the contour origin at  $\theta = -\pi/2$  is given by

$$Q_x(\theta) = \int_{-\pi/2}^{\theta} y(\theta) t a d\theta = -a^2 t \cos \theta \quad -\pi/2 \leq \theta \leq \pi/2. \quad (\text{d})$$

Since the product area moment  $I_{xy} = 0$ , eq. (4.4) yields the parameters  $n_x = n_y = 0$  and  $k = 1$ . The shear flow in eq. (4.13) on page 80 reduces to

$$q(s, z) = -\frac{V_y}{I_{xx}} Q_x(s), \quad (\text{e})$$

and the explicit equation for the shear flow is

$$q(\theta) = -V_y Q_x(\theta) / I_{xx} = \frac{2V_y}{(a\pi)} \cos \theta. \quad (\text{f})$$

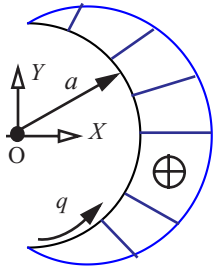


**Fig. 4.25** Distribution of the shear flow in the open section.  $V_y > 0$ .

The shear flow is plotted normal to the contour in figure 4.25, and it is apparent in the figure that the shear flow is a maximum at  $\theta = 0$ .

**Solution to part (c).** The coordinates of the shear center relative to the centroid are given in eq. (4.8) on page 80. In this example the equation for the coordinate  $x_{sc}$  reduces to

$$x_{sc} = -\left(\frac{1}{I_{xx}}\right) \left[ \int_c r_{nc}(\theta) Q_x(\theta) a d\theta \right], \quad (g)$$

where the coordinate normal to the contour with respect to the centroid is given in eq. (4.10). In this example the normal coordinate is

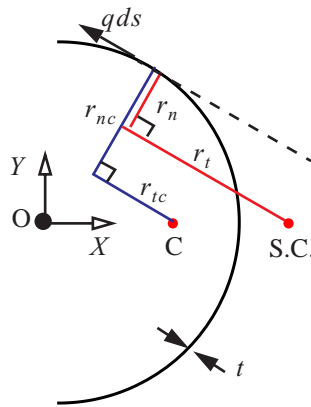
$$r_{nc} = x(s) \frac{dy}{ds} - y(s) \frac{dx}{ds} = a - \frac{2a}{\pi} \cos \theta. \quad (h)$$

Substitute eq. (h) for the normal coordinate and substitute eq. (d) for the distribution function, into eq. (g) to find

$$x_{sc} = \frac{-1}{I_{xx}} \int r_{nc}(\theta) Q_x(\theta) a d\theta = \frac{2a}{\pi}.$$

Relative to point O the coordinate of the shear center is given by  $X_{SC} = X_C + x_{sc} = (4a)/\pi$ . The shear center lies outside of the circular contour.

**Fig. 4.26** The shear flow located from the centroid and shear center by coordinates tangent and normal to the contour.



As a check on the shear flow we compute its torque with respect to the shear center by

$$M_z = \int_{-\pi/2}^{\pi/2} r_n(\theta) q(\theta) a d\theta, \quad (i)$$

where  $r_n(\theta)$  is the coordinate normal to the line of action of the shear flow as shown in figure 4.26. The normal coordinate is given by eq. (4.11). where  $r_{nc}(s)$  is the coordinate normal to the line of action of the shear flow with respect to the centroid as shown in figure 4.26. In this example the normal coordinate with respect to the centroid is

$$r_n = a \left( 1 - \frac{4}{\pi} \cos \theta \right), \quad (j)$$

Substitute eq. (k) for  $r_n(\theta)$  in eq. (i) followed by substitution eq. (f) for the shear flow to get

$$M_z = \int_{-\pi/2}^{\pi/2} \left[ a \left( 1 - \frac{4}{\pi} \cos \theta \right) \right] \left[ \frac{2V_y}{(a\pi)} \cos \theta \right] a d\theta = \frac{2a}{\pi} V_y \int_{-\pi/2}^{\pi/2} \left[ \cos \theta - \frac{4}{\pi} \cos^2 \theta \right] d\theta = \frac{2a}{\pi} V_y \left[ \sin \theta - \frac{4}{\pi} \left( \frac{\theta}{2} + \frac{1}{4} \sin 2\theta \right) \right] \Big|_{-\pi/2}^{\pi/2}. \quad (k)$$

Evaluating eq. (k) we find

$$M_z = \frac{2a}{\pi} V_y \left[ 1 - (-1) - \frac{4}{\pi} \left[ \frac{\pi}{4} - \left( -\frac{\pi}{4} \right) + \frac{1}{4} (0 - 0) \right] \right] = \frac{2a}{\pi} V_y \left[ 2 - \frac{4}{\pi} \left[ \frac{\pi}{2} + \frac{1}{4} (0 - 0) \right] \right] = \frac{2a}{\pi} V_y [2 - 2] = 0. \quad (l)$$

The result of the integration given by eq. (l) verifies that the shear flow results in no torque at the shear center.

**Solution to part (d).** The shear stress  $\sigma_{zs}$  is the sum of the shear stresses from the transverse shear force  $V_y$  and from the torque  $M_z$ , and is given by eq. (4.12) on page 80. For this example we find

$$\sigma_{zs} = q/t + 2(M_z/J)\zeta = 2(V_y/A)\cos\theta + 2(M_z/J)\zeta \quad -\pi/2 \leq \theta \leq \pi/2 \quad -t/2 \leq \zeta \leq t/2. \quad (m)$$

From eq. (4.14) the torsion constant  $J = (bt^3)/3 = (a\pi t^3)/3$ . The shear stress (m) is a maximum at  $\theta = 0$ , where the shear flow is maximum. At  $\theta = 0$  the maximum shear stress is determined from

$$\sigma_{zs}|_{\theta=0} = 2(V_y/A) \pm (M_z/J)t. \quad (n)$$

#### Example 4.8 Shear stress analysis for a closed cross-sectional contour

A closed contour in the shape of the letter D is shown in figure 4.27. The origin of the  $X$ - $Y$  system is taken at the center of the semicircular branch. The cross section is symmetric about the  $X$ -axis, so the centroid and shear center lie on the  $X$ -axis. To locate the shear center we take shear force  $V_x = 0$ , and note that the shear force  $V_y \neq 0$  and torque  $M_z \neq 0$  act at the shear center.

- Locate the centroid,
- determine the shear flow with respect to the centroid,
- locate the shear center,
- establish the shear flow with respect to the shear center, and
- determine the shear stress  $\sigma_{zs}$ .

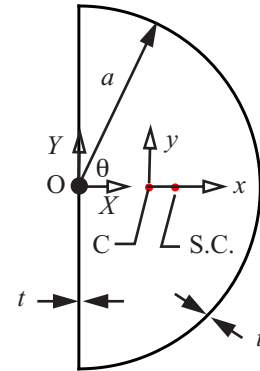


Fig. 4.27 Closed contour.

**Solution to part (a).** The cross section is composed of two branches. Branch 1 is the semicircular contour, and branch 2 is the vertical web connecting the ends of branch 1. The parametric equations of the contour for each branch are

$$\begin{aligned} [X_1(\theta), Y_1(\theta)] &= a[\cos(\theta), \sin(\theta)] & -\pi/2 \leq \theta \leq \pi/2 \\ [X_2(s), Y_2(s)] &= [0, a-s] & 0 \leq s \leq 2a \end{aligned} \quad (a)$$

Note that the contour coordinate  $s$  in branch 2 is defined in the negative  $y$ -direction. We compute the area  $A$ , the first area moment about the  $Y$ -axis  $Q_Y$ , and the location of the centroid as follows:

$$A = \int_{-\pi/2}^{\pi/2} t a d\theta + \int_0^{2a} t ds = (2 + \pi)at \quad Q_Y = \int_{-\pi/2}^{\pi/2} X_1 t a d\theta + \int_0^{2a} X_2 t ds = 2a^2 t \quad X_C = \frac{Q_Y}{A} = \frac{2a}{2 + \pi}. \quad (b)$$

**Solution part to (b).** The shear flow relative to the centroid is given by eq. (4.17) on page 81. For this example this shear flow function is

$$q_C(s, z) = \frac{M_{zc}(z)}{2A_c} - F_{yc}(s)V_y(z), \quad (\text{c})$$

The function  $F_{yc}(s)$  is given by eq. (4.19). For this symmetric section the product area moment  $I_{xy} = 0$ , and from eq. (4.4) on page 79 the cross-sectional coefficients  $n_x = n_y = 0$  and  $k = 1$ . Also, from eq. (4.7)  $\bar{y}(s) = y(s)$ . The function  $F_{yc}(s)$  in eq. (4.19) reduces to

$$F_{yc}(s) = \frac{1}{I_{xx}} \left[ Q_x(s) - \frac{1}{(2A_c)} \oint r_{nc}(s) Q_x(s) ds \right]. \quad (\text{d})$$

The distribution function given by eq. (4.23) in this example is simplified to

$$\bar{Q}_x = Q_x = \int_0^s y(s)t(s)ds, \quad (\text{e})$$

and the coordinate normal to the contour  $r_{nc}(s)$  in eq. (d) is given in eq. (4.10). The parametric equations of the contour with respect to the centroid are

$$\begin{aligned} x_1(\theta) &= X_1(\theta) - X_C = \frac{-2a}{2+\pi} + a \cos \theta & y_1(\theta) &= Y_1(\theta) \\ x_2(s) &= X_2(s) - X_C = \frac{-2a}{2+\pi} & y_2(s) &= Y_2(s) \end{aligned} \quad (\text{f})$$

The second area moment of the cross section about the  $x$ -axis through the centroid is

$$I_{xx} = \int_{-\pi/2}^{\pi/2} y_1^2 t a d\theta + \int_0^{2a} y_2^2 t ds = \left( \frac{4+3\pi}{6} \right) a^3 t = 2.23746 a^3 t. \quad (\text{g})$$

The distribution function about the  $x$ -axis beginning at the contour origin at  $\theta = -\pi/2$  and going counter-clockwise around the contour are determined for each branch from eq. (e) as

$$Q_{x1}(\theta) = \int_{-\pi/2}^{\theta} y_1 t a d\theta = -a^2 t \cos \theta \quad -\pi/2 \leq \theta \leq \pi/2, \text{ and} \quad (\text{h})$$

$$Q_{x2}(s) = Q_{x1}(\pi/2) + \int_0^s y_2 t ds = a t s - t \left( \frac{s^2}{2} \right) \quad 0 \leq s \leq 2a. \quad (\text{i})$$

Note that  $Q_{x2}(2a) = 0$ , since this represents the first area moment of the entire cross section about the centroidal  $x$ -axis. From eq. (4.10) the coordinates normal to the contour for each branch are

$$r_{nc1} = x_1 \left( \frac{dy_1}{ad\theta} \right) - y_1 \left( \frac{dx_1}{ad\theta} \right) = a \left( 1 - \frac{2}{2+\pi} \cos \theta \right) \quad r_{nc2} = x_2 \left( \frac{dy_2}{ds} \right) - y_2 \left( \frac{dx_2}{ds} \right) = \frac{2a}{2+\pi}. \quad (\text{j})$$

The area enclosed by the closed contour  $A_c$  is given by eq. (4.18), and we get the expected result as shown



below.

$$A_c = \int_{-\pi/2}^{\pi/2} r_{nc1} a d\theta + \int_0^{2a} r_{nc2} ds = \pi a^2 / 2. \quad (\mathbf{k})$$

Let the term containing the integral over the entire contour in eq. (d) be denoted by  $F_{yc0}$ . We compute  $F_{yc0}$  for this cross section as

$$F_{yc0} = \frac{1}{(2A_c)} \oint r_{nc}(s) Q_x(s) ds = \frac{1}{2A_c} \left( \int_{-\pi/2}^{\pi/2} r_{nc1} Q_{x1} a d\theta + \int_0^{2a} r_{nc2} Q_{x2} ds \right) = -\frac{8 + 3\pi}{3\pi(2 + \pi)} (a^2 t). \quad (\mathbf{l})$$

We now compute the shear flow distribution functions for each branch by substituting results from eqs. (h), (i), and (l) into eq. (d). The results are

$$F_{yc1} = \frac{(Q_{x1} - F_{yc0})}{I_{xx}} = \frac{1}{a} (0.16071 - 0.446935 \cos \theta), \text{ and} \quad (\mathbf{m})$$

$$F_{yc2} = \frac{(Q_{x2} - F_{yc0})}{I_{xx}} = \frac{1}{a} (0.16071 + 0.446935(s/a) - 0.223467(s/a)^2). \quad (\mathbf{n})$$

The shear flows with respect to the centroid in branch 1 and branch 2 are

$$q_{C1}(s, z) = \frac{M_{zc}(z)}{2A_c} - F_{yc1}(\theta) V_y(z) \quad q_{C2}(s, z) = \frac{M_{zc}(z)}{2A_c} - F_{yc2}(\theta) V_y(z). \quad (\mathbf{o})$$

**Solution to part (c).** The equation for the location of the shear center relative to the centroid is given in eq. (4.23). The shear modulus of the material is denoted by  $G$  in eq. (4.23), and we assume it is uniform around the contour in this example. Then the shear center relative to the centroid is

$$x_{sc} = \frac{2A_c}{\oint ds} \left[ \int_{-\pi/2}^{\pi/2} F_{yc1} a d\theta + \int_0^{2a} F_{yc2} ds \right], \text{ where } \oint ds = \int_{-\pi/2}^{\pi/2} a d\theta + \int_0^{2a} ds = (2 + \pi)a, \quad (\mathbf{p})$$

Performing the integrals for  $x_{sc}$  in eq. (p) we get

$$x_{sc} = \frac{\pi a^2 / 2}{(2 + \pi)a} \left[ \frac{16 - 2\pi}{4\pi + 3\pi^2} \right] = \frac{(16 - 2\pi)}{(2 + \pi)(4 + 3\pi)} a = 0.140773a. \quad (\mathbf{q})$$

The location of the shear center relative to point O is  $X_{SC} = X_C + x_{sc} = 0.529757a$ .

**Solution to part (d).** The shear flow relative to the shear center is given by eq. (4.25), which in this example is

$$q(s, z) = \frac{M_z(z)}{2A_c} - F_y(s) V_y(z), \quad (\mathbf{r})$$

where the shear flow distribution function relative to the shear center is given by eq. (4.26). The results for the shear flow distribution functions relative to the shear center for each branch are as follows:

$$F_{y1} = -\left(\frac{x_{sc}}{2A_c}\right) + F_{yc1} = \frac{1}{a}(0.1159 - 0.445635 \cos \theta), \text{ and} \quad (\text{s})$$

$$F_{y2} = -\left(\frac{x_{sc}}{2A_c}\right) + F_{yc2} = \frac{1}{a}\left[0.1159 + 0.446935\left(\frac{s}{a}\right) - 0.223467\left(\frac{s}{a}\right)^2\right]. \quad (\text{t})$$

Finally, from eq. (r) the shear flows in each branch are given by

$$q_1 = \frac{M_z}{2A_c} - F_{y1}V_y = \frac{M_z}{\pi a^2} - \frac{1}{a}(0.1159 - 0.445635 \cos \theta)V_y, \text{ and} \quad (\text{u})$$

$$q_2 = \frac{M_z}{2A_c} - F_{y2}V_y = \frac{M_z}{\pi a^2} - \frac{1}{a}\left[0.1159 + 0.446935\left(\frac{s}{a}\right) - 0.223467\left(\frac{s}{a}\right)^2\right]. \quad (\text{v})$$

A check on the shear flows is to compute the resultant for  $F_y$  and the resultant moment about the shear center  $C_z$ . Resolving the shear flows in the positive  $y$ -direction in each branch we compute the integrals

$$F_y = \int_{-\pi/2}^{\pi/2} q_1 \cos \theta a d\theta - \int_0^{2a} q_2 ds = V_y.$$

Thus, the resultant  $F_y$  is equal to the shear force. Note that  $q_2$  is positive in the negative  $y$ -direction. To compute the moment  $C_z$  we need the normal coordinate to the contour with respect to the shear center. From eq. (4.11) on page 80 the normal coordinates for each branch are determined by

$$r_{n1} = r_{nc1} - x_{sc}\left(\frac{dy_1}{ad\theta}\right) = a(1 - 0.529757 \cos \theta) \quad r_{n2} = r_{nc2} - x_{sc}\left(\frac{dy_2}{ds}\right) = 0.529757a. \quad (\text{w})$$

The resultant moment is

$$C_z = \int_{-\pi/2}^{\pi/2} r_{n1} q_1 a d\theta + \int_0^{2a} r_{n2} q_2 ds = M_z. \quad (\text{x})$$

The moment of the shear flows about the shear center equal the torque  $M_z$ . The shear flows in eqs. (u) and (v) are statically equivalent to the shear force  $V_y$  and the torque  $M_z$  resolved at the shear center.

**Solution to part (e).** The shear flows are plotted normal to the contour in figure 4.28. The shear flow from the torque is spatially uniform and equal to  $M_z/(2A_c)$ . The shear stress is equal to the shear flow divided by the thickness of the branch. From figure 4.28 it is apparent that the maximum magnitude of the shear stress occurs either at  $\theta = 0$  in the semicircular contour or at  $s = a$  in the vertical contour. These shear stress components are

$$\sigma_{zs1}(0) = \frac{M_z}{\pi a^2 t} + \frac{0.3297 V_y}{at} \quad \sigma_{zs2}(a) = \frac{M_z}{\pi a^2 t} - \frac{0.3394 V_y}{at}. \quad \blacksquare \quad (y)$$

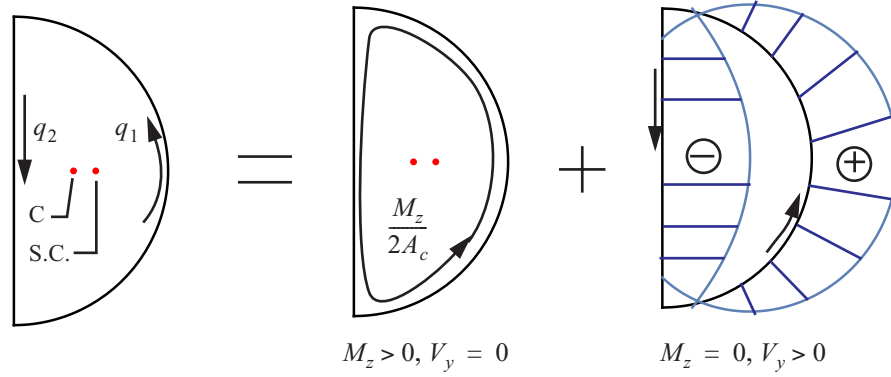
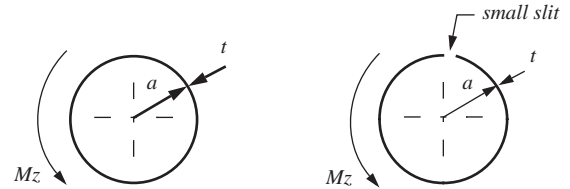


**Fig. 4.28** Shear flow distribution along the contour of the closed section shown in figure 4.27. The shear flow is the sum of a spatially uniform flow due to the torque plus a nonuniform flow due to the shear force.

#### Example 4.9 Torsional response of an open section and an equivalent closed section

A thin-walled circular tube with contour radius  $a$  and wall thickness  $t$  is subject to a torque  $M_z$ . The wall of a second identical tube is cut parallel to its longitudinal axis along its entire length to make the cross section of this second tube an open circular arc. See figure 4.29. Assume the saw kerf is very small. Compare the unit twist and maximum shear stress in the closed section to the open section.

**Fig. 4.29** Closed and open thin-walled circular sections.



**Solution.** For the closed section the shear flow  $q = \frac{M_z}{2(\pi a^2)}$  as shown in figure 4.28, and the torsion constant  $J = 2\pi a^3 t$  from eq. (3.128) on page 70. Hence the maximum shear stress and unit twist are

$$(\sigma_{zs})_{closed} = \frac{M_z}{2\pi a^2 t} \quad \left(\frac{d\theta_z}{dz}\right)_{closed} = \frac{M_z}{GJ} = \frac{M_z}{G(2\pi a^3 t)}. \quad (a)$$

For the open section the developed length  $b$  of the contour is essentially  $2\pi a$ , since the saw kerf is assumed to be very small. By the membrane analogy discussed in article 3.9.1 on page 63, the torsional response is the same as the thin-walled rectangular section of length  $b$  and thickness  $t$ . The maximum shear stress is given by eq. (3.129) on page 63, and the torsion constant is given in eq. (3.128). For  $b = 2\pi a$ , we have

$$(\sigma_{zs})_{open} = \frac{3M_z}{2\pi at^2} \quad \left(\frac{d\theta_z}{dz}\right)_{open} = \frac{M_z}{G\left(\frac{1}{3}2\pi at^3\right)} \quad (b)$$

Forming the ratio of the maximum shear stress of the open section to the closed section we find

$$\frac{(\sigma_{zs})_{open}}{(\sigma_{zs})_{closed}} = \frac{3M_z}{2\pi at^2} \cdot \frac{2\pi a^2 t}{M_z} = 3\frac{a}{t} \gg 1. \quad (c)$$

Likewise, the ratio of the unit twists are

$$\frac{(d\theta_z/dz)_{open}}{(d\theta_z/dz)_{closed}} = \frac{3M_z}{G2\pi at^3} \cdot \frac{G2\pi a^3 t}{M_z} = 3\left(\frac{a}{t}\right)^2 \gg 1. \quad (d)$$

Since the ratio of the radius to thickness is greater than ten for a thin-walled section, the above results show that the shear stress (c) and unit twist (d) of the open circular section are much larger than for the closed section if both sections are subject to the same torque.

Hence, if a bar is to resist torsional loading, a closed section is preferable to an equivalent open section bar. That is, the unit twist is smaller for the closed section bar (it is stiffer), and the maximum shear stress is smaller, than for the equivalent open section bar subject to the same torque. ■

#### 4.4.1 Resultant of uniform shear flow

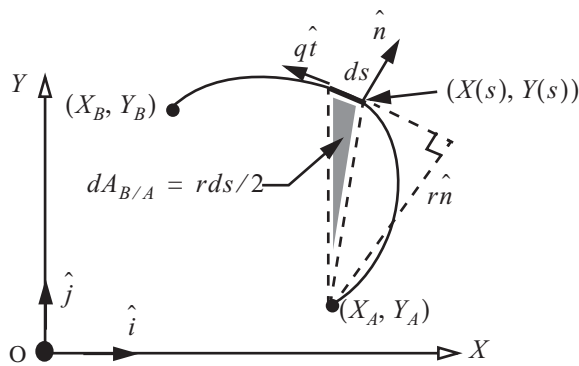


**Fig. 4.30 A constant shear flow in a curved branch.**

In torsion problems it is often necessary to find the resultant of a constant shear flow along the contour of a curved branch. This situation is depicted in figure 4.30, where the curved branch begins at point A with coordinates  $(X_A, Y_A)$  and ends at point B with coordinates  $(X_B, Y_B)$ . The resultant of the shear flow is resolved at point A in this figure.

The sense of the arc-length  $s$  and the shear flow  $q$  are assumed positive from A to B along the contour of the branch. The shear flow acts tangent to the contour, and the unit tangent vector to the contour is denoted by  $\hat{t}(s)$ . The unit tangent vector is given by eq. (3.4) on page 33, where we note that  $dX/ds = dx/ds$  and  $dY/ds = dy/ds$ . The differential force obtained from

the shear flow is

$$d\vec{F} = qds\hat{t} = qds\left[\left(\frac{dX}{ds}\right)\hat{i} + \left(\frac{dY}{ds}\right)\hat{j}\right] = q[(dX)\hat{i} + (dY)\hat{j}]. \quad (4.52)$$

Integrate eq. (4.52) from point A to point B on the contour to get

$$\vec{F} = q \left[ \int_A^B (dX\hat{i} + dY\hat{j}) \right] = q[(X_B - X_A)\hat{i} + (Y_B - Y_A)\hat{j}] = (qL_{B/A})\hat{u}_{B/A}, \quad (4.53)$$

where the length of the chord connecting the ends of contour is denoted by  $L_{B/A}$ . The length of the chord and the unit vector  $\hat{u}_{B/A}$  are given by

$$L_{B/A} = \sqrt{(X_B - X_A)^2 + (Y_B - Y_A)^2} \quad \hat{u}_{B/A} = \frac{(X_B - X_A)}{L_{B/A}}\hat{i} + \frac{(Y_B - Y_A)}{L_{B/A}}\hat{j}. \quad (4.54)$$

The differential torque about point A is

$$d\vec{M}_A = r(s)\hat{n}(s) \times qds\hat{k} = qr(s)ds\hat{k}, \quad (4.55)$$

where the position vector from point A to the line of action of the shear flow is  $r(s)\hat{n}(s)$ , and  $\hat{n}(s)$  is the unit vector normal to the contour at  $s$ . The product of  $r$  times  $ds$  is twice the enclosed area of the triangle with base  $ds$  and height  $r$ . As shown in figure 4.30  $r(s)ds = 2dA_{B/A}$ . Integrate eq. (4.55) from point A to point B to get

$$\vec{M}_A = q \int_A^B r(s)ds\hat{k} = q \int_A^B 2dA_{B/A}\hat{k} = 2qA_{B/A}\hat{k}. \quad (4.56)$$

The area between the contour and the chord is denoted by  $A_{B/A}$ . The force and torque resolved at point A is shown in figure 4.31(a). The force and torque at point A are statically equivalent to the force acting along a line of action that is parallel to the chord at a perpendicular distance  $e$  from the chord. The distance is determined from

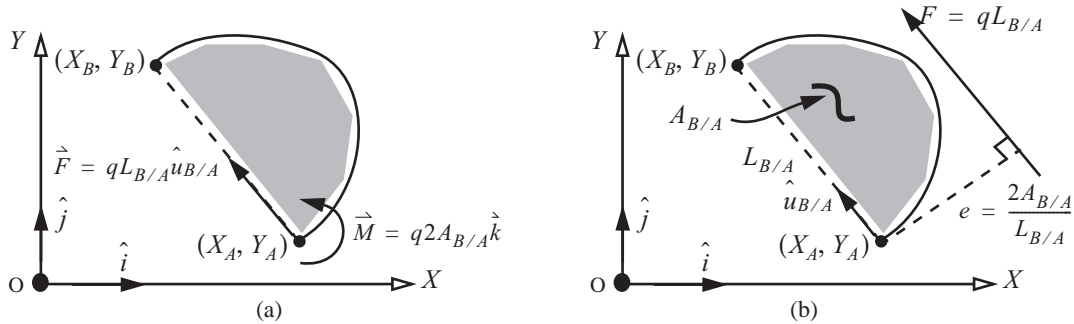


**Fig. 4.31 (a) The force and torque due to a constant shear flow resolved at point A. (b) The resultant of a constant shear flow is a force parallel to the chord at distance  $e$  from it.**

$M_A = eF = eqL_{A/B}$ . Solve for  $e$  and substitute  $2qA_{B/A}$  for the torque to get

$$e = \frac{M_A}{qL_{B/A}} = \frac{2qA_{B/A}}{qL_{B/A}}, \text{ or } e = \frac{2A_{B/A}}{L_{B/A}}. \quad (4.57)$$

The resultant of a constant shear flow is shown in figure 4.31(b).

Now consider a continuous contour that does not intersect itself except that point B coincides with point A as shown in figure 4.32. Since  $L_{B/A} = 0$  in eq. (4.53) the force  $\vec{F} = 0$ . For a closed contour let  $A_{B/A} = A_c$  and

$M_A = M_z$  in eq. (4.56). For a single-cell cross section subject to a torque  $M_z$  and no shear forces (pure torsion), the shear flow is given by

$$q = \frac{M_z}{2A_c}. \quad (4.58)$$

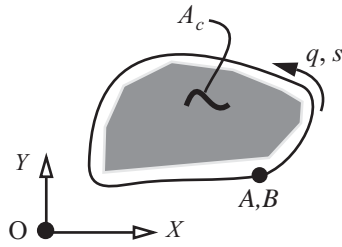


**Fig. 4.32** Constant shear flow on a closed contour of arbitrary shape.

Equation (4.58) is called **Bredt's formula**. (Also see eq. (3.165) on page 70.)

A constant shear flow in a closed contour is statically equivalent to a torque, and this torque is the same for any point in the plane about which moments are computed. The fact that the torque is a “free vector” is depicted in figure 4.33, in which it is shown that some of the enclosed area used in Bredt's formula can add as a negative quantity if the torque produced by the constant shear flow is clockwise over a segment of the branch. About point O in this figure, the torque produced by the shear flow from point B to A in the right half of the contour is counterclockwise, and the torque produced by the shear flow from A to B in the left half is clockwise.

Hence, the total torque is the sum of these two torques with due respect to the sign. This summation shows that the total torque is proportional to the area enclosed by the contour.

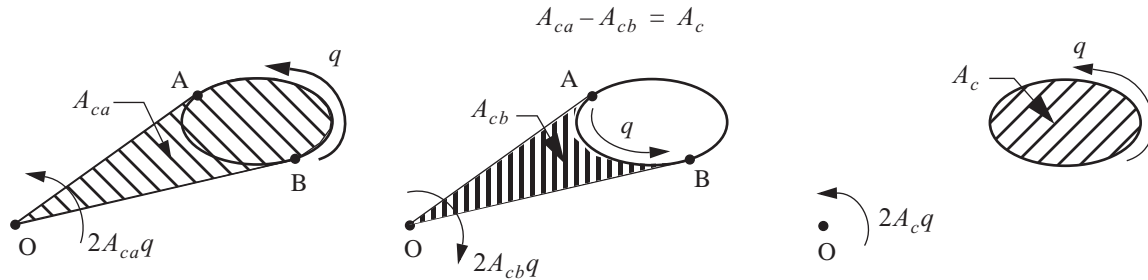


**Fig. 4.33** The torque about an arbitrary point O of a constant shear flow in a closed contour is twice the enclosed area of the circuit times the shear flow.

#### 4.4.2 Torsion of a hybrid section

Consider a hybrid section composed of a single closed cell and open branches, or fins, as shown in figure 4.34. The total torque carried by the section is the sum of the torques carried by the closed cell and open branches. For  $n$  open branches, we have

$$M_z = (M_z)_{closed} + \sum_{i=1}^n (M_z)_i, \quad (4.59)$$

where

$$(M_z)_{closed} = (GJ)_{closed} \left( \frac{d\phi_z}{dz} \right) \text{ and } (M_z)_i = (GJ)_i \left( \frac{d\phi_z}{dz} \right). \quad (4.60)$$

The torsional stiffness for the closed cell is

$$(GJ)_{closed} = \frac{4A_c^2}{\oint \frac{ds}{Gt}}, \quad (4.61)$$

and for each open branch the torsional stiffness is

$$(GJ)_i = G_i \left( \frac{1}{3} b_i t_i^3 \right). \quad (4.62)$$

Combining eqs. (4.59) and (4.60), we have

$$M_z = \left[ (GJ)_{closed} + \sum_{i=1}^n (GJ)_i \right] \frac{d\phi_z}{dz}. \quad (4.63)$$

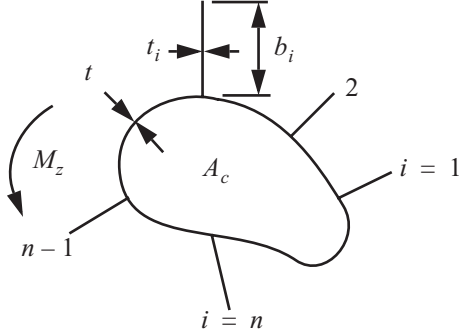


Fig. 4.34 Torsion of a hybrid section.

Comparing eq. (4.63) to the standard torsional formula

$M_z = (GJ)_{eff} \left( \frac{d\phi_z}{dz} \right)$ , the effective torsional stiffness for the entire section is

$$(GJ)_{eff} = (GJ)_{closed} + \sum_{i=1}^n (GJ)_i. \quad (4.64)$$

where the closed and open parts of the torsional stiffness are given by eqs. (4.61) and (4.62).

The shear stress in the closed cell is  $(\sigma_{zs})_{closed} = (M_z)_{closed} / (2A_c t)$ , where the portion of the torque carried by the closed cell is  $(M_z)_{closed} = (GJ)_{closed} (d\phi_z / dz)$ . The unit twist is given by  $(d\phi_z / dz) = M_z / (GJ)_{eff}$ . Combining these results, the shear stress in the closed cell is

$$(\sigma_{zs})_{closed} = \frac{(GJ)_{closed}}{(GJ)_{eff}} \cdot \frac{M_z}{2A_c t} \quad (4.65)$$

The shear stress in open branches is given by

$$(\sigma_{zs}|_{\max})_i = \frac{3M_{zi}}{b_i t_i^2}, \quad (4.66)$$

which was derived as eq. (3.132) on page 64. Substitute the second equation in (4.60) for the torque carried by the branch, and then substitute eq. (4.62) for the torsional stiffness of the branch, to write the shear stress as

$$(\sigma_{zs})_i = \frac{3(M_z)_i}{b_i t_i^2} = \frac{3}{b_i t_i^2} \cdot \left( G_i \frac{1}{3} b_i t_i^3 \right) \frac{d\phi_z}{dz}. \quad (4.67)$$

Substitute  $\frac{d\phi_z}{dz} = \frac{M_z}{(GJ)_{eff}}$  for the unit twist in eq. (4.67) to get

$$(\sigma_{zs})_i = \frac{G_i t_i}{(GJ)_{eff}} M_z. \quad (4.68)$$

If the shear modulus is the same in all branches, then eqs. (4.65) and (4.68) reduce to

$$(\sigma_{zs})_{closed} = \frac{J_{closed}}{J_{eff}} \cdot \frac{M_z}{2A_c t} \quad (\sigma_{zs})_i = \frac{t_i M_z}{J_{eff}}, \quad (4.69)$$

$$\text{where } J_{eff} = J_{closed} + \sum_{i=1}^n J_i.$$

#### Example 4.10 Torsion of a closed cross section composed of two cells

In multicell cross sections subject to pure torsion the shear flow is constant in each branch. In general the shear flows are different from branch to branch. Consider a cross section consisting of two cells with a horizontal axis of symmetry shown in figure 4.35. It is subject to a torque  $M_z$ . Cell 1 is enclosed by a semicircular exterior web

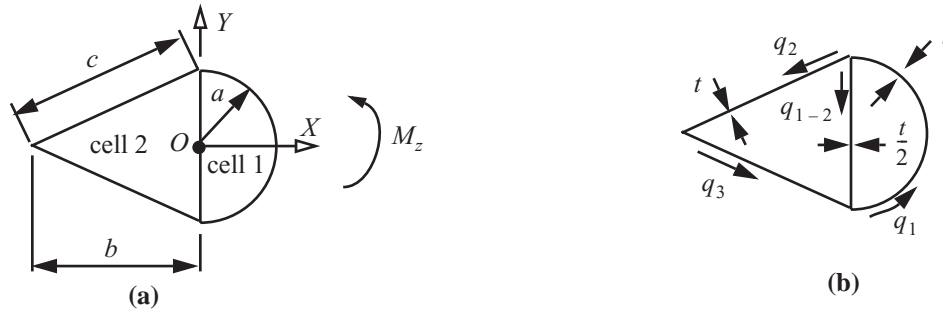


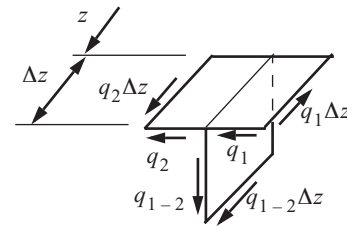
**Fig. 4.35 (a) Cross section composed of two cells and subject to pure torsion. (b) Shear flows and web thicknesses.**

of radius  $a$ , and a vertical web of length  $2a$ , which is common with cell 2. Cell 2 is enclosed by an isosceles triangle with equal exterior webs of length  $c$  and the common web of length  $2a$ . Take  $a = 5$  in.,  $b = 12$  in., and  $c = 13$  in. The thickness of the exterior webs  $t = 0.040$  in., and the thickness of the common web is  $t/2$ . The contour is composed of four branches. Branch 1 is the semicircular web with the contour coordinate denoted by  $s_1$ , branch 2 is the upper exterior straight web of cell 2 with contour coordinate  $s_2$ , branch 3 is the lower exterior straight web of cell 2 with contour coordinate  $s_3$ , and branch 4 is the vertical common web between cells with the contour coordinate denoted by  $s_{1-2}$ . The Cartesian coordinate system  $X-Y$  has its origin at point O, the center of the semicircular web. The  $X$ -axis is the axis of symmetry.

A free body diagram of the junction between branches 1, 2, and 1-2 is shown in figure 4.36. The sum of forces in the axial direction is  $q_{1-2}\Delta z + q_2\Delta z - q_1\Delta z = 0$ , Hence, axial equilibrium per unit  $z$ -length determines the shear flow in the common web as

$$q_{1-2} = q_1 - q_2. \quad (a)$$

**Fig. 4.36 Free body diagram of the junction between branches 1, 2, and 1-2.**





A simple rule to determine the axial equilibrium of the junction is to observe that the shear flow into the junction must equal the shear flow out of the junction. At the junction of branches 2 and 3 this rule results in  $q_3 = q_2$ . At the junction of branches 3, 1-2, and 1 the rule gives  $q_{1-2} + q_3 - q_1 = 0$ , but  $q_3 = q_2$ , which leads us to the same relation given by eq. (a). We started with four unknown shear flows  $q_1$ ,  $q_2$ ,  $q_3$ , and  $q_{1-2}$ . Axial equilibrium at the three junctions results in two relations between the four shear flows. Two shear flows remain unknown, say  $q_1$  and  $q_2$ , at this point in the analysis.

The remaining equation of static equivalence is to equate the torque due to the shear flows to  $M_z$ . The constant shear flows in each branch are shown in figure 4.37(a), and the resultants of these shear flows are determined by the analysis presented in article 4.4.1. As shown in figure 4.37(b) the resultant of the shear flow  $q_1$  in branch 1 is a vertical upward force of magnitude  $2aq_1$ , the resultant of the shear flow  $q_2$  in branches 2 and 3 is a vertical downward force of magnitude  $2aq_2$ , and the resultant of the shear flow in the common branch is a downward force of magnitude  $2a(q_1 - q_2)$ . The locations of the lines of action of the force resultants with respect to the common branch are also shown in figure 4.37(b). The vertical force  $F$  shown in figure 4.37(c) is determined from the branch forces by equilibrium. The result is

$$F = 2aq_1 - 2aq_2 - 2a(q_1 - q_2) = 0. \quad (b)$$

Take the moment of the branch forces in figure 4.37(b) about the common web to determine the torque  $M_z$  shown in figure 4.37(c). The result for static equivalence of the torque is

$$\begin{aligned} \left(\frac{2A_{c1}}{2a}\right)2aq_1 + \left(\frac{2A_{c2}}{2a}\right)2aq_2 &= M_z, \text{ or} \\ 2A_{c1}q_1 + 2A_{c2}q_2 &= M_z. \end{aligned} \quad (4.70)$$

Equation (4.70) is the extension of Bredt's formula in eq. (4.58) to two cells.

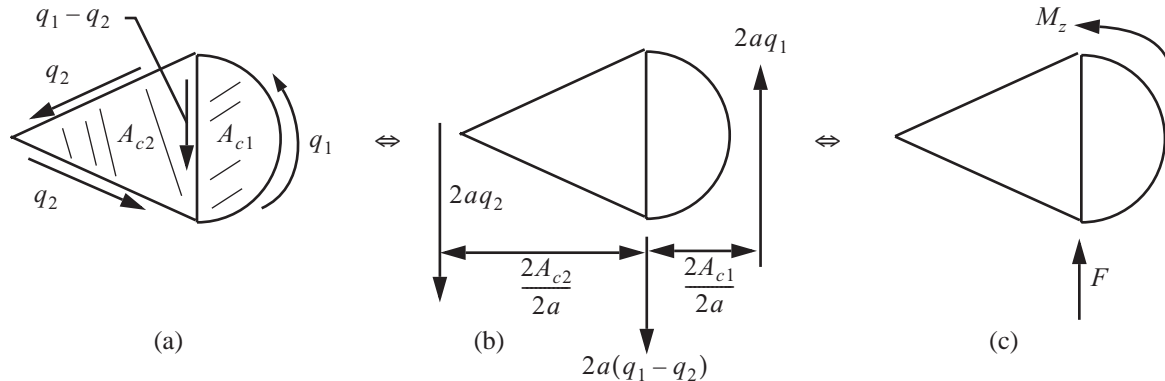


**Fig. 4.37 (a) Shear flows. (b) Statically equivalent branch forces. (c) Cross section resultant.**

We have used all the conditions of static equivalence, but the two shear flows  $q_1$  and  $q_2$  remain unknown. An additional equation relating the shear flows is based on the assumed rigidity of the cross section in its own plane. In torsion, this rigid cross section condition implies the unit twist of each cell is the same. The unit twist for a sin-

gle cell is given by eq. (4.20) on page 81. Since the shear modulus is the same for all branches in the cross section eq. (4.20) reduces to

$$\frac{d\phi_z}{dz} = \frac{1}{2A_c G} \oint \frac{q}{t} ds. \quad (4.71)$$

This unit twist formula was derived on the basis that a counterclockwise shear flow tends to produce a counterclockwise unit twist. Apply this equation to cell 1 to get

$$\left(\frac{d\phi_z}{dz}\right)_1 = \frac{1}{2A_{c1}G} \left[ \left(\frac{\pi a}{t}\right) q_1 + \left(\frac{2a}{t/2}\right) (q_1 - q_2) \right]. \quad (c)$$

For cell 2, the unit twist is

$$\left(\frac{d\phi_z}{dz}\right)_2 = \frac{1}{2A_{c2}G} \left[ \left(\frac{2c}{t}\right) q_2 - \left(\frac{2a}{t/2}\right) (q_1 - q_2) \right]. \quad (d)$$

Note that the contribution of the common branch shear flow is negative in the unit twist formula for cell 2. Relative to an observer in cell 2, a positive value for the shear flow  $q_{1-2}$  tends to produce a clockwise unit twist, and hence is negative by the convention that counterclockwise is positive. Since the unit twist of each cell is the same, we equate eqs. (c) and (d) to get

$$\frac{1}{A_{c1}} \left[ \left(\frac{2a}{t}\right) q_1 + \left(\frac{2a}{t/2}\right) (q_1 - q_2) \right] = \frac{1}{A_{c2}} \left[ \left(\frac{2c}{t}\right) q_2 - \left(\frac{2a}{t/2}\right) (q_1 - q_2) \right]. \quad (e)$$

After some algebraic manipulations eq. (e) is written in the form

$$\left[ \frac{4a + a\pi}{A_{c1}t} + \frac{4a}{A_{c2}t} \right] q_1 - \left[ \frac{4a}{A_{c1}t} + \frac{4a + 2c}{A_{c2}t} \right] q_2 = 0. \quad (f)$$

The enclosed areas of each cell are  $A_{c1} = \pi a^2$ , and  $A_{c2} = \frac{1}{2}b2a = ba$ . Numerical evaluations of eqs. (4.70) and (f) are

$$\begin{aligned} (50\pi \text{ in.}^2) q_1 + (120 \text{ in.}^2) q_2 &= M_z \\ (19.6995 \text{ in.}^2) q_1 - (25.5329 \text{ in.}^2) q_2 &= 0 \end{aligned} \quad (g)$$

The solutions of the two equations in (g) for the shear flows are

$$q_1 = (4.00538 \times 10^{-3} \text{ in.}^{-2}) M_z \quad q_2 = (3.00903 \times 10^{-3} \text{ in.}^{-2}) M_z \quad q_{1-2} = (0.915085 \times 10^{-3} \text{ in.}^{-2}) M_z. \quad (h)$$

The shear stresses in each branch are obtained from  $(\sigma_{zs})_1 = q_1/t$ ,  $(\sigma_{zs})_2 = q_2/t$ , and

$(\sigma_{zs})_{1-2} = q_{1-2}/(t/2)$ . The results are

$$(\sigma_{zs})_1 = (0.100135 \text{ in.}^{-3}) M_z \quad (\sigma_{zs})_2 = (0.0772575 \text{ in.}^{-3}) M_z \quad (\sigma_{zs})_{1-2} = (0.0457542 \text{ in.}^{-3}) M_z. \quad (i)$$

The twist per unit length for the entire cross section is obtained from either eq. (c) or eq. (d). For the shear flows given in eq. (h) the evaluation of unit twist is

$$\frac{d\phi_z}{dz} = \left(\frac{d\phi_z}{dz}\right)_1 = \left(\frac{d\phi_z}{dz}\right)_2 = (0.0129263 \text{ in.}^{-4})(M_z/G). \quad (\text{j})$$

Finally, we compute the torsion constant  $J$  by the following relation

$$J = \frac{M_z}{G\left(\frac{d\phi_z}{dz}\right)} = 77.3619 \text{ in.}^4 \quad (\text{k})$$

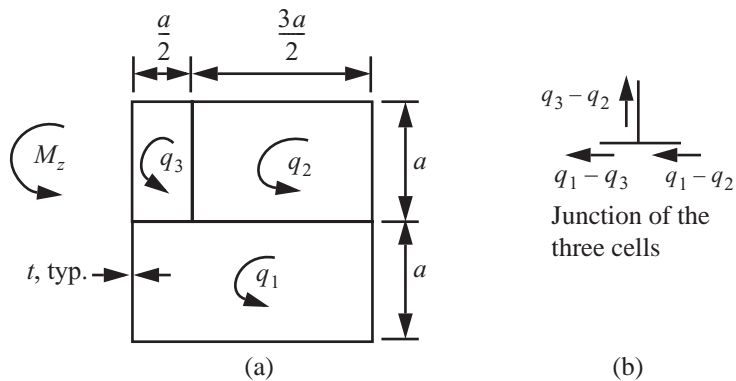
#### Example 4.11 Torsion of a closed section with three cells; circuit shear flow

Consider the cross section composed of three cells shown in figure 4.38(a). All branches have the same thickness  $t$  and shear modulus  $G$ . It is convenient to define **circuit shear flows** in each cell. Circuit shear flows are assumed to be positive counterclockwise in each cell and are equal to the actual shear flows in the exterior branches of the cell, if there are any exterior branches. However, the shear flow in a common branch between cells is the difference between the circuit shear flows sharing the common branch. At the junction of the three branches shown in figure 4.38(b) the shear flow into the junction is  $q_1 - q_2$ , and this equals the shear flow out of the junction, which is  $(q_1 - q_3) + (q_3 - q_2)$ . The method of defining circuit shear flows automatically satisfies axial equilibrium at the junction.

For an applied torque  $M_z$ , determine

- shear flows  $q_1$ ,  $q_2$ , and  $q_3$ ,
- the torsion constant  $J$ , and
- magnitude of the torque at the initiation of yielding.

**Fig. 4.38** (a) Circuit shear flows in the three-cell cross section. (b) Circuit shear flows at the junction of the three cells.



**Solution.** Bredt's formula for the section composed of two cells in eq. (4.70) is extended to three cells in this example to get

$$2A_{c1}q_1 + 2A_{c2}q_2 + 2A_{c3}q_3 = M_z. \quad (\text{a})$$

The areas enclosed by cells are

$$A_{c1} = 2a^2 \quad A_{c2} = 3a^2/2 \quad A_{c3} = a^2/2. \quad (\text{b})$$

From eq. (4.71) the twist per unit length for this example reduces to

$$\frac{d\phi_z}{dz} = \frac{1}{2A_c G t} \oint q ds = \frac{1}{2A_c G t} \sum \Delta s q. \quad (\text{c})$$

We apply eq.(c) to each cell and note that a shear flow is positive counterclockwise consistent with a positive counterclockwise unit twist. The results for each cell are as follows.

$$\left(\frac{d\phi_z}{dz}\right)_1 = \frac{1}{2A_{c1} G t} \left[ 4aq_1 + \frac{3a}{2}(q_1 - q_2) + \frac{a}{2}(q_1 - q_3) \right] \quad (\text{d})$$

$$\left(\frac{d\phi_z}{dz}\right)_2 = \frac{1}{2A_{c2} G t} \left[ \frac{5a}{2}q_2 + a(q_2 - q_3) + \frac{a}{2}(q_2 - q_1) \right] \quad (\text{e})$$

$$\left(\frac{d\phi_z}{dz}\right)_3 = \frac{1}{2A_{c3} G t} \left[ \frac{3a}{2}q_3 + \frac{a}{2}(q_3 - q_1) + a(q_3 - q_2) \right]. \quad (\text{f})$$

Since the cross section is assumed to be rigid in its own plane, the unit twist of each cell must be the same. This kinematic condition can be written between cells 1 and 2 as

$$\left(\frac{d\phi_z}{dz}\right)_1 - \left(\frac{d\phi_z}{dz}\right)_2 = 0. \quad (\text{g})$$

Evaluation of eq. (g) leads to

$$\frac{48q_1 - 49q_2 + 5q_3}{24Gat} = 0. \quad (\text{h})$$

Compatibility of the unit twist between cells 2 and 3 is

$$\left(\frac{d\phi_z}{dz}\right)_2 - \left(\frac{d\phi_z}{dz}\right)_3 = 0. \quad (\text{i})$$

Evaluation of eq. (i) leads to

$$\frac{2(4q_2 - 5q_3)}{3Gat} = 0. \quad (\text{j})$$

Solve eqs. (a), (h), and (j) for the shear flows to find

$$q_1 = \frac{75}{604} \frac{M_z}{a^2} \quad q_2 = \frac{20}{151} \frac{M_z}{a^2} \quad q_3 = \frac{16}{151} \frac{M_z}{a^2}. \quad (\text{k})$$

The unit twist of the section can be determined by substituting the shear flows (k) into any one of the eqs. (d), (e), or (f). The unit twist is

$$\frac{d\phi_z}{dz} = \frac{149}{1208Ga^3t} M_z. \quad (\text{l})$$

Compare this to the standard formula  $\frac{d\phi_z}{dz} = \frac{M_z}{GJ}$  to find to find the torsion constant  $J$ .

$$J = \frac{1208a^3t}{149}. \quad (\text{m})$$

The shear flows in the common branches are

$$\{(q_1 - q_2), (q_1 - q_3), (q_3 - q_2)\} = \{-0.0083, 0.0182, -0.0265\}(M_z/a^2). \quad (\text{n})$$

The magnitude of the largest shear flow is in the exterior branches of cell 2, which is also the location of the maximum shear stress. The maximum shear stress is

$$(\sigma_{zs})_{\max} = q_2/t = 0.13245M_z/(a^2t). \quad (\text{o})$$

According to von Mises criterion (4.31) yield initiates at  $\sqrt{3}(\sigma_{zs})_{\max} = \sigma_{\text{yield}}$ , so the magnitude of the torque at the initiation of yielding is

$$|M_z|_{\max} = 4.359(a^2t\sigma_{\text{yield}}). \quad (\text{p})$$

If all the common branches were removed to make the section shown in figure 4.38(a) a single-cell, square section  $2a$  by  $2a$ , then from eq. (3.161) on page 70 the torsion constant is

$$J|_{\text{single cell}} = \frac{4A_c^2}{\oint \frac{ds}{t}} = \frac{4(4a^2)^2}{\frac{8a}{t}} = 8a^3t. \quad (\text{q})$$

For this example, subdividing the single-cell section into three cells shown in figure 4.38(a) increases the torsional stiffness (m) by only 1.32 percent with respect to the single-cell section, while the weight of the three-cell section increases by 37.5 percent with respect to the weight of the single-cell section. However, a multicell section may be required for improved **damage tolerance**; i.e., if we modeled damage as a longitudinal fracture, or cut, of an exterior branch, then the loss of torsional stiffness of the single-cell would be substantial since it becomes an open section. Damage to an exterior branch of a multicell section on the other hand results in less of a reduction in torsional load carrying capability since some closed cells remain intact to carry the torsional load. ■

#### Example 4.12 Transverse bending of a two-cell cross section

Consider the cross section of example 4.10 on page 114 subject to a shear force  $V_y$  with  $V_x = M_z = 0$ . There are two cells with a horizontal axis of symmetry as shown in figure 4.39. I. Cell 1 is enclosed by a semicircular

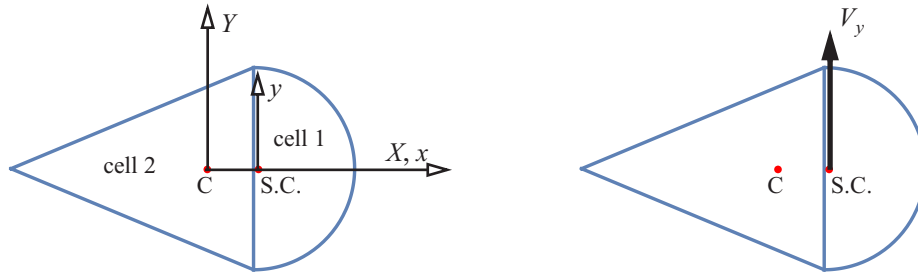


Fig. 4.39 Closed cross section consisting of two cells subject to transverse bending

exterior web of radius  $a$ , and a vertical web of length  $2a$ , which is common with cell 2. Cell 2 is enclosed by an isosceles triangle with equal exterior webs of length  $c$  and the common web of length  $2a$ . Take  $a = 5$  in.,  $b = 12$  in., and  $c = 13$  in. The thickness of the exterior webs  $t = 0.040$  in., and the thickness of the common web is  $t/2$ . The contour is composed of four branches. Branch 1 is the semicircular web with the contour coordinate denoted by  $s_1$ , branch 2 is the upper exterior straight web of cell 2 with contour coordinate  $s_2$ , branch 3 is the lower exterior straight web of cell 2 with contour coordinate  $s_3$ , and branch 4 is the vertical common web between cells with the contour coordinate denoted by  $s_{1-2}$ . The Cartesian coordinate system  $X$ - $Y$  has its origin at point  $O$ , the center of the semicircular web. The  $X$ -axis is the axis of symmetry. The Cartesian coordinates of each branch as a function of the contour coordinate are listed in table 4.5.

**Table 4.5 Parametric equations of the contour**

$i^{th}$ branch	$X_i(s) =$	$Y_i(s) =$	Range
$i = 1$	$a \sin(s_1/a)$	$-a \cos(s_1/a)$	$0 \leq s_1 \leq a\pi$
$i = 2$	$-b(s_2/c)$	$a(1 - s_2/c)$	$0 \leq s_2 \leq c$
$i = 3$	$-b(1 - s_3/c)$	$-a(s_3/c)$	$0 \leq s_3 \leq c$
$i = 1-2$	$0$	$a - s_{1-2}$	$0 \leq s_{1-2} \leq 2a$

The cross-sectional area  $A$ , first area moment  $Q_Y$ , and location of the centroid  $X_c$  are computed as follows:

$$A = \int_0^{a\pi} t ds_1 + \int_0^c t ds_2 + \int_0^c t ds_3 + \int_0^{2a} (t/2) ds_{1-2} = (a\pi + 2c + a)t = 1.86832 \text{ in.}^2 \quad (\text{a})$$

$$Q_Y = \int_0^{a\pi} X_1 t ds_1 + \int_0^c X_2 t ds_2 + \int_0^c X_3 t ds_3 + \int_0^{2a} X_{12} (t/2) ds_{1-2} = (2a^2 - bc)t = -4.24 \text{ in.}^3 \quad (\text{b})$$

$$X_c = Q_Y/A = -2.26942 \text{ in.} \quad (\text{c})$$

Symmetry about  $X$ -axis results in  $Q_X = 0$ , so that  $Y_c = 0$ . The Cartesian coordinates of the branches with respect to the centroid are  $x_i(s_i) = X_i(s_i) - X_c$ , and  $y_i(s_i) = Y_i(s_i)$ ,  $i = 1, 2, 3, 1-2$ . The second area moment about the  $x$ -axis is

$$I_{xx} = \int_0^{a\pi} y_1^2 t ds_1 + \int_0^c y_2^2 t ds_2 + \int_0^c y_3^2 t ds_3 + \int_0^{2a} y_{12}^2 (t/2) ds_{1-2} = \frac{\pi a^3 t}{2} + \frac{2a^2 c t}{3} + \frac{a^3 t}{3} = 18.1873 \text{ in.}^4. \quad (\text{d})$$

The shear flow is given by eq. (4.15) on page 81, and it is repeated as eq. (e) below.

$$q(s, z) = q_0(z) - \frac{k}{I_{yy}} V_x \overline{Q}_y(s) - \frac{k}{I_{xx}} V_y \overline{Q}_x(s). \quad (\text{e})$$

In this example the product area moment  $I_{xy} = 0$ . From eq. (4.4) cross-sectional coefficients  $n_x = n_y = 0$  and

$k = 1$ . The distribution function defined in eq. (4.9) simplifies to  $\bar{Q}_x(s) = Q_x(s)$  since  $\bar{y}(s) = y(s)$ . Hence, the shear flow equation in the  $i$ -th branch reduces to the form

$$q_i(s_i) = q_{0i} - (V_y/I_{xx})Q_{xi}(s_i). \quad (\text{f})$$

At the contour origin of the  $i$ -th branch where  $s_i = 0$  the shear flow in eq. (f) is denoted by  $q_{0i}$ , and the distribution function is given by

$$Q_{xi}(s_i) = \int_0^{s_i} y_i(s_i) t_i ds_i \quad i = 1, 2, 3, 1-2. \quad (\text{g})$$

Axial equilibrium per unit  $z$ -length at the three junctions connecting the branches leads to

$$q_1(a\pi) = q_{02} + q_{012} \quad q_2(c) = q_{03} \quad q_{1-2}(2a) + q_3(c) = q_{01}. \quad (\text{h})$$

The shear flows acting at the three junctions are shown in figure 4.40. We use the first two expressions in eq. (h) to eliminate  $q_{012}$  and  $q_{03}$ . After computing the first area moment functions, the shear flows are as follows:

$$q_1(s_1) = q_{01} + (V_y/I_{xx})a^2 t \sin(s_1/a) \quad (\text{i})$$

$$q_2(s_2) = q_{02} - (V_y/I_{xx}) \left[ ats_2 - \frac{ats_2^2}{2c} \right] \quad (\text{j})$$

$$q_3(s_3) = q_{02} - (V_y/I_{xx}) \left[ \frac{act}{2} - \frac{ats_3^2}{2c} \right] \quad (\text{k})$$

$$q_{1-2}(s_{1-2}) = q_{01} - q_{02} - (V_y/I_{xx}) \left[ \frac{ats_{1-2}}{2} - \frac{ts_{1-2}^2}{4} \right]. \quad (\text{l})$$

Note: If eqs. (k) and (l) are substituted into the third junction condition of eq. (h), then we obtain the identity  $q_{01} = q_{01}$ . Hence, the shear flows from the axial equilibrium conditions contain two unknowns  $q_{01}$  and  $q_{02}$ .

The resultant force acting on the section from the shear flows is given by the general relation

$$F_X \hat{i} + F_Y \hat{j} = \int_c \hat{q} t ds = \left[ \int_c q \frac{dx}{ds} ds \right] \hat{i} + \left[ \int_c q \frac{dy}{ds} ds \right] \hat{j}. \quad (\text{m})$$

Evaluation of the resultant forces gives

$$F_X = \int_0^{a\pi} q_1 \left( \frac{dx_1}{ds_1} \right) ds_1 + \int_0^c q_2 \left( \frac{dx_2}{ds_2} \right) ds_2 + \int_0^c q_3 \left( \frac{dx_3}{ds_3} \right) ds_3 + \int_0^{2a} q_{1-2} \left( \frac{dx_{12}}{ds_{12}} \right) ds_{1-2} = 0, \text{ and} \quad (\text{n})$$

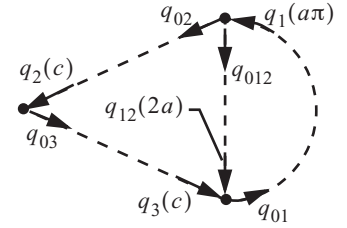


**Fig. 4.40 Junction shear flows.**

$$F_Y = \int_0^{a\pi} q_1 \left( \frac{dy_1}{ds_1} \right) ds_1 + \int_0^c q_2 \left( \frac{dy_2}{ds_2} \right) ds_2 + \int_0^c q_3 \left( \frac{dy_3}{ds_3} \right) ds_3 + \int_0^{2a} q_{1-2} \left( \frac{dy_{12}}{ds_{12}} \right) ds_{1-2} = V_y. \quad (\text{o})$$

The shear flow is statically equivalent to the shear force, as expected. No new information to determine  $q_{01}$  and  $q_{02}$  is obtained. The shear force acting at the shear center implies the twist per unit axial length of the cross section vanishes. This condition leads to two equations governing the shear flows in each cell. For a uniform shear modulus the twist per unit length is

$$\frac{d\phi_z}{dz} = \frac{1}{2A_c G} \oint_t q ds. \quad (\text{p})$$

Evaluate the twist per unit length for each cell and equate them to zero:

$$\left( \frac{d\phi_z}{dz} \right)_{\text{cell 1}} = 0 \rightarrow \frac{1}{t} \int_0^{a\pi} q_1 ds_1 + \frac{2}{t} \int_0^{2a} q_{1-2} ds_{1-2} = 0 \quad (\text{q})$$

$$\left( \frac{d\phi_z}{dz} \right)_{\text{cell 2}} = 0 \rightarrow \frac{1}{t} \int_0^c q_2 ds_2 + \frac{1}{t} \int_0^c q_3 ds_3 + \frac{2}{t} \int_{2a}^0 q_{1-2} ds_{1-2} = 0 \quad (\text{r})$$

Evaluation of eqs. (q) and (r), respectively, results in

$$\frac{a}{t}(4 + \pi)q_{01} - \frac{4a}{t}q_{02} + \frac{4a^3}{3I_{xx}}V_y = 0, \text{ and} \quad (\text{s})$$

$$-\frac{4a}{t}q_{01} + \frac{2(2a + c)}{t}q_{02} - \frac{2ab^2}{3I_{xx}}V_y = 0. \quad (\text{t})$$

Solve eqs. (s) and (t) for the shear flows  $q_{01}$  and  $q_{02}$  to get

$$q_{01} = \frac{-4at(3a^2 + ac - c^2)}{(4c + 2a\pi + c\pi)} \frac{V_y}{3I_{xx}} = (3.42199 \times 10^{-3} \text{ in.}^{-1})V_y, \text{ and} \quad (\text{u})$$

$$q_{02} = \frac{-t(12a^3 - 4ac^2 + a^3\pi - ac^2\pi)}{(4c + 2a\pi + c\pi)} \frac{V_y}{3I_{xx}} = (24.4374 \times 10^{-3} \text{ in.}^{-1})V_y. \quad (\text{v})$$

The final result for the shear flows are listed in eqs. (w) to (z) below.

$$q_1 = [3.42199 \times 10^{-3} \text{ in.}^{-1} + (54.9834 \times 10^{-3} \text{ in.}^{-1}) \sin(s_1/5)]V_y \quad 0 \leq s_1 \leq 5\pi \quad (\text{w})$$

$$q_2 = [24.4374 \times 10^{-3} \text{ in.}^{-1} - (10.9967 \times 10^{-3} \text{ in.}^{-2})s_2 + (0.422949 \times 10^{-3} \text{ in.}^{-3})s_2^2]V_y \quad 0 \leq s_2 \leq 13 \text{ in.} \quad (\text{x})$$

$$q_3 = [-47.041 \times 10^{-3} \text{ in.}^{-1} + (0.433949 \times 10^{-3} \text{ in.}^{-3})s_3^2]V_y \quad 0 \leq s_3 \leq 13 \text{ in.} \quad (\text{y})$$

$$q_{1-2} = [-21.0154 \times 10^{-3} \text{ in.}^{-1} - (5.49834 \times 10^{-3} \text{ in.}^{-2})s_{1-2} + (5.49834 \times 10^{-3} \text{ in.}^{-3})s_{1-2}^2]V_y \quad 0 \leq s_{1-2} \leq 10 \text{ in.} \quad (\text{z})$$



With the shear flows known we compute the torque about the centroid due to the shear flows by

$$M_{zc} = \int_0^{a\pi} r_{nc1} q_1 ds_1 + \int_0^c r_{nc2} q_2 ds_2 + \int_0^c r_{nc3} q_3 ds_3 + \int_0^{2a} r_{nc12} q_{1-2} ds_{1-2}, \quad (\text{aa})$$

where  $r_{nci}(s_i)$  is the normal coordinate to the contour with respect to the centroid in the  $i$ -th branch. From eq. (4.10) the normal coordinates are determined from

$$r_{nci} = x_i(s_i) \frac{dy_i}{ds_i} - y_i(s_i) \frac{dx_i}{ds_i}. \quad (\text{ab})$$

The results for the normal coordinates are

$$r_{nc1} = a - X_c \sin(s_1/a) \quad r_{nc2} = a(b + X_c)/c \quad r_{nc3} = a(b + X_c)/c \quad r_{nc1-2} = X_c. \quad (\text{ac})$$

Substitute eqs. (w) to (z) for the shear flows into eq. (y), followed by substitution of eq. (ac) for the normal coordinates. Numerical evaluation of the integrals after the substitutions leads to the expression for the torque in the form

$$M_{zc} = (2.50157 \text{ in.}) V_y. \quad (\text{ad})$$

The resultant force and torque at the centroid are shown in figure 4.41(a). We also added and subtracted the shear force at the shear center in figure 4.41(a), which does not change the static state. The upward shear force at the centroid and the downward shear force at the shear center form a clockwise couple whose moment is  $x_{sc} V_y$ . In figure 4.41(b) we resolved the torque  $M_z = (2.50157 \text{ in.}) V_y - x_{sc} V_y$  and shear force at the shear center. Since the torque at the shear center is equal to zero in this case, we can solve for the shear center location relative to the centroid to get

$$x_{sc} = 2.50157 \text{ in.} \quad (\text{ae})$$

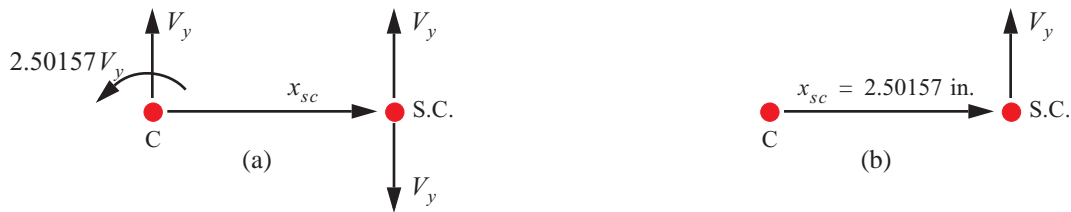


**Fig. 4.41 (a) Resultant of the shear flows at the centroid. (b) Resultant of the shear flows at the shear center.**

We perform one last check on the solution by computing the torque at the shear due to the shear flows from the equation

$$M_z = \int_0^{a\pi} r_{n1} q_1 ds_1 + \int_0^c r_{n2} q_2 ds_2 + \int_0^c r_{n3} q_3 ds_3 + \int_0^{2a} r_{n12} q_{1-2} ds_{1-2}, \quad (\text{af})$$

where the coordinates normal to contour with respect to the shear center are denoted by  $r_{ni}(s_i)$ . From eq. (3.10)

on page 34 the normal coordinates are related by

$$r_{ni} = r_{nci} - x_{sc} \frac{dy_i}{ds_i} + y_{sc} \frac{dx_i}{ds_i}. \quad (\text{ag})$$

In this example  $y_{sc} = 0$ , and the results for the coordinates  $r_{ni}(s_i)$  are given in eqs. (ah) and (ai) below.

$$r_{n1} = r_{nc1} - x_{sc} \left( \frac{\partial y_1}{\partial s_1} \right) = 5 - 0.232149 \sin(s_1/5) \quad r_{n2} = r_{nc2} - x_{sc} \left( \frac{\partial y_2}{\partial s_2} \right) = 4.70467 \text{ in.} \quad (\text{ah})$$

$$r_{n3} = r_{nc3} - x_{sc} \left( \frac{\partial y_3}{\partial s_3} \right) = 4.70467 \text{ in.} \quad r_{n1-2} = r_{nc1-2} - x_{sc} \left( \frac{\partial y_{1-2}}{\partial s_{1-2}} \right) = 0.232149 \text{ in.} \quad (\text{ai})$$

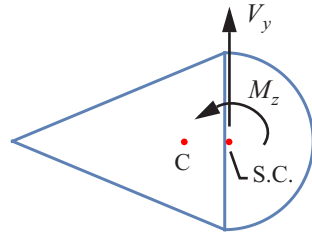
Substitute the shear flows from eqs. (w) to (z) into eq. (af), followed by the substitution of the coordinates normal to the contour in eqs. (ah) and (ai). After these substitutions we perform the integrations indicated in eq. (af) to find the result for torque at the shear center as

$$M_z = (-1.421 \times 10^{-14}) \frac{V_y}{I_{xx}} \approx 0. \quad (\text{aj})$$

Hence, the numerical result for the torque at the shear center with respect to finite precision arithmetic is equal to zero<sup>1</sup>. ■

#### Example 4.13 Superposition of example 4.10 and example 4.12

**Fig. 4.42** Transverse shear and torsion of the two-cell section.



Now consider that the cross section of example 4.10 and example 4.12 is subject to a torque  $M_z$  and a shear force  $V_y$  at the shear center as shown in figure 4.42. We simply add the results for the shear flows due to the torque from example 4.10 to the shear flows due to the transverse shear force  $V_y$  from example 4.12.

The results are

$$q_1(s_1) = (0.0040053 \text{ in.}^{-2})M_z + [0.00342199 \text{ in.}^{-1} + (0.0549834 \text{ in.}^{-1})\sin(s_1/5)]V_y, \quad 0 \leq s_1 \leq (5\pi) \text{ in.},$$

$$q_2(s_2) = (0.00300903 \text{ in.}^{-2})M_z + [0.0244374 \text{ in.}^{-1} - (0.0109967 \text{ in.}^{-2})s_2 + (0.000422949 \text{ in.}^{-3})s_2^2]V_y, \\ 0 \leq s_2 \leq 13 \text{ in.}$$

$$q_3(s_3) = (0.00300903 \text{ in.}^{-2})M_z + [-0.047041 \text{ in.}^{-1} + (0.000422949 \text{ in.}^{-3})s_3^2]V_y \quad 0 \leq s_3 \leq 13 \text{ in.}, \text{ and}$$

1. All computations performed numerically in a computer (MatLab, Mathematica, etc.) are performed with finite precision. That is, a decimal representation of a number that has been rounded or truncated. Computations performed numerically with decimal, or decimal floating point, representation are referred to as finite precision arithmetic.

$$q_{1-2}(s_{1-2}) = (0.000915085 \text{ in.}^{-2})M_z + [-0.0210154 \text{ in.}^{-1} - (0.00549834 \text{ in.}^{-2})s_{1-2} + (0.00549834 \text{ in.}^{-3})s_{1-2}^2]V_y$$

$$0 \leq s_{1-2} \leq 10 \text{ in.}$$

## 4.5 References

Dowling, N. E. **Mechanical Behavior of Materials: Engineering Methods for Deformation, Fracture, and Fatigue**. Englewood Cliffs, NJ: Prentice Hall, 1993, Chapter 7.

Muckle, W. **Strength of Ships' Structures**. London: Edward Arnold, Inc., 1967, pp. 5-12, 27-69.

Zubaly, R.M. **Applied Naval Architecture**. The Society of Naval Architects and Marine Engineers and Cornell Maritime Press, Inc., 1996, pp. 195-237.

## 4.6 Practice exercises

1. A 7 m long AH-1W Supercobra helicopter blade is rotating at 300 rpm and has a mass of 300 kg. Centrifugal forces due to the rotation of the blade lead to tension in the blade. Plot the distributed axial force intensity and the internal axial force distribution on the blade. Calculate the stress at the root for a blade cross-sectional area of  $0.02 \text{ m}^2$ . (Assume that the mass is evenly distributed and the center of mass of the cross section coincides with the tension axis.)

2. The cantilever wing is subject to a distributed air load  $f_y(z) = \frac{2L}{\pi z_{max}} \sqrt{1 - (z/z_{max})^2}$ , where the total lift (2 wings)  $L = 20,000 \text{ lb.}$  at cruise, wing length  $z_{max} = 32.5 \text{ ft.}$ , and  $z = z/z_{max}$ . Also, the wing supports an engine weighing 1000 lb. See figure 4.43. Plot the loading diagram, shear force diagram  $V_y(z)$ , and bending moment diagram  $M_x(z)$  as functions of  $z$  for  $0 \leq z \leq 32.5 \text{ ft.}$  Partial answer:  $V_y(0) = 9,000 \text{ lb.}$  and  $M_x(0) = -131,934 \text{ lb.-ft.}$

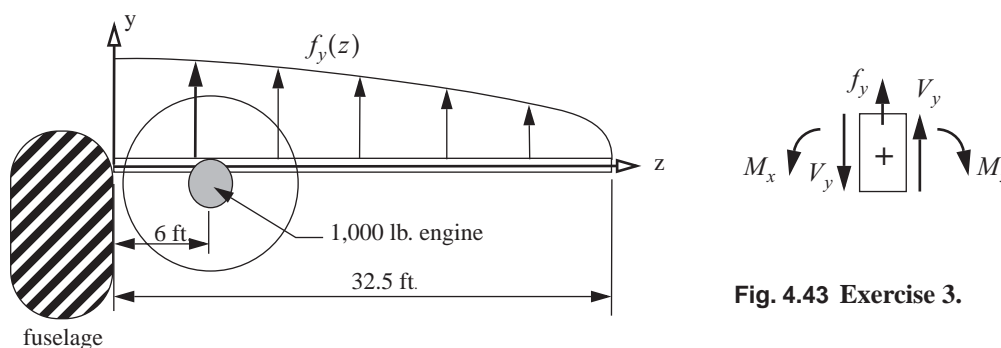


Fig. 4.43 Exercise 3.

3. The barge shown figure 4.44 is 20 m long and has a uniform cross section along its length that is the same cross section shown in figure 4.11 on page 89. It is subject to a uniformly distributed downward load with intensity  $f_0 = 100 \text{ kN/m}$ , and a buoyancy distribution in the hogging condition. The buoyancy distribution is given

by  $f_b = \gamma b d_m \left[ 1 - \cos\left(\pi \frac{z}{L}\right) \right]$ , where  $\gamma = 9.8 \text{ kN/m}^3$  is the specific weight of water,  $b = 10 \text{ m}$ ,  $d_m$  is the depth of the immersed cross section amidships, and  $L = 10 \text{ m}$ . Refer to figure 4.44

- Determine  $d_m$ .
- Determine the distributed loading intensity function  $f_y(z)$  for  $0 \leq z \leq 20 \text{ m}$
- Determine the shear force  $V_y(z)$  and bending moment  $M_x(z)$  for  $0 \leq z \leq 20 \text{ m}$ .
- Draw the distributed loading intensity, shear force, and bending moment diagrams in the manner shown in figure 4.10 on page 88. Label significant points.
- Determine the maximum value of the normal stress  $\sigma_{zz}$ .

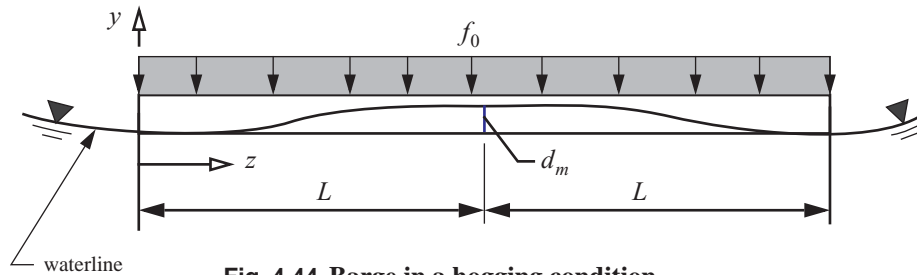
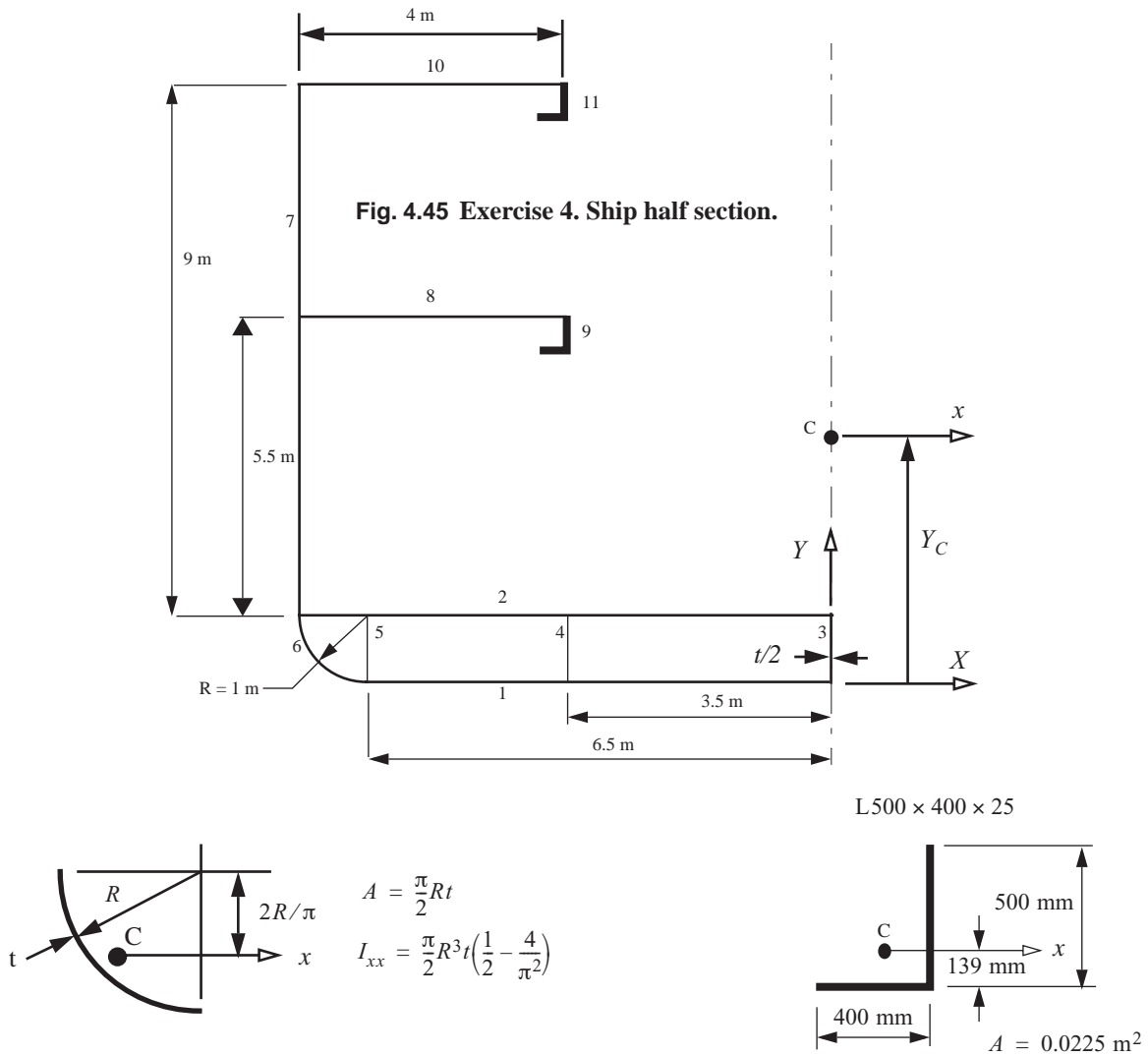


Fig. 4.44 Barge in a hogging condition.

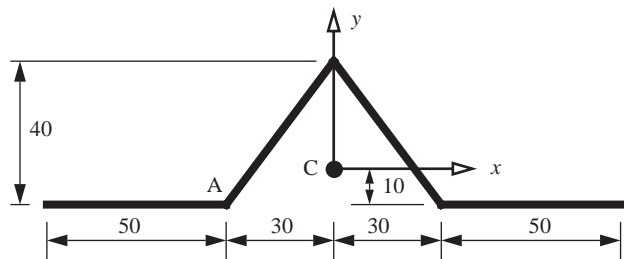
4. Half of the cross section of a ship is shown in figure 4.45. Only the material that is effective in the longitudinal bending is illustrated in the figure. Determine the area  $A$ , location of the centroid  $Y_C$ , and the second area moment about the  $x$ -axis ( $I_{xx}$ ) for the *full* section. Use the tabular format for the computations similar to table 4.2 on page 95. All plating has a thickness  $t = 14 \text{ mm}$  unless other wise noted. The descriptions of the numbered structural elements shown in the figure are listed in table 4.6.

Table 4.6 Description of structural member in figure 4.45.

Item #	Description
1	Outer bottom
2	Inner bottom
3	Center girder
4 & 5	Side girders
6	Bilge (curved portion)
7	Side plating
8	Second deck plating
9 & 11	Hatch side girders $L500 \times 400 \times 25$
10	Strength deck plating



5. The thickness of each branch in the thin-walled cross section shown in figure 4.46 is 3 mm and  $I_{xx} = 10^5 \text{ mm}^4$ . The shear force  $V_y = 5 \text{ kN}$ .
- Determine the shear flow distribution and sketch it on the cross section. Indicate on the sketch the positive sense along the branch.
  - Estimate the shear stress due to the transverse shear force at point A.
  - Estimate the maximum shear stress due to transverse shear.
6. The cross section shown in figure 4.46 is subject to a vertical shear force  $V_y$ , positive upward, and a counter-clockwise torque  $M_z$  acting at the shear center. Take dimensions  $b = 40 \text{ mm}$  and  $t = 0.635 \text{ mm}$ . Determine torsion constant  $J$  and the magnitude of the maximum shear stress  $(\sigma_{zs})_{max}$ .



Note: all dimensions in mm

**Fig. 4.46 Exercise 5.**

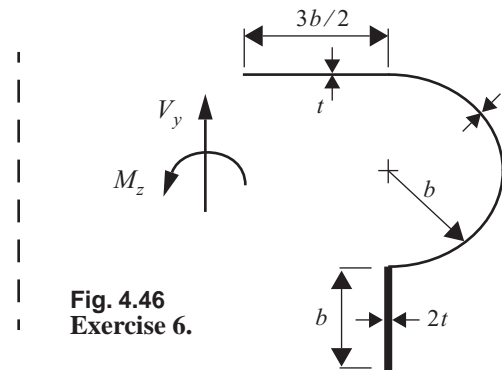
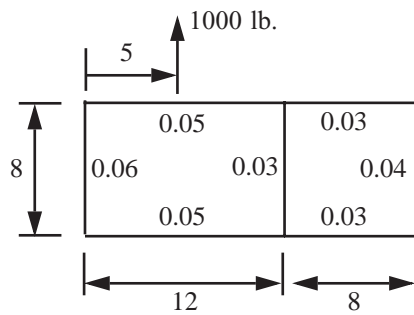


**Fig. 4.46 Exercise 6.**

7. Determine the shear flow in two-cell cross section shown in figure 4.47. The X-axis is a horizontal axis of symmetry,



All dimensions in inches

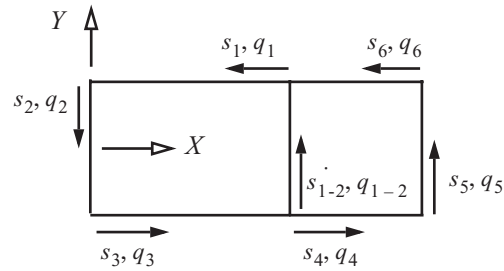


**Fig. 4.47 Two-cell box cross section.**

# Work and energy methods

In article 5.1 and article 5.2 Hooke's law is presented in terms of generalized forces and their corresponding generalized displacements acting on a body. Refer to eqs. (5.6) and (5.10). Corollaries to Hooke's law are the principle of superposition and the reciprocal theorem of Maxwell. Articles 5.3 to 5.6 develop expressions for the energy stored due to elastic deformation of a thin-walled bar. Castigliano's energy theorems are presented in articles 5.7 and 5.8.

## 5.1 Hooke's law and its corollaries

Consider a body, or structure, supported so that rigid body motion is impossible. If it is subject to a force, say by hanging a weight on it, then by Newton's law of action-reaction the body must resist the force by producing an equal and opposite force. The manner by which the body produces this reactive force is by deforming. That is, the body changes shape under the action of a mechanical force and it is the change in shape that enables it to supply the reactive force. If the force is removed and the body returns to its original shape, then the body is **elastic**.

Consider the action of force  $Q_1$  at point 1 on the body, and the action of force  $Q_2$  at point 2 on the body shown in figure 5.1. Let the forces be fixed in direction and in point of application. Let the displacements at points 1 and 2 be denoted by  $q_1$  and  $q_2$ , respectively, being measured with respect to a rectangular Cartesian reference frame. Define the displacements  $q_1$  and  $q_2$  at the points of application to be in the direction of the forces  $Q_1$  and  $Q_2$ , respectively. Displacements  $q_i$  and forces  $Q_i$ ,  $i = 1, 2$ , are said to **correspond**; they are defined at the same point and in the same direction.

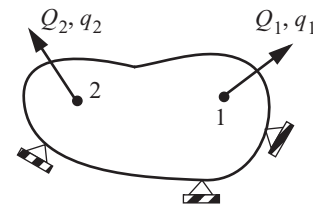


**Fig. 5.1** Static equilibrium of a body under external forces.

For a linear elastic body Hooke's law governs the response (Robert Hooke, 1635–1703). If only force  $Q_1$  is applied, Hooke's law is

$$\begin{aligned} q_1 &= c_{11}Q_1 & \text{for } Q_2 &= 0 \\ q_2 &= c_{21}Q_1 & \text{for } Q_2 &= 0 \end{aligned} \quad (5.1)$$

If force only force  $Q_2$  is applied, Hooke's law is

$$\begin{aligned} q_1 &= c_{12}Q_2 & \text{for } Q_1 &= 0 \\ q_2 &= c_{22}Q_2 & \text{for } Q_1 &= 0 \end{aligned} \quad (5.2)$$

The coefficients  $c_{11}$ ,  $c_{12}$ ,  $c_{21}$ , and  $c_{22}$  are called **flexibility influence coefficients**, and they depend on the points of application and the direction of the corresponding forces and displacements, and the size, shape, and the material of the body.

Note that the application of the force  $Q_1$  results in a displacement at point 2, and force  $Q_2$  results in a displacement at point 1. Under mechanical load Hooke recognized that the material from which the body is made deforms internally throughout its extent. We now know the scale of deformation is to the level of the distortion of interatomic bonds constituting the material. At the atomic scale the material is not continuous. However, for length scales greater than that of interatomic distances the atomic structure of the body is ignored and the body is idealized as a **continuum**. Points within the body are identified with the material particles, and continuity is defined in the mathematical sense. Neighboring points remain neighbors under any loading condition.

If both forces  $Q_1$  and  $Q_2$  act on the body, a questions that arises: Is Hooke's law given by eq. (5.3) below?

$$\begin{aligned} q_1 &= c_{11}Q_1 + c_{12}Q_2 \\ q_2 &= c_{21}Q_1 + c_{22}Q_2 \end{aligned} \quad (5.3)$$

From the hypothesis that the body returns to its original shape after the forces are removed it is proved that eq. (5.3) for two loads is the correct form of Hooke's law. The proof is given by Fung (1965, p. 3). Also, coefficients  $c_{11}$  and  $c_{21}$  are independent of force  $Q_2$ , and coefficients  $c_{12}$  and  $c_{22}$  are independent of force  $Q_1$ . This proof leads to the principle of superposition.

<b>Principle of superposition</b>
<b>For a linear elastic body the effects caused by two or more loads are the sum of the loads applied separately.</b>
<ul style="list-style-type: none"> <li>• The deformations are small, and</li> <li>• the order of loading is unimportant.</li> </ul>



### 5.1.1 Work of the external loads

Multiplying the first of eq. (5.3) by  $Q_1$ , the second equation by  $Q_2$ , and adding, we obtain

$$Q_1q_1 + Q_2q_2 = c_{11}Q_1^2 + c_{12}Q_1Q_2 + c_{21}Q_2Q_1 + c_{22}Q_2^2. \quad (5.4)$$

The quantity above is independent of the order in which the loads are applied. Hence, it has a definite meaning for each order of the application of loads  $Q_1$  and  $Q_2$ .



Consider the special case of proportional loading, where the ratio  $Q_2/Q_1$  is kept constant and the loading increases very slowly from zero to the final value (i.e., **quasi-static loading**). In this case, the corresponding displacements also increase proportionally and slowly. Force-displacement plots at points 1 and 2 are shown in figure 5.2 for this special case of proportional loading. It should be clear that the

work done by the force  $Q_1$  is exactly  $\frac{1}{2}Q_1q_1$ , and that of  $Q_2$  is

$$\frac{1}{2}Q_2q_2.$$

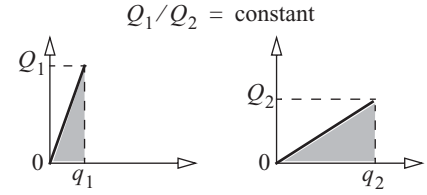


**Fig. 5.2** Load-displacement plots for proportional loading

Hence, we conclude from eq. (5.4) that the **total work done,  $W$ , by the set of forces is independent of the order in which the forces are applied.**

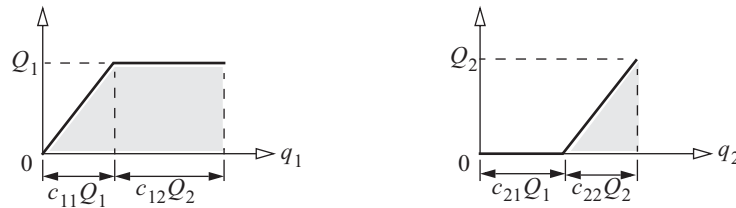
$$W = \frac{1}{2}(Q_1q_1 + Q_2q_2). \quad (5.5)$$

### 5.1.2 Maxwell's reciprocal theorem

Now consider the two different sequences in the application of forces  $Q_1$  and  $Q_2$ . First, apply  $Q_1$  slowly with  $Q_2 = 0$ . At the final value of  $Q_1$ , the displacement of point 1 is  $c_{11}Q_1$  and the displacement of point 2 is  $c_{21}Q_1$ . The work done is  $\frac{1}{2}c_{11}Q_1^2$ . With  $Q_1$  held fixed, apply  $Q_2$  slowly until  $Q_2$  attains its final value. The additional displacement at point 1 is  $c_{12}Q_2$  and the additional displacement at point 2 is  $c_{22}Q_2$ . The additional work done is  $Q_1c_{12}Q_2 + \frac{1}{2}c_{22}Q_2^2$ . When the forces are applied in the order  $Q_1, Q_2$ , the total work done, as shown in figure 5.3, is

$$W = \underbrace{\frac{1}{2}c_{11}Q_1^2 + c_{12}Q_1Q_2}_{\text{pt. 1}} + \underbrace{\frac{1}{2}c_{22}Q_2^2}_{\text{pt. 2}}.$$

**Fig. 5.3** Load-displacement plots for the loading sequence  $Q_1, Q_2$ .

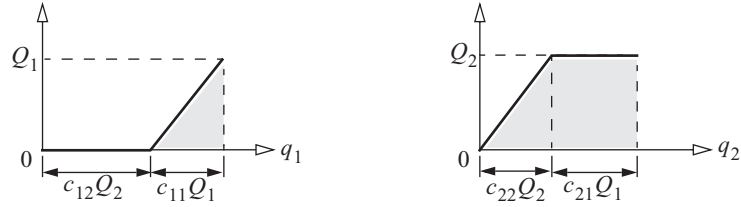


Second, apply  $Q_2$  slowly with  $Q_1 = 0$ . At the final value of  $Q_2$ , the displacement of point 1 is  $c_{12}Q_2$  and the displacement of point 2 is  $c_{22}Q_2$ . The work done is  $\frac{1}{2}c_{22}Q_2^2$ . With  $Q_2$  held fixed, apply  $Q_1$  slowly until  $Q_1$  attains its final value. The additional displacement at point 1 is  $c_{11}Q_1$  and the additional displacement at point 2

is  $c_{21}Q_1$ . The additional work done is  $Q_2c_{21}Q_1 + \frac{1}{2}c_{11}Q_1^2$ . When the forces are applied in the order  $Q_2, Q_1$  the total work done, as shown in figure 5.4, is

$$W' = \underbrace{\frac{1}{2}c_{11}Q_1^2}_{\text{pt. 1}} + \underbrace{\frac{1}{2}c_{22}Q_2^2 + c_{21}Q_1Q_2}_{\text{pt. 2}}.$$

**Fig. 5.4** Load-displacement plots for the loading sequence  $Q_2, Q_1$ .



However,  $W = W'$  for arbitrary order of application of  $Q_1, Q_2$ . Hence,  $c_{12} = c_{21}$ .

For a set of applied forces  $Q_1, Q_2, \dots, Q_n$  and their corresponding displacements  $q_1, q_2, \dots, q_n$ , eq. (5.3) generalizes to

$$q_i = \sum_{j=1}^n c_{ij}Q_j \quad i = 1, 2, \dots, n. \quad (5.6)$$

#### Maxwell's reciprocal theorem

**The influence coefficients for corresponding forces and displacements are symmetric.**

- $c_{ij} = c_{ji}$

**In other words, the displacement at point  $i$  due to a unit load at another point  $j$  is equal to the displacement at  $j$  due to a unit load at  $i$ , provided that the displacements and forces “correspond,” (i.e., that they are measured in the same direction at each point.)**

Since the flexibility influence coefficients  $c_{12} = c_{21}$ , the work done on the body can be written as

$$W = \frac{1}{2}(c_{11}Q_1^2 + 2c_{12}Q_1Q_2 + c_{22}Q_2^2). \quad (5.7)$$

Take the partial derivatives of the work function in eq. (5.7) with respect to forces  $Q_1$  and  $Q_2$ , and recognize the material law in eq. (5.3), to find that

$$q_1 = \frac{\partial W}{\partial Q_1} \quad q_2 = \frac{\partial W}{\partial Q_2}. \quad (5.8)$$

That is, the partial derivative of the work function with respect to a force equals the corresponding displacement.

## 5.2 Extensions of Hooke's law to include a couple and rotation

Hooke's law, eq. (5.3), can be extended to include the moment of a couple acting on the body and the rotation of the arm connecting the couple.

As shown in figure 5.5, the forces  $Q'_3$  and  $Q'_4$  form a couple with an arm of length  $a$  if  $Q'_3 = P$  and  $Q'_4 = P$ . That is, forces  $Q'_3$  and  $Q'_4$  are functions of the force  $P$ . Take the partial derivative of the work done by the forces with respect to force  $P$  and use the chain rule to get

$$\frac{\partial W}{\partial P} = \frac{\partial W}{\partial Q'_3} \frac{\partial Q'_3}{\partial P} + \frac{\partial W}{\partial Q'_4} \frac{\partial Q'_4}{\partial P}.$$

Let  $q'_3$  denote the displacement corresponding to force  $Q'_3$ , and let  $q'_4$  denote the displacement corresponding to force  $Q'_4$ . Then, with reference to eq. (5.8)  $q'_3 = \frac{\partial W}{\partial Q'_3}$ ,  $q'_4 = \frac{\partial W}{\partial Q'_4}$ , and note that  $\frac{\partial Q'_3}{\partial P} = \frac{\partial Q'_4}{\partial P} = 1$ . So

$$\frac{\partial W}{\partial P} = q'_3 + q'_4.$$

For small displacements,  $q'_3 + q'_4 = aq$ , where  $q$  is the small rotation of the moment arm in radians, as is shown in figure 5.6.

Thus,  $\frac{\partial W}{\partial P} = aq$ . Divide this last equation by the length of the

moment arm to get  $\frac{1}{a} \frac{\partial W}{\partial P} = q$ . Lastly, the moment of a couple is

$Q = aP$ , so we get

$$\frac{\partial W}{\partial Q} = q. \quad (5.9)$$

Thus, in Hooke's law if  $q_i$  is a rotation, then corresponding "force"  $Q_i$  is a moment.

We can consider a *concentrated couple* as the limiting case of two equal and opposite forces acting in a plane at the surface of the body that approach each other, but maintain a constant moment; i.e.,

$$\lim_{a \rightarrow 0} (aP) = Q$$

In this limiting process  $P \rightarrow \infty$ . Then, the angle of rotation  $q$  is interpreted as the rotation of an infinitesimal line element in the plane of the couple.

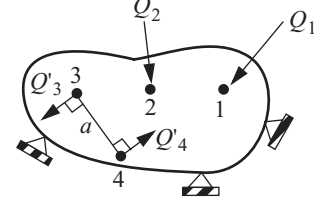


**Fig. 5.5** Static equilibrium of a body under external forces including a couple

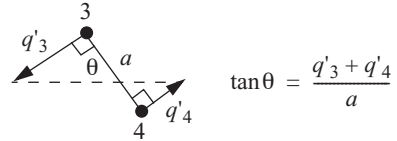


**Fig. 5.6** Rotation of the arm of the couple

### 5.2.1 Generalized forces and displacements

Define  $Q_i$  as the magnitude of the generalized force acting at point  $i$  on the body, and let  $q_i$  denote the corresponding generalized displacement at point  $i$ , where  $i = 1, 2, \dots, n$ . The product of  $Q_i q_i$  has dimensional units of work, or  $F \cdot L$ . If  $Q_i$  is a force, then  $q_i$  is the corresponding displacement. If  $Q_i$  is the moment of a concentrated couple with dimensional unit  $F \cdot L$ , then  $q_i$  is the corresponding rotation in radians of the infinitesimal line element in the plane of the couple at the point of its application. By defining generalized forces and moments, we can extend Hooke's law in eq. (5.6) to include moments and rotations as well as forces and displacements. In eq. (5.6), the flexibility influence coefficients can have different dimensional units. For example, if  $q_1$  is a displacement of point 1 on the body and  $Q_2$  is a moment of a couple acting point 2, then the dimensional unit of flexibility influence coefficient  $c_{12}$  is  $F^{-1}$ . Since the generalized displacement  $q_2$  corresponding to  $Q_2$  is a rotation in radians and the generalized force  $Q_1$  acting at point 1 is a force corresponding to  $q_1$ , then the dimensional unit of flexibility influence coefficient  $c_{21}$  is also  $F^{-1}$ . Also, the dimensional unit of  $c_{11}$  is  $LF^{-1}$ , and  $c_{22}$  is  $F^{-1}L^{-1}$ .

### 5.2.2 Stiffness influence coefficients

Assume that the displacement-force system given by eq. (5.6) can be inverted so that the forces may be expressed in terms of the displacements as

$$Q_i = \sum_{j=1}^n k_{ij} q_j \quad i = 1, 2, \dots, n, \quad (5.10)$$

where constants  $k_{ij}$  are called **stiffness influence coefficients**. In matrix notation, we write the displacement-force form of Hooke's law, eq. (5.6), as

$$\underbrace{\{q\}}_{n \times 1} = \underbrace{[c]}_{n \times n} \underbrace{\{Q\}}_{n \times 1}, \quad (5.11)$$

and the force-displacement form, eq. (5.10), as

$$\underbrace{\{Q\}}_{n \times 1} = \underbrace{[k]}_{n \times n} \underbrace{\{q\}}_{n \times 1}. \quad (5.12)$$

Matrix  $[c]$  is called the *flexibility matrix* and  $[k]$  is called the *stiffness matrix*. Both matrices are square of order  $n \times n$ . In matrix algebra the stiffness matrix is the inverse of the flexibility matrix, or

$$[k] = [c]^{-1}. \quad (5.13)$$

The inverse matrix has the property that

$$[c]^{-1}[c] = [c][c]^{-1} = [I], \quad (5.14)$$

where  $[I]$  is the  $n \times n$  identity matrix (i.e., the identity matrix is a square matrix with all diagonal elements equal to unity and all off-diagonal elements equal to zero).

Maxwell's theorem in article 5.1.2 states that the flexibility matrix is symmetric. In matrix algebra symmetry is written as

$$[c]^T = [c], \quad (5.15)$$

where the superscript  $T$  means matrix transpose (i.e., the matrix obtained by interchanging its rows with its columns). Since the flexibility matrix is symmetric, the stiffness matrix is also symmetric. That is,

$$[k]^T = [k]. \quad (5.16)$$

**Proof.** By definition

$$[c]^{-1}[c] = [I]. \quad (5.17)$$

Take the transpose of eq. (5.17) to get

$$([c]^{-1}[c])^T = [I]^T. \quad (5.18)$$

Use the fact that the transpose of the product of two matrices is equal to the product of the transpose of the second matrix times the transpose of the first matrix, and that the transpose of the identity matrix is equal to itself. Hence, eq. (5.18) is equal to

$$[c]^T([c]^{-1})^T = [I]. \quad (5.19)$$

By symmetry of the flexibility matrix eq. (5.19) is equal to

$$[c]([c]^{-1})^T = [I]. \quad (5.20)$$

Pre-multiply eq. (5.20) by the inverse of the flexibility matrix to get

$$[c]^{-1}[c]([c]^{-1})^T = [c]^{-1}[I] = [c]^{-1}. \quad (5.21)$$

Employ the relation in eq. (5.14) and write eq. (5.21) as

$$([c]^{-1})^T = [c]^{-1}. \quad (5.22)$$

Again, by definition  $[c]^{-1} \equiv [k]$ . Thus,

$$[k]^T = [k]. \quad (5.23)$$

Similarly in the generalized force and generalized displacement form of eq. (5.12), the stiffness influence coefficients,  $k_{ij}$ , also can have different dimensional units.

### 5.3 Strain energy density functions

External loads imposed on a body cause it to deform. The energy stored in an elastic body due to deformation is called the strain energy, and the strain energy per unit volume is called the strain energy density. For the thin wall bar theory discussed in article 3.4 on page 37, deformation is quantified by values of the axial normal strain  $\epsilon_{zz}$ , and shear strains  $\gamma_{zs}$  and  $\gamma_{z\zeta}$ . The three remaining strains  $\epsilon_{ss} = \epsilon_{\zeta\zeta} = \gamma_{s\zeta} = 0$ . In this article expressions for the strain energy density functions in terms of the non-zero strains are developed.

#### 5.3.1 Strain energy density in uniaxial normal strain

Begin with the axial equation of motion for an element of the bar of length  $\Delta z$  as shown in figure 5.7. The equation of motion is

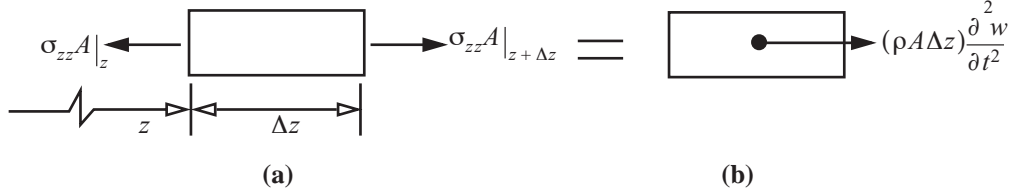


**Fig. 5.7 Axial bar element. (a) free body diagram. (b) time rate of change of linear momentum.**

$$\sigma_{zz}A|_{z+\Delta z} - \sigma_{zz}A|_z = (\rho A \Delta z) \frac{\partial^2 w}{\partial t^2}, \quad (5.24)$$

in which  $A$  denotes the cross-sectional area,  $\rho$  the mass density, and  $\frac{\partial w}{\partial t}$  the axial velocity. Division of eq. (5.24) by  $A\Delta z$  followed by letting  $\Delta z \rightarrow 0$  yields the differential equation at coordinate  $z$  and time  $t$  as

$$\frac{\partial \sigma_{zz}}{\partial z} = \rho \frac{\partial^2 w}{\partial t^2}. \quad (5.25)$$

Consider the first law of thermodynamics for a closed system of continuous matter not interchanging matter with its surroundings. Then the first law is (Malvern, 1969, p. 229)

$$P_{\text{input}} + Q_{\text{input}} = \frac{\partial E}{\partial t}, \quad (5.26)$$

where  $P_{\text{input}}$  is the power input of the external loads,  $Q_{\text{input}}$  is the rate of heat input, and  $E$  is the total energy of the system. Assume the process is **adiabatic** so  $Q_{\text{input}} = 0$ . The energy is the sum of the kinetic energy and internal energy. For the closed system consisting of the axial bar element shown in figure 5.7,  $P_{\text{input}}$  is the time rate of work of the normal stresses acting on the element. Expressions for  $P_{\text{input}}$  and the time rate of change of energy are

$$P_{\text{input}} = \sigma_{zz}A \frac{\partial w}{\partial t} \Big|_{z+\Delta z} - \sigma_{zz}A \frac{\partial w}{\partial t} \Big|_z, \quad \frac{\partial E}{\partial t} = \frac{\partial}{\partial t} \left[ \frac{1}{2} (\rho A \Delta z) \left( \frac{\partial w}{\partial t} \right)^2 \right] + A \Delta z \frac{\partial U_0}{\partial t}, \quad (5.27)$$

where  $U_0$  is the internal energy per unit volume, or internal energy density. Substitute eq. (5.27) into the first law (5.26) with  $Q_{\text{input}} = 0$ , followed by division by  $A\Delta z$ . In the result from these previous manipulations let  $\Delta z \rightarrow 0$  to get the differential equation of the first law at coordinate  $z$  and time  $t$  as

$$\frac{\partial}{\partial z} \left( \sigma_{zz} \frac{\partial w}{\partial t} \right) = \rho \frac{\partial w}{\partial t} \frac{\partial^2 w}{\partial t^2} + \frac{\partial U_0}{\partial t}. \quad (5.28)$$

Expand the derivative on the left-hand side of eq. (5.28) to get

$$\frac{\partial \sigma_{zz}}{\partial z} \frac{\partial w}{\partial t} + \sigma_{zz} \frac{\partial}{\partial z} \left( \frac{\partial w}{\partial t} \right) = \rho \frac{\partial w}{\partial t} \frac{\partial^2 w}{\partial t^2} + \frac{\partial U_0}{\partial t}. \quad (5.29)$$

Substitute the equation of motion (5.25) for  $\partial \sigma_{zz} / \partial z$  in the first term on the left-hand side of eq. (5.29). We

assume it is permissible to interchange the order of differentiation of the second term on the left-hand side and write it as

$$\frac{\partial}{\partial z} \left( \frac{\partial w}{\partial t} \right) = \frac{\partial}{\partial t} \left( \frac{\partial w}{\partial z} \right) = \frac{\partial \epsilon_{zz}}{\partial t}.$$

Hence, eq. (5.29) becomes

$$\left( \rho \frac{\partial^2 w}{\partial t^2} \right) \frac{\partial w}{\partial t} + \sigma_{zz} \frac{\partial \epsilon_{zz}}{\partial t} = \rho \frac{\partial w}{\partial t} \frac{\partial^2 w}{\partial t^2} + \frac{\partial U_0}{\partial t},$$

and note that the terms involving the acceleration cancel. We are left with

$$\sigma_{zz} \frac{\partial \epsilon_{zz}}{\partial t} = \frac{\partial U_0}{\partial t}. \quad (5.30)$$

For the response of an elastic body under an adiabatic conditions, it is assumed that the internal energy density is a function of the strain (Allen and Haisler, 1985, pp. 101,102). For  $U_0 = U_0(\epsilon_{zz})$ , and that the strain at point  $z$  is a function of time  $t$ , we use the change rule to write

$$\frac{\partial U_0}{\partial t} = \frac{\partial U_0}{\partial \epsilon_{zz}} \left( \frac{\partial \epsilon_{zz}}{\partial t} \right). \quad (5.31)$$

Substitute eq. (5.31) into the first law (5.30) to get

$$\left( \sigma_{zz} - \frac{\partial U_0}{\partial \epsilon_{zz}} \right) \left( \frac{\partial \epsilon_{zz}}{\partial t} \right) = 0. \quad (5.32)$$

Since the time rate of strain is, in general, not zero, it is concluded from (5.32) that

$$\sigma_{zz} = \frac{\partial U_0}{\partial \epsilon_{zz}}. \quad (5.33)$$

Thus, the derivative of the internal energy density function  $U_0(\epsilon_{zz})$  with respect normal strain equals the corresponding normal stress under the assumption of adiabatic deformation for an elastic material.

In elasticity a function having the property illustrated by eq. (5.33) is called the **strain energy density**. Thus, the internal energy density function is identified as the strain energy density. It is shown in continuum mechanics texts, e.g. Fung (1965, p. 348), that the strain energy density is identified with the internal energy in an adiabatic process and the free energy for an isothermal process. For a thermoelastic stress-strain law that is not associated with an adiabatic or isothermal process, it is assumed that a strain energy function exists. That is, **an elastic material is defined by postulating that a scalar function exists such that its derivative with respect to a strain component determines the corresponding stress component**. Consequently, the postulate of a strain energy function leads to the material law relating the stresses to the strains. Equation (A.110) in the appendix augments eq. (5.33) to include a three-dimensional state of stress and strain.

From eq. (3.65) on page 45 Hooke's law for the axial stress and strain is  $\sigma_{zz} = E\epsilon_{zz} - \beta\Delta T$ , where  $E$  is the modulus of elasticity,  $\beta = E\alpha$ , and  $\alpha$  is the coefficient of thermal expansion. Substitute the expression for stress  $\sigma_{zz}$  from Hooke's law into the left-hand side of eq. (5.33) and then integrate the result with respect to the strain  $\epsilon_{zz}$  to get

$$U_0 = \frac{1}{2}E\varepsilon_{zz}^2 - \beta\Delta T\varepsilon_{zz}. \quad (5.34)$$

The strain energy density is zero in the unstrained state, since it will be the change in strain energy that is important in subsequent applications. A graphical representation of the strain energy density is obtained in the plot of Hooke's law as shown in figure 5.8. It is interpreted as the "area" between Hooke's law and the strain axis. From the graph the "area" is

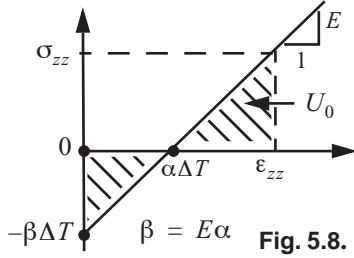


Fig. 5.8.

$$U_0 = \frac{1}{2}\sigma_{zz}(\varepsilon_{zz} - \alpha\Delta T) + \frac{1}{2}(-\beta\Delta T)(\alpha\Delta T), \text{ or}$$

$$U_0 = \frac{E}{2}[(\varepsilon_{zz} - \alpha\Delta T)^2 - (\alpha\Delta T)^2]. \quad (5.35)$$

Simplification of eq. (5.35) reduces it to eq. (5.34). The "area" represents the work done per unit volume of the stress acting through the strain. The static analog to eq. (5.30) is  $\sigma_{zz}\delta\varepsilon_{zz} = \delta U_0$ , where the incremental work per unit volume  $\delta W_0 = \sigma_{zz}\delta\varepsilon_{zz}$ . The work done during the deformation is

$$W_0 = \int_0^{\varepsilon_z} \sigma_{zz} \delta\varepsilon_{zz} = \int_0^{\varepsilon_z} \delta U_0 = U_0(\varepsilon_{zz}) - U_0(0) = U_0(\varepsilon_{zz}). \quad (5.36)$$

That is, the work done per unit volume is equal to the strain-energy-density function, and  $W_0$  only depends on the final state of strain and not the strain history.<sup>1</sup>

Strain energy density functions for a Hookean material subject to a three-dimensional state of strain, including thermal strains, are given by eq. (A.140) in the appendix. The three-dimensional strain energy density function reduces to eq. (5.34) for uniaxial strain if the Poisson effect is neglected.

### 5.3.2 Complementary energy density in uniaxial normal stress

Equation (5.33) is transformed to a conjugate form by introducing a new function  $U_0^*(\sigma_{zz})$  called the complementary-strain-energy density. The transformation was developed by A. M. Legendre. Refer to the discussion by Langhaar (1962, p. 120). It is defined by

$$U_0^*[\sigma_{zz}] \equiv -U_0[\varepsilon_{zz}] + \sigma_{zz}\varepsilon_{zz}. \quad (5.37)$$

Take the partial derivative of the complementary-strain-energy density with respect to the normal stress component to get

$$\frac{\partial U_0^*}{\partial \sigma_{zz}} = -\frac{\partial U_0}{\partial \varepsilon_{zz}} \frac{\partial \varepsilon_{zz}}{\partial \sigma_{zz}} + \varepsilon_{zz} + \sigma_{zz} \frac{\partial \varepsilon_{zz}}{\partial \sigma_{zz}} = \underbrace{\left[ \sigma_{zz} - \left( \frac{\partial U_0}{\partial \varepsilon_{zz}} \right) \right]}_{= 0} \left( \frac{\partial \varepsilon_{zz}}{\partial \sigma_{zz}} \right) + \varepsilon_{zz}, \quad (5.38)$$

1. Note that reversing the order of application of the mechanical load  $\sigma_z$  and thermal load  $\Delta T$  changes the "area" under the stress-strain plot, which implies  $W_0$  is path dependent. See, for example, the discussion in Donaldson (1993, p. 510) and Allen and Haisler (1985, p. 287). However, these authors use eq. (5.34) for  $U_0$ .



in which the leading term on the right-hand side of eq. (5.38) vanishes by eq. (5.33). Hence, complementary-strain-energy density has the property that

$$\epsilon_{zz} = \frac{\partial U_0^*}{\partial \sigma_{zz}}. \quad (5.39)$$

Equation (5.39) is the conjugate to eq. (5.33). Hooke's law for the normal strain is  $\epsilon_{zz} = (\sigma_{zz} + \beta\Delta T)/E$ , which is substituted for the strain in eq. (5.39). The result is integrated with respect to the stress to get

$$U_0^* = \int_{-\beta\Delta T}^{\sigma_{zz}} [(\sigma_{zz} + \beta\Delta T)/E] d\sigma_{zz} = \frac{1}{2E}(\sigma_{zz} + \beta\Delta T)^2. \quad (5.40)$$

As is shown in figure 5.9, the complementary-strain-energy density represents the “area” between Hooke's law and the stress axis. Expand the last result for the complementary strain energy density to find

$$U_0^* = \frac{1}{2E}(\sigma_{zz}^2 + 2\beta\Delta T\sigma_{zz}) + \frac{(\alpha\Delta T)^2}{2E}. \quad (5.41)$$

The third term in the complementary-strain-energy density above depends only on the change in temperature. This third term in the expression for  $U_0^*$  may be omitted under the assumption of one-way, thermal-mechanical coupling, since the change in temperature is specified independent of the mechanical state. (Refer to the discussion in article 3.7.1 on page 44.) It is the change in  $U_0^*$  with respect to the stress state that is important in subsequent analyses.

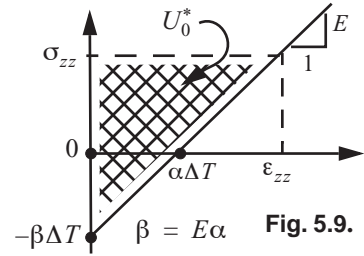


Fig. 5.9.

### 5.3.3 Strain energy density in shear

The properties of the strain-energy densities in shear are

$$\sigma_{zs} = \frac{\partial U_0}{\partial \gamma_{zs}} \quad \gamma_{zs} = \frac{\partial U_0^*}{\partial \sigma_{zs}}. \quad (5.42)$$

Hooke's law relates the shear stress to the shear strain by  $\sigma_{zs} = G\gamma_{zs}$ , where  $G$  is the shear modulus of the material. Substituting Hooke's law into eq. (5.42) followed by integration, we get the expressions for the strain energy densities as

$$U_0 = \frac{1}{2}G\gamma_{zs}^2 \quad U_0^* = \frac{1}{2G}\sigma_{zs}^2. \quad (5.43)$$

As is shown in figure 5.10, the strain-energy density is the “area” between Hooke's law and the strain axis, and the complementary-strain-energy density is the “area” between Hooke's law and the stress axis. Including shear strain  $\gamma_{z\zeta}$  and its corresponding shear stress  $\sigma_{z\zeta}$ , the combined strain energy densities in shear are

$$U_0 = \frac{G}{2}(\gamma_{zs}^2 + \gamma_{z\zeta}^2) \quad U_0^* = \frac{1}{2G}(\sigma_{zs}^2 + \sigma_{z\zeta}^2). \quad (5.44)$$

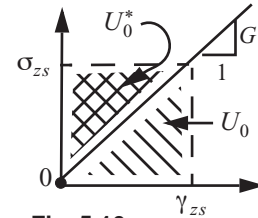


Fig. 5.10

### 5.4 Strain energy for extension and bending of a thin-walled bar

Assuming that the axial normal strain is uniform through the thickness of the wall, we obtain from eq. (3.30) on page 38 that the axial normal strain is related to the axial displacement  $w(z)$ , and bending rotations  $\phi_x(z)$  and  $\phi_y(z)$ , by

$$\epsilon_{zz} = \frac{dw}{dz} + y(s)\frac{d\phi_x}{dz} + x(s)\frac{d\phi_y}{dz}. \quad (5.45)$$

Substitute eq. (5.45) for the normal strain into the strain energy density (5.34) to get

$$U_0(\epsilon_{zz}) = \frac{E}{2} \left( \frac{dw}{dz} + y(s)\frac{d\phi_x}{dz} + x(s)\frac{d\phi_y}{dz} \right)^2 - \beta \Delta T \left( \frac{dw}{dz} + y(s)\frac{d\phi_x}{dz} + x(s)\frac{d\phi_y}{dz} \right). \quad (5.46)$$

The strain energy per unit axial length is defined by  $\bar{U} = \int_c U_0(\epsilon_{zz}) t(s) ds$ . Substitute eq. (5.46) for the strain

energy density into the strain energy per unit axial length, and note the geometric properties listed in eqs. (3.74) and (3.77) on page 46 relative to the centroid, to get

$$\bar{U} = \frac{E}{2} \left[ A \left( \frac{dw}{dz} \right)^2 + I_{xx} \left( \frac{d\phi_x}{dz} \right)^2 + I_{yy} \left( \frac{d\phi_y}{dz} \right)^2 + 2I_{xy} \left( \frac{d\phi_x}{dz} \right) \left( \frac{d\phi_y}{dz} \right) \right] - N_T \left( \frac{dw}{dz} \right) - M_{xT} \left( \frac{d\phi_x}{dz} \right) - M_{yT} \left( \frac{d\phi_y}{dz} \right). \quad (5.47)$$

The thermal actions appearing in eq. (5.47) are given by eqs. (3.75) and (3.78) on page 46.

Assuming that the axial normal stress is uniform through the thickness of the wall, then the axial normal stress is given by eq. (3.83) on page 47. Substitute eq. (3.83) for the normal stress into the expression (5.41) for the complementary strain energy density to get

$$U_0^*(\sigma_{zz}) = \left( \frac{1}{2E} \right) \left\{ \left[ \frac{N + N_T}{A} + k \frac{(M_x + M_{xT})^-}{I_{xx}} y(s) + k \frac{(M_y + M_{yT})^-}{I_{yy}} x(s) - \beta \Delta T \right]^2 + 2\beta \Delta T \left[ \frac{N + N_T}{A} + k \frac{(M_x + M_{xT})^-}{I_{xx}} y(s) + k \frac{(M_y + M_{yT})^-}{I_{yy}} x(s) - \beta \Delta T \right] \right\},$$

in which the quadratic term in the temperature change of eq. (5.41) is neglected. Expand and simplify the latter expression to find

$$U_0^*(\sigma_{zz}) = \frac{1}{2E} \left\{ \left( \frac{N + N_T}{A} \right)^2 + \left[ k \frac{(M_x + M_{xT})^-}{I_{xx}} y(s) \right]^2 + \left[ k \frac{(M_y + M_{yT})^-}{I_{yy}} x(s) \right]^2 + 2 \left( \frac{N + N_T}{A} \right) \left( k \frac{M_x + M_{xT}^-}{I_{xx}} y(s) \right) + 2 \left( \frac{N + N_T}{A} \right) \left( k \frac{M_y + M_{yT}^-}{I_{yy}} x(s) \right) + 2 \left( k \frac{M_x + M_{xT}^-}{I_{xx}} y(s) \right) \left( k \frac{M_y + M_{yT}^-}{I_{yy}} x(s) \right) \right\}. \quad (5.48)$$

Again, all terms in the simplification of eq. (5.48) that contain only the temperature are neglected. The complementary strain energy per unit axial length is defined by  $\bar{U}^* = \int_c U_0^*(\sigma_{zz}) t(s) ds$ . Substitute eq. (5.48) for the complementary strain energy density into the complementary strain energy per unit length. In the evaluation of  $\bar{U}^*$  we use the definitions given by eqs. (3.74), (3.81), and (3.84) in article 3.7.2 on page 45 to determine the fol-

lowing integrals:

$$\int_c \bar{x}(s) t ds = Q_y - n_x Q_x = 0 \quad \int_c \bar{y}(s) t ds = Q_x - n_y Q_y = 0, \text{ and} \quad (5.49)$$

$$\int_c \bar{y}^2 t ds = \frac{I_{xx}}{k} \quad \int_c \bar{x}^2 t ds = \frac{I_{yy}}{k} \quad \int_c \bar{x} \bar{y} t ds = \frac{-I_{xy}}{k}. \quad (5.50)$$

The final result for the complementary strain energy per unit length is

$$\bar{U}^* = \frac{1}{2E} \left[ \frac{(N + N_T)^2}{A} + k \frac{(M_x + M_{xT})^2}{I_{xx}} + k \frac{(M_y + M_{yT})^2}{I_{yy}} - 2k I_{xy} \frac{(M_x + M_{xT})(M_y + M_{yT})}{I_{xx} I_{yy}} \right]. \quad (5.51)$$

## 5.5 Strain energy for shear and torsion of a thin-walled bar

Consider the strain energy densities due to shear (5.44). Integrate these strain energy densities over the cross-sectional area to get the strain energies per unit axial length. That is,

$$\bar{U} = \frac{1}{2} \int_c \left[ \int_{-t/2}^{t/2} G(\gamma_{zs}^2 + \gamma_{z\zeta}^2) d\zeta \right] ds \quad \bar{U}^* = \frac{1}{2} \int_c \left[ \int_{-t/2}^{t/2} \frac{1}{G} (\sigma_{zs}^2 + \sigma_{z\zeta}^2) d\zeta \right] ds. \quad (5.52)$$

If we substituted the shear strains  $\gamma_{zs}$  and  $\gamma_{z\zeta}$  from eq. (3.31) on page 38 into the strain energy per unit length and performed the integration over the cross section we would get the strain energy function per unit length in the form

$$\bar{U} = \bar{U} \left[ \psi_x, \psi_y, \frac{d\phi_z}{dz} \right]. \quad (5.53)$$

Partial derivatives of  $\bar{U}$  with respect to the transverse shears and twist per unit length determine the material law for the transverse shear forces and torque. That is,

$$V_x = \frac{\partial \bar{U}}{\partial \psi_x} \quad V_y = \frac{\partial \bar{U}}{\partial \psi_y} \quad M_z = \frac{\partial \bar{U}}{\partial \left( \frac{d\phi_z}{dz} \right)}. \quad (5.54)$$

The shear stresses enter the definitions of the shear flow  $q$ , twisting moment resultant  $m_{zs}$ , and the transverse stress resultant  $q_z$ , given by eq. (3.37) on page 40. For a thin, curved wall we neglect the term  $\zeta/R_s$  in the factor  $(1 + \zeta/R_s)$  appearing in the integrand of eq. (3.37). It follows that the shear stresses consistent with stress resultant definitions are

$$\sigma_{zs}(s, z, \zeta) = \frac{q(s, z)}{t(s)} + \frac{12}{t^3(s)} m_{zs}(s, z) \zeta \quad \sigma_{z\zeta}(s, z) = q_z(s, z)/t(s). \quad (5.55)$$

Substitute eq. (5.55) for the stresses in complementary energy per unit length (5.52), followed by integration through the thickness to get

$$\bar{U}^* = \frac{1}{2} \int_c \frac{q^2}{Gt} ds + \frac{1}{2} \int_c \frac{1}{G} \left[ \frac{12}{t^3} m_{zs}^2 + \frac{q_z^2}{t} \right] ds. \quad (5.56)$$

### 5.5.1 Open cross-sectional contour

The shear flow in the first integral on the right-hand side of (5.56) is given by eq. (3.98) on page 51. It is repeated below.

$$q(s, z) = -\frac{k}{I_{yy}} V_x(z) \bar{Q}_y(s) - \frac{k}{I_{xx}} V_y(z) \bar{Q}_x(s). \quad (5.57)$$

Note that the shear flow is directly related to the shear forces and is independent of the torque. To account for the torque, evaluate the second integral on the right-hand side of eq. (5.56) for torsion of the open section with the straight contour presented in article 3.9 on page 57. From eq. (3.119) on page 60 these stress resultants are

$$m_{zs} = \frac{t^3}{6J} \left( 1 - \frac{\cosh ks}{\cosh \lambda} \right) M_z \quad q_z = -2Gt \frac{\sinh ks}{k \cosh \lambda} \left( \frac{d\phi_z}{dz} \right) \quad -b/2 \leq s \leq b/2, \quad (5.58)$$

where

$$\frac{d\phi_z}{dz} = \frac{M_z}{GJ} \quad J = \frac{bt^3}{3} \left( 1 - \frac{\tanh \lambda}{\lambda} \right) \quad k = \frac{2\sqrt{3}}{t} \quad \lambda = \frac{kb}{2} = \sqrt{3} \frac{b}{t}.$$

Substituting the stress resultants  $m_{zs}$  and  $q_z$  from eq. (5.58) into the second integral in the complementary strain energy (5.56), followed by evaluating the integral, we find

$$\frac{1}{2} \int_c \frac{1}{G} \left[ \frac{12}{t^3} m_{zs}^2 + \frac{q_z^2}{t} \right] ds = \frac{1}{2G} \int_{-b/2}^{b/2} \left[ \frac{12}{t^3} m_{zs}^2 + \frac{q_z^2}{t} \right] ds = \frac{M_z^2}{2GJ}. \quad (5.59)$$

Hence, the complementary strain energy per unit axial length is

$$\bar{U}^* = \frac{1}{2} \int_c \frac{1}{Gt} \left[ -\frac{k}{I_{yy}} V_x(z) \bar{Q}_y(s) - \frac{k}{I_{xx}} V_y(z) \bar{Q}_x(s) \right]^2 ds + \frac{M_z^2}{2GJ}. \quad (5.60)$$

We write the eq. (5.60) in the form

$$\bar{U}^* = \frac{1}{2} [c_{xx} V_x^2 + 2c_{xy} V_x V_y + c_{yy} V_y^2] + \frac{M_z^2}{2GJ}, \quad (5.61)$$

where  $c_{xx}$ ,  $c_{xy}$ ,  $c_{yx}$ , and  $c_{yy}$  are the flexibility influence coefficients for the cross section of the bar given by

$$c_{xx} = \left( \frac{k}{I_{yy}} \right)^2 \int_c \frac{[\bar{Q}_y(s)]^2}{Gt} ds \quad c_{xy} = c_{yx} = \frac{k^2}{I_{xx} I_{yy}} \int_c \frac{[\bar{Q}_x(s) \bar{Q}_y(s)]}{Gt} ds \quad c_{yy} = \left( \frac{k}{I_{xx}} \right)^2 \int_c \frac{[\bar{Q}_x(s)]^2}{Gt} ds. \quad (5.62)$$

### 5.5.2 Closed cross-sectional contour

The shear flow for the closed cross-sectional contour is directly related to the shear forces and the torque resolved at the shear center. Equation (3.163) on page 70 is

$$q(s, z) = \frac{M_z(z)}{2A_c} - F_x(s)V_x(z) - F_y(s)V_y(z),$$

where the shear flow distribution functions  $F_x(s)$  and  $F_y(s)$  are determined from eqs. (3.151) and (3.164) on page 69. For the closed section the stress resultants  $m_{zs}$  and  $q_z$  are assumed negligible with respect to the shear flow  $q$ . Consequently, in the complementary strain energy per unit axial length (5.56) the second integral on the right-hand side is neglected with respect to the first integral on the right-hand side. The complementary strain energy per unit axial length is then given by

$$\bar{U}^* = \frac{1}{2} \int_c \frac{1}{Gt} \left[ \frac{M_z(z)}{2A_c} - F_x(s)V_x(z) - F_y(s)V_y(z) \right]^2 ds. \quad (5.63)$$

Expand the integrand of latter equation and write it as

$$\bar{U}^* = \frac{1}{2} [c_{xx}V_x^2 + c_{yy}V_y^2 + c_{zz}M_z^2 + 2c_{xz}V_xM_z + 2c_{yz}V_yM_z + 2c_{xy}V_xV_y]. \quad (5.64)$$

The flexibility influence coefficients for the closed cross-sectional contour are

$$c_{xx} = \oint \frac{F_x^2}{Gt} ds \quad c_{yy} = \oint \frac{F_y^2}{Gt} ds \quad c_{zz} = \frac{1}{4A_c^2} \oint \frac{ds}{Gt} = \frac{1}{GJ}, \text{ and} \quad (5.65)$$

$$c_{xz} = c_{zx} = \left( \frac{1}{2A_c} \right) \int_c \frac{F_x}{Gt} ds = 0 \quad c_{yz} = c_{zy} = \left( \frac{1}{2A_c} \right) \int_c \frac{F_y}{Gt} ds = 0 \quad c_{xy} = c_{yx} = \oint \frac{F_x F_y}{Gt} ds. \quad (5.66)$$

The torsion constant  $J$  for a single-cell cross section is given by eq. (3.160) on page 70. Influence coefficients  $c_{xz} = c_{yz} = 0$ , since the shear flow distribution functions  $F_x(s)$  and  $F_y(s)$  are defined with respect to the shear center. (Refer to eq. (3.151) and eq. (3.164).)

### 5.5.3 Material law for transverse shear and torsion

The relation between the strain energy densities in shear is analogous to the one for normal stress and strain (5.37). This relation is

$$U_0^*[\sigma_{zs}] = -U_0[\gamma_{zs}, \gamma_{z\zeta}] + \sigma_{zs}\gamma_{zs} + \sigma_{z\zeta}\gamma_{z\zeta}. \quad (5.67)$$

Integrate eq. (5.67) over the cross-sectional area to get

$$\underbrace{\int_c \left[ \int_{-t/2}^{t/2} U_0^*[\sigma_{zs}] d\zeta \right] ds}_{\bar{U}^*[V_x, V_y, M_z]} = - \underbrace{\int_c \left[ \int_{-t/2}^{t/2} U_0[\gamma_{zs}, \gamma_{z\zeta}] d\zeta \right] ds}_{\bar{U}[\psi_x, \psi_y, \frac{d\phi_z}{dz}]} + \underbrace{\int_c \left[ \int_{-t/2}^{t/2} (\sigma_{zs}\gamma_{zs} + \sigma_{z\zeta}\gamma_{z\zeta}) d\zeta \right] ds}_I. \quad (5.68)$$

Substitute (5.55) for the stresses, and eq. (3.31) on page 38 for the strains, in the second integral labeled  $I$  on the right-hand side of eq. (5.68). After integration over the thickness the integral  $I$  is

$$I = \int_c \left[ q \left( -\psi_x \sin \theta + \psi_y \cos \theta + r_n s \frac{d\phi_z}{dz} \right) + m_{zs} \frac{d\phi_z}{dz} + q_z \left( \psi_x \cos \theta + \psi_y \sin \theta - r_t \frac{d\phi_z}{dz} \right) \right] ds. \quad (5.69)$$

Rearrange the integrand in eq. (5.69) to

$$I = \left[ \int_c (-q \sin \theta + q_z \cos \theta) ds \right] \psi_x + \left[ \int_c (q \cos \theta + q_z \sin \theta) ds \right] \psi_y + \left[ \int_c (r_n q + m_{zs} - r_t q_z) ds \right] \frac{d\phi_z}{dz}. \quad (5.70)$$

From eq. (3.40) on page 40 recognize that the coefficient of shear  $\psi_x$  is the shear force  $V_x$ , the coefficient of shear  $\psi_y$  is the shear force  $V_y$ , and the coefficient of the twist per unit length is the torque  $M_z$ . Hence, the integral  $I$  is given by

$$I = \int_c \left[ \int_{-t/2}^{t/2} (\sigma_{zs} \gamma_{zs} + \sigma_{z\zeta} \gamma_{z\zeta}) d\zeta \right] ds = V_x \psi_{xx} + V_y \psi_{yy} + M_z \frac{d\phi_z}{dz}. \quad (5.71)$$

The relation between the shear strain energies per unit axial length in eq. (5.68) becomes

$$\bar{U}^*[V_x, V_y, M_z] = -\bar{U}\left[\psi_x, \psi_y, \frac{d\phi_z}{dz}\right] + V_x \psi_x + V_y \psi_y + M_z \frac{d\phi_z}{dz}. \quad (5.72)$$

Take the partial derivative of (5.72) with respect to the shear force  $V_x$  as follows:

$$\frac{\partial \bar{U}^*}{\partial V_x} = -\frac{\partial \bar{U}}{\partial \psi_x} \frac{\partial \psi_x}{\partial V_x} + \psi_x + V_x \frac{\partial \psi_x}{\partial V_x} = \left( V_x - \frac{\partial \bar{U}}{\partial \psi_x} \right) \left( \frac{\partial \psi_x}{\partial V_x} \right) + \psi_x. \quad (5.73)$$

The term  $V_x - \partial \bar{U} / \partial \psi_x = 0$  in eq. (5.73) since it is the elastic material law for the shear force given by eq. (5.54). Consequently, eq. (5.73) leads to the material law for shear  $\psi_x$

$$\frac{\partial \bar{U}^*}{\partial V_x} = \psi_x. \quad (5.74)$$

Following steps similar to those used in eqs. (5.72) to (5.74) leads to the additional material laws

$$\frac{\partial \bar{U}^*}{\partial V_y} = \psi_y \text{ and } \frac{\partial \bar{U}^*}{\partial M_z} = \frac{d\phi_z}{dz}. \quad (5.75)$$

Substitute the complementary strain energy from either eq. (5.61) or (5.64) into eqs. (5.74) and (5.75) to obtain the material law governing the transverse shears and the twist per unit length. Since the expressions for the complementary strain energy per unit axial length with respect to the shear center are the same for the open contour (5.61) and the closed contour (5.64), the material law in both cases is

$$\begin{bmatrix} \psi_x \\ \psi_y \\ \frac{d\phi_z}{dz} \end{bmatrix} = \begin{bmatrix} c_{xx} & c_{xy} & 0 \\ c_{xy} & c_{yy} & 0 \\ 0 & 0 & 1/(GJ) \end{bmatrix} \begin{bmatrix} V_x \\ V_y \\ M_z \end{bmatrix}. \quad (5.76)$$

Assume we can invert the material law (5.76) and write it as

$$\begin{bmatrix} V_x \\ V_y \\ M_z \end{bmatrix} = \begin{bmatrix} s_{xx} & s_{xy} & 0 \\ s_{xy} & s_{yy} & 0 \\ 0 & 0 & GJ \end{bmatrix} \begin{bmatrix} \psi_x \\ \psi_y \\ \phi'_z \end{bmatrix}, \quad (5.77)$$

where

$$[s_{xx}, s_{yy}, s_{xy}] = [c_{yy}, c_{xx}, -c_{xy}] / (c_{xx}c_{yy} - c_{xy}^2). \quad (5.78)$$

The strain energy per unit axial length in shear and torsion is

$$\bar{U} = \frac{1}{2} \left[ s_{xx} \psi_x^2 + 2s_{xy} \psi_x \psi_y + s_{yy} \psi_y^2 + GJ \left( \frac{d\phi_z}{dz} \right)^2 \right]. \quad (5.79)$$

## 5.6 Total strain energy expressions for a thin-walled bar

The total strain energy is obtained from strain energy per unit axial length by integration with respect to axial coordinate  $z$ ,  $0 \leq z \leq L$ , where  $L$  is the length of the bar. The total strain energy is written as

$$U = U_\epsilon + U_\gamma, \quad (5.80)$$

where the strain energy obtained from axial normal strain  $\epsilon_{zz}$  is denoted by  $U_\epsilon$ , and the strain energy obtained from shear strains  $\gamma_{zs}$  and  $\gamma_{z\zeta}$  is denoted by  $U_\gamma$ . From eqs. (5.47) and (5.79) these strain energies are

$$U_\epsilon = \int_0^L \left\{ \frac{E}{2} \left[ A \left( \frac{dw}{dz} \right)^2 + I_{xx} \left( \frac{d\phi_x}{dz} \right)^2 + I_{yy} \left( \frac{d\phi_y}{dz} \right)^2 + 2I_{xy} \left( \frac{d\phi_x}{dz} \right) \left( \frac{d\phi_y}{dz} \right) \right] - N_T \left( \frac{dw}{dz} \right) - M_{xT} \left( \frac{d\phi_x}{dz} \right) - M_{yT} \left( \frac{d\phi_y}{dz} \right) \right\} dz, \quad (5.81)$$

and

$$U_\gamma = \frac{1}{2} \int_0^L \left[ s_{xx} \psi_x^2 + 2s_{xy} \psi_x \psi_y + s_{yy} \psi_y^2 + GJ \left( \frac{d\phi_z}{dz} \right)^2 \right] dz. \quad (5.82)$$

The stiffness coefficients in eq. (5.82) are computed from the compliance coefficients as shown in eq. (5.78).

The total complementary strain energy is written as

$$U^* = U_\sigma^* + U_\tau^*, \quad (5.83)$$

where the complementary strain energy obtained from axial normal stress  $\sigma_{zz}$  is denoted by  $U_\sigma^*$ , and the complementary strain energy obtained from shear stresses  $\sigma_{zs}$  and  $\sigma_{z\zeta}$  is denoted by  $U_\tau^*$ . From eqs. (5.51) and (5.61) these complementary strain energies are

$$U_\sigma^* = \frac{1}{2E} \int_0^L \left[ \frac{(N + N_T)^2}{A} + k \frac{(M_x + M_{xT})^2}{I_{xx}} + k \frac{(M_y + M_{yT})^2}{I_{yy}} - 2kI_{xy} \frac{(M_x + M_{xT})(M_y + M_{yT})}{I_{xx}I_{yy}} \right] dz, \quad (5.84)$$

and

$$U_\tau^* = \frac{1}{2} \int_0^L \left[ c_{xx} V_x^2 + 2c_{xy} V_x V_y + c_{yy} V_y^2 + \frac{M_z^2}{GJ} \right] dz. \quad (5.85)$$

The compliance coefficients in eq. (5.85) are determined by eq. (5.62) for the open contour and by eqs. (5.65) and (5.66) for the closed contour.

### 5.7 Castigliano's first theorem

The work function can be written in terms of the generalized displacements and stiffness influence coefficients by substituting  $n = 2$  in eq. (5.10), then substituting the result for the generalized forces into the work eq. (5.5). The result is

$$W = \left(\frac{1}{2}\right)(k_{11}q_1^2 + 2k_{12}q_1q_2 + k_{22}q_2^2). \quad (5.86)$$

Take the partial derivative of the work function with respect to  $q_1$  and  $q_2$  to get

$$\frac{\partial W}{\partial q_1} = k_{11}q_1 + k_{12}q_2 \quad \frac{\partial W}{\partial q_2} = k_{12}q_1 + k_{22}q_2.$$

Comparing these results for the partial derivatives of  $W$  to the eq. (5.10) for  $n = 2$ , we find

$$Q_1 = \frac{\partial W}{\partial q_1} \quad Q_2 = \frac{\partial W}{\partial q_2}. \quad (5.87)$$

That is, the partial derivative of the work function with respect to a displacement equals the corresponding force. Equation (5.87) yields the stiffness law, and it is the conjugate to eq. (5.8) that yields the compliance law.

For adiabatic deformation of a Hookean material the first law of thermodynamics shows that the work done per unit volume is equal to the strain energy density. Refer to eq. (5.36) on page 138. For the body composed of a Hookean material, we take the work done by the external loads equal to the strain energy of the entire body. Then  $W = U$  in eq. (5.87), which leads to Castigliano's first theorem in terms of generalized displacements and forces as follows:

#### Castigliano's first theorem

If the strain energy of an elastic structure is expressed in terms of the independent generalized displacement components  $q_i$ ,  $i = 1, 2, \dots, n$ , in the direction of the prescribed generalized point forces  $Q_1, Q_2, \dots, Q_n$ , then the first partial derivative of the strain energy with respect to the displacement  $q_i$  is equal to the corresponding force  $Q_i$  or

$$Q_i = \frac{\partial U}{\partial q_i} \quad i = 1, 2, \dots, n$$

For the thin-walled bar the strain energy  $U$  is given by eqs. (5.80) to (5.82), and it has the form

$$U = \int_0^L \bar{U}(w', \phi_x', \phi_y', \phi_z', \psi_x, \psi_y) dz.$$

The prime indicates ordinary derivative with respect to coordinate  $z$  (e.g.  $w' = \frac{dw}{dz}$ ), and the averaged shears from eq. (3.32) on page 38 are repeated below.



$$\psi_x(z) = \frac{du}{dz} + \phi_y(z) \quad \psi_y(z) = \frac{dv}{dz} + \phi_x(z).$$

The procedure in the application of the first theorem to structural analysis is to assume functions for the displacement components  $u(z)$ ,  $v(z)$ , and  $w(z)$  and rotations  $\phi_x(z)$ ,  $\phi_y(z)$ , and  $\phi_z(z)$  that satisfy the three conditions below.

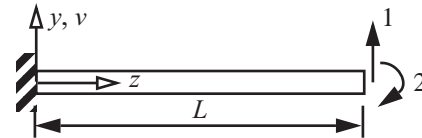
1. The displacement and rotations must be continuous functions of the coordinate  $z$ , so that their derivatives with respect to the coordinate, or strains, exist and are integrable over the domain of the bar.
2. The displacement and rotations must satisfy any prescribed conditions at the boundaries  $z = 0$  and  $z = L$ .
3. The displacement and rotation functions are selected such that they equate to the generalized displacements  $q_i$ ,  $i = 1, 2, \dots, n$ , at their defined points of application.

Displacement and rotation functions that satisfy continuity conditions and prescribed displacement boundary conditions are said to be **kinematically admissible**. Kinematically admissible displacements lead to a compatible deformation. Compatibility of a deformable body means the displacements are continuous and single-valued (i.e., no gaps or overlaps of material result in the deformed state). **Castigliano's first theorem is a condition of equilibrium consistent with the assumed kinematically admissible displacements.**

### Example 5.1 Response of cantilever beam by Castigliano's first theorem

The cantilever beam shown in figure 5.11 is subject to a vertical displacement  $q_1$  and a clockwise rotation  $q_2$  at its tip, and a uniform thermal moment  $M_{xT}$  along its length. The cross section is symmetric with respect to the  $y$ - $z$  plane.

**Fig. 5.11** Cantilever beam subject to a temperature gradient and end loads.



Assume a kinematically admissible displacement and bending rotation as

$$v(z) = q_1(z/L) \quad \phi_x(z) = q_2(z/L) \quad 0 \leq z \leq L. \quad (\text{a})$$

Continuous and differentiable functions for the generalized displacements are ensured by employing polynomial functions in coordinate  $z$ . Also, assumptions (a) satisfy the prescribed end conditions  $v(0) = 0$  and  $\phi_x(0) = 0$ . Therefore, assumptions (a) satisfy the conditions of kinematic admissibility. The strain energy reduces to a function generalized displacements  $q_1$  and  $q_2$ . For this example the expression for the strain energy from (5.81) and (5.82) is

$$U = \int_0^L \bar{U}[\phi'_x, \psi_y] dz \quad \text{where} \quad \bar{U}[\phi'_x, \psi_y] = \frac{1}{2} EI_{xx} (\phi'_x)^2 - M_{xT} (\phi'_x) + \frac{1}{2} s_{yy} \psi_y^2. \quad (\text{b})$$

The derivatives of the functions in (a) with respect to  $z$ , and the evaluation of the transverse shear strain are

$$v'(z) = q_1/L \quad \phi_x'(z) = q_2/L \quad \psi_y(z) = q_1/L + q_2(z/L). \quad (\text{c})$$

Substitute eq. (c) into eq. (b) to get

$$\bar{U} = \frac{EI_{xx}}{2L^2} q_2^2 + \frac{s_{yy}}{2} \left( \frac{q_1}{L} + \frac{q_2}{L} z \right)^2 - \frac{M_{xT}}{L} q_2. \quad (\text{d})$$

The definite integral of eq. (d) over the length of beam yields the discrete form of the strain energy (b). The result is

$$U(q_1, q_2) = \frac{EI_{xx}}{2L} q_2^2 + \frac{s_{yy}}{2L} q_1^2 + \frac{s_{yy}}{2} q_1 q_2 + \frac{s_{yy}L}{6} q_2^2 - M_{xT} q_2. \quad (\text{e})$$

The strain energy expression in eq. (b) is called a **functional** because its value is determined by the functions  $\phi_x(z)$  and  $\psi_y(z)$ . Assumption (a) results in a strain energy function given by eq. (e) where the generalized displacements  $q_1$  and  $q_2$  are the independent variables. The generalized forces  $Q_1$  and  $Q_2$  corresponding to  $q_1$  and  $q_2$ , respectively, are determined by Castiglano's first theorem. That is,

$$Q_1 = \frac{\partial U}{\partial q_1} \text{ and } Q_2 = \frac{\partial U}{\partial q_2}. \quad (\text{f})$$

Take the partial derivatives of eq. (e) with respect to  $q_1$  and  $q_2$  to find

$$Q_1 = \frac{s_{yy}}{L} q_1 + \frac{s_{yy}}{2} q_2 \text{ and } Q_2 = \frac{s_{yy}}{2} q_1 + \left( \frac{EI_{xx}}{L} + \frac{Ls_{yy}}{3} \right) q_2 - M_{xT}. \quad (\text{g})$$

The expressions in eq. (g) are written in the matrix form

$$\begin{bmatrix} Q_1 \\ Q_2 \end{bmatrix} = \begin{bmatrix} \frac{s_{yy}}{L} & \frac{s_{yy}}{2} \\ \frac{s_{yy}}{2} & \frac{EI_{xx}}{L} + \frac{Ls_{yy}}{3} \end{bmatrix} \begin{bmatrix} q_1 \\ q_2 \end{bmatrix} - \begin{bmatrix} 0 \\ 1 \end{bmatrix} M_{xT}. \quad (\text{h})$$

The elements of the 2X2 stiffness matrix in eq. (h) are the stiffness influence coefficients. Also note that the stiffness matrix is symmetric.

From eq. (3.79) Hooke's law for the bending moment is

$$M_x = EI_{xx} \phi_x'(z) - M_{xT}, \quad (\text{i})$$

and from eq. (5.77) the material law for the transverse shear force is

$$V_y = s_{yy} \psi_y. \quad (\text{j})$$

Substitute  $\phi_x'$  and  $\psi_y$  from eq. (c) into eqs. (i) and (j) to get

$$M_x = EI_{xx}(q_2/L) - M_{xT} \text{ and } V_y = s_{yy}(q_1/L + q_2(z/L)). \quad (\text{k})$$

Equilibrium differential equations (3.54) and (3.55) are

$$\frac{dV_y}{dz} = 0 \text{ and } \frac{dM_x}{dz} - V_y = 0 \text{ for } 0 < z < L. \quad (l)$$

Substitute the bending moment and shear force from eq. (k) into eq. (l) to get

$$\frac{dV_y}{dz} = \frac{s_{yy}}{L} q_2 \neq 0 \text{ and } \frac{dM_x}{dz} - V_y = 0 - \left( \frac{s_{yy}}{L} q_2 z + c \right) \neq 0, \quad (m)$$

where  $c$  denotes a constant of integration for the shear force. The differential equations are not satisfied for the assumption in eq. (a). Of all the possible kinematically admissible displacement functions those given by (a) lead to an approximate equilibrium solution but not the exact equilibrium solution. ■

## 5.8 Castigliano's second theorem

The generalized displacements from Hooke's law in eq. (5.3) are substituted into the work eq. (5.5) to express the work function as

$$W = \left( \frac{1}{2} \right) (c_{11} Q_1^2 + c_{12} Q_1 Q_2 + c_{21} Q_2 Q_1 + c_{22} Q_2^2).$$

Take the partial derivative of the work function with respect to  $Q_1$  and  $Q_2$  to get

$$\frac{\partial W}{\partial Q_1} = c_{11} Q_1 + c_{12} Q_2 \quad \frac{\partial W}{\partial Q_2} = c_{12} Q_1 + c_{22} Q_2.$$

Comparing these results for the partial derivatives of  $W$  to the two equations (5.3), we find

$$q_1 = \frac{\partial W}{\partial Q_1} \text{ and } q_2 = \frac{\partial W}{\partial Q_2}. \quad (5.88)$$

If the work function is written in terms of the forces and flexibility influence coefficients, then partial derivatives of the work with respect to a force equals the corresponding displacement. The work done on a Hookean body is equal to the change in energy stored due to elastic deformation. We use the complementary strain energy  $U^*$  in this case to represent the change in energy since  $U^* = 0$  in the reference state. Hence, set  $W = U^*$ , and we arrive at Castigliano's second theorem in terms of generalized displacements and forces, which is as follows:

### Castigliano's second theorem

If an elastic structure is mounted such that rigid body displacements are impossible and certain generalized point forces  $Q_1, Q_2, \dots, Q_n$  act on the structure, in addition to distributed loads and thermal strains, the displacement component  $q_i, i = 1, 2, \dots, n$  of the point of application of force  $Q_i$  in the direction of  $Q_i$  is determined by the equation

$$q_i = \frac{\partial U^*}{\partial Q_i}.$$

For a thin-walled bar the complementary strain energy given by eqs. (5.83) to (5.85) has the form

$$U^* = \int_0^L \bar{U}^*(V_x, V_y, N, M_x, M_y, M_z) dz. \quad (5.89)$$

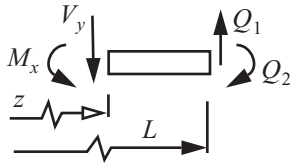
The procedure in the application of the second theorem to the analysis of thin-walled bars is to assume functions in the axial coordinate  $z$  for the bar resultants  $V_x$ ,  $V_y$ ,  $N$ ,  $M_x$ ,  $M_y$ , and  $M_z$ , that satisfy the three conditions below.

1. The bar resultants must be represented by functions of the Cartesian coordinates that satisfy the differential equations of equilibrium of article 3.6.1 on page 41 for  $0 < z < L$ .
2. The functions for the bar resultants must satisfy their prescribed values on the boundaries at  $z = 0$  and  $z = L$ .
3. The functions for the bar resultants must contain the generalized forces  $Q_i$ ,  $i = 1, 2, \dots, n$ , as parameters.

Functions for the bar resultants that satisfy the differential equations of equilibrium and prescribed force boundary conditions are said to be **statically admissible**. **Castigliano's second theorem is the condition of compatibility for the statically admissible bar resultants**. Compatibility of a deformable body means the displacements are continuous and single-valued (i.e., no gaps or overlaps of material result in the deformed state). Castigliano's second theorem is useful in determining displacements of a structure.

#### Example 5.2 Response of the cantilever beam by Castigliano's second theorem

**Fig. 5.12**  
**Free body**  
**diagram of**  
**the beam.**



Consider the cantilever beam in example 5.1 on page 147 again. Take the end loads  $Q_1$  and  $Q_2$  to be specified, and use Castigliano's second theorem to determine the corresponding displacements  $q_1$  and  $q_2$ . We note that the beam in this example is statically determinate. From equilibrium of the free body diagram shown in figure 5.12 the statically admissible internal actions are.

$$V_y = Q_1 \quad M_x = Q_2 - Q_1(L - z) \quad 0 \leq z \leq L. \quad (a)$$

The complementary strain energy from (5.84) and (5.85) is

$$U^* = \int_0^L \bar{U}^*[V_y, M_x] dz, \text{ where } \bar{U}^*[V_y, M_x] = \frac{1}{2} c_{yy} V_y^2 + \frac{1}{2EI_{xx}} (M_x + M_{xT})^2. \quad (b)$$

Substitute the shear force and bending moment from eq. (a) into the complementary strain energy per unit axial length given in eq. (b) to get

$$\bar{U}^* = \frac{c_{yy}}{2} Q_1^2 + \frac{[Q_2 - (L - z)Q_1 + M_{xT}]^2}{2EI_{xx}}. \quad (c)$$

Integrate eq. (c) over the length of the beam to find the complementary strain energy as

$$U^* = \left( \frac{c_{yy}L}{2} + \frac{L^3}{6EI_{xx}} \right) Q_1^2 - \frac{L^2}{2EI_{xx}} Q_1 Q_2 + \frac{L}{2EI_{xx}} Q_2^2 - \frac{L^2}{2EI_{xx}} M_{xT} Q_1 + \frac{L}{EI_{xx}} M_{xT} Q_2 + \frac{LM_{xT}^2}{2EI_{xx}}. \quad (d)$$

The statically admissible functions assumed in eq. (a) transform the complementary strain energy functional

given by eq. (b) to a function of the independent variables  $Q_1$  and  $Q_2$  in eq. (d). Castiglino's second theorem determines the generalized displacements  $q_1$  and  $q_2$  corresponding to the generalized forces  $Q_1$  and  $Q_2$ . That is,

$$q_1 = \frac{\partial \bar{U}^*}{\partial Q_1} \text{ and } q_2 = \frac{\partial \bar{U}^*}{\partial Q_2}. \quad (\text{e})$$

Substitute the complementary strain energy (d) into Castigliano's second theorem (e) to get

$$q_1 = \left( c_{yy}L + \frac{L^3}{3EI_{xx}} \right) Q_1 - \frac{L^2}{3EI_{xx}} Q_2 - \frac{L^2}{2EI_{xx}} M_{xT}, \text{ and} \quad (\text{f})$$

$$q_2 = -\frac{L^2}{EI_{xx}} Q_1 + \frac{L}{EI_{xx}} Q_2 + \frac{L}{EI_{xx}} M_{xT}. \quad (\text{g})$$

Equations (f) and (g) are written in the matrix form as

$$\begin{bmatrix} q_1 \\ q_2 \end{bmatrix} = \begin{bmatrix} c_{yy}L + \frac{L^3}{3EI_{xx}} & -\frac{L^2}{2EI_{xx}} \\ -\frac{L^2}{2EI_{xx}} & \frac{L}{EI_{xx}} \end{bmatrix} \begin{bmatrix} Q_1 \\ Q_2 \end{bmatrix} + \begin{bmatrix} -\frac{L^2}{2EI_{xx}} \\ \frac{L}{EI_{xx}} \end{bmatrix} M_{xT}. \quad (\text{h})$$

The elements of the 2X2 compliance matrix in eq. (h) are the flexibility influence coefficients. Also note that the compliance matrix is symmetric. ■

## References

- Allen, D. H., and Haisler, W. E. *Introduction to Aerospace Structural Analysis*, 2d ed. London:, John Wiley & Sons, 1985, pp. 101, 102, & 287.
- Donaldson, B. K. *Analysis of Aircraft Structures: An Introduction*. New York: McGraw-Hill, Inc., 1993, p. 510.
- Fung, Y. C. *Foundations of Solid Mechanics*. Englewood Cliffs, NJ: Prentice-Hall, Inc., 1965, pp. 1-7, 270-278, 348.
- Lanczos, C. *The Variational Principles of Mechanics*. 4th ed. New York: Dover Publications, Inc., 1970, pp.54-60, 68-73. (Originally published by the University of Toronto Press).
- Langhaar, H. L. *Energy Methods in Applied Mechanics*. New York: John Wiley & Sons, Inc., 1962, pp. 75-89, & 120.
- Malvern, L. E. *Introduction to the Mechanics of a Continuous Medium*. Englewood Cliffs, NJ: Prentice-Hall, Inc., 1969, p.229.

# Applications of Castigliano's Theorems

## 6.1 Coplanar trusses

### 6.1.1 Castigliano's first theorem

Consider a truss idealized as an assemblage of uniform bars connected by smooth ball-and-socket joints in three-dimensional trusses, or by smooth hinge joints in a coplanar truss. External forces are assumed to act only at the joints. The line connecting the joints at the end of each bar is assumed to coincide with the reference axis of the bar. Hence, the axial force and strain in each bar is uniform along its length, and the bar is either in tension or compression.

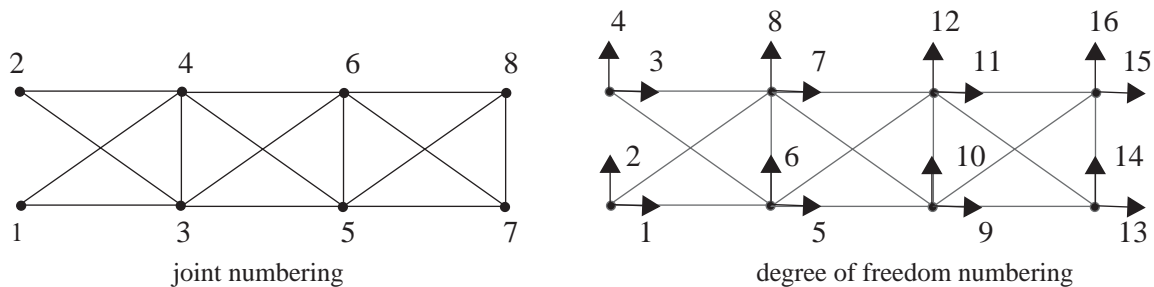


**Fig. 6.1** A fifteen-bar truss.

A coplanar truss consisting of fifteen bars and eight joints is shown in figure 6.1. Each joint in a coplanar truss has two degrees of freedom, one horizontal displacement and the one vertical displacement. Hence, there are sixteen displacement degrees of freedom for this truss. At joint  $i$ ,  $i = 1, 2, \dots, 8$ , the horizontal displacement is denoted by  $q_{2i-1}$  and the vertical displacement is denoted by  $q_{2i}$ . The positive directions for the displacements and corresponding forces in the fifteen bar truss are shown in figure 6.1. The original coordinates of the joints and the sixteen displacements completely define the configuration of the truss in the deformed state.

A typical bar in a truss connecting joints labeled  $i$  and  $j$  is shown in figure 6.2(a). The location of the bar in a  $X$ - $Y$  coordinate system is established by the coordinates of joint  $i$  ( $X_i, Y_i$ ) and those of joint  $j$  ( $X_j, Y_j$ ). The angle of

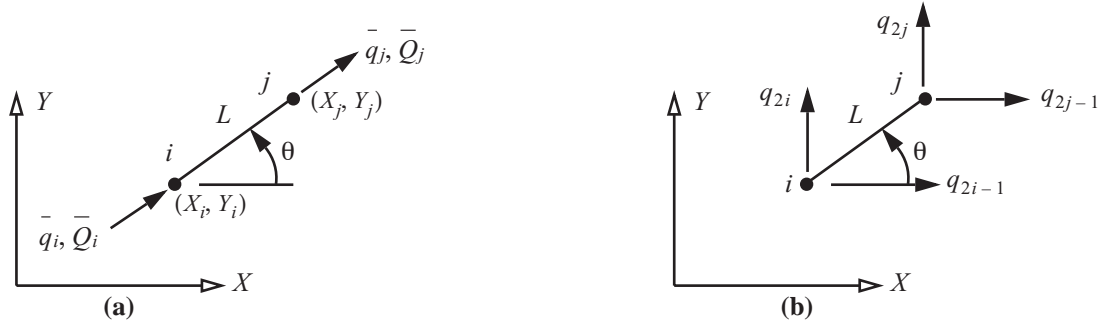


**Fig. 6.2** (a) Truss bar  $i$ - $j$  subject to axial displacements. (b) Truss bar  $i$ - $j$  subject to horizontal and vertical displacements.

the bar with respect to the  $X$ -axis is denoted by  $\theta$ . Trigonometric functions of the angle  $\theta$  are related to the coordinates of the joints and length  $L$  of the bar by

$$\cos \theta = (X_j - X_i)/L \quad \sin \theta = (Y_j - Y_i)/L \quad L = \sqrt{(X_j - X_i)^2 + (Y_j - Y_i)^2}. \quad (6.1)$$

As shown in figure 6.2(a), the axial displacement of the bar at joint  $i$  is  $\bar{q}_i$  and that of joint  $j$  is  $\bar{q}_j$ . Assume the axial displacement  $w(z) = \bar{q}_i(1 - z/L) + \bar{q}_j(z/L)$ ,  $0 \leq z \leq L$ . The axial strain  $\epsilon_{zz} = w' = (\bar{q}_j - \bar{q}_i)/L$ , and denote the elongation  $\Delta_{i-j} = \bar{q}_j - \bar{q}_i$ . Also, assume the temperature change is uniform in  $z$ . From eq. (3.79) on page 46 the axial force in the bar is

$$N_{i-j} = \left( \frac{EA}{L} \right)_{i-j} \Delta_{i-j} - (N_T)_{i-j}. \quad (6.2)$$

The differential equation of equilibrium  $\frac{dN}{dz} = 0$  (eq. (3.53) on page 42) is satisfied under assumptions of uniform axial strain and uniform axial change in temperature. The strain energy (5.81) on page 145 of the bar reduces to

$$U = \frac{1}{2} \frac{EA}{L} \Delta_{i-j}^2 - N_T \Delta_{i-j}. \quad (6.3)$$

Castigliano's first theorem determines the force  $\bar{Q}_i$  corresponding to displacement  $\bar{q}_i$ , and force  $\bar{Q}_j$  corresponding to displacement  $\bar{q}_j$ . The results are

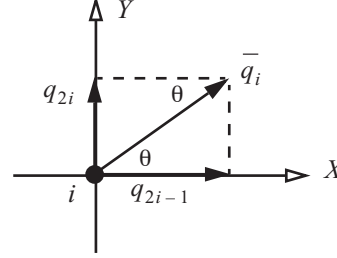
$$\bar{Q}_i = \frac{\partial U}{\partial \bar{q}_i} = \frac{EA}{L} (\bar{q}_i - \bar{q}_j) + N_T \quad \text{and} \quad \bar{Q}_j = \frac{EA}{L} (-\bar{q}_i + \bar{q}_j) - N_T. \quad (6.4)$$

Note that  $\bar{Q}_i + \bar{Q}_j = 0$ , which is the condition of equilibrium.



In figure 6.2(b) truss displacements of joint  $i$  are  $(q_{2i-1}, q_{2i})$  and for joint  $j$  are  $(q_{2j-1}, q_{2j})$ . At joint  $i$  the

**Fig. 6.3** Relation between the displacements components at joint  $i$ .



truss and axial displacements are related by  $q_{2i-1} = \bar{q}_i \cos \theta$  and  $q_{2i} = \bar{q}_i \sin \theta$  as shown in figure 6.3. Likewise at joint  $j$   $q_{2j-1} = \bar{q}_j \cos \theta$  and  $q_{2j} = \bar{q}_j \sin \theta$ . These relations can be solved for the axial displacement in terms of the truss displacements to get

$$\bar{q}_i = q_{2i-1} \cos \theta + q_{2i} \sin \theta \quad \bar{q}_j = q_{2j-1} \cos \theta + q_{2j} \sin \theta. \quad (6.5)$$

The elongation of the truss bar  $i-j$  in terms of the joint displacements is

$$\Delta_{i-j} = \bar{q}_j - \bar{q}_i = (q_{2j-1} - q_{2i-1}) \cos \theta + (q_{2j} - q_{2i}) \sin \theta. \quad (6.6)$$

The elongation (6.6) is the sum of the projections of the relative displacements onto the reference axis of the undeformed bar which is depicted in figure 6.4.

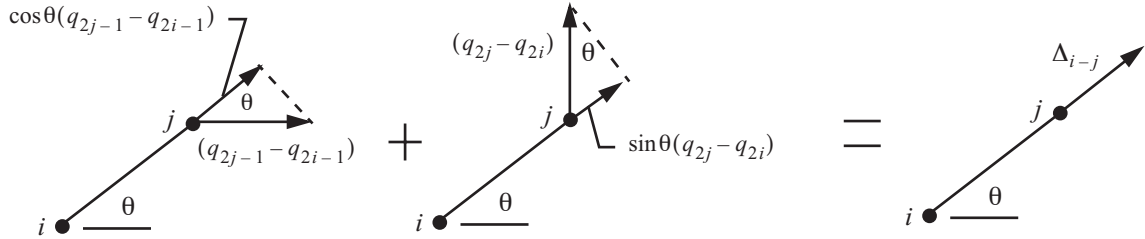


**Fig. 6.4** Elongation of the bar as the sum of projections of the relative horizontal and vertical displacements along the direction of the undeformed bar.

For the  $m$ -th bar of the truss shown in figure 6.1, where,  $m = 1, 2, \dots, 15$ , denote its extension stiffness by  $(EA/L)_m$ , its elongation by  $\Delta_m$ , and denote the thermal force by  $N_{Tm}$ . The temperature change is uniform in each bar, but can be different from bar to bar. The relation between bar index  $m$  and the joints  $i$  and  $j$  of the bar are defined by assignment. For example in figure 6.1, the bar identified by  $m = 2$  may be selected as the bar connecting joint 1 to joint 4, so its elongation (6.6) is

$$\Delta_2 = \Delta_{1-4} = (q_7 - q_1) \cos \theta_2 + (q_8 - q_2) \sin \theta_2.$$

The sine and cosine of angle  $\theta_2$  are determined from eq. (6.1). The strain energy of the assemblage is simply the sum of the strain energies in each bar, where (6.3) is the energy for one bar. Hence, the total strain energy is

$$U = \sum_{m=1}^{15} \left\{ \frac{1}{2} \left( \frac{EA}{L} \right)_m \Delta_m^2 - N_{Tm} \Delta_m \right\} \quad (6.7)$$

The displacements  $q_n$  and the corresponding forces  $Q_n$ ,  $n = 1, 2, \dots, 16$ , used in the formulation of Castigliano's theorem are the displacements and corresponding forces at the joints. Hence, Castigliano's first theorem for the truss shown in figure 6.1 is

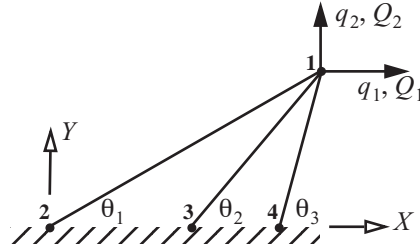
$$Q_n = \sum_{m=1}^{15} \left[ \left( \frac{EA}{L} \right) \Delta_m - N_{Tm} \right] \frac{\partial \Delta_m}{\partial q_n} \quad n = 1, 2, \dots, 16. \quad (6.8)$$

### Example 6.1 Three-bar coplanar truss

The coplanar truss shown in figure 6.5 consists of three bars ( $m = 1, 2, 3$ ) and four joints 1, 2, 3, 4. Beginning joint  $i$  and end joint  $j$  for each bar are listed in the figure. Joints 2, 3, and 4 are fixed so their displacements equal zero, and joint 1 is movable. The change in the thermal force in each bar is equal to zero. The spring stiffness of the bars are denoted by  $(EA/L)_m$ . Determine the  $2 \times 2$  stiffness matrix using Castigliano's first theorem.

**Fig. 6.5** Three-bar truss.

m	joint i	joint j
1	2	1
2	3	1
3	4	1



**Solution.** The elongation of each bar as determined from eq. (6.6) is

$$\Delta_m = \cos(\theta_m)q_1 + \sin(\theta_m)q_2 \quad m = 1, 2, 3. \quad (a)$$

Castigliano's theorem (6.8) applied to this example yields

$$Q_1 = \sum_{m=1}^3 \left( \frac{EA}{L} \right)_m [\cos(\theta_m)q_1 + \sin(\theta_m)q_2] [\cos(\theta_m)] \quad (b)$$

$$Q_2 = \sum_{m=1}^3 \left( \frac{EA}{L} \right)_m [\cos(\theta_m)q_1 + \sin(\theta_m)q_2] [\sin(\theta_m)] \quad (c)$$

These results are written in the matrix form

$$\begin{bmatrix} Q_1 \\ Q_2 \end{bmatrix} = \begin{bmatrix} k_{11} & k_{12} \\ k_{21} & k_{22} \end{bmatrix} \begin{bmatrix} q_1 \\ q_2 \end{bmatrix}, \quad (d)$$

where the elements of the stiffness matrix are

$$k_{11} = \sum_{m=1}^3 \left( \frac{EA}{L} \right)_m \cos^2(\theta_m) \quad k_{22} = \sum_{m=1}^3 \left( \frac{EA}{L} \right)_m \sin^2(\theta_m) \quad k_{12} = k_{21} = \sum_{m=1}^3 \left( \frac{EA}{L} \right)_m \cos(\theta_m) \sin(\theta_m). \quad (e)$$

Note that this example is statically indeterminate, since there are only two equilibrium equations at the movable

joint 1 but three unknown bar forces. For specified nodal forces  $Q_1$  and  $Q_2$ , matrix eq. (d) is solved for the nodal displacements  $q_1$  and  $q_2$ . From eq. (a) the elongation of each bar is then computed, and from these elongations the bar forces are determined from

$$N_m = \left( \frac{EA}{L} \right)_m \Delta_m \quad m = 1, 2, 3 \quad \blacksquare \quad (f)$$

### Example 6.2 Three-bar truss with lack of fit

Consider the same three bar-truss of example 6.1, but now assume that bar 1 was too short and had to be stretched an amount  $\bar{\Delta}_1$  in order to connect it to joint 1. This is a case of lack of fit, and lack of fit is common in the fabrication of structures. That is, before the external loads are applied ( $Q_1 = Q_2 = 0$ ), the truss bars experience initial forces due to the lack of fit of bar 1. Determine the initial forces in the bars using Castigliano's first theorem.

**Solution.** Lack of fit can be included in the energy analysis by modifying the specified thermal force term in the strain energy (6.7). For uniform material properties and uniform change in temperature, the thermal force in a truss bar is  $N_T = EA\alpha\Delta T$ . (Refer to eq. (3.75) on page 46.) The factor  $\alpha\Delta T = \varepsilon_0$  is the initial strain due to the temperature change. Note  $\varepsilon_0$  is dimensionless. Now interpret  $\varepsilon_0$  as the initial strain specified due to lack of fit.

The initial strain due to the specified displacement  $\bar{\Delta}$  required to connect a bar to a joint is  $\varepsilon_0 = \bar{\Delta}/L$ . Let  $N_T \rightarrow N_{\bar{\Delta}} = EA(\bar{\Delta}/L)$ . The strain energy is modified to

$$U = \sum_{m=1}^3 \left\{ \frac{1}{2} \left( \frac{EA}{L} \right)_m \Delta_m^2 - N_{\bar{\Delta}m} \Delta_m \right\}. \quad (a)$$

The specified initial strain is only for bar 1, so

$$U = \sum_{m=1}^3 \left\{ \frac{1}{2} \left( \frac{EA}{L} \right)_m \Delta_m^2 - \left( \frac{EA}{L} \right)_1 \bar{\Delta}_1 \Delta_1 \right\}. \quad (b)$$

Castigliano's theorem (6.8) leads to

$$Q_n = \sum_{m=1}^3 \left[ \left( \frac{EA}{L} \right)_m \Delta_m \right] \frac{\partial \Delta_m}{\partial q_n} - \left( \frac{EA}{L} \right)_1 \bar{\Delta}_1 \left( \frac{\partial \Delta_1}{\partial q_n} \right) \quad n = 1, 2. \quad (c)$$

The matrix form of eq. (c) is

$$\begin{bmatrix} Q_1 \\ Q_2 \end{bmatrix} = \begin{bmatrix} k_{11} & k_{12} \\ k_{21} & k_{22} \end{bmatrix} \begin{bmatrix} q_1 \\ q_2 \end{bmatrix} - \left( \frac{EA}{L} \right)_1 \bar{\Delta}_1 \begin{bmatrix} \cos(\theta_1) \\ \sin(\theta_1) \end{bmatrix}. \quad (d)$$

Elements of the stiffness matrix are the same as given by eq. (e) of example 6.1. Set  $Q_1 = 0$  and  $Q_2 = 0$ , since no external forces are applied to the joint just after assembly. Then solve the matrix equation (d) for the joint displacements to get

$$\begin{bmatrix} q_1 \\ q_2 \end{bmatrix} = \begin{bmatrix} k_{11} & k_{12} \\ k_{21} & k_{22} \end{bmatrix}^{-1} \begin{bmatrix} \cos(\theta_1) \\ \sin(\theta_1) \end{bmatrix} \left( \frac{EA}{L} \right)_1 \bar{\Delta}_1. \quad (e)$$

From this solution for the displacements we can calculate the elongation of each bar after assembly from eq. (a) in example 6.1. The initial bar forces after assembly are computed from

$$N_1 = \left( \frac{EA}{L} \right)_1 (\Delta_1 - \bar{\Delta}_1) \quad N_2 = \left( \frac{EA}{L} \right)_2 \Delta_2 \quad N_3 = \left( \frac{EA}{L} \right)_3 \Delta_3. \quad (f)$$

A specific case:  $\theta_1 = 30^\circ$ ,  $\theta_2 = 45^\circ$ ,  $\theta_3 = 60^\circ$ , and  $EA$  is the same for each bar. Take  $L_1 = L$ , so that  $L_2 = L/\sqrt{2}$ , and  $L_3 = L/(\sqrt{3})$ . The solution for the displacements from eq. (b) are  $q_1 = 1.458\bar{\Delta}_1$  and  $q_2 = -\bar{\Delta}_1$ . The elongations are  $\Delta_1 = 0.763\bar{\Delta}_1$ ,  $\Delta_2 = 0.324\bar{\Delta}_1$ , and  $\Delta_3 = -0.137\bar{\Delta}_1$ , and the bar forces from eq. (f) are

$$N_1 = -0.237EA(\bar{\Delta}_1/L) \quad N_2 = 0.458EA(\bar{\Delta}_1/L) \quad N_3 = -0.237EA(\bar{\Delta}_1/L). \quad (g)$$

## 6.1.2 Castigliano's second theorem for a statically determinate truss

### Example 6.3 Truss displacements

The truss shown in figure 6.6 consists of three bars labeled 1-2, 1-3, and 2-3. Joint 1 is a fixed pin, and pin joint 3 is free to move vertically but not horizontally. A downward applied force of a 84,000 N acts at joint 2. The cross-sectional areas of bars are  $A_{1-2} = 900\text{mm}^2$ ,  $A_{1-3} = 300\text{mm}^2$ , and  $A_{2-3} = 1,200\text{mm}^2$ . Each bar has a modulus of elasticity  $E = 70,000 \text{ N/mm}^2$ . The degree of freedom numbering is shown the figure. Determine displacements  $q_3$  and  $q_4$  by Castigliano's second theorem

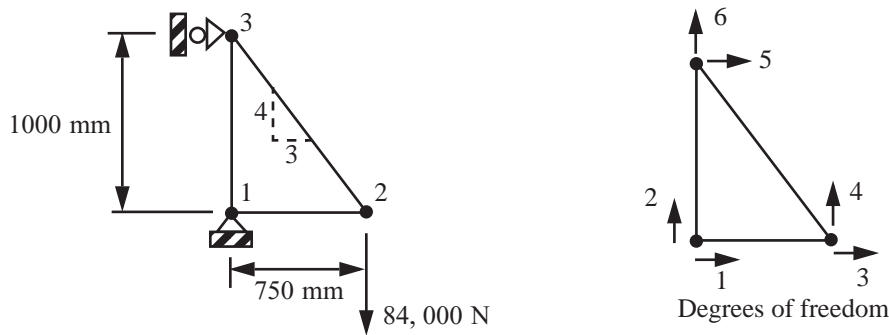


Fig. 6.6 A statically determinate three-bar truss.

**A note on static determinacy:** Let  $m$  = the number of unknown bar forces,  $r$  = the number of support reactions, and let  $j$  = the number of joints. There are two independent equilibrium equations per joint. For a statically determinate truss, the number of unknown forces is equal to number of independent equilibrium equations (i.e.,  $2j = m$

+  $r$ ). For the truss in this example  $j = 3$ ,  $m = 3$ , and  $r = 3$ . So it is statically determinate. For the truss in example 6.1,  $j = 3$ ,  $m = 3$ , and  $r = 6$ , and  $6 < 3 + 6$ . So the truss in example 6.1 is statically indeterminate.

**Solution.** Free body diagrams of joints 2 and 3 are shown figure 6.7. The diagrams are drawn assuming each bar is in tension, so the reaction of the bar force acting on a joint is an arrow aligned with the bar and pointing away from the joint. The objective is to determine each bar force in terms of external forces  $Q_3$  and  $Q_4$ . Note that  $Q_3 = 0$  and  $Q_4 = -84,000$  N, but we will wait to substitute these numerical values after the derivatives are evaluated in Castigliano's second theorem.

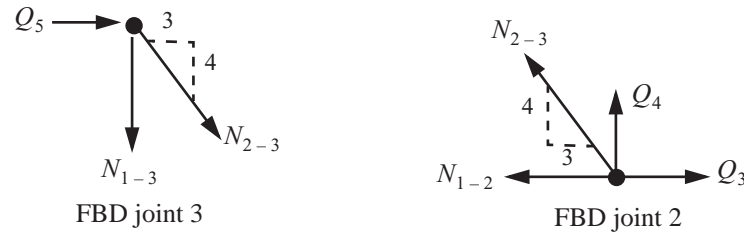


Fig. 6.7 Free body diagrams of two joints of the three-bar truss.

The only contribution to the complementary strain energy in (5.84) on page 145 is the axial normal force  $N$ , which is spatially uniform along the length of the bar. Also, there is no change in temperature from the reference state. Hence, the complementary strain energy for the truss is

$$U^* = \frac{1}{2} \left[ \left( \frac{L}{EA} \right)_{1-2} N_{1-2}^2 + \left( \frac{L}{EA} \right)_{1-3} N_{1-3}^2 + \left( \frac{L}{EA} \right)_{2-3} N_{2-3}^2 \right], \quad (\text{a})$$

Castigliano's second theorem for the displacement  $q_3$  is

$$q_3 = \frac{\partial U^*}{\partial Q_3} = \left( \frac{L}{EA} \right)_{1-2} N_{1-2} \frac{\partial N_{1-2}}{\partial Q_3} + \left( \frac{L}{EA} \right)_{1-3} N_{1-3} \frac{\partial N_{1-3}}{\partial Q_3} + \left( \frac{L}{EA} \right)_{2-3} N_{2-3} \frac{\partial N_{2-3}}{\partial Q_3}. \quad (\text{b})$$

The terms in eq. (b) are listed in table 6.1. Replace the derivatives of the bar forces with their values listed in the

Table 6.1 Terms in Castigliano's theorem for displacements  $q_3$  and  $q_4$

Bar	L, mm	A, mm <sup>2</sup>	L/(EA), mm/N	N	$\partial N / \partial Q_3$	$\partial N / \partial Q_4$
1-2	750	900	$11.90 \times 10^{-6}$	$Q_3 + 3Q_4/4$	1	3/4
1-3	1000	300	$47.62 \times 10^{-6}$	$Q_4$	0	1
2-3	1250	1200	$14.88 \times 10^{-6}$	$-5Q_4/4$	0	-5/4

table to get

$$q_3 = \left( \frac{L}{EA} \right)_{1-2} N_{1-2}(1) + \left( \frac{L}{EA} \right)_{1-3} N_{1-3}(0) + \left( \frac{L}{EA} \right)_{2-3} N_{2-3}(0). \quad (\text{c})$$

Substitute the equation for bar force  $N_{1-2}$  from the table in the previous equation and note that  $Q_3 = 0$  and

$Q_4 = -84,000 \text{ N}$  to get

$$q_3 = \left(\frac{L}{EA}\right)_{1-2} (Q_3 + 3Q_4/4) = (11.90 \times 10^{-6} \text{ mm/N}) \left(0 + \frac{3}{4}(-84,000 \text{ N})\right) = -0.750 \text{ mm} . \quad (\text{d})$$

Castigliano's second theorem for the displacement  $q_4$  is

$$q_4 = \frac{\partial U^*}{\partial Q_4} = \left(\frac{L}{EA}\right)_{1-2} N_{1-2} \frac{\partial N_{1-2}}{\partial Q_4} + \left(\frac{L}{EA}\right)_{1-3} N_{1-3} \frac{\partial N_{1-3}}{\partial Q_4} + \left(\frac{L}{EA}\right)_{2-3} N_{2-3} \frac{\partial N_{2-3}}{\partial Q_4} . \quad (\text{e})$$

Replace the bar forces and their derivatives in eq. (e) with their values listed in table 6.1 to get

$$q_4 = \left(\frac{L}{EA}\right)_{1-2} (0 + 3Q_4/4) \left(\frac{3}{4}\right) + \left(\frac{L}{EA}\right)_{1-3} (Q_4)(1) + \left(\frac{L}{EA}\right)_{2-3} (-5Q_4/4) \left(-\frac{5}{4}\right) . \quad (\text{f})$$

Substitute numerical values into eq. (f) to get

$$q_4 = \left[ (11.90 \times 10^{-6} \text{ mm/N}) \frac{9}{16} + (47.62 \times 10^{-6} \text{ mm/N}) + (14.88 \times 10^{-6} \text{ mm/N}) \frac{25}{16} \right] (-84,000 \text{ N}) . \quad (\text{g})$$

The final result from eq. (g) is

$$q_3 = -0.750 \text{ mm} \quad q_4 = -6.516 \text{ mm} \blacksquare \quad (\text{h})$$

## 6.2 Beam structures

### Example 6.4 Cross-sectional properties of a thin-walled tube

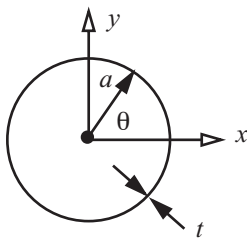


Fig. 6.8.

The cross section is a thin-walled tube with a circular contour of radius  $a$  and wall thickness  $t$ , as shown in figure 6.8.

**Solution.** The  $x$ - and  $y$ - axes are axes of symmetry in the cross section, so the centroid and shear center coincide with the center of the circular contour. The parametric coordinates of the circular contour are  $x = a \cos \theta$  and  $y = a \sin \theta$ , and the arc length along the contour  $s = a\theta$ ;  $0 \leq \theta \leq 2\pi$ . The cross-sectional area and first area moments are

$$A = \int_0^{2\pi} t a d\theta = 2\pi a t \quad Q_x = \int_0^{2\pi} y t a d\theta = 0 \quad Q_y = \int_0^{2\pi} x t a d\theta = 0 . \quad (\text{a})$$

The first area moments equal zero since the center of the circle is the centroid. The second area moments are

$$I_{xx} = \int_0^{2\pi} y^2 t a d\theta = \pi a^3 t \quad I_{yy} = \int_0^{2\pi} x^2 t a d\theta = \pi a^3 t \quad I_{xy} = \int_0^{2\pi} x y t a d\theta = 0 . \quad (\text{b})$$

Since the product area moment is zero, then coefficients  $n_x = n_y = 0$  and  $k = 1$  from eq. (4.4) on page 79. To

compute the transverse shear compliances given in eq. (4.30) on page 83, we need to compute the distribution functions from eq. (4.19) and eq. (4.26). The distribution functions for the first area moments for a segment of the contour from  $s = 0$  to  $s = a\theta$  are given by

$$Q_x(\theta) = \int_0^\theta y t a d\theta = a^2 t (1 - \cos \theta) \quad Q_y(\theta) = \int_0^\theta x t a d\theta = a^2 t \sin \theta. \quad (c)$$

The coordinates normal and tangent to the contour with respect to the shear center are

$$r_n = x \left( \frac{1}{a} \frac{dy}{d\theta} \right) - y \left( \frac{1}{a} \frac{dx}{d\theta} \right) = a \quad r_t = x \left( \frac{1}{a} \frac{dx}{d\theta} \right) + y \left( \frac{1}{a} \frac{dy}{d\theta} \right) = 0. \quad (d)$$

(Refer to eq. (3.10) on page 34.) The area enclosed by the contour is

$$A_c = \frac{1}{2} \int_0^{2\pi} r_n a d\theta = \pi a^2. \quad (e)$$

The shear flow distribution functions given by eqs.(4.19) and (4.26) on page 82 for the closed section are

$$F_x = \frac{1}{I_{yy}} \left[ Q_y(\theta) - \frac{1}{2A_c} \int_0^{2\pi} r_n Q_y(\theta) a d\theta \right] = \frac{a^2 t \sin \theta}{I_{yy}} = \frac{\sin \theta}{a\pi}, \text{ and} \quad (f)$$

$$F_y = \frac{1}{I_{xx}} \left[ Q_x(\theta) - \frac{1}{2A_c} \int_0^{2\pi} r_n Q_x(\theta) a d\theta \right] = -\left( \frac{a^2 t}{I_{xx}} \right) \cos \theta = \frac{-\cos \theta}{a\pi}. \quad (g)$$

Finally, the transverse shear compliances are

$$c_{xx} = \frac{1}{Gt} \int_0^{2\pi} F_x^2(\theta) a d\theta = \frac{\pi a^5 t}{G I_{yy}^2} = \frac{1}{\pi a t G} \quad c_{yy} = \frac{1}{Gt} \int_0^{2\pi} F_y^2(\theta) a d\theta = \frac{1}{\pi a t G}, \text{ and} \quad (h)$$

$$c_{xy} = \frac{1}{Gt} \int_0^{2\pi} [F_x(\theta) F_y(\theta)] a d\theta = 0. \quad (i)$$

For a uniform shear modulus around the contour, the torsion constant is determined from eq. (3.161) on page 70 as

$$J = \frac{4A_c^2}{\oint \frac{ds}{t}} = \frac{4(\pi a^2)^2}{\frac{2\pi a}{t}} = 2\pi a^3 t \blacksquare \quad (j)$$

### 6.2.1 Castigliano's second theorem

#### Example 6.5 Thin-walled tube subject to radiant heating

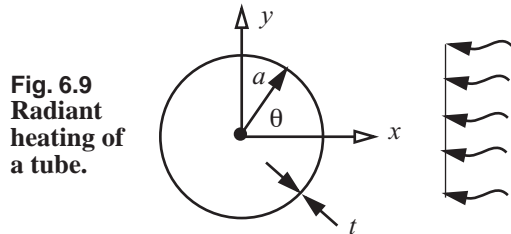


**Fig. 6.9**  
Radiant  
heating of  
a tube.

A common structural member in orbiting space structures is a thin-walled tube. Tubes are used as truss members and for satellite booms. Solar heating combined with heat conduction results in the distribution of temperature around the perimeter and along the length of the tube. The data in this example is for an aluminum 6061-T6 tube taken from Thornton (1996, pp. 118-121).

A thin-walled tube with a circular contour of radius  $a$ , and wall thickness  $t$  is subjected to radiant heating as shown in figure 6.9. The tube is cantilevered, that is, fixed at  $z = 0$  and free at  $z = L$ , where  $L$  is the length of tube. The change in temperature from the reference state is uniform along the length but it varies around the perimeter, and is specified by

$$\Delta T(\theta) = \bar{T} + T_m \cos \theta \quad \theta \in [0, 2\pi]. \quad (\text{a})$$

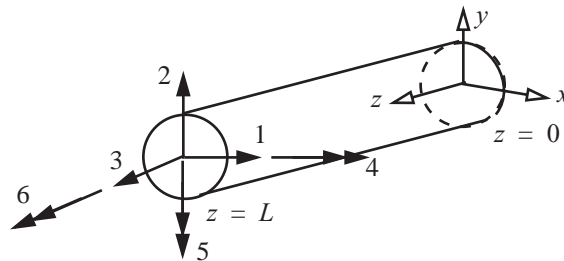
where the average temperature is denoted by  $\bar{T}$  and the perturbation in temperature is denoted by  $T_m$ . Data for this example are listed in table 6.2.

**Table 6.2 Numerical data for example 6.5**

radius	$a = 0.03812 \text{ m}$	Poisson's ratio	$\nu = 0.33$
wall thickness	$t = 7.14 \times 10^{-4} \text{ m}$	coefficient of thermal expansion	$\alpha = 23 \times 10^{-6} / ^\circ K$
tube length	$L = 0.8 \text{ m}$	average temperature	$\bar{T} = 462^\circ K$
modulus of elasticity	$E = 68.3 \text{ GPa}$	perturbation temperature	$T_m = 34^\circ K$

Determine the displacements  $q_1$  and  $q_3$ , and rotation  $q_5$  of the cross section at the free end using Castigliano's second theorem. The degree of freedom numbering is shown in figure 6.10.

**Fig. 6.10** Degree of freedom numbering at the free end of the cantilevered tube.



**Solution.** From eqs. (5.83) to (5.85) on page 145 the complementary strain energy in this example is



$$U^* = \frac{1}{2} \int_0^L \left[ \frac{(N + N_T)^2}{EA} + \frac{(M_x + M_{xT})^2}{EI_{xx}} + \frac{(M_y + M_{yT})^2}{EI_{yy}} + c_{xx} V_x^2 + c_{yy} V_y^2 + \frac{M_z^2}{GJ} \right] dz. \quad (\text{b})$$

The cross-sectional properties were determined in example 6.4, and they are

$$A = 2\pi at = 2\pi(0.03812\text{m})(7.14 \times 10^{-4}\text{m}) = 171.014 \times 10^{-6}\text{m}^2, \quad (\text{c})$$

$$I_{xx} = I_{yy} = \pi a^3 t = \pi(0.03812\text{m})^3(7.14 \times 10^{-4}\text{m}) = 124.25 \times 10^{-9}\text{m}^4, \text{ and } J = 2\pi a^3 t = 248.50 \times 10^{-9}\text{m}^4. \quad (\text{d})$$

The shear modulus is given by the isotropic formula  $G = E/(2(1 + \nu)) = 25.6 \text{ GPa}$ , so the transverse shear compliances are

$$c_{xx} = c_{yy} = \frac{1}{\pi at G} = \frac{1}{\pi(0.03812\text{m})(7.14 \times 10^{-4}\text{m})(25.6 \times 10^9 \text{N/m}^2)} = \frac{456.61 \times 10^{-9}}{\text{N}}. \quad (\text{e})$$

The thermal axial force is given by eq. (3.75) on page 46, and thermal moments are given in eq. (3.78). Material properties are uniform along the contour and  $x = a \cos \theta$ , and  $y = a \sin \theta$  in the thermal action formulas. The results for these thermal actions are

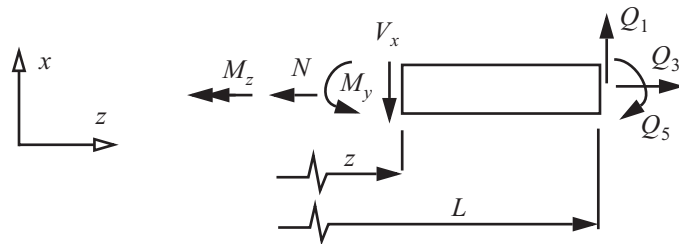
$$N_T = E\alpha \int_0^{2\pi} \Delta T t d\theta = 2\pi at E\alpha \bar{T} \quad M_{xT} = E\alpha \int_0^{2\pi} \Delta T y t d\theta = 0 \quad M_{yT} = E\alpha \int_0^{2\pi} \Delta T x t d\theta = \pi a^2 t E\alpha T_m, \quad (\text{f})$$

$$N_T = 2\pi(0.03812\text{m})(7.14 \times 10^{-4}\text{m})(68.3 \times 10^9 \text{N/m}^2)(23 \times 10^{-6}^\circ \text{K})(462^\circ \text{K}) = 124.11 \times 10^3 \text{N}, \text{ and} \quad (\text{g})$$

$$M_{yT} = \pi(0.03812\text{m})^2(7.14 \times 10^{-4}\text{m})(68.3 \times 10^9 \text{N/m}^2)(23 \times 10^{-6}^\circ \text{K})(34^\circ \text{K}) = 174.10 \text{N}\cdot\text{m}. \quad (\text{h})$$

The free body diagram of the tube in the  $x$ - $z$  plane is shown in figure 6.11. Generalized forces  $Q_1$ ,  $Q_3$ , and  $Q_5$  are introduced at the free end to facilitate computing the corresponding displacements via Castigliano's theorem, and they are set equal to zero at the end of the procedure (i.e., they are fictitious actions).

**Fig. 6.11** Fictitious actions acting at the free end of the cantilevered tube.



Equilibrium of the free body diagram in the  $x$ - $z$  plane yields

$$N = Q_3 \quad V_x = Q_1 \quad M_y = Q_5 - Q_1(L - z) \quad M_z = 0 \quad z \in [0, L]. \quad (\text{i})$$

Since generalized forces  $Q_2 = Q_4 = 0$ , equilibrium in the  $y$ - $z$  plane yields  $V_y = M_x = 0$  for  $z \in [0, L]$ . The complementary strain energy reduces to

$$U^* = \frac{1}{2} \int_0^L \left[ \frac{(Q_3 + N_T)^2}{EA} + \frac{[Q_5 - Q_1(L-z) + M_{yT}]^2}{EI_{yy}} + \frac{Q_1^2}{\pi atG} \right] dz. \quad (j)$$

Displacement  $q_1$  is determined from

$$q_1 = \frac{\partial U^*}{\partial Q_1} = \int_0^L \left[ \frac{(Q_3 + N_T) \partial(Q_3 + N_T)}{EA \partial Q_1} + \frac{[Q_5 - Q_1(L-z) + M_{yT}] \partial[Q_5 - Q_1(L-z) + M_{yT}]}{EI_{yy} \partial Q_1} + \frac{Q_1}{\pi atG} \left( \frac{\partial Q_1}{\partial Q_1} \right) \right] dz, \quad (k)$$

where we interchanged the derivative and integral since our functions are continuous. Performing the derivative inside the integral we get

$$q_1 = \frac{1}{EI_{yy}} \int_0^L [Q_5 - Q_1(L-z) + M_{yT}] [- (L-z)] dz + \frac{1}{\pi atG} \int_0^L Q_1(1) dz. \quad (l)$$

Now set  $Q_1$  and  $Q_5$  equal to zero and find

$$q_1 = \left( \frac{1}{EI_{yy}} \right) \int_0^L M_{yT} [- (L-z)] dz = \frac{-L^2 M_{yT}}{2EI_{yy}} = \frac{-(0.8 \text{ m})^2 (174.10 \text{ N-m})}{2(68.3 \times 10^9 \text{ N/m}^2)(124.25 \times 10^{-9} \text{ m}^4)} = -6.565 \times 10^{-3} \text{ m}. \quad (m)$$

Axial displacement  $q_3$  is given by

$$q_3 = \frac{\partial U^*}{\partial Q_3} = \int_0^L \left[ \frac{(Q_3 + N_T) \partial(Q_3 + N_T)}{EA \partial Q_3} + \frac{[Q_5 - Q_1(L-z) + M_{yT}] \partial[Q_5 - Q_1(L-z) + M_{yT}]}{EI_{yy} \partial Q_3} + \frac{Q_1}{\pi atG} \left( \frac{\partial Q_1}{\partial Q_3} \right) \right] dz. \quad (n)$$

Since  $Q_3 = 0$ , the latter equation reduces to

$$q_3 = \left( \frac{1}{EA} \right) \int_0^L (Q_3 + N_T)(1) dz \Bigg|_{Q_3=0} = \frac{L}{EA} N_T = \frac{(0.8 \text{ m})(124.11 \times 10^3 \text{ N})}{(68.3 \times 10^9 \text{ N/m}^2)(171.014 \times 10^{-6} \text{ m}^2)} = 8.5 \times 10^{-3} \text{ m}. \quad (o)$$

Finally, the rotation in radians about the  $y$ -axis is given by

$$q_5 = \left( \frac{1}{EI_{yy}} \right) \int_0^L [Q_5 - Q_1(L-z) + M_{yT}] [1] dz \Bigg|_{Q_1=Q_3=0},$$

$$q_5 = \frac{LM_{yT}}{EI_{yy}} = \frac{(0.8 \text{ m})(174.10 \text{ N-m})}{(68.3 \times 10^9 \text{ N/m}^2)(124.25 \times 10^{-9} \text{ m}^4)} = 16.41 \times 10^{-3} \text{ rad}. \quad (p)$$

**Example 6.6 Wing spar subject to a distributed spanwise air load**

A light airplane experiences a total lift  $L = 12,000$  lb. in a certain symmetric maneuver. Thus, the lift acting on each wing is  $L/2$ . Assume the airload is distributed elliptically over the wing, so that the airload intensity  $f_L$  per unit span is given as

$$f_L = \frac{2L}{\pi z_{max}} \sqrt{1 - \left(\frac{z}{z_{max}}\right)^2} \quad 0 \leq z \leq z_{max}, \quad (a)$$

where  $z$  is the spanwise coordinate,  $z = 0$  at the root, and  $z = z_{max}$  at the tip of the wing. See figure 6.12 (a). The spar of the wing is a uniform, longitudinal, thin-walled beam with a closed section stiffened by four longitudinal stringers as shown in figure 6.12 (b). This cross-section is the same one shown in figure 3.24 and analyzed in example 3.4 on page 71. Assume the spar is clamped at the root and free at the tip (i.e., a cantilever spar). At the tip of the spar we will use Castigliano's second theorem to find the vertical displacement of the shear center denoted by  $q_2$ , and to find the torsional rotation of the cross section denoted by  $q_6$ . To use the theorem, we introduce a fictitious force  $Q_2$  corresponding to displacement  $q_2$ , and a fictitious torque  $Q_6$  corresponding to rotation  $q_6$ . A typical cross section of the spar with the locations of the centroid ( $X_C$ ), the shear center ( $X_{SC}$ ), and the line of action of the airload ( $X_L$ ) with respect to the vertical web are shown in the left-hand sketch of figure 6.13. The right-hand sketch in figure 6.13 illustrates that the airload is statically equivalent to the external line load intensity  $f_y$  and line moment intensity  $m_z$  resolved at the shear center.

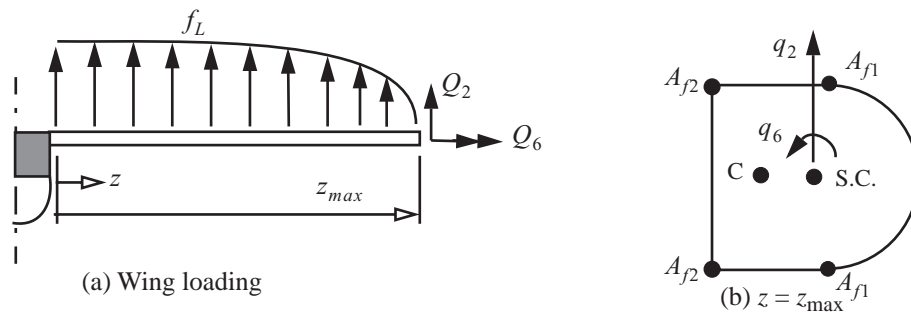


**Fig. 6.12 : (a) Wing spanwise airload intensity and fictitious actions  $Q_2$  and  $Q_6$  of example 6.6. (b) Wing tip cross section and the corresponding generalized displacements  $q_2$  and  $q_6$ .**

Numerical data for the cross-sectional dimensions are listed in table 6.3. The material is an aluminium alloy with

**Table 6.3 Cross-sectional data for the wing spar**

Dimensional data of the cross section			
$A_{f1}$ , stringer 1 flange area	0.30 in. <sup>2</sup>	$b$ , length horizontal web	7.0 in.
$A_{j2}$ , stringer 2 flange area	0.70 in. <sup>2</sup>	$t$ , wall thickness	0.030 in.
$a$ , nose web radius	6.0 in	$X_L$ , location of the airload	10.0 in.

a Young's modulus  $E = 10.5 \times 10^3$  ksi, a shear modulus  $G = 4.0 \times 10^3$  ksi, and with a yield strength  $\sigma_{yield} = 44$  ksi. Additional cross-sectional properties computed from example 3.4 on page 71 are listed in

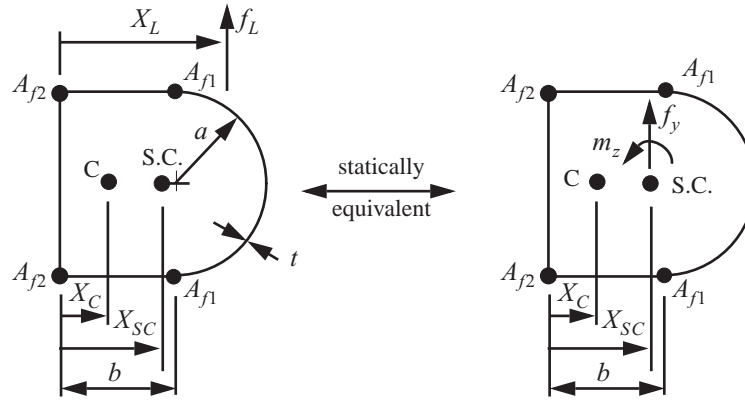


Fig. 6.13 example 6.6: Typical cross section of the uniform spar.

table 6.4.

Table 6.4 Data from example 3.4

$A$ , area of the cross section	3.3455 in. <sup>2</sup>		
$X_C$ , horizontal location of the centroid	3.52367 in.	$c_{yy}$ , compliance coefficient in transverse shear <sup>a</sup>	$\left(\frac{1.64758}{\text{in.}^2}\right) \frac{1}{G}$
$X_{SC}$ , horizontal location of the shear center	6.39638 in.	$c_{zz}$ , compliance coefficient in torsion <sup>b</sup>	$\left(\frac{0.0189201}{\text{in.}^4}\right) \frac{1}{G}$
$I_{xx}$ , second area moment about the $x$ -axis	101.619 in. <sup>4</sup>	$A_c$ , area enclosed by the contour	140.549 in. <sup>2</sup>

a. Note: from eq. (5.65) on page 143  $c_{yy} = \sum_{i=1}^4 \int_0^{(s_i)_{\max}} \frac{F_{yi}^2(s_i)}{Gt} ds_i$ , where the shear flow distribution functions  $F_{yi}(s_i)$  are given by eqs. (d) to (g) in part c of example 3.4.

b. Note:  $c_{zz} = (GJ)^{-1}$ , and from eq. (3.160) on page 70 the torsion constant  $J = (4A_c^2) / \left( \oint \frac{ds}{t} \right)$ .

- Determine the statically admissible bar resultants in the spar for  $0 \leq z \leq z_{\max}$ .
- Determine the generalized displacements  $q_2$  and  $q_6$  of the shear center at  $z = z_{\max}$ .
- Tabulate the displacement  $q_2$ , percentage of the displacement  $q_2$  due to transverse shear, and the rotation  $q_6$  of part (b) for the following spar lengths:  $z_{\max} = 12, 24, 60, 120, 1800, 240$ , and 300 in. Also, tabulate the ratio of the maximum von Mises effective stress (eq. (4.31) on p. 84) to the yield strength in the semi-circular web, or branch 1, at  $z = 0$  for the same set of spar lengths.

**Solution to part (a).** The external distributed line load intensities resolved at the shear center are shown figure 6.13. In terms of the specified airload  $f_y = f_L$  and  $m_z = ef_L$ , where  $e = X_L - X_{SC}$ . The differential equation for

the transverse shear force  $V_y$  is given by eq. (3.54) on page 43. Substitute the expression for the airload to get the shear force as

$$V_y = \int \left[ -\left( \frac{2L}{\pi z_{max}} \right) \sqrt{1 - \left( \frac{z}{z_{max}} \right)^2} \right] dz = \left( \frac{L}{\pi} \right) \left[ \operatorname{acos} \left( \frac{z}{z_{max}} \right) - \left( \frac{z}{z_{max}} \right) \sqrt{1 - \left( \frac{z}{z_{max}} \right)^2} \right] + c_1. \quad (\text{a})$$

Note that the integration is facilitated by the substitution  $z/z_{max} = \cos \theta$ , and using trigonometric identities.

The constant of integration  $c_1$  is determined by the boundary condition  $V_y(z_{maz}) = Q_2$ . Hence  $c_1 = Q_2$ , and the final result for the shear force is

$$V_y = \left( \frac{L}{\pi} \right) \left[ \operatorname{acos} \left( \frac{z}{z_{max}} \right) - \left( \frac{z}{z_{max}} \right) \sqrt{1 - \left( \frac{z}{z_{max}} \right)^2} \right] + Q_2. \quad (\text{b})$$

The shear force at the root for  $Q_2 = 0$  is  $V_y(0)|_{Q_2=0} = L/2$ .

The bending moment  $M_x$  is determined by eq. (3.55) on page 43. Substitute the result for the shear force  $V_y$  into eq. (3.55) to find

$$M_x = \int \left\{ \left( \frac{L}{\pi} \right) \left[ \operatorname{acos} \left( \frac{z}{z_{max}} \right) - \left( \frac{z}{z_{max}} \right) \sqrt{1 - \left( \frac{z}{z_{max}} \right)^2} \right] + Q_2 \right\} dz.$$

Again, the integration for  $M_x$  is facilitated by the substitution  $z/z_{max} = \cos \theta$ , and using trigonometric identities to get

$$M_x = \left( \frac{Lz_{max}}{\pi} \right) \left[ -\sqrt{1 - \left( \frac{z}{z_{max}} \right)^2} + \frac{1}{3} \left[ 1 - \left( \frac{z}{z_{max}} \right)^2 \right]^{3/2} + \left( \frac{z}{z_{max}} \right) \operatorname{acos} \left( \frac{z}{z_{max}} \right) \right] + Q_2 z + c_2. \quad (\text{c})$$

The constant of integration  $c_2$  is determined by the boundary condition  $M_x(z_{maz}) = 0$ . Hence  $c_2 = -z_{max}Q_2$ , and the final result for the bending moment is

$$M_x = \left( \frac{Lz_{max}}{\pi} \right) \left[ -\sqrt{1 - \left( \frac{z}{z_{max}} \right)^2} + \frac{1}{3} \left[ 1 - \left( \frac{z}{z_{max}} \right)^2 \right]^{3/2} + \left( \frac{z}{z_{max}} \right) \operatorname{acos} \left( \frac{z}{z_{max}} \right) \right] - Q_2(z_{max} - z). \quad (\text{d})$$

The bending moment at the root of the spar for  $Q_2 = 0$  is  $M_x(0)|_{Q_2=0} = \frac{-2Lz_{max}}{3\pi}$ .

From eq. (3.61) on page 43, and that  $m_z = ef_L$ , we can express the torque  $M_z$  as

$$\frac{dM_z}{dz} = -m_z = -ef_L. \quad (\text{e})$$

Hence,

$$M_z = -e \int \frac{2L}{\pi z_{max}} \sqrt{1 - \left( \frac{z}{z_{max}} \right)^2} dz + c_3 = -e \frac{L}{\pi} \left\{ \left( \frac{z}{z_{max}} \right) \sqrt{1 - \left( \frac{z}{z_{max}} \right)^2} + \operatorname{asin} \left( \frac{z}{z_{max}} \right) \right\} + c_3. \quad (\text{f})$$

The constant of integration  $c_3$  is determined from the boundary condition  $M_z(z_{max}) = Q_6$ , which yields

$c_3 = e\frac{L}{2} + Q_6$ . The final result for the torque is

$$M_z = \frac{eL}{2} - \frac{eL}{\pi} \left[ \left( \frac{z}{z_{max}} \right) \sqrt{1 - \left( \frac{z}{z_{max}} \right)^2} + \text{asin} \left( \frac{z}{z_{max}} \right) \right] + Q_6. \quad (g)$$

The torque at the root of the spar for  $Q_6 = 0$  is  $M_z(0)|_{Q_6=0} = eL/2$ . We have determined the statically admissible shear force  $V_y$ , bending moment  $M_x$ , and torque  $M_z$  in the wing spar in terms of the distributed airload, external force  $Q_2$ , and external torque  $Q_6$ .

**Solution to part (b).** From eqs. (5.84) and (5.85) on page 145, the total complementary strain energy for the bar in this example is

$$U^* = \frac{1}{2} \int_0^{z_{max}} \left( \frac{M_x^2}{EI_{xx}} + c_{yy} V_y^2 + c_{zz} M_z^2 \right) dz. \quad (h)$$

Castigliano's second theorem for the vertical displacement of the shear center is

$$q_2 = \frac{\partial U^*}{\partial Q_2} \bigg|_{Q_2=Q_6=0} = \int_0^{z_{max}} \left[ \frac{M_x}{EI_{xx}} \frac{\partial M_x}{\partial Q_2} + c_{yy} V_y \frac{\partial V_y}{\partial Q_2} + c_{zz} M_z \frac{\partial M_z}{\partial Q_2} \right] dz \bigg|_{Q_2=Q_6=0}. \quad (i)$$

Note that the torque is independent of force  $Q_2$ , so that  $\partial M_z / \partial Q_2 = 0$ . Let  $q_2 = q_{2m} + q_{2v}$ , where  $q_{2m}$  is the portion of the displacement due to bending moment  $M_x$  and  $q_{2v}$  is the portion due to transverse shear force  $V_y$ .

$$q_{2m} = \int_0^{z_{max}} \left[ \frac{M_x}{EI_{xx}} \frac{\partial M_x}{\partial Q_2} \right] dz \bigg|_{Q_2=Q_6=0} = \frac{1}{EI_{xx}} \int_0^{z_{max}} M_x [-(z_{max} - z)] dz \bigg|_{Q_2=Q_6=0}. \quad (j)$$

Substitute eq. (d) for  $M_x$  with  $Q_2 = 0$  into eq. (j), and perform the integration to get

$$q_{2m} = \frac{L(-32 + 45\pi)z_{max}^3}{720EI_{xx}\pi}. \quad (k)$$

The portion of the displacement due to transverse shear force  $V_y$  is

$$q_{2v} = \int_0^{z_{max}} \left[ c_{yy} V_y \frac{\partial V_y}{\partial Q_2} \right] dz \bigg|_{Q_2=Q_6=0} = c_{yy} \int_0^{z_{max}} \left\{ \left( \frac{L}{\pi} \right) \left[ \text{acos} \left( \frac{z}{z_{max}} \right) - \left( \frac{z}{z_{max}} \right) \sqrt{1 - \left( \frac{z}{z_{max}} \right)^2} \right] \right\} \{1\} dz = \frac{2c_{yy}Lz_{max}}{3\pi}. \quad (l)$$

Add eqs. (k) and (l) to get the total vertical displacement at the shear center as

$$q_2 = \frac{L(-32 + 45\pi)z_{max}^3}{720EI_{xx}\pi} + \frac{2c_{yy}Lz_{max}}{3\pi}. \quad (m)$$

Castigliano's second theorem for the rotation of the cross-section at  $z = z_{\max}$  about the shear center is

$$q_6 = \left. \frac{\partial U^*}{\partial Q_6} \right|_{Q_2 = Q_6 = 0} = \int_0^{z_{\max}} \left[ \frac{k}{EI_{xx}} M_x \frac{\partial M_x}{\partial Q_6} + c_{yy} V_y \frac{\partial V_y}{\partial Q_6} + c_{zz} M_z \frac{\partial M_z}{\partial Q_6} \right] dz \bigg|_{Q_2 = Q_6 = 0}. \quad (\text{n})$$

The bending moment  $M_x$  and transverse shear force  $V_y$  are independent of the external torque  $Q_6$ . Hence,

$$q_6 = \left. \frac{\partial U^*}{\partial Q_6} \right|_{Q_2 = Q_6 = 0} = c_{zz} \int_0^{z_{\max}} \left\{ \frac{eL}{2} - \frac{eL}{\pi} \left[ \left( \frac{z}{z_{\max}} \right) \sqrt{1 - \left( \frac{z}{z_{\max}} \right)^2} + \text{asin} \left( \frac{z}{z_{\max}} \right) \right] \right\} [1] dz. \quad (\text{o})$$

The integration of eq. (o) yields

$$q_6 = \frac{2c_{zz}eLz_{\max}}{3\pi}. \quad (\text{p})$$

**Solution to part (c).** Numerical evaluation of the displacements yields

$$q_{2m} = \left( \frac{5.438 \times 10^{-7}}{\text{in.}^2} \right) z_{\max}^3 \quad q_{2v} = (1.0489 \times 10^{-3}) z_{\max} \quad q_6 = (4.3905 \times 10^{-5} \text{ in.}^{-1}) z_{\max}. \quad (\text{q})$$

The expression for the shear flow is given by eq. (3.163) on page 70. At the root cross section the equation for the shear flow reduces to

$$q(s, 0) = M_z(0)/(2A_c) - F_y(s)V_y(0). \quad (\text{r})$$

The torque results in a spatially uniform component to the shear flow around the contour equal to

$$q_t = M_z(0)/(2A_c) = 76.9188 \text{ lb/in.} \quad (\text{s})$$

(Refer to eq. (3.165) on p. 70 ). The total shear flow in each branch is

$$q_i(s_i, 0) = 76.9188 \text{ lb/in.} - F_{yi}(s_i)(6000.0 \text{ lb.}) \quad i = 1, 2, 3, 4, \quad (\text{t})$$

where the contour coordinates  $s_i$  are shown in figure 3.24(b) on page 71, and the shear flow distribution functions  $F_{yi}(s_i)$  are given by eqs. (ab) to (ae) in part c of example 3.4. The shear stress distribution along the contour in each branch is given by

$$\sigma_{zi}(s_i, 0) = [q_i(s_i, 0)]/t \quad i = 1, 2, 3, 4. \quad (\text{u})$$

In this example  $I_{xy} = n_x = n_y = 0$  and  $k = 1$  in the axial normal stress given by eq. (4.6) on page 79. For no change in temperature and  $N = M_y = 0$ , the axial normal stress eq. (4.6) at the root cross section in each branch reduces to

$$\sigma_{zi}(s_i, 0) = \frac{M_x(0)y_i(s_i)}{I_{xx}} = \left[ \left( -25.0591 \frac{\text{lb.}}{\text{in.}^4} \right) z_{\max} \right] y_i(s_i) \quad i = 1, 2, 3, 4. \quad (\text{v})$$

The parametric equations for the y-coordinates of the contour in each branch are

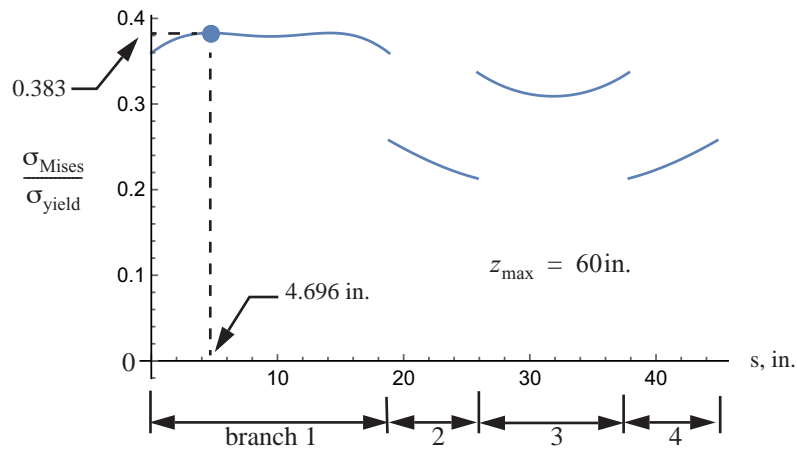
$$y_1(s_1) = -a \cos(s_1/a) \quad y_2 = a \quad y_3(s_3) = a - s_3 \quad y_4 = -a. \quad (\text{w})$$

(Refer to figure 3.24 on page 71.) From eq. (4.31) the von Mises effective stress is

$$(\sigma_{\text{Mises}})_i = \sqrt{[\sigma_{zi}(s_i, 0)]^2 + 3[\sigma_{zsi}(s_i, 0)]^2} \quad i = 1, 2, 3, 4. \quad (\text{x})$$

The von Mises effective stress normalized by the yield strength is plotted with respect to the contour coordinate for  $z_{\text{max}} = 60$  inches in figure 6.14. As shown in the figure the maximum normalized effective stress is 0.383 at  $s = 4.696$  inches in branch 1. In terms of an angular measurement in the semi-circular branch 1, we note the location as  $s_1/a = (4.696/6)(180^\circ/\pi) = 44.8^\circ$ . For the other values of  $z_{\text{max}}$ , the maximum value of the von Mises stress also occurs in branch 1 but at different angular locations. Discontinuities in the von Mises stress with respect to the contour coordinate are a result of the jumps in the shear flow across the stringers. (Refer to eq. (3.135) on p. 65 ).

**Fig. 6.14** Normalized von Mises effective stress plotted with respect to the contour coordinate  $s$  at the root cross section of the spar.



Numerical results are listed in table 6.5.

**Table 6.5** Wing tip displacements and wing root stresses as a function of the span

$z_{\text{max}}, \text{ in.}$	Wing tip			Wing root	
	$q_2, \text{ in.}$	$q_{2v}/q_2, \%$	$q_6, \text{ deg.}$	$\sigma_{\text{Mises}}/\sigma_{\text{yield}}$	$s_1/a, \text{ deg.}$
12.	0.0135	93.1	0.0298	0.379	90.0
24.	0.0327	77.0	0.0597	0.379	90.0
60.	0.180	34.9	0.149	0.383	44.8
120.	1.066	11.8	0.298	0.509	8.82
180.	3.360	5.62	0.448	0.683	3.81
240.	7.77	3.29	0.597	0.872	2.13
300.	15.0	2.10	0.746	1.07	1.36

Note that as the length of the spar increases the percentage of the vertical displacement at the tip due to transverse shear decreases and the von Mises effective stress increases. At  $z_{\text{max}} = 300$  in. the von Mises stress exceeds the yield strength of the material indicating failure by material yielding.



### 6.3 Coplanar Frames

Frames are also skeletal structures composed of slender bars that can transmit axial, bending, and transverse shear loads. The bars act as beams with a superimposed axial load. Joints in a frame are usually assumed rigid, which means that the rotation of all bars connected to the joint are the same. Moments can be transferred through a rigid joint, but not a hinge joint, nor ball-and-socket joint. A frame structure may also contain some hinge joints.

#### Example 6.7 A frame of two tubular bars

The tubular post shown in figure 6.15 supports a load of 250 N at the free end. The diameter of the cross-sectional contour is 100 mm and the wall thickness is 3 mm. The material is steel with modulus of elasticity of 206,000 N/mm<sup>2</sup> and a Poisson's ratio of 0.3. Each bar of the frame has the same uniform geometric cross section along its length. Find the vertical and horizontal displacement of the free end.

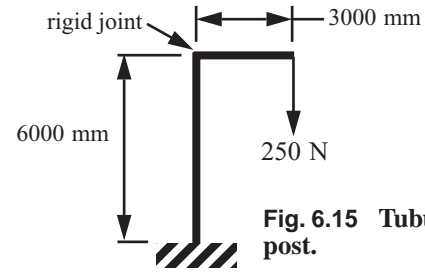


Fig. 6.15 Tubular post.

**Solution.** We use Castigliano's second theorem to determine the displacements of the free end for this statically determinate structure. A horizontal force  $Q$  is introduced at the free end so that the horizontal displacement can be computed from the theorem. Also, let  $P = 250$  N. The complementary strain energy is determined from eqs. (5.84) and (5.85). Since there is no change in temperature nor torsion, the complementary strain energy is

$$U^* = \sum_{\text{bars}} \int_0^L \left[ \frac{N^2}{2EA} + \frac{M_x^2}{2EI_{xx}} + \frac{1}{2} c_{yy} V_y^2 \right] dz. \quad (\text{a})$$

Let  $u_P$  denote the displacement corresponding to force  $P$ , and let  $u_Q$  denote the displacement corresponding to force  $Q$ . These displacements are given by

$$u_P = \left. \frac{\partial U^*}{\partial P} \right|_{P=250, Q=0} \quad u_Q = \left. \frac{\partial U^*}{\partial Q} \right|_{P=250, Q=0}. \quad (\text{b})$$

The coordinate system in each bar is shown in figure 6.16 (a), the free body diagram for the vertical bar in figure 6.16 (b), and the free body diagram of the horizontal bar is shown in figure 6.16 (c). The partial derivatives of the complementary strain energy for the frame with respect to the external loads are

$$\frac{\partial U^*}{\partial P} = \int_0^{L_1} \left( \frac{N_1}{EA} \frac{\partial N_1}{\partial P} + \frac{M_1}{EI_{xx}} \frac{\partial M_1}{\partial P} + c_{yy} V_1 \frac{\partial V_1}{\partial P} \right) dz_1 + \int_0^{L_2} \left( \frac{N_2}{EA} \frac{\partial N_2}{\partial P} + \frac{M_2}{EI_{xx}} \frac{\partial M_2}{\partial P} + c_{yy} V_2 \frac{\partial V_2}{\partial P} \right) dz_2, \text{ and} \quad (\text{c})$$

$$\frac{\partial U^*}{\partial Q} = \int_0^{L_1} \left( \frac{N_1}{EA} \frac{\partial N_1}{\partial Q} + \frac{M_1}{EI_{xx}} \frac{\partial M_1}{\partial Q} + c_{yy} V_1 \frac{\partial V_1}{\partial Q} \right) dz_1 + \int_0^{L_2} \left( \frac{N_2}{EA} \frac{\partial N_2}{\partial Q} + \frac{M_2}{EI_{xx}} \frac{\partial M_2}{\partial Q} + c_{yy} V_2 \frac{\partial V_2}{\partial Q} \right) dz_2, \quad (\text{d})$$

where  $L_1 = 6000$  mm and  $L_2 = 3000$  mm. Equilibrium determines the internal actions  $N$ ,  $V$ ,  $M$  in each bar. The results are

$$N_1 = -P \quad V_1 = -Q \quad M_1 = L_2 P + (L_1 - z_1) Q \quad z_1 \in [0, L_1], \text{ and} \quad (\text{e})$$

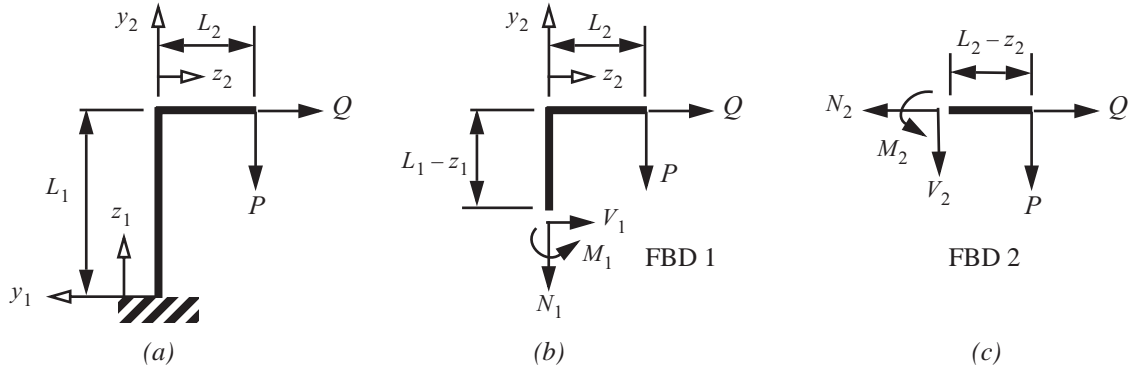


**Fig. 6.16** (a) Coordinates in each bar. (b) FBD of vertical bar. (c) FBD of horizontal bar.

$$N_2 = Q \quad V_2 = -P \quad M_2 = (L_2 - z_2)P \quad z_2 \in [0, L_2]. \quad (\text{f})$$

Evaluating the partial derivatives based on equilibrium conditions we get

$$\begin{aligned} \frac{\partial U^*}{\partial P} = & \int_0^{L_1} \left[ \frac{(-P)}{EA}(-1) + \frac{(L_2 P + (L_1 - z_1)Q)}{EI_{xx}}(L_2) + c_{yy}(-Q)(0) \right] dz_1 + \\ & \int_0^{L_2} \left( \frac{(Q)}{EA}(0) + \frac{(L_2 - z_2)P}{EI_{xx}}(L_2 - z_2) + c_{yy}(-P)(-1) \right) dz_2 \end{aligned} \quad , \text{ and} \quad (\text{g})$$

$$\begin{aligned} \frac{\partial U^*}{\partial Q} = & \int_0^{L_1} \left[ \frac{(-P)}{EA}(0) + \frac{(L_2 P + (L_1 - z_1)Q)}{EI_{xx}}(L_1 - z_1) + c_{yy}(-Q)(-1) \right] dz_1 + \\ & \int_0^{L_2} \left[ \frac{(Q)}{EA}(1) + \frac{(L_2 - z_2)P}{EI_{xx}}(0) + c_{yy}(-P)(0) \right] dz_2 \end{aligned} \quad . \quad (\text{h})$$

The displacements can now be computed from the expressions for the partial derivatives as

$$u_P = \int_0^{L_1} \left[ \frac{P}{EA} + \frac{L_2^2 P}{EI_{xx}} \right] dz_1 + \int_0^{L_2} \left[ \frac{(L_2 - z_2)^2 P}{EI_{xx}} + c_{yy} P \right] dz_2 \bigg|_{P=250} = \frac{L_1 P}{EA} + \underbrace{\frac{L_1 L_2^2 P}{EI_{xx}} + \frac{L_2^3 P}{3EI_{xx}}}_{\text{bending}} + c_{yy} L_2 P \bigg|_{P=250} \quad (\text{i})$$

$$u_Q = \frac{\partial U^*}{\partial Q} \bigg|_{P=250, Q=0} = \int_0^{L_1} \left[ \frac{(L_2 P)}{EI_{xx}}(L_1 - z_1) \right] dz_1 \bigg|_{P=250} = \frac{L_1^2 L_2 P}{2EI_{xx}} \bigg|_{P=250} \quad . \quad (\text{j})$$

The formulas for the section properties are given in example 6.4 on page 160. For  $a = 50$  mm and  $t = 3$  mm we get

$$A = 300\pi \text{ mm}^2 \quad c_{yy} = \frac{1}{G(150\pi \text{ mm}^2)} \quad I_{xx} = 375000\pi \text{ mm}^4. \quad (\text{k})$$

For an isotropic material the shear modulus is computed from  $G = E/[2(1 + \nu)]$ , which evaluates to  $G = 79231 \text{ N/mm}^2$ . Numerical evaluation of the displacements gives

$$u_P = \frac{(6000)250}{(206000)(300\pi)} + \frac{(6000)(3000)^2 250}{(206000)(375000\pi)} + \frac{(3000)^3 250}{3(206000)(375000\pi)} + \frac{(3000)250}{(79231)(150\pi)}, \quad (\text{l})$$

$$u_P = 0.0077259681 + 55.62697 + 9.2711617 + 0.020087459 = 64.925946 \text{ mm}, \text{ and} \quad (\text{m})$$

$$u_Q = \frac{(6000)^2(3000)250}{2(206000)(375000\pi)} = 55.62697 \text{ mm}. \quad (\text{n})$$

Note that the contribution to the displacement  $u_P$  due to bending is  $55.62697 + 9.2711617 = 64.898132$  mm,

which is  $\left(\frac{64.898132}{64.925946}\right) 100 = 99.957161\%$  of the total displacement. **As a general rule the deflections of**

**frames composed of slender bars is dominated by bending, and the contributions due to axial stretching and transverse shear deformations to the deflections can be neglected. ■**

## 6.4 Castigliano's second theorem and statically indeterminate structures

A statically indeterminate structure is one in which the number of unknown forces exceeds the number of independent equations of static equilibrium. The excess forces are called redundants. By removing supports and/or members in a statically indeterminate structure equal to the number of redundants, a stable statically base structure can be obtained. To determine the redundants, we can impose displacement compatibility using Castigliano's second theorem. A stable statically determinate base structure is capable of resisting the external loads. Removing a support reaction or a member in statically determinate structure renders it unstable – it is not capable of resisting external loads and it is classified as moving mechanical system (i.e., either a mechanism or linkage).

Consider a coplanar truss which consists of straight bars connected by smooth hinge joints with the external loads applied only to the joints. As discussed in example 6.3 on page 158, a truss is statically determinate if  $m = 2j - r$  and statically indeterminate if  $m > 2j - r$ , where  $m$  denotes the number of bars or members,  $j$  the number of joints, and  $r$  denotes the number of reaction forces at the supports. Even statically determinate trusses can be unstable if the members are not arranged properly. Statical determinacy is a necessary condition for stability, not a sufficient condition. Each truss must be examined individually to determine stability. For the truss shown in part (a) of figure 6.17,  $m = 9$ ,  $r = 4$ , and  $j = 6$ , so it is statically indeterminate. If the upper left support is removed and replaced with a horizontal force  $Q$ , then a statically determinate base structure results as shown in part (b) of figure 6.17. The force  $Q$  is the redundant and it is treated as an external load on the base structure. Equilibrium of the base structure determines the internal bar forces in terms of external forces  $P$  and  $Q$ . The solution to the truss in part (a) is effected by imposing the displacement corresponding to force  $Q$  to vanish via Castigliano's second theorem (i.e.,  $q = \partial U^* / \partial Q = 0$ ). This displacement compatibility condition determines the redundant  $Q$ .



Fig. 6.17 A singly redundant truss (a), and its stable statically determinate base structure (b).

### Example 6.8 Statically indeterminate truss

Consider the truss shown in part (a) of figure 6.18. The horizontal bars and the vertical bars have a length denoted by  $L$ , and each bar has the same elastic modulus  $E$  and same cross-sectional area  $A$ . For this truss  $m = 6$ ,  $r = 3$ , and  $j = 4$ . So the truss is statically indeterminate. Note that this truss is statically determinate externally, but is statically indeterminate internally. Determine the bar forces in terms of the external applied load  $P$ .

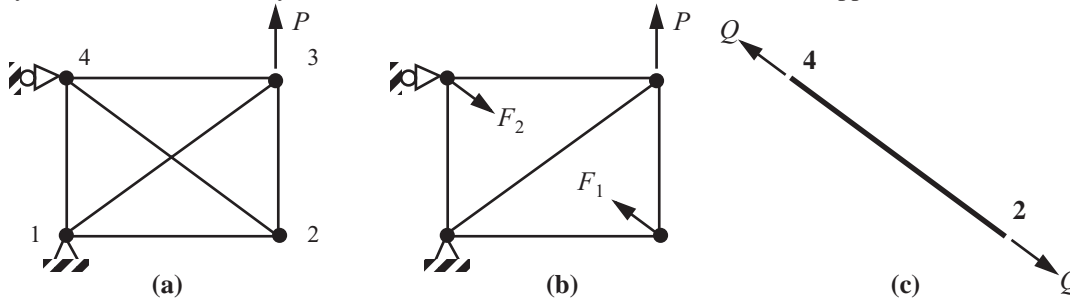


Fig. 6.18 (a) Statically indeterminate truss. (b) Statically determinant base structure with bar 2-4 replaced by forces  $F_1$  and  $F_2$ . (c) Bar 2-4 subject to equal and opposite forces.

**Solution.** Consider a statically determinate truss with bar 2-4 removed, and a force  $F_1$  acting at joint 2 and a force  $F_2$  acting at joint 4 as shown in figure 6.18 (b). These forces are oppositely directed along a line action coinciding with the removed bar 2-4. Let the complementary strain energy for this statically determinate, five-bar truss be denoted by  $\hat{U}^*$ . We employ Castigliano's second theorem to determine the displacement  $u_1$  corresponding to force  $F_1$  and displacement  $u_2$  corresponding to  $F_2$ . That is,

$$u_i = \frac{\partial \hat{U}^*}{\partial F_i} = \frac{1}{EA} \left[ LN_{12} \frac{\partial N_{12}}{\partial F_i} + \sqrt{2} LN_{13} \frac{\partial N_{13}}{\partial F_i} + LN_{14} \frac{\partial N_{14}}{\partial F_i} + LN_{23} \frac{\partial N_{23}}{\partial F_i} + LN_{34} \frac{\partial N_{34}}{\partial F_i} \right] \quad i = 1, 2. \quad (\text{a})$$

The bar forces are determined by joint equilibrium, and the results are shown in table 6.6. Bar forces are assumed

positive in tension.

**Table 6.6** Terms in eq. (a) for Castigliano's second theorem

						$F_1 = F_2 = Q$
Bar	Length $L$	Axial force $N$	$\partial N / \partial F_1$	$LN \frac{\partial N}{\partial F_1}$	$LN \frac{\partial N}{\partial F_2}$	$LN \frac{\partial N}{\partial Q}$
1-2	$L$	$-F_1 / \sqrt{2}$	$-1 / \sqrt{2}$	$LF_1 / 2$	0	$LQ / 2$
1-3	$\sqrt{2}L$	$F_1 + \sqrt{2}P$	1	$\sqrt{2}LF_1 + 2LP$	0	$\sqrt{2}LQ + 2LP$
1-4	$L$	$-F_2 / \sqrt{2}$	0	0	$(LF_2) / 2$	$(LQ) / 2$
2-3	$L$	$-F_1 / \sqrt{2}$	$-1 / \sqrt{2}$	$LF_1 / 2$	0	$LQ / 2$
3-4	$L$	$-F_1 / \sqrt{2} - P$	$-1 / \sqrt{2}$	$LF_1 / 2 + LP / \sqrt{2}$	0	$LQ / 2 + LP / \sqrt{2}$

The sum of elements in column five divided by the product  $EA$  determines displacement  $u_1$ , and the sum of column six divided by  $EA$  determines  $u_2$ . Simplifying the results leads to

$$u_1 = \frac{L}{EA} \left[ \frac{3 + 2\sqrt{2}}{2} \right] F_1 + \frac{L}{EA} \left[ \frac{4 + \sqrt{2}}{2} \right] P \text{ and } u_2 = \frac{L}{2EA} F_2. \quad (\text{b})$$

The relative inward displacement between joints 2 and joint 4 is given by the sum  $u_1 + u_2$ . For equal and opposite forces we set  $F_1 = F_2 = Q$ , and then the relative inward displacement reduces to

$$\Delta_{1/2} = u_1 + u_2 \Big|_{F_1 = F_2 = Q} = \frac{L}{EA} [2 + \sqrt{2}] Q + \frac{L}{EA} \left[ \frac{4 + \sqrt{2}}{2} \right] P. \quad (\text{c})$$

The seventh column in the table is obtained by setting  $F_1 = F_2 = Q$ . The sum of elements in the seventh column divided by  $EA$  is derivative of  $\hat{U}^*$  with respect to  $Q$ ; i.e.,

$$\frac{\partial \hat{U}^*}{\partial Q} = \frac{L}{EA} [2 + \sqrt{2}] Q + \frac{L}{EA} \left[ \frac{4 + \sqrt{2}}{2} \right] P. \quad (\text{d})$$

We conclude that the relative inward displacement between joints 2 and joint 4 is given by

$$\Delta_{1/2} = \frac{\partial \hat{U}^*}{\partial Q}. \quad (\text{e})$$

The elongation of bar 2-4 is denoted by  $\Delta_{24}$  and its complementary strain energy is denoted by  $U_{24}^*$ .

Hooke's law for bar 2-4 is given by eq. (6.2) on page 154, which for  $N \rightarrow Q$  and  $L \rightarrow \sqrt{2}L$  is solved for its elongation. The complementary strain energy is given by eq. (5.84) on page 145. These relations are

$$\Delta_{24} = \frac{\sqrt{2}L}{EA}Q \text{ and } U^*_{24} = \frac{1}{2EA} \int_0^{\sqrt{2}L} N^2 dz \Big|_{N=Q} = \frac{\sqrt{2}L}{2EA}Q^2. \quad (\text{f})$$

Castigliano's second theorem is  $\frac{\partial U^*_{24}}{\partial Q} = \frac{\sqrt{2}L}{EA}Q$ , which is equal to the elongation. Thus,  $\Delta_{24} = \frac{\partial U^*_{24}}{\partial Q}$ .

**Geometric compatibility** of the statically indeterminate, six-bar truss requires the relative inward displacement between joints 2 and 4 equals the negative of the elongation of bar 2-4. In other words, the sum  $\Delta_{1/2} + \Delta_{24} = 0$ . Hence,

$$\Delta_{1/2} + \Delta_{24} = \frac{\partial \hat{U}^*}{\partial Q} + \frac{\partial U^*_{24}}{\partial Q} = \frac{\partial U^*}{\partial Q} = 0, \quad (\text{g})$$

where the total complementary strain energy of the statically indeterminate six-bar truss is  $U^* = \hat{U}^* + U^*_{24}$ . Hence, Castigliano's second theorem applied to the six-bar truss is

$$\frac{\partial U^*}{\partial Q} = \underbrace{\frac{L}{EA}[2 + \sqrt{2}]Q + \frac{L}{EA}\left[\frac{4 + \sqrt{2}}{2}\right]P}_{\frac{\partial \hat{U}^*}{\partial Q}} + \underbrace{\frac{\sqrt{2}L}{EA}Q}_{\frac{\partial U^*_{24}}{\partial Q}} = \frac{L}{EA}\{2(1 + \sqrt{2})Q + [(4 + \sqrt{2})P]/2\} = 0 \quad (\text{h})$$

From eq. (h) we determine the redundant as

$$Q = -\left(\frac{4 + \sqrt{2}}{4(1 + \sqrt{2})}\right)P = -0.56066P. \quad (\text{i})$$

Finally, the bar forces are

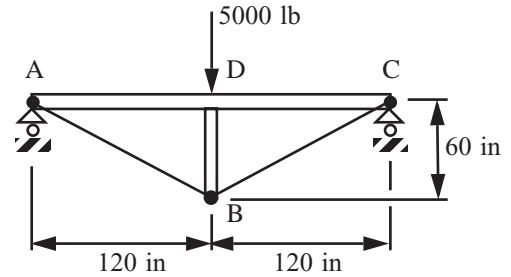
$$\begin{aligned} N_{1-2} &= 0.396447P & N_{1-3} &= 0.853553P & N_{1-4} &= 0.396447P \\ N_{2-3} &= 0.396447P & N_{2-4} &= -0.56066P & N_{3-4} &= -0.603553P \end{aligned} \quad (\text{j})$$

The condition that  $\partial U^*/\partial Q = 0$  is interpreted as the relative displacement between the faces of an imaginary cut in bar 2-4 is equal to zero. ■

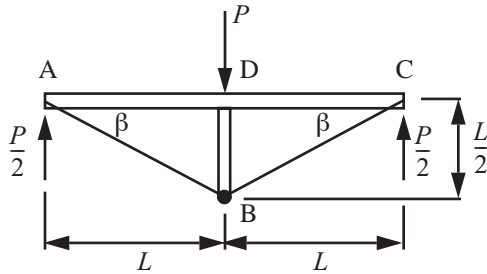
If the solution of the truss in example 6.8 was undertaken using Castigliano's first theorem, it would lead to five simultaneous linear equations for the unknown joint displacements  $q_3, q_4, q_5, q_6$ , and  $q_8$  in terms of the applied load  $P$ . (Refer to "Coplanar trusses" on page 153 for the displacement numbering convention.) After solving for these simultaneous equations for the joints displacements, the elongations of each bar,  $\Delta_{i-j}$ , would be computed from eq. (6.6) on page 155. Lastly, the bar forces are determined from  $N_{i-j} = (EA/L)_{i-j}\Delta_{i-j}$ . Using Castigliano's second theorem for this singly redundant truss, we only had to solve one equation for the unknown redundant  $Q$ . The number of simultaneous equations to be solved in a statically indeterminate structure by Castigliano's second theorem is equal to the number of redundants.

**Example 6.9 King Post truss**

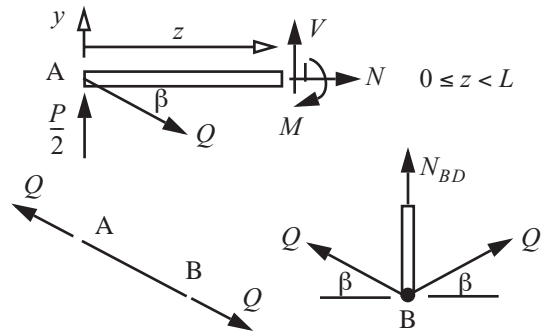
In this example we paraphrase the problem statement given in the text by Bruhn (1973, p. A8.42). The structure shown in figure 6.19 consists of members ADC, AB, BC, and BD. Continuous member ADC is simply supported at ends A and C, has an area of  $9.25 \text{ in}^2$ , and a second area moment of  $216 \text{ in}^4$ . Members AB, BC and BD have areas of  $2 \text{ in}^2$ . The modulus of elasticity is the same for all members. Determine the internal actions in each member using Castigliano's second theorem.

**Fig. 6.19 King Post Truss.**

**Solution.** This structure is statically determinant externally. Also, the structure, its support conditions, and the



(a) The structure removed from its supports



(b) Members AD, AB, and BD

**Fig. 6.20 Free body diagrams of the King Post truss.**

external loading are symmetric about the vertical line of action of the 5,000 lb. force. The support reactions of the truss removed from its supports at A and C are shown in figure 6.20(a). Consideration of the free body diagrams of members AD, AB, and BD in figure 6.20(b) leads to the conclusion that this structure is statically indeterminate internally. The redundant  $Q$  is taken as the axial force in member AB. If  $Q$  is known, then the forces and moments in the other members are determined by equilibrium. Neglecting the energy due to transverse shear in member ADC, the complementary strain energy is

$$U^* = 2 \int_0^L \left[ \frac{N^2}{2EA_{AC}} + \frac{M^2}{2EI} \right] dz + 2 \left[ \frac{L_{AB} Q^2}{2EA} \right] + \frac{(L/2) N_{BD}^2}{2EA}. \quad (a)$$

Note that the complementary strain energy in members AD and AB are multiplied by two to account for the energy in members DC and BC, respectively. The compatibility condition that the relative displacement of an imaginary cut in member AB vanishes is that the derivative of the complementary energy with respect to  $Q$  equals zero. Thus,

$$0 = 2 \int_0^L \left\{ \frac{N}{EA_{AC}} \left( \frac{\partial N}{\partial Q} \right) + \frac{M}{EI} \left( \frac{\partial M}{\partial Q} \right) \right\} dz + \frac{2L_{AB} Q}{EA} + \frac{(L/2) N_{BD}}{EA} \left( \frac{\partial N_{BD}}{\partial Q} \right). \quad (b)$$

Equilibrium equations of member AD are

$$N + Q \cos \beta = 0 \quad V + P/2 - Q \sin \beta = 0 \quad M + (P/2 - Q \sin \beta)z = 0 \quad 0 \leq z < L. \quad (\text{c})$$

The axial equilibrium equation for member BD is

$$N_{BD} + 2Q \sin \beta = 0. \quad (\text{d})$$

Substitute member axial forces and moment from the equilibrium eq. (c) into the compatibility condition (b) to get

$$0 = 2 \int_0^L \left[ \frac{(-Q \cos \beta)}{EA_{AC}} (-\cos \beta) + \frac{[-(P/2 - Q \sin \beta)z]}{EI} [(\sin \beta)z] \right] dz + \frac{2L_{AB}Q}{EA} + \frac{(L/2)(-2Q \sin \beta)}{EA} (-2 \sin \beta). \quad (\text{e})$$

Perform the integration in eq. (e) followed by the substitutions  $L_{AB} = (\sqrt{5}L)/2$ ,  $\cos \beta = 2/(\sqrt{5})$ , and  $\sin \beta = 1/(\sqrt{5})$  to find

$$0 = 2 \left( \frac{-L^3 P}{6\sqrt{5}EI} + \frac{4LQ}{5EA_{AC}} + \frac{L^3 Q}{15EI} \right) + \frac{2LQ}{5EA} + \frac{\sqrt{5}LQ}{EA}. \quad (\text{f})$$

Solve. (f) for the redundant  $Q$ :

$$Q = \frac{\sqrt{5}AA_{AC}L^2P}{24AI + 6A_{AC}I + 15\sqrt{5}A_{AC}I + 2AA_{AC}L^2}. \quad (\text{g})$$

Substitute the numerical values for the quantities on the right-hand side of eq. (g) to find the redundant:

$$Q = \frac{\sqrt{5}(2)(9.25)(120^2)(5000)}{24(2)(216) + 6(9.25)(216) + 15\sqrt{5}(9.25)(216) + 2(2)(9.25)(120^2)} = 4,787.18 \text{ lb.} \quad (\text{h})$$

The axial force in member BD from eq. (d) is

$$N_{BD} = -2(4787.18) \left( \frac{1}{\sqrt{5}} \right) = -4281.78 \text{ lb.} \quad (\text{i})$$

The negative value of  $N_{BD}$  means member BD is in compression. The axial force and bending moment in member AD is

$$N = -(4787.18)2/\sqrt{5} = -4281.78 \text{ lb.} \quad M = \left( -2500 + \frac{(4747.18)}{\sqrt{5}} \right) z = (-359.11 \text{ lb.})z \quad 0 \leq z < 120 \text{ in} \quad (\text{j})$$

### 6.4.1 Function of a Turnbuckle

A turnbuckle is a metal coupling device consisting of an oblong piece, or barrel, internally threaded at both ends into which the corresponding sections of two threaded rods are screwed in order to form a unit that can be adjusted for tension or length. A right-hand thread is used at one end and a left-hand thread at the other end. The device either lengthens or shortens when the barrel is rotated. Each full turn of the barrel causes it to travel a distance  $p$  along each screw, where  $p$  is the pitch of the threads. Tightening the turnbuckle by one turn causes the rods to be drawn closer together by a distance  $2p$ . That is, one turn to tighten causes the device to shorten by  $2p$ .



For  $n$  turns the shortening distance is  $2np$ , where  $n$  need not be an integer. Turnbuckles are widely used in aircraft. Biplanes may use turnbuckles to adjust the tension on structural wires bracing their wings as discussed in example 6.10 below. Turnbuckles are also widely used with flexible cables in flight control systems.

### Example 6.10 Rigging biplane landing and flying wires

An acrobatic biplane has a maximum gross weight of 1,700 lbs. and a wing span of 25 feet. The cross sections of the lower and upper wings are thin, so the wing structure is strengthened by external bracing. As shown in figure 6.21 the bracing consists of landing and flying wires connecting the fuselage to the wings at the interplane strut. Turnbuckles inserted in the landing and flying wires are used to pre-tension the wires by changing their length.

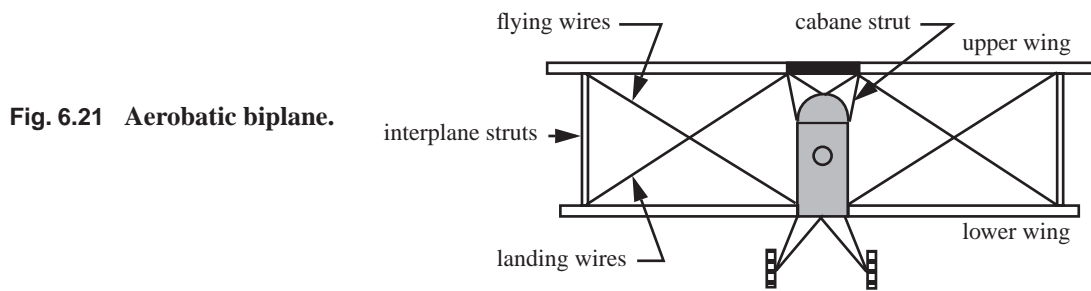


Fig. 6.21 Aerobatic biplane.

We will model the structural unit consisting of the lower wing, upper wing, interplane strut, landing wires, and flying wires as shown in figure 6.22 (a). The left-hand wings are modeled as a pin-jointed truss. Bars 1-2 and 3-4 represent the spars in the lower wing and upper wing, respectively, and are of length  $L = 10$  ft. The spars are made of Sitka spruce with a Young's modulus parallel to the grain of  $1.5 \times 10^6$  lb./in.<sup>2</sup>, and a cross-sectional area of  $1.25$  in.<sup>2</sup>. Bar 1-3 represents the landing wire, bar 2-4 the flying wire, and the wires are made of stainless steel with a modulus of  $30 \times 10^6$  lb./in.<sup>2</sup>. Each wire has a diameter of  $0.125$  in. Bar 1-4 is the interplane strut of length  $h$  equal to  $4.3$  ft., and it is assumed to be very stiff. The wings are specified to have a dihedral angle  $\Gamma = 4^\circ$ .

Determine the number of turns in the flying wire turnbuckle  $n_F$ , and the number of turns in the landing wire turnbuckle  $n_L$ , such that the flying wire tension is  $400$  lb., and the dihedral is maintained at four degrees. The pitch of the turnbuckle threads is  $p = 1$  in./( $10$  turns).

**Solution.** The structural model of the left-hand wing and bracing shown in figure 6.22 (a) consists of five truss bars. The turnbuckle displacements are determined from the horizontal position of the wing. Free body diagrams of joints 1 and 4 are shown in figure 6.22 (b). A vertical external force  $Q_2$  is introduced at joint 1 so that its corresponding displacement  $q_2$  can be determined in the application of Castigliano's theorem. Displacement  $q_2$  is specified from the wing's required dihedral. That is  $q_2 = L \sin \Gamma$ , and after its determination external force  $Q_2$  is set to zero.

From eq. (5.84) on page 145 the complementary energy for a homogenous truss bar subject to a uniform change in temperature is

$$U^* = \frac{L}{2EA}(N + N_T)^2. \quad (a)$$

To account for the displacements of the turnbuckles in Castigliano's second theorem we modify the axial temper-

ature term in the complementary strain energy. The thermal axial force in the truss bar is obtained from eq. (3.75) on page 46:

$$N_T = \int_c \beta \Delta T(s, z) t(s) ds = EA \alpha \Delta T. \quad (b)$$

Let the thermal strain  $\alpha \Delta T$  be replaced by the initial strain induced by the turnbuckle displacement  $\Delta_T = 2np$  divided by the length of the bar containing the turnbuckle. That is,  $\alpha \Delta T \rightarrow \Delta_T / L$ . Then the complementary strain energy in eq. (a) that includes the displacement caused by the turnbuckle is

$$U^* = \frac{c}{2} (N + \Delta_T / c)^2, \quad (c)$$

where the flexibility influence coefficient  $c = L / (EA)$ .

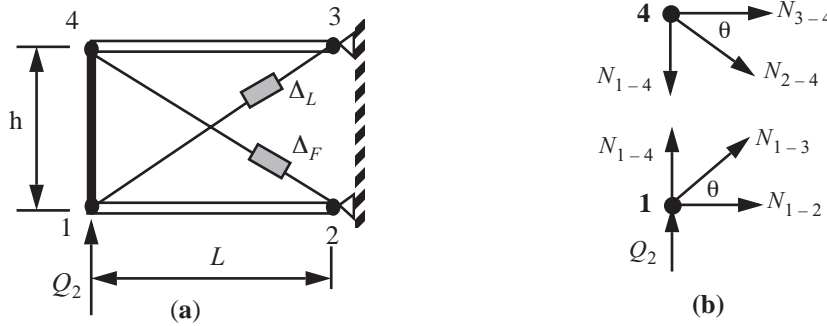


**Fig. 6.22 (a) Structural model of the left-hand wing and bracing. (b) Free body diagrams.**

The interplane strut subject to force  $N_{1-4}$  is assumed to be rigid. Its flexibility influence coefficients vanishes and it does not contribute the elastic complementary strain energy. The complementary strain energy is

$$U^* = \frac{1}{2} c_W (N_{1-2})^2 + \frac{1}{2} c_{ST} (N_{1-3} + \Delta_L / c_{ST})^2 + \frac{1}{2} c_{ST} (N_{2-4} + \Delta_F / c_{ST})^2 + \frac{1}{2} c_W (N_{3-4})^2. \quad (d)$$

The flexibility influence coefficients for the two wing spars is

$$c_W = \frac{L}{E_W A_W} = \frac{120}{(1.5 \times 10^6) 1.25} = 64 \times 10^{-6} \text{ in./lb}, \quad (e)$$

and the flexibility influence coefficients for the two wires is

$$c_{ST} = \frac{\sqrt{120^2 + 51.6^2}}{(30 \times 10^6) \pi (0.125/2)^2} = \frac{130.624}{(30 \times 10^6) (0.012272)} = 354.81 \times 10^{-6} \text{ in./lb}. \quad (f)$$

Equilibrium equations at joint 1 in figure 6.22(b) are

$$N_{1-3} \cos \theta + N_{1-2} = 0 \quad Q_2 + N_{1-4} + N_{1-3} \sin \theta = 0, \quad (g)$$

and equilibrium equations at joint 4 are

$$N_{3-4} + N_{2-4} \cos \theta = 0 \quad N_{1-4} + N_{2-4} \sin \theta = 0. \quad (\text{h})$$

The trigonometric functions of the angle  $\theta$  are

$$\cos \theta = \lambda = \frac{120}{\sqrt{120^2 + 51.6^2}} = 0.91866919 \quad \sin \theta = \mu = \frac{51.6}{\sqrt{120^2 + 51.6^2}} = 0.39502775. \quad (\text{i})$$

Now eliminate the bar force  $N_{1-4}$  between the four equilibrium equations to get the three equations

$$N_{1-3} \lambda + N_{1-2} = 0 \quad N_{3-4} + N_{2-4} \lambda = 0 \quad Q_2 - N_{2-4} \mu + N_{1-3} \mu = 0. \quad (\text{j})$$

The force  $N_{2-4}$  in the flying wire is taken as the redundant. Solve the remaining bar forces from eq. (j) in terms of the redundant and force  $Q_2$  to get

$$N_{1-2} = -N_{2-4} \lambda + Q_2 \lambda / \mu \quad N_{1-3} = N_{2-4} - Q_2 / \mu \quad N_{3-4} = -N_{2-4} \lambda. \quad (\text{k})$$

Substitute the results for  $N_{1-2}$ ,  $N_{1-3}$ , and  $N_{3-4}$  from eq. (k) into the complementary strain energy (d) to find the energy in the form  $U^*[N_{2-4}, Q_2]$  with turnbuckle displacements  $\Delta_L$  and  $\Delta_F$  appearing in  $U^*$  as parameters.

$$q_2 = \left. \frac{\partial U^*}{\partial Q_2} \right|_{Q_2=0} = -(c_{ST} + c_W \lambda^2)(N_{2-4} / \mu) - (\Delta L) / \mu. \quad (\text{l})$$

$$\frac{\partial U^*}{\partial N_{2-4}} = 2(c_{ST} + c_W \lambda^2)N_{2-4} - (c_{ST} + c_W \lambda^2)(Q_2 / \mu) + \Delta_L + \Delta_F = 0. \quad (\text{m})$$

Set  $q_2 = L \sin \Gamma$  in eq. (l) and solve for the landing wire turnbuckle displacement, followed by solving eq. (m) for the to find flying wire turnbuckle displacement. The results are

$$\Delta L = -(c_{ST} + c_W \lambda^2)N_{2-4} - \mu L \sin \Gamma \quad \text{and} \quad \Delta F = -(c_{ST} + c_W \lambda^2)N_{2-4} + \mu L \sin \Gamma. \quad (\text{n})$$

Set  $N_{2-4} = 400$  lb. to obtain the numerical results for the turnbuckle displacements and their number of turns as

$$\Delta L = -3.41912 \text{ in.} \quad n_L = -17.0956 \text{ turns} \quad \Delta F = 3.19425 \text{ in.} \quad n_F = 15.9713 \text{ turns.} \quad (\text{o})$$

The landing wire turnbuckle decreases the length between joints 1 and 3, and the flying wire turnbuckle increases the length between joints 2 and 4. The bar forces are

$$N_{1-2} = N_{3-4} = -367.468 \text{ lb.} \quad N_{1-3} = N_{2-4} = 400 \text{ lb.} \quad N_{1-4} = -158.011 \text{ lb.} \quad \blacksquare \quad (\text{p})$$

## 6.5 References

Bruhn, E. F., 1973, **Analysis and Design of Flight Vehicle Structures**, Jacobs Publishing, Inc., Carmel, Indiana, 46032, p. A8.42. (ISBN# 0-9615234-0-9)

Dowling, Norman E., 1993, **Mechanical Behavior of Materials**, Prentice Hall, Englewood Cliffs, New Jersey 07632, pp. 245-247.

Thornton, E. A., 1996, **Thermal Structures for Aerospace Applications**, AIAA Education Series, American Institute of Aeronautics and Astronautics, Inc., Reston, Virginia, pp. 118-121.

Warwick, Graham. "Big Fuel Savings Demand New Configurations," November 7, 2011. Aviation Week.com.

## 6.6 Practice exercises

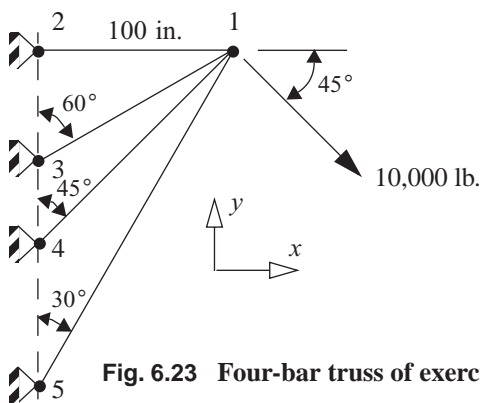


Fig. 6.23 Four-bar truss of exercise 1.

1. Each bar in the truss shown in figure 6.23 has a cross-sectional area of  $1.0 \text{ in.}^2$ , and a modulus of elasticity of  $10^7 \text{ psi}$ . There is no change in temperature. Use Castigliano's first theorem to find

- the horizontal and vertical displacements of joint 1,
- the stress in psi in each bar, and
- the horizontal and vertical support reactions at joint 5.

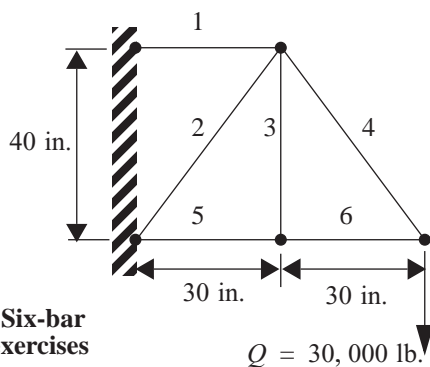


Fig. 6.24 Six-bar truss for exercises 2 and 3.

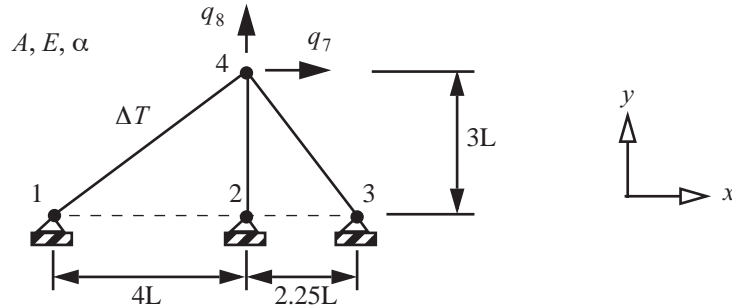
2. The bars in the truss shown in figure 6.24 have the following cross-sectional areas:  $A_1 = 1.0 \text{ in.}^2$ ,  $A_2 = A_4 = 2.0 \text{ in.}^2$ ,  $A_3 = 1/2 \text{ in.}^2$ ,  $A_5 = A_6 = 3/2 \text{ in.}^2$ . The modulus of elasticity of each bar is  $10^7 \text{ psi}$ . Compute the vertical displacement of the right-hand joint using Castigliano's second theorem. Note this truss is statically determinate and all bar forces can be determined in terms of external load  $Q$ .

3. Use Castigliano's second theorem to compute the horizontal displacement of the right-hand joint of exercise 2.

4. The truss shown figure 6.25 consists of three bars: 1-4, 2-4, and 3-4. Each bar has the same cross-sectional area  $A$ , modulus of elasticity  $E$ , and the same coefficient of thermal expansion  $\alpha$ . Bar 1-4 is subjected to a change in temperature  $\Delta T$  from ambient temperature (the unstressed state), while bars 2-4 and 3-4 remain at ambient temperature. Use Castigliano's first theorem to deter-

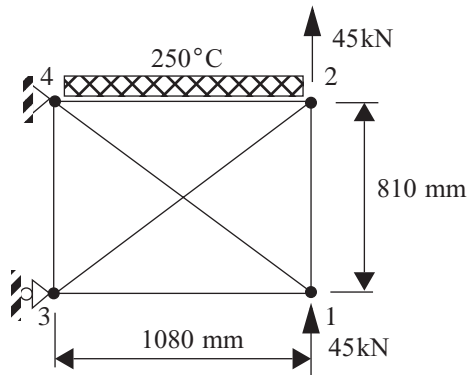
mine the horizontal displacement  $q_7$  and the vertical displacement  $q_8$  of joint 4.

**Fig. 6.25** Three-bar truss of exercise 4.



5. The plane truss shown in figure 6.26 represents a single bay of a wing spar truss. For all bars:  $E = 75 \text{ GPa}$  and  $\alpha = 23.0 \times 10^{-6} / ^\circ\text{C}$ . The cross-sectional areas of the bars are:  $2580 \text{ mm}^2$  for the horizontal bars,  $387 \text{ mm}^2$  for the vertical bars, and  $2690 \text{ mm}^2$  for the diagonal bars. The upper horizontal bar is heated to  $250^\circ\text{C}$  above the zero stress temperature, and all other bars remain at the zero stress temperature. Two  $45 \text{ kN}$  lift forces act at joints 1 and 2.

**Fig. 6.26** Six-bar truss in a single bay of a wing spar.



Use Castigliano's first theorem to find

- stiffness matrix in  $\text{kN/mm}$ ,
  - displacement of all joints in  $\text{mm}$ ,
  - all boundary reactions in  $\text{kN}$ , and
  - the stresses in  $\text{MPa}$  in each bar.
6. The truss shown in figure 6.27 consists of five bars: 1-2, 1-3, 1-4, 2-4, and 3-4. Each bar has the same cross-sectional area  $A$  and same modulus of elasticity  $E$ . The lengths of bars 1-2, 1-4, and 3-4 are the same, and are denoted by  $L$ . A horizontal force of magnitude  $P$  is applied to joint 1. Use Castigliano's second theorem to determine the horizontal displacement  $q_5$  of joint 3.
7. A simply supported, uniform beam of length  $L$  is subjected to a moment  $Q_1$  at its left end as shown in figure 6.28. The material is homogeneous and linear elastic, the cross section is symmetric ( $I_{xy} = 0$ ), and there are no thermal strains. The bending stiffness is  $EI$ . Use Castigliano's second theorem to determine the rotation at (a) the left end, and (b) the right end. Neglect energy due to transverse shear deformation.

**Fig. 6.27** Five-bar truss of exercise 6.

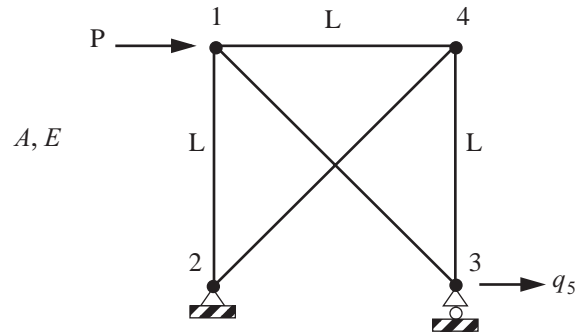


**Fig. 6.28** Simply supported beam of exercise 7.

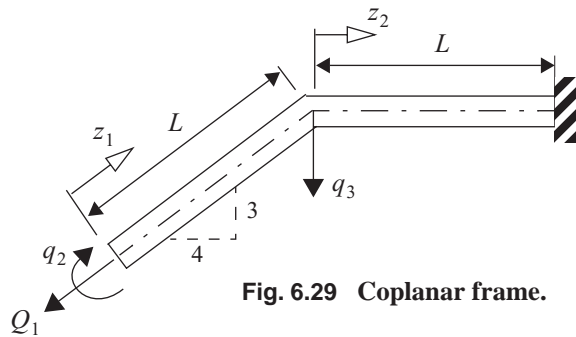
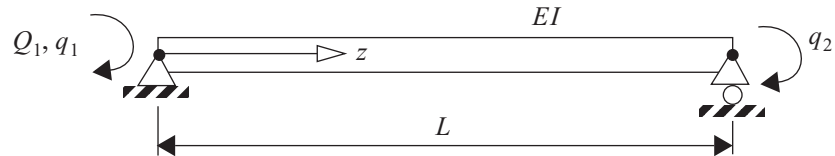


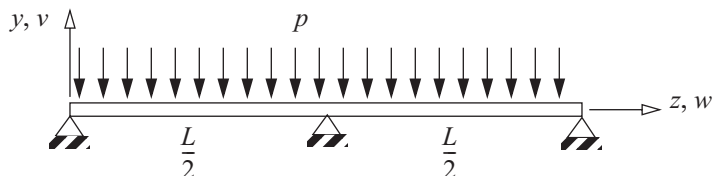
**Fig. 6.29** Coplanar frame.

8. A coplanar frame is subjected to an end force  $Q_1$  as shown in figure 6.29. The bars of the frame are uniform with axial stiffness  $EA$  and bending stiffness  $EI$ . Use Castigliano's second theorem to find

- the end rotation  $q_2$ , and
- the vertical displacement  $q_3$  at the joint.

9. Consider the statically indeterminate, uniform beam shown in figure 6.30 that is subjected to a uniform, downward distributed load of intensity  $p$ . For small displacements assume that only the complementary strain energy in bending is significant. If the center support moves downward by the amount  $0.01pL^4/EI_{xx}$  and remains attached to the beam, use Castigliano's second theorem to find the reactions at the left and right supports.

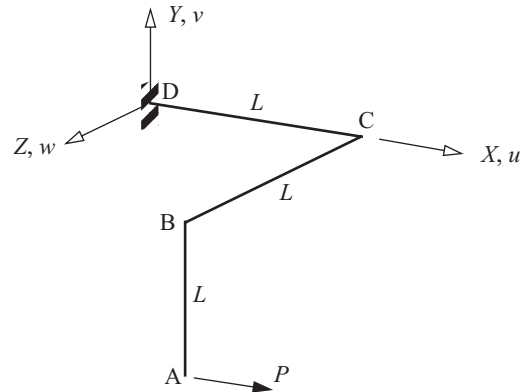
**Fig. 6.30** Uniform beam of exercise 9



10. The frame consists of three slender, uniform bars of length  $L$ , and two right angle bends. Assume the bends are rigid joints. Each member has a solid circular cross section of diameter  $d$ . A force  $P$  acts in the global  $X$ -direction at point A. Find the three displacement components  $u_A$ ,  $v_A$ ,  $w_A$  of point A in terms of  $P$ ,  $L$ ,  $d$ , and  $E$  using

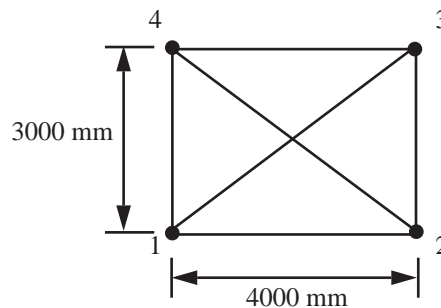
Castigliano's second theorem. Assume  $G = 0.4E$ . Neglect deformations due to transverse shear.

**Fig. 6.31** Space frame of exercise 10.



- 11.** The rectangular space truss shown in the sketch consists of six bars: 1-2, 1-3, 1-4, 2-3, 2-4, and 3-4. The cross-sectional area of each bar is  $200 \text{ mm}^2$ . The temperature of bar 2-3 is increased by  $30^\circ\text{C}$  above the stress free temperature, while the other five bars remain at the stress free temperature. Calculate the forces in all six bars. The coefficient of thermal expansion  $\alpha = 7 \times 10^{-6}/^\circ\text{C}$ , and the modulus of elasticity  $E = 200 \times 10^3 \text{ N/mm}^2$ .

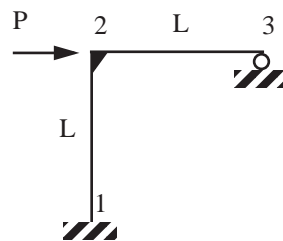
**Fig. 6.32** Space truss of exercise 11



Note that  $m = 6$ ,  $j = 4$ , and  $r = 0$ . Hence,  $m < 2j - r$ , and this truss cannot support an external load without accelerating. However, under the self-straining caused by the temperature change, it is statically indeterminate internally.

- 12.** Sketch the bending moment diagrams of bars 1-2 and 2-3 in the singly redundant frame shown in figure 6.33. Each bar has the same length  $L$  and flexural stiffness  $EI$ . Since the bars are slender, neglect deformations due to extension and transverse shear. Take the reaction moment at support point 1 as the redundant.

**Fig. 6.33** Two-bar frame of exercise 12.



**13.** The aerodynamic advantages of high aspect-ratio (AR) wings are well-known—long span reduces lift-induced drag and narrow chord promotes laminar flow to reduce skin-friction drag. However, a long wing span significantly increases the structural loads at the wing root requiring heavier components to safely transmit the loading to the fuselage. The truss-braced wing (TWB) is a method to reduce the load at the wing root. (It is the subject of research in AOE at Virginia Tech under a NASA program to achieve significant fuel savings for 737 type airplanes (Warwick, 2011)). A simplified model of TWB in this exercise is a single truss bar supporting a wing spar.

A wing spar is clamped at its root and supported by a truss bar that is pinned to the support at one end and pinned to the spar at the other end. Refer to figure 6.34. The spar is subjected to a span-wise distributed air load  $f_y(z)$  approximated by

$$f_y(z) = \frac{3L}{2b} \left[ 1 - \left( \frac{z}{b} \right)^2 \right] \quad 0 \leq \left( \frac{z}{b} \right) \leq 1. \quad (\text{a})$$

where the lift on the wing is denoted by  $L$  and the wing span is denoted by  $b$ . The pin connection of the truss bar to the spar is at the span-wise distance  $s \cdot b$  from the root, where the range of nondimensional parameter  $s$  is  $0 < s \leq 1$ .

The assemblage is statically indeterminate, and the statically determinate base structure is obtained by removing the lower pin support of the truss bar and replacing it by the redundant force  $Q$  which is also the tensile force in the truss bar. Refer to the right-hand sketch in figure 6.34. The condition of compatibility is the displacement corresponding to the redundant is equal to zero. Enforce compatibility by Castigliano's second theorem given by

$$q = \frac{\partial U^*}{\partial Q} = 0 \quad U^* = \int_0^{sb} \left( \frac{M_x^2}{2EI_{xx}} + \frac{N^2}{2EA} \right) dz + \int_{sb}^b \left( \frac{M_x^2}{2EI_{xx}} \right) dz + \frac{Q^2 l_s}{2EA_s}. \quad (\text{b})$$

where  $l_s$  is the length of the strut. Numerical data are listed in table 6.7.

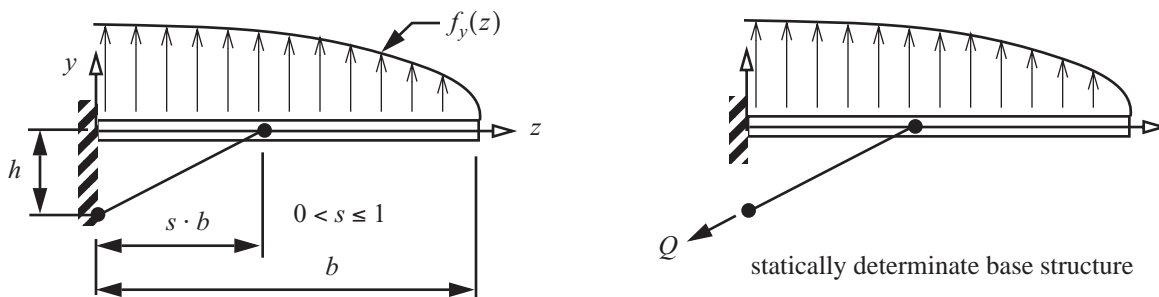


**Fig. 6.34 Truss braced wing.**

- Plot the normalized bending moment at the wing root  $(M_x(0))/M_0$  versus  $s$  for  $0.01 \leq s \leq 1$ , where  $M_0$  is the root bending moment of the cantilever wing; i.e.,  $M_0 = -(3/8)bL$
- Plot the tensile normal stress  $\sigma = Q/A_s$  in the strut versus  $s$  for  $0.01 \leq s \leq 1$ .
- If the allowable tensile stress in the strut is 30 ksi, what is the value of  $s$  to yield the smallest value of the



ratio  $(M_x(0))/M_0$ ? What is the value of  $(M_x(0))/M_0$  for this particular  $s$ ?

**Table 6.7 Numerical data for the strut-braced wing**

$b$ , wing span	390 in.
$h$ , vertical distance from the spar centroid to lower strut support	72 in.
$A$ , cross-sectional area of the spar	23.88 in. <sup>2</sup>
$I_{xx}$ , second area moment of the cross section of the spar	872.716 in. <sup>4</sup>
$A_s$ , cross-sectional area of the strut (1.75 in. diameter)	2.40528 in. <sup>2</sup>
$L$ , wing lift	50,000. lb.
$E$ , modulus of elasticity for the spar and strut material	$10 \times 10^6$ lb./in. <sup>2</sup>



# Arches, rings and fuselage frames

A common structural component in aerospace structures is a curved bar. For example, fuselage frames are often composed of slender curved elements and thin rings. The Winkler<sup>1</sup> theory for the linear elastic response of coplanar curved bars within their plane is presented in article 7.1. (Also refer to Langhaar, 1962). The Winkler theory models both thick and thin curved bars. A curved bar is generally considered thin if the ratio of the radius of curvature to its in-plane thickness is greater than ten. Ratios less than ten are considered thick bars. It is assumed that there is no out-of-plane bending and torsion of the bar in article 7.1. Consistent with this limitation and assumption is an idealization employed in aircraft structural analyses that a ring frame is coplanar structure supporting loads in its plane and not supporting loads normal to its plane. Out-of plane bending and torsion of planar, thin curved bars is reviewed in the article by Chidamparam and Leissa (1993).

## 7.1 Coplanar curved bars

The reference axis of the bar is defined as a uniformly continuous plane curve within a closed interval. It is assumed that the cross sections of the bar are symmetric with respect to the plane of the reference axis, and that the locus of points along the centroids of each cross section coincide with the reference axis. Only deformations of the bar in the plane of symmetry are considered.

The Cartesian coordinates of the reference axis with origin at point O are denoted by  $y_0(s)$  and  $z_0(s)$  in the plane of symmetry, where  $s$  denotes the curvilinear coordinate of the reference axis. Geometry of the curved bar in its plane of symmetry is shown in figure. 7.1. The position vector of the reference axis with respect to the origin O is  $\vec{r}(s) = y_0(s)\hat{j}_0 + z_0(s)\hat{k}_0$ , where  $\hat{j}_0$  and  $\hat{k}_0$  are fixed unit vectors along the positive  $y_0$  and  $z_0$  directions, respectively. The unit tangent vector to the reference axis at point  $s$  is

$$\hat{t}(s) = \frac{d\vec{r}}{ds} = \frac{dy_0}{ds}\hat{j}_0 + \frac{dz_0}{ds}\hat{k}_0. \quad (7.1)$$

1. Emil Winkler, 1835-1888, German civil engineer and professor.


$$\hat{i}(s) = -\sin\theta(s)\hat{j}_0 + \cos\theta(s)\hat{k}_0 \quad j(\hat{s}) = \cos\theta(s)\hat{j}_0 + \sin\theta(s)\hat{k}_0. \quad (7.2)$$
$$\frac{\hat{dt}}{ds} = \frac{-\hat{j}}{R(s)} \quad \frac{\hat{dj}}{ds} = \frac{\hat{t}}{R(s)} \quad \frac{1}{R(s)} = \frac{d\theta}{ds}, \quad (7.3)$$
$$dS = \left(1 + \frac{y}{R(s)}\right) ds. \quad (7.4)$$

### 7.1.1 Displacements and strain

Consider the displacement of a particle located by  $\vec{R}(S, y)$  on the parallel curve to the position located by displacement vector  $\vec{R}^*(S^*, y)$  with respect to origin O on the parallel curve in the deformed bar. Let  $S^*$  denote the arc-length along the parallel curve in the deformed bar, where the  $y$ -coordinate remains unchanged in the deformation. That is, **it is assumed the cross section remains rigid in its own plane**. We write the position of the particle in the deformed bar with respect to its position in the undeformed bar as  $\vec{R}^* = \vec{R} + \vec{u}$ , where the displacement vector is defined by

$$\vec{u}(S, y) = u_s(S, y)\hat{t}(s) + u_y(S, y)\hat{j}(s). \quad (7.5)$$

The differential of  $\vec{R}^*(S^*, y)$  along the parallel curve in the deformed bar is given by

$$d\vec{R}^* = dS\hat{t} + \frac{d}{dS}(u_s\hat{t} + u_y\hat{j})dS = dS\hat{t} + \left[\frac{d}{dS}(u_s\hat{t} + u_y\hat{j})\right]\left(1 + \frac{y}{R(s)}\right)^{-1}dS, \quad (7.6)$$

in which we use the chain rule of differentiation (i.e.,  $\frac{d\vec{u}}{dS} = \frac{d\vec{u}}{ds}\frac{ds}{dS}$ ) and eq. (7.4) to transform the derivative with respect  $S$  to the derivative with respect  $s$ . Performing the differentiations in eq. (7.6) and using the relations in eq. (7.3), we get

$$d\vec{R}^* = \left[\hat{t} + \frac{1}{\left(1 + \frac{y}{R}\right)}\frac{d}{ds}(u_s\hat{t} + u_y\hat{j})\right]dS = \left[\hat{t} + \frac{1}{\left(1 + \frac{y}{R}\right)}\left[\left(\frac{du_s}{ds} + \frac{u_y}{R}\right)\hat{t} + \left(\frac{du_y}{ds} - \frac{u_s}{R}\right)\hat{j}\right]\right]dS. \quad (7.7)$$

The last result is written as

$$d\vec{R}^* = [(1 + \varepsilon)\hat{t} - \omega\hat{j}]dS, \quad (7.8)$$

where

$$\varepsilon = \frac{R}{R + y}\left(\frac{du_s}{ds} + \frac{u_y}{R}\right) \quad \omega = -\left(\frac{R}{R + y}\right)\left(\frac{du_y}{ds} - \frac{u_s}{R}\right). \quad (7.9)$$

The differential arc-length along the parallel curve in the deformed bar is determined by  $(dS^*)^2 = d\vec{R}^* \cdot d\vec{R}^*$ , and the unit tangent vector to the parallel curve in the deformed bar is  $\hat{t}^* = (d\vec{R}^*)/(dS^*)$ . The stretch ratio  $\lambda$  is defined by  $dS^* = \lambda dS$ , and with regard to eq. (7.8)  $\lambda = \sqrt{(1 + \varepsilon)^2 + \omega^2}$ . Consider the binomial series  $\sqrt{1 + \xi} = 1 + \xi/2 - \xi^2/8 \pm \dots$ . For  $\xi = 2\varepsilon + \varepsilon^2 + \omega^2$ , the binomial series for the stretch ratio is  $\lambda = 1 + \varepsilon + \omega^2/2 + \dots$ . Since the engineering strain is defined by  $\lambda - 1 = \varepsilon + \omega^2/2 + \dots$ , we see that to the lowest degree in the series expansion of the engineering strain that  $\varepsilon$  is interpreted as the normal strain of a parallel curve for infinitesimal deformation. To interpret the physical meaning of  $\omega$  a graph of eq. (7.8) is shown in figure. 7.2(a). Let  $\Omega$  denote the angle between the unit tangent vector  $\hat{t}$  of the parallel curve in the undeformed bar and the unit tangent vector  $\hat{t}^*$  of the parallel curve in the deformed bar. From the geometry of the triangle in figure. 7.2(a) we see that  $\tan \Omega = \omega/(1 + \varepsilon)$ . Using the small angle approximation for the tangent function, and

the assumption of infinitesimal strain, we find  $\Omega \approx \omega$ . That is,  $\omega$  represents the rotation of the tangent line element to the parallel curve for infinitesimal deformations of the bar. Let  $\hat{j}^*$  denote unit normal vector to  $\hat{t}^*$ . From figure. 7.2(a) the unit normal vector  $\hat{j}^* = (\cos \Omega)\hat{j} + (\sin \Omega)\hat{t}$ . For small angles  $\Omega$ , the unit normal vector approximates as

$$\hat{j}^* \approx \hat{j} + \omega \hat{t}. \quad (7.10)$$

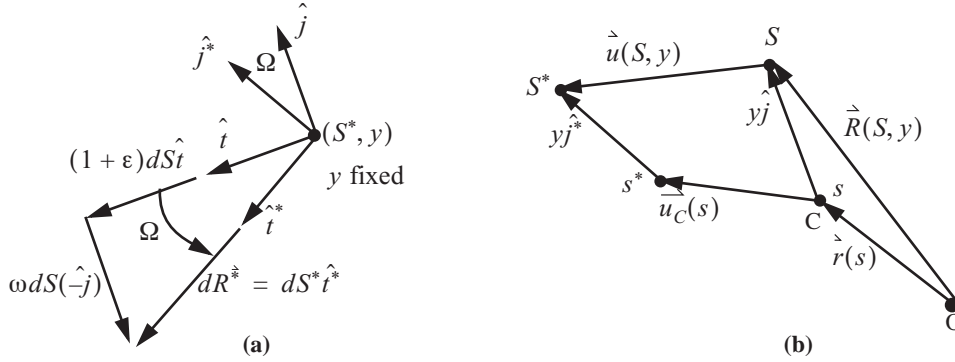


**Fig. 7.2** (a) Differential line element of a parallel curve in the deformed bar. (b) Relationship of the displacement of a particle on a parallel curve to the displacement of the corresponding particle on the reference axis.

The relationship between the displacement vector of the parallel curve to the displacement vector of the reference axis is based on the assumptions that plane cross sections normal to the reference axis remain normal to the reference axis in the deformed bar and that the cross section remains rigid in its own plane. These assumptions, which are the basis of classical beam theory, are depicted in figure. 7.2(b). Thus,

$$\vec{u}(S, y) = \vec{u}_C(s) + y(\hat{j}^* - \hat{j}), \quad (7.11)$$

where the displacement vector of the reference axis is defined by

$$\vec{u}_C(s) = w(s)\hat{t}(s) + v(s)\hat{j}(s). \quad (7.12)$$

Substitute eq. (7.5) for  $\vec{u}(S, y)$  in eq. (7.11), followed by substitutions of eq. (7.10) and (7.12) into eq. (7.11) to find

$$u_s = w(s) + y\omega(s) \quad u_y = v(s). \quad (7.13)$$

Substitute the displacements of eq. (7.13) into the expression in eq. (7.9) for  $\omega$  to get

$$\omega = -\left(\frac{R}{R+y}\right)\left(\frac{dv}{ds} - \frac{w(s)+y\omega}{R}\right) = -\left(\frac{R}{R+y}\right)\left(\frac{dv}{ds} - \frac{w(s)}{R}\right) + \frac{y\omega}{R+y}. \quad (7.14)$$

Solve eq. (7.14) for  $\omega$  to find

$$\omega = -\left(\frac{dv}{ds} - \frac{w}{R}\right). \quad (7.15)$$

Finally, substitute the displacements of eq. (7.13) into the expression for  $\epsilon$  in eq. (7.9), followed by the substitu-

tion of  $w$  from eq. (7.15), to get the strain-displacement relation for the curved bar as

$$\epsilon = \frac{dw}{ds} + \frac{v}{R+y} - \frac{y}{R+y} \left[ R \left( \frac{d^2 v}{ds^2} \right) + \frac{w}{R} \left( \frac{dR}{ds} \right) \right]. \quad (7.16)$$

Although the displacements (7.13) are linear in the thickness coordinate  $y$ , note that the strain (7.16) is nonlinear in  $y$ .

### 7.1.2 Normal stress, stress resultants, and strain energy

The material of the bar is assumed to linear elastic, isotropic, and homogeneous. Then, the normal stress  $\sigma$  acting on the cross section is related to the normal strain  $\epsilon$  via Hooke's law. As was discussed in article 3.7 we take  $\sigma = E\epsilon$ , where  $E$  is the modulus of elasticity of the material. The result for the normal stress is written as

$$\sigma = \frac{E}{R+y} \left\{ \left( v + R \frac{dw}{ds} \right) + y \left[ \frac{dw}{ds} - \left[ R \left( \frac{d^2 v}{ds^2} \right) + \frac{w}{R} \left( \frac{dR}{ds} \right) \right] \right] \right\}. \quad (7.17)$$

The normal force  $N$  and bending moment  $M$  about the centroidal  $x$ -axis of the cross section are related to the normal stress by

$$(N, M) = \int_A (1, y) \sigma dA, \quad (7.18)$$

where  $A$  denotes the cross-sectional area of the bar. Substitute Hooke's law for the normal stress (7.17) into eq. (7.18) to get the relation between the resultants and the displacements. In this substitution process the following integrals over the cross section occur:

$$\int_A \frac{dA}{R+y} = \frac{A}{R}(1+Y) \quad \int_A \frac{y dA}{R+y} = -YA \quad \int_A \frac{y^2 dA}{R+y} = YAR, \quad (7.19)$$

in which  $Y$  is the dimensionless parameter of Winkler's curved bar theory. Equivalence of the three integrals (7.19) with respect to parameter  $Y$  can be demonstrated by dividing the denominator into the numerator of the integrand in the first two integrals and noting  $\int_A y dA = 0$ , since  $y$  is measured from the centroid. Langhaar

(1962) states that the third expression in eq. (7.19) is the most convenient for the evaluation of the parameter  $Y$  if numerical integration is required. If  $R \gg y$ , then the third expression in eq. (7.19) approximates  $Y$  as

$$Y \cong Y_{\text{appx}} = I/(AR^2) \quad \text{where} \quad I = \int_A y^2 dA. \quad (7.20)$$

The equations for the resultants are

$$N = \frac{EA}{R} \left\{ \left( v + R \frac{dw}{ds} \right) + Y \left[ v + R \left[ R \left( \frac{d^2 v}{ds^2} \right) + \frac{w}{R} \left( \frac{dR}{ds} \right) \right] \right] \right\}, \text{ and} \quad (7.21)$$

$$M = -EAY \left\{ v + R \left[ R \left( \frac{d^2 v}{ds^2} \right) + \frac{w}{R} \left( \frac{dR}{ds} \right) \right] \right\}. \quad (7.22)$$

From eqs. (7.21) and (7.22), the following results are obtained:

$$v + R \frac{dw}{ds} = \frac{RN + M}{EA} \quad \frac{dw}{ds} - \left[ R \left( \frac{d^2 v}{ds^2} \right) + \frac{w}{R} \left( \frac{dR}{ds} \right) \right] = \frac{1}{REA} \left[ RN + \left( 1 + \frac{1}{Y} \right) M \right]. \quad (7.23)$$

Substitution of eq. (7.23) into the expression for the normal stress (7.17), yields the stress in terms of resultants as

$$\sigma = \frac{N}{A} + \left( 1 + \frac{y}{(R+y)Y} \right) \frac{M}{RA} \quad \text{or} \quad \sigma = \frac{1}{RA} \left( RN + M + \frac{y}{R+y} \frac{M}{Y} \right). \quad (7.24)$$

Note the normal stress at the centroid ( $y = 0$ ) in pure bending ( $N = 0$ ) is  $\sigma = M/(RA)$ . That is, the centroidal axis does not coincide with the neutral axis of the cross section for the curved bar. The neutral axis of the curved bar is located radially inward from the centroidal axis, i.e.,  $y = -RY/(1 + Y)$ . For pure bending of a straight bar the  $\sigma = 0$  at the centroid, so the centroidal axis and neutral axis coincide.

The complementary strain energy is given by

$$U^* = \frac{1}{2} \iint \frac{\sigma^2}{E} (R+y) d\theta dA, \quad (7.25)$$

where the volume element is  $(R+y)d\theta dA$ . Substitute eq. (7.24) for the normal stress into the complementary strain energy (7.25), followed by integration over the cross-sectional area, to get

$$U^* = \int \frac{1}{2ER^2A} \left[ (RN + M)^2 + \frac{M^2}{Y} \right] ds. \quad (7.26)$$

The final result for the complementary strain energy (7.26) was obtained using property of the centroid

$\int_A y dA = 0$ , the third integral in (7.19), and  $ds = R d\theta$ .

### Example 7.1 Pure bending of a circular bar with a rectangular cross section.

The reference axis is a segment of a circle of radius  $a$ . Thus, the radius of curvature is uniform with respect to the arc-length along the reference axis, and  $R = a$ . The cross section is a solid rectangle of height  $h$  and width  $b$ . The bar is subject to equal and opposite moments  $M$  at each end, and no other loads. See figure. 7.3. Equilibrium is satisfied by the fact that the bending moment in the bar at each cross section is equal to the applied moment  $M$ , and that the circumferential force  $N$  vanishes at each cross section. The normal stress distribution through the thickness at a typical cross section is determined from eq. (7.24).

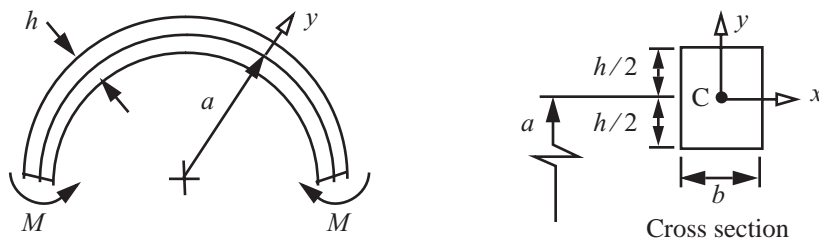


Fig. 7.3 Pure bending example 7.1.



The formula for the dimensionless Winkler parameter  $Y$  is evaluated from the third expression in eq. (7.19), where the cross-sectional area  $A = bh$ . That is,

$$Y = \frac{1}{bha} \int_{-h/2}^{h/2} \frac{y^2}{a+y} b dy = \frac{1}{ha} \int_{-h/2}^{h/2} \frac{y^2}{a+y} dy. \quad (\text{a})$$

For the simple rectangular section the following indefinite integral is obtained from a table of integrals:

$$\int \frac{y^2}{a+y} dy = (a+y)^2/2 - 2a(a+y) + a^2 \log(a+y). \quad (\text{b})$$

The natural logarithm is specified in eq. (b). After some algebra we get

$$Y = \rho \log\left(\frac{2\rho+1}{2\rho-1}\right) - 1 \quad \text{where} \quad \rho = a/h. \quad (\text{c})$$

Practical geometries require  $\rho > 1/2$ . That is,  $a > h/2$ . If  $a \gg y$ , then  $Y_{\text{appx}} = \left(\frac{bh^3}{12}\right)/(bha^2) = 1/(12\rho^2)$ .

For selected values of  $\rho$ , the values of  $Y$ ,  $Y_{\text{appx}}$ , and percentage error between the exact and approximate values of  $Y$  are listed in table 7.1. As can be seen in table 7.1, the parameter  $Y$  decreases rapidly with increasing radius

**Table 7.1 Winkler parameter for selected radius to thickness ratios**

$\rho = a/h$	$Y$	$Y_{\text{appx}}$	$(Y - Y_{\text{appx}})/Y \times 100 \%$
1	0.09861	0.08333	15.4
5	0.003353	0.003333	0.60
10	0.0008346	0.0008333	0.150
20	0.0002084	0.0002083	0.0375

to thickness ratios  $a/h$ , and that the approximate value of  $Y$  is less than 0.15 percent of the exact value for  $a/h > 10$ .

From eq. (7.24) the normal stress for the curved bar is  $\sigma = \frac{M}{aA} \left[ 1 + \frac{y}{a+y} \frac{1}{Y} \right]$ . For a straight bar subject to pure bending the normal stress is given by  $\sigma = (My)/I$ , where the second area moment about the  $x$ -axis is  $I = (bh^3)/12$ . Define the dimensionless thickness coordinate  $\eta = (2y)/h$ , and a dimensionless normal stress by  $\bar{\sigma} = \frac{2I\sigma}{hM}$ . Then  $\bar{\sigma} = \eta$  for the straight bar, and

$$\bar{\sigma} = \frac{1}{6\rho} \left[ 1 + \frac{\eta}{2\rho + \eta} \frac{1}{Y} \right], \text{ for the curved bar.} \quad (\text{d})$$

The distributions of the dimensionless stress through the thickness of the curved bar and the straight bar are shown in figure. 7.4 for radius to thickness ratios of 1 and 5. The normal stress for the curved bar is hyperbolic in the thickness coordinate  $y$ , whereas for the straight bar the distribution of the normal stress is linear in coordinate  $y$ . For  $M > 0$  the maximum tensile stress for the curved bar is less than that of the straight bar, but the magnitude

of the maximum compressive stress is larger for the curved bar than for the straight bar. The graph for  $a/h = 5$  in figure. 7.4 shows that the stress distribution in the curved bar is close to the linear distribution of the straight bar. The percentage error of the maximum compressive stress of the straight bar with respect to the curved bar for increasing radius to thickness ratios are listed in table 7.2.

**Table 7.2 Percentage error in the maximum compressive stress of a straight bar with respect to a curved bar**

$a/h$	$\frac{(\sigma_{\text{curved}} - \sigma_{\text{straight}})100}{\sigma_{\text{curved}}}$
1	34.4%
5	6.64%
10	3.32%
20	1.66%
50	0.67%

The error approximating the maximum stress from straight bar theory with respect to curved bar theory is 3.32 percent for  $a/h = 10$ , and less than 1.66 percent for  $a/h > 20$ . ■

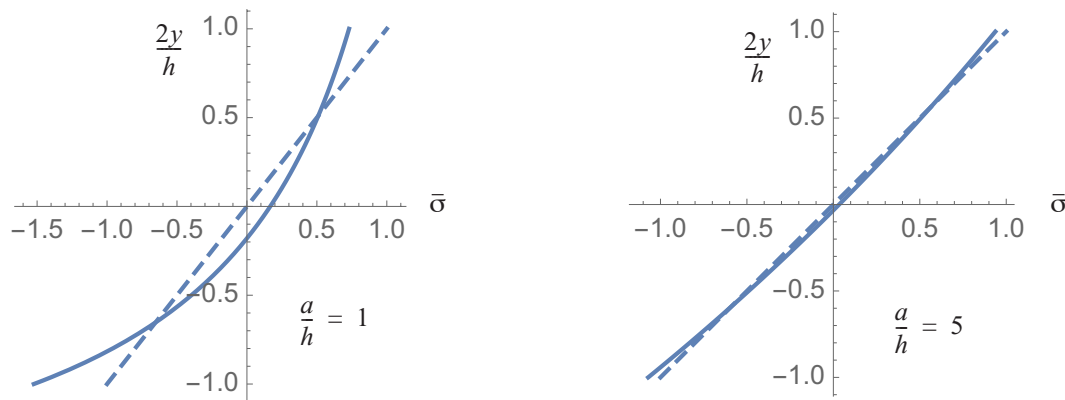


**Fig. 7.4 Thickness distributions of the dimensionless normal stress for  $a/h = 1$  and  $a/h = 5$ . The solid line corresponds to the curved bar and the dashed line to the straight bar.**

### Example 7.2 Displacement of a semicircular bar

A semicircular bar of radius  $a$  is connected to a fixed pin support at its left end and a pin support free to move horizontally at its right end. The right end support is subject to a horizontal force  $Q$  with a corresponding displacement denoted by  $q$ . The cross section of the bar is the thin-walled tube of example 6.4 on page 160 with the mean radius denoted by  $b$ , and a wall thickness denoted by  $t$ . See figure. 7.5. Determine the flexibility influence coefficient  $c$  in the relation  $q = cQ$  using Castigliano's second theorem.

**Solution.** The complementary strain energy in eq. (7.26) reduces to

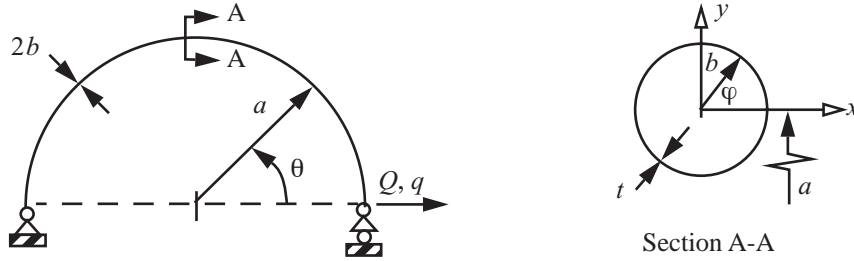


**Fig. 7.5** Configuration of the semicircular bar of example 7.2, and its thin-walled cross section.

$$U^* = \frac{1}{2Ea^2A} \int_0^\pi \left[ (aN + M)^2 + \frac{M^2}{Y} \right] a d\theta = \frac{1}{2Ea(2\pi bt)} \int_0^\pi \left[ (aN + M)^2 + \frac{M^2}{Y} \right] d\theta. \quad (\text{a})$$

A free body diagram of the segment of the bar is shown in figure. 7.6. The circumferential normal force  $N$  and the



Free body diagram of a segment of the base structure

Component of  $Q$  along direction of  $N$

**Fig. 7.6** Free body diagram of a segment of the semicircular bar.

bending moment  $M$  determined from equilibrium are

$$N = Q \sin \theta \quad M = -(a \sin \theta) Q. \quad (\text{b})$$

From Castigliano's theorem the displacement corresponding to force  $Q$  is given by

$$q = \frac{\partial U^*}{\partial Q} = \frac{1}{Ea(2\pi bt)} \int_0^\pi \left[ (aN + M) \left( a \frac{\partial N}{\partial Q} + \frac{\partial M}{\partial Q} \right) + \frac{M}{Y} \frac{\partial M}{\partial Q} \right] d\theta. \quad (\text{c})$$

Substitute for the actions  $N$  and  $M$  from eq. (b) into eq. (c) and perform the integral to get

$$q = \frac{Q}{Ea(2\pi bt)} \int_0^\pi \frac{a^2 \sin^2 \theta}{Y} d\theta = \left( \frac{a}{4Eb t Y} \right) Q. \quad (\text{d})$$

Thus, the flexibility influence coefficient is identified in eq. (d) as

$$c = \frac{a}{4Eb t Y} = \frac{\rho}{2EtY}, \quad (\text{e})$$

in which the radius-to-thickness ratio is defined by  $\rho = a/(2b)$ . The formula for the Winkler parameter  $Y$  is obtained from the third expression in eq. (7.19) as

$$Y = \frac{1}{aA} \int_A \frac{y^2}{a+y} dA = \frac{1}{a(2\pi bt)} \int_0^{2\pi} \frac{(b \sin \varphi)^2}{a + b \sin \varphi} t b d\varphi = \frac{1}{4\pi\rho} \int_0^{2\pi} \frac{\sin^2 \varphi}{2\rho + \sin \varphi} d\varphi. \quad (\text{f})$$

The integration was performed in *Mathematica* for  $\rho > 1/2$  to get

$$Y = \frac{2\rho}{\sqrt{4\rho^2 - 1}} - 1. \quad (\text{g})$$

Consider computing the flexibility influence coefficient from the complementary strain energy of a straight bar but applied to the semicircular bar. For this example eq. (5.51) on page 141 reduces to the complementary energy expression

$$U^* = \frac{1}{(2EI_{xx})} \int_0^\pi M^2 a d\theta + \frac{1}{2EA} \int_0^\pi N^2 a d\theta. \quad (\text{h})$$

Let the displacement obtained from Castigliano's theorem using the complementary strain energy expression in eq. (h) be denoted by  $q_a$ . Then,

$$q_a = \left( \frac{1}{EI_{xx}} \right) \int_0^\pi M \frac{\partial M}{\partial Q} a d\theta + \frac{1}{EA} \int_0^\pi N \frac{\partial N}{\partial Q} a d\theta. \quad (\text{i})$$

Substitute for the actions  $N$  and  $M$  from equilibrium eq. (b) into eq. (i) and perform the integral to get

$$q_a = \frac{a\pi Q}{2AE} + \frac{a^3\pi Q}{2I_{xx}E} = \frac{aQ}{4btE} + \frac{a^3Q}{2b^3tE}, \quad (\text{j})$$

in which we substitute for the area and second area moment  $A = 2\pi bt$  and  $I_{xx} = \pi b^3 t$ , respectively. The approximate flexibility influence coefficient, denoted by  $c_a$ , is

$$c_a = \frac{a}{4btE} + \frac{a^3}{2b^3tE} = \frac{\rho + 8\rho^3}{2tE}, \quad (\text{k})$$

where  $\rho = a/(2b)$ .

The ratio of the flexibility influence coefficient in eq. (e) to its approximate value in eq. (k) is

$$c_r = c/c_a = \frac{1}{(1 + 8\rho^2)Y}. \quad (\text{l})$$

Numerical results for selected values of the radius-to-thickness ratios  $\rho$  are presented in table 7.3. The third column in the table lists the ratio of the flexibility influence coefficient to its approximate value. For  $\rho = 1$  the approximate flexibility influence coefficient is about 1.39  $c$ , which means the displacement  $q_a$  is larger than the displacement determined from curved bar theory. For  $\rho = 10$   $c_a = 1.003c$ , and for  $\rho$  exceeding ten,  $c_a$  is essen-

tially equal to  $c$ . Hence, we can use the strain energy expression for a straight bar to determine the displacement of the curved bar if  $\rho \geq 10$ . ■

**Table 7.3 Ratio of the exact flexibility coefficient to the approximate value for selected radius-to-thickness ratios**

$\rho = a/(2b)$	$Y(\rho)$	$c/c_a$
1	0.154701	0.718234
2	0.0327956	0.923998
3	0.0141851	0.965705
4	0.00790526	0.980605
5	0.00503782	0.987556
10	0.00125235	0.996879

## 7.2 Strain-displacement and Hooke's law for thin curved bars

It was demonstrated in example 7.1 and example 7.2 that some equations of straight bar theory are applicable to the analysis of curved bars if the radius of curvature to the thickness in the plane of curvature is greater than ten. If the ratio of the minimum radius of curvature to the in-plane thickness is greater than ten, then the bar is identified as a **thin curved bar**. Ratios less than ten are considered **thick curved bars**. For example, thin curved bar formulas are applicable to fuselage ring-frames. Fittings, machine parts, crane hooks, and chain links are examples where thick curved bar theory is required. Thin curved bar formulas for strain, stress, stress resultants, and complementary strain energy are as follows:

$$\varepsilon = \frac{dw}{ds} + \frac{v}{R} - y \left( \frac{d^2 v}{ds^2} + \frac{w}{R^2} \frac{dR}{ds} \right), \quad (7.27)$$

$$N = EA \left( \frac{dw}{ds} + \frac{v}{R} \right) \quad M = -EI_{xx} \left( \frac{d^2 v}{ds^2} + \frac{w}{R^2} \frac{dR}{ds} \right), \text{ and} \quad (7.28)$$

$$\sigma = E\varepsilon = \frac{N}{A} + y \frac{M}{I_{xx}} \quad U^* = \frac{1}{2} \int \left( \frac{N^2}{EA} + \frac{M^2}{EI_{xx}} \right) ds. \quad (7.29)$$

### Example 7.3 Circular arch

Consider a thin curved bar that forms a circular arch as shown in figure. 7.7. It is supported by smooth pins at each end. The distance  $L$  between the end supports remains fixed as the arch is subject to a downward force  $P$  at midspan. The area of the cross section is denoted by  $A$ , the radius of the circular arc passing through the centroid of each cross section by  $a$ , and its semi-opening angle by  $\beta$ . The arch is statically indeterminate and the horizontal reaction force  $Q$  is the redundant. The overall free body diagram of the arch is shown in figure. 7.7.

(a) Using Castigliano's second theorem determine the redundant load  $Q$ . Neglect strain energy due to transverse shear.

(b) Take  $L = 1\text{ m}$ ,  $EA = 175 \times 10^6\text{ N}$ , and  $EI = 218,750\text{ N}\cdot\text{m}^2$ . Plot  $Q/P$  as function of the rise to span ratio  $H/L$  for  $1^\circ \leq \beta \leq 90^\circ$ .

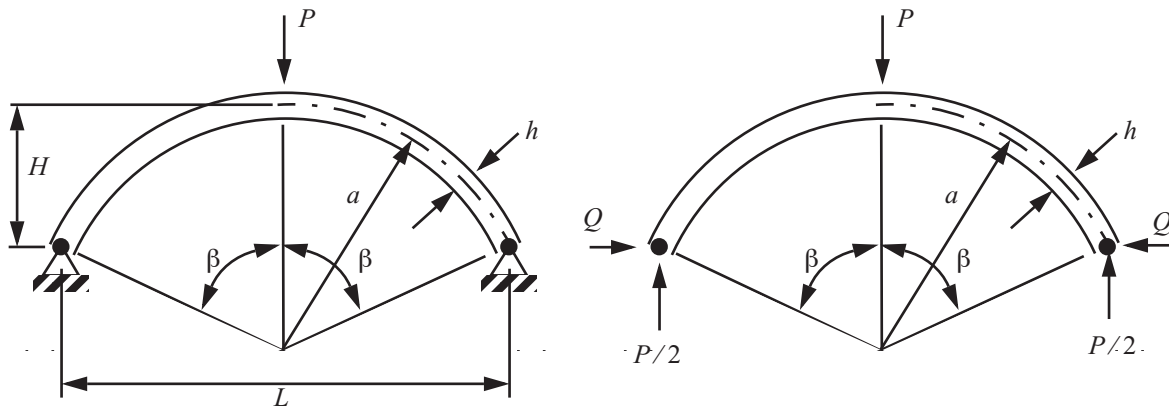
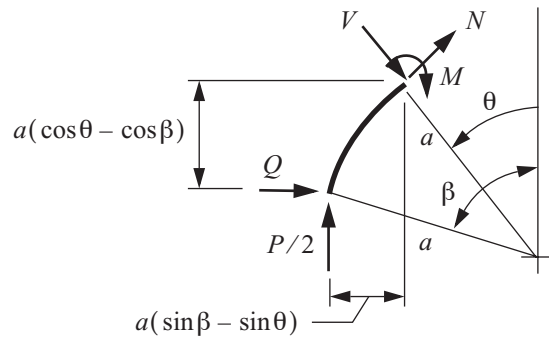


Fig. 7.7 Circular arch.  $a/h > 10$ .

**Solution to part (a).** The arch is symmetric about the vertical axis through the center, so only the left-half section is analyzed. The free body diagram shown in figure 7.8 cuts the arch at angle  $\theta$  measured counterclockwise from the vertical axis, and  $0 \leq \theta \leq \beta$ . The internal actions on the cut face are the circumferential normal force  $N$ , transverse shear force  $V$ , and the bending moment  $M$ . The cut face is a negative  $\theta$ -face with a positive normal force causing circumferential extension, a positive shear force is defined radially inward, and a positive bending moment causes tension on the radially outboard circumference.

Fig. 7.8 Free body diagram of a section of the arch.



Equilibrium in the direction of the normal force leads to the equation

$$N = -(P/2)\sin\theta - Q\cos\theta. \quad (\text{a})$$

Equilibrium in the direction of the shear force leads to the equation

$$V = (P/2)\cos\theta - Q\sin\theta. \quad (\text{b})$$

Moment equilibrium at the  $\theta$ -face leads to the equation

$$M = -a(\sin\beta - \sin\theta)(P/2) + a(\cos\theta - \cos\beta)Q. \quad (\text{c})$$

The complementary strain energy from eq. (7.29) reduces to

$$U^* = 2\left(\frac{1}{2}\right)\int_0^\beta \left[\frac{N^2}{2EA} + \frac{M^2}{2EI}\right]a d\theta. \quad (\text{d})$$

In the previous integral, integration is performed over the left-hand portion of the arch, and the total complementary energy stored in the arch is accounted for by the factor of two multiplying the integral. Since the displacement in the direction of the horizontal redundant force  $Q$  is zero, Castigliano's second theorem gives

$0 = (\partial U^*)/(\partial Q)$ . Thus,

$$0 = \int_0^\beta \left[ \frac{N}{EA} \left( \frac{\partial N}{\partial Q} \right) + \frac{M}{EI} \left( \frac{\partial M}{\partial Q} \right) \right] a d\theta. \quad (\text{e})$$

Substitute eq. (a) for  $N$  and eq. (c) for  $M$  in eq. (e) followed by integration to get

$$0 = \left( \frac{a}{2EA} \right) [\sin^2\beta P + (2\beta + \sin 2\beta)Q] + \left( \frac{a^3}{4EI} \right) [(1 - 4\cos\beta + 3\cos 2\beta + 2\beta \sin 2\beta)P + (8\beta + 4\beta \cos 2\beta - 6\sin 2\beta)Q] \quad (\text{f})$$

Solve eq. (f) for the redundant force  $Q$  to get

$$\frac{Q}{P} = \frac{a^2(-1 + 4\cos\beta - 3\cos 2\beta - 2\beta \sin 2\beta)EA - (2\sin^2\beta)EI}{a^2(8\beta + 4\beta \cos 2\beta - 6\sin 2\beta)EA + (4\beta + 2\sin 2\beta)EI}. \quad (\text{g})$$

**Solution to part (b).** The rise-to-span ratio in terms of the semi-opening angle  $\beta$  is

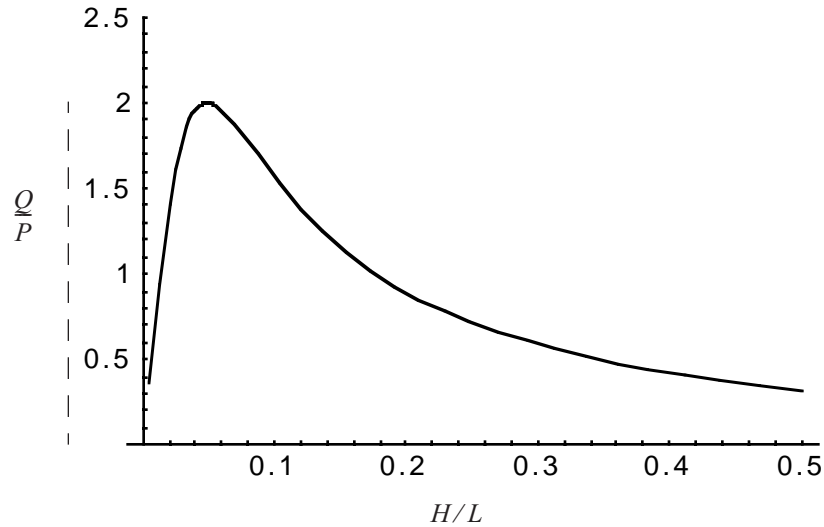
$$\frac{H}{L} = \frac{a(1 - \cos\beta)}{2a\sin\beta} = \frac{(1 - \cos\beta)}{2\sin\beta}. \quad (\text{h})$$

Note that this ratio is independent of the radius  $a$ . The distance  $L$  between the supports is fixed at one meter, and  $L = 2a\sin\beta$ . Hence, the radius of the arch is a function of the semi-opening angle  $\beta$  given by

$$a = (1\text{m})/(2\sin\beta). \quad (\text{i})$$

Specifying  $\beta$ , we compute  $a$  from eq. (i),  $H/L$  from eq. (h), and the ratio of  $Q/P$  from eq. (g). A graph of  $Q/P$  versus  $H/L$  is shown in figure. 7.9.

**Fig. 7.9** Ratio of the horizontal reaction force to the applied load as a function of the rise-to-span ratio for a circular arch.



The maximum value of the redundant is  $2P$  for  $H/L = 0.0485$  corresponding to  $\beta = 11.08^\circ$ . This maximum occurs for a shallow arch. A shallow arch is characterized by a small value of the angle  $\beta$ . ■

#### Example 7.4 Thin ring subject to diametric tension

A uniform, thin ring of radius  $a$  is subject to equal and opposite tension forces labeled  $P$  as shown in the left sketch in figure. 7.10. This configuration is symmetric about the horizontal diameter AB and the vertical diameter. Determine the bending moment distribution in the upper right-hand quarter segment of the ring where the angle  $\theta$  has the range  $0 \leq \theta \leq \pi/2$ . Include only bending deformations in Castigliano's second theorem to determine the redundant actions.

**Solution.** The right-hand sketch in figure. 7.10 shows the free body diagrams obtained by sectioning the ring across diameter AB. Action-reaction pairs of the internal circumferential normal forces, internal transverse shear forces, and internal bending moments are labeled in the free body diagrams. The upper and lower free body diagrams are mirror images of one another, which implies that the transverse shear forces  $V_A$  in the upper and lower free body diagrams should be drawn in the same direction at the cut at A. But this mirror image argument is in contradiction with the action-reaction pairing. So to resolve this contradiction means that the transverse shear force  $V_A = 0$ . A similar argument implies that the transverse shear force at cut B must vanish (i.e.,  $V_B = 0$ ).

From symmetry about the vertical diameter the circumferential normal forces  $N_A$  and  $N_B$  are equal and the bending moments  $M_A$  and  $M_B$  are equal. Vertical force equilibrium yields  $N_A = N_B = P/2$ . Thus, the only redundant is the bending moment  $M_A$ . A free body diagram of the section from point A to the cut at  $\theta$  is shown in figure. 7.11.

Moment equilibrium about the cut at  $\theta$  determines the bending moment as

$$M = M_A + a(1 - \cos\theta)(P/2). \quad (\text{a})$$



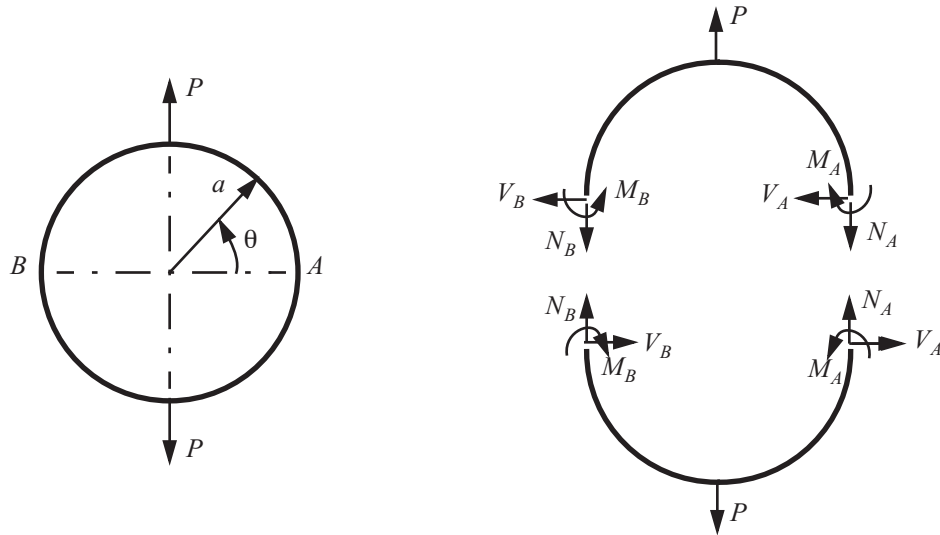
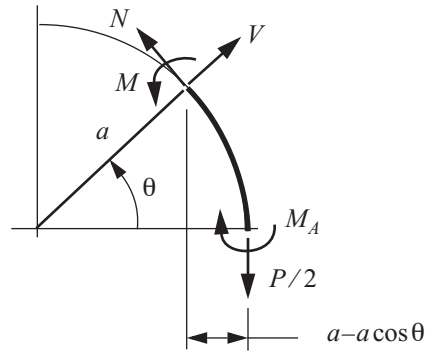


**Fig. 7.10** A thin ring subject to diametric tension. Free body diagrams obtained from a cut across the horizontal diameter.

**Fig. 7.11** Free body diagram of a circular sector of the ring in example 7.4.



The complementary strain energy including bending only is

$$U^* = \int_0^{\frac{\pi}{2}} \left[ \frac{M^2}{2EI} \right] a d\theta. \quad (\text{b})$$

By symmetry, the rotation corresponding to the moment  $M_A$  must vanish. Hence, Castigliano's second theorem gives

$$0 = \frac{\partial U^*}{\partial M_A} = \frac{1}{EI} \int_0^{\frac{\pi}{2}} [M] \left[ \frac{\partial M}{\partial M_A} \right] a d\theta = \frac{1}{EI} \int_0^{\frac{\pi}{2}} [M_A + a(1 - \cos\theta)(P/2)] [1] a d\theta. \quad (\text{c})$$

Perform the integration in eq. (c) to get

$$0 = \frac{1}{EI} \left[ \frac{M_A \pi a}{2} - \frac{Pa^2}{2} + \frac{1}{4} P \pi a^2 \right]. \quad (\text{d})$$

Solve eq. (d) for the redundant to find

$$M_A = \frac{Pa(2 - \pi)}{2\pi}. \quad (\text{e})$$

Substitute eq. (e) into eq. (a) to get the bending moment as

$$M = \frac{Pa}{\pi} - \frac{1}{2} Pa \cos \theta \quad 0 \leq \theta \leq \frac{\pi}{2}. \quad (\text{f})$$

The bending moment is plotted in figure. 7.12 as a radial coordinate with respect to the ring, where a positive moment is plotted outside the ring and a negative moment is plotted inside the ring. ■

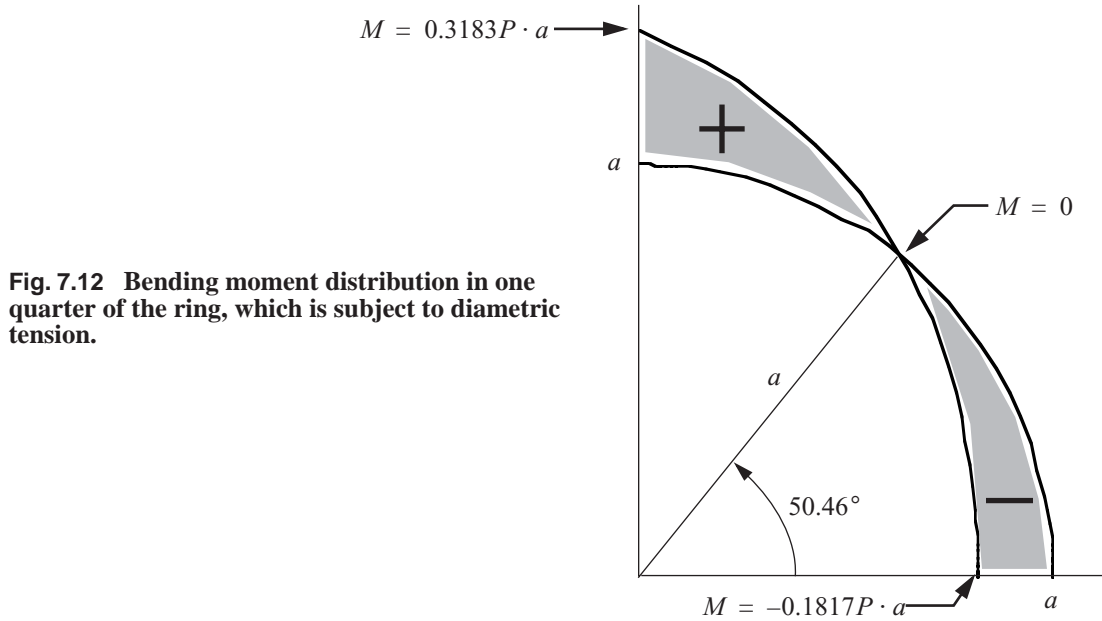


**Fig. 7.12** Bending moment distribution in one quarter of the ring, which is subject to diametric tension.

### 7.3 Differential equilibrium equations of a curved bar

Consider a differential element of a curved bar subject to prescribed line load per unit length along the reference axis. The vector of the external line load intensity is denoted by  $\vec{f}(s)$  with component  $q(s)$  tangent to the reference axis and component  $p(s)$  normal to the reference axis. That is

$$\vec{f}(s) = q(s)\hat{t}(s) + p(s)\hat{j}(s). \quad (7.30)$$

Denote the internal force vector acting on the cross section by  $\vec{F}(s)$  with component  $N(s)$  normal to the cross section positive in tension, and the shear component  $V(s)$  tangent to the cross section. That is,

$$\vec{F}(s) = N(s)\hat{t}(s) + V(s)\hat{j}(s). \quad (7.31)$$

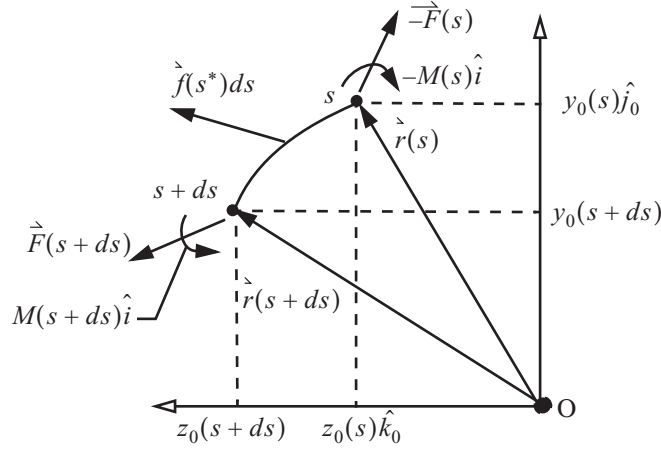


Fig. 7.13 Free body diagram of an element of a curved bar.

Summation of forces acting on the differential element shown in figure. 7.13 leads to

$$\vec{F}(s+ds) - \vec{F}(s) + \vec{f}(s^*)ds = 0 \quad s < s^* < s+ds. \quad (7.32)$$

Expanding the force vectors in a series we write eq. (7.32) as

$$\left\{ \frac{d\vec{F}}{ds} + \left[ \vec{f}(s) + \frac{d\vec{f}}{ds}(s^* - s) \right] \right\} ds + O(ds^2) = 0. \quad (7.33)$$

Divide eq. (7.33) by  $ds$ , followed by taking the limit as  $ds \rightarrow 0$ , and note that  $s^* \rightarrow s$  in the limit. The resulting differential equation is

$$\frac{d\vec{F}}{ds} + \vec{f}(s) = 0. \quad (7.34)$$

The derivative of the internal force vector in eq. (7.31) is

$$\frac{d\vec{F}}{ds} = \left( \frac{dN}{ds} \right) \hat{t} + N \left( \frac{d\hat{t}}{ds} \right) + \left( \frac{dV}{ds} \right) \hat{j} + V \left( \frac{d\hat{j}}{ds} \right) = \left( \frac{dN}{ds} + \frac{V}{R} \right) \hat{t} + \left( \frac{dV}{ds} - \frac{N}{R} \right) \hat{j},$$

where the derivatives of the unit vectors are given in eq. (7.3). Hence, the scalar differential equation of force equilibrium in the tangent direction is

$$\frac{dN}{ds} + \frac{V}{R} + q = 0, \quad (7.35)$$

and differential equation in the normal direction is

$$\frac{dV}{ds} - \frac{N}{R} + p = 0. \quad (7.36)$$

The bending moment acting on the cross section is denoted by  $M(s)$  with a positive moment causing an increase in curvature of the bar. Take the sum of moments about  $s$  in the free body diagram to get

$$M(s+ds)\hat{i} - M(s)\hat{i} + [\vec{r}(s+ds) - \vec{r}(s)] \times \vec{F}(s+ds) + [\vec{r}(s^*) - \vec{r}(s)] \times \vec{f}(s^*)ds = 0, \quad (7.37)$$

Expanding the moment and force vector in a series we write

$$\left\{ \frac{dM}{ds}\hat{i} + \frac{d\vec{r}}{ds} \times \vec{F}(s) + [\vec{r}(s^*) - \vec{r}(s)] \times \vec{f}(s^*) \right\} ds + O(ds^2) = 0. \quad (7.38)$$

Divide by  $ds$  and then take the limit as  $ds \rightarrow 0$ , and note that  $\vec{r}(s^*) \rightarrow \vec{r}(s)$  in the limit, to get

$$\frac{dM}{ds}\hat{i} + \hat{t} \times [N\hat{t} + V\hat{j}] = \left( \frac{dM}{ds} - V \right) \hat{i} = 0. \quad (7.39)$$

The moment differential equation is

$$\frac{dM}{ds} - V = 0. \quad (7.40)$$

### Example 7.5 Funicular arch

Consider a uniform, pinned-pinned arch subject to uniformly distributed load of intensity  $p_0$  that is directed vertically downward as shown in figure. 7.14. For example  $p_0$  could represent the weight per unit length of the arch. We determine the form or shape of the arch such that each cross section is in pure compression (i.e., there is no bending). This condition of pure compression under a uniform lateral load can be achieved with a curved bar, but not with a straight bar or beam. A beam carries a uniform lateral load by bending. Tailoring the shape of the arch for pure compression to the uniformly distributed loading defines the funicular arch. All of the parallel fibers in a cross section are under the same compressive stress, which means all of the material in the cross section is utilized in resisting the load.

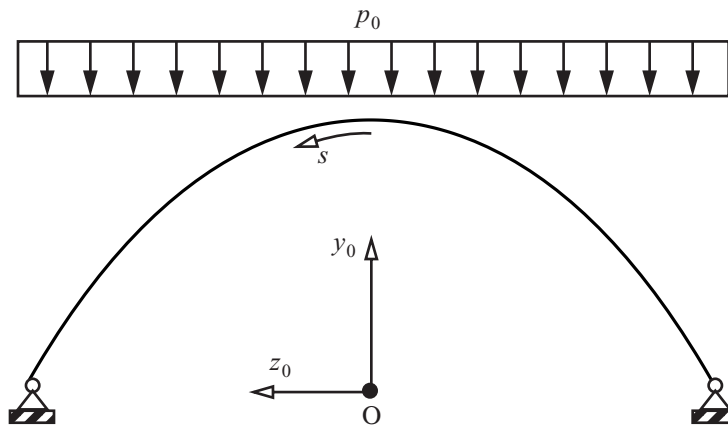


Fig. 7.14 Funicular arch subject to a uniformly distributed load.

Resolve the applied downward load intensity into the tangential and normal components of eq. (7.30) to find

$$q = p_0 \sin \theta \quad p = -p_0 \cos \theta . \quad (\text{a})$$

For the bending moment and shear force to vanish for all values of  $s$  the equilibrium equations (7.35) to (7.40) reduce to the following:

$$\frac{1}{R} \frac{dN}{d\theta} + p_0 \sin \theta = 0 \quad -\frac{N}{R} - p_0 \cos \theta = 0 . \quad (\text{b})$$

Eliminating the tangential force between the last two equations leads to the following differential equation for the radius of curvature:

$$\frac{dR}{d\theta} - (2 \tan \theta) R = 0 . \quad (\text{c})$$

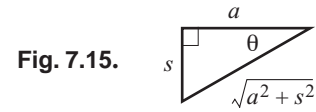
The solution for the radius of curvature is

$$R = \frac{a}{\cos^2 \theta} , \quad (\text{d})$$

where  $a$  is the constant of integration and is equal to the radius of curvature at  $\theta = 0$ . The curvature is  $1/R$  and from the third expression in eq. (7.3) we obtain

$$\frac{d\theta}{ds} = \frac{\cos^2 \theta}{a} \rightarrow \int \sec^2 \theta d\theta = \int \frac{1}{a} ds . \quad (\text{e})$$

Perform the integration in eq. (e) to find  $\tan \theta = s/a$ . From the result that the tangent of  $\theta$  is equal to the arc-length divided by  $a$ , we obtain the trigonometric relations (see figure. 7.15)



$$\sin \theta = \frac{s}{\sqrt{a^2 + s^2}} \quad \text{and} \quad \cos \theta = \frac{a}{\sqrt{a^2 + s^2}} . \quad (\text{f})$$

As shown by the insert in figure. 7.1,  $(dz_0)/(ds) = \cos \theta$ , which combined with the cosine relation from eq. (b) can be integrated to determine coordinate function  $z_0(s)$ ; i.e.,

$$z_0 = \int \frac{a}{\sqrt{a^2 + s^2}} ds = \int \frac{a}{\sqrt{1 + \left(\frac{s}{a}\right)^2}} d\left(\frac{s}{a}\right) = a \sinh^{-1} \frac{s}{a} .$$

Thus,

$$\sinh(z_0/a) = s/a . \quad (\text{g})$$

Also as shown by the insert in figure. 7.1,  $(dy_0)/(ds) = -\sin \theta$ , which combined with the sine relation from eq. (f) can be integrated to determine coordinate function  $y_0(s)$ ; i.e.,

$$y_0 = \int \frac{-s}{\sqrt{a^2 + s^2}} ds = -\sqrt{a^2 + s^2} + c . \quad (\text{h})$$

We specify  $y_0(0) = a$ , and find  $c = 2a$ . The coordinate function  $y_0(s)$  is

$$y_0 = 2a - \sqrt{a^2 + s^2}. \quad (\text{i})$$

Express eq. (i) as  $y_0 = 2a - a\sqrt{1 + (s/a)^2}$ , and use eq. (g) to replace the ratio  $s/a$  to get

$$y_0 = 2a - a\sqrt{1 + \sinh^2 \frac{z_0}{a}} = 2a - a\sqrt{\cosh^2 \frac{z_0}{a}}. \quad (\text{j})$$

The latter result in eq. (j) is the equation for the shape of the funicular arch, which is

$$y_0 = 2a - a \cosh(z_0/a). \quad (\text{k})$$

Equation (k) is the equation of a **catenary**. A catenary is a curve formed by a wire, rope, or chain hanging freely from two points that is in tension. The funicular arch is an inverted catenary and is in compression.

The tangential force in the arch is given by  $N = -p_0 R \cos \theta$ . Using eqs. (d), (f), and (g), it can be shown that the spanwise distribution of the tangential force is

$$N = -p_0 a \cosh(z_0/a), \quad (\text{l})$$

where  $-z_m/a \leq z_0/a \leq z_m/a$ . Set  $y_0 = 0$  in eq. (k) to find  $z_m/a = \text{ArcCosh}(2) = 1.317$ . Define the thrust as the negative of the tangential force. The spanwise distribution of the thrust scaled by  $p_0 a$  is shown in figure.

7.16. The minimum thrust is  $p_0 a$  at the crown and increases to a maximum of  $2p_0 a$  at each pin support.

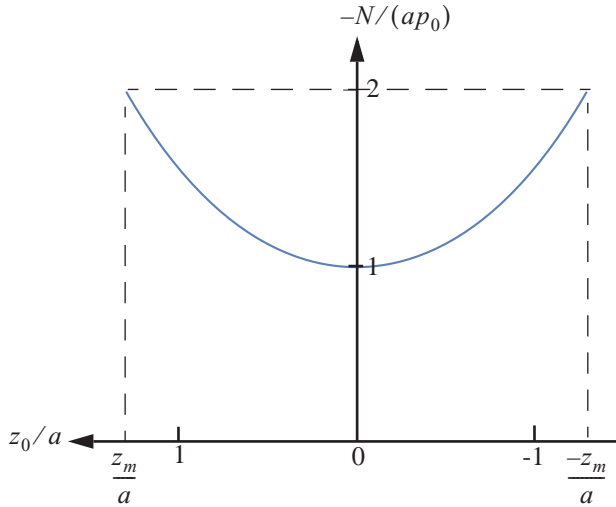


**Fig. 7.16** Distribution of the thrust with respect to the span of the funicular arch,  $z_m/a = 1.317$ .

## 7.4 Loads on fuselage frames

The skins, or webs, in semimonocoque construction are thin and cannot withstand large concentrated loads. Instead, stiffeners are located in the design of the structure where the concentrated loads are applied. The concentrated load acting on the stiffener diffuses the load to the attached skins or webs. For example, a fuselage structure has closely spaced frames or bulkheads that resist loads in the transverse planes, while the fuselage shell resists loads in the fore-and-aft direction. Typically, frames react to point loads from the wing spar attach-

ments and distributed loads from floor beams, and are often modeled as two-dimensional rings subject to in-plane loading. In the following analyses, we quantitatively determine how loads applied to frames are transferred to the attached skin, followed by the determination of the internal actions in the frame. Additional examples of loads acting on fuselage frames and wing ribs are given in Bruhn (1973), Curtis (1997), and Megson (1999).

Consider a transverse frame together with the attached skin of the fuselage. The frame is subject to forces  $P_x$  and  $P_y$ , and torque  $T_z$  as shown in figure. 7.17(a). Note that positive values of  $P_x$  and  $P_y$  are defined in the

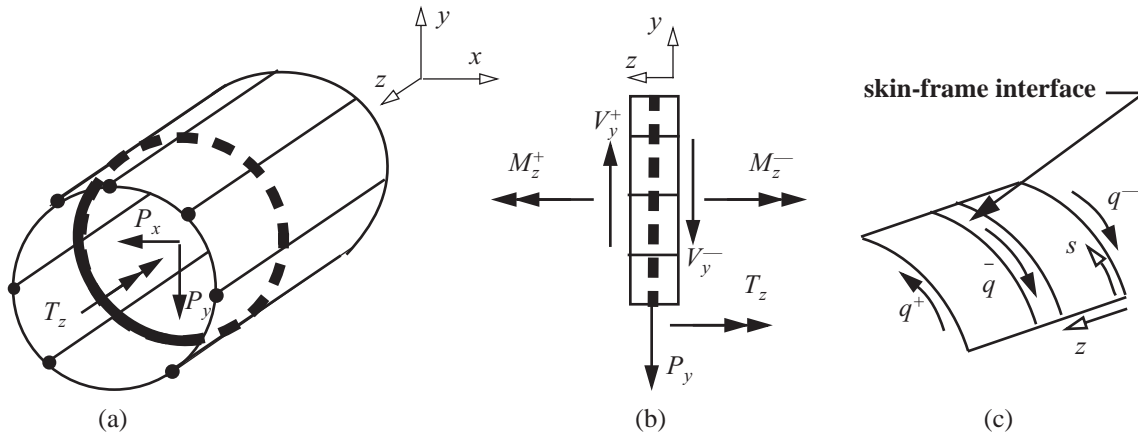


**Fig. 7.17 (a) Frame loads. (b) Forces and torques acting on frame and fuselage skin viewed from the  $y$ - $z$  plane. (c) Shear flows in the skin fore and aft of the frame and the interface shear flow from the frame acting on the skin.**

negative  $x$ - and  $y$ -directions, respectively, and a positive torque is defined in the negative  $z$ -direction by the right-hand screw rule. Equilibrium immediately fore and aft of the frame leads to jumps in the shear forces and torque acting on the fuselage skin. As depicted in figure. 7.17(b), the jump conditions are

$$\Delta V_x = V_x^+ - V_x^- = P_x \quad \Delta V_y = V_y^+ - V_y^- = P_y \quad \Delta M_z = M_z^+ - M_z^- = T_z. \quad (7.41)$$

As shown in figure. 7.17(c) the shear flows acting on the cross section of the fuselage immediately fore and aft of the frame are denoted by  $q^+$  and  $q^-$ , respectively. The shear flow exerted by the frame on the skin at the interface is denoted by  $\bar{q}$ . Equilibrium of the shear flows in figure. 7.17(c) yields

$$q^+ - q^- = \bar{q}. \quad (7.42)$$

The shear flow acting on a single-cell cross section is given by eq. (3.163) on page 70. For this situation

$$q(s, z) = \frac{M_z}{2A_c} - F_x(s)V_x(z) - F_y(s)V_y(z). \quad (7.43)$$

Assume the geometry of the fuselage shell is the same fore and aft of the frame. Substitute eq. (7.43) for the shear flows in the skin fore and aft of the frame into eq. (7.42) to find the shear flow exerted on the skin by the frame as

$$\bar{q} = -F_x(s)[V_x^+ - V_x^-] - F_y(s)[V_y^+ - V_y^-] + [M_z^+ - M_z^-]/(2A_c). \quad (7.44)$$

Now substitute the jump conditions from eq. (7.41) into eq. (7.44) to get

$$\bar{q} = -F_x(s)P_x - F_y(s)P_y + T_z/(2A_c). \quad (7.45)$$

Since the shear center and centroid coincide, the shear flow distribution functions from eqs. (3.151) and (3.164) on page 68 and page 70, respectively, are given by

$$F_x(s) = \frac{1}{I_{yy}} \left[ Q_y(s) - \frac{1}{2A_c} \oint (r_n Q_y) ds \right] \quad F_y(s) = \frac{1}{I_{xx}} \left[ Q_x(s) - \frac{1}{2A_c} \oint (r_n Q_x) ds \right]. \quad (7.46)$$

Equation (7.45) determines the interface shear flow exerted by the frame on the fuselage skin in terms of the concentrated loads acting on the frame as depicted in figure. 7.18(a). The reaction to this interface shear flow acts on the frame, and the free body diagram of the frame is shown in figure. 7.18(b).

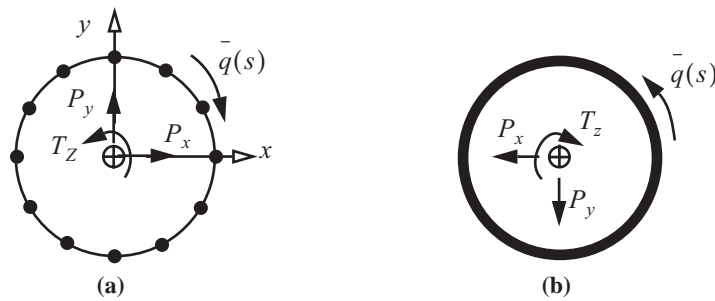


Fig. 7.18 (a) Free body diagram of the fuselage skin. (b) Free body diagram of the frame.

#### Example 7.6 Floor loading on a frame in a stringer-stiffened fuselage

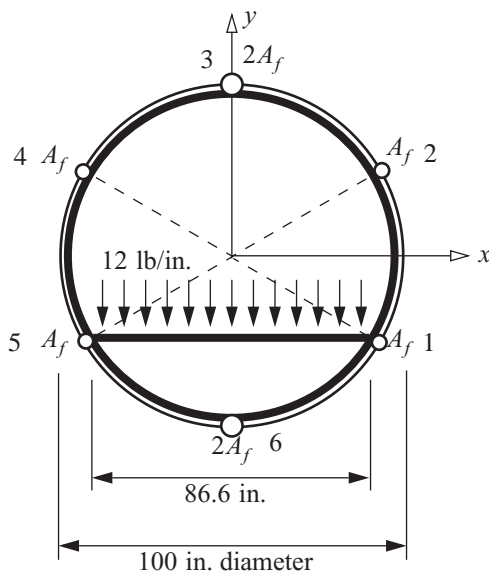


Fig. 7.19 Fuselage frame.

A frame in a circular fuselage is subject to a uniformly distributed line load with an intensity of 12 lb./in. acting on its floor support. See the adjacent sketch. The fuselage skin thickness  $t = 0.015 \text{ in.}$ , and it is stiffened by six stringers spaced  $60^\circ$  apart. Stringers 1, 2, 4, and 5 have flange areas  $A_f = 0.15 \text{ in.}^2$ , and stringers 3 and 6 have flange areas  $2A_f = 0.30 \text{ in.}^2$ . Determine the interface shear flows acting on the skin-stringer fuselage due to the contact with the frame.

**Solution.** The circular skin-stringer fuselage is symmetric with respect to the  $x$ - and  $y$ -axes through its center, so the centroid and shear center are both located at the center of the circle. The resultant downward force acting on the frame is  $P_y = 12 \times 86.6 = 1,039.2 \text{ lb.}$  When the frame is removed from the fuselage the action of the



frame on the fuselage is represented by a jump in the shear force in the fuselage. From eq. (7.41)  $\Delta V_y = P_y$ . A free body diagram of the skin-stringer structure is shown in figure. 7.20.

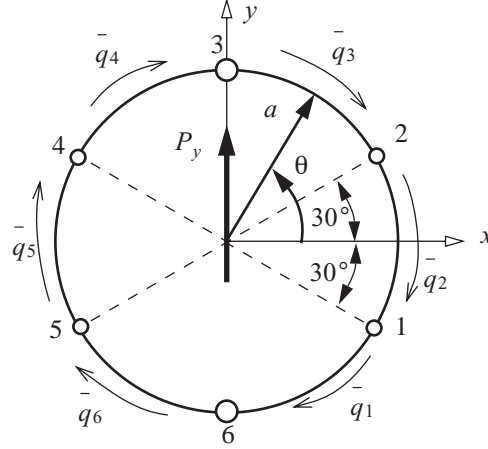


Fig. 7.20 Free body diagram of the skin-stringer structure.

The expression (7.45) for the interface shear flow in this example reduces to  $\bar{q} = -F_y(s)P_y$ . The contour coordinate  $s$  is related to the polar angle  $\theta$  by  $s = a\theta$ , where the radius of the circular contour  $a = 50$  in., and  $0 \leq \theta < 2\pi$  radians. The contour distribution function  $F_y(s)$ , or  $F_y(\theta)$ , is given by eq. (7.46), which is evaluated by computing the first area moment with respect to the  $x$ -axis of a portion of the skin-stringer fuselage from  $\theta = -\pi/2$  to a value in the range  $-\pi/2 < \theta < 3\pi/2$ . The expression for the first area moment  $Q_x(\theta)$  is facilitated by accumulating the first area moments in each of the six segments of the contour.

Beginning at  $\theta = -\pi/2$ , and proceeding counterclockwise around the contour, the first area moments of the skin-stringer structure with respect to the  $x$ -axis are denoted by  $Q_{xi}(\theta)$ ,  $i = 1, 2, \dots, 6$ . The first area moments are calculated as follows:

$$Q_{x1}(\theta) = -a(2A_f) + \int_{-\pi/2}^{\theta} (a \sin \theta) t a d\theta = -a(2A_f) - a^2 t \cos \theta \quad -\pi/2 \leq \theta < -\pi/6, \quad (a)$$

$$Q_{x2}(\theta) = Q_{x1}\left(-\frac{\pi}{6}\right) + \left(-\frac{a}{2}\right)A_f + \int_{-\pi/6}^{\theta} (a \sin \theta) t a d\theta = -\frac{a}{2}(5A_f + 2at \cos \theta) \quad -\pi/6 \leq \theta < \pi/6, \quad (b)$$

$$Q_{x3}(\theta) = Q_{x2}\left(\frac{\pi}{6}\right) + \left(\frac{a}{2}\right)A_f + \int_{\pi/6}^{\theta} (a \sin \theta) t a d\theta = -a(2A_f + at \cos \theta) \quad \pi/6 \leq \theta < \pi/2, \quad (c)$$

$$Q_{x4}(\theta) = Q_{x3}\left(\frac{\pi}{2}\right) + a(2A_f) + \int_{\pi/2}^{\theta} (a \sin \theta) t a d\theta = -a^2 t \cos \theta \quad \pi/2 \leq \theta < 5\pi/6, \quad (\text{d})$$

$$Q_{x5}(\theta) = Q_{x4}\left(\frac{5\pi}{6}\right) + \left(\frac{a}{2}\right)A_f + \int_{5\pi/6}^{\theta} (a \sin \theta) t a d\theta = \frac{a}{2}(A_f - 2at \cos \theta) \quad 5\pi/6 \leq \theta < 7\pi/6, \text{ and} \quad (\text{e})$$

$$Q_{x6}(\theta) = Q_{x5}\left(\frac{7\pi}{6}\right) + \left(-\frac{a}{2}\right)A_f + \int_{7\pi/6}^{\theta} (a \sin \theta) t a d\theta = -a^2 t \cos \theta \quad 7\pi/6 \leq \theta < 3\pi/2. \quad (\text{f})$$

Note that the first area moment of the entire cross section about the  $x$ -axis vanishes, or  $Q_{x6}(3\pi/2) = 0$ , since the  $x$ -axis passes through the centroid.

The expression for the shear flow distribution function from eq. (7.46) is written as

$$F_{yi}(\theta) = \frac{1}{I_{xx}} \left[ Q_{xi}(\theta) - \frac{1}{2A_c} \oint (r_n Q_x) a d\theta \right] \quad i = 1, 2, \dots, 6. \quad (\text{g})$$

The integral of  $r_n Q_x$  around the entire contour, where  $r_n = a$ , is given by

$$\begin{aligned} \oint (r_n Q_x) a d\theta = & \int_{-\pi/2}^{-\pi/6} a Q_{x1}(\theta) a d\theta + \int_{-\pi/6}^{\pi/6} a Q_{x2}(\theta) a d\theta + \int_{\pi/6}^{\pi/2} a Q_{x3}(\theta) a d\theta + \int_{\pi/2}^{5\pi/6} a Q_{x4}(\theta) a d\theta + \\ & \int_{5\pi/6}^{7\pi/6} a Q_{x5}(\theta) a d\theta + \int_{7\pi/6}^{3\pi/2} a Q_{x6}(\theta) a d\theta \end{aligned} \quad (\text{h})$$

which after integration yields

$$\oint (r_n Q_x) a d\theta = -2\pi a^3 A_f. \quad (\text{i})$$

The area enclosed by the contour is  $A_c = a^2 \pi$ . Hence, the interface shear flows are given by

$$\bar{q}_i(\theta) = -\left(\frac{1}{I_{xx}}\right) [Q_{xi}(\theta) + a A_f] P_y \quad i = 1, 2, \dots, 6. \quad (\text{j})$$

The second area moment about the  $x$ -axis is given by

$$I_{xx} = \int_0^{2\pi} (a \sin \theta)^2 t a d\theta + \sum_{i=1}^6 (y f_i)^2 A f_i = 5a^2 A_f + \pi a^3 t = 7,765.49 \text{ in.}^4 \quad (\text{k})$$

Results for the interface shear flows with dimensional units of lb./in. are listed below:

$$\bar{q}_1(\theta) = \left[ \frac{a(A_f + at \cos \theta)}{I_{xx}} \right] P_y = 1.00367 + 5.01836 \cos \theta \quad -\pi/2 \leq \theta < -\pi/6, \quad (\text{l})$$

$$\bar{q}_2(\theta) = \left[ \frac{a(3A_f + 2at\cos\theta)}{2I_{xx}} \right] P_y = 1.50551 + 5.01836\cos\theta \quad -\pi/6 \leq \theta < \pi/6, \quad (\text{m})$$

$$\bar{q}_3(\theta) = \frac{a[A_f + at\cos\theta]}{I_{xx}} P_y = 1.00367 + 5.01836\cos\theta \quad \pi/6 \leq \theta < \pi/2, \quad (\text{n})$$

$$\bar{q}_4(\theta) = \frac{-a(A_f - at\cos\theta)}{I_{xx}} P_y = -1.00367 + 5.01836\cos\theta \quad \pi/2 \leq \theta < 5\pi/6, \quad (\text{o})$$

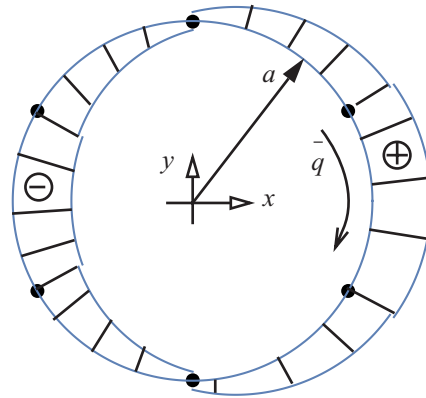
$$\bar{q}_5(\theta) = \frac{-a(3A_f - 2at\cos\theta)}{2I_{xx}} P_y = -1.50551 + 5.01836\cos\theta \quad 5\pi/6 \leq \theta < 7\pi/6, \text{ and} \quad (\text{p})$$

$$\bar{q}_6(\theta) = \frac{-a(A_f - at\cos\theta)}{I_{xx}} P_y = -1.00367 + 5.01836\cos\theta \quad 7\pi/6 \leq \theta < 3\pi/2. \quad (\text{q})$$

The shear flows are plotted normal to the contour in the graph shown in figure. 7.21.



**Fig. 7.21** Distribution of the interface shear flow acting skin-stringer fuselage in example 7.6.



### Example 7.7 Bending moment in the frame of example 7.6

We use symmetry of the frame about the  $y$ -axis and draw a free body diagram of the right half of the frame as shown in figure. 7.22. Consequently, the frame has three vertical cuts: cut  $a$  is at the bottom of the frame, cut  $b$  at the top, and cut  $c$  at the center of the floor beam. The action of the left half of the frame on the right half is represented by three forces  $N_a$ ,  $N_b$ , and  $N_c$ , and by three moments  $M_a$ ,  $M_b$ , and  $M_c$  at the location of the three cuts as shown in figure. 7.22. Shear forces at cuts  $a$ ,  $b$ , and  $c$  vanish by symmetry conditions similar to what was discussed in example 7.4. These six unknown actions at the cuts are related by the three independent equations of equilibrium for the overall free body diagram in figure. 7.22. Hence, this is a statically indeterminate structure. The redundants are determined from conditions of compatibility imposed via Castigliano's second theorem. The solution process is divided into six steps:

1. Overall frame equilibrium
2. Solutions to the differential equilibrium equations for the frame
3. Bending moments in segments 1, 2, and 3 of the frame

4. Floor beam equilibrium
5. Equilibrium at the junction of the floor beam and frame
6. Compatibility conditions

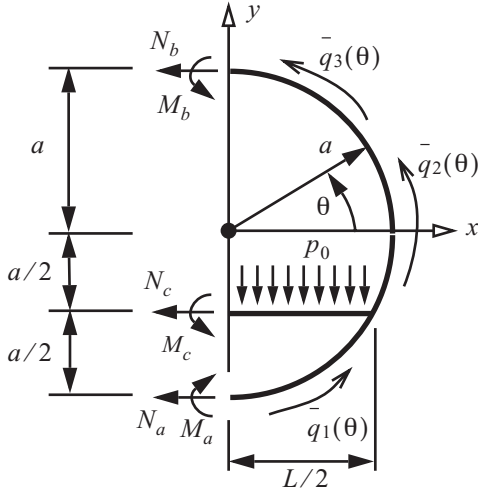


**Fig. 7.22** Free body diagram of the right-half section of the frame in example 7.6.

**Solution to part 1.** Overall frame equilibrium

Force equilibrium of the right half frame segment in the negative  $x$ -direction requires

$$N_a + N_b + N_c + \underbrace{\int_{-\pi/2}^{-\pi/6} (\bar{q}_1(\theta) \sin \theta) a d\theta + \int_{-\pi/6}^{\pi/6} (\bar{q}_2(\theta) \sin \theta) a d\theta + \int_{\pi/6}^{\pi/2} (\bar{q}_3(\theta) \sin \theta) a d\theta}_{= R_x} = 0 \quad . \quad (\text{a})$$

The resultant force  $R_x = 0$  as determined from the interface shear flows given in example 7.6. Hence, force equilibrium in the  $x$ -direction reduces to

$$N_a + N_b + N_c = 0 \quad . \quad (\text{b})$$

Force equilibrium of the right half frame segment in the  $y$ -direction requires

$$\underbrace{\int_{-\pi/2}^{-\pi/6} (\bar{q}_1(\theta) \cos \theta) a d\theta + \int_{-\pi/6}^{\pi/6} (\bar{q}_2(\theta) \cos \theta) a d\theta + \int_{\pi/6}^{\pi/2} (\bar{q}_3(\theta) \cos \theta) a d\theta}_{= R_y} - P_y/2 = 0 \quad . \quad (\text{c})$$

Substituting the interface shear flows from example 7.6 we find the force  $R_y = P_y/2$ . So force equilibrium in the  $y$ -direction is identically satisfied. Torsional equilibrium about the origin yields

$$M_z + M_b + M_c - M_a + aN_b - (a/2)N_c - aN_a - (L/4)(P_y/2) = 0 \quad , \quad (\text{d})$$

where the torque from the interface shear flows is given by

$$M_z = \int_{-\pi/2}^{-\pi/6} a \bar{q}_1(\theta) a d\theta + \int_{-\pi/6}^{\pi/6} a \bar{q}_2(\theta) a d\theta + \int_{\pi/6}^{\pi/2} a \bar{q}_3(\theta) a d\theta = 34,289.4 \text{ lb.-in.} \quad (\text{e})$$

**Solution to part 2.** Solutions to the differential equilibrium equations for the frame.

The differential equilibrium equations (7.35), (7.36), and (7.40) are solved for  $R = a$ ,  $ds = a d\theta$ ,  $p = 0$ , and

$q = \bar{q}(\theta)$ . Differentiate eq. (7.35) with respect to  $\theta$ , and then substitute eq. (7.36) for the derivative of the shear force to get

$$\frac{d^2 N}{d\theta^2} + N + a \frac{d\bar{q}}{d\theta} = 0. \quad (\text{f})$$

Each interface shear flow has the functional form

$$\bar{q}_i(\theta) = A_i + B \cos \theta \quad i = 1, 2, 3, \quad (\text{g})$$

where

$$A_1 = A_3 = \frac{a(a_f)P_y}{I_{xx}} = 1.0037 \text{ lb./in.} \quad A_2 = \frac{3}{2}A_1 = 1.50555 \text{ lb./in.} \quad B = \frac{a^2 t P_y}{I_{xx}} = 5.01836 \text{ lb./in.} \quad (\text{h})$$

Substitute eq. (g) for the shear flow in eq. (f), then the resulting differential equation is solved for  $N(\theta)$  to get

$$N(\theta) = c_1 \cos \theta + c_2 \sin \theta - (aB/2)\theta \cos \theta. \quad (\text{i})$$

Equilibrium equations (7.35) and (7.40) determine the shear force and bending moment as

$$V(\theta) = -a \bar{q}_i(\theta) - \frac{dN}{d\theta} \quad M(\theta) = a \int V(\theta) d\theta + c_3. \quad (\text{j})$$

It is convenient to determine the three constants  $c_1$ ,  $c_2$ , and  $c_3$  in terms of the forces and moment at the point  $\theta = \theta_\alpha$  by the following conditions

$$N(\theta_\alpha) = N_\alpha \quad V(\theta_\alpha) = V_\alpha \quad M(\theta_\alpha) = M_\alpha. \quad (\text{k})$$

The point  $\theta_\alpha$  on the contour is either the initial point or final point of the contour segment. The statically admissible solution for the normal force, shear force, and bending is

$$\begin{bmatrix} N(\theta; \theta_\alpha) \\ V(\theta; \theta_\alpha) \\ M(\theta; \theta_\alpha) \end{bmatrix} = N_\alpha \begin{bmatrix} \cos(\theta - \theta_\alpha) \\ \sin(\theta - \theta_\alpha) \\ a[1 - \cos(\theta - \theta_\alpha)] \end{bmatrix} + V_\alpha \begin{bmatrix} -\sin(\theta - \theta_\alpha) \\ \cos(\theta - \theta_\alpha) \\ a \sin(\theta - \theta_\alpha) \end{bmatrix} + M_\alpha \begin{bmatrix} 0 \\ 0 \\ 1 \end{bmatrix} + \begin{bmatrix} N_q(\theta; \theta_\alpha) \\ V_q(\theta; \theta_\alpha) \\ M_q(\theta; \theta_\alpha) \end{bmatrix}, \quad (\text{l})$$

where

$$\begin{bmatrix} N_q(\theta; \theta_\alpha) \\ V_q(\theta; \theta_\alpha) \\ M_q(\theta; \theta_\alpha) \end{bmatrix} = A_i \begin{bmatrix} -a \sin(\theta - \theta_\alpha) \\ -a[1 - \cos(\theta - \theta_\alpha)] \\ -a^2[\theta - \theta_\alpha - \sin(\theta - \theta_\alpha)] \end{bmatrix} - \left(\frac{aB}{4}\right) \begin{bmatrix} 2(\theta - \theta_\alpha) \cos \theta + 2 \cos \theta_\alpha \sin(\theta - \theta_\alpha) \\ \cos \theta - \cos(\theta - 2\theta_\alpha) + 2(\theta - \theta_\alpha) \sin \theta \\ a[-2(\theta - \theta_\alpha) \cos \theta + 3 \sin \theta - \sin(\theta - 2\theta_\alpha) - 4 \sin \theta_\alpha] \end{bmatrix} \quad (\text{m})$$

**Solution to part 3.** Bending moments in segments 1, 2, and 3 of the frame

The range for the solution interval in frame segment 1 is  $-\pi/2 \leq \theta \leq -\pi/6$ , and we let  $\theta_\alpha \rightarrow -\pi/2$ ,  $N_\alpha \rightarrow N_a$ ,  $V_\alpha \rightarrow 0$ , and  $M_\alpha \rightarrow M_a$  in eq. (i). The numerical result for the bending moment in segment 1 is

$$M_1(\theta) = 50N_a(1 + \sin \theta) + M_a - 16,487.8 - 2509.25\theta + 12,363.1 \cos \theta + 6,273.1\theta \cos \theta - 12,546.3 \sin \theta. \quad (\text{n})$$

The range for the solution interval in frame segment 3 is  $\pi/6 \leq \theta \leq \pi/2$ , and we let  $\theta_\alpha \rightarrow \pi/2$ ,  $N_\alpha \rightarrow N_b$ ,  $V_\alpha \rightarrow 0$ , and  $M_\alpha \rightarrow M_b$  in eq. (i). The numerical result for the bending moment in segment 3 is

$$M_3(\theta) = 50N_b(1 - \sin \theta) + M_b + 16,487.8 - 2,509.25\theta - 12,363.1 \cos \theta + 6,273.13\theta \cos \theta - 12,546.3 \sin \theta. \quad (\text{o})$$

The range for the solution interval in frame segment 2 is  $-\pi/6 \leq \theta \leq \pi/6$ , and we let  $\theta_\alpha \rightarrow \pi/6$ ,  $N_\alpha \rightarrow N_{2a}$ ,  $V_\alpha \rightarrow V_{2a}$ , and  $M_\alpha \rightarrow M_{2a}$  in eq. (i). At the junction of segment 2 and 3 where  $\theta = \pi/6$ , we impose continuity conditions

$$N_3(\pi/6) = N_{2a} \quad V_3(\pi/6) = V_{2a} \quad M_3(\pi/6) = M_{2a}. \quad (\text{p})$$

The result of imposing the previous continuity conditions is to express  $N_{2a}$ ,  $V_{2a}$ ,  $M_{2a}$  in terms of  $N_b$  and  $M_b$ . The numerical results for the bending moments in segments 2 is

$$M_2(\theta) = 50N_b(1 - \sin \theta) + M_b + 17,144.7 - 3,763.88\theta - 12,990.4 \cos \theta + 6,273.13\theta \cos \theta - 11,459.7 \sin \theta. \quad (\text{q})$$

**Solution to part 4.** Floor beam equilibrium

The internal shear force in the floor beam is denoted by  $V_4$  and the bending moment by  $M_4$ . Equilibrium of the floor beam yields

$$V_4(x) = P_y(x/L) \quad M_4(x) = M_c + \frac{P_y}{2L}x^2 \quad 0 \leq x \leq L/2. \quad (\text{r})$$

The axial force  $N_c$  is uniform in the beam.

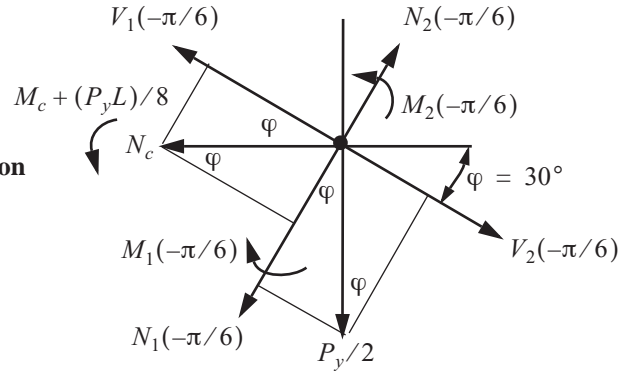
**Solution to part 5.** Equilibrium at the junction of the floor beam and frame.

A free body diagram of the junction of the frame and the floor beam is shown in figure. 7.23. Force equilibrium in the tangential direction to the frame yields

$$N_2(-\pi/6) - N_1(-\pi/6) - N_c \sin 30^\circ - (P_y/2) \cos 30^\circ = 0. \quad (\text{s})$$

Equation (s) leads to  $N_c = -N_a - N_b$ , which also satisfies eq. (b). Force equilibrium in the normal direction to the frame yields

**Fig. 7.23** Free body diagram of the junction of the frame and floor beam.



$$V_2(-\pi/6) - V_1(-\pi/6) - N_c \cos 30^\circ + (P_y/2) \sin 30^\circ = 0. \quad (\text{t})$$

Equation (t) leads to  $N_a + N_b + N_c = 0$ , which is satisfied by the solution for  $N_c$  from the tangential equilibrium equation. Torsional equilibrium at the junction yields

$$M_2(-\pi/6) - M_1(-\pi/6) + (M_c + P_y L/8) = 0. \quad (\text{u})$$

Numerical evaluation of the torsional equilibrium equation gives

$$23,039.4 - M_a + M_b + M_c - 25N_a + 75N_b = 0, \quad (\text{v})$$

which is solved for  $M_c$  to get

$$M_c = -23,039.4 + M_a - M_b + 25N_a - 75N_b. \quad (\text{w})$$

The overall torsional equilibrium equation (d) is identically satisfied for the results determined for  $N_c$  and  $M_c$  from equilibrium at the junction. At this point in the solution process all static equilibrium equations are satisfied, and the expressions for the bending moments in the frame are

$$M_1(\theta) = 50.N_a(1 + \sin\theta) + M_a - 16,487.8 - 2,509.25\theta + 12,363.1 \cos\theta + 6,273.13\theta \cos\theta - 12,546.3 \sin\theta, \quad (\text{x})$$

$$M_2(\theta) = 50.(1 - \sin\theta)N_b + M_b + 17,144.7 + (-12,990.4 + 6,273.13\theta) \cos\theta - 11,459.7 \sin\theta, \text{ and} \quad (\text{y})$$

$$M_3(\theta) = 50(1 - \sin\theta)N_b + M_b + 16,487.8 - 2,509.25\theta + (-12,363.1 + 6,273.13\theta) \cos\theta - 12,546.3 \sin\theta. \quad (\text{z})$$

The bending moment in the floor beam is

$$M_4(x) = -23,039.41 + M_a - M_b + 25N_a - 75N_b + 6x^2. \quad (\text{aa})$$

The unknown parameters  $N_a$ ,  $M_a$ ,  $N_b$ , and  $M_b$  in this statically admissible solution, eqs. (x) to (aa), are the redundants.

#### **Solution to part 6.** Compatibility conditions

To determine the redundants we impose compatibility by using Castigliano's second theorem. Neglect the complementary strain energies due to the tangential force  $N$  and the shear force  $V$ , which implies that complementary strain energy in bending is the main contributor to the deflections of the frame. Assume for simplicity that the flexural stiffness  $EI$  of the frame and the floor beam are the same. Symmetry about the vertical axis of the frame

requires the generalized displacements corresponding to the redundants to vanish. Then, setting the displacement corresponding to redundant  $N_a$  equal to zero is imposed by

$$0 = \int_{-\pi/2}^{-\pi/6} M_1 \left( \frac{\partial M_1}{\partial N_a} \right) a d\theta + \int_{-\pi/6}^{\pi/6} M_2 \left( \frac{\partial M_2}{\partial N_a} \right) a d\theta + \int_{\pi/6}^{\pi/2} M_3 \left( \frac{\partial M_3}{\partial N_a} \right) a d\theta + \int_0^{L/2} M_4 \left( \frac{\partial M_4}{\partial N_a} \right) dx. \quad (\text{ab})$$

After substituting eqs. (x) to (aa) into eq. (ab) we find

$$0 = -2.10978 \times 10^7 + 1,535.46 M_a - 1082.53 M_b + 33,969.8 N_a - 81,189.9 N_b. \quad (\text{ac})$$

Setting the rotation corresponding to redundant  $M_a$  equal to zero leads to the following equation

$$0 = \int_{-\pi/2}^{-\pi/6} M_1 \left( \frac{\partial M_1}{\partial M_a} \right) a d\theta + \int_{-\pi/6}^{\pi/6} M_2 \left( \frac{\partial M_2}{\partial M_a} \right) a d\theta + \int_{\pi/6}^{\pi/2} M_3 \left( \frac{\partial M_3}{\partial M_a} \right) a d\theta + \int_0^{L/2} M_4 \left( \frac{\partial M_4}{\partial M_a} \right) dx, \quad (\text{ad})$$

which evaluates as

$$0 = -847,565. + 95.6611 M_a - 43.3013 M_b + 1,535.46 N_a - 3,247.6 N_b. \quad (\text{ae})$$

Setting the displacement corresponding to redundant  $N_b$  equal to zero yields

$$0 = \int_{-\pi/2}^{-\pi/6} M_1 \left( \frac{\partial M_1}{\partial N_b} \right) a d\theta + \int_{-\pi/6}^{\pi/6} M_2 \left( \frac{\partial M_2}{\partial N_b} \right) a d\theta + \int_{\pi/6}^{\pi/2} M_3 \left( \frac{\partial M_3}{\partial N_b} \right) a d\theta + \int_0^{L/2} M_4 \left( \frac{\partial M_4}{\partial N_b} \right) dx, \quad (\text{af})$$

which evaluates as

$$0 = 7.73981 \times 10^7 - 3,247.6 M_a + 6,318.52 M_b - 81,189.9 N_a + 392,699. N_b. \quad (\text{ag})$$

Setting the rotation corresponding to redundant  $M_b$  equal to zero leads to the following equation

$$0 = \int_{-\pi/2}^{-\pi/6} M_1 \left( \frac{\partial M_1}{\partial M_b} \right) a d\theta + \int_{-\pi/6}^{\pi/6} M_2 \left( \frac{\partial M_2}{\partial M_b} \right) a d\theta + \int_{\pi/6}^{\pi/2} M_3 \left( \frac{\partial M_3}{\partial M_b} \right) a d\theta + \int_0^{L/2} M_4 \left( \frac{\partial M_4}{\partial M_b} \right) dx, \quad (\text{ah})$$

which evaluates as

$$0 = 1.09574 \times 10^6 - 43.3013 M_a + 148.021 M_b - 1,082.53 N_a + 6,318.52 N_b. \quad (\text{ai})$$

The solution for the redundants in eqs. (ac), (ae), (ag), and (ai) is

$$N_a = -361.122 \text{ lb.} \quad M_a = -1,756.43 \text{ in.-lb.} \quad N_b = -166.284 \text{ lb.} \quad M_b = 1,822.71 \text{ in.-lb.} \quad (\text{aj})$$

The remaining actions at cut  $c$  and the bending moment at the end of the floor beam are

$$N_c = -194.838 \text{ lb.} \quad M_c = -5,119.2 \text{ in.-lb.} \quad M_c + (P_y L)/8 = 6,130.8 \text{ in.-lb.} \quad (\text{ak})$$

A plot of the bending moment in segments one, two, and three of the frame is shown in figure. 7.24. The bending moment exhibits a step change in value at the junction of the frame and the floor beam. That is,



$$M_2(-\pi/6) - M_1(-\pi/6) = 102.182 - 6,232.98 = -6,130.8 \text{ in.-lb.}$$

This step change in the bending moment between curved segments one and two of the frame is equal to the magnitude of the bending moment at the end of the floor beam.

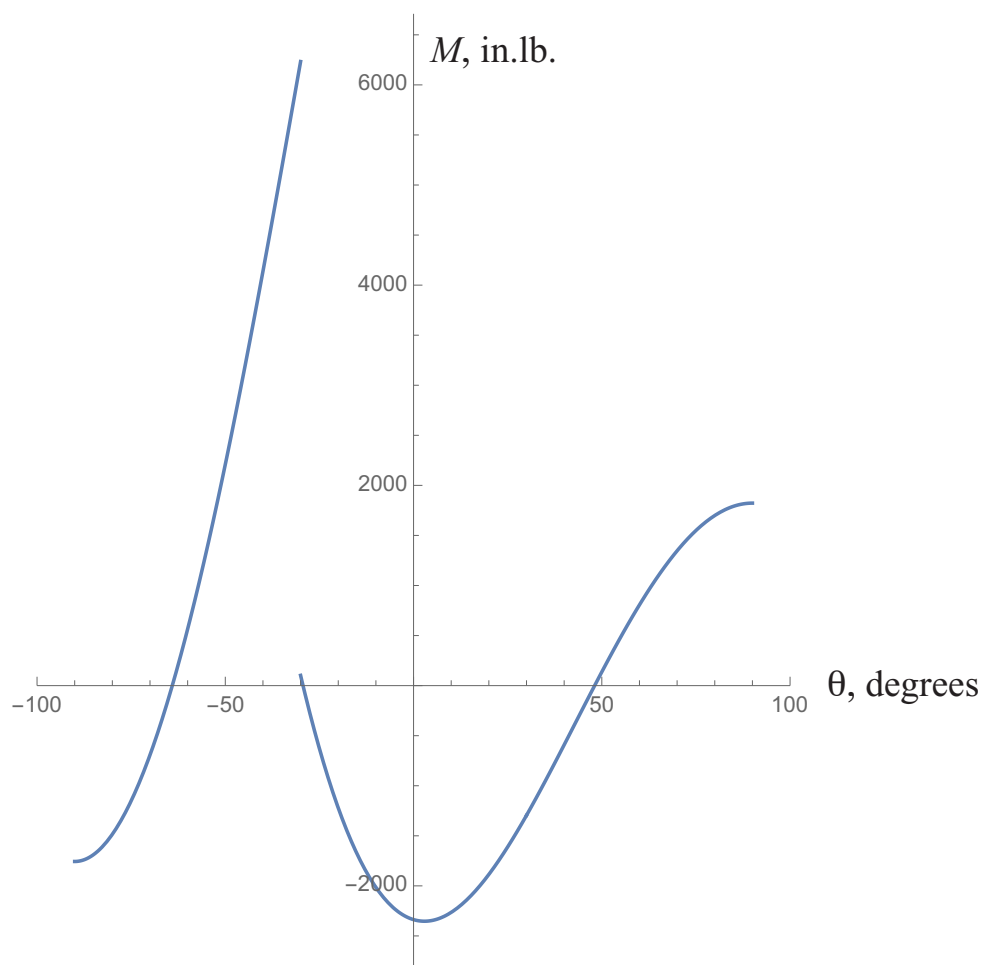


**Fig. 7.24** Frame bending moment distribution.

## 7.5 References

Bruhn, E. F. *Analysis and Design of Flight Vehicle Structures*. Carmel IN: Jacobs Publishing, Inc., 1973, p. A13.17., and Chapter A21

Chidamparam, P, and A. W. Leissa. "Vibrations of Planar Curved Beams, Rings, and Arches." *American Society of Mechanical Engineers, Applied Mechanics Reviews* 46, no. 9 (September 1993).

Curtis, Howard. D. *Fundamentals of Aircraft Structural Analysis*. Jefferson City, MO: Richard D. Irwin, a

Times Mirror Higher Education Group, Inc. Company, 1997, pp. 269, 270, 384-389.

Langhaar, H. L. *Energy Methods in Applied Mechanics*. New York: John Wiley & Sons, 1962, pp. 48-50.

Megson, T. H. G. *Aircraft Structures for Engineering Students*. 3d ed. London and New York: Arnold and John Wiley & Sons, Inc., 1999 Section 10.4.

## 7.6 Practice exercises

1. The radius of the centroidal arc of a thick, semicircular bar is 42 mm as shown in figure. 7.25. It is subject to two 5 kN loads symmetrically distributed with respect to midspan. Determine the normal stresses in the radial inboard flange ( $y_1$ ) and the radial outboard flange ( $y_3$ ) at midspan.

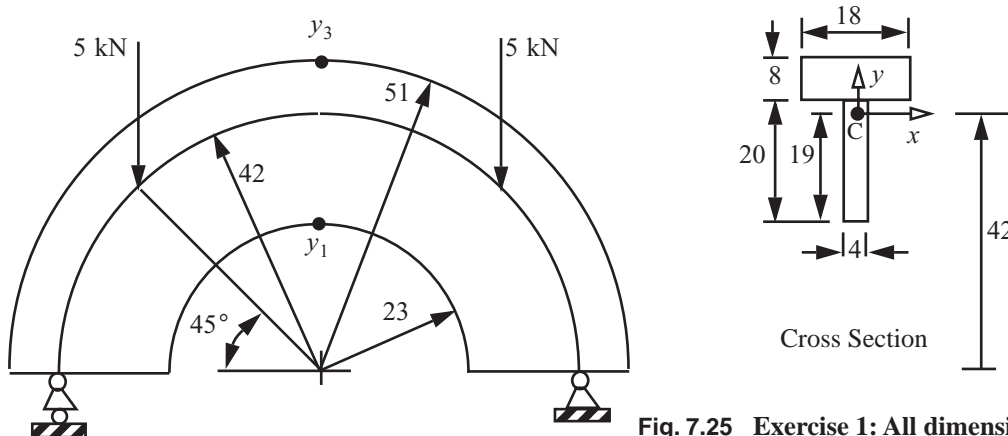
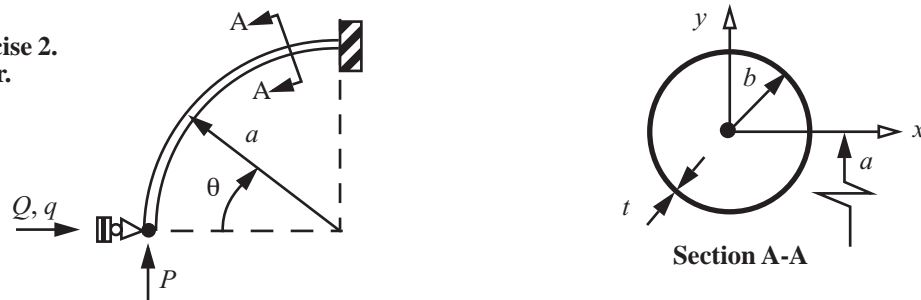


Fig. 7.25 Exercise 1: All dimensions in mm.

2. Consider a thin curved bar with a uniform, symmetrical cross section whose reference axis is one-quarter of a circle of radius  $a$  as shown in figure. 7.26. The cross section of the bar is the thin-walled tube of example 6.4 on page 160 with the mean radius denoted by  $a$  and a wall thickness denoted by  $t$ . The bar is clamped to a fixed support at its upper end, and supported by a roller at its lower end that is free to move vertically but not horizontally. An upward vertical force  $P$  is applied at the lower end of the bar. Determine the horizontal reaction force  $Q$  at its lower end in terms of the applied force  $P$  using Castigliano's second theorem.

Fig. 7.26 Exercise 2. Thin curved bar.



3. Continuing with the arch problem in example 7.3 do the following:

- Use Castigliano's second theorem to determine the displacement  $\Delta$  in the direction of the external force  $P$  in terms of  $P$ , the semi-opening angle  $\beta$ , redundant  $Q$ , extensional stiffness  $EA$ , and flexural stiffness

$EI$ . Note that the redundant was determined and is given by eq. (g).

- b) The structural stiffness of the arch is defined by  $K = P/\Delta$ . For a straight beam having the same flexural stiffness as the arch, spanning the distance  $L$  between the supports, and subject to force  $P$  at midspan, the structural stiffness is  $K_b = P/\Delta_b = (48EI)/L^3$ . Plot the ratio of the arch stiffness to the beam stiffness  $K/K_b$  as a function of the rise-to-span ratio given by eq. (h). Use the numerical data given in the example. Plot parametrically by selecting values of the semi-opening angle  $\beta$  in the range  $1^\circ \leq \beta \leq 90^\circ$ , then compute the sequence  $H/L$ ,  $R$ ,  $Q/P$ , and  $K/K_b$  for each  $\beta$ .

4. Consider a thin-walled, cylindrical shell stiffened by an internal frame. As shown in figure. 7.27, the frame consists of a thin-walled circular bar of radius  $a$ , and a horizontal bar of length  $2a$  clamped to the ends of the circular bar. A point load  $P$  is applied to the midspan of the horizontal bar. This load is equilibrated by interface shear flows, which were determined from a free body diagram of the shell with the following results:

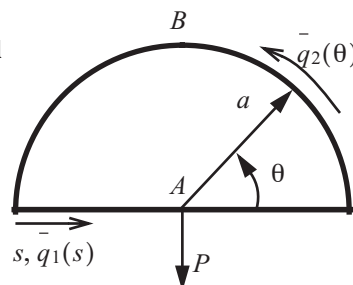
$$\bar{q}_1(s) = -k_1 \frac{P}{a^2}(a-s) \quad 0 \leq s \leq 2a, \text{ and} \quad (7.47)$$

$$\bar{q}_2(\theta) = \frac{P}{a}(-k_2 + k_3\theta + k_4\cos\theta) \quad 0 \leq \theta \leq \pi, \quad (7.48)$$

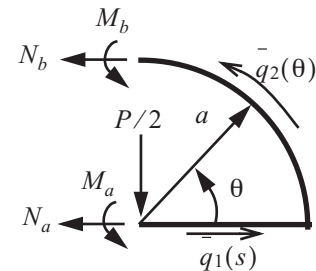
where  $k_1 = k_3 = \frac{4}{-8 + 2\pi + \pi^2}$ ,  $k_2 = \frac{2\pi}{-8 + 2\pi + \pi^2}$ ,  $k_4 = \frac{2(2 + \pi)}{-8 + 2\pi + \pi^2}$ . The frame is symmetric with respect to the vertical line A-B through the center of the circular part. A free body diagram of the right half of the frame is also shown in the sketch below. The action of the left half on the right half of the frame are represented by normal forces  $N_a$  and  $N_b$ , and bending moments  $M_a$  and  $M_b$ . The shear forces  $V_a$  and  $V_b$  acting on the cross sections at A and B vanish because of symmetry. There are four unknown actions at A and B but only three independent equilibrium equations for the right half of the frame. Hence, the half frame is singly redundant.

- Determine the redundant in terms of parameters  $a$  and  $P$  from the compatibility equation obtained by application of Castigliano's second theorem. Include only the bending moments in the complementary strain energy, and assume the flexural stiffness  $EI$  is uniform in the frame.
- List the values of  $N_a$ ,  $N_b$ ,  $M_a$ , and  $M_b$  in terms of parameters  $a$  and  $P$ .
- Determine the maximum bending moment in the frame, as well as the point, or points, where the bending moment is zero. (Partial answer: the magnitude of the maximum bending moment is  $0.3162 aP$ .)

**Fig. 7.27 Internal frame in a cylindrical shell.**



Overall FBD of the frame



FBD of the right half

**Hint.** Show that the following results for the normal force in the straight part  $N_1$  and in the circular part  $N_2$  satisfy equilibrium:

$$N_1(s) = N_a - k_1 P(s-a)^2 / (2a^2) \quad a \leq s \leq 2a, \quad (7.49)$$

$$N_2(\theta) = c_1 \cos \theta + c_2 \sin \theta - P(2k_3 + k_4 \theta \cos \theta) / 2 \quad 0 \leq \theta \leq \pi/2, \quad (7.50)$$

where  $c_1$  and  $c_2$  are constants to be determined.

## *Laminated bars of fiber-reinforced polymer composites*

### *8.1 Fibrous composites*

A composite material consists of two or more constituents that are chemically distinct on a macroscopic scale and have a recognizable interface between them. An important class of composites for aerospace applications are fiber-reinforced polymer composites (FRP). Fiber-reinforced polymer composites consist of continuous and aligned fibers embedded in a polymer matrix. Continuous glass fibers are 3-20  $\mu\text{m}$  in diameter, with most about 12  $\mu\text{m}$ . The diameter of carbon and graphite fibers is about 8  $\mu\text{m}$ . Fibers are inherently much stiffer and stronger than the same material in bulk form. The polymer matrix supports, protects, and transfers stresses to the fibers. Typically the matrix is of considerably lower density, stiffness, and strength than the fibers. Polymers are subdivided into thermosets and thermoplastics. Thermoset polymers, such as epoxies, become cross-linked during fabrication and do not soften on reheating. Thermoplastic polymers, such as PEEK, soften on heating and can be reshaped with heat and pressure. Usually fibers are bundled in tows, which can consist of 3,000 to 30,000 fibers.

The unidirectional lamina is the basic form of a continuous fiber composite (i.e., one with all fibers in the same direction as shown in figure. 8.1). It can be fabricated from pre-impregnated tape (filament tows pre-impregnated with epoxy), filament winding, pultrusion, or resin transfer molding (RTM). The thickness of lamina, denoted by  $t_{ply}$  in a laminate is typically about 0.127 mm (0.005 in.). Laminates are fabricated by stacking

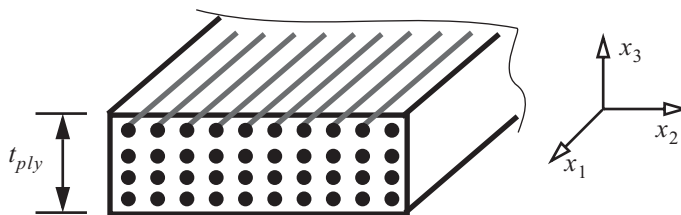


**Fig. 8.1** Unidirectional lamina of a continuous fiber composite.

unidirectional lamina at different fiber orientations followed by curing. Curing is a drying process of the matrix material to form a bond between the fibers and between the lamina.

The advantage of polymer-composites aerospace structures are many: They weigh less than equivalent-strength aluminum, do not corrode or fatigue, require less maintenance, and reduce the need for drilled holes and parts. Composite parts generally cost more than equivalent metal parts, but that premium is decreasing. And the cost premium is offset by operating savings in fuel and maintenance (Canada, 2015).

### 8.1.1 Material law in principal directions

Fiber-reinforced composites are usually treated as a linear elastic material with orthotropic material properties in the material principal directions (i.e. directions parallel and perpendicular to the fibers). In a right-handed Cartesian system denoted by  $x_1$ - $x_2$ - $x_3$ , let the  $x_1$ -axis be parallel to the fibers, the  $x_2$ -axis be transverse to the fibers, and the  $x_3$ -axis be parallel to the thickness of the lamina. (Also, refer to discussion with respect to eq. (A.131) in the appendix.) In the discussion of the material law, it is convenient to use a contracted notation for strain components and the corresponding stress components. The contracted notation defines the 6-by-1 engineering strain vector in principal material directions as

$$\{\gamma_m\} = [\epsilon_{11} \ \epsilon_{22} \ \epsilon_{33} \ \gamma_{23} \ \gamma_{31} \ \gamma_{12}]^T, \quad (8.1)$$

where the normal strains are denoted by  $\epsilon_{11}$ ,  $\epsilon_{22}$ , and  $\epsilon_{33}$ , and the shear strains are denoted by  $\gamma_{23}$ ,  $\gamma_{31}$ , and  $\gamma_{12}$ . The corresponding 6-by-1 stress vector in principal material directions is

$$\{\sigma_m\} = [\sigma_{11} \ \sigma_{22} \ \sigma_{33} \ \sigma_{23} \ \sigma_{31} \ \sigma_{12}]^T, \quad (8.2)$$

where the normal stresses are denoted by  $\sigma_{11}$ ,  $\sigma_{22}$ , and  $\sigma_{33}$ , and the shear stresses are denoted by  $\sigma_{23}$ ,  $\sigma_{31}$ , and  $\sigma_{12}$ . See figure. 8.2.

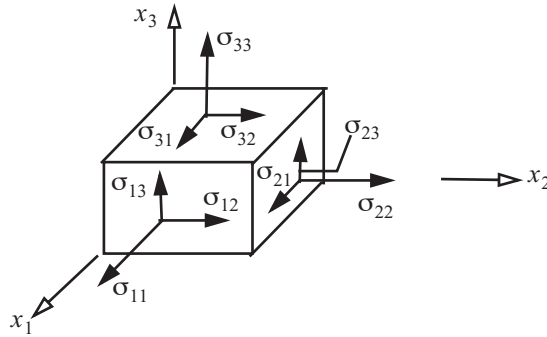


**Fig. 8.2** Stresses in material principal directions.

Hooke's law for an orthotropic material in the contracted notation is

$$\begin{bmatrix} \epsilon_{11} \\ \epsilon_{22} \\ \epsilon_{33} \\ \gamma_{23} \\ \gamma_{31} \\ \gamma_{12} \end{bmatrix} = \underbrace{\begin{bmatrix} C_{11} & C_{12} & C_{13} & 0 & 0 & 0 \\ C_{21} & C_{22} & C_{23} & 0 & 0 & 0 \\ C_{31} & C_{32} & C_{33} & 0 & 0 & 0 \\ 0 & 0 & 0 & C_{44} & 0 & 0 \\ 0 & 0 & 0 & 0 & C_{55} & 0 \\ 0 & 0 & 0 & 0 & 0 & C_{66} \end{bmatrix}}_{[C]} \begin{bmatrix} \sigma_{11} \\ \sigma_{22} \\ \sigma_{33} \\ \sigma_{23} \\ \sigma_{31} \\ \sigma_{12} \end{bmatrix}, \quad (8.3)$$

in which  $[C]$  is the symmetric 6X6 compliance matrix. The non-zero elements of the compliance matrix in terms of engineering constants are

$$C_{11} = \frac{1}{E_1} \quad C_{22} = \frac{1}{E_2} \quad C_{33} = \frac{1}{E_3} \quad C_{44} = \frac{1}{G_{23}} \quad C_{55} = \frac{1}{G_{31}} \quad C_{66} = \frac{1}{G_{12}}, \text{ and} \quad (8.4)$$

$$\begin{aligned} C_{21} &= -\nu_{21}/E_1 = C_{12} = -\nu_{12}/E_2 \\ C_{31} &= -\nu_{31}/E_1 = C_{13} = -\nu_{13}/E_3 \\ C_{32} &= -\nu_{32}/E_2 = C_{23} = -\nu_{23}/E_3 \end{aligned} \quad (8.5)$$

The nine independent engineering constants are described as follows:

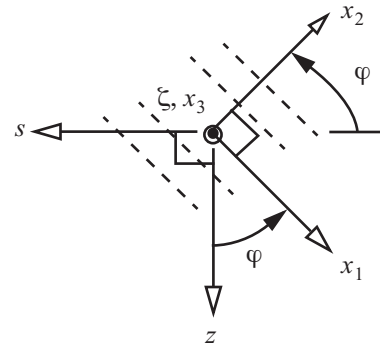
- Moduli of elasticity in the fiber direction, transverse direction, and thickness direction are denoted by  $E_1$ ,  $E_2$ , and  $E_3$ , respectively.
- The principal Poisson's ratios are  $\nu_{21}$ ,  $\nu_{31}$ , and  $\nu_{32}$ .
- Shear moduli in the 2-3 plane, 3-1 plane, and 1-2 plane are denoted by  $G_{23}$ ,  $G_{31}$ , and  $G_{12}$ , respectively.

The three minor Poisson's ratios,  $\nu_{12}$ ,  $\nu_{13}$ , and  $\nu_{23}$ , are determined from symmetry of the compliance matrix. Material characterization tests are conducted to measure the nine independent engineering constants. However, the most accurate measurements are made for the in-plane properties  $E_1$ ,  $E_2$ ,  $\nu_{21}$ , and  $G_{12}$ .

### 8.1.2 Compliance matrix in bar coordinate directions

Consider the thin-walled bar, or beam, analysis presented in article 3.2 to article 3.5. Instead of a the wall composed of a homogeneous, linear elastic material as in article 3.7, we now take the wall to be composed of a fibrous composite material. The fibers are parallel and contained in thin layers, or lamina, that are normal to the thickness coordinate direction  $\zeta$  of the wall. Within a lamina the bar contour coordinate direction  $s$ , and longitudinal direction  $z$ , are not, in general, aligned with the material principal coordinate directions  $x_1$  and  $x_2$ . Define a positive angle  $\varphi$  by the counterclockwise rotation from the positive  $z$ -axis to the positive  $x_1$ -axis as shown in figure. 8.3.

**Fig. 8.3** Material principal directions  $x_1$ ,  $x_2$ , and  $x_3$  with respect to bar axes  $s$ ,  $z$ , and  $\zeta$ .



The direction cosines between the principal material coordinate directions  $x_1$ - $x_2$ - $x_3$  and the bar coordinate directions  $s$ - $z$ - $\zeta$  are listed in table 8.1.

**Table 8.1 Direction cosines**

	s	z	ζ
$x_1$	$\cos(90^\circ + \varphi)$	$\cos\varphi$	0
$x_2$	$\cos(180^\circ - \varphi)$	$\cos(90^\circ + \varphi)$	0
$x_3$	0	0	1

Let  $m = \cos\varphi$  and  $n = \sin\varphi$ . Then, the matrix relations between the coordinate directions are written as

$$\begin{bmatrix} x_1 \\ x_2 \\ x_3 \end{bmatrix} = \underbrace{\begin{bmatrix} -n & m & 0 \\ -m & -n & 0 \\ 0 & 0 & 1 \end{bmatrix}}_{[\lambda]} \begin{bmatrix} s \\ z \\ \zeta \end{bmatrix} \quad \text{and} \quad \begin{bmatrix} s \\ z \\ \zeta \end{bmatrix} = \underbrace{\begin{bmatrix} -n & -m & 0 \\ m & -n & 0 \\ 0 & 0 & 1 \end{bmatrix}}_{[\lambda]^T} \begin{bmatrix} x_1 \\ x_2 \\ x_3 \end{bmatrix} \quad (8.6)$$

Matrix  $[\lambda]$  is an orthogonal matrix so that  $[\lambda][\lambda]^T = [\lambda]^T[\lambda] = [I]$ , and  $\text{Det}[\lambda] = 1$ . In the material coordinate directions the symmetric, Cartesian strain tensor is denoted by the 3X3 matrix  $[\varepsilon]$ , and the symmetric, stress tensor is denoted by the 3X3 matrix  $[\sigma]$ . The elements of these matrices are

$$[\varepsilon] = \begin{bmatrix} \varepsilon_{11} & \gamma_{12}/2 & \gamma_{13}/2 \\ \gamma_{12}/2 & \varepsilon_{22} & \gamma_{23}/2 \\ \gamma_{13}/2 & \gamma_{23}/2 & \varepsilon_{33} \end{bmatrix} \quad \text{and} \quad [\sigma] = \begin{bmatrix} \sigma_{11} & \sigma_{12} & \sigma_{13} \\ \sigma_{12} & \sigma_{22} & \sigma_{23} \\ \sigma_{13} & \sigma_{23} & \sigma_{33} \end{bmatrix}. \quad (8.7)$$

In the bar coordinate directions, the strain matrix  $[\varepsilon']$  and stress matrix  $[\sigma']$  are denoted by

$$[\varepsilon'] = \begin{bmatrix} \varepsilon_{ss} & \gamma_{zs}/2 & \gamma_{\zeta s}/2 \\ \gamma_{zs}/2 & \varepsilon_{zz} & \gamma_{\zeta z}/2 \\ \gamma_{\zeta s}/2 & \gamma_{\zeta z}/2 & \varepsilon_{\zeta\zeta} \end{bmatrix} \quad \text{and} \quad [\sigma'] = \begin{bmatrix} \sigma_{ss} & \sigma_{zs} & \sigma_{\zeta s} \\ \sigma_{zs} & \sigma_{zz} & \sigma_{\zeta z} \\ \sigma_{\zeta s} & \sigma_{\zeta z} & \sigma_{\zeta\zeta} \end{bmatrix}. \quad (8.8)$$

From eq. (A.63) and eq. (A.65) in the appendix the transformation relations between the Cartesian strain matrices are

$$[\varepsilon'] = [\lambda][\varepsilon][\lambda]^T \quad \text{and} \quad [\varepsilon] = [\lambda]^T[\varepsilon'][\lambda]. \quad (8.9)$$

From eq. (A.96) and eq. (A.97) in the appendix the transformation relations between the stress matrices are

$$[\sigma'] = [\lambda][\sigma][\lambda]^T \quad \text{and} \quad [\sigma] = [\lambda]^T[\sigma'][\lambda]. \quad (8.10)$$

After performing the matrix operations indicated for the strain matrices (8.9), we can establish the contracted notation for the transformation of the strain vectors. The results are as follows:



$$\begin{bmatrix} \epsilon_{ss} \\ \epsilon_{zz} \\ \epsilon_{\zeta\zeta} \\ \gamma_{z\zeta} \\ \gamma_{\zeta s} \\ \gamma_{sz} \end{bmatrix} = \underbrace{\begin{bmatrix} n^2 & m^2 & 0 & 0 & 0 & -mn \\ m^2 & n^2 & 0 & 0 & 0 & mn \\ 0 & 0 & 1 & 0 & 0 & 0 \\ 0 & 0 & 0 & -n & -m & 0 \\ 0 & 0 & 0 & m & -n & 0 \\ 2mn & -2mn & 0 & 0 & 0 & -m^2 + n^2 \end{bmatrix}}_{[T_{\epsilon 1}]} \begin{bmatrix} \epsilon_{11} \\ \epsilon_{22} \\ \epsilon_{33} \\ \gamma_{23} \\ \gamma_{31} \\ \gamma_{12} \end{bmatrix} \quad (8.11)$$

$$\begin{bmatrix} \epsilon_{11} \\ \epsilon_{22} \\ \epsilon_{33} \\ \gamma_{23} \\ \gamma_{31} \\ \gamma_{12} \end{bmatrix} = \underbrace{\begin{bmatrix} n^2 & m^2 & 0 & 0 & 0 & mn \\ m^2 & n^2 & 0 & 0 & 0 & -mn \\ 0 & 0 & 1 & 0 & 0 & 0 \\ 0 & 0 & 0 & -n & m & 0 \\ 0 & 0 & 0 & -m & -n & 0 \\ -2mn & 2mn & 0 & 0 & 0 & -m^2 + n^2 \end{bmatrix}}_{[T_{\epsilon 2}]} \begin{bmatrix} \epsilon_{ss} \\ \epsilon_{zz} \\ \epsilon_{\zeta\zeta} \\ \gamma_{z\zeta} \\ \gamma_{\zeta s} \\ \gamma_{sz} \end{bmatrix} \quad (8.12)$$

Note that  $\text{Det}[T_{\epsilon 1}] = \text{Det}[T_{\epsilon 2}] = 1$ , and  $[T_{\epsilon 1}][T_{\epsilon 2}] = [I]$ . That is,  $[T_{\epsilon 2}] = [T_{\epsilon 1}]^{-1}$ . After performing the matrix operations indicated for the stress matrices (8.10), we can establish the contracted notation for the transformation of the stress vectors. The results are as follows:

$$\begin{bmatrix} \sigma_{ss} \\ \sigma_{zz} \\ \sigma_{\zeta\zeta} \\ \sigma_{z\zeta} \\ \sigma_{\zeta s} \\ \sigma_{sz} \end{bmatrix} = \underbrace{\begin{bmatrix} n^2 & m^2 & 0 & 0 & 0 & -2mn \\ m^2 & n^2 & 0 & 0 & 0 & 2mn \\ 0 & 0 & 1 & 0 & 0 & 0 \\ 0 & 0 & 0 & -n & -m & 0 \\ 0 & 0 & 0 & m & -n & 0 \\ mn & -mn & 0 & 0 & 0 & -m^2 + n^2 \end{bmatrix}}_{[T_{\sigma 1}]} \begin{bmatrix} \sigma_{11} \\ \sigma_{22} \\ \sigma_{33} \\ \sigma_{23} \\ \sigma_{31} \\ \sigma_{12} \end{bmatrix} \quad (8.13)$$

$$\begin{bmatrix} \sigma_{11} \\ \sigma_{22} \\ \sigma_{33} \\ \sigma_{23} \\ \sigma_{31} \\ \sigma_{12} \end{bmatrix} = \underbrace{\begin{bmatrix} n^2 & m^2 & 0 & 0 & 0 & 2mn \\ m^2 & n^2 & 0 & 0 & 0 & -2mn \\ 0 & 0 & 1 & 0 & 0 & 0 \\ 0 & 0 & 0 & -n & m & 0 \\ 0 & 0 & 0 & -m & -n & 0 \\ -mn & mn & 0 & 0 & 0 & -m^2 + n^2 \end{bmatrix}}_{[T_{\sigma 2}]} \begin{bmatrix} \sigma_{ss} \\ \sigma_{zz} \\ \sigma_{\zeta\zeta} \\ \sigma_{z\zeta} \\ \sigma_{\zeta s} \\ \sigma_{sz} \end{bmatrix} \quad (8.14)$$

Note that  $\text{Det}[T_{\sigma 1}] = \text{Det}[T_{\sigma 2}] = 1$ , and  $[T_{\sigma 1}][T_{\sigma 2}] = [I]$ . That is,  $[T_{\sigma 2}] = [T_{\sigma 1}]^{-1}$ . Additionally, from the foregoing eqs. (8.11) to (8.14) the following matrix relations can be shown:

$$[T_{\varepsilon 1}]^T = [T_{\sigma 2}] \text{ and } [T_{\varepsilon 2}]^T = [T_{\sigma 1}]. \quad (8.15)$$

The elements of the 6X6 matrices in eq. (8.15) are as follows:

$$\underbrace{\begin{bmatrix} n^2 & m^2 & 0 & 0 & 0 & -mn \\ m^2 & n^2 & 0 & 0 & 0 & mn \\ 0 & 0 & 1 & 0 & 0 & 0 \\ 0 & 0 & 0 & -n & -m & 0 \\ 0 & 0 & 0 & m & -n & 0 \\ 2mn & -2mn & 0 & 0 & 0 & -m^2 + n^2 \end{bmatrix}}_{[T_{\varepsilon 1}]^T}^T = \underbrace{\begin{bmatrix} n^2 & m^2 & 0 & 0 & 0 & 2mn \\ m^2 & n^2 & 0 & 0 & 0 & -2mn \\ 0 & 0 & 1 & 0 & 0 & 0 \\ 0 & 0 & 0 & -n & m & 0 \\ 0 & 0 & 0 & -m & -n & 0 \\ -mn & mn & 0 & 0 & 0 & -m^2 + n^2 \end{bmatrix}}_{[T_{\sigma 2}]}, \text{ and}$$

$$\underbrace{\begin{bmatrix} n^2 & m^2 & 0 & 0 & 0 & mn \\ m^2 & n^2 & 0 & 0 & 0 & -mn \\ 0 & 0 & 1 & 0 & 0 & 0 \\ 0 & 0 & 0 & -n & m & 0 \\ 0 & 0 & 0 & -m & -n & 0 \\ -2mn & 2mn & 0 & 0 & 0 & -m^2 + n^2 \end{bmatrix}}_{[T_{\varepsilon 2}]^T}^T = \underbrace{\begin{bmatrix} n^2 & m^2 & 0 & 0 & 0 & -2mn \\ m^2 & n^2 & 0 & 0 & 0 & 2mn \\ 0 & 0 & 1 & 0 & 0 & 0 \\ 0 & 0 & 0 & -n & -m & 0 \\ 0 & 0 & 0 & m & -n & 0 \\ mn & -mn & 0 & 0 & 0 & -m^2 + n^2 \end{bmatrix}}_{[T_{\sigma 1}]}$$

To determine the off-axis compliance material law we pre-multiply the on-axis material law (8.3) by matrix  $[T_{\varepsilon 1}]$ , followed by substituting of eq. (8.14) for the on-axis stresses on the right-hand side of eq. (8.3). Use the fact that  $[T_{\varepsilon 1}]^T = [T_{\sigma 2}]$  from eq. (8.15). Denote the 6X6 off-axis compliance matrix by  $[C']$  and we find that  $[C'] = [T_{\varepsilon 1}][C][T_{\varepsilon 1}]^T$ . The form of the off-axis material law is

$$\begin{bmatrix} \varepsilon_{ss} \\ \varepsilon_{zz} \\ \varepsilon_{\zeta\zeta} \\ \gamma_{z\zeta} \\ \gamma_{\zeta s} \\ \gamma_{sz} \end{bmatrix} = \begin{bmatrix} C'_{11} & C'_{12} & C'_{13} & 0 & 0 & C'_{16} \\ C'_{21} & C'_{22} & C'_{23} & 0 & 0 & C'_{26} \\ C'_{31} & C'_{32} & C'_{33} & 0 & 0 & C'_{36} \\ 0 & 0 & 0 & C'_{44} & C'_{45} & 0 \\ 0 & 0 & 0 & C'_{54} & C'_{55} & 0 \\ C'_{61} & C'_{62} & C'_{63} & 0 & 0 & C'_{66} \end{bmatrix} \begin{bmatrix} \sigma_{ss} \\ \sigma_{zz} \\ \sigma_{\zeta\zeta} \\ \sigma_{z\zeta} \\ \sigma_{\zeta s} \\ \sigma_{sz} \end{bmatrix}. \quad (8.16)$$

Matrix  $[C']$  is symmetric with the compliance coefficients in terms of the engineering constants and the directions cosines given by eq. (8.17) to (8.23) below.

$$C'_{11} = \frac{m^4}{E_2} + \frac{m^2 n^2}{G_{12}} + \frac{n^4 - 2m^2 n^2 \nu_{21}}{E_1} \quad C'_{21} = C'_{12} = \frac{m^2 n^2 (G_{12} - E_2)}{E_2 G_{12}} + \frac{m^2 n^2 - (m^4 + n^4) \nu_{21}}{E_1} \quad (8.17)$$

$$C'_{31} = C'_{13} = \frac{-n^2 \nu_{31}}{E_1} - \frac{m^2 \nu_{32}}{E_2} \quad C'_{61} = C'_{16} = mn \left( \frac{-2m^2}{E_2} + \frac{m^2 - n^2}{G_{12}} - \frac{2m^2 \nu_{21}}{E_1} + \frac{2n^2 (1 + \nu_{21})}{E_1} \right) \quad (8.18)$$

$$C'_{22} = \frac{m^2 n^2}{G_{12}} + \frac{n^4}{E_2} + \frac{m^4 - 2m^2 n^2 \nu_{21}}{E_1} \quad C'_{23} = C'_{32} = \frac{-m^2 \nu_{31}}{E_1} - \frac{n^2 \nu_{32}}{E_2} \quad (8.19)$$

$$C'_{26} = C'_{62} = mn \left( \frac{-2n^2}{E_2} + \frac{n^2 - m^2}{G_{12}} + \frac{2m^2 (1 + \nu_{21}) - 2n^2 \nu_{21}}{E_1} \right) \quad (8.20)$$

$$C'_{33} = \frac{1}{E_3} \quad C'_{63} = C'_{36} = 2mn \left( \frac{\nu_{32}}{E_2} - \frac{\nu_{31}}{E_1} \right) \quad (8.21)$$

$$C'_{44} = \frac{m^2}{G_{13}} + \frac{n^2}{G_{23}} \quad C'_{54} = C'_{45} = mn \left( \frac{1}{G_{13}} - \frac{1}{G_{23}} \right) \quad C'_{55} = \frac{m^2}{G_{23}} + \frac{n^2}{G_{13}} \quad (8.22)$$

$$C'_{66} = \frac{(m^2 - n^2)^2}{G_{12}} + \frac{4m^2 n^2 (E_1 + (1 + 2\nu_{21})E_2)}{E_1 E_2} \quad (8.23)$$

### 8.1.3 Plane stress

Since composites used in many structural applications are thin plates or thin shells, the assumption of a plane stress state as used plate and shell theory is also made for a composite plate. In figure. 8.2 the in-plane stress components are  $\sigma_{11}$ ,  $\sigma_{22}$ , and  $\sigma_{12}$ . Thus, the following stress components are assumed negligible with respect to the in-plane stress components and set equal to zero in eq. (8.3):

$$\sigma_{33} = \sigma_{31} = \sigma_{13} = \sigma_{32} = \sigma_{23} = 0. \quad (8.24)$$

Hence, the compliance form of the orthotropic material law for a unidirectional lamina subject to plane stress is

$$\begin{bmatrix} \epsilon_{11} \\ \epsilon_{22} \\ \gamma_{12} \end{bmatrix} = \underbrace{\begin{bmatrix} C_{11} & C_{12} & 0 \\ C_{21} & C_{22} & 0 \\ 0 & 0 & C_{66} \end{bmatrix}}_{[C]} \begin{bmatrix} \sigma_{11} \\ \sigma_{22} \\ \sigma_{12} \end{bmatrix} = \begin{bmatrix} 1/E_1 & -\nu_{12}/E_2 & 0 \\ -\nu_{21}/E_1 & 1/E_2 & 0 \\ 0 & 0 & 1/G_{12} \end{bmatrix} \begin{bmatrix} \sigma_{11} \\ \sigma_{22} \\ \sigma_{12} \end{bmatrix}, \quad (8.25)$$

and the thickness normal strain is

$$\epsilon_{33} = C_{31}\sigma_{11} + C_{32}\sigma_{22}. \quad (8.26)$$

The stress-strain form of the material law (8.25) is written as

$$\begin{bmatrix} \sigma_{11} \\ \sigma_{22} \\ \sigma_{12} \end{bmatrix} = \underbrace{\begin{bmatrix} Q_{11} & Q_{12} & 0 \\ Q_{21} & Q_{22} & 0 \\ 0 & 0 & Q_{66} \end{bmatrix}}_{[Q]} \begin{bmatrix} \epsilon_{11} \\ \epsilon_{22} \\ \gamma_{12} \end{bmatrix} = \begin{bmatrix} E_1/(1 - \nu_{21}\nu_{12}) & (\nu_{12}E_1)/(1 - \nu_{21}\nu_{12}) & 0 \\ (\nu_{21}E_2)/(1 - \nu_{21}\nu_{12}) & E_2/(1 - \nu_{21}\nu_{12}) & 0 \\ 0 & 0 & G_{12} \end{bmatrix} \begin{bmatrix} \epsilon_{11} \\ \epsilon_{22} \\ \gamma_{12} \end{bmatrix}, \quad (8.27)$$

where the matrix  $[Q]$  is called the reduced stiffness matrix. Matrix  $[Q]$  is symmetric since  $\nu_{21}E_2 = \nu_{12}E_1$  (refer to eq. (8.5)). It follows from eq. (8.3) that the transverse shear strains  $\gamma_{23} = \gamma_{31} = 0$ , which leads to transverse shear strains  $\gamma_{z\zeta} = \gamma_{\zeta s} = 0$  by eq. (8.11). Also, the normal strain  $\epsilon_{\zeta\zeta} = \epsilon_{33}$ . From eq. (8.13) the stresses  $\sigma_{\zeta\zeta} = \sigma_{z\zeta} = \sigma_{\zeta s} = 0$ .

Transform eq. (8.27) to an off-axis material law as follows: For plane stress the stress transformation equation (8.13) reduces to

$$\begin{bmatrix} \sigma_{ss} \\ \sigma_{zz} \\ \sigma_{sz} \end{bmatrix} = \underbrace{\begin{bmatrix} n^2 & m^2 & -2mn \\ m^2 & n^2 & 2mn \\ mn & -mn & (-m^2 + n^2) \end{bmatrix}}_{[T_{\sigma 1}]} \begin{bmatrix} \sigma_{11} \\ \sigma_{22} \\ \sigma_{12} \end{bmatrix} \quad (8.28)$$

and the strain transformation eq. (8.11) reduces to

$$\begin{bmatrix} \epsilon_{11} \\ \epsilon_{22} \\ \gamma_{12} \end{bmatrix} = \underbrace{\begin{bmatrix} n^2 & m^2 & mn \\ m^2 & n^2 & -mn \\ -2mn & 2mn & (-m^2 + n^2) \end{bmatrix}}_{[T_{\epsilon 2}]} \begin{bmatrix} \epsilon_{ss} \\ \epsilon_{zz} \\ \gamma_{sz} \end{bmatrix} \quad (8.29)$$

Pre-multiply eq. (8.27)  $[T_{\sigma 1}]$ , and substitute the strain transformation eq. (8.29) on the right-hand side of eq.

(8.27). Use the fact that  $[T_{\epsilon 2}] = [T_{\sigma 1}]^T$  from eq. (8.15). These matrix manipulations result in the off-axis material law in plane stress given by

$$\begin{bmatrix} \sigma_{ss} \\ \sigma_{zz} \\ \sigma_{sz} \end{bmatrix} = \underbrace{\begin{bmatrix} \bar{Q} \end{bmatrix}}_{[Q]} \begin{bmatrix} \epsilon_{ss} \\ \epsilon_{zz} \\ \gamma_{sz} \end{bmatrix} = \begin{bmatrix} \bar{Q}_{11} & \bar{Q}_{12} & \bar{Q}_{16} \\ \bar{Q}_{21} & \bar{Q}_{22} & \bar{Q}_{26} \\ \bar{Q}_{61} & \bar{Q}_{62} & \bar{Q}_{66} \end{bmatrix} \begin{bmatrix} \epsilon_{ss} \\ \epsilon_{zz} \\ \gamma_{sz} \end{bmatrix} \quad (8.30)$$

where the transformed reduced stiffness matrix is given by  $\begin{bmatrix} \bar{Q} \end{bmatrix} = [T_{\sigma 1}][Q][T_{\sigma 1}]^T$ . Since the on-axis reduced stiffness matrix  $[Q]$  is symmetric, it follows from these matrix relations that the transformed stiffness matrix is symmetric ( $\begin{bmatrix} \bar{Q} \end{bmatrix}^T = \begin{bmatrix} \bar{Q} \end{bmatrix}$ ). Elements of the transformed reduced stiffness matrix in terms of the reduced matrix elements are given by

$$\begin{bmatrix} \bar{Q}_{11} \\ \bar{Q}_{22} \\ \bar{Q}_{21} \\ \bar{Q}_{66} \\ \bar{Q}_{16} \\ \bar{Q}_{26} \end{bmatrix} = \begin{bmatrix} n^4 & m^4 & 2m^2n^2 & 4m^2n^2 \\ m^4 & n^4 & 2m^2n^2 & 4m^2n^2 \\ m^2n^2 & m^2n^2 & (m^4 + n^4) & -4m^2n^2 \\ m^2n^2 & m^2n^2 & -2m^2n^2 & (-m^2 + n^2)^2 \\ mn^3 & -m^3n & mn(m^2 - n^2) & 2mn(m^2 - n^2) \\ m^3n & -mn^3 & -mn(m^2 - n^2) & -2mn(m^2 - n^2) \end{bmatrix} \begin{bmatrix} Q_{11} \\ Q_{22} \\ Q_{21} \\ Q_{66} \end{bmatrix}. \quad (8.31)$$

#### 8.1.4 Nomenclature of composite materials

Composite materials are identified by the name of the fiber followed by the name of the matrix. For example, AS4/3501-6 denotes the carbon fiber AS4 and the epoxy matrix 3501-6. The data in table 8.2 is taken from Herakovich (1998, p.14), and it lists typical properties for AS4/3501-6 and T300/5208 carbon fiber-reinforced epoxy composites.

**Table 8.2 Material properties of selected CFRP lamina**

Property	Units	AS4/3501-6	T300/5208
Axial modulus $E_1$	GPa	148	132
	Msi	21.5	19.2
Transverse modulus $E_2$	GPa	10.5	10.8
	Msi	1.46	1.56
Major Poisson's ratio $\nu_{21}$	dimensionless	0.30	0.24
Major Poisson's ratio $\nu_{23}$	dimensionless	0.59	0.59
Shear modulus $G_{12}$	GPa	5.61	5.65
	Msi	0.81	0.82
Shear modulus $G_{23}$	GPa	3.17	3.38
	Msi	0.46	0.49
Density	$g/cm^3$	1.52	1.54
	lb./in. <sup>3</sup>	0.055	0.056
Ply thickness $t_{ply}$	mm	0.127	0.127
	in.	0.005	0.005
Fiber volume fraction $V_f$	dimensionless	0.62	0.62

### Example 8.1 Transformed reduced stiffness matrix for an off-axis ply

Determine the transformed reduced stiffness matrix of T300/5208 carbon/epoxy for a 30-degree off-axis lamina in U.S. customary units.

**Solution.** From table 8.2  $E_1 = 19.2 \text{ Msi}$ ,  $E_2 = 1.56 \text{ Msi}$ ,  $\nu_{21} = 0.24$ , and  $G_{12} = 0.82 \text{ Msi}$ . The minor Poisson's ratio is  $\nu_{12} = 0.24[(1.56 \text{ Msi})/(19.2 \text{ Msi})] = 0.0195$ . The reduced stiffness matrix is computed from eq. (8.30) and eq. (8.31); i.e.,

$$[Q] = \begin{bmatrix} 19.3 & 0.376 & 0 \\ 0.376 & 1.57 & 0 \\ 0 & 0 & 0.82 \end{bmatrix} \text{ Msi.} \quad (\text{a})$$

The transformed reduced stiffness matrix is given by  $[\bar{Q}] = [T_{\sigma 1}][Q][T_{\sigma 1}]^T$ , the reduced stiffness by eq.

(8.27), and the transform matrix  $[T_{\sigma 1}]$  by eq. (8.28). The matrix product is

$$[\bar{Q}] = \begin{bmatrix} 1/4 & 3/4 & -\sqrt{3}/2 \\ 3/4 & 1/4 & \sqrt{3}/2 \\ \sqrt{3}/4 & -\sqrt{3}/4 & -1/2 \end{bmatrix} \begin{bmatrix} 19.3 & 0.376 & 0 \\ 0.376 & 1.57 & 0 \\ 0 & 0 & 0.82 \end{bmatrix} \begin{bmatrix} 1/4 & 3/4 & \sqrt{3}/4 \\ 3/4 & 1/4 & -\sqrt{3}/4 \\ -\sqrt{3}/2 & \sqrt{3}/2 & -1/2 \end{bmatrix}, \quad (\text{b})$$

and the result is

$$[\bar{Q}] = \begin{bmatrix} 2.84537 & 3.53313 & 2.01589 \\ 3.53313 & 11.7104 & 5.66142 \\ 2.01589 & 5.66142 & 3.97713 \end{bmatrix} \text{ Msi.} \quad (\text{c})$$

### 8.1.5 Laminated wall

Laminates are made by stacking the unidirectional lamina, also called plies, at different fiber orientations. The plies are usually bound together by the same matrix material that is used within the lamina. Laminates are designated by the ply angle stacking sequence. A  $[45 - 45 \ 0 \ 90]$  stacking sequence denotes a 4-ply laminate with plies at 45,  $-45$ , 0, and 90 degrees with respect to the longitudinal  $z$ -axis. A  $[45 - 45 \ 0 \ 90]_2$  stacking sequence denotes an 8-ply laminate with plies at 45,  $-45$ , 0, 90, 45,  $-45$ , 0, and 90 degrees. A  $[45 - 45 \ 0 \ 90]_s$  stacking sequence denotes an 8-ply symmetric laminate with plies at 45,  $-45$ , 0, 90, 90, 0,  $-45$ , and 45 degrees. The assumptions of lamination theory are

- The laminate consists of perfectly bonded layers or lamina.
- Each layer is a homogeneous material with known effective properties.
- Each layer is in a state of plane stress.
- Individual layers can be isotropic or orthotropic.

Consistent with thin-walled bar theory in chapter 3, we **assume that the strains  $\epsilon_{zz}$ ,  $\epsilon_{ss}$ , and  $\gamma_{zs}$  are spatially uniform through the thickness of the wall**. That is, there is no local bending of the laminated wall. The laminate can stretch and shear in-plane as membrane. For a laminate of  $Np$ -plies, the material law for the  $k$ -th ply, where  $k = 1, 2, \dots, Np$ , is obtained from eq. (8.30) as

$$\begin{bmatrix} \sigma_{ss} \\ \sigma_{zz} \\ \sigma_{sz} \end{bmatrix}^{(k)} = \begin{bmatrix} \bar{Q}_{11} & \bar{Q}_{12} & \bar{Q}_{16} \\ \bar{Q}_{21} & \bar{Q}_{22} & \bar{Q}_{26} \\ \bar{Q}_{61} & \bar{Q}_{62} & \bar{Q}_{66} \end{bmatrix}^{(k)} \begin{bmatrix} \epsilon_{ss} \\ \epsilon_{zz} \\ \gamma_{sz} \end{bmatrix} \quad k = 1, 2, \dots, Np. \quad (8.32)$$

Even though the strains are uniform through the thickness of the wall, note that the stresses are piecewise constant through the thickness of the wall since the transformed reduced stiffness matrix changes from ply to ply. Let the origin of the thickness coordinate  $\zeta$  be at the midplane of the laminate, such that  $-t/2 \leq \zeta \leq t/2$ , where  $t$  denotes the total thickness of the laminated wall. The stress resultant  $n_s$ , the axial stress resultant  $n_z$ , and the shear flow  $q$  are defined by integrals through the thickness of the wall of the corresponding stresses; i.e.,

$$\begin{bmatrix} n_s \\ n_z \\ q \end{bmatrix} = \int_{-t/2}^{t/2} \begin{bmatrix} \sigma_{ss} \\ \sigma_{zz} \\ \sigma_{zs} \end{bmatrix} d\zeta = \sum_{k=1}^{Np} \left( \int_{\zeta_k}^{\zeta_{k+1}} \begin{bmatrix} \sigma_{ss} \\ \sigma_{zz} \\ \sigma_{zs} \end{bmatrix}^{(k)} d\zeta \right), \quad (8.33)$$

where  $\zeta = \zeta_k$  at the bottom of the  $k$ -th ply, and  $\zeta = \zeta_{k+1}$  at the top of the  $k$ -th ply. Denote the thickness of the  $k$ -th ply by  $t_k$  such that  $\zeta_{k+1} - \zeta_k = t_k$ . Substitute for the stresses from Hooke's law (8.32) into eq. (8.33) to get

$$\begin{bmatrix} n_s \\ n_z \\ q \end{bmatrix} = \sum_{k=1}^{Np} \left\{ \int_{\zeta_k}^{\zeta_{k+1}} \begin{bmatrix} \bar{Q}_{11} & \bar{Q}_{12} & \bar{Q}_{16} \\ \bar{Q}_{21} & \bar{Q}_{22} & \bar{Q}_{26} \\ \bar{Q}_{61} & \bar{Q}_{62} & \bar{Q}_{66} \end{bmatrix}^{(k)} d\zeta \right\} \begin{bmatrix} \epsilon_{ss} \\ \epsilon_{zz} \\ \gamma_{sz} \end{bmatrix}. \quad (8.34)$$

The last result is written as

$$\begin{bmatrix} n_s \\ n_z \\ q \end{bmatrix} = \underbrace{\begin{bmatrix} A_{11} & A_{12} & A_{16} \\ A_{21} & A_{22} & A_{26} \\ A_{61} & A_{62} & A_{66} \end{bmatrix}}_{[A]}, \begin{bmatrix} \epsilon_{ss} \\ \epsilon_{zz} \\ \gamma_{sz} \end{bmatrix}, \quad (8.35)$$

where  $[A]$  is the in-plane stiffness matrix. Elements of the in-plane stiffness matrix are computed by the sum

$$\begin{bmatrix} A_{11} & A_{12} & A_{16} \\ A_{21} & A_{22} & A_{26} \\ A_{61} & A_{62} & A_{66} \end{bmatrix} = \sum_{k=1}^{Np} \begin{bmatrix} \bar{Q}_{11} & \bar{Q}_{12} & \bar{Q}_{16} \\ \bar{Q}_{21} & \bar{Q}_{22} & \bar{Q}_{26} \\ \bar{Q}_{61} & \bar{Q}_{62} & \bar{Q}_{66} \end{bmatrix}^{(k)} t_k. \quad (8.36)$$

Stiffness elements  $A_{11}$  and  $A_{22}$  correspond to in-plane extensional stiffnesses in the  $s$ - and  $z$ -directions, respectively. Element  $A_{66}$  corresponds to a shear stiffness in the  $s$ - $z$  plane, stiffnesses  $A_{21} = A_{12}$  are Poisson's type terms, and stiffnesses  $A_{61} = A_{16}$  and  $A_{62} = A_{26}$  couple in-plane shear and extension. The in-plane stiffness matrix depends on the content of the layers in the laminate, and is independent of the stacking sequence of the layers through the thickness of the laminate.

### Example 8.2 In-plane stiffness matrix for a laminate with two plies

Consider a two-ply  $[\varphi -\varphi]$  laminate with plies of equal thickness  $t/2$ .

- (a) Determine the  $[A]$  matrix  
 (b) Evaluate the  $[A]$  matrix for T300/5208 with  $\varphi = 30^\circ$  and  $t/2 = 0.005$  in.

**Solution to part (a).** The transformed reduced stiffnesses are given by eq. (8.31) in which  $m = \cos\varphi$  and  $n = \sin\varphi$ . Note that stiffnesses  $\bar{Q}_{11}$ ,  $\bar{Q}_{22}$ ,  $\bar{Q}_{66}$ , and  $\bar{Q}_{21}$  are even functions of the ply angle  $\varphi$ , and stiffnesses  $\bar{Q}_{61}$  and  $\bar{Q}_{62}$  are odd functions of  $\varphi$ . Thus,

$$[A] = \begin{bmatrix} \bar{Q}_{11}(\varphi) & \bar{Q}_{12}(\varphi) & \bar{Q}_{16}(\varphi) \\ \bar{Q}_{21}(\varphi) & \bar{Q}_{22}(\varphi) & \bar{Q}_{26}(\varphi) \\ \bar{Q}_{61}(\varphi) & \bar{Q}_{62}(\varphi) & \bar{Q}_{66}(\varphi) \end{bmatrix} \frac{t}{2} + \begin{bmatrix} \bar{Q}_{11}(\varphi) & \bar{Q}_{12}(\varphi) & -(\bar{Q}_{16}(\varphi)) \\ \bar{Q}_{21}(\varphi) & \bar{Q}_{22}(\varphi) & -(\bar{Q}_{26}(\varphi)) \\ -(\bar{Q}_{61}(\varphi)) & -(\bar{Q}_{62}(\varphi)) & \bar{Q}_{66}(\varphi) \end{bmatrix} \frac{t}{2}$$

$$[A] = \begin{bmatrix} \bar{Q}_{11}(\varphi) & \bar{Q}_{12}(\varphi) & 0 \\ \bar{Q}_{21}(\varphi) & \bar{Q}_{22}(\varphi) & 0 \\ 0 & 0 & \bar{Q}_{66}(\varphi) \end{bmatrix} t.$$

**Solution to part (b).** From the T300/5208 example on page 231  $\bar{Q}_{11}(30) = 2.843$  Msi,  $\bar{Q}_{22}(30) = 11.7$  Msi,  $\bar{Q}_{66}(30) = 3.975$  Msi, and  $\bar{Q}_{21}(30) = 3.531$  Msi. Thus,

$$[A] = \begin{bmatrix} 2.843 & 3.531 & 0 \\ 3.531 & 11.7 & 0 \\ 0 & 0 & 3.975 \end{bmatrix} (10^6 \text{ lb./in.}^2)(0.01 \text{ in.}) = \begin{bmatrix} 28.43 & 35.3 & 0 \\ 35.3 & 117. & 0 \\ 0 & 0 & 39.7 \end{bmatrix} 10^3 \text{ lb./in.} \blacksquare.$$

### 8.1.6 Balanced and specially orthotropic laminates

A laminate consisting of off-axis plies with positive fiber angles  $\varphi_i$  and off-axis plies with negative fiber angles  $-\varphi_i$ ,  $i = 1, 2, 3, \dots, i_{max}$ , with each  $\varphi_i$ -ply and  $-\varphi_i$ -ply having the same thickness and material properties, is called a **balanced laminate**. For example, a stacking sequence  $[30/-30]_{2S}$  is a balanced laminate consisting of eight plies if each  $30^\circ$ -ply and  $-30^\circ$ -ply have the same thickness and material properties. For a balanced lami-



nate the in-plane stiffness coefficients  $A_{16} = A_{61} = 0$ , and  $A_{26} = A_{62} = 0$  as example 8.2 illustrates. The in-plane material law for a balanced laminate reduces to the form

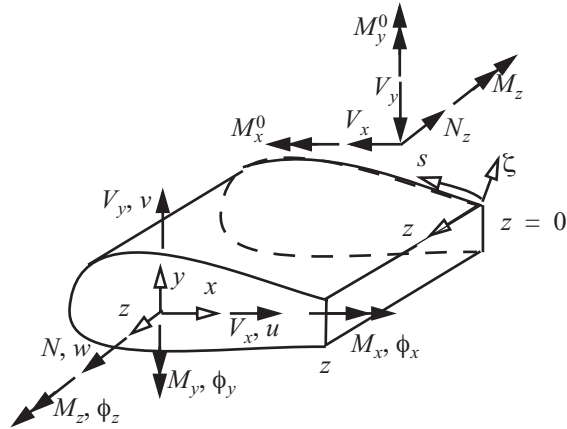
$$\begin{bmatrix} n_s \\ n_z \\ q \end{bmatrix} = \begin{bmatrix} A_{11} & A_{12} & 0 \\ A_{21} & A_{22} & 0 \\ 0 & 0 & A_{66} \end{bmatrix} \begin{bmatrix} \epsilon_{ss} \\ \epsilon_{zz} \\ \gamma_{zs} \end{bmatrix}. \quad (8.37)$$

In eq. (8.37) resultants  $n_s$  and  $n_z$  are independent of the shear strain  $\gamma_{zs}$ , and the shear flow  $q$  is independent of the normal strains  $\epsilon_{ss}$  and  $\epsilon_{zz}$ . That is, there is no coupling between in-plane extension and shear. Laminates whose material law is given by (8.37) are also said to be **specialy orthotropic**. Laminates consisting of only  $0^\circ$  and  $90^\circ$  plies are specially orthotropic laminates, since the product  $mn = \cos\varphi \sin\varphi = 0$  in the last two rows of (8.31) results in  $\bar{Q}_{16} = \bar{Q}_{26} = 0$  for these laminates. Hence, a  $[0/90]$  laminate has coupling stiffnesses  $A_{16} = A_{26} = 0$  as can be recognized from eq. (8.36). Another example of a specially orthotropic laminate is a stacking sequence  $[\pm 45/0/90]_S$ .

## 8.2 Composite thin-walled bar with a closed cross-sectional contour

The analysis in this section was published by Johnson, et al., (2001), and it is also reviewed by Vasiliev and Morozov (2013). We consider free bending and torsion of a thin-walled bar with a closed cross-sectional contour as depicted in figure. 8.4. The laminated wall consists of unidirectional FRP layers. The external traction compo-

**Fig. 8.4** Closed cross-sectional bar subject to free bending and torsion.



nents acting on the lateral surface of the bar  $p_n(s, z)$ ,  $p_s(s, z)$ , and  $p_z(s, z)$  appearing in eq. (3.42) on page 41 are prescribed to be zero for all values of  $s$  and  $z$ . Thus, distributed force intensities  $f_x = f_y = f_z = 0$  in eq. (3.42), and distributed moment intensities  $m_x = m_y = m_z = 0$  in eq. (3.45) all vanish. The differential equilibrium equations (3.53), (3.56), (3.54), and (3.61) on page 42 are satisfied for

$$\frac{dN}{dz} = 0 \quad \frac{dV_x}{dz} = 0 \quad \frac{dV_y}{dz} = 0 \quad \frac{dM_z}{dz} = 0 \quad 0 \leq z \leq L. \quad (8.38)$$

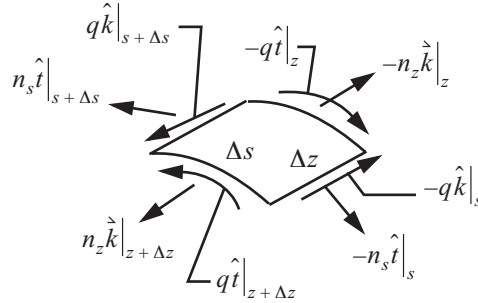
Hence, the axial force  $N$ , shear forces  $V_x$  and  $V_y$ , and the torque  $M_z$  are uniform along the length  $L$  of the bar. Bending moment equilibrium equations (3.55) and (3.57) on page 43 are satisfied by

$$M_x = M_x^0 + V_y z \quad M_y = M_y^0 + V_x z \quad 0 \leq z \leq L, \quad (8.39)$$

where  $M_x^0$  and  $M_y^0$  are the bending moments acting on the cross section at  $z = 0$ .

Consider a free body diagram of the stress resultants acting on a segment of the wall with dimensions  $\Delta s$ -by- $\Delta z$  is shown in figure. 8.5.

**Fig. 8.5** Stress resultants acting on an element of the wall



Force equilibrium leads to

$$[n_z \Delta s \hat{k}|_{z+\Delta z} - n_z \Delta s \hat{k}|_z] + [q \Delta z \hat{k}|_{s+\Delta s} - q \Delta z \hat{k}|_s] + [q \Delta s \hat{t}|_{z+\Delta z} - q \Delta s \hat{t}|_z] + [n_s \Delta z \hat{t}|_{s+\Delta s} - n_s \Delta z \hat{t}|_s] = 0. \quad (8.40)$$

Expand the functions  $n(s, z)$ ,  $q(s, z)$ , and  $n_s(s, z)$  in a Taylor series about  $s$  and  $z$  to get

$$\left(n_z + \frac{\partial n_z}{\partial z} \Delta z - n_z\right) \Delta s \hat{k} + \left(q + \frac{\partial q}{\partial s} \Delta s - q\right) \Delta z \hat{k} + \left(q + \frac{\partial q}{\partial z} \Delta z - q\right) \Delta s \hat{t} + \left(n_s \hat{t} + \frac{\partial n_s}{\partial s} \Delta s - n_s \hat{t}\right) \Delta z + O(\Delta s^2, \Delta z^2) = 0. \quad (8.41)$$

Division of eq. (8.41) by the product  $\Delta s \cdot \Delta z$ , followed by taking the limit as  $\Delta s \rightarrow 0$  and  $\Delta z \rightarrow 0$  leads to the differential equations

$$\left(\frac{\partial n_z}{\partial z} + \frac{\partial q}{\partial s}\right) \hat{k} + \left(\frac{\partial q}{\partial z} + \frac{\partial n_s}{\partial s}\right) \hat{t} + n_s \frac{\partial \hat{t}}{\partial s} = 0.$$

From eq. (3.6) on page 34 the derivative of the unit tangent vector is  $\frac{\partial \hat{t}}{\partial s} = \frac{-\hat{n}}{R_s}$ , where  $R_s$  is the radius of curvature of the contour. The differential equations of equilibrium at coordinates  $s$  and  $z$  in the wall are

$$\frac{\partial n_z}{\partial z} + \frac{\partial q}{\partial s} = 0 \quad \frac{\partial q}{\partial z} + \frac{\partial n_s}{\partial s} = 0 \quad \frac{-n_s}{R_s} = 0. \quad (8.42)$$

From the last two equations in (8.42) we get

$$n_s = 0 \quad \frac{\partial q}{\partial z} = 0. \quad (8.43)$$

That is, the circumferential stress resultant vanishes and the shear flow is independent of the longitudinal coordinate  $z$ .

### 8.2.1 Anisotropic Hooke's law for the cross section

Set  $n_s = 0$  in eq. (8.35), and solve for the normal strain  $\epsilon_{zz}$  to eliminate it in the material law. We write the resulting material law in several forms to be used in subsequent developments:

$$n_z = B\epsilon_{zz} + bq \quad q = B_s\gamma_{sz} + B_z\epsilon_{zz}, \text{ and} \quad (8.44)$$

$$\epsilon_{zz} = \frac{1}{B}(n_z - bq) \quad \gamma_{sz} = \frac{1}{B_s}(aq - bn_z). \quad (8.45)$$

The coefficients in the previous equations are

$$B = A_{22} - A_{12}A_{21}/A_{11} - bB_z, \quad (8.46)$$

$$B_s = A_{66} - A_{61}A_{16}/A_{11} \quad B_z = A_{62} - A_{12}A_{61}/A_{11}, \text{ and} \quad (8.47)$$

$$a = \frac{1}{B_s}(A_{22} - A_{12}A_{21}/A_{11}) \quad b = B_z/B_s. \quad (8.48)$$

The stiffness parameters  $b$  and  $B_z$  represent the shear-extension coupling of the laminated wall, since they are directly related to stiffnesses  $A_{61}$  and  $A_{62}$  by eqs. (8.47) and (8.48). In a specially orthotropic laminate  $A_{61} = A_{62} = 0$ , so  $b = B_z = 0$ . There is no material coupling between shear and extension in a specially orthotropic laminate.

The second assumption is traditional for the beam theory and states that the axial strain is a linear function of coordinates  $x$  and  $y$ . From eq. (3.30) on page 38 the axial normal strain along the contour ( $\zeta = 0$ ) is

$$\epsilon_{zz} = \frac{dw}{dz} + y(s)\frac{d\phi_x}{dz} + x(s)\frac{d\phi_y}{dz}. \quad (8.49)$$

where  $w(z)$  is the axial displacement of the cross section,  $\phi_x(z)$  is the rotation of the cross section about the  $x$ -axis, and  $\phi_y(z)$  is the rotation of the cross section about the negative  $y$ -axis. Refer to figure. 8.5. Substitute eq. (8.49) for the strain in the first equation of (8.44) to get the normal stress resultant as

$$n_z = B\left(\frac{dw}{dz} + y(s)\frac{d\phi_x}{dz} + x(s)\frac{d\phi_y}{dz}\right) + bq. \quad (8.50)$$

Substitute the previous expression for the normal stress resultant into the definition of the bar resultant  $N$  in eq. (3.39) on page 40 to get

$$N = \oint n_z ds = S\left(\frac{dw}{dz}\right) + S_x\left(\frac{d\phi_x}{dz}\right) + S_y\left(\frac{d\phi_y}{dz}\right) + \oint (bq) ds, \quad (8.51)$$

where

$$S = \oint B(s) ds \quad S_x = \oint B(s)y(s) ds \quad S_y = \oint B(s)x(s) ds. \quad (8.52)$$

In eq. (8.52) the modulus-weighted extensional stiffness of the cross section of the beam is denoted by  $S$ , the modulus-weighted first moment of the cross-sectional area about the  $x$ -axis by  $S_x$ , and the modulus-weighted first moment of the cross-sectional area about the  $y$ -axis by  $S_y$ . We now locate the origin of the  $x$ - $y$  coordinates at

the modulus-weighted centroid of the cross section. Let  $x(s) = X(s) - X_c$  and  $y(s) = Y(s) - Y_c$ , where  $X(s)$  and  $Y(s)$  are the Cartesian coordinates of the contour with respect to an arbitrary origin at point  $O$  (see Fig. 3.1 on page 31). The coordinates  $(X_c, Y_c)$  of the modulus-weighted centroid are determined from

$$S_x = 0 = \oint B(s)Y(s)ds - Y_c S \quad S_y = 0 = \oint B(s)X(s)ds - X_c S. \quad (8.53)$$

Since  $S_x = S_y = 0$ , eq. (8.51) is written as

$$\bar{N} = S\left(\frac{dw}{dz}\right) \quad \text{where} \quad \bar{N} = N - \oint (bq)ds. \quad (8.54)$$

The bending moments  $M_x$  and  $M_y$  acting in the cross section are determined from the normal stress resultant  $n_z$  by

$$M_x = \oint (yn_z)ds \quad M_y = \oint (xn_z)ds. \quad (8.55)$$

Substitute eq. (8.50) for the normal stress resultant into these expressions for the bending moments to get

$$M_x = D_{xx}\left(\frac{d\phi_x}{dz}\right) + D_{xy}\left(\frac{d\phi_y}{dz}\right) + \oint (ybq)ds \quad M_y = D_{xy}\left(\frac{d\phi_x}{dz}\right) + D_{yy}\left(\frac{d\phi_y}{dz}\right) + \oint (xbq)ds. \quad (8.56)$$

The modulus-weighted second moments of the cross section appearing in eq. (8.56) are defined by

$$\begin{bmatrix} D_{xx} & D_{yy} & D_{xy} \end{bmatrix} = \oint [y^2 \ x^2 \ xy] B ds. \quad (8.57)$$

Solve for the gradients of the bending rotations eq. (8.56) and write the result as

$$\begin{bmatrix} \frac{d\phi_x}{dz} \\ \frac{d\phi_y}{dz} \end{bmatrix} = k \begin{bmatrix} \frac{1}{D_{xx}} & \frac{-n_x}{D_{yy}} \\ \frac{-n_y}{D_{xx}} & \frac{1}{D_{yy}} \end{bmatrix} \begin{bmatrix} \bar{M}_x \\ \bar{M}_y \end{bmatrix}, \quad (8.58)$$

where

$$n_x = \frac{D_{xy}}{D_{xx}} \quad n_y = \frac{D_{xy}}{D_{yy}} \quad k = \frac{1}{1 - n_x n_y}, \quad (8.59)$$

and

$$\bar{M}_x = M_x - \oint (ybq)ds \quad \bar{M}_y = M_y - \oint (xbq)ds. \quad (8.60)$$

Substitute eq. (8.54) for the axial displacement gradient, and eq. (8.58) for the bending rotation gradients, into eq. (8.50) to express the normal stress resultant as

$$n_z = \frac{B}{S}\bar{N} + B\bar{y}(s)\frac{k}{D_{xx}}\bar{M}_x + B\bar{x}(s)\frac{k}{D_{yy}}\bar{M}_y + bq, \quad (8.61)$$

where

$$\bar{x}(s) = x(s) - n_x y(s) \quad \bar{y}(s) = y(s) - n_y x(s). \quad (8.62)$$

### 8.2.2 Expressions for the shear flow and normal stress resultant

Substitute the normal stress resultant from eq. (8.61) into the equilibrium differential equation (8.42), to get

$$\frac{dq}{ds} = -\left(\frac{B}{S}\frac{d\bar{N}}{dz} - \bar{B}_y\frac{k}{D_{xx}}\frac{d\bar{M}_x}{dz} - \bar{B}_x\frac{k}{D_{yy}}\frac{d\bar{M}_y}{dz}\right). \quad (8.63)$$

Recall that the stiffness parameter  $b$  and the shear flow  $q$  are independent of coordinate  $z$ . Derivatives of  $\bar{N}$ ,  $\bar{M}_x$ , and  $\bar{M}_y$  with respect to  $z$  are determined from eqs. (8.54) and (8.60) as

$$\frac{d\bar{N}}{dz} = \frac{dN}{dz} \quad \frac{d\bar{M}_x}{dz} = \frac{dM_x}{dz} \quad \frac{d\bar{M}_y}{dz} = \frac{dM_y}{dz}. \quad (8.64)$$

Derivatives of the bar resultants are given by equilibrium equations (8.38) and (8.39). Thus,

$$\frac{dN}{dz} = 0 \quad \frac{dM_x}{dz} = V_y \quad \frac{dM_y}{dz} = V_x. \quad (8.65)$$

The derivative of the shear flow with respect to the contour coordinate reduces to

$$\frac{dq}{ds} = -\bar{B}_y\frac{k}{D_{xx}}V_y - \bar{B}_x\frac{k}{D_{yy}}V_x. \quad (8.66)$$

Now we integrate the previous result with respect to the contour coordinate from  $s = 0$  to  $s = s$  and write the result as

$$q(s) = q_0 - \bar{S}_x(s)\frac{k}{D_{xx}}V_y - \bar{S}_y(s)\frac{k}{D_{yy}}V_x, \quad (8.67)$$

where

$$q_0 = q(0) \quad \bar{S}_x(s) = \int_0^s \bar{B}_y(s)ds \quad \bar{S}_y(s) = \int_0^s \bar{B}_x(s)ds. \quad (8.68)$$

Substitute eq. (8.62) for  $\bar{x}(s)$  and  $\bar{y}(s)$  into eq. (8.68) to get

$$\bar{S}_x(s) = S_x(s) - n_y S_y(s) \quad \bar{S}_y(s) = S_y(s) - n_x S_x(s), \quad (8.69)$$

where the modulus-weighted first moments of a segment of the cross-sectional area from  $s = 0$  to  $s = s$  are defined by

$$S_x(s) = \int_0^s B(s)y(s)ds \quad S_y(s) = \int_0^s B(s)x(s)ds. \quad (8.70)$$

Note that  $S_x(s)$  and  $S_y(s)$  evaluated at the end point of the closed contour vanish, which is consistent with eq. (8.53). The shear flow at the contour origin  $q_0$  is determined by torque equivalence of the shear flow with respect to the modulus-weighted centroid. That is,

$$M_{zc} = \oint r_{nc}(s)q(s)ds, \quad (8.71)$$

where  $r_{nc}(s)$  is the coordinate normal to the contour as depicted in Fig. 3.3 on page 33, and it is determined from

eq. (3.11) on page 34. Substitute eq. (8.67) for the shear flow in eq. (8.71) and solve for  $q_0$  to find

$$q_0 = \frac{1}{2A_c} \left[ M_{zc} + \left( \frac{kV_y}{D_{xx}} \right) \oint (r_{nc} \bar{S}_x) ds + \left( \frac{kV_x}{D_{yy}} \right) \oint (r_{nc} \bar{S}_y) ds \right], \quad (8.72)$$

where the area enclosed by the contour is given by

$$A_c = \frac{1}{2} \oint r_{nc} ds. \quad (8.73)$$

With  $q_0$  determined, we write the final expression for the shear flow in eq. (8.67) as

$$q(s) = \frac{M_{zc}}{2A_c} - F_{xc}(s)V_x - F_{yc}(s)V_y, \quad (8.74)$$

where the shear flow distribution functions are defined by

$$F_{xc}(s) = \frac{k}{D_{yy}} \left[ \bar{S}_y(s) - \frac{1}{2A_c} \oint (r_{nc} \bar{S}_y) ds \right] \quad F_{yc}(s) = \frac{k}{D_{xx}} \left[ \bar{S}_x(s) - \frac{1}{2A_c} \oint (r_{nc} \bar{S}_x) ds \right]. \quad (8.75)$$

Substitute eq. (8.54) for the normal stress resultant  $\bar{N}$  in eq. (8.61), and substitute for  $\bar{M}_x$  and  $\bar{M}_y$  from eq. (8.60) into eq. (8.61), to get

$$n_z = \frac{B}{S} [N - \oint (bq) ds] + B\bar{y} \frac{k}{D_{xx}} [M_x - \oint (ybq) ds] + B\bar{x} \frac{k}{D_{yy}} [M_y - \oint (xbq) ds] + bq. \quad (8.76)$$

Substitute eq. (8.74) for the shear flow into the previous equation for the normal stress resultant. After some algebraic manipulations we write the result as

$$n_z = \frac{B}{S} N + B\bar{y}(s) \frac{k}{D_{xx}} M_x + B\bar{x}(s) \frac{k}{D_{yy}} M_y + \Phi_x(s) V_x + \Phi_y(s) V_y + \Phi(s) \frac{M_{zc}}{2A_c}. \quad (8.77)$$

The functions  $\Phi_x(s)$ ,  $\Phi_y(s)$ , and  $\Phi(s)$  are a consequence of the coupling between extension and shear in the material law (i.e.,  $b \neq 0$ ). If the stiffness parameter  $b = 0$  over the entire contour, then

$\Phi_x(s) = \Phi_y(s) = \Phi(s) = 0$ . Equations for these functions are

$$\Phi_x(s) = -bF_{xc}(s) + \frac{B}{S} \oint bF_{xc} ds + \frac{Bk\bar{y}(s)}{D_{xx}} \oint byF_{xc} ds + \frac{Bk\bar{x}(s)}{D_{yy}} \oint bxF_{xc} ds, \quad (8.78)$$

$$\Phi_y(s) = -bF_{yc}(s) + \frac{B}{S} \oint bF_{yc} ds + \frac{Bk\bar{y}(s)}{D_{xx}} \oint byF_{yc} ds + \frac{Bk\bar{x}(s)}{D_{yy}} \oint bxF_{yc} ds, \quad (8.79)$$

$$\Phi(s) = b - \frac{B}{S} \oint b ds - \frac{Bk\bar{y}(s)}{D_{xx}} \oint by ds - \frac{Bk\bar{x}(s)}{D_{yy}} \oint bx ds. \quad (8.80)$$

### 8.2.3 Complementary work and energy

Consider a free bending and torsion state of the bar as shown in figure. 8.4 where the displacements, strains, and forces satisfy the compatibility conditions, Hooke's law, and the equilibrium conditions. In this state, the actual displacements of the modulus-weighted centroid are  $u_c(z)$ ,  $v_c(z)$ , and  $w(z)$ , and the corresponding forces are

$V_x(z)$ ,  $V_y(z)$ , and  $N(z)$ , respectively. The actual rotations of a cross section with respect to the modulus-weighted centroid are  $\phi_x(z)$ ,  $\phi_y(z)$ , and  $\phi_z(z)$ , and the corresponding moments are  $M_x(z)$ ,  $M_y(z)$ , and  $M_{zc}(z)$ , respectively. Now consider infinitesimal increments in the forces and moments denoted by  $\delta V_x$ ,  $\delta V_y$ ,  $\delta N$ ,  $\delta M_x$ ,  $\delta M_y$ , and  $\delta M_{zc}$  from the equilibrium state. For an element of the bar of length  $\Delta z$ , the complementary work is given by

$$\delta \bar{U}^* \Delta z = [\delta V_x u_c + \delta V_y v_c + \delta N w + \delta M_x \phi_x + \delta M_y \phi_y + \delta M_{zc} \phi_z] \Big|_z^{z+\Delta z}, \quad (8.81)$$

where  $\delta \bar{U}^*$  denotes the increment in the complementary work per unit axial length. Divide eq. (8.81) by  $\Delta z$ , and let  $\Delta z \rightarrow 0$ , to get in the limit

$$\delta \bar{U}^* = \frac{d}{dz} [\delta V_x u_c + \delta V_y v_c + \delta N w + \delta M_x \phi_x + \delta M_y \phi_y + \delta M_{zc} \phi_z]. \quad (8.82)$$

Statically admissible incremental actions requires that they satisfy the equilibrium differential equations (8.38) and (8.39): i.e.,

$$\frac{d}{dz} \delta V_x = \frac{d}{dz} \delta V_y = \frac{d}{dz} \delta N = \frac{d}{dz} \delta M_{zc} = 0 \quad \frac{d}{dz} \delta M_x = \delta V_y \quad \frac{d}{dz} \delta M_y = \delta V_x. \quad (8.83)$$

Imposing equilibrium (8.83) reduces eq. (8.82) to

$$\delta \bar{U}^* = \psi_{xc} \delta V_x + \psi_{yc} \delta V_y + \left( \frac{dw}{dz} \right) \delta N + \left( \frac{d\phi_x}{dz} \right) \delta M_x + \left( \frac{d\phi_y}{dz} \right) \delta M_y + \left( \frac{d\phi_z}{dz} \right) \delta M_{zc}, \quad (8.84)$$

where shear strains averaged over the cross section of the bar relative to the centroid are defined by

$$\psi_{xc} = \frac{du_c}{dz} + \phi_y \quad \psi_{yc} = \frac{dv_c}{dz} + \phi_x. \quad (8.85)$$

An elastic material is defined by the existence of a complementary strain energy function per unit axial length with the form  $\bar{U}^*(M_x, M_y, N, V_x, V_y, M_{zc})$ . Then, the total increment in function  $\bar{U}^*$  is

$$\delta \bar{U}^* = \frac{\partial \bar{U}^*}{\partial M_x} \delta M_x + \frac{\partial \bar{U}^*}{\partial M_y} \delta M_y + \frac{\partial \bar{U}^*}{\partial N} \delta N + \frac{\partial \bar{U}^*}{\partial V_x} \delta V_x + \frac{\partial \bar{U}^*}{\partial V_y} \delta V_y + \frac{\partial \bar{U}^*}{\partial M_{zc}} \delta M_{zc}, \quad (8.86)$$

Identify the complementary work (8.84) with the complementary energy (8.86) to get the important properties of complementary strain energy function. That is,

$$\frac{d\phi_x}{dz} = \frac{\partial \bar{U}^*}{\partial M_x} \quad \frac{d\phi_y}{dz} = \frac{\partial \bar{U}^*}{\partial M_y} \quad \frac{dw}{dz} = \frac{\partial \bar{U}^*}{\partial N} \quad \psi_{xc} = \frac{\partial \bar{U}^*}{\partial V_x} \quad \psi_{yc} = \frac{\partial \bar{U}^*}{\partial V_y} \quad \frac{d\phi_z}{dz} = \frac{\partial \bar{U}^*}{\partial M_{zc}}. \quad (8.87)$$

Now consider the complementary work for the free bending and torsion state of an element of the wall  $\Delta s$ -by- $\Delta z$  as shown in Fig. 8.5. On the contour ( $\zeta = 0$ ) the axial displacement  $u_z(s, z)$  corresponds to the stress resultant  $n_z$  and tangential displacement  $u_s(s, z)$  corresponds to the shear flow  $q$ . Let  $\delta U_o^*$  denote the increment in the complementary work per unit area for increments in the stress resultants  $\delta n_z$  and  $\delta q$  acting on the element  $\Delta s$ -by- $\Delta z$  of Fig. 8.5. Then, the complementary work is

$$\delta U_o^* \Delta s \Delta z = [(\delta n_z \Delta s) u_z + (\delta q \Delta s) u_s] \Big|_z^{z+\Delta z} + [(\delta q \Delta z) u_s] \Big|_{ss}^{s+\Delta s}. \quad (8.88)$$

Divide eq. (8.88) by  $\Delta s \Delta z$ , and let  $\Delta s \rightarrow 0$  and  $\Delta z \rightarrow 0$ , to get in the limit

$$\delta U_o^* = \frac{\partial}{\partial z}[(\delta n_z)u_z + (\delta q)u_s] + \frac{\partial}{\partial s}[(\delta q)u_z], \quad (8.89)$$

which expands to

$$\delta U_o^* = \left[ \frac{\partial}{\partial z}(\delta n_z) + \frac{\partial}{\partial s}(\delta q) \right] u_z + \left[ \frac{\partial}{\partial z}(\delta q) \right] u_s + \frac{\partial u_z}{\partial z} \delta n_z + \left( \frac{\partial u_z}{\partial s} + \frac{\partial u_s}{\partial z} \right) \delta q. \quad (8.90)$$

Statically admissible increments in the stress resultants  $\delta n_z$  and  $\delta q$  requires that they satisfy equilibrium equations (8.42) and (8.43), which are

$$\frac{\partial}{\partial z}(\delta n_z) + \frac{\partial}{\partial s}(\delta q) = 0 \quad \frac{\partial}{\partial z}(\delta q) = 0. \quad (8.91)$$

From the strain-displacement relations (3.27) and (3.28) on page 37 we identify the axial normal strain  $\epsilon_{zz}$  and the shear strain  $\gamma_{sz}$  as

$$\epsilon_{zz} = \frac{\partial u_z}{\partial z} \quad \gamma_{sz} = \frac{\partial u_z}{\partial s} + \frac{\partial u_s}{\partial z}. \quad (8.92)$$

Substitute eqs. (8.91) and (8.92) into eq. (8.90) to get the increment in the complementary work per unit area as

$$\delta U_o^* = \epsilon_{zz} \delta n_z + \gamma_{sz} \delta q. \quad (8.93)$$

For an elastic material we identify  $\delta U_o^*$  with the increment in the complementary strain energy function per unit area, which is a function of the stress resultants, or  $U_o^*(n_z, q)$ , with the properties

$$\epsilon_{zz} = \frac{\partial U_o^*}{\partial n_z} \quad \gamma_{sz} = \frac{\partial U_o^*}{\partial q}. \quad (8.94)$$

Now substitute Hooke's law (8.45) for the normal strain  $\epsilon_{zz}$  and for the shear strain  $\gamma_{sz}$  in the previous equation to get

$$\frac{\partial U_o^*}{\partial n_z} = \frac{1}{B}(n_z - bq) \quad \frac{\partial U_o^*}{\partial q} = \frac{1}{B}(aq - bn_z). \quad (8.95)$$

The complementary strain energy function per unit area consistent with these properties (8.95) is

$$U_o^* = \frac{1}{2B}(n_z^2 - 2bn_zq + aq^2). \quad (8.96)$$

The increment in the complementary energy per unit axial length  $\delta \bar{U}^*$  is defined  $\delta \bar{U}^* = \oint \delta U_o^* ds$ . Hence,

$$\bar{U}^* = \frac{1}{2} \oint \frac{1}{B}(n_z^2 - 2bn_zq + aq^2) ds. \quad (8.97)$$

Equations (8.74) and (8.77) relate the shear flow and normal stress resultant to the bar forces  $N$ ,  $V_x$ , and  $V_y$  and the moments  $M_x$ ,  $M_y$ , and  $M_z$ . Imposing the properties of the complementary strain energy for the bar given by (8.87) to the expression (8.97) for the complementary strain energy, we get the following relations:



$$\frac{d\phi_x}{dz} = \oint_B \frac{1}{B} \left[ (n_z - bq) \frac{\partial n_z}{\partial M_x} + (aq - bn_z) \frac{\partial q}{\partial M_x} \right] ds \quad (8.98)$$

$$\frac{d\phi_y}{dz} = \oint_B \frac{1}{B} \left[ (n_z - bq) \frac{\partial n_z}{\partial M_y} + (aq - bn_z) \frac{\partial q}{\partial M_y} \right] ds \quad (8.99)$$

$$\frac{dw}{dz} = \oint_B \frac{1}{B} \left[ (n_z - bq) \frac{\partial n_z}{\partial N} + (aq - bn_z) \frac{\partial q}{\partial N} \right] ds \quad (8.100)$$

$$\psi_{xc} = \oint_B \frac{1}{B} \left[ (n_z - bq) \frac{\partial n_z}{\partial V_x} + (aq - bn_z) \frac{\partial q}{\partial V_x} \right] ds \quad (8.101)$$

$$\psi_{yc} = \oint_B \frac{1}{B} \left[ (n_z - bq) \frac{\partial n_z}{\partial V_y} + (aq - bn_z) \frac{\partial q}{\partial V_y} \right] ds \quad (8.102)$$

$$\frac{d\phi_z}{dz} = \oint_B \frac{1}{B} \left[ (n_z - bq) \frac{\partial n_z}{\partial M_{zC}} + (aq - bn_z) \frac{\partial q}{\partial M_{zC}} \right] ds. \quad (8.103)$$

Equations (8.98) to (8.103) are statements of Castiglano's second theorem.

## 8.2.4 Cross-sectional compliance matrix

Substitute eq. (8.74) for the shear flow, and substitute eq. (8.77) for the normal stress resultant, into eqs. (8.98) to (8.103), followed by integration over the contour. The result from the integration leads to compliance form of the material law:

$$\begin{bmatrix} d\phi_x/dz \\ d\phi_y/dz \\ dw/dz \\ \psi_{xc} \\ \psi_{yc} \\ d\phi_z/dz \end{bmatrix} = \begin{bmatrix} c_{11} & c_{12} & c_{13} & c_{14} & c_{15} & c_{16} \\ c_{21} & c_{22} & c_{23} & c_{24} & c_{25} & c_{26} \\ c_{31} & c_{32} & c_{33} & c_{34} & c_{35} & c_{36} \\ c_{41} & c_{42} & c_{43} & c_{44} & c_{45} & c_{46} \\ c_{51} & c_{52} & c_{53} & c_{54} & c_{55} & c_{56} \\ c_{61} & c_{62} & c_{63} & c_{64} & c_{65} & c_{66} \end{bmatrix} \begin{bmatrix} M_x \\ M_y \\ N \\ V_x \\ V_y \\ M_{zC} \end{bmatrix}. \quad (8.104)$$

Elements of the compliance matrix are given below.

$$c_{11} = \frac{k}{D_{xx}} \quad c_{21} = \frac{-kn_y}{D_{xx}} = c_{12} = \frac{-kn_x}{D_{yy}} \quad c_{13} = c_{31} = 0 \quad c_{14} = c_{41} = \left( \frac{k}{D_{xx}} \right) \oint (by \bar{F}_{xc}) ds \quad (8.105)$$

$$c_{15} = c_{51} = \left( \frac{k}{D_{xx}} \right) \oint (by \bar{F}_{yc}) ds \quad c_{16} = c_{61} = \left( \frac{-k}{2A_c D_{xx}} \right) \oint (by \bar{F}) ds \quad (8.106)$$

$$c_{22} = \frac{k}{D_{yy}} \quad c_{23} = c_{32} = 0 \quad c_{24} = c_{42} = \left( \frac{k}{D_{yy}} \right) \oint (bx \bar{F}_{xc}) ds \quad (8.107)$$

$$c_{25} = c_{52} = \left( \frac{k}{D_{yy}} \right) \oint (bx \bar{F}_{yc}) ds \quad c_{26} = c_{62} = \left( \frac{-k}{2A_c D_{yy}} \right) \oint (bx \bar{F}) ds \quad c_{33} = 1/S \quad (8.108)$$

$$c_{34} = c_{43} = \left(\frac{1}{S}\right) \oint (bF_{xc}) ds \quad c_{35} = c_{53} = \left(\frac{1}{S}\right) \oint (bF_{yc}) ds \quad c_{36} = c_{63} = \left(\frac{-1}{2A_c S}\right) \oint (b) ds \quad (8.109)$$

$$c_{44} = \oint_B^1 (aF_{xc}^2 + 2bF_{xc}\Phi_x + \Phi_x^2) ds \quad c_{45} = c_{54} = \oint_B^1 (aF_{xc}F_{yc} + bF_{yc}\Phi_x + bF_{xc}\Phi_y + \Phi_x\Phi_y) ds \quad (8.110)$$

$$c_{46} = c_{64} = \left(\frac{1}{2A_c}\right) \oint_B^1 (-aF_{xc} + bF_{xc}\Phi - b\Phi_x + \Phi\Phi_x) ds \quad c_{55} = \oint_B^1 (aF_{yc}^2 + 2bF_{yc}\Phi_y + \Phi_y^2) ds \quad (8.111)$$

$$c_{56} = c_{65} = \left(\frac{1}{2A_c}\right) \oint_B^1 (-aF_{yc} + bF_{yc}\Phi - b\Phi_y + \Phi\Phi_y) ds \quad c_{66} = \left(\frac{1}{4A_c^2}\right) \oint_B^1 (a - 2b\Phi + \Phi^2) ds. \quad (8.112)$$

Matrix  $[c_{ij}]$  is symmetric so that twenty-one of the coefficients are independent. The fifteen of the off-diagonal coefficients correspond to different types of coupling effects as described in table 8.3.

**Table 8.3 Description of coupling coefficients**

Coefficients	Coupling effects	Comment
$c_{21}$	combined bending about $x$ - and $y$ -axes	$c_{21} = 0$ if $D_{xy} = 0$
$c_{31}$ & $c_{32}$	bending-extension	$c_{31} = c_{32} = 0$ , since origin is at modulus weighted centroid
$c_{41}$ , $c_{51}$ , $c_{42}$ , & $c_{52}$	bending-shearing	are zero if parameter $b = 0$ over entire contour
$c_{61}$ & $c_{62}$	bending-torsion	are zero if parameter $b = 0$ over entire contour
$c_{43}$ & $c_{53}$	shearing-extension	are zero if parameter $b = 0$ over entire contour
$c_{63}$	torsion-extension	is zero if parameter $b = 0$ over entire contour
$c_{64}$ & $c_{65}$	torsion-shearing	
$c_{45}$	combined transverse shear in $x$ - $z$ and $y$ - $z$ planes	

**Example 8.3 Graphite-epoxy circular tube**

Nixon (1987) conducted experiments on thin-walled tubes fabricated from T300/5208 graphite/epoxy. The test specimens had a mean radius  $R = 20.32$  mm, a wall thickness  $t = 1.016$  mm, and were composed of two unidirectional layers with angles  $\varphi_1 = -20^\circ$  and  $\varphi_2 = 70^\circ$ . The thickness of both layers is the same, and the properties of the material are  $E_1 = 146.7$  GPa (21.3 ksi),  $E_2 = 11.0$  GPa (1.6 ksi),  $G_{12} = 6.41$  GPa (0.93 ksi), principal Poisson's ratio  $\nu_{21} = 0.38$  and the minor Poisson's ratio  $\nu_{12} = 0.0285$ . The twist per unit length  $d\phi_z/dz$  was measured in the experiment for an applied axial force  $N$  and an applied torque  $M_z$ . Determine this relationship from the composite bar theory.

**Solution.** The in-plane stiffness matrix is determined from  $[A] = [\bar{Q}(\varphi_1)]\frac{t}{2} + [\bar{Q}(\varphi_2)]\frac{t}{2}$ , where the formulas for the elements of transformed reduced stiffness matrix are listed in eq. (8.35). The result is

$$\begin{bmatrix} A_{11} & A_{12} & A_{16} \\ A_{21} & A_{22} & A_{26} \\ A_{61} & A_{62} & A_{66} \end{bmatrix} = \begin{bmatrix} 67.8649 & 17.4628 & 15.6839 \\ 17.4628 & 67.8649 & -15.6839 \\ 15.6839 & -15.6839 & 19.6701 \end{bmatrix} \text{MN/m}. \quad (\text{a})$$

From eqs. (8.47) and (8.48) the stiffness parameters of the composite bar theory are

$$B_s = 16.0454 \text{ MN/m} \quad B_z = -19.7196 \text{ MN/m} \quad b = -1.22899 \quad B = 39.1363 \text{ MN/m} \quad a = 3.9495. \quad (\text{b})$$

Note that the stiffness parameters are spatially uniform over the entire contour. Cartesian coordinates relative to the center of the circular contour are  $x = R \cos \theta$  and  $y = R \sin \theta$ ,  $0 \leq \theta < 2\pi$ . From eq. (8.52) the axial stiffness is  $S = 4.99669 \text{ MN}$ , and the modulus-weighted first moments (8.70) are

$$S_x = \oint B(s)y(s)ds = B \int_0^{2\pi} y(\theta)Rd\theta = 0 \quad S_y = \oint B(s)x(s)ds = B \int_0^{2\pi} x(\theta)Rd\theta = 0. \quad (\text{c})$$

As a consequence of eq. (c) the modulus-weighted centroid coincides with the center of the circular contour. The modulus-weighted second moments are computed from eq. (8.57), and the results are

$$D_{xx} = D_{yy} = \pi BR^3 = 1,031.57 \text{ N-m}^2 \quad D_{xy} = 0. \quad (\text{d})$$

Thus, from eq. (8.59) and eq. (8.62) we find  $n_x = n_y = 0$ ,  $k = 1$ ,  $\bar{x} = x$ , and  $\bar{y} = y$ . The combined first moment functions in eq. (8.69) are computed from the first moment functions in eq. (8.70). The results are

$$\bar{S}_x(\theta) = BR^2(1 - \cos \theta) \quad \bar{S}_y(\theta) = BR^2 \sin \theta. \quad (\text{e})$$

Note that  $\bar{S}_x(0) = \bar{S}_y(0) = \bar{S}_x(2\pi) = \bar{S}_y(2\pi) = 0$ . The shear flow distribution functions  $F_{xc}$  and  $F_{yc}$  are computed from eq. (8.75). Functions  $\Phi_x$ ,  $\Phi_y$ ,  $\Phi$ , which couple shear and torsion to the normal stress resultant (8.77), are computed from eqs. (8.78) to (8.80). In this example, the results for these functions are

$$F_{xc} = \frac{\sin \theta}{\pi R} \quad F_{yc} = \frac{-\cos \theta}{\pi R} \quad \Phi_x = \Phi_y = \Phi = 0 \quad 0 \leq \theta < 2\pi. \quad (\text{f})$$

Elements of the compliance matrix are determined by eqs. (8.105) to (8.112). In this example the result for the cross-sectional compliance matrix is

$$\begin{bmatrix} d\phi_x/dz \\ d\phi_y/dz \\ dw/dz \\ \psi_x \\ \psi_y \\ d\phi_z/dz \end{bmatrix} = \frac{1}{\pi BR^3} \begin{bmatrix} 1 & 0 & 0 & bR & 0 & 0 \\ 0 & 1 & 0 & 0 & -bR & 0 \\ 0 & 0 & \frac{R^2}{2} & 0 & 0 & \frac{-bR}{2} \\ bR & 0 & 0 & aR^2 & 0 & 0 \\ 0 & -bR & 0 & 0 & aR^2 & 0 \\ 0 & 0 & \frac{-bR}{2} & 0 & 0 & \frac{a}{2} \end{bmatrix} \begin{bmatrix} M_x \\ M_y \\ N \\ V_x \\ V_y \\ M_z \end{bmatrix}. \quad (g)$$

The twist per unit length, or unit twist, for the circular tube is equal to  $c_{63}N + c_{66}M_z$ . The unit twist evaluates as

$$\frac{d\phi_z}{dz} = \left( \frac{-b}{2\pi BR^2} \right) N + \left( \frac{a}{2\pi BR^3} \right) M_z = (1.21043 \times 10^{-5}) N + (1.91431 \times 10^{-3}) M_z. \quad (h)$$

The unit twist in eq. (h) is plotted with respect to the torque in figure. 8.6 for two values of the axial force. Discrete measurements from the experiment reported by Nixon (1987) are shown by filled circles in the plot. ■

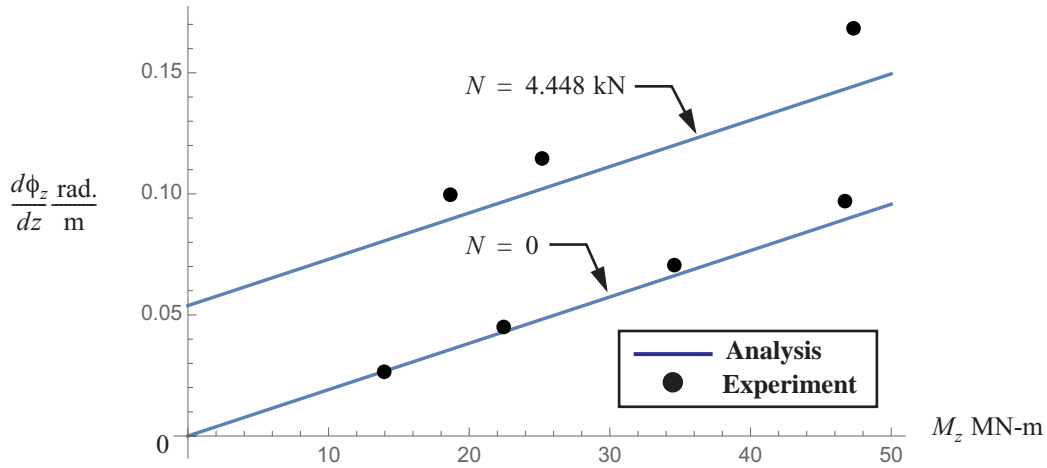


Fig. 8.6 example 8.3: Unit twist versus torque for the two values of the axial force.

### Example 8.4 Composite box beam

Consider the composite box beam in the experiments conducted by Smith and Chopra (1991) and Chandra et al. (1990). As shown in figure. 8.7, the beam is clamped at its left end where the axial coordinate  $z = 0$ ,  $0 \leq z \leq L$ , where the length of the beam  $L = 762$  mm. The cross-sectional dimensions of the rectangular contour are  $b_x = 24.2$  mm and  $b_y = 13.6$  mm, and the wall thickness  $t = 0.76$  mm over the entire contour. The material is unidirectional tape of carbon-epoxy with properties  $E_1 = 142$  GPa,  $E_2 = 9.8$  GPa,  $G_{12} = 6$  GPa,  $\nu_{21} = 0.42$ , and  $\nu_{12} = 0.029$ .

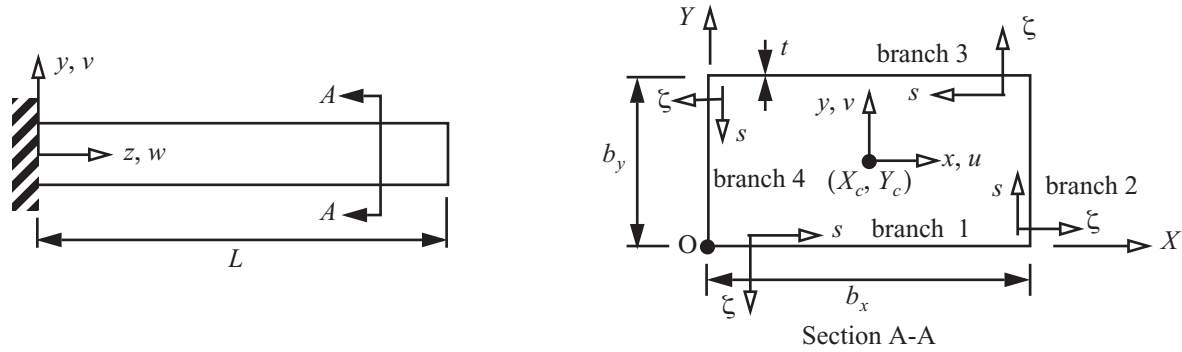
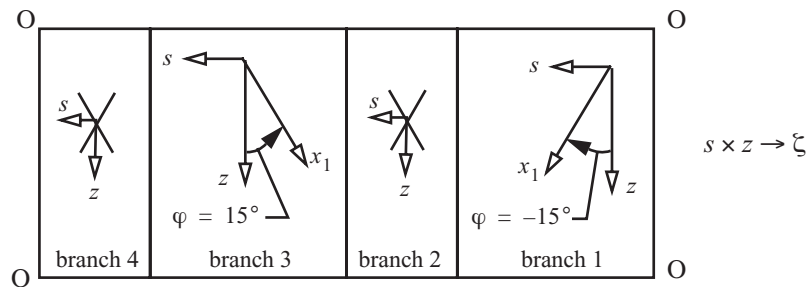


Fig. 8.7 Cantilever, thin-walled box beam.

The lower horizontal flange, or branch 1, is a unidirectional laminate with a ply angle  $\varphi = -15^\circ$ , and the upper horizontal flange, or branch 3, is also a unidirectional laminate with a ply angle of  $\varphi = 15^\circ$ . The vertical webs, or branches 2 and 4, are angle-ply laminates with a layout of  $(15^\circ, -15^\circ)$ . Imagine cutting the box beam parallel to the  $z$ -axis through point O. Then unfold the laminated walls and lay them flat such that the outside surface is facing up. The fiber directions with respect to  $s$ - $z$ - $\zeta$  coordinates in each branch are shown in figure. 8.8.

Fig. 8.8 Outside surface of the unfolded box.



- Determine the torsional rotation  $\phi_z(z)$  under transverse bending  $V_y = Q$ .
- Determine the slope  $dv/dz$  of the reference axis due to a torque  $M_z$ .

**Solution.** Stiffness coefficients of the four branches comprising the contour are listed in table 8.4.

**Table 8.4 Stiffness coefficients for each branch of the box beam**

Stiffness coefficient	Branch 1	Branch 3	Branches 2 & 4
$A_{11}$ , MN/m	8.59	8.59	8.59
$A_{12}$ , MN/m	8.93	8.93	8.93
$A_{22}$ , MN/m	9.67	9.67	9.67
$A_{66}$ , MN/m	10.3	10.3	10.3
$A_{16}$ , MN/m	-2.73	2.73	0
$A_{26}$ , MN/m	-2.27	2.27	0
$B_z$ , MN/m	-19.9	19.8	0
$B_s$ , MN/m	9.46	9.455	10.3
$B$ , MN/m	45.7	45.7	87.4
$b$ , (-)	-2.1	2.1	0
$a$ , (-)	9.242	9.242	8.465

Note that  $B_3 = B_1$ ,  $B_4 = B_2$ ,  $b_3 = -b_1$ ,  $a_3 = a_1$ , and  $a_4 = a_2$ . The origin of the contour coordinate where  $s = 0$  is at point O of section A-A of figure. 8.7. The Cartesian coordinate functions ( $X(s)$ ,  $Y(s)$ ) with origin also at point O are listed in table 8.5.

**Table 8.5 Parametric equations of the contour for the box beam**

Branch no.	Range of $s$ , in.	$X(s)$	$Y(s)$
1	$0 \leq s \leq b_x$	$s$	0
2	$b_x \leq s \leq b_x + b_y$	$b_x$	$s - b_x$
3	$b_x + b_y \leq s \leq 2b_x + b_y$	$2b_x + b_y - s$	$b_y$
4	$2b_x + b_y \leq s \leq 2(b_x + b_y)$	0	$2(b_x + b_y) - s$

The axial stiffness is

$$S = \oint B ds = 2(B_1 b_x + B_2 b_y) = 4.58819 \text{ MN}. \quad (\text{a})$$

The first moments with respect to the  $X$ - $Y$  coordinates are

$$S_X = \oint B Y ds = b_y(B_1 b_x + B_2 b_y) \quad S_Y = \oint B X ds = b_x(B_1 b_x + B_2 b_y). \quad (\text{b})$$

Consequently, the modulus-weighted centroid is located at

$$X_c = S_Y/S = b_x/2 \quad Y_c = S_X/S = b_y/2. \quad (\text{c})$$

In this example the modulus-weighted centroid coincides with the geometric centroid of the cross section. The Cartesian coordinates of the contour with respect to the modulus-weighted centroid are determined from  $x(s) = X(s) - X_c$  and  $y(s) = Y(s) - Y_c$ . The modulus-weighted second moments computed from eq. (8.57) are

$$D_{xx} = \frac{b_y^2}{6}(3B_1b_x + B_2b_y) = 138.884 \text{ Nm}^2 \quad D_{yy} = \frac{b_x^2}{6}(B_1b_x + 3B_2b_y) = 455.927 \text{ Nm}^2 \quad D_{xy} = 0. \quad (\text{d})$$

The values of the parameters listed in eq. (8.59) are  $n_x = n_y = 0$  and  $k = 1$ . Hence, from eq. (8.62) we find  $\bar{x}(s) = x(s)$  and  $\bar{y}(s) = y(s)$ . Also, from eq. (8.69)  $\bar{S}_x(s) = S_x(s)$  and  $\bar{S}_y(s) = S_y(s)$ . The modulus-weighted distribution functions  $S_x(s)$  and  $S_y(s)$  with respect to a segment of the cross-sectional area are defined in eq. (8.70), and the results for these functions are listed in table 8.6.

**Table 8.6 Modulus-weighted distribution functions for the first area moments**

Branch	$\bar{S}_x(s) = S_x(s)$	$\bar{S}_y(s) = S_y(s)$
1	$(-B_1b_ys)/2$	$B_1s[(-b_x + s)/2]$
2	$[-B_1b_xb_y + B_2(b_x - s)(b_x + b_y - s)]/2$	$[B_2b_x(-b_x + s)]/2$
3	$[-B_1b_y(2b_x + b_y - s)]/2$	$[B_2b_xb_y - B_1(2b_x^2 + 3b_x(b_y - s) + (b_y - s)^2)]/2$
4	$-B_2([4b_x^2 + 6b_xb_y + 2b_y^2 - 4b_xs - 3b_ys + s^2])/2$	$[B_2b_x(2b_x + 2b_y - s)]/2$

The procedure to determine  $S_x(s)$  and  $S_y(s)$  is the same procedure used to determine the first area moments  $Q_x(s)$  and  $Q_y(s)$  for a cross section with a wall made of an isotropic material. See example 3.4 on page 71. For the composite wall  $S_x(s)$  is analogous to  $Q_x(s)$  of the isotropic wall, and  $S_y(s)$  is analogous to  $Q_y(s)$ . Note that  $\bar{S}_x(0) = 0$  in branch 1, and that  $\bar{S}_x[2(b_x + b_y)] = 0$  in branch 4, which are necessary conditions for the first moment about the centroidal  $x$ -axis. Similarly,  $\bar{S}_y(0) = 0$  in branch 1, and  $\bar{S}_y[2(b_x + b_y)] = 0$  in branch 4, which are necessary conditions for the first moment about the centroidal  $y$ -axis.

The coordinates normal to the contour for each branch with respect to the centroid given by eq. (3.10) on page 34, and the area enclosed by the contour, are as follows:

$$r_{nc1} = r_{nc3} = b_y/2 = 6.8 \text{ mm}, r_{nc2} = r_{nc4} = b_x/2 = 12.1 \text{ mm}, \text{ and } A_c = b_xb_y = 329.12 \text{ mm}^2. \quad (\text{e})$$

The numerical evaluation of the shear flow distribution functions in eq. (8.75) can now be computed with the results shown in table 8.7.

**Table 8.7 Shear flow distribution functions for the box beam**

Branch	$F_{xc}, m^{-1}$ (s in meters)	$F_{yc}, m^{-1}$ (s in meters)
1	$-15.771 - 1,212.5s + 50,102.5s^2$	$-27.066 - 2,236.88s$
2	$-71.896 + 2,319.2s$	$-260.728 - 19,505.9s + 314,612s^2$

**Table 8.7 Shear flow distribution functions for the box beam**

Branch	$F_{xc}, m^{-1}$ (s in meters)	$F_{yc}, m^{-1}$ (s in meters)
3	$-101.65 + 5,000.2s - 50,102.5s^2$	$-111.62 + 2,236.88s$
4	$-159.564 - 2,319.24s$	$-1,447.58 + 43,290.5s - 314,612s^2$

For anisotropic wall properties, the normal stress resultant (8.77) is related to shear and torsion in addition to the axial normal force and bending moments. The coefficient functions of the shear terms ( $\Phi_x(s)$  and  $\Phi_y(s)$ ) and torsion term ( $\Phi(s)$ ) are given by eqs. (8.78) to (8.80), and the numerical results for these functions are listed below.

**Table 8.8 Coefficient functions for shear and torsion for the box beam (refer to eqs. (8.78) to (8.80)).**

Branch	$\Phi_x, m^{-1}$ (s in meters)	$\Phi_y, m^{-1}$ (s in meters)	$\Phi(s)$ , dimensionless and s in meters
1	$-12.209 - 2,546.37s + 105,222s^2$	$56.8427 - 4,697.75s$	$-0.554009$
2	$40.0001$	$0$	$13.482 - 434.916s$
3	$234.389 - 10,501.1s + 105,222s^2$	$234.418 - 4,697.75s$	$0.554009$
4	$40.0001$	$0$	$-29.9222 + 434.916s$

The numerical result for the compliance matrix (8.104) is

$$\begin{bmatrix} d\phi_x/dz \\ d\phi_y/dz \\ dw/dz \\ \psi_x \\ \psi_y \\ d\phi_z/dz \end{bmatrix} = 10^{-3} \begin{bmatrix} 7.200 & 0 & 0 & 0 & 0 & -7.561 \\ 0 & 2.193 & 0 & 0 & 0 & 0 \\ 0 & 0 & 2.180 \times 10^{-4} & 4.577 \times 10^{-4} & 0 & 0 \\ 0 & 0 & 4.577 \times 10^{-4} & 3.389 \times 10^{-3} & 0 & 0 \\ 0 & 0 & 0 & 0 & 4.861 \times 10^{-3} & 0 \\ -7.561 & 0 & 0 & 0 & 0 & 25.83 \end{bmatrix} \begin{bmatrix} M_x \\ M_y \\ N \\ V_x \\ V_y \\ M_z \end{bmatrix}.$$

The non-zero compliance coefficient  $c_{16}$  couples the torsional and bending responses of the beam. This coupling is illustrated in the following numerical examples.

- a. Take the beam subject to transverse shear with  $V_y = Q$ ,  $0 \leq z \leq L$ , and no other actions. The bending moment is  $M_x = -Q(L - z)$ . The twist per unit length under transverse bending is  $d\phi_z/dz = c_{61}M_x$ . The torsional rotation is given by

$$\phi_z = c_{61} \left[ -Q \left( Lz - \frac{z^2}{2} \right) \right] = -c_{61} L^2 Q \left[ \frac{z}{L} - \frac{1}{2} \left( \frac{z}{L} \right)^2 \right] = 0.00439 Q \left[ \frac{z}{L} - \frac{1}{2} \left( \frac{z}{L} \right)^2 \right].$$

The distributions of the torsional rotation for  $Q = 4.448$  N (1 lb.) from the present analysis, and from the experiment conducted by Smith and Chopra (1991), are shown in figure. 8.9.



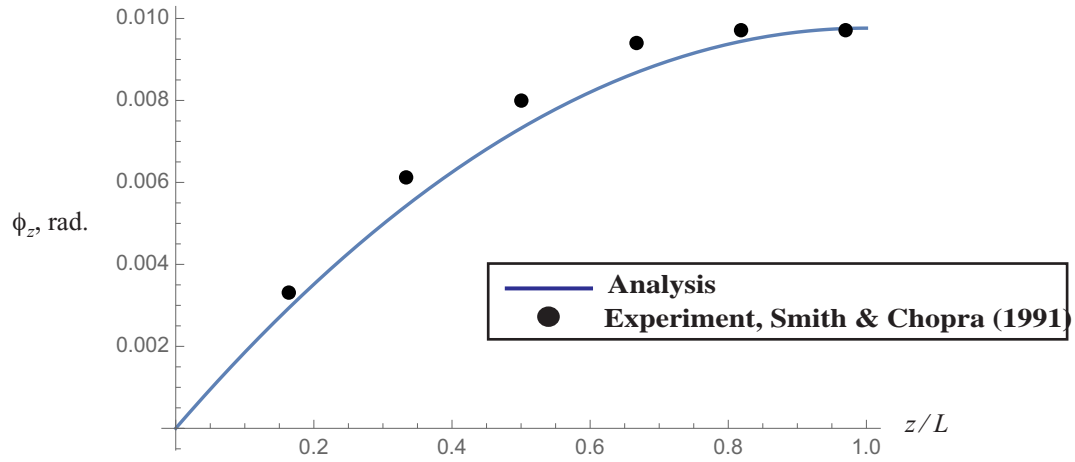


**Fig. 8.9** Spanwise distribution of the torsional rotation for  $V_y = Q = 4.448 \text{ N (1 lb.)}$ .

- b. Take the beam subject to a torque  $M_z$  and no other actions. From the compliance matrix we find  $\psi_y = c_{55} \cdot 0 = 0$ . From eq. (8.85) the slope of the reference axis  $dv/dz = -\phi_x$ , and from the compliance matrix  $d\phi_x/dz = c_{16}M_z$ , and  $\phi_x = c_{16}M_z z$ . Since  $c_{16} = c_{61}$ , the expression for the slope is

$$\frac{dv}{dz} = -c_{61}M_z z = -(-7.561 \times 10^{-3})LM_z(z/L) = 0.005761 \left( \frac{1}{\text{Nm}} \right) M_z(z/L).$$

The distributions of the slope of the reference axis from the present analysis, and from the experiment conducted by Chandra et al. (1990), for the torque  $M_z = 0.113 \text{ Nm (1.0 lb.-in.)}$  are shown in figure. 8.10.

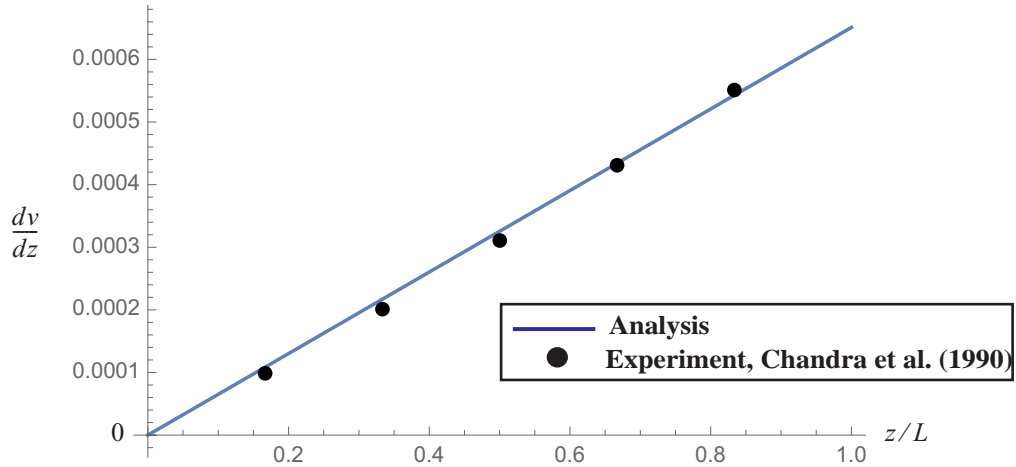


**Fig. 8.10** Slope of the reference axis for an applied torque of  $0.113 \text{ Nm (1.0 lb.-in.)}$

### 8.3 Open cross-sectional contour

For an open cross-sectional contour the shear flow is obtained from eq. (8.67) on page 239. The shear flow at the contour origin  $q_0 = 0$  if the origin is located at intersection with a longitudinal free edge. (Refer to the discussion in article 3.8.1 on page 51.) The equation for the shear flow for the FRP composite bar is

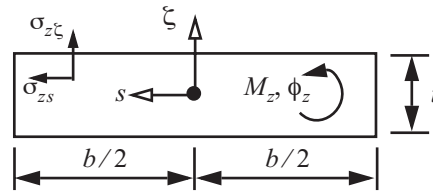
$$q(s) = -\bar{S}_x(s) \frac{k}{D_{xx}} V_y - \bar{S}_y(s) \frac{k}{D_{yy}} V_x. \quad (8.113)$$

The notes concerning the shear center in article 3.8.3 on page 57 apply as well to a bar made of an FRP composite. In particular from these notes, the resultant of the shear flow distribution over the contour is a force with components  $V_x$  and  $V_y$  acting through the shear center such that there is no torque acting at the shear center. If the cross section is subject to a torque, this torque cannot be balanced by the shear flow, which, according to eq. (8.113), is uniquely determined by the shear forces  $V_x$  and  $V_y$ . Part (b) of example 8.5 on page 263 shows how to find the shear center for an open section starting with eq. (8.113). After locating the shear center for the open cross-sectional contour, a material law for the torque acting at the shear center remains to be determined. This material law for torsion is developed in the next section.

### 8.4 Uniform torsion of an FRP bar with a rectangular cross section

We consider the uniform torsion of a prismatic bar with a rectangular cross section composed of a linear elastic, anisotropic material. Cartesian coordinates of the bar are denoted by  $s - z - \zeta$ , where the coordinate  $z$  is parallel to the longitudinal axis of the bar. The origin of the coordinates  $s$  and  $\zeta$  is at the center of the cross section;  $-b/2 \leq s \leq b/2$  where the width of the cross section is denoted by  $b$ , and  $-t/2 \leq \zeta \leq t/2$  where the thickness is denoted by  $t$ . See figure. 8.11.

**Fig. 8.11 Bar with a rectangular cross section subject to uniform torsion.**



The only applied load is a torque  $M_z$  about the  $z$ -axis, and the rotation about the  $z$ -axis corresponding to the torque is denoted by  $\phi_z$ . The torque and rotation are positive counterclockwise as shown in figure. 8.11. The shear stress components acting on the cross section are denoted by  $\sigma_{zs}$  and  $\sigma_{z\zeta}$ , and the torque is related to the shear stresses by the following integral over the cross section:

$$M_z = \int_{-b/2}^{b/2} \int_{-t/2}^{t/2} (\zeta \sigma_{zs} - s \sigma_{z\zeta}) d\zeta ds. \quad (8.114)$$

The lateral surfaces of the bar are not subject any loads or tractions. Hence, the stress components must satisfy the following conditions at the boundaries of the cross section:

$$\sigma_{\zeta s} = \sigma_{\zeta z} = \sigma_{zs} = \sigma_{z\zeta} = 0, \text{ for } -b/2 \leq s \leq b/2 \text{ at } \zeta = \pm t/2. \quad (8.115)$$

$$\sigma_{ss} = \sigma_{sz} = \sigma_{s\zeta} = 0, \text{ at } s = \pm b/2 \text{ for } -t/2 \leq \zeta \leq t/2. \quad (8.116)$$

**Under uniform torsion all stress components and their corresponding strains are independent of the axial coordinate  $z$ .** The exact elasticity formulation for the anisotropic bar is given in the monograph by Lekhnitskii (1981). We seek an approximate solution based on the following assumptions:

- Stress components  $\sigma_{ss}$ ,  $\sigma_{s\zeta}$ , and  $\sigma_{\zeta\zeta}$  are equal to zero in the domain of the cross section.
- The cross section is rigid in its own plane.

The procedure to develop the material law is as follows: (a) determine the displacements of the bar using the strain-displacement relations and the anisotropic form of Hooke's law, (b) satisfy the differential equation of equilibrium using a separable form of the stress function, (c) use static equivalence to determine the resultants of the axial normal stress, and (d) impose the principle of complementary virtual work to find the unknown part of the stress function. The final result for the material law in torsion is given by eqs. (8.193) and (8.194) on page 263.

#### 8.4.1 Displacements

The non-zero stress components are the axial normal stress  $\sigma_{zz}$ , and the shear stresses  $\sigma_{zs}$  and  $\sigma_{z\zeta}$ . To effect the rigidity assumption consider Hooke's law (8.16) for the strain components  $\epsilon_{ss}$ ,  $\epsilon_{\zeta\zeta}$ , and  $\gamma_{\zeta s}$ . Write these material laws as

$$\begin{aligned} \epsilon_{ss} &= \frac{\partial u_s}{\partial s} = \frac{1}{E_{ss}} \left[ \sigma_{ss} + \left( \frac{C'_{12}}{C'_{11}} \right) \sigma_{zz} + \left( \frac{C'_{13}}{C'_{11}} \right) \sigma_{\zeta\zeta} + \left( \frac{C'_{16}}{C'_{11}} \right) \sigma_{zs} \right] \\ \epsilon_{\zeta\zeta} &= \frac{\partial u_\zeta}{\partial \zeta} = \frac{1}{E_{\zeta\zeta}} \left[ \left( \frac{C'_{31}}{C'_{33}} \right) \sigma_{ss} + \left( \frac{C'_{32}}{C'_{33}} \right) \sigma_{zz} \right] + \sigma_{\zeta\zeta} + \left( \frac{C'_{36}}{C'_{33}} \right) \sigma_{zs}, \\ \gamma_{\zeta s} &= \frac{\partial u_\zeta}{\partial s} + \frac{\partial u_s}{\partial \zeta} = \frac{1}{G_{\zeta s}} \left[ \left( \frac{C'_{54}}{C'_{55}} \right) \sigma_{z\zeta} + \sigma_{\zeta s} \right] \end{aligned} \quad (8.117)$$

where  $E_{ss}$  is the modulus of elasticity for tension/compression along the  $s$ -axis,  $E_{\zeta\zeta}$  is the modulus along the  $\zeta$ -axis, and  $G_{\zeta s}$  is the shear modulus in the plane of the cross section. These moduli are related to the compliance coefficients by  $E_{ss} = (C'_{11})^{-1}$ ,  $E_{\zeta\zeta} = (C'_{33})^{-1}$ , and  $G_{\zeta s} = (C'_{55})^{-1}$ . Invoke the rigidity of the cross section by letting  $E_{ss} \rightarrow \infty$ ,  $E_{\zeta\zeta} \rightarrow \infty$ , and  $G_{\zeta s} \rightarrow \infty$ . The assumption of a rigid cross-sectional plane leads to the vanishing of the following strain-displacement relations:

$$\epsilon_{ss} = \frac{\partial u_s}{\partial s} = 0 \quad \epsilon_{\zeta\zeta} = \frac{\partial u_\zeta}{\partial \zeta} = 0 \quad \gamma_{\zeta s} = \frac{\partial u_\zeta}{\partial s} + \frac{\partial u_s}{\partial \zeta} = 0. \quad (8.118)$$

The normal strains in eq. (8.118) mean displacement functions  $u_s = u_s(z, \zeta)$  and  $u_\zeta = u_\zeta(z, s)$ . Hooke's law (8.16) for the remaining strains reduces to

$$\epsilon_{zz} = \frac{\partial u_z}{\partial z} = C'_{22} \sigma_{zz} + C'_{26} \sigma_{sz}, \quad (8.119)$$

$$\gamma_{z\zeta} = \frac{\partial u_\zeta}{\partial z} + \frac{\partial u_z}{\partial \zeta} = C'_{44} \sigma_{z\zeta}, \text{ and} \quad (8.120)$$

$$\gamma_{sz} = \frac{\partial u_z}{\partial s} + \frac{\partial u_s}{\partial z} = C'_{62}\sigma_{zz} + C'_{66}\sigma_{sz}. \quad (8.121)$$

Let the axial normal strain  $\epsilon_{zz} = D(s, \zeta)$ , where the function  $D(s, \zeta)$  is to be determined from the independence of the strains on axial coordinate  $z$ . Begin by integrating the strain-displacement equation for the axial normal strain with respect to  $z$  to determine the axial displacement as

$$u_z = zD(s, \zeta) + w(s, \zeta). \quad (8.122)$$

Solve eq. (8.119), for the axial normal stress to get

$$\sigma_{zz} = (D - C'_{26}\sigma_{zs})/(C'_{22}). \quad (8.123)$$

Substitute the axial displacement (8.122) into eq. (8.120) to find

$$\frac{\partial u_\zeta}{\partial z} = -z \frac{\partial D}{\partial \zeta} + \left( -\frac{\partial w}{\partial \zeta} + C'_{44}\sigma_{z\zeta} \right). \quad (8.124)$$

Integrate eq. (8.124) with respect to  $z$  to get

$$u_\zeta = \frac{-z^2 \partial D}{2 \partial \zeta} + z \left( -\frac{\partial w}{\partial \zeta} + C'_{44}\sigma_{z\zeta} \right) + v(s). \quad (8.125)$$

Substitute eq. (8.125) for the displacement  $u_\zeta$  for the expression for the strain  $\epsilon_{\zeta\zeta}$  in eq. (8.118) to get

$$\epsilon_{\zeta\zeta} = \frac{\partial u_\zeta}{\partial \zeta} = 0 = \frac{-z^2 \partial^2 D}{2 \partial \zeta^2} + z \frac{\partial}{\partial \zeta} \left( -\frac{\partial w}{\partial \zeta} + C'_{44}\sigma_{z\zeta} \right), \text{ for all values of } z. \quad (8.126)$$

Substitute eq. (8.123) for the axial normal stress into eq. (8.121) to get

$$\gamma_{sz} = \frac{\partial u_z}{\partial s} + \frac{\partial u_s}{\partial z} = (C'_{62}D)/C'_{22} + \beta_{66}\sigma_{sz}, \quad (8.127)$$

where  $\beta_{66} = (C'_{66} - C'^2_{26}/C'_{22})$ . Substitute eq. (8.122) for  $u_z$  into eq. (8.127) to get

$$\frac{\partial u_s}{\partial z} = -z \frac{\partial D}{\partial s} + \left( -\frac{\partial w}{\partial s} + (C'_{62}D)/C'_{22} + \beta_{66}\sigma_{sz} \right). \quad (8.128)$$

Integrate eq. (8.128) the with respect to  $z$  to find the displacement  $u_s$  as

$$u_s = \frac{-z^2 \partial D}{2 \partial s} + z \left( -\frac{\partial w}{\partial s} + \beta_{66}\sigma_{sz} + (C'_{62}D)/C'_{22} \right) + u(\zeta). \quad (8.129)$$

Substitute eq. (8.129) for displacement  $u_s$  in the expression for the strain  $\epsilon_{ss}$  in eq. (8.118) to get

$$\epsilon_{ss} = \frac{\partial u_s}{\partial s} = 0 = \frac{-z^2 \partial^2 D}{2 \partial s^2} + z \frac{\partial}{\partial s} \left( -\frac{\partial w}{\partial s} + \beta_{66}\sigma_{sz} + (C'_{62}D)/C'_{22} \right), \text{ for all values of } z. \quad (8.130)$$

Substitute displacement  $u_\zeta$  from eq. (8.125), and substitute displacement  $u_s$  from eq. (8.129), into the expression for the shear strain  $\gamma_{\zeta s}$  in eq. (8.118) to get

$$\gamma_{\zeta s} = 0 = -z^2 \frac{\partial^2 D}{\partial s \partial \zeta} + z \left[ \frac{\partial}{\partial s} \left( -\frac{\partial w}{\partial \zeta} + C'_{44}\sigma_{z\zeta} \right) + \frac{\partial}{\partial \zeta} \left( -\frac{\partial w}{\partial s} + \beta_{66}\sigma_{sz} + (C'_{62}D)/C'_{22} \right) \right] + \frac{dv}{ds} + \frac{du}{d\zeta}. \quad (8.131)$$

Equations (8.126), (8.130), and (8.131) are to be satisfied for all values of  $z$ , from which we conclude the following results:

$$\frac{\partial^2 D}{\partial \xi^2} = 0 \quad \frac{\partial^2 D}{\partial s^2} = 0 \quad \frac{\partial^2 D}{\partial s \partial \xi} = 0 \quad (8.132)$$

$$\frac{\partial}{\partial \xi} \left( -\frac{\partial w}{\partial \xi} + C'_{44} \sigma_{z\xi} \right) = 0 \quad \frac{\partial}{\partial s} \left( -\frac{\partial w}{\partial s} + \beta_{66} \sigma_{sz} + (C'_{62} D) / C'_{22} \right) = 0 \quad (8.133)$$

$$\frac{\partial}{\partial s} \left( -\frac{\partial w}{\partial \xi} + C'_{44} \sigma_{z\xi} \right) + \frac{\partial}{\partial \xi} \left( -\frac{\partial w}{\partial s} + \beta_{66} \sigma_{sz} + (C'_{62} D) / C'_{22} \right) = 0 \quad \frac{dv}{ds} + \frac{du}{d\xi} = 0. \quad (8.134)$$

To satisfy the vanishing of partial derivatives of  $D$  in eq. (8.132), we find that function  $D$  is linear in the coordinates. That is,

$$D = \bar{A}s + \bar{B}\xi + \bar{C}, \quad (8.135)$$

where  $\bar{A}$ ,  $\bar{B}$ , and  $\bar{C}$  are constants that will be determined later. Integrate the second expression eq. (8.133) with respect to  $s$ , and then integrate the first expression in eq. (8.133) with respect to  $\xi$ . The results of these integrations are

$$-\frac{\partial w}{\partial s} + \beta_{66} \sigma_{sz} + (C'_{62} D) / C'_{22} + F_1(\xi) = 0, \text{ and} \quad (8.136)$$

$$-\frac{\partial w}{\partial \xi} + C'_{44} \sigma_{z\xi} + F_2(s) = 0. \quad (8.137)$$

Substitute eq. (8.136) and eq. (8.137) into the first expression in eq. (8.134) to find

$$\frac{dF_1}{d\xi} + \frac{dF_2}{ds} = 0. \quad (8.138)$$

Equation (8.138) is satisfied by  $F_1(\xi) = -\lambda\xi$  and  $F_2(s) = \lambda s$ , where  $\lambda$  is called a separation constant. Substitute the result for  $F_1$  into eq. (8.136) to find

$$\frac{\partial w}{\partial s} = \beta_{66} \sigma_{sz} + (C'_{62} D) / C'_{22} - \lambda\xi. \quad (8.139)$$

Substitute the result for  $F_2$  into eq. (8.137) to find

$$\frac{\partial w}{\partial \xi} = C'_{44} \sigma_{z\xi} + \lambda s. \quad (8.140)$$

Substitute the derivative of displacement  $w$  with respect to  $\xi$  from eq. (8.140) into the displacement  $u_\xi$  given in eq. (8.125) to get

$$u_\xi = \frac{-z^2}{2} \bar{B} - \lambda z s + v(s). \quad (8.141)$$

Substitute the derivative of displacement  $w$  with respect to  $s$  from eq. (8.139) into the displacement  $u_s$  given in eq. (8.129) to get

$$u_s = \frac{-z^2}{2} \bar{A} + \lambda z \xi + u(\xi). \quad (8.142)$$

From eq. (8.134) consider the relation  $\frac{dv}{ds} + \frac{du}{d\zeta} = 0$ . The latter relation is satisfied by  $\frac{dv}{ds} = -\omega$  and  $\frac{du}{d\zeta} = \omega$ , where  $\omega$  is a second separation constant. Thus,  $v(s) = -\omega s + v(0)$  and  $u(\zeta) = \omega\zeta + u(0)$ . Substitute the equations for  $v(s)$  and  $u(\zeta)$  into eqs. eq. (8.141) and eq. (8.142) to get

$$u_{\zeta} = \frac{-z^2}{2}\bar{B} - \lambda z s - \omega s + v(0) \quad u_s = \frac{-z^2}{2}\bar{A} + \lambda z \zeta + \omega \zeta + u(0). \quad (8.143)$$

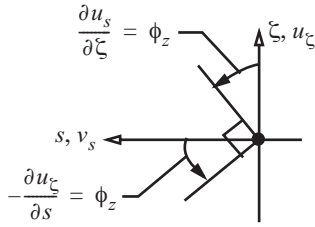


**Fig. 8.12 Rotation of the cross section about the  $z$ -axis.**

From eq. (8.118) the in-plane shear strain  $\gamma_{\zeta s} = \frac{\partial u_{\zeta}}{\partial s} + \frac{\partial u_s}{\partial \zeta} = 0$ . As shown in figure. 8.12 the partial derivative terms appearing in the shear strain can be related to rotation  $\phi_z$  of the cross section. Let  $\frac{\partial u_s}{\partial \zeta} = \phi_z$  and let  $-\frac{\partial u_{\zeta}}{\partial s} = \phi_z$ . The partial derivatives of the displacements in eq. (8.143) are equated to the rotation to get

$$\phi_z = \frac{\partial u_s}{\partial \zeta} = \lambda z + \omega, \text{ and } \phi_z = -\frac{\partial u_{\zeta}}{\partial s} = \lambda z + \omega. \quad (8.144)$$

Thus,  $\phi_z = \lambda z + \omega$ , from which we identify the separation constant  $\lambda = \frac{d\phi_z}{dz}$ . The separation constant  $\omega$  represents a rigid body rotation of the bar about the  $z$ -axis. To prevent rigid body rotation and displacement of the cross section set  $\omega = 0$ ,  $v(0) = 0$ , and  $u(0) = 0$ . The final results for the displacements are

$$u_z = z(\bar{A}s + \bar{B}\zeta + \bar{C}) + w(s, \zeta), \quad (8.145)$$

$$u_{\zeta} = \frac{-z^2}{2}\bar{B} - z s \frac{d\phi_z}{dz}, \text{ and} \quad (8.146)$$

$$u_s = \frac{-z^2}{2}\bar{A} + z \zeta \frac{d\phi_z}{dz}. \quad (8.147)$$

## 8.4.2 Equilibrium

The differential equation for axial equilibrium is

$$\frac{\partial \sigma_{sz}}{\partial s} + \frac{\partial \sigma_{\zeta z}}{\partial \zeta} + \underbrace{\frac{\partial \sigma_{zz}}{\partial z}}_{=0} = 0. \quad (8.148)$$

The axial normal stress  $\sigma_{zz}$  does not contribute to eq. (8.148) since it is independent of coordinate  $z$ . Equation (8.148) is identically satisfied by the introduction of the stress function  $\psi(s, \zeta)$  where the stress components are related to the stress function by

$$\sigma_{sz} = -\frac{\partial \psi}{\partial \zeta} \quad \sigma_{\zeta z} = \frac{\partial \psi}{\partial s}. \quad (8.149)$$

For shear stress  $\sigma_{\zeta z}$  to satisfy the boundary conditions (8.115) at  $\zeta = \pm t/2$  the stress function  $\partial \psi / \partial s = 0$ .

For shear stress  $\sigma_{sz}$  to satisfy the boundary conditions (8.116) at  $s = \pm b/2$  the stress function  $\partial\psi/\partial\zeta = 0$ . That is the stress function is a constant on the boundaries, and for convenience we take  $\psi = 0$  on the boundaries of the rectangular domain.

Substitute eq. (8.149) for the shear stresses in the expression (8.114) for the torque to get

$$M_z = \int_{-b/2}^{b/2} \left[ \int_{-t/2}^{t/2} \left( \zeta \left( -\frac{\partial\psi}{\partial\zeta} \right) - s \left( \frac{\partial\psi}{\partial s} \right) \right) d\zeta \right] ds. \quad (8.150)$$

Integrate eq. (8.150) by parts with respect to  $s$  and  $\zeta$  to get

$$M_z = \int_{-b/2}^{b/2} \left\{ -\zeta\psi \Big|_{t/2}^{t/2} + \int_{-t/2}^{t/2} \psi d\zeta \right\} ds + \int_{-t/2}^{t/2} \left\{ [-s\psi]_{-b/2}^{b/2} + \int_{-b/2}^{b/2} \psi ds \right\} d\zeta. \quad (8.151)$$

Since the stress function is equal to zero on the boundaries we find that the torque is given by integral of the stress function over the cross-sectional area:

$$M_z = 2 \int_{-b/2}^{b/2} \int_{-t/2}^{t/2} \psi d\zeta ds. \quad (8.152)$$

We make an additional assumption for the stress function that

$$\psi(s, \zeta) = \psi_1(s) [(t/2)^2 - \zeta^2], \quad (8.153)$$

which satisfies the boundary condition that  $\psi(s, \pm t/2) = 0$ . Function  $\psi_1(s)$  must satisfy the boundary condition  $\psi_1(\pm b/2) = 0$ . The shear stresses for this assumption are given by

$$\sigma_{sz} = 2\psi_1(s)\zeta \quad \sigma_{\zeta z} = \frac{d\psi_1}{ds} [(t/2)^2 - \zeta^2]. \quad (8.154)$$

Substitute the stress function (8.153) into the torque (8.152) to get

$$M_z = \frac{t^3}{3} \int_{-b/2}^{b/2} \psi_1(s) ds. \quad (8.155)$$

### 8.4.3 Static equivalence

In general, the resultants of the axial normal stress  $\sigma_{zz}$  acting over the cross section are a normal force denoted by  $N$ , a bending moment about the  $s$ -axis by  $M_s$ , and a bending moment about the  $\zeta$ -axis by  $M_\zeta$ . For a laminated wall these resultants are given by

$$(N, M_\zeta, M_s) = \int_{-b/2}^{b/2} \left[ \sum_{k=1}^{N_p} \int_{\zeta_k}^{\zeta_{k+1}} (1, \zeta, s) \sigma_{zz}^{(k)} d\zeta \right] ds, \quad (8.156)$$

where  $N_p$  is the number of plies, and  $k = 1, 2, \dots, N_p$ . At the bottom of the  $k$ -th ply  $\zeta = \zeta_k$ , and at the top of the  $k$ -th ply  $\zeta = \zeta_{k+1}$ ,  $\zeta_{k+1} > \zeta_k$ . From eqs. (8.123) and (8.149) the axial normal stress in the  $k$ -th ply is

$$\sigma_{zz}^{(k)} = \frac{D}{C'_{22}(k)} - \left( \frac{C'_{26}}{C'_{22}} \right)^{(k)} \sigma_{sz} = \frac{(\bar{A}s + \bar{B}\zeta + \bar{C})}{C'_{22}(k)} - \left( \frac{C'_{26}}{C'_{22}} \right)^{(k)} 2\zeta\psi_1(s). \quad (8.157)$$

Substitute eq. (8.157) for the axial normal stress into the equations for the axial force and bending moments given by eq. (8.156). In the process of computing the resultants, integrals that are explicit in coordinates  $s$  and  $\zeta$  are performed. Integrals of the stress function also appear in this process and from eq. (8.155), and we use the fact that

$$\int_{-b/2}^{b/2} \psi_1(s) ds = \frac{3M_z}{t^3}.$$

The results are

$$N = (bB_{22})\bar{B} + (bA_{22})\bar{C} - \frac{6}{t^3}\theta_{26}M_z, \quad (8.158)$$

$$M_s = (bD_{22})\bar{B} + (bB_{22})\bar{C} - \eta_{26}M_z, \text{ and} \quad (8.159)$$

$$M_\zeta = \left( \frac{b^3}{12}A_{22} \right)\bar{A} - 2\theta_{26} \int_{-b/2}^{b/2} s\psi_1(s) ds. \quad (8.160)$$

Stiffness coefficients in the previous equations are defined by

$$A_{22} = \sum_{k=1}^{Np} \frac{1}{C'_{22}(k)} (\zeta_{k+1} - \zeta_k) \quad B_{22} = \sum_{k=1}^{Np} \frac{1}{2C'_{22}(k)} (\zeta_{k+1}^2 - \zeta_k^2) \quad D_{22} = \sum_{k=1}^{Np} \frac{1}{3C'_{22}(k)} (\zeta_{k+1}^3 - \zeta_k^3). \quad (8.161)$$

Shear-extension coupling coefficients are defined by

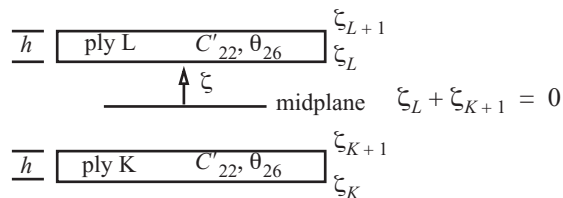
$$\theta_{26} = \sum_{k=1}^{Np} \left( \frac{C'_{26}}{C'_{22}} \right)^{(k)} \frac{1}{2} (\zeta_{k+1}^2 - \zeta_k^2) \quad \eta_{26} = \left( \frac{6}{t^3} \right) \sum_{k=1}^{Np} \left( \frac{C'_{26}}{C'_{22}} \right)^{(k)} \frac{1}{3} (\zeta_{k+1}^3 - \zeta_k^3). \quad (8.162)$$

We limit consideration to a **symmetric laminate** in which the stacking sequence of the plies is symmetric about the midplane. Symmetry leads to coefficients

$$B_{22} = \theta_{26} = 0. \quad (8.163)$$

To illustrate that symmetry results in the previous property consider two identical plies labeled  $K$  and  $L$  in figure. 8.13. The two plies have the same material properties, same thickness denoted by  $h$ , and are symmetrically

**Fig. 8.13 Identical plies symmetric about the midplane.**



located with respect to the midplane. Symmetry requires the coordinates  $\zeta_L + \zeta_{K+1} = 0$ . The remaining coordinates are  $\zeta_K = \zeta_{K+1} - h$  and  $\zeta_{L+1} = \zeta_L + h$ . The sum the of plies  $K$  and  $L$  that contribute to coefficient  $B_{22}$  are



$$\frac{1}{2C'_{22}}[\zeta_{L+1}^2 - \zeta_L^2 + \zeta_{K+1}^2 - \zeta_K^2] = \frac{1}{2C'_{22}}[(\zeta_L + h)^2 - \zeta_L^2 + (-\zeta_L)^2 - (-\zeta_L - h)^2] = 0. \quad (8.164)$$

Hence, for a symmetric laminate the normal force  $N = 0$  leads to coefficient  $\bar{C} = 0$ , bending moment  $M_\zeta = 0$  leads to coefficient  $\bar{A} = 0$ , and bending moment  $M_s = 0$  leads to coefficient  $B$  given by

$$\bar{B} = \frac{\eta_{26}}{bD_{22}}M_z. \quad (8.165)$$

The transverse shear resultants acting on the cross section are denoted by  $V_s$  and  $V_\zeta$ . They are given by

$$V_s = \int_{-b/2}^{b/2} \left[ \int_{-t/2}^{t/2} \sigma_{zs} d\zeta \right] ds \text{ and } V_\zeta = \int_{-t/2}^{t/2} \left[ \int_{-b/2}^{b/2} \sigma_{z\zeta} ds \right] d\zeta. \quad (8.166)$$

Substitute eq. (8.154) for the shear stresses in the integrals of the previous equations to get

$$V_s = \int_{-b/2}^{b/2} 2\psi_1 \left[ \int_{-t/2}^{t/2} \zeta d\zeta \right] ds = \int_{-b/2}^{b/2} 2\psi_1[0] ds = 0, \text{ and} \quad (8.167)$$

$$V_\zeta = \int_{-t/2}^{t/2} \left\{ [t/2^2 - \zeta^2] \left[ \int_{-b/2}^{b/2} \frac{d\psi_1}{ds} ds \right] \right\} d\zeta = \int_{-t/2}^{t/2} \{ [t/2^2 - \zeta^2] [\psi_1(b/2) - \psi_1(-b/2)] \} d\zeta = 0. \quad (8.168)$$

Therefore, the resultants acting on the cross section of the bar are  $N = V_s = V_\zeta = M_s = M_\zeta = 0$  and an applied torque  $M_z \neq 0$ .

#### 8.4.4 Principle of complementary virtual work

Consider uniform torsion state of the bar as shown in figure. 8.11 where the displacements, strains, and forces satisfy the compatibility conditions, Hooke's law, and the equilibrium conditions. In this state, the actual displacements are  $u_z$ ,  $u_\zeta$ , and  $u_s$  given by eqs. (8.145), (8.146), and (8.147), respectively. The actual non-zero strains are  $\epsilon_{zz}$ ,  $\gamma_{z\zeta}$ , and  $\gamma_{sz}$  and the corresponding stresses are  $\sigma_{zz}$ ,  $\sigma_{z\zeta}$ , and  $\sigma_{sz}$ , respectively. The only cross-sectional resultant is the torque  $M_z$  and its corresponding rotation is  $\phi_z$ . Now consider infinitesimal increments in the stresses denoted by  $\delta\sigma_{zz}$ ,  $\delta\sigma_{z\zeta}$ , and  $\delta\sigma_{sz}$  that satisfy equilibrium. For a bar of length  $L$ ,  $0 \leq z \leq L$ , the increment in the internal complementary work is given by

$$\delta W_{\text{int}} = \int_0^L \left\{ \int_{-b/2}^{b/2} \int_{-t/2}^{t/2} (\epsilon_{zz} \delta\sigma_{zz} + \gamma_{z\zeta} \delta\sigma_{z\zeta} + \gamma_{sz} \delta\sigma_{sz}) d\zeta ds \right\} dz = L \int_{-b/2}^{b/2} \int_{-t/2}^{t/2} (\epsilon_{zz} \delta\sigma_{zz} + \gamma_{z\zeta} \delta\sigma_{z\zeta} + \gamma_{sz} \delta\sigma_{sz}) d\zeta ds, \quad (8.169)$$

Note that the strains and stresses are independent of the axial coordinate  $z$ . The increment in the external complementary work is

$$\delta W_{\text{ext}} = \int_{-b/2}^{b/2} \int_{-t/2}^{t/2} (u_z \delta\sigma_{zz} + u_\zeta \delta\sigma_{z\zeta} + u_s \delta\sigma_{zs}) \Big|_{z=L} d\zeta ds - \int_{-b/2}^{b/2} \int_{-t/2}^{t/2} (u_z \delta\sigma_{zz} + u_\zeta \delta\sigma_{z\zeta} + u_s \delta\sigma_{zs}) \Big|_{z=0} d\zeta ds. \quad (8.170)$$

From eqs. (8.145) to (8.147), and with displacement coefficients  $\bar{A} = \bar{C} = 0$ , the displacements at the end cross sections are as follows:

$$\text{At } z = 0, u_z = w(s, \zeta), u_\zeta = 0, \text{ and } u_s = 0. \quad (8.171)$$

$$\text{At } z = L, u_z = L\bar{B}\zeta + w(s, \zeta), u_\zeta = -\frac{L^2\bar{B}}{2} - Ls\frac{d\phi_z}{dz}, \text{ and } u_s = L\zeta\frac{d\phi_z}{dz}. \quad (8.172)$$

Substitute the displacements at  $z = 0$  and  $z = L$  into the increment in the external work (8.170) to get

$$\delta W_{\text{ext}} = \int_{-b/2-t/2}^{b/2} \int_{-t/2}^{t/2} \left[ (L\bar{B}\zeta + w(s, \zeta))\delta\sigma_{zz} + \left(-\frac{L^2\bar{B}}{2} - Ls\frac{d\phi_z}{dz}\right)\delta\sigma_{z\zeta} + \left(L\zeta\frac{d\phi_z}{dz}\right)\delta\sigma_{zs} \right] d\zeta ds - \int_{-b/2-t/2}^{b/2} \int_{-t/2}^{t/2} [w(s, \zeta)\delta\sigma_{zz}] d\zeta ds,$$

in which we used the fact that the increments in the stresses are independent of the coordinate  $z$ . The integrals involving  $w\delta\sigma_{zz}$  add to zero. Hence,

$$\delta W_{\text{ext}} = \int_{-b/2-t/2}^{b/2} \int_{-t/2}^{t/2} \left[ (L\bar{B}\zeta)\delta\sigma_{zz} + \left(-\frac{L^2\bar{B}}{2} - Ls\frac{d\phi_z}{dz}\right)\delta\sigma_{z\zeta} + \left(L\zeta\frac{d\phi_z}{dz}\right)\delta\sigma_{zs} \right] d\zeta ds.$$

Rearrange the terms in the last equation, and note displacement coefficient  $\bar{B}$  is a constant, to get

$$\delta W_{\text{ext}} = L\bar{B} \int_{-b/2-t/2}^{b/2} \int_{-t/2}^{t/2} \zeta\delta\sigma_{xx} d\zeta ds - \frac{L^2\bar{B}}{2} \int_{-b/2-t/2}^{b/2} \int_{-t/2}^{t/2} \delta\sigma_{z\zeta} d\zeta ds + L\frac{d\phi_z}{dz} \int_{-b/2-t/2}^{b/2} \int_{-t/2}^{t/2} (\zeta\delta\sigma_{zs} - s\delta\sigma_{z\zeta}) d\zeta ds. \quad (8.173)$$

Integrals of the increments in the stresses are identified as increments in the resultants  $\delta M_s$ ,  $\delta V_\zeta$ , and  $\delta M_z$ .

Then, we find

$$\delta W_{\text{ext}} = L\bar{B}\delta M_s - \frac{L^2\bar{B}}{2}\delta V_\zeta + L\frac{d\phi_z}{dz}\delta M_z. \quad (8.174)$$

Since the bending moment  $M_s$  is prescribed then  $\delta M_s = 0$ . Similarly, shear force  $V_\zeta$  is prescribed, so

$\delta V_\zeta = 0$ . The final expression for the increment in the external work is

$$\delta W_{\text{ext}} = L\frac{d\phi_z}{dz}\delta M_z. \quad (8.175)$$

Equate the increment in the external work (8.175) to the increment in internal work (8.169), followed by division by  $L$ , to get the principle of complementary work as

$$\frac{d\phi_z}{dz}\delta M_z = \int_{-b/2-t/2}^{b/2} \int_{-t/2}^{t/2} (\epsilon_{zz}\delta\sigma_{zz} + \gamma_{z\zeta}\delta\sigma_{z\zeta} + \gamma_{sz}\delta\sigma_{sz}) d\zeta ds. \quad (8.176)$$

The strain-stress relations are given by Hooke's law in eqs. (8.119) to (8.121). In Hooke's law for the strains  $\epsilon_{zz}$  and  $\gamma_{sz}$  we substitute eq. (8.123) for the axial normal stress. After the process of eliminating the axial normal stress, we get the strain relations as

$$\varepsilon_{zz} = \bar{B}\bar{\zeta} \quad \gamma_{z\zeta} = C'_{44}\sigma_{z\zeta} \quad \gamma_{sz} = \left(\frac{C'_{26}}{C'_{22}}\right)\bar{B}\bar{\zeta} + \beta_{66}\sigma_{sz}, \quad (8.177)$$

where the compliance coefficient  $\beta_{66} = C'_{66} - C'^2_{26}/C'_{22}$ . Let  $\bar{B} \rightarrow \bar{B} + \delta\bar{B}$  and  $\sigma_{sz} \rightarrow \sigma_{sz} + \delta\sigma_{sz}$  in eq. (8.123) to find that the increment in the normal stress is

$$\delta\sigma_{zz} = \frac{\bar{\zeta}}{C'_{22}}\delta\bar{B} - \frac{C'_{26}}{C'_{22}}\delta\sigma_{sz}. \quad (8.178)$$

Substitute eq. (8.177) for the strains in eq. (8.176), followed by substitution of eq. (8.178) for the increment in the normal stress. The result of these substitutions is the following form for the principle of complementary work:

$$\frac{d\phi_z}{dz}\delta M_z = \int_{-b/2}^{b/2} \left\{ \int_{t/2}^{t/2} \left[ \left(\frac{\bar{\zeta}^2}{C'_{22}}\bar{B}\right)\delta\bar{B} + (C'_{44}\sigma_{z\zeta})\delta\sigma_{z\zeta} + (\beta_{66}\sigma_{sz})\delta\sigma_{sz} \right] d\bar{\zeta} \right\} ds. \quad (8.179)$$

Statically admissible increments  $\delta\sigma_{sz}$  and  $\delta\sigma_{z\zeta}$  in eq. (8.179) are defined in terms of the increment in the stress function  $\delta\psi_1$  by

$$\delta\sigma_{sz} = 2\bar{\zeta}\delta\psi_1(s) \quad \delta\sigma_{z\zeta} = \delta\left(\frac{d\psi_1}{ds}\right)\left[\left(\frac{t}{2}\right)^2 - \bar{\zeta}^2\right]. \quad (8.180)$$

Substitute eq. (8.180) for the increments in the stresses in eq. (8.179), followed by the substituting of eq. (8.154) for the stresses  $\sigma_{sz}$  and  $\sigma_{z\zeta}$  in eq. (8.179). The result of these substitutions is

$$\frac{d\phi_z}{dz}\delta M_z = \int_{-b/2}^{b/2} \left\{ \int_{t/2}^{t/2} \left[ \left(\frac{\bar{\zeta}^2}{C'_{22}}\bar{B}\right)\delta\bar{B} + \left(C'_{44}\left[\frac{t^2}{2} - \bar{\zeta}^2\right]^2 \frac{d\psi_1}{ds}\right)\delta\left(\frac{d\psi_1}{ds}\right) + (4\beta_{66}\bar{\zeta}^2\psi_1)\delta\psi_1 \right] d\bar{\zeta} \right\} ds. \quad (8.181)$$

In the case of laminated cross section the last equation is written as

$$\frac{d\phi_z}{dz}\delta M_z = \int_{-b/2}^{b/2} \left\{ \sum_{k=1}^{N_p} \int_{\zeta_k}^{\zeta_{k+1}} \left[ \left(\frac{\bar{\zeta}^2}{C'_{22}^{(k)}}\bar{B}\right)\delta\bar{B} + \left(C'_{44}^{(k)}\left[\frac{t^2}{2} - \bar{\zeta}^2\right]^2 \frac{d\psi_1}{ds}\right)\delta\left(\frac{d\psi_1}{ds}\right) + (4\beta_{66}^{(k)}\bar{\zeta}^2\psi_1)\delta\psi_1 \right] d\bar{\zeta} \right\} ds.$$

The integrations with respect to  $\bar{\zeta}$  are carried out in the previous equation, and the result is written as

$$\frac{d\phi_z}{dz}\delta M_z = \int_{-b/2}^{b/2} \left[ (D_{22}\bar{B})\delta\bar{B} + \left[\left(\frac{t^5}{30}a_{44}\right)\frac{d\psi_1}{ds}\right]\delta\left(\frac{d\psi_1}{ds}\right) + \left[\left(4\frac{t^3}{12}a_{66}\right)\psi_1\right]\delta\psi_1 \right] ds, \quad (8.182)$$

where the stiffness coefficient  $D_{22}$  is given in eq. (8.161). The laminate compliance coefficients in eq. (8.182) are defined by

$$a_{44} = \left(\frac{30}{t^5}\right) \sum_{k=1}^{N_p} C'_{44}^{(k)} \int_{\zeta_k}^{\zeta_{k+1}} \left[\frac{t^2}{2} - \bar{\zeta}^2\right]^2 d\bar{\zeta} = \left(\frac{30}{t^5}\right) \sum_{k=1}^{N_p} C'_{44}^{(k)} \left[ \frac{t^4}{16}(\zeta_{k+1} - \zeta_k) - \frac{t^2}{6}(\zeta_{k+1}^3 - \zeta_k^3) + \frac{1}{5}(\zeta_{k+1}^5 - \zeta_k^5) \right], \text{ and } (8.183)$$

$$a_{66} = \left(\frac{12}{t^3}\right) \sum_{k=1}^{Np} \beta_{66}^{(k)} \int_{\zeta_k}^{\zeta_{k+1}} \zeta^2 d\zeta = \left(\frac{12}{t^3}\right) \sum_{k=1}^{Np} \beta_{66}^{(k)} \frac{1}{3} (\zeta_{k+1}^3 - \zeta_k^3). \quad (8.184)$$

The terms involving the derivatives of  $\psi_1$  and  $\delta\psi_1$  in eq. (8.182) are integrated by parts with respect to  $s$ . Note that the boundary term vanishes since  $\delta\psi_1(\pm b/2) = 0$ . ( $\psi_1$  is specified at  $s = \pm b/2$ .) After integration by parts, eq. (8.182) reduces to

$$\frac{d\phi_z}{dz} \delta M_z = (bD_{22}\bar{B})\delta\bar{B} + \int_{-b/2}^{b/2} \left[ -\left(\frac{t^5}{30}a_{44}\right) \frac{d^2\psi_1}{ds^2} + \frac{t^3}{3}a_{66}\psi_1 \right] \delta\psi_1 ds. \quad (8.185)$$

From eq. (8.165) we substitute  $\delta\bar{B} = \frac{\eta_{26}}{bD_{22}}\delta M_z$  in eq. (8.185) and collect the terms multiplying  $\delta M_z$  to get

$$\delta M_z \left[ \frac{d\phi_z}{dz} - \eta_{26}\bar{B} \right] = \int_{-b/2}^{b/2} \left[ -\left(\frac{t^5}{30}a_{44}\right) \frac{d^2\psi_1}{ds^2} + \frac{t^3}{3}a_{66}\psi_1 \right] \delta\psi_1 ds. \quad (8.186)$$

Finally, substitute  $\delta M_z = \frac{t^3}{3} \int_{-b/2}^{b/2} \delta\psi_1 ds$  in eq. (8.186) to get the complementary work statement as

$$\int_{-b/2}^{b/2} \left[ \frac{t^3}{3} \left( \frac{d\phi_z}{dz} - \eta_{26}\bar{B} \right) \right] \delta\psi_1 ds = \int_{-b/2}^{b/2} \left[ -\left(\frac{t^5}{30}a_{44}\right) \frac{d^2\psi_1}{ds^2} + \frac{t^3}{3}a_{66}\psi_1 \right] \delta\psi_1 ds. \quad (8.187)$$

Since the increment in complementary work (8.187) holds for every continuous function  $\delta\psi_1(s)$  such that  $\delta\psi_1(\pm b/2) = 0$ , we find the following differential equation governing function  $\psi_1(s)$ :

$$-\left(\frac{t^5}{30}a_{44}\right) \frac{d^2\psi_1}{ds^2} + \frac{t^3}{3}a_{66}\psi_1 = \frac{t^3}{3} \left( \frac{d\phi_z}{dz} - \eta_{26}\bar{B} \right) \quad -b/2 < s < b/2. \quad (8.188)$$

Simplify eq. (8.188) by multiplying by  $-3/t^3$  to write the differential equation as

$$\frac{t^2}{10}a_{44} \frac{d^2\psi_1}{ds^2} - a_{66}\psi_1 = -\left(\frac{d\phi_z}{dz} - \eta_{26}\bar{B}\right) \quad -b/2 < s < b/2. \quad (8.189)$$

The solution of eq. (8.189) subject to  $\psi_1(\pm b/2) = 0$  is

$$\psi_1(s) = \frac{1}{a_{66}} \left( \frac{d\phi_z}{dz} - \eta_{26}\bar{B} \right) \left[ 1 - \frac{\cosh \mu s}{\cosh \mu b/2} \right], \text{ where } \mu = \frac{1}{t} \sqrt{10a_{66}/a_{44}}. \quad (8.190)$$

The torque is computed from eq. (8.155) to find

$$M_z = \frac{bt^3}{3a_{66}} \left( \frac{d\phi_z}{dz} - \eta_{26}\bar{B} \right) g\left(\mu \frac{b}{2}\right), \quad (8.191)$$

where the function  $g(\mu b/2)$  is defined as

$$g\left(\mu \frac{b}{2}\right) = 1 - \left(\mu \frac{b}{2}\right)^{-1} \tanh\left(\mu \frac{b}{2}\right), \text{ and } \mu \frac{b}{2} = \frac{b}{2t} \sqrt{10(a_{66}/a_{44})}. \quad (8.192)$$

Substitute eq. (8.165) for coefficient  $\bar{B}$  in eq. (8.191) to find

$$M_z = \frac{bt^3}{3a_{66}} \left( \frac{d\phi_z}{dz} - \frac{\eta_{26}^2}{bD_{22}} M_z \right) g\left(\mu \frac{b}{2}\right)$$

Solve the latter equation for the torque and write the result as

$$M_z = D_T \frac{d\phi_z}{dz}. \quad (8.193)$$

where  $D_T$  is the torsional stiffness of the bar given by

$$D_T = \frac{bt^3}{3} \frac{g\left(\mu \frac{b}{2}\right)}{a_{66} + \left[ t^3 \eta_{26}^2 g\left(\mu \frac{b}{2}\right) \right] / (3D_{22})}. \quad (8.194)$$

From eq. (8.146) and eq. (8.165), the lateral displacement of the bar is

$$u_\xi = -\frac{z^2}{2} \left( \frac{\eta_{26}}{bD_{22}} \right) M_z - zs \left( \frac{M_z}{D_T} \right). \quad (8.195)$$

Under the action of torsion the axis of the bar does not remain straight, but it is curved as shown in figure. 8.14(a).

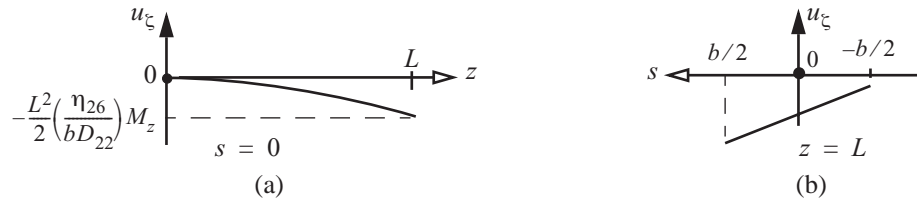


**Fig. 8.14** Lateral displacement of the bar under torsion: (a) in the plane  $s = 0$ , and (b) in the plane  $z = L$

### Example 8.5 Transverse bending and torsion of a composite channel section

The cross section of the bar shown in figure. 8.15(a) is composed of a lower horizontal flange with length  $b_1 = 16$  mm, an upper horizontal flange with length  $b_3 = 16$  mm. The flanges are joined by a vertical web with length  $b_2 = 32$  mm. The lower flange is denoted by branch 1, the web by branch 2, and the upper flange by branch 3. Each branch is fabricated from T300/5208 graphite/epoxy with material properties listed in Table 8.2 on page 231, and the dimensional units used in this example are Newtons and millimeters. The laminate in each branch consists of eight plies with a specially orthotropic, symmetric stacking sequence of  $[45^\circ/-45^\circ/0/90]_S$ .

The thickness of each branch  $t = 1.016$  mm. As shown in figure. 8.15(b), the cross section is symmetric about the X-axis both in geometry and material properties. The axial stiffness per unit length  $B$  is given in eq. (8.46),

the torsional stiffness per unit length  $B_s$  is given in eq. (8.47), and they are the same in each branch. For a specially orthotropic laminate the coupling coefficient  $b = 0$  in eq. (8.46). Numerical evaluation of these stiffness coefficients are

$$B = A_{22} - A_{12}A_{21}/A_{11} = 15,822.7 \text{ N/mm}, \text{ and } B_s = A_{66} = 5,565.23 \text{ N/mm}.$$

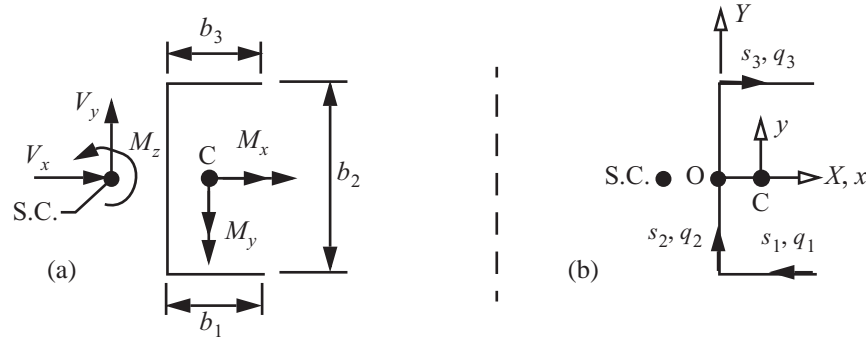


**Fig. 8.15 (a) Channel section subject to transverse bending and torsion. (b) Cross-sectional coordinate systems and shear flows.**

The section shown in figure. 8.15(a) is subject to an axial force  $N$  (not shown in figure. 8.15(a)), transverse shear forces  $V_x$  and  $V_y$ , bending moments  $M_x$  and  $M_y$ , and a torque  $M_z$ .

- Determine the material law for extension and bending of the bar.
- Determine the material law for shear and torsion of the bar.

**Solution to part (a).** The parametric equations of the contour in the  $X$ - $Y$  coordinates are

$$\begin{aligned} X_1(s_1) &= b_1 - s_1 & Y_1 &= -b_2/2 & 0 \leq s_1 \leq b_1, \\ X_2(s_2) &= 0 & Y_2(s_2) &= -b_2/2 + s_2 & 0 \leq s_2 \leq b_2, \text{ and} \\ X_3(s_3) &= s_3 & Y_3 &= b_2/2 & 0 \leq s_3 \leq b_3. \end{aligned}$$

To locate the modulus-weighted centroid on the  $X$ -axis, we first have to determine the modulus-weighted area  $S$  and the modulus-weighted first area moment about the  $Y$ -axis  $S_Y$  from eq. (8.52). These are given by

$$\begin{aligned} S &= \int_0^{b_1} B ds_1 + \int_0^{b_2} B ds_2 + \int_0^{b_3} B ds_3 = B(b_1 + b_2 + b_3) = 1.01265 \times 10^6 \text{ N}, \text{ and} \\ S_Y &= \int_0^{b_1} B X_1(s_1) ds_1 + \int_0^{b_2} B X_2(s_2) ds_2 + \int_0^{b_3} B X_3(s_3) ds_3 = B(b_1^2 + b_3^2)/2 = 4.05061 \times 10^6 \text{ N-mm}. \end{aligned}$$

The location of the modulus-weighted centroid (8.53) is

$$X_c = S_Y/S = \frac{b_1^2 + b_3^2}{2(b_1 + b_2 + b_3)} = 4 \text{ mm} \quad Y_c = 0.$$

The parametric equations of the contour with respect to the centroidal axes  $x$  and  $y$  are determined as follows:

$$x_1(s_1) = X_1(s_1) - X_c = 12 \text{ mm} - s_1 \quad y_1 = -16 \text{ mm} \quad 0 \leq s_1 \leq 16 \text{ mm} \quad (\text{a})$$

$$x_2(s_2) = -4 \text{ mm} \quad y_2(s_2) = -16 \text{ mm} + s_2 \quad 0 \leq s_2 \leq 32 \text{ mm} \quad (\text{b})$$

$$x_3(s_3) = -4 \text{ mm} + s_3 \quad y_3 = 16 \text{ mm} \quad 0 \leq s_3 \leq 16 \text{ mm} \quad (\text{c})$$

Equations (a), (b), and (c) are substituted into the formulas for the modulus-weighted second moments  $D_{xx}$  and  $D_{yy}$  given by eq. (8.57) to get

$$D_{xx} = \int_0^{b_1} B y_1^2 ds_1 + \int_0^{b_2} B y_2^2 ds_2 + \int_0^{b_3} B y_3^2 ds_3 = 1.72826 \times 10^8 \text{ N-mm}^2, \text{ and} \quad (\text{d})$$

$$D_{yy} = \int_0^{b_1} B x_1^2 ds_1 + \int_0^{b_2} B x_2^2 ds_2 + \int_0^{b_3} B x_3^2 ds_3 = 0.27004 \times 10^8 \text{ N-mm}^2. \quad (\text{e})$$

The modulus-weighted product moment  $D_{xy} = 0$ , because the  $x$ -axis is an axis of symmetry. The cross-sectional material law in extension and bending is

$$\begin{bmatrix} N \\ M_x \\ M_y \end{bmatrix} = \begin{bmatrix} S & 0 & 0 \\ 0 & D_{xx} & 0 \\ 0 & 0 & D_{yy} \end{bmatrix} \begin{bmatrix} \frac{dw}{dz} \\ \frac{d\phi_x}{dz} \\ \frac{d\phi_y}{dz} \end{bmatrix} = 10^6 \begin{bmatrix} 1.01265 \text{ N} & 0 & 0 \\ 0 & 172.826 \text{ N-mm}^2 & 0 \\ 0 & 0 & 27.004 \text{ N-mm}^2 \end{bmatrix} \begin{bmatrix} \frac{dw}{dz} \\ \frac{d\phi_x}{dz} \\ \frac{d\phi_y}{dz} \end{bmatrix}. \quad (\text{f})$$

**Solution to part (b).** To establish the material law for shear and torsion we start with the shear flow given by eq. (8.113). For the channel section the product moment  $D_{xy} = 0$ , which means coefficients  $n_x = n_y = 0$  and  $k = 1$  in eqs. (8.59) and (8.69). At the contour origin where  $s_1 = 0$  the shear flow must equal zero since the longitudinal edge is free of traction. Equation (8.113) for each branch reduces to

$$q_j(s_j) = -S_{xj}(s_j) \frac{V_y}{D_{xx}} - S_{yj}(s_j) \frac{V_x}{D_{yy}} \quad 0 \leq s_j \leq b_j \quad j = 1, 2, 3. \quad (\text{g})$$

The modulus-weighted, first area moments  $S_x$  and  $S_y$  are functions of the contour coordinate given by eq. (8.70), and have dimensional units of  $\text{N-mm}$ . The first area moment functions with respect to the  $x$ -axis are

$$S_{x1}(s_1) = \int_0^{s_1} B y_1 ds_1 = -253,163 s_1 \quad 0 \leq s_1 \leq 16 \text{ mm}, \quad (\text{h})$$

$$S_{x2}(s_2) = S_{x1}(16) + \int_0^{s_2} B y_2 ds_2 = -4.05061 \times 10^6 - 253,163 s_2 + 7,911.34 s_2^2 \quad 0 \leq s_2 \leq 32 \text{ mm}, \text{ and} \quad (\text{i})$$

$$S_{x3}(s_3) = S_{x2}(32) + \int_0^{s_3} B_3 y_3 ds_3 = -4.05061 \times 10^6 + 253,163.s_3 \quad 0 \leq s_3 \leq 16 \text{ mm}. \quad (\text{j})$$

Note that at the free longitudinal edges  $S_{x1}(0) = 0$  and  $S_{x3}(16) = -4.05061 \times 10^6 + 4.05061 \times 10^6 = 0$ . The first area moment functions with respect to the y-axis are

$$S_{y1}(s_1) = \int_0^{s_1} B x_1 ds_1 = 189,872.s_1 - 7,911.34 s_1^2 \quad 0 \leq s_1 \leq 16 \text{ mm}, \quad (\text{k})$$

$$S_{y2}(s_2) = S_{y1}(16) + \int_0^{s_2} B x_2 ds_2 = 1.01265 \times 10^6 - 63,290.7 s_2 \quad 0 \leq s_2 \leq 32 \text{ mm}, \text{ and} \quad (\text{l})$$

$$S_{y3}(s_3) = S_{y2}(32) + \int_0^{s_3} B_3 x_3 ds_3 = -1.01265 \times 10^6 - 63,290.7 s_3 + 7,911.34 s_3^2 \quad 0 \leq s_3 \leq 16 \text{ mm}. \quad (\text{m})$$

Also note that  $S_{y1}(0) = 0$  and  $S_{y3}(16) = 0$ . The resultant of the shear flow distribution is a horizontal force denoted by  $F_X$ , a vertical force  $F_Y$ , and a torque at the shear center  $M_z$ . The resultant forces are

$$F_X = \int_0^{b_3} q_3 ds_3 - \int_0^{b_1} q_1 ds_1 = \frac{V_x}{2} + \frac{3}{16} V_y - \left( -\frac{V_2}{2} + \frac{3}{16} V_y \right) = V_x, \text{ and } F_Y = \int_0^{b_2} q_2 ds_2 = V_y. \quad (\text{n})$$

Equation (n) yields the expected result that the horizontal force equals the shear force  $V_x$ , and the vertical force equals the shear force  $V_y$ . We cannot compute the torque until the location of the shear center is known. The coordinates of the shear center  $(x_{sc}, y_{sc})$  are determined by letting  $I_{xx} \rightarrow D_{xx}$ ,  $I_{yy} \rightarrow D_{yy}$ ,  $\bar{Q}_x(s) \rightarrow \bar{S}_x(s)$ , and  $\bar{Q}_y(s) \rightarrow \bar{S}_y(s)$  in eq. (3.106) on page 54. The transformation of eq. (3.106) to the composite laminate is

$$x_{sc} = -\left(\frac{k}{D_{xx}}\right) \int_c r_{nc}(s) \bar{S}_x(s) ds \quad y_{sc} = \left(\frac{k}{D_{yy}}\right) \int_c r_{nc}(s) \bar{S}_y(s) ds. \quad (\text{o})$$

The coordinate normal to the contour with respect to the centroid is denoted by  $r_{nc}(s)$ . It is depicted in figure. 3.3(b) on page 33, and the expression to compute it is given in eq. (3.11) on page 34. For the channel section the normal coordinates for each branch are

$$r_{nci} = x_i \frac{dy_i}{ds_i} - y_i \frac{dx_i}{ds_i} \quad i = 1, 2, 3. \quad (\text{p})$$

Evaluation of eq. (p) results in  $r_{nc1} = -16 \text{ mm}$ ,  $r_{nc2} = -4 \text{ mm}$ , and  $r_{nc3} = -16 \text{ mm}$ . For the channel section in this example the evaluation of eq. (o) is



$$x_{sc} = \left( \frac{-1}{D_{xx}} \right) \sum_{i=1}^3 \int_0^{b_i} r_{nci} S_{xi} ds_i = -10 \text{ mm} \quad y_{sc} = \left( \frac{1}{D_{yy}} \right) \sum_{i=1}^3 \int_0^{b_i} r_{nci} S_{yi} ds_i = 0. \quad (\mathbf{q})$$

The torque from the shear flows with respect to the shear center is

$$M_z = \sum_{i=1}^3 \int_0^{b_i} r_{ni} q_i ds_i, \quad (\mathbf{r})$$

where the coordinate normal to the contour with respect to the shear center is denoted by  $r_n(s)$ . This normal coordinate is depicted in figure. 3.3(b) on page 33, and the expression to compute it is given in eq. (3.10) on page 34. For this example the normal coordinate for each branch is given by

$$r_{ni} = r_{nci} - x_{sc} \frac{dy_i}{ds_i} \quad i = 1, 2, 3. \quad (\mathbf{s})$$

Evaluation of eq. (s) yields  $r_{n1} = -16 \text{ mm}$ ,  $r_{n2} = 6 \text{ mm}$ , and  $r_{n3} = -16 \text{ mm}$ . Evaluating the torque given by eq. (r) gives

$$M_z = \underbrace{(8V_x - 3V_y)}_{\text{branch 1}} + \underbrace{(6V_y)}_{\text{branch 2}} + \underbrace{(-8V_x - 3V_y)}_{\text{branch 3}} = 0. \quad (\mathbf{t})$$

Equation (t) shows that the torque due to the shear flows equals zero at the shear center. Hence, the resultant of the shear flow distribution is a force with its line of action passing through the shear center having components  $V_x$  and  $V_y$ .

The material law for transverse shear relates the shear strains  $\psi_x$  and  $\psi_y$  to the shear forces  $V_x$  and  $V_y$ . For the bar made of an homogeneous, isotropic material this material law is discussed in article 5.5.3 on page 143. Referring to eq. (5.76) the form of the material law is the same for the composite material. That is,

$$\begin{bmatrix} \psi_x \\ \psi_y \end{bmatrix} = \begin{bmatrix} c_{xx} & c_{xy} \\ c_{yx} & c_{yy} \end{bmatrix} \begin{bmatrix} V_x \\ V_y \end{bmatrix}, \quad (\mathbf{u})$$

where the flexibility influence coefficients  $c_{xx}$ ,  $c_{xy}$ ,  $c_{yx}$ , and  $c_{yy}$  are determined from the complementary strain energy per unit axial length  $\bar{U}^*$ . For the open section  $\bar{U}^*$  is obtained from eq. (8.97) on page 242, and it is

$$\bar{U}^* = \frac{1}{2} \int_c \frac{1}{A_{66}} q^2 ds. \quad (\mathbf{v})$$

The shear strains  $\psi_x$  and  $\psi_y$  are determined from derivatives of the complementary strain energy per unit axial length with respect to the shear forces. For the channel section in this example we get the following results:

$$\psi_x = \frac{\partial \bar{U}^*}{\partial V_x} = \sum_{i=1}^3 \int_0^{b_i} \frac{1}{(A_{66})_i} q_i \frac{\partial q_i}{\partial V_x} ds_i = c_{xx} V_x + c_{xy} V_y,$$

$$\psi_y = \sum_{i=1}^3 \int_0^{b_i} \frac{1}{(A_{66})_i} q_i \frac{\partial q_i}{\partial V_y} ds_i = c_{yx} V_x + c_{yy} V_y,$$

$$c_{xx} = 9.16404 \times 10^{-6} \text{ N}^{-1} \quad c_{xy} = c_{yx} = 0 \quad c_{yy} = 6.73827 \times 10^{-6} \text{ N}^{-1}. \quad (\text{w})$$

In general, external loads cause the bar to resist a torque. For an open cross-sectional contour the shear flows cannot provide this resistance to torsion. A separate analysis for the linear elastic response to uniform torsion of a symmetrically laminated bar was developed in article 8.4. The result of this development is the material law (8.193) that equates the torque to torsional stiffness  $D_T$  times the twist per unit length. The torsional stiffness is given by eq. (8.194). To compute  $D_T$  we evaluate the following laminate properties:

- the transverse shear compliance (8.183)  $a_{44} = 242.736 \times 10^{-6} \text{ mm}^2/\text{N}$ ,
- the torsional compliance (8.184)  $a_{66} = 200.446 \times 10^{-6} \text{ mm}^2/\text{N}$ ,
- the bending stiffness (8.161)  $D_{22} = 1,130.94 \text{ N-mm}$ ,
- the dimensionless shear-extension coefficient in bending (8.162)  $\eta_{26} = -0.0459727$ , and
- the solution parameter (8.190)  $\mu = 2.82838 \text{ mm}^{-1}$ .

The function  $g(\mu b/2)$  appearing in the equation for  $D_T$  depends on the length of the branch. For the channel section the values of this function are

$$g\left(\frac{\mu b_1}{2}\right) = g\left(\frac{\mu b_3}{2}\right) = 0.955805 \quad g\left(\frac{\mu b_2}{2}\right) = 0.977903. \quad (\text{x})$$

The torsional stiffnesses for each branch are

$$D_{T1} = D_{T3} = \frac{16t^3}{3} \frac{g\left(\mu \frac{16}{2}\right)}{a_{66} + \left[t^3 \eta_{26}^2 g\left(\mu \frac{16}{2}\right)\right] / (3D_{22})} = 26,589 \text{ N-mm}^2, \text{ and} \quad (\text{y})$$

$$D_{T2} = \frac{32t^3}{3} \frac{g\left(\mu \frac{32}{2}\right)}{a_{66} + \left[t^3 \eta_{26}^2 g\left(\mu \frac{32}{2}\right)\right] / (3D_{22})} = 54,403.4 \text{ N-mm}^2. \quad (\text{z})$$

The torsional stiffness of the channel is equal to the sum of the torsional stiffnesses of each of its branches. That is,

$$D_T = D_{T1} + D_{T2} + D_{T3} = 107,581 \text{ N-mm}^2. \quad (\text{aa})$$

Finally, the material law for transverse shear and torsion is

$$\begin{bmatrix} V_x \\ V_y \\ M_z \end{bmatrix} = \begin{bmatrix} 109,122. \text{ N} & 0 & 0 \\ 0 & 148,406. \text{ N} & 0 \\ 0 & 0 & 107,581. \text{ N-mm}^2 \end{bmatrix} \begin{bmatrix} \psi_x \\ \psi_y \\ \frac{d\phi_z}{dz} \end{bmatrix} \quad \blacksquare$$

## 8.5 References

- Canaday, H. "Composites vs. Metals," in *Aerospace America* 53, no. 5, (May, 2015): 18-23.
- Chandra, R., A. T. Stemple, and I. Chopra. "Thin-Walled Composite Beams Under Bending, Torsional, and Extensional Loads." *Journal of Aircraft* 27, no. 7 (July, 1990): 6116-626.
- Herakovich, Carl T. *Mechanics of Fibrous Composites*. New York: John Wiley & Sons, Inc., 1998.
- Johnson, E. R., V. V. Vasiliev, V. V., and D. V. Vasiliev, "Anisotropic Thin-Walled Beams with Closed Cross-Sectional Contours." *AIAA Journal* 39, no. 12 (2001): 2389-2393.
- Lekhnitskii, S. G. *Theory of Elasticity of an Anisotropic Body*. Moscow: Mir Publishers, 1981, Sections 18 - 20, and 49.
- Nixon, M. W. "Extension-Twist Coupling of Composite Circular Tubes with Application to Tilt Rotor Blade Design." *Proceedings of the 28th Structures, Structural Dynamics, and Materials Conference* (Monterey, CA). Reston VA: American Institute of Aeronautics and Astronautics, 1987, Part I: 295-303
- Smith, E.C., and I. Chopra. "Formulation and Evaluation of an Analytical Model for Composite Box-Beams." *Journal of the American Helicopter Society* 36, no. 3 (1991): 23-25.
- Tsai, S. W. *Theory of Composites Design*. Dayton OH: THINK COMPOSITES, a division of ILT Corporation, 1992.
- Vasiliev, V. V., and E. V. Morozov *Advanced Mechanics of Composite Materials and Structural Elements*, 3d ed., Waltham, MA: Elsevier, 2013 pp. 622-635.



---

## *Failure initiation in FRP composites*

---

### *9.1 Strength of a composite ply*

The strength of a laminated composite wall is assessed on a ply-by-ply basis. The main failure modes of unidirectional plies of fiber-reinforced polymer (FRP) composites are

- matrix compression failure,
- matrix tension failure,
- fiber compression failure,
- fiber tension failure,
- delamination.

The fiber modes and the matrix modes are intralaminar failure modes, meaning these failures occur within a ply. Intralaminar modes include fractures of the fiber and/or matrix, and fiber kinking or buckling in compression. Delamination is an interlaminar failure mode, and it refers to the formation of an interfacial crack, or a debonding, occurring between adjacent lamina with different fiber orientations. Delamination has been modeled with the concepts of fracture mechanics, where the displacements are discontinuous across the interfacial crack faces. An initial delamination crack is postulated and fracture mechanics principles are used to determine if the crack will propagate in a self-similar manner. Analysis of delamination by fracture mechanics is presented in article 13.7 on page 392.

Simple tests are conducted on unidirectional plies of FRP composites to determine its intralaminar failure strengths. There are five independent strengths of a unidirectional ply. Denote  $X_T$  as the longitudinal tensile strength along the fiber direction,  $X_C$  the longitudinal compression strength along the fiber direction,  $Y_T$  the transverse tensile strength perpendicular to the fibers,  $Y_C$  the transverse compression strength perpendicular to the fibers, and  $S_L$  the longitudinal shear strength in the  $x_1$ - $x_2$  plane. Typical values of the five basic strengths of selected composite materials are listed in table 9.1.

**Table 9.1 Strengths of selected composite materials in MPa from Tsai (1992 p. 8-2)**

Test and strength data				Composite ply				
Loading	Specimen	Strength MPa		T300/ 5208	AS/ 3501	E-glass/ epoxy	Kevlar 49/epoxy	IM6/ epoxy
Uniaxial	[0]	Longit tension	$X_T$	1,500	1,447	1,062	1,400	3,500
Uniaxial	[0]	Longit compr	$X_C$	1,500	1,447	610	235	1,540
Uniaxial	[90]	Trans tension	$Y_T$	40	52	31	12	56
Uniaxial	[90]	Trans compr	$Y_C$	246	206	118	53	150
Shear	[0] or [90]	Longit shear	$S_L$	68	93	72	34	98

Failure criteria for unidirectional FRP composites based on general states of stress  $\sigma_{11}$ ,  $\sigma_{22}$ , and  $\sigma_{12}$  are reviewed in Tsai (1992, Section 8) and in Herakovich (1998, Section 9.3). Several of these criteria are in the form of dimensionless quadratic equations in the stress components with the five basic strengths appearing as parameters. The reader is referred to these references and the other references cited therein to see the details of these criteria. In the next subsection we review a recent criterion based on observed damage states.

### 9.1.1 Puck's failure criterion

Intralaminar criteria for failure initiation have recently been assessed for FRP composites in the World-Wide Failure Exercise (WWFE) as summarized by Soden, et al. (2004). Nineteen theoretical approaches for predicting the deformation and failure response of FRP composite laminates were compared to test results. At the conclusion of the WWFE five leading theories were selected to create recommendations and guidelines for designers. The theory proposed by Puck, et al. (2002) was cited as one of the five producing the highest number of accurate predictions and capturing more general features of the experimental results. Puck's methodology assumes brittle fracture of polymer matrix composites, and distinguishes between fiber failure and inter-fiber failure (IFF) by separate criteria. Inter-fiber failure refers to cracks running parallel to the fibers through the thickness of a ply, with the plane of crack determined by three matrix-mode criteria denoted by A, B, and C.

With respect to the material principal directions  $x_1$ - $x_2$ - $x_3$ , the fracture plane is parallel to the  $x_1$ -axis as shown in figure. 9.1. Coordinates with respect to the fracture plane are denoted by  $x_1$ - $x_n$ - $x_t$  with the  $x_n$ -axis normal to the plane. The  $x_n$ -axis is located by a counterclockwise rotation through the angle  $\alpha$  about the  $x_1$ -axis. The relation between coordinate directions shown in figure. 9.1 is given by the direction cosines of the angle  $\alpha$ :

$$\begin{bmatrix} x_1 \\ x_2 \\ x_3 \end{bmatrix} = \begin{bmatrix} 1 & 0 & 0 \\ 0 & \cos \alpha & -\sin \alpha \\ 0 & \sin \alpha & \cos \alpha \end{bmatrix} \begin{bmatrix} x_1 \\ x_n \\ x_t \end{bmatrix}, \text{ or } \begin{bmatrix} x_1 \\ x_2 \\ x_3 \end{bmatrix} = [\lambda] \begin{bmatrix} x_1 \\ x_n \\ x_t \end{bmatrix}, \quad (9.1)$$

where  $[\lambda]$  is the direction cosine matrix. The transformation from the stress components in the material principal directions to the stress components in the  $x_1$ - $x_n$ - $x_t$  axis system is given eq. (A.96) in the appendix. With due regard to the notation in this article this matrix transformation is

$$\begin{bmatrix} \sigma_{11} & \sigma_{1n} & \sigma_{1t} \\ \sigma_{n1} & \sigma_{nn} & \sigma_{nt} \\ \sigma_{t1} & \sigma_{tn} & \sigma_{tt} \end{bmatrix} = [\lambda] \begin{bmatrix} \sigma_{11} & \sigma_{12} & \sigma_{13} \\ \sigma_{12} & \sigma_{22} & \sigma_{23} \\ \sigma_{13} & \sigma_{23} & \sigma_{33} \end{bmatrix} [\lambda]^T. \quad (9.2)$$

Complete the matrix multiplication in the previous equation to find the stress components  $\sigma_{nn}$ ,  $\sigma_{nt}$ , and  $\sigma_{n1}$  acting on the fracture plane in terms of the stress components in the principal material directions. The results are

$$\begin{aligned} \sigma_{nn} &= \frac{1}{2}(\sigma_{22} + \sigma_{33}) + \frac{1}{2}(\sigma_{22} - \sigma_{33})\cos 2\alpha + \sigma_{23}\sin 2\alpha \\ \sigma_{nt} &= -\frac{1}{2}(\sigma_{22} - \sigma_{33})\sin 2\alpha + \sigma_{23}\cos 2\alpha \\ \sigma_{n1} &= \sigma_{21}\cos \alpha + \sigma_{31}\sin \alpha \end{aligned} \quad (9.3)$$

Note that the stress component  $\sigma_{11}$  does not appear in a criterion formulated from the stress components on the fracture plane.

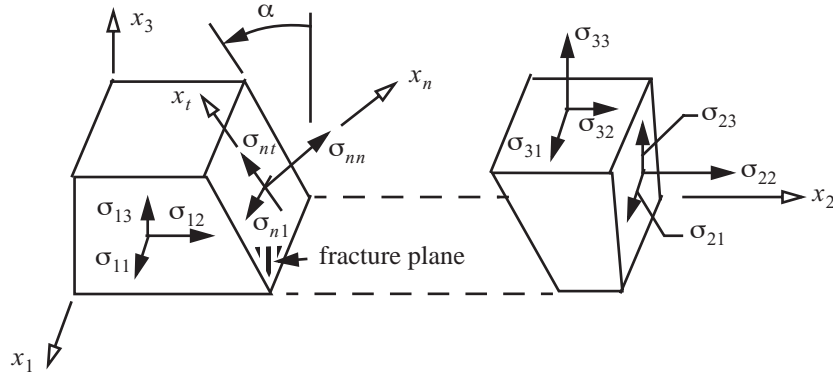


**Fig. 9.1** Inter-fiber fracture plane is located by rotation through angle  $\alpha$  about the  $x_1$ -axis.

Puck's criteria are expressed in terms of a dimensionless failure index denoted by  $FI$  for either a matrix mode  $FI_M$  or a fiber mode  $FI_F$ . The range of the failure indices are  $0 \leq FI < 1$  for no failure, and  $FI = 1$  at failure initiation.

**Matrix mode A.** In the uniaxial transverse tension test and the in-plane shear test, the plane of fracture is normal to the  $x_2$ -direction so  $\alpha = 0$ . From eq. (9.3) the stresses on the fracture plane are  $\sigma_{nn} = \sigma_{22}$ ,  $\sigma_{nt} = \sigma_{23}$ , and  $\sigma_{n1} = \sigma_{21}$ . In the transverse tension test  $\sigma_{22} = Y_T$  at failure, and all other stresses in the  $x_i$ -system vanish. For the in-plane shear test all stresses in the  $x_i$ -system vanish except that  $\sigma_{21} = S_L$  at failure. The proposed criterion including these test results is quadratic and of the form

$$(1 - c_1)\left(\frac{\sigma_{nn}}{Y_T}\right)^2 + c_1\left(\frac{\sigma_{nn}}{Y_T}\right) + \left(\frac{\sigma_{nt}}{S_T}\right)^2 + \left(\frac{\sigma_{n1}}{S_L}\right)^2 = 1 \quad \sigma_{nn} \geq 0. \quad (9.4)$$

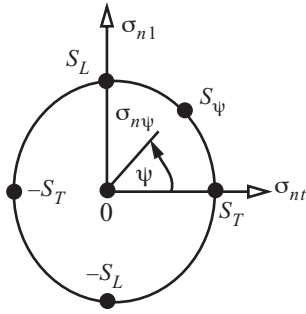


**Fig. 9.2**  $\sigma_{nn} = 0$  plane.

The shear strength transverse to the fibers in the fracture plane is denoted by  $S_T$  in eq. (9.4)<sup>1</sup>. In the Cartesian coordinates with axes  $\sigma_{nn}$ ,  $\sigma_{nt}$ , and  $\sigma_{n1}$  the surface given by eq. (9.4) is an ellipsoid if the constant  $c_I < 1$ . In the shear stress plane  $\sigma_{nt}$ - $\sigma_{n1}$  where  $\sigma_{nn}$  is equal to zero, the cross section of the ellipsoid is an ellipse shown in figure. 9.2. The equation for the ellipse in the plane  $\sigma_{nn}$  equal to zero is

$$\left(\frac{\sigma_{nt}}{S_T}\right)^2 + \left(\frac{\sigma_{n1}}{S_L}\right)^2 = 1 \quad \sigma_{nn} = 0. \quad (9.5)$$

The resultant of the shear stress components is denoted by  $\sigma_{n\psi}$ , and the angle between the line of action of the resultant and  $\sigma_{nt}$ -axis is denoted by  $\psi$ . The stress components are related to the resultant by

$$\sigma_{nt} = \sigma_{n\psi} \cos \psi \quad \sigma_{n1} = \sigma_{n\psi} \sin \psi. \quad (9.6)$$

Substitute eq. (9.6) for the stress components in eq. (9.5) to get

$$\sigma_{n\psi}^2 \left( \frac{\cos^2 \psi}{S_T^2} + \frac{\sin^2 \psi}{S_L^2} \right) = 1 \quad \sigma_{nn} = 0. \quad (9.7)$$

On the failure ellipse  $\sigma_{n\psi} = S_\psi$  in eq. (9.7). Hence, strength  $S_\psi$  is related to strengths  $S_T$  and  $S_L$  by

$$S_\psi^2 \left( \frac{\cos^2 \psi}{S_T^2} + \frac{\sin^2 \psi}{S_L^2} \right) = 1 \quad \sigma_{nn} = 0. \quad (9.8)$$

To interpret constant  $c_I$  we take the differential of (9.4) with respect to  $\sigma_{nn}$  followed by setting  $\sigma_{nn} = 0$  to get

$$\frac{c_I}{Y_T} + \frac{2\sigma_{nt}}{S_T^2} \frac{d\sigma_{nt}}{d\sigma_{nn}} + \frac{2\sigma_{n1}}{S_L^2} \frac{d\sigma_{n1}}{d\sigma_{nn}} = 0 \quad \sigma_{nn} = 0. \quad (9.9)$$

Along the curve on the ellipsoid defined by angle  $\psi$  equal to a constant, substitute the relations (9.6) with  $\sigma_{n\psi} = S_\psi$  into eq. (9.9) to get

$$\frac{c_I}{2Y_T} + S_\psi \left( \frac{\cos^2 \psi}{S_T^2} + \frac{\sin^2 \psi}{S_L^2} \right) \frac{d\sigma_{n\psi}}{d\sigma_{nn}} = 0 \quad \sigma_{nn} = 0. \quad (9.10)$$

Use the result in eq. (9.8) to write eq. (9.10) as

$$\frac{c_I}{2Y_T} + \frac{1}{S_\psi} \frac{d\sigma_{n\psi}}{d\sigma_{nn}} = 0 \quad \sigma_{nn} = 0. \quad (9.11)$$

Along the curve on the ellipsoid defined by angle  $\psi$  equal to a constant, let the negative of the slope of the  $\sigma_{n\psi}$  with respect to  $\sigma_{nn}$  at  $\sigma_{nn} = 0$  be denoted by  $p_{n\psi}^{(+)}$ . That is,

1. There is no simple test to determine  $S_T$  for FRP composites. In Puck's criterion  $S_T$  is determined from the pure transverse compression test. Refer to eq. (9.49) on page 280.



$$p_{n\psi}^{(+)} = - \frac{d\sigma_{n\psi}}{d\sigma_{nn}} \bigg|_{\sigma_{nn}=0} . \quad (9.12)$$

Puck defines  $p_{n\psi}^{(+)}$  as an inclination parameter. Therefore, the constant  $c_1$  is determined from

$$\frac{c_1}{2Y_T} = \frac{p_{n\psi}^{(+)}}{S_\psi} . \quad (9.13)$$

Substitute the constant  $c_1$  determined from eq. (9.13) into eq. (9.4) to get the failure criterion for mode A as

$$\left(1 - \frac{2Y_T}{S_\psi} p_{n\psi}^{(+)}\right) \left(\frac{\sigma_{nn}}{Y_T}\right)^2 + \frac{2Y_T}{S_\psi} p_{n\psi}^{(+)} \left(\frac{\sigma_{nn}}{Y_T}\right) + \left(\frac{\sigma_{nt}}{S_T}\right)^2 + \left(\frac{\sigma_{n1}}{S_L}\right)^2 = 1 \quad \sigma_{nn} \geq 0 . \quad (9.14)$$

The following failure index for mode A is given by Puck:

$$FI_M = \sqrt{\left[1 - \frac{Y_T}{S_\psi} p_{n\psi}^{(+)}\right]^2 \left(\frac{\sigma_{nn}}{Y_T}\right)^2 + \left(\frac{\sigma_{nt}}{S_T}\right)^2 + \left(\frac{\sigma_{n1}}{S_L}\right)^2} + p_{n\psi}^{(+)} \left(\frac{\sigma_{nn}}{S_\psi}\right) \quad \sigma_{nn} \geq 0 . \quad (9.15)$$

To show eqs. (9.14) and (9.15) are equivalent: Set  $FI_M = 1$  in (9.15) and subtract  $\frac{Y_T}{S_\psi} p_{n\psi}^{(+)} \left(\frac{\sigma_{nn}}{Y_T}\right)$  from each side.

Then square the result to arrive at eq. (9.14) after some algebraic manipulations.

The inclination parameter  $p_{n\psi}^{(+)}$  is related to the inclination parameters defined for the  $\psi = 0$  and  $\psi = \pi/2$  failure loci on the ellipsoid. The locus of failure initiation for  $\psi = 0$  is a curve in the  $\sigma_{nn}$ - $\sigma_{nt}$  plane. At the point on this curve where  $(\sigma_{nn}, \sigma_{n1}) = (0, 0)$  failure initiates when  $\sigma_{nt} = S_T = S_\psi$ . The gradient condition at this point from eq. (9.9) is

$$\frac{c_1}{2Y_T} + \frac{1}{S_T} \frac{d\sigma_{nt}}{d\sigma_{nn}} = 0 . \quad (9.16)$$

The locus of failure initiation for  $\psi = \pi/2$  is a curve in the  $\sigma_{nn}$ - $\sigma_{n1}$  plane. At the point on this curve where  $(\sigma_{nn}, \sigma_{nt}) = (0, 0)$  failure initiates when  $\sigma_{n1} = S_L = S_\psi$ . The gradient condition at this point from eq. (9.9) is

$$\frac{c_1}{2Y_T} + \frac{1}{S_L} \frac{d\sigma_{n1}}{d\sigma_{nn}} = 0 . \quad (9.17)$$

Define the inclination parameter on the  $\psi = 0$  curve as  $p_{nt}^{(+)} = - \frac{d\sigma_{nt}}{d\sigma_{nn}}$ , and on the  $\psi = \pi/2$  curve as

$p_{n1}^{(+)} = - \frac{d\sigma_{n1}}{d\sigma_{nn}}$ . Combine eqs. (9.13), (9.16), and (9.17) to find

$$\frac{p_{n\psi}^{(+)}}{S_\psi} = \frac{p_{nt}^{(+)}}{S_T} , \text{ and } \frac{p_{n\psi}^{(+)}}{S_\psi} = \frac{p_{n1}^{(+)}}{S_L} . \quad (9.18)$$

Multiply the first expression in eq. (9.18) by  $\cos^2\psi$ , and add it to the second expression in eq. (9.18) multiplied by  $\sin^2\psi$ , to get relationship between the inclination parameters on the tension side of the ellipse in figure. 9.2 as

$$\frac{p_{n\psi}^{(+)}}{S_\psi} = \frac{p_{nt}^{(+)}}{S_T} \cos^2 \psi + \frac{p_{n1}^{(+)}}{S_L} \sin^2 \psi. \quad (9.19)$$

**Matrix modes B and C.** These modes are defined for a compressive normal stress,  $\sigma_{nn} < 0$ , acting on the fracture plane. The motivation of Puck's criterion for modes B and C is the Coulomb-Mohr (C-M) criterion (Dowling, 1993, pp. 255-261) for failure of brittle materials. In the C-M criterion a compressive normal stress resists fracture caused by the shear stresses  $\sigma_{nt}$  and  $\sigma_{n1}$ . The C-M criterion can be considered to be a shear stress criterion in which the limiting shear stress increases for larger amounts of compression. Consider the case where  $\sigma_{n1} = 0$ , so on the fracture plane  $\sigma_{nn} < 0$  and  $\sigma_{nt} \neq 0$ . Then the C-M criterion can be written in the form

$|\sigma_{nt}| + \mu \sigma_{nn} = S_T$ , where  $\mu$  is a friction coefficient and  $S_T$  is the shear strength transverse to the fibers in the fracture plane. The friction effect,  $\mu \sigma_{nn}$ , can be used to increase the strength or to decrease the applied shear stress in a C-M criterion. Puck and Schürmann (1998) proposed the following criterion

$$\left( \frac{\sigma_{nt}}{S_T - p_{nt}^{(-)} \sigma_{nn}} \right)^2 + \left( \frac{\sigma_{n1}}{S_L - p_{n1}^{(-)} \sigma_{nn}} \right)^2 = 1 \quad \sigma_{nn} \leq 0, \quad (9.20)$$

in which the strengths in the denominators are increased by the compressive normal stress, and  $(p_{nt}^{(-)}, p_{n1}^{(-)})$  are the inclination parameters in compression. Set  $\sigma_{n1} = 0$  in eq. (9.20) to get  $\sigma_{nt} = S_T - p_{nt}^{(-)} \sigma_{nn}$ , and from this expression the inclination parameter is interpreted as the negative slope of  $\sigma_{nt}$  with respect to  $\sigma_{nn}$ , or

$$p_{nt}^{(-)} = - \left( \frac{d\sigma_{nt}}{d\sigma_{nn}} \right) \bigg|_{\sigma_{n1}=0}. \quad (9.21)$$

Set  $\sigma_{nt} = 0$  in eq. (9.20) to get  $\sigma_{n1} = S_L - p_{n1}^{(-)} \sigma_{nn}$ , and from this expression the inclination parameter is interpreted as the negative slope of  $\sigma_{n1}$  with respect to  $\sigma_{nn}$ , or

$$p_{n1}^{(-)} = - \left( \frac{d\sigma_{n1}}{d\sigma_{nn}} \right) \bigg|_{\sigma_{nt}=0}. \quad (9.22)$$

Citing better agreement with experimental results, the denominators of the shear stresses in eq. (9.20) are expanded and the quadratic terms in the normal stress  $\sigma_{nn}$  are neglected with respect to the linear terms in  $\sigma_{nn}$ , so the criterion reduces to

$$\frac{\sigma_{nt}^2}{S_T^2 - 2p_{nt}^{(-)} S_T \sigma_{nn}} + \frac{\sigma_{n1}^2}{S_L^2 - 2p_{n1}^{(-)} S_L \sigma_{nn}} = 1 \quad \sigma_{nn} \leq 0. \quad (9.23)$$

For mathematical simplification Puck and Shürmann assume that the inclination parameters are related in a similar way to eq. (9.18) by

$$\frac{p_{nt}^{(-)}}{S_T} = \frac{p_{n1}^{(-)}}{S_L} = \frac{p}{R}. \quad (9.24)$$

With this assumption eq. (9.23) reduces to the simpler form

$$\left(\frac{\sigma_{nt}}{S_T}\right)^2 + \left(\frac{\sigma_{nl}}{S_L}\right)^2 + 2\left(\frac{p}{R}\right)\sigma_{nn} = 1 \quad \sigma_{nn} \leq 0. \quad (9.25)$$

In the Cartesian coordinates with axes  $\sigma_{nn}$ ,  $\sigma_{nt}$ , and  $\sigma_{nl}$  the surface given by eq. (9.25) is an elliptic paraboloid. Note that the failure surface does not intersect the negative  $\sigma_{nn}$ -axis according to the hypothesis that a compressive normal stress impedes a shear fracture (i.e., the shear resistance to fracture means the contour lines in the failure surface increase with increasing compression). In the shear stress plane  $\sigma_{nt}$ - $\sigma_{nl}$  where  $\sigma_{nn}$  is equal to zero, the cross section of the ellipsoid is an ellipse shown in figure. 9.2. Substitute the relations given by eq. (9.6) into eq. (9.25) to get

$$\sigma_{n\psi}^2 \left( \frac{\cos^2 \psi}{S_T^2} + \frac{\sin^2 \psi}{S_L^2} \right) + 2\left(\frac{p}{R}\right)\sigma_{nn} = 1 \quad \sigma_{nn} \leq 0. \quad (9.26)$$

Differentiate eq. (9.26) with respect to  $\sigma_{nn}$  to get

$$\sigma_{n\psi} \left( \frac{\cos^2 \psi}{S_T^2} + \frac{\sin^2 \psi}{S_L^2} \right) \frac{d\sigma_{n\psi}}{d\sigma_{nn}} + \frac{p}{R} = 0. \quad (9.27)$$

Consider the  $\sigma_{nt}$ - $\sigma_{nl}$  plane at  $\sigma_{nn} = 0$ . On the failure ellipse  $\sigma_{n\psi} = S_\psi$  and (9.26) is

$$S_\psi^2 \left( \frac{\cos^2 \psi}{S_T^2} + \frac{\sin^2 \psi}{S_L^2} \right) = 1. \quad (9.28)$$

Evaluate eq. (9.27) at  $\sigma_{n\psi} = S_\psi$ , followed by the substitution of eq. (9.28). The result is

$$\frac{1}{S_\psi} \frac{d\sigma_{n\psi}}{d\sigma_{nn}} + \frac{p}{R} = 0 \quad \sigma_{nn} = 0. \quad (9.29)$$

Define the inclination parameter for the curve  $\psi$  equal to a constant by  $p_{n\psi}^{(-)} = -\frac{d\sigma_{n\psi}}{d\sigma_{nn}}$ . Hence,

$$\frac{p}{R} = \frac{p_{n\psi}^{(-)}}{S_\psi}. \quad (9.30)$$

Substitute the result (9.30) into the condition of failure initiation (9.25) to find

$$\left(\frac{\sigma_{nt}}{S_T}\right)^2 + \left(\frac{\sigma_{nl}}{S_L}\right)^2 + 2\left(\frac{p_{n\psi}^{(-)}}{S_\psi}\right)\sigma_{nn} = 1 \quad \sigma_{nn} \leq 0. \quad (9.31)$$

The following failure index for  $\sigma_{nn} \leq 0$  is given by Puck.

$$FI_M = \sqrt{\left(\frac{\sigma_{nt}}{S_T}\right)^2 + \left(\frac{\sigma_{nl}}{S_L}\right)^2 + \left(\frac{p_{n\psi}^{(-)}}{S_\psi}\sigma_{nn}\right)^2} + \left(\frac{p_{n\psi}^{(-)}}{S_\psi}\right)\sigma_{nn} \quad \sigma_{nn} \leq 0. \quad (9.32)$$

One can show eq. (9.32) is equivalent to eq. (9.31) if we set  $FI_M = 1$  in (9.32).

Combining eqs. (9.24) and (9.30) we get

$$\frac{p_{n\psi}^{(-)}}{S_\psi} = \frac{p_{nl}^{(-)}}{S_T}, \text{ and } \frac{p_{n\psi}^{(-)}}{S_\psi} = \frac{p_{nt}^{(-)}}{S_L}. \quad (9.33)$$

Similar to the manipulations to get eq. (9.19), the expressions in eq. (9.33) lead to the relationship between the inclination parameters on the compression side of the ellipse of figure. 9.2 as

$$\frac{p_{nt}^{(-)}}{S_\psi} = \frac{p_{nt}^{(-)}}{S_T} \cos^2 \psi + \frac{p_{n1}^{(-)}}{S_L} \sin^2 \psi. \quad (9.34)$$

For given values of the stress components  $\sigma_{22}$ ,  $\sigma_{33}$ ,  $\sigma_{23}$ ,  $\sigma_{21}$ , and  $\sigma_{31}$  for which  $\sigma_{nn} \leq 0$ , the failure index is a function of the angle  $\alpha$  of the fracture plane. The condition to find  $\alpha$  is to make the failure index a maximum. The necessary condition for a maximum is  $\frac{\partial FI_M}{\partial \alpha} = 0$ . To find  $\alpha$  that satisfies the necessary condition requires a numerical search.

The section of the failure surface in the  $\sigma_{nn}$ - $\sigma_{nt}$  plane where  $\sigma_{n1} = 0$  is shown in figure. 9.3(a), and the section of the failure surface in the  $\sigma_{nn}$ - $\sigma_{n1}$  plane where  $\sigma_{nt} = 0$  is shown in figure. 9.3(b). In addition to the five

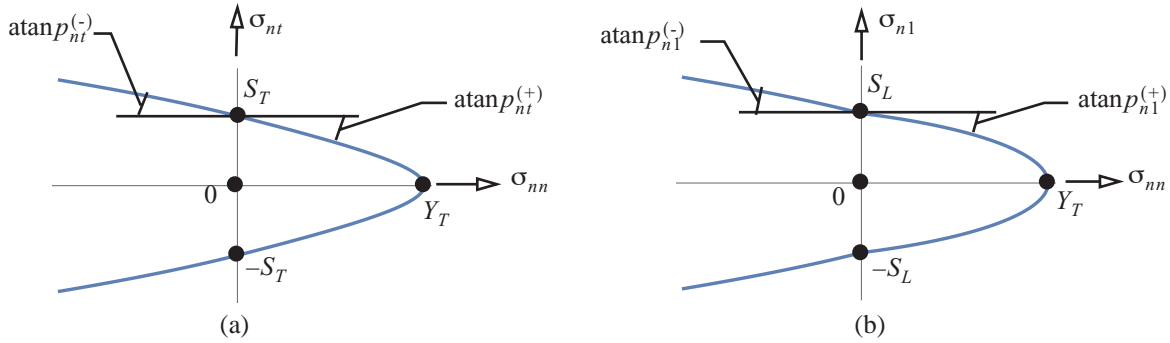


**Fig. 9.3** (a) Sections of the failure surface in the  $\sigma_{nn}$ - $\sigma_{nt}$  plane, and (b) in the  $\sigma_{nn}$ - $\sigma_{n1}$  plane.

basic strength data for an FRP composite ply listed in table 9.1, Puck's criterion introduces four new dimensionless parameters:  $p_{n1}^{(+)}$ ,  $p_{nt}^{(+)}$ ,  $p_{nt}^{(-)}$ , and  $p_{n1}^{(-)}$ . The inclination parameters  $p_{nt}^{(-)}$  and  $p_{nt}^{(+)}$  are the slopes of the failure locus at the  $\sigma_{nt}$ -axis in figure. 9.3(a). Inclination parameters  $p_{n1}^{(-)}$  and  $p_{n1}^{(+)}$  are the slopes of the failure locus at the  $\sigma_{n1}$ -axis shown in figure. 9.3(b). Puck, et al. (2002) recommend that  $p_{nt}^{(-)} = p_{nt}^{(+)}$ , which makes the slope of the  $\sigma_{nn}$ - $\sigma_{nt}$  curve continuous at the  $\sigma_{nt}$ -axis. The inclination parameters  $p_{n1}^{(-)} = 0.25$  and  $p_{n1}^{(+)} = 0.30$  with  $p_{nt}^{(-)}$  computed from eq. (9.24) were used in the WWFE. Recommended ranges of inclination parameters are listed table 9.2.

**Table 9.2 Recommended range for inclination parameter  $p_{nt}$  from Puck et al. (2002)**

	$p_{nt}^{(-)}$	$p_{nt}^{(+)}$
Glass-fiber/epoxy	0.20 to 0.25	0.20 to 0.25
Carbon-fiber/epoxy	0.25 to 0.30	0.25 to 0.30

**Fiber modes.** A simple fiber mode criterion that does not interact with the longitudinal shear stresses  $\sigma_{21}$  and  $\sigma_{31}$  is the maximum stress criterion along the fibers. The fiber failure index  $FI_F$  is defined by

$$FI_F = \begin{cases} \frac{-\sigma_{11}}{X_c} & \sigma_{11} < 0 \\ \frac{\sigma_{11}}{X_T} & \sigma_{11} > 0 \end{cases}, \quad (9.35)$$

where  $0 \leq FI_F < 1$  for no failure of the fiber, and  $FI_F = 1$  at failure.

### 9.1.2 Matrix failure criteria for a plane stress state

The assumption of plane stress is that out-of-plane stresses  $\sigma_{33}$ ,  $\sigma_{23}$ , and  $\sigma_{31}$  are negligible in comparison to the in-plane stress components  $\sigma_{22}$  and  $\sigma_{21}$ . Hence, the out-of-plane stresses can be neglected in the stress transformation equations (9.3). The stress transformation equations reduce to

$$\sigma_{nn} = \sigma_{22} \cos^2 \alpha \quad \sigma_{nt} = -\sigma_{22} \sin \alpha \cos \alpha \quad \sigma_{n1} = \sigma_{21} \cos \alpha. \quad (9.36)$$

In **mode A**  $\alpha = 0$ , and stresses  $\sigma_{nn} = \sigma_{22}$ ,  $\sigma_{nt} = 0$ , and  $\sigma_{n1} = \sigma_{21}$ . For  $\sigma_{nt} = 0$  the locus of failure initiation is a curve in the  $\sigma_{nn}$ - $\sigma_{n1}$  plane and  $\psi = \pi/2$ . From eq. (9.19) we find  $\frac{p_{n\psi}^{(+)}}{S_\psi} = \frac{p_{n1}^{(+)}}{S_L}$ . Therefore, the mode A failure index. (9.15) in plane stress reduces to

$$FI_M = \sqrt{\left[1 - p_{n1}^{(+)} \frac{Y_T}{S_L}\right]^2 \left(\frac{\sigma_{22}}{Y_T}\right)^2 + \left(\frac{\sigma_{21}}{S_L}\right)^2} + \frac{p_{n1}^{(+)} \sigma_{22}}{S_L} \quad \sigma_{22} \geq 0. \quad (9.37)$$

**Modes B and C for a plane stress state.** Substitute the stress transformation equations (9.36) into eq. (9.25) to get

$$FI_M = \left(\frac{\sigma_{22}}{S_T}\right)^2 \sin^2 \alpha \cos^2 \alpha + \left(\frac{\sigma_{21}}{S_L}\right)^2 \cos^2 \alpha + 2\left(\frac{p}{R}\right) \sigma_{22} \cos^2 \alpha \quad \sigma_{22} < 0. \quad (9.38)$$

The angle of the fracture plane is determined when index  $FI_M$  is a maximum value with respect to  $\alpha$ . Substitute  $\sin^2 \alpha = 1 - \cos^2 \alpha$  in (9.38) to express index  $FI_M$  as a function of  $\cos^2 \alpha$ . Then the necessary condition for a maximum can be written as

$$\frac{dFI_M}{d\alpha} = \frac{dFI_M}{d(\cos^2 \alpha)} (-2 \cos \alpha \sin \alpha) = 0. \quad (9.39)$$

One solution of eq. (9.39) is  $\alpha = 0$ , which is the mode B fracture where the fracture plane is normal to the  $x_2$ -direction.

$$1 = \left(\frac{\sigma_{21}}{S_L}\right)^2 + 2p_{n1}^{(-)} \left(\frac{\sigma_{22}}{S_L}\right) \quad \sigma_{22} < 0 \quad \text{mode B} \quad (9.40)$$

Now take the derivative of the failure index (9.38) with respect to  $\cos^2 \alpha$  and set it equal to zero. Solve the resulting expression for  $\cos^2 \alpha$  to find

$$\cos^2 \alpha = \frac{1}{2} \left[ 1 + \left(\frac{S_T}{S_L}\right)^2 \left(\frac{\sigma_{21}}{\sigma_{22}}\right)^2 \right] + p_{n1}^{(-)} \frac{S_T}{\sigma_{22}}. \quad (9.41)$$

Equation (9.41) is used to eliminate the trigonometric functions in the failure index (9.38) to get

$$FI_M = \left\{ \frac{1}{2} \left( \frac{S_T}{\sigma_{22}} \right) \left[ \left( \frac{\sigma_{22}}{S_T} \right)^2 + \left( \frac{\sigma_{21}}{S_L} \right)^2 \right] + p_{nt}^{(-)} \right\}^2. \quad (9.42)$$

Note that  $-1 \leq \sqrt{FI_M} \leq 1$ , so that the square root of eq. (9.42) is

$$-1 \leq \frac{1}{2} \left( \frac{S_T}{\sigma_{22}} \right) \left[ \left( \frac{\sigma_{22}}{S_T} \right)^2 + \left( \frac{\sigma_{21}}{S_L} \right)^2 + 2p_{nt}^{(-)} \left( \frac{\sigma_{22}}{S_T} \right) \right] \leq 1. \quad (9.43)$$

Take the left-hand inequality of eq. (9.43) and multiply by  $-1$  to get the form

$$1 \geq \frac{1}{2} \left( \frac{S_T}{-\sigma_{22}} \right) \left[ \left( \frac{\sigma_{22}}{S_T} \right)^2 + \left( \frac{\sigma_{21}}{S_L} \right)^2 \right] - p_{nt}^{(-)}. \quad (9.44)$$

Finally, add  $p_{nt}^{(-)}$  to each side of eq. (9.44) followed by division by  $1 + p_{nt}^{(-)}$  to get

$$\frac{1}{2(1 + p_{nt}^{(-)})} \left[ \left( \frac{\sigma_{22}}{S_T} \right)^2 + \left( \frac{\sigma_{21}}{S_L} \right)^2 \right] \left( \frac{S_T}{-\sigma_{22}} \right) = FI_M \quad \sigma_{22} \leq 0 \quad \text{mode C}, \quad (9.45)$$

where  $FI_M = 1$  at failure in mode C. Equation (9.41) is written in the equivalent form as

$$\cos^2 \alpha = \frac{1}{2} \left( \frac{S_T}{\sigma_{22}} \right)^2 \left[ \left( \frac{\sigma_{22}}{S_T} \right)^2 + \left( \frac{\sigma_{21}}{S_L} \right)^2 + 2p_{nt}^{(-)} \left( \frac{\sigma_{22}}{S_T} \right) \right]. \quad (9.46)$$

At failure eq. (9.45) is solved in the form

$$\left( \frac{\sigma_{22}}{S_T} \right)^2 + \left( \frac{\sigma_{21}}{S_L} \right)^2 = 2(1 + p_{nt}^{(-)}) \left( \frac{-\sigma_{22}}{S_T} \right). \quad (9.47)$$

Substitute eq. (9.47) into eq. (9.46) and perform some algebra to get final result for the angle of fracture plane for mode C:

$$\cos^2 \alpha = \frac{S_T}{-\sigma_{22}} \quad \sigma_{22} \leq -S_T \quad \text{mode C}. \quad (9.48)$$

**Transverse shear strength.** The shear strength transverse to the fibers in the fracture plane  $S_T$  cannot be determined from simple tests. Instead  $S_T$  is derived from the uniaxial transverse compression test in which  $\sigma_{22} = -Y_C$  at failure and all other stresses in the  $x_i$ -system vanish. In eq. (9.45) set  $FI_M = 1$ ,  $\sigma_{21} = 0$ , and  $\sigma_{22} = -Y_C$  to evaluate the transverse shear strength  $S_T$  at the pure transverse compression condition. The result is

$$S_T = \frac{Y_C}{2(1 + p_{nt}^{(-)})}. \quad (9.49)$$

To find the transition values of stresses  $\sigma_{21}$  and  $\sigma_{22}$  between modes B and C, solve the eq. (9.40) for  $\sigma_{21}$  and substitute this result for  $\sigma_{21}$  in eq. (9.45) with  $FI_M = 1$ . The results are

$$\sigma_{22} = -S_T \quad \sigma_{21} = S_L \sqrt{1 + 2p_{nt}^{(-)}}. \quad (9.50)$$

Thus, for **plane stress** the matrix failure indices are

$$FI_M = \sqrt{\left[1 - p_{n1}^{(+)} \frac{Y_T}{S_L}\right]^2 \left(\frac{\sigma_{22}}{Y_T}\right)^2 + \left(\frac{\sigma_{21}}{S_L}\right)^2} + \frac{p_{n1}^{(+)} \sigma_{22}}{S_L} \quad \sigma_{22} \geq 0 \quad \text{mode A} \quad (9.51)$$

$$FI_M = \left(\frac{\sigma_{21}}{S_L}\right)^2 + 2p_{n1}^{(-)} \left(\frac{\sigma_{22}}{S_L}\right) \quad -S_T \leq \sigma_{22} < 0 \quad S_L < |\sigma_{21}| \leq S_L \sqrt{1 + 2p_{nt}^{(-)}} \quad \text{mode B} \quad (9.52)$$

$$FI_M = \frac{1}{2(1 + p_{nt}^{(-)})} \left[ \left(\frac{\sigma_{22}}{S_T}\right)^2 + \left(\frac{\sigma_{21}}{S_L}\right)^2 \right] \left(\frac{S_T}{-\sigma_{22}}\right) \quad -Y_C \leq \sigma_{22} \leq -S_T \quad \text{mode C} \quad (9.53)$$

The matrix failure locus is plotted in  $(\sigma_{nn}, \sigma_{nt}, \sigma_{n1})$  stress space in figure. 9.4 for the lamina subject to plane stress. The stress components at selected points are listed in table 9.3.

**Fig. 9.4** Matrix failure locus in the  $\sigma_{nn}$ ,  $\sigma_{nt}$ , and  $\sigma_{n1}$  stress space for a unidirectional ply subject to plane stress. The failure locus is symmetric with respect to the  $\sigma_{nn} - \sigma_{n1}$  plane and the  $\sigma_{nn} - \sigma_{nt}$  plane.

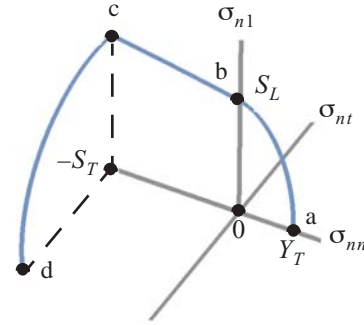


**Table 9.3** Stress components at selected points labeled in figure. 9.4

Point	$\sigma_{nn}$	$\sigma_{nt}$	$\sigma_{n1}$	$\sigma_{22}$	$\sigma_{21}$
a	$Y_T$	0	0	$Y_T$	0
b	0	0	$S_L$	0	$S_L$
c	$-S_T$	0	$S_L \sqrt{1 + 2p_{nt}^{(-)}}$	$-S_T$	$S_L \sqrt{1 + 2p_{nt}^{(-)}}$
d	$-S_T$	$-Y_C \cos \alpha_f \sin \alpha_f^a$	0	$-Y_C$	0

a.  $\cos \alpha_f = [2(1 + p_{nt}^{(-)})]^{-1/2}$

The matrix failure locus shown in figure. 9.4 is plotted in the  $\sigma_{22}$ - $\sigma_{21}$  stress plane in figure. 9.5.

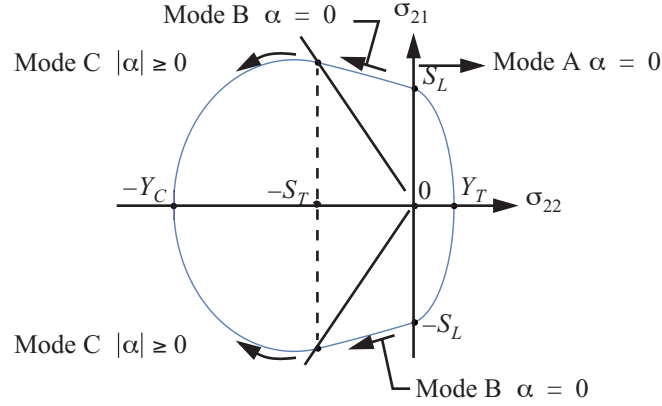


**Fig. 9.5** Matrix failure modes for Puck's criterion in the  $\sigma_{22}$  -  $\sigma_{21}$  stress plane for a unidirectional ply.

In multidirectional laminates the intralaminar failure predictions are made by the analysis of strains and/or stresses in each lamina, with failure criteria evaluated in each lamina. A failure initiated in one lamina predicts the onset of damage, or first ply failure (FPF), that is usually not the ultimate failure of the laminate. It is insufficient to predict ultimate failure with the failure initiation criteria alone if the composite structure can accumulate damage before ultimate failure.

## 9.2 Stresses in the principal material directions

The stresses in the  $k$ -th ply,  $k = 1, 2, \dots, Np$ , of the laminated wall are required to assess the strength of the ply. Starting from eq. (8.27) on page 229 we have for the  $k$ -th ply

$$\begin{bmatrix} \sigma_{11} \\ \sigma_{22} \\ \sigma_{12} \end{bmatrix}^{(k)} = [Q] \begin{bmatrix} \epsilon_{11} \\ \epsilon_{22} \\ \gamma_{12} \end{bmatrix}^{(k)}, \quad (9.54)$$

where the reduced stiffness matrix is

$$[Q] = \begin{bmatrix} E_1/(1-\nu_{21}\nu_{12}) & (\nu_{12}E_1)/(1-\nu_{21}\nu_{12}) & 0 \\ (\nu_{21}E_2)/(1-\nu_{21}\nu_{12}) & E_2/(1-\nu_{21}\nu_{12}) & 0 \\ 0 & 0 & G_{12} \end{bmatrix}. \quad (9.55)$$

The strains in the principal material directions are related to the strains in the beam coordinate directions by eq. (8.29), which is repeated below.



$$\begin{bmatrix} \epsilon_{11} \\ \epsilon_{22} \\ \gamma_{12} \end{bmatrix}^{(k)} = [T_{\epsilon 2}(\varphi_k)] \begin{bmatrix} \epsilon_{ss} \\ \epsilon_{zz} \\ \gamma_{zs} \end{bmatrix} = \begin{bmatrix} n^2 & m^2 & mn \\ m^2 & n^2 & -mn \\ -2mn & 2mn & (-m^2 + n^2) \end{bmatrix} \begin{bmatrix} \epsilon_{ss} \\ \epsilon_{zz} \\ \gamma_{zs} \end{bmatrix}, \quad (9.56)$$

where  $m = \cos \varphi_k$  and  $n = \sin \varphi_k$ . Substitute eq. (9.56) for the strains in eq. (9.54) to get

$$\begin{bmatrix} \sigma_{11} \\ \sigma_{22} \\ \sigma_{12} \end{bmatrix}^{(k)} = [Q] [T_{\epsilon 2}(\varphi_k)] \begin{bmatrix} \epsilon_{ss} \\ \epsilon_{zz} \\ \gamma_{zs} \end{bmatrix}. \quad (9.57)$$

The axial normal strain  $\epsilon_{zz}$  and the shear strain  $\gamma_{zs}$  are determined from the material law, eq. (8.45) on page 237; i.e.,

$$\epsilon_{zz} = \frac{1}{B}(n_z - bq) \quad \gamma_{zs} = \frac{1}{B}(aq - bn_z). \quad (9.58)$$

The normal strain  $\epsilon_{ss}$  is determined from the assumption  $n_s = 0$  in eq. (8.35) on page 233, which yields

$$\epsilon_{ss} = -(A_{12}/A_{11})\epsilon_{zz} - (A_{16}/A_{11})\gamma_{zs}. \quad (9.59)$$

With the strains  $\epsilon_{zz}$ ,  $\gamma_{zs}$ , and  $\epsilon_{ss}$  determined from eq. (9.58) and eq. (9.59), the stresses in the material principal directions in the  $k$ -th ply are obtained from eq. (9.57)

### Example 9.1 First ply failure envelope for the circular tube in example 8.3

The graphite-epoxy tube is subject to a prescribed axial force  $N$  and torque  $M_z$  at its free end, and no other external loads. Thus, the only internal actions at each cross section are an axial force  $N$  and a torque  $M_z$ . The shear flow  $q$  from eq. (8.74), and the normal stress resultant  $n$  from eq. (8.77), at each cross section reduce to

$$q = M_z/(2A_c) \quad n_z = (B/S)N. \quad (a)$$

From eq. (f) in example 8.3 on page 245 the function  $\Phi(\theta) = 0$ ,  $0 \leq \theta < 2\pi$ , so the torque does not contribute to the expression for the normal stress resultant. From example 8.3 we have the following data:

$$S = 4.99669 \text{ MN} \quad b = -1.22899 \quad B = 39.1363 \text{ MN/m} \quad a = 3.9495 \quad A_c = 0.00129717 \text{ m}^2.$$

Consider proportional loading and take

$$q/n_z = \tan \beta = [S/(2A_c B)](M_z/N). \quad (b)$$

For  $N = \lambda \cos \beta$ , the torque  $M_z = (2A_c B/S)\lambda \sin \beta = (0.02032 \text{ m})\lambda \sin \beta$ . A radial ray that runs from the origin to the point of failure initiation in the plane of the axial force and torque is shown in figure. 9.6. Use Puck's criterion, eqs. (9.51) to (9.53), to determine which of the two unidirectional layers with angles  $\varphi_1 = -20^\circ$  and  $\varphi_2 = 70^\circ$  fail first. That is, we find the minimum value of  $\lambda > 0$  for specified values of  $\beta$ ,  $0 \leq \beta \leq 2\pi$  to assess first ply failure. The strengths of T300/5208 graphite/epoxy are listed in table 9.4.

**Fig. 9.6** A load ray in the plane of the axial force and torque

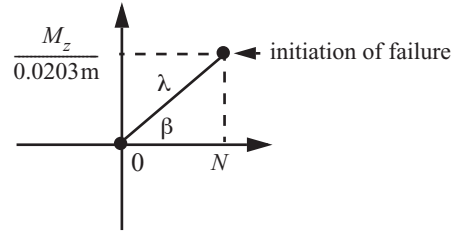


**Table 9.4** Strength parameters for Puck's criterion: eqs. (9.51) to (9.53)

$X_T^a$	1,454.72 MPa (211. ksi)	$p_{nt}^{(-)}$	0.25
$X_C$	1,454.72 MPa (211. ksi)	$p_{nt}^{(+)}$	0.25
$Y_T^a$	42.0559 MPa (6.1 ksi)	$p_{n1}^{(+)}$	0.25
$Y_C^b$	246 MPa	$p_{n1}^{(-)c}$	0.241725
$S_L^a$	95.1429 MPa (13.8 ksi)	$S_T$	98.4 MPa

a. Nixon (1987).

b. Tsai (1992).

c. Equation (9.24).

The strains from the compliance law (9.58) are

$$\epsilon_{zz} = N/S - [b/(2A_c B)]M_z \quad \gamma_{sz} = [a/(2A_c B)]M_z - (b/S)N, \quad (c)$$

The normal strain  $\epsilon_{ss}$  in eq. (9.59) is evaluated from in-plane stiffness matrix is given by eq. (a) of example 8.3.

The results for the laminate strains are

$$\begin{bmatrix} \epsilon_{ss} \\ \epsilon_{zz} \\ \gamma_{sz} \end{bmatrix} = \begin{bmatrix} 1.99988 \times 10^{-7} & 12.0956 \times 10^{-6} \\ -1.08262 \times 10^{-7} & -12.0956 \times 10^{-6} \\ 2.45783 \times 10^{-7} & 38.8707 \times 10^{-6} \end{bmatrix} \begin{bmatrix} N \\ M_z \end{bmatrix}. \quad (d)$$

The reduced stiffness matrix is determined from the material property data listed in example 8.3 which yields the result

$$[Q] = \begin{bmatrix} 148.461 & 4.2377 & 0 \\ 4.23777 & 11.152 & 0 \\ 0 & 0 & 6.4118 \end{bmatrix} \text{ GPa}. \quad (e)$$

The stresses in the principal directions of a ply are determined from eq. (9.57). For the  $\varphi_1 = -20^\circ$  ply,  $m = 0.939693$  and  $n = -0.342020$  in eq. (9.56). The stresses in the principal material directions are

$$\begin{bmatrix} \sigma_{11} \\ \sigma_{22} \\ \sigma_{12} \end{bmatrix}^{(1)} = [Q] [T_{\epsilon_2}(-20^\circ)] \begin{bmatrix} \epsilon_{ss} \\ \epsilon_{zz} \\ \gamma_{sz} \end{bmatrix} = \lambda \begin{bmatrix} 12,638.6 & -9,457.22 \\ 435.659 & 453.391 \\ -2,477.65 & -5,905.5 \end{bmatrix} \begin{bmatrix} \cos\beta \\ \sin\beta \end{bmatrix}. \quad (f)$$

For the  $\varphi_2 = 70^\circ$  ply,  $m = 0.342020$  and  $n = 0.939693$  in eq. (9.56). The stresses in the principal material directions are

$$\begin{bmatrix} \sigma_{11} \\ \sigma_{22} \\ \sigma_{12} \end{bmatrix}^{(2)} = [Q] [T_{\epsilon_2}(70^\circ)] \begin{bmatrix} \epsilon_{ss} \\ \epsilon_{zz} \\ \gamma_{sz} \end{bmatrix} = \lambda \begin{bmatrix} 1,367.92 & 9,347.22 \\ 975.989 & -453.391 \\ 2,477.65 & 5,905.5 \end{bmatrix} \begin{bmatrix} \cos\beta \\ \sin\beta \end{bmatrix}. \quad (g)$$

To illustrate the failure methodology we detail the first ply failure analysis for  $\beta = 30^\circ$  and  $\beta = 150^\circ$ . The stress components in the material directions in each ply are listed in table 9.5.

**Table 9.5 Stresses in the principal material directions in the  $-20^\circ$  ply and the  $70^\circ$  ply for two different load rays**

Stress	$\beta = 30^\circ$		$\beta = 150^\circ$	
	$-20^\circ$ ply	$70^\circ$ ply	$-20^\circ$ ply	$70^\circ$ ply
$\sigma_{11}$	$6,216.74\lambda$	$5,913.26\lambda$	$-15,674.\lambda$	$3,543.95\lambda$
$\sigma_{22}$	$603.987\lambda$	$618.536\lambda$	$-150.597\lambda$	$-1,071.93\lambda$
$\sigma_{21}$	$-5,098.46\lambda$	$5,098.46\lambda$	$-807.041\lambda$	$807.041\lambda$

**Computations for  $\beta = 30^\circ$ .** The stress component in the fiber direction  $\sigma_{11} > 0$  for both plies indicates a fiber tension mode of failure for  $\lambda > 0$ . Since  $\sigma_{11}$  is larger in the  $-20^\circ$  ply it leads to a smaller value of  $\lambda$ . From (9.35)

$$1 = \frac{(6,216.74 \text{ 1/m}^2)\lambda}{(1,454.72 \times 10^6 \text{ N/m}^2)}, \quad (h)$$

which is solved to find  $\lambda = 234,001 \text{ N}$ . In the  $-20^\circ$  ply the stress components  $\sigma_{22} > 0$  and  $\sigma_{21} < 0$  which corresponds to the quadrant IV of the stress plane of figure. 9.5. Evaluation of the mode A failure criterion (9.51) for the  $-20^\circ$  ply leads to

$$1.58705 \times 10^{-6} \lambda + 55.08999 \times 10^{-6} \sqrt{\lambda^2} = 1. \quad (i)$$

The positive root of eq. (i) is  $\lambda = 17,644.1 \text{ N}$ . In the  $70^\circ$  ply the stresses  $\sigma_{22} > 0$  and  $\sigma_{21} > 0$ , which corresponds to quadrant I of the stress plane. Evaluation of the mode A failure criterion (9.51) for the  $70^\circ$  ply leads to

$$1.62528 \times 10^{-6} \lambda + 55.1611 \times 10^{-6} \sqrt{\lambda^2} = 1. \quad (j)$$

The positive root of eq. (j) is  $\lambda = 17,609.8 \text{ N}$ . The results of first ply failure analysis for  $\beta = 30^\circ$  is a matrix mode A failure in the  $70^\circ$  ply at  $\lambda = 17,609.8 \text{ N}$ .

**Computations for  $\beta = 150^\circ$ .** The stress  $\sigma_{11} < 0$  in the  $-20^\circ$  ply, and  $\sigma_{11} > 0$  in the  $70^\circ$  ply for  $\lambda > 0$ . The magnitude of  $\sigma_{11}$  in the  $-20^\circ$  ply exceeds the magnitude of  $\sigma_{11}$  in the  $70^\circ$  ply, so for fiber failure the  $-20^\circ$  ply leads to a smaller value of  $\lambda$ . Equating the fiber failure index in compression to equal one leads to

$$1 = \frac{-(-15,674.1/\text{m}^2)\lambda}{(1454.72 \times 10^6 \text{ N/m}^2)}, \quad (\text{k})$$

which is solved to find  $\lambda = 92,811.4 \text{ N}$ .

In the  $-20^\circ$  ply stresses  $\sigma_{22} < 0$ , and  $\sigma_{21} < 0$ , which means the matrix failure index is evaluated in quadrant III of the stress plane shown in figure. 9.5. To determine if the failure index is evaluated in the mode B or mode C sub-domain of quadrant III, we calculate the slope of the line representing the stress ratio  $\sigma_{21}/\sigma_{22}$  and compare it to the slope of the line dividing the mode B and mode C sub-domains. Let  $m_\sigma$  denote the slope of the line determined by the stress ratio, and let  $m_{b/c}$  denote the slope of the line dividing sub-domains in quadrant III. Refer to figure. 9.5 to see that the stress coordinates  $\sigma_{21} = -S_L\sqrt{1+2p_{nl}^{(\cdot)}}$  and  $\sigma_{22} = -S_T$  define a point on the line subdividing mode B and mode C. The strength data is listed in table 9.4. Numerical evaluation of the slopes yields

$$m_\sigma = \frac{-807.041\lambda}{(-150.597\lambda)} = 5.359 \quad m_{b/c} = \frac{(-S_L\sqrt{1+2p_{nl}^{(\cdot)}})}{-S_T} = 1.184. \quad (\text{l})$$

Since  $m_{b/c} < m_\sigma < \infty$ , the matrix failure index is evaluated in the mode B sub-domain of quadrant III. Set the failure index in mode B (9.52) equal to one to get the quadratic equation

$$(-7.65227 \times 10^{-7} + 7.19512 \times 10^{-11}\lambda)\lambda = 1. \quad (\text{m})$$

The positive root of eq. (m) is  $\lambda = 123,329. \text{ N}$ .

In the  $70^\circ$  ply the matrix stresses  $\sigma_{22} < 0$  and  $\sigma_{21} > 0$ , so the matrix failure index is computed in quadrant II of the stress plane. To determine if the failure is a mode B or mode C, we again determine the slopes  $m_\sigma$  and  $m_{b/c}$  in quadrant II. The numerical results for the slopes are

$$m_\sigma = \frac{807.041\lambda}{-1,071.93\lambda} = -0.752 \quad m_{b/c} = \frac{(S_L\sqrt{1+2p_{nl}^{(\cdot)}})}{-S_T} = -1.184. \quad (\text{n})$$

Since  $m_{b/c} < m_\sigma < 0$ , the failure index is compute for mode C in quadrant II. Set the failure index in mode C (9.53) equal to one to get

$$6.9994 \times 10^{-6}\lambda = 1. \quad (\text{o})$$

Hence, for the matrix mode C in the  $70^\circ$  ply  $\lambda = 142,869 \text{ N}$ . For  $\beta = 150^\circ$  the minimum value of  $\lambda$  is

92,811.4 N, which corresponds to a fiber compression mode in the  $-20^\circ$  ply.

The following table lists first ply failure results for selected values of  $\beta$ .

**Table 9.6 First ply failure data for selected load rays**

$\beta$ , degrees	$\lambda$ , N	Axial force $N$ , kN	Torque $M_z$ , N-m	Mode of failure
0	27,936.9	27.94	0	$70^\circ$ ply matrix mode A
30	17,609.8	15.25	178.9	$70^\circ$ ply matrix mode A
35	16,658.1	13.65	194.2	$-20^\circ$ ply matrix mode A
90	15,625.6	0	317.5	$-20^\circ$ ply matrix mode A
135	39,199.9	-27.72	563.2	$-20^\circ$ ply matrix mode A
140	50,399.	-38.61	658.2	$-20^\circ$ ply matrix mode B
145	71,295.8	-58.40	831.0	$-20^\circ$ ply matrix mode B
150	92,811.4	-80.38	943.0	$-20^\circ$ ply fiber compression
155	94,149.1	-85.33	808.5	$-20^\circ$ ply fiber compression
160	96,269.3	-90.46	669.1	$-20^\circ$ ply fiber compression
165	99,260.1	-95.88	522.0	$-20^\circ$ ply fiber compression
170	71,408.	-101.7	364.3	$-20^\circ$ ply matrix mode B
180	40,067.3	-51.14	0	$-20^\circ$ ply matrix mode B
210	19,203.1	-17.91	-210.1	$-20^\circ$ ply matrix mode B
215	17,992.2	-15.73	-223.8	$-70^\circ$ ply matrix mode B
245	14,868.6	-6.352	-276.8	$-70^\circ$ ply matrix mode B
250	14,814.	-5.085	-283.9	$-70^\circ$ ply matrix mode A
270	15,625.6	0	-310.1	$-70^\circ$ ply matrix mode A
335	38,849.7	33.53	-317.8	$-70^\circ$ ply matrix mode A
355	30,944.9	34.02	-60.49	$70^\circ$ ply matrix mode A

Note that the majority of first ply failures are matrix modes A and B. For  $150^\circ \leq \beta \leq 165^\circ$  the mode of failure is fiber compression in the  $-20^\circ$  ply. The first ply failure locus is plotted in figure. 9.7.

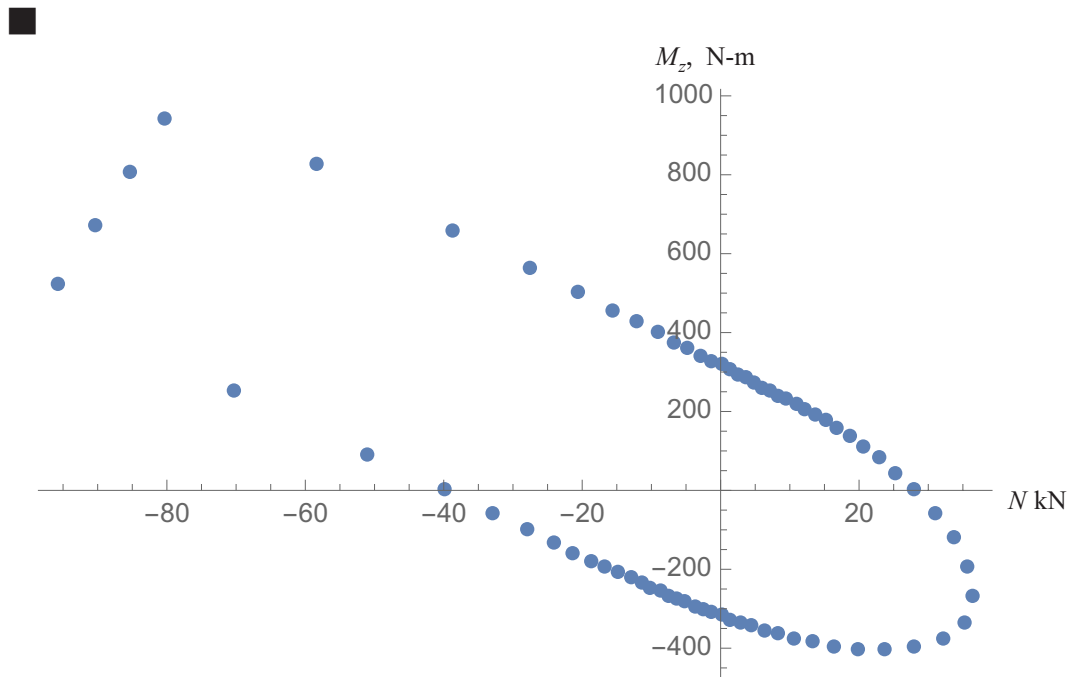


**Fig. 9.7** First ply failure locus for the graphite epoxy circular tube subject to an axial force and a torque.

### 9.3 References

- Dowling, N. E. *Mechanical Behavior of Materials*. Englewood Cliffs, NJ: Prentice Hall, Inc., 1993.
- Herakovich, Carl T. *Mechanics of Fibrous Composites*. New York: John Wiley & Sons, Inc., 1998.
- Nixon, M. W. "Extension-Twist Coupling of Composite Circular Tubes with Application to Tilt Rotor Blade Design." In *Proceedings of the 28th Structures, Structural Dynamics, and Materials Conference* (Monterey, CA). Reston, VA: American Institute of Aeronautics and Astronautics, 1987.
- Puck, A., and H. Schürmann. "Failure Analysis of FRP Laminates by Means of Physically Based Phenomenological Models." *Composites Science and Technology* 58 (1998):1045-1067.
- Puck, A., J. Kopp, and M. Knops., "Guidelines for the Determination of the Parameters in Puck's Action Plane Strength Criterion." *Composites Science and Technology*, 62 (2002): 371-378.
- Soden, P. D., A. S. Kaddour, and M. J. Hinton. "Recommendations for Designers and Researchers Resulting from the World Wide Failure Exercise." *Composites Science and Technology*, 64 (2004): 589-601.
- Tsai, S. W. *Theory of Composites Design*. Dayton, OH: THINK COMPOSITES, a Division of ILT Corporation, 1992.

---

# *Structural stability of discrete conservative systems*

---

Structures subject to compression fail in differently than those subject to tension. For some ductile metals that are short and thick, compression failure is associated with a shear mechanism with a fracture plane inclined with respect to the axis of the compressive load. Other ductile metals may not fracture in compression but crush during plastic deformation. Long and thin compression members fail by buckling in which the member responds by displacing sideways with respect to the direction of the compressive load. Buckling is characterized by

- failure due to excessive displacements (loss of structural stiffness), and/or
- loss of stability of an equilibrium configuration

*Stability of equilibrium* means that the response of the structure due to a small disturbance from its equilibrium configuration remains small; the smaller the disturbance the smaller the resulting magnitude of the displacement in the response. If a small disturbance causes large displacement, perhaps even theoretically infinite, then the equilibrium state is unstable. Practical structures in engineering are stable at no load. Now consider increasing the load slowly. We are interested in the value of the load, called the *critical load*, at which buckling occurs. That is, we are interested when a sequence of stable equilibrium states as a function of the load, one state for each value of the load, ceases to be stable.

In this chapter structural stability phenomena, concepts, and methods are presented by analyzing discrete systems composed of rigid bars and springs. Stability of discrete systems are also presented by Simites (1976), and in a monograph by Huseyin (1975). The latter author presents a general non-linear theory of elastic stability of discrete systems. Continuum analyses for the buckling of columns and plates are discussed in the next chapter.

## *10.1 Model A: stable symmetric bifurcation buckling*

This model is shown in figure 10.1 and it has one coordinate  $\theta$ ,  $-\pi < \theta < \pi$ , to describe the configuration of the model under the *deadweight load*  $P$ . (An external load independent of its corresponding displacement.) The model consists of a rigid rod of length  $L$ , connected by smooth hinge to a rigid base. The rod can rotate about the hinge, but it is restrained by a linear elastic torsional spring of stiffness  $K$  (dimensional units of F-L/ radian). The restoring moment of the spring acting on the bar is zero at  $\theta = 0$ . Neglect the weight of the rod with respect to the

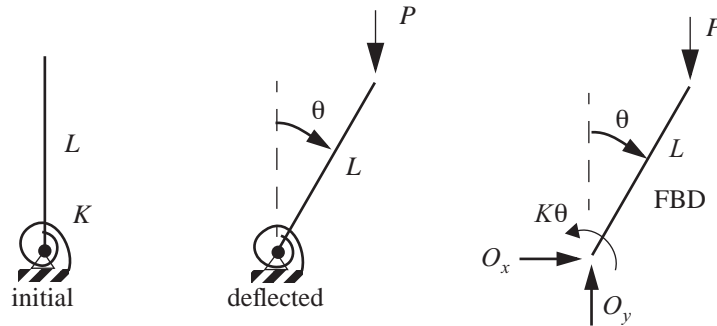


**Fig. 10.1 One degree-of-freedom structural model.**

applied load  $P$ . From the free body diagram of the rod shown in figure 10.1, the equation of motion for rotation about the fixed hinge is

$$PL \sin \theta - K\theta = I_0 \frac{d^2 \theta}{dt^2} \quad \theta = \theta(t) \quad t > 0 \quad (10.1)$$

where  $I_0$  is the moment of inertia of the rod about the fixed point and  $t$  is time.

### 10.1.1 Equilibrium method

This method is also known as the classical method or bifurcation method. Consider equilibrium states under the static, downward load  $P$  which are characterized by the angle  $\theta$  being independent of time  $t$ . Hence, the inertia term in eq. (10.1) vanishes and we have

$$PL \sin \theta - K\theta = 0 \quad |\theta| < \pi. \quad (10.2)$$

One solution to eq. (10.2) is

$$p1: \theta = 0 \text{ for any } P. \quad (10.3)$$

Equilibrium path (10.3) is called the trivial equilibrium configuration. The equilibrium method is characterized by the question

*What are the values of the load for which the perfect system admits non-trivial equilibrium configurations?* (Ziegler, 1968)

A second solution of eq. (10.2) is

$$p2: P = \left(\frac{K}{L}\right) \frac{\theta}{\sin \theta} \quad (10.4)$$

Recall from the calculus using l'Hôpital's rule that the limit of the indeterminate form  $\theta/(\sin \theta)$  as  $\theta \rightarrow 0$  is one. The two equilibrium paths are plotted in the load-deflection diagram shown in figure 10.2. Equilibrium path  $p2$  is called the secondary path and we note it is symmetric about  $\theta = 0$ . For  $P < K/L$  there is only one equilibrium position:  $\theta = 0$  on the primary path  $p1$ . For  $P > K/L$  there are three equilibrium positions:  $\theta = 0$  on path  $p1$ , and two on the secondary path  $p2$ .



The two equilibrium paths intersect at  $(\theta, P) = (0, K/L)$ . This intersection of the two paths is called a **bifurcation point**, and represents the equilibrium state or position common to two separate equilibrium paths. At no load the rod is vertical and this corresponds to the origin in the load-deflection diagram. As the load  $P$  is slowly increased from zero the rod remains vertical ( $\theta = 0$ ), and at  $P = K/L$  adjacent equilibrium states exist on the secondary path.

The existence of adjacent equilibrium states in the vicinity of the primary equilibrium path has been noted by investigators of structural stability as the onset of buckling. Hence, buckling is characterized by the bifurcation point on the load-deflection diagram. For this reason, the term bifurcation buckling is used to describe this condition. As we will show later, the rod will not remain vertical for loads  $P > K/L$  if there are infinitesimal disturbances present (there always are), but will rotate either to the left or right depending on type of infinitesimal disturbance. We note that the magnitude of the angle  $\theta$  becomes large as the load is increased from  $K/L$  on the secondary path. The load at the bifurcation point is called the critical load and is denoted as  $P_{cr}$ . Thus,

$$P_{cr} = K/L. \quad (10.5)$$

**Small  $\theta$  analysis** Consider the small angles of rotation such that  $\sin \theta \approx \theta$  for  $\theta$  measured in radians. Equilibrium eq. (10.2) becomes

$$PL\theta - K\theta = 0. \quad (10.6)$$

The solutions of this equation (10.6) are

$$p1': \quad \theta = 0 \text{ for any } P, \text{ and} \quad (10.7)$$

$$p2': \quad P = K/L \text{ for any small } \theta. \quad (10.8)$$

These solutions are shown in the load-deflection plane in figure 10.3. The equilibrium path  $p1'$  coincides with path  $p1$ , but path  $p2'$  is not a good approximation to path  $p2$  unless  $\theta$  is very small. However, the bifurcation point is the same as obtained in the large  $\theta$ -analysis. Hence, the critical load from the small  $\theta$ -analysis is the same as obtained in eq. (10.5) from the large  $\theta$ -analysis.

### 10.1.2 Kinetic method

The kinetic method, or the vibration method, is based on the definition of stability of equilibrium. The vibration method is characterized by the question

*What is the value of the load for which the most general free motion of the perfect system in the equilibrium position ceases to be bounded? (Ziegler, 1968)*

Let the rotation angle

$$\theta(t) = \theta_0 + \varphi(t), \quad (10.9)$$

where  $\theta_0$  is independent of time and satisfies the equilibrium eq. (10.2); i.e.,

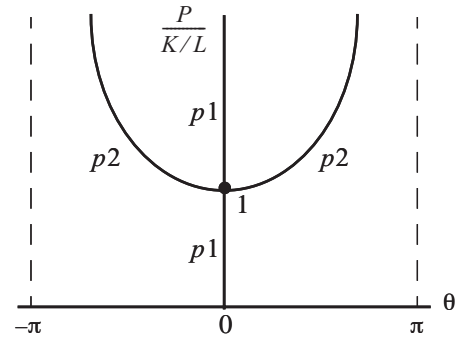


Fig. 10.2 Equilibrium paths

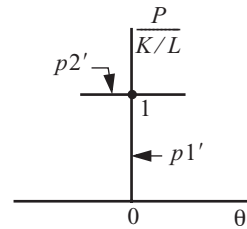
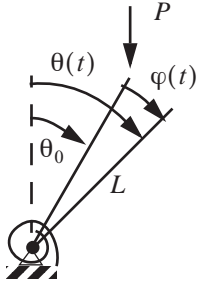


Fig. 10.3 Small  $\theta$  analysis.



**Fig. 10.4 Rotations in the stability analysis.**

$$PL \sin \theta_0 - K \theta_0 = 0. \quad (10.10)$$

Consider the additional rotation angle  $\varphi(t)$  to be small in magnitude but a function of time. Thus, we are considering small oscillations about an equilibrium state  $(P, \theta_0)$  as shown in figure 10.4. Substitute eq. (10.9) for  $\theta(t)$  in the equation of motion, eq. (10.1), to get

$$I_0 \ddot{\varphi} + K(\theta_0 + \varphi) - PL \sin(\theta_0 + \varphi) = 0, \quad (10.11)$$

where the dots denote derivatives with respect to time (e.g.,  $\ddot{\varphi} = \frac{d^2 \varphi}{dt^2}$ ). Using the trigonometric identity for the sine of the sum of two angles, and performing some minor rearrangements, equation (10.11) becomes

$$I_0 \ddot{\varphi} + K \theta_0 + K \varphi - PL [\sin \theta_0 \cos \varphi + \cos \theta_0 \sin \varphi] = 0. \quad (10.12)$$

Now expand the trigonometric functions of angle  $\varphi$  in a Taylor Series about  $\varphi = 0$  to get

$$I_0 \ddot{\varphi} + K \theta_0 + K \varphi - PL \sin \theta_0 \left[ 1 - \frac{1}{2} \varphi^2 + O(\varphi^4) \right] - PL \cos \theta_0 \left[ \varphi - \frac{1}{6} \varphi^3 + O(\varphi^5) \right] = 0, \quad (10.13)$$

in which  $O(\varphi^n)$  means terms of order  $\varphi^n$  and higher. Arrange eq. (10.13) in powers of  $\varphi$  to get

$$I_0 \ddot{\varphi} + \underbrace{(K \theta_0 - PL \sin \theta_0)}_{=0} + (K - PL \cos \theta_0) \varphi + \left( \frac{PL}{2} \sin \theta_0 \right) \varphi^2 + \left( \frac{PL}{6} \cos \theta_0 \right) \varphi^3 + O(\varphi^4) = 0 \quad (10.14)$$

Note that “coefficient” of the term  $\varphi^0$  vanishes because of the equilibrium condition given by eq. (10.10).

For very small additional rotation angles  $\varphi(t)$  about the equilibrium configuration, eq. (10.14) is approximated by

$$I_0 \ddot{\varphi} + (K - PL \cos \theta_0) \varphi = 0 \quad \text{or} \quad \ddot{\varphi} + \omega^2 \varphi = 0, \quad (10.15)$$

where

$$\omega^2 = (K - PL \cos \theta_0) / I_0. \quad (10.16)$$

The solution of the second order differential equation (10.15) for  $\omega^2 > 0$  is

$$\varphi(t) = A_1 \sin(\omega t) + A_2 \cos(\omega t) \quad \omega^2 > 0, \quad (10.17)$$

in which constants  $A_1$  and  $A_2$  are determined by initial conditions for  $\varphi(0)$  and  $\dot{\varphi}(0)$ . The solution given by eq. (10.17) is a harmonic oscillation about the equilibrium configuration and  $\omega$  is interpreted as the natural frequency in radians per second. Initial conditions  $\varphi(0)$  and  $\dot{\varphi}(0)$  are considered to be very small to simulate an arbitrary infinitesimal disturbance. The smaller the initial disturbance, the smaller the maximum amplitude of the oscillation in  $\varphi$ . Thus,  $\omega^2 > 0$  is a condition for a stable equilibrium configuration with respect to infinitesimal disturbances.

The solution of the second order differential equation, eq. (10.15), for  $\omega^2 < 0$  is

$$\varphi(t) = A_1 e^{\bar{\omega}t} + A_2 e^{-\bar{\omega}t} \quad \bar{\omega}^2 = -\omega^2 = -(K - PL \cos \theta_0)/I_0. \quad (10.18)$$

For arbitrary initial conditions, the term with the positive exponent in the dominates the solution. This corresponds to large values of the  $\varphi$  no matter how small the initial disturbance. Hence,  $\omega^2 < 0$  is a condition of unstable equilibrium configuration with respect to infinitesimal disturbances. The kinetic method for model A leads to the following criterion.

#### Dynamic criterion for stability of an equilibrium state

The equilibrium state is stable if	$\omega^2 > 0$
The equilibrium state is critical if	$\omega^2 = 0$
The equilibrium state is unstable if	$\omega^2 < 0$

On the primary equilibrium path  $pI$  given by eq. (10.3), we have from eq. (10.16) that

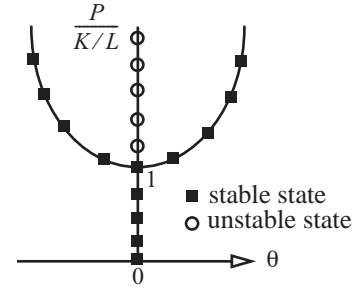
$$\omega^2 = (K - PL)/I_0 \quad \text{on } pI. \quad (10.19)$$

Thus, equilibrium configurations are stable if  $P < K/L$ , critical if  $P = K/L$ , and unstable if  $P > K/L$ . The primary equilibrium path ceases to be stable at  $P = P_{cr}$ , and  $P_{cr}$  is the buckling load. On the secondary path (10.4)  $\omega^2 = [K(1 - \theta_0 \cot \theta_0)]/I_0$ , and  $\omega^2 \geq 0$  for  $0 < |\theta_0| < \pi$ . Thus, the equilibrium configuration on the secondary path is critical at  $\theta_0 = 0$ , and the equilibrium configurations for  $0 < |\theta_0| < \pi$  are stable. Retaining the first non-zero term in the expansion of the differential equation of motion (10.13) at the bifurcation point  $(\theta_0, P) = (0, K/L)$  we get

$$\ddot{\varphi} + \left(\frac{K}{6I_0}\right)\varphi^3 = 0. \quad (10.20)$$

Differential equation of motion (10.20) is nonlinear. Since coefficient  $K/(6I_0) > 0$ , its solution is a nonlinear oscillation about the bifurcation point for small initial disturbances (Simitses, 1976). Hence, equilibrium at the bifurcation point is stable. The stability of the equilibrium states for model A are shown in figure 10.5.

**Fig. 10.5**  
Stability of the  
equilibrium  
states for  
model A.



### 10.1.3 Energy method

**Theorem.** A conservative mechanical system is in a configuration of stable equilibrium if, and only if, the value of the potential energy is a relative minimum, otherwise it is unstable.

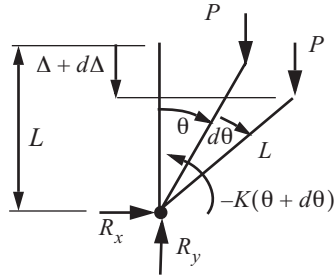
This method is characterized by the question:

*What is the value of the load for which the potential energy of the system in the equilibrium position ceases to be positive definite? (Ziegler, 1968)*

First we have to determine if model A is a conservative mechanical system. The incremental work of the external load and the rotational spring acting on the bar shown in figure 10.6 are given by

$$dW_{\text{ext}} = P(\Delta + d\Delta) - P\Delta = Pd\Delta \quad dW_{\text{int}} = -[K(\theta + d\theta) - K\theta] = -(K\theta)d\theta. \quad (10.21)$$

**Fig. 10.6**  
Forces acting on the bar of model A for an increment in its rotation.



The incremental external work is positive since load  $P$  and the shortening  $\Delta$  act in the same direction, but the incremental work of the spring on the bar opposes the increase in rotation. The shortening is given by

$$\Delta = L(1 - \cos\theta). \quad (10.22)$$

The increment in the shortening with respect to an infinitesimal change in the rotation is

$$d\Delta = \frac{d\Delta}{d\theta}d\theta = (L\sin\theta)d\theta. \quad (10.23)$$

The incremental external work is  $dW_{\text{ext}} = PL\sin\theta d\theta$ . Since the load  $P$  is independent of angle  $\theta$  for dead-weight loading, we can integrate incremental work expression to get  $W_{\text{ext}} = -PL\cos\theta + C$ . The constant  $C$  is determined if we define  $W_{\text{ext}} = 0$  when  $\theta = 0$ . The external work function is

$$W_{\text{ext}} = PL(1 - \cos\theta). \quad (10.24)$$

Note that the work of  $P$  is independent of path. For example, the value of  $W_{\text{ext}}$  is the same if the bar first rotated to  $2\theta$  and then rotated back to  $\theta$ . The expression for the incremental work of the spring acting on the bar is integrated with respect to  $\theta$  to get  $W_{\text{int}} = -\frac{1}{2}K\theta^2 + C'$ . The constant  $C'$  is determined if we define  $W_{\text{int}} = 0$  at  $\theta = 0$ . Hence,

$$W_{\text{int}} = -K\theta^2/2. \quad (10.25)$$

Since the work done by the external load and the spring force are independent of the process of how the final value of  $\theta$  is achieved, they are conservative forces. The potential energy is defined as the negative of the work function. The negative sign means that the work done by the spring force against the rotation increases the potential energy while the work done by the force  $P$  with the rotation decreases the potential energy. Let  $U$  denote the potential energy of the spring and let  $\Omega$  denote the potential energy of the external load. Then

$$U = \frac{1}{2}K\theta^2 \quad \Omega = -PL(1 - \cos\theta). \quad (10.26)$$

The total potential energy is denoted by  $V$ , where

$$V(\theta) = U(\theta) + \Omega(\theta) = \frac{1}{2}K\theta^2 - PL(1 - \cos\theta). \quad (10.27)$$

Second, we must determine the equilibrium positions and if these correspond to a relative minimum of  $V$ . A necessary condition for a relative minimum is that  $V$  is stationary with respect to  $\theta$ , and this leads to equilibrium. That is,

$$\frac{dV}{d\theta} = 0 = K\theta - PL\sin\theta, \quad (10.28)$$

which is the same equation (10.2) governing equilibrium found from the free body diagram approach. Let  $\theta_0$  denote the rotation of the bar in equilibrium under load  $P$ , or  $K\theta_0 - PL \sin \theta_0 = 0$ . The Taylor series of the potential energy about the equilibrium position is

$$V(\theta_0 + h) = V(\theta_0) + V_1(\theta_0)h + \frac{1}{2!}V_2(\theta_0)h^2 + \frac{1}{3!}V_3(\theta_0)h^3 + \frac{1}{4!}V_4(\theta_0)h^4 + \dots, \quad (10.29)$$

where

$$h = \theta - \theta_0 \quad V_1(\theta_0) = \left. \frac{dV}{d\theta} \right|_{\theta = \theta_0} \quad V_2(\theta_0) = \left. \frac{d^2V}{d\theta^2} \right|_{\theta = \theta_0} \quad \text{et cetera.} \quad (10.30)$$

At equilibrium  $V_1(\theta_0) = 0$ . The change in potential energy  $\Delta V = V(\theta_0 + d\theta) - V(\theta_0)$  is

$$\Delta V = \frac{1}{2!}V_2(\theta_0)h^2 + \frac{1}{3!}V_3(\theta_0)h^3 + \frac{1}{4!}V_4(\theta_0)h^4 + \dots \quad (10.31)$$

For infinitesimal changes in  $h \neq 0$  from the equilibrium position, the lowest degree term in  $h$  dominates the series of  $\Delta V$ . Consequently, the potential energy is positive definite if  $V_2(\theta_0) > 0$ , indefinite if  $V_2(\theta_0) = 0$ , and negative definite if  $V_2(\theta_0) < 0$ . The second derivative of  $V(\theta)$  is

$$\frac{d^2V}{d\theta^2} = K - PL \cos \theta_0. \quad (10.32)$$

On trivial equilibrium path  $\theta_0 = 0$  for any  $P$ , and the second derivative  $\left. \frac{d^2V}{d\theta^2} \right|_{p1} = K - PL$ . Therefore,

$$\left. \frac{d^2V}{d\theta^2} \right|_{p1} > 0, \text{ stable, } P < K/L \quad \left. \frac{d^2V}{d\theta^2} \right|_{p1} = 0, \text{ critical, } P = K/L \quad \left. \frac{d^2V}{d\theta^2} \right|_{p1} < 0, \text{ unstable, } P > K/L. \quad (10.33)$$

In answer to the question characterizing the energy method, the potential energy ceases to be positive definite on the primary equilibrium path when  $P > K/L$ . On the secondary path  $PL = K\theta_0/\sin \theta_0$ , and the second derivative of the potential energy is

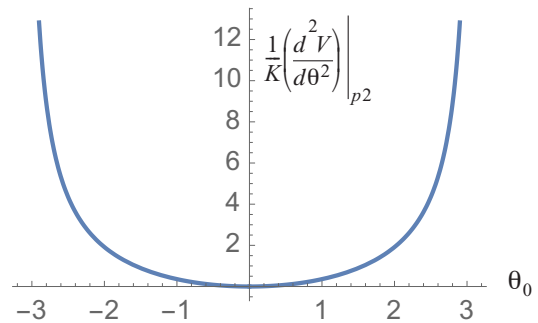
$$\left. \frac{d^2V}{d\theta^2} \right|_{p2} = K(1 - \theta_0 \cot \theta_0). \quad (10.34)$$

A graph of eq. (10.34) is shown in figure 10.7. Thus,

$$\left. \frac{d^2V}{d\theta^2} \right|_{p2} > 0, \text{ stable, } 0 < |\theta_0| < \pi \quad \left. \frac{d^2V}{d\theta^2} \right|_{p2} = 0, \text{ critical, } P = K/L \quad \left. \frac{d^2V}{d\theta^2} \right|_{p2} < 0, \text{ unstable, no } \theta \text{ of interest.} \quad (10.35)$$

These results from the energy method confirm the previous results from the kinetic method. At the bifurcation point  $(\theta_0, P) = (0, K/L)$ , and the second derivative  $V_2(\theta_0) = 0$ . Evaluate the next two terms in the series

**Fig. 10.7**  
Second derivative of the potential energy on the secondary equilibrium path.



(10.31) for  $\Delta V$  at the bifurcation point to find

$$V_3(\theta_0) = \frac{1}{\sin^2 \theta_0} (\theta_0 - \cos \theta_0 \sin \theta_0) \Big|_{\theta_0 \rightarrow 0} = 0 \quad V_4(\theta_0) = \frac{2}{\sin^3 \theta_0} (\sin \theta_0 - \theta_0 \cos \theta_0) \Big|_{\theta_0 \rightarrow 0} = \frac{2}{3}. \quad (10.36)$$

The series for  $\Delta V$  at the bifurcation point is

$$\Delta V = \frac{2}{3} h^4 + O(h^5). \quad (10.37)$$

Hence,  $V_4(0) > 0$ , and the bifurcation point  $(\theta_0, P) = (0, K/L)$  is stable.

#### 10.1.4 Eccentric load

Consider the applied load  $P$  applied slightly off the center line of the bar by  $\delta_0$  as shown in figure 10.8. Moment

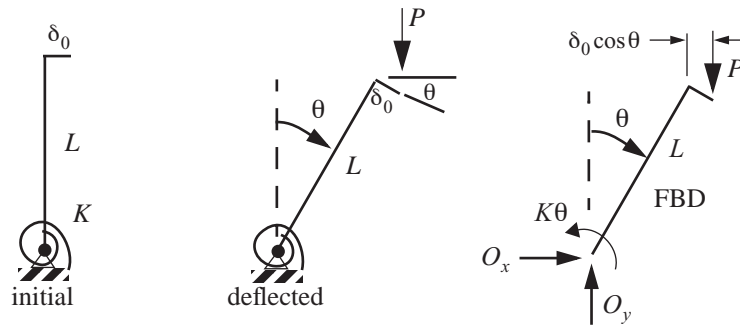


Fig. 10.8 Model A subject to eccentric load.

equilibrium about the fixed pin is

$$P(L \sin \theta + \delta_0 \cos \theta) - K\theta = 0. \quad (10.38)$$

The equilibrium equation (10.38) solved numerically and the equilibrium paths in the load-deflection plane are shown as dashed lines in figure 10.9. There are two equilibrium paths: the first one begins from the unloaded state ( $P = 0$ ,  $\theta = 0$ ), and a second complementary path that is not connected to the first path. As the load  $P$  increases from zero along the first path, the angle  $\theta$  increases slowly until  $P$  is in the vicinity of  $P_{cr} = K/L$ .

Equilibrium positions on the first path are stable ( $\Delta V > 0$ ).

Note the following characteristics.

- The deflection for the path beginning from the unloaded state is always the same sign as  $\delta_0$ .
- If  $\delta_0$  is small, the equilibrium path of the imperfect system approaches that of the perfect model as the deflection becomes large.
- There is no intersection of two equilibrium paths.
- Even if  $\delta_0 \neq 0$  there are three equilibrium states for  $P > P_{cr}$ .
- There is a minimum load on the complementary path that divides unstable and stable equilibrium states.

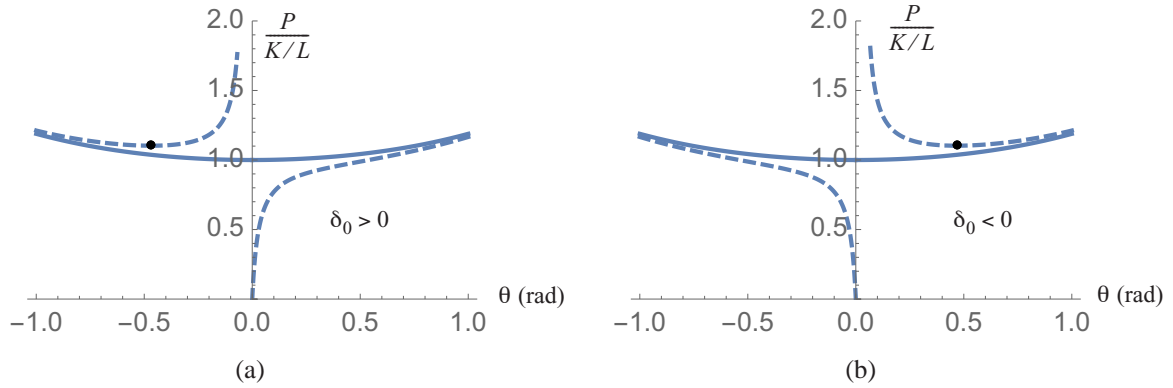


**Fig. 10.9** Load-deflection plots for model A subject to the eccentric load are shown by the dashed lines for (a)  $\delta_0 > 0$  and (b)  $\delta_0 < 0$ .

### 10.1.5 Initial angle

When  $P = 0$ , suppose the bar is not vertical but is at an initial angle  $\theta = \delta_0$  with the spring restoring moment equal to zero as shown in figure 10.10. Moment equilibrium about the fixed pin is

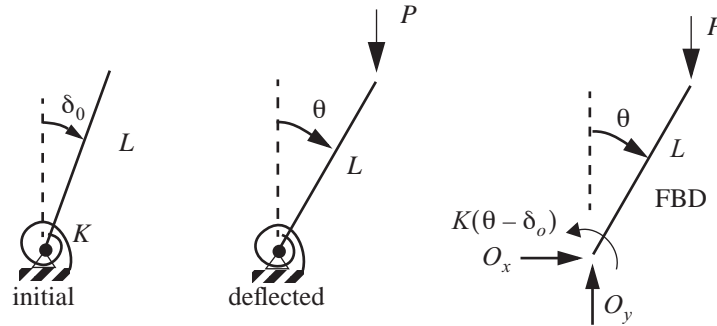


**Fig. 10.10** Model A with an initial angle.

$$PL \sin \theta - K(\theta - \delta_0) = 0. \quad (10.39)$$

Equilibrium equation (10.39) is plotted in figure 10.11. The response of model A with the initial angle is similar to the response of model A subject to the eccentric load in figure 10.9

**Discussion.** Eccentricity in load and the initial slope of the bar are examples of **imperfections**. The structural systems are imperfect. Small imperfections of model A do not change the fact that there are large displacements when  $P = P_{cr}$  of the perfect system. Model A is classified as **stable symmetric bifurcation**. The secondary equilibrium path  $p_2$  of the perfect system in figure 10.2 is symmetric about  $\theta = 0$  and it is stable.

Real structures exhibiting stable symmetric bifurcation are,

- long straight columns subject to axial compression, and

b. flat plates subject to in-plane edge loading.

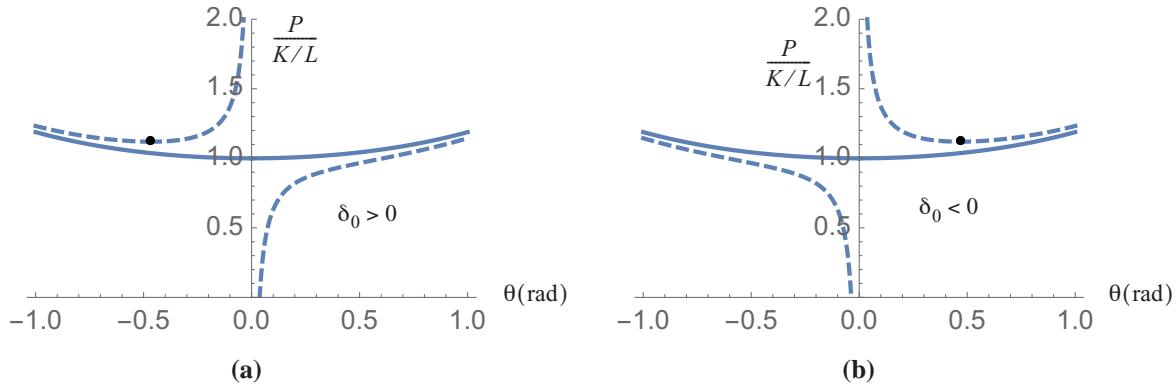


**Fig. 10.11** Load-deflection plots for model A with the initial angle are shown by the dashed lines for (a)  $\delta_0 > 0$  and (b)  $\delta_0 < 0$ .

## 10.2 Model B: unstable symmetric bifurcation

This model consists of a coplanar arrangement of two rigid bars of length  $L$  and a linear elastic spring of stiffness  $K$ . The bars are horizontal in the initial position and connect to a center hinge, with the opposite ends of each bar supported on roller support. The vertical spring connects to the center hinge and is not stretched when the bars are in the horizontal position. A horizontal load  $P$  acts at each roller support to subject the model to compression.

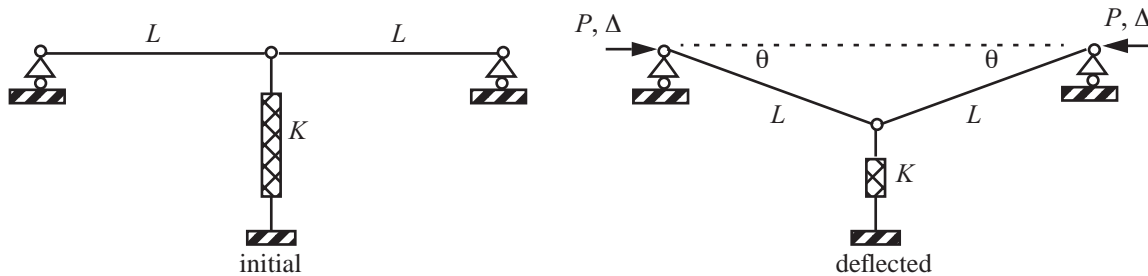


**Fig. 10.12** Model B.

The deflected configuration of the model is symmetric with respect to the vertical line through the spring, and each bar rotates through an angle  $\theta$  with respect to the original horizontal position. The deflection of the spring is  $L \sin \theta$ , and the load  $P$  is independent of the corresponding displacement  $\Delta(\theta)$ . The potential energy is

$$V = \frac{1}{2}K(L \sin \theta)^2 - 2P \underbrace{[L(1 - \cos \theta)]}_{\Delta} \quad (10.40)$$

The potential energy is stationary at equilibrium, or  $\frac{dV}{d\theta} = 0$ , which leads to



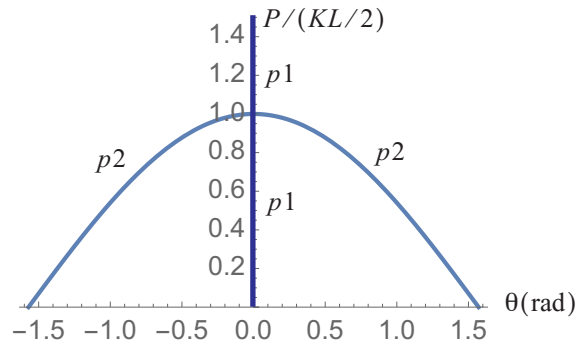
$$(KL^2 \cos \theta - 2PL) \sin \theta = 0. \quad (10.41)$$

The solutions of eq. (10.41) are

$$p1: \theta = 0 \text{ for any } P \quad p2: P = \frac{1}{2}KL \cos \theta. \quad (10.42)$$

The equilibrium paths are shown on the load-deflection plot in figure 10.13. Equilibrium paths intersect at the bifurcation point  $(\theta, P) = (0, KL/2)$ . By the equilibrium method the critical load is  $P_{cr} = KL/2$ . However, equilibrium states in figure 10.13 are different than those of model A shown in figure 10.2. Note that there are three equilibrium positions for  $P < P_{cr}$ .

Fig. 10.13 Model B equilibrium states.



The stability of the equilibrium states is assessed from the second derivative of the potential energy (10.40). The second derivative is

$$\frac{d^2 V}{d\theta^2} = V_2(\theta) = KL^2(\cos^2 \theta - \sin^2 \theta) - 2PL \cos \theta = KL^2 \cos 2\theta - 2PL \cos \theta. \quad (10.43)$$

On equilibrium path  $p1$

$$V_2(0) = KL^2 - 2PL. \quad (10.44)$$

Therefore, on equilibrium path  $p1$

$$V_2(0)|_{p1} > 0, \text{ stable, } P < \frac{KL}{2} \quad V_2(0)|_{p1} = 0, \text{ critical, } P = \frac{KL}{2} \quad V_2(0)|_{p1} < 0, \text{ unstable, } P > \frac{KL}{2} \quad (10.45)$$

On equilibrium path  $p2$   $P = (KL/2) \cos \theta_0$ . The second derivative is

$$V_2(\theta_0) = KL^2(\cos^2 \theta - \sin^2 \theta) - 2(KL/2) \cos^2 \theta = -KL^2 \sin^2 \theta_0. \quad (10.46)$$

Therefore, on equilibrium path  $p2$

$$V_2(\theta_0)|_{p2} > 0, \text{ stable, for no } 0 < |\theta_0| \leq \frac{\pi}{2} \quad V_2(\theta_0)|_{p2} = 0, \text{ critical, } \theta_0 = 0 \quad V_2(\theta_0)|_{p2} < 0, \text{ unstable, } 0 < |\theta_0| < \frac{\pi}{2} \quad (10.47)$$

At the bifurcation point  $(\theta_0, P) = (0, KL/2)$  on path  $p2$  the derivatives of the potential energy are

$$V_2(0) = 0 \quad V_3(0) = 0 \quad V_4(0) = -3KL^2. \quad (10.48)$$

The potential energy is a relative maximum at the bifurcation point, so the bifurcation point is unstable. Model B exhibits **unstable symmetric bifurcation**.

### 10.2.1 Initial angle imperfection

Consider a small deviation of the bars from the horizontal position represented by angle  $\delta_0$  as shown in figure 10.14. The spring is not stretched in the initial position.

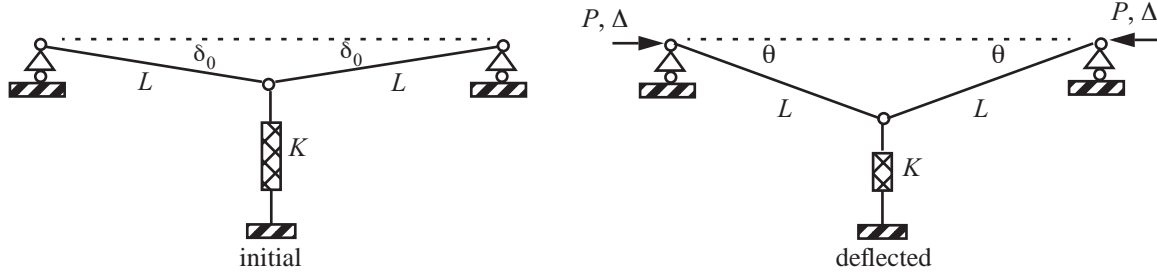


Fig. 10.14 Imperfect model B.

The potential energy of the system is

$$V = \frac{1}{2}K(L \sin \theta - L \sin \delta_0)^2 - 2PL(\cos \delta_0 - \cos \theta). \quad (10.49)$$

The potential energy is stationary at equilibrium, or  $\frac{dV}{d\theta} = 0$ . Hence, the equilibrium equation is

$$KL^2(\sin \theta - \sin \delta_0)\cos \theta - 2PL \sin \theta = 0. \quad (10.50)$$

Equation (10.50) is written in the equivalent form as

$$(\sin \theta - \sin \delta_0)\cos \theta - (P/P_{cr})\sin \theta = 0, \quad (10.51)$$

where the critical load of the perfect system is  $P_{cr} = KL/2$ . One solution to eq. (10.51) is the unloaded state at  $(\theta, P) = (\delta_0, 0)$ . Other solutions are plotted as dashed lines in the load-deflection plane of figure 10.15. Equilibrium states along the path beginning at the unloaded state are stable until a relative maximum on the path is encountered at  $(\theta_m, P_m)$ , which is indicated by the filled circles in figure 10.15. There are no stable adjacent equilibrium states if the load  $P$  increases from  $P_m$  or if  $\theta$  increases from  $\theta_m$ . Any small increase in load or rotation from the relative maximum results in a dynamic motion of the system that may lead to catastrophic collapse.

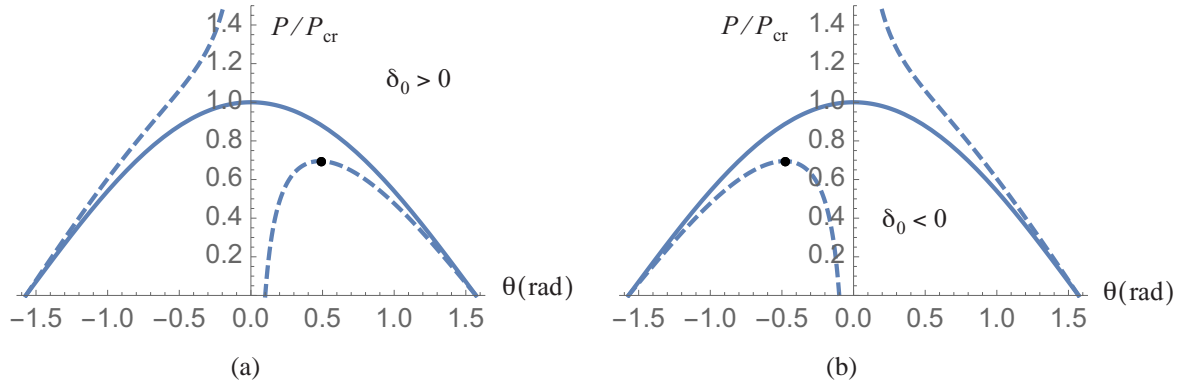


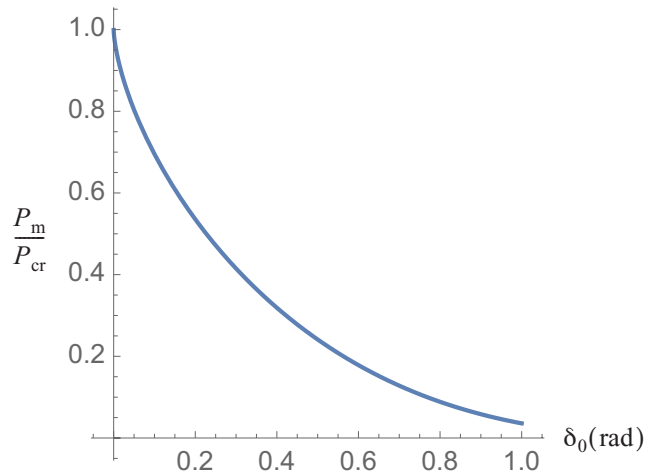
**Fig. 10.15** Equilibrium paths of the imperfect model B are shown in the load-deflection plane by dashed lines for (a)  $\delta_0 > 0$  and (b)  $\delta_0 < 0$ .

The relative maximum on the equilibrium path emanating from the unloaded state is determined from

$$(\sin \theta_m - \sin \delta_0) \cos \theta_m - (P_m/P_{cr}) \sin \theta_m = 0, \text{ where } \sin \theta_m = \sqrt[3]{\sin \delta_0}. \quad (10.52)$$

For selected values of angle  $\delta_0$  the values of  $P_m/P_{cr}$  are plotted from eq. (10.52) in figure 10.16. There is a rapid decrease in the maximum load for small increases in the imperfection angle. For example, at  $\delta_0 = 0.1$  rad

**Fig. 10.16** The maximum load as a function of the imperfection angle for model B.



( $5.7^\circ$ )  $P_m/P_{cr} = 0.70$ , which is a 30% reduction of the buckling load with respect to the perfect system. For  $\delta_0 = 0.1$  rad, the value of  $\theta_m = 0.482$  rad, or  $27.6^\circ$ , which is a large rotation at the maximum load.

**Discussion.** All real structures are imperfect. For columns and plates these imperfections if small did not significantly reduce the actual buckling load from the critical load  $P_{cr}$  obtained in the analysis of the perfect structure. However, the buckling loads for axially compressed cylindrical shells in experiments are significantly less than the critical load determined from the perfect analysis (small displacements and slopes). Refer to Brush and Alm-

roth (1975). Even for small imperfections in axially compressed shells the maximum load  $P_m$  is much lower than  $P_{cr}$ . The axially compressed cylindrical shell is sensitive to imperfections.

It is concluded then, that the value of  $P_{cr}$  may not be meaningful in practice. It depends on the nonlinear behavior of the equilibrium paths.

- Model B is imperfection sensitive.
- Model A is imperfection insensitive.

The question of whether a structure is imperfection sensitive is answered completely by the stability or instability of the bifurcation point or by the initial, nonlinear post-buckling path.

### 10.3 Model C: asymmetric bifurcation

Model C is a coplanar arrangement of two rigid bars of length  $L$  and a linear elastic spring with stiffness  $K$ . In the initial configuration the bars are horizontal and the spring is at a  $45^\circ$  angle with respect to the bars. The bars and the spring are connected to a smooth central pin. The opposite end of the left bar is pinned to a fixed point, and the opposite end of the spring is connected to a fixed pin at distance  $L$  below the fixed end of the left bar. The opposite end of the right bar is pinned to a roller support free to move horizontally. A compressive force  $P$  acts at the roller support and under its action the bars can rotate through an angle  $\theta$  with respect to the original horizontal position..

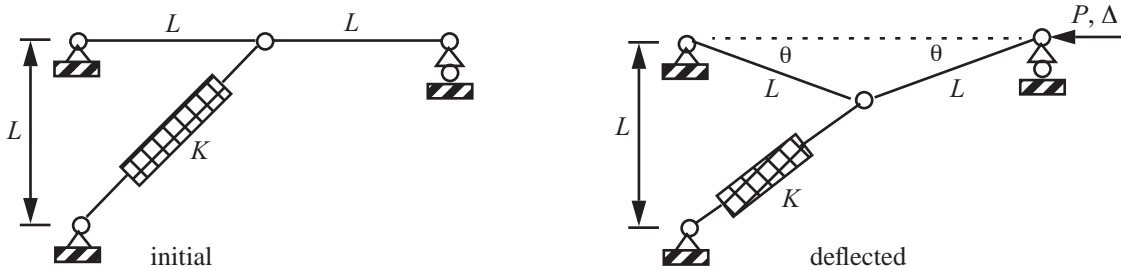


Fig. 10.17 Model C.

The potential energy is  $V = K\Delta_s^2/2 - P\Delta$ , where  $\Delta_s$  denotes the change in the length of the spring and  $\Delta$  denotes the shortening of the distance between supports. These changes in length are related to angle  $\theta$  by

$$\Delta_s = \sqrt{(L\cos\theta)^2 + (L - L\sin\theta)^2} - \sqrt{2}L = \sqrt{2}L(\sqrt{1 - \sin\theta} - 1) \quad \Delta = 2L - 2L\cos\theta. \quad (10.53)$$

The total potential energy  $V(\theta)$  is given by

$$V(\theta) = KL^2(\sqrt{1 - \sin\theta} - 1)^2 - 2PL(1 - \cos\theta). \quad (10.54)$$

The potential energy is stationary at equilibrium which leads to

$$KL^2\cos\theta[(1 - \sin\theta)^{-1/2} - 1] - 2PL\sin\theta = 0. \quad (10.55)$$

The solutions of eq. (10.55) are

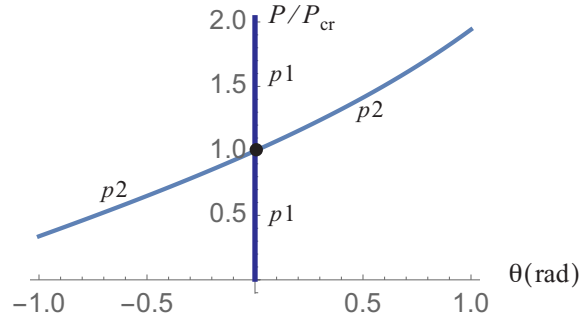
$$p1: \theta = 0 \text{ for any } P \quad p2: P = \frac{KL}{2} \cot \theta [(1 - \sin \theta)^{-1/2} - 1]. \quad (10.56)$$

On path  $p2$  as  $\theta \rightarrow 0$ , we get the indeterminate form  $\frac{KL}{2} \frac{1}{0} \left( \frac{1}{1} - 1 \right) = \frac{KL}{2} \frac{1}{0} \times 0$ . The limit of this indeterminate form is found from l'Hôpital's rule to be

$$P = P_{cr} = KL/4 \quad \text{at } \theta = 0. \quad (10.57)$$

The equilibrium paths are plotted on the load-deflection plane in figure 10.18. Equilibrium path  $p2$  is asymmetric about  $\theta = 0$ . Stability analysis leads to path  $p2$  being stable for  $\theta > 0$  and unstable for  $\theta < 0$ . Path  $p1$  is stable for  $0 \leq P < P_{cr}$  and unstable for  $P > P_{cr}$ . At the bifurcation point  $(\theta, P) = (0, P_{cr})$  higher derivatives of the potential energy are  $V_2 = 0$  and  $V_3 = (3KL^2)/4$ . That is, the potential energy is neither a minimum nor maximum, but has a horizontal inflection point at  $(\theta, P) = (0, P_{cr})$ .

Fig. 10.18 Model C equilibrium states.



Consider a geometric imperfection of model C in which the bars are at an angle  $\delta_0$  with respect to the horizontal before the load is applied as is shown in figure 10.19. In the unloaded configuration the spring is not stretched nor contracted. The change in spring length is

$$\Delta_s = \sqrt{2}L(\sqrt{1 - \sin \theta} - \sqrt{1 - \sin \delta_0}). \quad (10.58)$$

The potential energy is

$$V = KL^2(\sqrt{1 - \sin \theta} - \sqrt{1 - \sin \delta_0})^2 - 2PL(\cos \delta_0 - \cos \theta). \quad (10.59)$$

The potential energy is stationary at equilibrium, which leads to

$$KL^2 \cos \theta \left( \frac{\sqrt{1 - \sin \theta} - \sqrt{1 - \sin \delta_0}}{\sqrt{1 - \sin \theta}} \right) - 2PL \sin \theta = 0. \quad (10.60)$$

Solve eq. (10.60) for  $P$  and divide by  $P_{cr} = KL/4$  to get

$$\frac{P}{P_{cr}} = 2 \cot \theta \left( \frac{\sqrt{1 - \sin \theta} - \sqrt{1 - \sin \delta_0}}{\sqrt{1 - \sin \theta}} \right). \quad (10.61)$$

Note that a solution of eq. (10.61) is  $(\theta, P) = (\delta_0, 0)$ . The equilibrium paths determined from eq. (10.61) are

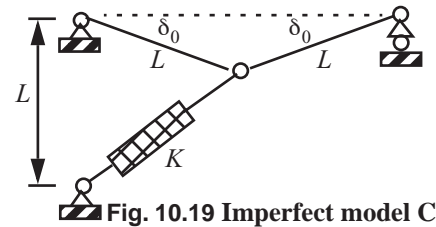
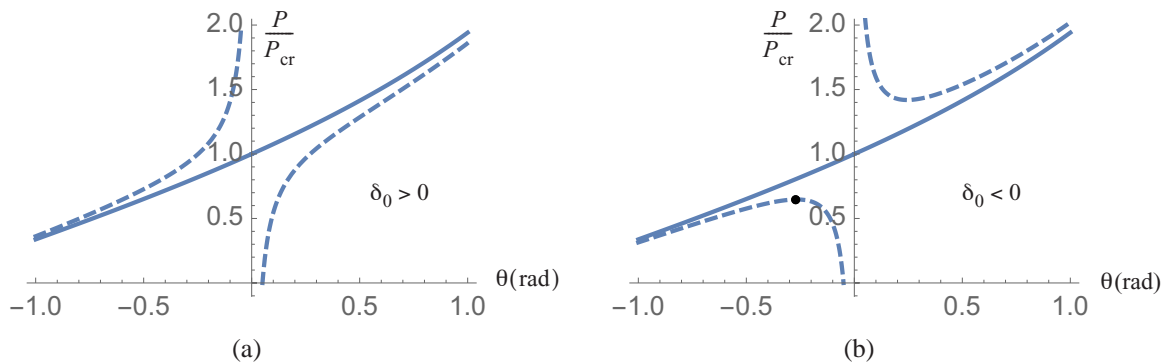


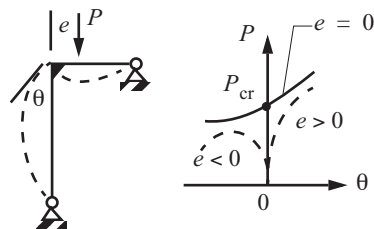
Fig. 10.19 Imperfect model C.

shown as dashed lines in the load-deflection plane of figure 10.20. The equilibrium path beginning at the unloaded state for  $\delta_0 > 0$  in figure 10.20(a) is stable and the deflection increases rapidly as the load approaches the critical load of the perfect system. The equilibrium path beginning at the unloaded state for  $\delta_0 < 0$  in figure 10.20(b) is stable until the maximum load  $P_m$  is encountered, which is indicated by the filled circle. There are no stable adjacent equilibrium states if  $P$  is increased from  $P_m$  or if  $\theta$  decreases from the maximum load point. Hence, model C is imperfection sensitive for  $\delta_0 < 0$ .



**Fig. 10.20** Equilibrium paths of the imperfect model C shown as dashed lines for (a)  $\delta_0 > 0$  and (b)  $\delta_0 < 0$ .

**Fig. 10.21**  
A frame of  
two  
members  
supported  
by smooth  
pins.



A real structure exhibiting asymmetric bifurcation is a pin-supported, two-member frame. The joint connecting the members is assumed rigid. Thus, each bar rotates through the same angle at the joint as shown in figure 10.21. For  $e > 0$  the horizontal member is in tension, which is a stabilizing effect. For  $e < 0$  the horizontal member is in compression, which is a destabilizing effect.

## 10.4 Discussion of models A, B, and C

We have considered three one-degree-of-freedom models (one coordinate is sufficient to describe the equilibrium configuration). The equilibrium paths were plotted on the  $(\theta, P)$  plane. For the perfect system  $\theta = 0$  for any  $P$  is an equilibrium state (trivial equilibrium). Two equilibrium paths of the perfect system cross at the **bifurcation point**  $(\theta, P) = (0, P_{cr})$ . There are three basic bifurcation points: stable symmetric, unstable symmetric, and asymmetric. The unstable symmetric and asymmetric cases are **imperfection sensitive**. A maximum load  $P_m$  below  $P_{cr}$  is possible when the system has imperfections. This theory was originally developed in the PhD dissertation by Koiter (1945 in Dutch, English translation 1970).

### 10.5 Model D: snap-through instability

Model D is a coplanar arrangement of two rigid bars and a linear elastic spring in the shape of an arch as shown in figure 10.22. Each bar has the same length  $L$ , and the bars connect to a central pin. The bars are at angle  $\alpha$  with respect to a horizontal line passing through the supported ends of the bars. The left end of the left bar is pin-connected to a fixed support. The right end of the right bar is pin-connected to a roller support restrained to move horizontally by a linear elastic spring with stiffness  $K$ . The model is subject to a downward, deadweight load  $P$  acting at the central pin.

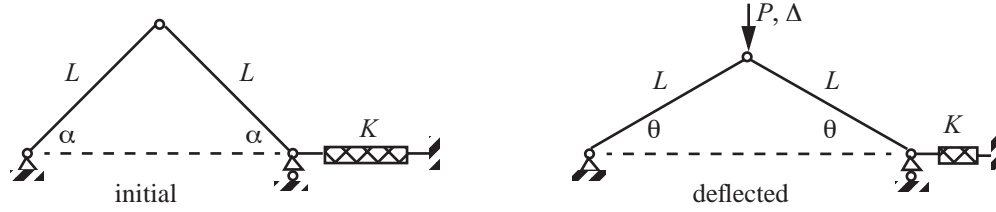


Fig. 10.22 Model D.

The total potential energy is  $V = K(\Delta_s)^2/2 - P\Delta$ , where  $\Delta_s$  is the change in length of the spring and  $\Delta$  is the downward displacement corresponding to the load  $P$ . The change in length of the spring and the downward displacement are

$$\Delta_s = 2L(\cos\theta - \cos\alpha) \quad \Delta = L(\sin\alpha - \sin\theta). \quad (10.62)$$

Hence, the total potential energy is

$$V(\theta) = 2KL^2(\cos\theta - \cos\alpha)^2 - PL(\sin\alpha - \sin\theta). \quad (10.63)$$

The total potential energy is stationary at equilibrium, which yields the equilibrium equation

$$4KL^2(\cos\theta - \cos\alpha)(-\sin\theta) + PL\cos\theta = 0. \quad (10.64)$$

Solve eq. (10.64) for load  $P$  to get

$$P = 4KL(\cos\theta - \cos\alpha)\tan\theta. \quad (10.65)$$

Note that the range of  $\theta$  in eq. (10.65) is  $-\pi/2 < \theta < \pi/2$  for finite values of the load  $P$ . On a plot of the load  $P$  as a function of  $\theta$ , horizontal slopes occur at  $\frac{dP}{d\theta} = 0$ . The derivative of eq. (10.65) with respect to  $\theta$  is

$$\frac{dP}{d\theta} = 4KL \left[ -\sin\theta \tan\theta + \frac{(\cos\theta - \cos\alpha)}{\cos^2\theta} \right] = 4KL \frac{(\cos^3\theta - \cos\alpha)}{\cos^2\theta}. \quad (10.66)$$

Therefore horizontal slopes occur at

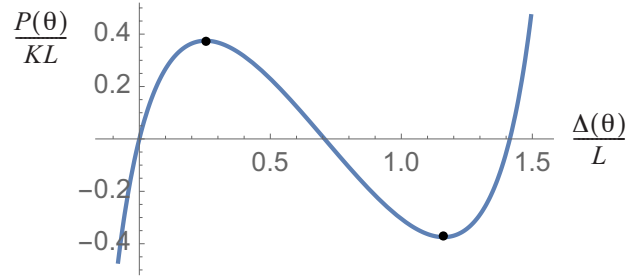
$$\theta_m = \pm \arccos[\sqrt[3]{\cos\alpha}], \quad (10.67)$$

Substitute  $\cos\theta = \cos^{1/3}\alpha$  into eq. (10.65) and use trigonometric identities to find the load at the horizontal slope to be

$$P_m = 4KL(1 - \cos^{2/3}\alpha)^{3/2}. \quad (10.68)$$

For  $\alpha = 45^\circ$ ,  $\theta_m = \pm 27.01^\circ$ . At  $\theta_m = -27.01^\circ$  the load  $P_m = -0.375KL$  with the corresponding displacement  $\Delta_m = 1.16L$ . At  $\theta_m = 27.01^\circ$  the load  $P_m = 0.375KL$  with the corresponding displacement  $\Delta_m = 0.253L$ . The load-displacement response is plotted in figure 10.23 by selecting  $\theta$  and computing  $P$  from eq. (10.65) and  $\Delta$  from eq. (10.62). There is one continuous path with no bifurcation. The loads at the horizontal slopes are indicated by filled circles in figure 10.23.

**Fig. 10.23** Equilibrium path on the load-displacement plane for model D.  $|\theta| \leq 52^\circ$  and  $\alpha = 45^\circ$ .



The stability of the equilibrium states are determined from the second derivative of the potential energy. The second derivative is

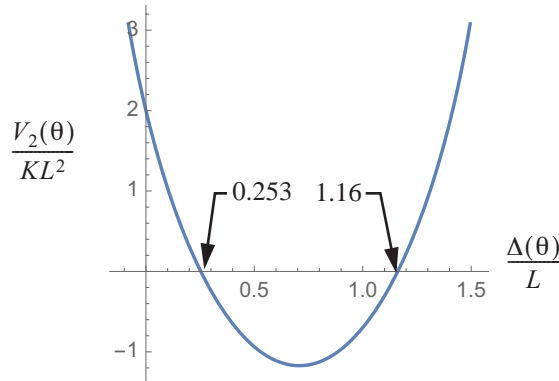
$$\frac{d^2 V}{d\theta^2} = 4KL^2[\sin^2\theta - \cos\theta(-\cos\alpha + \cos\theta)] - PL\sin\theta. \quad (10.69)$$

Substitute the expression for  $P$  from eq. (10.65) into eq. (10.69) to evaluate the second derivative on the equilibrium path to find

$$V_2(\theta) = \frac{d^2 V}{d\theta^2} = 4KL^2 \frac{(\cos^3\theta - \cos\alpha)}{\cos\theta}. \quad (10.70)$$

For  $|\theta| < \pi/2$ ,  $\cos\theta > 0$ . Select a value of  $\theta$  in the range  $|\theta| < \pi/2$ . Then, the value of  $\Delta$  is computed from eq. (10.62) and the value of the second derivative of the potential energy is computed from eq. (10.70). The plot of the second derivative divided by  $KL^2$  with respect to  $\Delta/L$  is shown in figure 10.24.

**Fig. 10.24** Parametric plot of the second derivative of the potential energy with respect to the displacement along the equilibrium path for model D.  $|\theta| \leq 52^\circ$  and  $\alpha = 45^\circ$ .





For  $\alpha = 45^\circ$  the range of  $\Delta$  is  $-0.2929L < \Delta < 1.707L$  when  $\theta$  is in the interval  $\pi/2 > \theta > -\pi/2$ . From figure 10.24 the stability of the equilibrium path is determined as

$$V_2 > 0, \text{ stable, } -0.293 < \Delta/L < 0.253 \text{ \& } 1.16 < \Delta/L < 1.1707, \quad (10.71)$$

$$V_2 = 0, \text{ critical } \Delta/L = 0.253 \text{ \& } \Delta/L = 1.16, \text{ and} \quad (10.72)$$

$$V_2 < 0, \text{ unstable, } 0.253 < \Delta/L < 1.16. \quad (10.73)$$

The stability of the equilibrium path is depicted in figure 10.25. As the load  $P$  is increased from  $\Delta = 0$  a maximum load  $P_m$  is encountered. If the load is increased further the system snaps-through. The maximum point is called a **limit point**. This is a different kind of instability from the perfect systems of models A, B, and C. In models A, B, and C  $\theta = 0$  was an equilibrium state of the perfect system. Model D is said to have pre-buckling “deformations.” That is  $\theta \neq 0$  before buckling. Snap-through is a dynamic event, and the system can settle to an inverted, stable equilibrium state. If the load is decreased from the inverted state to the lower limit point the system can snap back to a shape resembling the original configuration.

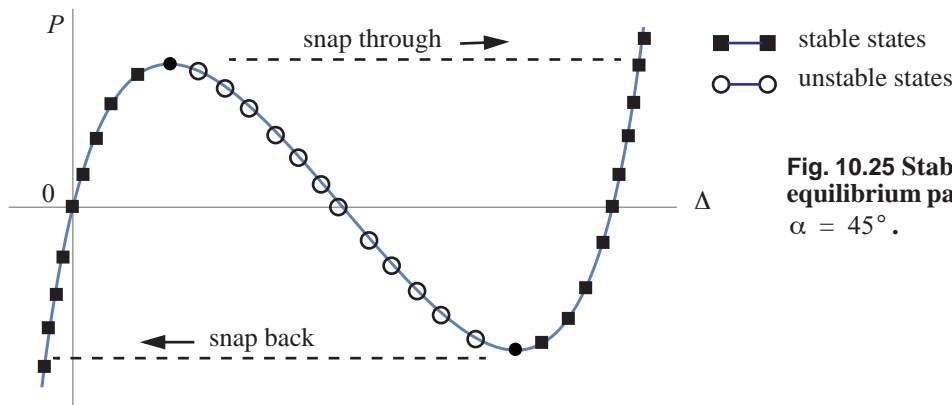


**Fig. 10.25** Stability of the equilibrium path for model D.  $\alpha = 45^\circ$ .

## 10.6 Model E: a two-degree-of freedom system

Models A to D are single-degree-of-freedom systems. Only one coordinate  $\theta$  determines the position of the system. Consider a two-degree-of-freedom system consisting of rigid bar restrained by two rotational springs with stiffnesses  $K_1$  and  $K_2$ , and subject to a vertical, deadweight load  $P$  as shown in figure 10.26. This model is known as Augusti's column. See Bazant and Cedolin (1991). The position of the bar is referenced to a right-handed Cartesian coordinate system  $x$ - $y$ - $z$ , with corresponding unit vectors  $\hat{i}, \hat{j}, \hat{k}$ . The initial position of the bar is vertical coinciding with the  $z$ -axis shown in figure 10.26(a), and in the deflected position it is located by two angles  $\theta_1$  and  $\theta_2$  shown in figure 10.26(b). The projection of the bar into the  $x$ - $z$  plane is at angle  $\theta_1$  with respect to the  $z$ -axis. The projection of the bar in the  $y$ - $z$  plane is at angle  $\theta_2$  with respect to the  $z$ -axis.

The angle between the bar and the  $z$ -axis is denoted by  $\varphi$ . The Cartesian coordinates at the end of the bar in its deflected position in shown in figure 10.26 (c) are  $(L \sin \theta_1, L \sin \theta_2, L \cos \varphi)$ . By the Pythagorean theorem the square of the length of the bar in the deflected position is given by

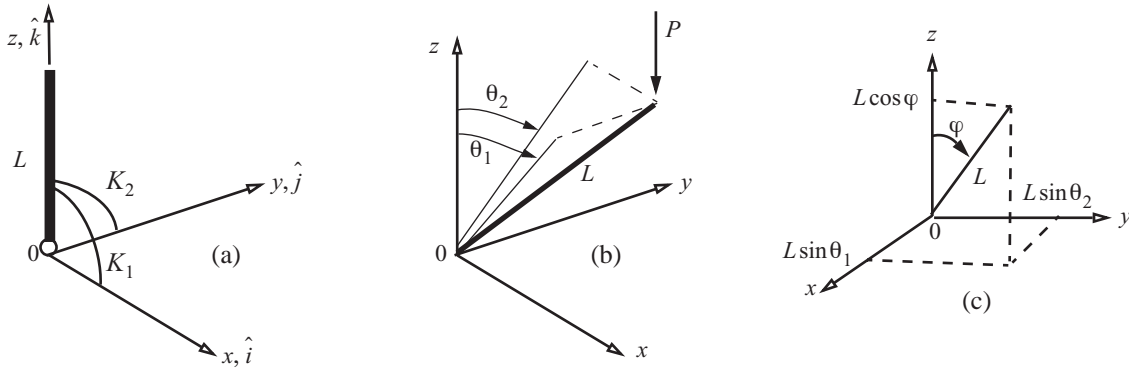


**Fig. 10.26 Model E. (a) Initial unloaded configuration. (b) Deflected configuration under a downward applied load. (c) Coordinates at end of the bar.**

$$L^2 = (L \sin \theta_1)^2 + (L \sin \theta_2)^2 + (L \cos \varphi)^2. \quad (10.74)$$

From eq. (10.74) we find that the cosine of the angle  $\varphi$  is

$$\cos \varphi = \sqrt{1 - \sin^2 \theta_1 - \sin^2 \theta_2}. \quad (10.75)$$

The displacement corresponding to load  $P$  is  $\Delta = L(1 - \cos \varphi)$ . The total potential energy is

$$V(\theta_1, \theta_2) = K_1 \theta_1^2 / 2 + K_2 \theta_2^2 / 2 - PL(1 - \sqrt{1 - \sin^2 \theta_1 - \sin^2 \theta_2}). \quad (10.76)$$

The series expansion of  $1 - \cos \varphi$  is

$$1 - \sqrt{1 - \sin^2 \theta_1 - \sin^2 \theta_2} = \frac{1}{2} \left( \theta_1^2 + \theta_2^2 + \frac{1}{2} \theta_1^2 \theta_2^2 - \frac{1}{12} \theta_1^4 - \frac{1}{12} \theta_2^4 + O(\theta^6) \right). \quad (10.77)$$

Neglect terms of order six and higher in the series expansion to get the total potential energy as

$$V(\theta_1, \theta_2) = K_1 \theta_1^2 / 2 + K_2 \theta_2^2 / 2 - PL \left( \theta_1^2 + \theta_2^2 + \frac{1}{2} \theta_1^2 \theta_2^2 - \frac{1}{12} \theta_1^4 - \frac{1}{12} \theta_2^4 \right) / 2. \quad (10.78)$$

Let  $\theta_1 = \theta_{10}$  and  $\theta_2 = \theta_{20}$  denote the angles in an equilibrium state, and let small changes in the angles with respect to the equilibrium state be denoted by

$$h_1 = \theta_1 - \theta_{10} \quad \text{and} \quad h_2 = \theta_2 - \theta_{20}. \quad (10.79)$$

The Taylor series of the potential energy about the equilibrium state is

$$V(\theta_1, \theta_2) = V(\theta_{10}, \theta_{20}) + \delta V + \delta^2 V + \delta^3 V + \delta^4 V + \dots, \quad (10.80)$$

where  $\delta V$  is called the first variation with terms linear in  $h_1$  and  $h_2$ , and  $\delta^2 V$  is called the second variation with terms quadratic in  $h_1$  and  $h_2$ , etc. The change in potential energy about the equilibrium state is

$\Delta V = V(\theta_1, \theta_2) - V(\theta_{10}, \theta_{20})$ . Thus,

$$\Delta V = \delta V + \delta^2 V + \delta^3 V + \delta^4 V + \dots \quad (10.81)$$

Partial derivatives of the potential energy evaluated at the equilibrium state are represented by the notation

$$V_0^{(m,n)} = \left. \frac{\partial^{(m+n)} V}{\partial \theta_1^m \partial \theta_2^n} \right|_{\theta_{10}, \theta_{20}} \quad m, n = 0, 1, 2, \dots \quad (10.82)$$

For example,

$$V_0^{(1,0)} = \left. \frac{\partial V}{\partial \theta_1} \right|_{\theta_{10}, \theta_{20}} \quad V_0^{(1,1)} = \left. \frac{\partial^2 V}{\partial \theta_1 \partial \theta_2} \right|_{\theta_{10}, \theta_{20}} \quad V_0^{(2,2)} = \left. \frac{\partial^4 V}{\partial \theta_1^2 \partial \theta_2^2} \right|_{\theta_{10}, \theta_{20}} \quad (10.83)$$

The terms in the Taylor series expansion (10.81) are

$$\begin{aligned} \delta V &= V_0^{(1,0)} h_1 + V_0^{(0,1)} h_2 \\ \delta^2 V &= \frac{1}{2} (V_0^{(2,0)} h_1^2 + 2 V_0^{(1,1)} h_1 h_2 + V_0^{(0,2)} h_2^2) \\ \delta^3 V &= \frac{1}{6} (V_0^{(3,0)} h_1^3 + 3 V_0^{(2,1)} h_1^2 h_2 + 3 V_0^{(1,2)} h_1 h_2^2 + V_0^{(0,3)} h_2^3) \\ \delta^4 V &= \frac{1}{24} (V_0^{(4,0)} h_1^4 + 4 V_0^{(3,1)} h_1^3 h_2 + 6 V_0^{(2,2)} h_1^2 h_2^2 + 4 V_0^{(1,3)} h_1 h_2^3 + V_0^{(0,4)} h_2^4) \end{aligned} \quad (10.84)$$

A necessary condition for the potential energy to be a relative minimum or maximum at the equilibrium state is  $\delta V = 0$  for every  $h_1$  and  $h_2$ , but both not equal to zero. Thus, “coefficients”  $V_0^{(1,0)} = 0$  and  $V_0^{(0,1)} = 0$ . The potential energy is stationary at equilibrium. Take the partial derivatives of the potential energy (10.78) to get the equilibrium equations

$$V_0^{(1,0)} = K_1 \theta_{10} - LP(\theta_{10} - \theta_{10}^3/6 + \theta_{10} \theta_{20}^2/2) = 0, \text{ and} \quad (10.85)$$

$$V_0^{(0,1)} = K_2 \theta_{20} - LP(\theta_{20} - \theta_{20}^3/6 + \theta_{10}^2 \theta_{20}/2) = 0. \quad (10.86)$$

A solution to the equilibrium equations (10.85) and (10.86) is

$$p1: \theta_{10} = \theta_{20} = 0 \text{ for any } P. \quad (10.87)$$

The next non-zero term in the expansion of  $\Delta V$  is the second variation. Evaluating the second order partial derivatives of the potential energy (10.78) followed by evaluation on equilibrium path  $p1$  we get

$$\delta^2 V = \frac{1}{2} [(K_1 - LP) h_1^2 + (K_2 - LP) h_2^2]. \quad (10.88)$$

Buckling loads are determined when second variation vanishes for every value of  $h_1$  and  $h_2$ , but both not equal to zero. This leads to two buckling loads and associated modes

$$P_1 = K_1/L \quad (h_1, h_2) = (1, 0), \text{ and} \quad (10.89)$$

$$P_2 = K_2/L \quad (h_1, h_2) = (0, 1). \quad (10.90)$$

The critical loads and modes are shown in the load-deflection plane of figure 10.27. Take the case of  $K_1 < K_2$ . Then, the critical load is  $P_{cr} = P_1 = K_1/L$  and the associated mode is  $(h_1, h_2) = (1, 0)$ .

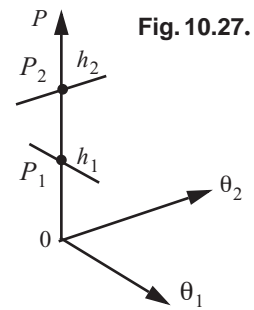


Fig. 10.27.

The second variation  $\delta^2 V$  is a quadratic form in variables  $h_1$  and  $h_2$ . Examples of quadratic forms and their descriptions are listed in Table 10.1.

**Table 10.1 Examples of quadratic forms**

$\delta^2 V$	Description
$h_1^2 + h_2^2$	Positive definite
$(h_1 + h_2)^2$	Positive semidefinite
$-h_1^2 - h_2^2$	Negative definite
$-(h_1 + h_2)^2$	Negative semidefinite
$h_1 h_2$	Indefinite

The second variation (10.88) is **positive definite** for  $0 \leq P < K_1/L$ . At the critical load the second variation is

$$\delta^2 V = \frac{1}{2}[0 \cdot h_1^2 + (K_2 - K_1)h_2^2]. \quad (10.91)$$

The second variation at the critical load is said to be **positive semidefinite**. It is zero for all non-zero values of  $h_1$  and  $h_2 = 0$ , but is positive for all non-zero values of  $h_2$  and  $h_1 = 0$ . The second variation ceases to be positive definite at the critical state. The stability of equilibrium path  $p_1$  is determined from eq. (10.88) as follows:

$$\delta^2 V|_{p_1} > 0, \text{ stable, } 0 \leq P < K_1/L \quad \delta^2 V|_{p_1} = 0, \text{ critical, } P = K_1/L \quad \delta^2 V|_{p_1} < 0, \text{ unstable, } P > K_1/L. \quad (10.92)$$

The stability of the bifurcation point  $(\theta_1, \theta_2, P) = (0, 0, K_1/L)$  is not determined from the second variation of the potential energy.

At the critical load  $\theta_2 = 0$ . This suggests we seek a solution to equilibrium equations (10.85) and (10.86) with  $\theta_{10} \neq 0$  and  $\theta_{20} = 0$ . Equation (10.86) is identically satisfied, and eq. (10.85) reduces to

$$K_1 \theta_{10} - LP(\theta_{10} - \theta_{10}^3/6) = 0. \quad (10.93)$$

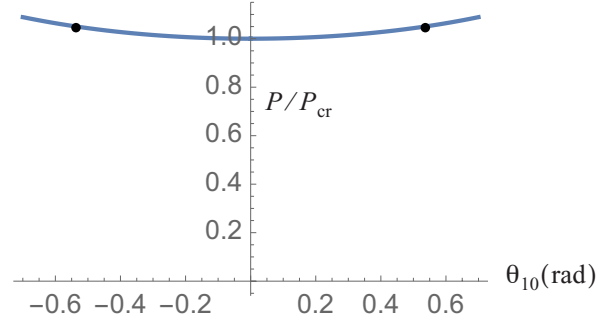
Solve eq. (10.93) for  $P$  to get

$$\frac{P}{P_{cr}} = \frac{\theta_{10}}{\theta_{10} - \theta_{10}^3/6}. \quad (10.94)$$

The equilibrium path described by eq. (10.94) is shown in figure 10.28. The load increases in the initial post-buckling response indicating the bifurcation point is stable.

Consider the case where  $K_1 = K_2 = K$ . The critical points  $P_1$  and  $P_2$  coincide on the path  $p_1$  and simultaneous buckling modes  $(h_1, h_2) = (1, 0)$  and  $(h_1, h_2) = (0, 1)$  interact at  $(\theta_1, \theta_2, P) = (0, 0, K/L)$ . In this case both  $\delta V = 0$  and  $\delta^2 V = 0$  at the bifurcation point, and we have to consider the next non-zero term in the expansion of the change in potential energy (10.81). To evaluate the third variation at the bifurcation point, the third partial derivatives of the total potential energy evaluated at the bifurcation point are

**Fig. 10.28** Post-buckling equilibrium path for model E with  $\theta_{20} = 0$  and  $K_1 < K_2$ .



$$V_0^{(3,0)} = V_0^{(2,1)} = V_0^{(1,2)} = V_0^{(0,3)} = 0. \quad (10.95)$$

Hence,  $\delta^3 V = 0$  for all values of  $h_1$  and  $h_2$ . Evaluate the fourth partial derivatives of the total potential energy at the bifurcation point to find

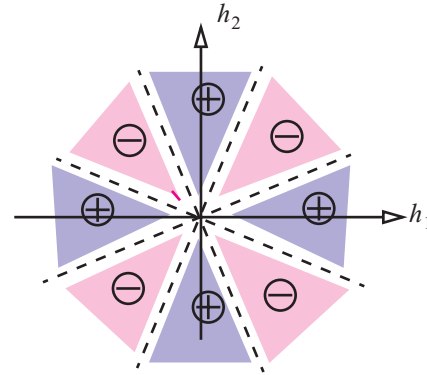
$$V_0^{(4,0)} = K_1 \quad V_0^{(3,1)} = 0 \quad V_0^{(2,2)} = -K_1 \quad V_0^{(1,3)} = 0 \quad V_0^{(0,4)} = K_1. \quad (10.96)$$

The fourth variation of the potential energy is

$$\delta^4 V = \frac{1}{24} (K_1 h_1^4 - 6K_1 h_1^2 h_2^2 + K_1 h_2^4). \quad (10.97)$$

The fourth variation vanishes at  $h_2 = \pm 0.414h_1$  and  $h_2 = \pm 2.414h_1$ . Regions in the  $h_1$ - $h_2$  plane where the fourth variation is positive and negative are established by plotting the locus where it is zero as shown in figure 10.29. The minimum values of the fourth variation occur along the directions  $h_2 = \pm\sqrt{3}h_1$  and are

**Fig. 10.29** Regions in the  $h_1$ - $h_2$  plane where the fourth variation is positive and negative, Along the dashed lines the fourth variation is zero.



$\delta^4 V = -K_1 h_1^4 / 3$ . Since the fourth variation can be positive, zero, and negative depending on the values of  $h_1$  and  $h_2$ , the fourth variation is **indefinite**. The bifurcation point is unstable. It is shown in Bazant and Cedolin (1991) that the condition for existence of a non-zero solution to equilibrium equations (10.85) and (10.86) is  $\theta_{10} = \theta_{20} = \theta$ . The two equilibrium equations reduce to the single equation

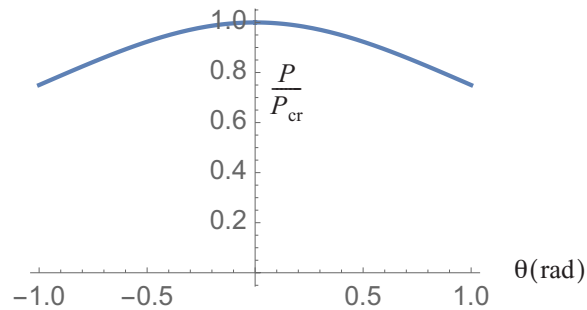
$$K\theta - PL(\theta + \theta^3/3) = 0. \quad (10.98)$$

Solve eq. (10.98) for the load  $P$  to get

$$P/P_{cr} = \frac{\theta}{\theta + \theta^3/3}. \quad (10.99)$$

The load decreases from the critical value on the post-buckling path for  $|\theta| > 0$  as shown in figure 10.30.

**Fig. 10.30** Model E post-buckling equilibrium path for  $K_1 = K_2$  and  $\theta_1 = \theta_2 = \theta$ .



For  $K_1 < K_2$  the bifurcation point stable and the system is imperfection insensitive. For  $K_1 = K_2 = K$  the bifurcation point is unstable and the system is imperfection sensitive.

## 10.7 References

- Bazant, Z., and L. Cedolin. **Stability of Structures: Elastic, Inelastic, Fracture, and Damage Theories**. New York: Oxford University Press, 1991, p.265.
- Brush, D. O., and BO O. Almroth. **Buckling of Bars, Plates, and Shells**. New York: McGraw-Hill, 1975, p. 185.
- Huseyin, K. **Nonlinear theory of elastic stability**. Leyden, The Netherlands: Noordhoff International Publishing, 1975.
- Koiter, W. T. "The Stability of Elastic Equilibrium." PhD diss., Technische Hoog School, Delft, The Netherlands. 1945. (English translation published as Technical Report AFFDL-TR-70-25, Air Force Flight Dynamics Laboratory, Wright-Patterson Air Force Base, OH, February 1970.)
- Simitses, G. **An Introduction to the Elastic Stability of Structures**. Englewood Cliffs, NJ: Prentice Hall, Inc., 1976, Chapter 2.
- Ziegler, Hans. **Principles of Structural Stability**. Waltham, Massachusetts: Blaisdell Publishing Company, A Division of Ginn and Company, 1968, Chapter 1.

## 10.8 Practice exercises

1. A rigid, straight bar of length  $L$  is pinned at point  $O$ , restrained by a linear elastic spring with stiffness  $K$ , and subject to a downward load  $P$ . Neglect the weight of the bar. The bar is vertical in the initial configuration as shown in figure 10.31(a). The spring remains horizontal as the bar rotates from the vertical through angle  $\theta$  as shown in figure 10.31(b). Refer to the free body diagram in figure 10.31(c) to find the equation of motion is

$$PL \sin \theta - [K(a \sin \theta)]a \cos \theta = I_0 \frac{d^2 \theta}{dt^2} \quad \theta = \theta(t), \quad (10.100)$$

where  $I_0$  is the moment of inertia of the rod about the fixed point and  $t$  is time.  $\theta > 0$  clockwise.

- Plot the equilibrium paths on the  $P - \theta$  plane for  $-\frac{\pi}{2} < \theta < \frac{\pi}{2}$  and  $P > 0$ . Note,  $\theta$  is independent of  $t$ .
- What is the critical load  $P_{cr}$ ?
- Let the rotation angle  $\theta(t) = \theta_0 + \varphi(t)$  where  $\theta_0$  is independent of time and satisfies the equilibrium equation of part (a), and where the additional rotation about the equilibrium configuration  $\varphi(t)$  is infinitesimal. Determine  $\omega^2$  on the equilibrium paths, and from the dynamic criterion state the stability of the equilibrium states on each equilibrium path.

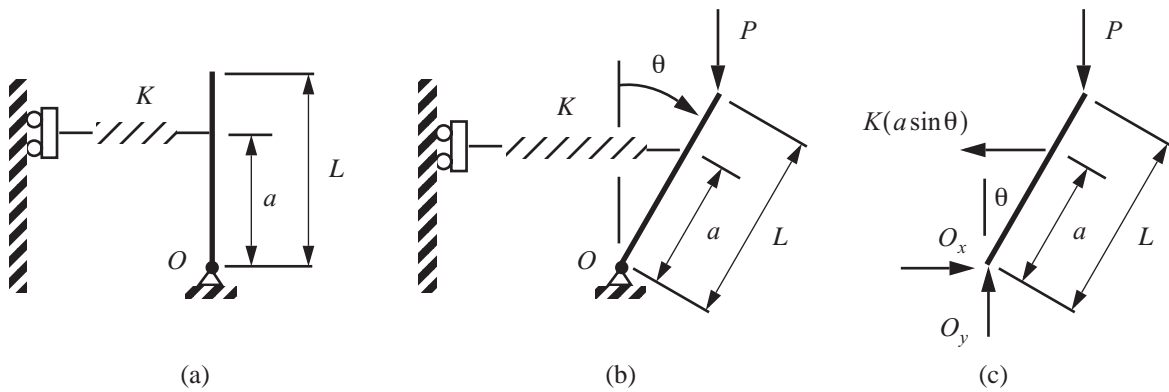


**Fig. 10.31 (a) initial configuration. (b) Deflected configuration. (c) Free body diagram.**

- Determine the stability of the post-buckling path for model E given by eq. (10.94) and shown in figure 10.28.





# Buckling of columns and plates

If buckling occurs before the elastic limit of the material, which is roughly the yield strength of the material, then it is called *elastic buckling*. If buckling occurs beyond the elastic limit, it is called *inelastic buckling*, or plastic buckling if the material exhibits plasticity during buckling (mainly metals). Many thin-walled structural components buckle in compression below the elastic limit. Therefore, buckling determines the limit state in compression rather than material yielding. In fact, about 50 percent of an airplane structure is designed based on buckling constraints.

## 11.1 Perfect columns

Consider a perfectly straight, uniform column of length  $L$  with cross-sectional area  $A$  subject to a centric end load  $P$  as shown in figure. 11.1. (The column is drawn horizontally for convenience.) The column is long relative to its largest cross-sectional dimension, and the column consists of a homogeneous, linear elastic material whose modulus of elasticity is denoted by  $E$ . Buckling analyses are inherently nonlinear. As the previous structural models discussed in chapter 10 demonstrate, nonlinear analysis results in more than one equilibrium state for a specified load, whereas in linear analysis there is only one equilibrium state for a specified load. A geometrically nonlinear analysis of a column is developed in this article in which the axial strain-displacement relation is nonlinear and equilibrium is taken on the displaced structure.

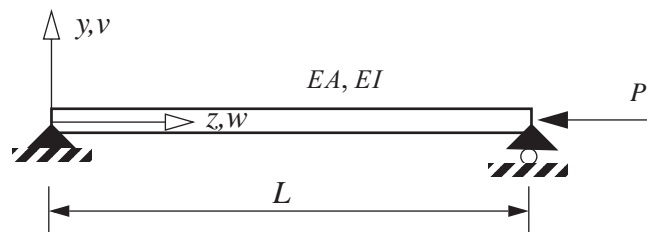


Fig. 11.1 A straight column subject to a centric, compressive axial force.

**Kinematics.** Consider a differential element  $dz$ -by- $dy$  in the initial, undeformed column, where  $dz$  is along the centroidal axis and  $dy$  is perpendicular to the centroidal axis as shown in figure. 11.2. In the  $z$ - $y$  coordinate system, the material point at coordinates  $(z, 0)$  displaces to coordinates  $(z^*, y^*)$  in the deformed bar, where  $(z^*, y^*)$  is referenced to the same  $z$ - $y$  system. These coordinates are related by

$$z^* = z + w(z) \quad y^* = 0 + v(z), \quad (11.1)$$

where  $w(z)$  is the displacement parallel to the  $z$ -axis and  $v(z)$  is the displacement parallel to the  $y$ -axis. The material points along length  $dz$  map to the differential length  $ds^*$  along the centroidal axis in the deformed bar. By the Pythagorean theorem  $(ds^*)^2 = (dz^*)^2 + (dy^*)^2$ . The differential lengths in the deformed bar are

$$dz^* = \left(1 + \frac{dw}{dz}\right) dz \quad \text{and} \quad dy^* = \left(\frac{dv}{dz}\right) dz. \quad (11.2)$$

Define the stretch ratio  $\lambda$  by  $\lambda = ds^*/dz$ . Consequently, the stretch ratio is related to the derivatives of the dis-

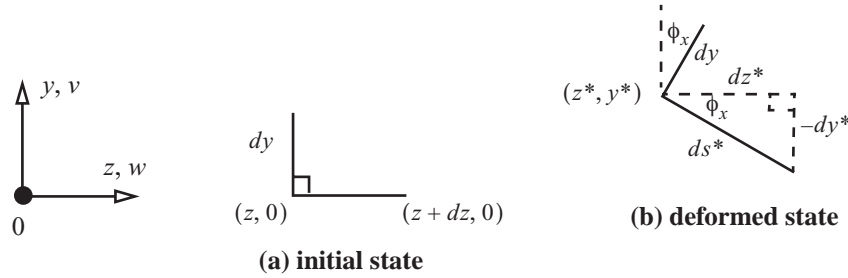


**Fig. 11.2** Differential elements in the initial state (a) and in the deformed state (b).

placements by

$$\lambda = \sqrt{\left(1 + \frac{dw}{dz}\right)^2 + \left(\frac{dv}{dz}\right)^2}. \quad (11.3)$$

The clockwise rotation angle of element  $ds^*$  with respect to the  $z$ -direction is denoted by  $\phi_x(z)$ . Trigonometric functions of this rotation angle are given by

$$\sin \phi_x = \frac{-dy^*}{ds^*} \quad \text{and} \quad \cos \phi_x = \frac{dz^*}{ds^*}. \quad (11.4)$$

Using the chain rule of differentiation and the definition of the stretch ratio these trigonometric functions can be written as

$$\sin \phi_x = \left(\frac{-dy^*}{dz}\right) \frac{dz}{ds^*} = \frac{1}{\lambda} \left(\frac{-dv}{dz}\right), \quad \text{and similarly} \quad \cos \phi_x = \frac{1}{\lambda} \left(1 + \frac{dw}{dz}\right). \quad (11.5)$$

We impose the hypothesis of classical theory that cross sections normal to the centroidal axis in the undeformed bar remain rigid and normal to the centroidal axis in the deformed bar. Thus, the differential line element  $dy$  in the undeformed bar does not change length in the deformed bar and remains normal to the centroidal axis in the deformed bar. That is, line element  $dy$  also rotates clockwise through angle  $\phi_x$ . The stretch ratio (11.3) is expanded in a binomial series to get

$$\lambda = 1 + \frac{1}{2} \left[ 2 \frac{dw}{dz} + \left( \frac{dw}{dz} \right)^2 + \left( \frac{dv}{dz} \right)^2 \right] - \frac{1}{8} \left[ 2 \frac{dw}{dz} + \left( \frac{dw}{dz} \right)^2 + \left( \frac{dv}{dz} \right)^2 \right]^2 + \dots = 1 + \frac{dw}{dz} + \frac{1}{2} \left( \frac{dv}{dz} \right)^2 + O \left( \frac{dw}{dz} \right)^3. \quad (11.6)$$

The engineering strain is defined as  $\epsilon_{zz} = \lambda - 1$ . If cubic powers and higher of the displacement derivatives in the series expansion of  $\lambda$  are neglected, then the strain-displacement relation is

$$\epsilon_{zz} = \frac{dw}{dz} + \frac{1}{2} \left( \frac{dv}{dz} \right)^2. \quad (11.7)$$

**Equilibrium.** The free body diagram of the element of the bar in the deformed state is shown in figure. 11.3(a).

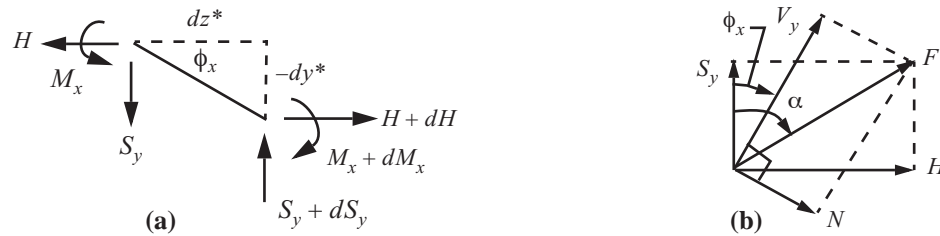


**Fig. 11.3** Free body diagram of the differential element in the deformed bar (a), and the resolution of the resultant force  $F$  into components acting on the cross section (b).

The force  $F$  acting on the cross section of the deformed bar is resolved in two sets of orthogonal components. Components  $H$  and  $S_y$  act in horizontal direction and the vertical direction, respectively. Components  $N$  and  $V_y$  act tangent and normal to the centroidal axis, respectively. Let  $\alpha$  denote the angle between the vertical and the line of action of force  $F$ . From figure. 11.3(b)  $H = F \sin \alpha$  and  $S_y = F \cos \alpha$ . Components  $N$  and  $V_y$  are given by

$$N = F \sin(\alpha - \phi_x) = (F \sin \alpha) \cos \phi_x - (F \cos \alpha) \sin \phi_x = H \cos \phi_x - S_y \sin \phi_x, \text{ and} \quad (11.8)$$

$$V_y = F \cos(\alpha - \phi_x) = (F \cos \alpha) \cos \phi_x + (F \sin \alpha) \sin \phi_x = S_y \cos \phi_x + H \sin \phi_x. \quad (11.9)$$

Equilibrium in the horizontal direction requires  $dH = 0$  and equilibrium in the vertical direction requires  $dS_y = 0$ . Thus, the horizontal component  $H$  and the vertical component  $S_y$  are spatially uniform along the length of the bar. Since the applied compressive force  $P$  is also horizontal then  $H = -P$ . The bending moment is denoted by  $M_x$ . Moment equilibrium about the right end of the element in figure. 11.3(a) leads to

$$M_x + dM_x - M_x - (-dy^*)H - (dz^*)S_y = 0. \quad (11.10)$$

The differential functions are expanded in a series. For example  $dM_x = \frac{dM_x}{dz} dz + \frac{d^2 M_x}{dz^2} (dz^2) + \dots$ . Then moment equilibrium becomes

$$\left[ \frac{dM_x}{dz} - \left( \frac{dy^*}{dz} \right) H - \left( \frac{dz^*}{dz} \right) S_y \right] dz + O(dz^2) = 0. \quad (11.11)$$

Division by  $dz$  followed by the limit as  $dz \rightarrow 0$  leads to the differential equation

$$\frac{dM_x}{dz} - \left(\frac{dv}{dz}\right)P - \left(1 + \frac{dw}{dz}\right)S_y = 0. \quad (11.12)$$

**Hooke's law.** The normal force component  $N$  is proportional to the axial strain  $\epsilon_{zz}$  of the centroidal axis, and the bending moment  $M_x$  is proportional to the rotation gradient  $\frac{d\phi_x}{dz}$  of the cross section. That is,

$$N = EA\epsilon_{zz} \quad M_x = EI\left(\frac{d\phi_x}{dz}\right), \quad (11.13)$$

where the modulus of elasticity is denoted by  $E$ , the cross-sectional area by  $A$ , and the second area moment of the cross section by  $I$ .

### 11.1.1 Pre-buckling equilibrium

The trivial equilibrium configuration of the column is straight and in compression subject to the applied axial force  $P$ . The lateral displacement  $v(z) = 0$ , rotation  $\phi_x(z) = 0$ , and  $M_x = 0$  for  $0 \leq z \leq L$ . From eq. (11.8)  $N = H = -P$ . From eq. (11.9)  $S_y = V_y$  but overall equilibrium requires  $S_y = 0$ . Let  $w_0(z)$  denote the axial displacement in pre-buckling equilibrium. Then, strain (11.7) and stretch ratio reduce to  $\epsilon_{zz} = \frac{dw_0}{dz}$  and

$\lambda = 1 + \frac{dw_0}{dz}$ , respectively. Hooke's law (11.13) for the axial force is  $-P = EA\left(\frac{dw_0}{dz}\right)$ . Integrate Hooke's law and take the axial displacement  $w_0(0) = 0$  to get

$$w_0(z) = \frac{-Pz}{EA}. \quad (11.14)$$

### 11.1.2 Buckling

To assess buckling of a slightly defected column, we introduce a small, dimensionless parameter  $\xi$  such that all dependent variables equal their pre-buckling equilibrium expressions as  $\xi \rightarrow 0$ . The displacements and rotation are expressed as

$$w(z) = w_0(z) + \xi w_1(z) \quad v(z) = \xi v_1(z) \quad \phi_x(z) = \xi \phi_1(z). \quad (11.15)$$

The trigonometric functions of the rotation angle are

$$\sin \phi_x = \xi \phi_1(z) + O(\xi^3) \quad \cos \phi_x = 1 + O(\xi^2). \quad (11.16)$$

In the following developments terms of  $\xi^2$  and higher degrees are neglected. The vertical shear force  $S_y = \xi S_{y1}$ . The axial strain (11.7) expansion is

$$\epsilon_{zz} = \frac{dw_0}{dz} + \xi \frac{dw_1}{dz}. \quad (11.17)$$

The first expression in (11.8) is written as  $N + P \cos \phi_x + S_y \sin \phi_x = 0$ , where  $N = EA\epsilon_{zz}$ . The expansion for this equation containing the force  $N$  is

$$\xi^0 \left[ EA \frac{dw_0}{dz} + P \right] + \xi \left[ EA \frac{dw_1}{dz} \right] + O(\xi^2) = 0. \quad (11.18)$$

To satisfy the last equation for each value of  $\xi \neq 0$ , the coefficients of  $\xi^0$  and  $\xi^1$  must vanish, which leads to

$$\frac{dw_0}{dz} = \frac{-P}{EA} \quad \frac{dw_1}{dz} = 0. \quad (11.19)$$

On the pre-buckling equilibrium path the stretch ratio  $\lambda = 1 - P/(EA)$ .

The expansion of the equilibrium equation for bending (11.12) combined with the moment from Hooke's law (11.13) is

$$\xi^0 \cdot 0 + \xi \left[ EI \frac{d^2 \phi_1}{dz^2} - P \frac{dv_1}{dz} - \left( 1 - \frac{P}{EA} \right) S_{y1} \right] + O(\xi^2) = 0. \quad (11.20)$$

Therefore, the significant result from eq. (11.20) is

$$EI \frac{d^2 \phi_1}{dz^2} - P \frac{dv_1}{dz} - \left( 1 - \frac{P}{EA} \right) S_{y1} = 0. \quad (11.21)$$

The first expression in eq. (11.5) relating the rotation, the stretch ratio, and the displacement  $v(z)$  is written as

$$\left[ 1 - P/(EA) \right] \sin \phi_x + \frac{dv}{dz} = 0. \quad (11.22)$$

The expansion of eq. (11.22) becomes

$$\xi^0 \cdot 0 + \xi \left[ \frac{dv_1}{dz} + \left( 1 - \frac{P}{EA} \right) \phi_1 \right] + O(\xi^2) = 0. \quad (11.23)$$

Therefore,

$$\frac{dv_1}{dz} + \left( 1 - \frac{P}{EA} \right) \phi_1 = 0. \quad (11.24)$$

Solve eq. (11.24) for  $\phi_1(z)$  and substitute the result into eq. (11.21) to get

$$-EI \left[ \frac{d^3 v_1}{dz^3} \right] - P \left( 1 - \frac{P}{EA} \right) \frac{dv_1}{dz} - \left( 1 - \frac{P}{EA} \right)^2 S_{y1} = 0. \quad (11.25)$$

Now differentiate eq. (11.25) with respect to  $z$  and note that  $\frac{dS_{y1}}{dz} = 0$  consistent with the equilibrium equation

$\frac{dS_y}{dz} = 0$ . The final result is

$$\frac{d^4 v_1}{dz^4} + K^2 \frac{d^2 v_1}{dz^2} = 0 \quad v_1 = v_1(z) \quad 0 < z < L, \quad (11.26)$$

where

$$K^2 = \frac{P}{EI} \left( 1 - \frac{P}{EA} \right). \quad (11.27)$$

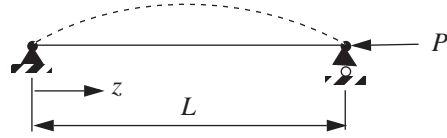
The expressions for the bending moment and vertical shear force are

$$\left( 1 - \frac{P}{EA} \right) M_{x1} = -EI \left( \frac{d^2 v_1}{dz^2} \right) \quad \left( 1 - \frac{P}{EA} \right)^2 S_{y1} = -EI \left[ \frac{d^3 v_1}{dz^3} + K^2 \frac{dv_1}{dz} \right]. \quad (11.28)$$

The solution of eq. (11.26) for  $v_1(z)$  is subject to boundary conditions at  $z = 0$  and  $z = L$ . There are four so-called standard boundary conditions. These are shown in figure. 11.4.

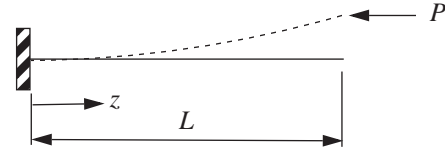
A. Pinned-pinned

$$\begin{aligned} v_1(0) &= 0 & v_1(L) &= 0 \\ M_{x1}(0) &= 0 & M_{x1}(L) &= 0 \end{aligned}$$



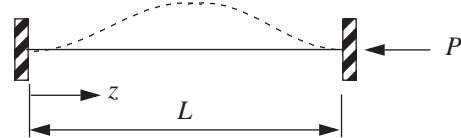
B. Clamped-free

$$\begin{aligned} v_1(0) &= 0 & M_{x1}(L) &= 0 \\ \phi_{x1}(0) &= 0 & S_{y1}(L) &= 0 \end{aligned}$$



C. Clamped-clamped

$$\begin{aligned} v_1(0) &= 0 & v_1(L) &= 0 \\ \phi_{x1}(0) &= 0 & \phi_{x1}(L) &= 0 \end{aligned}$$



D. Clamped-pinned

$$\begin{aligned} v_1(0) &= 0 & v_1(L) &= 0 \\ \phi_{x1}(0) &= 0 & M_{x1}(L) &= 0 \end{aligned}$$

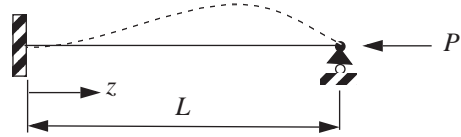


**Fig. 11.4 Standard buckling boundary conditions.**

One solution to the differential equation (11.26) subject to boundary conditions A-D is  $v_1(z) = 0$  for all values of the load  $P$ . This is the trivial solution. The general solution of eq. (11.26) for  $K^2 > 0$  is

$$v_1(z) = A_1 \sin(Kz) + A_2 \cos(Kz) + A_3 z + A_4, \quad (11.29)$$

where  $A_1, A_2, A_3$ , and  $A_4$  are arbitrary constants to be determined by boundary conditions.

**Example 11.1 Critical load for clamped-free boundary conditions in figure. 11.4(B)**

Consider the clamped-free boundary conditions denoted as (B). Determine the critical load  $P_{cr}$  for which the perfect column admits a non-trivial equilibrium state.

**Solution.** The bending moment and vertical shear force (11.28) vanish at  $z = L$ . The four boundary conditions in this case are

$$v_1(0) = 0 \quad v_1'(0) = 0 \quad EIv_1''(L) = 0 \quad [v_1''' + K^2v_1']_{z=L} = 0, \quad (\text{a})$$

where the primes denote derivatives with respect to  $z$ . Taking derivatives of eq. (11.29) we have

$$\begin{aligned} v_1 &= A_1 \sin(Kz) + A_2 \cos(Kz) + A_3 z + A_4 \\ v_1' &= A_1 K \cos(Kz) - A_2 K \sin(Kz) + A_3 \\ v_1'' &= -A_1 K^2 \sin(Kz) - A_2 K^2 \cos(Kz) \\ v_1''' &= -A_1 K^3 \cos(Kz) + A_2 K^3 \sin(Kz) \end{aligned} \quad (\text{b})$$

Substitute these solutions into the four boundary conditions to get

$$\begin{bmatrix} 0 & 1 & 0 & 1 \\ K & 0 & 1 & 0 \\ -K^2 \sin(KL) & -K^2 \cos(KL) & 0 & 0 \\ 0 & 0 & K^2 & 0 \end{bmatrix} \begin{bmatrix} A_1 \\ A_2 \\ A_3 \\ A_4 \end{bmatrix} = 0. \quad (\text{c})$$

A non-trivial solution for  $A_1$  to  $A_4$  requires the determinate of coefficients to vanish:

$$\det \begin{bmatrix} 0 & 1 & 0 & 1 \\ K & 0 & 1 & 0 \\ -K^2 \sin(KL) & -K^2 \cos(KL) & 0 & 0 \\ 0 & 0 & K^2 & 0 \end{bmatrix} = 0. \quad (\text{d})$$

After expanding this determinate we get

$$-K^5 \cos(KL) = 0, \quad (\text{e})$$

which is called the **characteristic equation**. The solution  $K = 0$  of the characteristic equation leads to the trivial solution for  $v(z)$ . Non-trivial solutions to the characteristic equation occur for  $\cos(KL) = 0$ , whose positive roots are

$$K_n L = (2n - 1)(\pi/2) \quad n = 1, 2, 3, \dots \quad (\text{f})$$

For the discrete values of  $K_n L$  in eq. (f) to satisfy the equation in the fourth row of matrix eq. (c) requires  $A_3 = 0$ . Setting  $A_3 = 0$  in the equation in the second row of matrix eq. (c) requires  $A_1 = 0$ . The equation of the first row of matrix eq. (c) yields  $A_2 = -A_4$ . Note that the equation obtained from the third row of matrix eq.

(c) is identically satisfied for  $A_1 = 0$  and the discrete values of  $K_n L$ . For each value of  $n$  we have an associated **buckling mode** ( $A_1 = A_3 = 0, A_2 = -A_4$ ):

$$v_1(z) = A_4[1 - \cos(K_n z)]. \quad (g)$$

The buckling loads are determined from the expression for  $K^2$  in eq. (11.27), which after some manipulation is written as

$$K^2 = \left(\frac{P}{EI}\right) \left(1 - \frac{P}{EI} \left(\frac{EI}{EA}\right)\right) = k^2(1 - k^2 r^2), \quad (h)$$

where  $k^2 = P/(EI)$  and  $r^2 = I/A$ . The radius of gyration of the cross section is denoted by  $r$ . At  $K = K_1 = \pi/(2L)$  we have

$$\left(\frac{\pi}{2L}\right)^2 = k_{cr}^2(1 - k_{cr}^2 r^2), \quad (i)$$

where  $k_{cr}^2 = P_{cr}/(EI)$ . Equation (i) is a quadratic equation for  $k_{cr}^2$ , and the lowest root is

$$k_{cr}^2 = \frac{L - \sqrt{L^2 - \pi^2 r^2}}{2Lr^2} = \frac{1}{2L^2} \left(\frac{L}{r}\right) \left[\left(\frac{L}{r}\right) - \sqrt{\left(\frac{L}{r}\right)^2 - \pi^2}\right], \quad (j)$$

where  $L/r$  is the *slenderness ratio* of the column. For selected values of the slenderness ratio the values of  $k_{cr}^2$  are listed in table 11.1.

**Table 11.1 Buckling coefficient for selected slenderness ratios.**

$L/r$	$k_{cr}^2$	$\frac{k_{cr}^2}{(k_{cr}^2)_{\min}}$
20	$2.48281/L^2$	1.00625
40	$2.47122/L^2$	1.00153
60	$2.46909/L^2$	1.00069
80	$2.46835/L^2$	1.00039
100	$2.46801/L^2$	1.00025
$\infty$	$\pi^2/(4L^2) = 2.4674/L^2$	1.0

Values of  $k_{cr}^2$  monotonically decrease with increasing slenderness ratios and approach a minimum value of  $\pi^2/(4L^2)$  as  $L/r \rightarrow \infty$ . At  $L/r = 20$  the value of  $k_{cr}^2$  is 0.63 percent higher than the minimum, and at  $L/r = 100$  the value of  $k_{cr}^2$  is 0.03 percent higher than the minimum. In design we use the minimum value of  $k_{cr}^2$  for the critical load. That is,



$$[k_{cr}^2 = P_{cr}/(EI) = \pi^2/(4L^2)] \rightarrow P_{cr} = \frac{\pi^2 EI}{4L^2}. \quad (\mathbf{k})$$

The result for the critical load in eq. (k) is obtained if the axial strain at the bifurcation point with is neglected with respect to unity. From eqs. (11.17) and (11.19) the strain at the bifurcation point is

$$\varepsilon_{zz} = \frac{dw_0}{dz} = -\left(\frac{P_{cr}}{EA}\right) = -\left(\frac{\pi^2}{4(L/r)^2}\right).$$

For  $20 \leq L/r \leq 100$  the range of the strain at bifurcation point is  $-0.0062 \leq \varepsilon_{zz} \leq -0.00025$ . For small strain at the bifurcation point the stretch ratio  $\lambda = 1 + \varepsilon_{zz} \approx 1$ . Equation (11.27) yields  $K_{cr}^2 = k_{cr}^2 \lambda \approx k_{cr}^2$ . Hence, the values of  $k$  are

$$k_n = \frac{(2n-1)\pi}{L} = \sqrt{\frac{P_n}{EI}} \quad n = 1, 2, 3, \dots \quad (\mathbf{l})$$

Solve eq. (l) for the loads to get

$$P_n = \left[(2n-1)\frac{\pi}{2}\right]^2 \frac{EI}{L^2} \quad n = 1, 2, 3, \dots, \quad (\mathbf{m})$$

where  $P_n$  are the **buckling loads**. The first three buckling modes and corresponding buckling loads are shown in figure. 11.5. Remember that in design we use the minimum  $EI$  for the cross section. ■

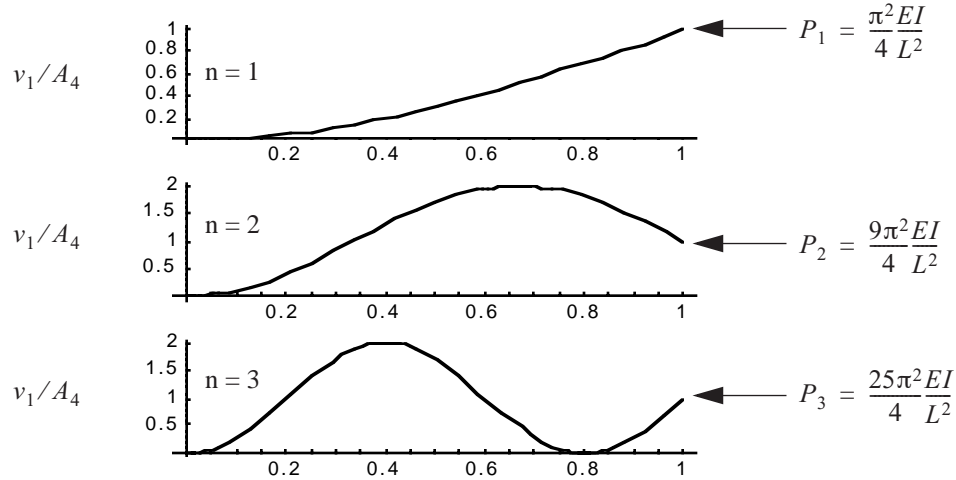


**Fig. 11.5** First three buckling modes for the clamped-free column.

### 11.1.3 Buckling equations for negligible strain at the bifurcation point

Neglecting the axial strain with respect to unity means the stretch ratio  $\lambda = 1 - P/(EA) \approx 1$ , and eqs. (11.21), (11.24), and (11.27) simplify to

$$EI \frac{d^2 \phi_1}{dz^2} - P \frac{dv_1}{dz} - S_{y1} = 0 \quad \frac{dv_1}{dz} + \phi_1 = 0 \quad K^2 = \frac{P}{EI} \quad 0 < z < L, \quad (11.30)$$

From eq. (11.26) the differential equation governing buckling is

$$\frac{d^4 v_1}{dz^4} + k^2 \frac{d^2 v_1}{dz^2} = 0 \quad v_1 = v_1(z) \quad 0 < z < L \quad k^2 = P/(EI). \quad (11.31)$$

The critical loads for boundary conditions A through D and for  $EI = \text{constant}$  are given in figure. 11.6.

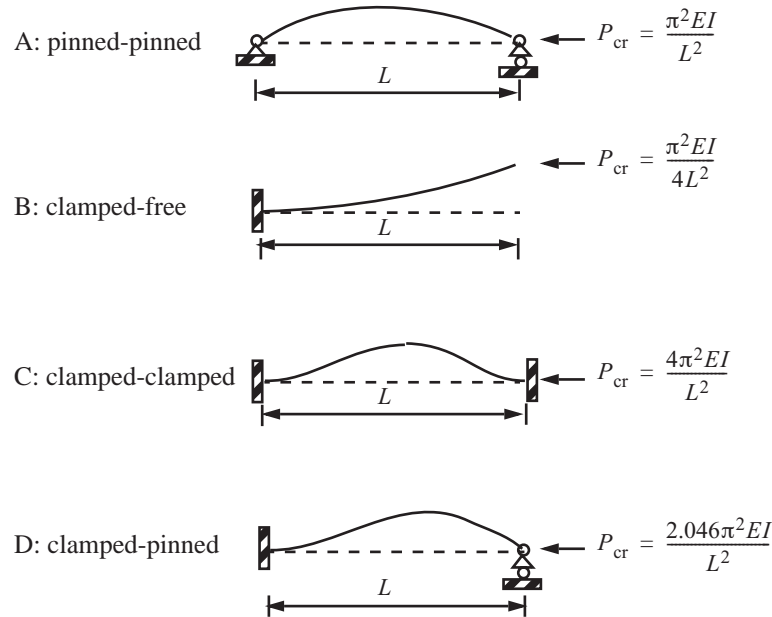


Fig. 11.6 Critical buckling loads for the standard boundary conditions A to D.

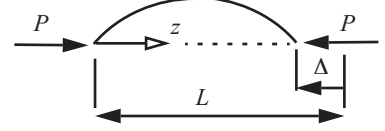
## 11.2 Initial post-buckling of the pinned-pinned column

The objective in this analysis is to seek an approximation for the displacement and load about the bifurcation point so that the early post-buckling behavior can be estimated. That is, does the load increase or decrease from its value at the bifurcation point on the post-buckling equilibrium path? The theory was originally due to Koiter using total potential energy (1945, in Dutch, English translation in 1970). Later Budiansky and Hutchinson (1964) and Budiansky (1966) employed the principal of virtual work to get results equivalent to Koiter's static post-buckling analysis. In this article the nonlinear equilibrium equations are used to develop the initial post-buckling behavior.

### 11.2.1 Summary of the nonlinear equations

The overall free body diagram of the column in a deflected configuration is shown in figure. 11.7. The shortening of the distance between support points is denoted by  $\Delta$ , where  $\Delta = -w(L)$ . If the column is cut at some point along its length, then equilibrium results in the vertical force component  $S_y = 0$  for  $0 \leq z \leq L$ .

**Fig. 11.7**  
FBD of  
deflected  
pinned-  
pinned  
column.



The relation of the force  $N$  to load  $P$  is obtained from eq. (11.8) with  $H = -P$  as

$$EA\epsilon_{zz} + P\cos\phi = 0 \quad (11.32)$$

In eq. (11.32) force  $N$  was replaced by Hooke's law (11.13), and we dropped the subscript  $x$  on the rotation  $\phi_x$  introduced in article 11.1 for convenience in the following developments. The strain  $\epsilon_{zz}$  is related to the derivatives of the displacements by the nonlinear relation (11.7). Substitute Hooke's law (11.13) for the bending moment into eq. (11.12) to get the differential equation for bending as

$$EI\left(\frac{d^2\phi}{dz^2}\right) - P\left(\frac{dv}{dz}\right) = 0 \quad 0 < z < L, \quad (11.33)$$

From eq. (11.5) the trigonometric functions of the rotation are related to the displacements by

$$\lambda\sin\phi + \frac{dv}{dz} = 0 \quad \lambda\cos\phi - \left(1 + \frac{dw}{dz}\right) = 0, \quad (11.34)$$

where the stretch ratio is  $\lambda = 1 + \epsilon_{zz}$ . The boundary conditions to be satisfied are

$$w(0) = 0 \quad v(0) = 0 \quad \left.\frac{d\phi}{dz}\right|_{z=0} = 0 \quad v(L) = 0 \quad \left.\frac{d\phi}{dz}\right|_{z=L} = 0. \quad (11.35)$$

### 11.2.2 The perturbation expansion.

From the expressions in eq. (11.30) the differential equation governing buckling in terms of the rotation is

$$EI\frac{d^2\phi_1}{dz^2} + P\phi_1 = 0 \quad \phi_1 = \phi_1(z) \quad 0 < z < L, \quad (11.36)$$

subject to the boundary conditions

$$\left.\frac{d\phi_1}{dz}\right|_{z=0} = 0 \quad \text{at} \quad z = 0, L. \quad (11.37)$$

The solution to this boundary value problem is

$$\phi_1(z) = -\cos\left(\frac{\pi z}{L}\right) \quad P = P_{cr} = \frac{\pi^2 EI}{L^2}. \quad (11.38)$$

The lateral displacement is determined from the second equation in (11.30) as

$$v_1(z) = \frac{L}{\pi} \sin\left(\frac{\pi z}{L}\right). \quad (11.39)$$

Consider the rotation and displacement in the differential equation (11.33) to be a function the dimensionless parameter  $\xi$  as well as independent variable  $z$  (i.e.,  $\phi(z, \xi)$  and  $v(z, \xi)$ ). An approximate solution to the nonlinear differential equation (11.33) and kinematic equation (11.34) is to be determined by perturbation expansions of the dependent variables in the parameter  $\xi$  for very small values of  $\xi$ . To effect the procedure, the displacements and rotation are expanded in a series in  $\xi$  as

$$\begin{aligned} w(z) &= w_0(z) + \xi w_1(z) + \xi^2 w_2(z) + \xi^3 w_3(z) + \dots \\ v(z) &= \xi v_1(z) + \xi^2 v_2(z) + \xi^3 v_3(z) + \dots \\ \phi &= \xi \phi_1(z) + \xi^2 \phi_2(z) + \xi^3 \phi_3(z) + \dots \end{aligned} \quad (11.40)$$

Functions  $w_0(z)$ ,  $\phi_1(z)$ , and  $v_1(z)$  are given by eqs. (11.14), (11.38), and (11.39), respectively. The remaining functions in the expansion (11.40) are to be determined. The expansion of the sine and cosine functions are

$$\begin{aligned} \sin \phi_x &= \sin[\xi \phi_1(z) + \xi^2 \phi_2(z) + \xi^3 \phi_3(z) + \dots] = \xi \phi_1 + \xi^2 \phi_2 + \xi^3 \left( \phi_3 - \frac{\phi_1^3}{6} \right) + O(\xi^4) \\ \cos \phi &= \cos(\xi \phi_1(z) + \xi^2 \phi_2(z) + \xi^3 \phi_3(z) + \dots) = 1 - \frac{1}{2} \xi^2 \phi_1^2(z) - \xi^3 \phi_1(z) \phi_2(z) + O(\xi^4) \end{aligned} \quad (11.41)$$

### 11.2.3 Relations between the expansion functions for the rotations and lateral displacement

With respect to the discussion in article 11.1.3 we take  $\lambda = 1$ , so the expansion of the first equation in (11.34) is

$$\xi \left[ \phi_1 + \frac{dv_1}{dz} \right] + \xi^2 \left[ \phi_2 + \frac{dv_2}{dz} \right] + \xi^3 \left[ \phi_3 + \frac{dv_3}{dz} - \frac{1}{6} \phi_1^3 \right] + O(\xi^4) = 0. \quad (11.42)$$

The previous series converges to zero for each sufficiently small value of  $\xi \neq 0$  requires that the coefficient of each power of  $\xi$  must vanish. Hence,

$$\frac{dv_1}{dz} = -\phi_1 \quad \frac{dv_2}{dz} = -\phi_2 \quad \frac{dv_3}{dz} = -\phi_3 + \frac{1}{6} \phi_1^3. \quad (11.43)$$

### 11.2.4 Perturbation expansion of the load P

We utilize the relations in eq. (11.43) to get the expansion of eq. (11.33) as

$$\xi \left( EI \frac{d^2 \phi_1}{dz^2} + P \phi_1 \right) + \xi^2 \left( EI \frac{d^2 \phi_2}{dz^2} + P \phi_2 \right) + \xi^3 \left( EI \frac{d^2 \phi_3}{dz^2} + P \phi_3 - \frac{P}{6} \phi_1^3 \right) + O(\xi^4) = 0. \quad (11.44)$$

To determine how the load  $P$  is a function of  $\xi$  multiply eq. (11.44) by  $\phi_1$  and integrate with respect to  $z$  from  $z = 0$  to  $z = L$ :

$$\xi \left[ \int_0^L \left( EI \frac{d^2 \phi_1}{dz^2} + P \phi_1 \right) \phi_1 dz \right] + \xi^2 \left[ \int_0^L \left( EI \frac{d^2 \phi_2}{dz^2} + P \phi_2 \right) \phi_1 dz \right] + \xi^3 \left[ \int_0^L \left( EI \frac{d^2 \phi_3}{dz^2} + P \phi_3 - \frac{P}{6} \phi_1^3 \right) \phi_1 dz \right] + O(\xi^4) = 0. \quad (11.45)$$

Integrate twice by parts with respect to  $z$  of the  $O(\xi^2)$  term in eq. (11.45) to get

$$\int_0^L EI \frac{d^2 \phi_2}{dz^2} \phi_1 dz = \int_0^L EI \frac{d^2 \phi_1}{dz^2} \phi_2 dz + \underbrace{\left[ EI \frac{d\phi_2}{dz} \phi_1 - EI \frac{d\phi_1}{dz} \phi_2 \right]_0^L}_{=0} = \int_0^L EI \frac{d^2 \phi_1}{dz^2} \phi_2 dz \quad (11.46)$$

The boundary terms in the expansion functions vanish consistent with the conditions in eq. (11.35). Also, integrate twice by parts with respect to  $z$  of the  $O(\xi^3)$  term. After integrating by parts, eq. (11.45) is

$$\xi \left[ \int_0^L \left( EI \frac{d^2 \phi_1}{dz^2} + P \phi_1 \right) \phi_1 dz \right] + \xi^2 \int_0^L \left( EI \frac{d^2 \phi_1}{dz^2} + P \phi_1 \right) \phi_2 dz + \xi^3 \left[ \int_0^L \left( EI \frac{d^2 \phi_1}{dz^2} + P \phi_1 \right) \phi_3 - \frac{P}{6} \phi_1^4 dz \right] + O(\xi^4) = 0. \quad (11.47)$$

From the differential equation (11.36) at buckling we have

$$EI \frac{d^2 \phi_1}{dz^2} = -P_{cr} \phi_1. \quad (11.48)$$

Substitute eq. (11.48) into eq. (11.47) to find

$$\xi (P - P_{cr}) \left( \int_0^L \phi_1^2 dz \right) + \xi^2 (P - P_{cr}) \int_0^L \phi_1 \phi_2 dz + \xi^3 \left[ (P - P_{cr}) \int_0^L \phi_1 \phi_3 dz - \frac{P}{6} \int_0^L \phi_1^4 dz \right] + O(\xi^4) = 0. \quad (11.49)$$

The last step is to impose the orthogonality conditions on the expansion functions, which are

$$\int_0^L \phi_1 \phi_2 dz = 0 \quad \int_0^L \phi_1 \phi_3 dz = 0. \quad (11.50)$$

Equation (11.49) reduces to

$$\xi (P - P_{cr}) \left( \int_0^L \phi_1^2 dz \right) - \xi^3 \frac{P}{6} \int_0^L \phi_1^4 dz + O(\xi^4) = 0. \quad (11.51)$$

Divide eq. (11.51) by  $\xi P_{cr} \left( \int_0^L \phi_1^2 dz \right)$  and rearrange terms to the form  $\frac{P}{P_{cr}} = \frac{1 + O(\xi^3)}{(1 - \xi^2 b)}$ ,

where

$$b = \frac{1}{6} \left[ \left( \int_0^L \phi_1^4 dz \right) / \left( \int_0^L \phi_1^2 dz \right) \right] = \frac{1}{8}. \quad (11.52)$$

The series of  $(1 - \xi^2 b)^{-1} = 1 + b \xi^2 + O(\xi^4)$ , which leads to

$$\frac{P}{P_{cr}} = 1 + b \xi^2 + O(\xi^3). \quad (11.53)$$

In general, the expansion of  $P/P_{cr}$  is written as

$$\frac{P}{P_{cr}} = 1 + a\xi + b\xi^2 + \dots \quad (11.54)$$

### 11.2.5 Solutions for the rotation and lateral displacement functions

Substitute the expansion of load  $P$  from eq. (11.54) into eq. (11.44), and arrange terms in powers of  $\xi$  to get

$$\xi \left[ EI \frac{d^2 \phi_1}{dz^2} + P_{cr} \phi_1 \right] + \xi^2 \left[ EI \frac{d^2 \phi_2}{dz^2} + P_{cr} \phi_2 + a P_{cr} \phi_1 \right] + \xi^3 \left[ EI \frac{d^2 \phi_3}{dz^2} + P_{cr} \phi_3 + a P_{cr} \phi_2 + b P_{cr} \phi_1 - \frac{1}{6} P_{cr} \phi_1^3 \right] + \dots = 0. \quad (11.55)$$

For the series (11.55) to converge to zero for each sufficiently small value of  $\xi$ , the coefficient of each power of  $\xi$  must vanish. The coefficient of  $\xi$  is the differential equation for buckling, eqs. (11.36) and (11.38). The coefficients of  $\xi^2$  and  $\xi^3$  lead to differential equations

$$EI \frac{d^2 \phi_k}{dz^2} + P_{cr} \phi_k = F_k \quad \phi_k = \phi_k(z) \quad 0 < z < L \quad k = 2, 3, \quad (11.56)$$

subject to boundary conditions

$$\left. \frac{d\phi_k}{dz} \right|_{z=0} = 0 \quad \left. \frac{d\phi_k}{dz} \right|_{z=L} = 0. \quad (11.57)$$

The non-homogeneous terms in eq. (11.56) depend on previous solutions of the expansion functions. That is,

$$F_2 = -a P_{cr} \phi_1 \quad F_3 = -a P_{cr} \phi_2 - b P_{cr} \phi_1 + \frac{1}{6} P_{cr} \phi_1^3. \quad (11.58)$$

Let  $k_{cr} = P_{cr}/(EI)$ . The general solution to differential equation (11.56) consists of a complementary function  $c_{1k} \cos(k_{cr} z) + c_{2k} \sin(k_{cr} z)$  that satisfies the homogeneous equation plus a particular solution denoted by  $\phi_k^*(z)$  that satisfies the non-homogeneous equation. Then, the general solution is

$$\phi_k(z) = c_{1k} \cos(k_{cr} z) + c_{2k} \sin(k_{cr} z) + \phi_k^*(z). \quad (11.59)$$

Consider conditions required to solve the boundary value problem presented by eqs. (11.56) and (11.57). Multiply eq. (11.56) by  $\phi_1(z)$  and integrate the result from  $z = 0$  to  $z = L$ . The result is

$$\int_0^L \left( EI \frac{d^2 \phi_k}{dz^2} \phi_1 + P_{cr} \phi_k \phi_1 \right) dz = \int_0^L F_k \phi_1 dz. \quad (11.60)$$

Integrate the first term on the left-hand side of eq. (11.60) by parts twice to get

$$\left[ \phi_1 EI \frac{d\phi_k}{dz} - \frac{d\phi_1}{dz} EI \phi_k \right] \Big|_{z=L} - \left[ \phi_1 EI \frac{d\phi_k}{dz} - \frac{d\phi_1}{dz} EI \phi_k \right] \Big|_{z=0} + \int_0^L \left( EI \frac{d^2 \phi_1}{dz^2} + P_{cr} \phi_1 \right) \phi_k dz = \int_0^L F_k \phi_1 dz. \quad (11.61)$$

Boundary conditions (11.37) and (11.57) result in the terms on the left-hand side of eq. (11.61) evaluated at the end points of the interval equal to zero. Also, the integrand on the left-hand side vanishes since rotation  $\phi_1$  satisfies eq. (11.36). We are left with the condition for the solution of the boundary value problem for  $\phi_k$  that

$$\int_0^L F_k \phi_1 dz = 0. \quad (11.62)$$

For  $k = 2$  condition (11.62) is

$$\int_0^L F_2 \phi_1 dz = -a P_{cr} \int_0^L \phi_1^2 dz = -a P_{cr} \left( \frac{L}{2} \right) = 0. \quad (11.63)$$

The only way to satisfy the condition in eq. (11.63) is to take the post-buckling coefficient  $a = 0$ . The solution for  $\phi_2$  that satisfies the boundary conditions (11.57) is  $\phi_2(z) = c_{12} \cos(k_{cr} z)$ . The orthogonality condition (11.50) determines  $c_{12} = 0$ . Thus,  $\phi_2(z) = 0$ . From eq. (11.43) and boundary condition (11.35) we find  $v_2(z) = 0$  for  $0 \leq z \leq L$ . For  $k = 3$ , condition (11.62) is

$$\int_0^L F_3 \phi_1 dz = \int_0^L \left( -b P_{cr} \phi_1 + \frac{1}{6} P_{cr} \phi_1^3 \right) \phi_1 dz = 0. \quad (11.64)$$

Equation (11.64) determines post-buckling coefficient  $b$ , and it is the same as given in eq. (11.52).

From eq. (11.56) the governing equation for  $\phi_3(z)$  with  $a = 0$  and  $b = 1/8$  is

$$EI \frac{d^2 \phi_3}{dz^2} + P_{cr} \phi_3 = -\left( \frac{1}{8} \right) P_{cr} \phi_1 + \frac{1}{6} P_{cr} \phi_1^3 = P_{cr} \left[ \left( \frac{1}{8} \right) \cos\left( \frac{\pi z}{L} \right) - \left( \frac{1}{6} \right) \cos^3\left( \frac{\pi z}{L} \right) \right]. \quad (11.65)$$

Use the trigonometric identity  $\cos^3 x = (3/4) \cos x + (1/4) \cos(3x)$  to find

$$EI \frac{d^2 \phi_3}{dz^2} + P_{cr} \phi_3 = \frac{-P_{cr}}{24} \cos\left( \frac{3\pi z}{L} \right). \quad (11.66)$$

The solution to differential equation (11.66) is

$$\phi_3(z) = c_{13} \cos(k_{cr} z) + c_{23} \sin(k_{cr} z) + \left( \frac{1}{192} \right) \cos\left( \frac{3\pi z}{L} \right). \quad (11.67)$$

Boundary conditions (11.57) lead to coefficient  $c_{23} = 0$ . Coefficient  $c_{13}$  is determined from the orthogonality condition (11.50)

$$\int_0^L \phi_3 \phi_1 dz = \frac{-c_{13} L}{2} = 0. \quad (11.68)$$

Therefore  $c_{13} = 0$  and the solution for function  $\phi_3(z)$  is

$$\phi_3(z) = \left( \frac{1}{192} \right) \cos\left( \frac{3\pi z}{L} \right). \quad (11.69)$$

The function  $v_3(z)$  can now be determined from eq. (11.43). The result that satisfies boundary conditions (11.35) is

$$v_3(z) = \left(\frac{-L}{8\pi}\right) \sin\left(\frac{\pi z}{L}\right) - \left(\frac{L}{64\pi}\right) \sin\left(\frac{3\pi z}{L}\right). \quad (11.70)$$

### 11.2.6 Solutions for the axial displacement functions

We make use of eq. (11.43) to find that the expansion of the strain  $\varepsilon_{zz}$  in (11.7) is

$$\varepsilon_{zz} = \frac{dw_0}{dz} + \xi \frac{dw_1}{dz} + \xi^2 \left[ \frac{dw_2}{dz} + \frac{1}{2} \phi_1^2 \right] + \xi^3 \left[ \frac{dw_3}{dz} + \phi_1 \phi_2 \right] + O(\xi^4). \quad (11.71)$$

Substitute expansions of the strain from eq. (11.71), the load  $P$  from eq. (11.54), and the cosine function from eq. (11.41), into eq. (11.32) to find the expansion of the axial equilibrium as

$$\xi^0 \left[ EA \frac{dw_0}{dz} + P_{cr} \right] + \xi \left[ EA \frac{dw_1}{dz} + a P_{cr} \right] + \xi^2 \left[ EA \frac{dw_2}{dz} + b P_{cr} - P_{cr} \phi_1^2 + EA \frac{1}{2} \phi_1^2 \right] + O(\xi^3) = 0. \quad (11.72)$$

For eq. (11.72) to converge to zero for each sufficiently small value of  $\xi$ , the coefficient of each power of  $\xi$  must vanish. Thus, we get to expressions for the derivatives of the expansion functions of displacement  $w(z)$  as

$$\frac{dw_0}{dz} = \frac{-P_{cr}}{EA} \quad \frac{dw_1}{dz} = \frac{-a P_{cr}}{EA} \quad \frac{dw_2}{dz} = \frac{-2b P_{cr} + (2P_{cr} - EA) \phi_1^2}{2EA}. \quad (11.73)$$

Since  $a = 0$  and  $w_1(0) = 0$ , the displacement function  $w_1(z) = 0$  for  $0 \leq z \leq L$ . The expression for the derivative of displacement function  $w_2(z)$  is integrated with respect to  $z$ , and we set  $w_2(0) = 0$  to find

$$w_2(z) = -\frac{z}{4} + \frac{7P_{cr}}{8EA} z - \frac{L}{8\pi} \sin\left(\frac{2\pi z}{L}\right). \quad (11.74)$$

### 11.2.7 Summary

From this initial post-buckling analysis the results for the expansions of the load, displacements, and rotation are

$$\frac{P}{P_{cr}} = 1 + \frac{\xi^2}{8} \quad w(z) = -\frac{P_{cr}}{EA} z + \xi^2 w_2(z) \quad v(z) = \xi v_1(z) + \xi^3 v_3(z) \quad \phi(z) = \xi \phi_1(z) + \xi^3 \phi_3(z). \quad (11.75)$$

The strain of the centroidal axis is

$$\varepsilon_{zz} = -\frac{P_{cr}}{EA} + \xi^2 \left[ \frac{dw_2}{dz} + \frac{1}{2} \left( \frac{dv_1}{dz} \right)^2 \right]. \quad (11.76)$$

Rotation functions  $\phi_1(z)$  and  $\phi_3(z)$  are given by eqs. (11.38) and (11.69), respectively. Lateral displacement functions  $v_1(z)$  and  $v_3(z)$  are given by eqs. (11.39) and (11.70), respectively, and the axial displacement function  $w_2(z)$  is given by eq. (11.74).



**Example 11.2 Numerical results for the initial post-buckling of the pinned-pinned column**

Consider the column with a solid, rectangular cross section of height  $h$  and width  $b$ , where  $h < b$ . The radius of gyration is  $r = \sqrt{I/A} = h/\sqrt{12}$ . The strain at the bifurcation point is obtained from eq. (11.76) for  $\xi \rightarrow 0$  is  $-P_{cr}/(EA)$ , and take this strain equal to  $-0.0006$ . Since  $P_{cr} = (\pi^2 EI)/L^2$ , we have

$$\frac{P_{cr}}{EA} = \frac{\pi^2 EI}{L^2} \left( \frac{1}{EA} \right) = \frac{\pi^2}{12} \left( \frac{h}{L} \right)^2 = 0.0006. \quad (\text{a})$$

Hence, the span-to-thickness ratio  $L/h = 37$ .

The restriction on the magnitude of the expansion parameter  $\xi$  in the initial post-buckling analysis is based on the strain at the elastic limit of 7075-T6 aluminum alloy, which is about 0.0068. Let  $\bar{\epsilon}_{zz}$  denote the strain of a line element parallel to the centroidal axis. It is the sum of the strain of centroidal axis  $\epsilon_{zz}$  plus the strain due to bending. That is,

$$\bar{\epsilon}_{zz} = \epsilon_{zz} + y \left( \frac{d\phi}{dz} \right), \quad (\text{b})$$

where  $(-h)/2 \leq y \leq h/2$  and  $d\phi/dz$  is the curvature of the centroidal axis. The magnitude of the maximum compressive strain in post-buckling occurs at midspan,  $z = L/2$ , and  $y = -h/2$ . That is,

$$\bar{\epsilon}_{zz} = \epsilon_{zz} - \frac{h}{2} \left( \frac{d\phi}{dz} \right) \Big|_{z=L/2}. \quad (\text{c})$$

The expansion for the curvature at midspan is determined from eqs. (11.75), (11.38) and (11.69). The result is

$$\left. \frac{d\phi}{dz} \right|_{z=L/2} = \left[ \frac{\pi}{L} \sin\left(\frac{\pi z}{L}\right) \right] \xi - \left[ \frac{\pi}{64L} \sin\left(\frac{3\pi z}{L}\right) \right] \xi^3 \Big|_{z=L/2} = \frac{\pi}{L} \xi + \frac{\pi}{64L} \xi^3. \quad (\text{d})$$

Substitute  $h = 0.270L$  and  $P_{cr} = 0.0006EA$  in the expansions for the strains. The numerical evaluations of the strain in eq. (11.76) and the strain from bending are

$$\epsilon_{zz} = -0.0006 - 0.000075\xi^2 \quad -\frac{h}{2} \left( \frac{d\phi}{dz} \right) = -0.0424264\xi - 0.000662193\xi^3. \quad (\text{e})$$

The axial strain on the concave side of the bar at midspan is set equal to the elastic limit strain of  $-0.0068$ . Thus,

$$\bar{\epsilon}_{zz} = -0.0006 - 0.042464\xi - 0.000075\xi^2 - 0.000662913\xi^3 = -0.0068.$$

The real root of the previous polynomial is the maximum value of parameter  $\xi$ , which is

$$\xi_{\max} = 0.14605. \quad (\text{f})$$

For post-buckling coefficients  $a = 0$  and  $b = 1/8$ , we get  $P/P_{cr} = 1.0027$  at  $\xi = \xi_{\max}$  from eq. (11.54).

There is a very small increase in the load during post-buckling. The lateral displacement of the column is determined from eqs. (11.75), (11.39), and (11.70), and it is a maximum at midspan. Evaluation of the maximum dis-

placement is

$$v_{\max} = v(L/2) = \frac{L\xi}{\pi} - \frac{7L\xi^2}{64\pi}, \quad (g)$$

and  $v_{\max} = 0.04638L$  at  $\xi = \xi_{\max}$ .

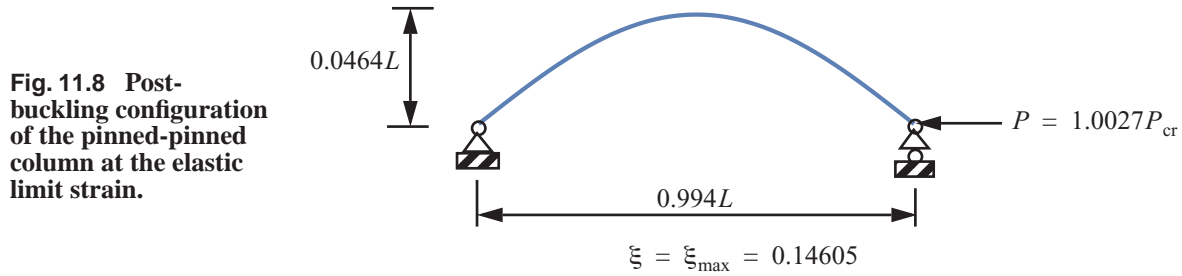
The axial displacement of the column is determined from eqs. (11.75) and (11.74). The shortening of distance between supports is

$$\Delta = -w(L) = L(0.0006) + \left(\frac{L}{4} + \frac{L(0.0006)}{8}\right)\xi^2. \quad (h)$$

The shortening at buckling is  $\Delta_{\text{cr}} = \Delta|_{\xi=0} = L(0.0006)$ , and the normalized shortening is defined by

$$\Delta/\Delta_{\text{cr}} = 1 + 416.792\xi^2. \quad (i)$$

At  $\xi = \xi_{\max}$ ,  $\Delta/\Delta_{\text{cr}} = 9.89$  on the post-buckling path. The configuration of the column at  $\xi_{\max}$  is shown in figure. 11.8.



The pre-buckling equilibrium path is determined from eq. (11.14) where  $\Delta = -w_0(L) = (PL)/(EA)$ , or  $P = (EA/L)\Delta$ . Divide by the critical load to get  $P/P_{\text{cr}} = (EA/P_{\text{cr}})(\Delta/L)$ . From eq. (a) the factor  $EA/P_{\text{cr}} = 1/0.0006$ . Thus,  $P/P_{\text{cr}} = \Delta/(0.0006L) = \Delta/\Delta_{\text{cr}}$  on the pre-buckling equilibrium path.

The load-deflection response is shown in figure. 11.9(a), and the load-shortening response is shown in figure. 11.9(b). The post-buckling behavior of the column is **stable symmetric bifurcation**, which is the same behavior as model A in article 10.1 on page 289. The load does not decrease in post-buckling. However, the increase in load is very small in post-buckling. From a practical point of view, the column is considered neutral in post-buckling. The structural stiffness is defined as  $dP/d\Delta$ . For post-buckling the structural stiffness is computed as

$$\frac{dP}{d\Delta} = \frac{dP}{d\xi} \frac{d\xi}{d\Delta} = \left(\frac{P_{\text{cr}}}{4}\xi\right) \frac{1}{2(L/4 + 0.0006(L/8))\xi} = \frac{P_{\text{cr}}}{L(2 + 0.0006)} = \frac{EA(0.0006)}{L(2.0006)} = \frac{EA}{L}(0.0003).$$

The structural stiffness in pre-buckling is  $(EA)/L$ . The ratio of the post-buckling stiffness to the pre-buckling stiffness is 0.0003, which indicates the dramatic loss of structural stiffness due to buckling. ■

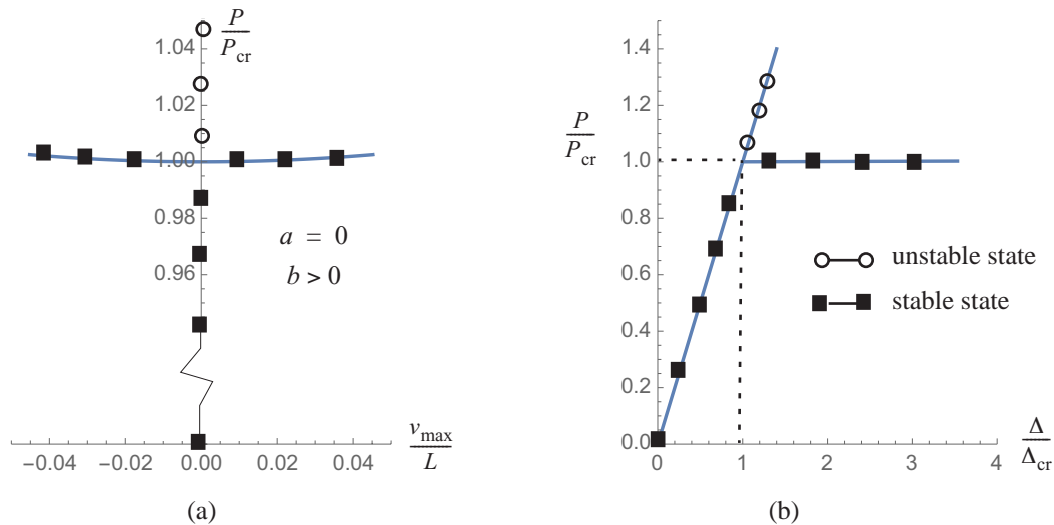


**Fig. 11.9** Equilibrium paths for the pinned-pinned column subject to axial compression (a) on the load-deflection plot, and (b) on the load-shortening plot.

From eq. (11.54) the perturbation expansion of the load in initial post-buckling is  $P/P_{cr} = 1 + a\xi + b\xi^2$ . The post-buckling coefficients  $a = 0$  and  $b < 0$  correspond to unstable symmetric bifurcation behavior illustrated by model B in article 10.2 on page 298. Post-buckling coefficient  $a \neq 0$  corresponds to asymmetric bifurcation behavior illustrated by model C in article 10.3 on page 302.

### 11.3 In-plane buckling of trusses

When a truss has all of its joints pinned, then there will be no interaction between the bending deflections of individual members. Hence the buckling load of the truss will be the load at which the weakest compression member buckles as an Euler column (case A in figure. 11.6). However, when a truss is rigidly jointed, as in a frame, there will be interaction between bending deflections of neighboring members through rotation of the common joint. A rigid-jointed truss is stiffer than a pin-jointed truss, and therefore its buckling load is increased relative to the pin-jointed truss.

#### Example 11.3 Buckling of a two-bar truss

A symmetric truss consisting of two identical bars of length  $L$  are connected together by a hinge joint at the center of the truss. The opposite end of each bar connects to a separate hinge joint at a fixed support. Both supports are at a distance  $H$  below central joint. The central joint is subject to downward load  $Q$  whose corresponding displacement is denoted by  $q$ .

We consider a linear analysis and a nonlinear analysis for the stability of the truss, where Hooke's law governs the material behavior in both analyses. The material of the bars is 7075-T6 aluminum alloy with a modulus of elasticity  $E = 71,000 \text{ N/mm}^2$  and yield strength of  $\sigma_{yield} = 469 \text{ MPa}$ . The remaining numerical data are

listed in table 11.2. From the data in table 11.2 the angle  $\beta = 5.16^\circ$ . A small value of  $\beta$  characterizes a shallow truss configuration.

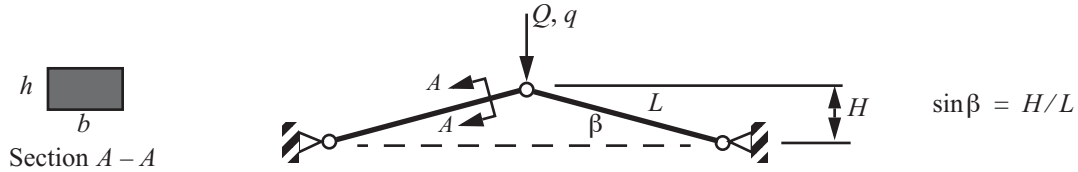


**Fig. 11.10** A shallow truss horizontally constrained between fixed points.

**Table 11.2** Numerical data for the truss in figure. 11.10

Length of truss bars $L$ , mm	300	Width of truss bar $b$ , mm	25
Truss rise above supports $H$ , mm	27	Area of truss bar $A$ , mm <sup>2</sup>	450
Thickness of truss bar $h$ , mm	18	Second area moment $I$ , mm <sup>4</sup>	12,150

**Axial strain-displacement relation.** The strain-displacement relation (11.7) for each bar is

$$\epsilon_{zz} = \frac{dw}{dz} + \frac{1}{2} \left( \frac{dv}{dz} \right)^2, \quad (\text{a})$$

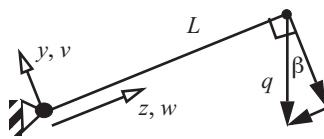


**Fig. 11.11** Left-hand bar of the truss.

where the axial displacement is denoted by  $w(z)$  and the lateral displacement is denoted by  $v(z)$ . Consider the bar on the left-hand side of the truss as shown in figure. 11.11. At the fixed end where  $z=0$ ,  $w(0) = v(0) = 0$ . At the end of the bar where  $z=L$  the axial displacement and the lateral displacement are related to the downward displacement  $q$  of the movable joint by  $w(L) = -q \sin \beta$  and  $v(L) = -q \cos \beta$ , respectively. The axial strain in a truss bar is uniform along its length, which means that the displacements are linear in coordinate  $z$ . Linear displacement functions for each displacement satisfying the end conditions are,

$$w(z) = (-q \sin \beta)(z/L) \quad v(z) = (-q \cos \beta)(z/L). \quad (\text{b})$$

Substitute eq. (b) for the displacement functions into eq. (a) to get the strain-displacement relation

$$\epsilon_{zz} = (\sin \beta) \left( \frac{-q}{L} \right) + \frac{1}{2} (\cos^2 \beta) \left( \frac{q}{L} \right)^2. \quad (\text{c})$$

Substitute  $\sin \beta = H/L$ , and  $\cos \beta = (\sqrt{L^2 - H^2})/L$  into eq. (c) to get

$$\epsilon_{zz} = \frac{H}{L} \left( \frac{-q}{L} \right) + \frac{(L^2 - H^2)}{2L^2} \left( \frac{-q}{L} \right)^2. \quad (\text{d})$$

Numerical evaluation of eq. (d) is

$$\epsilon_{zz} = (-3 \times 10^{-4} / \text{mm}) q + (5.51056 \times 10^{-6} / \text{mm}^2) q^2. \quad (\text{e})$$

The strain energy of the truss is

$$U = 2 \left( \frac{1}{2} EAL \epsilon_{zz}^2 \right), \quad (\text{f})$$

in which the leading factor of 2 accounts for the two bars. Castigliano's first theorem determines the force  $Q$  by

$$Q = \frac{\partial U}{\partial q} = 2EAL \epsilon_{zz} \frac{\partial \epsilon_{zz}}{\partial q}. \quad (\text{g})$$

Substitute eq. (d) for the strain into eq. (f) to get

$$Q = 2EA \left[ \frac{H^2}{L^3} q - \frac{3H(L^2 - H^2)}{2L^5} q^2 + \frac{(L^2 - H^2)^2}{2L^7} q^3 \right]. \quad (\text{h})$$

Numerical evaluation of eq. (h) is

$$Q = (1,725.3 \text{ N/mm})q - (95.0736 \text{ N/mm}^2)q^2 + (1.16424 \text{ N/mm}^3)q^3. \quad (\text{i})$$

**In-plane buckling of the truss bars based on linear analysis.** The expressions for the axial strain (e) and applied load (h) reduce to

$$\epsilon_{zz} = \frac{H}{L} \left( \frac{-q}{L} \right) = (-3 \times 10^{-4} \text{ mm}^{-1})q, \text{ and } Q = 2EA \left[ \frac{H^2}{L^3} q \right] = (1,725.3 \text{ N/mm})q. \quad (\text{j})$$

The axial force in each bar is given by

$$N = EA \epsilon_{zz} = (-9,585 \text{ N/mm})q. \quad (\text{k})$$

The Euler buckling force  $P_E = (\pi^2 EI)/L^2 = 94.60 \text{ kN}$ . Set  $-N = P_E$  to find the displacement for in-plane buckling of the truss bars  $q = 9.87 \text{ mm}$ . The corresponding load  $Q = 17.028 \text{ kN}$ .

Equations (i) and (j) are plotted on the graph of load  $Q$  versus displacement  $q$  in figure. 11.12. As the load is increased from zero on the nonlinear path (i) a **limit point** load of 9.038 kN at a displacement of 11.5 mm is encountered. As discussed in article 10.5 a dynamic snap-through motion occurs at the limit load that eventually (with damping) settles to a displacement of 58.65 mm. The linear response path (j) is the straight line in figure.

11.12, and the load causing in-plane buckling of the truss bars is 17.028 kN. Thus, the critical load for this structure is at the limit point. ■

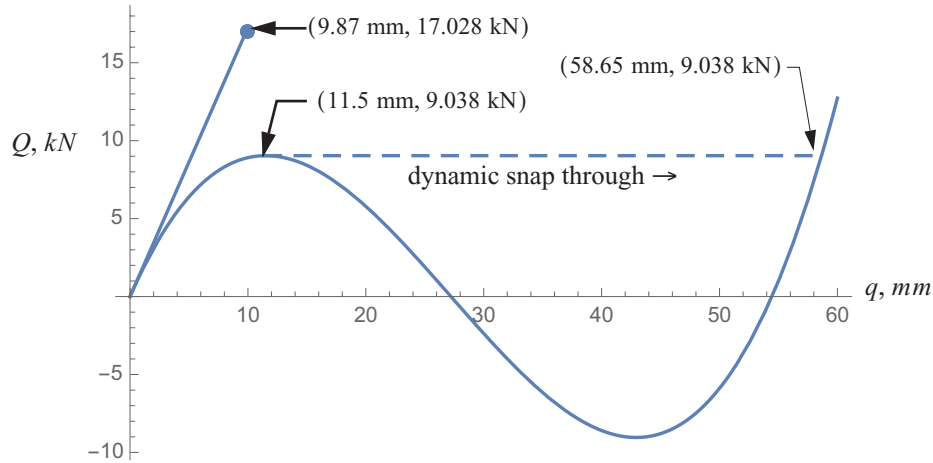
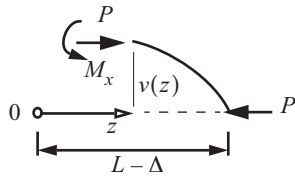


Fig. 11.12 Load-displacement responses of the two-bar truss from linear and nonlinear analyses.

### 11.4 Geometrically imperfect column

Fig. 11.13  
FBD of the  
right-hand  
part of a  
pinned-pinned  
column.



segment of the column shown in figure. 11.13 is

$$M_x - vP = 0. \quad (11.77)$$

The bending moment in the column is zero under no load, so we write the material law for bending as

$$M_x = EI \left( \frac{d\phi}{dz} - \frac{d\phi_0}{dz} \right), \quad (11.78)$$

where  $\phi_0(z)$  is the rotation of the initial shape of the column. For small slopes of the slightly deflected column the rotations are related to the lateral displacements by

$$\phi(z) = -\left( \frac{dv}{dz} \right) \quad \phi_0(z) = -\left( \frac{dv_0}{dz} \right). \quad (11.79)$$

Hence, the bending moment becomes

$$M_x = -EI \left( \frac{d^2 v}{dz^2} - \frac{d^2 v_0}{dz^2} \right). \quad (11.80)$$

Substitute the bending moment from eq. (11.80) into the moment equilibrium equation (11.77) to get

$$-EI \left( \frac{d^2 v}{dz^2} - \frac{d^2 v_0}{dz^2} \right) - vP = 0. \quad (11.81)$$

Equation (11.81) is arranged to the form

$$\frac{d^2 v}{dz^2} + k^2 v = \frac{d^2 v_0}{dz^2}, \quad (11.82)$$

where  $k^2 = P/(EI)$ . Take the initial shape of the column  $v_0(z) = a_1 \sin(\pi z/L)$ , where  $a_1$  is the amplitude of the initial shape at midspan. Then the differential equation for  $v(z)$  is

$$\frac{d^2 v}{dz^2} + k^2 v = -a_1 \left( \frac{\pi}{L} \right)^2 \sin(\pi z/L) \quad 0 < z < L. \quad (11.83)$$

The boundary conditions are  $v(0) = v(L) = 0$ . The solution of the differential equation (11.83) subject to boundary conditions is

$$v(z) = \frac{a_1}{1 - \left( \frac{kL}{\pi} \right)^2} \sin\left(\frac{\pi z}{L}\right) \quad 0 \leq z \leq L. \quad (11.84)$$

The term  $k^2 L^2 / \pi^2 = P/P_{cr}$  where the critical load of the perfect structure is  $P_{cr} = (\pi^2 EI)/L^2$ . It is convenient to measure the deflection of the imperfect column under load with respect to its original unloaded state. That is, let  $\delta$  define the additional displacement at midspan by  $\delta = v(L/2) - v_0(L/2)$ . Hence,

$$\delta = a_1 \frac{\left( \frac{P}{P_{cr}} \right)}{1 - \left( \frac{P}{P_{cr}} \right)}. \quad (11.85)$$

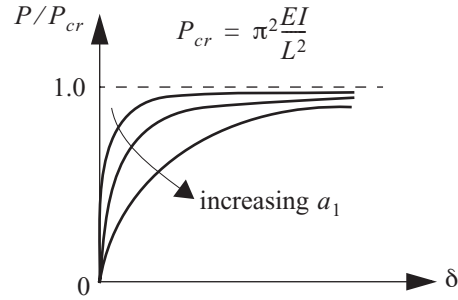
The load-displacement response is sketched in figure. 11.14. Note that  $|\delta| \rightarrow \infty$  as  $P \rightarrow P_{cr}$  for  $a_1 \neq 0$ . That is, for a non-zero value of the imperfection amplitude, the displacement gets very large as the axial force approaches the buckling load of the perfect column. Also, the imperfect column deflects in the direction of imperfection (e.g., if  $a_1 > 0$ , then  $\delta > 0$ ).

An arbitrary initial shape is represented by a Fourier Sine series as

$$v_0(z) = a_1 \sin \frac{\pi z}{L} + a_2 \sin \frac{2\pi z}{L} + \dots \quad (11.86)$$

Timoshenko and Gere (1961) show the solution for  $\delta(z) = v(z) - v_0(z)$  is

**Fig. 11.14 Load-deflection response plots for geometrically imperfect columns**



$$\delta(z) = \frac{P}{P_{cr}} \left[ \frac{a_1}{1 - P/P_{cr}} \sin\left(\frac{\pi z}{L}\right) + \frac{a_2}{2^2 - P/P_{cr}} \sin\left(\frac{2\pi z}{L}\right) + \dots \right]. \quad (11.87)$$

For  $P < P_{cr}$  as  $P \rightarrow P_{cr}$ , the first term dominates the solution for  $\delta(z)$ . Thus, for  $P$  near  $P_{cr}$

$$\delta_c = \delta\left(\frac{L}{2}\right) \sim \frac{P/P_{cr}}{1 - P/P_{cr}} a_1. \quad (11.88)$$

The buckling behavior of a long, straight column subject to centric axial compression (the perfect column) is classified as stable symmetric bifurcation. As such it is imperfection insensitive. Refer to the discussions in article 10.1.5 on page 297 and article 10.2.1 on page 300. Even for a well manufactured column whose geometric imperfections are small, and with the load eccentricity small, the displacements become excessive as the axial compressive force  $P$  approaches the critical load  $P_{cr}$  of the perfect column. *Hence, the critical load determined from the analysis of the perfect column is meaningful in practice.*

### 11.4.1 Southwell plot

Rearrange eq. (11.88) as follows:  $\delta_c(1 - P/P_{cr}) = (P/P_{cr})a_1$ , then  $\delta_c - (P/P_{cr})\delta_c = (P/P_{cr})a_1$ . Divide the last by  $P$  to get

$$\frac{\delta_c}{P} = \frac{(\delta_c + a_1)}{P_{cr}}. \quad (11.89)$$

We plot  $\delta_c/P$  versus  $\delta_c$  from eq. (11.89) in figure. 11.15, which is called the Southwell plot (Southwell, 1932).<sup>1</sup> The Southwell plot is very useful for determining  $P_{cr}$  from test data in the elastic range. As  $P \rightarrow P_{cr}$ ,  $P < P_{cr}$ ,  $\delta$  becomes large and the data  $((\delta/P) \text{ vs. } \delta)$  tends to plot on a straight line. Extrapolating this straight line back to toward the ordinate axis  $(\delta/P)$  one can estimate  $a_1$  and  $P_{cr}$ . It is more difficult to determine  $P_{cr}$  by the load-deflection curve obtained in experiments as illustrated in figure. 11.16.

1. Richard V. Southwell (1888 -1970), British mathematician specializing in applied mechanics. In his article "On the Analysis of Experimental Observations in Problems of Elastic Stability", he discussed the coordinates used in the plot to correlate the experimental data on elastic column buckling with linear theory.



Fig. 11.15 Southwell plot.

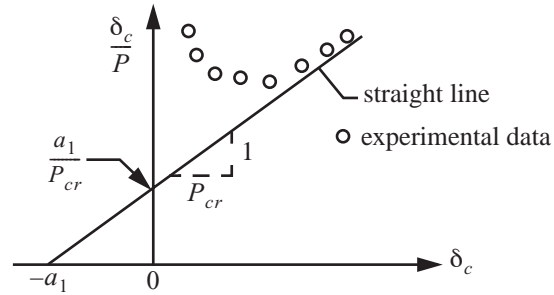
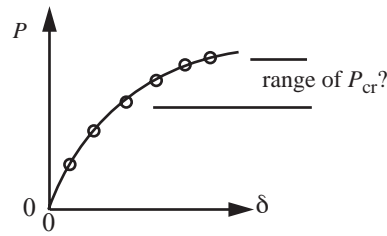


Fig. 11.16 Load-deflection plot from test data.

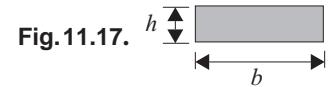


## 11.5 Column design curve

Consider the pinned-pinned uniform column whose critical load is given by  $P_{cr} = \pi^2(EI/L^2)$ . Let  $A$  denote the cross-sectional area of the column. At the onset of buckling the critical stress is defined as

$$\sigma_{cr} = P_{cr}/A = (\pi^2 EI)/(AL^2). \quad (11.90)$$

The second area moment is  $I = r^2 A$ , where  $r$  denotes the minimum radius of gyration of the cross section. For the rectangular section shown in figure. 11.17,  $I_{min} = (bh^3)/12$  and  $A = bh$ , so that  $r = h/\sqrt{12}$ , where  $0 < h < b$ . Thus, the critical stress becomes



$$\sigma_{cr} = \pi^2 \frac{E}{(L/r)^2}. \quad (11.91)$$

and  $L/r$  is called the *slenderness ratio*. The slenderness ratio is the column length divided by a cross-sectional dimension significant to bending.

For any set of boundary conditions define the *effective length*  $KL$  by the formula

$$P_{cr} = \pi^2 \frac{EI}{(KL)^2}. \quad (11.92)$$

The effective lengths for the four standard boundary conditions are as follows:

A: pinned-pinned	$P_{cr} = \pi^2 \frac{EI}{L^2} = \pi^2 \frac{EI}{(KL)^2}$	$KL = L$	$K = 1$
B: clamped-free	$P_{cr} = \frac{\pi^2 EI}{4 L^2} = \pi^2 \frac{EI}{(KL)^2}$	$KL = 2L$	$K = 2$
C: clamped-clamped	$P_{cr} = 4\pi^2 \frac{EI}{L^2} = \pi^2 \frac{EI}{(KL)^2}$	$KL = L/2$	$K = 1/2$
D: clamped-pinned	$P_{cr} = 20.2 \frac{EI}{L^2} = \pi^2 \frac{EI}{(KL)^2}$	$KL = 0.699L$	$K = 0.7$

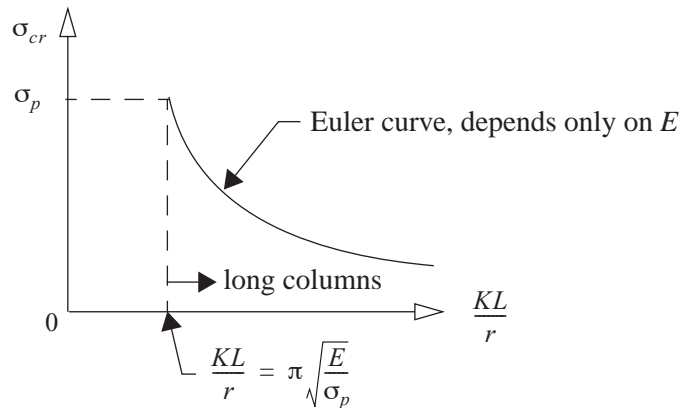
The definition of effective length uses case A boundary conditions as a reference. The concept of effective length accounts for boundary conditions other than simple support, or pinned-pinned end conditions.

The *column curve* is a plot of the critical stress versus the effective slenderness ratio (i.e.,  $\sigma_{cr}$  versus  $KL/r$ ). For elastic column buckling under all boundary conditions

$$\sigma_{cr} = \frac{\pi^2 E}{\left(\frac{KL}{r}\right)^2}, \quad (11.93)$$

which is a hyperbola that depends only on the modulus of elasticity  $E$  of the material. This equation governing elastic buckling is called the Euler curve, and columns that buckle in the elastic range are called long columns. See figure. 11.18.

**Fig. 11.18 Column curve for elastic buckling.**

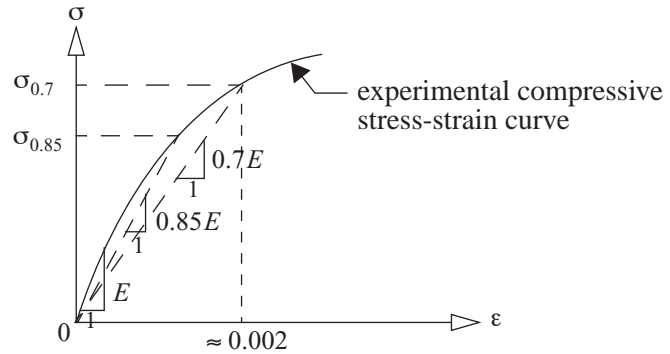


### 11.5.1 Inelastic buckling

The column curve equation, eq. (11.93), is valid up to the proportional limit of the material, denoted by  $\sigma_p$ . The proportional limit is defined as the stress where the compressive stress-strain curve of the material deviates from a straight line. If the stress at the onset of buckling is greater than the proportional limit, then the column is said to be of intermediate length, and the Euler formula, eq. (11.93), cannot be used. The proportional limit is difficult to measure from test data because its definition is based on the deviation from linearity. In particular, the compressive stress-strain curves for aluminum alloys typically used in aircraft construction do not exhibit a very pronounced linear range. For aluminum alloys a material law developed by Ramberg and Osgood (1943) is often

used to describe the nonlinear compressive stress-strain curve. The Ramberg-Osgood equation is a three-parameter fit to the compressive stress-strain curves of aluminum alloys. From the experimental compressive stress-strain curve the slope near the origin is the modulus of elasticity  $E$ . The stress where the secant line drawn from the origin with slope  $0.85 E$  intersects the stress-strain curve is denoted  $\sigma_{0.85}$ . The stress where a second secant line drawn from the origin with slope  $0.7E$  intersects the stress-strain curve is denoted by  $\sigma_{0.7}$ . These data are depicted in figure. 11.19. Note that the compressive normal strain corresponding to the stress  $\sigma_{0.7}$  is usually

**Fig. 11.19 Data used to fit the compression stress-strain curve of aluminum alloys.**



about the 0.2 percent offset yield strain for the material. Hence, stress  $\sigma_{0.7}$  is close to the 0.2 percent offset yield stress of the aluminum alloy. The Ramberg-Osgood equation is

$$\epsilon = \frac{\sigma}{E} \left[ 1 + \frac{3}{7} \left( \frac{\sigma}{\sigma_{0.7}} \right)^{n-1} \right], \quad (11.94)$$

where the shape parameter  $n$  is given by

$$n = 1 + \ln\left(\frac{17}{7}\right) / \ln\left(\frac{\sigma_{0.7}}{\sigma_{0.85}}\right). \quad (11.95)$$

Equation (11.94) is re-written as

$$\frac{E\epsilon}{\sigma_{0.7}} = \frac{\sigma}{\sigma_{0.7}} + \frac{3}{7} \left( \frac{\sigma}{\sigma_{0.7}} \right)^n, \quad (11.96)$$

and is plotted as  $\sigma/\sigma_{0.7}$  versus  $(E\epsilon)/\sigma_{0.7}$  for various values of the shape parameter  $n$ . This plot is shown in figure. 11.20. Some approximate values for common aluminum alloys are listed in table 11.3.

**Table 11.3 Ramberg-Osgood parameters for selected aluminum alloys**

<i>AL</i>	<i>E</i> in $10^6$ psi	$\sigma_{0.7}$ in $10^3$ psi	<i>n</i>
2014-T6	10.6	60	20
2024-T4	10.6	48	10
6061-T6	10.0	40	30
7075-T6	10.4	73	20

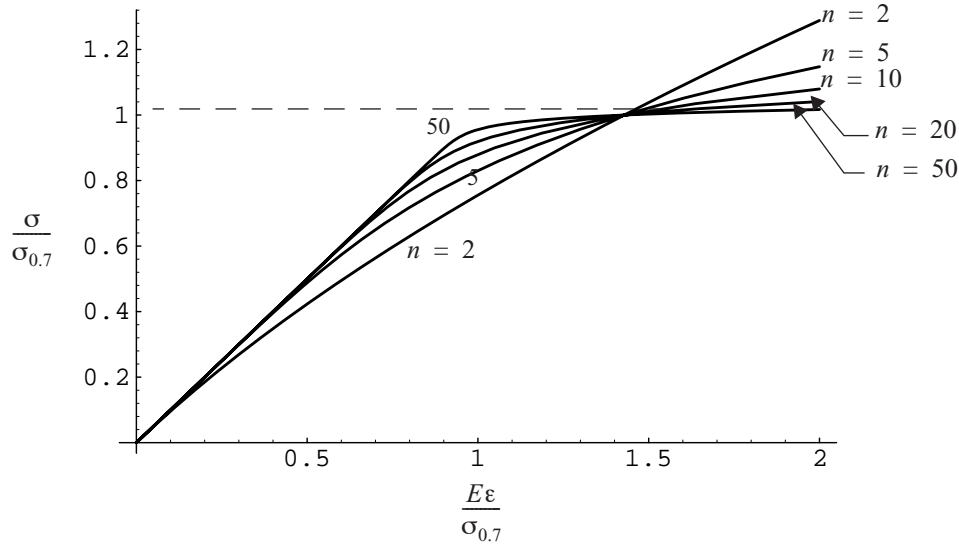


**Fig. 11.20** A normalized plot of the Ramberg-Osgood material law for various values of the shape parameter  $n$ .

From the Ramberg-Osgood equation, eq. (11.94), the local slope of the compressive stress-strain curve is determined as a function of the stress. This slope of the compressive stress-strain curve is called the tangent modulus (i.e.,  $\frac{d\sigma}{d\epsilon} = E_t$  where  $E_t$  is the tangent modulus). Differentiate eq. (11.94) to get

$$d\epsilon = \frac{d\sigma}{E} + \frac{3n\sigma^{n-1}}{7E\sigma_{0.7}^{n-1}}d\sigma \quad \frac{d\epsilon}{d\sigma} = \frac{1}{E_t} = \frac{1}{E} + \frac{3n}{7E}\left(\frac{\sigma}{\sigma_{0.7}}\right)^{n-1}. \quad (11.97)$$

Thus, the tangent modulus is

$$E_t = \frac{E}{1 + \frac{3n}{7}\left(\frac{\sigma}{\sigma_{0.7}}\right)^{n-1}}. \quad (11.98)$$

For intermediate length columns it has been demonstrated by extensive testing that the critical stress is reasonably well predicted using the Euler curve, eq. (11.93), with the modulus of elasticity replaced by the tangent modulus. This inelastic buckling analysis is called the *tangent modulus theory*. That is,

$$\sigma_{cr} = \pi^2 \frac{E_t}{\left(\frac{KL}{r}\right)^2}. \quad (11.99)$$

Now substitute eq. (11.98) for the tangent modulus in the latter equation, noting that  $\sigma = \sigma_{cr}$ , to get

$$\sigma_{cr} = \frac{\pi^2}{\left(\frac{KL}{r}\right)^2} \left[ \frac{E}{1 + \frac{3n}{7}\left(\frac{\sigma_{cr}}{\sigma_{0.7}}\right)^{n-1}} \right]. \quad (11.100)$$

After division by  $\sigma_{0.7}$ , eq. (11.100) can be written as

$$\frac{\sigma_{cr}}{\sigma_{0.7}} + \frac{3}{7}n\left(\frac{\sigma_{cr}}{\sigma_{0.7}}\right)^n = \frac{1}{\left[\frac{(KL/r)}{\pi\sqrt{E/\sigma_{0.7}}}\right]^2}. \quad (11.101)$$

A plot of the column curve given by eq. (11.101) is shown in figure. 11.21.

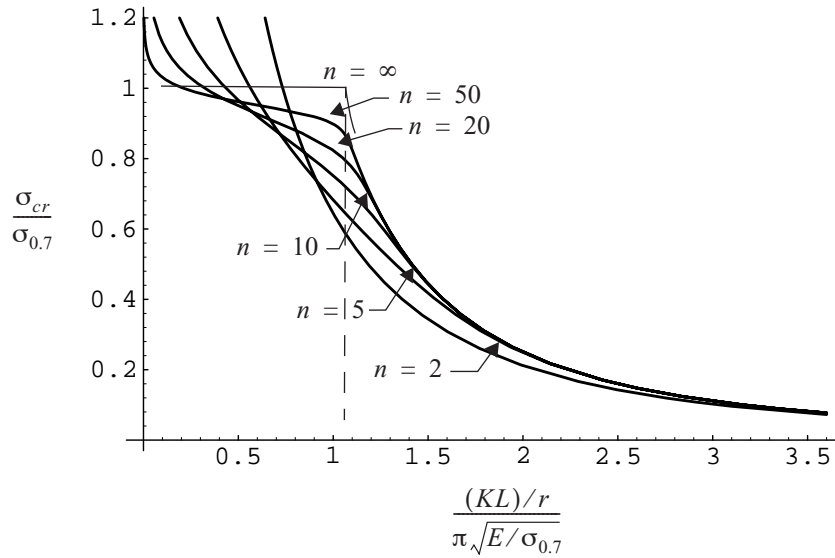
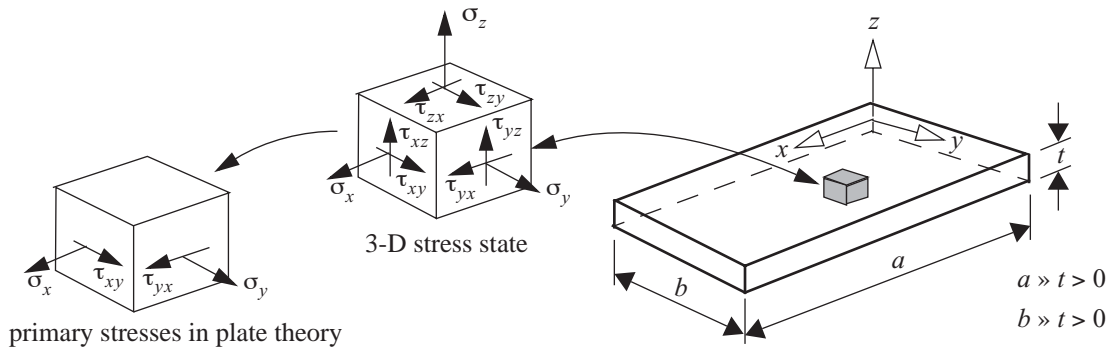


Fig. 11.21 Column curves for a Ramberg-Osgood material law with different shape factors.

## 11.6 Bending of thin plates

Recall that bars and beams are structural elements characterized by having two orthogonal dimensions, say the thickness and width, that are small compared to the third orthogonal dimension, the length. Thin plates, both flat and curved, are common structural elements in flight vehicle structures, and they are characterized by one dimension being small, say the thickness, with respect to the other two orthogonal dimensions, say the width and length. A thin, rectangular, flat plate shown in figure. 11.22 is referenced to Cartesian axes  $x$ ,  $y$ , and  $z$ , where the  $x$ -direction is parallel to the length, the  $y$ -direction is parallel to the width, and the  $z$ -axis is parallel to the thickness of the plate. We denote the length of the plate by  $a$ , the width by  $b$ , and the thickness by  $t$ , and  $0 \leq x \leq a$ ,  $0 \leq y \leq b$ , and  $-t/2 \leq z \leq t/2$ . The plane with  $z = 0$  is the midsurface, or reference surface, of the plate.

A beam resists the transverse loads, or lateral loads, primarily by the longitudinal normal stress  $\sigma_x$ , and the so-called lateral stresses  $\sigma_y$ ,  $\sigma_z$ ,  $\tau_{yx}$ , and  $\tau_{yz}$  are assumed to be negligible. Transverse loads, acting in the  $z$ -direction applied to the plate are primarily resisted by the in-plane stress components  $\sigma_x$ ,  $\sigma_y$ , and  $\tau_{xy}$ . Transverse shear stresses  $\tau_{xz}$  and  $\tau_{yz}$  are necessary for force equilibrium in the  $z$ -direction under transverse loads, but are smaller in magnitude with respect to the in-plane stresses. In plate theory, the transverse normal stress  $\sigma_z$  is very small



**Fig. 11.22** Illustration of the nomenclature and primary stresses for a flat, rectangular plate.

with respect to the in-plane normal stresses and, hence, is neglected. Bending of thin plates is discussed in many texts on plate theory; for example, see Ugural and Fenster (2003). Only some elements of the plate bending theory are discussed here. The assumptions of the linear theory for thin plates are as follows:

1. The deflection of the midsurface is small with respect to the thickness of the plate, and the slope of the deflected midsurface is much less than unity.
2. Straight lines normal to the midsurface in the undeformed plate remain straight and normal to the midsurface in the deformed plate, and do not change length.
3. The normal stress component  $\sigma_z$  is negligible with respect to the in-plane normal stresses and is neglected in Hooke's law.

Now consider the deformation, or strains, caused by the normal stresses. Hooke's law for the normal stresses and strains in a three-dimensional state of stress is

$$\begin{aligned}\epsilon_x &= \frac{1}{E}(\sigma_x - \nu\sigma_y - \nu\sigma_z) \\ \epsilon_y &= \frac{1}{E}(-\nu\sigma_x + \sigma_y + \nu\sigma_z), \\ \epsilon_z &= \frac{1}{E}(-\nu\sigma_x - \nu\sigma_y + \sigma_z)\end{aligned}\tag{11.102}$$

where  $E$  is the modulus of elasticity and  $\nu$  is Poisson's ratio. From assumption **3** the thickness normal stress  $\sigma_z$  is assumed negligible and is set to zero in Hooke's law. From assumption **2** the thickness normal strain  $\epsilon_z = 0$ , because the line element normal to the midsurface does not change length. Since the normal stress  $\sigma_z$  is also assumed to vanish, the third of eq. (11.102) leads to a contradiction. Hence, the third equation of Hooke's law is neglected. The material law for the in-plane normal strains and stresses for thin plates is

$$\begin{aligned}\epsilon_x &= \frac{1}{E}(\sigma_x - \nu\sigma_y) \\ \epsilon_y &= \frac{1}{E}(-\nu\sigma_x + \sigma_y)\end{aligned}\tag{11.103}$$

Consider two cases of pure bending of a plate or a beam subject to moment  $M$ . In the first case the cross section is compact with dimension  $b$  nearly equal to thickness  $t$ , and in the second case dimension  $b$  is much larger

than thickness  $t$ . In the first case the structure is a beam, and in the second case it is a plate. In pure bending the

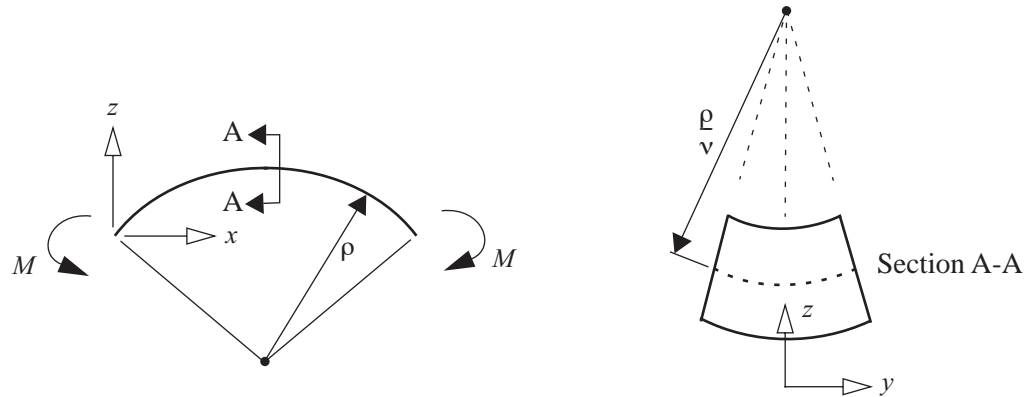


**Fig. 11.23** Pure bending of a beam in the  $x$ - $z$  plane and the associated anticlastic curvature of its cross section.

neutral axis of the beam deforms into an arc of a circle with radius  $\rho$ , and the normal strain in the  $x$ -direction is  $\epsilon_x = z/\rho$ . Note that we assumed that the  $x$ -axis coincided with the neutral axis in the undeformed beam. Hence, longitudinal line elements above the neutral axis,  $z > 0$ , are stretched, and line elements below the neutral axis,  $z < 0$ , are compressed. In the case of a beam, the normal stress in the  $y$ -direction,  $\sigma_y$ , is also very small and is neglected with respect to the longitudinal normal stress  $\sigma_x$ . That is, the beam resists the applied bending moment by the longitudinal normal stress  $\sigma_x$ . Since  $\sigma_y = 0$ , we get from Hooke's law, eq. (11.103), that

$$\begin{aligned}\sigma_x &= E\epsilon_x \\ \epsilon_y &= -\nu\epsilon_x = -\frac{\nu}{\rho}z = -\frac{z}{\left(\frac{\rho}{\nu}\right)}.\end{aligned}\quad (11.104)$$

Hence, the longitudinal normal stress is the modulus of elasticity times the longitudinal normal strain, and the normal strain in the  $y$ -direction is just Poisson's ratio times the longitudinal normal strain. The form of the last expression for  $\epsilon_y$  in eq. (11.104) shows that the line elements in the cross section parallel to the  $y$ -axis before deformation also bend into circular arcs. The line element parallel to the  $y$ -direction at  $z = 0$  in the undeformed beam has a radius of curvature of  $\frac{\rho}{\nu}$  in the deformed beam. This transverse curvature is called *anticlastic curvature*, and is illustrated in figure. 11.23.

Now consider pure bending of a plate under the same moment  $M$ , where now the dimension  $b$  is much larger than thickness  $t$ . In this case experiments show that the transverse line elements remain straight over the central section of the plate, so that the anticlastic curvature is suppressed. In this central section of the plate the transverse normal stress  $\sigma_y$  is non-zero. However, the transverse normal stress must vanish at the free edges at  $y = 0$  and  $y = b$ , so that anticlastic curvature develops only in narrow zones near the free edges to adjust to vanishing of the normal stress  $\sigma_y$  at the free edges. In the central portion of the plate, the associated normal strain is zero. The suppression of anticlastic curvature is characterized by the vanishing of the normal strain  $\epsilon_y$ . Hence from Hooke's law, eq. (11.103), for  $\epsilon_y = 0$  we get

$$\sigma_x = \frac{E}{1-\nu^2} \epsilon_x \quad \sigma_y = \nu \sigma_x. \quad (11.105)$$

Since the denominator in the expression for  $\sigma_x$  is positive but less than unity, the plate is stiffer than the beam owing to the presence of the non-zero transverse normal stress  $\sigma_y$  to help in resisting the applied moment. Compare eqs. (11.104) and (11.105) for the normal stress  $\sigma_x$ . The quantity  $E/(1-\nu^2)$  is an effective modulus of the plate.

### 11.7 Compression buckling of thin rectangular plates

Consider the perfectly flat plate subject to a longitudinal compressive force of magnitude  $P_x$  applied in a spatially uniform manner along edges  $x = 0$  and  $x = a$ , as shown in figure. 11.24. The equilibrium response of the

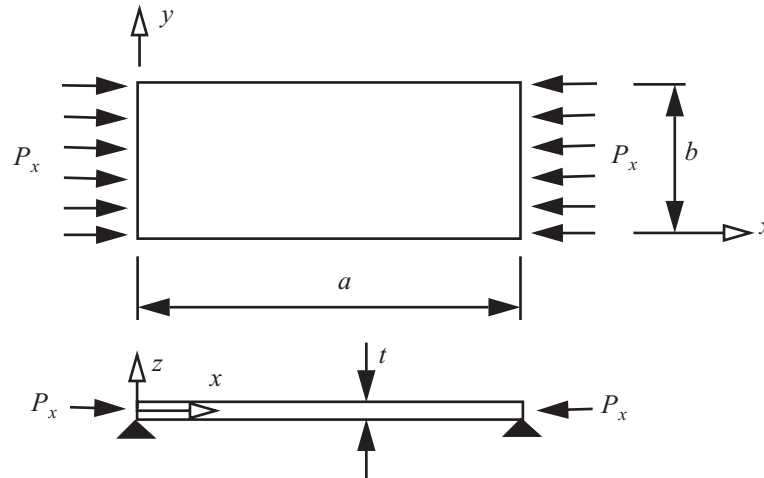


**Fig. 11.24** Uniformly applied compressive forces applied to opposite longitudinal edges of a rectangular plate.

plate in linear theory is that of pure compression in the  $x$ - $y$  plane with no out-of-plane deflection of the midsurface. That is, in the pre-buckling equilibrium state the plate remains flat. The normal stress  $\sigma_x$  in the plate is spatially uniform, and we write it as  $\sigma_x = -\sigma$ , where  $\sigma = P_x/(bt)$  is the applied compressive stress.

At a critical value of the compressive force  $P_{xcr}$  the plate will buckle, or deflect out of the flat pre-buckling equilibrium state. To determine this critical force we have to consider a slightly deflected equilibrium configuration of the plate, similar to the analysis of the perfect column presented in article 11.1. Refer to Brush and Almroth (1975) for the details of this adjacent equilibrium analysis for the critical force.

Instead of a detailed adjacent equilibrium analysis of the plate, we can make a comparison to the critical force determined for the pinned-pinned column in figure. 11.6. The configuration of the plate comparable to the pinned-pinned column has simply supported, or hinged, edges at  $x = 0$  and  $x = a$ , and has free edges at  $y = 0$  and  $y = b$ . The compressively loaded plate for these boundary conditions is called a *wide column*. The critical force for the pinned-pinned column is



$$P_{cr} = \pi^2 \frac{EI}{L^2}. \quad (11.106)$$

For the plate, replace the modulus of elasticity  $E$  in the column formula by  $E/(1 - \nu^2)$ , since the plate is stiffer than the column. Also set  $L = a$  for the plate. The formula for the second area moment of a rectangular cross section is  $I = (bt^3)/12$ . Hence, eq. (11.106) transforms to

$$P_{xcr} = \pi^2 \left( \frac{E}{1 - \nu^2} \right) \left( \frac{1}{a^2} \right) \left( \frac{bt^3}{12} \right) = \pi^2 \left( \frac{Et^3}{12(1 - \nu^2)} \right) \frac{b}{a^2}. \quad (11.107)$$

For the *wide column* configuration of the plate, the critical load is written in the form

$$P_{xcr} = \frac{\pi^2 D b}{a^2}, \quad (11.108)$$

where the bending stiffness, or flexural rigidity, of the plate is defined as

$$D = \frac{Et^3}{12(1 - \nu^2)}. \quad (11.109)$$

The critical compressive stress at buckling is simply  $\sigma_{cr} = P_{xcr}/(bt)$ . Divide eq. (11.107) by area  $bt$  to get

$$\sigma_{cr} = \pi^2 \left( \frac{Et^3}{12(1 - \nu^2)} \right) \frac{b}{a^2} \frac{1}{bt} = \pi^2 \frac{E}{12(1 - \nu^2)} \left( \frac{t}{b} \right)^2 \left( \frac{b}{a} \right)^2.$$

By convention, this critical compressive stress is written in the form

$$\sigma_{cr} = k_c \pi^2 \frac{E}{12(1 - \nu^2)} \left( \frac{t}{b} \right)^2 \quad (11.110)$$

where  $k_c$  is a nondimensional buckling coefficient for compressive loading, which is a function of the plate aspect ratio  $a/b$ . For the unloaded edges free and the loaded edges simply supported, this buckling coefficient is

$$k_c = \frac{1}{(a/b)^2} \quad \text{wide column}. \quad (11.111)$$

For other support conditions on the edges  $x = 0$ ,  $x = a$ ,  $y = 0$ , and  $y = b$ , the critical compressive stress is also given by eq. (11.110) but the compressive buckling coefficient is a different function of the plate aspect ratio. The transition from column to plate as supports are added along the unloaded edges ( $y = 0$  and  $y = b$ ) are depicted in figure. 11.25 on page 349. The compressive buckling coefficient is plotted for various support conditions as shown in figure. 11.26 on page 350. Note that some of the curves for the buckling coefficient exhibit cusps, or discontinuous slopes, at selected values of the plate aspect ratio. The cusps correspond to changes in the half wave length of the buckle pattern along the  $x$ -direction. In particular, for the plate with simple support on all four edges, case C in figure. 11.26 on page 350, note that  $k_c = 4$  for integer aspect ratios.

### 11.7.1 Simply supported rectangular plate

Consider a plate simply supported on all four edges and subject to uniform compressive on edges  $x = 0$  and  $x = a$ . In the pre-buckling equilibrium configuration the plate remains flat,  $w_0(x, y) = 0$ , with a spatially uniform compressive stress equal to the applied compressive stress  $\sigma$ . From the method of adjacent equilibrium, the out-of-plane displacement of the plate at the onset of buckling is

$$w_1(x, y) = A_1 \sin\left(\frac{m\pi x}{a}\right) \sin\left(\frac{n\pi y}{b}\right), \quad (11.112)$$

where  $m$  and  $n$  are positive integers and  $A_1$  is an arbitrary amplitude. Integer  $m$  corresponds to the number of half waves in the  $x$ -direction and integer  $n$  corresponds to the number of half waves in the  $y$ -direction. Thus, specific values of integers  $m$  and  $n$  in eq. (11.112) characterize a buckling mode, and for each buckling mode there is a corresponding buckling stress. Equation (11.110) is the formula for the compressive stress at buckling, with the compressive buckling coefficient given by

$$k_c = \left( \frac{m}{a/b} + n^2 \frac{(a/b)}{m} \right)^2 \quad m, n = 1, 2, \dots \quad (11.113)$$

The critical stress is the lowest buckling stress, which occurs for a certain choice of  $m$  and  $n$ . Since  $k_c$  is directly proportional to powers of integer  $n$ , the minimum value of  $k_c$  occurs for  $n = 1$ . Then minimum values of  $k_c$  are related to  $a/b$  and integer  $m$  by

$$k_c = \left( \frac{m}{a/b} + \frac{(a/b)}{m} \right)^2. \quad (11.114)$$

Fig. 11.25 Transition from column to plate as supports are added along unloaded edges. Note changes in buckle configurations (NACA TN 3781, figure 1).

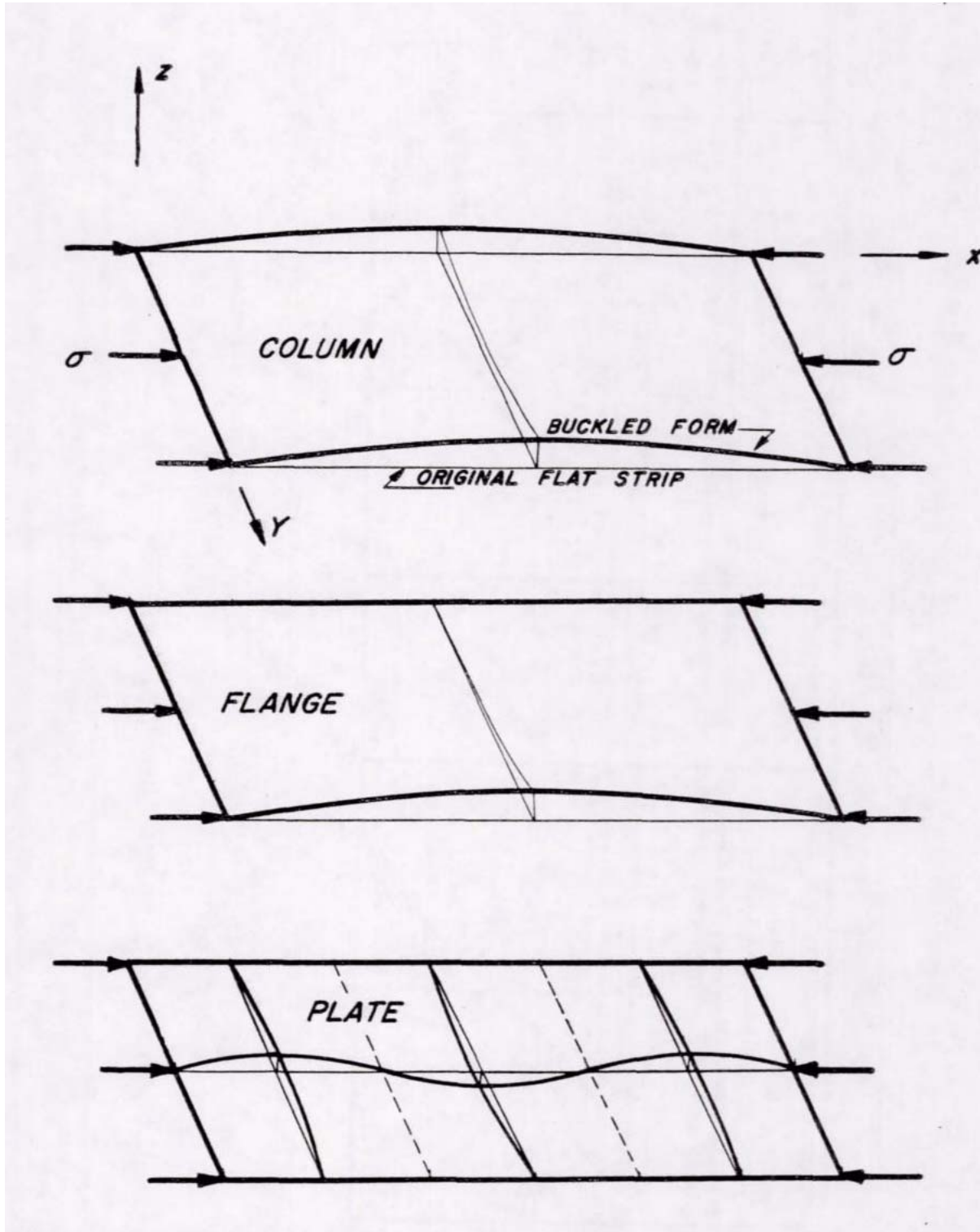
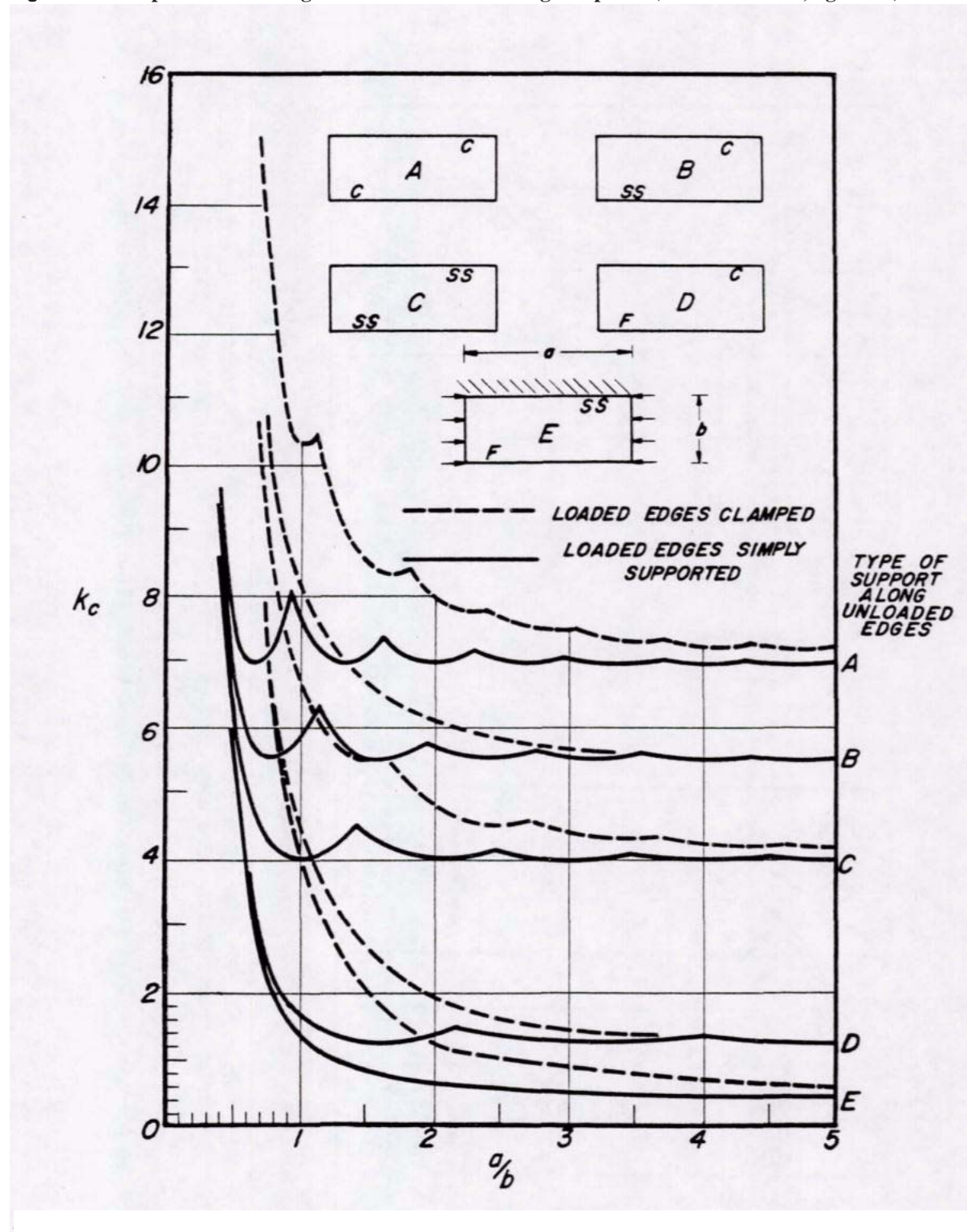


Fig. 11.26 Compression buckling coefficient for flat rectangular plates (NACA TN 3781, figure 14).



Critical values of the compressive buckling coefficient as a function of a few aspect ratios are listed in table 11.4.

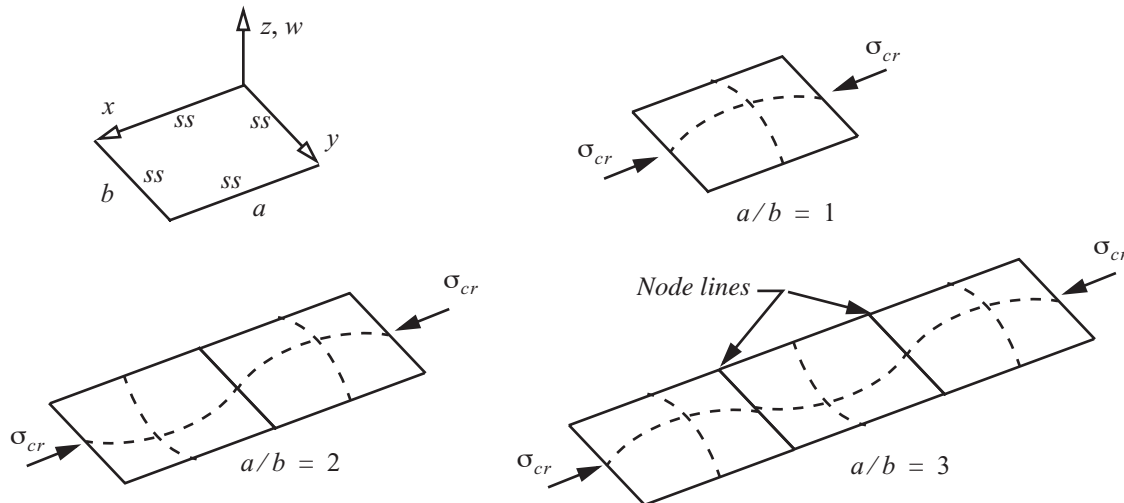
**Table 11.4** Compression buckling coefficient for selected plate aspect ratios

Plate aspect ratio	Number of half waves in the x-direction	Critical compressive buckling coefficient
$0 < a/b \leq \sqrt{2}$	$m = 1$	$k_{cr} = \left( \frac{1}{a/b} + \frac{a/b}{1} \right)^2$
$\sqrt{2} \leq a/b \leq \sqrt{6}$	$m = 2$	$k_{cr} = \left( \frac{2}{a/b} + \frac{a/b}{2} \right)^2$
$\sqrt{6} \leq a/b \leq \sqrt{12}$	$m = 3$	$k_{cr} = \left( \frac{3}{a/b} + \frac{a/b}{3} \right)^2$

These critical values of the compression buckling coefficient are plotted as case C in figure. 11.26 on page 350. The buckling modes for three integer values of the aspect ratio are depicted in figure. 11.27. There is one half wave across the width ( $n = 1$ ) and the number of half waves across the length,  $m$ , increases with increasing aspect ratio. For integer values of the aspect ratio the critical value of the compressive buckling coefficient  $k_{cr} = 4$ , and it follows that the critical compressive stress is

$$\sigma_{cr} = 4\pi^2 \frac{E}{12(1-\nu^2)} \left( \frac{t}{b} \right)^2 \quad \frac{a}{b} = m = 1, 2, 3, \dots \quad n = 1. \quad (11.115)$$

From eq. (11.112) the length of a half wave in the  $x$ -direction is  $a/m$ , and the length of a half wave in the  $y$ -direction is the plate width  $b$  for  $n = 1$ . These half wave lengths are the same when  $a/m = b$ , or  $a/b = m$ . That is, the half wave lengths in the  $x$ - and  $y$ -directions are the same for integer values of the aspect ratio. Hence, for integer values of the plate aspect ratio the buckling mode consists of a sequence of *square buckles*.



**Fig. 11.27** Compression buckling modes for integer aspect ratios of a simply supported rectangular plate.

**Example 11.4 Critical load for simply supported rectangular plate in compression**

Let  $a = 20$  in.,  $b = 10$  in.,  $t = 0.10$  in.,  $E = 10 \times 10^6$  lb./in.<sup>2</sup>, and  $\nu = 0.3$ . From eq. (11.110) the critical compressive stress

$$\sigma_{cr} = k_c(903.81 \text{ lb./in.}^2). \quad (\text{a})$$

From eq. (11.114) the compression buckling coefficient is

$$k_c = \left( \frac{m}{2} + \frac{2}{m} \right)^2. \quad (\text{b})$$

For  $m = 1, 2, 3$ ,  $k_c = 6.25, 4.0, 4.694$ , respectively. For larger values of  $m$ , coefficient  $k_c$  is larger. The minimum value of  $k_c$  is 4 corresponding to  $m = 2$ . Hence, the critical stress is

$$\sigma_{cr} = 3,615.24 \text{ lb./in.}^2. \quad (\text{c})$$

The critical compressive load  $P_{cr} = \sigma_{cr}bt$ . Hence,

$$P_{cr} = 3,615 \text{ lb.} \quad (\text{d})$$

The buckling mode for  $(m, n) = (2, 1)$  has one half sine wave in the transverse direction and two half waves in the longitudinal direction. The load  $P_{cr} = 3,615$  lb. is the lowest load at which such a plate can lose its stability. ■

**11.8 Buckling of flat rectangular plates under shear loads**

Consider a thin, rectangular plate with a thickness denoted by  $t$ , and the in-plane dimensions denoted by  $a$  and  $b$ , where  $0 < t \ll b \leq a$ . Note that  $a$  denotes the long dimension of the plate and  $b$  denotes the short dimension. It is subject to uniformly distributed shear stress  $\tau$  as illustrated in figure. 11.28. From Mohr's circle for plane stress,

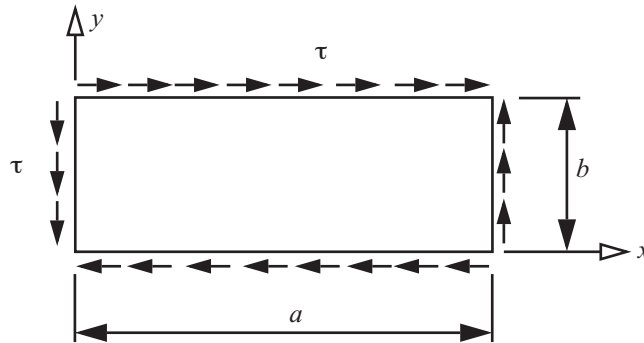


**Fig. 11.28 Plate subject to in-plane shear loading.**

the state of pure shear is equivalent to tensile and compressive normal stresses at forty-five degrees to the direction of pure shear. It is this compressive normal stress that leads to buckling of the thin plate subjected to shear.

The critical value of the shear stress per unit length,  $\tau_{cr}$ , is given by the formula

$$\tau_{cr} = k_s \pi^2 \frac{E}{12(1-\nu^2)} \left(\frac{t}{b}\right)^2, \quad (11.116)$$

where  $k_s$  is a nondimensional buckling coefficient for shear loading. This buckling coefficient is a function of the plate aspect ratio  $a/b$  and the boundary conditions applied to the plate. Values of the shear buckling coefficient are given in figure. 11.30 on page 354. The buckling mode labeled the symmetric mode in the figure pertains to a buckled form that is symmetric with respect to a diagonal across the plate at the node line slope. For a narrow range of aspect ratios the plate buckles in an antisymmetric mode. For an infinitely long strip, or  $a/b \rightarrow \infty$ ,  $k_s = 5.35$  for simply supported, or hinged, edges at  $y = 0, b$ , and  $k_s = 8.98$  for clamped edges.

A least squares fit of the shear buckling coefficient as a function of the plate aspect ratio is convenient in problem solving. For the simply supported plate, or the plate with hinged edges, the data listed in table 11.5 was read from the graph in figure. 11.30.

**Table 11.5 Shear buckling coefficient for selected plate aspect ratios**

$a/b$	$k_s$
1	9.6
2	6.4
3	5.8
4	5.7
5	5.5

These data are fit to the functions 1 and  $\frac{1}{a/b}$ . The result of the least squares fit to these data is

$$k_s = 4.22565 + \frac{5.19931}{a/b} \quad 1 \leq a/b \leq 5. \quad (11.117)$$

The least squares fit and the input data are plotted in figure. 11.29.

**Fig. 11.29 Graph of eq. (11.117) compared to discrete data listed in table 11.5.**

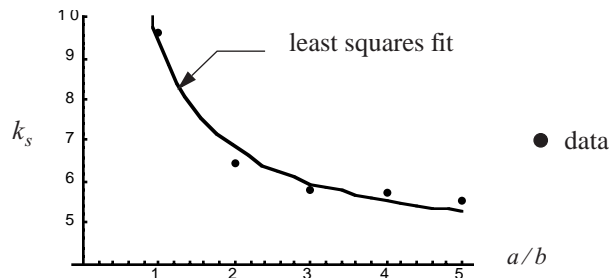
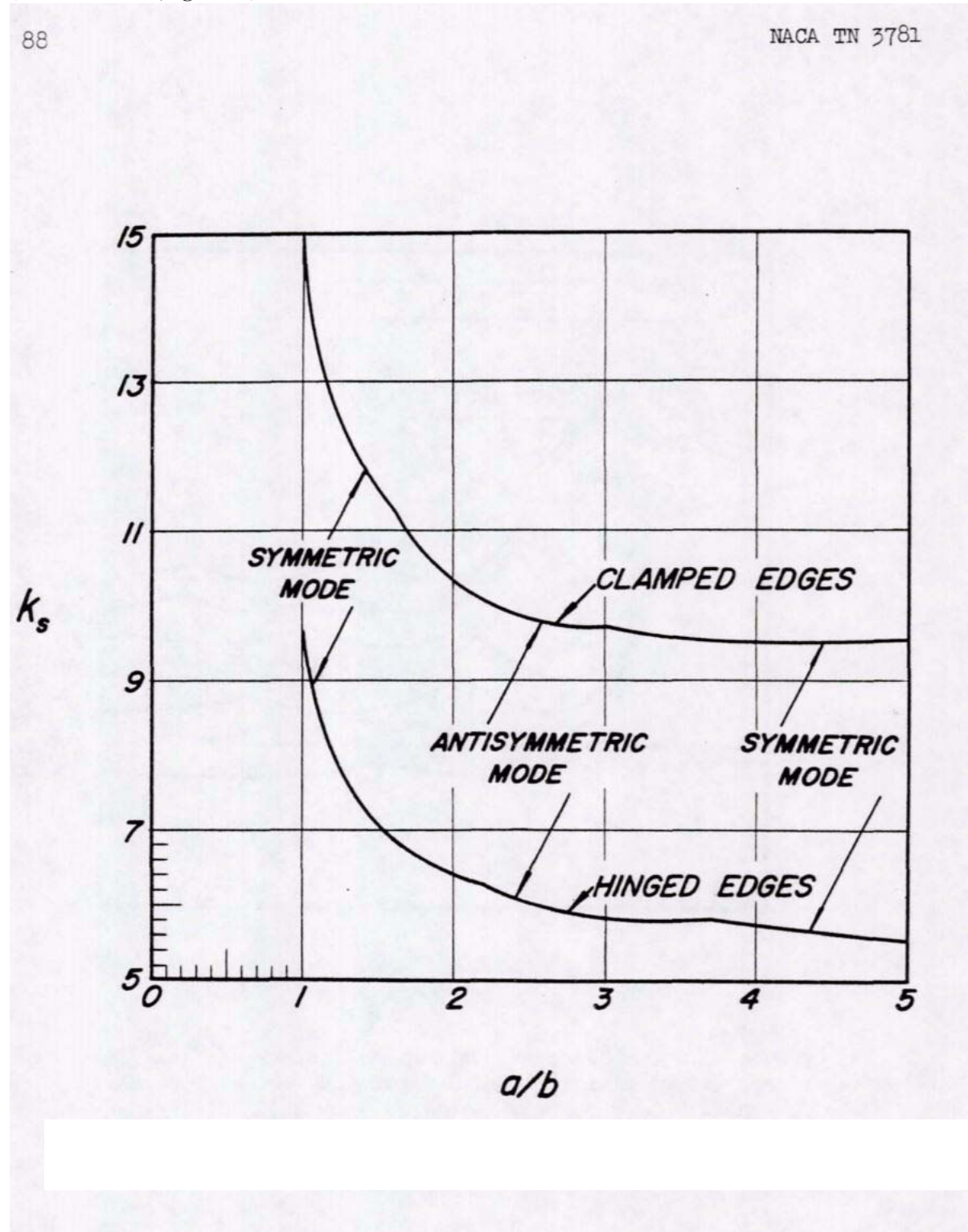




Fig. 11.30 Shear-buckling-stress coefficient of plates as a function of  $a/b$  for clamped and hinged edges (NACA TN 3781, figure 22).





### 11.9 Buckling of flat rectangular plates under combined compression and shear

A plate subject to uniformly applied longitudinal compression and shear is shown in figure. 11.31. The critical

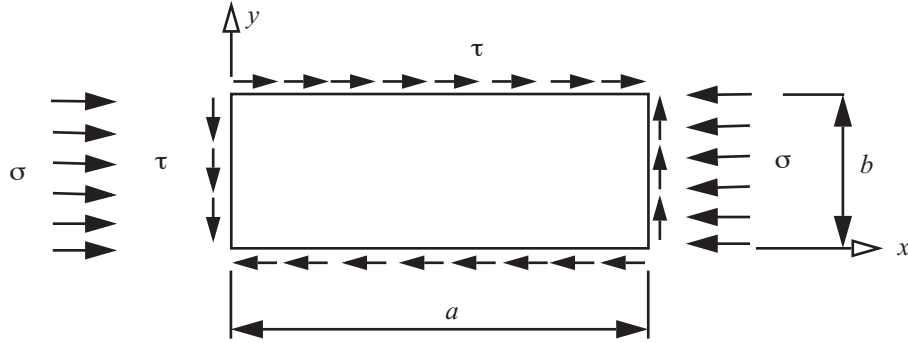


Fig. 11.31 Plate subject to longitudinal compression and in-plane shear loading.

combination of shear and compression stresses under different boundary conditions and different aspect ratios of the plate can be approximated to a sufficient accuracy by

$$\left(\frac{\tau}{\tau_{cr}}\right)^2 + \left(\frac{\sigma}{\sigma_{cr}}\right) = 1, \quad (11.118)$$

where  $\tau_{cr}$  and  $\sigma_{cr}$  are the critical values of the separately acting shear stress and the compression normal stress, respectively (NACA TN 3781, pp. 38, 39). Equation (11.118) is plotted in figure. 11.32.

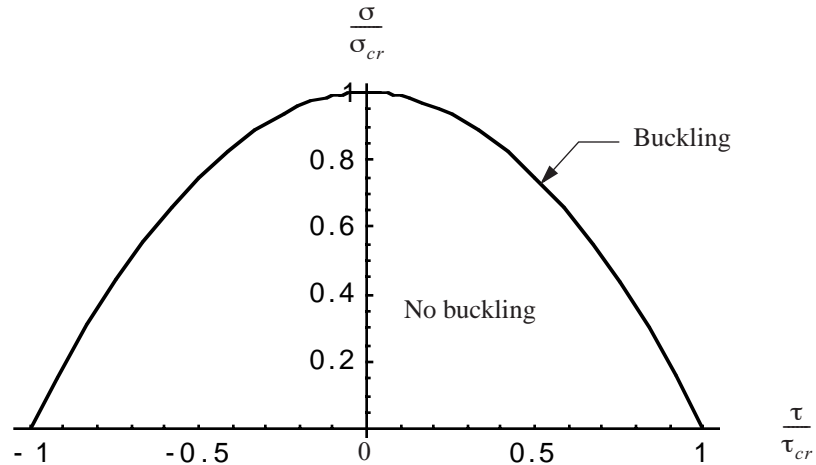


Fig. 11.32 Buckling interaction relationship for critical combinations of shear and compression.

### Example 11.5 Wing rib spacing based on a buckling constraint

The stringer stiffened box beam that is the main spar in a wing is shown in figure. 11.33. For a pull-up maneuver, the calculated transverse shear force  $V_y = 25,000$  lb. and the bending moment  $M_x = -4.14 \times 10^6$  lb-in. at the wing root. The thickness and width of the upper and lower cover skins are  $t_f = 0.5$  in. and  $b_f = 24$  in., respectively. The thickness and height of the left and right webs are  $t_w = 0.30$  in. and  $b_w = 13$  in., respectively, and the flange area of the stringers  $A_f = 2.0$  in.<sup>2</sup>. The material is isotropic with properties  $E = 10 \times 10^6$  lb/in.<sup>2</sup> and  $\nu = 0.3$ . For  $M_x < 0$ , the upper skin is in compression. Determine the rib spacing, denoted by  $a$ , such that the margin of safety for buckling of the upper skin is slightly positive.

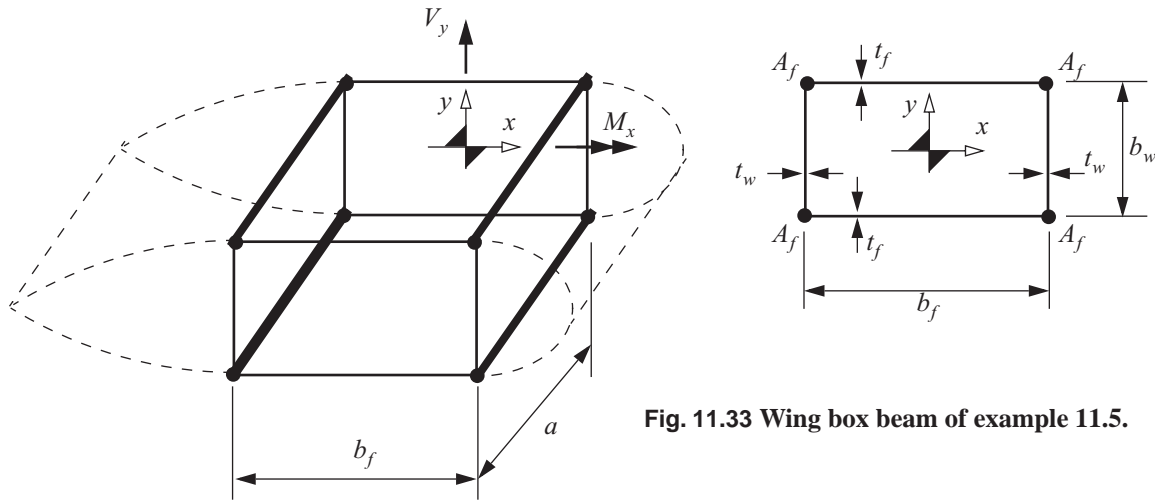


Fig. 11.33 Wing box beam of example 11.5.

**Solution.** The centroid and the shear center of the cross section coincide with the center of the box beam due to symmetry. The normal stress due to bending in the upper skin is calculated from the flexure formula; i.e.,

$$\sigma_z = \frac{M_x(b_w/2)}{I_{xx}}, \quad (a)$$

where the second area moment of the cross section about the  $x$ -axis is

$$I_{xx} = b_w^2 A_f + \frac{1}{2} b_f b_w^2 t_f + \frac{1}{6} b_w^3 t_w = 1,461.85 \text{ in.}^4 \quad (b)$$

Hence, the bending normal stress in the upper skin is

$$\sigma_z = -18,408.2 \text{ lb./in.}^2. \quad (c)$$

The shear stress in the upper skin is determined from the analysis of the shear flow distribution around the contour of the cross section, which is shown in figure. 11.34.

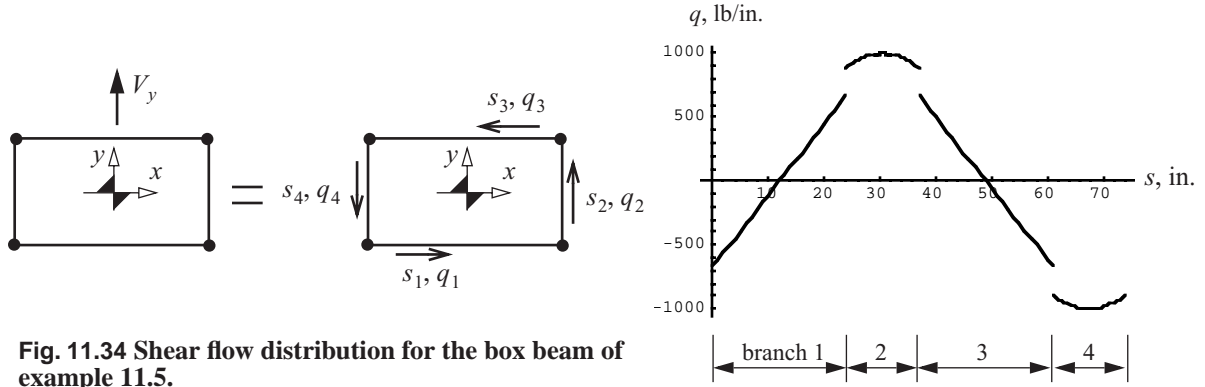


**Fig. 11.34** Shear flow distribution for the box beam of example 11.5.

The shear flow in the upper skin is

$$q_3 = \frac{b_w t_f (b_f - 2s_3)}{4I_{xx}} V_y \quad 0 \leq s_3 \leq b_f. \quad (d)$$

The shear stress  $\tau_3 = q_3/t_f$ , and its evaluation is

$$\tau_3 = 55.5803(24 - 2s_3) \text{ lb./in.}^2 \quad 0 \leq s_3 \leq 24 \text{ in.} \quad (e)$$

Computing the maximum magnitude and the average value of this shear stress results in

$$|\tau_3|_{\max} = 1,333.93 \text{ lb/in.}^2 \quad (\tau_3)_{\text{ave}} = \frac{1}{b_f} \int_0^{b_f} \tau_3 ds_3 = 0. \quad (f)$$

The maximum magnitude of the shear stress in the upper skin is 7.25 percent of the magnitude of the bending normal stress. Moreover, the average value of the shear stress is zero in the upper skin. Hence, it is reasonable to neglect the effect of the shear stress on the buckling of the upper skin.

Assume the upper skin is a simply supported rectangular plate between the stringers and ribs. Actually, the stringer and ribs provide rotational constraint to the upper skin, but the assumption of no rotational constraint is conservative with respect to design. The critical compressive stress for simple support on all four edges of the upper skin underestimates its actual value. Equation (11.110) for the top cover skin is

$$\sigma_{cr} = k_c \pi^2 \frac{E}{12(1 - \nu^2)} \left( \frac{t_f}{b_f} \right)^2, \quad (g)$$

and eq. (11.114) for the compression buckling coefficient is

$$k_c = \left( \frac{m}{a/b_f} + \frac{a/b_f}{m} \right)^2 \quad m \text{ a positive integer to minimize } k_c. \quad (a)$$

The margin of safety is defined by

$$MS = \frac{\text{Excess strength}}{\text{Required strength}} = \frac{\sigma_{cr} - |\sigma_z|}{|\sigma_z|}. \quad (11.119)$$

The margin of safety (11.119) is positive for a feasible design, otherwise the design is infeasible. It should be a small positive value for a design of least weight. The computations for the margin of safety are listed in table 11.6.

**Table 11.6** Margin of safety for selected rib spacings

a, in.	a/b <sub>f</sub>	k <sub>c</sub>	σ <sub>cr</sub> , lb./in. <sup>2</sup>	Margin of safety	Design
14	0.583	5.27905	20,708.6	0.12497	feasible
15	0.625	4.95063	19,420.2	0.05498	feasible
16	0.667	4.69444	18,415.3	0.000387	feasible
17	0.708	4.49482	17,632.20	− 0.04215	infeasible
18	0.750	4.34028	17,026.0	− 0.07509	infeasible
19	0.792	4.2223	16,563.2	− 0.1002	infeasible

A rib spacing of 16 in. is a feasible design with a slightly positive margin of safety. ■

## 11.10 References

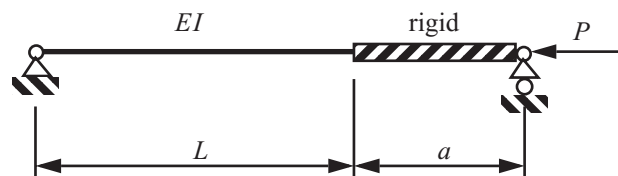
- Brush, D. O., and B. O. Almroth. *Buckling of Bars, Plates, and Shells*. New York: McGraw-Hill, 1975, pp. 75-105.
- Budiansky, B., and J. W. Hutchinson. "Dynamic Buckling of Imperfection-Sensitive Structures." In *Proceedings of the Eleventh International Congress of Applied Mechanics* (Munich, Germany). 1964, pp. 639-643.
- Budiansky, B. "Dynamic Buckling of Elastic Structures: Criteria and Estimates." In *Proceedings of an International Conference at Northwestern University* (Evanston IL). New York and Oxford: Pergamon Press, 1966.
- Gerard, G., and H. Becker. *Handbook of Structural Stability: Part I, Buckling of Flat Plates*. Technical Report NACA-TN 3781. Washington, DC: Office of Scientific and Technical Information, U.S. Department of Energy, 1957.
- Koiter, W. T. "The Stability of Elastic Equilibrium." PhD diss., Technische Hoog School, Delft, The Netherlands, 1945. (English translation published as Technical Report AFFDL-TR-70-25, Air Force Flight Dynamics Laboratory, Wright-Patterson Air Force Base, OH, February 1970.)
- National Advisory Committee for Aeronautics (NACA), Technical Note 3781 (NACA-TN-3781) July 1957. <https://ntrs.nasa.gov/api/citations/1930084505/downloads/19930084505.pdf>.
- Ramberg, W., and Osgood, W. *Description of Stress-Strain Curves by Three Parameters*. Technical Report NACA-TN-902. Washington DC: NASA, 1943.
- Southwell, Richard V. "On the Analysis of Experimental Observations in Problems of Elastic Stability." *Proc. Roy. Soc. London A*, no. 135 (April 1932): 601-616.
- Timoshenko, S. P., and J. M. Gere. *Theory of Elastic Stability*. New York: McGraw-Hill Book Company, 1961, p.33.

Ugural A. C., and S. K. Fenster. **Advanced Strength and Applied Elasticity**, 4th ed., Upper Saddle River, NJ: Pearson Education, Inc., Publishing as Prentice Hall Professional Technical Reference, 2003, pp. 472-490.

### 11.11 Practice exercises

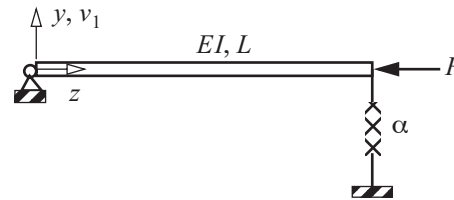
1. An ideal column of length  $L$  is pinned at one end and fixed to a rigid bar of length  $a$  at the other end. The second end of the rigid bar is pinned on rollers. Refer to figure. 11.35 Find the critical load  $P_{cr}$  and discuss the extreme cases of  $a \rightarrow 0$  and  $a \rightarrow \infty$ .

Fig. 11.35 Exercise 1.



2. The column shown in figure. 11.36 is pinned at the left end and supported by an extensional spring of stiffness  $\alpha$  at the loaded right end.

Fig. 11.36 Exercise 2.



- a) Use the **adjacent equilibrium method** to show that the characteristic equation is

$$-k^2 \sin kL \left[ -k^2 + \frac{\alpha L}{EI} \right] = 0.$$

- b) Plot the critical load  $P_{cr}$  as a function of  $\alpha$ ,  $0 \leq \alpha$ . For what values of  $\alpha$  will the column buckle in the Euler mode? (i.e., case A in figure. 11.6).
3. The statically indeterminate truss shown in figure. 11.37 consists of six bars, labeled 1-2, 1-3, 1-4, 2-3, 2-4, and 3-4. It is subject to a vertical force  $F$  at joint number 2. The cross-sectional area of each bar is  $2,000 \text{ mm}^2$ , the second area moment of each bar is  $160,000 \text{ mm}^4$ , and the modulus of elasticity of each bar is  $75,000 \text{ N/mm}^2$ .

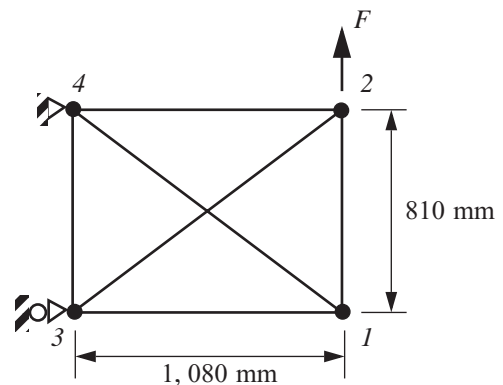


Fig. 11.37 Truss for exercise 3.

- a) Take bar force 1-4 as the redundant (i.e.,  $N_{1-4} = Q$ ). Using Castiglano's second theorem to determine the redundant  $Q$  in terms of the external load  $F$ .
- b) Determine the value of  $F$  in kN to initiate buckling of

the truss.

- c) If the yield strength of the material is 400 MPa in tension, determine the value of  $F$  in kN to initiate yielding of the truss.

4. Bars 1-2, 2-3, and 2-4 of the truss shown figure. 11.38 are unstressed at the ambient temperature. Only bar 1-2 is heated above the ambient temperature. Determine the increase in temperature, denoted by  $\Delta T$ , of bar 1-2 to cause buckling of the truss. The cross section of each bar is a thin-walled tube with radius  $R = 13$  mm and wall thickness  $t = 1.5$  mm. Take length  $L = 762$  mm. All three bars are made of the same material with properties  $E = 75,000$  N/mm<sup>2</sup> and  $\alpha = 23 \times 10^{-6}$  /°C.

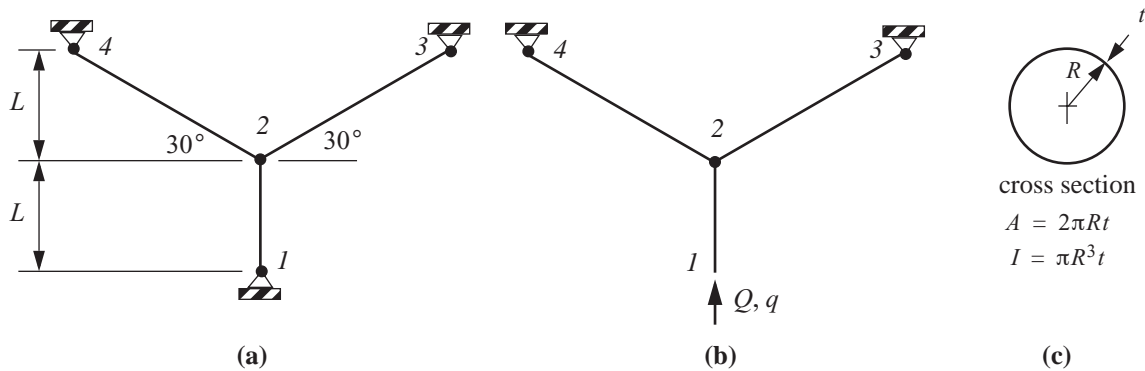


Fig. 11.38 Exercise 4. (a) three-bar truss, (b) base structure. (c) cross section of the bars.

5. Consider the wing spar in example 11.5. A counterclockwise torque  $T = 6 \times 10^6$  lb.-in. is specified to act at the root cross section in addition to the specified transverse shear force and bending moment. Determine the rib spacing, denoted by  $a$ , such that the margin of safety with respect to buckling of the upper skin is slightly positive. Report the value of  $a$  to two significant figures and the associated margin of safety. The margin of safety is defined by the formula

$$MS = \frac{1 - f_b}{f_b} \quad \text{where} \quad f_b = \left( \frac{\tau}{\tau_{cr}} \right)^2 + \frac{\sigma}{\sigma_{cr}}.$$

Use the average value of the shear stress over the width of the upper skin for the shear stress  $\tau$  in the margin of safety formula. Remember that dimension  $b$  is smaller than dimension  $a$  in the formula for the critical value of the shear stress, and that  $b$  is the width of the plate/skin on which the compressive normal stress acts in the formula for  $\sigma_{cr}$ .

---

## *Introduction to aeroelasticity*

---

### *12.1 The Collar diagram of aeroelastic forces*

The following paragraphs are excerpted from *Aeroelasticity* by R. L. Bisplinghoff, H. Ashley, and R. L. Halfman (1996).

Aeroelasticity is defined as a science which studies the mutual interaction between aerodynamic forces and elastic forces, and the influence of this interaction on airplane design. Aeroelastic problems would not exist if the airplane structure were perfectly rigid. Modern airplane structures are very flexible, and this flexibility is fundamentally responsible for the various types of aeroelastic phenomena. Structural flexibility itself may not be objectionable; however, aeroelastic phenomena arise when structural deformations induce additional aerodynamic forces. Such interactions may become smaller and smaller until a condition of stable equilibrium is reached, or they may tend to diverge and destroy the structure.

The term aeroelasticity, however, is not completely descriptive, since many important aeroelastic phenomena involve inertial forces as well as aerodynamic and elastic forces. We shall apply a definition in which the term aeroelasticity includes phenomena involving interactions among inertial, aerodynamic, and elastic forces, and other phenomena involving interactions between aerodynamic and elastic forces. The former will be referred to as *dynamic* and the latter as *static* aeroelastic phenomena.

Collar has ingeniously classified problems in aeroelasticity by means of a triangle of forces. Referring to Fig. 1-1 [figure. 12.1 below], the three types of forces, aerodynamic, elastic, and inertial are represented by the symbols  $A$ ,  $E$ , and  $I$ , respectively, are placed at the vertices of a triangle. Each aeroelastic phenomenon can be located on the diagram according to its relation to the three vertices. For example, dynamic aeroelastic phenomena such as flutter  $F$ , lie within the triangle, since they involve all three types of forces and must be bonded to all three vertices. Static aeroelastic phenomena such as wing divergence,  $D$ , lie outside the triangle on the upper left side, since they involve only aerodynamic and elastic forces. Although it is difficult to define precise limits on the field of aeroelasticity, the classes of problems connected by solid lines to the vertices in Fig. 1-1 are usually accepted as the principal ones. Of course, other borderline fields of mechanical vibrations,  $V$ , and rigid-body aerodynamic stability,  $DS$ , are connected to the vertices by dotted lines. It is very likely that in certain cases the dynamic

stability problem is influenced by airplane flexibility and it would therefore be moved within the triangle to correspond with *DSA*, where it would be regarded as a dynamic aeroelastic problem.

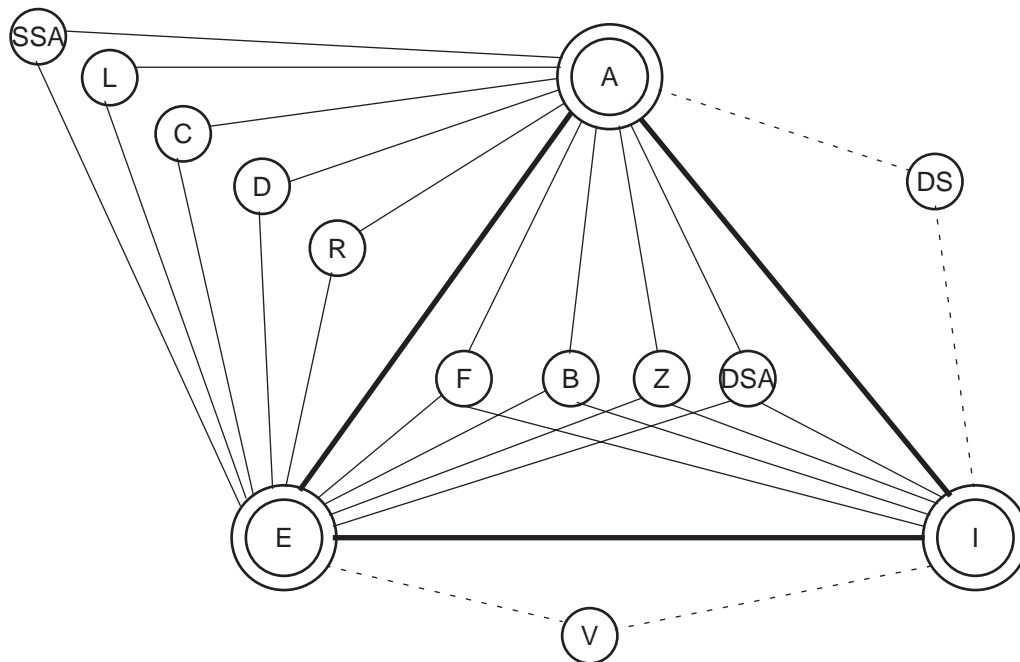


**Fig. 12.1** The aeroelastic triangle of forces.

It would be convenient to state concise definitions of each aeroelastic phenomenon which appears on the diagram in Fig. 1-1.

*Flutter, F.* A dynamic instability occurring in an aircraft in flight at a speed called the flutter speed, where the elasticity of the structure plays an essential part in the instability.

*Buffeting, B.* Transient vibrations of aircraft structural components due to aerodynamic impulses produced by the wake behind wings, nacelles, fuselage pods, or other components of the airplane.

*Dynamic response, Z.* Transient response of aircraft structural components produced by rapidly applied loads due to gusts, landing, gun reactions, abrupt control motions, moving shock waves, or other dynamic loads.

*Aeroelastic effects on stability, DSA & SSA.* Influence of elastic deformations of the structure on dynamic and static airplane stability.

*Load distribution, L.* Influence of elastic deformations of the structure on the distribution of aerodynamic pressures over the structure.

*Divergence, D.* A static instability of a lifting surface of an aircraft in flight, at a speed called the divergence speed, where the elasticity of lifting surface plays an essential role in the instability.

*Control effectiveness, C.* Influence of elastic deformations of the structure on the controllability of an airplane.

*Control system reversal, R.* A condition occurring in flight, at a speed called the control



reversal speed, at which the intended effects of displacing a given component of the control system are completely nullified by elastic deformations of the structure.

*Mechanical vibrations*, V. A related field.

*Dynamic stability*, DS. A related field.

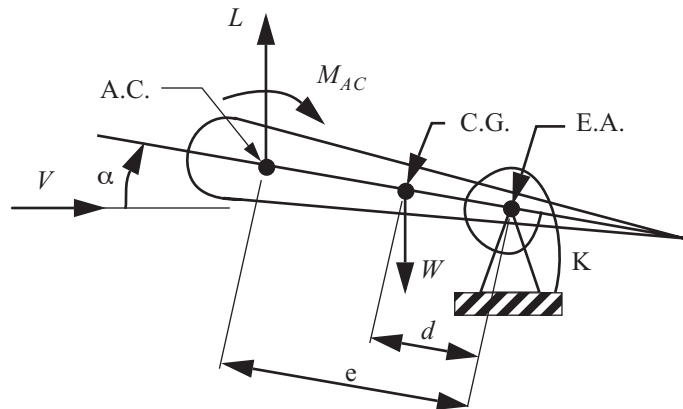
## 12.2 Divergence analysis of a rigid wing segment

A model to illustrate the phenomenon of wing divergence consists of a uniform, rigid wing segment hinged to a fixed support in a wind tunnel as is shown in figure. 12.2. The hinge line is located at the **elastic axis** (E.A.) of the wing. The elastic axis coincides with the locus of shear centers of the wing sections.

Recall that the **shear center** of the cross section of a bar (wing) is a reference point in the cross section where the lateral deflections due to bending are de-coupled from the twist due to torsion (i.e., a shear force acting at the elastic axis results in bending deflections and no twist, and a torque acting at the elastic axis causes twist but no lateral deflection of the elastic axis due to bending).

The rigid wing segment is restrained against rotation, or twist, about the E.A. by a linear elastic rotational spring of stiffness  $K$ . This rotational spring is analogous the torsional stiffness per unit span, or  $(GJ)/L$ , of a wing.

**Fig. 12.2** Rigid wing segment model for divergence analysis



We assume two-dimensional, incompressible aerodynamics is applicable. Let  $V$  denote the airspeed,  $\alpha$  the angle of attack relative to the zero lift angle,  $L$  the lift,  $M_{AC}$  the pitching moment, and let  $W$  denote the weight of the wing segment acting at the center of gravity (C.G.). The lift and pitching moment act at the aerodynamic center (A.C.), which is the point about which the pitching moment is independent of the angle of attack. Usually the A.C. is close to the quarter chord. We neglect the drag force  $D$  relative to the lift since  $D \ll L$ .

The angle of attack is written as

$$\alpha = \alpha_0 + \theta, \quad (12.1)$$

where  $\alpha_0$  is the initial wing incidence, or the angle of attack if there are no aerodynamic and gravity loads, and

$\theta$  is the rotation angle due to elastic deformations of the spring. Assume small angles such that  $\sin \alpha \approx \alpha$ ,  $\cos \alpha \approx 1$ , and  $\tan \alpha \approx \alpha$ . The lift is given by

$$L = qSC_L, \quad (12.2)$$

where  $q$  is the dynamic pressure,  $S$  is the wing planform area, and  $C_L$  is the lift coefficient. Let  $\rho$  denote the density of air,  $c$  the chord length, and  $s$  the wing span. The dynamic pressure, planform area, and lift coefficient are given by

$$q = \frac{1}{2} \rho V^2 \quad S = cs \quad C_L = \left( \frac{\partial C_L}{\partial \alpha} \right) \alpha. \quad (12.3)$$

In the above equation  $(\partial C_L)/(\partial \alpha)$  is the lift curve slope, which is assumed constant between stall points.

The pitching moment is given by

$$M_{AC} = qScC_{MAC}, \quad (12.4)$$

where  $C_{MAC}$  is the pitching moment coefficient about the A.C., and is independent of  $\alpha$ .

Moment equilibrium about the E.A. gives

$$eL + M_{MAC} - Wd - K\theta = 0, \quad (12.5)$$

where  $e$  is the distance from the E. A. to the A. C., assuming the E.A. is behind the A.C.

Substituting for the elastic twist, lift, and pitching moment from eqs. (12.1) to (12.4), the moment equation becomes

$$eqS\left(\frac{\partial C_L}{\partial \alpha}\right)\alpha + qScC_{MAC} - Wd - K(\alpha - \alpha_0) = 0. \quad (12.6)$$

Rearrange eq. (12.6) to

$$\left[ qS\left(\frac{\partial C_L}{\partial \alpha}\right)e - K \right] \alpha = Wd - qScC_{MAC} - K\alpha_0. \quad (12.7)$$

Now divide eq. (12.7) by  $-K$  to get

$$\left[ 1 - \frac{qS\left(\frac{\partial C_L}{\partial \alpha}\right)e}{K} \right] \alpha = \alpha_0 - \frac{Wd}{K} + \frac{qScC_{MAC}}{K}. \quad (12.8)$$

Let

$$q_D = \frac{K}{S\left(\frac{\partial C_L}{\partial \alpha}\right)e}. \quad (12.9)$$

Hence, equation (12.8) for the equilibrium value of the angle of attack reduces to

$$\alpha = \frac{\left[ \alpha_0 - (Wd)/K + \left( \frac{q}{q_D} \right) \left( \frac{c}{e} \right) \frac{C_{MAC}}{\left( \frac{\partial C_L}{\partial \alpha} \right)} \right]}{1 - q/q_D}. \quad (12.10)$$

A plot of  $q/q_D$  versus the angle of attack obtained from eq. (12.10) is shown in figure. 12.3.

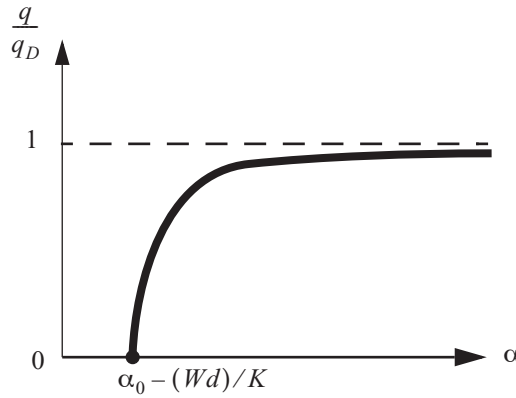


**Fig. 12.3 Response of the rigid wing segment model.**

From eq. (12.10) we see that  $\alpha \rightarrow \infty$  as  $q \rightarrow q_D$  for  $0 \leq q < q_D$ . That is, the angle of attack grows without bound as  $q \rightarrow q_D$ . Of course, this excessive twist is a theoretical result. In reality the wing will stall or twist off due to a strength failure. Hence, the divergence dynamic pressure is defined as

$$q_D = \frac{K}{S \left( \frac{\partial C_L}{\partial \alpha} \right) e}, \quad (12.11)$$

and the divergence speed is

$$V_D = \sqrt{\frac{2q_D}{\rho}}. \quad (12.12)$$

Divergence corresponds to static instability. At  $V = V_D$  we get excessive rotation in twist of the wing.

### 12.2.1 Responses of the rigid wing segment and the imperfect column

The response plots of the rigid wing segment model of article 12.2 and the geometrically imperfect column in article 11.4 on page 336 are repeated in figure. 12.4. Comparing the two response plots reveals that these phenomena are the same. Both the column buckling and the wing divergence are static instabilities. The critical load  $P_{cr}$  for the column and the divergence dynamic pressure  $q_D$  of the rigid wing segment model are determined from a static analysis of the slightly deflected structure.

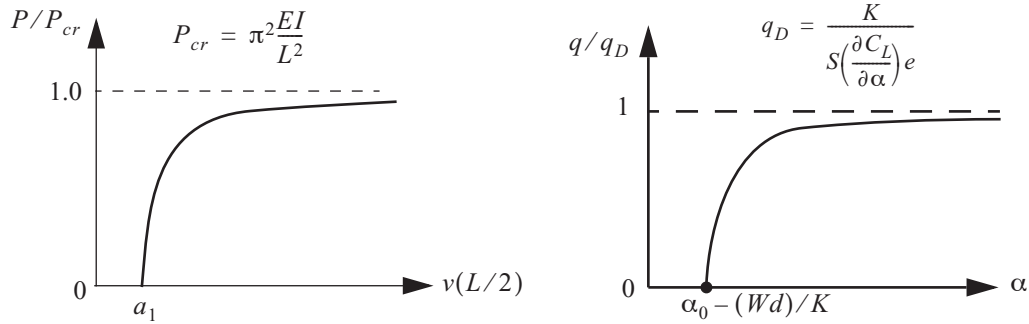


**Fig. 12.4** Response plots of the geometrically imperfect column and the rigid wing segment model.

### 12.2.2 Divergence experiments

Experiments to measure the divergence dynamic pressure of an elastic wing confront the issue of damaging the wing and its supporting structure if the dynamic pressure is near or at its critical value. A nondestructive method to measure the critical dynamic pressure is accomplished by plotting the data on a Southwell plot, which was developed for elastic column buckling in article 11.4.1 on page 338. The Southwell plotting coordinates are determined from eq. (12.10) by formulating the change in the angle of attack  $\Delta\alpha$ , where

$\Delta\alpha = \alpha - (\alpha_0 - (Wd)/K)$ . After some algebraic manipulations, the change in the angle of attack is written as

$$\Delta\alpha = \frac{C_0(q/q_D)}{1 - q/q_D}, \quad (12.13)$$

where

$$C_0 = \alpha_0 - (Wd)/K + \left(\frac{c}{e}\right) \frac{C_{MAC}}{\left(\frac{\partial C_L}{\partial \alpha}\right)}. \quad (12.14)$$

Equation (12.13) is rearranged as follows: (1), Multiply each side by  $1 - q/q_D$ , and write

$$\Delta\alpha - \Delta\alpha(q/q_D) = C_0(q/q_D).$$

(2) Divide by the dynamic pressure and write the final result as

$$\frac{\Delta\alpha}{q} = \frac{(\Delta\alpha + C_0)}{q_D}. \quad (12.15)$$

On the Southwell plot  $(\Delta\alpha)/q$  is the ordinate and  $\Delta\alpha$  is the abscissa. Thus, eq. (12.15) is a straight line on the plot as shown in figure. 12.5. The important aspect of the Southwell plot from the experimental viewpoint is that the slope of the graph is the reciprocal of the divergence dynamic pressure. As the dynamic pressure is increased from magnitudes less than the divergence dynamic pressure, the changes in angle of attack  $\Delta\alpha$  become large, and the data of  $(\Delta\alpha)/q$  versus  $\Delta\alpha$  tends to plot as a straight line. The experimental divergence

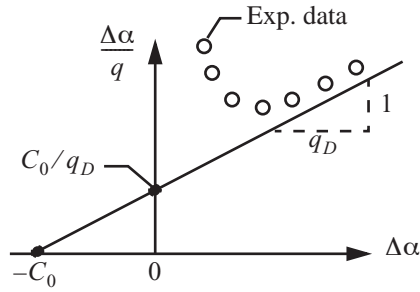


Fig. 12.5 Southwell plot.

dynamic pressure is determined from the slope of this fitted straight line. The actual value of  $C_0$  is not significant with respect to the determination of the experimental divergence dynamic pressure.

### 12.3 Straight, uniform, unswept, high aspect ratio, cantilever wing in steady incompressible flow

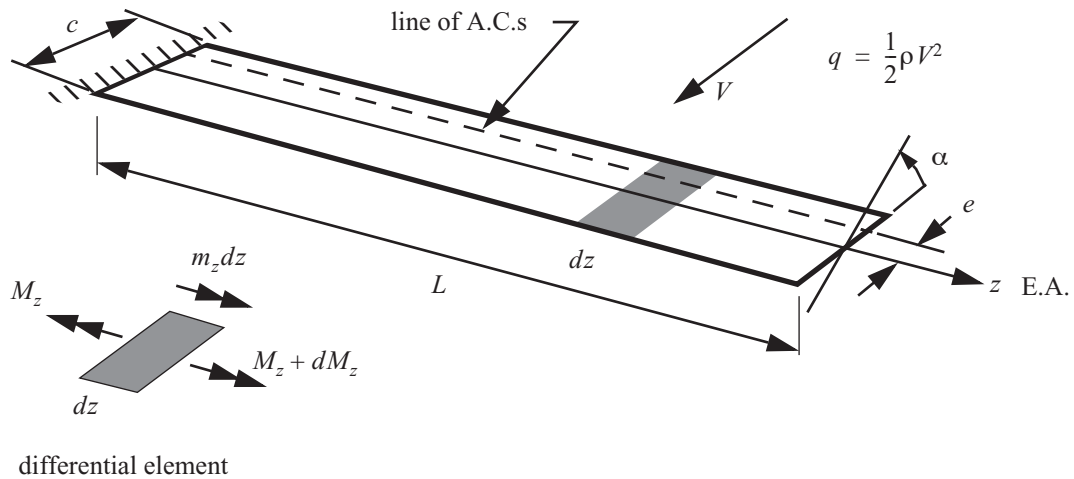


Fig. 12.6 Wing model for torsional divergence analysis.

Let  $\alpha(z)$  denote the total wing incidence, and let  $\alpha_0$  denote the fixed incidence at the wing root. The fixed incidence could be a function of  $z$  for a variable in built-in twist, but we will consider it constant along the span. So

$$\alpha = \alpha_0 + \phi_z(z), \quad (12.16)$$

where  $\phi_z(z)$  is the twist angle of the wing due to elastic deformation. Neglect airfoil weight, since we saw for the rigid wing segment that this factor played no role in the divergence dynamic pressure.

From eq. (3.61) on page 43 the differential equation in torsion is

$$\frac{dM_z}{dz} + m_z = 0 \quad 0 < z < L, \quad (12.17)$$

where  $m_z$  denotes the external torque per unit span. In this case the external torque per unit span is due to the aerodynamic loads acting on the wing.

In reference to eq. (3.121) on page 60, St. Venant's torsion theory relates the torque to the unit twist as

$$M_z = GJ \frac{d\phi_z}{dz}, \quad (12.18)$$

where  $GJ$  is the torsional stiffness of the wing box. From eq. (3.161) page 70, the torsion constant for a single-cell cross section is given by

$$J = (4A_c^2) / \left( \oint \frac{ds}{t} \right), \quad (12.19)$$

where  $A_c$  is the area enclosed by the cross-sectional contour,  $s$  is the arc-length along the contour, and  $t$  is the thickness of the contour. Substitute eq. (12.18) into (12.17) and use the fact that the wing is uniform along the span to get

$$GJ \frac{d^2 \phi_z}{dz^2} + m_z = 0 \quad \phi_z = \phi_z(z) \quad 0 < z < L. \quad (12.20)$$

### 12.3.1 Aerodynamic strip theory

Strip theory assumes aerodynamic lift and moment at station  $z$  depends only on the angle of attack, or incidence, at  $z$ , and is independent of the angle of attack at any other spanwise locations. Physically, this is reasonable for high aspect ratio wings.

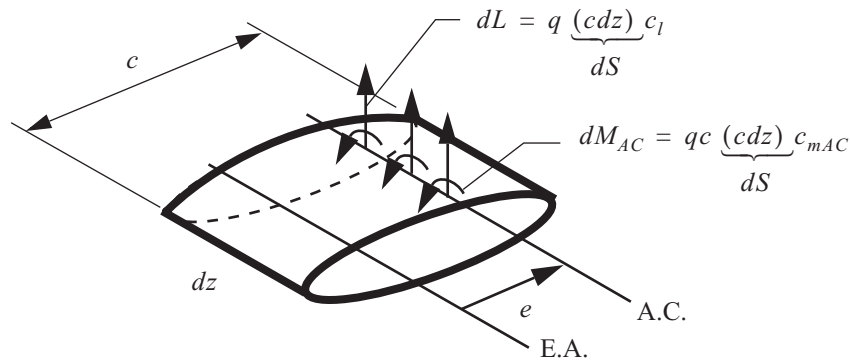


Fig. 12.7 Lift and pitching moment acting on the differential element of a wing.

The differential lift and differential pitching moment acting at the A.C. on an typical element of the wing are shown in the figure. 12.7, where  $c_l$  is the local lift coefficient and  $c_{mAC}$  is the local moment coefficient about the A.C. Hence, the external torque acting on the differential element about the elastic axis is

$$m_z dz = e dL + dM_{AC} = [eqc c_l + qc^2 c_{mAC}] dz, \quad (12.21)$$

or

$$m_z(z) = qce c_l + qc^2 c_{mAC}. \quad (12.22)$$

According to strip theory

$$c_l = \left( \frac{\partial c_l}{\partial \alpha} \right) \alpha = a_0 \alpha, \quad (12.23)$$

where  $a_0$  is the lift curve slope. Substituting eq. (12.16) into (12.23), we get

$$c_l = a_0 [\alpha_0 + \phi_z(z)]. \quad (12.24)$$

Hence,

$$m_z(z) = qcea_0 [\alpha_0 + \phi_z(z)] + qc^2 c_{mAC}. \quad (12.25)$$

### 12.3.2 Differential equation of torsional divergence

Now substitute eq. (12.25) into (12.20) and rearrange the terms to get

$$GJ \frac{d^2 \phi_z}{dz^2} + (qcea_0) \phi_z = -qcea_0 \alpha_0 - qc^2 c_{mAC}. \quad (12.26)$$

Equation (12.26) is the governing, second order, ordinary differential equation for  $\phi_z(z)$  with  $0 < z < L$ . The boundary conditions at  $z = 0$  and  $z = L$  are to specify either  $\phi_z$  or  $M_z$ , but not both. For a cantilever wing, which is clamped at the root and free at the tip, the boundary conditions are

$$\phi_z(0) = 0 \quad M_z(L) = GJ \frac{d\phi_z}{dz} \Big|_{z=L} = 0. \quad (12.27)$$

The general solution of the ordinary differential eq. (12.26) is the sum of a particular solution and a homogenous solution.

$$\phi_z(z) = \phi_p(z) + \phi_h(z). \quad (12.28)$$

By the method of undetermined coefficients the particular solution is

$$\phi_p = -\alpha_0 - \frac{cc_{mAC}}{ea_0}. \quad (12.29)$$

The homogenous equation is

$$GJ \frac{d^2 \phi_h}{dz^2} + (qcea_0) \phi_h = 0, \quad (12.30)$$

and its solution is given by

$$\phi_h = A_1 \sin(\lambda z) + A_2 \cos(\lambda z), \quad (12.31)$$

where

$$\lambda^2 = (q c e a_0) / (GJ). \quad (12.32)$$

Hence, the general solution for the wing twist is

$$\phi_z(z) = A_1 \sin(\lambda z) + A_2 \cos(\lambda z) - \alpha_0 - \frac{c c_{mAC}}{e a_0}. \quad (12.33)$$

Substitute the general solution (12.33) into the boundary conditions (12.27) to determine constants  $A_1$  and  $A_2$ :

$$A_2 - \alpha_0 - \frac{c c_{mAC}}{e a_0} = 0 \quad A_1 \lambda \cos(\lambda L) - A_2 \lambda \sin(\lambda L) = 0. \quad (12.34)$$

Solving eq. (12.34) for the constants, we get

$$A_1 = \left( \alpha_0 + \frac{c c_{mAC}}{e a_0} \right) \tan(\lambda L) \quad A_2 = \alpha_0 + \frac{c c_{mAC}}{e a_0}. \quad (12.35)$$

Substitute eq. (12.35) for  $A_1$  and  $A_2$  into eq. (12.33) to get the angle of twist for the cantilever wing as

$$\phi_z(z) = \left( \alpha_0 + \frac{c c_{mAC}}{e a_0} \right) [\tan(\lambda L) \sin(\lambda z) + \cos(\lambda z) - 1]. \quad (12.36)$$

Hence from eqs. (12.16) and (12.36), the total wing incidence is

$$\alpha(z) = \alpha_0 + \left( \alpha_0 + \frac{c c_{mAC}}{e a_0} \right) \left[ \frac{\sin(\lambda L) \sin(\lambda z) + \cos(\lambda L) \cos(\lambda z)}{\cos(\lambda L)} - 1 \right]. \quad (12.37)$$

Using the trigonometric identity for the cosine of the sum of two angles, this last result can be written as

$$\alpha(z) = \alpha_0 + \left( \alpha_0 + \frac{c c_{mAC}}{e a_0} \right) \left[ \frac{\cos[\lambda(L-z)]}{\cos(\lambda L)} - 1 \right]. \quad (12.38)$$

From eq. (12.38) we see that  $\alpha \rightarrow \infty$  if  $\cos(\lambda L) = 0$ . Vanishing of the cosine function occurs when  $\lambda L = \frac{\pi}{2}, 3\frac{\pi}{2}, \dots$ . The lowest root gives the critical divergence dynamic pressure as

$$\left( \lambda_D L = \frac{\pi}{2} = \sqrt{\frac{q_D c e a_0}{GJ}} L \right) \rightarrow q_D = \left( \frac{\pi}{2L} \right)^2 \frac{GJ}{c e a_0}. \quad (12.39)$$

The value of  $q_D$  in eq. (12.39) is the **wing's torsional divergence dynamic pressure**.



The analogy between the divergence dynamic pressure for the rigid wing model and the elastic wing model is summarized in table 12.1.

**Table 12.1 Expressions for divergence dynamic pressure of the rigid wing and of the elastic wing**

Rigid, eq. (12.10)	Elastic, eq. (12.39)
$K$	$(GJ)/L$
$S$	$Lc$
$e$	$e$
$(\partial C_L)/(\partial \alpha)$	$a_0$

## 12.4 Effect of wing sweep on divergence

Divergence of a slender straight wing that is approximately perpendicular to the airplane plane of symmetry is dependent on wing twist, referred to as torsional divergence, and bending is not a factor in the instability. For slender swept wings bending of the wing has an important and complicating affect on divergence and is referred to as bending-torsional divergence.

Let the angle  $\Lambda$  denote the wing sweep measured relative to the unswept wing with  $\Lambda > 0$  for a swept-back wing, and  $\Lambda < 0$  for a swept-forward wing. See figure. 12.8. When a swept-back wing ( $\Lambda > 0$ ) bends, its angle of attack in the streamwise direction is reduced. Bending causes a nose-down twist in the streamwise direction. To understand this bending effect, consider an upward force applied to the reference axis. Points  $A$  and  $B$  deflect upward about the same amount. Point  $A'$  has less upward deflection since it is closer to the wing root. Hence, streamwise segment  $A'B$  will have a smaller angle of attack due to bending and a negative increment in lift results. This negative lift increment due to bending is a stabilizing influence, since it opposes the nose-up twist of segment  $A'B$ .

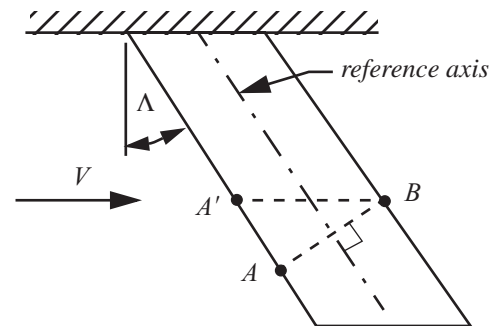


**Fig. 12.8 Streamwise and chordwise segments of a swept-back wing.**

Consider a swept-forward wing with  $\Lambda < 0$  as shown in figure. 12.9. Bending causes an increase in the angle of attack, or nose-up twist, for the streamwise segment  $A'B$ . This increase in angle of attack due to bending is a destabilizing influence. Divergence essentially rules out swept-forward metallic wings. For wings made of composite materials, it is possible to materially couple bending and torsion in such a way to have an acceptable divergence speed for forward-swept wings (e.g., the X-29 demonstrator).

From NASA Armstrong Fact Sheet: X-29 Advanced Technology Demonstrator Aircraft (Gibbs, 2015): The X-29's thin supercritical wing was of composite construction. State-of-the-art composites permit aeroelastic tailoring, which allows the wing some bending but limits

twisting and eliminates structural divergence within the flight envelope (deformation of the wing or breaking off in flight).

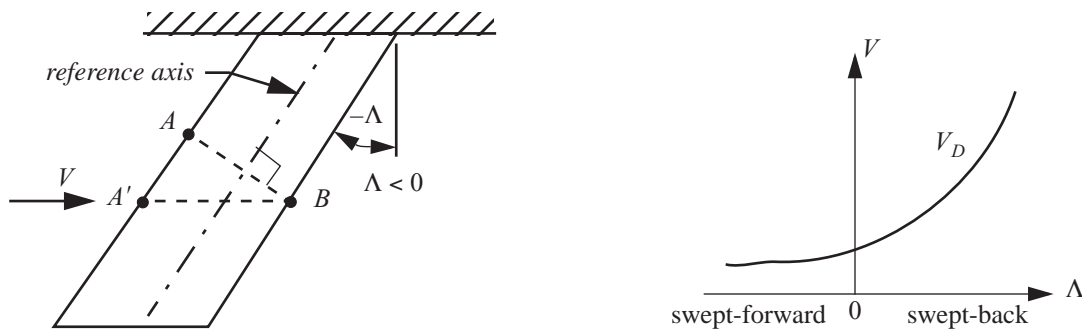


**Fig. 12.9** Streamwise and chordwise segments of a swept-forward wing.

## 12.5 References

- Bisplinghoff, R.L., H. Ashley, and R.L. Halfman. *Aeroelasticity*. Mineola, NY: Dover Publications, Inc., 1996. pp. 1-3, 421-432, 474 & 475. (Originally published by Addison-Wesley, 1955.)
- Gibbs, Y. "NASA Armstrong Fact Sheet: X-29 Advanced Technology Demonstrator Aircraft." NASA.gov, November 5, 2015. <https://www.nasa.gov/centers/armstrong/news/FactSheets/FS-008-DFRC.html>.
- Gordon, J. E. *Structures, or Why Things Don't Fall Down*. Boston: Da Capo Press, 2003. (Originally published by Harmondsworth: Penguin Books. 1978.)

## 12.6 Practice exercises

1. An interesting historical account of wing torsional divergence is given by Gordon (2003); An excerpt follows.

During World War I Antony Fokker developed an advanced monoplane fighter – the Fokker D8 – with performance better than available or in immediate prospect on the Allied side. As soon as the D8 was flown in combat conditions it was found out that, when the aircraft was pulled out of a dive in a dog fight, the wings came off. Since many lives were lost – including those of some of the best and most experienced German fighter pilots – this was a matter of very grave concern to the Germans at the time, and is still instructive to study the cause of the trouble.

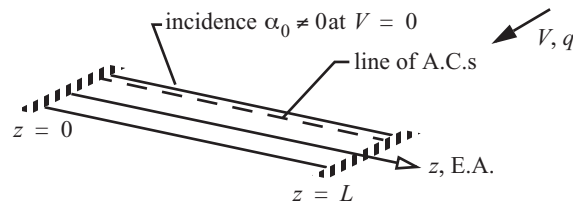
Read pages 260-271 in the book by Gordon and answer the following questions.

- a) For a given engine power, why is a monoplane generally faster than a biplane?
- b) What was the material of wing skin on the D8? Is it effective in resisting shear?
- c) What was the method of loading in the structural test of the wings of the D8?
- d) What was the ultimate load factor from the structural test?

- e) What was the first attempt to strengthen the rear wing spar?
- f) What was the best method to strengthen the rear wing spar? and why did it work?
- g) What is aileron reversal?
- h) What common geometric feature do a tube and the torsion box of the old-fashioned biplane have that makes them so effective in resisting torsion?
2. The uniform wing sketched in figure. 12.10 is fixed at both ends. Starting with the general solution eq. (12.33), derive the algebraic expression for

- a. total incidence  $\alpha(z) = \alpha_0 + \phi_z(z)$ , and
- b. divergence dynamic pressure  $q_D$ .

Fig. 12.10 Wing with fixed ends.



3. Consider a rigid wing segment of weight  $W$  mounted on an elastic sting in a wind tunnel. The sting is modeled as a uniform, elastic, cantilever beam with bending stiffness  $EI_{xx} = EI$  and length  $2c$ . Neglect the weight of the sting. The model is mounted in such a way to have the angle of attack  $\alpha_0$  when the beam is undeformed. Thus, the angle of attack  $\alpha = \alpha_0 + \theta$ , where  $\theta$  is the nose-up rotation of the wing resulting from the bending of the sting. Denote the lift and the pitching moment acting at the aerodynamic center (A.C.) as  $L$  and  $M_{AC}$ , respectively.

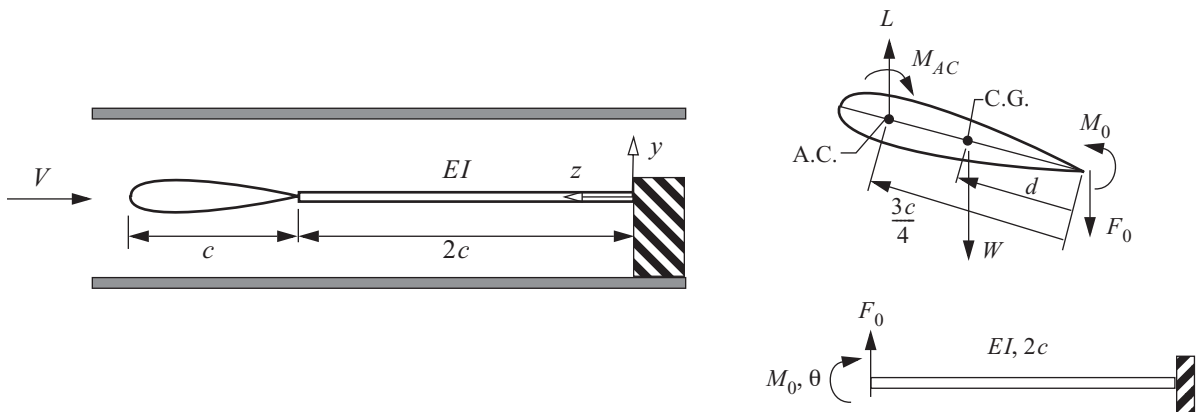


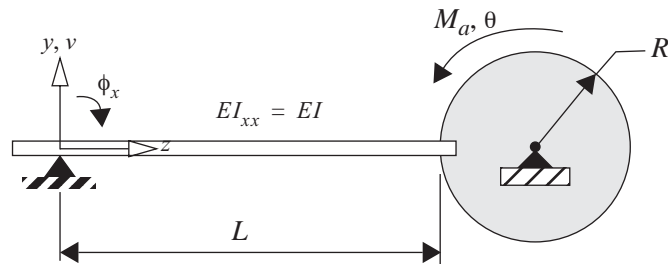
Fig. 12.11 Rigid wing mounted on an elastic sting in a wind tunnel.

Assume

- steady, two-dimensional incompressible flow at airspeed  $V$  and density  $\rho$ ,
  - the lift curve slope  $\frac{\partial C_L}{\partial \alpha} = a_0$  is constant between stall points,
  - and that the angle of attack is small.
- a. Use the second theorem of Castigliano to determine the rotation  $\theta$  of the cantilever beam due to end force  $F_0$  and moment  $M_0$  as shown in the sketch above. Consider bending only.
  - b. Determine the angle of attack  $\alpha$  as a function of the dynamic pressure  $q = (\rho V^2)/2$ ,  $\alpha_0$ , wing reference area  $S$ , flexural stiffness  $EI$ , chord length  $c$ ,  $a_0$ , pitching moment coefficient  $C_{MAC}$ , distance  $d$ , and weight  $W$ .
  - c. Determine the divergence dynamic pressure,  $q_D$ .

4. A uniform beam with a rectangular cross section rests on a knife edge at its left end, while the right end is clamped in rigid disk. This configuration is shown in figure. 12.12. The bending stiffness  $EI_{xx} = EI$ , the distance between the knife edge and the beam's connection to the disk is  $L$ , and the radius of the disk is  $R$ . This disk rotates about a fixed smooth pin through its center under the action of applied moment  $M_a$  as shown. Determine the relation between the applied moment  $M_a$  and rotation angle  $\theta$  of the disk under the assumption that the angle of rotation  $\theta$  is small. In a wind tunnel test the disk is connected to a rigid airfoil, then this structural configuration is used to provide the rotational spring of stiffness  $K$  depicted in figure. 12.2.

**Fig. 12.12 Apparatus to provide rotational stiffness in a wind tunnel test of an airfoil.**



## *Fracture of cracked members*

---

The strength of ductile metals is limited by yielding. However, the presence of a crack in a structure may weaken it so that it fails by fracturing in two or more pieces. The study of crack propagation in bodies is the subject of **fracture mechanics**. Linear elastic fracture mechanics (**LEFM**) is the study of crack propagation in linear elastic bodies.

**Damage tolerant design** allows for the presence of subcritical cracks that will not grow to critical length between inspection intervals. Cracks can nucleate and grow in airplane structures under cyclic loading, or fatigue. This important structural issue of fatigue crack growth is tragically illustrated by the Comet disasters of 1954.

### *13.1 Comet disasters of 1954*

The content of this article is taken from Wikipedia, the free encyclopedia, and Cawthon (2005).

The de Havilland Comet was the world's first commercial jet airliner to reach production. Developed and manufactured by de Havilland, it first flew in 1949 and was considered a landmark British aeronautical design. The Comet is an all-metal low-wing cantilever monoplane powered by four jet engines, approximately the length of a Boeing 737 but carrying fewer people in greater comfort. The clean, low-drag design featured many unique or innovative design elements, including a swept leading edge, integral wing fuel tanks, and four-wheel bogie main undercarriage units designed by de Havilland. The Comet was also the first pressurized jet-propelled commercial aircraft. Comet went into commercial service with BOAC on 22 January 1952. In May, the first paying passengers flew from Heathrow Airport to Johannesburg, South Africa. The Comet could fly higher and faster than any other airliner of the day and passengers loved it. They especially liked the Comet's big, rectangular windows, which allowed a much better view than those on competing planes. See figure. 13.1.

**Fig. 13.1 BOAC De Havilland DH106 Comet 1G-ALYX on tarmac. (c) British Airways Speedbird Heritage Centre. Released under CC BY NC SA license 4.0**



The structural flaws in the Comet's design caused two fatal accidents in 1954. The first came just after the New Year, on January 10. BOAC Comet G-ALYP left Ciampino airport in Rome on its way to London. Less than a half-hour after takeoff, a routine radio call was cut off in mid-transmission. The Comet had crashed into the Mediterranean Sea about 16 miles from the island of Elba. The investigators determined the cabin failed because of metal fatigue. Just three months later, another Comet crashed, this time it was South African Airways G-ALYY, which was also flying out of Ciampino and also wound up in the Mediterranean, killing all twenty-one people on board. Authorities were unable to retrieve much wreckage, but cited the circumstances that caused the January incident.

Engineers subjected an identical airframe, G-ALYU ("Yoke Uncle"), to repeated repressurization and over pressurization and after 3,057 flight cycles (1,221 actual and 1,836 simulated), Yoke Uncle failed due to metal fatigue near the front port-side escape hatch. Investigators began considering fatigue as the most likely cause of both accidents, and further research into measurable strain on the skin began. Stress around the window corners was found to be much higher than expected, "probably over 40,000 psi," and stresses on the skin were generally more than previously expected or tested. This was due to stress concentration, a consequence of the window's square shape. The stresses caused by thousands of takeoffs and landings were causing the plane's aluminum skin to begin to crack around the right-angle edges of those nice, big windows that were so popular with the passengers. Eventually the metal would completely fail, causing immediate depressurization of the cabin and catastrophic structure failure.

The problem was exacerbated by the punch rivet construction technique employed. The windows had been engineered to be glued and riveted, but had been punch riveted only. Unlike drill riveting, the imperfect nature of the hole created by punch riveting may cause the start of fatigue cracks around the rivet.

The square windows of the Comet 1 were redesigned as oval for the Comet 2, which first flew in 1953. The skin sheeting was thickened slightly. The remaining Comet 1s and 1As were either scrapped or modified with oval window rip-stop doublers. All production Comet 2s were modified to alleviate the fatigue problems, and most of these served with the Royal Air Force as the Comet C2. The Comet did not resume commercial airline service until 1958, when the much-improved Comet 4 was introduced and became the first jet airliner to enter transatlantic service. As is often the case in aeronautical engineering, other aircraft manufacturers learned from and profited by de Havilland's hard-learned lessons. Representatives from American manufacturers such as Boeing and Douglas "admitted that if it hadn't been for our problems, it would have happened to one of them."

The Comet 4 not only had a stronger airframe and rounded windows, it was also longer, carried more passengers, and had four new Rolls-Royce Avon engines, which produced twice the thrust of the original de Havilland Ghosts. BOAC had ordered nineteen of the new Comets in 1955, before the redesign was completed. The Comet 4 made its maiden flight on 27 April 1958 and de Havilland began delivering planes to BOAC in September. BOAC started Comet passenger service with London to New York on 4 October 1958, beating Pan Am's inaugural 707 Clipper Service by three weeks.

But it was too late. The Comet, unbeatable in 1954, was an also-ran in 1958. In addition to its early problems, the Comet's dated design and smaller size convinced most carriers to select the newer 707 or Douglas DC-8. Only seventy-six Comet 4s were built from 1958 to 1964, and it was America, not Great Britain, that owned the commercial jetliner market for the rest of the twentieth century.

### 13.2 Cracks as stress raisers

Some of the discussion in this article paraphrases that given by Dowling (1993, p.279). Consider the linear elastic response of a rectangular plate containing a centrally located elliptical hole that is subject to a remote tensile stress  $\sigma$ . See figure. 13.2. The major axis of the through hole is denoted by  $a$  and the minor axis by  $d$ . The radius of curvature  $\rho$  at the tip of the major axis is given by  $\rho = d^2/a$ .

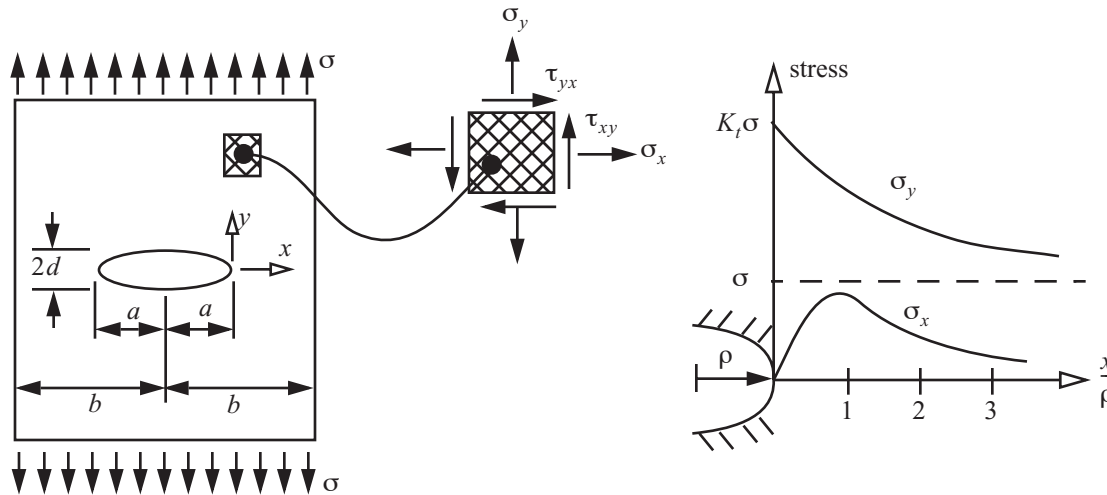


Fig. 13.2 Stresses at the tip of an elliptical through hole in a rectangular plate subject to remote tension.

The stress concentration factor,  $K_t$ , at the edge of the hole is defined by

$$K_t = \frac{\sigma_y(x, y)|_{x=y=0}}{\sigma}. \quad (13.1)$$

From linear elasticity for a plate half width  $b \gg a$ , this stress concentration factor for an isotropic material is given by

$$K_t = 1 + 2\frac{a}{d} = 1 + 2\sqrt{\frac{a}{\rho}}. \quad (13.2)$$

For selected values of the ratio  $a/d$ , the stress concentration factors are listed in table 13.1.

**Table 13.1 Stress concentration factors for selected elliptical hole sizes**

$a/d$	$K_t$
1 (circular hole)	3
2	5
3	7

As  $d \rightarrow 0$ , or  $\rho \rightarrow 0$ ,  $K_t \rightarrow \infty$ . This limiting geometry is a crack-like slit. Consequently the plate experiences a strength failure at no load. Clearly, this is a theoretical result from linear elasticity. Real materials cannot support infinite stress. In ductile metals, large plastic deformation exists in the vicinity of the crack tip. The stress is not infinite and the sharp crack tip is blunted.

There are generally three modes of loading, which involve different crack surface displacements as depicted in the sketches of figure. 13.3. The three modes are:

Mode I: opening or tensile mode (the crack faces are pulled apart)

Mode II: sliding or in-plane shear (the crack surfaces slide over each other)

Mode III: tearing or anti-plane shear (the crack surfaces move parallel to the leading edge of the crack and relative to each other)

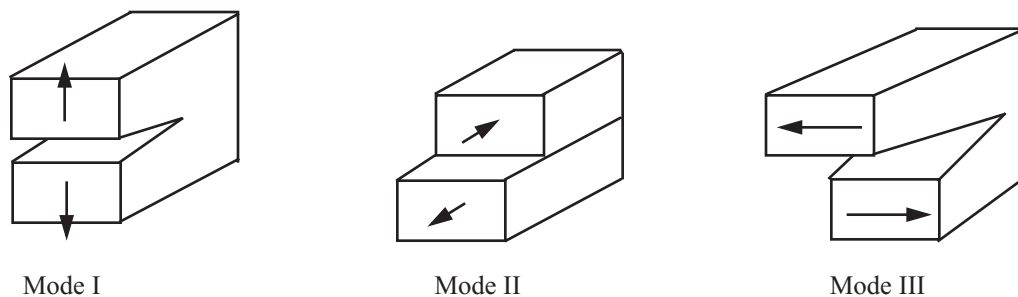


**Fig. 13.3 Basic displacement modes of a cracked body.**

### 13.3 LEFM stress field in the vicinity of the crack tip for mode I

A center-cracked plate subject to remote tension, or mode I loading, is shown in figure. 13.4. This loading is symmetric with respect to the crack surface. The crack length is  $2a$ , plate width  $2b$ , and the plate thickness  $t$ . The two free surface areas of the crack are  $2a$ -by- $t$ . The remote tensile stress is denoted by  $\sigma$ . Let  $r$  and  $\theta$  denote the



polar coordinates in the  $x$ - $y$  plane measured from the crack tip. From linear elastic fracture mechanics (Anderson, 1995, pp. 31-96), LEFM, the dominant terms in the stress field near the crack tip are as follows:

$$\sigma_x = \frac{K_I}{\sqrt{2\pi r}} \cos \frac{\theta}{2} \left[ 1 - \sin \frac{\theta}{2} \sin \frac{3\theta}{2} \right] + \dots, \quad (13.3)$$

$$\sigma_y = \frac{K_I}{\sqrt{2\pi r}} \cos \frac{\theta}{2} \left[ 1 + \sin \frac{\theta}{2} \sin \frac{3\theta}{2} \right] + \dots, \quad (13.4)$$

$$\tau_{xy} = \frac{K_I}{\sqrt{2\pi r}} \cos \frac{\theta}{2} \sin \frac{\theta}{2} \cos \frac{3\theta}{2} + \dots, \quad (13.5)$$

$$\sigma_z = \begin{cases} 0, & \text{plane stress where } \varepsilon_z \neq 0 \\ \nu(\sigma_x + \sigma_y), & \text{plane strain where } \varepsilon_z = 0 \end{cases}, \quad (13.6)$$

$$\tau_{zx} = \tau_{zy} = 0. \quad (13.7)$$

Poisson's ratio is denoted by  $\nu$ . The plane stress solution is more appropriate if the thickness  $t$  is relatively small, and the plane strain solution is more appropriate if the thickness is relatively large. At  $\theta = 0$ , stress components

$\sigma_x = \sigma_y \approx \frac{K_I}{\sqrt{2\pi r}}$  near  $r \approx 0$ . So  $\sigma_x$  and  $\sigma_y \rightarrow \infty$  as  $r \rightarrow 0$ . For small values of  $r$ , stress components  $\sigma_x$  and  $\sigma_y$

are proportional to  $K_I$ .

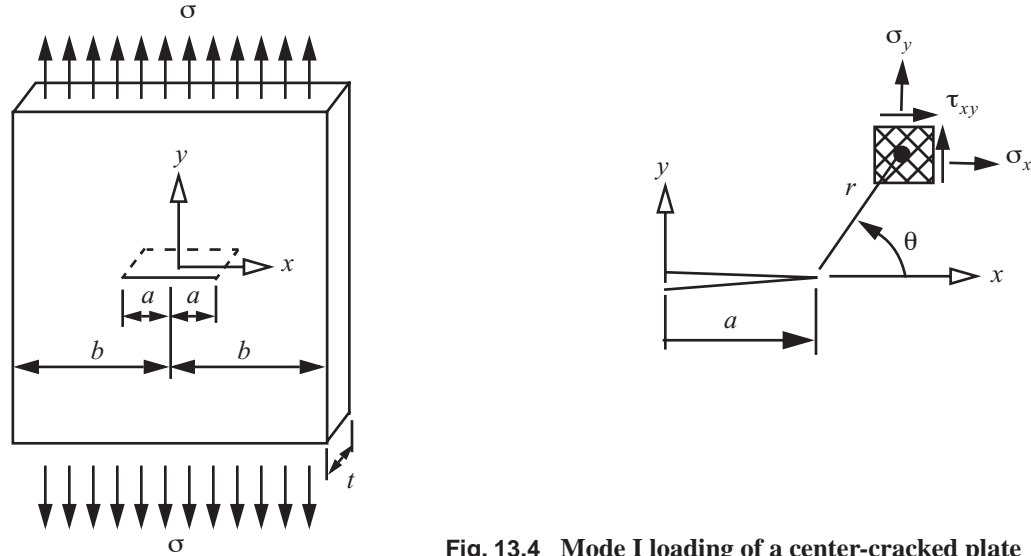


Fig. 13.4 Mode I loading of a center-cracked plate

The magnitude of the stress field in the vicinity of the crack tip is characterized by  $K_I$ . Hence,  $K_I$  is a measure of the severity of the crack. **The parameter  $K_I$  is called the mode I stress intensity factor.** For an infinite plate, where  $b \rightarrow \infty$  with  $a > 0$ , LEFM yields the result that

$$K_I = \sigma \sqrt{\pi a}. \quad (13.8)$$

For finite plate geometries

$$K_I = F\sigma\sqrt{\pi a}, \quad (13.9)$$

where  $F$  is a dimensionless width-correction factor that is a function of the geometry and the ratio of  $a/b$ . For the center-cracked plate, the quantity  $F$  is given by

$$F = \begin{cases} \frac{1 - 0.5(a/b) + 0.326(a/b)^2}{\sqrt{1 - (a/b)}} & , \text{ and} \\ 1 & a/b \leq 0.4 \end{cases} \quad (13.10)$$

$$F = 1 \text{ if } 0 < \frac{a}{b} \ll 1. \quad (13.11)$$

In general the correction factor is a function of the loading configuration as well as the geometry and ratio of  $a/b$ . The reader is referred to Dowling (1999) and the references cited there for additional relations for  $F$ .

The following facts are noted:

- The mode I stress intensity factor  $K_I$  depends on the remote stress  $\sigma$ , and  $\sigma$  is the stress  $\sigma_y$  if **no** crack is present.
- The mode I stress intensity factor  $K_I$  depends on the square root of the half crack length.
- The dimensional units of  $K_I$  are stress times the square root of length (e.g., ksi $\sqrt{\text{in}}$  in U.S. customary units, or MPa $\sqrt{\text{m}}$  in SI units.)

The crack opening displacement  $v(x)$  along the crack surface is also of interest, where the origin of the  $x$ -axis is located at the center of the crack as is shown in figure. 13.7. For the infinite plate geometry under mode I

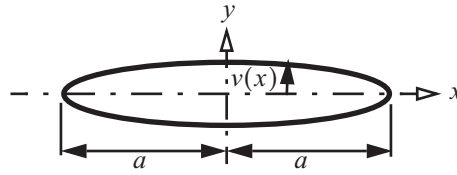


**Fig. 13.5 Opening displacement of the crack under mode I loading of the center-cracked plate.**

loading, the displacement at the upper and lower crack faces are symmetrical, so only the displacement on the upper crack surface needs to be described. The expression for  $v(x)$  as given by Sun (1998, p. 162) is

$$v(x) = \frac{(\kappa + 1)(1 + \nu)}{2E} \sigma \sqrt{a^2 - x^2} \quad |x| \leq a, \quad (13.12)$$

where

$$\kappa = \begin{cases} 3 - 4\nu & \text{for plane strain} \\ \frac{3 - \nu}{1 + \nu} & \text{for plane stress} \end{cases}. \quad (13.13)$$

The critical mode I stress intensity factor is denoted by  $K_{Ic}$ , and it is assumed to be a material parameter.

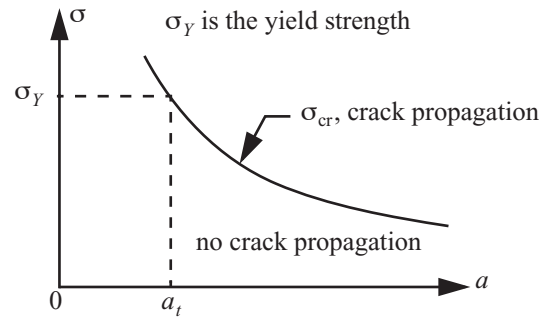
- $K_I < K_{Ic}$ . There is no crack growth, and the material resists the crack without brittle fracture.
- $K_I = K_{Ic}$ . The crack begins to propagate and brittle fracture occurs.

The critical mode I stress intensity factor is also called the **fracture toughness**. A tough material has a large value of  $K_{Ic}$ , which means it is effective in resisting crack growth. At crack growth, the remote stress is denoted by  $\sigma_{cr}$  and is given by

$$\sigma_{cr} = \frac{K_{Ic}}{F\sqrt{\pi a}}. \quad (13.14)$$

A representative graph of eq. (13.14) is shown in figure. 13.6. The value of the half crack length when  $\sigma_{cr} = \sigma_Y$ ,

**Fig. 13.6** Representative graph of the critical stress for crack propagation as a function of the half crack length.



is called the transition crack length  $a_t$ , where  $\sigma_Y$  denotes the yield strength of the material. Set  $\sigma_{cr} = \sigma_Y$  in eq. (13.14) to find

$$a_t = \frac{1}{\pi} \left( \frac{K_{Ic}}{\sigma_Y} \right)^2. \quad (13.15)$$

The transition crack length is the approximate length above which strength is limited by fracture. If  $a > a_t$  then fracture limits strength. If  $a < a_t$  then yielding dominates strength. Materials with

- high  $K_{Ic}$  and low  $\sigma_Y$  imply a long  $a_t$  and small cracks are no problem, and
- low  $K_{Ic}$  and high  $\sigma_Y$  imply a short  $a_t$  and small cracks can be a problem.

Typical values of the fracture toughness at room temperature are listed in table 13.2.

**Table 13.2 Fracture toughness and corresponding tensile properties for selected metals at room temperature (Dowling, 1999).**

Material	Toughness $K_{Ic}$		Yield strength $\sigma_Y$		Ultimate Strength $\sigma_U$	
	MPa $\sqrt{m}$	ksi $\sqrt{in}$	MPa	ksi	MPa	ksi
<i>Steels</i>						
AISI 1144	66	60	540	78	840	122
AISI 4130	110	100	1090	158	1150	167
<i>Aluminum and titanium alloys (L-T Orientation)</i>						
2014-T651	24	22	415	60	485	70
2024-T351	34	31	325	47	470	68
2219-T851	36	33	350	51	455	66
7075-T651	29	26	505	73	570	83
7475-T7351	52	47	435	63	505	73
Ti-6Al-4V annealed	66	60	925	134	1000	145

### Example 13.1 ASTM compact tension configuration

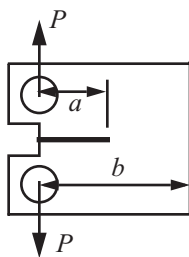


**Fig. 13.7**

The configuration shown in figure. 13.7 is subject to a tensile load  $P$ , has a crack length denoted by  $a$ , and a thickness denoted by  $t$ . It is the configuration of the ASTM standard compact specimen. The mode I stress intensity factor is given by (Dowling, p. 295)

$$K = F_P(\alpha) \frac{P}{t\sqrt{b}}, \quad (a)$$

where  $\alpha = a/b$ . The nondimensional function  $F_P$  is

$$F_P(\alpha) = \frac{(2 + \alpha)}{(1 - \alpha)^{3/2}} [0.866 + 4.64\alpha - 13.32\alpha^2 + 14.72\alpha^3 - 5.6\alpha^4] \quad \alpha \geq 0.2. \quad (b)$$

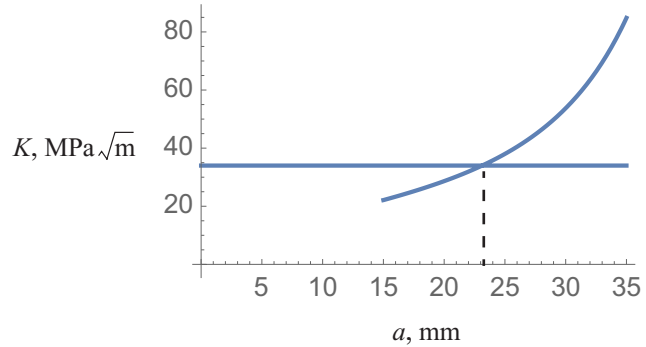
For  $P = 22 \text{ kN}$ ,  $b = 50 \text{ mm}$ , and  $t = 25 \text{ mm}$ , determine the critical crack length for brittle fracture of 2024-T351 aluminum alloy. The numerical factor multiplying  $F_P$  is

$$\frac{P}{t\sqrt{b}} = \frac{22,000 \text{ N}}{25 \text{ mm} \sqrt{50 \text{ mm} (10^3 \text{ mm/m})}} = \frac{22,000}{25 \sqrt{50,000}} \left( \frac{\text{N}}{\text{mm}^2} \right) \sqrt{\text{m}} = 3.93548 \text{ MPa} \sqrt{\text{m}}. \quad (c)$$

A graph of the stress intensity factor as a function of the crack length in the range from 15 mm to 35 mm is shown in figure. 13.8. The critical mode I stress intensity factor is  $34 \text{ MPa} \sqrt{\text{m}}$  from table 13.2, and it plots as horizontal line in the graph. Using a root finding procedure, or a trial and error method, the intersection of the

two lines in the graph occurs at 23.1 mm. Thus, the critical crack length for brittle fracture is 23.1 mm. ■

**Fig. 13.8** Stress intensity factor as a function of crack length.



The example that follows illustrates how the methods of strength of materials and fracture mechanics are employed to analyze the strength of a cantilever beam.

### Example 13.2 Strength of a cantilever beam.

This example is adapted from Kanninen and Popelar (1985, pp. 10-12). Determine the maximum value of the tip load  $Q$  acting on a cantilever beam depicted in figure. 13.9 by the strength of materials method and the fracture mechanics method. The beam has a length  $L = 300$  mm, height  $h = 30$  mm, and rectangular cross section with width  $b = 15$  mm. Assume a factor of safety (FS) of 1.5. The material is aluminum alloy 2014-T651 with properties listed in table 13.2. Plot the maximum value of  $Q$  versus the crack length  $a$ .

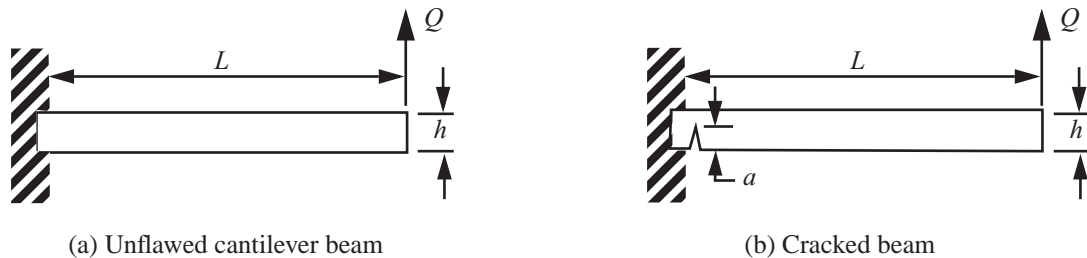


**Fig. 13.9** Basis for the comparison of strength of materials and fracture mechanics approaches.

**(a) Strength of materials approach.** The maximum load is determined such that the maximum stress in the beam is less than the yield strength of the material. The maximum tensile normal stress occurs at the bottom of the beam at its built-in end. The bending moment at the built-in end is  $M = LQ$ , and the flexure formula for the maximum normal stress is

$$\sigma_{\max} = \frac{M(h/2)}{I}, \quad (\text{a})$$

where the second area moment of the rectangular cross section is  $I = (bh^3)/12$ . Hence,

$$\sigma_{\max} = \frac{6QL}{bh^2} < \frac{\sigma_Y}{FS}. \quad (\text{b})$$

Solve the inequality for the load in eq. (b) to get

$$Q < \frac{bh^2}{6(FS)L} \sigma_Y = \frac{(15 \text{ mm})(30 \text{ mm})^2}{6(1.5)(300 \text{ mm})} (415 \text{ N/mm}^2). \quad (\text{c})$$

Hence,  $Q < 2075 \text{ N}$ .

**(b) Fracture mechanics approach.** Consider that the beam, instead of being defect free, contains an edge crack of length  $a$  normal to the free edge. Further suppose that, as shown in figure. 13.9(b), the crack is located where the maximum tensile stress is anticipated. This geometry and loading configuration is not the center-cracked plate. However, for a relatively small crack, an LEFM-based analysis of the flawed beam shown in figure. 13.9(b) would give a reasonable approximation in the following expression for the stress intensity factor:

$$K_I = 1.12 \sigma_{\max} \sqrt{\pi a}, \quad (\text{d})$$

where  $\sigma_{\max}$  is the stress that would occur at the crack location *in the absence of the crack*. The beam is safe from fracture if  $K_I \leq K_{Ic}$ . Further assurance can be obtained by having  $K_I < K_{Ic}/(FS)$ , where, just as in the strength of materials approach, the number  $FS$  is the factor of safety. Using eq. (d) to replace  $\sigma_{\max}$  in eq. (d) then leads to

$$K_I = 1.12 \left( \frac{6QL}{bh^2} \right) \sqrt{\pi a} < \frac{K_{Ic}}{FS}. \quad (\text{f})$$

Solve eq. (e) for the load to get

$$Q < \left( \frac{bh^2}{6(FS)L} \right) \frac{K_{Ic}}{1.12 \sqrt{\pi a}}. \quad (\text{g})$$

Substitute numerical values into eq. (f) to get

$$Q < \left[ \frac{(15 \text{ mm})(30 \text{ mm})^2}{6(1.5)(300 \text{ mm})} \right] \frac{(24 \text{ N/mm}^2) \sqrt{\text{m}(10^3 \text{ mm/m})}}{1.12 \sqrt{\pi a}}. \quad (\text{h})$$

Hence,  $Q < \frac{1911.56 \text{ N}\sqrt{\text{mm}}}{\sqrt{a}}$ , which is the fracture mechanics estimate of the safe operating load. A graph of the failure load is shown in figure. 13.10. From the plots in the graph, yielding governs failure for  $0 < a < 0.849 \text{ mm}$ , whereas fracture governs failure for  $a > 0.849 \text{ mm}$ . The transition crack length,  $a_t = 0.849 \text{ mm}$ , determines the crack length for which it can be expected that fracture rather than yielding governs the mode of failure. In this example the transition crack length is only 2.8 percent of the height,  $h$ , of the beam.

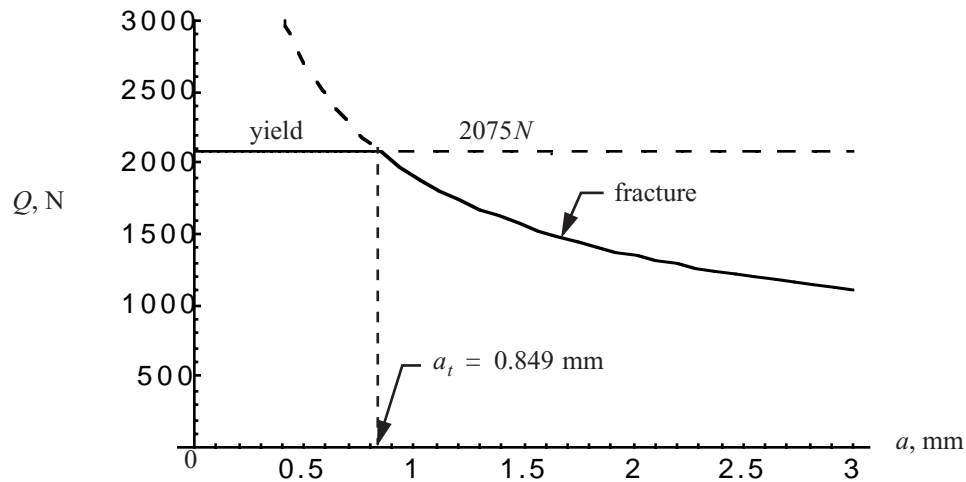


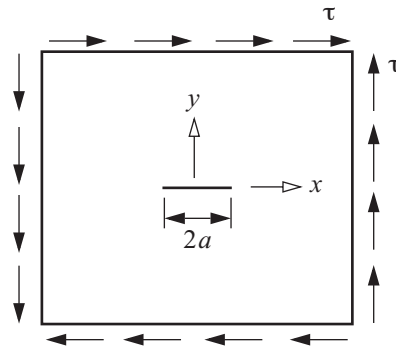
Fig. 13.10 Failure load versus crack length for the cantilever beam of example 13.2.

A comparison between eq. (c) and eq. (g) is instructive. It can be seen that the structural geometry and the factor of safety enter both relations in exactly the same way – that is, through the multiplicative parameter  $(bh^2)/(6(FS)L)$ . Also, both relations contain a basic, albeit different, material property. The essential difference is that the fracture mechanics approach explicitly introduces a new physical parameter: the size of a (real or postulated) crack-like flaw. In fracture mechanics the size of the crack is the dominant structural parameter. It is the specification of this parameter that distinguishes fracture mechanics from conventional failure analyses. ■

### 13.4 LEFM stress field in the vicinity of the crack tip for mode II

Mode II fracture is associated with loading that is antisymmetric with respect to the crack surface. Shear loading is shown in figure. 13.11 and is a mode II fracture problem.

Fig. 13.11 Antisymmetric shear loading.



From the linear elastic fracture mechanics analysis, the singular stress field near the crack tip in terms of the polar coordinates shown in figure. 13.4 is

$$\sigma_x = -\left(\frac{K_{II}}{\sqrt{2\pi r}}\right) \sin \frac{\theta}{2} \left[ 2 + \cos \frac{\theta}{2} \cos \frac{3\theta}{2} \right] + \dots, \quad (13.16)$$

$$\sigma_y = \frac{K_{II}}{\sqrt{2\pi r}} \sin \frac{\theta}{2} \cos \frac{\theta}{2} \cos \frac{3\theta}{2} + \dots, \quad (13.17)$$

$$\tau_{xy} = \frac{K_{II}}{\sqrt{2\pi r}} \cos \frac{\theta}{2} \left( 1 - \sin \frac{\theta}{2} \sin \frac{3\theta}{2} \right) + \dots, \quad (13.18)$$

where  $K_{II}$  is the mode II stress intensity factor, and  $r = 0$  at the crack tip. Along the  $x$ -axis where  $\theta = 0$ , the stresses near the crack tip are

$$\sigma_x = \sigma_y = 0 \quad \tau_{xy} = \frac{K_{II}}{\sqrt{2\pi r}} + \dots \quad (13.19)$$

Hence, the linear elastic analysis gives  $\tau_{xy} \rightarrow \infty$  as  $r \rightarrow 0$ . For an infinite plate subject to a uniform shear  $\tau$  as shown in figure. 13.11,

$$K_{II} = \tau \sqrt{\pi a} \quad \text{LEFM infinite plate solution.} \quad (13.20)$$

**The critical mode II stress intensity factor is denoted by  $K_{IIc}$ , and it is assumed to be a material parameter.**

- $K_{II} < K_{IIc}$ . There is no crack growth, and the material resists the crack without brittle fracture.
- $K_{II} = K_{IIc}$ . The crack begins to propagate and brittle fracture occurs.

The critical mode II stress intensity factor is also called the **mode II fracture toughness**.

The displacements on the two crack surfaces are antisymmetric with respect to the  $x$ -axis. Let  $u$  denote the displacement component in the  $x$ -direction, and let  $v$  denote the displacement component in the  $y$ -direction. The expression for the upper surface displacement  $u(x)$  as given by Sun (1998, p. 163) is

$$u = \frac{(\kappa + 1)(1 + \nu)}{2E} \tau \sqrt{a^2 - x^2} \quad \text{and} \quad v(x) = 0, \quad |x| \leq a. \quad (13.21)$$

The origin of the  $x$ -axis is located at the center of the crack as is shown in figure. 13.5, and  $\kappa$  depends on Poisson's ratio, which is given by eq. (13.13). Under antisymmetric loading the crack surfaces are in sliding contact with each other and do not open as they do in mode I.



### 13.5 Energy criterion for crack growth

The text that follows is taken from Gordon (1978).

The paradox that a material with a sharp crack has infinite stress at the tip, so that it fails at infinitesimal load, motivated Griffith to develop a fracture theory based on energy.

From chemistry, the surface energy needed to break chemical bonds on any one plane is from 0.1 to 1.0 J/m<sup>2</sup> for most structural solids. For brittle materials – stone, brick, concrete – 1 J/m<sup>2</sup> is nearly all the energy, or work, required to produce a new fracture surface. Ductile materials – many metals – yield before fracture, so much work goes into plastic deformation ahead of the crack tip. Some approximate values of the work of fracture are listed in the table [table 13.3] that follows.

**Table 13.3 Work of fracture for selected materials from Gordon (1978)**

Material	Approximate work of fracture J/m <sup>2</sup>	Approximate tensile strength MPa
glass, pottery	1 – 10	170
cement, brick	3 – 40	4
epoxy resins	100	50
wood	10,000	100
mild steel	10 <sup>4</sup> – 10 <sup>6</sup>	4,000
high tensile steel	10 <sup>4</sup>	1,000

A tough material has a work of fracture between 10<sup>3</sup> – 10<sup>6</sup> J/m<sup>2</sup>.

#### 13.5.1 Griffith criterion

The rationale for the Griffith energy criterion is the first law of thermodynamics and the theorem of minimum potential energy for an elastic body. The critical condition for equilibrium crack growth is that there is no net change in the total energy (Anderson, 1995, p. 36). Consider a cracked plate of thickness  $t$  with a through crack of length  $a$  as shown in figure. 13.12. Then the infinitesimal increase in the crack area is  $dA = t da$ .

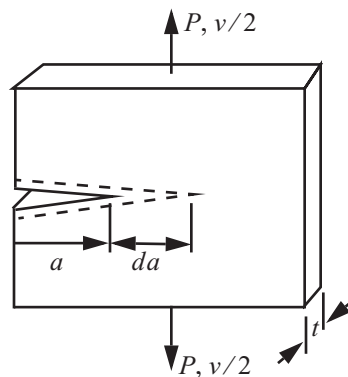


**Fig. 13.12 Mode I loading of a cracked plate.**

Let  $E$  denote the total energy,  $U$  the total strain energy contained in the plate,  $W_e$  the work performed by the

external force, and  $W_s$  the work to create new surfaces. Then,  $E = U - W_e + W_s$  and the **critical condition** for crack growth in the plate is given by

$$\frac{dE}{tda} = \frac{d}{tda}[U - W_e + W_s] = 0. \quad (13.22)$$

Rearrange the previous equation to

$$\underbrace{\frac{1}{t} \frac{dW_s}{da}}_R = \underbrace{\frac{1}{t} \frac{d}{da}[W_e - U]}_G. \quad (13.23)$$

In the latter equation  $R$  denotes the material resistance to crack growth, and  $G$  denotes the energy release rate. The energy release rate is a measure of the energy available for an increment of crack extension, and since it is obtained from the derivative of a potential, it is also called the crack extension force or crack driving force.

If  $G < R$  no crack growth  
If  $G = R$  crack growth

(13.24)

When  $G = R$  there is sufficient energy in the system to form an additional crack size  $dA$ . For the plate under the action of the load  $P$ , the load application points undergo a relative displacement  $v$ . When the crack length increases by  $da$ , the displacement will increase by  $dv$ . The work done by the external load is  $Pdv$ . Hence, for mode I loading

$$G = \frac{1}{t} \frac{d}{da}[W_e - U] = \frac{1}{t} \left[ P \frac{dv}{da} - \frac{dU}{da} \right]. \quad (13.25)$$

Prior to crack growth  $v = cP$ , where  $c$  is the compliance of the plate, and the strain energy  $U = \frac{1}{2}Pv = \frac{1}{2}cP^2$ , as is shown in figure. 13.13.

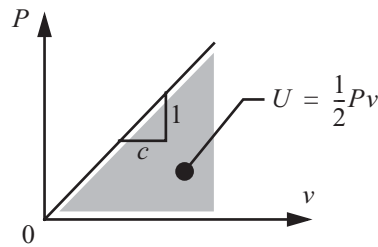


**Fig. 13.13 Elastic response prior to crack growth.**

Hence,

$$G = \frac{1}{t} \left[ P \frac{d}{da}(cP) - \frac{d}{da} \left( \frac{1}{2} cP^2 \right) \right]. \quad (13.26)$$

Performing the differentiations in eq. (13.26) we get

$$G = \frac{1}{t} \left[ P^2 \frac{dc}{da} + cP \frac{dP}{da} - \frac{P^2}{2} \frac{dc}{da} - cP \frac{dP}{da} \right] \quad \text{add to zero} \quad (13.27)$$

Therefore, the strain energy release rate is independent of whether the load changes or not during crack growth, and we get

$$G = \frac{P^2 dc}{2t da}. \quad (13.28)$$

Consider two types of loading as shown in figure. 13.14.

a. Load  $P = \text{constant}$  during crack growth

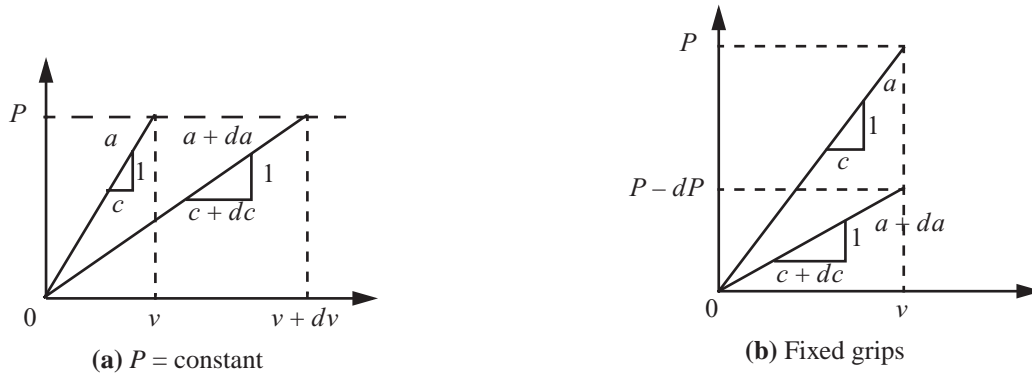


Fig. 13.14 Two types of loading under mode I crack growth.

The strain energy and its differential with respect to the compliance at a fixed value of the load is

$$U = \frac{1}{2}cP^2 \quad dU|_P = \frac{P^2}{2}dc,$$

or

$$\left. \frac{1}{t} \frac{dU}{da} \right|_P = \frac{P^2 dc}{2t da}. \quad (13.29)$$

Comparing eq. (13.28) and eq. (13.29), we find

$$G = \left. \frac{1}{t} \frac{dU}{da} \right|_P. \quad (13.30)$$

That is,  $dU > 0$  for  $da > 0$ , and for  $P$  fixed in value.

b. Fixed grips with  $v = \text{constant}$

In this case  $U = (cP^2)/2 = \left(c\left(\frac{v}{c}\right)^2\right)/2 = v^2/(2c)$  since  $P = v/c$ . Hence, the differential of the strain energy with fixed grips is

$$dU|_v = d\left(\frac{v^2}{2c}\right) = \left(\frac{v^2}{2}\right)\left(-\frac{dc}{c}\right) = -\frac{1}{2}\left(\frac{v}{c}\right)^2 dc. \quad (13.31)$$

Substitute  $v = cP$  for  $v$  in eq. (13.31) to get

$$\left. \frac{1}{t} \frac{dU}{da} \right|_v = - \left( \frac{P^2}{2t} \frac{dc}{da} \right). \quad (13.32)$$

Comparing eq. (13.28) and eq. (13.32), we find

$$G = - \left( \frac{1}{t} \frac{dU}{da} \right) \bigg|_v. \quad (13.33)$$

So  $dU < 0$  for  $da > 0$ , and for  $v$  fixed in value, and no external work is done by load  $P$ .

Equations (13.30) and (13.33) show that the strain energy release rate is always equal to the derivative of the strain energy apart from the sign. Crack extension occurs when  $G_I = R$  where  $R$  is the work of fracture, or the material resistance to crack extension. For an ideally brittle material, like glass,  $R \sim 2 \text{ J/m}^2$ , which is twice the surface energy to create two new surfaces. For ductile metals, the work of fracture is much larger than the surface energy to create new free surfaces because of plastic deformation occurring in front of the crack tip. During crack extension energy is expended by deformation of a new plastic zone at the tip of the advancing crack. Note that the Griffith energy criterion is based on linear elastic material behavior, so the formation of a nonlinear effect such as plasticity seems to negate the analysis. However, if the plastic zone ahead of the crack tip is very small compared to the bulk material remaining elastic, then the criterion is applicable. If the increase in energy required for plastic deformation is independent of the increase in crack area, then  $R = \text{constant}$ . From fracture tests of a material, the value of  $G$  at crack growth, which equals  $R$ , is called the **critical strain energy release rate**, denoted by  $G_c$ , and is assumed to be a material parameter.

If  $G < G_c$  no crack growth

If  $G = G_c$  crack growth initiates. (13.34)

### 13.6 Relation between $K$ and $G$

Consider the through-the-thickness crack in a infinite plate of unit thickness subject to uniform tension, or mode I loading, as shown in figure. 13.4. The through-crack opening displacement for a crack length of  $2a$  is shown in figure. 13.5 and given by eq. (13.12). The relation between  $K$  and  $G$  is established by computing the work done to close a crack of length  $2a$ , and restore the uniform stress  $\sigma$  in the plate to its pre-cracked value. This crack closure method is presented in several texts on fracture mechanics (e.g., Broek (1986, p. 126), Anderson (1995, p. 70), and Sun (1998, p. 164)). The analysis for the crack closure method that follows is from Sun. Denote the work done to close the crack as  $W_s(a)$  where

$$W_s(a) = 2 \int_{-a}^a \frac{1}{2} \sigma v(x) dx. \quad (13.35)$$

The factor of 2 preceding the integral in the expression for  $W_s(a)$  accounts for two crack surfaces. The crack opening displacement  $v(x)$  given by eq. (13.12) is symmetric with respect to  $x$ , and  $\sigma$  is independent of the displacement. Perform the integration to get the work done to close the crack as

$$W_s(a) = 4 \int_0^a \frac{1}{2} \sigma v(x) dx = \frac{a^2 \pi (1 + \kappa)(1 + \nu) \sigma^2}{4E}. \quad (13.36)$$

The mode I strain energy release rate per crack tip is

$$G_I = \frac{1}{2} \frac{\partial W_s}{\partial a} = \frac{a \pi (1 + \kappa)(1 + \nu) \sigma^2}{4E}. \quad (13.37)$$

Substitute  $\sigma = K_I / \sqrt{\pi a}$  from (13.8), and substitute eq. (13.13) for  $\kappa$ , in the previous equation to get

$$G_I = \frac{K_I^2}{E'}, \quad (13.38)$$

where

$$E' = E \text{ for plane stress and } E' = E/(1 - \nu^2) \text{ for plane strain.} \quad (13.39)$$

For mode II fracture the relation between  $K_{II}$  and  $G_{II}$  is

$$G_{II} = \frac{K_{II}^2}{E'}. \quad (13.40)$$

Equations (13.38) to (13.40) are also valid for finite dimensions and arbitrary loading, however,  $K_I$  and  $K_{II}$  depend on the configuration and loading of the plate. Thin plates that are closer to the ideal plane stress condition have higher fracture toughness than thick plates that are closer to the state of plane strain. Most standard fracture tests are performed using thick specimens, and thus they give fracture toughness under the plane strain condition. Fracture toughness of a material can be given by either  $G_c$  or  $K_c$ .

### 13.6.1 Mixed mode fracture

Generally, crack growth occurs under mixed mode loading. Under this type of loading, crack growth might occur before any of the energy release rate components attain their individual critical value. Failure interaction criteria are established from mixed mode fracture test configurations. The following criterion has been shown to fit test data for many materials quite well:

$$\frac{G_I}{G_{Ic}} + \frac{G_{II}}{G_{IIc}} = 1, \quad (13.41)$$

where  $G_{Ic}$  and  $G_{IIc}$  are the single mode critical energy release rates for modes I and II, respectively. From the relations between  $G$  and  $K$  in eqs. (13.38) and (13.40), the previous criterion (13.41) in terms of the **stress intensity factors** is

$$\left( \frac{K_I}{K_{Ic}} \right)^2 + \left( \frac{K_{II}}{K_{IIc}} \right)^2 = 1. \quad (13.42)$$

### 13.7 Interlaminar failure in composites: delamination

The main failure modes of fiber-reinforced polymer (FRP) composites were discussed in article 9.1 on page 271. Laminated composite structures can fail within lamina, which is intralaminar failure; between lamina, which is interlaminar failure; or by interacting together in a complex manner. Interlaminar failure refers to debonding of adjacent lamina, or delamination, which can initiate from an interfacial crack.

Delamination is the chief vulnerability of composites. However, Boeing's Chief Technology Officer states: "We designed [composite parts] so they carry loads even if delaminated. We know how to inspect and we know how to repair." (Canaday, 2015)

In this section delamination is analyzed with the concepts from fracture mechanics. An initial delamination crack is postulated and fracture mechanics principles are used to determine if the crack will propagate in a self-similar manner. The examples analyzed here are standard fracture test configurations. The tests are performed on unidirectional composites with the fibers oriented such that they are parallel to the length of the initial delamination. Consequently, the fracture configurations are modeled as laminated beams. The material is carbon fiber-reinforced epoxy with the properties listed in table 13.4.

**Table 13.4 T300/977-2 carbon fiber composite**

$E_1$	$E_2$	$\nu_{21}$	$G_{12}$	$G_{Ic}$	$G_{IIc}$
150 GPa	11.0 GPa	0.25	6.0 GPa	352 J/m <sup>2</sup>	1,450 J/m <sup>2</sup>

Note that the critical mode I strain energy release rate  $G_{Ic}$  for interface fracture is the order of the work of fracture listed for epoxy resins in article 13.5 on page 387.

#### Example 13.3 Double cantilever beam (DCB) fracture test specimen

Consider a cantilever, laminated beam subject to equal and oppositely directed forces of magnitude  $P$  applied at the free end. Under the action of the forces there is a crack at the free end perpendicular to the forces of length  $a$  and centered with respect to the depth of the beam. The length of the beam is  $L$ , depth is  $2h$ , and its thickness is  $t$ . This is a case of mode I loading, and the initial crack length  $a_0 = 50$  mm when  $P = 0$ . See figure. 13.15. The

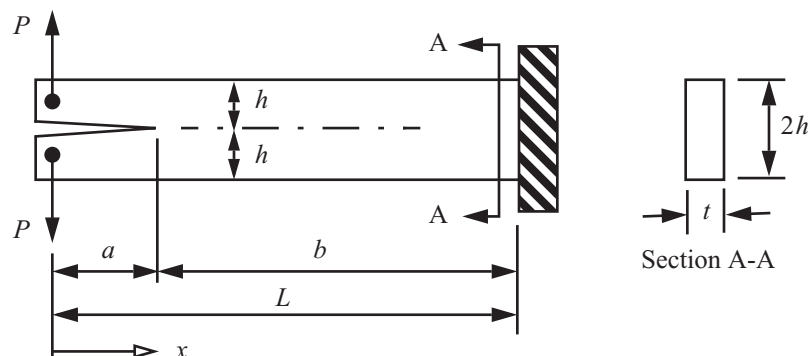


**Fig. 13.15 Double cantilever beam configuration of example 13.3.**

following data is specified:  $h = 1.98$  mm,  $t = 20$  mm, and  $L \gg 2h$ . Material properties are listed in table 13.4. Let  $v$  denote the relative vertical displacement of the load points. Determine static response of the beam and plot

it on the  $P$ - $v$  plane. Analytical and numerical solutions for this example were originally given by Mi, et al., (1998).

**Solution.** We use Castigliano's second theorem to determine the relative displacement  $v$ . Complementary strain energy is stored in each arm of the beam for  $0 \leq x \leq a$ , and not in the un-stressed section of the beam from  $a < x \leq L$ . The complementary strain energy is

$$U^* = \frac{1}{2} \int_0^a \frac{M_1^2}{EI} dx + \frac{1}{2} \int_0^a \frac{M_2^2}{EI} dx, \quad (\text{a})$$

where the bending moment in the upper arm is  $M_1$ , the bending moment in the lower arm is  $M_2$ , and the second area moment of each arm is

$$I = \frac{th^3}{12} = 12.9373 \text{ mm}^4. \quad (\text{b})$$

Note that the modulus of elasticity  $E = E_1$ . The distribution of the bending moment in each arm is determined from equilibrium. The results are

$$M_1(x) = -M_2(x) = -Px \quad 0 \leq x \leq a. \quad (\text{c})$$

Hence,

$$v = \frac{\partial U^*}{\partial P} = \frac{1}{EI} \left\{ \int_0^a (-Px)(-x) dx + \int_0^a (Px)(x) dx \right\} = \frac{2P}{EI} \int_0^a x^2 dx. \quad (\text{d})$$

Performing the integration in eq. (d) we get

$$v = \frac{2Pa^3}{3EI}. \quad (\text{e})$$

From this last equation, the compliance of the beam is given by  $c = (2a^3)/(3EI)$ . The strain energy release rate is determined from eq. (13.28), which yields

$$G_I = \frac{P^2 dc}{2t da} = \frac{P^2 a^2}{tEI}. \quad (\text{f})$$

At the initiation of crack growth  $G_I = G_{Ic}$ , so

$$G_{Ic} = \frac{P^2 a^2}{tEI} \text{ at crack growth.} \quad (\text{g})$$

Solve eq. (g) for the crack length  $a$  to get

$$a = (tEI G_{Ic})^{1/2} \left( \frac{1}{P} \right). \quad (\text{h})$$

Substitute eq. (h) for crack length  $a$  into eq. (e) to get

$$v = \frac{2(tG_{Ic}EI)^{3/2}}{3EIP^2} \text{ for the propagating crack.} \quad (i)$$

Prior to crack growth eq. (e) determines the response as

$$v = \frac{2}{3} \frac{(50 \text{ mm})^3 P}{(150,000 \text{ N/mm}^2)(12.9373 \text{ mm}^4)} = (0.04294 \text{ mm/N})P. \quad (j)$$

For the propagating crack eq. (h) evaluates to

$$a = [(20 \text{ mm})(150,000 \text{ N/mm}^2)(12.9373 \text{ mm}^4)(0.352 \text{ N/mm})]^{1/2} \left( \frac{1}{P} \right) = \frac{3,696.19 \text{ Nmm}}{P}. \quad (k)$$

For the initial crack length  $a_0 = 50 \text{ mm}$  eq. (k) determines the maximum load, and then either eq. (e) or eq. (j) determines the corresponding displacement; i.e.,

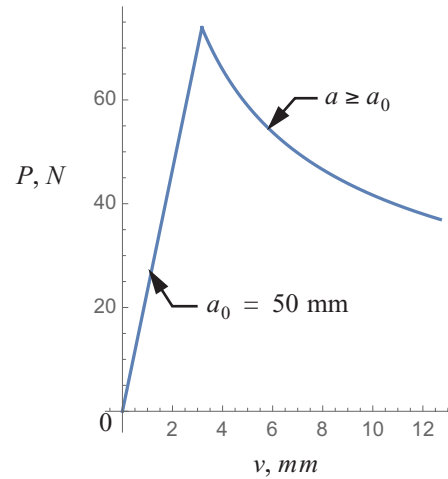
$$P = 73.9238 \text{ N and } v = 3.1744 \text{ mm at the initiation of crack growth.}$$

For the propagating crack eq. (i) evaluates to

$$v = \frac{2}{3} \frac{[20 \text{ mm}(0.352 \text{ N/mm})(150,000 \text{ N/mm}^2)(12.9373 \text{ mm}^4)]^{3/2} \left( \frac{1}{P^2} \right)}{(150,000 \text{ N/mm}^2)(12.9373 \text{ mm}^4)} = 17,347.4 \text{ N}^2 \text{mm} \left( \frac{1}{P^2} \right). \quad (l)$$

Equations (j) and (l) are used to plot the load-displacement response shown in figure. 13.16.

**Fig. 13.16 Static response of the DCB configuration. Crack growth begins at 73.92 N and 3.17 mm.**



In load control, where  $P$  is specified and increased slowly from zero, a sudden dynamic increase in crack growth occurs at  $P = 73.9238 \text{ N}$  since there is no stable adjacent equilibrium state. In displacement control, where  $v$  is specified and is increased slowly from zero to 3.17 mm, the load  $P$  increases to 73.92 N. For  $v > 3.17 \text{ mm}$  the load decreases as the crack increases in length.



**Example 13.4 End load split (ELS) configuration**

The end load split (ELS) configuration shown in figure. 13.17 has an initial crack length denoted by  $a = a_0$ , length by  $L$ , height by  $2h$ , and thickness normal to the  $x$ - $y$  plane by  $t$ . The lower arm at the tip is subject to vertical force  $P$ . Both arms below and above the crack are identical and are subject to the same load as shown in the free body diagrams of figure. 13.18. Hence, both arms have the same lateral displacement  $v(x)$  and rotation  $-v'(x)$ . The  $x$ -direction displacement at the crack tip of the upper arm is  $\frac{h}{2}[v'(a)]$ , and the  $x$ -direction displacement of the lower arm at the crack tip is  $\frac{h}{2}[-v'(a)]$ . Thus, the relative axial displacement between the lower surface of the upper arm and the upper surface of the lower arm is  $h[v'(a)]$ , which is a mode II displacement loading. Determine the strain energy release rate  $G_{II}$ . Analytical and numerical solutions for this example were originally given by Chen et al. (1999).

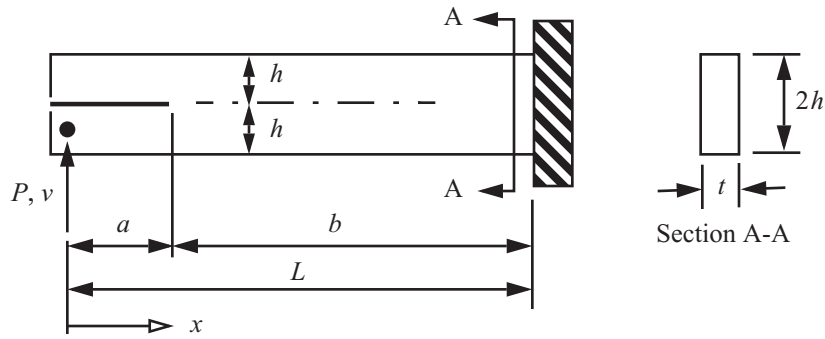


**Fig. 13.17** End load split configuration of example 13.4.

**Solution.** The strain energy is

$$U = \int_0^a \frac{M_1^2}{2EI} dx + \int_0^a \frac{M_2^2}{2EI} dx + \int_a^L \frac{M_3^2}{2E(8I)} dx, \quad (\text{a})$$

where  $M_1$  denotes the bending moment in the arm below the crack,  $M_2$  the bending moment in the arm above the crack, and  $M_3$  the bending moment in the segment not containing the crack. The second area moment of each arm is denoted by  $I$ , and  $I = (th^3)/12$ . From the free body diagrams shown in figure. 13.18, equilibrium determines the bending moments as

$$M_1(x) = M_2(x) = -\left(\frac{P}{2}\right)x \quad 0 \leq x \leq a, \text{ and} \quad (\text{b})$$

$$M_3(x) = -(x-a)P + M_1(a) + M_2(a) = -Px \quad a \leq x \leq L. \quad (\text{c})$$

Substitute eqs. (b) and (c) for the bending moments in eq. (a), and perform the integrations to get

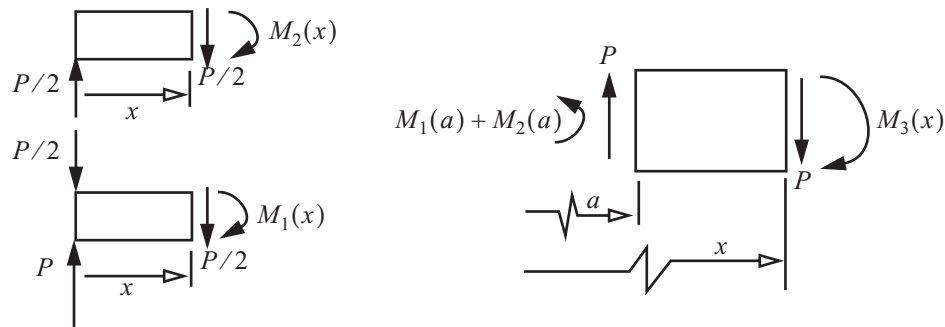


Fig. 13.18 Free body diagrams of the three segments of the ELS configuration.

$$U = \frac{(3a^3 + L^3)P^2}{48EI}. \quad (d)$$

The mode II strain energy release rate is

$$G_{II} = \frac{\partial U}{\partial a} = \frac{3a^2 P^2}{16tEI}. \quad (e)$$

### 13.7.1 Mixed mode fracture

Consider a cantilever beam of length  $L$  containing a through crack of length  $a$  centered at its free end. This configuration subject to load  $P$  shown in part (a) of figure. 13.19 is labeled FRMM, which means fixed ratio mixed mode. By the method of superposition FRMM is equivalent to the DCB test configuration shown in part (b) of the figure plus the ELS test configuration shown in part (c) of the figure. Hence, the FRMM configuration is a mixed mode I and II fracture test.

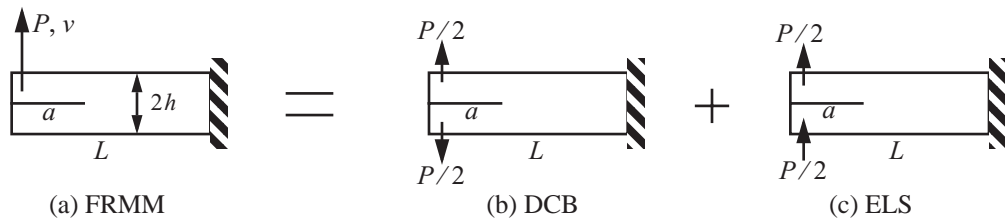


Fig. 13.19 Mixed mode I and II loading: (a) fixed ratio mixed mode, (b) double cantilever beam, and (c) end load split.

From eq. (f) in example 13.3 the mode I strain energy release rate for the configuration in part (b) of figure. 13.19 is

$$G_I = \left. \frac{P^2 a^2}{tEI} \right|_{P \rightarrow P/2} = \frac{P^2 a^2}{4tEI}. \quad (13.43)$$

From eq.(e) in example 13.4 the mode II strain energy release rate for the configuration in part (c) of figure. 13.19 is

$$G_{II} = \frac{3a^2P^2}{16tEI}. \quad (13.44)$$

Therefore, the mixed mode ratio for the FRMM configuration is  $G_I/G_{II} = 4/3$ .

### Example 13.5 Response of the FRMM configuration shown in figure. 13.19

Take the height of the arms  $h = 1.5$  mm, thickness  $t = 10$  mm, length  $L = 100$  mm, so that  $I = 2.8125$  mm<sup>4</sup>. The initial crack length  $a_0 = 40$  mm. From table 13.4 where  $E = 150,000$  N/mm<sup>2</sup>,  $GI_c = 0.352$  N/mm and  $GII_c = 1.45$  N/mm. Determine the load-displacement response, and the crack-length-displacement response.

**Solution.** The bending moment in the FRMM configuration is  $M = -Px$ ,  $0 \leq x \leq L$ . The strain energy is

$$U = \int_0^a \frac{M^2}{2EI} dx + \int_a^L \frac{M^2}{2E(8I)} dx = \frac{(7a^3 + L^3)P^2}{48EI}, \quad (a)$$

where  $I = th^3/12$ . The displacement corresponding to load  $P$  is given by

$$v = \frac{\partial U}{\partial P} = \frac{(7a^3 + L^3)P}{24EI}. \quad (b)$$

The displacement prior to crack growth

$$v = v_0 = (0.143012 \text{ mm/N})P. \quad (c)$$

The mode I (13.43) and mode II (13.44) strain energy release rates are

$$G_I = \left[ 5.92593 \times 10^{-8} \left( \frac{1}{\text{mm}^3 \text{N}} \right) \right] a^2 P^2 \quad G_{II} = \left[ 4.44444 \times 10^{-8} \left( \frac{1}{\text{mm}^3 \text{N}} \right) \right] a^2 P^2. \quad (d)$$

Evaluate the mixed mode fracture criterion (13.41) to get

$$\left[ 1.99002 \times 10^{-7} \left( \frac{1}{\text{mm}^2 \text{N}^2} \right) \right] a^2 P^2 = 1. \quad (e)$$

Solve eq. (e) for  $a$  to find

$$a = \frac{2241.67 \text{ mmN}}{P}. \quad (f)$$

Substitute the crack length from eq. (f) into eq. (b) to get the displacement for the propagating crack

$$v = \frac{7,797.87 \text{ mmN}^2}{P^2} + (0.0987654 \text{ mm/N})P. \quad (g)$$

The transition from the initial crack to the propagating crack is obtained by equating eq. (c) to eq. (g). The result

is

$$(v, P) = (8.01466 \text{ mm}, 56.04 \text{ N}). \quad (\text{h})$$

For the crack length  $a = L$ , eq. (f) yields  $P = 22.41 \text{ N}$ . Hence, at completed separation

$$(v, P) = (17.32 \text{ mm}, 22.41 \text{ N}). \quad (\text{i})$$

The response plots for the FRMM fracture specimen are shown in figure. 13.20. ■

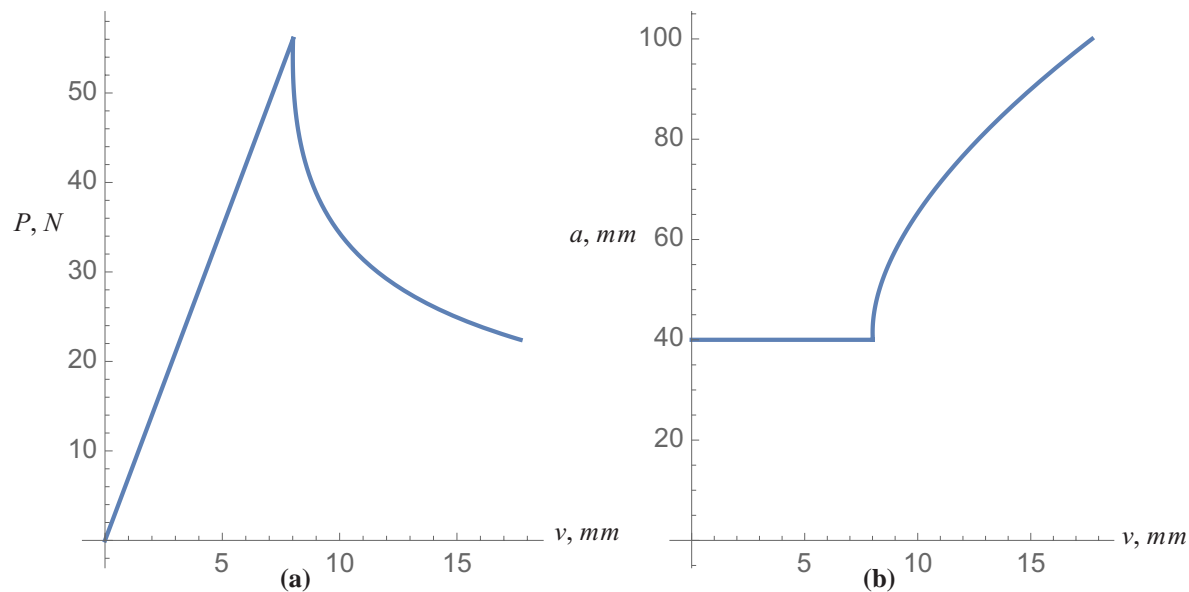


Fig. 13.20 (a) Load-displacement, and (b) crack length vs. displacement for the FRMM fracture test.

## 13.8 References

- Anderson, T.L. **Fracture Mechanics**, 2d ed. Boca Raton, FL: CRC Press, Inc., 1995.
- Broek, David. **Elementary Engineering Fracture Mechanics**, 4d ed., Dordrecht, The Netherlands: Martinus Nijhoff Publishers, 1986, p. 126.
- Canaday, H. "Composites vs. Metals." *Aerospace America*, May 2015, p. 18.
- Cawthon, Bill. "De Havilland's Comet: The Original Jetliner." Promotex Online, June 15, 2005, [http://www.promotex.ca/articles/cawthon/2005/2005-06-15\\_article.html](http://www.promotex.ca/articles/cawthon/2005/2005-06-15_article.html).
- Chen, J., M. Crisfield, A. Kinloch, E. Busso, E., F. Matthews, and Y. Qiu. "Predicting Progressive Delamination of Composite Material Specimens via Interface Elements." *Mechanics of Composite Materials and Structures* 6, (1999): 301-317.
- Dowling, Norman. **Mechanical Behavior of Materials: Engineering Methods for Deformation, Fracture and Fatigue**, 2d ed. Upper Saddle River, NJ: Prentice Hall, 1999, pp. 291, 292.

Gordon, J. E. *Structures or Why Things Don't Fall Down*. Boston: Da Capo Press, 2003. (Originally published by Harmondsworth: Penguin Books, 1978.)

Kanninen, Melvin F., and Carl H. Popelar. *Advanced Fracture Mechanics*. New York: Oxford University Press, 1985.

Mi, Y., M. Crisfield, G. Davies, and H-B. Hellweg. "Progressive Delamination Using Interface Elements." *Journal of Composite Materials* 332 (1998): 1246-1273.

Sun, C. T. *Mechanics of Aircraft Structures*. New York: John Wiley & Sons, 1998.

"de Havilland Comet." Wikipedia, [https://en.wikipedia.org/wiki/De\\_Havilland\\_Comet](https://en.wikipedia.org/wiki/De_Havilland_Comet) (accessed February 2008).

### 13.9 Practice exercises

1. A monocoque fuselage consists of a circular cylindrical shell with a mean radius  $R = 50.0$  in. and wall thickness denoted by  $t$ , where  $R \gg t$ . It is subject to internal pressure  $p$ , with the design ultimate pressure specified as  $p = 18.2$  psi. A damage tolerance philosophy allows for the presence of a subcritical crack that will not grow to critical length between periodic inspections. Assume an axial crack through the thickness of the wall of the shell with a length  $2a = 2.0$  in. **Determine the minimum thickness of the shell such that crack growth does not occur at the design ultimate pressure.** The material is 2024-T351 aluminum alloy with a fracture toughness  $K_{Ic} = 31 \text{ ksi}\sqrt{\text{in.}}$ , and a yield strength of 47 ksi.

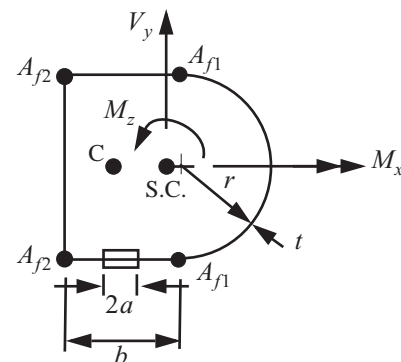
The mode I stress intensity factor for an axial crack through the thickness of a cylindrical shell subject to internal pressure is (Anderson, p. 636)

$$K_I = \sigma_\theta \sqrt{\pi a} \sqrt{1 + 0.52\chi + 1.29\chi^2 - 0.074\chi^3}, \quad (\text{a})$$

where the dimensionless parameter  $\chi = a/(\sqrt{Rt})$ . The circumferential normal stress, or hoop stress, is  $\sigma_\theta = (pR)/t$ .

2. Consider the cross section at the root of the wing spar in example 6.6 on page 165 as shown in figure. 13.21.

**Fig. 13.21** Cross section at the root of the wing spar in Exercise 8.2.



During an inspection a one-inch crack ( $2a = 1.0$ ) is detected that is parallel to the chord in the center of the lower web at the root section. (This web is labeled branch 4 in Fig. 3.24 on page 71.) At the root cross section the transverse shear force  $V_y$ , bending moment  $M_x$ , and torque  $M_z$  are given by

$$V_y = \frac{L}{2} \quad M_x = \frac{-2Lz_{\max}}{3\pi} \quad M_z = \frac{eL}{2}. \quad (\text{b})$$

The total lift force acting on the airplane is denoted by  $L$ , the span of the wing spar by  $z_{\max}$ , and  $e$  denotes the distance from the shear center to the line of action of the lift force acting on the wing. Take  $z_{\max} = 120$ . in.

Pertinent data are listed in table 13.5.

**Table 13.5 Data from example 6.6**

$r$ , nose web radius	6.0 in	$I_{xx}$ , second area moment about the $x$ -axis	101.619 in. <sup>4</sup>
$b$ , length horizontal web	7.0 in.	$A_c$ , area enclosed by the contour	140.549 in. <sup>2</sup>
$t$ , wall thickness	0.030 in.	$e = X_L - X_{SC}$	3.604 in.

To aid in computing the shear stress, the shear flow in the lower web is given by

$$q_4(s_4) = \frac{M_z}{2A_c} - F_{y4}(s_4)V_y. \quad (\text{c})$$

Repeating eq. (ae) in example 3.4 on page 71, the shear flow distribution function is

$$F_{y4}(s_4) = 0.00542827 - 0.00177133s_4 \quad 0 \leq s_4 \leq 7 \text{ in.} \quad (\text{d})$$

The critical mode I stress intensity factor  $K_{Ic} = 31 \text{ ksi}\sqrt{\text{in.}}$ , and the critical mode II stress intensity factor  $K_{IIc} = 23.5 \text{ ksi}\sqrt{\text{in.}}$ . **Determine the lift force  $L$  to initiate crack growth using a factor of safety FS = 1.5.**

**3.** Consider the end load split (ELS) fracture configuration in example 13.4 on page 395. It is modeled as a laminated beam made of unidirectional plies of the carbon-epoxy listed in table 13.4. Take  $E_1$  for the modulus of elasticity. For  $a_0 = 30 \text{ mm}$ ,  $L = 100 \text{ mm}$ ,  $t = 30 \text{ mm}$ , and  $h = 1.5 \text{ mm}$ , complete the following steps:

- Use Castigliano's second theorem to determine the tip displacement  $v$  at the point of load application.
- Determine the crack length  $a$  for  $G_{II} = G_{IIc}$ .
- Determine the displacement  $v$  for the crack length in part (b).
- Plot the load  $P$  versus displacement  $v$  for  $a_0 \leq a \leq L$ . Comment on the  $P$ - $v$  plot for the propagating crack as compared to the same plot for the DCB configuration shown in figure. 13.16.

Partial answer: The maximum load is 571.183 N.

4. Consider the fixed ratio mixed mode (FRMM) fracture configuration in article 13.7.1. It is modeled as a laminated beam of made of unidirectional plies of the carbon-epoxy listed in table 13.4. Take  $E_1$  for the modulus of elasticity. For  $a_0 = 40$  mm ,  $L = 100$  mm ,  $t = 10$  mm , and  $h = 1.5$  mm , complete the following steps:

- a) Use Castigliano's second theorem to determine the tip displacement  $v$  at the point of load application.
- b) Determine the crack length  $a$  from eq. (13.41).
- c) Determine the displacement  $v$  for the crack length in part (b).
- d) Plot the load  $P$  versus displacement  $v$  for  $a_0 \leq a \leq L$ .

Partial answer: The maximum load is 56.04 N.





---

## *Design of a landing strut and wing spar*

---

The methodology for the design of a landing strut and a wing spar are discussed in this chapter. Simultaneous satisfaction of the strength and deflection are required in the design of the landing strut. The objective for the wing spar design is to determine two design variables that minimize the weight of the spar subject to constraints on material yielding, buckling, and fracture. Practice exercises in design are included for the reader to complete. The exercise in article 14.1.2 requires a re-design of the strut. The exercise in article 14.2.3 involves a mono-coque spar, and the exercise in article 14.3.3 involves a stringer-stiffened spar.

### *14.1 Landing strut*

Private aircraft are certified in the United States under the FAA Federal Aviation Regulation (FAR) Part 23 – Normal, utility, acrobatic, and commuter category. Landing gear struts, or shock struts, are designed to absorb dynamic loads due severe impact. Design of a simple steel leaf spring strut is discussed in this article, which augments the original design methodology presented by Thurston (1995). FAA design conditions require each main wheel to carry a vertical load at least equal to the airplane gross weight per FAR 23.473(g) and FAR 23 Appendix C. The gross weight of the airplane  $W = 2,000$  lb., and the configuration of the landing strut is shown in figure 14.1.

#### **14.1.1 Strut deflection**

When developing a strut design it is necessary to vary the spring strut dimensions  $b$  and  $h$  as shown in figure 14.1 until sufficient deflection is obtained to provide acceptable vertical force load factors. If the spring strut is too stiff, the deflection is too low and the vertical load factor is high. If the spring strut is too compliant, the deflection is too large and the landing gear is springy, but the vertical load factor may be acceptable. We use Castigliano's second theorem to determine the formula for vertical deflection of the strut:

$$\Delta = \frac{\partial U^*}{\partial R}, \quad (14.1)$$

where  $U^*$  is the complementary strain energy. Energy is stored in the strut due to bending, compression, and

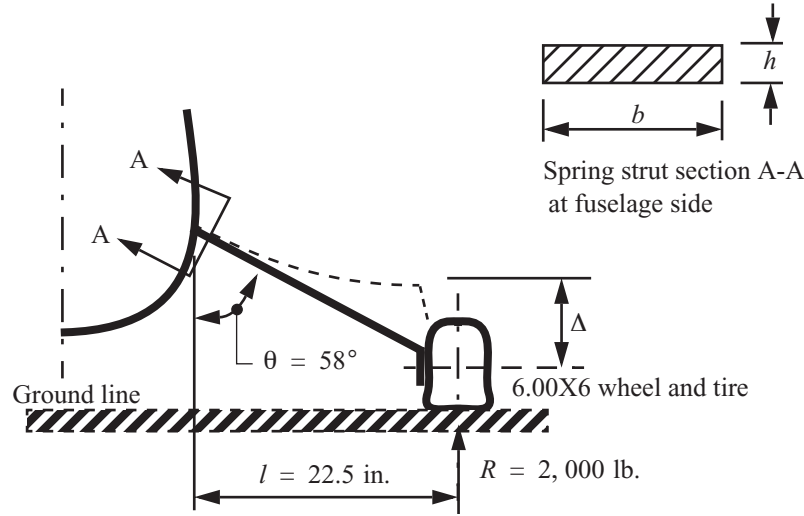


**Fig. 14.1** Sketch of the steel leaf spring strut configuration.

transverse shear deformation. However, the deflection is dominated by bending, so

$$U^* = \int_0^L \left[ \frac{M_x^2}{2EI_{xx}} \right] dz, \quad (14.2)$$

where  $L$  is the length of the strut,  $z$  is the axial coordinate;  $z = 0$  @ axel,  $M_x(z)$  is the bending moment,  $E$  is Young's modulus, and  $I_{xx}$  is the second area moment about the centroidal  $x$ -axis. Interchanging the derivative and definite integral in eq. (14.2), the deflection in the direction of  $R$  is

$$\Delta = \frac{\partial U^*}{\partial R} = \int_0^L \left[ \frac{M_x}{EI_{xx}} \frac{\partial M_x}{\partial R} \right] dz. \quad (14.3)$$

To determine how the bending moment, axial force, and shear force depend on  $R$ , impose static equilibrium conditions on the strut. From the free-body diagram shown in figure. 14.2, we get

$$V_y + R \sin \theta = 0 \quad N + R \cos \theta = 0 \quad M_x + zR \sin \theta = 0 \quad 0 \leq z \leq L. \quad (14.4)$$

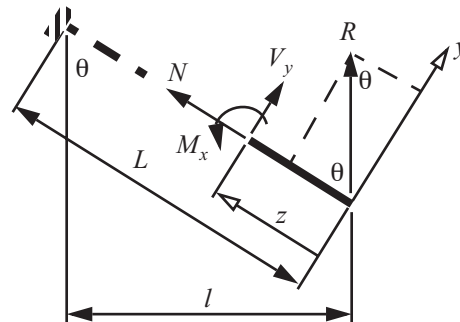


**Fig. 14.2** Free body diagram of the strut.

Substitute the bending moment from eq. (14.4) into eq. (14.3) to find

$$\Delta = \frac{1}{EI_{xx}} \int_0^L (-zR \sin \theta)(-z \sin \theta) dz = \frac{RL^3 \sin^2 \theta}{3EI_{xx}}. \quad (14.5)$$

The horizontal length  $l = L \sin \theta$ . Eliminate strut length in terms of the horizontal length in eq. (14.5) to get

$$\Delta = \frac{Rl^3}{3EI_{xx} \sin \theta}. \quad (14.6)$$

Take the strut to be made of steel having a Young's modulus of  $30 \times 10^6$  psi. Consider an initial size of

$$b = 3.0 \text{ in.} \quad h = 0.69 \text{ in.} \quad (14.7)$$

The cross-sectional area  $A = 3(0.69) = 2.07 \text{ in.}^2$ . The second area moment about the centroidal  $x$ -axis in the cross section is

$$I_{xx} = \frac{bh^3}{12} = \frac{3(0.69)^3}{12} = 0.0821 \text{ in.}^4 \quad (14.8)$$

Numerical evaluation of the strut deflection is

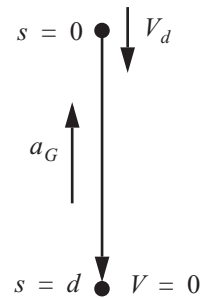
$$\Delta = \frac{(2,200 \text{ lb.})(22.5 \text{ in.})^3}{3(30 \times 10^6 \text{ lb./in.}^2)(0.0821 \text{ in.}^4) \sin 58^\circ} = 4.00 \text{ in.} \quad (14.9)$$

The stopping distance  $d$  is equal to the stroke of the strut plus the tire deflection. From 6.00X6 tire deflection charts at an inflation pressure of 20 psi, the tire deflection is 3.14 in. at 2,200 lb. loading. Hence,

$$d = \Delta + 3.14 \text{ in.} = 7.14 \text{ in.} = 0.595 \text{ ft.} \quad (14.10)$$

According to FAR 23.473(d), the initial descent velocity, in feet per second, for landing gear design calculations cannot be less than  $4.4(W/S)^{1/4}$ , where  $W$  is the gross weight in pounds and  $S$  is the wing reference area in sq. ft. Assuming  $S = 157 \text{ ft.}^2$  we get  $V_d = 8.5 \text{ ft./s.}$  Now assume the acceleration of the mass center is constant during the period of landing. Let descent velocity at touchdown be denoted by  $V_d$ , and during the period of landing the vertical speed reduces from  $V_d$  to zero. The acceleration of the mass center is computed from the uniform acceleration formula given by eq. (2.14) on page 12. See figure. 14.3.

**Fig. 14.3**  
Uniform  
deceleration  
along a  
straight line.



$$a_G = V_d^2 / (2d) = \frac{(8.5)^2}{2(0.595)} = 60.714 \text{ ft/s}^2. \quad (14.11)$$

The load factor at touchdown is

$$n = 1 + \frac{60.714}{32.2} = 2.89. \quad (14.12)$$

The load reduction due to wing lift is 0.67 as stipulated in FAR 23.473(e), so the landing gear limit load factor is

$$n = 2.89 - 0.67 = 2.2. \quad (14.13)$$

**Strength consideration.** The axial normal stress is due to the superposition of the bending component and the compression component.

$$\sigma_z = \frac{M_x y}{I_{xx}} + \frac{N}{A} \quad -\frac{h}{2} \leq y \leq \frac{h}{2} \quad 0 \leq z \leq L. \quad (14.14)$$

Substitute  $M_x$  and  $N$  from eq. (14.4), and substitute  $I_{xx}$  from eq. (14.8), into eq. (14.14) to get

$$\sigma_z = \frac{-zR \sin \theta (h/2)}{(bh^3)/12} - \frac{R \cos \theta}{bh} = \frac{-6zR \sin \theta}{bh^2} - \frac{R \cos \theta}{bh}. \quad (14.15)$$

The axial normal stress (14.15) attains maximum magnitude at  $z = L$ . For  $b = 3$  in. and  $h = 0.69$  in. the maximum magnitude is

$$\sigma_z|_{z=L} = -208,503. - 563.2 = -209,066.2 \text{ psi}.$$

Steel alloy 4340, oil quenched and tempered, has a yield strength of 230 ksi and an ultimate tensile strength of 250 ksi. A major application of alloy 4340 is to aircraft landing gears because of its high strength. For design assume an allowable stress of 160 ksi, which implies a factor of safety of 1.4 with respect to yield. The margin of safety is defined by

$$MS = \frac{\text{excess strength}}{\text{required strength}} = \frac{\sigma_{\text{allowable}} - |\sigma_z|_{\text{max}}}{|\sigma_z|_{\text{max}}}. \quad (14.16)$$

The margin of safety is positive for a feasible design, and negative for an infeasible design. For the design  $b = 3$  in. and  $h = 0.69$  in., the  $MS = -0.233$ . Therefore, with respect to strength the design (14.7) is infeasible.

Moreover, the landing gear limit load factor is specified as 2.0 in FAR 23.473(g), and not the 2.2 determined for the initial design (14.7). To achieve the required landing gear load factor we compute new values for the acceleration, the stopping distance and the stroke of the strut as follows:

$$a_G = (2 - 1 + 0.67)g = 53.77 \text{ ft./s}^2 \quad d = V_d^2 / (2a_G) = 8.09 \text{ in.} \quad \Delta = d - 3.14 = 4.95 \text{ in.} \quad (14.17)$$

The new second area moment for the leaf spring strut is obtained by a rearrangement of (14.9):

$$I_{xx} = \frac{Rl^3}{3E(4.95) \sin \theta} = 0.06638 \text{ in.}^4 = \frac{bh^3}{12}. \quad (14.18)$$

Solve eq. (14.18) for  $h$  to get

$$h = 0.9269883 / b^{1/3}. \quad (14.19)$$

Substitute eq. (14.19) for  $h$  into axial normal stress (14.15) and evaluate it at  $z = L$  to get

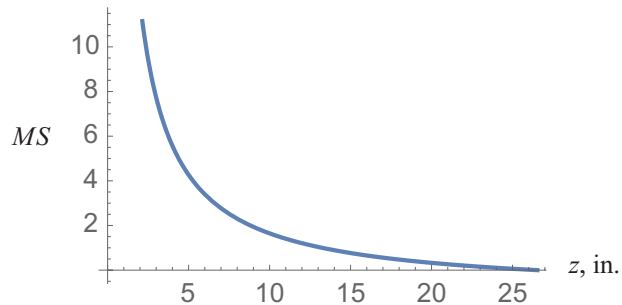
$$\sigma_z = \frac{-1,257.65}{b^{2/3}} - \frac{345,632.}{b^{1/3}}. \quad (14.20)$$

Set  $|\sigma_z| = 160,000$  psi in eq. (14.20), and by a root finding routine, or by a trial and error method, find

$$b = 10.13 \text{ in.} \quad h = 0.4284 \text{ in.} \quad (14.21)$$

For the design (14.21), the margin of safety (14.16) is positive for  $0 \leq z \leq L$  as shown in figure. 14.4. At  $z = L = 26.53$  in. it is  $6.7 \times 10^{-16} \sim 0$  and at  $z = 0$  it is 594.7. The design (14.21) is feasible with respect to strength and also satisfies the landing gear load factor of 2.

**Fig. 14.4** Distribution of the margin of safety along the length of the strut for design (14.21).



### 14.1.2 Strut design exercise

Although the margin of safety is positive along the length of the strut in figure. 14.4, it is very large over most of the length of the strut. An efficient use of material to carry the load has a margin of safety that is slightly positive. The large positive values of the margin of safety shown in figure. 14.4 indicate that the design is too heavy. The specific weight of steel is  $0.284 \text{ lb./in.}^3$ , so the weight of the leaf spring strut (14.21) is

$$W = (0.284 \text{ lb./in.}^3)(10.13 \text{ in.})(0.4284 \text{ in.})(26.53 \text{ in.}) = 32.7 \text{ lb.} \quad (14.22)$$

Since the axial normal stress (14.15) is linear in the coordinate  $z$ , it is reasonable to assume that the cross-sectional area of the strut should be linear in  $z$ . Take the thickness of the strut  $h$  to be independent of  $z$ , and let the width of the strut be a linear function of  $z$ . That is,

$$b(z) = b_L \left( \frac{z}{L} \right) + b_0 \left( 1 - \frac{z}{L} \right) \quad 0 \leq z \leq L, \quad (14.23)$$

where  $b_0$  is the width at the axel and  $b_L$  is the width at the fuselage. Of course, this means that the second area moment of the cross section,  $I_{xx} = (bh^3)/12$ , is a linear function of  $z$ .

1. Determine the value of the design variables  $h$ ,  $b_0$ , and  $b_L$  such that stroke is equal to 4.95 in. and the magnitude of the normal stress  $\sigma_z$  is less than, or equal to, an allowable value of 160,000 psi.
2. Plot the margin of safety for strength of the design in step 1 with respect to  $z$  for  $0 \leq z \leq L$ .
3. Compute the weight of the design determined in step 1.

## 14.2 Wing spar design

The wing spar is the primary load bearing structure in the wing. Consider the design of a spar for minimum weight under a particular maneuver condition subject to different design limit states. The example is the Mohawk commuter airplane shown in figure. 14.5. The wing is slightly tapered, but to simplify the analysis we will treat it as uniform. The wing span is 74 feet, and the wing area is 592 square feet, so that the average chord is 8 feet. About 9 feet of this wing span is the fuselage width, so that we will assume that each wing is a 32.5-foot-long cantilever beam. At the root of the wing, the airfoil is NACA 23016, with a thickness-to-chord ratio ( $t/c$ ) of 16

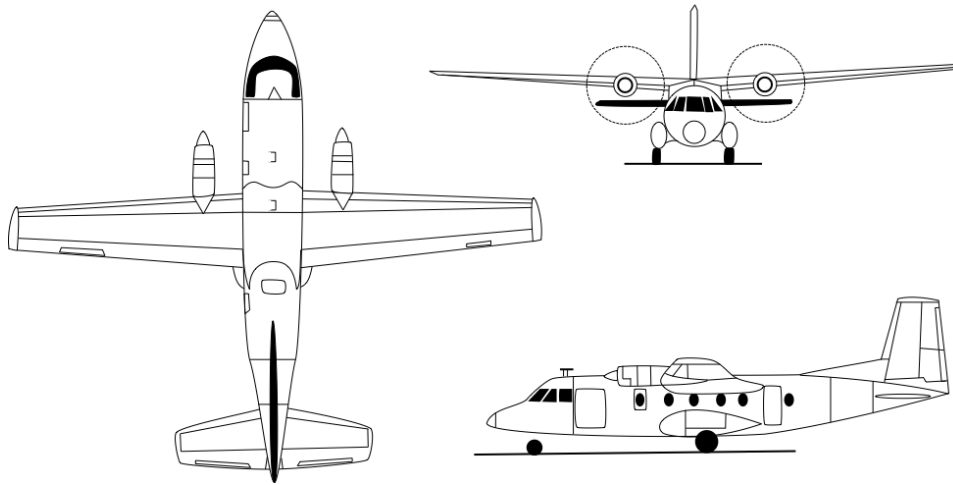


Fig. 14.5 Mohawk 298 commuter airplane

percent, while at the tip, the airfoil is NACA 32012, with a thickness-to-chord ratio of 12 percent. Assume a constant  $t/c = 0.14$ , corresponding to a maximum thickness of the airfoil of 1.12 ft.

**Design load condition.** The load condition that usually designs most of the wing box is a pull-up maneuver. For transport aircraft the FAA specifies a maneuver of 2.5 g, with a safety factor of 1.5. That is, the wings need to be able to carry about 2.5 times the weight of the airplane without suffering material failure. The maximum takeoff weight is 23,810 lb., but in this condition there is a lot of fuel in the wing, and this fuel provides inertia relief, reducing the stresses in the wing. Also, part of the lift of the wing is provided by the area over the fuselage, so we will assume that the two wings carry 20,000 lb. in cruise, and 50,000 lb. in the design pull-up maneuver.

**Wing box overall dimensions.** Assume a wing box that is 24 in. in the chord-wise direction and 13 in. deep so that it can fit into the airfoil. See figure. 14.6.

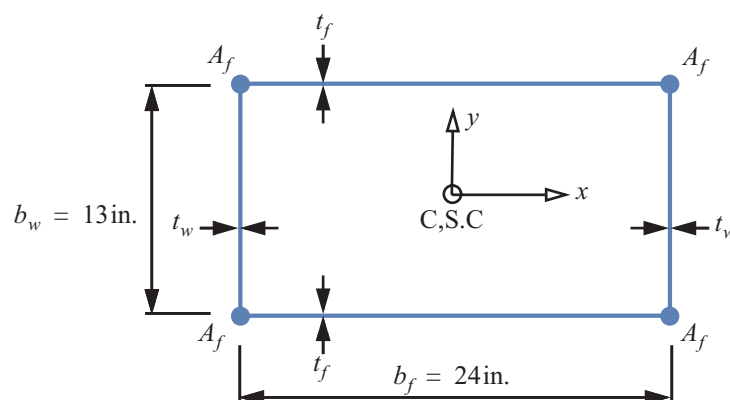


Fig. 14.6 Semimonocoque wing spar cross section. Design variables are the thicknesses  $t_f$  and  $t_w$ , and the stringer flange area  $A_f$ .

**Material data.** 1. The wing is made of aluminum alloy 2024-T351 with Young's modulus of

$E = 10 \times 10^6$  psi, Poisson's ratio of 0.3, a specific weight of  $0.1 \text{ lb./in.}^3$ , a yield strength in tension or compression of 47,000 psi, and a mode I fracture toughness

$$K_{Ic} = 31,000 \text{ psi}\sqrt{\text{in.}}$$

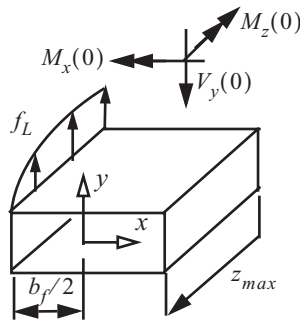
**Spanwise airload distribution.** Let  $z$  denote the spanwise axis along the locus of shear centers of each cross section. The  $z$ -axis measured from the root to tip, with  $0 \leq z \leq z_{max}$ , and  $z_{max} = 32.5 \times 12 = 390 \text{ in.}$  Assume that the load is distributed elliptically over the wing as in example 6.6 on page 165, so that the load intensity  $f_L$  per unit span is given as

$$f_L(\zeta) = \frac{2L}{\pi z_{max}} \sqrt{1 - \zeta^2} \quad 0 \leq \zeta \leq 1 \quad \zeta = \frac{z}{z_{max}}, \quad (14.24)$$

where the total lift  $L = 50,000 \text{ lb.}$ , and the wing span  $z_{max} = 32.5 \text{ ft.}$

It is given that the line of action of the lift is acting on the front web of the box beam. Equilibrium conditions shown in figure. 14.7 determine the shear force, bending moment, and torque at the wing root as

$$V_y(0) = \frac{L}{2} = 25,000 \text{ lb.} \quad M_x(0) = \frac{-2Lz_{max}}{3\pi} = -4.13803 \times 10^6 \text{ lb.-in.} \quad M_z(0) = \left(-\frac{bf}{2}\right) \frac{L}{2} = -300,000 \text{ lb.-in.}$$



$$\begin{aligned} -V_y(0) + z_{max} \int_0^1 f_L(\zeta) d\zeta &= 0 \\ -M_x(0) - z_{max}^2 \int_0^1 \zeta f_L(\zeta) d\zeta &= 0 \\ -M_z(0) - \left(\frac{bf}{2}\right) z_{max} \int_0^1 f_L(\zeta) d\zeta &= 0 \end{aligned}$$

**Fig. 14.7 Free body diagram of the spar and the equilibrium equations.**

### 14.2.1 Evaluation of stresses at root cross section

Since the wing box is uniform along the span, the thicknesses are sized by the conditions at the root. Ten locations for evaluation of the Mises effective stresses and the margins of safety are shown in figure. 14.8.

The axial normal stress at the root due to flexure is determined from eq. (4.6) on page 79. For this symmetric cross section we get from eq. (4.4) that  $n_x = n_y = 0$ ,  $k = 1$ , and  $\bar{y}(s) = y(s)$  by eq. (4.7). In the absence of an axial normal force and no thermal loads, the normal stress in eq. (4.6) reduces to

$$\sigma_{zz} = \frac{M_x(0)}{I_{xx}} y(s). \quad (14.25)$$

The second area moment about the  $x$ -axis through the centroid of the cross section is given by

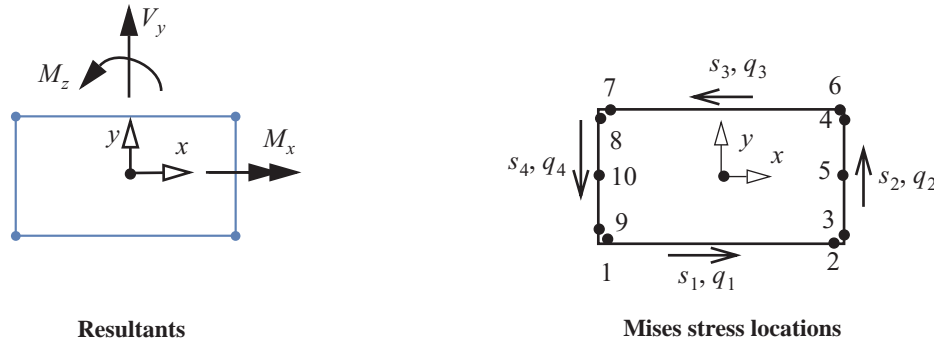


**Fig. 14.8** Locations for the evaluation of stresses at the wing root.

$$I_{xx} = A_f b_w^2 + (b_f b_w^2 t_f)/2 + (b_w^3 t_w)/6. \quad (14.26)$$

The shear stresses tangent to the contour are determined from the shear flows and thicknesses of the panels of the box beam (i.e.,  $\sigma_{zs} = q(s, z)/t(s)$ ). For the box beam the shear stresses in each branch are

$$\sigma_{zs}|_i = \tau_i(s_i) = q_i(s_i)/t_i \quad i = 1, 2, 3, 4, \quad (14.27)$$

where  $q_i(s_i)$  denotes the shear flow in the  $i$ -th branch, and  $s_i$  denotes the branch contour coordinate. The total shear flows are the summation of the shear flow due to the transverse shear force acting through the shear center and the torque. From eq. (4.25) on page 82, the total shear flow at a given contour location is

$$q_i(s_i) = \frac{M_z(0)}{2A_c} - F_y(s_i)V_y(0) \quad i = 1, 2, 3, 4. \quad (14.28)$$

The shear flow distribution function with respect to the shear center  $F_y(s)$  is obtained from eq. (4.19) and eq. (4.26), where  $x_{sc} = 0$ . For each branch we write

$$F_y(s_i) = \frac{1}{I_{xx}} \left[ Q_{xi}(s_i) - \frac{1}{2A_c} \oint r_n Q_x ds \right], \quad (14.29)$$

where the area enclosed by the cell  $A_c = b_f b_w$ . The functions  $Q_{xi}(s_i)$  in eq. (14.29) are distribution functions defined by first area moments, and are obtained from eq. (4.9) on page 80. For each branch functions  $Q_{xi}(s_i)$  are determined from

$$\begin{aligned} Q_{x1}(s_1) &= \left(\frac{-b_w}{2}\right) A_f + \int_0^{s_1} y_1(s_1) t_f ds_1, \quad Q_{x2}(s_2) = Q_{x1}(b_f) + \left(\frac{-b_w}{2}\right) A_f + \int_0^{s_2} y_2(s_2) t_w ds_2, \\ Q_{x3}(s_3) &= Q_{x2}(b_w) + \left(\frac{b_w}{2}\right) A_f + \int_0^{s_3} y_3(s_3) t_f ds_3, \quad \text{and} \quad Q_{x4}(s_4) = Q_{x3}(b_f) + \left(\frac{b_w}{2}\right) A_f + \int_0^{s_4} y_4(s_4) t_w ds_4. \end{aligned} \quad (14.30)$$

The contour coordinate functions  $[x(s), y(s)]$ , functions  $Q_{xi}(s_i)$ , and the evaluation of coordinates normal to



contour  $r_{ni}$  are listed in table 14.1.

**Table 14.1 Geometric functions of the contour**

Branch	$s_i$	$x_i$	$y_i$	$Qx_i$	$r_{ni}$ , eq. (4.11)
i = 1	$0 \leq s_1 \leq b_f$	$-(b_f)/2 + s_1$	$-b_w/2$	$(-b_w t_f s_1)/2$	$b_w/2$
i = 2	$0 \leq s_2 \leq b_w$	$b_f/2$	$(-b_w)/2 + s_2$	$-\frac{b_f b_w t_f}{2} - \frac{b_w t_w s_2}{2} + \frac{t_w s_2^2}{2}$	$b_f/2$
i = 3	$0 \leq s_3 \leq b_f$	$b_f/2 - s_3$	$b_w/2$	$-\frac{b_f b_w t_f}{2} + \frac{b_w t_f s_3}{2}$	$b_w/2$
i = 4	$0 \leq s_4 \leq b_w$	$(-b_f)/2$	$b_w/2 - s_4$	$\frac{b_w t_w s_4}{2} - \frac{t_w s_4^2}{2}$	$b_f/2$

From the results listed in table 14.1, the integral term on the right-hand side of eq. (14.29) evaluates as

$$\frac{1}{2A_c} \oint [r_n Q_x] ds = -\left(A_f b_f b_w^2 + \frac{b_f^2 b_w^2 t_f}{2}\right) / 2b_f b_w. \quad (14.31)$$

The shear flow distribution functions are given in eq. (14.32) below.

$$\begin{aligned} F_y(s_1) &= \frac{b_w t_f (b_f - 2s_1)}{4I_{xx}} & F_y(s_2) &= -\left(\frac{2A_f b_w + b_f b_w t_f + 2(b_w - s_2)s_2 t_w}{4I_{xx}}\right) \\ F_y(s_3) &= \frac{-b_w t_f (b_f - 2s_3)}{4I_{xx}} & F_y(s_4) &= \frac{2A_f b_w + b_f b_w t_f + 2(b_w - s_4)s_4 t_w}{4I_{xx}}. \end{aligned} \quad (14.32)$$

**Strength limit state.** The Von Mises criterion given by eq. (4.31) on page 84 is used to predict the initiation of material yielding. The Mises effective stress is defined by

$$\sigma_{\text{Mises}} = \sqrt{\sigma_{zz}^2 + 3\sigma_{zs}^2}. \quad (14.33)$$

If  $\sigma_{\text{Mises}} < \sigma_{\text{yield}}$ , then the material response is elastic, and if  $\sigma_{\text{Mises}} = \sigma_{\text{yield}}$  yielding initiates. The margin of safety (14.16) in this case is

$$MS = \frac{\sigma_{\text{allowable}} - \sigma_{\text{Mises}}}{\sigma_{\text{Mises}}} = \frac{\sigma_{\text{allowable}}}{\sigma_{\text{Mises}}} - 1. \quad (14.34)$$

The allowable stress for the strength limit state is the yield strength of the material divided by the factor of safety (FS). That is

$$\sigma_{\text{allowable}} = \sigma_{\text{yield}} / (FS). \quad (14.35)$$

The margin of safety is nonnegative for a feasible design, otherwise the design is infeasible. It should be zero or a small positive number.

### 14.2.2 Trial design of the monocoque box beam spar

A computer program was written to evaluate the Mises effective stresses at the ten locations of the root cross section using a factor of safety of 1.5. For  $t_f = 0.40$  in.,  $t_w = 0.30$  in., and  $A_f = 0$  the weight of the spar is 1,053. lb. The values of the ten margins of safety for this design are listed in table 14.2.

**Table 14.2 Margins of safety for the trial design**

MS <sub>1</sub>	0.0528	MS <sub>6</sub>	0.0714
MS <sub>2</sub>	0.0714	MS <sub>7</sub>	0.0528
MS <sub>3</sub>	0.0702	MS <sub>8</sub>	0.0378
MS <sub>4</sub>	0.0702	MS <sub>9</sub>	0.0378
MS <sub>5</sub>	9.086	MS <sub>10</sub>	2.619

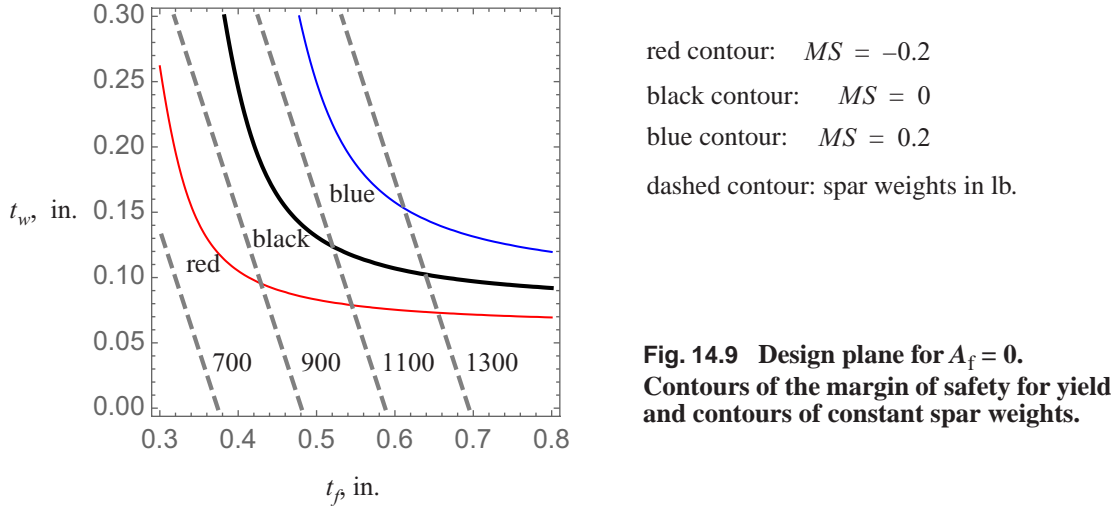
Since the margins of safety are all positive, this design is feasible. Although feasible, this design is too heavy and, consequently, not optimal. Lower weight feasible designs will have a nonnegative minimum margin of safety close to zero.

To aid in the search for the best design, consider the design plane shown in figure. 14.9. The thickness  $t_f$  is the abscissa and the thickness  $t_w$  is the ordinate. Each point in the plane represents a design, some are feasible some are not. Contours of constant margins of safety and constant spar weights are plotted in the design plane<sup>1</sup>. Only designs with a nonnegative margin of safety are feasible. The least weight design occurs at a point  $(t_f^*, t_w^*)$  on the margin of safety contour equal to zero. A second condition is needed to determine point  $(t_f^*, t_w^*)$ . This second condition is to equate the slope  $t_w/t_f = -\left(\frac{\partial MS}{\partial t_f}\right)/\frac{\partial MS}{\partial t_w}$  on the margin of safety contour  $MS = 0$  to the slope of the constant weight contour  $t_w/t_f = (-b_f)/b_w$ . That is, the point  $(t_f^*, t_w^*)$  on the contour  $MS = 0$  is tangent to the contour of least weight.

### 14.2.3 Design exercise A

Write a computer program to find the thicknesses  $t_f$  and  $t_w$  of the wing box for  $A_f = 0$  that will minimize the weight and carry the load without experiencing material yield using a factor of safety of 1.5. Calculate the weight of the spar and the margins of safety at the ten locations shown in figure. 14.8. Although the design given in article 14.2.2 is too heavy, it can be used to assess if the computer program is correct. Include a print out of the program and the output for the best design, which includes the ten margins of safety and the weight.

1. Fig. 14.9 was generated by the *Mathematica* function **ContourPlot[Min[MS[tf,tw,0]] == 0, {tf, 0.3, 0.8},{tw, 0.0, 0.3}]**, where definition of function **MS[tf,tw,Af]** is determined by eq. (14.34) and the ten points shown in figure. 14.8.



### 14.3 Additional limit states for buckling and fracture

Consider design variables  $t_f > 0$ ,  $t_w > 0$ , and  $A_f \geq 0$  for the Mohawk 298 wing spar subject to constraints on yielding, buckling, and fracture. The locations in the cross section at the wing root where the design constraints are evaluated are shown in figure. 14.10.

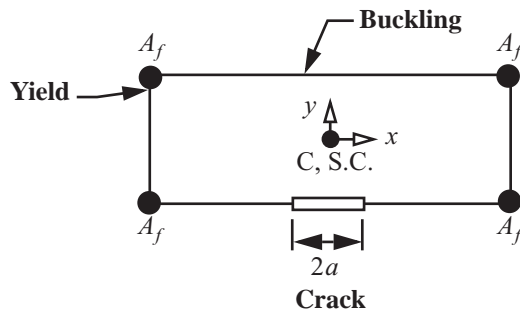


**Fig. 14.10** Cross section of the stringer-stiffened box beam, and locations of constraint evaluations

#### 14.3.1 Buckling margin of safety

Let rib spacing along the span, or  $z$ -axis, at the root of the wing be denoted by  $a_r$ , and take  $a_r = b_f/2$ . The upper cover skin, or branch 3 with coordinates  $[x_3(s_3), y_3]$ , is subject to compression and shear. The normal stress is  $\sigma_{zz} = (M_x y_3)/I_{xx}$  and the shear stress  $\tau_3(s_3)$  is a linear function in the contour coordinate  $s_3$ . Assume the skin can be modeled as simply supported flat plate between stiffeners for the buckling analysis. From eq. (11.118) on page 355 the combined compression and shear index for buckling is defined by

$$f_b = \left( \frac{\tau_{\text{ave}}}{\tau_{\text{cr}}} \right)^2 + \left( \frac{|\sigma_z|}{\sigma_{\text{cr}}} \right)^2, \quad (14.36)$$

where  $0 \leq f_b < 1$  for no buckling and  $f_b = 1$  at the onset of buckling. The average shear stress is

$$\tau_{\text{ave}} = \left( \frac{1}{b_f} \right) \int_0^{b_f} \tau_3(s_3) ds_3. \quad (14.37)$$

The critical stresses for compression (11.110) and shear (11.116) are

$$\sigma_{\text{cr}} = k_c \frac{\pi^2 E}{12(1-\nu^2)} \left( \frac{t_f}{b_f} \right)^2 \quad \tau_{\text{cr}} = k_s \frac{\pi^2 E}{12(1-\nu^2)} \left( \frac{t_f}{b_f} \right)^2. \quad (14.38)$$

The buckling coefficients are

$$k_c = \left( \frac{1}{(a_r/b_f)} + \left( \frac{a_r}{b_f} \right) \right)^2 = 6.25 \quad k_s = 4.22565 + \frac{5.19931}{a_r/b_f} = 14.624. \quad (14.39)$$

The margin of for the buckling limit state is

$$MS_b = \frac{1-f_b}{f_b}. \quad (14.40)$$

### 14.3.2 Fracture margin of safety

The design damage condition is a through crack centered in the lower left skin that is 1.00 in. long ( $2a = 1.00$  in.) with the crack faces perpendicular to the  $z$ -axis. The lower skin, or branch 1 with coordinates  $[x_1(s_1), y_1]$ , is subject to a tensile stress  $\sigma_{zz} = (M_x y_1)/I_{xx}$  and a shear stress  $\tau_1(s_1)$  that is a linear function of contour coordinate  $s_1$ . Thus, the crack is exposed to tension and shear, which leads to mixed mode cracking (i.e., a mixture of mode I and mode II). The stress intensity factor for mode I is  $K_I = \sigma_{zz} \sqrt{\pi a}$ , and the stress intensity factor for mode II is  $K_{II} = \tau_1 \sqrt{\pi a}$ . The fracture toughness for mode I loading only is  $K_{Ic}$ , and the fracture toughness for mode II loading only is  $K_{IIc}$ . A fracture criterion for mixed mode loading is given by eq. (13.42) on page 391. The plane strain fracture toughness for mode I loading is usually readily available in the literature, but the mode II fracture toughness is not usually available. Tests for mode II are more difficult to design than for mode I. Usually mode II loading does not lead to fracture (Anderson, 1995)<sup>1</sup>. In other words  $K_{IIc} > K_{Ic}$ . In addition for the design  $(t_f, t_w, A_f) = (0.4, 0.3, 0)$ , the stresses at the center of branch 1 are  $\sigma_{zz} = 29,202.8$  psi and  $\tau_3(b_f/2) = -1,201.92$  psi. The shear stress is about 4 percent of the normal stress, and so it is expected that shear would have a small influence on fracture. Thus, we assume fracture is in mode I. The margin of safety for fracture is

$$MS_f = \frac{K_{Ic}/(FS_f) - K_I}{K_I}, \quad (14.41)$$

1. Mode II loading is important if there is weak interface in the material, which is the case for delamination of filamentary composites as discussed in article 13.7 on page 392.

where the factor of safety for fracture is specified as  $FS_f = 1.2$ .

### 14.3.3 Design exercise B

Consider a longitudinally stiffened configuration of the wing box for the Mohawk 298 commuter airplane described in article 14.3. Write a computer program to determine the thicknesses  $t_f$  and  $t_w$  of the wing box for selected values of the flange area  $A_f$  listed in the table below. The objective is to minimize the weight. The design limit states are material yield (14.34) using a factor of safety of 1.5, that the compression panel of the upper skin does not buckle (14.40), and that the crack in the lower panel does not propagate (14.41). Evaluate the margin of safety for yield at point 8 shown in figure. 14.8. The minimum margin of safety should not be negative for a feasible design, but should be a small positive number. Write a computer program to determine the thicknesses  $t_f$  and  $t_w$  of the wing box for selected values of the flange area  $A_f$  listed in table 14.3.

**Table 14.3 Design exercise B**

$A_f, \text{in.}^2$	$t_f, \text{in.}$	$t_w, \text{in.}$	weight, lb.	Margins of safety		
				Yield	Buckling	Fracture
0						
1.0						
2.0						
3.0						

### *14.4 References*

Anderson, T.L. *Fracture Mechanics*, 2d ed. Boca Raton, FL: CRC Press Inc., 1995, p. 87.

Dowling, N. *Mechanical Behavior of Materials*. Englewood Cliffs, NJ: Prentice-Hall, Inc., 1993, pp. 245-252.

Thurston, David B. *Design For Flying*. 2d ed. New York: TAB Books, a Division of McGraw-Hill, Inc., 1995, pp. 237-245.

Unit action states and unit displacement states are defined in the first section followed by an example to show how these definitions can be used to find flexibility and stiffness influence coefficients. To introduce the basic methods of matrix structural analysis, the analyses of structures modeled with linear elastic springs are presented in article 15.2 to article 15.6. The objective is to illustrate the steps in the **direct stiffness method**, which is summarized in article 15.7. The approach followed here is based on chapters 2, 3, 4, and 6 of Martin (1966).

### 15.1 Physical interpretation of influence coefficients

Consider the structural model of a cantilever wing with two degrees of freedom shown in figure. 15.1. The gener-

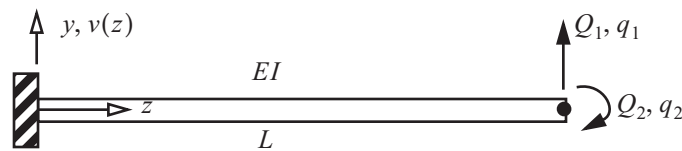


Fig. 15.1 Two-degree-of-freedom model of the cantilever wing.

alized forces are denoted by  $Q_i$  and the corresponding generalized displacements by  $q_i$ ,  $i = 1, 2$ . Refer to the discussion in article 5.2.1 and article 5.2.2 on page 134. The linear elastic response of the wing is determined from the matrix relations

$$\begin{bmatrix} Q_1 \\ Q_2 \end{bmatrix} = \underbrace{\begin{bmatrix} k_{11} & k_{12} \\ k_{21} & k_{22} \end{bmatrix}}_{[k]} \begin{bmatrix} q_1 \\ q_2 \end{bmatrix} \quad \begin{bmatrix} q_1 \\ q_2 \end{bmatrix} = \underbrace{\begin{bmatrix} c_{11} & c_{12} \\ c_{21} & c_{22} \end{bmatrix}}_{[c]} \begin{bmatrix} Q_1 \\ Q_2 \end{bmatrix} \quad (15.1)$$

Elements  $k_{ij}$  of the stiffness matrix are stiffness influence coefficients, and elements  $c_{ij}$  of the flexibility matrix

are flexibility influence coefficients. Matrices  $[k]$  and  $[c]$  are symmetric, and they are the inverse of one another; i.e.,

$$[k]^T = [k] \quad [c]^T = [c] \quad [k][c] = [c][k] = [I]. \quad (15.2)$$

The following definition of the stiffness influence coefficients is the basis of the unit displacement state (UDS) method:

*The stiffness influence coefficient  $k_{ij}$  represents the generalized force at point  $i$  in the direction  $q_i$  due to a unit generalized displacement  $q_j$ , all other generalized displacements equal to zero.*

For UDS 1 take the displacement vector  $\begin{bmatrix} q_1 \\ q_2 \end{bmatrix} = \begin{bmatrix} 1 \\ 0 \end{bmatrix}$ , then the generalized forces from the first of eqs. (15.1) are

$$\begin{bmatrix} Q_1 \\ Q_2 \end{bmatrix} = \begin{bmatrix} k_{11} \\ k_{21} \end{bmatrix} \cdot 1. \text{ For UDS 1 the force vector is equal to the first column of the stiffness matrix. For UDS 2 take}$$

$$\begin{bmatrix} q_1 \\ q_2 \end{bmatrix} = \begin{bmatrix} 0 \\ 1 \end{bmatrix}, \text{ then the generalized force vector is } \begin{bmatrix} Q_1 \\ Q_2 \end{bmatrix} = \begin{bmatrix} k_{12} \\ k_{22} \end{bmatrix} \cdot 1. \text{ For UDS 2 the force vector is equal to the}$$

second column of the stiffness matrix. For the wing example the generalized force vectors in terms of the elements of the stiffness matrix are depicted in figure. 15.2.

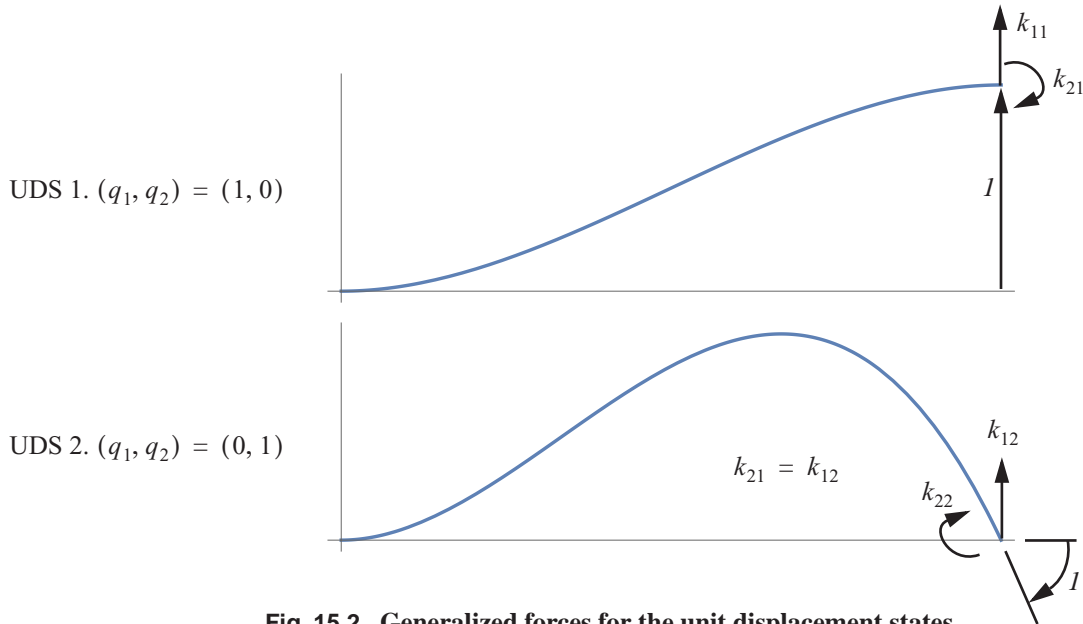


**Fig. 15.2 Generalized forces for the unit displacement states.**

The following definition of the flexibility influence coefficients is the basis of the unit action state (UAS) method:



The flexibility influence coefficient  $c_{ij}$  represents the generalized displacement at point  $i$  in the direction  $Q_i$  due to a unit generalized force  $Q_j$ , all other generalized forces equal to zero.

For UAS 1 take the generalized force vector  $\begin{bmatrix} Q_1 \\ Q_2 \end{bmatrix} = \begin{bmatrix} 1 \\ 0 \end{bmatrix}$ , then the generalized displacements from the second of

eq. (15.1) are  $\begin{bmatrix} q_1 \\ q_2 \end{bmatrix} = \begin{bmatrix} c_{11} \\ c_{21} \end{bmatrix} \cdot 1$ . For UAS 1 the displacement vector is equal to the first column of the flexibility

matrix. For UAS 2 take  $\begin{bmatrix} Q_1 \\ Q_2 \end{bmatrix} = \begin{bmatrix} 0 \\ 1 \end{bmatrix}$ , then the generalized displacement vector is  $\begin{bmatrix} q_1 \\ q_2 \end{bmatrix} = \begin{bmatrix} c_{12} \\ c_{22} \end{bmatrix} \cdot 1$ . For UAS 2

the displacement vector is equal to the second column of the flexibility matrix. For the wing example the generalized displacement vectors in terms of the elements of the flexibility matrix are depicted in figure. 15.3.

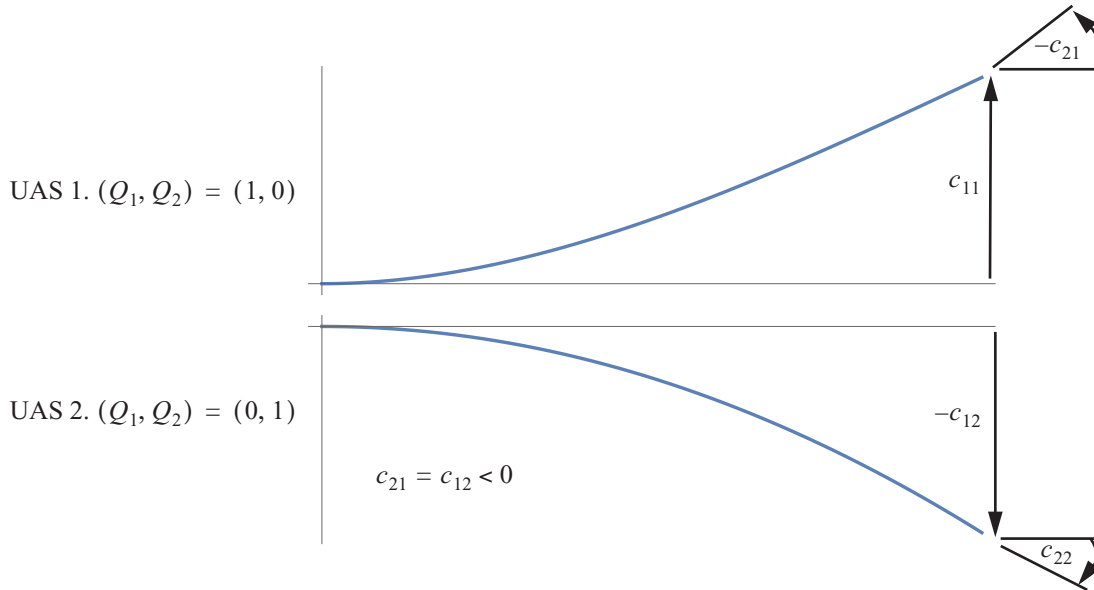
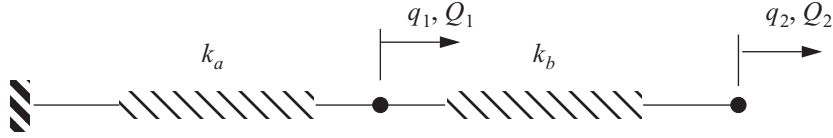


Fig. 15.3 Generalized displacements for unit action states.

#### Example 15.1 Two springs in series restrained at one end.

Construct the flexibility influence matrix  $[C]$  by the method of unit action states (UAS), and the stiffness influence matrix  $[K]$ , by the method of unit displacement states (UDS) for the two-degree-of freedom structural model shown in figure 15.4. The model consists of two linear elastic springs in series with the left end fixed against translation. The left spring has stiffness  $k_a$  and the right spring has stiffness  $k_b$ .

The flexibility and stiffness matrix relations are of the form



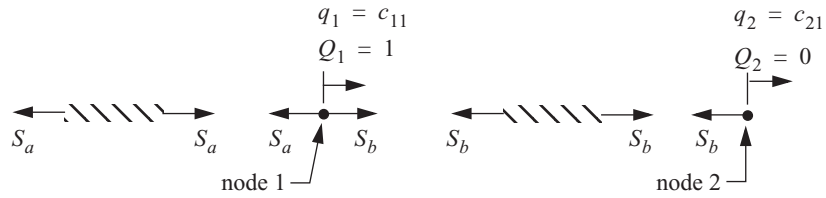
**Fig. 15.4** Two linear elastic springs in series restrained against rigid body translation.

$$\begin{bmatrix} q_1 \\ q_2 \end{bmatrix} = \begin{bmatrix} c_{11} & c_{12} \\ c_{21} & c_{22} \end{bmatrix} \begin{bmatrix} Q_1 \\ Q_2 \end{bmatrix} \quad \begin{bmatrix} Q_1 \\ Q_2 \end{bmatrix} = \begin{bmatrix} k_{11} & k_{12} \\ k_{21} & k_{22} \end{bmatrix} \begin{bmatrix} q_1 \\ q_2 \end{bmatrix}. \quad (\text{a})$$

**Solution.**

**UAS 1.**  $Q_1 = 1$  and  $Q_2 = 0$ . The free body diagrams of the springs, with the spring forces assumed positive in tension, and of joints 1 and 2 are shown in figure. 15.4.

**Fig. 15.5** Unit action state 1.



Equilibrium at joints 1 and 2 gives

$$-S_a + S_b + 1 = 0 \quad S_b = 0. \quad (\text{b})$$

Therefore,

$$S_a = 1 \quad S_b = 0. \quad (\text{c})$$

The material laws for the linear elastic springs are

$$S_a = k_a \Delta_a \quad S_b = k_b \Delta_b. \quad (\text{d})$$

where  $\Delta_a$  is the elongation of spring **a** and  $\Delta_b$  is the elongation of spring **b**. Spring elongations are related to the nodal displacements by geometric compatibility, and for this example we have

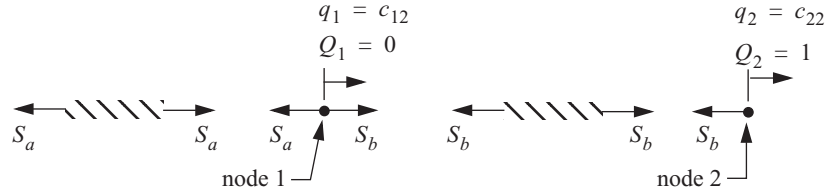
$$\Delta_a = q_1 \quad \Delta_b = q_2 - q_1. \quad (\text{e})$$

Thus,  $1 = k_a q_1$  and  $0 = k_b(q_2 - q_1)$ . Solve for the displacements to get

$$q_1 = \frac{1}{k_a} = c_{11} \quad q_2 = \frac{1}{k_a} = c_{21}. \quad (\text{f})$$

**UAS 2.**  $Q_1 = 0$  and  $Q_2 = 1$ . The free body diagrams are shown in figure. 15.5.

**Fig. 15.6 Unit action state 2.**



Equilibrium at the joints gives

$$-S_a + S_b = 0 \quad -S_b + 1 = 0. \quad (\text{g})$$

Therefore,

$$S_a = 1 \quad S_b = 1. \quad (\text{h})$$

The material laws for each spring and the elongation-displacement relations give

$$1 = k_a q_1 \quad 1 = k_b (q_2 - q_1). \quad (\text{i})$$

Solve for the displacements to get

$$q_1 = \frac{1}{k_a} = c_{12} \quad q_2 = \frac{1}{k_a} + \frac{1}{k_b} = c_{22}. \quad (\text{j})$$

From the method of unit action states we have determined the flexibility matrix to be

$$[C] = \begin{bmatrix} \frac{1}{k_a} & \frac{1}{k_a} \\ \frac{1}{k_a} & \left( \frac{1}{k_a} + \frac{1}{k_b} \right) \end{bmatrix}. \quad (\text{k})$$

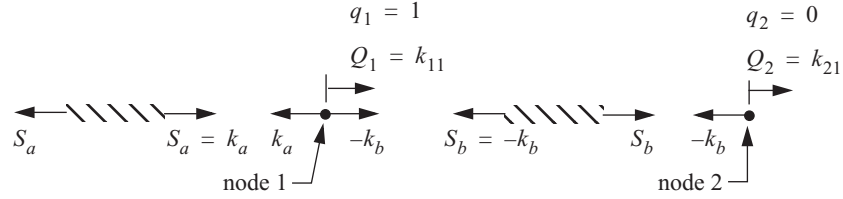
The flexibility matrix is symmetric, which it must be for a linear elastic structure by Maxwell's reciprocal theorem: See article 5.1.2 on page 131.

**UDS 1.**  $q_1 = 1$  and  $q_2 = 0$ . From the material laws for each spring and the elongation-displacement relations we have

$$S_a = k_a q_1 = k_a \cdot 1 = k_a \quad S_b = k_b (q_2 - q_1) = k_b (-1) = -k_b. \quad (\text{l})$$

Free body diagrams of the two joints are shown in figure. 15.6.

**Fig. 15.7 Unit displacement state 1.**



Equilibrium at the joints gives

$$-S_a + S_b + Q_1 = 0 \quad -S_b + Q_2 = 0. \quad (\text{m})$$

But  $S_a = k_a$  and  $S_b = -k_b$  for UDS 1. Also, we identify  $Q_1 = k_{11}$  and  $Q_2 = k_{21}$  for UDS 1. So

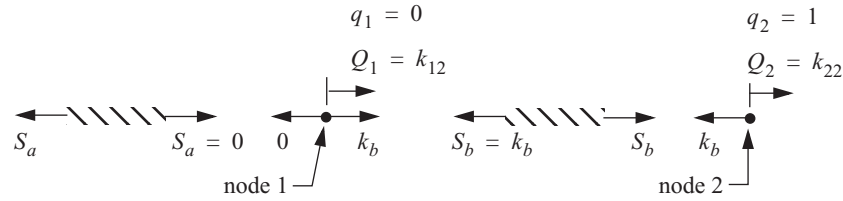
$$k_{11} = k_a + k_b \quad k_{21} = -k_b. \quad (\text{n})$$

**UDS 2.**  $q_1 = 0$  and  $q_2 = 1$ . From the material laws for each spring and the elongation-displacement relations we have

$$S_a = k_a(0) = 0 \quad S_b = k_b(q_2 - q_1) = k_b(1 - 0) = k_b. \quad (\text{o})$$

Free body diagrams of the two joints are shown in figure. 15.7.

**Fig. 15.8 Unit displacement state 2.**



Nodal equilibrium gives

$$-S_a + S_b + Q_1 = 0 \quad -S_b + Q_2 = 0. \quad (\text{p})$$

But  $S_a = 0$  and  $S_b = k_b$  for UDS 1. Also, we identify  $Q_1 = k_{12}$  and  $Q_2 = k_{22}$  for UDS 1. So

$$k_{12} = -k_b \quad k_{22} = k_b. \quad (\text{q})$$

Therefore, the stiffness matrix is

$$[K] = \begin{bmatrix} (k_a + k_b) & -k_b \\ -k_b & k_b \end{bmatrix}. \quad (\text{r})$$

The stiffness matrix is also symmetric, which was proved based on symmetry of the flexibility matrix. Refer to article 5.2.2.

Note that the matrix product

$$[C][K] = \begin{bmatrix} \frac{1}{k_a} & \frac{1}{k_a} \\ \frac{1}{k_a} \left( \frac{1}{k_a} + \frac{1}{k_b} \right) & \frac{1}{k_b} \left( \frac{1}{k_a} + \frac{1}{k_b} \right) \end{bmatrix} \begin{bmatrix} (k_a + k_b) & -k_b \\ -k_b & k_b \end{bmatrix} = \begin{bmatrix} \left( \frac{(k_a + k_b)}{k_a} - \frac{k_b}{k_a} \right) & \left( -\frac{k_b}{k_a} + \frac{k_b}{k_a} \right) \\ \left( \frac{(k_a + k_b)}{k_a} - k_b \left( \frac{1}{k_a} + \frac{1}{k_b} \right) \right) & \left( -\frac{k_b}{k_a} + k_b \left( \frac{1}{k_a} + \frac{1}{k_b} \right) \right) \end{bmatrix} = \begin{bmatrix} 1 & 0 \\ 0 & 1 \end{bmatrix}.$$

That is, the product of flexibility matrix and the stiffness matrix is the identity matrix. In other words, the inverse of the flexibility matrix is the stiffness matrix. ■

## 15.2 Unrestrained structural stiffness matrix

The flexibility influence coefficients  $c_{ij}$  are defined for a structure restrained against rigid body motion. However, it is not necessary to impose this rigid body constraint when forming the stiffness influence coefficients  $k_{ij}$  of a structure. Specifying the generalized displacements in the method of unit displacement states encompasses both rigid body displacements and those causing deformation. Consider a single, linear elastic spring element with two-degrees-of-freedom (DOFs) connected between joints  $i$  and  $j$ , where integers  $i \neq j$ , as shown in figure 15.9. Let  $k$  denote the stiffness of the spring, which has dimensional units of  $F/L$ .

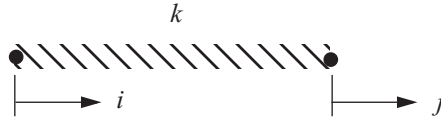


Fig. 15.9 A two-degree-of-freedom spring element.

The unrestrained structural stiffness matrix is, in general, given by

$$\begin{bmatrix} Q_i \\ Q_j \end{bmatrix} = \begin{bmatrix} k_{ii} & k_{ij} \\ k_{ji} & k_{jj} \end{bmatrix} \begin{bmatrix} q_i \\ q_j \end{bmatrix}, \quad (15.3)$$

in which  $i \neq j$ . Free body diagrams of the joints and spring are shown in figure 15.10. Equilibrium at the joints

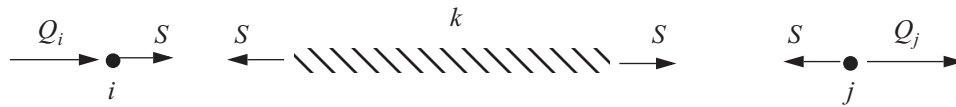


Fig. 15.10 Free body diagram of the two-degree-of-freedom spring element.

yields

$$Q_i + S = 0 \quad Q_j - S = 0. \quad (15.4)$$

The spring force is related to the nodal displacements by the material law

$$S = k(q_j - q_i). \quad (15.5)$$

**UDS 1.**  $q_i = 1$  and  $q_j = 0$ . Therefore eq. (15.5) gives  $S = -k \cdot 1$ . Nodal equilibrium, eq. (15.4), and the matrix relation, eq. (15.3), give

$$Q_i = -(-k \cdot 1) = k_{ii} \quad Q_j = -k \cdot 1 = k_{ji}. \quad (15.6)$$

**UDS 2.**  $q_i = 0$  and  $q_j = 1$ . Therefore eq. (15.5) gives  $S = k \cdot 1$ . Nodal equilibrium, eq. (15.4), and the matrix relation, eq. (15.3), give

$$Q_i = -k \cdot 1 = k_{ij} \quad Q_j = k \cdot 1 = k_{jj}. \quad (15.7)$$

So that the unrestrained structural stiffness matrix is given by

$$[K] = \begin{bmatrix} k & -k \\ -k & k \end{bmatrix} = k \begin{bmatrix} 1 & -1 \\ -1 & 1 \end{bmatrix}. \quad (15.8)$$

Note that the unrestrained structural stiffness matrix (15.8) has the following properties:

1. Matrix  $[K]$  is symmetric (i.e.,  $[K]^T = [K]$ ).
2. The sum of the column elements equals zero.  $\sum_{i=1}^2 k_{ij} = 0$  for  $j = 1, 2$ . The vanishing of this sum results from  $Q_i + Q_j = 0$  for each UDS.
3. The  $\det[K] = k^2 - (-k)^2 = 0$ . That is, the unrestrained structural stiffness matrix is *singular*. This occurs because the structure is not restrained against rigid body translation in the horizontal direction. Under the action of no external loads (i.e.,  $Q_i = 0$  and  $Q_j = 0$ ), the structure can translate horizontally at a constant speed. Rigid body motion can be used to establish constraints between elements of the unrestrained structural stiffness matrix. For example, let  $v$  denote the horizontal speed and let  $t$  denote time, then

$$q_i = q_j = vt. \quad (15.9)$$

Equation (15.3) gives

$$\begin{bmatrix} 0 \\ 0 \end{bmatrix} = \begin{bmatrix} k_{ii} & k_{ij} \\ k_{ji} & k_{jj} \end{bmatrix} \begin{bmatrix} vt \\ vt \end{bmatrix}, \quad (15.10)$$

or

$$(k_{ii} + k_{ij})q = 0 \quad (k_{ji} + k_{jj})q = 0 \quad q = vt \neq 0. \quad (15.11)$$

Therefore, the constraints between elements of the unrestrained stiffness matrix are

$$k_{ii} + k_{ij} = 0 \quad k_{ji} + k_{jj} = 0. \quad (15.12)$$

4. Diagonal elements of  $[K]$  are positive. This must be true based on physical grounds. If  $Q_i > 0$  and  $q_j = 0$ , then we expect  $q_i > 0$ . Thus, in the relation  $Q_i = k_{ii}q_i$ , the stiffness influence coefficient  $k_{ii} > 0$ .



Write eq. (15.17) in matrix form

$$\begin{bmatrix} Q_1 \\ Q_2 \\ Q_3 \end{bmatrix} = \begin{bmatrix} k_a & -k_a & 0 \\ -k_a & (k_a + k_b) & -k_b \\ 0 & -k_b & k_b \end{bmatrix} \begin{bmatrix} q_1 \\ q_2 \\ q_3 \end{bmatrix}. \quad (15.18)$$

Hence, the *unrestrained structural stiffness matrix* is

$$[K] = \begin{bmatrix} k_a & -k_a & 0 \\ -k_a & (k_a + k_b) & -k_b \\ 0 & -k_b & k_b \end{bmatrix}. \quad (15.19)$$

Note the following properties of the unrestrained structural stiffness matrix in eq. (15.19):

1. The matrix is symmetric, or  $[K]^T = [K]$ .
2. Using a co-factor expansion by the third column, the determinate of the matrix is computed as follows:

$$\begin{aligned} \det[K] &= (0)\det \begin{bmatrix} -k_a & (k_a + k_b) \\ 0 & -k_b \end{bmatrix} - (-k_b)\det \begin{bmatrix} k_a & -k_a \\ 0 & -k_b \end{bmatrix} + (k_b)\det \begin{bmatrix} k_a & -k_a \\ -k_a & (k_a + k_b) \end{bmatrix} \\ \det[K] &= 0 - k_a k_b^2 + (k_b)[k_a(k_a + k_b) - k_a^2] = -k_a k_b^2 + k_a k_b^2 = 0. \end{aligned}$$

Since the determinate is zero, the matrix is singular. The unrestrained structural stiffness matrix is singular because rigid body translation is not restrained.

3. The sum of the column elements is zero.  $\sum_{i=1}^3 k_{ij} = 0$  for  $j = 1, 2, 3$ .
4. Diagonal elements are positive  $k_{ii} > 0$ .

Of course, we could have used the method of unit displacement states to determine the unrestrained structural stiffness matrix (15.19) for the two springs in series rather than the assembly procedure given above.

Another way to obtain the unrestrained structural stiffness matrix is to first expand the element unrestrained stiffness matrices to size 3X3 by adding rows and columns of zeros, and then add the 3X3 element stiffness matrices. For spring element stiffness matrix given by eq. (15.13), displacement compatibility, eq. (15.15), identifies  $q_i = q_1$  and  $q_j = q_2$ . That is, columns one and two of the element stiffness matrix are associated with global degrees of freedom one and two. We write the element stiffness matrix as

$$[K_a] = \begin{matrix} & \begin{matrix} q_1 & q_2 & q_3 \end{matrix} \\ \begin{bmatrix} k_a & -k_a & 0 \\ -k_a & k_a & 0 \\ 0 & 0 & 0 \end{bmatrix} \end{matrix} \quad (15.20)$$

The global degrees of freedom are written above the appropriate columns of the expanded element stiffness matrix in eq. (15.20) to aid in keeping the order of the element columns consistent with the ordering of the global



displacements. For the spring element stiffness matrix given by eq. (15.14), displacement compatibility, eq. (15.15), identifies  $q_k = q_2$  and  $q_l = q_3$ . That is, columns one and two of the element stiffness matrix are associated with global degrees of freedom two and three. We write the element stiffness matrix as

$$[K_b] = \begin{matrix} & \begin{matrix} q_1 & q_2 & q_3 \end{matrix} \\ \begin{matrix} 0 & 0 & 0 \\ 0 & k_b & -k_b \\ 0 & -k_b & k_b \end{matrix} \end{matrix} \quad (15.21)$$

Note that the only non-zero elements in the expanded element stiffness matrix (15.21) are in rows and columns two and three. Since matrices (15.20) and (15.21) are of the same dimensions we can add them to get the unrestrained stiffness matrix of the structure; i.e.,

$$[K] = [K_a] + [K_b] = \begin{matrix} & \begin{matrix} q_1 & q_2 & q_3 \end{matrix} \\ \begin{matrix} k_a & -k_a & 0 \\ -k_a & (k_a + k_b) & -k_b \\ 0 & -k_b & k_b \end{matrix} \end{matrix} \quad (15.22)$$

The unrestrained structural stiffness matrix in eq. (15.22) is the same as the matrix in eq. (15.19). Thus, the superposition of individual element stiffness matrices to obtain the unrestrained structural stiffness matrix is equivalent to imposing displacement compatibility and equilibrium at the joints.

## 15.4 Prescribed nodal displacements and forces

At a joint we can prescribe either the displacement or the corresponding force, *but not both*. Consider the unrestrained structure of the last section in which we prescribe the values of the displacement  $q_1$ , force  $Q_2$ , and force  $Q_3$ . That is, nodal values of  $q_1$ ,  $Q_2$ , and  $Q_3$  are known, and nodal values of  $Q_1$ ,  $q_2$ , and  $q_3$  are unknown. Nodal forces  $Q_2$ , and  $Q_3$  are the applied loads, and nodal force  $Q_1$  is a reactive force, or support reaction. Nodal displacements  $q_2$ , and  $q_3$  are the unknown, or active, displacement degrees of freedom. We partition the unrestrained stiffness matrix given in eq. (15.22) by drawing lines between rows and columns to separate active and reactive nodal variables. In this example, we partition row 1 and column 1 as

$$\begin{bmatrix} Q_1 \\ Q_2 \\ Q_3 \end{bmatrix} = \begin{bmatrix} k_a & -k_a & 0 \\ -k_a & (k_a + k_b) & -k_b \\ 0 & -k_b & k_b \end{bmatrix} \begin{bmatrix} q_1 \\ q_2 \\ q_3 \end{bmatrix} \quad (15.23)$$

Now rearrange the order of the equations and the order of the displacements in eq. (15.23). The equations for the applied loads  $Q_2$ , and  $Q_3$  are moved to correspond with rows one and two, and the reactive force equation for  $Q_1$  is put in row three. Simultaneously, the unknown displacements  $q_2$ , and  $q_3$  are ordered such that they appear in columns one and two, and the prescribed displacement  $q_1$  appears in column three. The equations in matrix form now read as

$$\begin{bmatrix} Q_2 \\ Q_3 \\ Q_1 \end{bmatrix} = \begin{bmatrix} (k_a + k_b) & -k_b & -k_a \\ -k_b & k_b & 0 \\ -k_a & 0 & k_a \end{bmatrix} \begin{bmatrix} q_2 \\ q_3 \\ q_1 \end{bmatrix}. \quad (15.24)$$

The rearranged stiffness matrix is

$$[K] = \begin{bmatrix} & q_2 & q_3 & q_1 \\ (k_a + k_b) & -k_b & -k_a \\ -k_b & k_b & 0 \\ -k_a & 0 & k_a \end{bmatrix}. \quad (15.25)$$

In terms of matrix algebra, the unrestrained stiffness matrix in eq. (15.22) was rearranged to the matrix in eq. (15.25) by the following four-step sequence: First interchange elements in rows 1 and 3. Second, interchange elements in columns 1 and 3. Third, interchange elements in rows 1 and 2. Fourth, interchange elements in columns 1 and 2.

Let the vector of unknown displacement degrees of freedom be denoted by  $\{q_\alpha\}$ , the vector of prescribed displacements by  $\{q_\beta\}$ , the vector of applied forces by  $\{Q_\alpha\}$ , and the vector of reactive forces by  $\{Q_\beta\}$ . In the example of this and the last section these vectors are

$$\{q_\alpha\} = \begin{bmatrix} q_2 \\ q_3 \end{bmatrix} \quad \{q_\beta\} = \begin{bmatrix} q_1 \end{bmatrix} \quad \{Q_\alpha\} = \begin{bmatrix} Q_2 \\ Q_3 \end{bmatrix} \quad \{Q_\beta\} = \begin{bmatrix} Q_1 \end{bmatrix}. \quad (15.26)$$

The unrestrained structural stiffness matrix is rearranged to separate unknown and known nodal variables. In general, this partitioned matrix is written in the form

$$[K] = \begin{bmatrix} [K_{\alpha\alpha}] & [K_{\alpha\beta}] \\ [K_{\beta\alpha}] & [K_{\beta\beta}] \end{bmatrix}. \quad (15.27)$$

For the example in this and the last section, a comparison to the matrix in eq. (15.25) gives the submatrices in eq. (15.27) as

$$[K_{\alpha\alpha}] = \begin{bmatrix} (k_a + k_b) & -k_b \\ -k_b & k_b \end{bmatrix} \quad [K_{\alpha\beta}] = \begin{bmatrix} -k_a \\ 0 \end{bmatrix} \quad [K_{\beta\alpha}] = \begin{bmatrix} -k_a & 0 \end{bmatrix} \quad [K_{\beta\beta}] = \begin{bmatrix} k_a \end{bmatrix}. \quad (15.28)$$

The matrix equations for the structure in partitioned form are now written as

$$\begin{bmatrix} \{Q_\alpha\} \\ \{Q_\beta\} \end{bmatrix} = \begin{bmatrix} [K_{\alpha\alpha}] & [K_{\alpha\beta}] \\ [K_{\beta\alpha}] & [K_{\beta\beta}] \end{bmatrix} \begin{bmatrix} \{q_\alpha\} \\ \{q_\beta\} \end{bmatrix}. \quad (15.29)$$

Submatrix  $[K_{\alpha\alpha}]$  is called the **restrained structural stiffness matrix**. It is a square, symmetric matrix. For the example of this section it is seen from eq. (15.28) that the restrained stiffness matrix is 2X2, and its determinate is positive (i.e.,  $\det[K_{\alpha\alpha}] = k_a k_b > 0$ ). The restrained structural stiffness matrix is nonsingular if the prescribed

nodal displacements are sufficient to prevent rigid body motion of the structure. The restrained structural stiffness matrix for this example was determined by the method of unit displacement states in example 15.1. See eq.(r). The submatrix  $[K_{\beta\beta}]$  is, in general, square and symmetric. For the example in this section, eq. (15.28) shows  $[K_{\beta\beta}]$  is 1X1. The off-diagonal submatrices are, in general, rectangular, but they satisfy the relationship

$$[K_{\beta\alpha}] = [K_{\alpha\beta}]^T. \quad (15.30)$$

### 15.5 Solution for the unknown nodal variables

Multiply out the matrix equations (15.29) following the ordinary matrix product formula to get

$$\{Q_\alpha\} = [K_{\alpha\alpha}]\{q_\alpha\} + [K_{\alpha\beta}]\{q_\beta\} \quad (15.31)$$

$$\{Q_\beta\} = [K_{\beta\alpha}]\{q_\alpha\} + [K_{\beta\beta}]\{q_\beta\}. \quad (15.32)$$

Since the applied load vector  $\{Q_\alpha\}$  and the prescribed displacement vector  $\{q_\beta\}$  are known, solve eq. (15.31) for the unknown nodal displacement vector to get

$$\{q_\alpha\} = [K_{\alpha\alpha}]^{-1}\{Q_\alpha\} - [K_{\alpha\alpha}]^{-1}[K_{\alpha\beta}]\{q_\beta\}. \quad (15.33)$$

Continuing with the example of the last two sections, the restrained structural stiffness matrix is given in first of eqs. (15.28). Its inverse can be computed from

$$[K_{\alpha\alpha}]^{-1} = \frac{adj[K_{\alpha\alpha}]}{det[K_{\alpha\alpha}]}.$$

where  $adj[K_{\alpha\alpha}]$  is the *adjoint matrix*. The adjoint matrix<sup>1</sup> is the transpose of the matrix of co-factors of matrix  $[K_{\alpha\alpha}]$ . For the 2X2 restrained structural stiffness matrix (15.28)<sub>1</sub> in this example, the adjoint matrix is simple to compute. It is

$$adj[K_{\alpha\alpha}] = \begin{bmatrix} k_b & k_b \\ k_b & (k_a + k_b) \end{bmatrix}^T = \begin{bmatrix} k_b & k_b \\ k_b & (k_a + k_b) \end{bmatrix}. \quad (15.34)$$

Hence, the inverse matrix is

1. Many determinates must be evaluated to compute the adjoint matrix. For large matrices, evaluating many determinates is computationally inefficient. Other, more efficient methods to solve large linear systems of equations are used in numerical algorithms.

$$[K_{\alpha\alpha}]^{-1} = \frac{1}{(k_a + k_b)k_b - k_b^2} \begin{bmatrix} k_b & k_b \\ k_b & (k_a + k_b) \end{bmatrix} = \begin{bmatrix} \frac{1}{k_a} & \frac{1}{k_a} \\ \frac{1}{k_a} & \left(\frac{1}{k_a} + \frac{1}{k_b}\right) \end{bmatrix}. \quad (15.35)$$

Of course, the inverse of the restrained structural stiffness matrix is recognized as the flexibility matrix. Equation (15.35) was also obtained by the method of unit action state in example 15.1 eq. (k). Continuing with the computations indicated in eq. (15.33) for this example, we have

$$\begin{bmatrix} q_2 \\ q_3 \end{bmatrix} = \begin{bmatrix} \frac{1}{k_a} & \frac{1}{k_a} \\ \frac{1}{k_a} & \left(\frac{1}{k_a} + \frac{1}{k_b}\right) \end{bmatrix} \begin{bmatrix} Q_2 \\ Q_3 \end{bmatrix} - \begin{bmatrix} \frac{1}{k_a} & \frac{1}{k_a} \\ \frac{1}{k_a} & \left(\frac{1}{k_a} + \frac{1}{k_b}\right) \end{bmatrix} \begin{bmatrix} -k_a \\ 0 \end{bmatrix} [q_1]$$

$$\begin{bmatrix} q_2 \\ q_3 \end{bmatrix} = \begin{bmatrix} \frac{1}{k_a} & \frac{1}{k_a} \\ \frac{1}{k_a} & \left(\frac{1}{k_a} + \frac{1}{k_b}\right) \end{bmatrix} \begin{bmatrix} Q_2 \\ Q_3 \end{bmatrix} - \begin{bmatrix} -1 \\ -1 \end{bmatrix} [q_1] = \begin{bmatrix} \frac{(Q_2 + Q_3)}{k_a} + q_1 \\ \frac{Q_2}{k_a} + \left(\frac{1}{k_b} + \frac{1}{k_a}\right) Q_3 + q_1 \end{bmatrix}. \quad (15.36)$$

Equation (15.36) is the solution for the unknown nodal displacements.

To find the reactive nodal force vector, substitute the solution for the active nodal displacement vector from eq. (15.33) into eq. (15.32) to get

$$\{Q_\beta\} = [K_{\beta\alpha}] \left\{ [K_{\alpha\alpha}]^{-1} \{Q_\alpha\} - [K_{\alpha\alpha}]^{-1} [K_{\alpha\beta}] \{q_\beta\} \right\} + [K_{\beta\beta}] \{q_\beta\}. \quad (15.37)$$

Multiply the matrix products and collect terms in the prescribed nodal displacement vector to get

$$\{Q_\beta\} = [K_{\beta\alpha}] [K_{\alpha\alpha}]^{-1} \{Q_\alpha\} + \left\{ [K_{\beta\beta}] - [K_{\beta\alpha}] [K_{\alpha\alpha}]^{-1} [K_{\alpha\beta}] \right\} \{q_\beta\}. \quad (15.38)$$

Let's evaluate eq. (15.38) for the example problem. From eqs. (15.28) and (15.35)

$$Q_1 = [-k_a \ 0] \begin{bmatrix} \frac{1}{k_a} & \frac{1}{k_a} \\ \frac{1}{k_a} & \left(\frac{1}{k_a} + \frac{1}{k_b}\right) \end{bmatrix} \begin{bmatrix} Q_2 \\ Q_3 \end{bmatrix} + \left\{ k_a - [-k_a \ 0] \begin{bmatrix} \frac{1}{k_a} & \frac{1}{k_a} \\ \frac{1}{k_a} & \left(\frac{1}{k_a} + \frac{1}{k_b}\right) \end{bmatrix} \begin{bmatrix} -k_a \\ 0 \end{bmatrix} \right\} q_1. \quad (15.39)$$

Performing some of the matrix products, we get

$$Q_1 = [-1 \ -1] \begin{bmatrix} Q_2 \\ Q_3 \end{bmatrix} + \{k_a - k_a\} q_1. \quad (15.40)$$

This last matrix expression is equivalent to the scalar equation

$$Q_1 = -Q_2 - Q_3. \quad (15.41)$$

The result (15.41) for the reactive nodal force is as expected from overall equilibrium of the structure shown in figure. 15.11.

## 15.6 Stress matrix

The stress matrix is a matrix that directly yields the internal forces or stresses in an element in terms of the nodal displacements. Consider a typical spring element between joints  $i$  and  $j$  as shown in figure. 15.13. From the over-

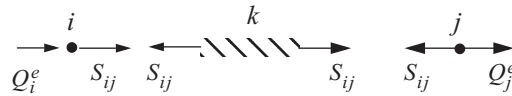


**Fig. 15.13 Typical spring element and equivalent joint forces.**

all solution for the structural response, the nodal displacement vector  $\{q_\alpha\}$  is determined. Hence, the actual nodal displacements  $q_i$  and  $q_j$  for the typical spring element are known. Define a vector of *equivalent nodal forces* as the element stiffness matrix times the known nodal displacement vector, or

$$\begin{bmatrix} Q_i \\ Q_j \end{bmatrix}^e = \begin{bmatrix} k & -k \\ -k & k \end{bmatrix} \begin{bmatrix} q_i \\ q_j \end{bmatrix}. \quad (15.42)$$

These equivalent nodal forces are not the actual forces at the joints, so they are fictitious. From this equation, the equivalent nodal forces at the joint are

$$Q_i^e = \begin{bmatrix} k & -k \end{bmatrix} \begin{bmatrix} q_i \\ q_j \end{bmatrix} \quad Q_j^e = \begin{bmatrix} -k & k \end{bmatrix} \begin{bmatrix} q_i \\ q_j \end{bmatrix}. \quad (15.43)$$

From the free body diagram shown in figure. 15.13, the spring force  $S_{ij}$  is related to the equivalent nodal forces by

$$Q_i^e = -S_{ij} \quad Q_j^e = S_{ij}. \quad (15.44)$$

Substitute eqs. (15.43) into (15.44) to eliminate the equivalent nodal forces to find that both of eqs. (15.44) lead to the same expression for the spring element force. The result is

$$S_{ij} = \begin{bmatrix} -k & k \end{bmatrix} \begin{bmatrix} q_i \\ q_j \end{bmatrix} = \begin{bmatrix} S \end{bmatrix} \begin{bmatrix} q_i \\ q_j \end{bmatrix}, \quad (15.45)$$

where  $\begin{bmatrix} S \end{bmatrix}$  is the stress matrix for the spring element given by

$$\begin{bmatrix} S \end{bmatrix} = \begin{bmatrix} -k & k \end{bmatrix}. \quad (15.46)$$

For the example problem, the stress matrix for the spring between joints 1 and 2 is  $\begin{bmatrix} -k_a & k_a \end{bmatrix}$ . Then, force in the spring element is

$$S_{12} = \begin{bmatrix} -k_a & k_a \end{bmatrix} \begin{bmatrix} q_1 \\ q_2 \end{bmatrix}.$$

From eq. (15.36), the displacement at joint 2 is

$$q_2 = \left( \frac{Q_2}{k_a} + \frac{Q_3}{k_a} \right) + q_1.$$

Hence, the force in the spring element between joints 1 and 2 is

$$S_{12} = -k_a q_1 + k_a q_2 = -k_a q_1 + k_a \left[ \left( \frac{Q_2}{k_a} + \frac{Q_3}{k_a} \right) + q_1 \right] = Q_2 + Q_3.$$

The stress matrix for the spring between joints 2 and 3 is  $\begin{bmatrix} -k_b & k_b \end{bmatrix}$ . Then the force in this spring element is

$$S_{23} = \begin{bmatrix} -k_b & k_b \end{bmatrix} \begin{bmatrix} q_2 \\ q_3 \end{bmatrix}.$$

Substitute the solution for the nodal displacements from eq. (15.36) into previous equation to get

$$S_{23} = \begin{bmatrix} -k_b & k_b \end{bmatrix} \begin{bmatrix} \frac{1}{k_a} & \frac{1}{k_a} \\ \frac{1}{k_a} \left( \frac{1}{k_a} + \frac{1}{k_b} \right) \end{bmatrix} \begin{bmatrix} Q_2 \\ Q_3 \end{bmatrix} - \begin{bmatrix} -k_b & k_b \end{bmatrix} \begin{bmatrix} -1 \\ -1 \end{bmatrix} \begin{bmatrix} q_1 \end{bmatrix}.$$

Perform the matrix products in this last equation to find the force in the element between joints 2 and 3 is

$$S_{23} = \left[ -k_b \left( \frac{Q_2}{k_a} + \frac{Q_3}{k_a} \right) + k_b \left( \frac{Q_2}{k_a} + Q_3 \left( \frac{1}{k_a} + \frac{1}{k_b} \right) \right) \right] - [0] q_1 = Q_3.$$

## 15.7 Summary of the direct stiffness method

We have completed all the steps of the direct stiffness method for the structure shown in figure. 15.11 in the discussions beginning in article 15.2 through article 15.6. The method is summarized as follows:

1. Formulate the member stiffness matrix, and expand it to the overall structural degrees of freedom by adding rows and columns of zeros.
2. Assemble of the member stiffness matrices to form the unrestrained structural stiffness matrix.

$$[K] = \sum_{\text{elements}} [K]_{\text{element}}. \quad (15.47)$$

3. Prescribe boundary displacement restraints  $\{q_\beta\}$  and applied nodal forces  $\{Q_\alpha\}$ :

$$\begin{Bmatrix} \{Q_\alpha\} \\ \{Q_\beta\} \end{Bmatrix} = \begin{bmatrix} [K_{\alpha\alpha}] & [K_{\alpha\beta}] \\ [K_{\beta\alpha}] & [K_{\beta\beta}] \end{bmatrix} \begin{Bmatrix} \{q_\alpha\} \\ \{q_\beta\} \end{Bmatrix}. \quad (15.48)$$

4. Solve for the unknown nodal displacements.

$$\{q_\alpha\} = [K_{\alpha\alpha}]^{-1} \{Q_\alpha\} - [K_{\alpha\alpha}]^{-1} [K_{\alpha\beta}] \{q_\beta\}. \quad (15.49)$$

5. Solve for the unknown support reactions.

$$\{Q_\beta\} = [K_{\beta\alpha}] \{q_\alpha\} + [K_{\beta\beta}] \{q_\beta\}. \quad (15.50)$$

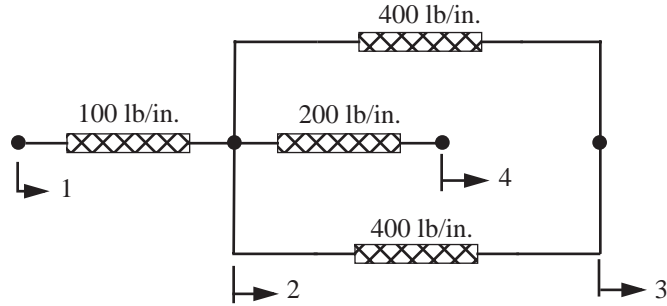
6. Determine the member forces/stresses:

$$S_{ij} = [S] \{q\}. \quad (15.51)$$

### Example 15.2 Partitioning an unrestrained structural stiffness matrix

A spring model with four degrees of freedom is shown in figure. 15.14.

**Fig. 15.14 Spring model of example 15.2.**



The unrestrained structural stiffness matrix is given as

$$[K] = \begin{bmatrix} q_1 & q_2 & q_3 & q_4 \\ 100 & -100 & 0 & 0 \\ -100 & 1,100 & -800 & -200 \\ 0 & -800 & 800 & 0 \\ 0 & -200 & 0 & 200 \end{bmatrix} \text{ lb./in.} \quad (a)$$

It is prescribed that the displacement  $q_1 = 1$  in., force  $Q_2 = 0$ , force  $Q_3 = -400$  lb., and that the displacement  $q_4 = 0$ .

- Determine the nodal displacement vectors  $\{q_\alpha\}$  and  $\{q_\beta\}$ , and the nodal force vectors  $\{Q_\alpha\}$  and  $\{Q_\beta\}$ .
- Determine the submatrices  $[K_{\alpha\alpha}]$ ,  $[K_{\alpha\beta}]$ ,  $[K_{\beta\alpha}]$ , and  $[K_{\beta\beta}]$ .
- Solve for the unknown nodal displacements and forces.

**Solution to part (a).** The known and unknown quantities are listed in table 15.1.

**Table 15.1 Classification of the nodal quantities**

Known	$q_1$	$Q_2$	$Q_3$	$q_4$
Unknown	$Q_1$	$q_2$	$q_3$	$Q_4$

Therefore, the  $\alpha$ -indices are 2 and 3, and the  $\beta$ -indices are 1 and 4. The unknown nodal displacement vector and the corresponding known nodal force vector are

$$\{q_\alpha\} = \begin{bmatrix} q_2 \\ q_3 \end{bmatrix} \quad \{Q_\alpha\} = \begin{bmatrix} Q_2 \\ Q_3 \end{bmatrix} = \begin{bmatrix} 0 \\ -400 \end{bmatrix}. \quad (\text{d})$$

The known displacement vector and the corresponding unknown force vector are

$$\{q_\beta\} = \begin{bmatrix} q_1 \\ q_4 \end{bmatrix} = \begin{bmatrix} 1 \\ 0 \end{bmatrix} \quad \{Q_\beta\} = \begin{bmatrix} Q_1 \\ Q_4 \end{bmatrix}. \quad (\text{e})$$

**Solution to part (b).** We change the order of the columns in the unrestrained structural stiffness matrix to correspond to displacements  $q_2, q_3, q_1$ , and  $q_4$ . Simultaneously we change the order of the rows to correspond to forces  $Q_2, Q_3, Q_1$ , and  $Q_4$ . The re-ordered unrestrained structural stiffness matrix is

$$\begin{array}{c} q_2 \quad q_3 \quad q_1 \quad q_4 \\ \begin{array}{l} Q_2: \\ Q_3: \\ Q_1: \\ Q_4: \end{array} \end{array} \begin{bmatrix} 1, & 100 & -800 & -100 & -200 \\ -800 & 800 & 0 & 0 \\ -100 & 0 & 100 & 0 \\ -200 & 0 & 0 & 200 \end{bmatrix}. \quad (\text{f})$$

Compare the partition form of the previous matrix to the general partitioned form given by eq. (15.27) to find

$$\begin{aligned} [K_{\alpha\alpha}] &= \begin{bmatrix} 1, & 100 & -800 \\ -800 & 800 \end{bmatrix} & [K_{\alpha\beta}] &= \begin{bmatrix} -100 & -200 \\ 0 & 0 \end{bmatrix} \\ [K_{\beta\alpha}] &= \begin{bmatrix} -100 & 0 \\ -200 & 0 \end{bmatrix} & [K_{\beta\beta}] &= \begin{bmatrix} 100 & 0 \\ 0 & 200 \end{bmatrix}. \end{aligned} \quad (\text{g})$$

**Solution to part (c).** The general form for the solution to the unknown nodal displacement vector is given by eq. (15.33). For this example the general form of the solution becomes

$$\begin{bmatrix} q_2 \\ q_3 \end{bmatrix} = \begin{bmatrix} 1, & 100 & -800 \\ -800 & 800 \end{bmatrix}^{-1} \begin{bmatrix} 0 \\ -400 \end{bmatrix} - \begin{bmatrix} 1, & 100 & -800 \\ -800 & 800 \end{bmatrix}^{-1} \begin{bmatrix} -100 & -200 \\ 0 & 0 \end{bmatrix} \begin{bmatrix} 1 \\ 0 \end{bmatrix} = \begin{bmatrix} -1 \\ -1.5 \end{bmatrix} \text{ in.} \quad (\text{h})$$

Since the nodal displacement vector  $\{q_\alpha\}$  has been determined, we use eq. (15.32) to find the unknown nodal force vector; i.e.,



$$\begin{bmatrix} Q_1 \\ Q_4 \end{bmatrix} = \begin{bmatrix} -100 & 0 \\ -200 & 0 \end{bmatrix} \begin{bmatrix} -1 \\ -1.5 \end{bmatrix} + \begin{bmatrix} 100 & 0 \\ 0 & 200 \end{bmatrix} \begin{bmatrix} 1 \\ 0 \end{bmatrix} = \begin{bmatrix} 200 \\ 200 \end{bmatrix} \text{ lb.} \quad (i)$$

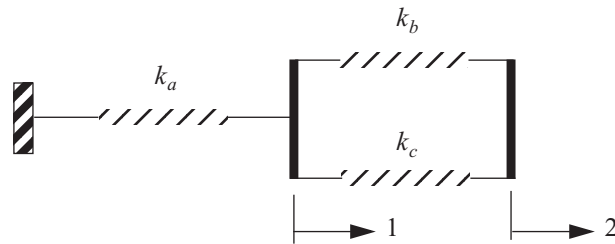
## 15.8 Reference

Martin, Harold C. *Introduction to Matrix Methods of Structural Analysis*. New York: McGraw-Hill Book Company, 1966.

## 15.9 Practice exercises

- For the spring assembly shown in figure. 15.15, determine the 2X2 flexibility influence matrix  $[C]$  by the method of unit action states.

**Fig. 15.15 Spring assembly of exercise 1.**



- Consider a three-degree-of-freedom model of the string in tension shown in figure. 15.16. Let  $T$  denote the horizontal component of the tension force. The three degrees of freedom are the vertical displacements and corresponding forces at the quarter points. The analysis of this structure is different from the analyses we have been using in that *we have to take equilibrium on a slightly deflected configuration rather than on the undeformed configuration even though the displacements are small*. A typical free body diagram to be used in the analysis is shown in the figure. Note that it is the horizontal component of the string tension that is equal to  $T$ .

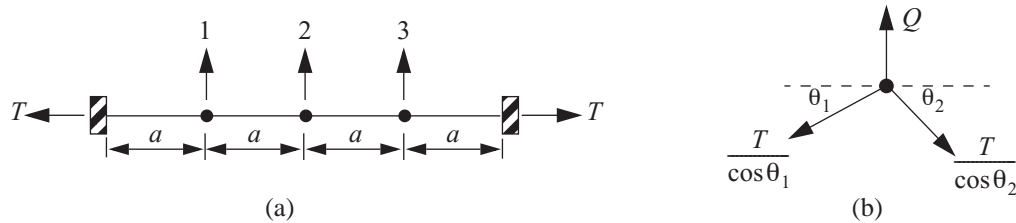
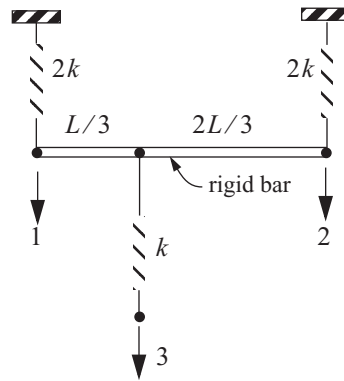


**Fig. 15.16 (a) String in tension. (b) Typical free body diagram**

- Use unit action states and the physical definition of flexibility influence coefficients to calculate the 3X3 flexibility matrix  $[C]$ . Write the elements of the matrix in terms of tension  $T$  and dimension  $a$ . Recall the vertical displacements are assumed small compared to length  $a$ . Partial answer:  $c_{11} = \frac{3}{4} \left( \frac{a}{T} \right)$ .

- b) Use unit displacement states and the physical definition of stiffness matrix elements to calculate the 3X3 stiffness matrix  $[K]$ . Partial answer:  $k_{11} = 2\left(\frac{T}{a}\right)$ .
- c) Check the plausibility of the matrices determined in parts **a** and **b**. Are they symmetric? Are diagonal elements positive? Does  $[K][C] = [I]$ ?
3. Derive by the method of unit displacement states the 3X3 stiffness matrix  $[K]$  for the structure shown in figure. 15.17. Assume small displacements and rotations of the horizontal rigid bar. Partial answer:  $k_{21} = 2k/9$ .

Fig. 15.17 Exercise 3.



4. For the spring model in example 15.2, use eq. (15.45) and determine the stress matrix and spring force in spring elements 1-2, 2-3, and 2-4. State if the spring element is in tension or compression. Note: the spring force 2-3 is the force in the upper and lower spring between joints 2 and 3.

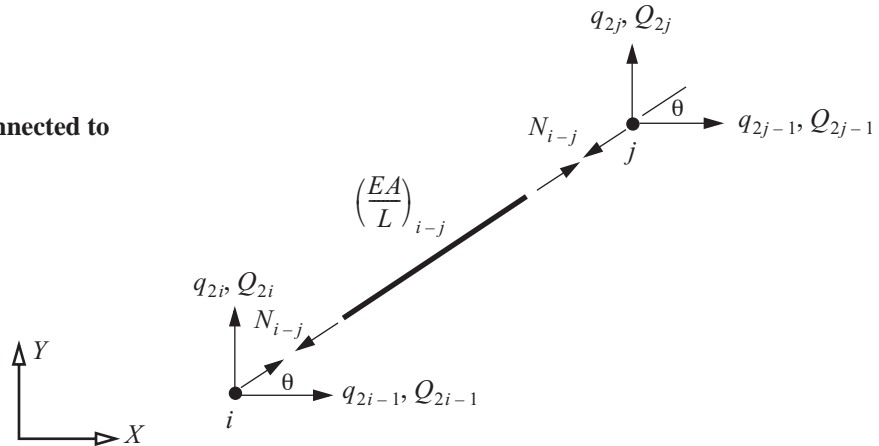
# Applications of the direct stiffness method

## 16.1 Coplanar trusses

The member stiffness matrix for a truss bar in the  $X$ - $Y$  plane is developed from the analysis in article 6.1.1 on page 153. A typical bar of length  $L$  located between joints  $i$  and  $j$  is shown in figure. 16.1. The coordinates of beginning joint  $i$  are  $(X_i, Y_i)$ , and coordinates of the end joint  $j$  are  $(X_j, Y_j)$ , in the undeformed state. The angle between the positive  $X$ -direction and directed line element  $i$ - $j$  is denoted as  $\theta$ , and is determined from

$$(\cos\theta)_{i-j} = \frac{X_j - X_i}{L_{i-j}} \quad (\sin\theta)_{i-j} = \frac{Y_j - Y_i}{L_{i-j}} \quad L_{i-j} = \sqrt{(X_j - X_i)^2 + (Y_j - Y_i)^2}. \quad (16.1)$$

**Fig. 16.1** Truss bar connected to joints  $i$  and  $j$ .



The axial force  $N_{i-j}$  from eq. (6.2) on page 154 is

$$N_{i-j} = \left(\frac{EA}{L}\right)_{i-j} \Delta_{i=j} - (N_T)_{i-j}. \quad (16.2)$$

The elongation  $\Delta_{i-j}$  is related to the joint displacements by eq. (6.6) on page 155, which is repeated as (16.3)

below.

$$\Delta_{i-j} = (\cos\theta)_{i-j}(q_{2j-1} - q_{2i-1}) + (\sin\theta)_{i-j}(q_{2j} - q_{2i}), \quad (16.3)$$

In matrix notation (16.3) is written as

$$\Delta_{i-j} = \begin{bmatrix} -c & -s & c & s \end{bmatrix} \begin{bmatrix} q_{2i-1} \\ q_{2i} \\ q_{2j} \\ q_{2j-1} \end{bmatrix} = \begin{bmatrix} b \end{bmatrix}^T \{q\}_{i-j}, \quad (16.4)$$

where we introduce the shorthand notation for the trigonometric functions

$$c = (\cos\theta)_{i-j} \quad s = (\sin\theta)_{i-j}. \quad (16.5)$$

Elements of the 4X1 matrix  $[b]$  and the 4X1 displacement vector are

$$\begin{bmatrix} b \end{bmatrix}^T = \begin{bmatrix} -c & -s & c & s \end{bmatrix} \quad \{q\}_{i-j}^T = \begin{bmatrix} q_{2i-1} & q_{2i} & q_{2j-1} & q_{2j} \end{bmatrix}. \quad (16.6)$$

Substitute the elongation-displacement relation (16.4) into Hooke's law (16.2) to get

$$N_{i-j} = \left(\frac{EA}{L}\right)_{i-j} \begin{bmatrix} b \end{bmatrix}^T \{q\}_{i-j} - (N_T)_{i-j}. \quad (16.7)$$

Free body diagrams of the bar and joints  $i$  and  $j$  are shown figure. 16.1. External forces in the  $X$ - and  $Y$ -directions at joint  $i$  are denoted by  $Q_{2i-1}$  and  $Q_{2i}$ , respectively, and external forces in the  $X$ - and  $Y$ -directions at joint  $j$  are denoted by  $Q_{2j-1}$  and  $Q_{2j}$ , respectively. Equilibrium at joints  $i$  and  $j$  yield

$$Q_{2i-1} + N_{i-j}\cos\theta = 0, \quad Q_{2i} + N_{i-j}\sin\theta = 0, \quad Q_{2j-1} - N_{i-j}\cos\theta = 0, \quad \text{and} \quad Q_{2j} - N_{i-j}\sin\theta = 0. \quad (16.8)$$

In matrix notation, equilibrium equations (16.8) are written as

$$\begin{bmatrix} Q_{2i-1} \\ Q_{2i} \\ Q_{2j-1} \\ Q_{2j} \end{bmatrix} = \begin{bmatrix} -c \\ -s \\ c \\ s \end{bmatrix} N_{i-j} \quad \text{or} \quad \{Q\}_{i-j} = \begin{bmatrix} b \end{bmatrix} N_{i-j}, \quad (16.9)$$

where  $\{Q\}_{i-j}$  is the joint force vector and matrix  $\begin{bmatrix} b \end{bmatrix}$  is defined in eq. (16.6). Substitute eq. (16.7) for the axial force in eq. (16.9) to get

$$\{Q\}_{i-j} = \left(\frac{EA}{L}\right)_{i-j} \begin{bmatrix} b \end{bmatrix} \begin{bmatrix} b \end{bmatrix}^T \{q\}_{i-j} - \begin{bmatrix} b \end{bmatrix} (N_T)_{i-j}. \quad (16.10)$$

The latter equation is written in the form

$$\{Q\}_{i-j} = \begin{bmatrix} K \end{bmatrix} \{q\}_{i-j} + \{Q^0\}_{i-j}, \quad (16.11)$$

where  $\begin{bmatrix} K \end{bmatrix} = \left(\frac{EA}{L}\right)_{i-j} \begin{bmatrix} b \end{bmatrix} \begin{bmatrix} b \end{bmatrix}^T$  is the truss stiffness matrix, and  $\{Q^0\}_{i-j} = -\begin{bmatrix} b \end{bmatrix} (N_T)_{i-j}$  is the fixed-end force

vector. The stiffness matrix for the truss bar is

$$[K] = \left( \frac{EA}{L} \right)_{i-j} \begin{bmatrix} c^2 & cs & -c^2 & -cs \\ cs & s^2 & -cs & -s^2 \\ -c^2 & -cs & c^2 & cs \\ -cs & -s^2 & cs & s^2 \end{bmatrix}. \quad (16.12)$$

Properties of the truss stiffness matrix (16.12):

- It is symmetric since the bar is linear elastic and the displacements are small.
- The sum of column elements is zero. This results from equilibrium of the bar for each unit displacement state.

For example UDS 1  $\{q\} = [1 \ 0 \ 0 \ 0]^T$  and the joint forces are

$$\{Q\} = [Q_{2i-1} \ Q_{2i} \ Q_{2j-1} \ Q_{2j}]^T = (EA/L) [c^2 \ cs \ -c^2 \ -cs]^T (1).$$

$$\text{Sum forces horizontally } Q_{2i-1} + Q_{2j-1} = (EA/L)(c^2 + (-c^2))(1) = 0.$$

$$\text{Sum forces vertically } Q_{2i} + Q_{2j} = (EA/L)(cs + (-cs))(1) = 0.$$

$$\text{Sum moments about joint } i \ LcQ_{2j} - LsQ_{2j-1} = L(EA/L)[c(-cs) - s(-c^2)](1) = 0.$$

- $\text{Det}[K] = 0$  since the bar is not restrained against rigid body displacements.
- Diagonal elements are positive.

The fixed-end force vector is

$$\{Q^0\}_{i-j} = \begin{bmatrix} Q_{2i-1}^0 \\ Q_{2i}^0 \\ Q_{2j-1}^0 \\ Q_{2j}^0 \end{bmatrix} = -[b](N_T)_{i-j} = -\begin{bmatrix} -c \\ -s \\ c \\ s \end{bmatrix} (N_T)_{i-j}. \quad (16.13)$$

Note that the nodal force vector is equal to the fixed-end vector when the joints are fixed and cannot displace; i.e.,

$$\{Q\}_{i-j} = \{Q^0\}_{i-j} \text{ if } \{q\}_{i-j}^T = [0 \ 0 \ 0 \ 0].$$

Equation (16.7) is rewritten for bar  $i-j$  as

$$N_{i-j} = [S]\{q\}_{i-j} - (N_T)_{i-j}, \quad (16.14)$$

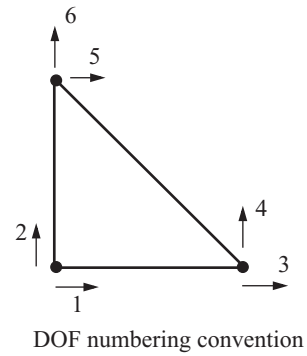
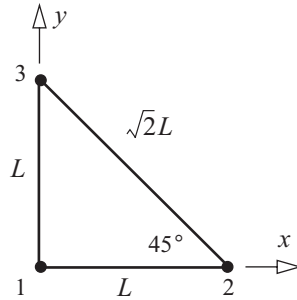
where the 1X4 stress matrix  $[S]$  is defined as

$$[S] = \left( \frac{EA}{L} \right)_{i-j} [-c \ -s \ c \ s] = \left( \frac{EA}{L} \right)_{i-j} [b]^T. \quad (16.15)$$

### Example 16.1 A three-bar truss

Each bar in the three-bar truss shown in figure. 16.2 has the same axial stiffness  $EA$ , and the joints are numbered as shown. The thermal forces in bar 1-2, 1-3, and 2-3 are denoted by  $(N_T)_{1-2}$ ,  $(N_T)_{1-3}$ , and  $(N_T)_{2-3}$ , respectively. Determine the 6X6 unrestrained structural stiffness matrix and the 6X1 fixed-end action vector.

**Fig. 16.2** Three-bar truss example.



**Solution.** The direction cosines and their products for each bar are listed in table 16.1.

**Table 16.1** Direction cosines for the three-bar truss

bar	$\theta$	$c$	$s$	$c^2$	$s^2$	$cs$
1-2	$0^\circ$	1	0	1	0	0
1-3	$90^\circ$	0	1	0	1	0
2-3	$135^\circ$	$-1/\sqrt{2}$	$1/\sqrt{2}$	$1/2$	$1/2$	$-1/2$

The direction cosines from table 16.1 are inserted into eqs. (16.12) and (16.13), to get the 4X4 stiffness matrices and the 4X1 fixed-end actions for the truss member. The stiffness matrices are expanded to 6X6 by adding two rows and two columns of zeros, and the column vectors are expanded to 6X1 by adding two rows of zeros. Refer to the discussion in article 15.3 on page 425. The 6X1 vector of forces for bar 1-2 is

$$\begin{bmatrix} Q_1 \\ Q_2 \\ Q_3 \\ Q_4 \\ Q_5 \\ Q_6 \end{bmatrix}_{1-2} = \left( \frac{EA}{L} \right) \begin{bmatrix} 1 & 0 & -1 & 0 & 0 & 0 \\ 0 & 0 & 0 & 0 & 0 & 0 \\ -1 & 0 & 1 & 0 & 0 & 0 \\ 0 & 0 & 0 & 0 & 0 & 0 \\ 0 & 0 & 0 & 0 & 0 & 0 \\ 0 & 0 & 0 & 0 & 0 & 0 \end{bmatrix} \begin{bmatrix} q_1 \\ q_2 \\ q_3 \\ q_4 \\ q_5 \\ q_6 \end{bmatrix} - \begin{bmatrix} -1 \\ 0 \\ 1 \\ 0 \\ 0 \\ 0 \end{bmatrix} (N_T)_{1-2}. \quad (\mathbf{a})$$

Rows five and six, and columns five and six, of the stiffness matrix in eq. (a) contain zeros entries since degrees of freedom five and six do not influence the response of truss bar 1-2. The 6X1 vector of forces for bar 1-3 is

$$\begin{bmatrix} Q_1 \\ Q_2 \\ Q_3 \\ Q_4 \\ Q_5 \\ Q_6 \end{bmatrix}_{1-3} = \left( \frac{EA}{L} \right) \begin{bmatrix} 0 & 0 & 0 & 0 & 0 & 0 \\ 0 & 1 & 0 & 0 & 0 & -1 \\ 0 & 0 & 0 & 0 & 0 & 0 \\ 0 & 0 & 0 & 0 & 0 & 0 \\ 0 & 0 & 0 & 0 & 0 & 0 \\ 0 & -1 & 0 & 0 & 0 & 1 \end{bmatrix} \begin{bmatrix} q_1 \\ q_2 \\ q_3 \\ q_4 \\ q_5 \\ q_6 \end{bmatrix} - \begin{bmatrix} 0 \\ -1 \\ 0 \\ 0 \\ 0 \\ 1 \end{bmatrix} (N_T)_{1-3}. \quad (\text{b})$$

Rows three and four, and columns three and four, of the stiffness matrix in eq. (b) contain zeros entries since degrees of freedom three and four do not influence the response of truss bar 1-3. The 6X1 vector of forces for bar 2-3 is

$$\begin{bmatrix} Q_1 \\ Q_2 \\ Q_3 \\ Q_4 \\ Q_5 \\ Q_6 \end{bmatrix}_{2-3} = \left( \frac{EA}{\sqrt{2}L} \right) \begin{bmatrix} 0 & 0 & 0 & 0 & 0 & 0 \\ 0 & 0 & 0 & 0 & 0 & 0 \\ 0 & 0 & 1/2 & -1/2 & -1/2 & 1/2 \\ 0 & 0 & -1/2 & 1/2 & 1/2 & -1/2 \\ 0 & 0 & -1/2 & 1/2 & 1/2 & -1/2 \\ 0 & 0 & 1/2 & -1/2 & -1/2 & 1/2 \end{bmatrix} \begin{bmatrix} q_1 \\ q_2 \\ q_3 \\ q_4 \\ q_5 \\ q_6 \end{bmatrix} - \begin{bmatrix} 0 \\ 0 \\ 1/\sqrt{2} \\ -1/\sqrt{2} \\ -1/\sqrt{2} \\ 1/\sqrt{2} \end{bmatrix} (N_T)_{2-3}. \quad (\text{c})$$

Rows one and two, and columns one and two, of the stiffness matrix in eq.(c) contain zeros entries since degrees of freedom one and two do not influence the response of truss bar 1-3. Let  $a = \frac{1}{2\sqrt{2}}$ , so that

$$\begin{bmatrix} Q_1 \\ Q_2 \\ Q_3 \\ Q_4 \\ Q_5 \\ Q_6 \end{bmatrix}_{2-3} = \left( \frac{EA}{L} \right) \begin{bmatrix} 0 & 0 & 0 & 0 & 0 & 0 \\ 0 & 0 & 0 & 0 & 0 & 0 \\ 0 & 0 & a & -a & -a & a \\ 0 & 0 & -a & a & a & -a \\ 0 & 0 & -a & a & a & -a \\ 0 & 0 & a & -a & -a & a \end{bmatrix} \begin{bmatrix} q_1 \\ q_2 \\ q_3 \\ q_4 \\ q_5 \\ q_6 \end{bmatrix} - \begin{bmatrix} 0 \\ 0 \\ 1/\sqrt{2} \\ -1/\sqrt{2} \\ -1/\sqrt{2} \\ 1/\sqrt{2} \end{bmatrix} (N_T)_{2-3}. \quad (\text{d})$$

Addition of the 6X1 force vectors for each truss member equals the external joint force vector acting on the truss. This addition of force vectors satisfies equilibrium at the joints assuming the procedure to expand each truss element to six degrees of freedom to four degrees of freedom is done correctly. Hence, the condition of equilibrium is

$$\begin{bmatrix} Q_1 \\ Q_2 \\ Q_3 \\ Q_4 \\ Q_5 \\ Q_6 \end{bmatrix} = \begin{bmatrix} Q_1 \\ Q_2 \\ Q_3 \\ Q_4 \\ Q_5 \\ Q_6 \end{bmatrix}_{1-2} + \begin{bmatrix} Q_1 \\ Q_2 \\ Q_3 \\ Q_4 \\ Q_5 \\ Q_6 \end{bmatrix}_{1-3} + \begin{bmatrix} Q_1 \\ Q_2 \\ Q_3 \\ Q_4 \\ Q_5 \\ Q_6 \end{bmatrix}_{2-3}. \quad (\text{e})$$

Equations (a), (b), and (d) for the force vectors are substituted into eq. (e) to get the unrestrained stiffness matrix

of the truss as

$$\begin{bmatrix} Q_1 \\ Q_2 \\ Q_3 \\ Q_4 \\ Q_5 \\ Q_6 \end{bmatrix} = \frac{EA}{L} \begin{bmatrix} 1 & 0 & -1 & 0 & 0 & 0 \\ 0 & 1 & 0 & 0 & 0 & -1 \\ -1 & 0 & 1+a & -a & -a & a \\ 0 & 0 & -a & a & a & -a \\ 0 & 0 & -a & a & a & -a \\ 0 & -1 & a & -a & -a & 1+a \end{bmatrix} \begin{bmatrix} q_1 \\ q_2 \\ q_3 \\ q_4 \\ q_5 \\ q_6 \end{bmatrix} + \begin{bmatrix} (N_T)_{1-2} \\ (N_T)_{1-3} \\ -(N_T)_{1-2} - (N_T)_{2-3}/\sqrt{2} \\ (N_T)_{2-3}/\sqrt{2} \\ (N_T)_{2-3}/\sqrt{2} \\ -(N_T)_{1-3} - (N_T)_{2-3}/\sqrt{2} \end{bmatrix}. \quad (\text{f})$$

In compact notation eq. (f) is

$$\{Q\} = [K]\{q\} + \{Q^0\}, \quad (\text{g})$$

where the 6X6 unrestrained structural stiffness matrix is

$$[K] = \left( \frac{EA}{L} \right) \begin{matrix} & \begin{matrix} q_1 & q_2 & q_3 & q_4 & q_5 & q_6 \end{matrix} \\ \begin{matrix} q_1 \\ q_2 \\ q_3 \\ q_4 \\ q_5 \\ q_6 \end{matrix} & \begin{bmatrix} 1 & 0 & -1 & 0 & 0 & 0 \\ 0 & 1 & 0 & 0 & 0 & -1 \\ -1 & 0 & 1+a & -a & -a & a \\ 0 & 0 & -a & a & a & -a \\ 0 & 0 & -a & a & a & -a \\ 0 & -1 & a & -a & -a & 1+a \end{bmatrix} \end{matrix}, \quad (\text{h})$$

and the 6X1 fixed-end action vector is

$$\{Q^0\} = \begin{bmatrix} (N_T)_{1-2} \\ (N_T)_{1-3} \\ -(N_T)_{1-2} - (N_T)_{2-3}/\sqrt{2} \\ (N_T)_{2-3}/\sqrt{2} \\ (N_T)_{2-3}/\sqrt{2} \\ -(N_T)_{1-3} - (N_T)_{2-3}/\sqrt{2} \end{bmatrix}. \quad (\text{i})$$

Note that the stiffness matrix in eq. (h) is symmetric; the sum of column elements equals zero; diagonal elements are positive; and its determinate vanishes. ■



### 16.1.1 Assembly algorithm

Consider again the three-bar truss in example 16.1 on page 440. For computer implementation an algorithm is presented to assemble the 6X6 unrestrained structural stiffness matrix from the three 4X4 truss stiffness matrices, and to assemble the 6X1 fixed-end vector from the three 4X1 fixed-end action vectors. Let a truss member be denoted by  $m$ , where  $m = 1$  for bar 1-2,  $m = 2$  for bar 1-3, and  $m = 3$  for bar 2-3. A description of symbols used in the of assembly algorithm is given in table 16.2.

**Table 16.2 Nomenclature**

Symbol	Description
$[K]$	6X6 unrestrained stiffness matrix
$K(row, col)$	row and column elements of the unrestrained stiffness matrix
$[K_m]$	4X4 stiffness matrix for truss member $m$
$K_m(i, j)$	matrix elements of the truss member stiffness matrix
$\{Q^0\}$	6X1 fixed-end action vector
$Q^0(row)$	row elements of the fixed-end action vector
$\{Q_m^{(0)}\}$	4X1 fixed-end action vector of truss member $m$
$Q_m^0(i)$	row elements of the truss member fixed-end action vector

Define the 3X1 "spring" stiffness vector  $[K_I]$  and the 3X1 thermal force vector  $[NT]$  by

$$[K_I] = \left[ \frac{EA}{L} \quad \frac{EA}{L} \quad \frac{EA}{\sqrt{2}L} \right]^T \quad [NT] = \left[ (N_T)_{1-2} \quad (N_T)_{1-3} \quad (N_T)_{2-3} \right]^T. \quad (16.16)$$

Direction cosines for each truss bar are specified in the 4X1 matrices  $[b_i]$ ,  $i = 1, 2, 3$ , in eq. (16.17) below:

$$[b_1] = \begin{bmatrix} -1 & 0 & 1 & 0 \end{bmatrix}^T \quad [b_2] = \begin{bmatrix} 0 & -1 & 0 & 1 \end{bmatrix}^T \quad [b_3] = \begin{bmatrix} \frac{1}{\sqrt{2}} & -\frac{1}{\sqrt{2}} & -\frac{1}{\sqrt{2}} & \frac{1}{\sqrt{2}} \end{bmatrix}^T. \quad (16.17)$$

Defined a 3X4 **connectivity matrix**  $[C]$  by

$$[C] = \begin{array}{c} \begin{array}{cccc} q_{2i-1} & q_{2i} & q_{2j-1} & q_{2j} \\ \swarrow & \swarrow & \swarrow & \swarrow \\ \begin{bmatrix} 1 & 2 & 3 & 4 \\ 1 & 2 & 5 & 6 \\ 3 & 4 & 5 & 6 \end{bmatrix} & \begin{array}{l} \text{member 1} \\ \text{member 2} \\ \text{member 3} \end{array} \end{array} \end{array}. \quad (16.18)$$

Row one of matrix  $[C]$  is assigned to member 1 (bar 1-2), row two to member 2 (bar 1-3), and row three to

member 3 (bar 2-3).

Column one contains the DOF for horizontal displacement  $q_{2i-1}$  at the beginning joint  $i$  of the member, column two contains the DOF for the vertical displacement  $q_{2i}$  of the beginning joint  $i$  of the member, column three contains the DOF of the horizontal displacement  $q_{2j-1}$  at the end joint  $j$  of the member, and column four contains the DOF for the vertical displacement  $q_{2j}$  at the end joint  $j$  of the member.

Refer to the nomenclature in table 16.2, and to matrices defined in eqs. (16.16), (16.17), and (16.18), to understand the flow chart for the assembly algorithm in figure. 16.3.

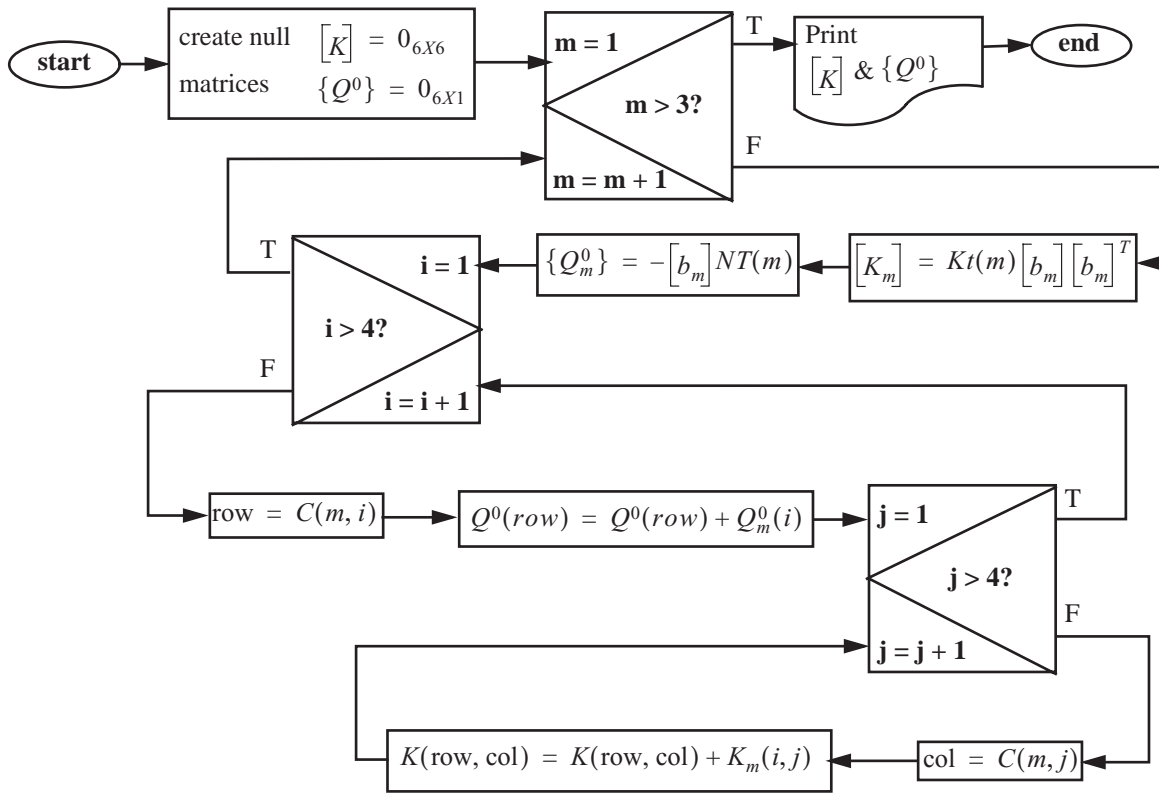


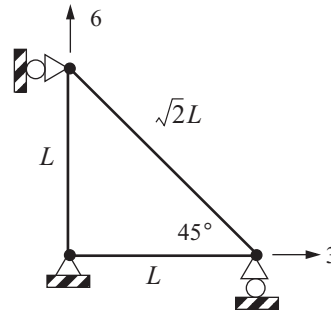
Fig. 16.3 Flow chart of the assembly algorithm.

### Example 16.2 Restrained three-bar truss of example 16.1

Consider the truss of example 16.1 supported in such a manner that joint displacements  $q_1 = q_2 = q_4 = q_5 = 0$  as is shown in figure. 16.4. The unknown displacements are  $q_3$  and  $q_6$ , and take the corresponding joint forces  $Q_3 = Q_6 = 0$ . The thermal forces in bars 1-2, 1-3, and 2-3 are specified as  $(N_T)_{1-2} = 0$ ,  $(N_T)_{1-3} \neq 0$ , and  $(N_T)_{2-3} = 0$ , respectively.

- a) Determine the restrained structural stiffness matrix  $[K_{\alpha\alpha}]$ , and submatrices  $[K_{\alpha\beta}]$ ,  $[K_{\beta\alpha}]$ , and  $[K_{\beta\beta}]$ .

**Fig. 16.4** Statically indeterminate three-bar truss.



- b) Determine the unknown joint displacements  $q_3$ , and  $q_6$ .
- c) Determine the unknown support reactions  $Q_1$ ,  $Q_2$ ,  $Q_4$ , and  $Q_5$ .
- d) Determine the bar forces  $N_{1-2}$ ,  $N_{1-3}$ , and  $N_{2-3}$ .

**Solution to part (a).** Rearrange the unrestrained stiffness matrix in eq. (h) of example 16.1 so that the order of the rows and columns correspond to degrees of freedom 3, 6, 1, 2, 4, and 5.

$$[K] = \left( \frac{EA}{L} \right) \begin{bmatrix} q_3 & q_6 & q_1 & q_2 & q_4 & q_5 \\ 1+a & a & -1 & 0 & -a & -a \\ -a & 1+a & 0 & -1 & -a & -a \\ -1 & 0 & 1 & 0 & 0 & 0 \\ 0 & -1 & 0 & 1 & 0 & 0 \\ -a & -a & 0 & 0 & a & a \\ -a & -a & 0 & 0 & a & a \end{bmatrix} \quad (a)$$

Compare the matrix in eq. (a) to the general form (15.27) on page 428 to identify

$$[K_{\alpha\alpha}] = \left( \frac{EA}{L} \right) \begin{bmatrix} 1+a & a \\ a & 1+a \end{bmatrix} \quad [K_{\alpha\beta}] = \left( \frac{EA}{L} \right) \begin{bmatrix} -1 & 0 & -a & -a \\ 0 & -1 & -a & -a \end{bmatrix}, \quad (b)$$

and

$$[K_{\beta\alpha}] = \left( \frac{EA}{L} \right) \begin{bmatrix} -1 & 0 \\ 0 & -1 \\ -a & -a \\ -a & -a \end{bmatrix} \quad [K_{\beta\beta}] = \left( \frac{EA}{L} \right) \begin{bmatrix} 1 & 0 & 0 & 0 \\ 0 & 1 & 0 & 0 \\ 0 & 0 & a & a \\ 0 & 0 & a & a \end{bmatrix}. \quad (c)$$

The restrained structural stiffness matrix  $[K_{\alpha\alpha}]$  is symmetric, and the sum of its column elements is not zero.

Also note that the restrained stiffness structural matrix can be obtained from the unrestrained structural stiffness matrix in eq. (h) by merely crossing out rows and columns 1, 2, 4, and 5:

$$[K] = \left( \frac{EA}{L} \right) \begin{bmatrix} 1 & 0 & -1 & 0 & 0 & 0 \\ 0 & 1 & 0 & 0 & 0 & 1 \\ -1 & 0 & 1+a & -a & -a & a \\ 0 & 0 & -a & a & a & -a \\ 0 & 0 & -a & a & a & -a \\ 0 & -1 & a & -a & -a & 1+a \end{bmatrix} \quad (d)$$

The fixed-end action vector in eq. (i) of example 16.1 for the unrestrained truss reduces to

$$\{Q^0\} = \begin{bmatrix} 0 & (N_T)_{1-3} & 0 & 0 & 0 & -(N_T)_{1-3} \end{bmatrix}^T \quad (e)$$

Elements in rows 3 and 6 constitute  $\{Q_\alpha^0\}$  while the remaining rows constitute  $\{Q_\beta^0\}$ . Thus,

$$\{Q_\alpha^0\} = \begin{bmatrix} 0 \\ -(N_T)_{1-3} \end{bmatrix} \quad \{Q_\beta^0\} = \begin{bmatrix} 0 \\ (N_T)_{1-3} \\ 0 \\ 0 \end{bmatrix} \quad (f)$$

**Solution to part (b).** Equation (15.31) on page 429 with the addition of the fixed-end action vector is

$$\{Q_\alpha\} = [K_{\alpha\alpha}]\{q_\alpha\} + [K_{\alpha\beta}]\{q_\beta\} + \{Q_\alpha^0\} \quad (g)$$

The fixed-end action vector is subtracted from each side of this equation, since it is a known vector determined from the specified temperature changes in the bars. That is, eq. (g) is written in the form

$$\underbrace{\{Q_\alpha\} + (-\{Q_\alpha^0\})}_{\text{equivalent joint force vector}} = [K_{\alpha\alpha}]\{q_\alpha\} + [K_{\alpha\beta}]\{q_\beta\} \quad (h)$$

The vector  $-\{Q_\alpha^0\}$  is called the **equivalent joint force vector**. In this example the prescribed joint displacement vector is  $\{q_\beta\} = [q_1 \ q_2 \ q_4 \ q_5]^T = [0 \ 0 \ 0 \ 0]^T$ , and the prescribed joint force vector is

$\{Q_\alpha\}^T = [Q_3 \ Q_6] = [0 \ 0]$ . The solution for the unknown joint displacement vector is

$$\{q_\alpha\} = [K_{\alpha\alpha}]^{-1}\{-Q_\alpha^0\}, \text{ where the inverse matrix is } [K_{\alpha\alpha}]^{-1} = \left( \text{adj}[K_{\alpha\alpha}] \right) / \left( \det[K_{\alpha\alpha}] \right) \quad (i)$$

The adjoint of the restrained structural stiffness matrix and its determinate are<sup>1</sup>

1. The  $\det(k[A])$ , where  $k$  is a scalar and  $[A]$  is an  $n$ -by- $n$  matrix, is equal to  $k^n \det[A]$ .

$$\text{adj}[K_{\alpha\alpha}] = \left(\frac{EA}{L}\right) \begin{bmatrix} 1+a & -a \\ -a & 1+a \end{bmatrix} \quad \det[K_{\alpha\alpha}] = \left(\frac{EA}{L}\right)^2 ((1+a)^2 - a^2) = \left(\frac{EA}{L}\right)^2 (1+2a). \quad (\text{j})$$

So the inverse of the restrained structural stiffness matrix is

$$[K_{\alpha\alpha}]^{-1} = \left(\frac{L}{EA}\right) \left(\frac{1}{1+2a}\right) \begin{bmatrix} 1+a & -a \\ -a & 1+a \end{bmatrix}. \quad (\text{k})$$

Perform a check of this inverse. Is  $[K_{\alpha\alpha}][K_{\alpha\alpha}]^{-1} = [I]$ ?

$$\begin{aligned} \left(\frac{EA}{L}\right) \begin{bmatrix} 1+a & a \\ a & 1+a \end{bmatrix} \left(\frac{L}{EA}\right) \left(\frac{1}{1+2a}\right) \begin{bmatrix} 1+a & -a \\ -a & 1+a \end{bmatrix} &= \left(\frac{1}{1+2a}\right) \begin{bmatrix} 1+a & a \\ a & 1+a \end{bmatrix} \begin{bmatrix} 1+a & -a \\ -a & 1+a \end{bmatrix} \\ &= \frac{1}{1+2a} \begin{bmatrix} (1+a)^2 + (-a^2) & (1+a)(-a) + a(1+a) \\ a(1+a) + (1+a)(-a) & -a^2 + (1+a)^2 \end{bmatrix} = \frac{1}{1+2a} \begin{bmatrix} 1+2a & 0 \\ 0 & 1+2a \end{bmatrix} = \begin{bmatrix} 1 & 0 \\ 0 & 1 \end{bmatrix}. \end{aligned} \quad (\text{l})$$

Hence, the inverse satisfies  $[K_{\alpha\alpha}][K_{\alpha\alpha}]^{-1} = [I]$ . The solution for the unknown nodal displacement vector is

$$\begin{bmatrix} q_3 \\ q_6 \end{bmatrix} = \left(\frac{L}{EA}\right) \begin{bmatrix} \frac{-\sqrt{2}}{4+2\sqrt{2}} \\ \frac{4+\sqrt{2}}{4+2\sqrt{2}} \end{bmatrix} (N_T)_{1-3}. \quad (\text{m})$$

**Solution to part (c).** The support reactions are determined from eq. (15.32) on page 429, which is repeated below as eq. (n).

$$\{Q_\beta\} = [K_{\beta\alpha}]\{q_\alpha\} + [K_{\beta\beta}]\{q_\beta\} + \{Q_\beta^0\}. \quad (\text{n})$$

The prescribed joint displacement vector  $\{q_\beta\} = 0_{4 \times 1}$ , and submatrix  $[K_{\beta\alpha}]$  was determined in part (a).

Hence,

$$\begin{bmatrix} Q_1 \\ Q_2 \\ Q_4 \\ Q_5 \end{bmatrix} = \left(\frac{EA}{L}\right) \begin{bmatrix} -1 & 0 \\ 0 & -1 \\ -a & -a \\ -a & -a \end{bmatrix} \begin{bmatrix} q_3 \\ q_6 \end{bmatrix} + \begin{bmatrix} 0 \\ 0 \\ 0 \\ 0 \end{bmatrix} (N_T)_{1-3}. \quad (\text{o})$$

Substitute eq. (m) for the displacement vector into eq. (o) to get

$$\begin{bmatrix} Q_1 \\ Q_2 \\ Q_4 \\ Q_5 \end{bmatrix} = \left( \frac{EA}{L} \right) \begin{bmatrix} -1 & 0 \\ 0 & -1 \\ -a & -a \\ -a & -a \end{bmatrix} \left( \frac{L}{EA} \right) \begin{bmatrix} -1 \\ 2 + 2\sqrt{2} \\ 4 + \sqrt{2} \\ 4 + 2\sqrt{2} \end{bmatrix} (N_T)_{1-3} + \begin{bmatrix} 0 \\ (N_T)_{1-3} \\ 0 \\ 0 \end{bmatrix}. \quad (\text{p})$$

After matrix algebra the reactive joint forces are

$$\begin{bmatrix} Q_1 \\ Q_2 \\ Q_4 \\ Q_5 \end{bmatrix} = \begin{bmatrix} \frac{1}{2 + 2\sqrt{2}} \\ \frac{1}{2 + 2\sqrt{2}} \\ \frac{1}{2} - \frac{1}{\sqrt{2}} \\ \frac{1}{2} - \frac{1}{\sqrt{2}} \end{bmatrix} (N_T)_{1-3}. \quad (\text{q})$$

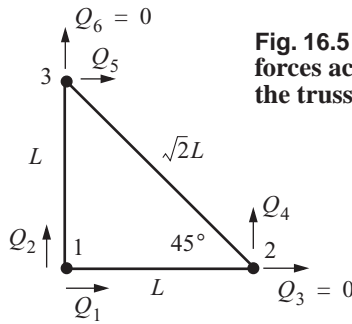


**Fig. 16.5 Joint forces acting on the truss.**

A free body diagram of all the joint forces is shown in figure. 16.5.

The condition for horizontal equilibrium is  $Q_1 + Q_5 = 0$ . Substitute the results for these reactive forces from eq. (q) into condition for horizontal equilibrium to get

$$Q_1 + Q_5 = \left( \frac{1}{2 + 2\sqrt{2}} + \frac{1}{2} - \frac{1}{\sqrt{2}} \right) (N_T)_{1-3}. \quad (\text{r})$$

Extract a common denominator in eq. (r):

$$Q_1 + Q_5 = \left( \frac{1}{2 + 2\sqrt{2}} \right) \left[ 1 + (1 + \sqrt{2}) - \frac{(2 + 2\sqrt{2})}{\sqrt{2}} \right] (N_T)_{1-3}. \quad (\text{s})$$

Combine terms in eq. (s) to get the final result

$$Q_1 + Q_5 = \left( \frac{1}{2 + 2\sqrt{2}} \right) [2 + \sqrt{2} - (\sqrt{2} + 2)] (N_T)_{1-3} = \left( \frac{1}{2 + 2\sqrt{2}} \right) [0] (N_T)_{1-3} = 0. \quad (\text{t})$$

Hence, the matrix solution for reactive forces  $Q_1$  and  $Q_5$  satisfy horizontal equilibrium. The condition for vertical equilibrium is  $Q_2 + Q_4 = 0$ . Substitute the results for these reactive forces from eq. (q) into the condition for vertical equilibrium to get

$$Q_2 + Q_4 = \left[ \frac{1}{2 + 2\sqrt{2}} + \frac{1}{2} - \frac{1}{\sqrt{2}} \right] (N_T)_{1-3} = 0. \quad (\text{u})$$

Note that the algebra in eq. (u) is the same as the algebra detailed in eq. (r) to eq. (t). So the condition for vertical equilibrium is satisfied. Vanishing of the moment about joint 1 requires  $LQ_4 - LQ_5 = 0$ . Substitute the results for these reactive forces from eq. (q) into the condition for moment equilibrium to get

$$LQ_4 - LQ_5 = L \left[ \frac{1}{2} - \frac{1}{\sqrt{2}} - \left( \frac{1}{2} - \frac{1}{\sqrt{2}} \right) \right] (N_T)_{1-3} = 0. \quad (\text{v})$$

Hence, the matrix solution for the reactive forces plus the applied forces satisfies equilibrium of the free body diagram for the entire truss.

**Solution to part (d).** The axial normal force in the bar between joints  $i$  and  $j$  from eq. (16.14) is

$$N_{i-j} = [S_{i-j}] \{q\}_{i-j} - (N_T)_{i-j}, \quad (\text{w})$$

where the stress matrix (16.15) is

$$[S_{i-j}] = \left( \frac{EA}{L} \right)_{i-j} [-c \ -s \ c \ s]_{i-j}. \quad (\text{x})$$

The direction cosines for each bar are listed in table 16.1.

For bar 1-2, the axial normal force is

$$N_{1-2} = \left( \frac{EA}{L} \right) [-1 \ 0 \ 1 \ 0] \begin{bmatrix} q_1 \\ q_2 \\ q_3 \\ q_4 \end{bmatrix} - (N_T)_{1-2} = \left( \frac{EA}{L} \right) [-1 \ 0 \ 1 \ 0] \begin{bmatrix} 0 \\ 0 \\ q_3 \\ 0 \end{bmatrix} - 0 = \left( \frac{EA}{L} \right) q_3. \quad (\text{y})$$

From eq. (m) the solution for the displacement is  $q_3 = \left( \frac{L}{EA} \right) \left( \frac{-\sqrt{2}}{4 + 2\sqrt{2}} \right) (N_T)_{1-3}$ , Substitute the result for  $q_3$  into eq. (y) to find

$$N_{1-2} = \left( \frac{EA}{L} \right) \left( \frac{L}{EA} \right) \left( \frac{-\sqrt{2}}{4 + 2\sqrt{2}} \right) (N_T)_{1-3} = \left( \frac{-\sqrt{2}}{4 + 2\sqrt{2}} \right) (N_T)_{1-3}.$$

For bar 1-3, the axial normal force is

$$N_{1-3} = \left( \frac{EA}{L} \right) [0 \ -1 \ 0 \ 1] \begin{bmatrix} 0 \\ 0 \\ 0 \\ q_6 \end{bmatrix} - (N_T)_{1-3} = \left( \frac{EA}{L} \right) q_6 - (N_T)_{1-3}. \quad (\text{z})$$

From eq. (m) the solution for the displacement is  $q_6 = \left( \frac{L}{EA} \right) \frac{4 + \sqrt{2}}{4 + 2\sqrt{2}} (N_T)_{1-3}$ . Substitute the result for  $q_6$  into eq. (z) to find

$$N_{1-3} = \left( \frac{EA}{L} \right) \left[ \left( \frac{L}{EA} \right) \frac{4 + \sqrt{2}}{4 + 2\sqrt{2}} (N_T)_{1-3} \right] - (N_T)_{1-3} = \left( \frac{-1}{2 + 2\sqrt{2}} \right) (N_T)_{1-3}. \quad (\text{aa})$$

For bar 2-3, the axial normal force is

$$N_{2-3} = \left( \frac{EA}{\sqrt{2}L} \right) \begin{bmatrix} 1/\sqrt{2} & -1/\sqrt{2} & -1/\sqrt{2} & 1/\sqrt{2} \end{bmatrix} \begin{bmatrix} q_3 \\ q_4 \\ q_5 \\ q_6 \end{bmatrix} - (N_T)_{2-3} = \left( \frac{EA}{\sqrt{2}L} \right) \begin{bmatrix} 1/\sqrt{2} & -1/\sqrt{2} & -1/\sqrt{2} & 1/\sqrt{2} \end{bmatrix} \begin{bmatrix} q_3 \\ 0 \\ 0 \\ q_6 \end{bmatrix} - 0. \quad (\text{ab})$$

Expand eq. (ab) to get

$$\begin{aligned} N_{2-3} &= \left( \frac{EA}{2L} \right) \begin{bmatrix} 1 & 1 \end{bmatrix} \begin{bmatrix} q_3 \\ q_6 \end{bmatrix} - (N_T)_{2-3} = \frac{EA}{2L} (q_3 + q_6) - 0 = \frac{EA}{2L} \left[ \left( \frac{L}{EA} \right) \left( \frac{-\sqrt{2}}{4 + 2\sqrt{2}} \right) (N_T)_{1-3} + \left( \frac{L}{EA} \right) \frac{4 + \sqrt{2}}{4 + 2\sqrt{2}} (N_T)_{1-3} \right] \\ &= \left( \frac{1}{2} \right) \left[ \frac{-\sqrt{2}}{4 + 2\sqrt{2}} + \frac{4 + \sqrt{2}}{4 + 2\sqrt{2}} \right] (N_T)_{1-3} = \left( \frac{1}{2} \right) \left[ \frac{4}{4 + 2\sqrt{2}} \right] (N_T)_{1-3} \end{aligned} \quad (\text{ac})$$

The final result for the force in bar 2-3 is

$$N_{2-3} = \frac{(N_T)_{1-3}}{2 + \sqrt{2}}. \quad (\text{ad})$$

Note that for this statically indeterminate truss all three bar forces are proportional to the change in temperature of bar 1-3. ■

### 16.1.2 Self-strained truss

Strain of the bars in a truss can occur due to temperature changes and also due to the **lack of fit** during assembly, even in the absence of applied nodal forces. The analysis for lack of fit of bar 1-3 in example 16.2 is achieved by replacing the thermal force by

$$(N_T)_{1-3} \rightarrow EA(\bar{\Delta}/L)_{1-3},$$

where  $\bar{\Delta}$  is the specified displacement of the bar to connect it to joints 1 and 3. For a gap between joints  $\bar{\Delta} > 0$  and for an overlap  $\bar{\Delta} < 0$ . Hence, the solution for the bar forces in example 16.2 can be interpreted for the problem of lack of fit of bar 1-3 by replacing  $(N_T)_{1-3}$  with  $EA(\bar{\Delta}/L)_{1-3}$ .

#### Example 16.3 Self-strained configuration of the truss in example 16.2

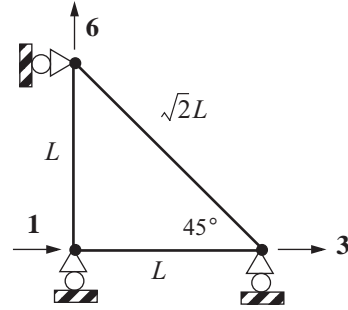
Now consider a statically determinate configuration of the truss in figure. 16.2, which is shown in figure. 16.6. Support conditions impose displacements  $q_2 = q_4 = q_5 = 0$ . The applied external forces are specified as  $Q_1 = Q_3 = Q_6 = 0$ , and only bar 1-3 is subject to a thermal force  $(N_T)_{1-3} = EA(\alpha\Delta T)$ .

- Determine the unknown joint displacements.
- Determine the unknown joint forces.
- Determine the elongation of each bar.

**Solution to part (a).** The matrix equation to determine the unknown joint displacements is



**Fig. 16.6** Statically determinate three-bar truss.



$$\{Q_\alpha\} = [K_{\alpha\alpha}]\{q_\alpha\} + [K_{\alpha\beta}]\{q_\beta\} + \{Q_\alpha^0\}. \quad (\text{a})$$

Refer to the stiffness matrix in eq.(h) and the fixed-end vector in eq. (i) of example 16.1. Then the matrices in eq. (a) are

$$\{Q_\alpha\} = \begin{bmatrix} Q_1 \\ Q_3 \\ Q_6 \end{bmatrix} = \begin{bmatrix} 0 \\ 0 \\ 0 \end{bmatrix}, [K_{\alpha\alpha}] = \frac{EA}{L} \begin{bmatrix} 1 & -1 & 0 \\ -1 & 1+a & a \\ 0 & a & 1+a \end{bmatrix}, \{q_\alpha\} = \begin{bmatrix} q_1 \\ q_3 \\ q_6 \end{bmatrix}, [K_{\alpha\beta}] = \frac{EA}{L} \begin{bmatrix} 0 & 0 & 0 \\ 0 & -a & -a \\ -1 & -a & -a \end{bmatrix}, \quad (\text{b})$$

$$\{q_\beta\} = \begin{bmatrix} q_2 \\ q_4 \\ q_5 \end{bmatrix} = \begin{bmatrix} 0 \\ 0 \\ 0 \end{bmatrix}, \text{ and } \{Q_\alpha^0\} = \begin{bmatrix} Q_1^0 \\ Q_3^0 \\ Q_6^0 \end{bmatrix} = \begin{bmatrix} 0 \\ 0 \\ -(N_T)_{1-3} \end{bmatrix}. \quad (\text{c})$$

The solution to eq. (a) for the joint displacements is

$$q_1 = -L(\alpha\Delta T) \quad q_3 = -L(\alpha\Delta T) \quad q_6 = L(\alpha\Delta T). \quad (\text{d})$$

**Solution to part (b).** The matrix equation to determine the unknown joint forces is

$$\{Q_\beta\} = [K_{\beta\alpha}]\{q_\alpha\} + [K_{\beta\beta}]\{q_\beta\} + \{Q_\beta^0\}. \quad (\text{e})$$

The matrices in eq. (e) are

$$\{Q_\beta\} = \begin{bmatrix} Q_2 \\ Q_4 \\ Q_5 \end{bmatrix}, [K_{\beta\alpha}] = \frac{EA}{L} \begin{bmatrix} 0 & 0 & -1 \\ 0 & -a & -a \\ 0 & -a & -a \end{bmatrix}, [K_{\beta\beta}] = \frac{EA}{L} \begin{bmatrix} 1 & 0 & 0 \\ 0 & a & a \\ 0 & a & a \end{bmatrix}, \text{ and } \{Q_\beta^0\} = \begin{bmatrix} Q_2^0 \\ Q_4^0 \\ Q_5^0 \end{bmatrix} = \begin{bmatrix} (N_T)_{1-3} \\ 0 \\ 0 \end{bmatrix}. \quad (\text{f})$$

The solution of eq. (e) for the unknown joint forces, or the reactive forces, is

$$Q_2 = Q_4 = Q_5 = 0. \quad (\text{g})$$

There no external forces acting on the truss since both the applied and reactive forces are zero. Consequently, it is reasonable to surmise that the internal forces in the bars vanish. That is,

$$N_{1-2} = N_{1-3} = N_{2-3} = 0, \quad (\text{h})$$

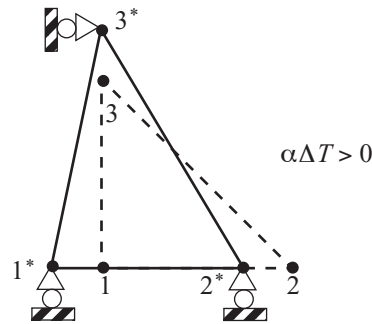
which can be verified using eq. (16.14).

**Solution to part (c).** The elongation of a truss is determined from eq. (16.4). Using the direction cosines listed in table 16.1, the elongation of each bar is given by

$$\begin{aligned}\Delta_{1-2} &= (1)(q_3 - q_1) + (0)(q_4 - q_2) = 0 \\ \Delta_{1-3} &= (0)(q_5 - q_1) + (1)(q_6 - q_2) = L(\alpha\Delta T) \\ \Delta_{2-3} &= \left(\frac{-1}{\sqrt{2}}\right)(q_5 - q_3) + \left(\frac{1}{\sqrt{2}}\right)(q_6 - q_4) = \left(\frac{1}{\sqrt{2}}\right)(q_6 + q_3) = 0\end{aligned}\quad (i)$$

Hence, bars 1-2 and 2-3 do not change in length, and the new length of bar 1-3 is  $L(1 + \alpha\Delta T)$ . Assuming  $\alpha\Delta T > 0$ , the displaced truss is shown with respect to initial configuration in figure. 16.7. ■

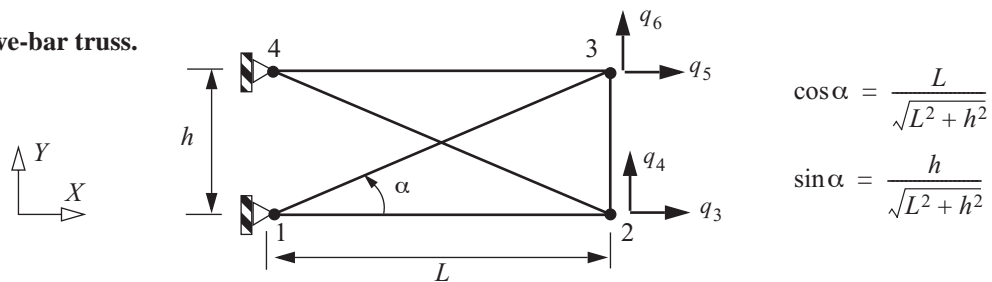
**Fig. 16.7** Initial configuration (dashed lines) and the displaced configuration (solid lines) of the self-strained truss in figure. 16.6.



#### Example 16.4 Five-bar truss

The five-bar truss shown in figure. 16.8 is restrained against rigid body motion, since joints 1 and 4 are fixed. pins All bars have the same extensional stiffness  $EA$ . Determine the restrained structural stiffness matrix  $[K_{\alpha\alpha}]$ .

**Fig. 16.8** Five-bar truss.



**Solution.** The dimensions of the restrained structural stiffness matrix is 4X4 in displacement degrees of freedom  $q_3, q_4, q_5$ , and  $q_6$ . The direction cosines for the truss bars are listed in table 16.3.

Table 16.3 Direction cosines for the five-bar truss

Bar	$\theta$	$c$	$s$	$c^2$	$s^2$	$cs$
1-2	$0^\circ$	1	0	1	0	0
1-3	$\alpha$	$\cos \alpha$	$\sin \alpha$	$\cos^2 \alpha$	$\sin^2 \alpha$	$\cos \alpha \sin \alpha$
2-3	$90^\circ$	0	1	0	1	0
2-4	$180^\circ - \alpha$	$-\cos \alpha$	$\sin \alpha$	$\cos^2 \alpha$	$\sin^2 \alpha$	$-\cos \alpha \sin \alpha$
3-4	$180^\circ$	-1	0	1	0	0

From eq. (16.12) the following member stiffness matrices are constructed using the direction cosines in table 16.3. Only elements contributing to rows and columns 3, 4, 5, and 6 of the restrained structural stiffness matrix are extracted from the individual element stiffness matrices. These member stiffness matrices follow:

$$[K_{\alpha\alpha}]_{1-2} = \begin{bmatrix} q_3 & q_4 \\ EA/L & 0 \\ 0 & 0 \end{bmatrix} \quad [K_{\alpha\alpha}]_{1-3} = \frac{EA}{L/(\cos \alpha)} \begin{bmatrix} q_5 & q_6 \\ \cos^2 \alpha & \cos \alpha \sin \alpha \\ \cos \alpha \sin \alpha & \sin^2 \alpha \end{bmatrix} = \frac{EA}{L} \begin{bmatrix} q_5 & q_6 \\ \cos^3 \alpha & \cos^2 \alpha \sin \alpha \\ \cos^2 \alpha \sin \alpha & \cos \alpha \sin^2 \alpha \end{bmatrix}. \quad (a)$$

$$[K_{\alpha\alpha}]_{2-3} = \left( \frac{EA}{L \tan \alpha} \right) \begin{bmatrix} q_3 & q_4 & q_5 & q_6 \\ 0 & 0 & 0 & 0 \\ 0 & 1 & 0 & -1 \\ 0 & 0 & 0 & 0 \\ 0 & -1 & 0 & 1 \end{bmatrix} = \left( \frac{EA}{L} \right) \begin{bmatrix} 0 & 0 & 0 & 0 \\ 0 & \cot \alpha & 0 & -\cot \alpha \\ 0 & 0 & 0 & 0 \\ 0 & -\cot \alpha & 0 & \cot \alpha \end{bmatrix} \quad [K_{\alpha\alpha}]_{3-4} = \begin{bmatrix} q_5 & q_6 \\ EA/L & 0 \\ 0 & 0 \end{bmatrix}. \quad (b)$$

$$[K_{\alpha\alpha}]_{2-4} = \left( \frac{EA}{L/(\cos \alpha)} \right) \begin{bmatrix} q_3 & q_4 \\ \cos^2 \alpha & -\cos \alpha \sin \alpha \\ -\cos \alpha \sin \alpha & \sin^2 \alpha \end{bmatrix} = \frac{EA}{L} \begin{bmatrix} q_3 & q_4 \\ \cos^3 \alpha & -\cos^2 \alpha \sin \alpha \\ -\cos^2 \alpha \sin \alpha & \cos \alpha \sin^2 \alpha \end{bmatrix}. \quad (c)$$

Assemblage of the restrained structural stiffness matrix is accomplished by adding like row and column elements from the stiffness matrices of each truss bar. The result for the restrained structural stiffness matrix is

$$[K_{\alpha\alpha}] = \left( \frac{EA}{L} \right) \begin{bmatrix} q_3 & q_4 & q_5 & q_6 \\ (1 + \cos^3 \alpha) & -\cos^2 \alpha \sin \alpha & 0 & 0 \\ -\cos^2 \alpha \sin \alpha & (\cot \alpha + \cos \alpha \sin^2 \alpha) & 0 & -\cot \alpha \\ 0 & 0 & (\cos^3 \alpha + 1) & \cos^2 \alpha \sin \alpha \\ 0 & -\cot \alpha & \cos^2 \alpha \sin \alpha & (\cos \alpha \sin^2 \alpha + \cot \alpha) \end{bmatrix}. \quad (d)$$

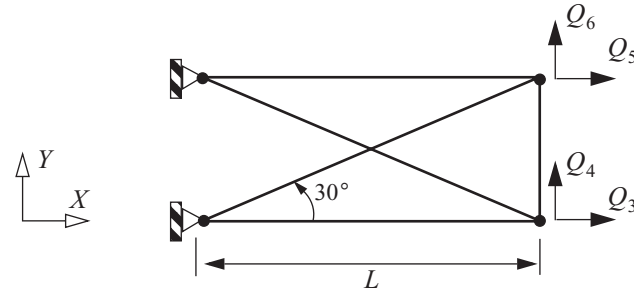
Note that the matrix is symmetric and the sum of the column elements do not add to zero. If we take  $\alpha = 30^\circ$ , then the restrained structural stiffness matrix reduces to

$$[K_{\alpha\alpha}] = \left(\frac{EA}{L}\right) \begin{bmatrix} q_3 & q_4 & q_5 & q_6 \\ 1 + (3\sqrt{3})/8 & -3/8 & 0 & 0 \\ -3/8 & \sqrt{3}(9/8) & 0 & -\sqrt{3} \\ 0 & 0 & 1 + (3\sqrt{3})/8 & 3/8 \\ 0 & -\sqrt{3} & 3/8 & \sqrt{3}(9/8) \end{bmatrix} \quad (e)$$

### Example 16.5 Using symmetry to reduce problem size

Consider the five-bar truss problem of example 16.4 with  $\alpha = 30^\circ$  that is subject to prescribed nodal forces  $Q_3, Q_4, Q_5$ , and  $Q_6$ . Use symmetry to reduce the problem size to solve for the unknown joint displacements.

**Fig. 16.9** Five-bar truss of example 16.5.



**Solution.** We note that the structure and boundary conditions are symmetric about a horizontal axis through the center of the truss. The joint displacements and corresponding forces can be decomposed into a symmetric and antisymmetric sets about this horizontal axis of symmetry as shown in figure. 16.10. The joint displacements and

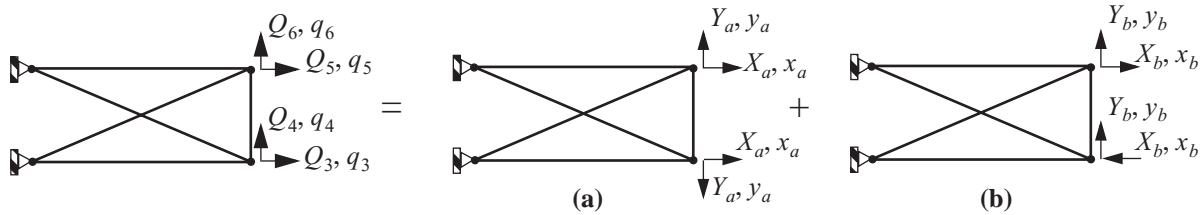


**Fig. 16.10** (a) Symmetric truss. (b) Antisymmetric truss.

the corresponding forces are related to the symmetric and antisymmetric counterparts by

$$\begin{bmatrix} q_3 \\ q_4 \\ q_5 \\ q_6 \end{bmatrix} = \begin{bmatrix} x_a \\ -y_a \\ x_a \\ y_a \end{bmatrix} + \begin{bmatrix} -x_b \\ y_b \\ x_b \\ y_b \end{bmatrix} = \begin{bmatrix} 1 & 0 & -1 & 0 \\ 0 & -1 & 0 & 1 \\ 1 & 0 & 1 & 0 \\ 0 & 1 & 0 & 1 \end{bmatrix} \begin{bmatrix} x_a \\ y_a \\ x_b \\ y_b \end{bmatrix}, \text{ and } \begin{bmatrix} Q_3 \\ Q_4 \\ Q_5 \\ Q_6 \end{bmatrix} = \begin{bmatrix} X_a \\ -Y_a \\ X_a \\ Y_a \end{bmatrix} + \begin{bmatrix} -X_b \\ Y_b \\ X_b \\ Y_b \end{bmatrix} = \begin{bmatrix} 1 & 0 & -1 & 0 \\ 0 & -1 & 0 & 1 \\ 1 & 0 & 1 & 0 \\ 0 & 1 & 0 & 1 \end{bmatrix} \begin{bmatrix} X_a \\ Y_a \\ X_b \\ Y_b \end{bmatrix}. \quad (a)$$

The expressions in eq. (a) are written in compact form as

$$\{q_\alpha\} = [A]\{x\}, \text{ and } \{Q_\alpha\} = [A]\{X\}, \quad (\text{b})$$

where the elements of the 4X4 matrix  $[A]$  are either  $-1$ ,  $0$ , or  $1$ . The force vector is related to the displacement vector by  $\{Q_\alpha\} = [K_{\alpha\alpha}]\{q_\alpha\}$ , where matrix  $[K_{\alpha\alpha}]$  is given by eq. (e) in example 16.4. Substitute eq. (b) into the matrix equation relating the force vector to the displacement vector to get

$$[A]\{X\} = [K_{\alpha\alpha}][A]\{x\}. \quad (\text{c})$$

Pre-multiply eq. (c) by the inverse of matrix  $[A]$  to find

$$\{X\} = [A]^{-1}[K_{\alpha\alpha}][A]\{x\}. \quad (\text{d})$$

Define stiffness matrix by  $[\bar{K}_{\alpha\alpha}] = [A]^{-1}[K_{\alpha\alpha}][A]$ . The the matrices to compute  $[\bar{K}_{\alpha\alpha}]$  are

$$[\bar{K}_{\alpha\alpha}] = \frac{1}{2} \begin{bmatrix} 1 & 0 & 1 & 0 \\ 0 & -1 & 0 & 1 \\ -1 & 0 & 1 & 0 \\ 0 & 1 & 0 & 1 \end{bmatrix} \left( \frac{EA}{L} \right) \begin{bmatrix} 1 + (3\sqrt{3})/8 & -3/8 & 0 & 0 \\ -3/8 & \sqrt{3}(9/8) & 0 & -\sqrt{3} \\ 0 & 0 & 1 + (3\sqrt{3})/8 & 3/8 \\ 0 & -\sqrt{3} & 3/8 & \sqrt{3}(9/8) \end{bmatrix} \begin{bmatrix} 1 & 0 & -1 & 0 \\ 0 & -1 & 0 & 1 \\ 1 & 0 & 1 & 0 \\ 0 & 1 & 0 & 1 \end{bmatrix}. \quad (\text{e})$$

The result of the matrix multiplications in eq. (e) is

$$[\bar{K}_{\alpha\alpha}] = \frac{EA}{L} \begin{bmatrix} 1 + (3\sqrt{3})/8 & 3/8 & 0 & 0 \\ 3/8 & (17\sqrt{3})/8 & 0 & 0 \\ 0 & 0 & 1 + (3\sqrt{3})/8 & 3/8 \\ 0 & 0 & 3/8 & (\sqrt{3})/8 \end{bmatrix} = \begin{bmatrix} [\bar{K}_a] & [0_{2 \times 2}] \\ [0_{2 \times 2}] & [\bar{K}_b] \end{bmatrix}. \quad (\text{f})$$

Note that the partitioned form of  $[\bar{K}_{\alpha\alpha}]$  is diagonal, and the 2X2 sub-matrices on the diagonal are

$$[\bar{K}_a] = \frac{EA}{L} \begin{bmatrix} 1 + \frac{3\sqrt{3}}{8} & \frac{3}{8} \\ \frac{3}{8} & \frac{17\sqrt{3}}{8} \end{bmatrix}, \text{ and } [\bar{K}_b] = \frac{EA}{L} \begin{bmatrix} 1 + \frac{3\sqrt{3}}{8} & \frac{3}{8} \\ \frac{3}{8} & \frac{\sqrt{3}}{8} \end{bmatrix}. \quad (\text{g})$$

The inverses of the matrices in eq. (g) are

$$[\bar{K}_a]^{-1} = \frac{L}{EA} \begin{bmatrix} \frac{17}{181}(17 - 6\sqrt{3}) & \frac{1}{181}(18 - 17\sqrt{3}) \\ \frac{1}{181}(18 - 17\sqrt{3}) & \frac{1}{543}(9 + 82\sqrt{3}) \end{bmatrix}, \text{ and } [\bar{K}_b]^{-1} = \frac{L}{EA} \begin{bmatrix} 1 & -\sqrt{3} \\ -\sqrt{3} & (3 + 8/\sqrt{3}) \end{bmatrix}. \quad (\text{h})$$

Then the inverse of eq. (f) is given by

$$\begin{bmatrix} \bar{K}_{\alpha\alpha} \end{bmatrix}^{-1} = \begin{bmatrix} \begin{bmatrix} \bar{K}_a \end{bmatrix}^{-1} & \begin{bmatrix} 0_{2 \times 2} \end{bmatrix} \\ \begin{bmatrix} 0_{2 \times 2} \end{bmatrix} & \begin{bmatrix} \bar{K}_b \end{bmatrix}^{-1} \end{bmatrix}. \quad (\text{i})$$

Hence, the solution for the displacement vector  $\{x\}$  in terms of the force vector  $\{X\}$  is

$$\{x\} = \begin{bmatrix} \bar{K}_{\alpha\alpha} \end{bmatrix}^{-1} \{X\}. \quad (\text{j})$$

From eq. (b)  $\{x\} = \begin{bmatrix} A \end{bmatrix}^{-1} \{q_\alpha\}$  and  $\{X\} = \begin{bmatrix} A \end{bmatrix}^{-1} \{Q_\alpha\}$ . Substitute the latter relations into eq. (j) to get

$$\begin{bmatrix} A \end{bmatrix}^{-1} \{q_\alpha\} = \begin{bmatrix} \bar{K}_{\alpha\alpha} \end{bmatrix}^{-1} \begin{bmatrix} A \end{bmatrix}^{-1} \{Q_\alpha\}. \quad (\text{k})$$

Pre-multiply eq. (k) by matrix  $\begin{bmatrix} A \end{bmatrix}$  to write the result for the unknown displacements as

$$\{q_\alpha\} = \begin{bmatrix} C_{\alpha\alpha} \end{bmatrix} \{Q_\alpha\}, \quad (\text{l})$$

where the compliance matrix is

$$\begin{bmatrix} C_{\alpha\alpha} \end{bmatrix} = \begin{bmatrix} A \end{bmatrix} \begin{bmatrix} \bar{K}_{\alpha\alpha} \end{bmatrix}^{-1} \begin{bmatrix} A \end{bmatrix}^{-1} = \frac{L}{EA} \begin{bmatrix} 0.810306 & 0.897641 & -0.189694 & 0.83441 \\ 0.897641 & 3.94847 & -0.83441 & 3.67033 \\ -0.189694 & -0.83441 & 0.810306 & -0.897641 \\ 0.83441 & 3.67033 & -0.897641 & 3.94847 \end{bmatrix}. \quad (\text{m})$$

The compliance matrix in eq. (m) was obtained by inverting two 2X2 sub-matrices, rather than directly inverting the 4X4 stiffness matrix  $\begin{bmatrix} K_{\alpha\alpha} \end{bmatrix}$ . Exploiting the symmetry conditions as illustrated in figure. 16.10, reduces the number of computations to find the inverse of matrix  $\begin{bmatrix} K_{\alpha\alpha} \end{bmatrix}$ . ■

## 16.2 Structures containing beam members

Consider a prismatic, homogeneous beam that is referenced to the Cartesian system  $x$ - $y$ - $z$ . The  $z$ -coordinate is the longitudinal axis, and the coordinates  $x$  and  $y$  define cross-sectional axes with the origin at the centroid. Assume at least one axis  $x$  and/or  $y$  is an axis of symmetry so that the product area moment  $I_{xy} = 0$ . External loads are specified as a transverse distributed load  $f_y(z)$  as shown in figure. 3.8 on page 41, and we assume a change in temperature in the form  $\Delta T(y, z) = \tau_y(z)y(s)$ . For this form of the prescribed change in temperature the thermal axial force  $N_T = 0$  in eq. (3.75), and thermal bending moment  $M_{xT} \neq 0$  in eq. (3.78). The plane of loading  $f_y(z)$  coincides with the locus of shear centers. Hence, the beam bends in the  $y$ - $z$  plane. Assume the **Euler-Bernoulli** theory in which the transverse shears in eq. (4.28) on page 82 equal zero. That is,

$$\psi_y = \frac{dv}{dz} + \phi_x = 0. \quad (16.19)$$

(Refer to the discussion about the Euler-Bernoulli theory following table 4.4 on page 102.) Equilibrium differential equations (3.54) and (3.55) are

$$\frac{dV_y}{dz} + f_y = 0 \quad \frac{dM_x}{dz} - V_y = 0. \quad (16.20)$$

Hooke's law (3.79) on page 46 for bending is

$$M_x + M_{xT} = EI_{xx} \frac{d\phi_x}{dz}, \quad (16.21)$$

where the thermal bending moment is given by eq. (3.78) on page 46. The change in temperature on the contour is  $\Delta T = \tau_y(z)y(s)$  and eq. (3.78) simplifies to

$$M_{xT} = EI_{xx} \alpha \tau_y(z). \quad (16.22)$$

Combine eqs. (16.20), (16.21), and (16.22) to get the governing differential equation for the deflection of the beam as

$$EI_{xx} \frac{d^4 v}{dz^4} = f_y(z) - EI_{xx} \alpha \frac{d^2 \tau_y}{dz^2} \quad 0 < z < L. \quad (16.23)$$

Let  $q_1$  denote the y-direction displacement of the neutral axis at  $z = 0$ ,  $q_2$  the rotation of the cross section about the x-axis at  $z = 0$ ,  $q_3$  the y-direction displacement of the neutral axis at  $z = L$ , and  $q_4$  the rotation of the cross section about the x-axis at  $z = L$ . Then the boundary conditions at the ends of the beam are

$$v(0) = q_1 \quad \phi_x(0) = q_2 \quad v(L) = q_3 \quad \phi_x(L) = q_4. \quad (16.24)$$

The governing boundary value problem defined by (16.23) and (16.24) is depicted in figure. 16.11(a). Actions

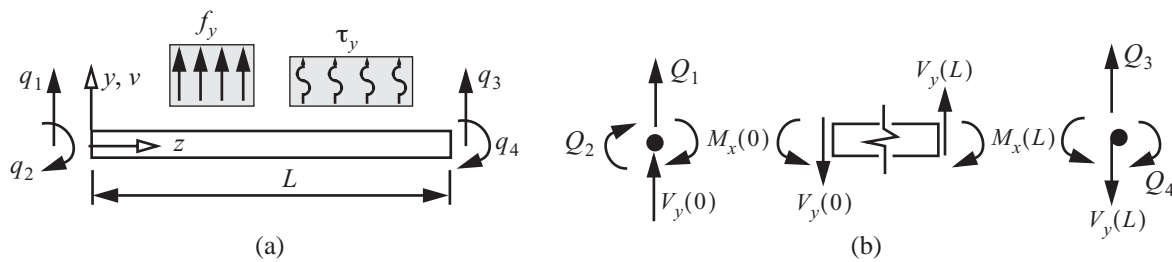


**Fig. 16.11 (a) The boundary value problem for the beam. (b) Joint equilibrium.**

corresponding to the generalized displacements  $q_1$ ,  $q_2$ ,  $q_3$ , and  $q_4$  are denoted by  $Q_1$ ,  $Q_2$ ,  $Q_3$ , and  $Q_4$ , respectively. Free body diagrams at the beginning joint ( $z = 0$ ) and the end joint ( $z = L$ ) are shown in figure. 16.11(b). Equilibrium at the joints leads to

$$Q_1 + V_y(0) = 0 \quad Q_2 + M_x(0) = 0 \quad Q_3 - V_y(L) = 0 \quad Q_4 - M_x(L) = 0. \quad (16.25)$$

The solution to the governing boundary value problem is sought by the method of superposition. Let the lateral displacement be represented by the sum of displacements in the form

$$v(z) = v_0(z) + v_1(z) . \quad (16.26)$$

The boundary value problem for  $v_0(z)$  is selected as

$$\begin{aligned} EIV_0'''' &= f_y(z) - EI\alpha\tau_y'' & 0 < z < L \\ v_0(0) &= 0 & -v_0'(0) &= 0 & v_0(L) &= 0 & -v_0'(L) &= 0 \end{aligned} \quad (16.27)$$

As a consequence the boundary value problem for  $v_1(z)$  is

$$\begin{aligned} EIV_1'''' &= 0 & 0 < z < L \\ v_1(0) &= q_1 & -v_1'(0) &= q_2 & v_1(L) &= q_3 & -v_1'(L) &= q_4 \end{aligned} \quad (16.28)$$

In eqs. (16.27) and (16.28) ordinary derivatives with respect to  $z$  are denoted by primes (e.g.,  $v' = \frac{dv}{dz}$ ). Also, we

let  $EI_{xx} = EI$ . The boundary value problem (16.27) for displacement function  $v_0(z)$  consists of an inhomogeneous differential equation with homogeneous boundary conditions, while the boundary value problem (16.28) for displacement function  $v_1(z)$  consists of a homogeneous differential equation with inhomogeneous boundary conditions. Since the displacements and rotations vanish at the end points of the beam in the boundary value problem for  $v_0(z)$ , the solution for it will lead to **fixed-end actions** in the matrix structural analysis method. That is, the fixed-end action problem accounts for distributed load intensity  $f_y(z)$ , and the distributed temperature gradient  $\tau_y(z)$ . By superposition the total bending moment is

$$M_x(z) = -EI(v_0'' + v_1'') - EI\alpha\tau_y = M_x^0 + M_x^1, \quad (16.29)$$

where the bending moments from the separate boundary value problems are

$$M_x^0 = -EIV_0'' - EI\alpha\tau_y, \quad M_x^1 = -EIV_1''. \quad (16.30)$$

The shear force is the sum

$$V_y(z) = V_y^0 + V_y^1, \quad (16.31)$$

where the shear forces from the separate boundary value problems are

$$V_y^0 = \frac{d}{dz}(M_x^0) \quad V_y^1 = \frac{d}{dz}(M_x^1). \quad (16.32)$$

### 16.2.1 Boundary value problem (16.28). Generalized displacements at the boundaries

The general solution for  $v_1(z)$  satisfying the differential equation in boundary value problem (16.28) is a cubic polynomial in the longitudinal coordinate, which is written as

$$v_1(z) = c_3 \frac{z^3}{6} + c_2 \frac{z^2}{2} + c_1 z + c_0, \quad (16.33)$$

where the constants  $c_3$ ,  $c_2$ ,  $c_1$ , and  $c_0$  are to be determined by the four boundary conditions specified in eq. (16.28). Substitute the general solution (16.33) into these four boundary conditions and write result as



$$\begin{bmatrix} 0 & 0 & 0 & 1 \\ 0 & 0 & -1 & 0 \\ L^3/6 & L^2/2 & L & 1 \\ -L^2/2 & -L & -1 & 0 \end{bmatrix} \begin{bmatrix} c_3 \\ c_2 \\ c_1 \\ c_0 \end{bmatrix} = \begin{bmatrix} q_1 \\ q_2 \\ q_3 \\ q_4 \end{bmatrix}. \quad (16.34)$$

Solve eq. (16.34) for the constants  $c_3$ ,  $c_2$ ,  $c_1$ , and  $c_0$  to get

$$\begin{bmatrix} c_3 \\ c_2 \\ c_1 \\ c_0 \end{bmatrix} = \begin{bmatrix} 12/L^3 & -6/L^2 & -12/L^3 & -6/L^2 \\ -6/L^2 & 4/L & 6/L^2 & 2/L \\ 0 & -1 & 0 & 0 \\ 1 & 0 & 0 & 0 \end{bmatrix} \begin{bmatrix} q_1 \\ q_2 \\ q_3 \\ q_4 \end{bmatrix}. \quad (16.35)$$

Substituting eq. (16.35) for the constants  $c_3$ ,  $c_2$ ,  $c_1$ , and  $c_0$  into eq. (16.33) leads to

$$v_1(z) = \frac{1}{6} \left( \frac{12}{L^3} q_1 - \frac{6}{L^2} q_2 - \frac{12}{L^3} q_3 - \frac{6}{L^2} q_4 \right) z^3 + \frac{1}{2} \left( -\frac{6}{L^2} q_1 + \frac{4}{L} q_2 + \frac{6}{L^2} q_3 + \frac{2}{L} q_4 \right) z^2 + (-q_2)z + q_1. \quad (16.36)$$

Rearrange eq. (16.36) to the form

$$v_1(z) = \left( 2\frac{z^3}{L^3} - 3\frac{z^2}{L^2} + 1 \right) q_1 + \left( -\frac{z^3}{L^2} + 2\frac{z^2}{L} - z \right) q_2 + \left( -2\frac{z^3}{L^3} + 3\frac{z^2}{L^2} \right) q_3 + \left( -\frac{z^3}{L^2} + \frac{z^2}{L} \right) q_4. \quad (16.37)$$

Equation (16.37) is further written in the matrix form

$$v_1(z) = \begin{bmatrix} \eta_1(z) & \eta_2(z) & \eta_3(z) & \eta_4(z) \end{bmatrix} \begin{bmatrix} q_1 \\ q_2 \\ q_3 \\ q_4 \end{bmatrix} = [\eta(z)]\{q\}. \quad (16.38)$$

The *shape functions*, or *interpolation functions*, are defined as

$$\eta_1(z) \equiv 2\frac{z^3}{L^3} - 3\frac{z^2}{L^2} + 1 \quad \eta_2(z) \equiv -\frac{z^3}{L^2} + 2\frac{z^2}{L} - z \quad \eta_3(z) \equiv -2\frac{z^3}{L^3} + 3\frac{z^2}{L^2} \quad \eta_4(z) \equiv -\frac{z^3}{L^2} + \frac{z^2}{L}. \quad (16.39)$$

From eq. (16.19) the rotation associated with the lateral displacement function  $v_1(z)$  is given by

$$\phi_x(z) = -v_1'(z) = \begin{bmatrix} -\eta_1'(z) & -\eta_2'(z) & -\eta_3'(z) & -\eta_4'(z) \end{bmatrix} \begin{bmatrix} q_1 \\ q_2 \\ q_3 \\ q_4 \end{bmatrix}, \quad (16.40)$$

where

$$\eta_1'(z) = \frac{6}{L^3} z^2 - 6\frac{z}{L^2} \quad \eta_2'(z) = -3\frac{z^2}{L^2} + 4\frac{z}{L} - 1 \quad \eta_3'(z) = -6\frac{z^2}{L^3} + 6\frac{z}{L^2} \quad \eta_4'(z) = -3\frac{z^2}{L^2} + 2\frac{z}{L}. \quad (16.41)$$

These interpolation functions have the following properties at the end points, or joints, of the beam member:

$$\begin{aligned}
\eta_1(0) &= 1 & \eta_2(0) &= 0 & \eta_3(0) &= 0 & \eta_4(0) &= 0 \\
\eta_1'(0) &= 0 & \eta_2'(0) &= -1 & \eta_3'(0) &= 0 & \eta_4'(0) &= 0 \\
\eta_1(L) &= 0 & \eta_2(L) &= 0 & \eta_3(L) &= 1 & \eta_4(L) &= 0 \\
\eta_1'(L) &= 0 & \eta_2'(L) &= 0 & \eta_3'(L) &= 0 & \eta_4'(L) &= -1
\end{aligned} \tag{16.42}$$

The distributions of the shear force (16.32) and the bending moment (16.30) for the boundary value problem (16.28) are

$$\begin{bmatrix} V_y^1(z) \\ M_x^1(z) \end{bmatrix} = EI \begin{bmatrix} -v_1''' \\ -v_1'' \end{bmatrix} = EI \begin{bmatrix} -\eta_1''' & -\eta_2''' & -\eta_3''' & -\eta_4''' \\ -\eta_1'' & -\eta_2'' & -\eta_3'' & -\eta_4'' \end{bmatrix} \begin{bmatrix} q_1 \\ q_2 \\ q_3 \\ q_4 \end{bmatrix}. \tag{16.43}$$

Substitute for the shape functions from eq. (16.39) into eq. (16.43) to find

$$\begin{bmatrix} V_y^1(z) \\ M_x^1(z) \end{bmatrix} = EI \begin{bmatrix} -\frac{12}{L^3} & \frac{6}{L^2} & \frac{12}{L^3} & \frac{6}{L^2} \\ \frac{6}{L^2} - \frac{12z}{L^3} & -\frac{4}{L} + \frac{6z}{L^2} & -\frac{6}{L^2} + \frac{12z}{L^3} & -\frac{2}{L} + \frac{6z}{L^2} \end{bmatrix} \begin{bmatrix} q_1 \\ q_2 \\ q_3 \\ q_4 \end{bmatrix}. \tag{16.44}$$

Since eq. (16.44) relates the internal actions consisting of the shear force and the bending moment to the joint displacement vector, it defines the 2X4 *stress matrix* as

$$[S^1(z)] \equiv EI \begin{bmatrix} -\frac{12}{L^3} & \frac{6}{L^2} & \frac{12}{L^3} & \frac{6}{L^2} \\ \frac{6}{L^2} - \frac{12z}{L^3} & -\frac{4}{L} + \frac{6z}{L^2} & -\frac{6}{L^2} + \frac{12z}{L^3} & -\frac{2}{L} + \frac{6z}{L^2} \end{bmatrix}, \tag{16.45}$$

such that

$$\begin{bmatrix} V_y^1(z) \\ M_x^1(z) \end{bmatrix} = [S^1(z)] \begin{bmatrix} q_1 \\ q_2 \\ q_3 \\ q_4 \end{bmatrix} \quad 0 \leq z \leq L. \tag{16.46}$$

Equilibrium at the joints  $z = 0$  and  $z = L$  in (16.25) leads to

$$\begin{bmatrix} Q_1^1 \\ Q_2^1 \end{bmatrix} = \begin{bmatrix} -V_y^1(0) \\ -M_x^1(0) \end{bmatrix} = [-S^1(0)] \begin{bmatrix} q_1 \\ q_2 \\ q_3 \\ q_4 \end{bmatrix} \quad \begin{bmatrix} Q_3^1 \\ Q_4^1 \end{bmatrix} = \begin{bmatrix} V_y^1(L) \\ M_x^1(L) \end{bmatrix} = [S^1(L)] \begin{bmatrix} q_1 \\ q_2 \\ q_3 \\ q_4 \end{bmatrix}. \tag{16.47}$$

Combine these results into one matrix equation to get

$$\begin{bmatrix} Q_1^1 \\ Q_2^1 \\ Q_3^1 \\ Q_4^1 \end{bmatrix} = \begin{bmatrix} [-S^1(0)] \\ [S^1(L)] \end{bmatrix} \begin{bmatrix} q_1 \\ q_2 \\ q_3 \\ q_4 \end{bmatrix} \quad \text{or} \quad \begin{matrix} \{Q^1\} \\ 4 \times 1 \end{matrix} = \begin{matrix} [K] \\ 4 \times 4 \end{matrix} \begin{matrix} \{q\} \\ 4 \times 1 \end{matrix} \quad (16.48)$$

The beam element stiffness matrix is defined by

$$[K] = \begin{bmatrix} [-S^1(0)] \\ [S^1(L)] \end{bmatrix}, \text{ which evaluates to } [K] = EI \begin{bmatrix} \frac{12}{L^3} & \frac{-6}{L^2} & \frac{-12}{L^3} & \frac{-6}{L^2} \\ \frac{-6}{L^2} & \frac{4}{L} & \frac{6}{L^2} & \frac{2}{L} \\ \frac{-12}{L^3} & \frac{6}{L^2} & \frac{12}{L^3} & \frac{6}{L^2} \\ \frac{-6}{L^2} & \frac{2}{L} & \frac{6}{L^2} & \frac{4}{L} \end{bmatrix}. \quad (16.49)$$

The stiffness matrix of the beam member (16.49) has the following properties:

- It is symmetric, because the material is linear elastic and the displacements and rotations of the beam are assumed small.
- The column elements satisfy equilibrium for each unit displacement state.

For example consider unit displacement state one with  $\{q\} = [1 \ 0 \ 0 \ 0]^T$ .

The corresponding generalized joint forces are  $\{Q^1\} = [Q_1^1 \ Q_2^1 \ Q_3^1 \ Q_4^1]^T = EI \left[ \frac{12}{L^3} \ \frac{-6}{L^2} \ \frac{-12}{L^3} \ \frac{-6}{L^2} \right]^T (1)$ .

The sum of the vertical forces is  $Q_1^1 + Q_3^1 = EI \left[ \frac{12}{L^3} + \left( \frac{-12}{L^3} \right) \right] (1) = 0$ .

The sum of moments about the center of the beam clockwise positive are:

$\frac{L}{2} Q_1^1 + Q_2^1 - \frac{L}{2} Q_3^1 + Q_4^1 = EI \left[ \frac{L}{2} \left( \frac{12}{L^3} \right) + \left( \frac{-6}{L^2} \right) - \frac{L}{2} \left( \frac{-12}{L^3} \right) + \frac{-6}{L^2} \right] (1) = 0$ .

As result of the four unit displacement states the elements of the beam stiffness matrix satisfy the following relationships.

The sum of rows one and three equals zero.  $\sum_{j=1}^4 k_{1j} + k_{3j} = 0$ .

The sum of  $L/2$  times row one plus row two minus  $L/2$  times row three plus row four is equal to zero.

$\sum_{j=1}^4 (L/2) k_{1j} + k_{2j} - (L/2) k_{3j} + k_{4j} = 0$ .

Since the stiffness matrix is symmetric, the column elements satisfy the same relationships as do the row elements

- $\text{Det}[K] = 0$ , since the beam member is not restrained against rigid body displacement.

- Its diagonal elements are positive.

### 16.2.2 Boundary value problem (16.27). Fixed-end actions

The fixed-end action vector is computed from the boundary value problem (16.27) to account for the distributed load and the temperature distribution in the direct stiffness method. Many practical problems can be analyzed with a linear distribution of the load intensity and a linear distribution of the cross-sectional temperature gradient. These linear distributions are specified as

$$f_y(z) = f_{y1}(1 - z/L) + f_{y2}(z/L) \text{ and } \tau_y(z) = \tau_{y1}(1 - z/L) + \tau_{y2}(z/L). \quad (16.50)$$

The values of the distributed load and temperature gradient at  $z = 0$  are  $f_{y1}$  and  $\tau_{y1}$ , respectively. At  $z = L$ , the distributed load intensity is  $f_{y2}$  and the temperature gradient is  $\tau_{y2}$ . The boundary value problem (16.27) reduces to

$$\begin{aligned} EIV_0'''' &= f_{y1}(1 - z/L) + f_{y2}(z/L) & 0 < z < L \\ v_0(0) &= 0 & -v_0'(0) = 0 & v_0(L) = 0 & -v_0'(L) = 0 \end{aligned} \quad (16.51)$$

The solution for displacement  $v_0(z)$  is

$$v_0(z) = \left[ \frac{(L-z)^2(3L-z)z^2}{120EIL} \right] f_{y1} + \left[ \frac{(L-z)^2(2L+z)z^2}{120EIL} \right] f_{y2}. \quad (16.52)$$

The distribution of the transverse shear force (16.32) and the bending moment (16.30) and are

$$\begin{bmatrix} V_y^0 \\ M_x^0 \end{bmatrix} = \frac{1}{60L} \begin{bmatrix} 21L^2 - 60Lz + 30z^2 & 9L^2 - 30z^2 \\ -3L^3 + 21L^2z - 30Lz^2 + 10z^3 & -2L^3 + 9L^2z - 10z^3 \end{bmatrix} \begin{bmatrix} f_{y1} \\ f_{y2} \end{bmatrix} - \frac{EI\alpha}{L} \begin{bmatrix} -1 & 1 \\ (L-z) & z \end{bmatrix} \begin{bmatrix} \tau_{y1} \\ \tau_{y2} \end{bmatrix}. \quad (16.53)$$

Substitute the results in (16.53) into joint equilibrium (16.25) to find the fixed-end actions

$$\{Q^0\} = \begin{bmatrix} Q_1^0 \\ Q_2^0 \\ Q_3^0 \\ Q_4^0 \end{bmatrix} = \begin{bmatrix} -7L/20 & -3L/20 \\ L^2/20 & L^2/30 \\ -3L/20 & -7L/20 \\ -L^2/30 & -L^2/20 \end{bmatrix} \begin{bmatrix} f_{y1} \\ f_{y2} \end{bmatrix} - \frac{EI\alpha}{L} \begin{bmatrix} -1 & 1 \\ L & 0 \\ 1 & -1 \\ 0 & L \end{bmatrix} \begin{bmatrix} \tau_{y1} \\ \tau_{y2} \end{bmatrix}. \quad (16.54)$$

In the case of uniform distributions where  $f_{y1} = f_{y2} = f_{y0}$  and  $\tau_{y1} = \tau_{y2} = \tau_{y0}$ , the bending moment and shear force simplify to

$$\begin{bmatrix} V_y^0 \\ M_x^0 \end{bmatrix} = \begin{bmatrix} (L-2z)/2 \\ (-L^2 + 6Lz - 6z^2)/12 \end{bmatrix} f_{y0} - EI\alpha \begin{bmatrix} 0 \\ 1 \end{bmatrix} \tau_{y0}, \quad (16.55)$$

and the fixed-end actions are

$$\{Q^0\} = \begin{bmatrix} Q_1^0 \\ Q_2^0 \\ Q_3^0 \\ Q_4^0 \end{bmatrix} = \begin{bmatrix} -L/2 \\ L^2/12 \\ -L/2 \\ -L^2/12 \end{bmatrix} f_{y0} - EI\alpha \begin{bmatrix} 0 \\ -1 \\ 0 \\ 1 \end{bmatrix} \tau_{y0}. \quad (16.56)$$

### 16.2.3 Results of the combined superposition solutions for the beam

Joint equilibrium (16.25) leads to the sum

$$\begin{bmatrix} Q_1 \\ Q_2 \\ Q_3 \\ Q_4 \end{bmatrix} = \begin{bmatrix} -V_y^0(0) \\ -M_x^0(0) \\ V_y^0(L) \\ M_x^0(L) \end{bmatrix} + \begin{bmatrix} -V_y^1(0) \\ -M_x^1(0) \\ V_y^1(L) \\ M_x^1(L) \end{bmatrix} = \begin{bmatrix} Q_1^0 \\ Q_2^0 \\ Q_3^0 \\ Q_4^0 \end{bmatrix} + \begin{bmatrix} Q_1^1 \\ Q_2^1 \\ Q_3^1 \\ Q_4^1 \end{bmatrix}, \quad (16.57)$$

where  $\{Q^0\}$  is the 4X1 joint force vector from the fixed-end action boundary value problem (16.27), and  $\{Q^1\}$  is the 4X1 joint force vector from the boundary value problem (16.28). That is, the total joint force vector is  $\{Q\} = \{Q^0\} + \{Q^1\}$ . From eq. (16.48) we have

$$\{Q^1\} = [K] \{q\}, \quad (16.58)$$

where the 4X4 beam stiffness matrix is given by eq. (16.49) and  $\{q\}$  is the 4X1 joint displacement vector. Hence, the total joint force vector is given by

$$\{Q\} = \{Q^0\} + [K] \{q\}. \quad (16.59)$$

Equation (16.59) is written in the form

$$\{Q\} + (-\{Q^0\}) = [K] \{q\}, \quad (16.60)$$

where the vector  $-\{Q^0\}$  is called the **equivalent joint force vector**. It is the negative of the fixed-end action vector.

To summarize, the analysis of a structure composed of beam members, with some members subject to distributed loads and temperature gradients, is as follows:

1. Lock every joint of the structure against translation and rotation, and calculate the fixed-end actions.
2. Apply the fixed-end actions with the **opposite** sign.
3. Analyze the structure with the specified joint forces and the negative of the fixed-end actions;  $\{Q\} + (-\{Q^0\})$ . Note that the joint displacements computed in this step are the actual joint displacements.
4. Obtain the internal actions consisting of the shear force and bending moment by superposition.

$$\begin{bmatrix} V_y(z) \\ M_x(z) \end{bmatrix} = \begin{bmatrix} V_y^0(z) \\ M_x^0(z) \end{bmatrix} + \begin{bmatrix} V_y^1(z) \\ M_x^1(z) \end{bmatrix} = \begin{bmatrix} V_y^0(z) \\ M_x^0(z) \end{bmatrix} + [S^1(z)] \{q\}. \quad (16.61)$$

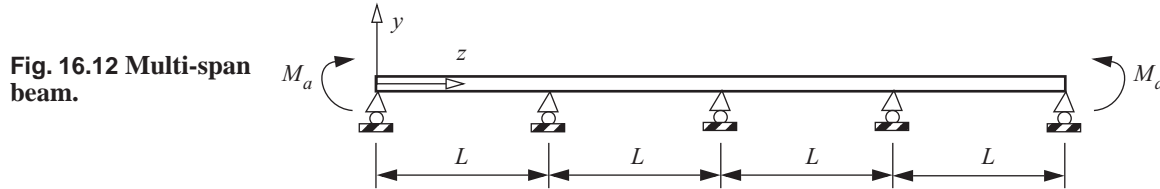
For the linear distributions of the specified external loads, the shear force  $V_y^0(z)$  and bending moment  $M_x^0(z)$  are

given by (16.53). The 2X4 stress matrix  $[S^1(z)]$  is given by (16.46), and  $\{q\}$  is the 4X1 joint displacement vector of the beam member obtained from the solution of the assembly of the structural members.

### Example 16.6 Multispan beam

Consider the multispan uniform beam in figure. 16.12. It is subject to equal and opposite couples in the  $y$ - $z$  plane at  $z = 0$  and  $z = L$ . The magnitude of the moment of these couples is denoted by  $M_a$ . The bending stiffness  $EI$  is the same constant in each span.

- Determine the unknown joint displacements using symmetry to reduce problem size.
- Draw the shear force and bending moment diagrams.
- Determine the support reactions.



**Solution for the unknown joint displacements.** The joints are taken at the support locations and are numbered one to five from left to right. Hence, there are ten degrees of freedom (DOFs) as is shown in the top sketch in figure. 16.13. The support conditions mean the vertical displacements vanish; i.e.,

$$\{q_\beta\} = [q_1 \ q_3 \ q_5 \ q_7 \ q_9]^T = 0_{5 \times 1}. \quad (\text{a})$$

The geometry, boundary conditions, and material properties of the structure are symmetric about the vertical centerline. If the top sketch of the beam and its DOFs are rotated  $180^\circ$  about this vertical centerline, the bottom sketch is obtained. See figure. 16.13. The displacements and rotations at the joints in the top and bottom sketch must be the same. Hence, symmetry implies the joint rotations must satisfy

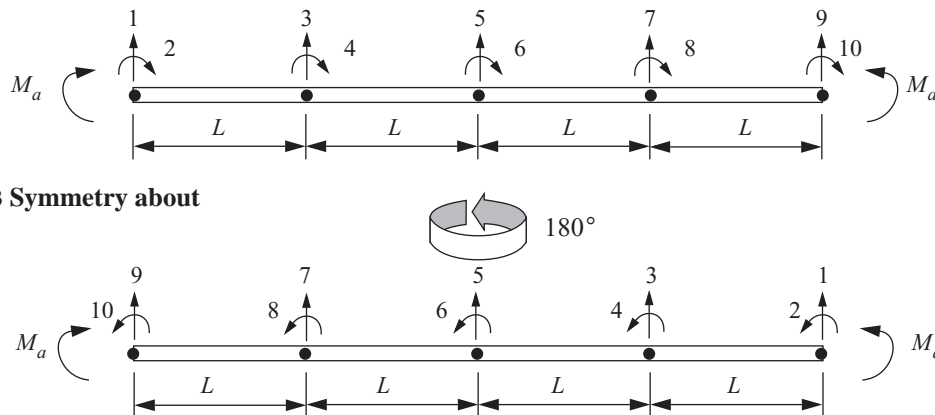
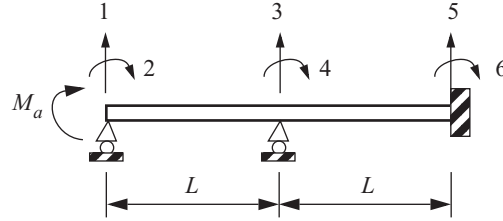


**Fig. 16.13 Symmetry about midspan.**

$$q_{10} = -q_2 \quad q_8 = -q_4 \quad q_6 = -q_6. \quad (b)$$

Clearly, the last symmetry condition on the rotations means rotation of the center joint vanishes;  $q_6 = 0$ . Then, the analysis for the response of the beam reduces to a two-span beam, clamped at its right end as is shown in figure. 16.14. The two active degrees of freedom are rotations  $q_2$  and  $q_4$ . The stiffness matrices (16.49) for beam

**Fig. 16.14** Equivalent two-span beam model.



members 1-2 and 2-3 are

$$[K_{1-2}] = EI \begin{bmatrix} q_1 & q_2 & q_3 & q_4 \\ 12/L^3 & -6/L^2 & -12/L^3 & -6/L^2 \\ -6/L^2 & 4/L & 6/L^2 & 2/L \\ -12/L^3 & 6/L^2 & 12/L^3 & 6/L^2 \\ -6/L^2 & 2/L & 6/L^2 & 4/L \end{bmatrix} \quad [K_{2-3}] = EI \begin{bmatrix} q_3 & q_4 & q_5 & q_6 \\ 12/L^3 & -6/L^2 & -12/L^3 & -6/L^2 \\ -6/L^2 & 4/L & 6/L^2 & 2/L \\ -12/L^3 & 6/L^2 & 12/L^3 & 6/L^2 \\ -6/L^2 & 2/L & 6/L^2 & 4/L \end{bmatrix}. \quad (c)$$

The 6X6 unrestrained structural stiffness matrix is the sum  $[K_{1-2}] + [K_{2-3}]$  with each member stiffness matrix expanded to 6X6 by adding two rows and two columns of zeros for degrees of freedom not contained in the member. The result is

$$[K] = EI \begin{bmatrix} q_1 & q_2 & q_3 & q_4 & q_5 & q_6 \\ 12/L^3 & -6/L^2 & -12/L^3 & -6/L^2 & 0 & 0 \\ -6/L^2 & 4/L & 6/L^2 & 2/L & 0 & 0 \\ -12/L^3 & 6/L^2 & 24/L^3 & 0 & -12/L^3 & -6/L^2 \\ -6/L^2 & 2/L & 0 & 8/L & 6/L^2 & 2/L \\ 0 & 0 & -12/L^3 & 6/L^2 & 12/L^3 & 6/L^2 \\ 0 & 0 & -6/L^2 & 2/L & 6/L^2 & 4/L \end{bmatrix}. \quad (d)$$

Partition the unrestrained structural stiffness matrix in terms of unknowns and knowns to get

$$[K] = EI \begin{bmatrix} q_2 & q_4 & q_1 & q_3 & q_5 & q_6 \\ 4/L & 2/L & -6/L^2 & 6/L^2 & 0 & 0 \\ 2/L & 8/L & -6/L^2 & 0 & 6/L^2 & 2/L \\ -6/L^2 & -6/L^2 & 12/L^3 & -12/L^3 & 0 & 0 \\ 6/L^3 & 0 & -12/L^3 & 24/L^3 & -12/L^3 & -6/L^2 \\ 0 & 6/L^2 & 0 & -12/L^3 & 12/L^3 & 6/L^2 \\ 0 & 2/L & 0 & -6/L^2 & 6/L^2 & 4/L \end{bmatrix} = \begin{bmatrix} [K_{\alpha\alpha}] & [K_{\alpha\beta}] \\ [K_{\beta\alpha}] & [K_{\beta\beta}] \end{bmatrix}. \quad (e)$$

The restrained structural stiffness matrix is

$$[K_{\alpha\alpha}] = EI \begin{matrix} & q_2 & q_4 \\ \begin{bmatrix} 4/L & 2/L \\ 2/L & 8/L \end{bmatrix} \end{matrix} \quad (f)$$

The unknown rotations are determined from

$$\begin{bmatrix} Q_2 \\ Q_4 \end{bmatrix} = \begin{bmatrix} M_a \\ 0 \end{bmatrix} = EI \begin{bmatrix} 4/L & 2/L \\ 2/L & 8/L \end{bmatrix} \begin{bmatrix} q_2 \\ q_4 \end{bmatrix} \quad (g)$$

Solve eq. (g) for the nodal rotations to find

$$\begin{bmatrix} q_2 \\ q_4 \end{bmatrix} = \frac{L}{EI(32-4)} \begin{bmatrix} 8 & -2 \\ -2 & 4 \end{bmatrix} \begin{bmatrix} M_a \\ 0 \end{bmatrix} = \frac{M_a L}{14EI} \begin{bmatrix} 4 \\ -1 \end{bmatrix} \quad (h)$$

By symmetry the joint rotations for the entire structure are

$$\begin{bmatrix} q_2 \\ q_4 \\ q_6 \\ q_8 \\ q_{10} \end{bmatrix} = \frac{M_a L}{14EI} \begin{bmatrix} 4 \\ -1 \\ 0 \\ 1 \\ -4 \end{bmatrix} \quad (i)$$

**Solution for the shear force and bending moment distributions.** The shear force and bending moment distribution in beam members 1-2 and 2-3 are determined from eq. (16.44). For member 1-2, we have

$$\begin{bmatrix} V_1(z) \\ M_1(z) \end{bmatrix}_{1-2} = EI \begin{bmatrix} -\frac{12}{L^3} & \frac{6}{L^2} & \frac{12}{L^3} & \frac{6}{L^2} \\ \left(\frac{6}{L^2} - \frac{12z}{L^3}\right) & \left(-\frac{4}{L} + \frac{6z}{L^2}\right) & \left(-\frac{6}{L^2} + \frac{12z}{L^3}\right) & \left(-\frac{2}{L} + \frac{6z}{L^2}\right) \end{bmatrix} \begin{bmatrix} q_1 \\ q_2 \\ q_3 \\ q_4 \end{bmatrix} \quad (j)$$

But  $q_1 = q_3 = 0$ , so

$$\begin{bmatrix} V_1(z) \\ M_1(z) \end{bmatrix}_{1-2} = EI \begin{bmatrix} \frac{6}{L^2} & \frac{6}{L^2} \\ \left(-\frac{4}{L} + \frac{6z}{L^2}\right) & \left(-\frac{2}{L} + \frac{6z}{L^2}\right) \end{bmatrix} \begin{bmatrix} q_2 \\ q_4 \end{bmatrix} \quad (k)$$

Substitute the solution for the rotations from eq. (h) into eq. (k) to get



$$\begin{bmatrix} V_1(z) \\ M_1(z) \end{bmatrix}_{1-2} = EI \begin{bmatrix} \frac{6}{L^2} & \frac{6}{L^2} \\ \left(-\frac{4}{L} + \frac{6z}{L^2}\right) & \left(-\frac{2}{L} + \frac{6z}{L^2}\right) \end{bmatrix} \frac{M_a L}{14EI} \begin{bmatrix} 4 \\ -1 \end{bmatrix} = \frac{M_a L}{14} \begin{bmatrix} \frac{18}{L^2} \\ -\frac{14}{L} + 18\frac{z}{L^2} \end{bmatrix} = \begin{bmatrix} \frac{9M_a}{7L} \\ -M_a + \frac{9M_a z}{7L} \end{bmatrix}. \quad (l)$$

Note that the coordinate  $z$  is local to the member in the formulas for the shear force and bending moment. For member 2-3, we have

$$\begin{bmatrix} V_1(z) \\ M_1(z) \end{bmatrix}_{2-3} = EI \begin{bmatrix} -\frac{12}{L^3} & \frac{6}{L^2} & \frac{12}{L^3} & \frac{6}{L^2} \\ \frac{6}{L^2} - \frac{12z}{L^3} - \frac{4}{L} + \frac{6z}{L^2} & -\frac{6}{L^2} + \frac{12z}{L^3} - \frac{2}{L} + \frac{6z}{L^2} \end{bmatrix} \begin{bmatrix} q_3 \\ q_4 \\ q_5 \\ q_6 \end{bmatrix}. \quad (m)$$

But  $q_3 = q_5 = q_6 = 0$ , so

$$\begin{bmatrix} V_1(z) \\ M_1(z) \end{bmatrix}_{2-3} = EI \begin{bmatrix} \frac{6}{L^2} \\ -\frac{4}{L} + \frac{6z}{L^2} \end{bmatrix} q_4. \quad (n)$$

Substitute the solution for rotation  $q_4$  from eq. (h) into eq. (n) to get

$$\begin{bmatrix} V_1(z) \\ M_1(z) \end{bmatrix}_{2-3} = EI \begin{bmatrix} \frac{6}{L^2} \\ -\frac{4}{L} + \frac{6z}{L^2} \end{bmatrix} \left( -\frac{M_a L}{14EI} \right) = \begin{bmatrix} -\frac{3M_a}{7L} \\ \frac{2M_a}{7} - \frac{3M_a z}{7L} \end{bmatrix}. \quad (o)$$

Again, note that the  $z$ -coordinate in these formulas for the shear force and bending moment in member 2-3 is local to the member and runs from zero to  $L$ . However, the beginning joint 2 corresponds to the global longitudinal coordinate  $L$ , and end joint 3 corresponds to the global longitudinal coordinate  $2L$ . The relationship between the member local coordinate and the global structural coordinate has to be taken into account when drawing the shear force and bending moment diagrams. The shear force and bending moment diagrams are shown in figure. 16.15. In this example, the shear force diagram is antisymmetric, and the moment diagram is symmetric, about the center of the multispan beam.

**Solution for the support reactions.** The support reactions are  $[Q_\beta] = [K_{\beta\alpha}] \{q_\alpha\}$ , since  $\{q_\beta\} = 0_{4 \times 1}$ .

Hence,

$$\begin{bmatrix} Q_1 \\ Q_3 \\ Q_5 \\ Q_6 \end{bmatrix} = EI \begin{bmatrix} -6/L^2 & -6/L^2 \\ 6/L^2 & 0 \\ 0 & 6/L^2 \\ 0 & 2/L \end{bmatrix} \begin{bmatrix} q_2 \\ q_4 \end{bmatrix} = EI \begin{bmatrix} -6/L^2 & -6/L^2 \\ 6/L^2 & 0 \\ 0 & 6/L^2 \\ 0 & 2/L \end{bmatrix} \frac{M_a L}{14EI} \begin{bmatrix} 4 \\ -1 \end{bmatrix} = M_a \begin{bmatrix} -9/(7L) \\ 12/(7L) \\ -3/(7L) \\ -1/7 \end{bmatrix}. \quad (p)$$

Note that these are the support reactions for the left half of the beam. By symmetry the support reactions on the

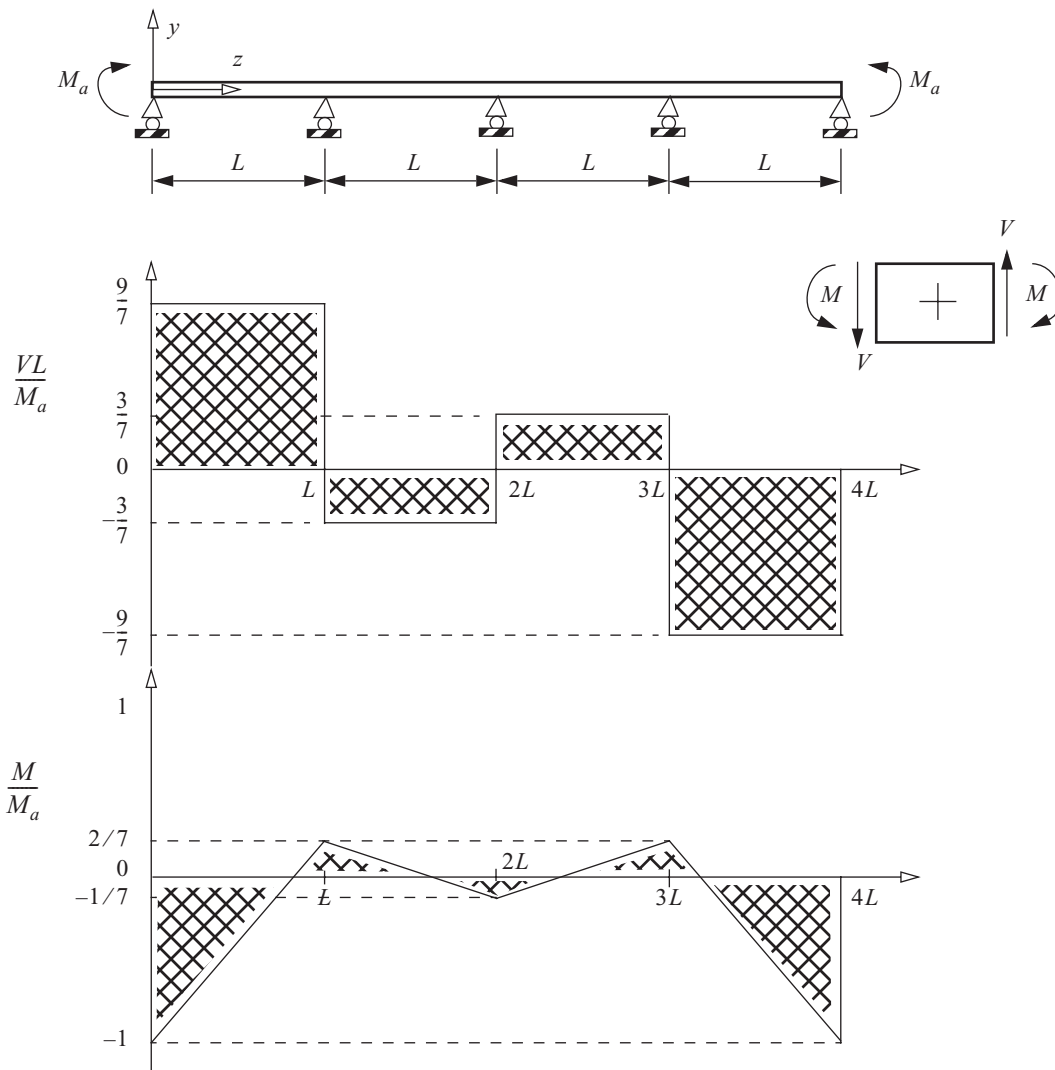


Fig. 16.15 Shear force and bending moment diagrams for the multispan beam.

right half of the beam are obtained by a rotation of the left half by  $180^\circ$  as shown in figure. 16.16. Joining the left half and right half we get the support reactions for the overall free body diagram of the multispan beam as shown in figure. 16.17. ■

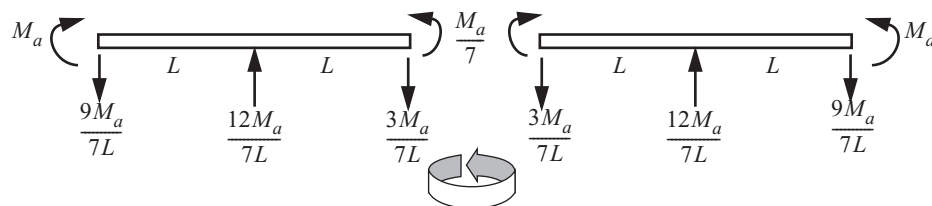


Fig. 16.16 Support reactions from the half models of the multispan beam.

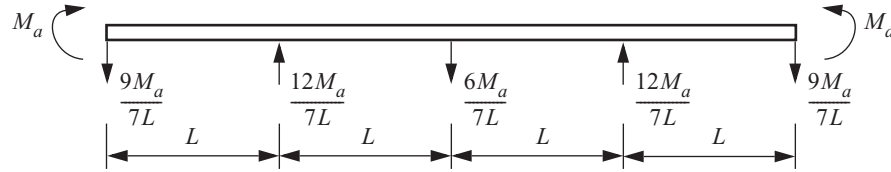


Fig. 16.17 Support reactions of the intact multispan beam.

### Example 16.7 Clamped-clamped, stepped beam restrained by a spring

The beam structure shown in figure. 16.18(a) has a step change in thickness at midspan, and is clamped at each end. The left half of has a uniform flexural stiffness  $2EI$ , and the right half has a uniform flexural stiffness  $EI$ . Each half has a length denoted by  $a$ . A vertical linear elastic spring of stiffness  $k = 6EI/a^3$  is connected at midspan. The structure is subject to a vertical distributed load and a vertical point force  $P$  applied at midspan. The distributed load is uniform on the left half with intensity  $f_{y0}$ , and decreases linearly from  $f_{y0}$  to zero on the right half. Model the response of the beam with two beam members, one in each half, and a spring member. Determine

- The restrained structural stiffness matrix.
- The fixed-end action vector.
- The unknown joint displacements.
- The support reactions.
- The shear force and bending moment in the left half of the beam.

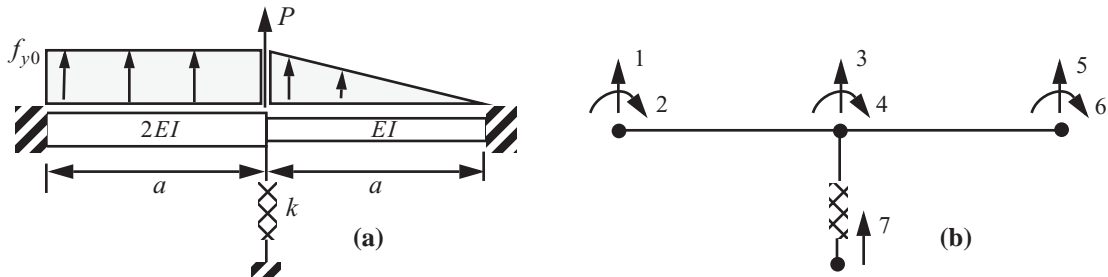


Fig. 16.18 (a) Beam with a step change in thickness. (b) Degree of freedom numbering.

**Solution to part (a).** The unrestrained structure has four joints and seven degrees of freedom as shown in figure. 16.18(b). The size of the unrestrained structural stiffness matrix is  $7 \times 7$ . The support conditions impose the vanishing of the following generalized displacement vector:  $\{q_\beta\} = [q_1 \ q_2 \ q_5 \ q_6 \ q_7]^T = 0_{5 \times 1}$ . The active, or unknown, displacement vector is  $\{q_\alpha\} = [q_3 \ q_4]^T$ .

The stiffness matrices for the two beam members are obtained from eq. (16.49) as

$$\begin{aligned}
[K_{1-2}] &= EI \begin{bmatrix} q_1 & q_2 & q_3 & q_4 \\ 24/a^3 & -12/a^2 & -24/a^3 & -12/a^2 \\ -12/a^2 & 8/a & 12/a^2 & 4/a \\ -24/a^3 & 12/a^2 & 24/a^3 & 12/a^2 \\ -12/a^2 & 4/a & 12/a^2 & 8/a \end{bmatrix} \quad [K_{2-3}] = EI \begin{bmatrix} q_3 & q_4 & q_5 & q_6 \\ 12/a^3 & -6/a^2 & -12/a^3 & -6/a^2 \\ -6/a^2 & 4/a & 6/a^2 & 2/a \\ -12/a^3 & 6/a^2 & 12/a^3 & 6/a^2 \\ -6/a^2 & 2/a & 6/a^2 & 4/a \end{bmatrix}. \quad (a)
\end{aligned}$$

The spring stiffness matrix is obtained from eq. (15.8) on page 424 as

$$[K_{4-2}] = EI \begin{bmatrix} q_7 & q_3 \\ 6/a^3 & -6/a^3 \\ -6/a^3 & 6/a^3 \end{bmatrix}. \quad (b)$$

Assembly of the element stiffness matrices is by summation of the element stiffness matrices with attention to the location of the matrix elements in the 7X7 unrestrained structural stiffness matrix. The result is

$$[K] = EI \begin{bmatrix} q_1 & q_2 & q_3 & q_4 & q_5 & q_6 & q_7 \\ 24/a^3 & -12/a^2 & -24/a^3 & -12/a^2 & 0 & 0 & 0 \\ -12/a^2 & 8/a & 12/a^2 & 4/a & 0 & 0 & 0 \\ -24/a^3 & 12/a^2 & 42/a^3 & 6/a^2 & 12/a^3 & -6/a^2 & -6/a^3 \\ -12/a^2 & 4/a & 6/a^2 & 12/a & 6/a^2 & 2/a & 0 \\ 0 & 0 & -12/a^3 & 6/a^2 & 12/a^3 & 6/a^2 & 0 \\ 0 & 0 & -6/a^2 & 2/a & 6/a^2 & 4/a & 0 \\ 0 & 0 & -6/a^3 & 0 & 0 & 0 & 6/a^3 \end{bmatrix}. \quad (c)$$

Partition the unrestrained structural stiffness matrix in eq. (c) so that rows and columns are in the order 3, 4, 1, 2, 5, 6, 7:

$$[K] = EI \begin{bmatrix} q_3 & q_4 & q_1 & q_2 & q_5 & q_6 & q_7 \\ 42/a^3 & 6/a^2 & -24/a^3 & 12/a^2 & -12/a^3 & -6/a^2 & -6/a^3 \\ 6/a^2 & 12/a & -12/a^2 & 4/a & 6/a^2 & 2/a & 0 \\ -24/a^3 & -12/a^2 & 24/a^3 & -12/a^2 & 0 & 0 & 0 \\ 12/a^2 & 4/a & -12/a^2 & 8/a & 0 & 0 & 0 \\ -12/a^3 & 6/a^2 & 0 & 0 & 12/a^3 & 6/a^2 & 0 \\ -6/a^2 & 2/a & 0 & 0 & 6/a^2 & 4/a & 0 \\ -6/a^3 & 0 & 0 & 0 & 0 & 0 & 6/a^3 \end{bmatrix} = \begin{bmatrix} [K_{\alpha\alpha}] & [K_{\alpha\beta}] \\ [K_{\beta\alpha}] & [K_{\beta\beta}] \end{bmatrix}. \quad (d)$$

From the partitioned form of eq. (d) the restrained structural stiffness matrix is

$$[K_{\alpha\alpha}] = EI \begin{bmatrix} 42/a^3 & 6/a^2 \\ 6/a^2 & 12/a \end{bmatrix}. \quad (e)$$

**Solution to part (b).** From eqs. (16.54) and (16.56) fixed-end actions of the beam member are

$$\begin{bmatrix} Q_1^0 \\ Q_2^0 \\ Q_3^0 \\ Q_4^0 \end{bmatrix}_{1-2} = \begin{bmatrix} -af_{y0}/2 \\ a^2f_{y0}/12 \\ -af_{y0}/2 \\ -a^2f_{y0}/12 \end{bmatrix} \quad \begin{bmatrix} Q_3^0 \\ Q_4^0 \\ Q_5^0 \\ Q_6^0 \end{bmatrix}_{2-3} = \begin{bmatrix} -7af_{y0}/20 \\ a^2f_{y0}/20 \\ -3af_{y0}/20 \\ -a^2f_{y0}/30 \end{bmatrix}. \quad (f)$$

The assembled 7X1 fixed-end action vector in the natural order 1, 2, 3, 4, 5, 6, 7 is

$$\{Q^0\} = \begin{bmatrix} -a/2 & a^2/12 & -17a/20 & -a^2/30 & -3a/20 & -a^2/30 & 0 \end{bmatrix}^T f_{y0}.$$

Partitioning the fixed-end action vector in the order 3, 4, 1, 2, 5, 6, 7 we get

$$\{Q^0\} = \begin{bmatrix} -17a/20 & -a^2/30 & -a/2 & a^2/12 & -3a/20 & -a^2/30 & 0 \end{bmatrix}^T f_{y0} = \{Q_\alpha^0\} + \{Q_\beta^0\},$$

where

$$\{Q_\alpha^0\} = \begin{bmatrix} -17a/20 & -a^2/30 \end{bmatrix}^T f_{y0} \quad \{Q_\beta^0\} = \begin{bmatrix} -a/2 & a^2/12 & -3a/20 & -a^2/30 & 0 \end{bmatrix}^T f_{y0}. \quad (g)$$

**Solution to part (c).** The matrix equation to determine the unknown joint displacement  $\{q_\alpha\}$  is

$$\{Q_\alpha\} = [K_{\alpha\alpha}]\{q_\alpha\} + [K_{\alpha\beta}]\{q_\beta\} + \{Q_\alpha^0\}. \quad (h)$$

The prescribed joint force vector  $\{Q_\alpha\}$  is

$$\begin{bmatrix} Q_3 \\ Q_4 \end{bmatrix}_\alpha = \begin{bmatrix} P \\ 0 \end{bmatrix}. \quad (i)$$

The specified displacement vector  $\{q_\beta\} = 0_{5 \times 1}$ . The matrix equation for the solution of the displacement vector  $\{q_\alpha\}$  reduces to

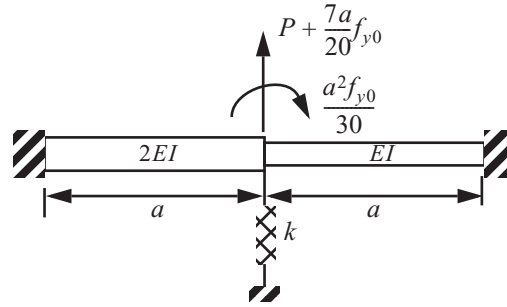
$$[K_{\alpha\alpha}]\{q_\alpha\} = \{Q_\alpha\} + (-\{Q_\alpha^0\}), \quad (j)$$

where  $(-\{Q_\alpha^0\})$  is the equivalent joint force vector. See figure. 16.19. The explicit form of the matrix equation to determine the unknown displacements is

$$EI \begin{bmatrix} 42/a^3 & 6/a^2 \\ 6/a^2 & 12/a \end{bmatrix} \begin{bmatrix} q_3 \\ q_4 \end{bmatrix} = \begin{bmatrix} P \\ 0 \end{bmatrix} + \begin{bmatrix} 17a/20 \\ a^2/30 \end{bmatrix} f_{y0}.$$

The solution for the generalized displacements is

**Fig. 16.19** Applied load  $P$  and the equivalent joint forces from the distributed loading.



$$\begin{bmatrix} q_3 \\ q_4 \end{bmatrix} = \frac{1}{EI} \begin{bmatrix} a^3/39 & -a^2/78 \\ -a^2/78 & 7a/78 \end{bmatrix} \begin{bmatrix} P + 17af_{y0}/20 \\ a^2f_{y0}/30 \end{bmatrix} = \frac{1}{39EI} \begin{bmatrix} a^3(P + 5af_{y0}/18) \\ -\frac{a^2}{2}(P + 37af_{y0}/60) \end{bmatrix}. \quad (\text{k})$$

**Solution to part (d).** The governing matrix equation for the unknown joint forces, or the support reactions, is

$$\{Q_\beta\} = [K_{\beta\alpha}]\{q_\alpha\} + [K_{\beta\beta}]\{q_\beta\} + \{Q_\beta^0\}. \quad (\text{l})$$

The matrix  $5 \times 2$   $[K_{\beta\alpha}]$  is obtained from the partitioned form eq. (d). Writing eq. (l) in detail we have

$$\begin{bmatrix} Q_1 \\ Q_2 \\ Q_5 \\ Q_6 \\ Q_7 \end{bmatrix} = EI \begin{bmatrix} -24/a^3 & -12/a^2 \\ 12/a^2 & 4/a \\ -12/a^3 & 6/a^2 \\ -6/a^2 & 2/a \\ -6/a^3 & 0 \end{bmatrix} \frac{1}{39EI} \begin{bmatrix} a^3P + 5af_{y0}/18 \\ -\frac{a^2}{2}P + 37af_{y0}/60 \end{bmatrix} + \begin{bmatrix} -a/2 \\ a^2/12 \\ -3a/20 \\ -a^2/30 \\ 0 \end{bmatrix} f_{y0}. \quad (\text{m})$$

After performing the matrix algebra in eq.(m) the result for the support reactions is

$$\begin{bmatrix} Q_1 \\ Q_2 \\ Q_5 \\ Q_6 \\ Q_7 \end{bmatrix} = \begin{bmatrix} -6/13 & -179/195 \\ 10a/39 & 721a/2,340 \\ -5/13 & -59/130 \\ 7a/39 & -83a/468 \\ 2/13 & -5/39 \end{bmatrix} \begin{bmatrix} P \\ af_{y0} \end{bmatrix}. \quad (\text{n})$$

**Solution to part e.** Referring to eq. (16.61) on page 463, the shear force and bending moment in beam member 1-2 is given by the superposition of the fixed-end solution and the displacement solution as

$$\begin{bmatrix} V_y(z) \\ M_x(z) \end{bmatrix}_{1-2} = \begin{bmatrix} V_y^0(z) \\ M_x^0(z) \end{bmatrix}_{1-2} + \begin{bmatrix} V_y^1(z) \\ M_x^1(z) \end{bmatrix}_{1-2} = \begin{bmatrix} V_y^0(z) \\ M_x^0(z) \end{bmatrix}_{1-2} + [S^1(z)]_{1-2} \{q\}_{1-2}. \quad (\text{o})$$

From the fixed-end action solution (16.55) the vector of the shear force and bending moment is

$$\begin{bmatrix} V_y^0(z) \\ M_x^0(z) \end{bmatrix}_{1-2} = \begin{bmatrix} (a-2z)/2 \\ (-a^2+6az-6z^2)/12 \end{bmatrix} f_{y0} \quad 0 \leq z \leq a. \quad (\text{p})$$

Equations (16.45) and (16.46) combine to determine the shear and moment from the displacements of the member. That is,

$$\begin{bmatrix} V_y^1(z) \\ M_x^1(z) \end{bmatrix}_{1-2} = [S^1(z)]_{1-2} \begin{bmatrix} q_1 \\ q_2 \\ q_3 \\ q_4 \end{bmatrix} = EI \begin{bmatrix} -\frac{12}{a^3} & \frac{6}{a^2} & \frac{12}{a^3} & \frac{6}{a^2} \\ \frac{6}{a^2} - \frac{12z}{a^3} & -\frac{4}{a} + \frac{6z}{a^2} & -\frac{6}{a^2} + \frac{12z}{a^3} & -\frac{2}{a} + \frac{6z}{a^2} \end{bmatrix} \begin{bmatrix} 0 \\ 0 \\ q_3 \\ q_4 \end{bmatrix}. \quad (\text{q})$$

Perform the matrix algebra in eq. (q) to find

$$\begin{bmatrix} V_y^1(z) \\ M_x^1(z) \end{bmatrix}_{1-2} = EI \begin{bmatrix} \frac{12}{a^3} & \frac{6}{a^2} \\ -\frac{6}{a^2} + \frac{12z}{a^3} & -\frac{2}{a} + \frac{6z}{a^2} \end{bmatrix} \frac{1}{39EI} \begin{bmatrix} a^3P + 5af_{y0}/18 \\ -\frac{a^2}{2}P + 37af_{y0}/60 \end{bmatrix} = \begin{bmatrix} \frac{6}{13} & \frac{163a}{390} \\ \left(-\frac{10a}{39} + \frac{6z}{13}\right) & \left(-\frac{263a^2}{1170} + \frac{163az}{390}\right) \end{bmatrix} \begin{bmatrix} P \\ f_{y0} \end{bmatrix}. \quad (\text{r})$$

Finally, substitute eqs. (p) and (r) into (o) to get

$$\begin{bmatrix} V_y(z) \\ M_x(z) \end{bmatrix}_{1-2} = \begin{bmatrix} \frac{6}{13} & \frac{179a}{195} - z \\ \left(-\frac{10a}{39} + \frac{6z}{13}\right) & \left(-\frac{721a^2}{2,340} + \frac{179az}{195} - \frac{z^2}{2}\right) \end{bmatrix} \begin{bmatrix} P \\ f_{y0} \end{bmatrix} \quad 0 \leq z \leq a. \quad \blacksquare$$

### 16.3 Coplanar frame structures

Frame members in a skeletal structure resist applied loads both by axial deformation and bending deformation. Frames are often modeled by assuming the joints are rigid, which means that members meeting at a joint have the same rotation. That is, instead of frictionless pins or ball and socket joints used to model trusses, the connections at a joint under the rigid joint assumption implies that bending moments in the members at the joint do not vanish. When distributed lateral loads act on the member, frame elements may be required even if the joints at the end of the member are modeled as frictionless pins. In a truss the loads are assumed to only act on the joints, and the members are not subject to lateral distributed loads. The stiffness matrix for a frame member is the superposition of the stiffness matrix for a truss member and the stiffness matrix for a beam member. There are three degrees of freedom at each joint in a coplanar frame member: two displacements and a rotation as shown in figure. 16.20. In this figure, degrees of freedom labeled one and four account for axial deformation, degrees of freedom two and five account for lateral deformation in bending, and degrees of freedom three and six account for rotations in bending. These degrees of freedom are referred to Cartesian coordinate directions along the longitudinal axis and the axis perpendicular to the member. Let the coordinate along the longitudinal, centroidal axis be denoted by  $z$ ,  $0 \leq z \leq L$ , and let  $y$  be the coordinate perpendicular to the member.

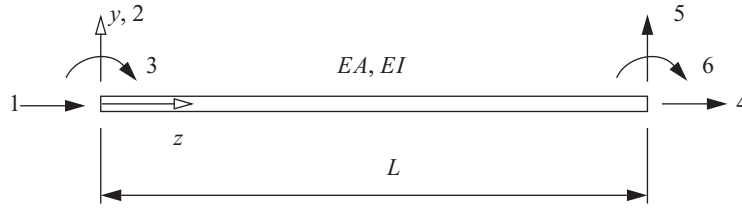


**Fig. 16.20** Frame member with six degrees of freedom.

Consider a typical plane frame member between joints  $i$  and  $j$  in a structure. Joint  $i$  is the beginning joint and joint  $j$  is the end joint, so that the  $z$ -axis is directed from joint  $i$  to joint  $j$ . Then, the 6X1 generalized displacement vector for the frame member in local coordinate directions is uniquely numbered by

$$\{\bar{q}\} = [\bar{q}_{3i-2} \quad \bar{q}_{3i-1} \quad \bar{q}_{3i} \quad \bar{q}_{3j-2} \quad \bar{q}_{3j-1} \quad \bar{q}_{3j}]^T. \quad (16.62)$$

These displacement components are shown in figure. 16.21. The 6X6 frame stiffness matrix in local coordinate

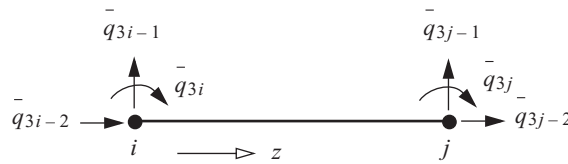


**Fig. 16.21** Generalized displacements for a frame element between joints  $i$  and  $j$ .

directions is the sum of the truss stiffness matrix and the beam stiffness matrix, where

$$[K_{\text{truss}}] = \begin{bmatrix} EA/L & -EA/L \\ -EA/L & EA/L \end{bmatrix} \quad [K_{\text{beam}}] = \begin{bmatrix} 12EI/L^3 & -6EI/L^2 & -12EI/L^3 & -6EI/L^2 \\ -6EI/L^2 & 4EI/L & 6EI/L^2 & 2EI/L \\ -12EI/L^3 & 6EI/L^2 & 12EI/L^3 & 6EI/L^2 \\ -6EI/L^2 & 2EI/L & 6EI/L^2 & 4EI/L \end{bmatrix}. \quad (16.63)$$

Now add the stiffness matrices in eq. (16.63) with due regard to the element locations in the 6X6 frame member stiffness matrix to get

$$[\bar{K}] = \begin{bmatrix} EA/L & 0 & 0 & -EA/L & 0 & 0 \\ 0 & 12EI/L^3 & -6EI/L^2 & 0 & -12EI/L^3 & -6EI/L^2 \\ 0 & -6EI/L^2 & 4EI/L & 0 & 6EI/L^2 & 2EI/L \\ -EA/L & 0 & 0 & EA/L & 0 & 0 \\ 0 & -12EI/L^3 & 6EI/L^2 & 0 & 12EI/L^3 & 6EI/L^2 \\ 0 & -6EI/L^2 & 2EI/L & 0 & 6EI/L^2 & 4EI/L \end{bmatrix}. \quad (16.64)$$



The frame member stiffness matrix (16.64) is symmetric, singular, and its diagonal elements are positive. Let the  $6 \times 1$  generalized joint force vector corresponding to the generalized displacement vector for the member in local coordinates be denoted by

$$\{\bar{Q}\} = [\bar{Q}_{3i-2} \ \bar{Q}_{3i-1} \ \bar{Q}_{3i} \ \bar{Q}_{3j-2} \ \bar{Q}_{3j-1} \ \bar{Q}_{3j}]^T. \quad (16.65)$$

Then, the matrix relationship between the generalized force and displacement vectors is

$$\{\bar{Q}\} = [\bar{K}] \{q\} \quad \begin{matrix} 6 \times 1 & 6 \times 6 & 6 \times 1 \end{matrix}, \quad (16.66)$$

where the frame member stiffness matrix in local coordinate directions is given by eq. (16.64).

### 16.3.1 Transformation of Cartesian coordinates

Let a coplanar frame assembly be defined with respect to global Cartesian coordinate directions  $(X, Y, Z)$ . The local Cartesian coordinates of a frame member are  $(z, y, x)$  with the  $z$ -coordinate along the reference axis of the member. The  $z$ -axis lies in the  $X$ - $Y$  plane at an angle  $\theta$  with respect to the positive  $X$ -direction as shown in figure. 16.22. To effect the assembly of member stiffness matrices it is necessary to transform the stiffness matrix (16.64) of a member from local coordinate directions  $(z, y, x)$  to the global coordinate directions  $(X, Y, Z)$ . The transformation from one Cartesian system  $(X, Y, Z)$  to another Cartesian system  $(z, y, x)$  at joint  $i$  is effected by the direction cosines of the latter with respect to the former. For example, denote the cosine of the angle of the  $z$ -direction with respect to the  $Z$ -direction as  $\cos(z, Z)$ , the cosine of the angle of the  $z$ -direction with respect to the

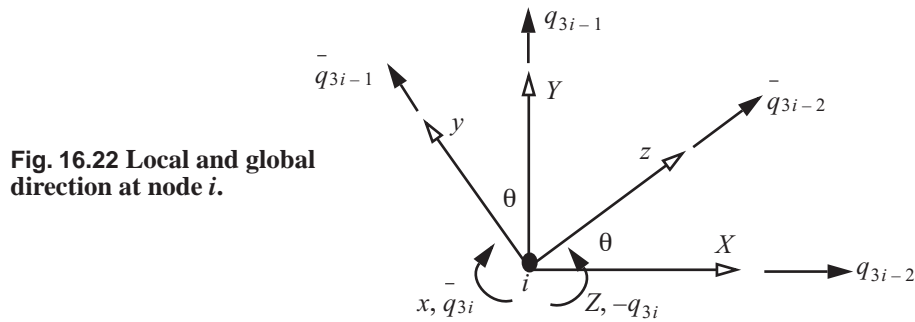


**Fig. 16.22** Local and global direction at node  $i$ .

$Y$ -direction as  $\cos(z, Y)$ , etc. Then the Cartesian coordinate transformation from global to local directions in terms of the direction cosines is

$$\begin{aligned} z &= \cos(z, X)X + \cos(z, Y)Y + \cos(z, Z)Z \\ y &= \cos(y, X)X + \cos(y, Y)Y + \cos(y, Z)Z \\ x &= \cos(x, X)X + \cos(x, Y)Y + \cos(x, Z)Z \end{aligned} \quad (16.67)$$

From figure. 16.22 the directions cosines in terms of angle  $\theta$  are as follows.

$$\cos(z, X) = \cos\theta, \cos(z, Y) = \cos(-\theta + 90^\circ) = \sin\theta, \cos(z, Z) = \cos 90^\circ = 0 \quad (16.68)$$

$$\cos(y, X) = \cos(\theta + 90^\circ) = -\sin\theta, \cos(y, Y) = \cos\theta, \cos(y, Z) = \cos 90^\circ = 0, \quad (16.69)$$

$$\cos(x, X) = \cos 90^\circ = 0, \cos(x, Y) = \cos 90^\circ = 0, \cos(x, Z) = \cos 180^\circ = -1. \quad (16.70)$$

Combine the direction cosines from eqs. (16.68) to (16.70) (b) into (16.67) to get the matrix transformation

$$\begin{bmatrix} z \\ y \\ x \end{bmatrix} = \begin{bmatrix} \cos\theta & \sin\theta & 0 \\ -\sin\theta & \cos\theta & 0 \\ 0 & 0 & -1 \end{bmatrix} \begin{bmatrix} X \\ Y \\ Z \end{bmatrix}. \quad (16.71)$$

The inverse Cartesian coordinate transformation from local to global directions is determined from the reverse direction cosines as

$$\begin{aligned} X &= \cos(X, z) \cdot z + \cos(X, y) \cdot y + \cos(X, x) \cdot x \\ Y &= \cos(Y, z) \cdot z + \cos(Y, y) \cdot y + \cos(Y, x) \cdot x. \\ Z &= \cos(Z, z) \cdot z + \cos(Z, y) \cdot y + \cos(Z, x) \cdot x \end{aligned} \quad (16.72)$$

The direction cosines of the global directions with respect to the local directions as functions of  $\theta$  are

$$\cos(X, z) = \cos\theta, \cos(X, y) = \cos(\theta + 90^\circ) = -\sin\theta, \cos(X, x) = \cos 90^\circ = 0, \quad (16.73)$$

$$\cos(Y, z) = \cos(-\theta + 90^\circ) = \sin\theta, \cos(Y, y) = \cos\theta, \cos(Y, x) = \cos 90^\circ = 0, \text{ and} \quad (16.74)$$

$$\cos(Z, z) = \cos 90^\circ = 0, \cos(Z, y) = \cos 90^\circ = 0, \cos(Z, x) = \cos 180^\circ = -1. \quad (16.75)$$

Substitute the direction cosines from eqs. (16.73) to (16.75) into eq. (16.72) to get the inverse matrix transformation as

$$\begin{bmatrix} X \\ Y \\ Z \end{bmatrix} = \begin{bmatrix} \cos\theta & -\sin\theta & 0 \\ \sin\theta & \cos\theta & 0 \\ 0 & 0 & -1 \end{bmatrix} \begin{bmatrix} z \\ y \\ x \end{bmatrix}. \quad (16.76)$$

The generalized displacements corresponding to local coordinates ( $z, y, x$ ) at joint  $i$  are

$$\{\bar{q}_i\} = \begin{bmatrix} \bar{q}_{3i-2} & \bar{q}_{3i-1} & \bar{q}_{3i} \end{bmatrix}^T, \text{ and the generalized displacements corresponding to global coordinates } (X, Y, Z) \text{ at}$$

joint  $i$  are  $\{q_i\} = \begin{bmatrix} q_{3i-2} & q_{3i-1} & q_{3i} \end{bmatrix}^T$ . The directions of the generalized displacements coincide with the coordinate directions as is shown in figure. 16.22. It follows from the coordinate transformation eq. (16.71) that the transformation of the generalized displacements from local to global directions is

$$\begin{bmatrix} \bar{q}_{3i-2} \\ \bar{q}_{3i-1} \\ \bar{q}_{3i} \end{bmatrix} = \begin{bmatrix} \cos\theta & \sin\theta & 0 \\ -\sin\theta & \cos\theta & 0 \\ 0 & 0 & -1 \end{bmatrix} \begin{bmatrix} q_{3i-2} \\ q_{3i-1} \\ -q_{3i} \end{bmatrix} = \begin{bmatrix} \cos\theta & \sin\theta & 0 \\ -\sin\theta & \cos\theta & 0 \\ 0 & 0 & 1 \end{bmatrix} \begin{bmatrix} q_{3i-2} \\ q_{3i-1} \\ q_{3i} \end{bmatrix}. \quad (16.77)$$

In matrix notation transformation eq. (16.77) is written as

$$\{\bar{q}_i\} = [\tau] \{q_i\}, \quad (16.78)$$

where

$$[\tau] = \begin{bmatrix} \cos\theta & \sin\theta & 0 \\ -\sin\theta & \cos\theta & 0 \\ 0 & 0 & 1 \end{bmatrix}. \quad (16.79)$$

It follows from the coordinate transformation in eq. (16.76) that the transformation of the generalized displacements from global to local directions is

$$\begin{bmatrix} q_{3i-2} \\ q_{3i-1} \\ -q_{3i} \end{bmatrix} = \begin{bmatrix} \cos\theta & -\sin\theta & 0 \\ \sin\theta & \cos\theta & 0 \\ 0 & 0 & -1 \end{bmatrix} \begin{bmatrix} \bar{q}_{3i-2} \\ \bar{q}_{3i-1} \\ \bar{q}_{3i} \end{bmatrix}. \quad (16.80)$$

In matrix notation the transformation in eq. (16.80) is written as

$$\{q_i\} = [\tau]^T \{\bar{q}_i\}. \quad (16.81)$$

The matrix of direction cosines has the following properties:

$$[\tau]^T [\tau] = \begin{bmatrix} \cos\theta & -\sin\theta & 0 \\ \sin\theta & \cos\theta & 0 \\ 0 & 0 & 1 \end{bmatrix} \begin{bmatrix} \cos\theta & \sin\theta & 0 \\ -\sin\theta & \cos\theta & 0 \\ 0 & 0 & 1 \end{bmatrix} = \begin{bmatrix} \cos^2\theta + \sin^2\theta & 0 & 0 \\ 0 & \sin^2\theta + \cos^2\theta & 0 \\ 0 & 0 & 1 \end{bmatrix} = \begin{bmatrix} 1 & 0 & 0 \\ 0 & 1 & 0 \\ 0 & 0 & 1 \end{bmatrix} = [I], \quad (16.82)$$

and  $\det [\tau] = 1$ . Hence, the inverse of matrix  $[\tau]$  is equal to its transpose. Matrix  $[\tau]$  is said to be an **orthogonal matrix**.

Let  $c = \cos\theta$  and  $s = \sin\theta$ . The transformation of the displacements at joint  $j$  is the same matrix equation as at joint  $i$  except that the components of the vectors are those corresponding to joint  $j$ . Hence, the transformation of the generalized displacement vector from global to local coordinate directions for frame member  $i$ - $j$  can be written in matrix form as

$$\begin{bmatrix} \bar{q}_{3i-2} \\ \bar{q}_{3i-1} \\ \bar{q}_{3i} \\ \bar{q}_{3j-2} \\ \bar{q}_{3j-1} \\ \bar{q}_{3j} \end{bmatrix} = \begin{bmatrix} c & s & 0 & 0 & 0 & 0 \\ -s & c & 0 & 0 & 0 & 0 \\ 0 & 0 & 1 & 0 & 0 & 0 \\ 0 & 0 & 0 & c & s & 0 \\ 0 & 0 & 0 & -s & c & 0 \\ 0 & 0 & 0 & 0 & 0 & 1 \end{bmatrix} \begin{bmatrix} q_{3i-2} \\ q_{3i-1} \\ q_{3i} \\ q_{3j-2} \\ q_{3j-1} \\ q_{3j} \end{bmatrix}. \quad (16.83)$$

Equation (16.83) is written in compact form as

$$\begin{matrix} \{\bar{q}\} \\ 6 \times 1 \end{matrix} = \begin{matrix} [T] \\ 6 \times 6 \end{matrix} \begin{matrix} \{q\} \\ 6 \times 1 \end{matrix}, \quad (16.84)$$

where the 6X6 transformation matrix is

$$[T] = \begin{bmatrix} [\tau] & 0_{3 \times 3} \\ 0_{3 \times 3} & [\tau] \end{bmatrix} = \begin{bmatrix} c & s & 0 & 0 & 0 & 0 \\ -s & c & 0 & 0 & 0 & 0 \\ 0 & 0 & 1 & 0 & 0 & 0 \\ 0 & 0 & 0 & c & s & 0 \\ 0 & 0 & 0 & -s & c & 0 \\ 0 & 0 & 0 & 0 & 0 & 1 \end{bmatrix}. \quad (16.85)$$

Transformation matrix  $[T]$  is also an orthogonal matrix. That is, its determinate is equal to one and its inverse is equal to its transpose.

### 16.3.2 Frame stiffness matrix in global coordinate directions

The generalized joint force vector for frame member  $i$ - $j$  transforms from global coordinate directions to local coordinate directions in the same manner as the generalized displacement vector does for the member. Hence, from eq. (16.84) the transformation of the 6X1 generalized force vector for element  $i$ - $j$  is

$$\{\bar{Q}\} = [T]\{Q\}, \quad (16.86)$$

where the 6X1 generalized force vector in global directions is  $\{Q\} = [Q_{3i-2} \ Q_{3i-1} \ Q_{3i} \ Q_{3j-2} \ Q_{3j-1} \ Q_{3j}]^T$ .

Since the 6X6 transformation matrix is orthogonal, the inverse transformation from local to global directions is

$$\{Q\} = [T]^T\{\bar{Q}\}. \quad (16.87)$$

To obtain the 6X6 frame element stiffness matrix in global coordinate directions, substitute (16.84) for the generalized displacement vector, and substitute (16.86) for the generalized force vector, into eq. (16.66) to get

$$[T]\{Q\} = [\bar{K}][T]\{q\}. \quad (16.88)$$

Pre-multiply this equation by  $[T]^T$ , recognizing that  $[T]^T[T] = [I]$ , to get

$$\{Q\} = [T]^T[\bar{K}][T]\{q\} = [K]\{q\}. \quad (16.89)$$

The 6X6 matrix  $[K] = [T]^T[\bar{K}][T]$  is the frame member stiffness matrix in global coordinate directions, and is given by

$$[K] = \begin{bmatrix} \frac{EA}{L}c^2 + \frac{12EI}{L^3}s^2 & \left(\frac{EA}{L} - \frac{12EI}{L^3}\right)cs & \frac{6EI}{L^2}s & -\left(\frac{EA}{L}c^2 + \frac{12EI}{L^3}s^2\right) & -\left(\frac{EA}{L} - \frac{12EI}{L^3}\right)cs & \frac{6EI}{L^2}s \\ \left(\frac{EA}{L} - \frac{12EI}{L^3}\right)cs & \frac{EA}{L}s^2 + \frac{12EI}{L^3}c^2 & \frac{-6EI}{L^2}c & -\left(\frac{EA}{L}c^2 + \frac{12EI}{L^3}s^2\right) & \left(\frac{EA}{L} - \frac{12EI}{L^3}\right)cs & \frac{-6EI}{L^2}c \\ \frac{6EI}{L^2}s & \frac{-6EI}{L^2}c & \frac{4EI}{L} & \frac{-6EI}{L^2}s & \frac{6EI}{L^2}c & \frac{2EI}{L} \\ -\left(\frac{EA}{L}c^2 + \frac{12EI}{L^3}s^2\right) & -\left(\frac{EA}{L} - \frac{12EI}{L^3}\right)cs & \frac{-6EI}{L^2}s & \frac{EA}{L}c^2 + \frac{12EI}{L^3}s^2 & \left(\frac{EA}{L} - \frac{12EI}{L^3}\right)cs & \frac{-6EI}{L^2}s \\ -\left(\frac{EA}{L} - \frac{12EI}{L^3}\right)cs & -\left(\frac{EA}{L}s^2 + \frac{12EI}{L^3}c^2\right) & \frac{6EI}{L^2}c & \left(\frac{EA}{L}c^2 + \frac{12EI}{L^3}s^2\right) & \frac{EA}{L}s^2 + \frac{12EI}{L^3}c^2 & \frac{6EI}{L^2}c \\ \frac{6EI}{L^2}s & \frac{-6EI}{L^2}c & \frac{2EI}{L} & \frac{-6EI}{L^2}s & \frac{6EI}{L^2}c & \frac{4EI}{L} \end{bmatrix}. \quad (16.90)$$

The frame member  $i$ - $j$  referenced to global coordinate directions is shown in figure. 16.23.

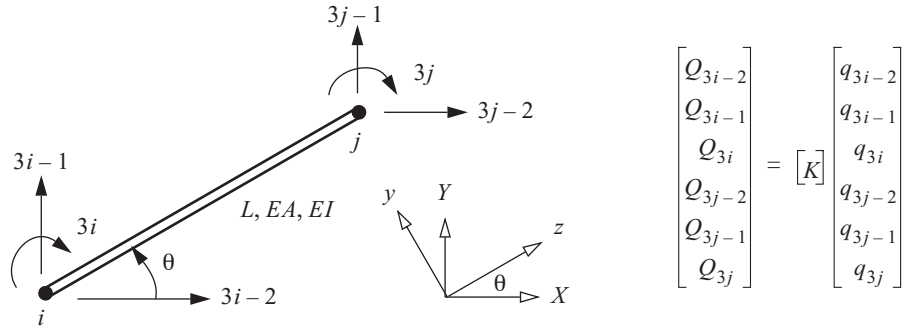


**Fig. 16.23** Frame member with an arbitrary orientation referenced to global coordinate directions.

The frame stiffness matrix (16.90) is symmetric and singular, and the diagonal elements are positive. Equilibrium of the frame member shown in figure. 16.23 for each of the six unit displacement states leads to the following relations for the elements of the stiffness matrix.

- Horizontal equilibrium:  $k_{1j} + k_{4j} = 0$ ,  $j = 1, 2, \dots, 6$ , which implies row 1 plus row 4 = 0.
- Vertical equilibrium:  $k_{2j} + k_{5j} = 0$ ,  $j = 1, 2, \dots, 6$ , which leads to row 2 plus row 5 = 0.
- Moment equilibrium about joint  $i$ :  $k_{3j} + (L \sin \theta)k_{4j} - (L \cos \theta)k_{5j} + k_{6j} = 0$ ,  $j = 1, 2, \dots, 6$ , which leads to row 3 plus  $(L \sin(\theta))$  times row 4 minus  $(L \cos(\theta))$  times row 5 plus row 6 = 0.

### 16.3.3 Frame stress matrix

The stress matrix for the frame member  $i$ - $j$  relates the internal axial force  $N$ , the transverse shear force  $V$ , and the bending moment  $M$  to the generalized joint displacement vector. We can combine the stress matrix for the truss member, eq. (16.14), and the stress matrix for the beam member, eq. (16.44), if local coordinate direction displacements are employed. With due regard for the joint numbering convention for the frame member relative to the numbering convention of the truss and beam members, the following relationship can be obtained from the stress matrices of the truss and beam members:

$$\begin{bmatrix} N \\ V \\ M \end{bmatrix}_{i-j} = \underbrace{\begin{bmatrix} -EA/L & 0 & 0 & EA/L & 0 & 0 \\ 0 & -12EI/L^3 & 6EI/L^2 & 0 & 12EI/L^3 & 6EI/L^2 \\ 0 & EI\left(\frac{6}{L^2} - \frac{12z}{L^3}\right) & EI\left(-\frac{4}{L} + \frac{6z}{L^2}\right) & 0 & EI\left(-\frac{6}{L^2} + \frac{12z}{L^3}\right) & EI\left(-\frac{2}{L} + \frac{6z}{L^2}\right) \end{bmatrix}}_{\left[\bar{S}(z)\right]_{i-j}} \begin{bmatrix} - \\ q_{3i-2} \\ - \\ q_{3i-1} \\ - \\ q_{3i} \\ - \\ q_{3j-2} \\ - \\ q_{3j-1} \\ - \\ q_{3j} \end{bmatrix}. \quad (16.91)$$

Recall that the axial coordinate  $z$  is a local coordinate in the frame element, which is zero at the beginning joint  $i$  and equal to the length  $L$  of the frame element at end joint  $j$ . The 3X6 stress matrix  $\left[\bar{S}(z)\right]_{i-j}$  (16.91) is referenced to the generalized displacement vector in local coordinate directions. The stress matrix in terms of the generalized displacement vector in global coordinate directions is obtained by substituting (16.84) for the displacement vector in eq. (16.91) to get

$$\begin{bmatrix} N \\ V \\ M \end{bmatrix}_{i-j} = \left[\bar{S}(z)\right]_{i-j} \begin{bmatrix} T \end{bmatrix}_{i-j} \begin{bmatrix} q_{3i-2} \\ q_{3i-1} \\ q_{3i} \\ q_{3j-2} \\ q_{3j-1} \\ q_{3j} \end{bmatrix} = \left[S(z)\right]_{i-j} \begin{bmatrix} q_{3i-2} \\ q_{3i-1} \\ q_{3i} \\ q_{3j-2} \\ q_{3j-1} \\ q_{3j} \end{bmatrix} \quad 0 \leq z \leq L, \quad (16.92)$$

where

$$\left[S(z)\right]_{i-j} = \begin{bmatrix} -EA/L & 0 & 0 & EA/L & 0 & 0 \\ 0 & -12EI/L^3 & 6EI/L^2 & 0 & 12EI/L^3 & 6EI/L^2 \\ 0 & EI\left(\frac{6}{L^2} - \frac{12z}{L^3}\right) & EI\left(-\frac{4}{L} + \frac{6z}{L^2}\right) & 0 & EI\left(-\frac{6}{L^2} + \frac{12z}{L^3}\right) & EI\left(-\frac{2}{L} + \frac{6z}{L^2}\right) \end{bmatrix} \begin{bmatrix} c & s & 0 & 0 & 0 & 0 \\ -s & c & 0 & 0 & 0 & 0 \\ 0 & 0 & 1 & 0 & 0 & 0 \\ 0 & 0 & 0 & c & s & 0 \\ 0 & 0 & 0 & -s & c & 0 \\ 0 & 0 & 0 & 0 & 0 & 1 \end{bmatrix}.$$

Perform the matrix multiplication in the last equation to find

$$\left[S(z)\right]_{i-j} = \begin{bmatrix} -cEA/L & -sEA/L & 0 & cEA/L & sEA/L & 0 \\ s12EI/L^3 & -c12EI/L^3 & 6EI/L^2 & -s12EI/L^3 & c12EI/L^3 & 6EI/L^2 \\ -EIs\left(\frac{6}{L^2} - \frac{12z}{L^3}\right) & EIs\left(\frac{6}{L^2} - \frac{12z}{L^3}\right) & EI\left(-\frac{4}{L} + \frac{6z}{L^2}\right) & -EIs\left(-\frac{6}{L^2} + \frac{12z}{L^3}\right) & EIs\left(-\frac{6}{L^2} + \frac{12z}{L^3}\right) & EI\left(-\frac{2}{L} + \frac{6z}{L^2}\right) \end{bmatrix}_{i-j}. \quad (16.93)$$

The 3X6 stress matrix  $\left[S(z)\right]_{i-j}$ ,  $0 \leq z \leq L$ , for the frame member relates the internal actions in local coordinate directions  $z$  and  $y$  to the generalized displacement vector in global coordinate directions.

**Example 16.8 Portal frame**

The coplanar rectangular frame shown in figure. 16.24 consists of three members: 1-2, 2-3, and 3-4. Joints 1 and 4 are restrained against displacement and rotation. At joint 2 there is a rigid connection between members 1-2 and 2-3, and at joint 3 there is a rigid connection between members 2-3 and 3-4. Joints 2 and 3 are moveable, and the generalized displacement vector for these joints is  $\{q_\alpha\} = [q_4 \ q_5 \ q_6 \ q_7 \ q_8 \ q_9]^T$ . Each member has a cross-sectional area  $A = 1,500 \text{ mm}^2$ , second area moment  $I = 2.8 \times 10^6 \text{ mm}^4$ , and the same modulus of elasticity  $E = 70 \times 10^3 \text{ N/mm}^2$ . The direction cosines for member 1-2 are  $(c, s) = (0, 1)$ , for member 2-3  $(c, s) = (1, 0)$ , and for member 3-4  $(c, s) = (0, -1)$ . Determine the generalized displacements of the movable joints 2 and 3, and the bending moment in each member.

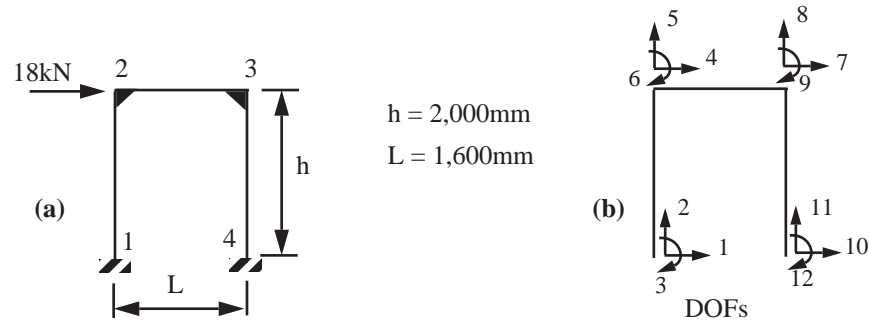


**Fig. 16.24 (a) Portal frame. (b) Degree of freedom numbering.**

The stiffness matrix (16.90) for each member including only the generalized displacements of joints 2 and 3 are as follows:

$$[K_{1-2}] = \begin{bmatrix} q_4 & q_5 & q_6 \\ (12EI)/h^3 & 0 & (-6EI)/h^2 \\ 0 & (EA)/h & 0 \\ (-6EI)/h^2 & 0 & (4EI)/h \end{bmatrix} = \begin{bmatrix} q_4 & q_5 & q_6 \\ 294. & 0 & -294,000 \\ 0 & 52,500 & 0 \\ -294,000 & 0 & 3.92 \times 10^8 \end{bmatrix}, \quad (a)$$

$$[K_{2-3}] = \begin{bmatrix} q_4 & q_5 & q_6 & q_7 & q_8 & q_9 \\ (EA)/L & 0 & 0 & (-EA)/L & 0 & 0 \\ 0 & (12EI)/L^3 & (-6EI)/L^2 & 0 & (-12EI)/L^3 & (6EI)/L^2 \\ 0 & (-6EI)/L^2 & (4EI)/L & 0 & (6EI)/L^2 & (2EI)/L \\ (-EA)/L & 0 & 0 & (EA)/L & 0 & 0 \\ 0 & (-12EI)/L^3 & (6EI)/L^2 & 0 & (12EI)/L^3 & (-6EI)/L^2 \\ 0 & (6EI)/L^2 & (2EI)/L & 0 & (-6EI)/L^2 & (4EI)/L \end{bmatrix},$$

$$\begin{aligned}
[K_{2-3}] &= \begin{bmatrix} q_4 & q_5 & q_6 & q_7 & q_8 & q_9 \\ 65,625 & 0 & 0 & -65,625 & 0 & 0 \\ 0 & 574.219 & -459,375 & 0 & -574.219 & -459,375 \\ 0 & -459,375 & 4.9 \times 10^8 & 0 & 459,375 & 2.45 \times 10^8 \\ -65,625 & 0 & 0 & 65,625 & 0 & 0 \\ 0 & -574.219 & 459,375 & 0 & 574.219 & 459,375 \\ 0 & -459,375 & 2.45 \times 10^8 & 0 & 459,375 & 4.9 \times 10^8 \end{bmatrix}, \text{ and} \quad (b) \\
[K_{3-4}] &= \begin{bmatrix} q_7 & q_8 & q_9 \\ (12EI)/h^3 & 0 & (6EI)/h^2 \\ 0 & (EA)/h & 0 \\ (6EI)/h^2 & 0 & (4EI)/h \end{bmatrix} = \begin{bmatrix} q_7 & q_8 & q_9 \\ 294,000 & 0 & 294,000 \\ 0 & 52,500 & 0 \\ 294,000 & 0 & 3.92 \times 10^8 \end{bmatrix}. \quad (c)
\end{aligned}$$

The restrained structural stiffness matrix is obtained by the sum of the member stiffness matrices in eqs.(a), (b), and (c) with due regard to the location of the matrix elements from the individual members to their place in the restrained stiffness matrix. The result is

$$[K_{\alpha\alpha}] = \begin{bmatrix} q_4 & q_5 & q_6 & q_7 & q_8 & q_9 \\ 65,919 & 0 & -294,000 & -65,625 & 0 & 0 \\ 0 & 53,074.2 & -459,375 & 0 & -574.219 & -459,375 \\ -294,000 & -459,375 & 8.82 \times 10^8 & 0 & 459,375 & 2.45 \times 10^8 \\ -65,625 & 0 & 0 & 65,919 & 0 & -294,000 \\ 0 & -574.219 & 459,375 & 0 & 53,074.2 & 459,375 \\ 0 & -459,375 & 2.45 \times 10^8 & -294,000 & 459,375 & 8.82 \times 10^8 \end{bmatrix}. \quad (d)$$

The prescribed external load vector is  $\{Q_\alpha\} = [Q_4 \ Q_5 \ Q_6 \ Q_7 \ Q_8 \ Q_9]^T = [18,000 \text{ N} \ 0 \ 0 \ 0 \ 0 \ 0]^T$ , and the matrix equation to determine the generalized displacements is  $\{Q_\alpha\} = [K_{\alpha\alpha}]\{q_\alpha\}$ . The solution for the generalized displacements from the latter equation is

$$\begin{aligned}
q_4 &= 41.6931 \text{ mm} & q_5 &= 0.18859 \text{ mm} & q_6 &= 0.0110439 \text{ rad.} \\
q_7 &= 41.5561 \text{ mm} & q_8 &= -0.18859 \text{ mm} & q_9 &= 0.0109807 \text{ rad.} \quad (e)
\end{aligned}$$

The bending moment in member 1-2 is determined from its stress matrix (16.93) and the generalized displacement vector for the member. Reading the third row of the stress matrix determines the bending moment as

$$(M_x)_{1-2} = [-EI(6/h^2 - 12z/h^3) \ 0 \ EI(-4/h + 6z/h^2) \ -EI(-6/h^2 + 12z/h^3) \ 0 \ EI(-2/h + 6z/h^2)] \{q_{1-2}\}, \quad (f)$$

where  $\{q_{1-2}\} = [0 \ 0 \ 0 \ q_4 \ q_5 \ q_6]^T$ . Numerical evaluation results in

$$\begin{aligned}
(M_x)_{1-2} &= (294,000 - 294z)q_4 + (-1.96 \times 10^8 + 294,000z)q_6 = 1.00931 \times 10^7 - 9,010.84z \\
&0 \leq z \leq 2,000 \text{ mm}
\end{aligned}$$



(g)

Following the same procedure for members 2-3 and 3-4 we find

$$(M_x)_{2-3} = (459,375 - 574.219z)q_5 + (-4.9 \times 10^8 + 459,375z)q_6 + (-459,375 + 574.219z)q_8 + (-2.45 \times 10^8 + 459,375z)q_9 = -7.92854 \times 10^6 + 9,900.99z \quad 0 \leq z \leq 1,600 \text{ mm} \quad , \text{ and} \quad (\text{h})$$

$$(M_x)_{3-4} = (294,000 - 294z)q_7 + (-3.92 \times 10^8 + 294,000z)q_9 = 7.91305 \times 10^6 - 8,989.16z, \quad 0 \leq z \leq 2,000 \text{ mm} \quad . \quad (\text{i})$$

The bending moment in each member is plotted with respect to the axial coordinate in figure. 16.25. The bending moment distribution is linear in each member and it passes through zero as it changes sign. ■

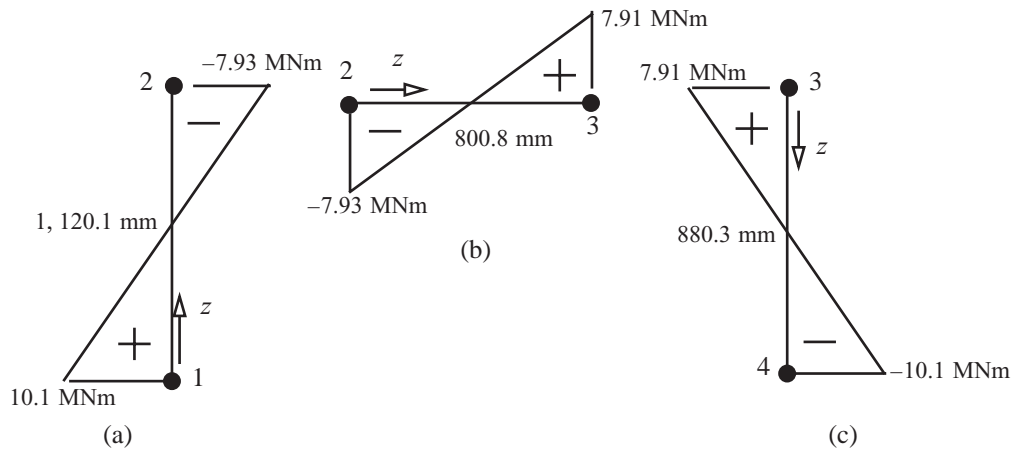
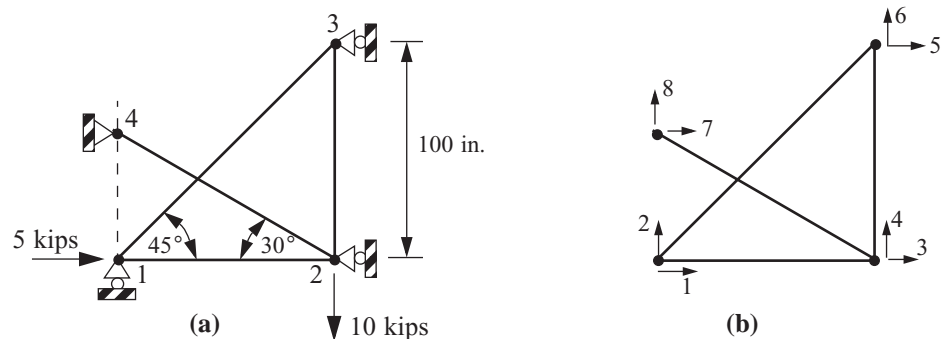


**Fig. 16.25** Bending moments in the members of the portal frame: (a) member 1-2, (b) member 2-3, (c) member 3-4.

## 16.4 Practice exercises

1. Consider the plane truss restrained against rigid body motion and subject to the loads shown in figure. 16.26(a). Use the degree of freedom numbering convention based on the joint numbering as shown in figure.

**Fig. 16.26**  
(a) Truss with four joints and four members.  
(b) Degree of freedom numbering.



16.26(b). All four bars have the same modulus of elasticity  $E = 10 \times 10^6$  psi, and the same  $A/L$  where the cross-

sectional area for bar 1-2 is  $0.5 \text{ in.}^2$ . Solve by hand the computations for the

- unrestrained structural stiffness matrix,
- restrained structural stiffness matrix, and
- unknown joint displacements.

2. Consider the plane truss consisting of five bars shown in figure. 16.27(a). Each bar has the same extensional stiffness  $EA$ . Use the degree of freedom numbering convention based on the joint numbers labeled in the figure.

- Determine the unrestrained structural stiffness matrix.
- Joints 1 and 3 are restrained such that  $q_1 = q_2 = q_6 = 0$ , and it is assumed the loads are applied in the remaining degrees of freedom. Determine the submatrix  $[K_{\beta\alpha}]$ .

3. For the seven-bar truss shown in figure. 16.27(b) all bars have the same value for  $EA/L$ . The horizontal displacement of joint 5 is prescribed as  $q_9 = 1$ . All applied forces are zero. Use symmetry to reduce the order of the restrained structural stiffness matrix  $[K_{\alpha\alpha}]$  and then determine the unknown nodal displacements  $q_3, q_4, q_5$ , and  $q_6$ .

4. In the three-bar truss shown in figure. 16.27(c) the temperature of bar 1-2 is increased  $100^\circ\text{C}$  above ambient temperature, while bars 1-3 and 1-4 remain at ambient temperature. The bars are made of aluminum alloy with a modulus of elasticity  $E = 69 \text{ GPa}$  and coefficient of thermal expansion  $\alpha = 23.6 \times 10^{-6}/^\circ\text{C}$ . The length of each bar  $L = 250 \text{ mm}$ , and the cross-sectional area of each bar  $A = 400 \text{ mm}^2$ . Determine

- the  $8 \times 1$  fixed-end action vector,
- the  $8 \times 8$  unrestrained structural stiffness matrix,
- the joint displacements  $q_1$  and  $q_2$  of movable joint 1,
- the support reactions, and
- the bar forces. State if they are in tension or compression.

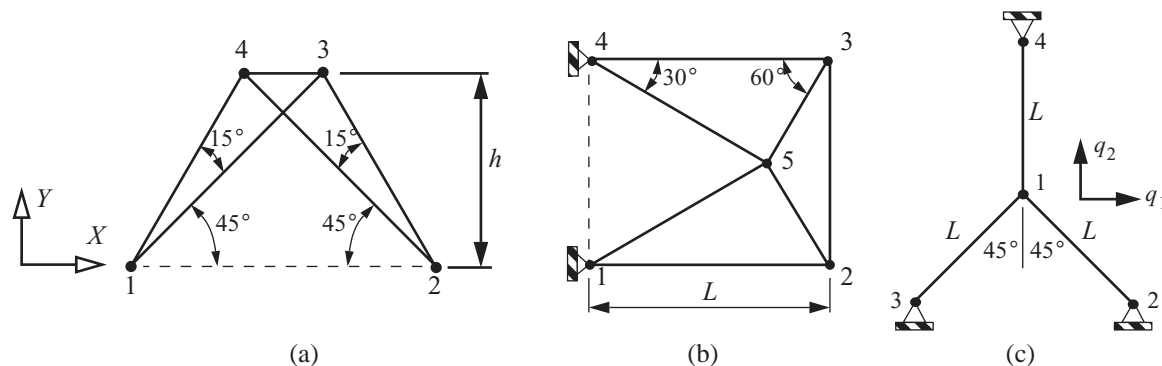
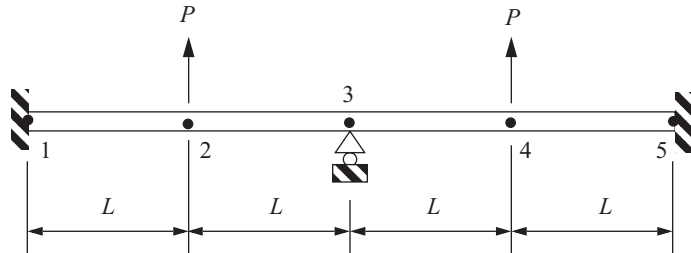


Fig. 16.27 Truss configurations. (a) Exercise 2. (b) Exercise 3. (c) Exercise 4.

5. The uniform, multispan beam shown in figure. 16.28 is clamped at each end and subject to vertical point loads at joints 2 and 4. Use the joint numbers indicated in the figure, and the degree of freedom numbering convention associated with the joint numbers.

Fig. 16.28 Multispan beam.



- Use symmetry to reduce the problem size and compute the joint displacement vector in terms of  $P$ ,  $L$ , and  $EI$ .
  - Determine the shear force and bending moment distributions in each span in terms of  $P$  and  $L$ . Sketch the shear force and bending moment diagrams.
  - Determine the support reactions.
6. The flexural stiffness of the uniform beam shown in figure. 16.29 is  $EI$ , and it has a length  $2L$ . It is supported by linear elastic springs at each end, each with a stiffness  $k = 6EI/L^3$ . It is subject to the linearly varying distributed load whose intensity is  $f_{y1}$  at midspan.

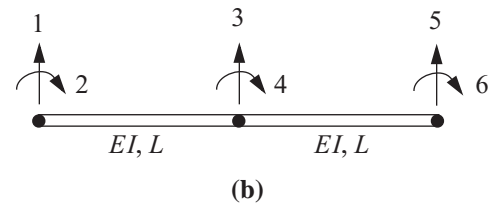
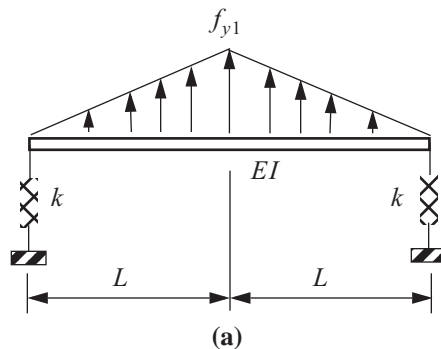
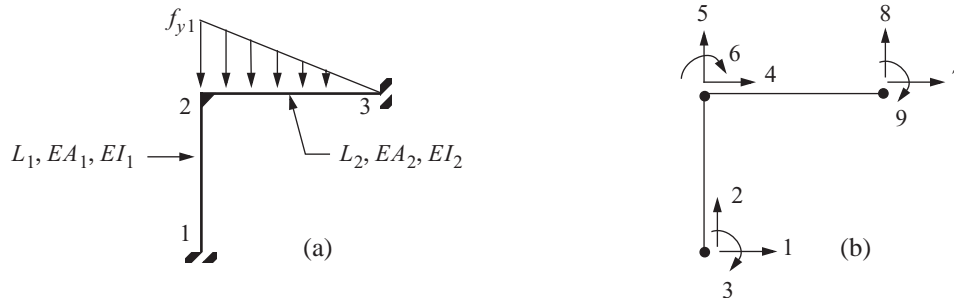


Fig. 16.29 (a) Beam with spring supports. (b) Degree of freedom numbering.

Use two members to model the beam, and use the degrees of freedom (DOFs) numbering shown in the figure.

- Use symmetry about the vertical centerline and determine the restrained structural stiffness matrix in DOFs 1, 2, and 3, and in terms of parameters  $EI$  and  $L$ .
  - Determine the  $6 \times 1$  fixed-end action vector  $\{Q^0\}$  in terms of  $f_{y1}$  and  $L$ .
  - Solve for the unknown joint displacement vector  $[q_1 \ q_2 \ q_3 \ q_4 \ q_5 \ q_6]^T$  in terms of  $EI$ ,  $L$ , and  $f_{y1}$ .
7. Consider the frame shown in figure. 16.30(a) consisting of a vertical bar 1-2 and a horizontal bar 2-3, which are joined together by a rigid connection at joint 2. The ends of the bars opposite to their common joint are

clamped. The horizontal bar 1-2 is subject to a linearly distributed load. The degree of freedom numbering convention is shown in figure. 16.30(b).



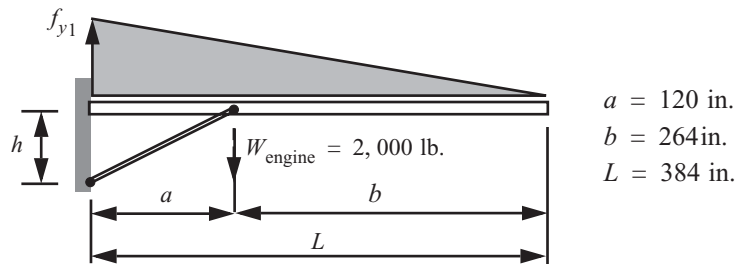
**Fig. 16.30 (a) Frame configuration. (b) Degree of freedom numbering.**

- Determine the restrained structural stiffness matrix  $[K_{\alpha\alpha}]$ .
- Determine the 9X1 fixed-end action vector  $\{Q^0\}$ .

8. Consider the model of a strut-braced wing spar shown in figure. 16.31 subject to the span-wise air load approximated as a linearly varying distributed line load. The intensity of the distributed load at the root

$f_{y1} = 130.2083 \text{ lb./in.}$  and the resultant lift acting on the spar is  $\frac{1}{2}f_{y1}(32 \times 12) = 25,000 \text{ lb.}$

**Fig. 16.31**  
**Strut-braced wing spar.**



The spar is clamped at the root and free at the tip, and the strut is pinned-connected to the spar and the support. The matrix structural model consists of three members as shown in figure. 16.32(a). Since the air load bends the spar which in turn stretches the strut, the structure is modeled with a frame member between joints 1 and 2, a beam member between joints 2 and 3, and a truss bar between joints 2 and 4. The degree of freedom numbering convention is shown in figure. 16.32(b).

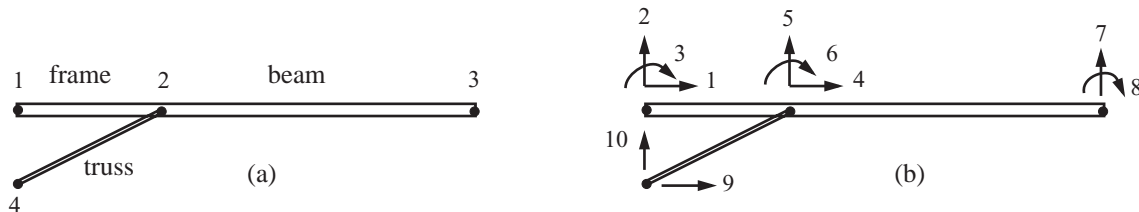


**Fig. 16.32 (a) Joint numbers for a three-member model. (b) Degrees of freedom.**

- Determine the fixed-end action vector  $\{Q^0\}$  and its partitions  $\{Q_{\alpha}^0\}$  and  $\{Q_{\beta}^0\}$ . The  $\alpha$ -indices are 4,

5, 6, 7, and 8, and the  $\beta$  -indices are 1, 2, 3, 9, and 10.

- b) Additional numerical data are listed in table 16.7. Determine the unknown nodal displacements.

**Table 16.7 Additional numerical data for the strut-braced wing**

$h$ , vertical distance from the spar centroid to lower strut support	60 in.
$A$ , cross-sectional area of the spar	23.88 in. <sup>2</sup>
$I_{xx}$ , second area moment of the cross section of the spar	872.716 in. <sup>4</sup>
$A_s$ , cross-sectional area of the strut (1.75 in. diameter)	2.40528 in. <sup>2</sup>
$L$ , wing lift	25,000 lb.
$E$ , modulus of elasticity for the spar and strut material	$10 \times 10^6$ lb./in. <sup>2</sup>



The direct stiffness method presented in chapters 15 and 16 developed matrix structural analyses for the linear elastic response of truss and frame members connected at a finite number of joints. Engineering bar theory modeled the frame members so that the deflection and stresses were readily computed in the member once the generalized displacements of the joints were determined by matrix methods. The direct stiffness method is a finite element method applied to trusses and frames. In the finite element method the joints are called nodes and the members are called elements. The development of the finite element method arose out of the need to determine influence coefficients for semimonocoque construction used in aerospace structures. Stiffened shells and flat plates are continuum structures with an infinite number of interconnection points. In this chapter we present the finite element method to continuum structures in one dimension. Developments for two- and three-dimensional continuum formulations are found in the large literature on the finite element method. We mention only two of the many references on finite elements for engineering students: Reddy (2019), and Huebner, Thornton, and Byrom (1995).

### 17.1 Elastic bar subject to axial loads

The presentation in this section follows, in part, that given by Szabo and Babuska (1991). A prismatic bar of

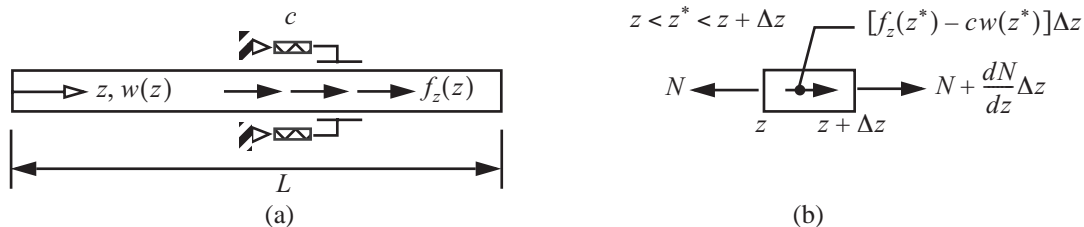


**Fig. 17.1** (a) Elastic bar subject to axial loading. (b) Free body of a segment of length  $\Delta z$ .

length  $L$  and a cross-sectional area  $A$  is shown in figure 17.1(a). The bar is made of a homogeneous, linear elastic material whose modulus of elasticity is denoted by  $E$  and its coefficient of thermal expansion by  $\alpha$ . Let the axial

displacement function be denoted by  $w(z)$  where  $z$  is the axial coordinate and  $0 \leq z \leq L$ . Prescribed external loads consist of an axial distributed load with intensity  $f_z(z)$  (F/L) and a change in temperature that is independent of the contour coordinate  $s$  but a function of the axial coordinate  $z$  (i.e.,  $\Delta T(s, z) = \tau_0(z)$ ). The bar is restrained by a distributed spring proportional to the axial displacement with an intensity given by  $-cw(z)$  and  $c \geq 0$  (F/L<sup>2</sup>). A free body diagram of a segment of the bar is shown in figure 17.1(b). The internal axial normal force is denoted by  $N(z)$ . Axial equilibrium of the segment as  $\Delta z \rightarrow 0$  leads to the differential equation

$$-\left(\frac{dN}{dz}\right) + cw = f_z(z) \quad 0 < z < L. \quad (17.1)$$

Hooke's law including the prescribed thermal force is  $N + N_T = EA dw/dz$ , where  $N_T = EA\alpha\tau_0(z)$ . Thus,

$$N = EA\left(\frac{dw}{dz} - \alpha\tau_0\right). \quad (17.2)$$

Substitute (17.2) for the axial force in equilibrium equation (17.1) to get the governing differential equation for axial displacement  $w(z)$  as

$$-\frac{d}{dz}\left[EA\left(\frac{dw}{dz} - \alpha\tau_0\right)\right] + cw = f_z(z). \quad (17.3)$$

The boundary conditions at  $z = 0$  and  $z = L$  are to prescribe either the displacement  $w$  or the axial normal force  $N$ . The displacement prescribed at the boundary is also called the essential boundary condition and the force prescribed at the boundary is called the natural boundary condition.

Multiply (17.3) by an arbitrary axial displacement function  $\bar{w}(z)$  and integrate:

$$-\int_0^L \left\{ \frac{d}{dz} \left[ EA \left( \frac{dw}{dz} - \alpha\tau_0 \right) \right] - cw \right\} \bar{w}(z) dz = \int_0^L f_z(z) \bar{w}(z) dz. \quad (17.4)$$

Integrate the left-hand side of the previous equation by parts:

$$-\left\{ N\bar{w} \Big|_{z=L} - N\bar{w} \Big|_{z=0} - \int_0^L \left[ EA \left( \frac{dw}{dz} - \alpha\tau_0 \right) \right] \frac{d\bar{w}}{dz} + cw\bar{w} \right\} dz = \int_0^L f_z(z) \bar{w}(z) dz. \quad (17.5)$$

Rearrange the terms in eq. (17.5) to get

$$\int_0^L \left\{ EA \frac{dw}{dz} \frac{d\bar{w}}{dz} + cw\bar{w} \right\} dz = \int_0^L f_z(z) \bar{w}(z) dz + N\bar{w} \Big|_{z=L} - N\bar{w} \Big|_{z=0} + \int_0^L \left( EA \frac{d\bar{w}}{dz} \right) \alpha\tau_0 dz. \quad (17.6)$$

If the governing boundary value problem for  $w(z)$  (17.3) is satisfied, then (17.6) is also satisfied for any  $\bar{w}(z)$  for which the operations in (17.6) are defined. Note that in (17.6) the highest derivative of the displacement is  $dw/dz$ , whereas the highest derivative in the differential equation (17.3) is  $\frac{d^2 w}{dz^2}$ . Integration by parts results in



a derivative of one less in  $w(z)$  than what occurs in the differential equation. Equation (17.6) is called the **weak form** of the differential equation (17.3).

In the finite element method the function  $w(z)$  is called a **trial function**. The function  $\bar{w}(z)$  is called a **test function** or a **virtual displacement**, and  $d\bar{w}/dz$  is the virtual strain. Function  $\bar{w}(z)$  is called a virtual displacement because it is not the actual physical displacement, but merely a hypothetical, admissible displacement. Each term in (17.6) represents virtual work, that is, the work done by the internal action  $EAdw/dz$  through the virtual strain, work done by the distributed spring through the virtual displacement, work done by the prescribed distributed load and boundary forces through the virtual displacement, and the work of the virtual thermal force  $EAdw/dz$  due to the prescribed thermal strain  $\alpha\tau_0$ . Define

$$B[w, \bar{w}] = \int_0^L \left\{ EA \frac{dw}{dz} \frac{d\bar{w}}{dz} + c w \bar{w} \right\} dz, \text{ and} \quad (17.7)$$

$$F[\bar{w}] = \int_0^L f_z(z) \bar{w}(z) dz + N\bar{w}|_{z=L} - N\bar{w}|_{z=0} + \int_0^L \left( EA \frac{d\bar{w}}{dz} \right) \alpha\tau_0 dz. \quad (17.8)$$

The bilinear form  $B[w, \bar{w}]$  associates a real number with any two functions  $w(z)$  and  $\bar{w}(z)$ , and the linear form  $F[\bar{w}]$  associates a real number for any function  $\bar{w}(z)$ . The bilinear form  $B[w, \bar{w}]$  represents the internal virtual work and the linear form  $F[\bar{w}]$  represents the external virtual work. Let  $U[w]$  denote the portion of the strain energy due to mechanical strain<sup>1</sup> and that from the distributed spring. The expression for the strain energy is

$$U[w] = \frac{1}{2} \int_0^L \left\{ EA \left( \frac{dw}{dz} \right)^2 + c w^2 \right\} dz = \frac{1}{2} B[w, w]. \quad (17.9)$$

All continuous functions  $w(z)$  defined on the open interval  $\Omega = \{z | 0 < z < L\}$  have a finite strain energy  $0 \leq U < \infty$ , and  $U = 0$  only if  $w(z) = 0$  on  $\Omega$ . The conditions that restrict the set of all continuous functions having a finite strain energy are called displacement, kinematic, and essential boundary conditions. For example, if it is prescribed that the trial function  $w(0) = q_1$  where  $q_1$  has a numerical value, and the total displacement at  $z = 0$  is  $w(0) + \bar{w}(0) = q_1$ , then the virtual displacement  $\bar{w}(0) = 0$ . The external virtual work for  $\bar{w}(0) = 0$  reduces to

$$F[\bar{w}] = \int_0^L f_z(z) \bar{w}(z) dz + N\bar{w}|_{z=L} + \int_0^L \left( EA \frac{d\bar{w}}{dz} \right) \alpha\tau_0 dz. \quad (17.10)$$

For displacement prescribed boundary conditions the virtual displacement must vanish at the boundaries. Kinetically admissible trial functions  $w(z)$  are continuous, single valued, and equal the prescribed displacement boundary conditions.

1. Refer to eq. (5.81) on page 145.

The **principle of virtual work** is to find a kinematically admissible displacement function  $w(z)$  such that

$$B[w, \bar{w}] = F[\bar{w}] \quad \text{for all kinematically admissible } \bar{w}(z). \quad (17.11)$$

The principle of virtual work (17.11) is a statement of equilibrium for the linear elastic bar, and it depends on the boundary conditions. The trial function  $w(z)$  is selected to satisfy displacement boundary conditions, if any, on the closed domain  $\bar{\Omega} = \{z | 0 \leq z \leq L\}$ . In the applications of the principle of virtual work it is not practical to consider an infinite number of kinematically admissible test functions. Instead, a subset of kinematically admissible functions is assumed. For example, polynomials in  $z$  are often selected because they are easy to differentiate and integrate. Consider an approximate polynomial for the trial function  $w(z)$  and a similar polynomial for the test function  $\bar{w}(z)$  by selecting

$$w(z) = a_1 + a_2 z + a_3 z^2 \quad \text{and} \quad \bar{w}(z) = b_1 + b_2 z + b_3 z^2. \quad (17.12)$$

Unknown coefficients  $a_i$  in the trial function are determined from the principle of virtual work for every choice of the coefficients  $b_i$ ,  $i = 1, 2, 3$ , in the test function. Coefficients  $b_i$  are independent of the coefficients  $a_i$  in the trial function.

### Example 17.1 An approximate solution by the principle of virtual work

Dimensional and material data for the bar shown in figure 17.1 are  $L = 500$  mm,  $A = 400$  mm<sup>2</sup>,  $E = 70,000$  N/mm<sup>2</sup>,  $\alpha = 23 \times 10^{-6}/(^{\circ}\text{C})$ , and  $c = 5 \times 10^3$  N/mm<sup>2</sup>. Uniform external loads are prescribed as  $f_z(z) = 0$  and a prescribed change in temperature  $\tau_0(z) = 40^{\circ}\text{C}$  for  $0 < z < L$ . Boundary conditions are  $w(0) = q_1 = -0.20$  mm and  $N(L) = F_L = -40,000$  N. Assume the trial and test functions for the displacements as

$$w(z) = q_1 + a_1 z \quad \text{and} \quad \bar{w}(z) = b_1 z. \quad (a)$$

Note that the trial function  $w(z)$  satisfies the prescribed displacement boundary condition at  $z = 0$ , and that the test function, or virtual displacement function,  $\bar{w}(z)$  vanishes at  $z = 0$ . The internal virtual work (17.7) is

$$B[w, \bar{w}] = \int_0^L \{EA(a_1)(b_1) + c(q_1 + a_1 z)(b_1 z)\} dz = b_1[(EAL + cL^3/3)a_1 + (cL^2/2)q_1], \quad (b)$$

The external virtual work (17.8) is

$$F[\bar{w}] = N(L)(\bar{w}(L)) + \int_0^L \left(EA \frac{d\bar{w}}{dz}\right) \alpha \tau_0 dz = b_1[LF_L + EAL\alpha\tau_0]. \quad (c)$$

The principle of virtual work (17.11) for the assumed displacement functions is

$$b_1[(EAL + cL^3/3)a_1 + (cL^2/2)q_1] = b_1[LF_L + EAL\alpha\tau_0] \quad \forall b_1 \neq 0. \quad (d)$$

Hence, the equation to determine coefficient  $a_1$  is

$$(EAL + (cL^3)/3)a_1 + (cL^2/2)q_1 = LF_L + EAL\alpha\tau_0. \quad (\text{e})$$

Solve (e) for  $a_1$  to get

$$a_1 = \frac{3(2FL - cLq_1 + 2EA\alpha\tau_0)}{2(3EA + cL^2)} = 530.195 \times 10^{-6}. \quad (\text{f})$$

Note that  $a_1$  is dimensionless. The following equations are the results for the axial displacement in eq. (a), axial normal force in eq. (17.2), and the strain energy in eq. (17.9):

$$w(z) = -0.20 + (530.195 \times 10^{-6})z \quad 0 \leq z \leq 500 \text{ mm}. \quad (\text{g})$$

$$N = EA[530.195 \times 10^{-6} - (23. \times 10^{-6} / ^\circ\text{C})40^\circ\text{C}] = -10,914.5 \text{ N} \quad 0 \leq z \leq 500 \text{ mm}, \quad (\text{h})$$

$$U[w] = \frac{1}{2} \int_0^L \left\{ EA \left( \frac{dw}{dz} \right)^2 + cw^2 \right\} dz = \frac{1}{2} \int_0^L \{ EA(a_1)^2 + c(q_1 + a_1 z)^2 \} dz = 14,975.3 \text{ N-mm}. \quad (\text{i})$$

The exact solution to the differential equation (17.3) subject to the prescribed external loads and the prescribed boundary conditions is

$$w_{\text{ex}}(z) = -0.20 \cosh \lambda z + 0.199904 \sinh \lambda z \quad 0 \leq z \leq 500 \text{ mm}, \quad (\text{j})$$

where  $\lambda = \sqrt{c/(EA)} = 0.0133631 \text{ mm}^{-1}$ . The axial normal force and strain energy for the exact solution are

$$N_{\text{ex}} = -25,760 + 74,797.2 \cosh \lambda z - 74,833.1 \sinh \lambda z \quad 0 \leq z \leq 500 \text{ mm}, \text{ and} \quad (\text{k})$$

$$U_{\text{ex}} = 7,754.26 \text{ N-mm}. \quad (\text{l})$$

The strain energy of the approximate solution exceeds that of the exact solution. The error in the strain energy is

$$\frac{(U - U_{\text{ex}})100}{U_{\text{ex}}} = 93.1\%. \quad (\text{m})$$

At  $z = L$ ,  $N_{\text{ex}} = -40,000 \text{ N}$  and for the approximate solution  $N = -10,914.5 \text{ N}$ , an error of  $-72.7$  percent. Graphs of the axial displacement distribution and axial force distribution are shown in figure 17.2 and figure 17.3, respectively.

**Fig. 17.2** Axial displacement distribution for example 17.1. The exact solution is compared to the approximate solution by the principle of virtual work.

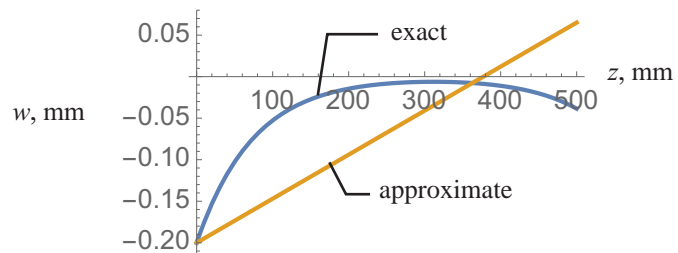
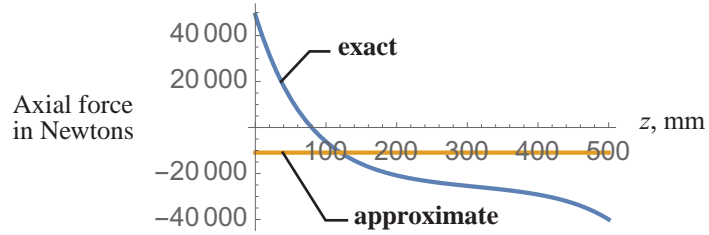


**Fig. 17.3** Axial normal force distribution in Newtons for example 17.1. The exact solution compared to the approximate solution.



The displacement and axial force in the approximate solution do not compare well with the exact solution. Including polynomial terms of higher degree for the trial function and test functions (a) results in improved approximate solutions. Rather than selecting polynomials of higher degree in the principle of virtual work, consider a finite element approximation using piecewise, linear polynomials as is discussed next in article 17.2. ■

## 17.2 Finite elements in one dimension

As stated in eq. (17.11) the principle of virtual work applies over the whole domain  $\Omega$  of the bar. However, the principle of virtual work can also be applied to subdomains of the bar. In the finite element method we partition  $\Omega$  into subdomains called finite elements. Partitions are called meshes, and finite element meshes are characterized by the selection of nodal points. Consider the mesh

$$0 = z_1 < z_2 < z_3 < \dots < z_M < z_{M+1} = L, \quad (17.13)$$

where  $M$  denotes the number of elements and  $M+1$  is the number of nodes. The  $k$ th element is denoted by

$$\Omega_k = \{z | z_k \leq z \leq z_{k+1}\} \quad k = 1, 2, \dots, M. \quad (17.14)$$

Each element is mapped onto a standard element denoted by

$$\Omega_{st} = \{\xi | -1 < \xi < 1\}. \quad (17.15)$$

The standard element is mapped onto the  $k$ th element by

$$z = \eta_1(\xi)z_k + \eta_2(\xi)z_{k+1}, \text{ where } \eta_1(\xi) = (1 - \xi)/2 \text{ and } \eta_2(\xi) = (1 + \xi)/2. \quad (17.16)$$

The inverse mapping is

$$\xi = \frac{2z - z_k - z_{k+1}}{z_{k+1} - z_k} = \frac{2z - z_k - z_{k+1}}{h_k} \quad z \in \Omega_k. \quad (17.17)$$

The length of the element is denoted by  $h_k$  where  $h_k = z_{k+1} - z_k$ . Functions  $\eta_i(\xi)$ ,  $i = 1, 2$ , are called **shape functions** or **interpolation functions**, which have the properties

$$\eta_1(-1) = 1 \quad \eta_1(1) = 0 \quad \eta_2(-1) = 0 \quad \eta_2(1) = 1. \quad (17.18)$$

Kinematic admissibility requires the displacement function  $w(z)$  to be continuous between elements and within an element. Continuity insures the derivative of the displacement is a square integrable function on  $\Omega$  so

that the strain energy (17.9) is finite. The displacement in the  $k$ th element is denoted by  $w^{(k)}(z)$ ,  $z \in \Omega_k$ . Let the displacements at the nodes  $z_k$  and  $z_{k+1}$  be denoted by  $w^{(k)}(z_k) = q_k$  and  $w^{(k)}(z_{k+1}) = q_{k+1}$ , respectively. A linear polynomial in the axial coordinate with two coefficients is sufficient to interpolate the displacement at the two nodes, and it meets the continuity requirement within the element. The simple choice is to use the same linear interpolation functions for the displacement of the  $k$ th element as were used to interpolate coordinate  $z \in \Omega_k$  (17.16). Hence, the trial function for the axial displacement of the  $k$ th element is

$$w^{(k)} = \eta_1(\zeta)q_k + \eta_2(\zeta)q_{k+1} \quad \zeta \in \Omega_{st}. \quad (17.19)$$

At node  $z_{k+1}$  the displacement from the end of the  $k$ th element is  $w^{(k)}(z_{k+1}) = \eta_2(1)q_{k+1} = q_{k+1}$ , and the beginning displacement of the  $k+1$  element is  $w^{(k+1)}(z_{k+1}) = \eta_1(-1)q_{k+1} = q_{k+1}$ . Thus, interelement continuity is satisfied. The virtual displacement for the  $k$ th element is assumed to be the same functional form as the trial function:

$$\bar{w}^{(k)} = \eta_1(\zeta)b_k + \eta_2(\zeta)b_{k+1} \quad \zeta \in \Omega_{st}, \quad (17.20)$$

where coefficients  $b_k$  are independent of the trial function.

The axial strain in the  $k$ th element is  $\varepsilon^{(k)} = \frac{dw^{(k)}}{dz}$ . By the chain rule and the inverse mapping (17.17) we transform the derivative with respect to  $z$  to the derivative with respect to  $\zeta$  by

$$\frac{d}{dz} = \frac{d}{d\zeta} \frac{d\zeta}{dz} = \left(\frac{2}{h_k}\right) \frac{d}{d\zeta}. \quad (17.21)$$

Thus, the strain in the  $k$ th element is

$$\varepsilon^{(k)} = \frac{dw^{(k)}}{dz} = \left(\frac{dw^{(k)}}{d\zeta}\right)\left(\frac{d\zeta}{dz}\right) = \left(\frac{d\eta_1}{d\zeta}q_k + \frac{d\eta_2}{d\zeta}q_{k+1}\right)\left(\frac{2}{h_k}\right) = \begin{bmatrix} -1/h_k & 1/h_k \end{bmatrix} \begin{bmatrix} q_k \\ q_{k+1} \end{bmatrix}. \quad (17.22)$$

Note that the strain (17.22) is spatially uniform in the element. The virtual strain  $\bar{\varepsilon}^{(k)}$  is

$$\bar{\varepsilon}^{(k)} = \frac{d\bar{w}^{(k)}}{dz} = \left(\frac{d\eta_1}{d\zeta}b_k + \frac{d\eta_2}{d\zeta}b_{k+1}\right)\left(\frac{2}{h_k}\right) = \begin{bmatrix} -1/h_k & 1/h_k \end{bmatrix} \begin{bmatrix} b_k \\ b_{k+1} \end{bmatrix}. \quad (17.23)$$

The bilinear form (17.7), or internal virtual work, for the  $k$ th element is

$$B_k[w^{(k)}, \bar{w}^{(k)}] = \int_{z_k}^{z_{k+1}} \bar{\varepsilon}^{(k)} EA \varepsilon^{(k)} dz + \int_{z_k}^{z_{k+1}} \bar{w}^{(k)} c w^{(k)} dz. \quad (17.24)$$

Substitute (17.22) and (17.23) for the strains, and (17.19) and (17.20) for the displacements, into the internal virtual work (17.24) to get

$$B_k[w^{(k)}, \bar{w}^{(k)}] = \int_{-1}^1 \begin{bmatrix} b_k & b_{k+1} \end{bmatrix} \begin{bmatrix} -1/h_k \\ 1/h_k \end{bmatrix} EA \begin{bmatrix} -1/h_k & 1/h_k \end{bmatrix} \begin{bmatrix} q_k \\ q_{k+1} \end{bmatrix} \frac{h_k}{2} d\zeta + \int_{-1}^1 \begin{bmatrix} b_k & b_{k+1} \end{bmatrix} \begin{bmatrix} \eta_1 \\ \eta_2 \end{bmatrix} c \begin{bmatrix} \eta_1 & \eta_2 \end{bmatrix} \begin{bmatrix} q_k \\ q_{k+1} \end{bmatrix} \frac{h_k}{2} d\zeta, \quad (17.25)$$

where  $dz = (h_k/2)d\zeta$ . Perform the matrix algebra in the latter equation to get

$$B_k[w^{(k)}, \bar{w}^{(k)}] = [b_k \ b_{k+1}] \left\{ \int_{-1}^1 \left( \begin{bmatrix} \frac{EA}{h_k^2} & \frac{-EA}{h_k^2} \\ \frac{-EA}{h_k^2} & \frac{EA}{h_k^2} \end{bmatrix} \frac{h_k}{2} + c \begin{bmatrix} \eta_1^2 & \eta_1 \eta_2 \\ \eta_1 \eta_2 & \eta_2^2 \end{bmatrix} \frac{h_k}{2} \right) d\zeta \right\} \begin{bmatrix} q_k \\ q_{k+1} \end{bmatrix} = [b_k \ b_{k+1}] [K^{(k)}] \begin{bmatrix} q_k \\ q_{k+1} \end{bmatrix}. \quad (17.26)$$

Perform the integration in eq. (17.26) to determine the element stiffness matrix  $[K^{(k)}]$ . The result is

$$[K^{(k)}] = \begin{bmatrix} k_{11}^{(k)} & k_{12}^{(k)} \\ k_{21}^{(k)} & k_{22}^{(k)} \end{bmatrix} = \begin{bmatrix} \frac{EA}{h_k} + \frac{ch_k}{3} & \frac{-EA}{h_k} + \frac{ch_k}{6} \\ \frac{-EA}{h_k} + \frac{ch_k}{6} & \frac{EA}{h_k} + \frac{ch_k}{3} \end{bmatrix}. \quad (17.27)$$

Take the virtual displacement equal to the trial displacement, or  $\bar{w}^{(k)} = w^{(k)}$ , in (17.26), which implies  $b_k = q_k$  and  $b_{k+1} = q_{k+1}$ . Then, multiply the result by one-half to identify the strain energy in the kth element as

$$U^{(k)} = \frac{1}{2} (B_k[w^{(k)}, w^{(k)}]) = \frac{1}{2} [q_k \ q_{k+1}] [K^{(k)}] \begin{bmatrix} q_k \\ q_{k+1} \end{bmatrix}. \quad (17.28)$$

The linear form (17.8), or the external virtual work, for the kth element is

$$F_k[\bar{w}^{(k)}] = \int_{z_k}^{z_{k+1}} f_z^{(k)}(z) \bar{w}^{(k)}(z) dz + N^{(k)} \bar{w}^{(k)} \Big|_{z=z_{k+1}} - N^{(k)} \bar{w}^{(k)} \Big|_{z=z_k} + \int_{z_k}^{z_{k+1}} (EA \bar{\epsilon}^{(k)}) \alpha \tau_0^{(k)}(z) dz. \quad (17.29)$$

Substitute (17.20) for the virtual displacement and (17.23) for the virtual strain into the external virtual work (17.29), followed by employing the mapping of  $z \rightarrow \zeta$  (17.16). The result is

$$F_k[\bar{w}^{(k)}] = \int_{-1}^1 f_z^{(k)}(\zeta) [\eta_1(\zeta) b_k + \eta_2(\zeta) b_{k+1}] (h_k/2) d\zeta + \int_{-1}^1 \left[ EA \left( b_k \left( \frac{-1}{h_k} \right) + b_{k+1} \left( \frac{1}{h_k} \right) \right) \right] \alpha \tau_0^{(k)}(\zeta) \left( \frac{h_k}{2} \right) d\zeta + N^{(k)}(z_{k+1}) b_{k+1} - N^{(k)}(z_k) b_k, \quad (17.30)$$

where

$$f_z^{(k)}(\zeta) = f_z[\eta_1(\zeta) z_k + \eta_2(\zeta) z_{k+1}] \quad \tau_0^{(k)}(\zeta) = \tau_0[\eta_1(\zeta) z_k + \eta_2(\zeta) z_{k+1}] \quad \zeta \in \Omega_{st}. \quad (17.31)$$

Arrange the terms in (17.30) to

$$F_k[\bar{w}^{(k)}] = b_k \left[ \int_{-1}^1 f_z^{(k)}(\zeta) \eta_1(\zeta) \frac{h_k}{2} d\zeta + \int_{-1}^1 EA \left( \frac{-1}{2} \right) \alpha \tau_0^{(k)}(\zeta) d\zeta - N^{(k)}(z_k) \right] + b_{k+1} \left[ \int_{-1}^1 f_z^{(k)}(\zeta) \eta_2(\zeta) \frac{h_k}{2} d\zeta + \left( \int_{-1}^1 EA \left( \frac{1}{2} \right) \alpha \tau_0^{(k)}(\zeta) d\zeta \right) + N^{(k)}(z_{k+1}) \right]. \quad (17.32)$$

The last expression for the external virtual work is written as

$$F_k[\bar{w}^{(k)}] = b_k[Q_k^{(k)} + F_k^{(k)}] + b_{k+1}[Q_{k+1}^{(k)} + F_{k+1}^{(k)}], \quad (17.33)$$

where we define

$$F_k^{(k)} = \int_{-1}^1 f_z^{(k)}(\zeta) \eta_1(\zeta) \frac{h_k}{2} d\zeta + \int_{-1}^1 EA \left( \frac{-1}{2} \right) \alpha \tau_0^{(k)}(\zeta) d\zeta, \quad Q_k^{(k)} = -N^{(k)}(z_k), \quad (17.34)$$

$$F_{k+1}^{(k)} = \int_{-1}^1 f_z^{(k)}(\zeta) \eta_2(\zeta) \frac{h_k}{2} d\zeta + \int_{-1}^1 EA \left( \frac{1}{2} \right) \alpha \tau_0^{(k)}(\zeta) d\zeta, \quad \text{and } Q_{k+1}^{(k)} = N^{(k)}(z_{k+1}). \quad (17.35)$$

The forces acting on the element separated from the nodes, and the forces acting on the nodes are depicted in figure 17.4.

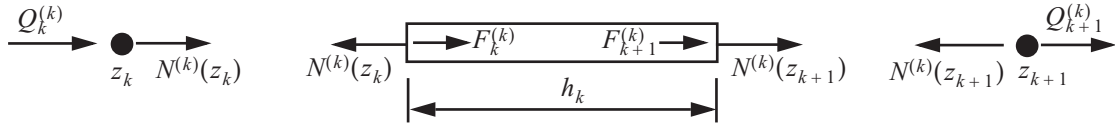


**Fig. 17.4** Forces acting on the bar and the nodes for element  $\Omega_k$ .

Finally, the external virtual work expression (17.33) for the  $k$ th element is written as

$$F_k[\bar{w}^{(k)}] = \{b_k\}^T (\{Q^{(k)}\} + \{F^{(k)}\}), \quad \text{where} \quad (17.36)$$

$$\{b_k\} = \begin{bmatrix} b_k \\ b_{k+1} \end{bmatrix}, \quad \{Q^{(k)}\} = \begin{bmatrix} Q_k^{(k)} \\ Q_{k+1}^{(k)} \end{bmatrix}, \quad \text{and } \{F^{(k)}\} = \begin{bmatrix} F_k^{(k)} \\ F_{k+1}^{(k)} \end{bmatrix}. \quad (17.37)$$

The axial force in the  $k$ th element is

$$N^{(k)} = EA \left[ \frac{2}{h_k} \frac{dw^{(k)}}{d\zeta} - \alpha \tau_0^{(k)}(\zeta) \right] \quad \zeta \in \Omega_{st}. \quad (17.38)$$

The virtual work expressions for the  $M$ -elements spanning  $\Omega$  are

$$B[w, \bar{w}] = \sum_{k=1}^M B_k[w^{(k)}, \bar{w}^{(k)}] \quad F[\bar{w}] = \sum_{k=1}^M F_k[\bar{w}^{(k)}]. \quad (17.39)$$

Consider in the summation of the external virtual work the terms from the  $k-1$  element and the  $k$ th element. From (17.33) these terms are

$$\underbrace{b_{k-1}[F_{k-1}^{(k-1)} + Q_{k-1}^{(k-1)}] + b_k[F_k^{(k-1)} + Q_k^{(k-1)}]}_{\text{element k-1}} + \underbrace{b_k[F_k^{(k)} + Q_k^{(k)}] + b_{k+1}[F_{k+1}^{(k)} + Q_{k+1}^{(k)}]}_{\text{element k}}. \quad (17.40)$$

Combine the terms multiplying virtual displacement  $b_k$  in eq. (17.40) to write the external virtual work as

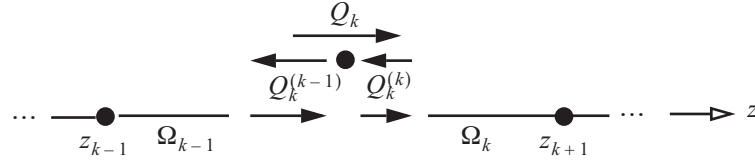
$$F[\bar{w}] = \dots + b_k[F_k^{(k-1)} + Q_k^{(k-1)} + F_k^{(k)} + Q_k^{(k)}] + \dots. \quad (17.41)$$

At the common node  $z_k$  let

$$Q_k = Q_k^{(k-1)} + Q_k^{(k)} = N^{(k-1)}(z_k) - N^{(k)}(z_k), \quad (17.42)$$

where  $Q_k$  is the external axial force at node  $z_k$ . The definition of force  $Q_k$  is based on equilibrium at node  $z_k$  as shown by the free body diagram in figure 17.5. Force  $Q_k$  is prescribed if displacement  $q_k$  is unknown, or it is an

**Fig. 17.5** Free body diagram of node  $z_k$ .



unknown reactive force if displacement  $q_k$  is prescribed. At node  $z_k$  the total external axial force consists of the contribution from the axial force  $Q_k$  plus the distributed loading from the  $k-1$  element and the  $k$ th element (i.e.,  $Q_k + F_k$ , where  $F_k = F_k^{(k-1)} + F_k^{(k)}$ ). A depiction of a finite element model with a mesh consisting of four nodes and three elements is shown in figure 17.6.

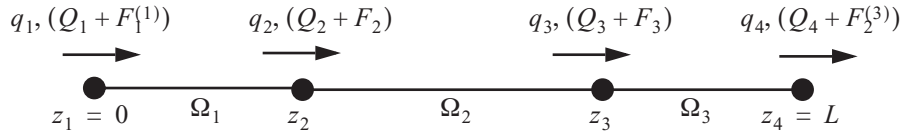


**Fig. 17.6** A mesh consisting of four nodes and an assembly of three elements. Displacements and the corresponding external forces are shown at each node.

If at node  $z_k$  there is no prescribed externally applied point force, then we have the following relation from eq. (17.42):

$$Q_k = 0 = N^{(k-1)}(z_k) - N^{(k)}(z_k). \quad (17.43)$$

Equation (17.43) implies that the axial force is continuous at the node connecting the  $k-1$  element to the  $k$ th element if  $Q_k = 0$ . Displacement continuity at the common nodes is imposed in the finite element method. However, for the linear interpolation functions (17.20) the axial force is, in general, discontinuous at the common nodes (i.e.,  $N^{(k-1)}(z_k) - N^{(k)}(z_k) \neq 0$ ). The jump in the axial force at common nodes decreases with mesh refinement as is illustrated in example 17.2 below.

### Example 17.2 Solution of example 17.1 using two finite elements

First consider a uniform mesh with  $M = 2$  using the interpolation functions (17.16). The nodes are  $z_1 = 0$ ,  $z_2 = L/2$ , and  $z_3 = L$ . The lengths of the elements are  $h_1 = h_2 = L/2$ . The total displacements for each element are

$$w^{(1)}(\xi) = \eta_1(\xi)q_1 + \eta_2(\xi)q_2, \text{ and } w^{(2)}(\xi) = \eta_1(\xi)q_2 + \eta_2(\xi)q_3. \quad (a)$$

The virtual displacements for each element are



$$\bar{w}^{(1)}(\xi) = \eta_2(\xi)b_2 \text{ and } \bar{w}^{(2)}(\xi) = \eta_1(\xi)b_2 + \eta_2(\xi)b_3. \quad (\text{b})$$

Note that virtual displacement in the first element at node one  $\bar{w}^{(1)}(-1) = 0$ , since the displacement  $q_1$  is prescribed at node one in the trial function.

The internal virtual work for elements one and two are

$$B_1[w^{(1)}, \bar{w}^{(1)}] = \left(\frac{2}{h_1}\right) \int_{-1}^1 EA \left(\frac{dw^{(1)}}{d\xi}\right) \left(\frac{d\bar{w}^{(1)}}{d\xi}\right) d\xi + \left(\frac{h_1}{2}\right) \int_{-1}^1 c w^{(1)} \bar{w}^{(1)} d\xi = b_2(k_{21}^{(1)}q_1 + k_{22}^{(1)}q_2), \text{ and} \quad (\text{c})$$

$$B_2[w^{(2)}, \bar{w}^{(2)}] = \left(\frac{2}{h_2}\right) \int_{-1}^1 EA \left(\frac{dw^{(2)}}{d\xi}\right) \left(\frac{d\bar{w}^{(2)}}{d\xi}\right) d\xi + \left(\frac{h_2}{2}\right) \int_{-1}^1 c w^{(2)} \bar{w}^{(2)} d\xi = b_2[k_{11}^{(2)}q_2 + k_{12}^{(2)}q_3] + b_3[k_{21}^{(2)}q_2 + k_{22}^{(2)}q_3]. \quad (\text{d})$$

The element stiffness coefficients in eqs. (c) and (d) are given by eq. (17.27). For the assembly of the elements the total internal virtual work is

$$B = B_1[w^{(1)}, \bar{w}^{(1)}] + B_2[w^{(2)}, \bar{w}^{(2)}] = b_2[k_{21}^{(1)}q_1 + (k_{22}^{(1)} + k_{11}^{(2)})q_2 + k_{12}^{(2)}q_3] + b_3[k_{21}^{(2)}q_2 + k_{22}^{(2)}q_3]. \quad (\text{e})$$

In matrix notation the internal virtual work for the assembly is

$$B = [b_2 \ b_3] \left( \begin{bmatrix} k_{22} & k_{23} \\ k_{32} & k_{33} \end{bmatrix} \begin{bmatrix} q_2 \\ q_3 \end{bmatrix} + \begin{bmatrix} k_{21}^{(1)}q_1 \\ 0 \end{bmatrix} \right), \text{ where} \quad (\text{f})$$

$$k_{22} = k_{22}^{(1)} + k_{11}^{(2)} \quad k_{23} = k_{12}^{(2)} \quad k_{32} = k_{21}^{(2)} \quad k_{33} = k_{22}^{(2)} \quad k_{21}^{(1)} = -\frac{EA}{h_1} + \frac{ch_1}{6}. \quad (\text{g})$$

Use the relation that  $h_1 = h_2 = L/2$  to find that the stiffness matrix of the assembly is

$$\begin{bmatrix} k_{22} & k_{23} \\ k_{32} & k_{33} \end{bmatrix} = \begin{bmatrix} \frac{4EA}{L} + \frac{cL}{3} & \frac{-2EA}{L} + \frac{cL}{12} \\ \frac{-2EA}{L} + \frac{cL}{12} & \frac{2EA}{L} + \frac{cL}{6} \end{bmatrix}. \quad (\text{h})$$

The external virtual work (17.33) for the first element is

$$F[\bar{w}^{(1)}] = b_2(Q_2^{(1)} + F_2^{(1)}). \quad (\text{i})$$

The external force from the change in temperature (17.35) for the first element is

$$F_2^{(1)} = \int_{-1}^1 EA \left(\frac{1}{2}\right) \alpha \tau_0^{(1)}(\xi) d\xi = EA \alpha \tau_0. \quad (\text{j})$$

The external virtual work for the second element (17.33) is

$$F_2[\bar{w}_2] = b_2(Q_2^{(2)} + F_2^{(2)}) + b_3(Q_3^{(2)} + F_3^{(2)}). \quad (\text{k})$$

The external forces from the change in temperature for the second element are determined from eqs. (17.34) and (17.35):

$$F_2^{(2)} = \int_{-1}^1 EA \left( \frac{-1}{2} \right) \alpha \tau_0^{(2)}(\xi) d\xi = -EA \alpha \tau_0, \text{ and } F_3^{(2)} = \int_{-1}^1 EA \left( \frac{1}{2} \right) \alpha \tau_0^{(2)}(\xi) d\xi = EA \alpha \tau_0. \quad (\text{l})$$

The total external virtual work is the sum of the contributions from eqs. (i) and (k) is

$$F[\bar{w}] = F_1[\bar{w}_1] + F_2[\bar{w}_2] = b_2(Q_2^{(1)} + F_2^{(1)} + Q_2^{(2)} + F_2^{(2)}) + b_3(Q_3^{(2)} + F_3^{(2)}). \quad (\text{m})$$

At node 2 there is no prescribed external force, so  $Q_2 = Q_2^{(1)} + Q_2^{(2)} = 0$ . Also at node 2 the sum of the thermal forces (j) and (l) is zero: that is,  $F_2 = F_2^{(1)} + F_2^{(2)} = EA \alpha \tau_0 + (-EA \alpha \tau_0) = 0$ . Hence, the total external force at node 2 vanishes. At node 3 the prescribed force  $Q_3 = Q_3^{(2)} = F_L$ , and the thermal force  $F_3 = F_3^{(2)} = EA \alpha \tau_0$ . The total external virtual work is

$$F[\bar{w}] = \begin{bmatrix} b_2 & b_3 \end{bmatrix} \begin{bmatrix} 0 \\ F_L + EA \alpha \tau_0 \end{bmatrix}. \quad (\text{n})$$

Equate expressions (f) and (n) to get the principle of virtual work:

$$\begin{bmatrix} b_2 & b_3 \end{bmatrix} \left( \begin{bmatrix} k_{22} & k_{23} \\ k_{32} & k_{33} \end{bmatrix} \begin{bmatrix} q_2 \\ q_3 \end{bmatrix} + \begin{bmatrix} k_{21}^{(1)} q_1 \\ 0 \end{bmatrix} \right) = \begin{bmatrix} b_2 & b_3 \end{bmatrix} \begin{bmatrix} 0 \\ F_L + EA \alpha \tau_0 \end{bmatrix} \quad \forall \begin{bmatrix} b_2 & b_3 \end{bmatrix} \neq 0_{1 \times 2}. \quad (\text{o})$$

It follows from eq. (o) that the matrix equation to determine the displacements is

$$\begin{bmatrix} k_{22} & k_{23} \\ k_{32} & k_{33} \end{bmatrix} \begin{bmatrix} q_2 \\ q_3 \end{bmatrix} = \begin{bmatrix} -k_{21}^{(1)} q_1 \\ F_L + EA \alpha \tau_0 \end{bmatrix} \quad \text{where} \quad k_{21}^{(1)} = -\frac{2EA}{L} + \frac{cL}{12}, \quad (\text{p})$$

Note that the term involving displacement  $q_1$  is known and so it is moved to the right-hand side of eq. (p).

Numerical evaluation of matrix equation (p) is

$$\begin{bmatrix} 1.05733 \times 10^6 & 96,333.3 \\ 96,333.3 & 528,667 \end{bmatrix} \begin{bmatrix} q_2 \\ q_3 \end{bmatrix} = \begin{bmatrix} 19,266.7 \\ -14,240 \end{bmatrix}. \quad (\text{q})$$

The solution to matrix equation (o) for the nodal displacements is  $q_2 = 0.0210251$  mm and  $q_3 = -0.0307669$  mm. The external forces acting on the bar modeled with two elements is shown in the free body diagram of figure 17.7. Force  $Q_1 = Q_1^{(1)}$  is the reactive force at node 1 where the displacement is prescribed. The thermal force at node 1  $F_1 = F_1^{(1)} = -EA \alpha \tau_0 = -25,760$  N, which is evaluated from (17.34).



The thermal force at node 3 is  $F_3 = F_3^{(2)} = EA \alpha \tau_0 = 25,760$  N, which is evaluated from (17.35). Then, axial equilibrium of the bar determines the reactive force  $Q_1 = 40,000$  N.

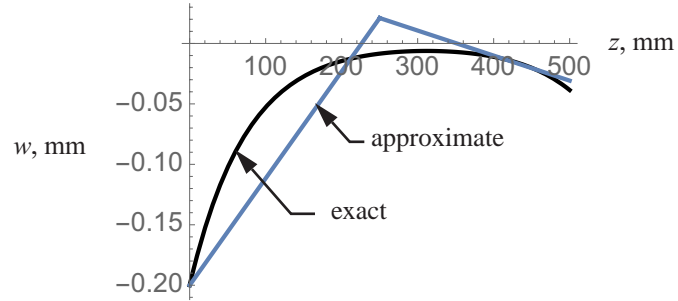
The trial functions for the displacements of the two elements are

$$w^{(1)} = -0.1(1 - \zeta) + 0.0105126(1 + \zeta), \text{ and} \quad (\text{r})$$

$$w^{(2)} = 0.0105126(1 - \zeta) - 0.0153834(1 + \zeta). \quad (\text{s})$$

The axial coordinate in element 1 is  $z = \eta_2(\zeta)(250 \text{ mm})$  and in element 2 it is  $z = \eta_1(\zeta)(250 \text{ mm}) + \eta_2(\zeta)(500 \text{ mm})$ . The axial displacement is plotted with respect to  $z$  from the exact solution given by eq. (j) in example 17.1 and from the finite element solution given by eqs. (r) and (s) in figure 17.8. The finite element representation of the axial displacement is a piecewise linear polynomial, which is an improvement with respect to the virtual work result shown in figure 17.2.

**Fig. 17.8** Axial displacement. Exact solution and an approximate solution using two finite elements.



The strain energy for the two element model is

$$U = \left(\frac{1}{2}\right) \sum_{k=1}^M \left[ \frac{2}{h_k} \int_{-1}^1 EA \left( \frac{dw^{(k)}}{d\zeta} \right)^2 d\zeta + \frac{h_k}{2} \int_{-1}^1 c (w^{(k)})^2 d\zeta \right] = 10,589.9 \text{ N-mm}. \quad (\text{t})$$

The error in the strain energy with respect to the exact value given by eq. (l) in example 17.1 is

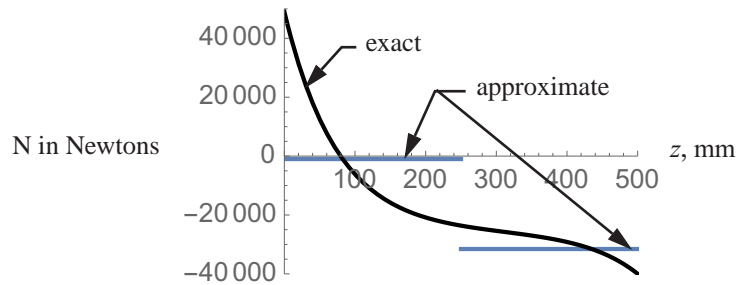
$$\frac{(U - U_{\text{ex}})100}{U_{\text{ex}}} = 36.6\%. \quad (\text{u})$$

From (17.38) the axial forces in each element are

$$N^{(1)} = EA \left[ \frac{2}{h_1} \left( \frac{dw^{(1)}}{d\zeta} \right) - \alpha \tau_0 \right] = -1,005.19 \text{ N} \text{ and } N^{(2)} = EA \left[ \frac{2}{h_2} \left( \frac{dw^{(2)}}{d\zeta} \right) - \alpha \tau_0 \right] = -31,560.7 \text{ N}. \quad (\text{v})$$

The distributions of the axial force  $N$  from the exact solution given by eq. (k) in example 17.1 and the finite element solution (v) are plotted in figure 17.9. The finite element result for  $N$  is piecewise constant, which is a improvement with respect to the virtual work result shown in figure 17.3. ■

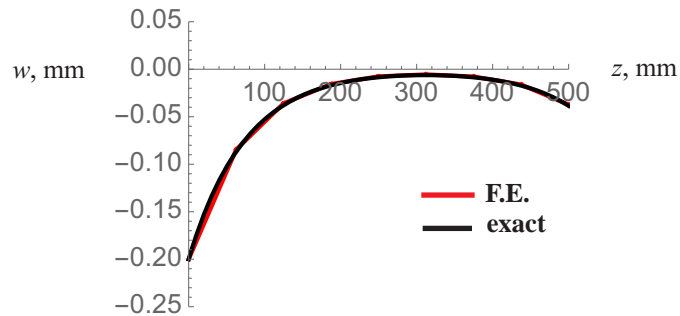
**Fig. 17.9** Axial force. Exact solution and an approximate solution using two finite elements.



### 17.2.1 Results from 4, 8, and 16 finite element solutions to example 17.1

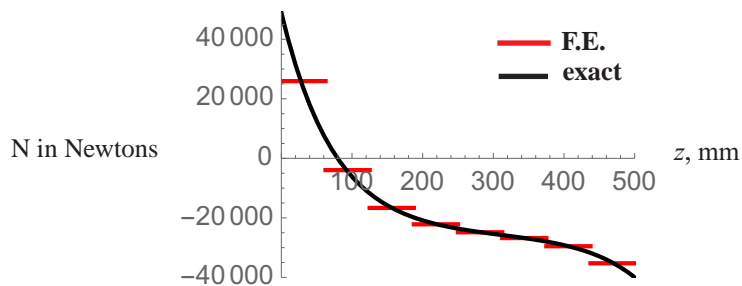
Improved numerical solutions are obtained by considering uniform meshes of four, eight, sixteen, etc., elements. As shown in figure 17.10, the piecewise polynomial approximation for the axial displacement using eight uniform elements is, to the scale of the plot, very close to the exact solution. The axial force from the exact solution

**Fig. 17.10 Axial displacement. Exact solution and an approximate solution using eight finite elements.**



and from the finite element solution with eight uniform elements is shown in figure 17.11. The piecewise constant axial force from the solution with eight elements is an improvement with respect to the two element model shown in figure 17.9.

**Fig. 17.11 Axial force. Exact solution and an approximate solution using eight finite elements.**



The strain energy and the natural boundary condition at  $z = L$  are used to measure the error in the finite element solutions with respect to the exact solution. Results for uniform meshes of one to sixteen elements are listed in table 17.1. The data in the table demonstrates that the strain energy converges faster than the natural boundary condition to the exact solution as the number of elements is increased.

**Table 17.1 Errors in the strain energies and natural boundary conditions of example 17.1 as the number of element is increased.**

M, number of uniform elements	U, strain energy, N-mm	Percentage error in the strain energy	N(L), Axial force in Newtons	Percentage error in the axial force at $z = L$
		$(U - U_{ex})100/U_{ex}$		$[F_L - N(L)]100/F_L$
1 <sup>a</sup>	14,975.3	93.1 <sup>b</sup>	-10,914.5	72.7 <sup>c</sup>
2	10,589.9	36.6	-31,560.7	21.1
4	8,551.95	10.3	-32,260.1	19.3
8	7,961.15	2.67	-35,260.1	11.8
16	7,806.5	0.674	-37,347.6	6.63

- 
- a. From example 17.1.
  - b.  $U_{ex} = 7,754.26 \text{ N-mm}$
  - c.  $FL = -40,000 \text{ N}$

### 17.2.2 Convergence requirements

Heubner et al. (1995, p. 85) list the following requirements for mathematical convergence of the finite element solution to the exact solution as an increasing number of smaller elements are used in the remeshing process.

- The elements must be made smaller in such a way that every point in the solution domain can always be within an element regardless of how small the element may be.
- All previous meshes must be contained in the refined meshes.
- The form of the interpolation functions must remain unchanged.

For example, the nodes in the mesh for  $M = 2$  are also contained in the mesh for  $M = 4$ , nodes in the mesh for  $M = 4$  are also contained in the mesh for  $M = 8$ , etc. The same linear interpolation functions (17.16) are used in each discretization.

### 17.2.3 Apparent loadings from the 8- and 16-element solutions of example 17.1

As illustrated in figure 17.11, the axial force exhibits jumps at the nodes between neighboring elements. These jumps can be interpreted as a series of concentrated forces applied at the nodes, and these forces are called the **apparent loading** (Szabo and Babuska, p. 63). Let  $\underline{Q}_k$  denote the apparent axial force at node  $z_k$ . From (17.42), the apparent axial force in the positive  $z$ -direction at an interior node is

$$\underline{Q}_k = N^{(k-1)}(z_k) - N^{(k)}(z_k) \quad k = 2, 3, \dots, M-1. \quad (17.44)$$

The forces at the nodes computed from the jump in the internal axial force are listed in table 17.2 for the 8-element model and for the 16-element model. Note that the sum of these forces  $\underline{Q}_k$  vanishes in each model, which is a consequence of the principle work as a statement of equilibrium. At common interior nodes the force  $\underline{Q}_k$  is smaller in the 16-element model than in the 8-element model.

**Table 17.2 Apparent loading from the finite element solutions of example 17.1.**

	8 elements, 9 nodes		16 elements, 17 nodes	
<i>z</i>	<i>k</i>	$\underline{Q}_k, \text{ N}$	<i>k</i>	$\underline{Q}_k, \text{ N}$
0	1	−25,950.	1	−35,743.3
L/16		-----	2	21,139.1
L/8	2	29,906.9	3	13,889.4
3 L/16		-----	4	9,134.26
L/4	3	12,697.5	5	6,019.91
5 L/16		-----	6	3,986.67
3 L/8	4	5,510.35	7	2,669.461
7 L/16		-----	8	1,831.7
L/2	5	2,672.57	9	1,322.93
9 L/16		-----	10	1,051.76
5 L/8	6	1,944.26	11	969.5
11 L/16		-----	12	1,061.37
3 L/4	7	2,750.58	13	1,343.86
13 L/16		-----	14	1,867.72
7 L/8	8	5,727.95	15	2,727.03
15 L/16		-----	16	4,076.14
L = 500 mm	9	−35,250.1	17	−37,347.6
	$\sum_{k=1}^9 \underline{Q}_k = 0$		$\sum_{k=1}^{17} \underline{Q}_k = 0$	

#### 17.2.4 Adaptive mesh refinement beginning with the 8-element solution to example 17.1

A uniform mesh may converge slowly to the exact solution with continued refinement. In practice, finite element simulations are performed on a structure where the exact solution is not known. For those structures whose exact solutions are unknown, the apparent loading from the finite element solution can be used in adaptive procedures to refine the mesh. Adaptive mesh refinement is based on assessing the relative error of the energy norm in each element between the original loading and the apparent loading (Szabo and Babuska, p. 63). The energy norm for a kinematically admissible function  $w(z)$  is denoted by  $\|w(z)\|$ , and it is defined as the square root of the strain energy (17.9) (i.e.,  $\|w\| = \sqrt{U[w]}$ ). The mesh and shape functions of the original model are not changed in the second solution of the model subject to the apparent loading. Those elements exhibiting the largest discrepancy in the energy norm between the original loading and the apparent loading are subdivided to generate a new mesh. The new mesh will not be uniform, and is called quasi-uniform. The adaptive mesh procedure is repeated with respect to the new mesh. This repeated use of mesh refinement generates a sequence of meshes. An optimum mesh is achieved when the local error is distributed uniformly through the mesh (Heubner et al., p. 514).

Consider the eight-element model ( $M = 8$ ) with nine nodes. The nine nodes in the uniform mesh are

$$\{z_9\} = \{0, 1/8, 1/4, 3/8, 1/2, 5/8, 3/4, 7/8, 1\}L. \quad (17.45)$$

Each element has the same length  $h_k = z_{k+1} - z_k = L/8$ ,  $k = 1, 2, \dots, 8$ . The dimensions of the restrained structural stiffness matrix  $[K_{\alpha\alpha}]$  is  $8 \times 8$ . The displacement degrees of freedom and the corresponding forces are

$$\{q_\alpha\} = [q_2, q_3, q_4, q_5, q_6, q_7, q_8, q_9]^T, \text{ and } \{Q_\alpha\} = [Q_2, Q_3, Q_4, Q_5, Q_6, Q_7, Q_8, Q_9]^T. \quad (17.46)$$

The nodal force vector for the original loading is

$$\{Q_\alpha\} = [(8EA/L - cL/48)q_1, 0, 0, 0, 0, 0, 0, 0, EA\alpha\tau_0 + F_L]^T = [-79, 183.3, 0, 0, 0, 0, 0, 0, -14240]^T. \quad (17.47)$$

The matrix equation  $[K_{\alpha\alpha}]\{q_\alpha\} = \{Q_\alpha\}$  is solved numerically to determine the displacement vector  $\{q_\alpha\}$ .

The axial displacement  $w^{(k)}$  in each of the eight elements is computed from  $\{q_\alpha\}$ , followed by the computation of the energy norm in each element  $\|w^{(k)}\|$ ,  $k = 1, 2, \dots, 8$ .

For the apparent loading the nodal force vector from table 17.2 is

$$\{\underline{Q}_\alpha\} = [29, 906.9, 12, 679.5, 5, 510.35, 2, 672.57, 1, 944.26, 2, 750.58, 5, 727.95, -35, 260.1]^T. \quad (17.48)$$

Without changing the restrained structural stiffness matrix, the equation  $[K_{\alpha\alpha}]\{\underline{q}_\alpha\} = \{\underline{Q}_\alpha\}$  is solved numerically for the displacement vector  $\{\underline{q}_\alpha\}$ . Note that  $\{\underline{q}_\alpha\} \neq \{q_\alpha\}$ . From the displacement vector  $\{\underline{q}_\alpha\}$  the axial displacement in the  $k$ th element  $\underline{w}^{(k)}$  is determined. The energy norm for the displacement in each element from the apparent loading is denoted by  $\|\underline{w}^{(k)}\|$ ,  $k = 1, 2, \dots, 8$ . Results for the energy norms from the original loading and apparent loading are listed in table 17.3. Elements 1, 8, 2, 7, 3, 5, 4, and 6 have the largest to the smallest discrepancy in the energy norms.

**Table 17.3 Element energy norms from the original and apparent loadings.**

	Original loading	Apparent loading	Discrepancy
Element	$\ w_k\ $	$\ \underline{w}_k\ $	$\ w_k\  - \ \underline{w}_k\ $
1	79.5058	120.577	-41.0708
2	33.5923	14.4801	19.1122
3	14.1945	12.1357	2.05885
4	6.01526	7.86369	-1.84843
5	2.76845	4.69067	-1.92222
6	2.84924	4.61159	-1.76235
7	6.26583	12.0038	-5.738
8	14.7925	34.9373	-20.1448

Based on the data in table 17.3, a quasi-uniform mesh is selected to increase the number of elements in the domain where the errors in energy norm are large. For example, a mesh of fifteen nodes and fourteen elements is illustrated below:

$$\{z_{15}\} = \{0, 1/24, 1/12, 1/8, 3/16, 1/4, 3/8, 1/2, 5/8, 3/4, 13/16, 7/8, 11/12, 23/24, 1\}L, \quad (17.49)$$

where the lengths of the elements are

$$\{h_{14}\} = \left\{ \frac{L}{24}, \frac{L}{24}, \frac{L}{24}, \frac{L}{16}, \frac{L}{16}, \frac{L}{8}, \frac{L}{8}, \frac{L}{8}, \frac{L}{8}, \frac{L}{16}, \frac{L}{16}, \frac{L}{24}, \frac{L}{24}, \frac{L}{24} \right\}. \quad (17.50)$$

The mesh with nine nodes and the mesh with fifteen nodes are depicted in figure 17.12. Nodes are clustered at the

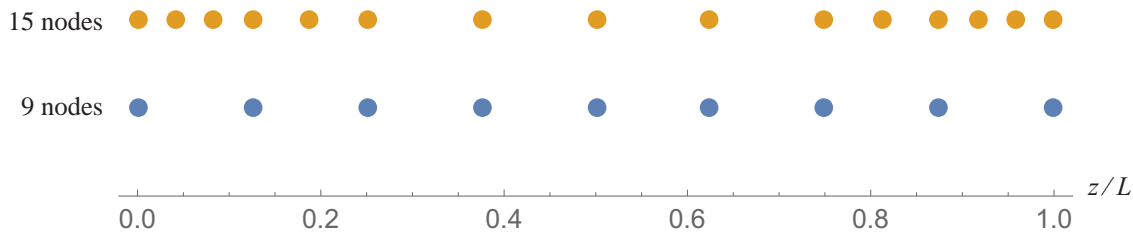


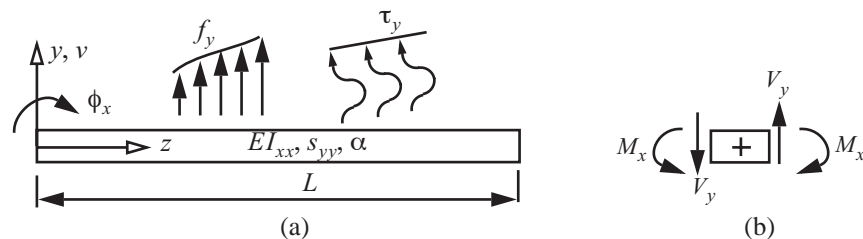
**Fig. 17.12 The nine-node uniform mesh and the fifteen-node quasi-uniform mesh.**

beginning and end of the domain of the 14-element model where discrepancies in the energy norm were the largest. A finite element analysis of this 14-element model resulted in a strain energy of the assembly of 7,788.23 N-mm, and a natural boundary condition  $N(L) = -38,164.2$  N. Compared to the exact solution the percentage error in the strain energy is 0.438 percent, and the error in the natural boundary condition is 4.59 percent. Moreover, compared to the results from the 16-element model with a uniform mesh in table 17.1, the 14-element model has a smaller error in the strain energy and a smaller error in the natural boundary condition.

### 17.3 A beam element including transverse shear deformation

The principle of virtual work is developed for a uniform beam of length  $L$  that is symmetric about the  $y$ - $z$  plane as shown in figure 17.13. It is subject to a lateral distributed load intensity  $f_y(z)$  (F/L) and a change in temperature  $\Delta T = \tau_y(z)y$ ,  $0 \leq z \leq L$ , where  $\tau_y(z)$  ( $^{\circ}\text{C}/L$ ) is the prescribed through the thickness temperature gradient. The  $y$ -direction displacement of the centroidal axis is denoted by  $v(z)$  (L), and the rotation of the cross section about the  $x$ -axis is denoted by  $\phi_x(z)$  (radians).

**Fig. 17.13 (a) Symmetric beam subject to an external load and temperature gradient. (b) Definition for positive shear and moment.**





The governing equations are as follows.

$$\text{equilibrium: } \frac{dV_y}{dz} + f_y(z) = 0, \text{ and } \frac{dM_x}{dz} - V_y = 0, \quad 0 < z < L. \quad (17.51)$$

$$\text{Hooke's law: } V_y = s_{yy}\psi_y, \text{ and } M_x = EI_{xx}(\kappa - \alpha\tau_y). \quad (17.52)$$

$$\text{strain-displacement: } \kappa = \frac{d\phi_x}{dz}, \text{ and } \psi_y = \frac{dv}{dz} + \phi_x. \quad (17.53)$$

The boundary conditions at  $z = 0$  and  $z = L$  are to

$$\text{prescribe either } v \text{ or } V_y, \text{ and to prescribe either } \phi_x \text{ or } M_x. \quad (17.54)$$

For a symmetric cross section the transverse shear stiffness  $s_{yy} = 1/c_{yy}$ , where  $c_{yy}$  ( $F^{-1}$ ) is the transverse shear compliance. (Equations for the shear compliances are given by eq. (5.62) on page 142 for an open cross-sectional contour and eq. (5.85) on page 145 for a closed cross-sectional contour.)

Combine the equations associated with the shear force to get

$$\frac{d}{dz} \left[ s_{yy} \left( \frac{dv}{dz} + \phi_x \right) \right] + f_y = 0. \quad (17.55)$$

Multiply (17.55) by the virtual displacement  $\bar{v}(z)$  and integrate over the domain. Then integrate the result by parts to get

$$\bar{v} V_y \Big|_0^L - \int_0^L s_{yy} \left( \frac{dv}{dz} + \phi_x \right) \left( \frac{d\bar{v}}{dz} \right) dz + \int_0^L f_y \bar{v} dz = 0. \quad (17.56)$$

Combine the equations associated with the bending moment to get

$$\frac{d}{dz} \left[ EI_{xx} \left( \frac{d\phi_x}{dz} - \alpha\tau_y \right) \right] - s_{yy} \left( \frac{dv}{dz} + \phi_x \right) = 0. \quad (17.57)$$

Multiply (17.57) by the virtual rotation  $\bar{\phi}_x(z)$  and integrate over the domain. Then integrate the result by parts to find

$$\bar{\phi}_x M_x \Big|_0^L - \int_0^L \left[ EI_{xx} \left( \frac{d\phi_x}{dz} - \alpha\tau_y \right) \right] \left( \frac{d\bar{\phi}_x}{dz} \right) dz - \int_0^L s_{yy} \left( \frac{dv}{dz} + \phi_x \right) \bar{\phi}_x dz = 0. \quad (17.58)$$

Equations (17.55) and (17.57) are coupled in the dependent variables  $v(z)$  and  $\phi_x(z)$ , as are (17.56) and (17.58). To obtain the principle of virtual work for the two dependent variables we add (17.56) and (17.58) to find

$$\bar{v} V_y \Big|_0^L + \bar{\phi}_x M_x \Big|_0^L - \int_0^L \left[ EI_{xx} \left( \frac{d\phi_x}{dz} - \alpha\tau_y \right) \right] \left( \frac{d\bar{\phi}_x}{dz} \right) dz - \int_0^L s_{yy} \left( \frac{dv}{dz} + \phi_x \right) \left( \frac{d\bar{v}}{dz} + \bar{\phi}_x \right) dz + \int_0^L f_y \bar{v} dz = 0. \quad (17.59)$$

Rearrange the terms in eq. (17.59) to get the **weak form**

$$\int_0^L \left[ EI_{xx} \left( \frac{d\phi_x}{dz} \right) \left( \frac{d\bar{\phi}_x}{dz} \right) + s_{yy} \psi_y \bar{\psi}_y \right] dz = \bar{v} V_y \Big|_0^L + \bar{\phi}_x M_x \Big|_0^L + \int_0^L f_y \bar{v} dz + \int_0^L \left( EI_{xx} \frac{d\bar{\phi}_x}{dz} \right) \alpha \tau_y dz, \quad (17.60)$$

where the virtual shear strain is

$$\bar{\psi}_y = \frac{d\bar{v}}{dz} + \bar{\phi}_x. \quad (17.61)$$

The **principle of virtual work** is determined from (17.60) is written in the form

$$B[\phi_x, \bar{\phi}_x, v, \bar{v}] = F[\bar{\phi}_x, \bar{v}] \quad \text{for every kinematically admissible } \bar{\phi}_x \text{ and } \bar{v}. \quad (17.62)$$

The internal virtual work is

$$B[\phi_x, \bar{\phi}_x, v, \bar{v}] = \int_0^L \left[ EI_{xx} \left( \frac{d\phi_x}{dz} \right) \left( \frac{d\bar{\phi}_x}{dz} \right) + s_{yy} \psi_y \bar{\psi}_y \right] dz, \quad (17.63)$$

and the external virtual work is

$$F[\bar{\phi}_x, \bar{v}] = \bar{v} V_y \Big|_0^L + \bar{\phi}_x M_x \Big|_0^L + \int_0^L f_y \bar{v} dz + \int_0^L \left( EI_{xx} \frac{d\bar{\phi}_x}{dz} \right) \alpha \tau_y dz. \quad (17.64)$$

Equations (5.81) and (5.82) on page 145 are the expressions for the strain energy. For the beam under consideration the strain energy from the mechanical strains is

$$U = \left( \frac{1}{2} \right) \int_0^L \left[ EI_{xx} \left( \frac{d\phi_x}{dz} \right)^2 + s_{yy} (\psi_y)^2 \right] dz = \left( \frac{1}{2} \right) B[\phi_x, \phi_x, v, v]. \quad (17.65)$$

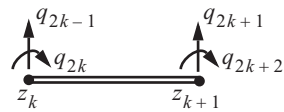
The first term in the integral (17.65) is the contribution of the bending to the strain energy, and the second term in the integral is the contribution of the transverse shear.

### 17.3.1 Element displacement functions and strains

The  $k$ th element is denoted by  $\Omega_k = \{z | z_k \leq z \leq z_{k+1}\}$ , where  $z_k < z_{k+1}$ . The standard element  $\Omega_{st} = \{\xi | -1 < \xi < 1\}$  (17.15) is mapped to the  $k$ th element by eq. (17.16), and the inverse mapping is given by eq. (17.17). The lateral displacement of the  $k$ th element is denoted by  $v^{(k)}(z)$  and the rotation by  $\phi_x^{(k)}(z)$ . Define the generalized nodal displacements as

$$v^{(k)}(z_k) = q_{2k-1} \quad \phi_x^{(k)}(z_k) = q_{2k} \quad v^{(k)}(z_{k+1}) = q_{2k+1} \quad \phi_x^{(k)}(z_{k+1}) = q_{2k+2}. \quad (17.66)$$

**Fig. 17.14**  
**Generalized**  
**nodal**  
**displacements.**



See figure 17.14. Admissible functions  $v(z)$  and  $\phi_x(z)$  must be continuous within an element and be continuous between elements. The following basis functions will be used for the beam element:

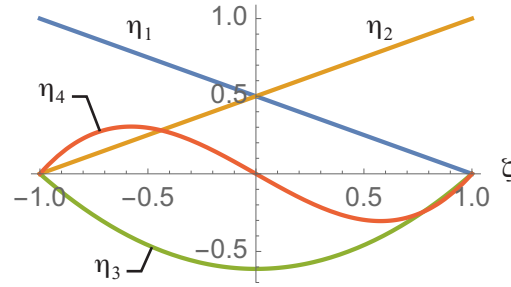
$$\eta_1(\xi) = (1 - \xi)/2 \quad \eta_2(\xi) = (1 + \xi)/2 \quad \eta_3(\xi) = \left(\frac{1}{2}\sqrt{\frac{3}{2}}\right)(\xi^2 - 1) \quad \eta_4(\xi) = \left(\frac{1}{2}\sqrt{\frac{5}{2}}\right)\xi(\xi^2 - 1). \quad (17.67)$$

The basis functions  $\eta_1(\xi)$  and  $\eta_2(\xi)$  are the **external shape functions** with the interpolation properties (17.18). The basis functions  $\eta_3(\xi)$  and  $\eta_4(\xi)$  are called **internal shape functions**. The internal shape functions vanish at the nodes  $\xi = \mp 1$ . The selection of the internal shape functions is based on Legendre polynomials. From Szabo and Babuska (1991, p. 38) the expressions for the internal shape function are

$$\eta_j(\xi) = \frac{1}{\sqrt{2(2j-1)}}[P_j(\xi) - P_{j-1}(\xi)] \quad j = 3, 4, \quad (17.68)$$

where  $P_j(\xi)$  is the Legendre polynomial of degree  $j$  in  $\xi$ .<sup>1</sup> Graphs of these basis functions are shown in figure 17.15.

**Fig. 17.15** Graphs of the basis functions for the beam element.



Consider the strain  $\kappa = d\phi_x/dz$  appearing in the bending moment (17.52), and the rotation  $\phi_x$  appearing in the transverse shear strain  $\psi_y(\xi)$  (17.53). As discussed by Reddy (2019, p. 294), in order to avoid the numerical problem of “shear locking” in the thin beam limit where  $\psi_y \rightarrow 0$ , a consistent interpolation procedure is employed. That is, a consistent interpolation of the shear strain  $\psi_y(\xi)$  requires that the polynomial for the displacement  $v(\xi)$  be one degree greater in  $\xi$  than the polynomial for the rotation  $\phi_x(\xi)$ . The beam element developed here is capable of representing a linear distribution of the bending moment  $M_x(\xi)$  and a constant shear force  $V_y$ . Then  $d\phi_x/dz$  is linear in  $\xi$ , which implies the rotation is quadratic in  $\xi$ . It follows that displacement  $v(\xi)$  is cubic in  $\xi$ . The trial functions for the  $k$ th element are

$$\begin{aligned} \phi_x^{(k)}(\xi) &= \eta_1(\xi)q_{2k} + \eta_2(\xi)q_{2k+2} + \eta_3(\xi)a_2^{(k)} \\ v^{(k)}(\xi) &= \eta_1(\xi)q_{2k-1} + \eta_2(\xi)q_{2k+1} + \eta_3(\xi)a_1^{(k)} + \eta_4(\xi)a_3^{(k)}. \end{aligned} \quad (17.69)$$

Internal degrees of freedom  $a_1^{(k)}$  and  $a_3^{(k)}$  are displacements with dimensions of length, and  $a_2^{(k)}$  is a rotation in radians. The internal degrees of freedom are not associated with a particular point in  $\Omega_{st}$ . That is, the beam element under consideration does not have internal nodes. Equation (17.69) is written in the matrix notation as

1.  $P_0 = 1$ ,  $P_1 = \xi$ ,  $P_2 = (3\xi^2 - 1)/2$ ,  $P_3 = (5\xi^3 - 3\xi)/2$ ,  $P_4 = (35\xi^4 - 30\xi^2 + 3)/8$ .

$$\begin{bmatrix} \phi_x^{(k)} \\ v^{(k)} \end{bmatrix} = [N_q(\xi)] \{q^{(k)}\} + [N_a(\xi)] \{a^{(k)}\}, \quad (17.70)$$

where the 4X1 and the 3X1 vectors of generalized displacements are

$$\{q^{(k)}\} = [q_{2k-1} \ q_{2k} \ q_{2k+1} \ q_{2k+2}]^T \quad \{a^{(k)}\} = [a_1^{(k)} \ a_2^{(k)} \ a_3^{(k)}]^T. \quad (17.71)$$

The shape function matrices are

$$[N_q(\xi)] = \begin{bmatrix} 0 & \eta_1 & 0 & \eta_2 \\ \eta_1 & 0 & \eta_2 & 0 \end{bmatrix} \quad [N_a(\xi)] = \begin{bmatrix} 0 & \eta_3 & 0 \\ \eta_3 & 0 & \eta_4 \end{bmatrix}. \quad (17.72)$$

This beam element has seven degrees of freedom. The virtual rotation and displacement for the kth element have the same functional form as (17.70) but with different coefficients:

$$\begin{bmatrix} \bar{\phi}_x^{(k)} \\ \bar{v}^{(k)} \end{bmatrix} = [N_q(\xi)] \{b^{(k)}\} + [N_a(\xi)] \{c^{(k)}\}, \quad (17.73)$$

where

$$\{b^{(k)}\} = [b_{2k-1} \ b_{2k} \ b_{2k+1} \ b_{2k+2}]^T \quad \{c^{(k)}\} = [c_1^{(k)} \ c_2^{(k)} \ c_3^{(k)}]^T. \quad (17.74)$$

Virtual degrees of freedom  $[b_{2k-1} \ b_{2k} \ b_{2k+1} \ b_{2k+2}]$  are associated with the nodal displacements (external shape functions), and virtual degrees of freedom  $[c_1^{(k)} \ c_2^{(k)} \ c_3^{(k)}]$  are associated with the internal shape functions. Elements of the virtual displacement vectors  $\{b_k\}$  and  $\{c^{(k)}\}$  are independent of the trial functions (17.69).

Using the chain rule and the inverse mapping (17.17), the strains for the kth element are

$$\frac{d\phi_x^{(k)}}{dz} = \left(\frac{2}{h_k}\right) \frac{d\phi_x^{(k)}}{d\xi} \quad \psi_y^{(k)} = \left(\frac{2}{h_k}\right) \frac{dv^{(k)}}{d\xi} + \phi_x^{(k)}, \quad (17.75)$$

Substitute (17.70) and (17.72) into the expressions for the strains (17.75) and write the strain-displacement relationship as

$$\{\epsilon^{(k)}\} = \begin{bmatrix} \frac{d\phi_x^{(k)}}{dz} \\ \psi_y^{(k)} \end{bmatrix} = \begin{bmatrix} 0 & \frac{2}{h_k} \frac{d\eta_1}{d\xi} & 0 & \frac{2}{h_k} \frac{d\eta_2}{d\xi} \\ \frac{2}{h_k} \frac{d\eta_1}{d\xi} & \eta_1 & \frac{2}{h_k} \frac{d\eta_2}{d\xi} & \eta_2 \end{bmatrix} \begin{bmatrix} q_{2k-1} \\ q_{2k} \\ q_{2k+1} \\ q_{2k+2} \end{bmatrix} + \begin{bmatrix} 0 & \frac{2}{h_k} \frac{d\eta_3}{d\xi} & 0 \\ \frac{2}{h_k} \frac{d\eta_3}{d\xi} & \eta_3 & \frac{2}{h_k} \frac{d\eta_4}{d\xi} \end{bmatrix} \begin{bmatrix} a_1^{(k)} \\ a_2^{(k)} \\ a_3^{(k)} \end{bmatrix}. \quad (17.76)$$

In compact notation the strain-displacement relation (17.76) is

$$\{\epsilon^{(k)}\} = [\epsilon_q(\xi)] \{q^{(k)}\} + [\epsilon_a(\xi)] \{a^{(k)}\}, \quad (17.77)$$

where the strain-displacement matrices associated with the external shape functions and internal shape functions are

$$\begin{bmatrix} \varepsilon_q(\zeta) \end{bmatrix} = \begin{bmatrix} 0 & \frac{-1}{h_k} & 0 & \frac{1}{h_k} \\ \frac{-1}{h_k} & \frac{(1-\zeta)}{2} & \frac{1}{h_k} & \frac{(1+\zeta)}{2} \end{bmatrix} \quad \begin{bmatrix} \varepsilon_a(\zeta) \end{bmatrix} = \begin{bmatrix} 0 & \left(\frac{\sqrt{6}\zeta}{h_k}\right) & 0 \\ \left(\frac{\sqrt{6}\zeta}{h_k}\right) & \left(\frac{1}{2}\sqrt{\frac{3}{2}}(\zeta^2-1)\right) & \left(\frac{1}{h_k}\sqrt{\frac{5}{2}}(3\zeta^2-1)\right) \end{bmatrix}. \quad (17.78)$$

The virtual strains are polynomials of the same degree as strains (17.77), but with independent coefficients:

$$\{\bar{\varepsilon}^{(k)}\} = \begin{bmatrix} \frac{d\bar{\Phi}_x^{(k)}}{dz} \\ \bar{\Psi}_y^{(k)} \end{bmatrix} = \begin{bmatrix} \varepsilon_q(\zeta) \end{bmatrix} \{b^{(k)}\} + \begin{bmatrix} \varepsilon_a(\zeta) \end{bmatrix} \{c^{(k)}\}. \quad (17.79)$$

### 17.3.2 Principle of virtual work for a typical element

The internal virtual work (17.63) for the kth element in matrix notation is

$$B[\Phi_x^{(k)}, \bar{\Phi}_x^{(k)}, v^{(k)}, \bar{v}^{(k)}] = \frac{h_k}{2} \int_{-1}^1 \{\bar{\varepsilon}^{(k)}\}^T [D] \{\varepsilon^{(k)}\} d\zeta, \quad (17.80)$$

where the material matrix is defined by

$$[D] = \begin{bmatrix} EI_{xx} & 0 \\ 0 & s_{yy} \end{bmatrix}. \quad (17.81)$$

Substitute the strain-displacement matrices (17.77) and (17.79) into (17.80) to get

$$B[\Phi_x^{(k)}, \bar{\Phi}_x^{(k)}, v^{(k)}, \bar{v}^{(k)}] = \frac{h_k}{2} \int_{-1}^1 \left( \{b^{(k)}\}^T [\varepsilon_q(\zeta)]^T + \{c^{(k)}\}^T [\varepsilon_a(\zeta)]^T \right) ([D] [\varepsilon_q(\zeta)] \{q^{(k)}\} + [D] [\varepsilon_a(\zeta)] \{a^{(k)}\}) d\zeta. \quad (17.82)$$

Perform the matrix multiplications in (17.82) and arrange the result to

$$\begin{aligned} B[\Phi_x^{(k)}, \bar{\Phi}_x^{(k)}, v^{(k)}, \bar{v}^{(k)}] = & \{b^{(k)}\}^T \left\{ \left( \frac{h_k}{2} \int_{-1}^1 [\varepsilon_q(\zeta)]^T [D] [\varepsilon_q(\zeta)] d\zeta \right) \{q^{(k)}\} + \left( \frac{h_k}{2} \int_{-1}^1 [\varepsilon_q(\zeta)]^T [D] [\varepsilon_a(\zeta)] d\zeta \right) \{a^{(k)}\} \right\} + \\ & \{c^{(k)}\}^T \left\{ \left( \frac{h_k}{2} \int_{-1}^1 [\varepsilon_a(\zeta)]^T [D] [\varepsilon_q(\zeta)] d\zeta \right) \{q^{(k)}\} + \left( \frac{h_k}{2} \int_{-1}^1 [\varepsilon_a(\zeta)]^T [D] [\varepsilon_a(\zeta)] d\zeta \right) \{a^{(k)}\} \right\} \end{aligned} \quad (17.83)$$

The expression for the internal virtual work (17.83) is written as

$$B[\Phi_x^{(k)}, \bar{\Phi}_x^{(k)}, v^{(k)}, \bar{v}^{(k)}] = \{b_k\}^T \{[K_{qq}]\{q^{(k)}\} + [K_{qa}]\{a^{(k)}\}\} + \{c^{(k)}\}^T \{[K_{aq}]\{q^{(k)}\} + [K_{aa}]\{a^{(k)}\}\}, \quad (17.84)$$

where the stiffness matrices are defined by

$$[K_{qq}] = \frac{h_k}{2} \int_{-1}^1 [\varepsilon_q(\zeta)]^T [D] [\varepsilon_q(\zeta)] d\zeta \quad [K_{qa}] = \frac{h_k}{2} \int_{-1}^1 [\varepsilon_q(\zeta)]^T [D] [\varepsilon_a(\zeta)] d\zeta, \text{ and} \quad (17.85)$$

$$[K_{aq}] = \frac{h_k}{2} \int_{-1}^1 [\varepsilon_a(\zeta)]^T [D] [\varepsilon_q(\zeta)] d\zeta \quad [K_{aa}] = \frac{h_k}{2} \int_{-1}^1 [\varepsilon_a(\zeta)]^T [D] [\varepsilon_a(\zeta)] d\zeta. \quad (17.86)$$

Evaluate the stiffness matrices to find

$$[K_{qq}] = \begin{bmatrix} \frac{s_{yy}}{h_k} & \frac{-s_{yy}}{2} & \frac{-s_{yy}}{h_k} & \frac{-s_{yy}}{2} \\ \frac{-s_{yy}}{2} & \frac{EI_{xx}}{h_k} + \frac{h_k s_{yy}}{3} & \frac{s_{yy}}{2} & \frac{-EI_{xx}}{h_k} + \frac{h_k s_{yy}}{6} \\ \frac{-s_{yy}}{h_k} & \frac{s_{yy}}{2} & \frac{s_{yy}}{h_k} & \frac{s_{yy}}{2} \\ \frac{-s_{yy}}{2} & \frac{-EI_{xx}}{h_k} + \frac{h_k s_{yy}}{6} & \frac{s_{yy}}{2} & \frac{EI_{xx}}{h_k} + \frac{h_k s_{yy}}{3} \end{bmatrix}, \text{ and} \quad (17.87)$$

$$[K_{qa}] = [K_{aq}]^T = \begin{bmatrix} 0 & \vdots & (s_{yy}/\sqrt{6}) & \vdots & 0 \\ (-s_{yy}/\sqrt{6}) & \vdots & (-h_k s_{yy}/(2\sqrt{6})) & \vdots & 0 \\ 0 & \vdots & (-s_{yy}/\sqrt{6}) & \vdots & 0 \\ (s_{yy}/\sqrt{6}) & \vdots & (-h_k s_{yy}/(2\sqrt{6})) & \vdots & 0 \end{bmatrix} \quad [K_{aa}] = \begin{bmatrix} \frac{2s_{yy}}{h_k} & 0 & \vdots & 0 \\ 0 & \frac{EI_{xx}}{h_k} + \frac{h_k s_{yy}}{5} & \vdots & \frac{s_{yy}}{\sqrt{15}} \\ 0 & \frac{s_{yy}}{\sqrt{15}} & \vdots & \frac{2s_{yy}}{h_k} \end{bmatrix}. \quad (17.88)$$

Take  $\{b^{(k)}\} = \{q^{(k)}\}$  and  $\{c^{(k)}\} = \{a^{(k)}\}$  in (17.84), and multiply the result by one-half, to find the strain energy in kth element as

$$U^{(k)} = \frac{1}{2} B[\phi_x^{(k)}, \phi_x^{(k)}, v^{(k)}, v^{(k)}] = \frac{1}{2} (\{q^{(k)}\}^T [K_{qq}] \{q^{(k)}\} + 2 \{q^{(k)}\}^T [K_{qa}] \{a^{(k)}\} + \{a^{(k)}\}^T [K_{aa}] \{a^{(k)}\}). \quad (17.89)$$

From the mapping (17.16), the distributed line load intensity and the thermal gradient are evaluated in the kth element as

$$f_y[z_k(\zeta)] = f_y[z_k \eta_1(\zeta) + z_{k+1} \eta_2(\zeta)] = f_y^{(k)}(\zeta) \\ \tau_y[z_k(\zeta)] = \tau_y[z_k \eta_1(\zeta) + z_{k+1} \eta_2(\zeta)] = \tau_y^{(k)}(\zeta). \quad (17.90)$$

The external virtual work (17.65) for the kth element is

$$F[\bar{\phi}_x^{(k)}, \bar{v}^{(k)}] = \bar{v}^{(k)} V_y^{(k)} \Big|_{z_k}^{z_{k+1}} + \bar{\phi}_x^{(k)} M_x^{(k)} \Big|_{z_k}^{z_{k+1}} + \int_{-1}^1 \bar{v}^{(k)} f_y^{(k)}(\zeta) \frac{h_k}{2} d\zeta + \int_{-1}^1 \left( EI_{xx} \frac{d\bar{\phi}_x^{(k)}}{d\zeta} \frac{2}{h_k} \right) \alpha \tau_y^{(k)}(\zeta) \left( \frac{h_k}{2} \right) d\zeta. \quad (17.91)$$

The boundary terms for the kth element are expressed in the form

$$\bar{v}^{(k)} V_y^{(k)} \Big|_{z_k}^{z_{k+1}} + \bar{\phi}_x^{(k)} M_x^{(k)} \Big|_{z_k}^{z_{k+1}} = b_{2k+1} Q_{2k+1}^{(k)} + b_{2k-1} Q_{2k-1}^{(k)} + b_{2k+2} Q_{2k+2}^{(k)} + b_{2k} Q_{2k}^{(k)}, \quad (17.92)$$

where generalized forces acting on the cross sections at  $z = z_k$  and  $z = z_{k+1}$  are defined by

$$Q_{2k-1}^{(k)} \equiv -V_y(z_k) \quad Q_{2k}^{(k)} \equiv -M_x(z_k) \quad Q_{2k+1}^{(k)} \equiv V_y(z_{k+1}) \quad Q_{2k+2}^{(k)} \equiv M_x(z_{k+1}). \quad (17.93)$$

The integral term with respect to the line load  $f_y^{(k)}(\zeta)$  in (17.91) expands to

$$\int_{-1}^1 v^{(k)} f_y^{(k)}(\zeta) \frac{h_k}{2} d\zeta = \frac{h_k}{2} \left( \int_{-1}^1 (b_{2k-1} \eta_1 + b_{2k+1} \eta_2 + c_1^{(k)} \eta_3 + c_3^{(k)} \eta_4) f_y^{(k)}(\zeta) d\zeta \right). \quad (17.94)$$

The integral term with respect to the temperature gradient  $\tau_y^{(k)}(\zeta)$  in (17.91) expands to

$$\int_{-1}^1 \left( EI_{xx} \frac{d\bar{\phi}_x^{(k)}}{d\zeta} \frac{2}{h_k} \right) \alpha \tau_y^{(k)}(\zeta) \left( \frac{h_k}{2} \right) d\zeta = \int_{-1}^1 EI_{xx} \left( b_{2k} \frac{d\eta_1}{d\zeta} + b_{2k+2} \frac{d\eta_2}{d\zeta} + c_2^{(k)} \frac{d\eta_3}{d\zeta} \right) \alpha \tau_y^{(k)}(\zeta) d\zeta. \quad (17.95)$$

Combining (17.92), (17.94), and (17.95), the external virtual work (17.91) is written in the matrix form

$$F[\bar{\phi}_x^{(k)}, v^{(k)}] = \{b^{(k)}\}^T (\{Q^{(k)}\} + \{FE^{(k)}\}) + \{c^{(k)}\}^T \{FI^{(k)}\}, \quad (17.96)$$

where the generalized nodal force vector is denoted by  $\{Q^{(k)}\}$ , the generalized force vector associated with the external shape functions by  $\{FE^{(k)}\}$ , and the generalized force vector associated with the internal shape functions by  $\{FI^{(k)}\}$ . These vectors are

$$\{Q^{(k)}\} = \begin{bmatrix} Q_{2k-1}^{(k)} \\ Q_{2k}^{(k)} \\ Q_{2k+1}^{(k)} \\ Q_{2k+2}^{(k)} \end{bmatrix}, \quad \{FE^{(k)}\} = \begin{bmatrix} FE_{2k-1}^{(k)} \\ FE_{2k}^{(k)} \\ FE_{2k+1}^{(k)} \\ FE_{2k+2}^{(k)} \end{bmatrix} = \begin{bmatrix} \frac{h_k}{2} \int_{-1}^1 \eta_1 f_y^{(k)} d\zeta \\ \int_{-1}^1 EI_{xx} \frac{d\eta_1}{d\zeta} \alpha \tau_y^{(k)} d\zeta \\ \frac{h_k}{2} \int_{-1}^1 \eta_2 f_y^{(k)} d\zeta \\ \int_{-1}^1 EI_{xx} \frac{d\eta_2}{d\zeta} \alpha \tau_y^{(k)} d\zeta \end{bmatrix}, \quad \{FI^{(k)}\} = \begin{bmatrix} FI_1^{(k)} \\ FI_2^{(k)} \\ FI_3^{(k)} \end{bmatrix} = \begin{bmatrix} \frac{h_k}{2} \int_{-1}^1 \eta_3 f_y^{(k)} d\zeta \\ \int_{-1}^1 EI_{xx} \frac{d\eta_3}{d\zeta} \alpha \tau_y^{(k)} d\zeta \\ \frac{h_k}{2} \int_{-1}^1 \eta_4 f_y^{(k)} d\zeta \end{bmatrix}. \quad (17.97)$$

Equate the internal virtual work (17.84) to the external virtual work (17.96) to get

$$\{b^{(k)}\}^T ([K_{qq}]\{q^{(k)}\} + [K_{qa}]\{a^{(k)}\}) + \{c^{(k)}\}^T ([K_{aq}]\{q^{(k)}\} + [K_{aa}]\{a^{(k)}\}) = \{b^{(k)}\}^T (\{Q^{(k)}\} + \{FE^{(k)}\}) + \{c^{(k)}\}^T \{FI^{(k)}\}. \quad (17.98)$$

The principle of virtual work leads to the governing matrix relations for the kth element:

$$[K_{qq}]\{q^{(k)}\} + [K_{qa}]\{a^{(k)}\} = \{Q^{(k)}\} + \{FE^{(k)}\} \quad \forall \{b^{(k)}\} \neq 0_{4 \times 1}, \quad (17.99)$$

$$[K_{aq}]\{q^{(k)}\} + [K_{aa}]\{a^{(k)}\} = \{FI^{(k)}\} \quad \forall \{c^{(k)}\} \neq 0_{3 \times 1}. \quad (17.100)$$

### 17.3.3 Static condensation

The internal degrees of freedom  $a_1^{(k)}$ ,  $a_2^{(k)}$ , and  $a_3^{(k)}$  associated with the internal shape functions do not affect interelement continuity. To reduce the number of system equations to solve resulting from the assembly of elements, the internal degrees of freedom can be eliminated at the element level in the process called static condensation. Further, the assembly algorithm is simplified if only the nodal displacements, or external degrees of freedom are employed. The internal degrees of freedom are eliminated in terms of the nodal displacements  $\{q^{(k)}\}$  and the generalized force vector  $\{FI^{(k)}\}$  by solving (17.100). Thus, from (17.100)

$$\{a^{(k)}\} = [K_{aa}]^{-1} \{FI^{(k)}\} - [K_{aa}]^{-1} [K_{aq}] \{q^{(k)}\} = [K_{aa}]^{-1} \{FI^{(k)}\} + [G_{aq}] \{q^{(k)}\}, \quad (17.101)$$

where

$$[K_{aa}]^{-1} = \begin{bmatrix} \frac{h_k}{2s_{yy}} & 0 & 0 \\ 0 & \frac{6h_k\mu}{EI_{xx}} & -\frac{\sqrt{\frac{3}{5}}h_k^2\mu}{EI_{xx}} \\ 0 & -\frac{\sqrt{\frac{3}{5}}h_k^2\mu}{EI_{xx}} & \frac{30EI_{xx}h_k + 3h_k^3s_{yy}}{60EI_{xx}s_{yy} + 5h_k^2s_{yy}^2} \end{bmatrix} \quad [G_{aq}] = \begin{bmatrix} 0 & \frac{h_k}{2\sqrt{6}} & 0 & \frac{-h_k}{2\sqrt{6}} \\ -\frac{\sqrt{6}h_k s_{yy}\mu}{EI_{xx}} & \frac{\sqrt{\frac{3}{2}}h_k^2 s_{yy}\mu}{EI_{xx}} & \frac{\sqrt{6}h_k s_{yy}\mu}{EI_{xx}} & \frac{\sqrt{\frac{3}{2}}h_k^2 s_{yy}\mu}{EI_{xx}} \\ \frac{h_k^2 s_{yy}\mu}{\sqrt{10}EI_{xx}} & \frac{-h_k^3 s_{yy}\mu}{2\sqrt{10}EI_{xx}} & \frac{-h_k^2 s_{yy}\mu}{\sqrt{10}EI_{xx}} & \frac{-h_k^3 s_{yy}\mu}{2\sqrt{10}EI_{xx}} \end{bmatrix}. \quad (17.102)$$

We define  $[G_{aq}]$  as the Guyan matrix, because the method of static condensation was first proposed by Guyan (1965), and it was also introduced by Irons (1965). In eq. (17.102) we have introduced the dimensionless factor

$$\mu = \frac{EI_{xx}}{12EI_{xx} + h_k^2 s_{yy}}. \quad (17.103)$$

Substitute the displacement vector  $\{a^{(k)}\}$  from (17.101) into eq. (17.99) and write the final result as

$$[K^{(k)}] \{q^{(k)}\} = \{Q^{(k)}\} + \{F^{(k)}\}, \quad (17.104)$$

where

$$[K^{(k)}] = [K_{qq}] + [K_{qa}] [G_{aq}] \quad (17.105)$$

$$\{F^{(k)}\} = \{FE^{(k)}\} - [K_{qa}] [K_{aa}]^{-1} \{FI^{(k)}\} = \{FE^{(k)}\} + [G_{aq}]^T \{FI^{(k)}\}.$$

The 4X4 matrix  $[K^{(k)}]$  is the condensed stiffness matrix for the kth element, and the 4X1 vector  $\{F^{(k)}\}$  is the condensed generalized force vector for the kth element. The generalized forces acting on the beam element separated from the nodes, and the generalized forces acting on the nodes, are depicted in figure 17.16.

The 4X4 condensed stiffness matrix is



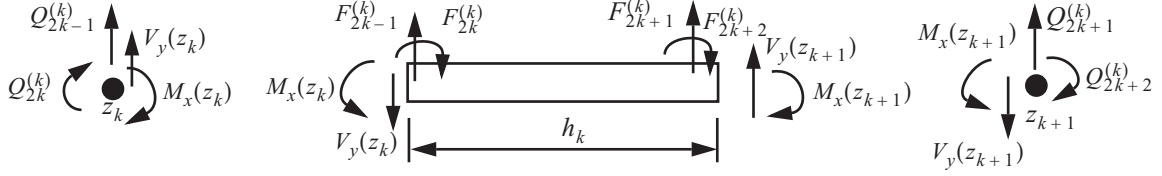


Fig. 17.16 Generalized forces acting on the beam and the nodes for element  $\Omega_k$ .

$$[K^{(k)}] = \mu \begin{bmatrix} \frac{12s_{yy}}{h_k} & -6s_{yy} & -\frac{12s_{yy}}{h_k} & -6s_{yy} \\ -6s_{yy} & \frac{12EI_{xx}}{h_k} + 4h_k s_{yy} & 6s_{yy} & -\frac{12EI_{xx}}{h_k} + 2h_k s_{yy} \\ -\frac{12s_{yy}}{h_k} & 6s_{yy} & \frac{12s_{yy}}{h_k} & 6s_{yy} \\ -6s_{yy} & -\frac{12EI_{xx}}{h_k} + 2h_k s_{yy} & 6s_{yy} & \frac{12EI_{xx}}{h_k} + 4h_k s_{yy} \end{bmatrix}. \quad (17.106)$$

### 17.3.4 Bending moment and shear force

Substitute vector  $\{a^{(k)}\}$  from (17.101) into the strain vector (17.77) to get

$$\{\epsilon^{(k)}\} = [\epsilon_q(\zeta)] \{q^{(k)}\} + [\epsilon_a(\zeta)] \{a^{(k)}\} = \left( [\epsilon_q(\zeta)] + [\epsilon_a] [G_{aq}] \right) \{q^{(k)}\} + [\epsilon_a(\zeta)] [K_{aa}]^{-1} \{FI^{(k)}\}. \quad (17.107)$$

The bending moment and shear force are determined from the matrix relation

$$\begin{bmatrix} M_x^{(k)} \\ V_y^{(k)} \end{bmatrix} = [D] \left( \{\epsilon^{(k)}\} - \begin{bmatrix} \alpha \tau_y^{(k)} \\ 0 \end{bmatrix} \right). \quad (17.108)$$

Substitute the strain (17.107) into (17.108) to find the matrix relation for the moment and shear:

$$\begin{bmatrix} M_x^{(k)} \\ V_y^{(k)} \end{bmatrix} = [D] \left( [\epsilon_q(\zeta)] + [\epsilon_a] [G_{aq}] \right) \{q^{(k)}\} + [D] \left( [\epsilon_a(\zeta)] [K_{aa}]^{-1} \{FI^{(k)}\} - \begin{bmatrix} \alpha \tau_y^{(k)} \\ 0 \end{bmatrix} \right). \quad (17.109)$$

The previous equation is written as

$$\begin{bmatrix} M_x^{(k)} \\ V_y^{(k)} \end{bmatrix} = [S_q(\zeta)] \begin{bmatrix} q_{2k-1} \\ q_{2k} \\ q_{2k+1} \\ q_{2k+2} \end{bmatrix} + [S_F(\zeta)] \begin{bmatrix} FI_1^{(k)} \\ FI_2^{(k)} \\ FI_3^{(k)} \end{bmatrix} - \begin{bmatrix} EI_{xx} \alpha \tau_y^{(k)}(\zeta) \\ 0 \end{bmatrix}, \quad (17.110)$$

where the stress matrices are defined as

$$[S_q(\zeta)] = \begin{bmatrix} -6s_{yy}\mu\zeta \left( \frac{-EI_{xx}}{h_k} + 3h_k s_{yy}\mu\zeta \right) & 6s_{yy}\mu\zeta \left( \frac{EI_{xx}}{h_k} + 3h_k s_{yy}\mu\zeta \right) \\ \frac{-12\mu s_{yy}}{h_k} & 6s_{yy}\mu & \frac{12\mu s_{yy}}{h_k} & 6s_{yy}\mu \end{bmatrix}, \text{ and} \quad (17.111)$$

$$[S_F(\zeta)] = \begin{bmatrix} 0 & 6\sqrt{6}\mu\zeta & -3\sqrt{\frac{2}{5}}h_k\mu\zeta \\ \sqrt{\frac{3}{2}}\zeta \left( \frac{-\sqrt{6}h_k s_{yy}\mu}{EI_{xx}} \right) & \frac{3[20EI_{xx}(-1 + 3\zeta^2) + h_k^2 s_{yy}(-1 + 5\zeta^2)]\mu}{2\sqrt{10}EI_{xx}} \end{bmatrix}. \quad (17.112)$$

### 17.3.5 Requirements of the interpolation functions.

The remeshing procedure for an increasing number of elements presented in article 17.2.2 has the old mesh embedded in the new mesh. Monotonic convergence of this sequence of finite element meshes also requires the interpolation functions to be **compatible** and **complete** (Bathe, 1982). Compatibility means the displacements must be continuous within the elements and between elements. Completeness means the displacement functions of the element must be able to represent the rigid body displacements and uniform strain states. Consequently, the beam element under consideration must be capable of representing zero strain states for rigid body displacements when the element is not subject to external loads. Note that the determinate of the stiffness matrix (17.106) is zero, since the element is not restrained against rigid body displacements. Now consider the response of the beam element under the two rigid body modes:

$$\{q^{(k)}\}_1 = [1 \ 0 \ 1 \ 0]^T \text{ and } \{q^{(k)}\}_2 = [h_k/2 \ 1 \ -h_k/2 \ 1]^T. \quad (17.113)$$

Generalized displacement vector  $\{q^{(k)}\}_1$  is a vertical displacement of the element, and the generalized displacement vector  $\{q^{(k)}\}_2$  is a clockwise rotation of the element about its center. In the absence of external loading the generalized force vectors  $\{Q^{(k)}\} = 0_{4 \times 1}$ ,  $\{FE^{(k)}\} = 0_{4 \times 1}$ ,  $\{FI^{(k)}\} = 0_{3 \times 1}$ , and  $\{F^{(k)}\} = 0_{4 \times 1}$ . The internal degrees of freedom (17.101) for the rigid body modes and no external loading also vanish; i.e.,

$$\{a^{(k)}\}_1 = [G_{aq}] \{q^{(k)}\}_1 = 0_{3 \times 1} \text{ and } \{a^{(k)}\}_2 = [G_{aq}] \{q^{(k)}\}_2 = 0_{3 \times 1}. \quad (17.114)$$

Also, evaluation of eq. (17.104) for the rigid body displacements results in  $[K^{(k)}] \{q^{(k)}\}_1 = 0_{4 \times 1}$  and

$[K^{(k)}] \{q^{(k)}\}_2 = 0_{4 \times 1}$ , which are consistent with vanishing external loads. Finally, the strains (17.77) in the element vanish for the rigid body displacements:

$$\{\epsilon^{(k)}\}_1 = [\epsilon_q(\zeta)] \{q^{(k)}\}_1 = 0_{2 \times 1} \text{ and } \{\epsilon^{(k)}\}_2 = [\epsilon_q(\zeta)] \{q^{(k)}\}_2 = 0_{2 \times 1}. \quad (17.115)$$

Therefore, the beam element satisfies part of the completeness requirement of vanishing strains under rigid body displacements. Constant strain states are demonstrated in the next two examples.

**Example 17.3 Pure bending**

A simply supported, uniform beam is shown in figure 17.17(a). It is subject to equal and opposite moments  $M_a$  at each end, and a temperature gradient through the thickness  $\tau_y$  that is uniform along the length of the beam. The lateral distributed load intensity  $f_y = 0$ ,  $0 < z < L$ . The beam is modeled with one finite element, and the two nodes are  $z_1 = 0$  and  $z_2 = L$  as shown in figure 17.17(b). The mapping (17.16) is  $z = \frac{1}{2}(1 + \xi)L$ .

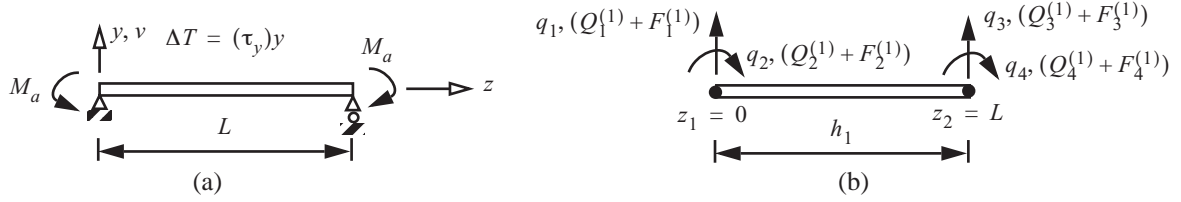


**Fig. 17.17 (a) Pure bending of a simply supported beam. (b) Finite element model.**

The generalized displacement vector  $\{q^{(1)}\} = [q_1 \ q_2 \ q_3 \ q_4]^T$  is partitioned to unknown components  $\{q_\alpha\}$  and known components  $\{q_\beta\}$ :

$$\{q^{(1)}\} = \begin{bmatrix} \{q_\alpha\} \\ \{q_\beta\} \end{bmatrix}, \quad \{q_\alpha\} = \begin{bmatrix} q_2 \\ q_4 \end{bmatrix}, \quad \text{and} \quad \{q_\beta\} = \begin{bmatrix} q_1 \\ q_3 \end{bmatrix} = \begin{bmatrix} 0 \\ 0 \end{bmatrix}. \quad (\text{a})$$

The generalized displacement vector (17.69) is

$$\begin{bmatrix} \phi_x^{(1)}(\xi) \\ v^{(1)}(\xi) \end{bmatrix} = \begin{bmatrix} 0 & \eta_1 & 0 & \eta_2 \\ \eta_1 & 0 & \eta_2 & 0 \end{bmatrix} \begin{bmatrix} 0 \\ q_2 \\ 0 \\ q_4 \end{bmatrix} + \begin{bmatrix} 0 & \eta_3 & 0 \\ \eta_3 & 0 & \eta_4 \end{bmatrix} \begin{bmatrix} a_1 \\ a_2 \\ a_3 \end{bmatrix} = \begin{bmatrix} \eta_1(\xi)q_2 + \eta_2(\xi)q_4 + \eta_3(\xi)a_2 \\ \eta_3(\xi)a_1 + \eta_4(\xi)a_3 \end{bmatrix}. \quad (\text{b})$$

Displacement boundary conditions  $v(-1) = 0$  and  $v(1) = 0$  are satisfied by (b). Matrix (17.106) represents the unrestrained structural stiffness matrix  $[K_u]$ . The rows and columns of  $[K_u]$  are interchanged to the order 2, 4, 1, and 3 to facilitate partitioning it into submatrices:

$$[K_u] = \mu \begin{bmatrix} q_2 & q_4 & q_1 & q_3 \\ \frac{12EI_{xx}}{L} + 4Ls_{yy} & \frac{-12EI_{xx}}{L} + 2Ls_{yy} & -6s_{yy} & 6s_{yy} \\ \frac{-12EI_{xx}}{L} + 2Lk_{yy} & \frac{12EI_{xx}}{L} + 4Lk_{yy} & -6s_{yy} & 6s_{yy} \\ -6s_{yy} & -6s_{yy} & \frac{12s_{yy}}{L} & -\frac{12s_{yy}}{L} \\ 6s_{yy} & 6s_{yy} & -\frac{12s_{yy}}{L} & \frac{12s_{yy}}{L} \end{bmatrix} = \begin{bmatrix} [K_{\alpha\alpha}] & [K_{\alpha\beta}] \\ [K_{\beta\alpha}] & [K_{\beta\beta}] \end{bmatrix} \quad (c)$$

The restrained structural stiffness matrix is

$$[K_{\alpha\alpha}] = \frac{EI_{xx}}{12EI_{xx} + L^2s_{yy}} \begin{bmatrix} \frac{12EI_{xx}}{L} + 4Ls_{yy} & \frac{-12EI_{xx}}{L} + 2Ls_{yy} \\ \frac{-12EI_{xx}}{L} + 2Ls_{yy} & \frac{12EI_{xx}}{L} + 4Ls_{yy} \end{bmatrix}, \quad (d)$$

where  $\mu$  is defined in eq. (17.103). From (17.97) actions  $FI_1^{(1)} = FI_2^{(1)} = FI_3^{(1)} = 0$ , since  $f_y = 0$  and  $\tau_y$  is spatially uniform in  $\zeta$ . Hence, from (17.105) the generalized nodal force vector is  $\{F^{(1)}\} = \{FE^{(1)}\}$ , which is evaluated from (17.97). The generalized nodal force vector  $\{Q^{(1)}\} = [Q_1^{(1)} \ Q_2^{(1)} \ Q_3^{(1)} \ Q_4^{(1)}]^T$  is partitioned into known components  $\{Q_\alpha\}$  and unknown components  $\{Q_\beta\}$ :

$$\{Q_\alpha\} = \begin{bmatrix} Q_2 \\ Q_4 \end{bmatrix} = \begin{bmatrix} -M_a \\ M_a \end{bmatrix}, \text{ and } \{Q_\beta\} = \begin{bmatrix} Q_1 \\ Q_3 \end{bmatrix}. \quad (e)$$

The generalized force vector  $\{F^{(1)}\} = [F_1^{(1)} \ F_2^{(1)} \ F_3^{(1)} \ F_4^{(1)}]^T$  (17.97) is prescribed and is partitioned as

$$\{F_\alpha\} = \begin{bmatrix} F_2^{(1)} \\ F_4^{(1)} \end{bmatrix} = \begin{bmatrix} \int_{-1}^1 \frac{(-EI_{xx}\alpha\tau_y)}{2} d\zeta \\ \int_{-1}^1 \frac{(EI_{xx}\alpha\tau_y)}{2} d\zeta \end{bmatrix} = \begin{bmatrix} -EI_{xx}\alpha\tau_y \\ EI_{xx}\alpha\tau_y \end{bmatrix}, \text{ and } \{F_\beta\} = \begin{bmatrix} F_1^{(1)} \\ F_3^{(1)} \end{bmatrix} = \begin{bmatrix} 0 \\ 0 \end{bmatrix}. \quad (f)$$

The matrix equation to determine the unknown displacements is  $[K_{\alpha\alpha}]\{q_\alpha\} = \{Q_\alpha\} + \{F_\alpha\}$ , or

$$\frac{EI_{xx}}{12EI_{xx} + L^2s_{yy}} \begin{bmatrix} \frac{12EI_{xx}}{L} + 4Ls_{yy} & \frac{-12EI_{xx}}{L} + 2Ls_{yy} \\ \frac{-12EI_{xx}}{L} + 2Ls_{yy} & \frac{12EI_{xx}}{L} + 4Ls_{yy} \end{bmatrix} \begin{bmatrix} q_2 \\ q_4 \end{bmatrix} = \begin{bmatrix} -M_a - EI_{xx}\alpha\tau_y \\ M_a + EI_{xx}\alpha\tau_y \end{bmatrix}. \quad (g)$$

The solution for  $\{q_\alpha\}$  from eq. (g) is

$$\{q_\alpha\} = \begin{bmatrix} q_2 \\ q_4 \end{bmatrix} = \frac{L(M_a + EI_{xx}\alpha\tau_y)}{2EI_{xx}} \begin{bmatrix} -1 \\ 1 \end{bmatrix}. \quad (\text{h})$$

The rotations are equal magnitude and of the opposite sense. The reactive force vector is determined from  $[K_{\beta\alpha}]\{q_\alpha\} + [K_{\beta\beta}]\{q_\beta\} = \{Q_\beta\} + \{F_\beta\}$ , which is

$$\frac{EI_{xx}}{12EI_{xx} + L^2s_{yy}} \begin{bmatrix} -6s_{yy} & -6s_{yy} \\ 6s_{yy} & 6s_{yy} \end{bmatrix} \frac{L(M_a + EI_{xx}\alpha\tau_y)}{2EI_{xx}} \begin{bmatrix} -1 \\ 1 \end{bmatrix} = \frac{L(M_a + EI_{xx}\alpha\tau_y)}{2(12EI_{xx} + L^2s_{yy})} \begin{bmatrix} 6s_{yy} - 6s_{yy} \\ -6s_{yy} + 6s_{yy} \end{bmatrix} = \begin{bmatrix} 0 \\ 0 \end{bmatrix}. \quad (\text{i})$$

Hence, the reactive force vector  $\{Q_\beta\}$  vanishes. The vector  $\{a^{(1)}\}$  associated with internal shape function is determined from (17.101) and (17.102). These computations are

$$\{a^{(1)}\} = [K_{aa}]^{-1}\{FI^{(1)}\} + [G_{aq}]\{q_k\} = \mathbf{0}_{3 \times 1} + \begin{bmatrix} 0 & \frac{L}{2\sqrt{6}} & 0 & \frac{-L}{2\sqrt{6}} \\ -\frac{\sqrt{6}Ls_{yy}\mu}{EI_{xx}} & \frac{\sqrt{\frac{3}{2}}L^2\mu}{EI_{xx}} & \frac{\sqrt{6}Ls_{yy}\mu}{EI_{xx}} & \frac{\sqrt{\frac{3}{2}}L^2\mu}{EI_{xx}} \\ \frac{L^2s_{yy}\mu}{\sqrt{10}EI_{xx}} & \frac{-L^3s_{yy}\mu}{2\sqrt{10}EI_{xx}} & \frac{-L^2s_{yy}\mu}{\sqrt{10}EI_{xx}} & \frac{-L^3s_{yy}\mu}{2\sqrt{10}EI_{xx}} \end{bmatrix} \begin{bmatrix} 0 \\ q_2 \\ 0 \\ q_4 \end{bmatrix}. \quad (\text{j})$$

Since  $q_2 = -q_4$ , we get

$$\{a^{(1)}\} = \begin{bmatrix} \frac{-L}{\sqrt{6}} \\ 0 \\ 0 \\ 0 \end{bmatrix} q_4 = \begin{bmatrix} \frac{-L^2(M_a + EI_{xx}\alpha\tau_y)}{2\sqrt{6}EI_{xx}} \\ 0 \\ 0 \\ 0 \end{bmatrix}. \quad (\text{k})$$

The generalized displacement vector in eq. (b) is

$$\begin{bmatrix} \phi_x^{(1)} \\ v^{(1)} \end{bmatrix} = \begin{bmatrix} \frac{L(M_a + EI_{xx}\alpha\tau_y)\xi}{2EI_{xx}} \\ \frac{L^2(M_a + EI_{xx}\alpha\tau_y)(1 - \xi^2)}{8EI_{xx}} \end{bmatrix}. \quad (\text{l})$$

From (17.110) the bending moment and shear force are

$$\begin{bmatrix} M_x \\ V_y \end{bmatrix} = [S_q] \begin{bmatrix} 0 \\ q_2 \\ 0 \\ q_4 \end{bmatrix} + [S_F] \begin{bmatrix} 0 \\ 0 \\ 0 \\ 0 \end{bmatrix} - \begin{bmatrix} EI_{xx}\alpha\tau_y \\ 0 \end{bmatrix} = [S_q] \begin{bmatrix} 0 \\ -1 \\ 0 \\ 1 \end{bmatrix} q_4 - \begin{bmatrix} EI_{xx}\alpha\tau_y \\ 0 \end{bmatrix}. \quad (\text{m})$$

The matrix multiplication of  $[S_q]$  times the 4X1 vector in eq. (m) is

$$\begin{bmatrix} -6s_{yy}\mu\zeta \left( \frac{-EI_{xx}}{L} + 3Ls_{yy}\mu\zeta \right) & 6s_{yy}\mu\zeta \left( \frac{EI_{xx}}{L} + 3Ls_{yy}\mu\zeta \right) \\ \frac{-12\mu s_{yy}}{L} & \frac{12\mu s_{yy}}{L} \\ 6s_{yy}\mu & 6s_{yy}\mu \end{bmatrix} \begin{bmatrix} 0 \\ -1 \\ 0 \\ 1 \end{bmatrix} = \begin{bmatrix} -\left( \frac{-EI_{xx}}{L} + 3\mu\zeta Ls_{yy} \right) + \left( \frac{EI_{xx}}{L} + 3\mu\zeta Ls_{yy} \right) \\ 0 \\ 0 \\ 0 \end{bmatrix}. \quad (n)$$

The final result for the bending moment and shear force is

$$\begin{bmatrix} M_x \\ V_y \end{bmatrix} = \begin{bmatrix} \frac{2EI_{xx}}{L} \\ 0 \end{bmatrix} \frac{L(M_a + EI_{xx}\alpha\tau_y)}{2EI_{xx}} - \begin{bmatrix} EI_{xx}\alpha\tau_y \\ 0 \end{bmatrix} = \begin{bmatrix} M_a \\ 0 \end{bmatrix}. \quad (o)$$

The bending moment is constant in the element and it is equal to the prescribed external moment  $M_a$ . The shear force vanishes within the element. If  $M_a = 0$  and  $\tau_y \neq 0$ , then bending moment  $M_x = 0$ . However, the rotation and displacement are not zero; i.e.,

$$\begin{bmatrix} \phi_x \\ v \end{bmatrix} = \begin{bmatrix} (L\alpha\tau_y)\zeta/2 \\ \frac{L^2}{8}\alpha\tau_y(1-\zeta^2) \end{bmatrix} \Big|_{M_a=0}. \quad (p)$$

This one-element solution is the same as the exact solution. ■

#### Example 17.4 Transverse bending

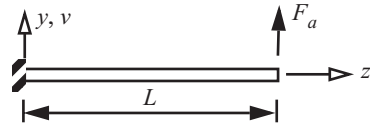


**Fig. 17.18 Transverse bending of a cantilever beam.**

A cantilever, uniform beam of length  $L$  is subject to a vertical force  $F_a$  at its free end as shown in figure 17.18. The distributed load intensity  $f_y = 0$ , and the through-the-thickness temperature gradient  $\tau_y(z) = 0$ ,  $0 < z < L$ . One element models the entire beam as shown in figure 17.17(b). Since  $f_y = 0$  and  $\tau_y(z) = 0$ , prescribed actions (17.97)  $\{FE^{(1)}\} = 0_{4 \times 1}$  and  $\{FI^{(1)}\} = 0_{3 \times 1}$ . It follows from (17.105) that  $\{F^{(1)}\} = 0_{4 \times 1}$ . The 4X1

generalized nodal displacement vector  $\{q^{(1)}\}$  and the 4X1 generalized force vector  $\{Q^{(1)}\}$  are partitioned into known and unknown components as follows:

$$\{q_\alpha\} = [q_3 \ q_4]^T, \{Q_\alpha\} = [Q_3 \ Q_4]^T = [F_a \ 0]^T, \{q_\beta\} = [q_1 \ q_2]^T = 0_{2 \times 1}, \text{ and } \{Q_\beta\} = [Q_1 \ Q_2]^T. \quad (a)$$

Matrix (17.106) represents the unrestrained structural stiffness matrix  $[K_u]$ . The rows and columns of  $[K_u]$  are interchanged to the order 3, 4, 1, and 2 to facilitate partitioning it into submatrices:

$$[K_u] = \mu \begin{bmatrix} q_3 & q_4 & q_1 & q_2 \\ \frac{12s_{yy}}{L} & 6s_{yy} & -\frac{12s_{yy}}{L} & 6s_{yy} \\ 6s_{yy} & \frac{12EI_{xx}}{L} + 4Ls_{yy} & -6s_{yy} & \frac{-12EI_{xx}}{L} + 2Ls_{yy} \\ -\frac{12s_{yy}}{L} & -6s_{yy} & \frac{12s_{yy}}{L} & -6s_{yy} \\ 6s_{yy} & \frac{-12EI_{xx}}{L} + 2Ls_{yy} & -6s_{yy} & \frac{12EI_{xx}}{L} + 4Ls_{yy} \end{bmatrix} = \begin{bmatrix} [K_{\alpha\alpha}] & [K_{\alpha\beta}] \\ [K_{\beta\alpha}] & [K_{\beta\beta}] \end{bmatrix} \quad (b)$$

The matrix equation to determine the unknown displacements is  $[K_{\alpha\alpha}]\{q_\alpha\} + [K_{\alpha\beta}]\{q_\beta\} = \{Q_\alpha\}$ , or

$$\frac{EI_{xx}}{12EI_{xx} + L^2s_{yy}} \begin{bmatrix} \frac{12s_{yy}}{L} & 6s_{yy} \\ 6s_{yy} & \frac{12EI_{xx}}{L} + 4Ls_{yy} \end{bmatrix} \begin{bmatrix} q_3 \\ q_4 \end{bmatrix} = \begin{bmatrix} F_a \\ 0 \end{bmatrix}. \quad (c)$$

The solution of eq. (c) for the displacements is

$$\begin{bmatrix} q_3 \\ q_4 \end{bmatrix} = \begin{bmatrix} \frac{F_a L^3}{3EI_{xx}} + \frac{F_a L}{s_{yy}} \\ -\frac{F_a L^2}{2EI_{xx}} \end{bmatrix}. \quad (d)$$

The matrix formulation to determine the generalized reactive force vector is  $[K_{\beta\alpha}]\{q_\alpha\} + [K_{\beta\beta}]\{q_\beta\} = \{Q_\beta\}$ , or

$$\begin{bmatrix} Q_1 \\ Q_2 \end{bmatrix} = \mu \begin{bmatrix} -\frac{12s_{yy}}{L} & -6s_{yy} \\ 6s_{yy} & \frac{-12EI_{xx}}{L} + 2Ls_{yy} \end{bmatrix} \begin{bmatrix} \frac{L^2}{3EI_{xx}} + \frac{1}{s_{yy}} \\ \frac{-L}{2EI_{xx}} \end{bmatrix} F_a L = \mu L F_a \begin{bmatrix} \frac{-(12EI_{xx} + L^2s_{yy})}{EI_{xx}L} \\ \frac{12EI_{xx} + L^2s_{yy}}{EI_{xx}} \end{bmatrix} = \begin{bmatrix} -F_a \\ L F_a \end{bmatrix}. \quad (e)$$

The generalized displacement vector  $\{a^{(1)}\}$  associated with internal shape function is determined from (17.101) and (17.102). The result is

$$\{a^{(1)}\} = [K_{aa}]^{-1} \{F I^{(1)}\} + [G_{aq}]\{q_k\} = 0_{3 \times 1} + [G_{aq}] \begin{bmatrix} 0 \\ q_3 \\ q_4 \end{bmatrix} = \begin{bmatrix} \frac{F_a L^2}{4\sqrt{6}EI_{xx}} \\ \frac{F_a L^2}{2\sqrt{6}EI_{xx}} \\ -\frac{F_a L^3}{12\sqrt{10}EI_{xx}} \end{bmatrix}. \quad (f)$$

The generalized displacement vector (17.70) is

$$\begin{bmatrix} \phi_x^{(1)} \\ v^{(1)} \end{bmatrix} = \begin{bmatrix} 0 & \eta_1 & 0 & \eta_2 \\ \eta_1 & 0 & \eta_2 & 0 \end{bmatrix} \begin{bmatrix} 0 \\ 0 \\ q_3 \\ q_4 \end{bmatrix} + \begin{bmatrix} 0 & \eta_3 & 0 \\ \eta_3 & 0 & \eta_4 \end{bmatrix} \begin{bmatrix} a_1^{(1)} \\ a_2^{(1)} \\ a_3^{(1)} \end{bmatrix} = \begin{bmatrix} \frac{F_a L^3}{8EI_{xx}}(-3 - 2\zeta + \zeta^2) \\ \frac{F_a L(1 + \zeta)[24EI_{xx} + L^2 s_{yy}(5 + 4\zeta - \zeta^2)]}{48EI_{xx}s_{yy}} \end{bmatrix}. \quad (g)$$

The vector of the bending moment and shear force (17.110) is

$$\begin{bmatrix} M_x \\ V_y \end{bmatrix} = [S_q] \begin{bmatrix} 0 \\ 0 \\ q_3 \\ q_4 \end{bmatrix} = \begin{bmatrix} (6\mu s_{yy}\zeta)\left(\frac{F_a L^3}{3EI_{xx}} + \frac{F_a L}{s_{yy}}\right) + \left(\frac{EI_{xx}}{L} + 3\mu L_k s_{yy}\zeta\right)\left(\frac{-F_a L^2}{2EI_{xx}}\right) \\ (12\mu s_{yy})\left(\frac{F_a L^3}{3EI_{xx}} + \frac{F_a L}{s_{yy}}\right) + (6\mu s_{yy})\left(\frac{-F_a L^2}{2EI_{xx}}\right) \end{bmatrix} = \begin{bmatrix} \frac{F_a L(-1 + \zeta)}{2} \\ F_a \end{bmatrix}. \quad (h)$$

The shear force is constant in the beam and is equal to the prescribed external force  $F_a$ . For  $F_a > 0$  the bending moment decreases linearly from zero at the free end to a minimum  $(-F_a L)$  at the clamped end. The finite element solution for transverse bending is the same as the exact solution of the governing boundary value problem. ■

### Example 17.5 Cantilever wing spar

The wing spar of a light airplane described in example 6.6 on page 165 is modeled as a cantilever beam as shown in figure 17.19(a). In a symmetric maneuver of the airplane the total lift  $L = 12,000$  lb., and the lift acting on each

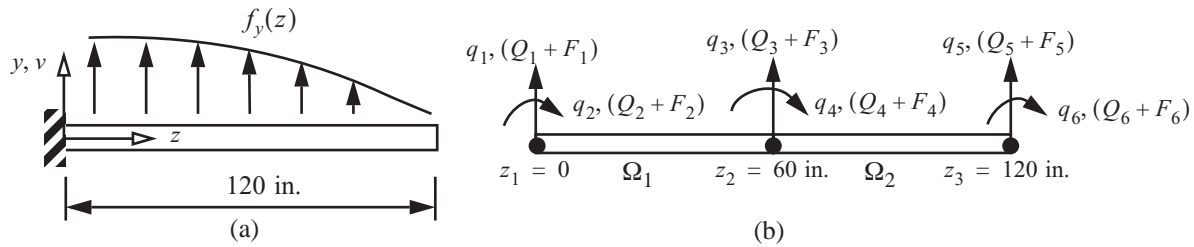


Fig. 17.19 (a) Cantilever wing spar. (b) Finite element model.

wing is  $L/2$ . Assume the airload acts along the locus of shear centers so that spar bends without twist in torsion. The airload is distributed elliptically over the wing, so that the airload intensity  $f_y(z)$  per unit span is given as

$$f_y(z) = \frac{2L}{\pi z_{max}} \sqrt{1 - \left(\frac{z}{z_{max}}\right)^2} \quad 0 \leq z \leq z_{max}, \quad (a)$$

where  $z$  is the spanwise coordinate,  $z = 0$  at the root, and  $z = z_{max} = 120$  in. at the tip of the wing spar. The transverse temperature gradient  $\tau_y(z) = 0$ ,  $0 < z < z_{max}$ . Data taken from example 6.6 are: the modulus of elas-



tivity  $E = 10.5 \times 10^6$  lb./in.<sup>2</sup>, the second area moment of the cross section about the  $x$ -axis  $I_{xx} = 101.619$  in.<sup>4</sup>, and the transverse shear coefficient  $s_{yy} = 2.4278 \times 10^6$  lb.

The finite element model shown in figure 17.19(b) has three nodes  $\{z_3\} = \{0, 60, 120\}$  in. , and two equal length elements  $h_1 = h_2 = 60$  in. . The stiffness matrices (17.106) for each element are

$$[K^{(1)}] = \begin{bmatrix} q_1 & q_2 & q_3 & q_4 \\ 24,048 & -721,441 & -24,048 & -721,441 \\ -721,441 & 3.94266 \times 10^7 & 721,441 & 3.85991 \times 10^6 \\ -24,048 & 721,441 & 24,048 & 721,441 \\ -721,441 & 3.85991 \times 10^6 & 721,441 & 3.94266 \times 10^7 \end{bmatrix} \text{ and} \quad (b)$$

$$[K^{(2)}] = \begin{bmatrix} q_3 & q_4 & q_4 & q_5 \\ 24,048 & -721,441 & -24,048 & -721,441 \\ -721,441 & 3.94266 \times 10^7 & 721,441 & 3.85991 \times 10^6 \\ -24,048 & 721,441 & 24,048 & 721,441 \\ -721,441 & 3.85991 \times 10^6 & 721,441 & 3.94266 \times 10^7 \end{bmatrix}. \quad (c)$$

The assembly process effects the matrix addition  $[K_u] = [K^{(1)}] + [K^{(2)}]$  to get the unrestrained structural stiffness matrix as

$$[K_u] = \begin{bmatrix} q_1 & q_2 & q_3 & q_4 & q_5 & q_6 \\ 24,048 & -721,441 & -24,048 & -721,441 & 0 & 0 \\ -721,441 & 3.94266 \times 10^7 & 721,441 & 3.85991 \times 10^6 & 0 & 0 \\ -24,048 & 721,441 & 48,096.1 & 0 & -24,048 & -721,441 \\ -721,441 & 3.85991 \times 10^6 & 0 & 7.88531 \times 10^7 & 721,441 & 3.85991 \times 10^6 \\ 0 & 0 & -24,048 & 721,441 & 24,048 & 721,441 \\ 0 & 0 & -721,441 & 3.85991 \times 10^6 & 721,441 & 3.94266 \times 10^7 \end{bmatrix}. \quad (d)$$

The generalized nodal displacement vector  $[q_1 \ q_2 \ q_3 \ q_4 \ q_5 \ q_6]^T$  is partitioned into unknown components  $\{q_\alpha\}$  and known components  $\{q_\beta\}$ :

$$\{q_\alpha\} = [q_3 \ q_4 \ q_5 \ q_6]^T \quad \{q_\beta\} = [q_1 \ q_2]^T = 0_{2 \times 1}. \quad (e)$$

We partition the unrestrained structural stiffness in eq. (d) in the form

$$[K_u] = \begin{bmatrix} [K_{\beta\beta}] & [K_{\beta\alpha}] \\ [K_{\alpha\beta}] & [K_{\alpha\alpha}] \end{bmatrix}, \text{ where} \quad (f)$$

$$[K_{\alpha\alpha}] = \begin{bmatrix} q_3 & q_4 & q_5 & q_6 \\ 48,096.1 & 0 & -24,048 & -721,441 \\ 0 & 7.88531 \times 10^7 & 721,441 & 3.85991 \times 10^6 \\ -24,048 & 721,441 & 24,048 & 721,441 \\ -721,441 & 3.85991 \times 10^6 & 721,441 & 3.94266 \times 10^7 \end{bmatrix}, \quad [K_{\alpha\beta}] = \begin{bmatrix} q_1 & q_2 \\ -24,048 & 721,441 \\ -721,441 & 3.85991 \times 10^6 \\ 0 & 0 \\ 0 & 0 \end{bmatrix} = [K_{\beta\alpha}]^T, \quad (g)$$

and

$$[K_{\beta\beta}] = \begin{bmatrix} q_1 & q_2 \\ 24,048 & -721,441 \\ -721,441 & 3.94266 \times 10^7 \end{bmatrix}. \quad (h)$$

The generalized forces acting at the nodes of elements 1 and 2 are shown in figure 17.20. The external general-

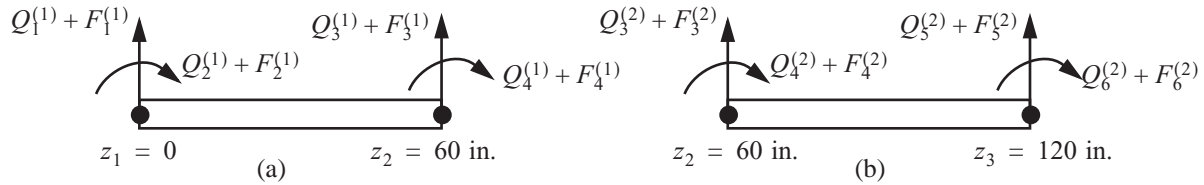


**Fig. 17.20** Generalized forces acting on (a) element  $\Omega_1$ , and (b) element  $\Omega_2$ .

ized forces acting on elements  $\Omega_1$  and  $\Omega_2$  from the distributed airload (a) are computed by numerical integration because of the complexity of the integrands (17.97). (Refer to article 17.3.6 for details on numerical integration.) The external generalized forces acting on each element are determined from eq. (17.105). The transpose of the Guyan matrix used to compute the generalized force vectors  $\{F^{(1)}\}$  and  $\{F^{(2)}\}$  in eq. (17.105) is the same for each element in this example. It is given by

$$[G_{aq}^{(1)}]^T = [G_{aq}^{(2)}]^T = \begin{bmatrix} 0 & -0.016526 & 0.128289 \\ 12.2474 & 0.496859 & -3.84866 \\ 0 & 0.016562 & -0.128289 \\ -12.2474 & 0.496859 & -3.84866 \end{bmatrix}. \quad (i)$$

The results for the generalized forces are

$$\{FE^{(1)}\} = \begin{bmatrix} 1,869 \text{ lb.} \\ 0 \\ 1,784.98 \text{ lb.} \\ 0 \end{bmatrix} \quad \{FI^{(1)}\} = \begin{bmatrix} -1,499.03 \text{ lb.} \\ 0 \\ 266.3992 \text{ lb.} \end{bmatrix} \quad \{F^{(1)}\} = \begin{bmatrix} F_1^{(1)} \\ F_2^{(1)} \\ F_3^{(1)} \\ F_4^{(1)} \end{bmatrix} = \begin{bmatrix} 1,872.39 \text{ lb.} \\ -18,460.9 \text{ lb.-in.} \\ 1,781.6 \text{ lb.} \\ 18,257.7 \text{ lb.-in.} \end{bmatrix}, \quad (j)$$

$$\{FE^{(2)}\} = \begin{bmatrix} 1,384.05 \text{ lb.} \\ 0 \\ 961.96 \text{ lb.} \\ 0 \end{bmatrix} \quad \{FI^{(2)}\} = \begin{bmatrix} -991.799 \text{ lb.} \\ 0 \\ 125.595 \text{ lb.} \end{bmatrix}, \text{ and } \{F^{(2)}\} = \begin{bmatrix} F_3^{(2)} \\ F_4^{(2)} \\ F_5^{(2)} \\ F_6^{(2)} \end{bmatrix} = \begin{bmatrix} 1,400.17 \text{ lb.} \\ -12,630.4 \text{ lb.-in.} \\ 945.848 \text{ lb.} \\ 11,663.6 \text{ lb.-in.} \end{bmatrix}. \quad (\mathbf{k})$$

Assembly of the two elements is shown in figure 17.19(b). The external generalized force vectors for the assembly are

$$\begin{bmatrix} F_1 \\ F_2 \\ F_3 \\ F_4 \\ F_5 \\ F_6 \end{bmatrix} = \begin{bmatrix} F_1^{(1)} \\ F_2^{(1)} \\ F_3^{(1)} + F_3^{(2)} \\ F_4^{(1)} + F_4^{(2)} \\ F_5^{(2)} \\ F_6^{(2)} \end{bmatrix} = \begin{bmatrix} 1,872.39 \text{ lb.} \\ -18,460.9 \text{ lb.-in.} \\ 3,181.77 \text{ lb.} \\ 5,627.30 \text{ lb.-in.} \\ 945.848 \text{ lb.} \\ 11,663.6 \text{ lb.-in.} \end{bmatrix} \quad \begin{bmatrix} Q_1 \\ Q_2 \\ Q_3 \\ Q_4 \\ Q_5 \\ Q_6 \end{bmatrix} = \begin{bmatrix} Q_1^{(1)} \\ Q_2^{(2)} \\ Q_3^{(1)} + Q_3^{(2)} \\ Q_4^{(1)} + Q_4^{(2)} \\ Q_5^{(2)} \\ Q_6^{(2)} \end{bmatrix}. \quad (\mathbf{l})$$

The 6X1 generalized nodal force vector  $[Q_1 \ Q_2 \ Q_3 \ Q_4 \ Q_5 \ Q_6]^T$  is partitioned into known components  $\{Q_\alpha\}$  and unknown components  $\{Q_\beta\}$  as follows:

$$\{Q_\alpha\} = [Q_3 \ Q_4 \ Q_5 \ Q_6]^T = 0_{4 \times 1}, \text{ and } \{Q_\beta\} = [Q_1 \ Q_2]^T. \quad (\mathbf{m})$$

There are no generalized point forces acting at nodes 2 and 3. Generalized point forces acting at node 1 are reactive. The generalized forces from the airload are also partitioned as

$$\{F_\alpha\} = [F_3 \ F_4 \ F_5 \ F_6]^T = [3,181.76 \ 5,627.37 \ 945.848 \ 11,663.6]^T, \text{ and} \quad (\mathbf{n})$$

$$\{F_\beta\} = [F_1 \ F_2]^T = [1,872.39 \ -18,460.9]^T. \quad (\mathbf{o})$$

The matrix equation to determine the unknown generalized displacements is

$$[K_{\alpha\alpha}]\{q_\alpha\} + [K_{\alpha\beta}]\{q_\beta\} = \{Q_\alpha\} + \{F_\alpha\}. \text{ The solution for the unknown displacement vector is}$$

$$\{q_\alpha\} = [0.447103 \ -0.0091821 \ 1.06555 \ -0.0101218]^T. \quad (\mathbf{p})$$

The matrix equation to determine the unknown forces is  $[K_{\beta\alpha}]\{q_\alpha\} + [K_{\beta\beta}]\{q_\beta\} = \{Q_\beta\} + \{F_\beta\}$ , or

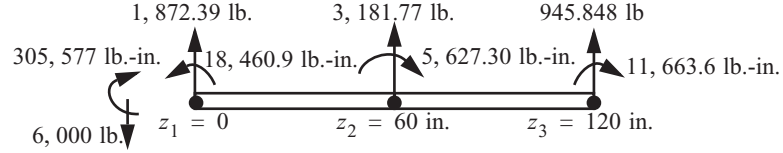
$$\begin{bmatrix} -24,048 & -721,441 & 0 & 0 \\ 721,441 & 3.85991 \times 10^6 & 0 & 0 \end{bmatrix} \begin{bmatrix} 0.447103 \\ -0.0091821 \\ 1.06555 \\ -0.0101218 \end{bmatrix} + \begin{bmatrix} 24,048 & -721,441 \\ -721,441 & 3.94266 \times 10^7 \end{bmatrix} \begin{bmatrix} 0 \\ 0 \end{bmatrix} = \begin{bmatrix} Q_1 \\ Q_2 \end{bmatrix} + \begin{bmatrix} 1,872.39 \\ -18,460.9 \end{bmatrix}. \quad (\mathbf{q})$$

Perform the matrix algebra in eq. (q) to find that the generalized reactive forces are

$$Q_1 = -6,000.0 \text{ lb.} \quad Q_2 = 305,577 \text{ lb.-in.} \quad (\mathbf{r})$$

The external generalized forces acting on the two-element model of wing spar are shown in the free body diagram in figure 17.21. ■

**Fig. 17.21 Generalized forces acting on the model with two elements.**



### 17.3.6 Gaussian integration

Consider the integral to compute the external force component  $FE_{2k+1}^{(k)}$  in eq. (17.97) for element two in example 17.5. The expression for this force component is

$$FE_5^{(2)} = \frac{h_2}{2} \int_{-1}^1 \frac{1}{2} (1 + \zeta) \frac{2L}{\pi z_{max}} \sqrt{1 - \left( \frac{z^{(2)}(\zeta)}{z_{max}} \right)^2} d\zeta, \quad (17.116)$$

where

$$z^{(2)} = \eta_1(\zeta)(60.) + \eta_2(\zeta)(120) = 90 + 30\zeta. \quad (17.117)$$

Numerical evaluation of eq. (17.116) leads to

$$FE_5^{(2)} = \int_{-1}^1 [954.930(1 + \zeta) \sqrt{0.4357 - 0.375\zeta - 0.0625\zeta^2}] d\zeta. \quad (17.118)$$

We carry out Gaussian integration of eq. (17.118) after a discussion of the method.

The method of Gaussian quadrature is to approximate the integral  $I = \int_{-1}^1 f(\zeta) d\zeta$  by

$$I \approx I_{\text{appr}} = \sum_{i=1}^n w_i f(\zeta_i), \quad (17.119)$$

where  $\zeta_i$  are the abscissas of the Legendre polynomial  $P_i(\zeta)$ , and  $w_i$  are the weight factors. The abscissas, or roots, of the Legendre polynomial are symmetrically located in the interval  $-1 \leq \zeta \leq 1$ . The weight factors are determined such that a polynomial of degree  $p$  is exactly equal to the sum in (17.119). Consider a polynomial of second degree  $f(\zeta) = c_0 + c_1\zeta + c_2\zeta^2$ . The exact integral is

$$I = \int_{-1}^1 (c_0 + c_1\zeta + c_2\zeta^2) d\zeta = 2c_0 + \frac{2}{3}c_2. \quad (17.120)$$

The exact integral is determined by two coefficients,  $c_0$  and  $c_2$ . The Legendre polynomial for  $n = 2$  is

$P_2(\zeta) = (-1 + 3\zeta^2)/2$ . The roots of  $P_2(\zeta) = 0$  are

$$-1/\sqrt{3} \text{ and } 1/(\sqrt{3}). \quad (17.121)$$

Equation (17.119) for  $n = 2$  is

$$I = I_{\text{appr.}} = w_1 f\left(\frac{-1}{\sqrt{3}}\right) + w_2 f\left(\frac{1}{\sqrt{3}}\right). \quad (17.122)$$

Evaluating eq. (17.122) we get

$$I = I_{\text{appr.}} = 2(w_1 + w_2)c_0 + \frac{(w_2 - w_1)}{\sqrt{3}}c_1 + \frac{1}{3}(w_1 + w_2). \quad (17.123)$$

Equate like coefficients in (17.120) and (17.123) to get three linear equations for the weight factors  $w_1$ , and  $w_2$ :

$$2 = w_1 + w_2 \quad 0 = (w_2 - w_1)/(\sqrt{3}) \quad \frac{2}{3} = \frac{1}{3}(w_1 + w_2). \quad (17.124)$$

The solution of eq. (17.124) is  $w_1 = w_2 = 1$ . Note that the weight factors of the positive root and the corresponding negative root are the same because the term with the odd power of  $\zeta$  does not contribute to  $I$  (17.120). Thus, a polynomial of degree 2 can be integrated exactly by evaluating it at  $\mp 1/\sqrt{3}$  and multiplying by the appropriate equal weight factors.

Consider the cubic polynomial  $f(\zeta) = c_0 + c_1\zeta + c_2\zeta^2 + c_3\zeta^3$  whose exact integral is  $I = 2c_0 + (2/3)c_2$ . The Legendre polynomial for  $n = 3$  is  $P_3(\zeta) = (-3\zeta + 5\zeta^3)/2$ . The roots of  $P_3(\zeta) = 0$  are 0, and  $\mp\sqrt{3/5}$ . Equation (17.119) for  $n = 3$  is

$$I = I_{\text{appr.}} = w_1 f(0) + w_2 f(-\sqrt{3/5}) + w_2 f(\sqrt{3/5}) = c_0(w_1 + w_2) + c_2(6w_2/5). \quad (17.125)$$

Equating like coefficients between the last equation and the exact integral we find the weight factors  $w_1 = 8/9$  and  $w_2 = 5/9$ . In general, a polynomial of degree  $p$  is integrated exactly if  $n \geq (p + 1)/2$ .

Now consider the integrand in the definite integral (17.118). The integrand is

$$f(\zeta) = 954.930(1 + \zeta)\sqrt{0.4357 - 0.375\zeta - 0.0625\zeta^2}. \quad (17.126)$$

Function  $f(\zeta)$  is continuous in the interval  $|\zeta| \leq 1$  as shown in figure 17.22. Its Taylor's formula is an infinite

series  $f(\zeta) = \sum_{m=0}^{\infty} a_m \zeta^m$ , where the  $a_m$  are real numbers. Consequently if  $f(\zeta)$  is replaced by its Taylor series,

then the integrand is a polynomial of infinite degree. The integral of a polynomial of infinite degree implies an infinite number of abscissas and weights for Gaussian quadrature, which, of course, is not practical. Only a finite number of abscissas and weights in Gaussian quadrature are considered in the sequence of numerical integrations to follow.

Gaussian quadrature of the integrand (17.119) for  $n = 2$  is

$$I_{\text{appr.}} = w_1 f(-1/\sqrt{3}) + w_1 f(1/\sqrt{3}) = (1)(321.154) + (1)(673.889) = 995.043 \text{ lb.} \quad (17.127)$$

Gaussian quadrature of the integrand (17.119) for  $n = 3$  is

$$I_{\text{appr.}} = w_1 f(0) + w_2 f(-\sqrt{3/5}) + w_2 f(\sqrt{3/5}) = \left(\frac{8}{9}\right)(631.627) + \left(\frac{5}{9}\right)(178.857) + \left(\frac{5}{9}\right)(560.829) = 972.382 \text{ lb.} \quad (17.128)$$

For  $n = 2, 3, 4, 5, 6, 7, 8, 9$ , and  $10$  the abscissa and weight factors are listed in table 17.4. Approximate values of the integrals of (17.126) are listed in table 17.5 based on the data in table 17.4. The results in table 17.5 show the integrals are slowly decreasing as the number of terms in the Gaussian integration increase. Apparently, the approximate values of the integrals are asymptotically approaching the value of 961.96 lb., which is the value of the integral of (17.126) computed from the function `NIntegrate[f( $\zeta$ ), { $\zeta$ , -1, 1}]` in *Mathematica*.

**Fig. 17.22** Graph of function (17.126) with the filled circles corresponding to the function evaluated at the abscissas in Gaussian quadrature for  $n = 10$ .

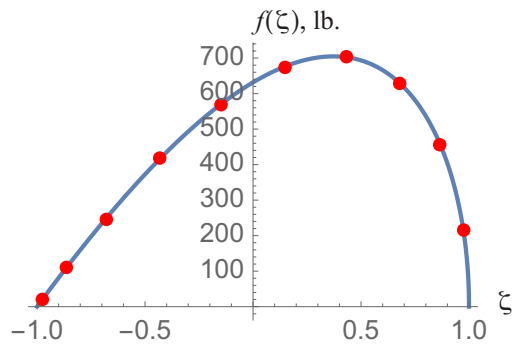


Table 17.4 Abscissas and weight factors for Gaussian integration

$\pm \zeta_i$	$w_i$	$\pm \zeta_i$	$w_i$
$n = 2$		$n = 8$	
$1/(\sqrt{3})$	1.0	0.18343 46424 95650	0.36268 37833 78362
$n = 3$		0.52553 24099 16329	0.31370 66458 77877
0	8/9	0.79666 64774 13627	0.22238 10344 53374
$\sqrt{3}/5$	5/9	0.96028 98564 97536	0.10122 85362 90376
$n = 4$		$n = 9$	
0.33998 10435 84856	0.65214 51548 62546	0	0.33023 93550 01260
0.86113 63115 94053	0.34785 48451 37454	0.32425 34234 03809	0.31234 7 0770 40003
$n = 5$		0.61337 14327 0 0590	0.26061 06964 02935
0	0.56888 88888 88889	0.83603 11073 26636	0.18064 81606 94857
0.53846 93101 05683	0.47862 86704 99366	0.96816 02395 07626	0.08127 43883 61574
0.90617 98459 38664	0.23692 68850 56189	$n = 10$	
$n = 6$		0.14887 43389 81631	0.29552 42247 14753
0.23861 91860 83197	0.46791 39345 72691	0.43339 53941 29247	0.26926 67193 09996
0.66120 93864 66265	0.36076 15730 4 8139	0.67940 95682 99024	0.21908 63625 15982
0.93246 95142 03152	0.17132 44923 79170	0.86506 33666 88985	0.14945 13491 50581
$n = 7$		0.97390 65285 17172	0.06667 13443 08688
0	0.417959183673470		
0.405845151377397	0.381830050505119		
0.741531185599395	0.279705391489277		
0.949107912342759	0.129484966168870		

**Table 17.5 Approximate integrals of (17.126).**

<b>n</b>	$I_{\text{appr. lb.}}$
2	995.043
3	972.382
4	966.61
5	964.443
6	963.443
7	962.917
8	962.613
9	962.426
10	962.304

### 17.4 Euler-Bernoulli beam element

The Euler-Bernoulli beam theory was discussed following table 4.4 on page 102, and in this theory we set the transverse shear strain  $\psi_y = 0$ . Hence, from eq. (17.53) the rotation of the cross section is related to the rotation of the centroidal axis by  $\phi_x = -(dv/dz)$ . The material law for the shear force (i.e  $V_y$  in eq. (17.52) is not valid). The shear force is reactive and it is determined by the first equilibrium equation (17.51). Combine the equilibrium equations (17.51) by eliminating the shear force to get

$$\frac{d^2 M_x}{dz^2} + f_y(z) = 0 \quad 0 < z < L. \quad (17.129)$$

The material law for the bending moment in eq. (17.52) becomes

$$M_x = EI_{xx} \left[ -\left( \frac{d^2 v}{dz^2} + \alpha \tau_y \right) \right]. \quad (17.130)$$

Substitute the material law for the bending moment (17.130) into the equilibrium equation (17.129) to find the fourth order differential equation for the lateral displacement  $v(z)$ :

$$\frac{d^2}{dz^2} \left[ EI_{xx} \left( -\frac{d^2 v}{dz^2} - \alpha \tau_y \right) \right] + f_y(z) = 0 \quad 0 < z < L. \quad (17.131)$$

The boundary conditions at  $z = 0$  and  $z = L$  in eq. (17.54) become

$$\text{prescribe either } v \text{ or } V_y, \text{ and prescribe either } \left( -\frac{dv}{dz} \right) \text{ or } M_x. \quad (17.132)$$

Multiply (17.131) by the virtual displacement  $\bar{v}(z)$  and integrate over the domain. Then integrate the result by parts twice with respect to  $z$  to get



$$\int_0^L \left[ EI_{xx} \left( -\frac{d^2 \bar{v}}{dz^2} - \alpha \tau_y \right) \right] \frac{d^2 \bar{v}}{dz^2} dz + \left\{ \bar{v} \frac{d}{dz} EI_{xx} \left[ -\left( \frac{d^2 \bar{v}}{dz^2} + \alpha \tau_y \right) \right] - \frac{d \bar{v}}{dz} EI_{xx} \left[ -\left( \frac{d^2 \bar{v}}{dz^2} + \alpha \tau_y \right) \right] \right\} \Big|_0^L + \int_0^L (f_y \bar{v}) dz = 0. \quad (17.133)$$

Note that the shear force is determined from equilibrium and the material law for the bending moment; i.e.,

$$V_y = \frac{dM_x}{dz} = \frac{d}{dz} EI_{xx} \left[ -\left( \frac{d^2 \bar{v}}{dz^2} + \alpha \tau_y \right) \right]. \quad (17.134)$$

Equation (17.133) is rearranged as follows:

$$\begin{aligned} \int_0^L \left[ EI_{xx} \left( -\frac{d^2 \bar{v}}{dz^2} \right) \right] \frac{d^2 \bar{v}}{dz^2} dz + \left[ \bar{v} V_y - \frac{d \bar{v}}{dz} M_x \right] \Big|_0^L + \int_0^L \left[ (-EI_{xx} \alpha \tau_y) \frac{d^2 \bar{v}}{dz^2} + f_y \bar{v} \right] dz &= 0 \\ \int_0^L \left[ EI_{xx} \frac{d^2 \bar{v}}{dz^2} \frac{d^2 \bar{v}}{dz^2} \right] dz = \left[ \bar{v} V_y - \frac{d \bar{v}}{dz} M_x \right] \Big|_0^L + \int_0^L \left[ (-EI_{xx} \alpha \tau_y) \frac{d^2 \bar{v}}{dz^2} + f_y \bar{v} \right] dz. \end{aligned} \quad (17.135)$$

The **principle of virtual work** is determined from (17.135) and is written in the form

$$B[\bar{v}, \bar{v}] = F[\bar{v}] \quad \text{for every kinematically admissible } \bar{v}. \quad (17.136)$$

The internal virtual work is

$$B[\bar{v}, \bar{v}] = \int_0^L \left[ EI_{xx} \frac{d^2 \bar{v}}{dz^2} \frac{d^2 \bar{v}}{dz^2} \right] dz, \quad (17.137)$$

and the external virtual work is

$$F[\bar{v}] = \bar{v} V_y \Big|_0^L + \left( -\frac{d \bar{v}}{dz} \right) M_x \Big|_0^L + \int_0^L f_y \bar{v} dz + \int_0^L \left[ EI_{xx} \left( -\frac{d^2 \bar{v}}{dz^2} \right) \right] \alpha \tau_y dz. \quad (17.138)$$

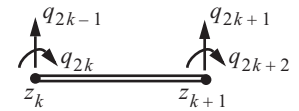
### 17.4.1 Element displacement functions and strains

The  $k$ th element is denoted by  $\Omega_k \equiv \{z | z_k \leq z \leq z_{k+1}\}$ , where  $z_k < z_{k+1}$ . The standard element  $\Omega_{st} \equiv \{\xi | -1 < \xi < 1\}$  (17.15) is mapped to the  $k$ th element by (17.16), and the inverse mapping is given by (17.17). The lateral displacement of the  $k$ th element is denoted by  $v^{(k)}(z)$  and the clockwise rotation by  $-\left(\frac{dv^{(k)}}{dz}\right)$ . Define the generalized nodal displacements as

$$v^{(k)}(z_k) = q_{2k-1} \quad -\left(\frac{dv^{(k)}}{dz}\right) \Big|_{z=z_k} = q_{2k} \quad v^{(k)}(z_{k+1}) = q_{2k+1} \quad -\left(\frac{dv^{(k)}}{dz}\right) \Big|_{z=z_{k+1}} = q_{2k+2}. \quad (17.139)$$

See figure 17.23. Admissible functions  $v(z)$  and its derivative must be continuous within an element and be continuous between elements. Interpolation functions that satisfy these continuity requirements are Hermite cubic interpolation functions, which are

**Fig. 17.23**  
**Generalized**  
**nodal**  
**displacements.**



denoted by  $\phi_i(\xi)$ ,  $i = 1, 2, 3, 4$ . These interpolation functions are

$$\begin{aligned}\phi_1(\xi) &= (2 - 3\xi + \xi^3)/4 & \phi_2(\xi) &= (h_k/8)(-1 + \xi + \xi^2 - \xi^3) \\ \phi_3(\xi) &= (2 + 3\xi - \xi^3)/4 & \phi_4(\xi) &= (h_k/8)(1 + \xi - \xi^2 - \xi^3)\end{aligned}\quad (17.140)$$

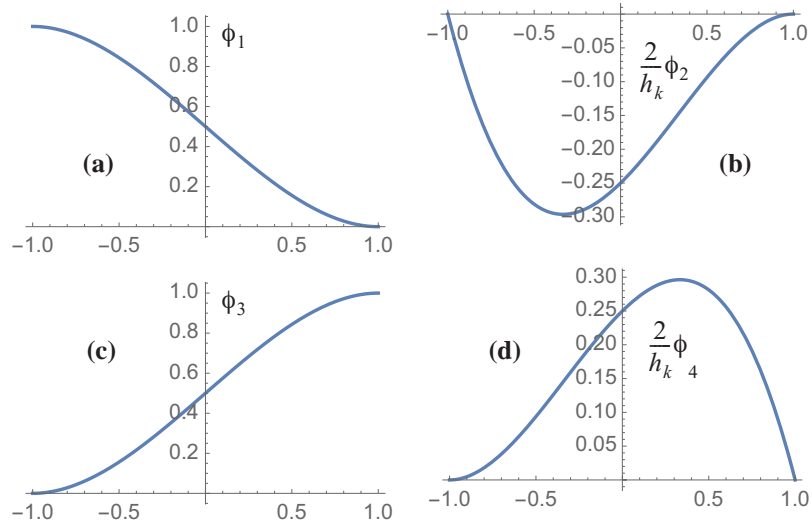
Let the derivative  $\frac{d\phi_i}{d\xi}$  be denoted by  $\phi_i'$ . The interpolation properties of the Hermite cubic functions are

$$\begin{aligned}\phi_1(-1) &= 1 & \phi_1'(-1) &= 0 & \phi_1(1) &= 0 & \phi_1'(1) &= 0 \\ \phi_2(-1) &= 0 & \phi_2'(-1) &= -h_k/2 & \phi_2(1) &= 0 & \phi_2'(1) &= 0 \\ \phi_3(-1) &= 0 & \phi_3'(-1) &= 0 & \phi_3(1) &= 1 & \phi_3'(1) &= 0 \\ \phi_4(-1) &= 0 & \phi_4'(-1) &= 0 & \phi_4(1) &= 0 & \phi_4'(1) &= -h_k/2\end{aligned}\quad (17.141)$$

Graphs of Hermite cubic functions are shown in figure 17.24. The displacement for element  $\Omega_k$  is

**Fig. 17.24 Hermite cubic interpolation functions.**

- (a)  $\phi_1(\xi)$ ,  
 (b)  $\frac{2}{h_k}\phi_2(\xi)$ ,  
 (c)  $\phi_3(\xi)$ , and  
 (d)  $\frac{2}{h_k}\phi_4(\xi)$ .  
 where  $-1 \leq \xi \leq 1$ .



$v^{(k)}(\xi) = [N(\xi)]\{q^{(k)}\}$ , where  $[N(\xi)]$  is the  $1 \times 4$  matrix of interpolation functions, and  $\{q^{(k)}\}$  is the  $4 \times 1$  vector of the generalized displacements at the nodes. The interpolation matrix and nodal displacement vector are

$$[N(\xi)] = [\phi_1(\xi) \ \phi_2(\xi) \ \phi_3(\xi) \ \phi_4(\xi)], \text{ and } \{q^{(k)}\} = [q_{2k-1} \ q_{2k} \ q_{2k+1} \ q_{2k+2}]^T. \quad (17.142)$$

The virtual displacement is  $\bar{v}(\xi) = [N(\xi)]\{b\}$ , where  $\{b\} = [b_1 \ b_2 \ b_3 \ b_4]^T$ . The second derivative of the displacement, or curvature  $\kappa$  of the centroidal axis in bending, is expressed as

$$\kappa = -\left(\frac{d^2v}{dz^2}\right) = -\left(\frac{d^2v}{d\xi^2}\right)\left(\frac{2}{h_k}\right)^2 = -\left(\frac{2}{h_k}\right)^2 \frac{d^2}{d\xi^2} [N(\xi)]\{q^{(k)}\} = [N_\kappa(\xi)]\{q^{(k)}\}, \text{ where} \quad (17.143)$$

$$[N_\kappa(\xi)] = \frac{1}{h_k^2} \begin{bmatrix} -6\xi & h_k(-1 + 3\xi) & 6\xi & h_k(1 + 3\xi) \end{bmatrix}. \quad (17.144)$$

The virtual curvature is  $\bar{\kappa} = -\left(\frac{d^2 \bar{v}^{(k)}}{dz^2}\right) = [N_{\kappa}(\zeta)] \{b\} = \{b\}^T [N_{\kappa}(\zeta)]^T$ . The bilinear form evaluates as

$$B[v, \bar{v}] = \int_0^L (\bar{\kappa} EI_{xx} \kappa) dz = \{b\}^T \left( \int_{-1}^1 [N_{\kappa}(\zeta)]^T EI_{xx} [N_{\kappa}(\zeta)] \frac{h_k}{2} d\zeta \right) \{q^{(k)}\} = \{b\}^T [K] \{q^{(k)}\}. \quad (17.145)$$

The element stiffness matrix is

$$[K] = \frac{EI_{xx}}{h_k^3} \begin{bmatrix} 12 & -6h_k & -12 & -6h_k \\ -6h_k & 4h_k^2 & 6h_k & 2h_k^2 \\ -12 & 6h_k & 12 & 6h_k \\ -6h_k & 2h_k^2 & 6h_k & 4h_k^2 \end{bmatrix}. \quad (17.146)$$

Referring to Fig. 17.16 on page 515, we express the boundary terms in the external virtual work (17.138) as

$$\bar{v} V_y \Big|_{z_{k+1}} - \bar{v} V_y \Big|_{z_k} + \left( -\frac{d\bar{v}}{dz} \right) M_x \Big|_{z_{k+1}} - \left( -\frac{d\bar{v}}{dz} \right) M_x \Big|_{z_k} = b_3 Q_{2k+1} - b_1 (-Q_{2k-1}) + b_4 Q_{2k+2} - b_2 (-Q_{2k}) = \{b\}^T \{Q^{(k)}\} \quad (17.147)$$

The prescribed distributed load terms in the external virtual work are

$$\int_0^L f_y \bar{v} dz + \int_0^L \left[ EI_{xx} \left( -\frac{d^2 \bar{v}}{dz^2} \right) \right] \alpha \tau_y dz = \{b\}^T \left( \int_{-1}^1 f_y^{(k)} [N(\zeta)] \frac{h_k}{2} d\zeta + \int_{-1}^1 EI_{xx} [N_{\kappa}(\zeta)]^T \alpha \tau_y^{(k)}(\zeta) \frac{h_k}{2} d\zeta \right), \quad (17.148)$$

where the distributed loading in the element is

$$f_y^{(k)} = f_y [\eta_1(\zeta) z_k + \eta_2(\zeta) z_{k+1}] \quad \tau_y^{(k)} = \tau_y [\eta_1(\zeta) z_k + \eta_2(\zeta) z_{k+1}]. \quad (17.149)$$

The final result for the external virtual work for element  $\Omega_k$  is

$$F[\bar{v}] = \{b\}^T (\{Q^k\} + \{F^{(k)}\}), \text{ where} \quad (17.150)$$

$$\{Q^k\} = [Q_{2k-1} \ Q_{2k} \ Q_{2k+1} \ Q_{2k+2}]^T \text{ and } \{F^{(k)}\} = [F_{2k-1} \ F_{2k} \ F_{2k+1} \ F_{2k+2}]^T. \quad (17.151)$$

Explicit expressions for the components of the generalized force vector from the distributed load are

$$F_{2k-1} = \int_{-1}^1 [f_y^{(k)}(\zeta)] \phi_1(\zeta) \frac{h_k}{2} d\zeta + \int_{-1}^1 \left[ EI_{xx} \left( \frac{-6\zeta}{h_k^2} \right) \right] [\alpha \tau_y^{(k)}(\zeta)] \frac{h_k}{2} d\zeta, \quad (17.152)$$

$$F_{2k} = \int_{-1}^1 [f_y^{(k)}(\zeta)] \phi_2(\zeta) \frac{h_k}{2} d\zeta + \int_{-1}^1 \left[ EI_{xx} \left( \frac{-1+3\zeta}{h_k} \right) \right] [\alpha \tau_y^{(k)}(\zeta)] \frac{h_k}{2} d\zeta, \quad (17.153)$$

$$F_{2k+1} = \int_{-1}^1 [f_y^{(k)}(\zeta)] \phi_3(\zeta) \frac{h_k}{2} d\zeta + \int_{-1}^1 \left[ EI_{xx} \left( \frac{6\zeta}{h_k^2} \right) \right] [\alpha \tau_y^{(k)}(\zeta)] \frac{h_k}{2} d\zeta, \text{ and} \quad (17.154)$$

$$F_{2k+2} = \int_{-1}^1 [f_y^{(k)}(\zeta)] \phi_4(\zeta) \frac{h_k}{2} d\zeta + \int_{-1}^1 \left[ EI_{xx} \frac{(1+3\zeta)}{h_k} \right] [\alpha \tau_y^{(k)}(\zeta)] \frac{h_k}{2} d\zeta. \quad (17.155)$$

## 17.5 References

- Bathe, K-J. *Finite Element Procedures in Engineering Analysis*. Englewood Cliffs, NJ: Prentice-Hall, Inc., 1982, p. 167.
- Guyan, R.J. “Reduction of Stiffness and Mass Matrices.” *AIAA Journal* 3, no.2, (1965): 380.
- Huebner, K. H., E. A. Thornton, and T. G. Byrom. *The Finite Element Method for Engineers*. 3d ed. New York: John Wiley & Sons, Inc., 1995.
- Irons, B.M. “Structural Eigenvalue Problems: Elimination of Unwanted Variables.” *AIAA Journal* 3, no.5 (1965): 961-962
- Reddy, J. N. *An Introduction to the Finite Element Method*, 4th ed. New York: McGraw Hill-Education, 2019.
- Szabo, B., and I. Babuska. *Finite Element Analysis*. New York: John Wiley & Sons, Inc., 1991.

---

## *Introduction to flexible body dynamics*

---

The transient response of a rocket at liftoff is presented to motivate the subject of structural dynamics. The accelerations at launch result in significant load factors imposed on the spacecraft, or payload. User guides for a launch vehicle specify load factors for preliminary design of the primary structure of the spacecraft. Often there are limits placed on the lowest natural frequency of the payload to ensure its dynamic characteristics do not adversely affect the control system of the booster (Sarafin, 1995). Thus, the capability to predict the load factor for the primary structure of the payload/spacecraft at launch, and the frequencies of the payload package, are necessary in the payload design. The example we begin with is the Atlas I.

### *18.1 Description of Atlas I*

A spacecraft consists of mission-specific equipment called the payload and a collection of subsystem components called a bus. Typical subsystem components may include attitude control, propulsion, communications, electrical power, etc. (Sarafin, 1995, p. 451). The spacecraft bus may be able to support different payloads for different missions. As shown in figure 18.1, the main components of the Atlas I space launch vehicle from bottom to top are an expendable booster, an expendable second stage called Centaur, and the payload/spacecraft (Isakowitz, 1995). The spacecraft is covered by a fairing. An adapter, also known as a launch vehicle adapter, structurally links the spacecraft and Atlas I. The spacecraft developer usually designs the adapter.

Selected weights and thrust data for the Atlas I in table 18.1 are from Isakowitz (1995).

**Table 18.1 Selected data for Atlas I**

Gross weight	362,200 lb.
Booster weight	321,100 lb.
Centaur (upper stage)	34,300 lb.
Payload fairing	3,027 lb
Payload	3,773 lb
Engine thrust at liftoff	439,300 lb.

Atlas I Space Launch Vehicle

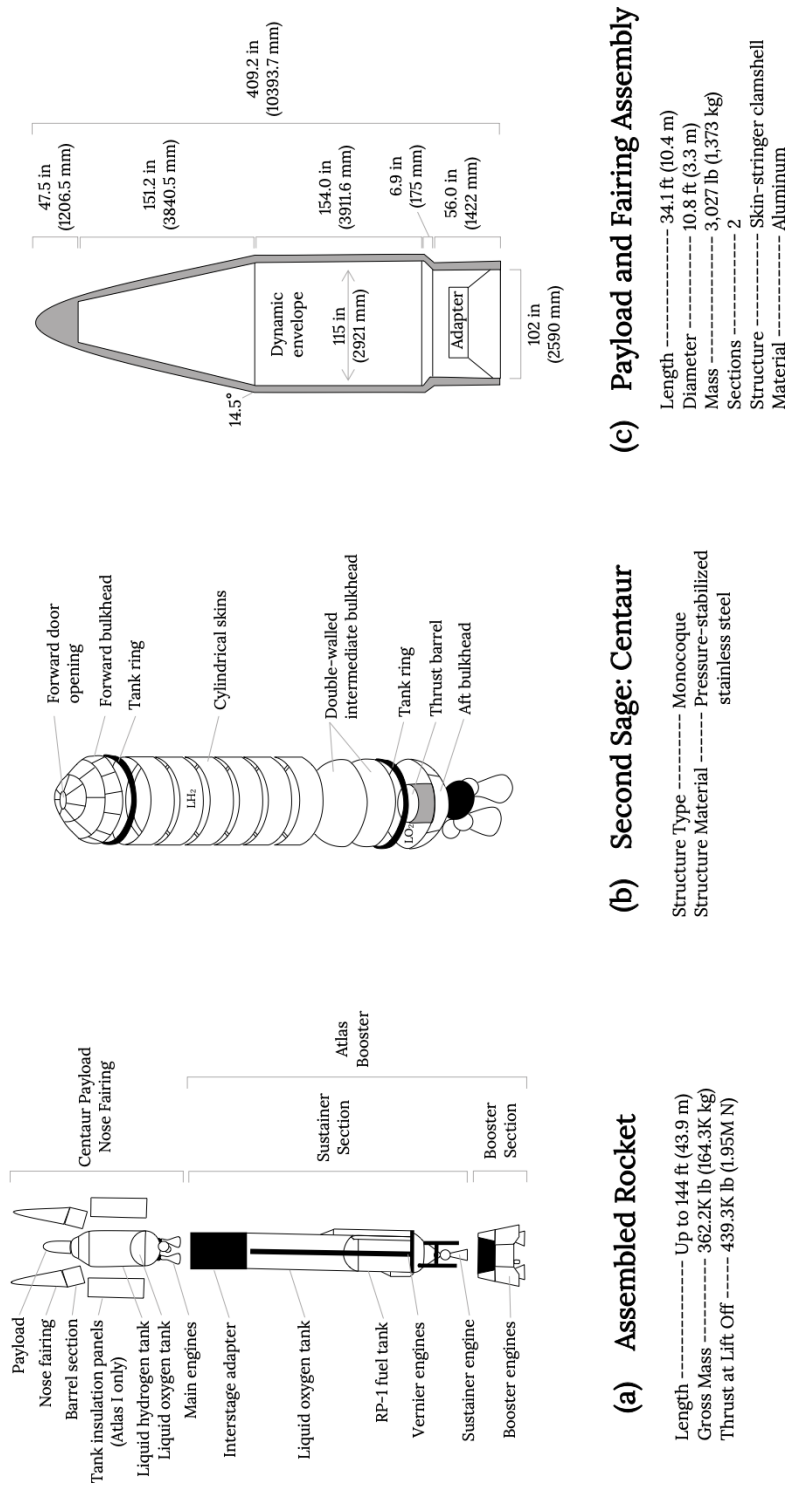


Fig. 18.1 .

Propellant weights in the booster and second stage, and the approximate structural weight are listed in table 18.2.

**Table 18.2 Weights of propellants and structure for Atlas I**

Booster propellant	305,500 lb.
Centaur propellant	30,000 lb.
Approximate structural weight <sup>a</sup>	22,927 lb.

a. Gross weight of 362,200 lb. less the sum of propellant weights of 335,500 lb. and the payload weight of 3,773 l.

In terms of percentages

92.6 percent of the total weight is propellant,  
6.33 percent of the total weight is structure, and  
1.04 percent of the total weight is payload.

Clearly, most of the weight is propellant.

**Objective.** Determine the maximum vertical load factor of the payload at liftoff. We assume the loss of mass due to propellant burn-off is small and can be neglected in the initial instants after liftoff.

## 18.2 Rigid body load factor

First, we assume Atlas I is a rigid body and determine the load factor from dynamic equilibrium. This analysis is shown in figure 18.2, where it is determined that the load factor is 1.213. However, this rigid body analysis omits information on frequencies. To determine frequencies of the structure we must consider flexible body dynamics, which is discussed beginning in the next section.

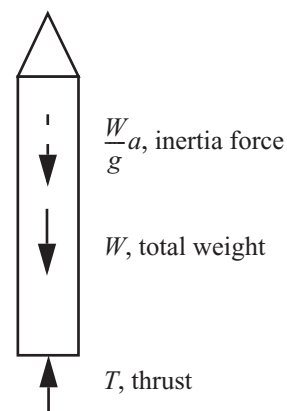
**Fig. 18.2 Rigid body analysis of Atlas I to determine the load factor at liftoff.**

$$T - W - \frac{W}{g}a = 0$$

$$T - W \underbrace{\left(1 + \frac{a}{g}\right)}_n = 0$$

$$n = \frac{T}{W} = \frac{439,300 \text{ lb.}}{362,200 \text{ lb.}}$$

$$n = 1.213$$



### 18.3 Steps in flexible body dynamics

1. Equations of motion relative to the equilibrium state.
2. Free vibration problem; normal modes.
3. Coordinate transformation from physical coordinates to modal coordinates.
4. Transform initial conditions from physical coordinates to modal coordinates. Solve for the time history of the modal coordinates.
5. Transform back to physical coordinates.
6. Calculate the payload acceleration time history.

**Step 1: Equations of motion about equilibrium.** Consider a three-degree-of-freedom model of Atlas I shown in figure 18.3(a). The model consists of three particles with lumped masses  $m_1$ ,  $m_2$ , and  $m_3$  and two springs with stiffnesses  $k_{12}$ , and  $k_{23}$ . Mass  $m_1$  is one-half the mass of the booster and Centaur, mass  $m_2$  is one-half of the mass of the booster and Centaur plus the mass of the fairing, and mass  $m_3$  is the mass of the payload. The stiffness of the booster and Centaur is represented by  $k_{12}$ , and the stiffness of the launch vehicle adapter is represented by  $k_{23}$ .

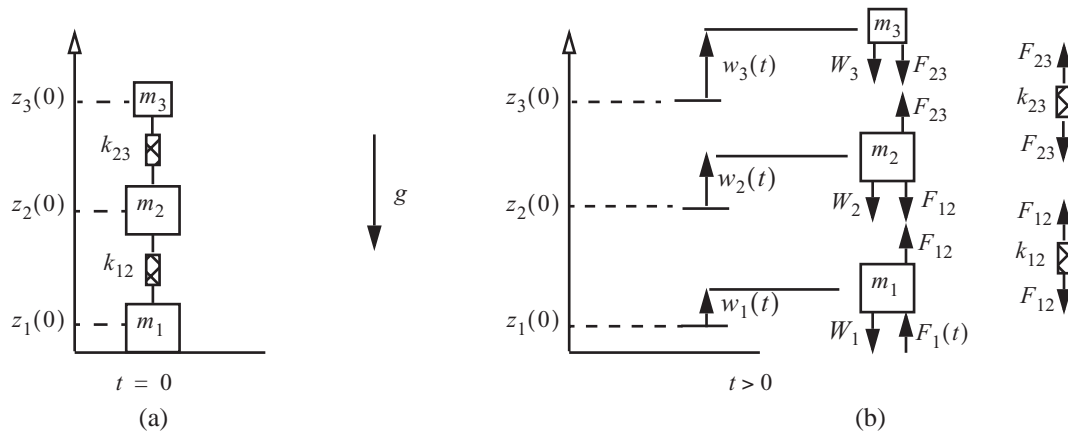


**Fig. 18.3** Three-degree-of-freedom model of Atlas I. (a) At rest. (b) Free body diagrams.

The axial coordinates of the particles in the equilibrium state at  $t = 0$  are  $z_i(0)$ ,  $i = 1, 2, 3$ , and the displacements of the masses from their equilibrium state are denoted by  $w_i(t)$ , and  $w_i(0) = 0$ . The weight of each particle is denoted by  $W_i$ ,  $i = 1, 2, 3$ . From the free body diagram shown in figure 18.3(b) the equations of motion are

$$F_1(t) - W_1 + F_{12} = m_1 \ddot{w}_1, \quad (18.1)$$

$$-W_2 - F_{12} + F_{23} = m_2 \ddot{w}_2, \text{ and} \quad (18.2)$$

$$-W_3 - F_{23} = m_3 \ddot{w}_3. \quad (18.3)$$

The two dots over the displacements is shorthand notation for the second derivative in time:



$$\ddot{w}_i(t) = \frac{d^2 w_i}{dt^2}. \quad (18.4)$$

The spring forces are related to the relative coordinates between the particles. That is,

$$\begin{aligned} F_{12} &= k_{12}[(z_2(0) + w_2(t)) - (z_1(0) + w_1(t))] \\ F_{23} &= k_{23}[(z_3(0) + w_3(t)) - (z_2(0) + w_2(t))] \end{aligned} \quad (18.5)$$

Substitute the spring force relations (18.5) into the equations of motion (18.1) to (18.3) to get

$$F_1(t) - W_1 + k_{12}(z_2(0) - z_1(0)) = m_1 \ddot{w}_1 + k_{12}w_1 - k_{12}w_2, \quad (18.6)$$

$$-W_2 - k_{12}(z_2(0) - z_1(0)) + k_{23}(z_3(0) - z_2(0)) = m_2 \ddot{w}_2 - k_{12}w_1 + (k_{12} + k_{23})w_2 - k_{23}w_3, \text{ and} \quad (18.7)$$

$$-W_3 - k_{23}(z_3(0) - z_2(0)) = m_3 \ddot{w}_3 - k_{23}w_2 + k_{23}w_3. \quad (18.8)$$

In the equilibrium state the eqs. (18.6) to (18.8) are

$$\begin{aligned} F_1(0) - W_1 + k_{12}(z_2(0) - z_1(0)) &= 0 \\ -W_2 - k_{12}(z_2(0) - z_1(0)) + k_{23}(z_3(0) - z_2(0)) &= 0 \\ -W_3 - k_{23}(z_3(0) - z_2(0)) &= 0 \end{aligned} \quad (18.9)$$

The solution of the equilibrium equation (18.9) is

$$\begin{aligned} F_1(0) &= W_1 + W_2 + W_3 = 362,200 \text{ lb.} \\ k_{23}[z_3(0) - z_2(0)] &= -W_3 \\ k_{12}[z_2(0) - z_1(0)] &= -W_2 - W_3 \end{aligned} \quad (18.10)$$

Force  $F_1(0)$  is the reaction force from the launch pad acting on the rocket in the equilibrium state prior to liftoff.

The equations of motion with respect to the equilibrium state are obtained by substituting eq. (18.10) into the equations of motion (18.6) to (18.8). Writing these equations in matrix form we get

$$\begin{bmatrix} m_1 & 0 & 0 \\ 0 & m_2 & 0 \\ 0 & 0 & m_3 \end{bmatrix} \begin{bmatrix} \ddot{w}_1 \\ \ddot{w}_2 \\ \ddot{w}_3 \end{bmatrix} + \begin{bmatrix} k_{12} & -k_{12} & 0 \\ -k_{12} & k_{12} + k_{23} & -k_{23} \\ 0 & -k_{23} & k_{23} \end{bmatrix} \begin{bmatrix} w_1 \\ w_2 \\ w_3 \end{bmatrix} = \begin{bmatrix} T(t) \\ 0 \\ 0 \end{bmatrix}, \quad (18.11)$$

where the net thrust after liftoff is  $T(t) = F_1(t) - F_1(0)$ . Numerical evaluation for the masses of the particles are

$$m_1 = \frac{(321,100 + 34,300)}{2(32.2)} = 5,518.63 \frac{\text{lb.}\cdot\text{s}^2}{\text{ft.}}, \quad m_2 = m_1 + 3,027/32.2 = 5,612.64 \frac{\text{lb.}\cdot\text{s}^2}{\text{ft.}}, \text{ and}$$

$$m_3 = 3,773/32.2 = 117.17 \frac{\text{lb.}\cdot\text{s}^2}{\text{ft.}}.$$

To estimate the structural stiffness of the booster and Centaur, assume the vehicle structure is a thin-walled cylindrical shell with a mean radius of 5 ft., and with an effective wall thickness  $t_w$ . We estimate the effective wall

thickness in the following way: The approximate structural weight of the booster is 15,600 lb., and its length is 72.7 ft. The approximate weight of Centaur is 4,300 lb., and its length is 30 ft. We equate this structural weight to the volume of material in the shell wall of the booster and Centaur times the specific weight of stainless steel; i.e.,

$$19,900 \text{ lb.} = 2\pi(5 \text{ ft.})t_w(102.7 \text{ ft.})(12 \text{ in./ft.})^2 0.286 \text{ lb./in.}^3.$$

Solve this equation for the booster shell wall thickness to get  $t_w = 0.149763 \text{ in.}$  Hence the equivalent cross-sectional area of the booster and Centaur is  $56.459 \text{ in.}^2$ . The structural stiffness is given by

$$k_{12} = \frac{EA}{L} = \frac{(28 \times 10^6 \text{ lb./in.}^2)(56.459 \text{ in.}^2)}{(102.7 \text{ ft.})} = 15.393 \times 10^6 \text{ lb./ft.}$$

The estimate of the stiffness of the launch vehicle adapter is

$$k_{23} = k_{12}/2 = 7.7014 \times 10^6 \text{ lb./ft.}$$

We neglect the loss of mass due to fuel burn during the initial period of liftoff, and assume the net thrust is a step function of time. That is,

$$T(t) = [439,300 - 362,200]H(t) = (77,100 \text{ lb.})H(t),$$

where the unit step function  $H(t) = 0$  for  $t < 0$ , and  $H(t) = 1$  for  $t > 0$ . Numerical evaluation of eq. (18.11) is

$$\begin{bmatrix} 5,518.63 & 0 & 0 \\ 0 & 5,612.64 & 0 \\ 0 & 0 & 117.174 \end{bmatrix} \begin{bmatrix} \ddot{w}_1 \\ \ddot{w}_2 \\ \ddot{w}_3 \end{bmatrix} + 10^6 \begin{bmatrix} 15.4027 & -15.4027 & 0 \\ -15.4027 & 23.1041 & -7.70136 \\ 0 & -7.70136 & 7.70136 \end{bmatrix} \begin{bmatrix} w_1 \\ w_2 \\ w_3 \end{bmatrix} = \begin{bmatrix} 76,100 \\ 0 \\ 0 \end{bmatrix}. \quad (18.12)$$

The initial conditions for the rocket at rest are:

$$w_i(0) = 0 \quad \dot{w}_i(0) = 0 \quad i = 1, 2, 3. \quad (18.13)$$

In compact notation the matrix equations of motion (18.12) are

$$[M]\{\ddot{w}\} + [K]\{w\} = \{T\}. \quad (18.14)$$

The linear ordinary differential equation (18.14) with constant coefficients can be solved numerically by step-by-step integration with respect to time, or they can be solved by the mode-separation method. The mode-separation method is limited to linear differential equations, but the step-by-step method can be used for linear and nonlinear ordinary differential equations. Step-by-step methods are discussed by Craig (1981, pp. 455-464) and Schiesser (1994), which contain many references to the literature. The mode-separation method is detailed in the following steps.

**Step 2: Free vibration problem.** For the free vibration problem set  $\{T\} = 0_{3 \times 1}$ , and seek a solution of the form

$$\{w(t)\} = \{\phi\} \cos(\omega t - \alpha). \quad (18.15)$$

Substitute eq. (18.15) into the free vibration equation of motion to get

$$([K] - \omega^2 [M])\{\phi\}(\cos \omega t - \alpha) = 0 \quad \forall t > 0. \quad (18.16)$$

Satisfying eq. (18.16) leads to

$$(\left[K\right] - \lambda \left[M\right])\{\phi\} = 0, \text{ where } \lambda = \omega^2. \quad (18.17)$$

One solution to eq. (18.17) is for the amplitude vector  $\{\phi\} = 0_{3 \times 1}$ , which leads to  $w(t) = 0$  for all time. For non-zero solutions of the amplitude vector we require

$$\text{Det}(\left[K\right] - \lambda \left[M\right]) = 0. \quad (18.18)$$

Evaluating the determinate (18.18) leads to the characteristic equation for  $\lambda$ , which in this case is a cubic polynomial:

$$\lambda[-k_{12}k_{23}(m_1 + m_2 + m_3) + (k_{12}m_3(m_1 + m_2) + k_{23}m_1(m_2 + m_3))\lambda - m_1m_2m_3\lambda^2] = 0. \quad (18.19)$$

Numerical solution for the roots of (18.19), which are called eigenvalues, are

$$\lambda_1 = 67159.2 \quad \lambda_2 = 5474.23 \quad \lambda_3 = 0. \quad (18.20)$$

For each eigenvalue (18.20) there are three linear equations to determine the amplitude vector  $\{\phi\}$  obtained from eq. (18.17). Since the determinate of eq. (18.17) vanishes for each eigenvalue, the three linear equations to determine the amplitude vector  $\{\phi\}$  corresponding to each  $\lambda$  are not independent. Solutions for  $\{\phi\}$  are called eigenvectors. From eigensystem software we find the following eigen pairs:

$$(\lambda_1, \{\phi_1\}) = \left( 67, 159.2, \begin{bmatrix} 0.945544 \times 10^{-3} \\ -0.0218065 \\ 1 \end{bmatrix} \right), (\lambda_2, \{\phi_2\}) = \left( 5, 474.23, \begin{bmatrix} -0.953559 \\ 0.916711 \\ 1 \end{bmatrix} \right), \& (\lambda_3, \{\phi_3\}) = \left( 0, \begin{bmatrix} 1 \\ 1 \\ 1 \end{bmatrix} \right). \quad (18.21)$$

The eigen pairs  $(\lambda_1, \{\phi_1\})$  and  $(\lambda_2, \{\phi_2\})$  correspond to elastic modes, and  $(\lambda_3, \{\phi_3\})$  corresponds to a rigid body mode. An eigenvector  $\{\phi_i\}$  can be multiplied by a non-zero constant and still be a solution to eq. (18.17) with  $\lambda = \lambda_i$ .

**Step 3: Coordinate transformation.** Now consider the solution to the forced vibration problem (18.14). Define the modal matrix  $[\Phi]$  whose columns are the eigenvectors:

$$[\Phi] = [\{\phi_1\} \{\phi_2\} \{\phi_3\}] = \begin{bmatrix} 0.945544 \times 10^{-3} & -0.953559 & 1 \\ -0.0218065 & 0.916711 & 1 \\ 1 & 1 & 1 \end{bmatrix}. \quad (18.22)$$

Transform from physical coordinates  $\{w(t)\}$  to modal coordinates  $\{q(t)\}$  using the modal matrix:

$$\begin{bmatrix} w_1(t) \\ w_2(t) \\ w_3(t) \end{bmatrix} = [\Phi] \begin{bmatrix} q_1(t) \\ q_2(t) \\ q_3(t) \end{bmatrix}. \quad (18.23)$$

**Step 4: Solutions for the time history of modal coordinates.** Substitute transformation (18.23) into the force vibration problem (18.14) to get

$$[M][\Phi]\{\ddot{q}(t)\} + [K][\Phi]\{q(t)\} = \{T\}. \quad (18.24)$$

Pre-multiply the previous matrix equation by the transpose of the modal matrix and write the result as

$$[M_g]\{\ddot{q}(t)\} + [K_g]\{q(t)\} = \{T_g\}. \quad (18.25)$$

The generalized mass matrix is defined by  $[M_g] = [\Phi]^T[M][\Phi]$ , the generalized stiffness matrix by

$[K_g] = [\Phi]^T[K][\Phi]$ , and the generalized force vector by  $\{T_g\} = [\Phi]^T\{T\}$ . The generalized mass and stiffness matrices are diagonal matrices; that is, the off-diagonal elements in these matrices are zero and the diagonal elements are non-zero. Numerical results for these generalized matrices are

$$[M_g] = \begin{bmatrix} 119.848 & 0 & 0 \\ 0 & 9,851.76 & 0 \\ 0 & 0 & 11,248.4 \end{bmatrix} \quad [K_g] = \begin{bmatrix} 8.04888 \times 10^6 & 0 & 0 \\ 0 & 5.39308 \times 10^7 & 0 \\ 0 & 0 & 0 \end{bmatrix} \quad \{T_g\} = \begin{bmatrix} 72.9014 \\ -73,549.4 \\ 77,100 \end{bmatrix}. \quad (18.26)$$

The equations of motion for the modal displacements are decoupled. Equations (18.13) and (18.23) determine the initial conditions for the modal displacements as

$$\begin{bmatrix} q_1(0) \\ q_2(0) \\ q_3(0) \end{bmatrix} = [\Phi]^{-1} \begin{bmatrix} w_1(0) \\ w_2(0) \\ w_3(0) \end{bmatrix} \quad \text{and} \quad \begin{bmatrix} \dot{q}_1(0) \\ \dot{q}_2(0) \\ \dot{q}_3(0) \end{bmatrix} = [\Phi]^{-1} \begin{bmatrix} \dot{w}_1(0) \\ \dot{w}_2(0) \\ \dot{w}_3(0) \end{bmatrix}$$

A convenient way to find the inverse of the modal matrix is to start with definition  $[\Phi][\Phi]^{-1} = [I]$ , pre-multiply it by  $[\Phi]^T[M]$  to find  $[\Phi]^T[M][\Phi][\Phi]^{-1} = [\Phi]^T[M]$ . But  $[\Phi]^T[K][\Phi] = [M_g]$ . Hence,

$$[\Phi]^{-1} = [M_g]^{-1}[\Phi]^T[M]. \quad (18.27)$$

The inverse of the generalized mass matrix is equal to the reciprocal of the diagonal elements of  $[M_g]$ . For this example the initial conditions for the modal coordinates are

$$q_i(0) = 0 \quad \dot{q}_i(0) = 0 \quad i = 1, 2, 3. \quad (18.28)$$

The differential equation for the first modal displacement is

$$119.848\ddot{q}_1 + 8.04888 \times 10^6 q_1 = 72.9014 \quad q_1 = q_1(t) \quad t \geq 0. \quad (18.29)$$

The solution to differential equation (18.29) is

$$q_1(t) = 9.05734 \times 10^{-6} + c_2 \cos \omega_1 t + c_1 \sin \omega_1 t, \quad (18.30)$$

where  $\omega_1 = \sqrt{\lambda_1} = 259.151$  rad/s. The constants  $c_1$  and  $c_2$  are determined from initial conditions (18.28). The final result for the first modal displacement is

$$q_1(t) = 9.05734 \times 10^{-6} (1 - \cos \omega_1 t) \quad \omega_1 = 259.151 \text{ rad/s}. \quad (18.31)$$

The differential equation for the second modal displacement is

$$9,851.76\ddot{q}_2 + 5.39308 \times 10^7 q_2 = -73,549.4 \quad q_2 = q_2(t) \quad t \geq 0. \quad (18.32)$$

The solution to differential equation (18.32) subject to initial conditions (18.28) is

$$q_2(t) = -0.00136322(1 - \cos \omega_2 t) \quad \omega_2 = \sqrt{\lambda_2} = 73.988 \text{ rad/s}. \quad (18.33)$$

The differential equation for the third modal displacement is

$$11,248.4\ddot{q}_3 = 77,100 \quad q_3 = q_3(t) \quad t \geq 0. \quad (18.34)$$

The solution to differential equation (18.34) subject to initial conditions (18.28) is

$$q_3(t) = 3.42714t^2. \quad (18.35)$$

**Step 5: Transform back to physical coordinates.** Equations (18.30), (18.33), and (18.35) are substituted for  $q_1$ ,  $q_2$ , and  $q_3$ , respectively, into the transformation (18.23) to determine the physical displacements. The payload displacement is

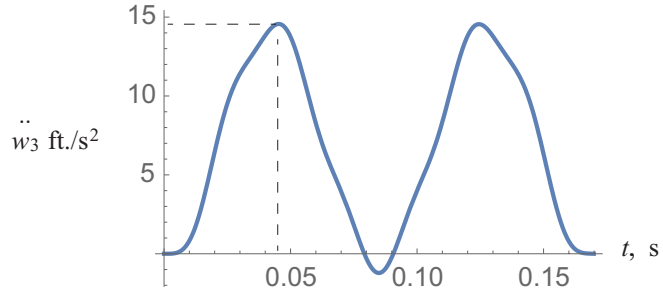
$$w_3(t) = -0.00135416 + 3.42714t^2 + 0.00136322 \cos(73.988t) - 9.05734 \times 10^{-6} \cos(259.151t). \quad (18.36)$$

**Step 6: Payload acceleration.** The payload acceleration computed from the second derivative of eq. (18.36) is

$$\ddot{w}_3(t) = 6.85428 - 7.46257 \cos(73.988t) + 0.608283 \cos(259.151t). \quad (18.37)$$

The payload acceleration over one period of the lowest frequency is plotted in figure 18.4. Maximum acceleration is  $14.56 \text{ ft./s}^2$  at  $t = 0.0453 \text{ s}$ . The payload load factor is  $n = 1 + 14.56/32.2 = 1.452$ , which is a 19.7 percent increase with respect to the rigid body load factor.

**Fig. 18.4** Time history of the payload acceleration.



## 18.4 Eigenvalue problems for real symmetric matrices

In general an  $n \times n$  real matrix  $[A]$  acts on an  $n \times 1$  vector  $\{\phi\}$  by changing both its magnitude and direction. For example consider

$$[A] = \begin{bmatrix} 2 & 1 \\ 1 & 2 \end{bmatrix} \quad \{\phi\} = \begin{bmatrix} 2 \\ 0 \end{bmatrix} \quad [A]\{\phi\} = \begin{bmatrix} 4 \\ 2 \end{bmatrix}. \quad (a)$$

Vectors  $\{\phi\}$  and  $[A]\{\phi\}$  are depicted in figure 18.5(a). Matrix  $[A]$  may act on certain vectors by changing only their magnitude, and leaving their direction unchanged; e.g.,

$$\begin{bmatrix} 2 & 1 \\ 1 & 2 \end{bmatrix} \begin{bmatrix} 1 \\ 1 \end{bmatrix} = \begin{bmatrix} 3 \\ 3 \end{bmatrix} = 3 \begin{bmatrix} 1 \\ 1 \end{bmatrix}. \quad (b)$$

Vector  $\begin{bmatrix} 1 & 1 \end{bmatrix}^T$  is an eigenvector of matrix  $[A]$  and the number “3” is an eigenvalue. Consider the vector  $\begin{bmatrix} -1 & 1 \end{bmatrix}^T$ . Then, the matrix  $[A]$  operating on this second vector is

$$\begin{bmatrix} 2 & 1 \\ 1 & 2 \end{bmatrix} \begin{bmatrix} -1 \\ 1 \end{bmatrix} = \begin{bmatrix} -1 \\ 1 \end{bmatrix}. \quad (c)$$

Thus, vector  $\begin{bmatrix} -1 & 1 \end{bmatrix}^T$  is an eigenvector and the number “1” is the eigenvalue. The eigenvectors of matrix  $[A]$  are depicted in figure 18.5(b).

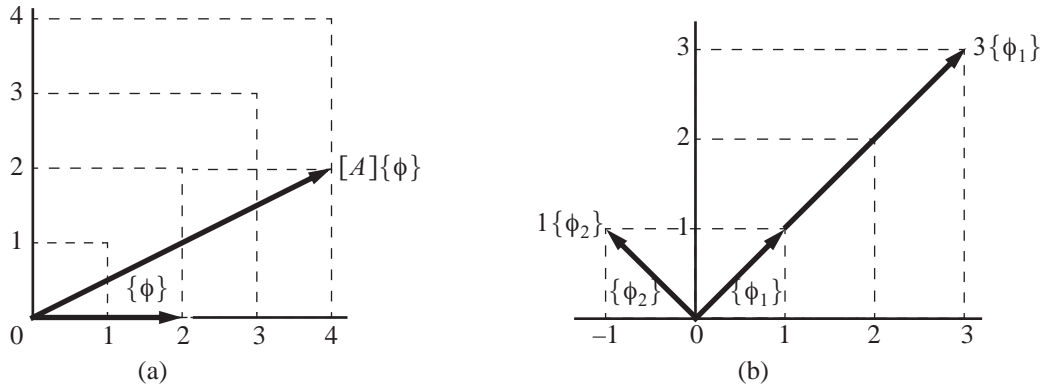


**Fig. 18.5 (a) Matrix A operating on a vector. (b) Matrix A operating on eigenvectors**

The eigenpairs of matrix  $[A]$  are written as

$$(\lambda_1, \{\phi_1\}) = \left(3, \begin{bmatrix} 1 \\ 1 \end{bmatrix}\right) \quad \text{and} \quad (\lambda_2, \{\phi_2\}) = \left(1, \begin{bmatrix} -1 \\ 1 \end{bmatrix}\right). \quad (d)$$

The standard matrix eigenvalue problem is

$$[A]\{\phi\} = \lambda\{\phi\}, \quad (18.38)$$

where  $[A]$  is a real  $nxn$  matrix and  $\{\phi\}$  is an  $nx1$  vector. It is also written as

$$([A] - \lambda[I])\{\phi\} = 0. \quad (e)$$

where  $[I]$  is the  $nxn$  identity matrix. (i.e., a diagonal matrix with each diagonal element equal to one). One solution to eq. (18.38) is  $\{\phi\} = 0_{nx1}$ , which is called the trivial solution. Non-trivial solutions for  $\{\phi\}$  require

$$\text{Det}([A] - \lambda[I]) = p(\lambda) = 0, \quad (18.39)$$

where  $p(\lambda)$  is a polynomial of degree  $n$  having  $n$  roots. The polynomial  $p(\lambda)$  is called the characteristic equation. The roots of  $p(\lambda) = 0$  are the eigenvalues of matrix  $[A]$ . The eigenvalue problem for the  $r$ -th mode is

$$[A]\{\phi_r\} = \lambda_r\{\phi_r\}. \quad (18.40)$$

The eigenpairs are denoted by  $(\lambda_r, \{\phi_r\})$ . If  $\{\phi_r\}$  is a solution to eq. (18.40), then  $c_r\{\phi_r\}$  is also a solution where  $c_r$  is an arbitrary constant. Thus, the solution for the eigenvector is not unique. Scaling, or normalization, is the process to make the amplitude of the eigenvector unique. One method to normalize the amplitude is to require  $\{\phi_r\}$  be a unit vector in the  $n$ -dimensional space. That is, we specify

$$\{\phi_r\}^T\{\phi_r\} = 1. \quad (18.41)$$

Consider the eigenvalue problem for  $s$ -th mode

$$[A]\{\phi_s\} = \lambda_s\{\phi_s\}. \quad (18.42)$$

Pre-multiply the  $r$ -th mode in eq. (18.40) by  $\{\phi_s\}^T$  to get

$$\{\phi_s\}^T[A]\{\phi_r\} = \lambda_r\{\phi_s\}^T\{\phi_r\}. \quad (18.43)$$

Pre-multiply the  $s$ -th mode in eq. (18.42) by  $\{\phi_r\}^T$ :

$$\{\phi_r\}^T[A]\{\phi_s\} = \lambda_s\{\phi_r\}^T\{\phi_s\}. \quad (18.44)$$

Take the transpose of eq. (18.43) and use the property of symmetry  $[A]^T = [A]$  to find

$$\{\phi_r\}^T[A]\{\phi_s\} = \lambda_r\{\phi_r\}^T\{\phi_s\}. \quad (18.45)$$

Subtract eq. (18.45) from eq. (18.44) to find

$$0 = (\lambda_r - \lambda_s)\{\phi_r\}^T\{\phi_s\}. \quad (18.46)$$

For  $\lambda_r \neq \lambda_s$

$$\{\phi_r\}^T\{\phi_s\} = 0 \quad r \neq s \quad r, s = 1, 2, \dots, n. \quad (18.47)$$

The eigenvectors for distinct eigenvalues are orthogonal. The eigenvectors are said to be orthonormal if

$$\{\phi_r\}^T\{\phi_s\} = \begin{cases} 1 & r = s \\ 0 & r \neq s \end{cases}. \quad (18.48)$$

Since the characteristic equation  $p(\lambda) = 0$  has real coefficients, the roots  $\lambda$  are real or occur as complex conjugate pairs. It can be shown that roots are real (Boresi, 1965, p. 34).

Let  $[\Phi]$  denote the  $n \times n$  modal matrix whose columns are the orthonormal eigenvectors. The  $r$ -th column contains the eigenvector  $\{\phi_r\}$  associated with eigenvalue  $\lambda_r$ ,  $r = 1, 2, \dots, n$ . Since the eigenvectors are orthonormal, the modal matrix has the property

$$[\Phi]^T[\Phi] = [\Phi][\Phi]^T = [I]. \quad (18.49)$$

The modal matrix is called an **orthogonal matrix**, and it has the properties

$$[\Phi]^{-1} = [\Phi]^T \quad \text{Det}[\Phi] = 1. \quad (18.50)$$

Using the modal matrix the standard eigenvalue problem can be written as

$$[A][\Phi] = [\Phi][D], \quad (18.51)$$

where  $[D]$  is a diagonal matrix of the eigenvalues:

$$[D] = \text{diag}[\lambda_1, \lambda_2, \dots, \lambda_n]. \quad (18.52)$$

Post-multiply eq. (18.51) by  $[\Phi]^T$  to get

$$[A] \underbrace{[\Phi][\Phi]^T}_{[I]} = [\Phi][D][\Phi]^T. \quad (18.53)$$

Hence, matrix  $[A]$  has the decomposition

$$[A] = [\Phi][D][\Phi]^T. \quad (18.54)$$

An  $n \times n$  real, symmetric matrix is **positive definite** if all eigenvalues  $\lambda_r > 0$ ,  $r = 1, 2, \dots, n$ . It is **positive semidefinite** if the eigenvalues  $\lambda_r \geq 0$ , that is, some of its eigenvalues may equal zero. For structures having rigid body freedoms the stiffness matrix  $[K]$  has as many zero eigenvalues as it has rigid body modes.

The mode superposition method leads to the generalized eigenvalue problem

$$[K]\{\phi\} = \lambda[M]\{\phi\}, \quad (18.55)$$

where the  $n \times n$  matrices  $[K]$  and  $[M]$  are real and symmetric,  $\{\phi\}$  is the  $n \times 1$  eigenvector, or modal vector, and the eigenvalue  $\lambda$  is equal to the square of the natural frequency  $\omega$ . Refer to eq. (18.17). The generalized eigenvalue problem (18.55) can be reduced to the standard form in eq. (18.38) if the mass matrix is positive definite (Bathe, p. 573). Then all the properties of the eigenvalues, eigenvectors, and characteristic polynomials can be derived from the properties of the standard eigenvalue problem. In particular, for the generalized eigenvalue problem

- all  $n$  of the  $\lambda_r$ 's are real (no complex conjugates), and
- for  $r \neq s$ ,  $\{\phi_r\}^T [M] \{\phi_s\} = 0$  (i.e., the eigenvectors are  $M$ -orthogonal).

Vanishing of the determinate  $\text{Det}([K] - \lambda[M]) = p(\lambda) = 0$  is equivalent to finding the roots of a polynomial of degree  $n$ . If  $n \geq 5$ , iterative solution procedures have to be employed (Graig, 1981). There are many efficient subroutines available in various scientific subroutine libraries to numerically solve eigenvalue problems. In *Mathematica* the function "Eigensystem[{K,M}]" finds numerical eigenvalues and eigenvectors of the generalized eigenvalue problem. In MATLAB the statement "[V,D] = EIG(K,M)" finds a diagonal matrix D of generalized eigenvalues and a full matrix V whose columns are the corresponding eigenvectors so that  $[K][V] = [M][V][D]$ . For the numerical solutions to the practice exercises listed in article 18.11 it is assumed the reader has access to a subroutine to find eigenvalues and eigenvectors.



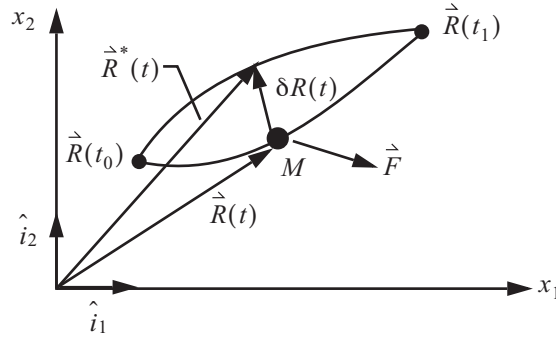
### 18.5 Hamilton's principle and Lagrange's equations

Consider a particle of mass  $M$  in motion along the  $x_1$ - $x_2$  plane as shown in figure 18.6. The position vector of the particle at time  $t$  is denoted by  $\vec{R}(t)$ , where

$$\vec{R}(t) = x_1(t)\hat{i}_1 + x_2(t)\hat{i}_2, \quad (18.56)$$

where  $\hat{i}_1$  and  $\hat{i}_2$  are unit vectors in the  $x_1$ -, and  $x_2$ -directions, respectively. From Newton's second law the equation of motion for the particle is solved for its motion  $\vec{R}(t)$ ,  $t > t_0$ , given its position  $\vec{R}(t_0)$  and the velocity  $\frac{d\vec{R}}{dt}(t_0)$  at  $t = t_0$ . In contrast to Newton's method, Hamilton's approach to this moving particle is to determine the motion  $\vec{R}(t)$  given the positions  $\vec{R}(t_0)$  and  $\vec{R}(t_1)$ ,  $t_1 > t_0$ . All positions in the interval  $t_0 \leq t \leq t_1$  describe a time-dependent path illustrated by a curve in figure 18.6. The path labeled  $\vec{R}(t)$  represents the actual motion. The path labeled  $\vec{R}^*(t)$  represents a motion from  $\vec{R}(t_0)$  to  $\vec{R}(t_1)$  in the vicinity of the actual motion.

**Fig. 18.6** Dynamical paths for a particle in plane motion.



Begin with D'Alembert's principle and introduce the inertia force in addition the applied force  $\vec{F}$  and write the dynamic equation of equilibrium as follows:

$$\vec{F} - M \frac{d^2 \vec{R}}{dt^2} = 0. \quad (18.57)$$

At a *fixed* time introduce an infinitesimal virtual displacement denoted by the function  $\delta \vec{R}(t)$ . We can imagine the motion is stopped at time  $t$  when the virtual displacement is imposed on the particle with both the applied force and inertia force acting on the particle. The virtual changes in the coordinates imposed on the particle at a fixed time are denoted by  $\delta x_1(t)$  and  $\delta x_2(t)$ , so that

$$\delta \vec{R}(t) = \delta x_1(t)\hat{i}_1 + \delta x_2(t)\hat{i}_2. \quad (18.58)$$

The varied path  $\vec{R}^*(t)$  in the vicinity of the actual path  $\vec{R}(t)$  is

$$\vec{R}^*(t) = \vec{R}(t) + \delta \vec{R}(t). \quad (18.59)$$

Since the varied path and actual path coincide at  $t = t_0$  and  $t = t_1$  the virtual displacement vanishes at these times:

$$\delta \vec{R}(t_0) = \delta \vec{R}(t_1) = 0\hat{i}_1 + 0\hat{i}_2. \quad (18.60)$$

The virtual work of the applied force and the inertia force acting through the virtual displacement is given by the scalar product of eq. (18.57) with the virtual displacement in eq. (18.58):

$$\vec{F} \cdot \delta \vec{R} - M \frac{d^2 \vec{R}}{dt^2} \cdot \delta \vec{R} = 0. \quad (18.61)$$

Consider the relation

$$\frac{d}{dt} \left( \frac{d\vec{R}}{dt} \cdot \delta \vec{R} \right) = \frac{d^2 \vec{R}}{dt^2} \cdot \delta \vec{R} + \frac{d\vec{R}}{dt} \cdot \frac{d}{dt} (\delta \vec{R}). \quad (18.62)$$

The virtual change in velocity is defined by

$$\delta \left( \frac{d\vec{R}}{dt} \right) \equiv \frac{d\vec{R}^*}{dt} - \frac{d\vec{R}}{dt} = \frac{d}{dt} (\vec{R}^* - \vec{R}) = \frac{d}{dt} (\delta \vec{R}). \quad (18.63)$$

Equation (18.63) shows we can interchange the virtual operator  $\delta(\ )$  and the differential operator  $d(\ )/dt$ . Use the result from eq. (18.63) to write eq. (18.62) as

$$\frac{d}{dt} \left( \frac{d\vec{R}}{dt} \cdot \delta \vec{R} \right) = \frac{d^2 \vec{R}}{dt^2} \cdot \delta \vec{R} + \frac{d\vec{R}}{dt} \cdot \delta \left( \frac{d\vec{R}}{dt} \right). \quad (18.64)$$

Equation (18.64) is incorporated into the virtual work eq. (18.61) to get

$$\vec{F} \cdot \delta \vec{R} + M \frac{d\vec{R}}{dt} \cdot \delta \left( \frac{d\vec{R}}{dt} \right) - \frac{d}{dt} \left( M \frac{d\vec{R}}{dt} \cdot \delta \vec{R} \right) = 0. \quad (18.65)$$

The virtual work of the applied force is written as  $\delta W = \vec{F} \cdot \delta \vec{R}$ , and let the velocity of the particle be denoted by  $\vec{v} = \frac{d\vec{R}}{dt}$ , and its virtual velocity by  $\delta \vec{v} = \delta \left( \frac{d\vec{R}}{dt} \right)$ . Then, eq. (18.65) for the virtual work is

$$\delta W + M \vec{v} \cdot \delta \vec{v} - \frac{d}{dt} (M \vec{v} \cdot \delta \vec{R}) = 0. \quad (18.66)$$

The kinetic energy of the particle is  $T = \frac{1}{2} M \vec{v} \cdot \vec{v}$ , and its kinetic energy on the varied path is

$$T + \Delta T = \frac{1}{2} M (\vec{v} + \delta \vec{v}) \cdot (\vec{v} + \delta \vec{v}) = \underbrace{\frac{1}{2} M \vec{v} \cdot \vec{v}}_T + \underbrace{M \vec{v} \cdot \delta \vec{v}}_{\delta T} + \underbrace{\frac{1}{2} M \delta \vec{v} \cdot \delta \vec{v}}_{\delta^2 T}. \quad (18.67)$$

For infinitesimal virtual velocities  $\Delta T \approx \delta T$ . Integrate eq. (18.66) with respect to time from  $t_0$  to  $t_1$  to get

$$\int_{t_0}^{t_1} (\delta W + \delta T) dt - (M \vec{v} \cdot \delta \vec{R}) \Big|_{t_0}^{t_1} = 0. \quad (18.68)$$

The virtual displacement  $\delta \vec{R}$  vanishes at times  $t_0$  and  $t_1$ . Then eq. (18.68) becomes

$$\int_{t_0}^{t_1} (\delta W + \delta T) dt = 0. \quad (18.69)$$

Equation (18.69) is Hamilton's principle. Note that  $\delta W$  is not the total virtual work. It is the virtual work of the non-inertial forces.

### 18.5.1 Lagrange's equations

Deriving equations of motion for connected bodies using Newton's laws as was done in step 1 of article 18.3 requires separate free body diagrams of each component, and the forces of interaction had to be eliminated to arrive at the final set of equations. An alternative method is to use the scalar functions kinetic energy  $T$  and the potential energy  $V$  of the system in Lagrange's equations to obtain the equations of motion. Lagrange's equations are derived from Hamilton's variational principle (18.69). In general, the kinetic energy of a particle as depicted in figure 18.6 is a function of its position  $(x_1, x_2)$  and its velocities  $(\dot{x}_1, \dot{x}_2)$  at time  $t$  (i.e.,  $T = T(x_1, x_2, \dot{x}_1, \dot{x}_2)$ ). The virtual change in kinetic energy is

$$\delta T = \frac{\partial T}{\partial x_1} \delta x_1 + \frac{\partial T}{\partial x_2} \delta x_2 + \frac{\partial T}{\partial \dot{x}_1} \delta \dot{x}_1 + \frac{\partial T}{\partial \dot{x}_2} \delta \dot{x}_2. \quad (18.70)$$

The virtual work of the applied force acting on the particle is  $\delta W = \vec{F} \cdot \delta \vec{R} = F_1 \delta x_1 + F_2 \delta x_2$ . The applied forces can be decomposed as  $F_i = Q_i + R_i$ ,  $i = 1, 2$ , where  $Q_i$  are non-conservative forces and  $R_i$  are the conservative forces. Conservative forces are determined in terms of the potential energy function  $V(x_1, x_2)$  by the relations

$$R_1 = -\left(\frac{\partial V}{\partial x_1}\right) \quad R_2 = -\left(\frac{\partial V}{\partial x_2}\right). \quad (18.71)$$

The virtual work is expressed as

$$\delta W = (Q_1 + R_1) \delta x_1 + (Q_2 + R_2) \delta x_2 = \left(Q_1 - \frac{\partial V}{\partial x_1}\right) \delta x_1 + \left(Q_2 - \frac{\partial V}{\partial x_2}\right) \delta x_2. \quad (18.72)$$

Substitute the virtual kinetic energy from eq. (18.70) and the virtual work from eq. (18.72) into Hamilton's principle (18.69) to get

$$\int_{t_0}^{t_1} \left[ \left(Q_1 - \frac{\partial V}{\partial x_1}\right) \delta x_1 + \left(Q_2 - \frac{\partial V}{\partial x_2}\right) \delta x_2 + \frac{\partial T}{\partial x_1} \delta x_1 + \frac{\partial T}{\partial x_2} \delta x_2 + \frac{\partial T}{\partial \dot{x}_1} \delta \dot{x}_1 + \frac{\partial T}{\partial \dot{x}_2} \delta \dot{x}_2 \right] dt = 0. \quad (18.73)$$

Rearrange the terms in eq. (18.73) to

$$\int_{t_0}^{t_1} \left[ \left(Q_1 - \frac{\partial V}{\partial x_1} + \frac{\partial T}{\partial x_1}\right) \delta x_1 + \left(Q_2 - \frac{\partial V}{\partial x_2} + \frac{\partial T}{\partial x_2}\right) \delta x_2 + \frac{\partial T}{\partial \dot{x}_1} \delta \dot{x}_1 + \frac{\partial T}{\partial \dot{x}_2} \delta \dot{x}_2 \right] dt = 0. \quad (18.74)$$

Integrate by parts the last two terms in the integrand of eq. (18.74) and note that the virtual coordinates  $\delta x_1$  and  $\delta x_2$  vanish at the beginning and end time. Hence, eq. (18.74) becomes

$$\int_{t_0}^{t_1} \left( \frac{\partial T}{\partial \dot{x}_1} \delta \dot{x}_1 + \frac{\partial T}{\partial \dot{x}_2} \delta \dot{x}_2 \right) dt = \int_{t_0}^{t_1} \left[ -\frac{d}{dt} \left( \frac{\partial T}{\partial \dot{x}_1} \right) - \frac{d}{dt} \left( \frac{\partial T}{\partial \dot{x}_2} \right) \right] dt + \underbrace{\left[ \left( \frac{\partial T}{\partial \dot{x}_1} \right) \delta x_1 + \left( \frac{\partial T}{\partial \dot{x}_2} \right) \delta x_2 \right]}_{= 0} \bigg|_{t_0}^{t_1} . \quad (18.75)$$

The result of the manipulations from eq. (18.73) to eq. (18.75) is

$$\int_{t_0}^{t_1} \left[ \left( Q_1 - \frac{\partial V}{\partial x_1} + \frac{\partial T}{\partial x_1} - \frac{d}{dt} \left( \frac{\partial T}{\partial \dot{x}_1} \right) \right) \delta x_1 + \left( Q_2 - \frac{\partial V}{\partial x_2} + \frac{\partial T}{\partial x_2} - \frac{d}{dt} \left( \frac{\partial T}{\partial \dot{x}_2} \right) \right) \delta x_2 \right] dt = 0 . \quad (18.76)$$

Define the Lagrangian function  $L$  by

$$L = T - V . \quad (18.77)$$

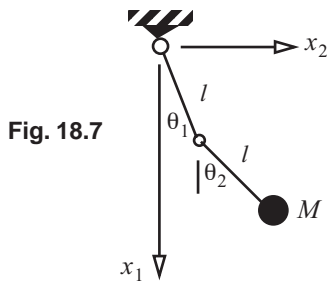
Incorporating the Lagrangian function in eq. (18.76) we get

$$\int_{t_0}^{t_1} \left[ \left( Q_1 + \frac{\partial L}{\partial x_1} - \frac{d}{dt} \left( \frac{\partial L}{\partial \dot{x}_1} \right) \right) \delta x_1 + \left( Q_2 + \frac{\partial L}{\partial x_2} - \frac{d}{dt} \left( \frac{\partial L}{\partial \dot{x}_2} \right) \right) \delta x_2 \right] dt = 0 . \quad (18.78)$$

Equation (18.78) vanishes for every choice of the virtual coordinates  $\delta x_1$  and  $\delta x_2$ , which leads to Lagrange's equations of motion given by eq. (18.79) below.

$$\frac{d}{dt} \left( \frac{\partial L}{\partial \dot{x}_1} \right) - \frac{\partial L}{\partial x_1} = Q_1 \quad \frac{d}{dt} \left( \frac{\partial L}{\partial \dot{x}_2} \right) - \frac{\partial L}{\partial x_2} = Q_2 . \quad (18.79)$$

### Example 18.1 Double pendulum



The pendulum shown figure 18.7 oscillates in the  $x_1$ - $x_2$  plane under the action of gravity. The mass is concentrated in the particle at the end of the lower bar. The hinges are frictionless. Two coordinates, angles  $\theta_1$  and  $\theta_2$ , describe the configuration the pendulum and are called *generalized coordinates*.<sup>1</sup> The coordinates of the particle are

$$\begin{aligned} x_1(t) &= l \cos \theta_1(t) + l \cos \theta_2(t) \\ x_2(t) &= l \sin \theta_1(t) + l \sin \theta_2(t) \end{aligned} . \quad (a)$$

The kinetic energy is

$$T = \frac{1}{2} M [(\dot{x}_1)^2 + (\dot{x}_2)^2] = \frac{1}{2} M l^2 [(\dot{\theta}_1)^2 + (\dot{\theta}_2)^2 + 2 \dot{\theta}_1 \dot{\theta}_2 \cos(\theta_1 - \theta_2)] . \quad (b)$$

The potential energy is

1. Requirements for generalized coordinates are (1) that there is a one-to-one correspondence between the coordinates and the configuration of the mechanical system, and (2) that infinitesimal increments in the generalized coordinates result in infinitesimal increments in the configuration. Requirement (1) precludes constraint equations between the generalize coordinates.

$$V = Mg(2l - x_1 - x_2) = Mgl[(1 - \cos\theta_1) + (1 - \cos\theta_2)]. \quad (\text{c})$$

Lagrange's equations (18.79) for the pendulum are

$$\frac{d}{dt}\left(\frac{\partial L}{\partial \dot{\theta}_1}\right) - \frac{\partial L}{\partial \theta_1} = 0 \quad \frac{d}{dt}\left(\frac{\partial L}{\partial \dot{\theta}_2}\right) - \frac{\partial L}{\partial \theta_2} = 0. \quad (\text{d})$$

Derivatives of the Lagrangian function (18.77) with respect to  $\theta_1$  and  $\dot{\theta}_1$  follow.

$$\frac{\partial L}{\partial \theta_1} = -Ml^2\dot{\theta}_1\dot{\theta}_2\sin(\theta_1 - \theta_2) - Mgl\sin\theta_1, \quad (\text{e})$$

$$\frac{\partial L}{\partial \dot{\theta}_1} = Ml^2[\dot{\theta}_1 + \dot{\theta}_2\cos(\theta_1 - \theta_2)], \text{ and } \frac{d}{dt}\left(\frac{\partial L}{\partial \dot{\theta}_1}\right) = Ml^2[\ddot{\theta}_1 + \ddot{\theta}_2\cos(\theta_1 - \theta_2) - \dot{\theta}_2(\dot{\theta}_1 - \dot{\theta}_2)\sin(\theta_1 - \theta_2)]. \quad (\text{f})$$

Substitute eqs. (e) and (f) into the Lagrangian equation for  $\theta_1$  in eq. (d) to get the equation of motion

$$Ml^2[\ddot{\theta}_1 + \ddot{\theta}_2\cos(\theta_1 - \theta_2) + (\dot{\theta}_2)^2\sin(\theta_1 - \theta_2)] + Mgl\sin\theta_1 = 0. \quad (\text{g})$$

Similar mathematical manipulations for Lagrange's equation in coordinate  $\theta_2$  lead to the second equation of motion

$$Ml^2[\ddot{\theta}_2 + \ddot{\theta}_1\cos(\theta_1 - \theta_2) - (\dot{\theta}_1)^2\sin(\theta_1 - \theta_2)] + Mgl\sin\theta_2 = 0. \quad (\text{h})$$

## 18.6 The dynamic response of an elastic thin-walled bar

Starting with Hamilton's principle we develop a weak form for the dynamic response of a thin-walled bar suitable for a finite element analysis. Assume the bar is homogenous with a uniform cross section along the  $z$ -axis,  $0 \leq z \leq L$ , where  $L$  denotes the length of the bar. Since the bar is a one-dimensional continuum, Hamilton's principle (18.69) is expressed as

$$\int_{t_0}^{t_1} \int_0^L (\delta \bar{T} + \delta \bar{W}) dz dt = 0, \quad (\text{18.80})$$

where  $\delta \bar{T}$  is the virtual kinetic energy per unit axial length, and  $\delta \bar{W}$  is the virtual work of the non-inertial forces per unit axial length. From eqs. (3.20) and (3.22) on page 36, and eq. (3.26) on page 37, the displacements of a material point on the contour of the cross section are

$$u_s(s, z, t) = -u(z, t)\sin\theta(s) + v(z, t)\cos\theta(s) + r_n(s)\phi_z(z, t), \quad (\text{18.81})$$

$$u_\zeta(s, z, t) = u(z, t)\cos\theta(s) + v(z, t)\sin\theta(s) - r_t(s)\phi_z(z, t), \text{ and} \quad (\text{18.82})$$

$$u_z(s, z, t) = w(z, t) + y(s)\phi_x(z, t) + x(s)\phi_y(z, t). \quad (\text{18.83})$$

The virtual kinetic energy term in Hamilton's principle (18.80) is written as

$$\int_{t_0}^{t_1} \left( \int_0^L \delta \bar{T} dz \right) dt = \int_{t_0}^{t_1} \left[ \int_0^L \left( \int_c \delta T t ds \right) dz \right] dt, \quad (18.84)$$

where the kinetic energy per unit volume, or the kinetic energy density, is

$$T = \frac{1}{2} \rho [(\dot{u}_s)^2 + (\dot{u}_\zeta)^2 + (\dot{u}_z)^2], \quad (18.85)$$

The mass density is denoted by  $\rho$ . The dot over the displacement function is a shorthand notation for the partial derivative of the function with respect to time; e.g.,

$$\dot{u}_s = \frac{\partial u_s}{\partial t}. \quad (18.86)$$

The virtual kinetic energy density at a fixed time is

$$\delta T = \frac{\partial T}{\partial \dot{u}_s} \delta \dot{u}_s + \frac{\partial T}{\partial \dot{u}_\zeta} \delta \dot{u}_\zeta + \frac{\partial T}{\partial \dot{u}_z} \delta \dot{u}_z = \rho (\dot{u}_s \delta \dot{u}_s + \dot{u}_\zeta \delta \dot{u}_\zeta + \dot{u}_z \delta \dot{u}_z), \quad (18.87)$$

where  $\delta \dot{u}_s$ ,  $\delta \dot{u}_\zeta$ , and  $\delta \dot{u}_z$  are the infinitesimal virtual velocity components. Interchange the order of the temporal and spatial integrals in eq. (18.84) to write the virtual kinetic energy term as

$$\int_{t_0}^{t_1} \left[ \int_0^L \left( \int_c \delta T t ds \right) dz \right] dt = \int_0^L \left[ \int_c \left( \int_{t_0}^{t_1} \delta T t dt \right) t ds \right] dz. \quad (18.88)$$

The interior integral in eq. (18.88) with respect to time is integrated by parts as follows:

$$\begin{aligned} \int_{t_0}^{t_1} \delta T t dt &= \rho \int_{t_0}^{t_1} (\dot{u}_s \delta \dot{u}_s + \dot{u}_\zeta \delta \dot{u}_\zeta + \dot{u}_z \delta \dot{u}_z) dt \\ &= -\rho \int_{t_0}^{t_1} (\ddot{u}_s \delta u_s + \ddot{u}_\zeta \delta u_\zeta + \ddot{u}_z \delta u_z) dt + \rho (\dot{u}_s \delta u_s + \dot{u}_\zeta \delta u_\zeta + \dot{u}_z \delta u_z) \Big|_{t_0}^{t_1}. \end{aligned} \quad (18.89)$$

By Hamilton's principle the virtual displacements  $\{\delta u_s, \delta u_\zeta, \delta u_z\}$  vanish at times  $t_0$  and  $t_1$ . Return to eq. (18.84) and identify

$$\int_{t_0}^{t_1} \left[ \int_0^L \left( \int_c \delta T t ds \right) dz \right] dt = \int_{t_0}^{t_1} \left[ \int_0^L \delta \bar{T} dz \right] dt, \quad (18.90)$$

where the virtual kinetic energy per unit axial length is

$$\delta \bar{T} = \int_c \delta T t ds = -\rho \int_c (\ddot{u}_s \delta u_s + \ddot{u}_\zeta \delta u_\zeta + \ddot{u}_z \delta u_z) t ds. \quad (18.91)$$

We assume the density of mass  $\rho$  is independent of the contour coordinate  $s$ . The individual terms in the integral for  $\delta \bar{T}$  are as follows:

$$\rho \int_c (\ddot{u}_s \delta u_s) t ds = \rho \int_c [-\ddot{u} \sin \theta + \ddot{v} \cos \theta + r_n \ddot{\phi}_z] [-\delta u \sin \theta + \delta v \cos \theta + r_n \delta \phi_z] t ds, \quad (18.92)$$

$$\rho \int_c (\ddot{u}_\zeta \delta u_\zeta) t ds = \rho \int_c [\ddot{u} \cos \theta + \ddot{v} \sin \theta - r_t \ddot{\phi}_z] [\delta u \cos \theta + \delta v \sin \theta - r_t \delta \phi_z] t ds, \text{ and} \quad (18.93)$$

$$\rho \int_c (\ddot{u}_z \delta u_z) t ds = \rho \int_c [\ddot{w} + y \ddot{\phi}_x + x \ddot{\phi}_y] [\delta w + y \delta \phi_x + x \delta \phi_y] t ds. \quad (18.94)$$

Sum eqs. (18.92) to (18.94) and collect terms in the integral multiplying the virtual displacements and virtual rotations. In the process of evaluating and simplifying the result for  $\delta \bar{T}$ , the following terms are identified or defined:

- From eq. (3.9) on page 34 the relationship between normal and tangential coordinates of the contour and the Cartesian coordinates  $\{x(s), y(s)\}$  of the contour is

$$r_n \cos \theta - r_t \sin \theta = x(s) - x_{sc} \quad r_n \sin \theta + r_t \cos \theta = y(s) - y_{sc}. \quad (18.95)$$

- From eqs. (4.2) and (4.3) on page 79 the geometric properties of the cross section are identified as

$$A = \int_c t ds \quad \int_c x t ds = 0 \quad \int_c y t ds = 0 \quad (I_{xx}, I_{yy}, I_{xy}) = \int_c (y^2, x^2, xy) t ds. \quad (18.96)$$

- Terms associated with the mass are defined by

$$m = \rho \int_c t ds = \rho A, \quad (18.97)$$

$$\rho (I_{xx}, I_{yy}, I_{xy}) = \rho A (I_{xx}/A, I_{yy}/A, I_{xy}/A) = m (r_x^2, r_y^2, r_{xy}^2), \text{ and} \quad (18.98)$$

$$I_z = \rho \int_c (r_n^2 + r_t^2) t ds = \rho A \left[ \frac{1}{A} \int_c (r_n^2 + r_t^2) t ds \right] = m r_z^2. \quad (18.99)$$

The mass per unit length is denoted by  $m$ , rotary inertial moments due to bending by  $\rho (I_{xx}, I_{yy}, I_{xy})$ , and the polar moment of inertia about the  $z$ -axis through the shear center by  $I_z$ . The final result for virtual kinetic energy per unit length in eq. (18.91) is

$$\begin{aligned} \delta \bar{T} = & -\{m(\ddot{u} + y_{sc} \ddot{\phi}_z) \delta u + m(\ddot{v} - x_{sc} \ddot{\phi}_z) \delta v + m \ddot{w} \delta w + m(r_x^2 \ddot{\phi}_x + r_{xy}^2 \ddot{\phi}_y) \delta \phi_x + m(r_{xy}^2 \ddot{\phi}_x + r_y^2 \ddot{\phi}_y) \delta \phi_y + \\ & m(r_z^2 \ddot{\phi}_z + y_{sc} \ddot{u} - x_{sc} \ddot{v}) \delta \phi_z\} \end{aligned} \quad (18.100)$$

The virtual work per unit axial length is determined from conservative forces and non-conservative forces. It is expressed as

$$\delta \bar{W} = -\delta \bar{U} + \delta \bar{W}_{n.c.}, \quad (18.101)$$

where  $\bar{U}$  is the potential energy of the conservative forces and  $\delta \bar{W}_{n.c.}$  is the virtual work of the non-conservative forces acting at point  $z$  in the bar. The potential energy per unit length represents the energy due to elastic deformation of the bar and it is given by

$$\bar{U} = \bar{U}_\varepsilon + \bar{U}_\gamma. \quad (18.102)$$

The strain energy due extension and bending is denoted by  $\bar{U}_\varepsilon$ , and the strain energy due to transverse shear and torsion by  $\bar{U}_\gamma$ . From eq. (5.47) on page 140

$$\bar{U}_\varepsilon = \frac{1}{2}[EA(w')^2 + EI_{xx}(\phi_x')^2 + EI_{yy}(\phi_y')^2 + 2EI_{xy}(\phi_x')(\phi_y')], \quad (18.103)$$

and from eq. (5.82) on page 145

$$\bar{U}_\gamma = \frac{1}{2}[s_{xx}\psi_x^2 + 2s_{xy}\psi_x\psi_y + s_{yy}\psi_y^2 + GJ(\phi_z')^2]. \quad (18.104)$$

Note that the partial derivatives of the axial displacement and bending rotations are denoted by a prime superscript in eq. (18.103). That is,

$$w' = \frac{\partial w}{\partial z} \quad \phi_x' = \frac{\partial \phi_x}{\partial z} \quad \phi_y' = \frac{\partial \phi_y}{\partial z}. \quad (18.105)$$

The transverse shear strains in eq. (18.104) are related to the displacements and rotations by

$$\psi_x = u' + \phi_y \quad \psi_y = v' + \phi_x. \quad (18.106)$$

Refer to figure 3.6 on page 38. The virtual strains are denoted by  $\delta w'$ ,  $\delta \phi_x'$ ,  $\delta \phi_y'$ ,  $\delta \psi_x$ ,  $\delta \psi_y$ , and  $\delta \phi_z'$ , where

$$\delta \psi_x = \delta u' + \delta \phi_y, \text{ and } \delta \psi_y = \delta v' + \delta \phi_x. \quad (18.107)$$

At a fixed value of the coordinate  $z$  the virtual strain energies per unit axial length are

$$\delta \bar{U}_\varepsilon = \frac{\partial \bar{U}_\varepsilon}{\partial w'} \delta w' + \frac{\partial \bar{U}_\varepsilon}{\partial \phi_x'} \delta \phi_x' + \frac{\partial \bar{U}_\varepsilon}{\partial \phi_y'} \delta \phi_y' = N \delta w' + M_x \delta \phi_x' + M_y \delta \phi_y', \text{ and} \quad (18.108)$$

$$\delta \bar{U}_\gamma = \frac{\partial \bar{U}_\gamma}{\partial \psi_x} \delta \psi_x + \frac{\partial \bar{U}_\gamma}{\partial \psi_y} \delta \psi_y + \frac{\partial \bar{U}_\gamma}{\partial \phi_z'} \delta \phi_z' = V_x \delta \psi_x + V_y \delta \psi_y + M_z \delta \phi_z'. \quad (18.109)$$

The generalized forces corresponding to the virtual strains in eqs. (18.108) and (18.109) are given by

$$N = EA w' \quad M_x = EI_{xx} \phi_x' + EI_{xy} \phi_y' \quad M_y = EI_{xy} \phi_x' + EI_{yy} \phi_y', \text{ and} \quad (18.110)$$

$$V_x = s_{xx} \psi_x + s_{xy} \psi_y \quad V_y = s_{xy} \psi_x + s_{yy} \psi_y \quad M_z = GJ \phi_z'. \quad (18.111)$$

The total virtual strain energy is the sum of eqs. (18.108) and (18.109). That is,

$$\delta \bar{U} = \delta \bar{U}_\varepsilon + \delta \bar{U}_\gamma = N \delta w' + M_x \delta \phi_x' + M_y \delta \phi_y' + V_x \delta \psi_x + V_y \delta \psi_y + M_z \delta \phi_z'. \quad (18.112)$$

Substitute eq. (18.101) into Hamilton's principle (18.80) to get

$$\int_{t_0}^{t_1} \left[ \int_0^L (\delta \bar{T} + \delta \bar{W}) dz \right] dt = - \int_{t_0}^{t_1} \left[ \int_0^L (-\delta \bar{T} + \delta \bar{U} - \delta \bar{W}_{n.c.}) dz \right] dt = 0. \quad (18.113)$$

Equation (18.113) is satisfied for  $t_0 \leq t \leq t_1$  by



$$\left[ \int_0^L (-\delta \bar{T} + \delta \bar{U} - \delta \bar{W}_{n.c.}) dz \right] = 0. \quad (18.114)$$

Substitute eq. (18.100) for  $\delta \bar{T}$  and eq. (18.112) for  $\delta \bar{U}$  into eq. (18.114) to get the weak form for the elastodynamics of the thin-walled bar as

$$\int_0^L \{ [m(\ddot{u} + y_{sc}\ddot{\phi}_z)\delta u + m(\ddot{v} - x_{sc}\ddot{\phi}_z)\delta v + m\ddot{w}\delta w + m(r_x^2\ddot{\phi}_x + r_{xy}^2\ddot{\phi}_y)\delta\phi_x + m(r_{xy}^2\ddot{\phi}_x + r_y^2\ddot{\phi}_y)\delta\phi_y + m(r_z^2\ddot{\phi}_z + y_{sc}\ddot{u} - x_{sc}\ddot{v})\delta\phi_z] + [N\delta w' + M_x\delta\phi_x' + M_y\delta\phi_y' + V_x\delta\psi_x + V_y\delta\psi_y + M_z\delta\phi_z'] \} dz = \int_0^L \delta \bar{W}_{n.c.} dz. \quad (18.115)$$

The non-conservative virtual work is expressed in terms of the prescribed external loads acting on the bar shown in figure 18.8. The generalized forces acting on the cross sections at  $z = 0$  and  $z = L$  are denoted by  $Q_i(t)$ ,  $i = 1, 2, \dots, 12$ . The prescribed distribution of force intensities (F/L) and distribution of moments intensities (F-L/L) are functions of coordinate  $z$  and time  $t$ . Distributions  $f_x(z, t)$  and  $f_y(z, t)$  are resolved at the shear center, and distribution  $f_z(z, t)$  is resolved at the centroid. Distributions of moments  $m_x(z, t)$  and  $m_y(z, t)$  are resolved at the centroid, and distribution  $m_z(z, t)$  is resolved at the shear center. Also, refer to figure 3.8(b) on page 41.

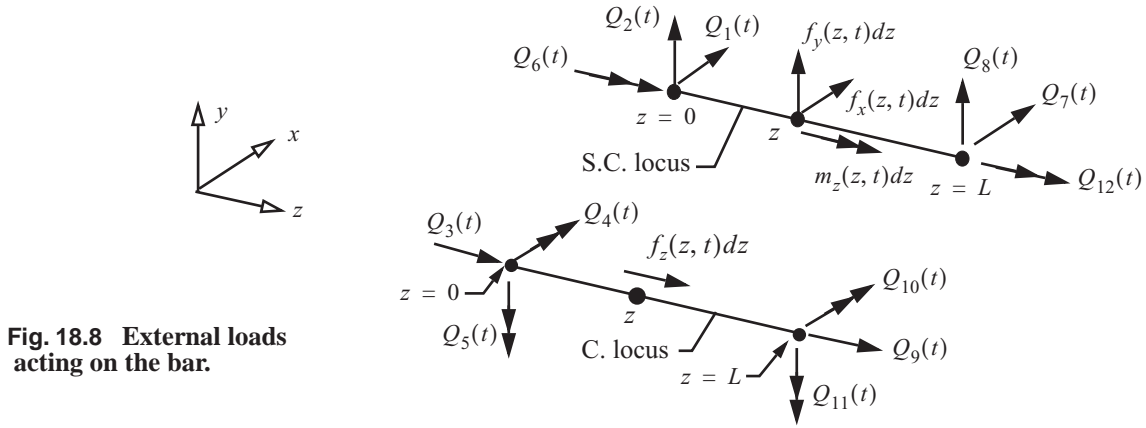


**Fig. 18.8** External loads acting on the bar.

The virtual displacements and rotations are independent variables. We can take  $\delta u$  and its derivative  $\delta u'$  not equal to zero, and the remaining virtual displacements and rotations equal to zero in eq. (18.115). Then the weak form governing virtual displacement  $\delta u$  is

$$\int_0^L [m(\ddot{u} + y_{sc}\ddot{\phi}_z)\delta u + V_x\delta u'] dz = \int_0^L f_x(z, t)\delta u(z, t) dz + Q_1(t)\delta u(0, t) + Q_7(t)\delta u(L, t). \quad (18.116)$$

From eq. (18.115) and eq. (18.107) the weak form governing  $\delta v$  and its derivative is

$$\int_0^L [m(\ddot{v} - x_{sc}\ddot{\phi}_z)\delta v + V_y\delta v']dz = \int_0^L f_y(z, t)\delta v(z, t)dz + Q_2(t)\delta v(0, t) + Q_8(t)\delta v(L, t). \quad (18.117)$$

The weak form governing  $\delta w$  and its derivative is

$$\int_0^L [m\ddot{w}\delta w + N\delta w']dz = \int_0^L f_z(z, t)\delta w(z, t)dz + Q_3(t)\delta w(0, t) + Q_9(t)\delta w(L, t). \quad (18.118)$$

The remaining weak forms governing the virtual rotations in the order  $\delta\phi_x$ ,  $\delta\phi_y$ , and  $\delta\phi_z$  are as follows:

$$\int_0^L [m(r_x^2\ddot{\phi}_x + r_{xy}^2\ddot{\phi}_y)\delta\phi_x + M_x\delta\phi_x' + V_y\delta\phi_x]dz = \int_0^L m_x(z, t)\delta\phi_x(z, t)dz + Q_4(t)\delta\phi_x(0, t) + Q_{10}(t)\delta\phi_x(L, t), \quad (18.119)$$

$$\int_0^L [m(r_{xy}^2\ddot{\phi}_x + r_y^2\ddot{\phi}_y)\delta\phi_y + M_y\delta\phi_y' + V_x\delta\phi_y]dz = \int_0^L m_y(z, t)\delta\phi_y(z, t)dz + Q_5(t)\delta\phi_y(0, t) + Q_{11}(t)\delta\phi_y(L, t), \text{ and } \quad (18.120)$$

$$\int_0^L [m(r_z^2\ddot{\phi}_z + y_{sc}\ddot{u} - x_{sc}\ddot{v})\delta\phi_z + M_z\delta\phi_z']dz = \int_0^L m_z(z, t)\delta\phi_z(z, t)dz + Q_6(t)\delta\phi_z(0, t) + Q_{12}(t)\delta\phi_z(L, t). \quad (18.121)$$

## 18.7 Finite element model for the dynamics of an axial bar

The weak form governing the response of the bar is given by eq. (18.118). Following the discussion in article 17.2 on page 494 consider the mesh

$$0 = z_1 < z_2 < z_3 < \dots < z_M < z_{M+1} = L, \quad (18.122)$$

where  $M$  denotes the number of elements, and  $M+1$  is the number of nodes. The  $k$ th element is denoted by

$$\Omega_k = \{z | z_k \leq z \leq z_{k+1}\} \quad k = 1, 2, \dots, M. \quad (18.123)$$

Each element is mapped into a standard element denoted by

$$\Omega_{st} = \{\xi | -1 < \xi < 1\}. \quad (18.124)$$

The standard element is mapped onto the  $k$ th element by

$$z = \eta_1(\xi)z_k + \eta_2(\xi)z_{k+1}, \text{ where } \eta_1(\xi) = (1 - \xi)/2 \text{ and } \eta_2(\xi) = (1 + \xi)/2. \quad (18.125)$$

The inverse mapping is

$$\xi = \frac{2z - z_z - z_{k+1}}{z_{k+1} - z_k} = \frac{2z - z_z - z_{k+1}}{h_k} \quad z \in \Omega_k. \quad (18.126)$$

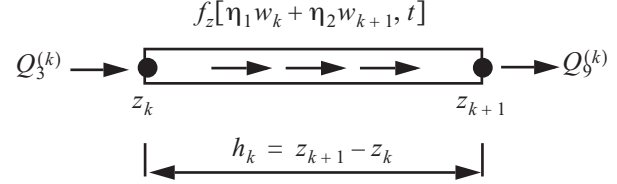
The length of the element is denoted by  $h_k$  where  $h_k = z_{k+1} - z_k$ . Let  $w^{(k)}(z, t)$  denote the axial displacement in  $\Omega_k$ , which expressed in terms of the nodal displacements and the shape functions is

$$w^{(k)}(\xi, t) = \eta_1(\xi)w_k(t) + \eta_2(\xi)w_{k+1}(t) \quad \xi \in \Omega_{st}. \quad (18.127)$$

$$\delta w^{(k)} = b_k \eta_1(\xi) + b_{k+1} \eta_2(\xi) \quad (18.128)$$

The external loads acting on element  $\Omega_k$  are shown in figure 18.9.

**Fig. 18.9** External loads acting on axial bar element  $\Omega_k$ .



Let  $\eta_1' = \frac{d\eta_1}{d\xi}$ . The finite element representation of eq. (18.118) is

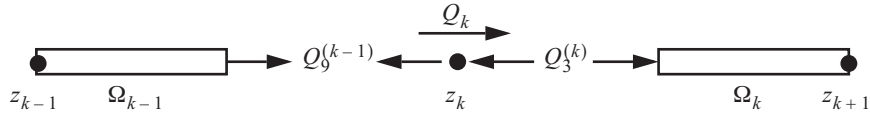
$$\begin{aligned} & \sum_{k=1}^M b_k \left\{ \int_{-1}^1 \left[ m(\eta_1 \ddot{w}_k + \eta_2 \ddot{w}_{k+1}) \eta_1 + EA \frac{2}{h_k} (\eta_1' w_k + \eta_2' w_{k+1}) \frac{2}{h_k} \eta_1' \right] \frac{h_k}{2} d\xi \right\} + \\ & b_{k+1} \left\{ \int_{-1}^1 \left[ m(\eta_1 \ddot{w}_k + \eta_2 \ddot{w}_{k+1}) \eta_2 + EA \frac{2}{h_k} (\eta_1' w_k + \eta_2' w_{k+1}) \frac{2}{h_k} \eta_2' \right] \frac{h_k}{2} d\xi \right\} = \\ & \sum_{k=1}^M b_k [Q_k(t) + F_k(t)] + b_{k+1} [Q_{k+1}(t) + F_{k+1}(t)]. \end{aligned} \quad (18.129)$$

External loads at a common node between elements are defined by

$$Q_k(t) = Q_9^{(k-1)}(t) + Q_3^{(k)}(t) \quad k = 2, 3, \dots, M-1, \quad (18.130)$$

which are depicted in figure 18.10.

**Fig. 18.10**



At the first node  $z_I$  and the last node  $z_{M+I}$  the external forces are

$$Q_1(t) = Q_3^{(1)}(t), \text{ and } Q_M(t) = Q_9^{(M)}. \quad (18.131)$$

The distributed loads lead to forces

$$F_k(t) = \int_{-1}^1 f_z[\eta_1 z_k + \eta_2 z_{k+1}, t] \eta_1 \frac{h_k}{2} d\xi \quad F_{k+1}(t) = \int_{-1}^1 f_z[\eta_1 z_k + \eta_2 z_{k+1}, t] \eta_2 \frac{h_k}{2} d\xi. \quad (18.132)$$

For  $b_k \neq 0$ , and  $b_{k+1} = 0$ , eq. (18.129) leads to

$$mh_k \left( \frac{1}{3} \ddot{w}_k + \frac{1}{6} \ddot{w}_{k+1} \right) + \frac{EA}{h_k} (w_k - w_{k+1}) = Q_k(t) + F_k(t). \quad (18.133)$$

For  $b_k = 0$  and  $b_{k+1} \neq 0$  eq. (18.129) leads to

$$mh_k \left( \frac{1}{6} \ddot{w}_k + \frac{1}{3} \ddot{w}_{k+1} \right) + \frac{EA}{h_k} (-w_k + w_{k+1}) = Q_{k+1}(t) + F_{k+1}(t).$$

Finally we write the matrix form for element  $\Omega_k$  as

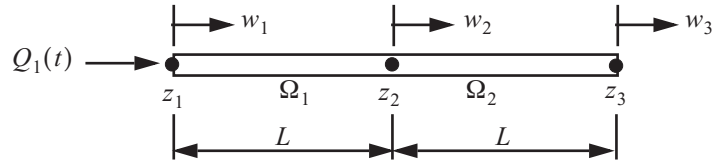
$$\frac{mh_k}{6} \begin{bmatrix} 2 & 1 \\ 1 & 2 \end{bmatrix} \begin{bmatrix} \ddot{w}_k \\ \ddot{w}_{k+1} \end{bmatrix} + \frac{EA}{h_k} \begin{bmatrix} 1 & -1 \\ -1 & 1 \end{bmatrix} \begin{bmatrix} w_k \\ w_{k+1} \end{bmatrix} = \begin{bmatrix} Q_k(t) + F_k(t) \\ Q_{k+1}(t) + F_{k+1}(t) \end{bmatrix} \quad (18.134)$$

Note that the mass matrix in eq. (18.134) is not diagonal, but it is symmetric. This mass matrix is called a **consistent mass matrix**, since the spatial distribution of the velocity function is consistent with the assumed spatial distribution of the axial displacement function (18.127).

### Example 18.2 Unrestrained axial motion of a bar

Consider a three-degree-of freedom model of a uniform bar shown in figure 18.11 that undergoes unrestrained axial motion. The mass per unit length  $m$  and the axial stiffness  $EA$  are constant. The bar is modeled with two finite elements  $\Omega_1$  and  $\Omega_2$ , each with lengths  $h_1 = h_2 = L$ .

**Fig. 18.11** Unrestrained axial motion of bar modeled with two elements.



For element  $\Omega_1$  the mass and stiffness matrices are

$$M^{(1)} = \frac{mL}{6} \begin{bmatrix} 2 & 1 \\ 1 & 2 \end{bmatrix} \quad \text{and} \quad K^{(1)} = \frac{EA}{L} \begin{bmatrix} 1 & -1 \\ -1 & 1 \end{bmatrix}. \quad (a)$$

For element  $\Omega_2$  the mass and stiffness matrices are

$$M^{(2)} = \frac{mL}{6} \begin{bmatrix} 2 & 1 \\ 1 & 2 \end{bmatrix} \quad \text{and} \quad K^{(2)} = \frac{EA}{L} \begin{bmatrix} 1 & -1 \\ -1 & 1 \end{bmatrix}. \quad (b)$$

The matrix equation of motion after assembly is

$$\frac{mL}{6} \begin{bmatrix} 2 & 1 & 0 \\ 1 & 4 & 1 \\ 0 & 1 & 2 \end{bmatrix} \begin{bmatrix} \ddot{w}_1 \\ \ddot{w}_2 \\ \ddot{w}_3 \end{bmatrix} + \frac{EA}{L} \begin{bmatrix} 1 & -1 & 0 \\ -1 & 2 & -1 \\ 0 & -1 & 1 \end{bmatrix} \begin{bmatrix} w_1 \\ w_2 \\ w_3 \end{bmatrix} = \begin{bmatrix} Q_1(t) \\ 0 \\ 0 \end{bmatrix}. \quad (c)$$

For the bar at rest at time  $t = 0$  the initial axial displacements are

$$w_1(0) = w_2(0) = w_3(0) = 0. \quad (\text{d})$$

Consider the impulsive response of the bar  $Q_1(t) = \hat{Q}\delta(t)$ , where  $\hat{Q}$  is the magnitude of the impulse and  $\delta(t)$  is the Dirac delta function. The Dirac delta function is defined by

$$\delta(t) = 0 \text{ for } t \neq 0, \text{ and } \int_{-\infty}^{\infty} \delta(t) dt = 1. \quad (\text{e})$$

The Dirac delta function is depicted in figure 18.12, in which we take the limit as  $\varepsilon \rightarrow 0$ . The amplitude of  $\delta(0)$  is undefined, but the area under the function is well defined. Note the dimensional units of the Dirac delta function are reciprocal seconds, and the dimensional units of impulse  $\hat{Q}$  are force-seconds. The impulsive force causes an initial velocity of the bar. To determine the initial velocity of the bar we integrate the equations of motion (c) with respect to time over an infinitesimal interval at  $t = 0$  from  $t = -0$  to  $t = +0$ . During this time

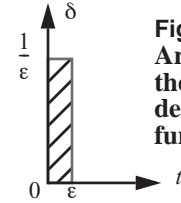


**Fig. 18.12**  
Area under  
the Dirac  
delta  
function.

interval there is no displacement of the bar and the velocities  $\dot{w}_i(-0) = 0$ ,  $i = 1, 2, 3$ . Integration of eq. (c) over the infinitesimal time interval is

$$\frac{mL}{6} \begin{bmatrix} 2 & 1 & 0 \\ 1 & 4 & 1 \\ 0 & 1 & 2 \end{bmatrix} \begin{bmatrix} \dot{w}_1(+0) \\ \dot{w}_2(+0) \\ \dot{w}_2(+0) \end{bmatrix} = \hat{Q} \int_{-0}^{+0} \begin{bmatrix} \delta(t) \\ 0 \\ 0 \end{bmatrix} dt = \hat{Q} \begin{bmatrix} 1 \\ 0 \\ 0 \end{bmatrix}. \quad (\text{f})$$

Solve eq. (f) for the initial velocities to get

$$\begin{bmatrix} \dot{w}_1(+0) \\ \dot{w}_2(+0) \\ \dot{w}_2(+0) \end{bmatrix} = \frac{\hat{Q}}{mL} \begin{bmatrix} 7/2 \\ -1 \\ 1/2 \end{bmatrix}. \quad (\text{g})$$

**Free vibration solution.** Assume a solution  $\{w(t)\} = \{\phi\} \cos(\omega t - \alpha)$  to eq. (c), which leads to the generalized eigenvalue problem

$$\begin{bmatrix} 1 & -1 & 0 \\ -1 & 2 & -1 \\ 0 & -1 & 1 \end{bmatrix} \begin{bmatrix} \phi_1 \\ \phi_2 \\ \phi_3 \end{bmatrix} = \lambda \begin{bmatrix} 2 & 1 & 0 \\ 1 & 4 & 1 \\ 0 & 1 & 2 \end{bmatrix} \begin{bmatrix} \phi_1 \\ \phi_2 \\ \phi_3 \end{bmatrix}, \quad (\text{h})$$

where  $\lambda = \left(\frac{mL^2}{6EA}\right) \omega^2$ . The eigenvalues and modal matrix are

$$(\lambda_1, \{\phi_1\}) = \left(2, \begin{bmatrix} 1 \\ -1 \\ 1 \end{bmatrix}\right), (\lambda_2, \{\phi_2\}) = \left(\frac{1}{2}, \begin{bmatrix} -1 \\ 0 \\ 1 \end{bmatrix}\right) \text{ and } (\lambda_3, \{\phi_3\}) = \left(0, \begin{bmatrix} 1 \\ 1 \\ 1 \end{bmatrix}\right). \quad (\text{i})$$

The eigenvalue  $\lambda_3 = 0$  and its associate mode  $\{\phi_3\} = \begin{bmatrix} 1 & 1 & 1 \end{bmatrix}^T$  correspond to a rigid body motion of the bar.

The non-zero eigenvalues  $\lambda_1$  and  $\lambda_2$ , and their associated modes correspond to elastic modes of the bar. The frequencies are

$$\omega_1 = \frac{2\sqrt{3}}{L} \sqrt{\frac{EA}{m}} \quad \omega_2 = \frac{\sqrt{3}}{L} \sqrt{\frac{EA}{m}} \quad \omega_3 = 0. \quad (\text{j})$$

**Transient response.** The transformation from physical displacements to modal displacements is given by

$$\begin{bmatrix} w_1(t) \\ w_2(t) \\ w_3(t) \end{bmatrix} = \begin{bmatrix} 1 & -1 & 1 \\ -1 & 0 & 1 \\ 1 & 1 & 1 \end{bmatrix} \begin{bmatrix} q_1(t) \\ q_2(t) \\ q_3(t) \end{bmatrix}. \quad (\text{k})$$

Substitute the transformation (k) into the equations of motion (c) to get equations of motion in modal coordinates:

$$\begin{bmatrix} \frac{2Lm}{3} & 0 & 0 \\ 0 & \frac{2Lm}{3} & 0 \\ 0 & 0 & 2Lm \end{bmatrix} \begin{bmatrix} \ddot{q}_1 \\ \ddot{q}_2 \\ \ddot{q}_3 \end{bmatrix} + \begin{bmatrix} \frac{8EA}{L} & 0 & 0 \\ 0 & \frac{2EA}{L} & 0 \\ 0 & 0 & 0 \end{bmatrix} \begin{bmatrix} q_1 \\ q_2 \\ q_3 \end{bmatrix} = \begin{bmatrix} 0 \\ 0 \\ 0 \end{bmatrix}, \quad t > +0. \quad (\text{l})$$

The initial conditions in modal coordinates are (refer to eq. (18.27))

$$\begin{bmatrix} q_1(0) \\ q_2(0) \\ q_3(0) \end{bmatrix} = \begin{bmatrix} 0 \\ 0 \\ 0 \end{bmatrix}, \text{ and } \begin{bmatrix} \dot{q}_1(0) \\ \dot{q}_2(0) \\ \dot{q}_3(0) \end{bmatrix} = \begin{bmatrix} \frac{2Lm}{3} & 0 & 0 \\ 0 & \frac{2Lm}{3} & 0 \\ 0 & 0 & 2Lm \end{bmatrix}^{-1} \begin{bmatrix} 1 & -1 & 1 \\ -1 & 0 & 1 \\ 1 & 1 & 1 \end{bmatrix}^T \frac{mL}{6} \begin{bmatrix} 2 & 1 & 0 \\ 1 & 4 & 1 \\ 0 & 1 & 2 \end{bmatrix} \frac{\hat{Q}}{mL} \begin{bmatrix} 7/2 \\ -1 \\ 1/2 \end{bmatrix} = \frac{\hat{Q}}{2mL} \begin{bmatrix} 3 \\ -3 \\ 1 \end{bmatrix}. \quad (\text{m})$$

The solution of eq. (l) for the modal displacements are

$$\begin{bmatrix} q_1(t) \\ q_2(t) \\ q_3(t) \end{bmatrix} = \frac{\hat{Q}}{2Lm} \begin{bmatrix} \frac{3}{\omega_1} \sin \omega_1 t \\ -\frac{3}{\omega_2} \sin \omega_2 t \\ t \end{bmatrix}. \quad (\text{n})$$

Substitute the modal displacements (n) into eq. (k) to find the results for the response of the physical displacements:

$$\begin{bmatrix} w_1(t) \\ w_2(t) \\ w_3(t) \end{bmatrix} = \frac{\hat{Q}}{2Lm} \begin{bmatrix} t + (3/\omega_1)\sin\omega_1 t + (3/\omega_2)\sin\omega_2 t \\ t - (3/\omega_1)\sin\omega_1 t \\ t + (3/\omega_1)\sin\omega_1 t - (3/\omega_2)\sin\omega_2 t \end{bmatrix}. \quad (o)$$

We specify the following data for an aluminum alloy bar:  $L = 16 \text{ in.}$ ,  $A = 0.2651 \text{ in.}^2$ ,  $I_{xx} = 0.2985 \text{ in.}^4$ , and  $E = 9.9 \times 10^6 \text{ lb./in.}^2$ . The mass density  $\rho = 0.0978 \text{ lbm/in.}^3$ . Convert the pound-mass (lbm) to pound-force (lb.) in the U.S. customary units by recognizing that one pound-force accelerates one pound-mass at the local acceleration of gravity  $g$ . Thus,  $\rho = (0.0978 \text{ lbm/in.}^3) \left( \frac{\text{lb.}}{(\text{lbm})386.4 \text{ in./s}^2} \right) = (2.531 \times 10^{-4}) \frac{\text{lb.-s}^2}{\text{in.}^4}$ , and the mass per unit length is

$$m = \rho A = (2.531 \times 10^{-4}) \frac{\text{lb.-s}^2}{\text{in.}^4} (0.2651 \text{ in.}^2) = 67.0968 \times 10^{-6} \frac{\text{lb.-s}^2}{\text{in.}^2}. \quad (p)$$

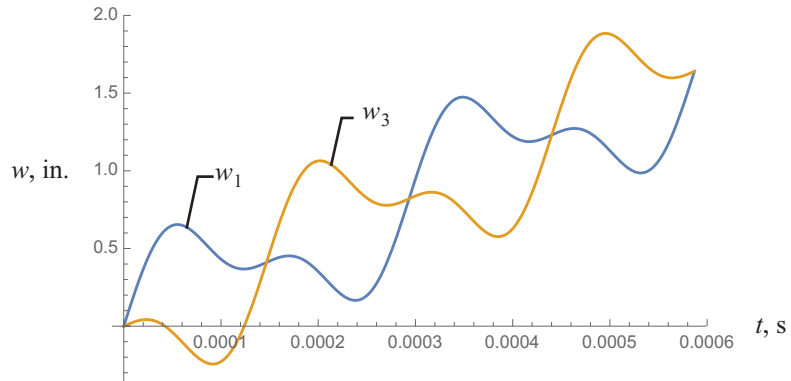
The natural frequencies are

$$\omega_1 = 42,819.6 \text{ r/s} = 6,814.94 \text{ Hz} \quad \omega_2 = 21,409.8 \text{ r/s} = 3,407.47 \text{ Hz} \quad \omega_3 = 0. \quad (q)$$

Take the impulse  $\hat{Q} = 6 \text{ lb.-s}$ , and compute  $\hat{Q}/(2Lm) = 2,794.47 \text{ in./s}$ . The transient response for displacements  $w_1(t)$  and  $w_3(t)$  for  $0 \leq t \leq 2\tau$  is shown in figure 18.13. The period for one complete oscillation at the lowest frequency is denoted by  $\tau$ , where

$$\tau = (2\pi)/(21,409.8 \text{ s}^{-1}) = 0.00029347 \text{ s.} \blacksquare$$

**Fig. 18.13** Transient response of the axial displacements in example 18.2.



### 18.7.1 Truss element

Take one element to represent a truss bar of length  $L$  at an angle  $\theta$  with respect to the  $X$ -axis connected between the nodes labeled  $i$  and  $j$  as shown in figure 18.14(a). Let  $h_k = L$ . The nodal displacements tangent and normal to the bar at node  $i$  are denoted by  $(w_i, v_i)$ , respectively, and the nodal displacements tangent and normal to the bar at node  $j$  are denoted by  $(w_j, v_j)$ , respectively. The nodal displacements in the  $X$ - and  $Y$ -directions to the bar

at node  $i$  are denoted by  $(u_{2i-1}, u_{2i})$ , respectively, and the corresponding nodal displacements at node  $j$  are denoted by  $(u_{2j-1}, u_{2j})$ , respectively. See figure 18.14(b).

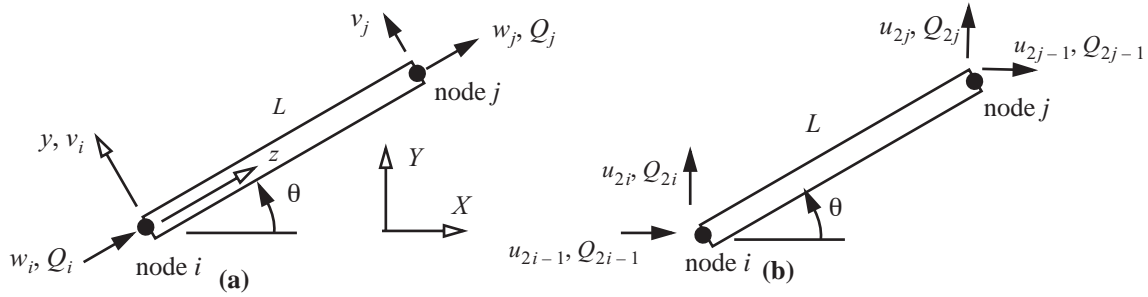


**Fig. 18.14 (a) Axial bar at an oblique angle. (b) Truss element.**

Expand eq. (18.134) to include displacements normal to the bar by adding rows and columns of zeros to get

$$\begin{bmatrix} mL/3 & 0 & mL/6 & 0 \\ 0 & 0 & 0 & 0 \\ mL/6 & 0 & mL/3 & 0 \\ 0 & 0 & 0 & 0 \end{bmatrix} \begin{bmatrix} \ddots \\ w_i \\ \ddots \\ v_i \\ \ddots \\ w_j \\ \ddots \\ v_j \end{bmatrix} + \begin{bmatrix} EA/L & 0 & -EA/L & 0 \\ 0 & 0 & 0 & 0 \\ -EA/L & 0 & EA/L & 0 \\ 0 & 0 & 0 & 0 \end{bmatrix} \begin{bmatrix} w_i \\ v_i \\ w_j \\ v_j \end{bmatrix} = \begin{bmatrix} Q_i \\ 0 \\ Q_j \\ 0 \end{bmatrix}. \quad (\text{a})$$

At node  $i$  the displacements in figure 18.14(a) are related to the displacements in figure 18.14(b) by  $w_i = (\cos\theta)u_{2i-1} + (\sin\theta)u_{2i}$ , and  $v_i = (-\sin\theta)u_{2i-1} + (\cos\theta)u_{2i}$ . At node  $j$  we have similar displacement relations. The nodal displacements are related by matrix

$$\begin{bmatrix} w_i \\ v_i \\ w_j \\ v_j \end{bmatrix} = \begin{bmatrix} c & s & 0 & 0 \\ -s & c & 0 & 0 \\ 0 & 0 & c & s \\ 0 & 0 & -s & c \end{bmatrix} \begin{bmatrix} u_{2i-1} \\ u_{2i} \\ u_{2j-1} \\ u_{2j} \end{bmatrix} = [T(\theta)] \{u\}, \quad (\text{b})$$

where  $c = \cos\theta$  and  $s = \sin\theta$ . Substitute eq. (b) into eq. (a), followed by pre-multiplication by  $[T(\theta)]^T$  to get

$$[T]^T \begin{bmatrix} mL/3 & 0 & mL/6 & 0 \\ 0 & 0 & 0 & 0 \\ mL/6 & 0 & mL/3 & 0 \\ 0 & 0 & 0 & 0 \end{bmatrix} [T] \begin{bmatrix} \ddots \\ u_{2i-1} \\ \ddots \\ u_{2i} \\ \ddots \\ u_{2j-1} \\ \ddots \\ u_{2j} \end{bmatrix} + [T]^T \begin{bmatrix} EA/L & 0 & -EA/L & 0 \\ 0 & 0 & 0 & 0 \\ -EA/L & 0 & EA/L & 0 \\ 0 & 0 & 0 & 0 \end{bmatrix} [T] \begin{bmatrix} u_{2i-1} \\ u_{2i} \\ u_{2j-1} \\ u_{2j} \end{bmatrix} = [T]^T \begin{bmatrix} Q_i \\ 0 \\ Q_j \\ 0 \end{bmatrix} = \begin{bmatrix} Q_{2i-1} \\ Q_{2i} \\ Q_{2j-1} \\ Q_{2j} \end{bmatrix}. \quad (\text{c})$$

The mass matrix for the truss bar is



$$[M] = \begin{bmatrix} c & -s & 0 & 0 \\ s & c & 0 & 0 \\ 0 & 0 & c & -s \\ 0 & 0 & s & c \end{bmatrix} \begin{bmatrix} mL/3 & 0 & mL/6 & 0 \\ 0 & 0 & 0 & 0 \\ mL/6 & 0 & mL/3 & 0 \\ 0 & 0 & 0 & 0 \end{bmatrix} \begin{bmatrix} c & s & 0 & 0 \\ -s & c & 0 & 0 \\ 0 & 0 & c & s \\ 0 & 0 & -s & c \end{bmatrix} = \frac{mL}{6} \begin{bmatrix} 2c^2 & 2cs & c^2 & cs \\ 2sc & 2s^2 & cs & s^2 \\ c^2 & cs & 2c^2 & 2cs \\ cs & s^2 & 2sc & 2s^2 \end{bmatrix}. \quad (18.135)$$

The stiffness matrix for the truss bar is

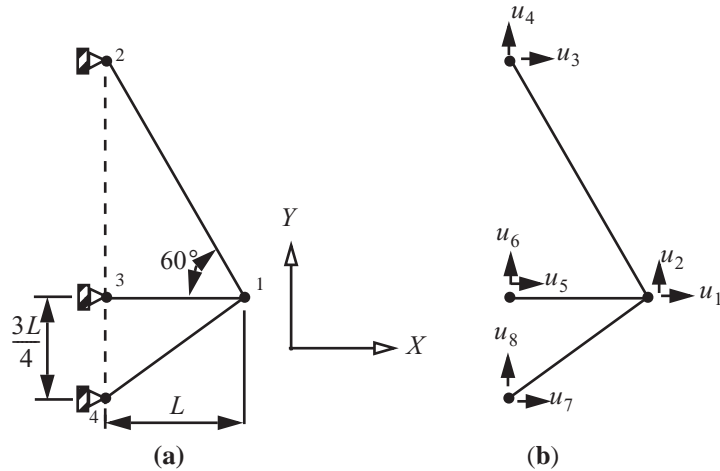
$$[K] = \begin{bmatrix} c & -s & 0 & 0 \\ s & c & 0 & 0 \\ 0 & 0 & c & -s \\ 0 & 0 & s & c \end{bmatrix} \begin{bmatrix} EA/L & 0 & -EA/L & 0 \\ 0 & 0 & 0 & 0 \\ -EA/L & 0 & EA/L & 0 \\ 0 & 0 & 0 & 0 \end{bmatrix} \begin{bmatrix} c & s & 0 & 0 \\ -s & c & 0 & 0 \\ 0 & 0 & c & s \\ 0 & 0 & -s & c \end{bmatrix} = \frac{EA}{L} \begin{bmatrix} c^2 & cs & -c^2 & -cs \\ cs & s^2 & -cs & -s^2 \\ -c^2 & -cs & c^2 & cs \\ -cs & -s^2 & cs & s^2 \end{bmatrix}. \quad (18.136)$$

The stiffness matrix (18.136) is the same stiffness matrix as determined by the direct stiffness method. See eq. (16.12) on page 439.

### Example 18.3 Free vibrations of a three-bar truss

The truss shown in figure 18.15 consists of three bars: 1-2, 1-3, and 1-4. Joints, or nodes, 2, 3, and 4 are fixed and only joint 1 is movable. For all three bars the cross-sectional area  $A = 475 \times 10^{-6} \text{ m}^2$ , the modulus of elasticity  $E = 70 \text{ GPa}$ , and the mass density  $\rho = 2710 \text{ Kg/m}^3$ . The length  $L = 2 \text{ m}$ . Determine the natural frequencies in Hz and the corresponding modal vectors. Normalize the modal vectors such that the component with the largest magnitude is equal to one.

**Fig. 18.15 Free vibration.**  
(a) Three-bar truss configuration. (b) Nodal displacements.



**Solution.** The unknown nodal displacement vector  $\{u_\alpha(t)\} = [u_1(t) \ u_2(t)]^T$ , and the known nodal displacement vector  $\{u_\beta(t)\} = [u_3(t) \ u_4(t) \ u_5(t) \ u_6(t) \ u_7(t) \ u_8(t)]^T = [0 \ 0 \ 0 \ 0 \ 0 \ 0]^T$ ,  $t \geq 0$ . The length of each bar and the direction cosines are listed in table 18.3.

**Table 18.3** Direction cosines for each truss bar

Bar	Length	$\theta$ , deg.	c	s	$c^2$	$s^2$	cs
1-2	$2L$	120	$-1/2$	$\sqrt{3}/2$	$1/4$	$3/4$	$-\sqrt{3}/4$
1-3	$L$	180	$-1$	0	1	0	0
1-4	$5L/4$	216.87	$-4/5$	$-3/5$	$16/25$	$9/25$	$12/25$

From the mass matrix (18.135) and stiffness matrix (18.136) for the generic truss bar, we formulate the mass and stiffness matrices for each truss bar in degrees of freedom one and two as follows:

$$[K_{1-2}] = \frac{EA}{2L} \begin{bmatrix} 1 & 2 & 3 & 4 \\ 1/4 & -\sqrt{3}/4 & \blacksquare & \blacksquare \\ -\sqrt{3}/4 & 3/4 & \blacksquare & \blacksquare \\ \blacksquare & \blacksquare & \blacksquare & \blacksquare \\ \blacksquare & \blacksquare & \blacksquare & \blacksquare \end{bmatrix} \quad [M_{1-2}] = \frac{\rho A(2L)}{6} \begin{bmatrix} 1 & 2 & 3 & 4 \\ 1/2 & -\sqrt{3}/2 & \blacksquare & \blacksquare \\ -\sqrt{3}/2 & 3/2 & \blacksquare & \blacksquare \\ \blacksquare & \blacksquare & \blacksquare & \blacksquare \\ \blacksquare & \blacksquare & \blacksquare & \blacksquare \end{bmatrix} \quad (a)$$

$$[K_{1-3}] = \frac{EA}{L} \begin{bmatrix} 1 & 2 & 5 & 6 \\ 1 & 0 & \blacksquare & \blacksquare \\ 0 & 0 & \blacksquare & \blacksquare \\ \blacksquare & \blacksquare & \blacksquare & \blacksquare \\ \blacksquare & \blacksquare & \blacksquare & \blacksquare \end{bmatrix} \quad [M_{1-3}] = \frac{\rho AL}{6} \begin{bmatrix} 1 & 2 & 5 & 6 \\ 2 & 0 & \blacksquare & \blacksquare \\ 0 & 0 & \blacksquare & \blacksquare \\ \blacksquare & \blacksquare & \blacksquare & \blacksquare \\ \blacksquare & \blacksquare & \blacksquare & \blacksquare \end{bmatrix} \quad (b)$$

$$[K_{1-4}] = \frac{EA}{5L/4} \begin{bmatrix} 1 & 2 & 7 & 8 \\ 16/25 & 12/25 & \blacksquare & \blacksquare \\ 12/25 & 9/25 & \blacksquare & \blacksquare \\ \blacksquare & \blacksquare & \blacksquare & \blacksquare \\ \blacksquare & \blacksquare & \blacksquare & \blacksquare \end{bmatrix} \quad [M_{1-4}] = \frac{\rho A(5L/4)}{6} \begin{bmatrix} 1 & 2 & 7 & 8 \\ 32/25 & 24/25 & \blacksquare & \blacksquare \\ 24/25 & 18/25 & \blacksquare & \blacksquare \\ \blacksquare & \blacksquare & \blacksquare & \blacksquare \\ \blacksquare & \blacksquare & \blacksquare & \blacksquare \end{bmatrix} \quad (c)$$

Assembly of the structural stiffness matrix in DOFs 1 and 2 results in

$$[K_{\alpha\alpha}] = \frac{EA}{L} \begin{bmatrix} \frac{1}{8} + 1 + \left(\frac{4}{5}\right)\left(\frac{16}{25}\right) & \frac{-\sqrt{3}}{8} + 0 + \left(\frac{4}{5}\right)\left(\frac{12}{25}\right) \\ \frac{-\sqrt{3}}{8} + 0 + \left(\frac{4}{5}\right)\left(\frac{12}{25}\right) & \frac{3}{8} + 0 + \left(\frac{4}{5}\right)\left(\frac{9}{25}\right) \end{bmatrix} = \begin{bmatrix} 2.72151 \times 10^7 & 2.78458 \times 10^6 \\ 2.78458 \times 10^6 & 1.10224 \times 10^7 \end{bmatrix} \text{N/m}, \quad (d)$$

in which  $EA/L = 16.625 \times 10^6$  N/m was used to get the numerical result for  $[K_{\alpha\alpha}]$ . Assembly of the structural mass matrix in DOFs 1 and 2 results in

$$[M_{\alpha\alpha}] = \frac{\rho AL}{6} \begin{bmatrix} 1 + 2 + \left(\frac{5}{4}\right)\left(\frac{32}{25}\right) & -\sqrt{3} + 0 + \left(\frac{5}{4}\right)\left(\frac{24}{25}\right) \\ -\sqrt{3} + 0 + \left(\frac{5}{4}\right)\left(\frac{24}{25}\right) & 3 + 0 + \left(\frac{5}{4}\right)\left(\frac{18}{25}\right) \end{bmatrix} = \begin{bmatrix} 1.97378 & -0.22829 \\ -0.22829 & 1.67343 \end{bmatrix} \text{Kg}, \quad (\text{e})$$

in which  $\rho AL = 2.5745 \text{ Kg}$  was used to get the numerical result for  $[M_{\alpha\alpha}]$ . The matrix eigenvalue problem for the natural frequencies and modes is  $[K_{\alpha\alpha}]\{\phi\} - \lambda[M_{\alpha\alpha}]\{\phi\} = \{0\}$ , where the eigenvalue is  $\lambda$  and  $\lambda = \omega^2$ . Written in detail for this structure the matrix eigenvalue problem is

$$\begin{bmatrix} 2.72151 \times 10^7 & 2.78458 \times 10^6 \\ 2.78458 \times 10^6 & 1.10224 \times 10^7 \end{bmatrix} \begin{bmatrix} \phi_1 \\ \phi_2 \end{bmatrix} - \lambda \begin{bmatrix} 1.97378 & -0.22829 \\ -0.22829 & 1.67343 \end{bmatrix} \begin{bmatrix} \phi_1 \\ \phi_2 \end{bmatrix} = \begin{bmatrix} 0 \\ 0 \end{bmatrix}. \quad (\text{f})$$

This eigenvalue system in eq. (f) was solved in *Mathematica* using the function `Eigensystem[{Kαα, Mαα}]`, which finds the generalized eigenvalues and eigenvectors. The eigen pairs are

$$(\lambda_1, \{\phi_1\}) = \left( 5.92732 \times 10^6, \begin{bmatrix} -0.266679 \\ 1.0 \end{bmatrix} \right), \text{ and } (\lambda_2, \{\phi_2\}) = \left( 1.51655 \times 10^7, \begin{bmatrix} 1.0 \\ 0.435137 \end{bmatrix} \right). \quad (\text{g})$$

The natural frequencies are

$$\omega_1 = \sqrt{5.92732 \times 10^6} = 2,434.61 \text{ rad/s} = 387.48 \text{ Hz}, \text{ and } \omega_2 = \sqrt{1.51655 \times 10^7} = 3,894.28 \text{ rad/s} = 619.795 \text{ Hz} \quad (\text{h})$$

## 18.8 Dynamic bending of a bar with two axes of symmetry

If the cross section is symmetric with respect to both the  $x$ - and  $y$ -axes through the centroid, then  $x_{sc} = y_{sc} = 0$ ,  $I_{xy} = 0$ ,  $r_{xy} = 0$ , and  $s_{xy} = 0$ . In this case of double symmetry, transverse bending is decoupled from torsion in both the inertia and stiffness terms. That is, the inertia axis and elastic axis coincide. However, the motions of the lateral displacement  $v(z, t)$  and the rotation  $\phi_x(z, t)$  are linked because of the presence of transverse shear deformation  $\psi_y$ . The governing weak forms (18.117) and (18.119) are

$$\begin{aligned} \int_0^L [m(\ddot{v})\delta v + s_{yy}(v' + \phi_x)\delta v'] dz &= \int_0^L f_y(z, t)\delta v(z) dz + Q_2(t)\delta v(0, t) + Q_8(t)\delta v(L, t). \\ \int_0^L [m(r_x^2 \ddot{\phi}_x)\delta \phi_x + EI_{xx}\phi_x'\delta \phi_x' + s_{yy}(v' + \phi_x)\delta \phi_x] dz &= \int_0^L m_x(z, t)\delta \phi_x(z, t) dz + Q_4(t)\delta \phi_x(0, t) + Q_{10}(t)\delta \phi_x(L, t) \end{aligned}$$

The previous two equations are combined to the matrix form

$$\int_0^L \left\{ [\delta\phi_x \ \delta v] \begin{bmatrix} mr_x^2 & 0 \\ 0 & m \end{bmatrix} \begin{bmatrix} \ddot{\phi}_x \\ \ddot{v} \end{bmatrix} + \delta\phi_x' EI_{xx} \phi_x' + (\delta v' + \delta\phi_x) s_{yy} (v' + \phi_x) \right\} dz = \delta W_{n.c.}, \quad (18.137)$$

where the virtual work of the non-conservative forces is

$$\delta W_{n.c.} = \int_0^L [\delta\phi_x \ \delta v] \begin{bmatrix} m_z(z, t) \\ f_y(z, t) \end{bmatrix} dz + [\delta\phi_x(0, t) \ \delta v(0, t)] \begin{bmatrix} Q_2(t) \\ Q_4(t) \end{bmatrix} + [\delta\phi_x(L, t) \ \delta v(L, t)] \begin{bmatrix} Q_8(t) \\ Q_{10}(t) \end{bmatrix}. \quad (18.138)$$

### 18.8.1 Finite element

The development of the generalized displacements in  $\Omega_k$  follows the discussion in article 17.3.1 on page 508.

The lateral displacement of the  $k$ th element is denoted by  $v^{(k)}(\zeta, t)$  and the rotation by  $\phi_x^{(k)}(\zeta, t)$ . Define the generalized external displacements in terms of the rotation and displacement at the nodes by

$$v^{(k)}(-1, t) = u_{2k-1}(t) \quad \phi_x^{(k)}(-1, t) = u_{2k}(t) \quad v^{(k)}(1, t) = u_{2k+1}(t) \quad \phi_x^{(k)}(1, t) = u_{2k+2}(t). \quad (18.139)$$

See figure 18.16. The 7X1 displacement vector of element  $\Omega_k$  is denoted by,

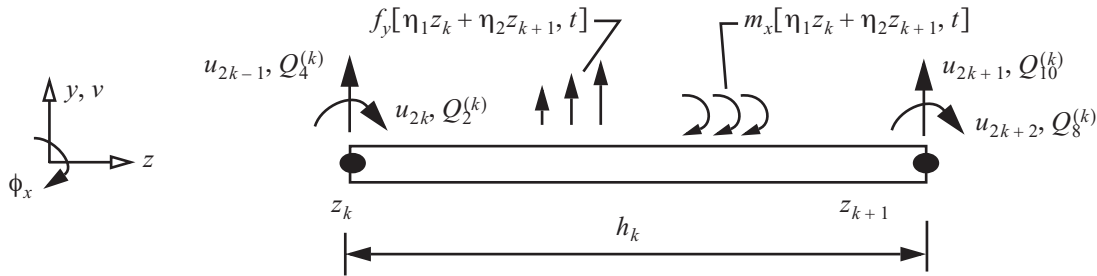


Fig. 18.16 Beam element  $\Omega_k$ .

$$\{u^{(k)}(t)\} = [u_{2k-1}(t) \ u_{2k}(t) \ u_{2k+1}(t) \ u_{2k+2}(t) \ u_1^{(k)}(t) \ u_2^{(k)}(t) \ u_3^{(k)}(t)]^T, \quad (18.140)$$

where  $u_1^{(k)}(t)$ ,  $u_2^{(k)}(t)$ , and  $u_3^{(k)}(t)$  are internal generalized displacement degrees of freedom. Rotation and displacement functions within the element are expressed in terms of the 2X7 shape function matrix and the 7X1 displacement vector:

$$\begin{bmatrix} \phi_x^{(k)}(\zeta, t) \\ v^{(k)}(\zeta, t) \end{bmatrix} = [N(\zeta)] \{u^{(k)}(t)\}, \quad (18.141)$$

where the shape function matrix is

$$[N(\zeta)] = \begin{bmatrix} 0 & \eta_1(\zeta) & 0 & \eta_2(\zeta) & 0 & \eta_3(\zeta) & 0 \\ \eta_1(\eta) & 0 & \eta_2(\zeta) & 0 & \eta_3(\zeta) & 0 & \eta_4(\zeta) \end{bmatrix}. \quad (18.142)$$

The basis functions for the element are

$$\eta_1(\xi) = (1 - \xi)/2 \quad \eta_2(\xi) = (1 + \xi)/2 \quad \eta_3(\xi) = \left(\frac{1}{2}\sqrt{\frac{3}{2}}\right)(\xi^2 - 1) \quad \eta_4(\xi) = \left(\frac{1}{2}\sqrt{\frac{5}{2}}\right)\xi(\xi^2 - 1). \quad (18.143)$$

The virtual rotation and displacement within the element are

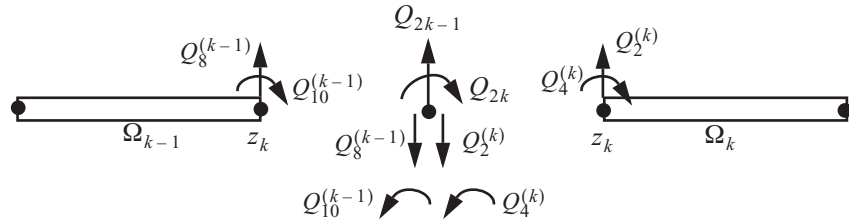
$$\begin{bmatrix} \delta\phi_x \\ \delta v \end{bmatrix} = [N(\xi)] \{b^{(k)}\}, \quad (18.144)$$

where the 7X1 vector  $\{b^{(k)}\} = [b_{2k-1} \ b_{2k} \ b_{2k+1} \ b_{2k+2} \ b_1^{(k)} \ b_2^{(k)} \ b_3^{(k)}]^T$ . The virtual generalized displacements  $b_1^{(k)}$ ,  $b_2^{(k)}$ , and  $b_3^{(k)}$  correspond to the internal degrees of freedom  $u_1^{(k)}(t)$ ,  $u_2^{(k)}(t)$ , and  $u_3^{(k)}(t)$ , respectively. The virtual generalized displacement vector  $\{b^{(k)}\}$  is independent of the physical generalized displacement vector  $\{u^{(k)}\}$ . The external virtual work of the non-conservative forces (18.138) for the elements is given by

$$\delta W_{\text{n.c.}} = \sum_{k=1}^M b_{2k-1} Q_2^{(k)} + b_{2k} Q_4^{(k)} + b_{2k+1} Q_8^{(k)} + b_{2k+2} Q_{10}^{(k)} + \sum_{k=1}^M \{b^{(k)}\} \int_{-1}^1 [N]^T \begin{bmatrix} m_x \\ f_y \end{bmatrix} \frac{h_k}{2} d\xi. \quad (18.145)$$

At the common node  $z_k$  between elements  $\Omega_{k-1}$  and  $\Omega_k$  there is an equilibrium relation between the externally applied force  $Q_{2k-1}$  and the externally applied moment  $Q_{2k}$  and the internal actions at the end of element  $\Omega_{k-1}$  and the beginning of element  $\Omega_k$ . Refer figure 18.17. These relations are

**Fig. 18.17 Free body diagram at a node between two elements**



$$Q_{2k-1} = Q_8^{(k-1)} + Q_2^{(k)} \quad Q_{2k} = Q_{10}^{(k-1)} + Q_4^{(k)} \quad k = 2, 3, \dots, M-1, \text{ and} \quad (18.146)$$

$$Q_1 = Q_2^{(1)} \quad Q_2 = Q_4^{(1)} \quad Q_{2M+1} = Q_8^{(M)} \quad Q_{2M+2} = Q_{10}^{(M)}. \quad (18.147)$$

We now write the virtual work of the non-conservative generalized forces as

$$\delta W_{\text{n.c.}} = \sum_{k=1}^M \{b^{(k)}\} (\{Q^{(k)}\} + \{F^{(k)}\}), \quad (18.148)$$

where

$$\{Q^{(k)}\} = [Q_{2k-1} \ Q_{2k} \ Q_{2k+1} \ Q_{2k+2} \ 0 \ 0 \ 0]^T, \text{ and } \{F^{(k)}(t)\} = \int_{-1}^1 [N]^T \begin{bmatrix} m_x [\eta_1(\xi)z_k + \eta_2(\xi)z_{k+1}, t] \\ f_y [\eta_1(\xi)z_k + \eta_2(\xi)z_{k+1}, t] \end{bmatrix} \frac{h_k}{2} d\xi. \quad (18.149)$$

The partial derivatives with respect to coordinate  $z$  in eq. (18.137) are replaced by derivatives with respect to dimensionless coordinate  $\xi$  using the chain rule. That is,

$$\frac{\partial \phi_x}{\partial z} = \frac{\partial \phi_x}{\partial \xi} \frac{d\xi}{dz} = \frac{2}{h_k} \frac{\partial \phi_x}{\partial \xi} = \frac{2}{h_k} \phi_x', \quad dz = \frac{dz}{d\xi} d\xi = \frac{h_k}{2} d\xi. \quad (18.150)$$

Note that in the following finite element development the prime superscript denotes a derivative with respect to  $\xi$ . The derivative of the rotation for element  $\Omega_k$  and the virtual rotation are

$$\phi_x' = [N_\phi(\xi)] \{u^{(k)}\} \quad \delta\phi_x' = [N_\phi(\xi)] \{b^{(k)}\}, \quad (18.151)$$

where the  $1 \times 7$  matrix is given by

$$[N_\phi(\xi)] = [0 \ \eta_1' \ 0 \ \eta_2' \ 0 \ \eta_3' \ 0]. \quad (18.152)$$

The shear strain for element  $\Omega_k$  and the virtual shear strain are

$$\left(\frac{2}{h_k} v' + \phi_x\right) = [N_\psi(\xi)] \{u^{(k)}\} \quad \left(\frac{2}{h_k} \delta v' + \delta\phi_x\right) = [N_\psi(\xi)] \{b\}, \quad (18.153)$$

where the  $1 \times 7$  matrix is given by

$$[N_\psi(\xi)] = \left[\frac{2}{h_k} \eta_1' \ \eta_1 \ \frac{2}{h_k} \eta_2' \ \eta_2 \ \frac{2}{h_k} \eta_3' \ \eta_3 \ \frac{2}{h_k} \eta_4'\right]. \quad (18.154)$$

Substitute eqs. (18.151) and (18.153) into the finite element representation of eq. (18.137), and substitute eq. (18.148) for the virtual work, to get

$$\sum_{k=1}^M \left( \{b^{(k)}\}^T \int_{-1}^1 [N]^T \begin{bmatrix} mr_x^2 & 0 \\ 0 & m \end{bmatrix} [N] \{u^{(k)}\} + \frac{2}{h_k} [N_\phi]^T EI_{xx} \frac{2}{h_k} [N_\phi] \{u^{(k)}\} + \frac{2}{h_k} [N_\psi]^T s_{yy} [N_\psi] \{u^{(k)}\} \right) \frac{h_k}{2} d\xi = \sum_{k=1}^M \{b^{(k)}\}^T (\{Q^{(k)}\} + \{F^{(k)}\}) \quad (18.155)$$

We satisfy eq. (18.155) for each element in the mesh by

$$\{b^{(k)}\}^T ([M] \{\ddot{u}^{(k)}\} + [K] \{u^{(k)}\} - (\{Q^{(k)}\} + \{F^{(k)}\})) = 0 \quad \forall (\{b^{(k)}\} \neq 0_{7 \times 1}). \quad (18.156)$$

Hence, the equation of motion for element  $\Omega_k$  is

$$[M] \{\ddot{u}^{(k)}\} + [K] \{u^{(k)}\} = \{Q^{(k)}\} + \{F^{(k)}\}. \quad (18.157)$$

The mass, and stiffness matrices are

$$[M] = \int_{-1}^1 [N]^T \begin{bmatrix} mr_x^2 & 0 \\ 0 & m \end{bmatrix} [N] \frac{h_k}{2} d\xi, \text{ and } [K] = \int_{-1}^1 \left( \frac{2}{h_k} [N_\phi]^T EI_{xx} \frac{2}{h_k} [N_\phi] + \frac{2}{h_k} [N_\psi]^T s_{yy} [N_\psi] \right) \frac{h_k}{2} d\xi. \quad (18.158)$$

Perform the matrix algebra in eq. (18.158) to find the  $7 \times 7$  mass matrix

$$[M] = mh_k \begin{bmatrix} 1/3 & 0 & 1/6 & 0 & -1/2\sqrt{6} & 0 & 1/6\sqrt{10} \\ 0 & r_x^2/3 & 0 & r_x^2/6 & 0 & -r_x^2/2\sqrt{6} & 0 \\ 1/6 & 0 & 1/3 & 0 & -1/2\sqrt{6} & 0 & -1/6\sqrt{10} \\ 0 & r_x^2/6 & 0 & r_x^2/3 & 0 & -r_x^2/2\sqrt{6} & 0 \\ -1/2\sqrt{6} & 0 & -1/2\sqrt{6} & 0 & 1/5 & 0 & 0 \\ 0 & -r_x^2/(2\sqrt{6}) & 0 & -r_x^2/2\sqrt{6} & 0 & r_x^2/5 & 0 \\ 1/(6\sqrt{10}) & 0 & -1/6\sqrt{10} & 0 & 0 & 0 & 1/21 \end{bmatrix}. \quad (18.159)$$

Perform the matrix algebra in of eq. (18.158) to find the 7X7 stiffness matrix

$$[K] = \begin{bmatrix} s_{yy}/h_k & -s_{yy}/2 & -s_{yy}/h_k & -s_{yy}/2 & 0 & s_{yy}/\sqrt{6} & 0 \\ -s_{yy}/2 & EI_{xx}/h_k + h_k s_{yy}/3 & s_{yy}/2 & -EI_{xx}/h_k + h_k s_{yy}/6 & -s_{yy}/\sqrt{6} & -h_k s_{yy}/2\sqrt{6} & 0 \\ -s_{yy}/h_k & s_{yy}/2 & s_{yy}/h_k & s_{yy}/2 & 0 & -s_{yy}/\sqrt{6} & 0 \\ -s_{yy}/2 & -EI_{xx}/h_k + h_k s_{yy}/6 & s_{yy}/2 & EI_{xx}/h_k + h_k s_{yy}/3 & s_{yy}/\sqrt{6} & -h_k s_{yy}/2\sqrt{6} & 0 \\ 0 & -s_{yy}/\sqrt{6} & 0 & s_{yy}/\sqrt{6} & 2s_{yy}/h_k & 0 & 0 \\ s_{yy}/\sqrt{6} & -h_k s_{yy}/2\sqrt{6} & -s_{yy}/\sqrt{6} & -h_k s_{yy}/2\sqrt{6} & 0 & 2EI_{xx}/h_k + h_k s_{yy}/5 & s_{yy}/\sqrt{15} \\ 0 & 0 & 0 & 0 & 0 & s_{yy}/\sqrt{15} & 2s_{yy}/h_k \end{bmatrix}. \quad (18.160)$$

### 18.8.2 Method of dynamic condensation

To eliminate the internal degrees of freedom we employ the Guyan reduction method (Craig, p. 413) and (Qu, 2004, p. 52). The Guyan condensation matrix is determined by ignoring the inertia terms in the internal degrees of freedom. Of course, an error is introduced with respect to the full dynamic model of element  $\Omega_k$ . Refer to the discussions about the error in the latter references. Let

$$\underbrace{\{u^{(k)}\}}_{7 \times 1} = \underbrace{\begin{bmatrix} I_{4 \times 4} \\ G_{au} \end{bmatrix}}_{7 \times 4} \begin{bmatrix} u_{2k-1} \\ u_{2k} \\ u_{2k+1} \\ u_{2k+2} \end{bmatrix} = [T_R] \begin{bmatrix} u_{2k-1} \\ u_{2k} \\ u_{2k+1} \\ u_{2k+2} \end{bmatrix}, \quad (18.161)$$

where the 3X4 matrix  $[G_{au}]$  is the Guyan condensation matrix which was developed in the static condensation procedure of article 17.3.3 on page 514. Matrix  $[G_{aq}]$  in eq. (17.102) on page 514 is equal to the matrix  $[G_{au}]$ . The explicit form of eq. (18.161) is

$$\begin{bmatrix} u_{2k-1} \\ u_{2k} \\ u_{2k+1} \\ u_{2k+2} \\ u_1^{(k)} \\ u_2^{(k)} \\ u_3^{(k)} \end{bmatrix} = \begin{bmatrix} 1 & 0 & 0 & 0 \\ 0 & 1 & 0 & 0 \\ 0 & 0 & 1 & 0 \\ 0 & 0 & 0 & 1 \\ \hline 0 & \frac{h_k}{2\sqrt{6}} & 0 & \frac{-h_k}{2\sqrt{6}} \\ \frac{-\sqrt{6}h_k s_{yy}}{12EI_{xx} + h_k^2 s_{yy}} & \frac{\sqrt{3/2}h_k^2 s_{yy}}{12EI_{xx} + h_k^2 s_{yy}} & \frac{\sqrt{6}h_k s_{yy}}{12EI_{xx} + h_k^2 s_{yy}} & \frac{\sqrt{3/2}h_k^2 s_{yy}}{12EI_{xx} + h_k^2 s_{yy}} \\ \frac{h_k^2 s_{yy}}{\sqrt{10}(12EI_{xx} + h_k^2 s_{yy})} & \frac{-h_k^3 s_{yy}}{2\sqrt{10}(12EI_{xx} + h_k^2 s_{yy})} & \frac{-h_k^2 s_{yy}}{\sqrt{10}(12EI_{xx} + h_k^2 s_{yy})} & \frac{-h_k^3 s_{yy}}{2\sqrt{10}(12EI_{xx} + h_k^2 s_{yy})} \end{bmatrix} \begin{bmatrix} u_{2k-1} \\ u_{2k} \\ u_{2k+1} \\ u_{2k+2} \end{bmatrix}. \quad (18.162)$$

The coefficients in the virtual generalized displacements (18.144) are also transformed through matrix  $[T_R]$ :

$$\underbrace{\{b^{(k)}\}}_{7 \times 1} = \underbrace{[T_R]}_{7 \times 4} \begin{bmatrix} b_{2k-1} \\ b_{2k} \\ b_{2k+1} \\ b_{2k+2} \end{bmatrix}. \quad (18.163)$$

Substitute the transformation for the generalized displacement  $\{u^{(k)}\}$  in eq. (18.161), and the transformation of the virtual coefficients (18.163), into the matrix form of Hamilton's principle (18.156) to get

$$\begin{bmatrix} b_{2k-1} & b_{2k} & b_{2k+1} & b_{2k+2} \end{bmatrix} \left( \begin{bmatrix} T_R \end{bmatrix}^T \begin{bmatrix} M \end{bmatrix} \begin{bmatrix} T_R \end{bmatrix} \begin{bmatrix} \ddots \\ u_{2k-1} \\ \ddots \\ u_{2k} \\ \ddots \\ u_{2k+1} \\ \ddots \\ u_{2k+2} \end{bmatrix} + \begin{bmatrix} T_R \end{bmatrix}^T \begin{bmatrix} K \end{bmatrix} \begin{bmatrix} T_R \end{bmatrix} \begin{bmatrix} u_{2k-1} \\ u_{2k} \\ u_{2k+1} \\ u_{2k+2} \end{bmatrix} - \begin{bmatrix} T_R \end{bmatrix}^T \{Q^{(k)}\} + \{F^{(k)}\} \right) = 0. \quad (18.164)$$

The previous equation is to be satisfied for every choice of  $\begin{bmatrix} b_{2k-1} & b_{2k} & b_{2k+1} & b_{2k+2} \end{bmatrix} \neq 0_{1 \times 4}$ . Consequently, we obtain the reduced form of the equations of motion in the external degrees of freedom for element  $\Omega_k$ :

$$\begin{bmatrix} M_R \end{bmatrix} \begin{bmatrix} \ddots \\ u_{2k-1} \\ \ddots \\ u_{2k} \\ \ddots \\ u_{2k+1} \\ \ddots \\ u_{2k+2} \end{bmatrix} + \begin{bmatrix} K_R \end{bmatrix} \begin{bmatrix} u_{2k-1} \\ u_{2k} \\ u_{2k+1} \\ u_{2k+2} \end{bmatrix} = \{R\}. \quad (18.165)$$

The 4X4 symmetric mass matrix  $[M_R]$ , the 4X4 symmetric stiffness matrix  $[K_R]$ , and the 4X1 generalized force vector, are given by

$$[M_R] = [T_R]^T [M] [T_R], \quad [K_R] = [T_R]^T [K] [T_R], \quad \text{and} \quad \{R\} = [T_R]^T \{Q^{(k)}\} + \{F^{(k)}\}. \quad (18.166)$$

The explicit form of the mass matrix is



$$[M_R] = mh_k \begin{bmatrix} \mu_{11} & -h_k \mu_{12} & \mu_{13} & h_k \mu_{14} \\ -h_k \mu_{21} & h_k^2 \mu_{22} & -h_k \mu_{23} & -h_k^2 \mu_{24} \\ \mu_{31} & -h_k \mu_{32} & \mu_{33} & h_k \mu_{34} \\ h_k \mu_{41} & -h_k^2 \mu_{42} & h_k \mu_{43} & h_k^2 \mu_{44} \end{bmatrix}, \quad (18.167)$$

where formulas for the dimensionless coefficients  $\mu_{ij}$ ,  $i, j = 1, 2, 3, 4$  follow:

$$\mu_{11} = \mu_{33} = \frac{1680(EI_{xx})^2 + 294EI_{xx}h_k^2s_{yy} + h_k^2(13h_k^2 + 42r_x^2)s_{yy}^2}{35(12EI_{xx} + h_k^2s_{yy})^2} \quad (18.168)$$

$$\mu_{21} = \mu_{12} = \mu_{43} = \mu_{34} = \frac{1260(EI_{xx})^2 + 21EI_{xx}(11h_k^2 - 60r_x^2)s_{yy} + h_k^2(11h_k^2 + 21r_x^2)s_{yy}^2}{210(12EI_{xx} + h_k^2s_{yy})^2} \quad (18.169)$$

$$\mu_{31} = \mu_{13} = \frac{3(560(EI_{xx})^2 + 84EI_{xx}h_k^2s_{yy} + h_k^2(3h_k^2 - 28r_x^2)s_{yy}^2)}{70(12EI_{xx} + h_k^2s_{yy})^2} \quad (18.170)$$

$$\mu_{41} = \mu_{14} = \mu_{32} = \mu_{23} = \frac{2520(EI_{xx})^2 + 126EI_{xx}(3h_k^2 + 20r_x^2)s_{yy} + h_k^2(13h_k^2 - 42r_x^2)s_{yy}^2}{420(12EI_{xx} + h_k^2s_{yy})^2} \quad (18.171)$$

$$\mu_{22} = \mu_{44} = \frac{126(EI_{xx})^2(h_k^2 + 40r_x^2) + 21EI_{xx}h_k^2(h_k^2 + 10r_x^2)s_{yy} + h_k^4(h_k^2 + 14r_x^2)s_{yy}^2}{105h_k^2(12EI_{xx} + h_k^2s_{yy})^2} \quad (18.172)$$

$$\mu_{42} = \mu_{24} = \frac{504(EI_{xx})^2(h_k^2 - 20r_x^2) + 84EI_{xx}h_k^2(h_k^2 + 10r_x^2)s_{yy} + h_k^4(3h_k^2 + 14r_x^2)s_{yy}^2}{420h_k^2(12EI_{xx} + h_k^2s_{yy})^2}, \quad (18.173)$$

Note that of the sixteen coefficients  $\mu_{ij}$  only six are independent. The 4X4 stiffness matrix  $[K_R]$  is the same 4X4 stiffness matrix given by eq. (17.106) on page 515.

#### Example 18.4 Free vibration of a cantilever beam

Consider the homogeneous, uniform cantilever beam shown in figure 18.18(a). The beam is a thin-walled tube with the data from example 6.5 on page 162. The length  $l = 0.8$  m, cross-sectional area  $A = 171.014 \times 10^{-6} \text{ m}^2$ , second area moment  $I_{xx} = 124.25 \times 10^{-9} \text{ m}^4$ , radius of gyration  $r_x = \sqrt{I_{xx}/A} = 0.026955$  m, modulus of elasticity  $E = 68.3 \text{ GPa}$ , transverse shear coefficient  $s_{yy} = 2.195 \text{ MN}$ , and the mass density  $\rho = 2,710 \text{ Kg./m}^3$ . The flexural stiffness  $EI_{xx} = 8,486.28 \text{ N-m}^2$ .

Determine the natural frequencies in Hz and the corresponding vibration modes for the one-element model shown in figure 18.18(b).

**Solution.** Generalized displacements  $u_1(t) = u_2(t) = 0$  for all  $t \geq 0$ . So formulate the restrained structural stiffness matrix, and the mass matrix, in DOFs 3 and 4. The total mass of the beam is  $mh_1 = \rho Ah_1 = 0.37075 \text{ Kg}$ . The numerical result for the 4X4 mass matrix (18.167) is

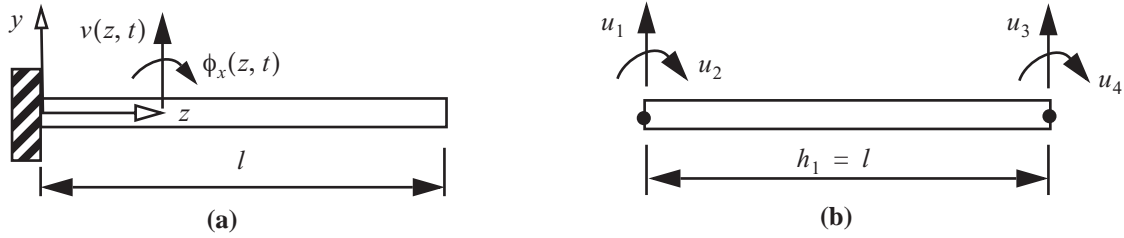


Fig. 18.18 (a) Cantilever beam. (b) One-element model.

$$[M_R] = \frac{mh_1}{420} \begin{bmatrix} \ddot{u}_1 & \ddot{u}_2 & \ddot{u}_3 & \ddot{u}_4 \\ 155.29 & -17.3257 & 54.7098 & 10.6725 \\ -17.3257 & 2.55726 & -10.6725 & -1.9736 \\ 54.7098 & -10.6725 & 155.29 & 17.3275 \\ 10.6725 & -1.9736 & 17.3275 & 2.55726 \end{bmatrix} = \begin{bmatrix} [M_{\beta\beta}] & [M_{\beta\alpha}] \\ [M_{\alpha\beta}] & [M_{\alpha\alpha}] \end{bmatrix} \quad (a)$$

The numerical evaluation of the 4X4 stiffness matrix is

$$[K_R] = \begin{bmatrix} u_1 & u_2 & u_3 & u_4 \\ 185461. & -74184.2 & -185461. & -74184.2 \\ -74184.2 & 40281.8 & 74184.2 & 19065.6 \\ -185461. & 74184.2 & 185461. & 74184.2 \\ -74184.2 & 19065.6 & 74184.2 & 40281.8 \end{bmatrix} = \begin{bmatrix} [K_{\beta\beta}] & [K_{\beta\alpha}] \\ [K_{\alpha\beta}] & [K_{\alpha\alpha}] \end{bmatrix} \quad (b)$$

The mass and stiffness matrices are partitioned in terms of known and unknown generalized displacements as shown in eqs. (a) and (b). The equations of motion for the generalized displacements  $u_3(t)$  and  $u_4(t)$  are

$$[M_{\alpha\alpha}] \begin{bmatrix} \ddot{u}_3 \\ \ddot{u}_4 \end{bmatrix} + [K_{\alpha\alpha}] \begin{bmatrix} u_3 \\ u_4 \end{bmatrix} = \begin{bmatrix} 0 \\ 0 \end{bmatrix} \quad (c)$$

Assume a harmonic motion given by the equation

$$\begin{bmatrix} u_3(t) \\ u_4(t) \end{bmatrix} = \begin{bmatrix} q_3 \\ q_4 \end{bmatrix} \cos(\omega t - \alpha) \quad (d)$$

Substitute eq. (d) into the equation of motion (c) to get

$$\left( [K_{\alpha\alpha}] - \lambda [M_{\alpha\alpha}] \right) \begin{bmatrix} q_3 \\ q_4 \end{bmatrix} = 0, \text{ or } \left( \begin{bmatrix} 18,5461 & 74,184.2 \\ 74,184.2 & 40,281.8 \end{bmatrix} - \lambda \begin{bmatrix} 0.137083 & 0.0152959 \\ 0.0152959 & 0.00225743 \end{bmatrix} \right) \begin{bmatrix} q_3 \\ q_4 \end{bmatrix} = \begin{bmatrix} 0 \\ 0 \end{bmatrix}, \quad (e)$$

where  $\lambda = \omega^2$ . The eigenvalues and eigenvectors are

$$(\lambda_1, \{q_1\}) = \left(541, 936, \begin{bmatrix} -0.509895 \\ 0.860236 \end{bmatrix}\right) \quad (\lambda_2, \{q_2\}) = \left(4.80887 \times 10^7, \begin{bmatrix} -0.102686 \\ 0.994714 \end{bmatrix}\right). \quad (f)$$

The frequencies in Hertz are

$$\omega_1 = \sqrt{\lambda_1}/(2\pi) = 117.164 \text{ Hz} \quad \omega_2 = \sqrt{\lambda_2}/(2\pi) = 1,103.68 \text{ Hz}. \quad (g)$$

The lateral displacement for the first vibration mode is given by

$$v_1(\zeta) = \eta_2(\zeta)(q_3)_1 + \eta_3(\zeta)(u_1^{(1)})_1 + \eta_4(\zeta)(u_3^{(1)})_1, \quad (h)$$

where the interior generalized displacements for mode one are determined from

$$\begin{bmatrix} u_1^{(1)} \\ u_2^{(1)} \\ u_3^{(1)} \end{bmatrix}_1 = [G_{au}] \begin{bmatrix} 0 \\ 0 \\ q_3 \\ q_4 \end{bmatrix}_1. \quad (i)$$

The 3X4 matrix  $[G_{au}]$  is obtained from the last three rows of eq. (18.162). Its numerical evaluation is

$$[G_{au}] = \begin{bmatrix} 0 & 0.163299 & 0 & -0.163299 \\ -2.85495 & 1.14198 & 2.85495 & 1.14198 \\ 0.294858 & -0.117943 & -0.294858 & -0.117943 \end{bmatrix}. \quad (j)$$

The interior generalized displacement vector for the first mode is

$$\begin{bmatrix} u_1^{(1)} \\ u_2^{(1)} \\ u_3^{(1)} \end{bmatrix}_1 = \begin{bmatrix} 0 & 0.163299 & 0 & -0.163299 \\ -2.85495 & 1.14198 & 2.85495 & 1.14198 \\ 0.294858 & -0.117943 & -0.294858 & -0.117943 \end{bmatrix} \begin{bmatrix} 0 \\ 0 \\ -0.509895 \\ 0.860236 \end{bmatrix} = \begin{bmatrix} -0.14047568 \\ -0.47335242 \\ 0.048887805 \end{bmatrix}. \quad (k)$$

Hence, the expression for the lateral displacement in the first mode is

$$v_1(\zeta) = \eta_2(\zeta)(-0.509895) + \eta_3(\zeta)(-0.14047568) + \eta_4(\zeta)(0.048887805). \quad (l)$$

The lateral displacement for the second vibration mode is given by

$$v_2(\zeta) = \eta_2(\zeta)(q_3)_2 + \eta_3(\zeta)(u_1^{(1)})_2 + \eta_4(\zeta)(u_3^{(1)})_2, \quad (m)$$

where the interior generalized displacements for mode two are determined from

$$\begin{bmatrix} u_1^{(1)} \\ u_2^{(1)} \\ u_3^{(1)} \end{bmatrix}_2 = [G_{au}] \begin{bmatrix} 0 \\ 0 \\ q_3 \\ q_4 \end{bmatrix}_2. \quad (n)$$

Numerical evaluation for the interior generalized displacement vector in the second mode is

$$\begin{bmatrix} u_1^{(1)} \\ u_2^{(1)} \\ u_3^{(1)} \end{bmatrix}_2 = \begin{bmatrix} 0 & 0.163299 & 0 & -0.163299 \\ -2.85495 & 1.14198 & 2.85495 & 1.14198 \\ 0.294858 & -0.117943 & -0.294858 & -0.117943 \end{bmatrix} \begin{bmatrix} 0 \\ 0 \\ -0.102686 \\ 0.994714 \end{bmatrix} = \begin{bmatrix} -0.1624358 \\ 0.8427801 \\ -0.087041765 \end{bmatrix}. \quad (\text{o})$$

Hence, the lateral displacement in the second mode is

$$v_2(\zeta) = \eta_2(\zeta)(-0.102686) + \eta_3(\zeta)(-0.1624358) + \eta_4(\zeta)(-0.087041765). \quad (\text{p})$$

For this two-degree-of-freedom model there is no prediction of the third and higher frequencies. ■

For the cantilever beam of example 18.4, numerical analyses were conducted with two to sixteen equally spaced condensed elements. The details are omitted here, but the results for the first four frequencies are listed in table 18.4. The frequencies decrease with increasing mesh refinement, and the lowest two frequencies are converging to 116.4 Hz and 668 Hz, respectively. The last row in the table lists the frequencies from a continuum analysis of the cantilever beam using Euler-Bernnolli beam theory. The inclusion of transverse shear deformation and rotary inertia in the finite element model result in lower values for the frequencies with respect to the Euler-Bernnolli theory, particularly in the higher frequencies.

**Table 18.4 Free vibration frequencies of the cantilever beam**

Number of condensed elements	$\omega_1$ , Hz	$\omega_2$ , Hz	$\omega_3$ , Hz	$\omega_4$ , Hz
1	117.2	1,103.7	-----	-----
2	116.5	682.0	2,344.4	6,153.1
4	116.4	672.5	1,735.9	3,109.9
8	116.4	669.2	1,691.1	2,979.9
16	116.4	668.4	1,679.2	2,920.3
Euler-Bernoulli <sup>a</sup>	118.3	741.5	2,076.2	4,068.8

a. The free vibration analysis of a continuum model of the cantilever beam using Euler-Bernoulli theory ( $\psi_y = 0$  and  $s_{yy} \rightarrow \infty$ ) is from the text by Craig (1981, p. 215).

The lateral displacement for the first four modes of the cantilever beam are shown in figure 18.19. The mode shapes were plotted such that the tip displacement was set equal to 0.2 m for clarity in the plots. The lateral displacement passes through zero in the open domain  $0 < z < 0.8$  m once for mode two, twice for mode three, and thrice for mode four. These zeros crossings are called vibration nodes. Vibration nodes are not to be confused

with finite element nodes.

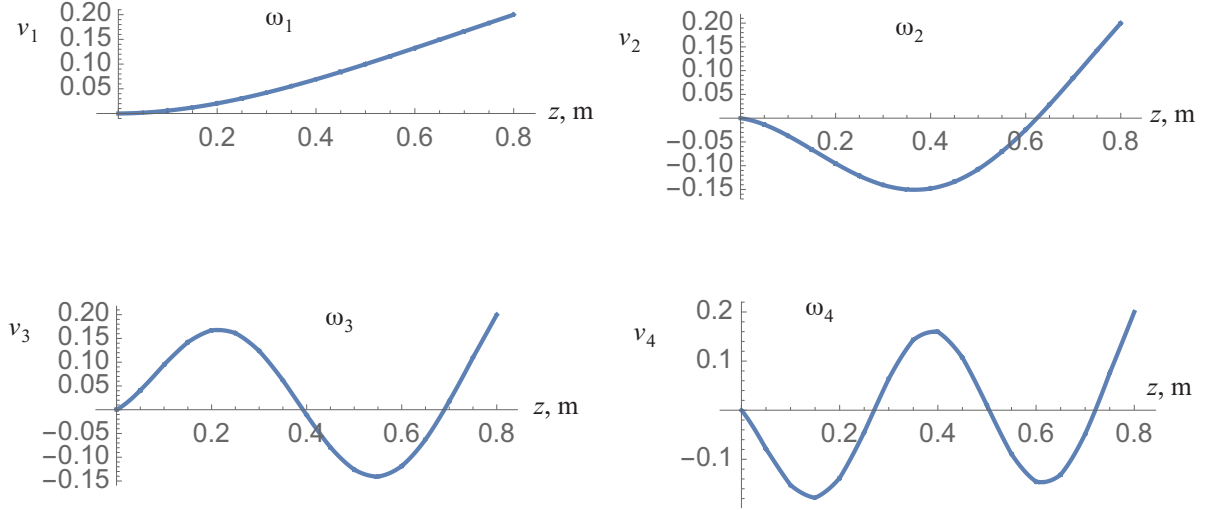


Fig. 18.19 First four vibration modes of the cantilever beam.

## 18.9 Vibrations of a coplanar frame

A bar in a coplanar frame is subject to extension and bending. In the local  $x$ - $y$ - $z$  coordinates of a bar, we assume that it is symmetric with the respect to the longitudinal  $x$ - $z$  plane and the  $y$ - $z$  plane as in article 18.8. The dynamic response of the bar for extension and bending in its  $y$ - $z$  plane is governed by eq. (18.115) on page 555, which reduces to

$$\int_0^L \left( m \ddot{v} \delta v + m \ddot{w} \delta w + m r_x^2 \ddot{\phi}_x \delta \phi_x + N \delta \left( \frac{\partial w}{\partial z} \right) + M_x \delta \left( \frac{\partial \phi_x}{\partial z} \right) + V_y \delta \psi_y \right) dz =$$

$$\left[ Q_2 \delta v + Q_3 \delta w + Q_4 \delta \phi_x \right] \Big|_{z=0} + \left[ Q_8 \delta v + Q_9 \delta w + Q_{10} \delta \phi_x \right] \Big|_{z=L} + \int_0^L f_y(z, t) \delta v(z) dz + \int_0^L f_z(z, t) \delta w(z) dz \quad (18.174)$$

We use Euler-Bernoulli theory so that transverse shear strain  $\psi_y = 0$ , which means the cross-sectional rota-

tion.  $\phi_x = -\left(\frac{\partial v}{\partial z}\right)$ . Also, neglect the rotary inertia  $m r_x^2 \ddot{\phi}_x$  in eq. (18.174). Ignoring rotary inertia and transverse

shear deformation has negligible effect on the first few modes of vibration for slender bars (Langhaar, p. 288)<sup>1</sup>. Let one finite element model the bar so that  $L = h_k$  and  $z = \eta_1(\xi)L$ . The frame element is shown in its reference configuration in figure 18.20(a) and in rotated configuration in figure 18.20(b). The 6X1 displacement vector of the frame element shown in figure 18.20(a) is

1. In regard to the effects of rotary inertia and shear deformation, Langhaar states: "they may cause appreciable perturbations of all modes when the theory of beams is employed as a basis for a study of vibrations of complicated structures, such as airplane wings and hulls of ships."

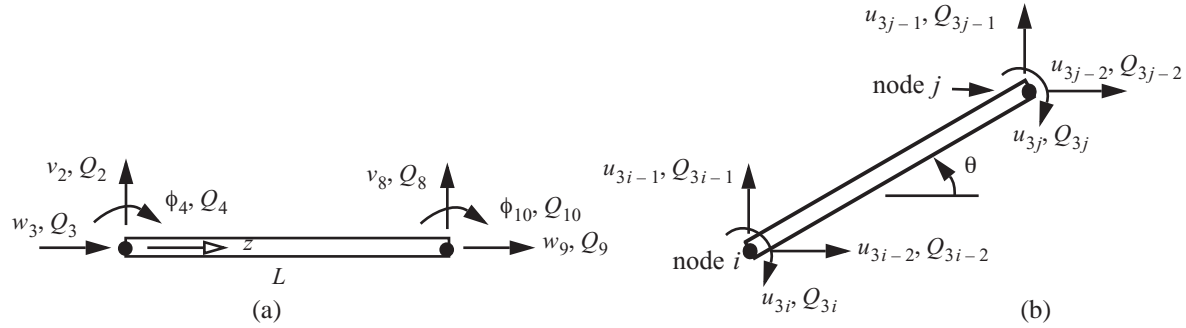


**Fig. 18.20 (a) Reference frame element. (b) Rotated frame element.**

$$\{\bar{u}(t)\} = [w_3 \ v_2 \ \phi_4 \ w_9 \ v_8 \ \phi_{10}]^T. \quad (18.175)$$

The displacements are expressed as

$$\begin{bmatrix} v(\zeta, t) \\ w(\zeta, t) \end{bmatrix} = [N(\zeta)] \{\bar{u}(t)\}, \quad (18.176)$$

where the interpolation matrix is

$$[N(\zeta)] = \begin{bmatrix} 0 & \phi_1(\zeta) & \phi_2(\zeta) & 0 & \phi_3(\zeta) & \phi_4(\zeta) \\ \eta_1(\zeta) & 0 & 0 & \eta_2(\zeta) & 0 & 0 \end{bmatrix}. \quad (18.177)$$

The interpolation functions for the lateral displacement  $\phi_i(\zeta)$ ,  $i = 1, 2, 3, 4$ , are the Hermite cubic interpolation functions given by eq. (17.140) on page 532. The virtual displacements have the same interpolation as the displacements,

$$\begin{bmatrix} \delta v(\zeta, t) \\ \delta w(\zeta, t) \end{bmatrix} = [N(\zeta)] \{b\}, \quad (18.178)$$

where the 6X1 vector  $\{b\}$  given in the following equation is independent of the nodal displacements

$$\{b\} = [b_3 \ b_2 \ b_4 \ b_9 \ b_8 \ b_{10}]^T. \quad (18.179)$$

The weak form for the element is

$$\int_{-1}^1 \left[ \begin{bmatrix} \delta v & \delta w \end{bmatrix} \begin{bmatrix} m & 0 \\ 0 & m \end{bmatrix} \begin{bmatrix} \ddot{v} \\ \ddot{w} \end{bmatrix} + \left( \frac{2}{L} \right)^2 \delta v'' \left( \frac{2}{L} \right) \delta w' \right] \begin{bmatrix} EI_{xx} & 0 \\ 0 & EA \end{bmatrix} \begin{bmatrix} \left( \frac{2}{L} \right)^2 v'' \\ \left( \frac{2}{L} \right) w' \end{bmatrix} \right] \frac{L}{2} d\zeta =$$

$$\{b\}^T \{Q\} + \int_{-1}^1 \begin{bmatrix} \delta v & \delta w \end{bmatrix} \begin{bmatrix} f_y(\eta_1(L, t)) \\ f_x(\eta_1(L, t)) \end{bmatrix} \frac{L}{2} d\zeta, \quad (18.180)$$

where the prime superscript means the derivative with respect to  $\zeta$ , and the generalized force vector is

$$\{Q\} = [Q_3 \ Q_2 \ Q_4 \ Q_9 \ Q_8 \ Q_{10}]^T. \quad (18.181)$$

The displacement derivatives with respect to  $\zeta$  appearing in the stiffness terms of eq. (18.180) are written in the matrix form

$$\begin{bmatrix} \left(\frac{2}{L}\right)^2 v'' \\ \left(\frac{2}{L}\right) w' \end{bmatrix} = \begin{bmatrix} \left(\frac{2}{L}\right)^2 \frac{d^2}{d\zeta^2} & 0 \\ 0 & \left(\frac{2}{L}\right) \frac{d}{d\zeta} \end{bmatrix} \begin{bmatrix} v \\ w \end{bmatrix} = [DN(\zeta)] \{\bar{u}\}, \quad (18.182)$$

where the 2X6 matrix relating the derivatives of the displacements to the displacement vector is given by

$$[DN(\zeta)] = \begin{bmatrix} \left(\frac{2}{L}\right)^2 \frac{d^2}{d\zeta^2} & 0 \\ 0 & \left(\frac{2}{L}\right) \frac{d}{d\zeta} \end{bmatrix} [N(\zeta)] = \begin{bmatrix} 0 & \left(\frac{2}{L}\right)^2 \phi_1'' & \left(\frac{2}{L}\right)^2 \phi_2'' & 0 & \left(\frac{2}{L}\right)^2 \phi_3'' & \left(\frac{2}{L}\right)^2 \phi_4'' \\ \frac{2}{L} \eta_1' & 0 & 0 & \frac{2}{L} \eta_2' & 0 & 0 \end{bmatrix}. \quad (18.183)$$

Substitute eqs. (18.176), (18.178), and (18.182) into (18.180) to get

$$\{b\}^T \int_{-1}^1 [N]^T \begin{bmatrix} m & 0 \\ 0 & m \end{bmatrix} [N] \frac{d^2}{dt^2} \{\bar{u}\} + [DN]^T \begin{bmatrix} EI_{xx} & 0 \\ 0 & EA \end{bmatrix} [DN] \{\bar{u}\} \frac{L}{2} d\zeta = \{b\}^T (\{Q\} + \{F\}), \quad (18.184)$$

where the external force vector due to the distributed loading is

$$\{F(t)\} = \int_{-1}^1 [N]^T \begin{bmatrix} f_y(\eta_1(L, t)) \\ f_x(\eta_1(L, t)) \end{bmatrix} \frac{L}{2} d\zeta = [F_3 \ F_2 \ F_4 \ F_9 \ F_8 \ F_{10}]^T. \quad (18.185)$$

We identify the mass matrix for the reference element as

$$[\bar{M}] = \int_{-1}^1 [N]^T \begin{bmatrix} m & 0 \\ 0 & m \end{bmatrix} [N] \frac{L}{2} d\zeta = \frac{mL}{420} \begin{bmatrix} 140 & 0 & 0 & 70 & 0 & 0 \\ 0 & 156 & -44 & 0 & 54 & 26 \\ 0 & -44 & 16 & 0 & -26 & -12 \\ 70 & 0 & 0 & 140 & 0 & 0 \\ 0 & 54 & -26 & 0 & 156 & 44 \\ 0 & 26 & -12 & 0 & 44 & 16 \end{bmatrix}. \quad (18.186)$$

and the stiffness matrix for the element as

$$[\bar{K}] = \int_{-1}^1 [DN]^T \begin{bmatrix} EI_{xx} & 0 \\ 0 & EA \end{bmatrix} [DN] \frac{L}{2} d\zeta = \frac{EI_{xx}}{L^3} \begin{bmatrix} (L/r_x)^2 & 0 & 0 & -(L/r_x)^2 & 0 & 0 \\ 0 & 12 & -6L & 0 & -12 & -6L \\ 0 & -6L & 4L^2 & 0 & 6L & 2L^2 \\ -(L/r_x)^2 & 0 & 0 & (L/r_x)^2 & 0 & 0 \\ 0 & -12 & 6L & 0 & 12 & 6L \\ 0 & -6L & 2L^2 & 0 & 6L & 4L^2 \end{bmatrix}. \quad (18.187)$$

In the stiffness matrix (18.187)  $r_x^2 = I_{xx}/A$ . Equation (18.184) is valid for every choice of  $\{b\} \neq 0_{6 \times 1}$ , which leads to the equation of motion (18.188) for the reference element below.

$$\left[\bar{M}\right] \frac{d^2}{dt^2} \{\bar{u}(t)\} + \left[\bar{K}\right] \{\bar{u}(t)\} = (\{Q\} + \{F\}). \quad (18.188)$$

The matrix equation of motion for the rotated frame element in figure 18.20(b) is obtained by using the transformation matrix in eq. (16.85) on page 478. This transformation equation is repeated below as eq. (18.189):

$$\left[T\right] = \begin{bmatrix} c & s & 0 & 0 & 0 & 0 \\ -s & c & 0 & 0 & 0 & 0 \\ 0 & 0 & 1 & 0 & 0 & 0 \\ 0 & 0 & 0 & c & s & 0 \\ 0 & 0 & 0 & -s & c & 0 \\ 0 & 0 & 0 & 0 & 0 & 1 \end{bmatrix}, \quad (18.189)$$

where  $c = \cos\theta$  and  $s = \sin\theta$ . The generalized displacement vector for the rotated frame element is given by  $\{u^{(k)}\} = \left[T\right] \{\bar{u}^{(k)}\}$ . The equation of motion for the rotated element is determined from eq. (18.188) by pre-multiplying it by  $\left[T\right]^T$ :

$$\left[T\right]^T \left[\bar{M}\right] \left[T\right] \frac{d^2}{dt^2} \{u\} + \left[T\right]^T \left[\bar{K}\right] \left[T\right] \{u\} = \left[T\right]^T (\{Q\} + \{F\}). \quad (18.190)$$

Equation Eq. (18.190) is written as

$$\left[M\right] \frac{d^2}{dt^2} \{u\} + \left[K\right] \{u\} = \{Q_{i-j}\} + \{F_{i-j}\}. \quad (18.191)$$

The 6X1 transformed generalized force vectors are

$$\begin{aligned} \{Q_{i-j}\} &= \left[ (cQ_3 + sQ_2) \ (cQ_2 - sQ_3) \ Q_9 \ (cQ_9 + sQ_8) \ (cQ_8 - sQ_9) \ Q_{10} \right]^T \\ &= \left[ Q_{3i-2} \ Q_{3i-1} \ Q_{3i} \ Q_{3j-2} \ Q_{3j-1} \ Q_{3j} \right]^T, \text{ and} \end{aligned} \quad (18.192)$$

$$\{F_{i-j}\} = \left[ (cF_3 + sF_2) \ (cF_2 - sF_3) \ F_9 \ (cF_9 + sF_8) \ (cF_8 - sF_9) \ F_{10} \right]^T. \quad (18.193)$$

The mass and stiffness matrices for the rotated frame element are

$$\left[M\right] = \frac{mL}{420} \begin{bmatrix} 140c^2 + 156s^2 & -16cs & 44s & 70c^2 + 54s^2 & 16cs & -26cs \\ -16cs & 156c^2 + 140s^2 & -44c & 16cs & 54c^2 + 70s^2 & 26c \\ 44s & -44c & 16 & 26s & -26c & -12 \\ 70c^2 + 54s^2 & 16cs & 26s & 140c^2 + 156s^2 & -16cs & -44s \\ 16cs & 54c^2 + 70s^2 & -26c & -16cs & 156c^2 + 140s^2 & 44c \\ -26cs & 26c & -12 & -44s & 44c & 16 \end{bmatrix}, \text{ and} \quad (18.194)$$



$$[K] = \frac{EI}{L^3} \begin{bmatrix} \left(\frac{L}{r_x}\right)^2 c^2 + 12s^2 & \left[\left(\frac{L}{r_x}\right)^2 - 12\right]cs & -6Ls & -\left[\left(\frac{L}{r_x}\right)^2 c^2 + 12s^2\right] & \left[12 - \left(\frac{L}{r_x}\right)^2\right]cs & 6Ls \\ \left[\left(\frac{L}{r_x}\right)^2 - 12\right]cs & 12c^2 + \left(\frac{L}{r_x}\right)^2 s^2 & -6Lc & \left[12 - \left(\frac{L}{r_x}\right)^2\right]cs & -\left[12c^2 + \left(\frac{L}{r_x}\right)^2 s^2\right] & -6Lc \\ -6Ls & -6Lc & 4L^2 & -6Ls & 6Lc & 2L^2 \\ -\left[\left(\frac{L}{r_x}\right)^2 c^2 + 12s^2\right] & \left[12 - \left(\frac{L}{r_x}\right)^2\right]cs & -6Ls & \left(\frac{L}{r_x}\right)^2 c^2 + 12s^2 & \left[\left(\frac{L}{r_x}\right)^2 - 12\right]cs & -6Ls \\ \left[12 - \left(\frac{L}{r_x}\right)^2\right]cs & -\left[12c^2 + \left(\frac{L}{r_x}\right)^2 s^2\right] & 6Lc & \left[\left(\frac{L}{r_x}\right)^2 - 12\right]cs & 12c^2 + \left(\frac{L}{r_x}\right)^2 s^2 & 6Lc \\ 6Ls & -6Lc & 2L^2 & -6Ls & 6Lc & 4L^2 \end{bmatrix}. \quad (18.195)$$

### Example 18.5 A two-bar frame subject to harmonic excitation

The frame shown in figure 18.21(a) consists of two identical bars of length  $L$ . It is modeled with two finite elements. Element  $\Omega_1$  is vertical with  $c = 0$  and  $s = 1$ , and element  $\Omega_2$  is horizontal with  $c = 1$  and  $s = 0$ . The base of the vertical bar is subject to a horizontal harmonic displacement  $a \sin(\Omega t)$ , where the amplitude is denoted by  $a$  and the driving frequency by  $\Omega$ . There are nine degrees of freedom as shown in figure 18.21(b) for the unre-

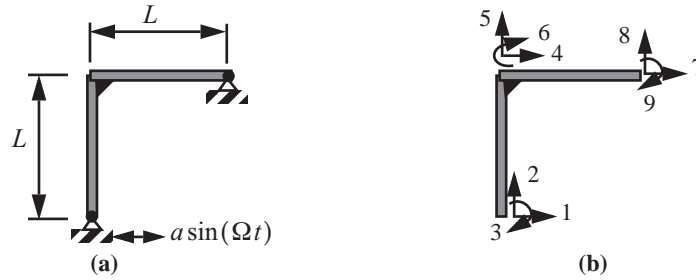


Fig. 18.21 (a) Two-bar frame subject to harmonic excitation. (b) Degree of freedom numbering.

strained frame. model. The active, or unknown, generalized displacement vector is

$$\{u_\alpha(t)\} = [u_3(t) \ u_4(t) \ u_5(t) \ u_6(t) \ u_9(t)]^T. \quad (a)$$

The prescribed displacement vector is

$$\{u_\beta(t)\} = [u_1(t) \ u_2(t) \ u_7(t) \ u_8(t)]^T = [a \sin(\Omega t) \ 0 \ 0 \ 0]^T. \quad (b)$$

The mass and stiffness matrices for element  $\Omega_1$  are

$$\begin{aligned}
[M^{(1)}] &= \frac{mL}{420} \begin{bmatrix} \ddot{u}_1 & \ddot{u}_2 & \ddot{u}_3 & \ddot{u}_4 & \ddot{u}_5 & \ddot{u}_6 \\ 156 & 0 & 44 & 54 & 0 & -26 \\ 0 & 140 & 0 & 0 & 70 & 0 \\ 44 & 0 & 16 & 26 & 0 & -12 \\ 54 & 0 & 26 & 156 & 0 & -44 \\ 0 & 70 & 0 & 0 & 140 & 0 \\ -26 & 0 & -12 & -44 & 0 & 16 \end{bmatrix} & [K^{(1)}] = \frac{EI_{xx}}{L^3} \begin{bmatrix} u_1 & u_2 & u_3 & u_4 & u_5 & u_6 \\ 12 & 0 & 6L & -12 & 0 & 6L \\ 0 & (L/r_x)^2 & 0 & 0 & -(L/r_x)^2 & 0 \\ 6L & 0 & 4L^2 & -6L & 0 & 2L^2 \\ -12 & 0 & -6L & 12 & 0 & -6L \\ 0 & -(L/r_x)^2 & 0 & 0 & (L/r_x)^2 & 0 \\ 6L & 0 & 2L^2 & -6L & 0 & 4L^2 \end{bmatrix}. \quad (c)
\end{aligned}$$

For element  $\Omega_2$  the mass matrix is given by eq. (18.186), and the stiffness matrix is given by eq. (18.187), where the order of the columns is associated with generalized displacements  $[u_4 \ u_5 \ u_6 \ u_7 \ u_8 \ u_9]$ . Assemble the mass matrices to get the 9X9 unrestrained mass matrix  $[M_u] = [M^{(1)}] + [M^{(2)}]$  with due regard in the summation of the matrix elements from the individual mass matrices to their location in  $[M_u]$ . Similarly, the 9X9 unrestrained stiffness matrix is assembled as  $[K_u] = [K^{(1)}] + [K^{(2)}]$ . After assembly, the unrestrained matrix equation of motion is reordered by simultaneously interchanging the rows and columns to  $[u_3 \ u_4 \ u_5 \ u_6 \ u_9 \ u_1 \ u_2 \ u_7 \ u_8]$ . The resulting matrix equation of motion in partitioned form is

$$\begin{bmatrix} [M_{\alpha\alpha}] & [M_{\alpha\beta}] \\ [M_{\beta\alpha}] & [M_{\beta\beta}] \end{bmatrix} \begin{bmatrix} \{\ddot{u}_\alpha\} \\ \{\ddot{u}_\beta\} \end{bmatrix} + \begin{bmatrix} [K_{\alpha\alpha}] & [K_{\alpha\beta}] \\ [K_{\beta\alpha}] & [K_{\beta\beta}] \end{bmatrix} \begin{bmatrix} \{u_\alpha\} \\ \{u_\beta\} \end{bmatrix} = \begin{bmatrix} \{Q_\alpha\} \\ \{Q_\beta\} \end{bmatrix}. \quad (d)$$

The submatrices are

$$[M_{\alpha\alpha}] = \frac{mL}{420} \begin{bmatrix} 16 & 26 & 0 & -12 & 0 \\ 26 & 296 & 0 & -44 & 0 \\ -12 & -44 & -44 & 32 & -12 \\ 0 & 0 & 26 & -12 & 16 \\ 0 & 0 & 26 & -12 & 16 \end{bmatrix} \quad [M_{\alpha\beta}] = \frac{mL}{420} \begin{bmatrix} 44 & 0 & 0 & 0 \\ 54 & 0 & 70 & 0 \\ 0 & 70 & 0 & 54 \\ -26 & 0 & 0 & -26 \\ 0 & 0 & 0 & 44 \end{bmatrix} = [M_{\beta\alpha}]^T \quad (e)$$

$$[M_{\beta\beta}] = \frac{mL}{420} \begin{bmatrix} 156 & 0 & 0 & 0 \\ 0 & 140 & 0 & 0 \\ 0 & 0 & 140 & 0 \\ 0 & 0 & 0 & 156 \end{bmatrix} \quad [K_{\alpha\alpha}] = \frac{EI_{xx}}{L^3} \begin{bmatrix} 4L^2 & -6L & 0 & 2L^2 & 0 \\ -6L & 12 + (L/r_x)^2 & 0 & -6L & 0 \\ 0 & 0 & 12 + (L/r_x)^2 & -6L & -6L \\ 2L^2 & -6L & -6L & 8L^2 & 2L^2 \\ 0 & 0 & -6L & 2L^2 & 4L^2 \end{bmatrix} \quad (f)$$

$$[K_{\alpha\beta}] = \frac{EI_{xx}}{L^3} \begin{bmatrix} 6L & 0 & 0 & 0 \\ -12 & 0 & -(L/r_x)^2 & 0 \\ 0 & -(L/r_x)^2 & 0 & 12 \\ 6L & 0 & 0 & 6L \\ 0 & 0 & 0 & 6L \end{bmatrix} = [K_{\beta\alpha}]^T \quad [K_{\beta\beta}] = \frac{EI_{xx}}{L^3} \begin{bmatrix} 12 & 0 & 0 & 0 \\ 0 & (L/r_x)^2 & 0 & 0 \\ 0 & 0 & (L/r_x)^2 & 0 \\ 0 & 0 & 0 & 12 \end{bmatrix} \quad (g)$$

$$\{Q_\alpha\} = 0_{5 \times 1} \quad \{Q_\beta\} = [Q_1 \ Q_2 \ Q_7 \ Q_9]^T. \quad (h)$$

There are no generalized forces prescribed in degrees of freedom 3, 4, 5, 6, and 9. The unknown generalized reaction force vector  $\{Q_\beta\}$  corresponds to the prescribed generalized displacement vector  $\{u_\beta\}$ . The matrix equation of motion for the unknown generalized displacements is

$$[M_{\alpha\alpha}]\{\ddot{u}_\alpha\} + [M_{\alpha\beta}]\{\ddot{u}_\beta\} + [K_{\alpha\alpha}]\{u_\alpha\} + [K_{\alpha\beta}]\{u_\beta\} = 0_{5 \times 1}.$$

Numerical data are taken from example 6.5 on page 162:  $a = 0.03812$  m,  $A = 171.014 \times 10^{-6}$  m<sup>2</sup>,  $I_{xx} = 124.25 \times 10^{-9}$  m<sup>4</sup>,  $L = 0.8$  m,  $r_x = 0.0269546$  m,  $E = 68.3 \times 10^9$  N/m<sup>2</sup>,  $\rho = 2,710$  Kg/m<sup>3</sup>, and  $m = \rho A = 0.463448$  Kg/m. The eigenvalue problem for the free vibrations of the frame is

$$[K_{\alpha\alpha}]\{\phi\} - \lambda[M_{\alpha\alpha}]\{\phi\} = 0_{5 \times 1}. \quad (i)$$

The numerical results for the eigenvalues and corresponding eigen vectors are

$$(\lambda_1, \{\phi_1\}) = \left( 9.99471 \times 10^7, \begin{bmatrix} 0.324108 \\ 0.268035 \\ 0.268035 \\ 0.324108 \end{bmatrix} \right) \quad (\lambda_2, \{\phi_2\}) = \left( 6.783 \times 10^7, \begin{bmatrix} -1 \\ 0.595335 \\ -0.595335 \\ -1.026 \times 10^{-15} \\ 1 \end{bmatrix} \right) \quad (j)$$

$$(\lambda_3, \{\phi_3\}) = \left( 1.78362 \times 10^7, \begin{bmatrix} 1 \\ -0.105789 \\ -0.105789 \\ 0.972216 \\ 1 \end{bmatrix} \right) \quad (\lambda_4, \{\phi_4\}) = \left( 2.89664 \times 10^6, \begin{bmatrix} 1 \\ 0.0104001 \\ -0.0104001 \\ -2.72413 \times 10^{-15} \\ -1 \end{bmatrix} \right) \quad (k)$$

$$(\lambda_5, \{\phi_5\}) = \left( 854, 421, \begin{bmatrix} 1 \\ 0.00365009 \\ 0.00365009 \\ -0.991238 \\ 1 \end{bmatrix} \right). \quad (l)$$

The natural frequencies are given by  $\omega_i = \sqrt{\lambda_i}$ ,  $i = 1, 2, \dots, 5$ .

$$\begin{bmatrix} \omega_1 & \omega_2 & \omega_3 & \omega_4 & \omega_5 \end{bmatrix} = \begin{bmatrix} 9,997.36 & 8,235.9 & 4,223.3 & 1,701.95 & 924.346 \end{bmatrix} \text{rad/s} \quad (\text{m})$$

The prescribed displacement terms in the matrix equation of motion lead to a generalized force vector defined by

$$\{\bar{Q}_\alpha\} = -[M_{\alpha\beta}]\{\ddot{u}_\beta\} - [K_{\alpha\beta}]\{u_\beta\}. \quad (\text{n})$$

Numerical evaluation of this generalized force vector is

$$\{\bar{Q}_\alpha\} = \begin{bmatrix} -3,032.78 + 0.00148063\Omega^2 \\ 7,581.96 + 0.00181714\Omega^2 \\ 0 \\ -3,032.78 - 0.000874919\Omega^2 \\ 0 \end{bmatrix} \sin \Omega t. \quad (\text{o})$$

The matrix equation of motion governing the unknown displacements is rewritten as

$$[M_{\alpha\alpha}]\{\ddot{u}_\alpha\} + [K_{\alpha\alpha}]\{u_\alpha\} = \{\bar{Q}_\alpha\}. \quad (\text{p})$$

The initial conditions are  $\{u_\alpha(0)\} = 0_{5 \times 1}$  and  $\{\dot{u}_\alpha(0)\} = 0_{5 \times 1}$ . Transform from the physical displacements to the modal displacements by  $\{u_\alpha(t)\} = [\Phi]\{q(t)\}$ , where the columns of the modal matrix  $[\Phi]$  are the eigenvectors. Equations of motion in modal coordinates are

$$[M_g]\ddot{q} + [K_g]\{q\} = \{F_g(t)\}, \quad (\text{q})$$

where the generalized mass, stiffness, and force vector are

$$[M_g] = \text{diag}[0.02135 \ 0.140492 \ 0.0144387 \ 0.0292596 \ 0.098909] \quad (\text{r})$$

$$[K_g] = \text{diag}[2134.77 \ 9529.59 \ 257.532 \ 84.7545 \ 84.5099]10^3,$$

$$\{F_g(t)\} = \{A(\Omega)\}\sin \Omega t, \text{ and where} \quad (\text{s})$$

$$\{A(\Omega)\} = \begin{bmatrix} -1,983.5 + 92.0225 \times 10^{-6} \Omega^2 \\ 7,275.15 - 463.879 \times 10^{-6} \Omega^2 \\ -6,061.51 + 610.799 \times 10^{-6} \Omega^2 \\ -2,953.93 + 1,499.53 \times 10^{-6} \Omega^2 \\ 1.10169 + 2,354.52 \times 10^{-6} \Omega^2 \end{bmatrix}. \quad (\text{t})$$

The equation of motion for each modal coordinate is in the form

$$\ddot{q}_i + \omega_i^2 q_i = \frac{1}{M_g(i,i)} A_i(\Omega) \sin(\Omega t) \quad i = 1, 2, \dots, 5, \quad (\text{u})$$

subject to initial conditions  $q_i(0) = 0$ , and  $\dot{q}_i(0) = 0$ . The solution for  $\Omega \neq \omega_i$  is

$$q_i(t) = \frac{A_i(\Omega)}{M_g(i, i)(\omega_i^2 - \Omega^2)} \left[ \frac{-\Omega}{\omega_i} \sin(\omega_i t) + \sin(\Omega t) \right]. \quad (\text{v})$$

The solution for  $\Omega = \omega_i$  is

$$q_i(t) = \frac{-A_i(\omega_i)}{2M_g(i, i)\omega_i^2} [(\omega_i t) \cos(\omega_i t) - \sin(\omega_i t)]. \quad (\text{w})$$

Transform from modal coordinates to physical coordinates by  $\{u_\alpha(t)\} = [\Phi] \{q(t)\}$ . The vertical displacement at the joint connecting the frame members is  $u_5(t)$ , and for  $\Omega = 0.9\omega_1$  it is

$$u_5(t) = 256.346 \times 10^{-6} \sin(\Omega t) - 333.609 \times 10^{-6} \sin(\omega_5 t) - 151.009 \times 10^{-6} \sin(\omega_4 t) - 47.4688 \times 10^{-6} \sin(\omega_3 t) + 41.6693 \times 10^{-6} \sin(\omega_2 t) + 20.1981 \times 10^{-6} \sin(\omega_1 t) \quad (\text{x})$$

The first term on the right-hand side of  $u_5(t)$  is the forced motion and has the same frequency as the excitation. The remaining five terms on the right-hand side constitute the natural motion with contributions from the five natural frequencies of the frame. A graph of the displacement response is shown in figure 18.9 for  $0 \leq t \leq 20\tau$ , where  $\tau$  is the period of the lowest natural frequency (i.e.,  $\tau = (2\pi)/\omega_5 = 0.006797$  s). The displacement response exhibits the phenomena of *beating*.

Pure undamped beating, in general, is the combination of two sinusoids that have different but closely spaced frequencies, as the two sinusoids pass into and out of phase with each other. (Hallauer, 2016).

In the case of the frame response shown in figure 18.22, the driving frequency  $\Omega$  is close to the lowest natural frequency  $\omega_5$ , and it is the combination of the two sinusoids  $\sin(\Omega t)$  and  $\sin(\omega_5 t)$  that are the source of beating.

For  $\Omega = \omega_5$ , the displacement  $u_5(t)$  is

$$u_5(t) = -0.406236t \cos(\Omega t) + 319.34 \times 10^{-6} \sin(\omega_5 t) - 158.115 \times 10^{-6} \sin(\omega_4 t) - 52.3109 \times 10^{-6} \sin(\omega_3 t) + 45.9088 \times 10^{-6} \sin(\omega_2 t) + 22.3042 \times 10^{-6} \sin(\omega_1 t) \quad (\text{y})$$

A graph of the displacement response is shown in figure 18.23 for  $0 \leq t \leq 10\tau$ , where  $\tau$  is the period of the lowest natural frequency. As shown in the graph, the amplitude of the vibrations for  $\Omega = \omega_5$  increase linearly in time, which is the condition of *resonance*.

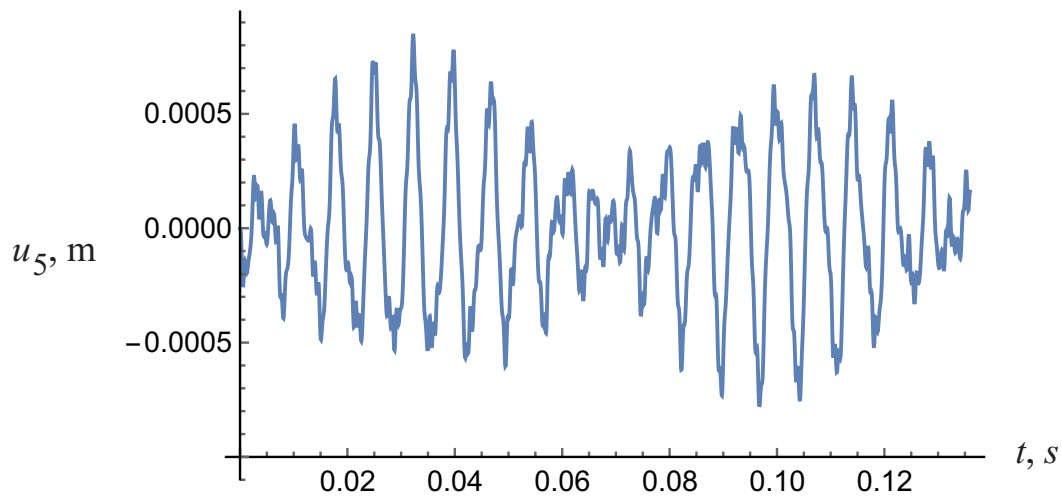


Fig. 18.22 Response of  $u_5(t)$  for  $\Omega = 0.90 \omega_5$ .

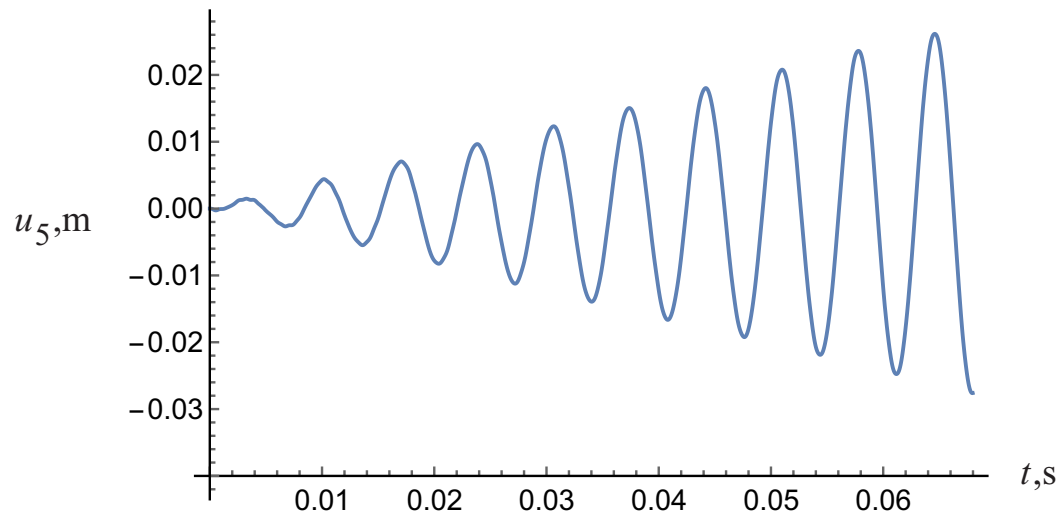


Fig. 18.23 Response of  $u_5(t)$  for  $\Omega = \omega_5$ .

## 18.10 References

- Bathe, K-L. *Finite Element Procedures in Engineering Analysis*. Englewood Cliffs, NJ: Prentice-Hall Inc., 1982.
- Boresi, A. P. *Elasticity In Engineering Mechanics*. Englewood Cliffs, N.J: Prentice-Hall, Inc. 1965, p. 34.
- Craig, Roy R., Jr. *Structural Dynamics: An Introduction to Computer Methods*. New York: John Wiley & Sons,

Inc., 1981, pp. 212-217, 321-340, 455-464.

Hallauer, W. L., Jr., *Introduction to Linear, Time-Invariant, Dynamic Systems for Students of Engineering*. Blacksburg, VA: Self-published, 2016. <http://hdl.handle.net/10919/78864>.

Isakowitz, Steven J. *Space Launch Systems*, 2d ed. Updated by Jeff Samella. Washington DC: American Institute of Aeronautics and Astronautics, 1995, pp. 201-218.

Langhaar, H. L. *Energy Methods in Applied Mechanics*. New York: John Wiley, and Sons, Inc., 1962.

Qu, Zu-Qing. *Model Order Reduction Techniques, With Application to Finite Element Analysis*. London: Springer-Verlag, 2004.

Sarafin, Thomas, P., ed. *Spacecraft Structures and Mechanisms – From Concept to Launch*. Torrance, CA, and Dordrecht, The Netherlands: Microcosom Press, and Kluwer, 1995, pp. 49 & 50.

Schiesser, W. E. *Computational Mathematics in Engineering and Applied Science*. Boca Raton, FL: CRC Press, 1994, Chapter 2.

Szabó, B., and I. Babuska. *Finite Element Analysis*. New York: John Wiley & Sons, 1991, pp. 163-166.

## 18.11 Practice exercises

1. The Lagrangian for a three-degree-of-freedom model of Atlas I is

$$L = \frac{m_1}{6}[(\dot{w}_1)^2 + \dot{w}_1\dot{w}_2 + (\dot{w}_2)^2] + \frac{1}{2}m_2(\dot{w}_2)^2 + \frac{1}{2}m_3(\dot{w}_3)^2 - \frac{1}{2}k_{12}(w_1 - w_2)^2 - \frac{1}{2}k_{23}(w_3 - w_2)^2, \quad (18.196)$$

where  $w_1(t)$  is the displacement at the bottom of the booster,  $w_2(t)$  is the displacement at the top of Centaur, and  $w_3(t)$  is the displacement of the payload. These displacements are defined with respect to the equilibrium state. The combined mass of the booster and Centaur is denoted by  $m_1$ , the mass of the fairing by  $m_2$ , and the mass of the payload by  $m_3$ . Masses are determined from the weight data given in “Description of Atlas I” on page 535. The spring stiffness  $k_{12}$  and  $k_{23}$  are listed in “Step 1: Equations of motion about equilibrium.” on page 538. Lagrange’s equations of motion are

$$\frac{d}{dt}\left(\frac{\partial L}{\partial \dot{w}_1}\right) - \frac{\partial L}{\partial w_1} = R_1 \quad \frac{d}{dt}\left(\frac{\partial L}{\partial \dot{w}_2}\right) - \frac{\partial L}{\partial w_2} = 0 \quad \frac{d}{dt}\left(\frac{\partial L}{\partial \dot{w}_3}\right) - \frac{\partial L}{\partial w_3} = 0, \quad (18.197)$$

where  $R_1 = 77,100$  lb is the net thrust. Determine the maximum payload load factor during the initial instants of lift off. Partial answer: the value and its associated eigenvector for the smallest elastic mode is

$$(\lambda_2, \{\phi_2\}) = \left( 15, 710.5, \begin{bmatrix} -0.795164 \\ 0.760969 \\ 1 \end{bmatrix} \right). \quad (18.198)$$

The eigenvector is normalized such that the magnitude of its largest component is a positive one.

2. Determine the natural frequencies in Hz and the corresponding modal vectors for the five-bar, pin-jointed truss shown in figure 18.24. Normalize the modal vectors such that the largest component in the vector is a positive 1. Sketch the mode shapes.

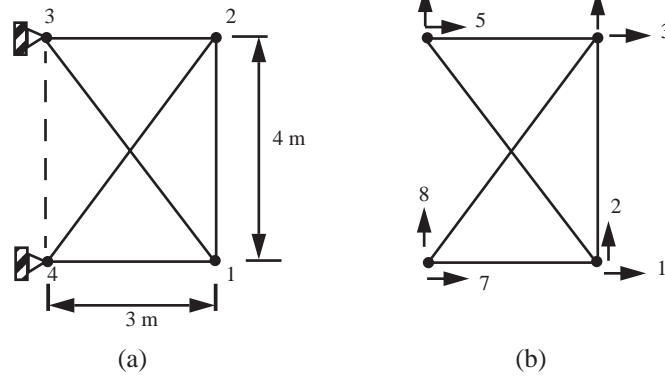
**Fig. 18.24 (a) Five-bar truss, (b) Degrees of freedom.**

All bars

$$E = 70 \text{ GPa}$$

$$A = 475 \times 10^{-6} \text{ m}^2$$

$$\rho = 2,710 \text{ Kg/m}^3$$

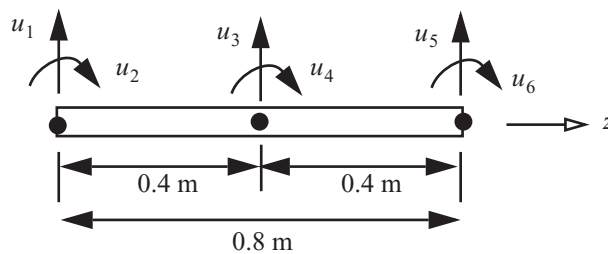


3. The three-bar truss in example 18.3 on page 563 is subjected to the following initial conditions

$$\begin{bmatrix} u_1(0) \\ u_2(0) \end{bmatrix} = \begin{bmatrix} 0 \\ 0 \end{bmatrix} \quad \left. \begin{bmatrix} \frac{du_1}{dt} \\ \frac{du_2}{dt} \end{bmatrix} \right|_{t=0} = \begin{bmatrix} 0 \\ 1 \end{bmatrix} \text{ m/s.} \quad (18.199)$$

- Determine the generalized mass matrix  $[M_g]$ , the generalized stiffness matrix  $[K_g]$ , and the initial conditions in modal coordinates (begin with eqs. (d) and (e)).
  - Determine the solution in modal coordinates and in physical coordinates.
  - Determine the transient bar forces  $N_{1-2}(t)$ ,  $N_{1-3}(t)$ , and  $N_{1-4}(t)$ .
  - Plot the bar forces found in part (c) for  $0 \leq t \leq 0.015 \text{ s}$ .
4. Model the cantilever beam in example 18.4 on page 571 with two equal length elements as shown in figure 18.25.
- Determine the natural frequencies in Hz and the corresponding modal vectors. Normalize the modal vectors such that the tip displacement  $u_5$  is equal to one in each mode. Refer to table 18.4.
  - Determine the percentage error of each frequency with respect to the exact frequency from the continuous beam vibration analysis.
  - Plot the lateral displacement of the beam,  $0 \leq z \leq 0.8 \text{ m}$ , for each mode using eq. (17.69) on page 509 and matrix  $[G_{aq}]$  from the last three rows of eq. (18.162).

**Fig. 18.25 Beam of example 18.4 modeled with two elements.**





5. The uniform beam shown in figure 18.26 is simply supported at each end. The material and geometric properties are the same as those given in example 18.4,

- a. Determine the first two natural frequencies in Hz for the beam modeled with **one** element. Use the condensed mass matrix (18.167) and stiffness matrix (17.106) on page 515.
- b. Compute the percent discrepancy of the frequencies with respect to the continuous beam solution. The frequencies for the continuous beam vibration analysis in rad/s are listed in Graig

$$(1981) \text{ as } \omega_n = \left(\frac{n\pi}{l}\right)^2 \sqrt{\frac{EI_{xx}}{\rho A}} \quad n = 1, 2.$$

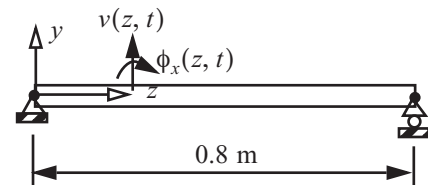


Fig. 18.26 Simply supported beam.



# *Linear elasticity of solid bodies*

Solid mechanics is a branch of continuum mechanics that studies the behavior of solid materials under the action of forces, temperature changes, or other external agents. Elasticity is a branch of solid mechanics that refers to the ability of the body to return to its original size and shape after the forces causing deformation are removed. In this appendix the basic equations of the three-dimensional elasticity theory are developed at material point in the body. A material point, or particle, is identified by its position in a rectangular cartesian coordinate system  $(x_1, x_2, x_3)$ . The fundamental equations of elasticity consist of the geometry of deformation in Article A.1, the stresses and equilibrium in Article A.2, and the stress-deformation relations in Article A.3. The focus is on the classical linear elasticity theory in which the strains are small with respect to unity and the material is linear elastic. The basic equations are summarized in Article A.4 along with a description of the boundary value problems of elasticity ,

## *A.1 Geometry of deformation*

A continuous three-dimensional body occupies a closed region denoted by  $B_0$  in the reference state. Let every point of  $B_0$  be defined in a fixed rectangular cartesian system of axes  $x_1, x_2, x_3$ . Let  $B$  denote the closed region of the body after it undergoes a deformation. The position vector of the point  $P_0$  in region  $B_0$  with respect to the origin is

$$\vec{r} = x_1 \hat{i}_1 + x_2 \hat{i}_2 + x_3 \hat{i}_3, \quad (\text{A.1})$$

where the unit vectors along the fixed axes are  $\hat{i}_1, \hat{i}_2, \hat{i}_3$ . The particle at  $P_0(x_1, x_2, x_3)$  passes to point  $P(y_1, y_2, y_3)$  in region  $B$ , where coordinates  $(y_1, y_2, y_3)$  are defined in the same fixed coordinate system. See Fig. A.1. The position vector of point  $P$  referred to the same origin is

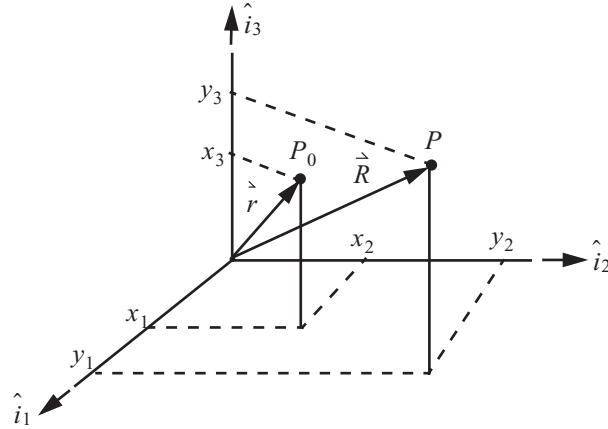
$$\vec{R} = y_1 \hat{i}_1 + y_2 \hat{i}_2 + y_3 \hat{i}_3. \quad (\text{A.2})$$

The deformation of the body is defined by the equations

$$y_1 = y_1(x_1, x_2, x_3) \quad y_2 = y_2(x_1, x_2, x_3) \quad y_3 = y_3(x_1, x_2, x_3), \quad (\text{A.3})$$

where  $x_1, x_2, x_3$  are restricted to  $B_0$  and  $(y_1, y_2, y_3)$  are restricted to  $B$ . In eq. (A.3) the  $y_i$ ,  $i = 1, 2, 3$ , on the

**Fig. A.1** A particle at point  $P_0:(x_1, x_2, x_3)$  in the reference configuration of the body and its position  $P:(y_1, y_2, y_3)$  in the body after deformation.



right-hand side denotes a function of three variables  $x_1, x_2, x_3$ , and  $y_i$  on the left-hand side denotes the value of the function. Equation (A.3) defines the final location of the particle in  $B$  that is located at point  $P_0$  in  $B_0$ . To prohibit the possibility that a particle at point  $P$  in region  $B$  maps to more than one point in region  $B_0$ , or visa versa, it is required that there is a one-to-one correspondence between points in regions  $B_0$  and  $B$ . It follows that in region  $B$  eqs. (A.3) have single-valued solutions

$$x_1 = x_1(y_1, y_2, y_3) \quad x_2 = x_2(y_1, y_2, y_3) \quad x_3 = x_3(y_1, y_2, y_3) \quad (\text{A.4})$$

The functions defined in eqs. (A.3) and (A.4) are assumed to be continuous and differentiable in their respective variables. Continuity insures no fracture of the body results in the deformation. If we choose eq. (A.3) to describe the deformation of the body then  $x_1, x_2, x_3$  are the independent variables, and the formulation is called the Lagrangian or the referential or material description. In the Lagrangian formulation we follow the particle originally at point  $P_0:(x_1, x_2, x_3)$  as the deformation proceeds. If we choose eq. (A.4) to describe the deformation of the body then  $y_1, y_2, y_3$  are the independent variables, and the formulation is called the Eulerian or spatial description. In the Eulerian formulation the same fixed spatial position  $y_1, y_2, y_3$  is occupied by different particles as the deformation proceeds. The Lagrangian description of the deformation is selected for the developments that follow in this appendix. The position vector of point  $P$  relative to point  $P_0$  is denoted by  $\vec{u}$  and is called the displacement vector. Thus,

$$\vec{u} = \vec{R} - \vec{r} = (y_1 - x_1)\hat{i}_1 + (y_2 - x_2)\hat{i}_2 + (y_3 - x_3)\hat{i}_3. \quad (\text{A.5})$$

Components of the displacement vector are

$$\begin{aligned} u_1(x_1, x_2, x_3) &= y_1(x_1, x_2, x_3) - x_1 \\ u_2(x_1, x_2, x_3) &= y_2(x_1, x_2, x_3) - x_2 \\ u_3(x_1, x_2, x_3) &= y_3(x_1, x_2, x_3) - x_3 \end{aligned} \quad (\text{A.6})$$

Deformation is quantified by the change in distance between any two points in a body. Consider two infinitesimally close points  $P_0$  and  $Q_0$  in region  $B_0$  that pass to points  $P$  and  $Q$ , respectively, in region  $B$ . The differential line element  $\widehat{P_0Q_0}$  in region  $B_0$  shown in Fig. A.2(a) passes to the differential line element  $\widehat{PQ}$  in region  $B$  shown in Fig. A.2(b). The differential position vector of line element  $\widehat{P_0Q_0}$  is  $\vec{dr} = dx_1\hat{i}_1 + dx_2\hat{i}_2 + dx_3\hat{i}_3$ . The square of the length of  $\vec{dr}$  is given by  $ds^2 = \vec{dr} \cdot \vec{dr} = (dx_1)^2 + (dx_2)^2 + (dx_3)^2$ . The unit vector of point  $Q_0$  with respect to point  $P_0$  is given by

$$\hat{n} = \frac{\vec{dr}}{ds} = \frac{dx_1}{ds}\hat{i}_1 + \frac{dx_2}{ds}\hat{i}_2 + \frac{dx_3}{ds}\hat{i}_3.$$

Write this unit vector as

$$\hat{n} = n_1\hat{i}_1 + n_2\hat{i}_2 + n_3\hat{i}_3, \quad (\text{A.7})$$

where  $n_i = \frac{dx_i}{ds}$ ,  $i = 1, 2, 3$ . The differential position vector of  $\widehat{PQ}$  is  $\vec{dR} = dy_1\hat{i}_1 + dy_2\hat{i}_2 + dy_3\hat{i}_3$ , and the square of its length is  $dS^2 = \vec{dR} \cdot \vec{dR} = (dy_1)^2 + (dy_2)^2 + (dy_3)^2$ . Write the differential vector as  $\vec{dR} = dS\hat{N}$  where the unit vector of point  $Q$  with respect to point  $P$  is

$$\hat{N} = \frac{dy_1}{dS}\hat{i}_1 + \frac{dy_2}{dS}\hat{i}_2 + \frac{dy_3}{dS}\hat{i}_3 = N_1\hat{i}_1 + N_2\hat{i}_2 + N_3\hat{i}_3 \quad (\text{A.8})$$

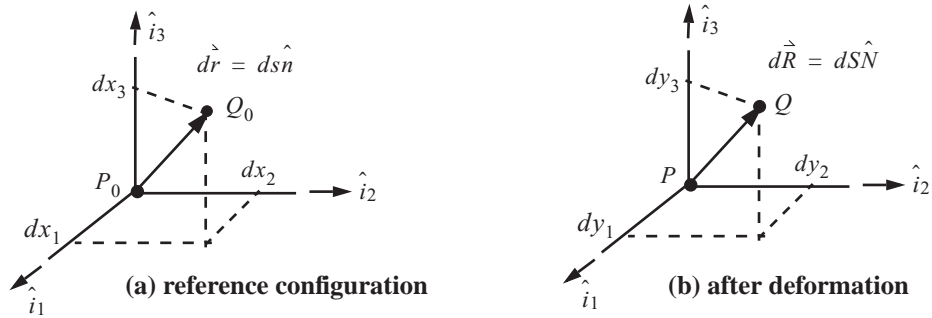


**Fig. A.2** (a) Line element  $\widehat{P_0Q_0}$  passes to (b) line element  $\widehat{PQ}$

The total differentials  $(dy_1, dy_2, dy_3)$  of the functions  $y_1(x_1, x_2, x_3)$ ,  $y_2(x_1, x_2, x_3)$ ,  $y_3(x_1, x_2, x_3)$ , are written in terms of the total differentials  $(dx_1, dx_2, dx_3)$  by

$$\begin{bmatrix} dy_1 \\ dy_2 \\ dy_3 \end{bmatrix} = \begin{bmatrix} \frac{\partial y_1}{\partial x_1} & \frac{\partial y_1}{\partial x_2} & \frac{\partial y_1}{\partial x_3} \\ \frac{\partial y_2}{\partial x_1} & \frac{\partial y_2}{\partial x_2} & \frac{\partial y_2}{\partial x_3} \\ \frac{\partial y_3}{\partial x_1} & \frac{\partial y_3}{\partial x_2} & \frac{\partial y_3}{\partial x_3} \end{bmatrix} \begin{bmatrix} dx_1 \\ dx_2 \\ dx_3 \end{bmatrix}. \quad (\text{A.9})$$

The determinate of the 3X3 matrix in eq. (A.3) is

$$J = \det \begin{bmatrix} \frac{\partial y_1}{\partial x_1} & \frac{\partial y_1}{\partial x_2} & \frac{\partial y_1}{\partial x_3} \\ \frac{\partial y_2}{\partial x_1} & \frac{\partial y_2}{\partial x_2} & \frac{\partial y_2}{\partial x_3} \\ \frac{\partial y_3}{\partial x_1} & \frac{\partial y_3}{\partial x_2} & \frac{\partial y_3}{\partial x_3} \end{bmatrix}, \quad (\text{A.10})$$

where  $J$  is called the Jacobian. Equations (A.3) possess a continuous single-valued solution satisfying the inverse (A.4) if and only if the Jacobian is positive for all points in region  $B_0$  (Batra, 2006). The strain of line element

$\widehat{PQ}$  is defined by

$$\epsilon_L = \frac{1}{2} \left[ \frac{dS^2 - ds^2}{ds^2} \right] = \frac{1}{2} \left[ \left( \frac{dS}{ds} \right)^2 - 1 \right]. \quad (\text{A.11})$$

Use the chain rule to write the square of the length of line element  $\widehat{PQ}$  with respect to the square of the length of line element  $\widehat{P_0Q_0}$  as

$$dS^2 = \left[ \left( \frac{dy_1}{ds} \right)^2 + \left( \frac{dy_2}{ds} \right)^2 + \left( \frac{dy_3}{ds} \right)^2 \right] ds^2. \quad (\text{A.12})$$

From eq. (A.9) use the chain rule again to write the differential  $dy_1$  as follows:

$$dy_1 = \frac{\partial y_1}{\partial x_1} dx_1 + \frac{\partial y_1}{\partial x_2} dx_2 + \frac{\partial y_1}{\partial x_3} dx_3 = \left[ \frac{\partial y_1}{\partial x_1} \frac{dx_1}{ds} + \frac{\partial y_1}{\partial x_2} \frac{dx_2}{ds} + \frac{\partial y_1}{\partial x_3} \frac{dx_3}{ds} \right] ds$$

Substitute  $dx_i/ds = n_i$  from eq. (A.7), and substitute  $u_1 + x_1$  for coordinate  $y_1$  from eq. (A.6), into the last expression for  $dy_1$  to get

$$\frac{dy_1}{ds} = \left[ \left( 1 + \frac{\partial u_1}{\partial x_1} \right) n_1 + \frac{\partial u_1}{\partial x_2} n_2 + \frac{\partial u_1}{\partial x_3} n_3 \right]. \quad (\text{A.13})$$

Starting with differentials  $dy_2$  and  $dy_3$  from eq. (A.9), we perform similar manipulations leading to eq. (A.13) to find

$$\frac{dy_2}{ds} = \left[ \frac{\partial u_2}{\partial x_1} n_1 + \left( 1 + \frac{\partial u_2}{\partial x_2} \right) n_2 + \frac{\partial u_2}{\partial x_3} n_3 \right] \quad \frac{dy_3}{ds} = \left[ \frac{\partial u_3}{\partial x_1} n_1 + \frac{\partial u_3}{\partial x_2} n_2 + \left( 1 + \frac{\partial u_3}{\partial x_3} \right) n_3 \right]. \quad (\text{A.14})$$

Substitute eq. (A.12) into eq. (A.11) to write the equivalent expression for the strain in eq. (A.11) as

$$\epsilon_L = \frac{1}{2} \left[ \left( \frac{dy_1}{ds} \right)^2 + \left( \frac{dy_2}{ds} \right)^2 + \left( \frac{dy_3}{ds} \right)^2 - (n_1^2 + n_2^2 + n_3^2) \right], \quad (\text{A.15})$$

and use the fact that  $n_1^2 + n_2^2 + n_3^2 = 1$ . Substitute the results from eqs. (A.13) and (A.14) into eq. (A.15) and write the result as

$$\varepsilon_L = \varepsilon_{11}n_1^2 + \varepsilon_{12}n_1n_2 + \varepsilon_{13}n_1n_3 + \varepsilon_{21}n_2n_1 + \varepsilon_{22}n_2^2 + \varepsilon_{23}n_2n_3 + \varepsilon_{31}n_3n_1 + \varepsilon_{32}n_3n_2 + \varepsilon_{33}n_3^2. \quad (\text{A.16})$$

The expression (A.16) for the strain can be written in the matrix form

$$\varepsilon_L = \begin{bmatrix} n_1 & n_2 & n_3 \end{bmatrix} \begin{bmatrix} \varepsilon_{11} & \varepsilon_{12} & \varepsilon_{13} \\ \varepsilon_{21} & \varepsilon_{22} & \varepsilon_{23} \\ \varepsilon_{31} & \varepsilon_{32} & \varepsilon_{33} \end{bmatrix} \begin{bmatrix} n_1 \\ n_2 \\ n_3 \end{bmatrix}. \quad (\text{A.17})$$

The coefficients in the expression for the strain are as follows:

$$\varepsilon_{11} = \frac{\partial u_1}{\partial x_1} + \frac{1}{2} \left[ \left( \frac{\partial u_1}{\partial x_1} \right)^2 + \left( \frac{\partial u_2}{\partial x_1} \right)^2 + \left( \frac{\partial u_3}{\partial x_1} \right)^2 \right] \quad (\text{A.18})$$

$$\varepsilon_{22} = \frac{\partial u_2}{\partial x_2} + \frac{1}{2} \left[ \left( \frac{\partial u_1}{\partial x_2} \right)^2 + \left( \frac{\partial u_2}{\partial x_2} \right)^2 + \left( \frac{\partial u_3}{\partial x_2} \right)^2 \right] \quad (\text{A.19})$$

$$\varepsilon_{33} = \frac{\partial u_3}{\partial x_3} + \frac{1}{2} \left[ \left( \frac{\partial u_1}{\partial x_3} \right)^2 + \left( \frac{\partial u_2}{\partial x_3} \right)^2 + \left( \frac{\partial u_3}{\partial x_3} \right)^2 \right] \quad (\text{A.20})$$

$$\varepsilon_{12} = \varepsilon_{21} = \frac{1}{2} \left[ \frac{\partial u_1}{\partial x_2} + \frac{\partial u_2}{\partial x_1} + \frac{\partial u_1}{\partial x_1} \frac{\partial u_1}{\partial x_2} + \frac{\partial u_2}{\partial x_1} \frac{\partial u_2}{\partial x_2} + \frac{\partial u_3}{\partial x_1} \frac{\partial u_3}{\partial x_2} \right] \quad (\text{A.21})$$

$$\varepsilon_{13} = \varepsilon_{31} = \frac{1}{2} \left[ \frac{\partial u_1}{\partial x_3} + \frac{\partial u_3}{\partial x_1} + \frac{\partial u_1}{\partial x_1} \frac{\partial u_1}{\partial x_3} + \frac{\partial u_2}{\partial x_1} \frac{\partial u_2}{\partial x_3} + \frac{\partial u_3}{\partial x_1} \frac{\partial u_3}{\partial x_3} \right] \quad (\text{A.22})$$

$$\varepsilon_{23} = \varepsilon_{32} = \frac{1}{2} \left[ \frac{\partial u_2}{\partial x_3} + \frac{\partial u_3}{\partial x_2} + \frac{\partial u_1}{\partial x_2} \frac{\partial u_1}{\partial x_3} + \frac{\partial u_2}{\partial x_2} \frac{\partial u_2}{\partial x_3} + \frac{\partial u_3}{\partial x_2} \frac{\partial u_3}{\partial x_3} \right] \quad (\text{A.23})$$

### A.1.1 Physical interpretation of strain components $\varepsilon_{ij}$

For the line element parallel to the  $x_1$ -axis in the reference configuration the components of the unit vector are  $(n_1, n_2, n_3) = (1, 0, 0)$ , and from eq. (A.16) its strain is given by  $\varepsilon_L = \varepsilon_{11}$ . For line element parallel to the  $x_2$ -axis the components of the unit vector are  $(n_1, n_2, n_3) = (0, 1, 0)$ , and its strain is given by  $\varepsilon_L = \varepsilon_{22}$ . For the line element parallel to the  $x_3$  axis its strain is  $\varepsilon_L = \varepsilon_{33}$ . The physical interpretation of component  $\varepsilon_{12}$  is determined from the passing of line elements  $dx_1 \hat{i}_1$  and  $dx_2 \hat{i}_2$  in region  $B_0$  to directions  $(\hat{N})_1$  and  $(\hat{N})_2$ , respectively, in region  $B$ . In general the components of unit vector  $\hat{N}$  are given by

$$N_i = \frac{dy_i}{dS} = \frac{dy_i ds}{ds dS} = \frac{dy_i}{ds} \left( \frac{1}{\sqrt{1 + 2\varepsilon_L}} \right) = \left( \frac{\partial y_i}{\partial x_1} n_1 + \frac{\partial y_i}{\partial x_2} n_2 + \frac{\partial y_i}{\partial x_3} n_3 \right) \left( \frac{1}{\sqrt{1 + 2\varepsilon_L}} \right), \quad i = 1, 2, 3. \quad (\text{A.24})$$

If we take  $(n_1, n_2, n_3) = (1, 0, 0)$  in eq. (A.24), then  $\varepsilon_L = \varepsilon_{11}$  and in the transition from region  $B_0$  to region  $B$  the unit vector  $\hat{i}_1 \rightarrow (\hat{N})_1$ . The unit vector  $(\hat{N})_1$  is given by

$$(\hat{N})_1 = \left[ \frac{\partial y_1}{\partial x_1} \hat{i}_1 + \frac{\partial y_2}{\partial x_1} \hat{i}_2 + \frac{\partial y_3}{\partial x_1} \hat{i}_3 \right] \left( \frac{1}{\sqrt{1 + 2\varepsilon_{11}}} \right). \quad (\text{A.25})$$

If we take  $(n_1, n_2, n_3) = (0, 1, 0)$  in eq. (A.24), then  $\varepsilon_L = \varepsilon_{22}$  and the transition of the unit vector is  $\hat{i}_2 \rightarrow (\hat{N})_2$ . The result for  $(\hat{N})_2$  is

$$(\hat{N})_2 = \left[ \frac{\partial y_1}{\partial x_2} \hat{i}_1 + \frac{\partial y_2}{\partial x_2} \hat{i}_2 + \frac{\partial y_3}{\partial x_2} \hat{i}_3 \right] \left( \frac{1}{\sqrt{1 + 2\varepsilon_{22}}} \right). \quad (\text{A.26})$$

The scalar product of the two unit vectors  $(\hat{N})_1$  and  $(\hat{N})_2$  is equal to the cosine of the angle between them. Let this angle be denoted by  $\pi/2 - \theta_{12}$  such that,

$$(\hat{N})_1 \cdot (\hat{N})_2 = \cos\left(\frac{\pi}{2} - \theta_{12}\right) = \sin\theta_{12}, \quad (\text{A.27})$$

where  $\theta_{12}$  denotes the change in the angle with respect to a right angle. Substitute eq. (A.25) for  $(\hat{N})_1$  and eq. (A.26) for  $(\hat{N})_2$  in the left-hand side of eq. (A.27) to get

$$\sin\theta_{12} = \left[ \frac{\partial y_1}{\partial x_1} \frac{\partial y_1}{\partial x_2} + \frac{\partial y_2}{\partial x_1} \frac{\partial y_2}{\partial x_2} + \frac{\partial y_3}{\partial x_1} \frac{\partial y_3}{\partial x_2} \right] \frac{1}{\sqrt{1 + 2\varepsilon_{11}} \sqrt{1 + 2\varepsilon_{22}}}.$$

Next substitute  $y_i = u_i + x_i$ ,  $i = 1, 2, 3$ , in the terms in the square brackets of the previous equation, and compare the result to eq. (A.21) to find

$$\sin\theta_{12} = \frac{2\varepsilon_{12}}{\sqrt{1 + 2\varepsilon_{11}} \sqrt{1 + 2\varepsilon_{22}}}. \quad (\text{A.28})$$

Thus, the right angle between line elements  $dx_1 \hat{i}_1$  and  $dx_2 \hat{i}_2$  in region  $B_0$  is changed in the transition to region  $B$  in direct proportion to the strain component  $\varepsilon_{12}$ . If  $\varepsilon_{12} = 0$ , then  $\theta_{12} = 0$ , and the right angle is preserved in the deformed body. Similarly, the strain component  $\varepsilon_{13}$  is proportional the change in the right angle between line elements  $dx_1$  and  $dx_3$  in the transition to the deformed body.

### A.1.2 Engineering strain

Engineering strain is defined by

$$\varepsilon_E = \frac{dS - ds}{ds} = \frac{dS}{ds} - 1 \quad (\text{A.29})$$

Substitute for  $dS/ds$  from eq. (A.29) into eq. (A.11) to get  $\varepsilon_L = \varepsilon_E + \varepsilon_E^2/2$ . Equation (A.16) can be written in the equivalent form

$$\varepsilon_L = \varepsilon_E + \frac{1}{2} \varepsilon_E^2 = \varepsilon_{11} n_1^2 + \varepsilon_{22} n_2^2 + \varepsilon_{33} n_3^2 + \gamma_{12} n_1 n_2 + \gamma_{13} n_1 n_3 + \gamma_{23} n_2 n_3, \quad (\text{A.30})$$

since the product of the direction cosines commute. In eq. (A.30) the engineering the shear strains are defined by

$$\gamma_{12} = \varepsilon_{12} + \varepsilon_{21} \quad \gamma_{13} = \varepsilon_{13} + \varepsilon_{31} \quad \gamma_{23} = \varepsilon_{23} + \varepsilon_{32}. \quad (\text{A.31})$$



### A.1.3 Linear strain-displacement relations

For many materials the strains are very small in the elastic range. A linear theory of deformation is characterized by the magnitude of the nine displacement gradients  $\left| \frac{\partial u_i}{\partial x_j} \right| \sim 10^{-3}$ . Hence, we neglect the quadratic terms in the displacement gradients with respect to the linear terms in the strain-displacement eqs. (A.18) to (A.23). The resulting linear strain-displacement relations are

$$\epsilon_{11} = \frac{\partial u_1}{\partial x_1} \quad \epsilon_{22} = \frac{\partial u_2}{\partial x_2} \quad \epsilon_{33} = \frac{\partial u_3}{\partial x_3}, \quad (\text{A.32})$$

$$\gamma_{12} = \frac{\partial u_1}{\partial x_2} + \frac{\partial u_2}{\partial x_1} \quad \gamma_{13} = \frac{\partial u_1}{\partial x_3} + \frac{\partial u_3}{\partial x_1} \quad \gamma_{23} = \frac{\partial u_2}{\partial x_3} + \frac{\partial u_3}{\partial x_2}, \text{ and} \quad (\text{A.33})$$

$$\epsilon_E = \epsilon_{11}n_1^2 + \epsilon_{22}n_2^2 + \epsilon_{33}n_3^2 + \gamma_{12}n_1n_2 + \gamma_{13}n_1n_3 + \gamma_{23}n_2n_3. \quad (\text{A.34})$$

### A.1.4 Transformation of the strains between two cartesian coordinate systems

In the reference configuration  $B_0$  consider the two orthogonal cartesian coordinate systems  $(x_1, x_2, x_3)$  and  $(x_1', x_2', x_3')$  which have the same origin. In  $(x_1, x_2, x_3)$  system, or simply the  $x_i$  system, the corresponding unit vectors are  $(\hat{i}_1, \hat{i}_2, \hat{i}_3)$ . In the  $(x_1', x_2', x_3')$  system, or the  $x_i'$  system, the corresponding unit vectors are  $(\hat{i}_1', \hat{i}_2', \hat{i}_3')$ . The position vector  $\vec{r}$  of a point  $P_0$  in space is the same if written in the  $x_i$ -system or in the  $x_i'$ -system. That is,

$$\vec{r} = x_1\hat{i}_1 + x_2\hat{i}_2 + x_3\hat{i}_3 = x_1'\hat{i}_1' + x_2'\hat{i}_2' + x_3'\hat{i}_3' \quad (\text{A.35})$$

The linear form  $x_1\hat{i}_1 + x_2\hat{i}_2 + x_3\hat{i}_3$  is said to remain **invariant** under the transformation of variables. Take the scalar product, or dot product, of eq. (A.35) with unit vector  $\hat{i}_1'$  to get

$$x_1\hat{i}_1 \cdot \hat{i}_1' + x_2\hat{i}_2 \cdot \hat{i}_1' + x_3\hat{i}_3 \cdot \hat{i}_1' = x_1'. \quad (\text{A.36})$$

Define the nine direction cosines  $\lambda_{ij}$ ,  $i, j = 1, 2, 3$ , by

$$\hat{i}_i' \cdot \hat{i}_j \equiv \lambda_{ij} = \cos(x_i', x_j). \quad (\text{A.37})$$

For example,  $\lambda_{12} = \cos(x_1', x_2)$  is the cosine of the angle between the  $x_1'$  axis and the  $x_2$  axis, and  $\lambda_{21} = \cos(x_2', x_1)$  is the cosine of the angle between the  $x_2'$  axis and the  $x_1$  axis. From the definition of  $\lambda_{ij}$  eq. (A.36) is  $x_1' = \lambda_{11}x_1 + \lambda_{12}x_2 + \lambda_{13}x_3$ . If we take the dot product of eq. (A.35) with  $\hat{i}_2'$  and use the definition (A.37), then we find  $x_2' = \lambda_{21}x_1 + \lambda_{22}x_2 + \lambda_{23}x_3$ . The relation between the  $x_i'$  coordinates and the  $x_i$  coordinates at point  $P_0$  is given by the linear transformation

$$\begin{bmatrix} x_1' \\ x_2' \\ x_3' \end{bmatrix} = \begin{bmatrix} \lambda_{11} & \lambda_{12} & \lambda_{13} \\ \lambda_{21} & \lambda_{22} & \lambda_{23} \\ \lambda_{31} & \lambda_{32} & \lambda_{33} \end{bmatrix} \begin{bmatrix} x_1 \\ x_2 \\ x_3 \end{bmatrix}. \quad (\text{A.38})$$

The compact form of matrix eq. (A.38) is

$$\{x'\} = [\lambda] \{x\}, \text{ where} \quad (\text{A.39})$$

$$\{x'\} = \begin{bmatrix} x_1' \\ x_2' \\ x_3' \end{bmatrix} \quad [\lambda] = \begin{bmatrix} \lambda_{11} & \lambda_{12} & \lambda_{13} \\ \lambda_{21} & \lambda_{22} & \lambda_{23} \\ \lambda_{31} & \lambda_{32} & \lambda_{33} \end{bmatrix} \quad \{x\} = \begin{bmatrix} x_1 \\ x_2 \\ x_3 \end{bmatrix}. \quad (\text{A.40})$$

The unit vectors in the  $x_i'$  system are related to those in the  $x_i$  system by the same relation given in eq. (A.38):

$$\begin{bmatrix} \hat{i}_1' \\ \hat{i}_2' \\ \hat{i}_3' \end{bmatrix} = \begin{bmatrix} \lambda_{11} & \lambda_{12} & \lambda_{13} \\ \lambda_{21} & \lambda_{22} & \lambda_{23} \\ \lambda_{31} & \lambda_{32} & \lambda_{33} \end{bmatrix} \begin{bmatrix} \hat{i}_1 \\ \hat{i}_2 \\ \hat{i}_3 \end{bmatrix}. \quad (\text{A.41})$$

Consider the dot product  $\hat{i}_1' \cdot \hat{i}_1' = 1$ , and from eq. (A.41) write it in terms of the unit vectors in the  $x_i$  system; i.e.,

$$1 = (\lambda_{11}\hat{i}_1 + \lambda_{12}\hat{i}_2 + \lambda_{13}\hat{i}_3) \cdot (\lambda_{11}\hat{i}_1 + \lambda_{12}\hat{i}_2 + \lambda_{13}\hat{i}_3).$$

Since unit vectors  $(\hat{i}_1, \hat{i}_2, \hat{i}_3)$  are mutually perpendicular we find the relation

$$1 = \lambda_{11}^2 + \lambda_{12}^2 + \lambda_{13}^2.$$

Consider the dot product  $\hat{i}_1' \cdot \hat{i}_2' = 0$  and write  $\hat{i}_1'$  and  $\hat{i}_2'$  from eq. (A.41) to get

$$0 = (\lambda_{11}\hat{i}_1 + \lambda_{12}\hat{i}_2 + \lambda_{13}\hat{i}_3) \cdot (\lambda_{21}\hat{i}_1 + \lambda_{22}\hat{i}_2 + \lambda_{23}\hat{i}_3).$$

Again  $(\hat{i}_1, \hat{i}_2, \hat{i}_3)$  are mutually perpendicular, so we find the relation

$$0 = \lambda_{11}\lambda_{21} + \lambda_{12}\lambda_{22} + \lambda_{13}\lambda_{23}.$$

We can proceed by performing the scalar products  $\hat{i}_1' \cdot \hat{i}_3' = 0$ ,  $\hat{i}_2' \cdot \hat{i}_2' = 1$ ,  $\hat{i}_2' \cdot \hat{i}_3' = 0$ , and  $\hat{i}_3' \cdot \hat{i}_3' = 1$ . Collectively we find the following relations between the direction cosines:

$$\begin{aligned} 1 &= \lambda_{11}^2 + \lambda_{12}^2 + \lambda_{13}^2, & 1 &= \lambda_{21}^2 + \lambda_{22}^2 + \lambda_{23}^2, & \text{and } 1 &= \lambda_{31}^2 + \lambda_{32}^2 + \lambda_{33}^2. \\ 0 &= \lambda_{11}\lambda_{21} + \lambda_{12}\lambda_{22} + \lambda_{13}\lambda_{23}, & 0 &= \lambda_{21}\lambda_{31} + \lambda_{22}\lambda_{32} + \lambda_{23}\lambda_{33}, & & \\ 0 &= \lambda_{11}\lambda_{31} + \lambda_{12}\lambda_{32} + \lambda_{13}\lambda_{33} \end{aligned} \quad (\text{A.42})$$

There are six relations in eq. (A.42) between the nine direction cosines. Hence, only three of direction cosines are independent. We show some interesting properties of the direction cosine matrix  $[\lambda]$  beginning with the matrix

product  $[\lambda][\lambda]^T$ . The result is

$$[\lambda][\lambda]^T = \begin{bmatrix} \lambda_{11}^2 + \lambda_{12}^2 + \lambda_{13}^2 & \lambda_{11}\lambda_{21} + \lambda_{12}\lambda_{22} + \lambda_{13}\lambda_{23} & \lambda_{11}\lambda_{31} + \lambda_{12}\lambda_{32} + \lambda_{13}\lambda_{33} \\ \lambda_{11}\lambda_{21} + \lambda_{12}\lambda_{22} + \lambda_{13}\lambda_{23} & \lambda_{21}^2 + \lambda_{22}^2 + \lambda_{23}^2 & \lambda_{21}\lambda_{31} + \lambda_{22}\lambda_{32} + \lambda_{23}\lambda_{33} \\ \lambda_{11}\lambda_{31} + \lambda_{12}\lambda_{32} + \lambda_{13}\lambda_{33} & \lambda_{21}\lambda_{31} + \lambda_{22}\lambda_{32} + \lambda_{23}\lambda_{33} & \lambda_{31}^2 + \lambda_{32}^2 + \lambda_{33}^2 \end{bmatrix}. \quad (\text{A.43})$$

Compare the elements of the matrix in eq. (A.43) to the relations in eq. (A.42) to find

$$[\lambda][\lambda]^T = \begin{bmatrix} 1 & 0 & 0 \\ 0 & 1 & 0 \\ 0 & 0 & 1 \end{bmatrix} = [I]. \quad (\text{A.44})$$

Equation (A.44) shows that the matrix  $[\lambda]$  is an **orthogonal matrix**. That is, the inverse  $[\lambda]^{-1}$  is equal to its transpose  $[\lambda]^T$ . Also  $\det([\lambda][\lambda]^T) = \det[\lambda]\det[\lambda]^T$ , but  $\det[\lambda]^T = \det[\lambda]$ . Hence,

$$\det([\lambda][\lambda]^T) = (\det[\lambda])^2 = (\det[I])^2 = 1.$$

The determinate of an orthogonal matrix is either 1 or -1. The inverse of eq. (A.39) is  $\{x\} = [\lambda]^T\{x'\}$  which written in expanded form is

$$\begin{bmatrix} x_1 \\ x_2 \\ x_3 \end{bmatrix} = \begin{bmatrix} \lambda_{11} & \lambda_{12} & \lambda_{13} \\ \lambda_{21} & \lambda_{22} & \lambda_{23} \\ \lambda_{31} & \lambda_{32} & \lambda_{33} \end{bmatrix} \begin{bmatrix} x_1' \\ x_2' \\ x_3' \end{bmatrix}. \quad (\text{A.45})$$

From eq. (A.35) with obtain the unit vector  $\hat{n}$  in both the  $x_i$  system and the  $x_i'$  system in the invariant forms

$$\hat{n} = \frac{dr}{ds} = \frac{dx_1}{ds}\hat{i}_1 + \frac{dx_2}{ds}\hat{i}_2 + \frac{dx_3}{ds}\hat{i}_3 = \frac{dx_1'}{ds}\hat{i}_1' + \frac{dx_2'}{ds}\hat{i}_2' + \frac{dx_3'}{ds}\hat{i}_3'. \quad (\text{A.46})$$

The derivatives of the coordinates in eq. (A.46) are obtained from eq. (A.38). These derivatives are

$$\begin{bmatrix} \frac{dx_1'}{ds} \\ \frac{dx_2'}{ds} \\ \frac{dx_3'}{ds} \end{bmatrix} = \begin{bmatrix} \lambda_{11} & \lambda_{12} & \lambda_{13} \\ \lambda_{21} & \lambda_{22} & \lambda_{23} \\ \lambda_{31} & \lambda_{32} & \lambda_{33} \end{bmatrix} \begin{bmatrix} \frac{dx_1}{ds} \\ \frac{dx_2}{ds} \\ \frac{dx_3}{ds} \end{bmatrix}. \quad (\text{A.47})$$

Let  $n_i = \frac{dx_i}{ds}$  and  $n_i' = \frac{dx_i'}{ds}$ ,  $i = 1, 2, 3$ . The matrix form of eq. (A.47) is

$$\{n'\} = [\lambda]\{n\}, \quad (\text{A.48})$$

where we write the unit vector in matrix notation as  $\{n\} = [n_1 \ n_2 \ n_3]^T$  and  $\{n'\} = [n_1' \ n_2' \ n_3']^T$ . The inverse of eq. (A.48) is

$$\{n\} = [\lambda]^T \{n'\}. \quad (\text{A.49})$$

The strain components  $\varepsilon_{ij}$  are functions in the variables  $(x_1, x_2, x_3)$ , and the strains  $\varepsilon_{ij}'$  are functions in the variables  $(x_1', x_2', x_3')$ . These strain matrices are

$$[\varepsilon] = \begin{bmatrix} \varepsilon_{11} & \varepsilon_{12} & \varepsilon_{13} \\ \varepsilon_{21} & \varepsilon_{22} & \varepsilon_{23} \\ \varepsilon_{31} & \varepsilon_{32} & \varepsilon_{33} \end{bmatrix}, \text{ and } [\varepsilon'] = \begin{bmatrix} \varepsilon_{11}' & \varepsilon_{12}' & \varepsilon_{13}' \\ \varepsilon_{21}' & \varepsilon_{22}' & \varepsilon_{23}' \\ \varepsilon_{31}' & \varepsilon_{32}' & \varepsilon_{33}' \end{bmatrix}. \quad (\text{A.50})$$

Note that the strain matrix  $[\varepsilon]$  is symmetric. The strain of line element  $P_0\widehat{Q}_0$  must be the same if computed in the  $x_i$  system or in the  $x_i'$  system. The expression for the strain (A.17) in matrix notation is

$$\varepsilon_L = \{n\}^T [\varepsilon] \{n\} \quad (\text{A.51})$$

Substitute eq. (A.49) for the unit vector into eq. (A.51) to get

$$\begin{aligned} \varepsilon_L &= ([\lambda]^T \{n'\})^T [\varepsilon] [\lambda]^T \{n'\}, \text{ or} \\ \varepsilon_L &= \{n'\}^T [\lambda] [\varepsilon] [\lambda]^T \{n'\} \end{aligned} \quad (\text{A.52})$$

For eq. (A.52) to be an invariant form of eq. (A.51) we conclude

$$[\varepsilon'] = [\lambda] [\varepsilon] [\lambda]^T. \quad (\text{A.53})$$

Hence,

$$\varepsilon_L = \{n'\}^T [\varepsilon'] \{n'\}. \quad (\text{A.54})$$

Compare the forms of eq. (A.51) and eq. (A.54) to note their similarity. Also, we have the inverse transformation

$$[\varepsilon] = [\lambda]^T [\varepsilon'] [\lambda]. \quad (\text{A.55})$$

If we take the transpose of eq. (A.53) and use the fact that matrix  $[\varepsilon]$  is symmetric, then  $[\varepsilon']^T = [\varepsilon']$ . The engineering shear strain  $\gamma_{12} = \varepsilon_{12} + \varepsilon_{21}$ , and  $\varepsilon_{12} = \varepsilon_{21}$ . Thus  $\varepsilon_{12} = \varepsilon_{21} = \gamma_{12}/2$ . In terms of engineering shear strains (A.31) the strain transformation (A.53) is

$$\begin{bmatrix} \varepsilon_{11}' & \gamma_{12}'/2 & \gamma_{13}'/2 \\ \gamma_{12}'/2 & \varepsilon_{22}' & \gamma_{23}'/2 \\ \gamma_{13}'/2 & \gamma_{23}'/2 & \varepsilon_{33}' \end{bmatrix} = [\lambda] \begin{bmatrix} \varepsilon_{11} & \gamma_{12}/2 & \gamma_{13}/2 \\ \gamma_{12}/2 & \varepsilon_{22} & \gamma_{23}/2 \\ \gamma_{13}/2 & \gamma_{23}/2 & \varepsilon_{33} \end{bmatrix} [\lambda]^T. \quad (\text{A.56})$$

## A.2 Stress

The reference configuration  $B_0$  the body is assumed to be the natural or unstressed state. External forces acting on the body cause a state of stress in the deformed configuration  $B$ , and it is in the configuration  $B$  where the study of stresses is to be carried out. However, for infinitesimal displacement gradients the point  $P_0$  in region  $B_0$  and point  $P$  in region  $B$  lie very close together so that we do not distinguish between them. For small deformation theory, the study of equilibrium at a point in a deformable body is performed in the reference configuration.

Consider a continuous deformable body acted on by external forces shown in Fig. A.3(a). Due to the action of the external forces there will be internal forces acting between particles of the body. To examine the internal forces we pass a plane labeled  $mm$  through point  $P$  that is parallel to the  $x_2x_3$  plane. Consider the free body to the left of the plane  $mm$  shown in Fig. A.3(b). Plane  $mm$  is divided into a large number of small areas, each  $\Delta x_2$  by  $\Delta x_3$ . The internal forces acting on each of these areas varies in magnitude and in direction.

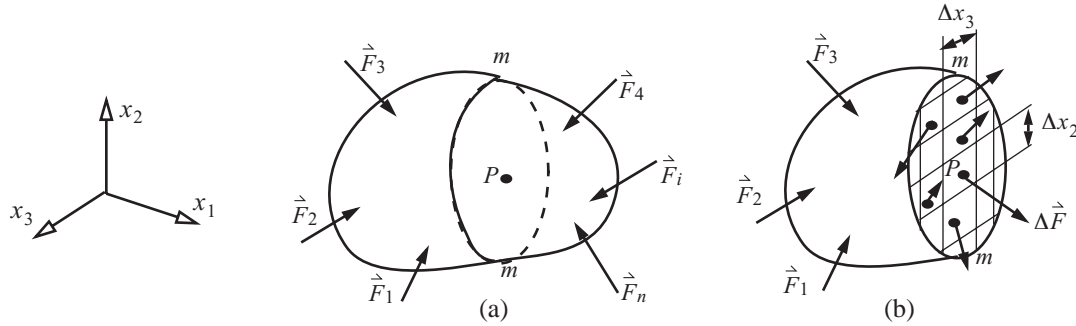


**Fig. A.3** (a) Isolated, continuous body acted on by external forces.  
(b) Internal forces acting on plane  $mm$ .

The internal force  $\Delta \vec{F}$  acting at point  $P$  is a resultant of distributed force intensities acting over area  $\Delta x_2 \Delta x_3$ . Let  $\Delta A_1$  denote the area  $\Delta x_2 \Delta x_3$ . Force  $\Delta \vec{F}$  represents the action exerted by the material outside the plane  $mm$  through area  $\Delta A_1$  on the material inside the plane  $mm$ . Point forces do not occur in nature. Forces are always distributed throughout regions which can have dimensions of length, area or volume. (However, point forces are an essential concept in the mechanics of solid bodies.) Consequently, as  $\Delta A_1 \rightarrow 0$  the resultant of the distributed force intensities acting over  $\Delta A_1$  vanishes; i.e.  $\Delta \vec{F} \rightarrow 0$ . The stress vector or traction vector acting at point  $P$  is defined as

$$\hat{T}^{(i_1)} = \lim_{\Delta A_1 \rightarrow 0} (\Delta \vec{F} / \Delta A_1), \quad (\text{A.57})$$

where the unit normal to area  $\Delta A_1$  is  $\hat{i}_1$ . Now consider a rectangular parallelepiped with edges  $\Delta x_1$ ,  $\Delta x_2$ , and  $\Delta x_3$  cut out of the body. It will have six separate plane surfaces which enclose the volume containing point  $P$ . Identify a surface face in terms of the coordinate axis normal to the surface. A face is defined as a positive face when its outwardly directed normal vector points in the direction of the positive coordinate direction, and as a

negative face when its outward normal vector points in the negative coordinate direction. The projection of the parallelepiped in the  $x_1$ - $x_2$  plane is shown Fig. A.4, where only the internal forces acting on the positive and negative faces normal to the  $x_1$ -axis are explicitly shown. Not shown in the figure are the surface forces acting on the four lateral faces and the body force acting in the volume. Let  $\Delta x_1 \rightarrow 0$  without changing the values of  $\Delta x_2$  and  $\Delta x_3$ . In the limit the forces acting on the lateral surfaces and the body force vanish, and force equilibrium yields

$$\vec{T}^{(-i_1)} \Delta A_1 + \vec{T}^{(i_1)} \Delta A_1 = 0.$$

Since  $\Delta A_1 > 0$ , we find from equilibrium that the stress vector on the negative  $x_1$ -face is equal to the negative of the stress vector on the positive  $x_1$ -face; i.e.,

$$\vec{T}^{(-i_1)} = -\vec{T}^{(i_1)}. \quad (\text{A.58})$$

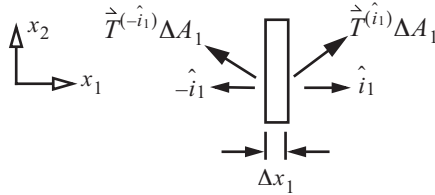


**Fig. A.4** Traction acting on the positive  $x_1$ -face and negative  $x_1$ -face of a narrow width parallelepiped

To simplify the notation let  $\vec{T}_1 = \vec{T}^{(i_1)}$ . Stress vectors acting on the positive  $x_2$ -face and the positive  $x_3$ -face are denoted by  $\vec{T}_2 = \vec{T}^{(i_2)}$  and  $\vec{T}_3 = \vec{T}^{(i_3)}$ , respectively. Stress vectors acting on the negative  $x_2$ -face and the negative  $x_3$ -face are  $-\vec{T}_2$  and  $-\vec{T}_3$ , respectively.

Define the stress components  $\sigma_{ij} = \vec{T}_i \cdot \hat{i}_j$ ,  $i, j = 1, 2, 3$ . The

first subscript on  $\sigma_{ij}$  is associated with the direction normal to the face and the second subscript is associated with the direction of the stress component. Thus the stress vectors in terms of components are

$$\begin{aligned} \vec{T}_1 &= \sigma_{11} \hat{i}_1 + \sigma_{12} \hat{i}_2 + \sigma_{13} \hat{i}_3 \\ \vec{T}_2 &= \sigma_{21} \hat{i}_1 + \sigma_{22} \hat{i}_2 + \sigma_{23} \hat{i}_3 \\ \vec{T}_3 &= \sigma_{31} \hat{i}_1 + \sigma_{32} \hat{i}_2 + \sigma_{33} \hat{i}_3 \end{aligned} \quad \text{or equivalently} \quad \begin{bmatrix} \vec{T}_1 \\ \vec{T}_2 \\ \vec{T}_3 \end{bmatrix} = \begin{bmatrix} \sigma_{11} & \sigma_{12} & \sigma_{13} \\ \sigma_{21} & \sigma_{22} & \sigma_{23} \\ \sigma_{31} & \sigma_{32} & \sigma_{33} \end{bmatrix} \begin{bmatrix} \hat{i}_1 \\ \hat{i}_2 \\ \hat{i}_3 \end{bmatrix}. \quad (\text{A.59})$$

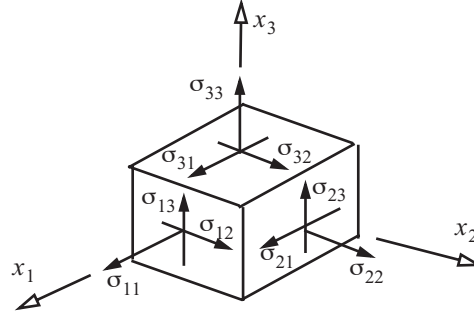
Positive stress components acting on the positive faces of the rectangular parallelepiped are shown in Fig. A.5. The stress components on the negative faces of the parallelepiped are equal and oppositely directed to those on the positive faces according to conditions like eq. (A.58). Hence, there are nine stress components at a point, not eighteen. We express the nine stress components at a point in the matrix form

$$[\sigma] = \begin{bmatrix} \sigma_{11} & \sigma_{12} & \sigma_{13} \\ \sigma_{21} & \sigma_{22} & \sigma_{23} \\ \sigma_{31} & \sigma_{32} & \sigma_{33} \end{bmatrix}. \quad (\text{A.60})$$

The diagonal elements in the stress matrix (A.60) are the normal stresses, and the off-diagonal elements are the

shear stresses. The nine stresses in matrix (A.60) are shown in Fig. A.5.

**Fig. A.5** Stresses acting on the positive coordinate faces of a rectangular parallelepiped



We pose the following question: Are the nine stress components at point  $P$  sufficient to determine the stresses on an arbitrarily orientated plane face through the point? To answer this question we consider equilibrium of a tetrahedron cut from the body at point  $P$ . The external surfaces of the tetrahedron shown in Fig. A.6 (a)

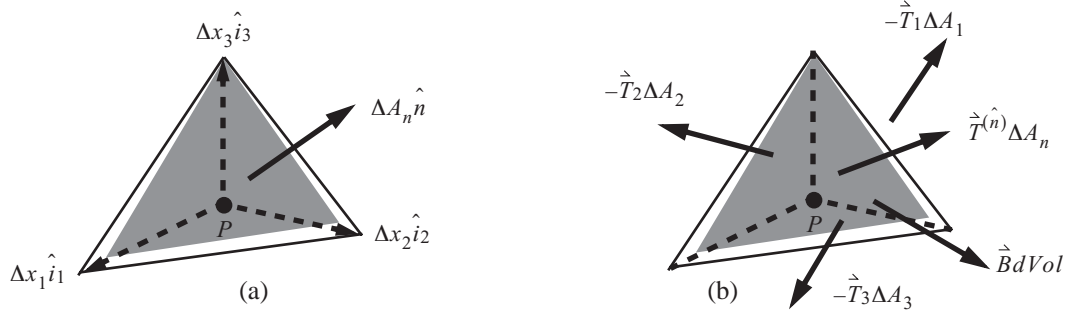


**Fig. A.6** (a) Geometry of the tetrahedron at point  $P$ . (b) Free body diagram of the tetrahedron

consist of three right triangles normal to the coordinate axes, and one oblique triangular area that is shaded in Fig. A.6. For the surface with unit outward normal vector  $-\hat{i}_1$  the area is  $\Delta A_1 = (\Delta x_2 \Delta x_3)/2$ , for the surface with unit outward normal  $-\hat{i}_2$  the area is  $\Delta A_2 = (\Delta x_1 \Delta x_3)/2$ , and for the surface with unit outward normal vector  $-\hat{i}_3$  the area is  $\Delta A_3 = (\Delta x_1 \Delta x_2)/2$ . The area of the oblique surface is denoted by  $\Delta A_n$  and its unit outward normal vector is  $\hat{n}$ . To calculate the area of the oblique face we use the fact the cross product of two position vectors is equal to the area of a parallelogram formed by the vectors and in a direction normal to the plane of the parallelogram. The vectors along the edges of the oblique face are  $-\Delta x_1 \hat{i}_1 + \Delta x_2 \hat{i}_2$  and  $-\Delta x_1 \hat{i}_1 + \Delta x_3 \hat{i}_3$ , and the area of the parallelogram formed by these vectors is equal to  $2\Delta A_n$ . Thus,

$$2\Delta A_n \hat{n} = (-\Delta x_1 \hat{i}_1 + \Delta x_2 \hat{i}_2) \times (-\Delta x_1 \hat{i}_1 + \Delta x_3 \hat{i}_3) = (\Delta x_2 \Delta x_3 \hat{i}_1 + \Delta x_1 \Delta x_3 \hat{i}_2 + \Delta x_1 \Delta x_2 \hat{i}_3),$$

which simplifies to

$$\Delta A_n \hat{n} = \Delta A_1 \hat{i}_1 + \Delta A_2 \hat{i}_2 + \Delta A_3 \hat{i}_3. \quad (\text{A.61})$$

From eq. (A.61) we find that area of the oblique face  $\Delta A_n = \sqrt{(\Delta A_1)^2 + (\Delta A_2)^2 + (\Delta A_3)^2}$ , and the components of the unit normal vector are

$$n_1 = \Delta A_1 / \Delta A_n \quad n_2 = \Delta A_2 / \Delta A_n \quad n_3 = \Delta A_3 / \Delta A_n. \quad (\text{A.62})$$

Equilibrium of the free body diagram in Fig. A.6(b) leads to

$$\vec{T}^{(\hat{n})} \Delta A_n + (-\vec{T}_1 \Delta A_1) + (-\vec{T}_2 \Delta A_2) + (-\vec{T}_3 \Delta A_3) + \vec{B}(dVol) = 0, \quad (\text{A.63})$$

where  $\vec{B}$  is the body force vector per unit volume. The tetrahedron is also a triangular pyramid where  $\Delta A_n$  is the area of its triangular base, and the volume of the pyramid is  $h \Delta A_n / 3$  where  $h$  is its height. Divide eq. (A.63) by  $\Delta A_n$  to get

$$\vec{T}^{(n)} = \vec{T}_1 n_1 + \vec{T}_2 n_2 + \vec{T}_3 n_3 - \vec{B}(h/3),$$

It can be shown that the height in this case is given by  $h = \Delta x_1 n_1 = \Delta x_2 n_2 = \Delta x_3 n_3$ . In the limit where  $\Delta x_1 \rightarrow 0$ ,  $\Delta x_2 \rightarrow 0$  and  $\Delta x_3 \rightarrow 0$ , the height  $h \rightarrow 0$ . Hence, in the limit the equilibrium equation is

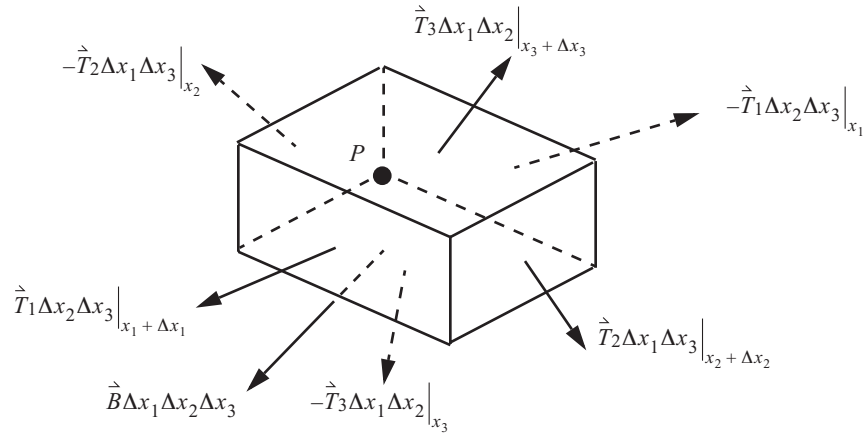
$$\vec{T}^{(n)} = \vec{T}_1 n_1 + \vec{T}_2 n_2 + \vec{T}_3 n_3. \quad (\text{A.64})$$

The implication of eq. (A.64) is that the nine stress components  $\sigma_{ij}$  at point  $P$  are sufficient to determine the traction, or stresses, on any face through the point.

### A.2.1 Equilibrium differential equations

Consider the forces acting on a rectangular parallelepiped at point  $P$ . The free body diagram is shown in Fig. A.7.

**Fig. A.7** Surface forces and a body force acting on a rectangular parallelepiped  $\Delta x_1 \Delta x_2 \Delta x_3$



The vector sum of forces is

$$\vec{T}_1 \Delta x_2 \Delta x_3 \Big|_{x_1 + \Delta x_1} - \vec{T}_1 \Delta x_2 \Delta x_3 \Big|_{x_1} + \vec{T}_2 \Delta x_1 \Delta x_3 \Big|_{x_2 + \Delta x_2} - \vec{T}_2 \Delta x_1 \Delta x_3 \Big|_{x_2} + \vec{T}_3 \Delta x_1 \Delta x_2 \Big|_{x_3 + \Delta x_3} - \vec{T}_3 \Delta x_1 \Delta x_2 \Big|_{x_3} + \vec{B} \Delta x_1 \Delta x_2 \Delta x_3.$$

For small increments in  $\Delta x_i$ ,  $i = 1, 2, 3$ , the Taylor series representation of surface forces results in the equilibrium equation



$$\frac{\partial}{\partial x_1}(\vec{T}_1 \Delta x_2 \Delta x_3) \Delta x_1 + \frac{\partial}{\partial x_2}(\vec{T}_2 \Delta x_1 \Delta x_3) \Delta x_2 + \frac{\partial}{\partial x_3}(\vec{T}_3 \Delta x_1 \Delta x_2) \Delta x_3 + \vec{B} \Delta x_1 \Delta x_2 \Delta x_3 + O((\Delta x_i)^4) = 0. \quad (\text{A.65})$$

$$\left( \frac{\partial \vec{T}_1}{\partial x_1} + \frac{\partial \vec{T}_2}{\partial x_2} + \frac{\partial \vec{T}_3}{\partial x_3} + \vec{B} \right) \Delta x_1 \Delta x_2 \Delta x_3 + O((\Delta x_i)^4) = 0 \quad (\text{A.66})$$

Divide eq. (A.66) by the volume followed by the limit as  $\Delta x_1 \Delta x_2 \Delta x_3 \rightarrow 0$  to get the vector differential equation of force equilibrium at point P as

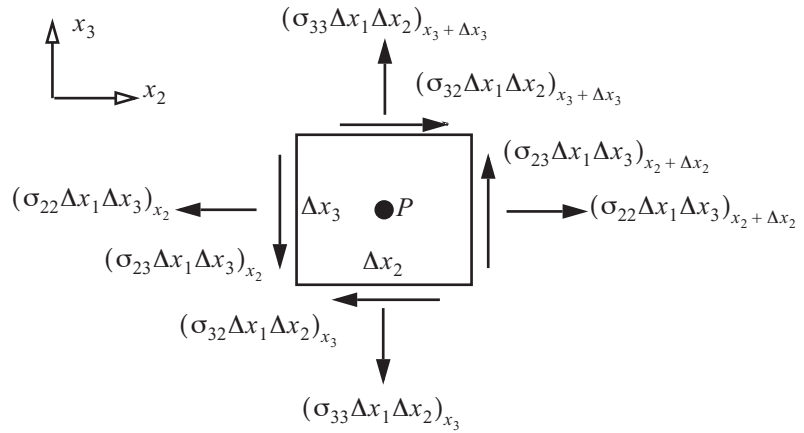
$$\frac{\partial \vec{T}_1}{\partial x_1} + \frac{\partial \vec{T}_2}{\partial x_2} + \frac{\partial \vec{T}_3}{\partial x_3} + \vec{B} = 0. \quad (\text{A.67})$$

Substitute eq. (A.59) for the traction vectors in eq. (A.67) to write the equilibrium differential equations in the  $x_i$  coordinate directions. In the order of  $x_1, x_2, x_3$  coordinate directions these equations are

$$\begin{aligned} \frac{\partial \sigma_{11}}{\partial x_1} + \frac{\partial \sigma_{21}}{\partial x_2} + \frac{\partial \sigma_{31}}{\partial x_3} + B_1 &= 0 \\ \frac{\partial \sigma_{12}}{\partial x_1} + \frac{\partial \sigma_{22}}{\partial x_2} + \frac{\partial \sigma_{32}}{\partial x_3} + B_2 &= 0. \\ \frac{\partial \sigma_{13}}{\partial x_1} + \frac{\partial \sigma_{23}}{\partial x_2} + \frac{\partial \sigma_{33}}{\partial x_3} + B_3 &= 0 \end{aligned} \quad (\text{A.68})$$

Now consider moment equilibrium about the coordinate axes of the rectangular parallelepiped at point P. For moment equilibrium about the  $x_1$  axis refer to the free body diagram in Fig. A.8.

**Fig. A.8** A free body diagram of the parallelepiped at point P for moment equilibrium about the  $x_1$  axis. The  $x_1$  axis points normal to the page towards the reader.



The moment arm from point P to the line of action of the normal force  $(\sigma_{22} \Delta x_1 \Delta x_3)_{x_2 + \Delta x_2}$  acting on the positive  $x_2$  face is denoted by  $\epsilon \Delta x_3$ , where  $0 \leq |\epsilon| < 1/2$ . Parameter  $\epsilon$  is not known, but this will not matter in the end result. The moment arm from point P to the line of action of the shear force  $(\sigma_{23} \Delta x_1 \Delta x_3)_{x_2 + \Delta x_2}$  acting on the positive  $x_2$  face is  $\Delta x_2/2$ . Including all the forces shown in Fig. A.8, the sum of moments about the  $x_1$  axis through point P, counterclockwise positive, is

$$\begin{aligned}
& -\varepsilon \Delta x_3 (\sigma_{22} \Delta x_1 \Delta x_3)_{x_2 + \Delta x_2} + \varepsilon \Delta x_3 (\sigma_{22} \Delta x_1 \Delta x_3)_{x_2} + \frac{\Delta x_2}{2} (\sigma_{23} \Delta x_1 \Delta x_3)_{x_2 + \Delta x_2} + \frac{\Delta x_2}{2} (\sigma_{23} \Delta x_1 \Delta x_3)_{x_2} + \\
& \varepsilon \Delta_2 (\sigma_{33} \Delta x_1 \Delta x_2)_{x_3 + \Delta x_3} - \varepsilon \Delta_2 (\sigma_{33} \Delta x_1 \Delta x_2)_{x_3} - \frac{\Delta x_3}{2} (\sigma_{32} \Delta x_1 \Delta x_2)_{x_3 + \Delta x_3} - \frac{\Delta x_3}{2} (\sigma_{32} \Delta x_1 \Delta x_2)_{x_3} = 0
\end{aligned} \quad (A.69)$$

Use the Taylor series to expand the forces acting on the positive coordinate faces with respect to the forces acting on the negative coordinate faces to get

$$\begin{aligned}
& -\varepsilon \Delta x_3 \left[ \frac{\partial \sigma_{22}}{\partial x_2} \Delta x_2 + O(\Delta x_2^2) \right] \Delta x_1 \Delta x_3 + \frac{\Delta x_2}{2} \left[ 2\sigma_{23} + \frac{\partial \sigma_{23}}{\partial x_2} \Delta x_2 + O(\Delta x_2^2) \right] \Delta x_1 \Delta x_3 + \\
& \varepsilon \Delta x_2 \left[ \frac{\partial \sigma_{33}}{\partial x_3} \Delta x_3 + O(\Delta x_3^2) \right] \Delta x_1 \Delta x_2 - \frac{\Delta x_3}{2} \left[ 2\sigma_{32} + \frac{\partial \sigma_{32}}{\partial x_3} \Delta x_3 + O(\Delta x_3^2) \right] \Delta x_1 \Delta x_2 = 0
\end{aligned} \quad (A.70)$$

Expand eq. (A.70) in powers of  $\Delta x_i$  to write it as

$$(\sigma_{23} - \sigma_{32}) \Delta x_1 \Delta x_2 \Delta x_3 + \varepsilon \left[ -\frac{\partial \sigma_{22}}{\partial x_2} \Delta x_1 \Delta x_2 \Delta x_3^2 + \frac{\partial \sigma_{33}}{\partial x_3} \Delta x_1 \Delta x_2^2 \Delta x_3 \right] + \text{H.O.T.} = 0, \quad (A.71)$$

where H.O.T. means higher order terms. That is, terms of quartic powers and higher in the increments in the coordinates. Notice the terms multiplied by  $\varepsilon$  are quartic powers of the increments in the coordinates. Division of eq. (A.71) by  $\Delta x_1 \Delta x_2 \Delta x_3$ , followed by the limit of  $\Delta x_i \rightarrow 0$  leads the condition of moment equilibrium about the  $x_1$  axis that  $\sigma_{23} - \sigma_{32} = 0$ . Moment equilibrium about the  $x_2$ -axis leads to  $\sigma_{13} - \sigma_{31} = 0$ , and moment equilibrium about the  $x_3$ -axis leads to  $\sigma_{12} - \sigma_{21} = 0$ . The equations of moment equilibrium are

$$\sigma_{12} = \sigma_{21} \quad \sigma_{13} = \sigma_{31} \quad \sigma_{23} = \sigma_{32}. \quad (A.72)$$

Hence, the stress matrix (A.59) is symmetric.

### A.2.2 Transformation of stresses between two cartesian coordinate systems

At point  $P$  coordinates  $(x_1', x_2', x_3')$  are linearly related to coordinates  $(x_1, x_2, x_3)$  by eq. (A.38). The stress components  $\sigma_{ij}$  are functions in the variables  $(x_1, x_2, x_3)$ , and the stresses  $\sigma_{ij}'$  are functions in the variables  $(x_1', x_2', x_3')$ . The stress vectors acting on the  $x_i$ -faces are denoted by  $\vec{T}_i$ , and those acting on the  $x_i'$ -faces are denoted by  $\vec{T}_i'$ . These stress vectors are written in their respective coordinate systems by

$$\begin{bmatrix} \vec{T}_1 \\ \vec{T}_2 \\ \vec{T}_3 \end{bmatrix} = \begin{bmatrix} \sigma_{11} & \sigma_{12} & \sigma_{13} \\ \sigma_{21} & \sigma_{22} & \sigma_{23} \\ \sigma_{31} & \sigma_{32} & \sigma_{33} \end{bmatrix} \begin{bmatrix} \hat{i}_1 \\ \hat{i}_2 \\ \hat{i}_3 \end{bmatrix}, \text{ and } \begin{bmatrix} \vec{T}_1' \\ \vec{T}_2' \\ \vec{T}_3' \end{bmatrix} = \begin{bmatrix} \sigma_{11}' & \sigma_{12}' & \sigma_{13}' \\ \sigma_{21}' & \sigma_{22}' & \sigma_{23}' \\ \sigma_{31}' & \sigma_{32}' & \sigma_{33}' \end{bmatrix} \begin{bmatrix} \hat{i}_1' \\ \hat{i}_2' \\ \hat{i}_3' \end{bmatrix}. \quad (A.73)$$

In eq. (A.73) the stress matrices are

$$[\sigma] = \begin{bmatrix} \sigma_{11} & \sigma_{12} & \sigma_{13} \\ \sigma_{21} & \sigma_{22} & \sigma_{23} \\ \sigma_{31} & \sigma_{32} & \sigma_{33} \end{bmatrix}, \text{ and } [\sigma'] = \begin{bmatrix} \sigma_{11}' & \sigma_{12}' & \sigma_{13}' \\ \sigma_{21}' & \sigma_{22}' & \sigma_{23}' \\ \sigma_{31}' & \sigma_{32}' & \sigma_{33}' \end{bmatrix}. \quad (A.74)$$

Equation (A.72) shows that the stress matrix  $[\sigma]$  is symmetric. The stress transformation equations between the cartesian coordinate systems  $(x_1, x_2, x_3)$  and  $(x_1', x_2', x_3')$  is determined by selecting the unit normal in eq. (A.64) to be either  $\hat{i}_1'$ ,  $\hat{i}_2'$ , or  $\hat{i}_3'$ . First let  $\hat{n} = \hat{i}_1'$  such that  $\vec{T}^{(n)} = \vec{T}_1'$  in eq. (A.64), and from eq. (A.41) we have  $\hat{n} = \lambda_{11}\hat{i}_1 + \lambda_{12}\hat{i}_2 + \lambda_{13}\hat{i}_3$ . Hence, eq. (A.64) becomes

$$\vec{T}_1' = \lambda_{11}\vec{T}_1 + \lambda_{12}\vec{T}_2 + \lambda_{13}\vec{T}_3.$$

Second, let  $\hat{n} = \hat{i}_2'$  such that  $\vec{T}^{(n)} = \vec{T}_2'$  and from eq. (A.41) we have  $\hat{n} = \lambda_{21}\hat{i}_1 + \lambda_{22}\hat{i}_2 + \lambda_{23}\hat{i}_3$ . Hence, eq. (A.64) becomes

$$\vec{T}_2' = \lambda_{21}\vec{T}_1 + \lambda_{22}\vec{T}_2 + \lambda_{23}\vec{T}_3.$$

Third, let  $\hat{n} = \hat{i}_3'$  such that  $\vec{T}^{(n)} = \vec{T}_3'$  and  $\hat{n} = \lambda_{31}\hat{i}_1 + \lambda_{32}\hat{i}_2 + \lambda_{33}\hat{i}_3$ . Hence,

$$\vec{T}_3' = \lambda_{31}\vec{T}_1 + \lambda_{32}\vec{T}_2 + \lambda_{33}\vec{T}_3.$$

The three selections for the unit normal in eq. (A.64) relate the tractions acting on the  $x_i'$  coordinate faces to the tractions acting on the  $x_i$  faces by

$$\begin{bmatrix} \vec{T}_1' \\ \vec{T}_2' \\ \vec{T}_3' \end{bmatrix} = \begin{bmatrix} \lambda_{11} & \lambda_{12} & \lambda_{13} \\ \lambda_{21} & \lambda_{22} & \lambda_{23} \\ \lambda_{31} & \lambda_{32} & \lambda_{33} \end{bmatrix} \begin{bmatrix} \vec{T}_1 \\ \vec{T}_2 \\ \vec{T}_3 \end{bmatrix}. \quad (\text{A.75})$$

Substitute the expressions for the stress vectors from eq. (A.73) into eq. (A.75) to get

$$\begin{bmatrix} \sigma_{11}' & \sigma_{12}' & \sigma_{13}' \\ \sigma_{21}' & \sigma_{22}' & \sigma_{23}' \\ \sigma_{31}' & \sigma_{32}' & \sigma_{33}' \end{bmatrix} \begin{bmatrix} \hat{i}_1' \\ \hat{i}_2' \\ \hat{i}_3' \end{bmatrix} = \begin{bmatrix} \lambda_{11} & \lambda_{12} & \lambda_{13} \\ \lambda_{21} & \lambda_{22} & \lambda_{23} \\ \lambda_{31} & \lambda_{32} & \lambda_{33} \end{bmatrix} \begin{bmatrix} \sigma_{11} & \sigma_{12} & \sigma_{13} \\ \sigma_{21} & \sigma_{22} & \sigma_{23} \\ \sigma_{31} & \sigma_{32} & \sigma_{33} \end{bmatrix} \begin{bmatrix} \hat{i}_1 \\ \hat{i}_2 \\ \hat{i}_3 \end{bmatrix} \quad (\text{A.76})$$

The unit vectors in the  $x_i$ -coordinates are related to the unit vectors in  $x_i'$ -coordinates by

$$\begin{bmatrix} \hat{i}_1 \\ \hat{i}_2 \\ \hat{i}_3 \end{bmatrix} = \begin{bmatrix} \lambda_{11} & \lambda_{21} & \lambda_{31} \\ \lambda_{12} & \lambda_{22} & \lambda_{32} \\ \lambda_{13} & \lambda_{23} & \lambda_{33} \end{bmatrix} \begin{bmatrix} \hat{i}_1' \\ \hat{i}_2' \\ \hat{i}_3' \end{bmatrix}. \quad (\text{A.77})$$

Substitute eq. (A.77) into the right-hand side of eq. (A.76) and rearrange the result to find

$$\left( \begin{bmatrix} \sigma_{11}' & \sigma_{12}' & \sigma_{13}' \\ \sigma_{21}' & \sigma_{22}' & \sigma_{23}' \\ \sigma_{31}' & \sigma_{32}' & \sigma_{33}' \end{bmatrix} - \begin{bmatrix} \lambda_{11} & \lambda_{12} & \lambda_{13} \\ \lambda_{21} & \lambda_{22} & \lambda_{23} \\ \lambda_{31} & \lambda_{32} & \lambda_{33} \end{bmatrix} \begin{bmatrix} \sigma_{11} & \sigma_{12} & \sigma_{13} \\ \sigma_{21} & \sigma_{22} & \sigma_{23} \\ \sigma_{31} & \sigma_{32} & \sigma_{33} \end{bmatrix} \begin{bmatrix} \lambda_{11} & \lambda_{21} & \lambda_{31} \\ \lambda_{12} & \lambda_{22} & \lambda_{32} \\ \lambda_{13} & \lambda_{23} & \lambda_{33} \end{bmatrix} \right) \begin{bmatrix} \hat{i}_1' \\ \hat{i}_2' \\ \hat{i}_3' \end{bmatrix} = \begin{bmatrix} 0 \\ 0 \\ 0 \end{bmatrix}. \quad (\text{A.78})$$

To satisfy eq. (A.78) we find that the stress components  $\sigma_{ij}'$  in the  $x_i'$  system are related to the stress components  $\sigma_{ij}$  in the  $x_i$  system by

$$\begin{bmatrix} \sigma_{11}' & \sigma_{12}' & \sigma_{13}' \\ \sigma_{21}' & \sigma_{22}' & \sigma_{23}' \\ \sigma_{31}' & \sigma_{32}' & \sigma_{33}' \end{bmatrix} = \begin{bmatrix} \lambda_{11} & \lambda_{12} & \lambda_{13} \\ \lambda_{21} & \lambda_{22} & \lambda_{23} \\ \lambda_{31} & \lambda_{32} & \lambda_{33} \end{bmatrix} \begin{bmatrix} \sigma_{11} & \sigma_{12} & \sigma_{13} \\ \sigma_{21} & \sigma_{22} & \sigma_{23} \\ \sigma_{31} & \sigma_{32} & \sigma_{33} \end{bmatrix} \begin{bmatrix} \lambda_{11} & \lambda_{21} & \lambda_{31} \\ \lambda_{12} & \lambda_{22} & \lambda_{32} \\ \lambda_{13} & \lambda_{23} & \lambda_{33} \end{bmatrix}. \quad (\text{A.79})$$

Equation (A.79) in compact form is

$$[\sigma'] = [\lambda] [\sigma] [\lambda]^T. \quad (\text{A.80})$$

Pre-multiply eq. (A.80) by  $[\lambda]^T$ , post-multiply it by  $[\lambda]$ , and note that  $[\lambda]^T [\lambda] = [\lambda] [\lambda]^T = [I]$  to find the inverse transformation

$$[\sigma] = [\lambda]^T [\sigma'] [\lambda]. \quad (\text{A.81})$$

The transpose of eq. (A.80) is  $[\lambda] [\sigma]^T [\lambda]^T$ , but  $[\sigma]^T = [\sigma]$ , so the stress matrix  $[\sigma']$  is also symmetric. Comparing the strain transformation eq. (A.53) to the stress transformation eq. (A.80), it is clear that the transformation of strains  $\epsilon_{ij}$  is the same form as the transformation of the stresses  $\sigma_{ij}$ .

### A.2.3 Cartesian tensors

A **tensor** is a system of numbers or functions, whose components obey a certain law of transformation when the independent variables undergo a linear transformation. If the independent variables are the rectangular cartesian systems  $x_i$  and  $x_i'$  transforming by the linear relations given by  $\{x'\} = [\lambda] \{x\}$  at point  $P$ , then the systems obeying certain laws of transformation are called cartesian tensors.

**Definition.** A system of order two may be defined to have nine components  $\epsilon_{ij}$  in  $x_i$  and nine components  $\epsilon_{ij}'$  in  $x_i'$ . If

$$[\epsilon_{ij}'] = [\lambda] [\epsilon_{ij}] [\lambda]^T$$

then the functions  $\epsilon_{ij}$  and  $\epsilon_{ij}'$  are the components in their respective variables of a second order cartesian tensor. Similarly, functions  $\sigma_{ij}$  and  $\sigma_{ij}'$  are the components in their respective variables of a second order cartesian tensor.

## A.3 Linear elastic material law

To this point in the study of the mechanics of a solid body we have eighteen unknown functions of the cartesian coordinates  $x_1, x_2, x_3$ . These are the three displacements  $u_1, u_2, u_3$ , the six strains  $\epsilon_{11}, \epsilon_{22}, \epsilon_{33}, \gamma_{23}, \gamma_{31}, \gamma_{12}$ , and nine stresses  $\sigma_{11}, \sigma_{12}, \sigma_{13}, \sigma_{21}, \sigma_{22}, \sigma_{23}, \sigma_{31}, \sigma_{32}, \sigma_{33}$ . There are twelve equations relating these unknowns; the six strain-displacement equations (A.32) and (A.33), and the six equilibrium equations (A.68) and (A.72). There-

fore we need six more equation to get the number of unknowns equal to number of equations. The additional six equations come from the relations between the strains and the stresses which express the material law. This relation between strains and stresses for different materials is established by material characterization tests on standard test specimens.

Solid bodies that can instantly recover their original size and shape when the forces producing the deformation are removed are called perfectly elastic. The elastic limit is defined as the greatest stress which can be applied without resulting in permanent strain on release of the stress. Elasticity is applicable to any body provided the stresses do not exceed the elastic limit. For many solid bodies there is a region where the stress is very nearly proportional to strain. The proportional limit is defined as the greatest stress for which the stress is still proportional to the strain. Both the elastic limit and proportional limit cannot be precisely determined from test data since they are defined by the limiting cases of no permanent deformation and no deviation from linearity. In practice the definition of the yield strength of a material is used to determine the limit of elastic behavior.

The theoretical basis for an elastic material law is the first law of thermodynamics applied to an arbitrary infinitesimal rectangular parallelepiped isolated from the body. We assume the deformation process is adiabatic. That is, no heat is lost or gained in the body during the deformation. The work expended in the transition from the reference state to the final deformed state is independent of the manner in which the process proceeds. The first law of thermodynamics states that work done on the rectangular parallelepiped is equal to the change in internal energy of the material contained in the parallelepiped.<sup>1</sup> In elasticity the internal energy is called the strain energy. The strain energy per unit volume of the reference configuration, or strain energy density, is a function of the six strain components and is denoted by  $U(\epsilon_{11}, \epsilon_{22}, \epsilon_{33}, \gamma_{23}, \gamma_{31}, \gamma_{12})$ . The strain energy density function depends on the physical properties of the material. The incremental work of the tractions and body force acting on the parallelepiped is formulated in terms of incremental displacements from the equilibrium state. These incremental displacement functions are denoted by  $\delta u_i(x_1, x_2, x_3)$ ,  $i = 1, 2, 3$ , and to be kinematically admissible they are continuous and single-valued in the independent variables. In addition, functions  $\delta u_i$  are assumed to be infinitesimal in magnitude. The total displacement is  $\tilde{u}_i = u_i + \delta u_i$ , where  $u_i$  are the displacement components in the equilibrium state.

**The distinction between  $\delta u_1$  and  $du_1$**  In one-dimension we define  $u_1(x_1)$  as the displacement function of a particle originally at coordinate  $x_1$  in the reference configuration of the body. (region  $B_0$ ). The definition of incremental work necessitates consideration of the incremental displacement of a particle in the body. The distinction between  $\delta u_1$  and  $du_1$  is illustrated in Fig. A.9. The incremental displacement  $\delta u_1$  is at fixed value of the independent variable  $x_1$  and the differential  $du_1$  is the change in displacement with respect to the change in the independent variable  $x_1$ . In the formulation of incremental work

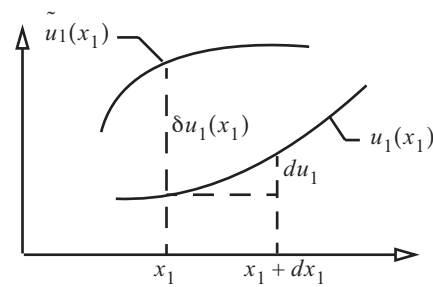


Fig. A.9 Graph of  $u_1(x_1)$  and  $\tilde{u}_1(x_1)$

1. We are not considering the change in kinetic energy for simplicity. If kinetic energy were actuated for in the first law of thermodynamics, then the final results obtained in this article would be unchanged.

we interpret  $\delta u_1$  as the infinitesimal change in the displacement of one particle identified by its coordinate in region  $B_0$ . The interpretation of  $du_1$  is the relative displacement between two particles, one originally at  $x_1 + dx_1$  and the other originally at  $x_1$  in region  $B_0$ .

For an adiabatic deformation process the first law of thermodynamics for the material in the rectangular parallelepiped of Fig. A.7 is

$$\begin{aligned} \vec{T}_1 \Delta x_2 \Delta x_3 \cdot \delta \vec{u} \Big|_{x_1 + \Delta x_1} + (-\vec{T}_1 \Delta x_2 \Delta x_3 \cdot \delta \vec{u}) \Big|_{x_1} + \vec{T}_2 \Delta x_1 \Delta x_3 \cdot \delta \vec{u} \Big|_{x_2 + \Delta x_2} + (-\vec{T}_2 \Delta x_1 \Delta x_3 \cdot \delta \vec{u}) \Big|_{x_2} + \\ \vec{T}_3 \Delta x_1 \Delta x_2 \cdot \delta \vec{u} \Big|_{x_3 + \Delta x_3} + (-\vec{T}_3 \Delta x_1 \Delta x_2 \cdot \delta \vec{u}) \Big|_{x_3} + \vec{B} \Delta x_1 \Delta x_2 \Delta x_3 = \delta U \Delta x_1 \Delta x_2 \Delta x_3, \end{aligned}$$

where the incremental displacement vector is  $\delta \vec{u} = \delta u_1 \hat{i}_1 + \delta u_2 \hat{i}_2 + \delta u_3 \hat{i}_3$ . Expand the tractions acting on the faces of the rectangular parallelepiped at point  $P$  in a Taylor series keeping only those terms to the first degree in the differentials  $\Delta x_i$  to get

$$\frac{\partial(\vec{T}_1 \cdot \delta \vec{u})}{\partial x_1} \Delta x_1 \Delta x_2 \Delta x_3 + \frac{\partial(\vec{T}_2 \cdot \delta \vec{u})}{\partial x_2} \Delta x_1 \Delta x_2 \Delta x_3 + \frac{\partial(\vec{T}_3 \cdot \delta \vec{u})}{\partial x_3} \Delta x_1 \Delta x_2 \Delta x_3 + \vec{B} \Delta x_1 \Delta x_2 \Delta x_3 = \delta U \Delta x_1 \Delta x_2 \Delta x_3.$$

Divide by the volume  $\Delta x_1 \Delta x_2 \Delta x_3$  to get

$$\left( \frac{\partial \vec{T}_1}{\partial x_1} + \frac{\partial \vec{T}_2}{\partial x_2} + \frac{\partial \vec{T}_3}{\partial x_3} + \vec{B} \right) \cdot \delta \vec{u} + \vec{T}_1 \cdot \frac{\partial}{\partial x_1} (\delta \vec{u}) + \vec{T}_2 \cdot \frac{\partial}{\partial x_2} (\delta \vec{u}) + \vec{T}_3 \cdot \frac{\partial}{\partial x_3} (\delta \vec{u}) = \delta U \quad (\text{A.82})$$

The first term on the left-hand side vanishes via equilibrium eq. (A.67). Hence, (A.82) reduces to

$$\vec{T}_1 \cdot \frac{\partial}{\partial x_1} (\delta \vec{u}) + \vec{T}_2 \cdot \frac{\partial}{\partial x_2} (\delta \vec{u}) + \vec{T}_3 \cdot \frac{\partial}{\partial x_3} (\delta \vec{u}) = \delta U \quad (\text{A.83})$$

Consider the term

$$\vec{T}_1 \cdot \frac{\partial}{\partial x_1} (\delta \vec{u}) = [\sigma_{11} \hat{i}_1 + \sigma_{12} \hat{i}_2 + \sigma_{13} \hat{i}_3] \cdot \left[ \frac{\partial}{\partial x_1} (\delta u_1) \hat{i}_1 + \frac{\partial}{\partial x_1} (\delta u_2) \hat{i}_2 + \frac{\partial}{\partial x_1} (\delta u_3) \hat{i}_3 \right]. \quad (\text{A.84})$$

The variation in the derivative of a function is defined as

$$\delta \left( \frac{du_i}{dx_j} \right) \equiv \frac{\tilde{du}_i}{dx_j} - \frac{du_i}{dx_j}, \quad i, j = 1, 2, 3. \quad (\text{A.85})$$

Substitute  $\tilde{u}_i = u_i + \delta u_i$  into eq. (A.85) to get

$$\delta \left( \frac{du_i}{dx_j} \right) = \frac{d}{dx_j} (u_i + \delta u_i) - \frac{du_i}{dx_j} = \frac{d}{dx_j} (\delta u_i)$$

Hence,

$$\delta \left( \frac{du_i}{dx_j} \right) = \frac{d}{dx_j} (\delta u_i) \quad (\text{A.86})$$

Employing the result of eq. (A.86) in eq. (A.84) we write the latter as

$$\begin{aligned}\dot{T}_1 \cdot \frac{\partial}{\partial x_1}(\delta \dot{u}) &= [\sigma_{11}\hat{i}_1 + \sigma_{12}\hat{i}_2 + \sigma_{13}\hat{i}_3] \cdot \left[ \delta\left(\frac{\partial u_1}{\partial x_1}\right)\hat{i}_1 + \delta\left(\frac{\partial u_2}{\partial x_1}\right)\hat{i}_2 + \delta\left(\frac{\partial u_3}{\partial x_1}\right)\hat{i}_3 \right] \\ &= \sigma_{11}\delta\left(\frac{\partial u_1}{\partial x_1}\right) + \sigma_{12}\delta\left(\frac{\partial u_2}{\partial x_1}\right) + \sigma_{13}\delta\left(\frac{\partial u_3}{\partial x_1}\right)\end{aligned}\quad (\text{A.87})$$

Similarly the remaining terms on the left-hand side of eq. (A.83) can be evaluated as was done starting with eq. (A.84). The result is

$$\begin{aligned}&\sigma_{11}\delta\left(\frac{\partial u_1}{\partial x_1}\right) + \sigma_{22}\delta\left(\frac{\partial u_2}{\partial x_2}\right) + \sigma_{33}\delta\left(\frac{\partial u_3}{\partial x_3}\right) + \\ &\sigma_{23}\left[\delta\left(\frac{\partial u_2}{\partial x_3}\right) + \delta\left(\frac{\partial u_3}{\partial x_2}\right)\right] + \sigma_{31}\left[\delta\left(\frac{\partial u_1}{\partial x_3}\right) + \delta\left(\frac{\partial u_3}{\partial x_1}\right)\right] + \sigma_{12}\left[\delta\left(\frac{\partial u_1}{\partial x_2}\right) + \delta\left(\frac{\partial u_2}{\partial x_1}\right)\right] = \delta U\end{aligned}\quad (\text{A.88})$$

The increments in the strains are determined from eq. (A.32) and eq. (A.33) by letting  $u_i \rightarrow u_i + \delta u_i$ , The strain increments are

$$\delta \varepsilon_{11} = \delta \frac{\partial u_1}{\partial x_1} \quad \delta \varepsilon_{22} = \delta \left( \frac{\partial u_2}{\partial x_2} \right) \quad \dots \quad \delta \gamma_{12} = \delta \left( \frac{\partial u_1}{\partial x_2} \right) + \delta \left( \frac{\partial u_2}{\partial x_1} \right)$$

Thus eq. (A.88) is

$$\sigma_{11}\delta \varepsilon_{11} + \sigma_{22}\delta \varepsilon_{22} + \sigma_{33}\delta \varepsilon_{33} + \sigma_{23}\delta \gamma_{23} + \sigma_{31}\delta \gamma_{31} + \sigma_{12}\delta \gamma_{12} = \delta U. \quad (\text{A.89})$$

The change in the strain energy for the material in the rectangular parallelepiped as the strains are incremented is determined from the series

$$\begin{aligned}U(\varepsilon_{11} + \delta \varepsilon_{11}, \varepsilon_{22} + \delta \varepsilon_{22}, \dots, \gamma_{12} + \delta \gamma_{12}) &= U(\varepsilon_{11}, \varepsilon_{22}, \dots, \gamma_{12}) + \frac{\partial U}{\partial \varepsilon_{11}}\delta \varepsilon_{11} + \frac{\partial U}{\partial \varepsilon_{22}}\delta \varepsilon_{22} + \frac{\partial U}{\partial \varepsilon_{33}}\delta \varepsilon_{33} + \dots + \frac{\partial U}{\partial \gamma_{12}}\delta \gamma_{12} \\ &\quad + \text{H.O.T.},\end{aligned}$$

where H.O.T. are higher order terms that contain quadratic and higher powers in the strain increments. The change in strain energy is given by

$$\Delta U = U(\varepsilon_{11} + \delta \varepsilon_{11}, \varepsilon_{22} + \delta \varepsilon_{22}, \dots, \gamma_{12} + \delta \gamma_{12}) - U(\varepsilon_{11}, \varepsilon_{22}, \dots, \gamma_{12}) + \delta U + \text{H.O.T}$$

For infinitesimal increments in the strains  $\Delta U \sim \delta U$  where

$$\delta U = \frac{\partial U}{\partial \varepsilon_{11}}\delta \varepsilon_{11} + \frac{\partial U}{\partial \varepsilon_{22}}\delta \varepsilon_{22} + \frac{\partial U}{\partial \varepsilon_{33}}\delta \varepsilon_{33} + \frac{\partial U}{\partial \gamma_{23}}\delta \gamma_{23} + \frac{\partial U}{\partial \gamma_{31}}\delta \gamma_{31} + \frac{\partial U}{\partial \gamma_{12}}\delta \gamma_{12} \quad (\text{A.90})$$

Compare eqs. (A.89) and (A.90) to identify

$$\sigma_{11} = \frac{\partial U}{\partial \varepsilon_{11}} \quad \sigma_{22} = \frac{\partial U}{\partial \varepsilon_{22}} \quad \sigma_{33} = \frac{\partial U}{\partial \varepsilon_{33}} \quad \sigma_{23} = \frac{\partial U}{\partial \gamma_{23}} \quad \sigma_{31} = \frac{\partial U}{\partial \gamma_{31}} \quad \sigma_{12} = \frac{\partial U}{\partial \gamma_{12}}. \quad (\text{A.91})$$

To simplify further developments of the material law, we introduce the following short hand notation for the stresses and strains

$$\sigma_1 = \sigma_{11} \quad \sigma_2 = \sigma_{22} \quad \sigma_3 = \sigma_{33} \quad \sigma_4 = \sigma_{23} \quad \sigma_5 = \sigma_{31} \quad \sigma_6 = \sigma_{12}, \text{ and} \quad (\text{A.92})$$

$$\varepsilon_1 = \varepsilon_{11} \quad \varepsilon_2 = \varepsilon_{22} \quad \varepsilon_3 = \varepsilon_{33} \quad \varepsilon_4 = \gamma_{23} \quad \varepsilon_5 = \gamma_{31} \quad \varepsilon_6 = \gamma_{12}. \quad (\text{A.93})$$

The strain energy function  $U(\epsilon_1, \epsilon_2, \dots, \epsilon_6)$  is expanded in a series

$$U = \sum_{i=1}^6 S_i \epsilon_i + \frac{1}{2} \sum_{i=1}^6 \sum_{j=1}^6 S_{ij} \epsilon_i \epsilon_j + \dots, \quad (\text{A.94})$$

in which the strain energy is assumed to vanish when all the strain components are zero. Employing the properties given in eq. (A.91) we get

$$\sigma_k = \frac{\partial U}{\partial \epsilon_k} = S_k + \sum_{j=1}^6 \frac{1}{2} (S_{kj} + S_{jk}) \epsilon_j, \quad k = 1, 2, \dots, 6. \quad (\text{A.95})$$

Note that when all strain components equal zero, eq. (A.95) yields  $\sigma_k = S_k$ . Non-zero stresses can occur in a state of vanishing strains when there is a change in temperature. Let the change in temperature from the reference state be denoted by  $T - T_0$ . For the change in temperature let

$$S_k = -\beta_k (T - T_0), \quad (\text{A.96})$$

where the  $\beta_k$  are thermal coefficients. For  $k = 1$  and  $k = 2$  eq. (A.95) expands to

$$\begin{aligned} \sigma_1 &= S_1 + S_{11} \epsilon_1 + \frac{1}{2} (S_{12} + S_{21}) \epsilon_2 + \dots + \frac{1}{2} (S_{16} + S_{61}) \epsilon_6 \\ \sigma_2 &= S_2 + \frac{1}{2} (S_{21} + S_{12}) \epsilon_1 + S_{22} \epsilon_2 + \dots + \frac{1}{2} (S_{26} + S_{62}) \epsilon_6 \end{aligned}$$

Clearly,  $\frac{1}{2} (S_{12} + S_{21}) = \frac{1}{2} (S_{21} + S_{12})$ , so we can take  $S_{12} = S_{21}$  without changing the stress-strain relation. By implication  $S_{ij} = S_{ji}$ . The full expression for the linear elastic material law is

$$\begin{bmatrix} \sigma_1 \\ \sigma_2 \\ \sigma_3 \\ \sigma_4 \\ \sigma_5 \\ \sigma_6 \end{bmatrix} = - \begin{bmatrix} \beta_1 \\ \beta_2 \\ \beta_3 \\ \beta_4 \\ \beta_5 \\ \beta_6 \end{bmatrix} (T - T_0) + \underbrace{\begin{bmatrix} S_{11} & S_{12} & S_{13} & S_{14} & S_{15} & S_{16} \\ S_{21} & S_{22} & S_{23} & S_{24} & S_{25} & S_{26} \\ S_{31} & S_{32} & S_{33} & S_{34} & S_{35} & S_{36} \\ S_{41} & S_{42} & S_{43} & S_{44} & S_{45} & S_{46} \\ S_{51} & S_{52} & S_{53} & S_{54} & S_{55} & S_{56} \\ S_{61} & S_{62} & S_{63} & S_{64} & S_{65} & S_{66} \end{bmatrix}}_{[S]} \begin{bmatrix} \epsilon_1 \\ \epsilon_2 \\ \epsilon_3 \\ \epsilon_4 \\ \epsilon_5 \\ \epsilon_6 \end{bmatrix} \quad (\text{A.97})$$

The 6X6 elasticity matrix  $[S]$  is symmetric which means there are twenty-one independent elastic constants, and there are six independent thermal coefficients. Equation (A.97) is the material law for an **anisotropic** material where the number of independent elastic constants is determined by the existence of the strain energy density function and the symmetry of the strain and stress tensors.

### A.3.1 Material symmetry

Consider a monoclinic material for which the  $x_1 x_2$  plane at a point  $P$  is a plane of elastic symmetry. This means that the elastic constants at point  $P$  have the same values for a pair of Cartesian coordinate systems which are



mirror images of one another in the elastic plane. The elastic constants  $S_{ij}$  are invariant under the reflection coordinate transformation  $x_1' = x_1$ ,  $x_2' = x_2$ , and  $x_3' = -x_3$ . The direction cosines for this reflection transformation are listed in Table 1

TABLE 1. Direction cosines

	$x_1$	$x_2$	$x_3$
$x_1'$	1	0	0
$x_2'$	0	1	0
$x_3'$	0	0	-1

From strain and stress transformations in eq. (A.53) and eq. (A.79), respectively, we find

$$\begin{aligned} \sigma_i' &= \sigma_i & \epsilon_i' &= \epsilon_i & i &= 1, 2, 3, 6 \\ \sigma_4' &= -\sigma_4 & \sigma_5' &= -\sigma_5 & \epsilon_4' &= -\epsilon_4 & \epsilon_5' &= -\epsilon_5 \end{aligned}$$

In the  $x_i'$  system the first of eq. (A.97) becomes

$$\sigma_1' = -\beta_1(T - T_0) + S_{11}\epsilon_1' + S_{12}\epsilon_2' + S_{13}\epsilon_3' + S_{14}\epsilon_4' + S_{15}\epsilon_5' + S_{16}\epsilon_6'.$$

Substitute the stress and strain transformation relations into the latter equation to find

$$\sigma_1 = -\beta_1(T - T_0) + S_{11}\epsilon_1 + S_{12}\epsilon_2 + S_{13}\epsilon_3 - S_{14}\epsilon_4 - S_{15}\epsilon_5 + S_{16}\epsilon_6.$$

Comparison of last equation to the first equation from (A.97) shows that  $S_{14} = 0$  and  $S_{15} = 0$ . Constructing material law for  $\sigma_2'$  and following a similar procedure used for the  $\sigma_1'$  material law leads to  $S_{24} = 0$  and  $S_{25} = 0$ . Considerations for the material law for  $\sigma_3'$  leads to  $S_{34} = 0$  and  $S_{35} = 0$ , material law  $\sigma_4'$  leads to  $\beta_4 = 0$  and  $S_{46} = 0$ , and finally material law  $\sigma_5'$  leads to  $\beta_5 = 0$  and  $S_{56} = 0$ . The material law for the  $x_1x_2$  plane of elastic symmetry is

$$\begin{bmatrix} \sigma_1 \\ \sigma_2 \\ \sigma_3 \\ \sigma_4 \\ \sigma_5 \\ \sigma_6 \end{bmatrix} = - \begin{bmatrix} \beta_1 \\ \beta_2 \\ \beta_3 \\ 0 \\ 0 \\ \beta_6 \end{bmatrix} (T - T_0) + \begin{bmatrix} S_{11} & S_{12} & S_{13} & 0 & 0 & S_{16} \\ S_{21} & S_{22} & S_{23} & 0 & 0 & S_{26} \\ S_{31} & S_{32} & S_{33} & 0 & 0 & S_{36} \\ 0 & 0 & 0 & S_{44} & S_{45} & 0 \\ 0 & 0 & 0 & S_{54} & S_{55} & 0 \\ S_{61} & S_{62} & S_{63} & 0 & 0 & S_{66} \end{bmatrix} \begin{bmatrix} \epsilon_1 \\ \epsilon_2 \\ \epsilon_3 \\ \epsilon_4 \\ \epsilon_5 \\ \epsilon_6 \end{bmatrix}. \quad (\text{A.98})$$

There are thirteen independent elastic constants  $S_{ij}$ , and four independent thermal coefficients. Equation (A.98) is the material law for a **monoclinic** material

Certain elastic constants in eq. (A.98) vanish if in addition to the  $x_1x_2$  plane of elastic symmetry the  $x_2x_3$  plane is a plane of elastic symmetry. The reflection coordinate transformation is  $x_1' = -x_1$ ,  $x_2' = x_2$ , and  $x_3' = x_3$ . The direction cosines are listed in Table 2.

**TABLE 2. Direction cosines**

	$x_1$	$x_2$	$x_3$
$x_1'$	-1	0	0
$x_2'$	0	1	0
$x_3'$	0	0	1

The strain and stress transformation equations for the direction cosines in Table 2 are

$$\begin{aligned} \sigma_i' &= \sigma_i & \epsilon_i' &= \epsilon_i & i &= 1, 2, 3, 4 \\ \sigma_5' &= -\sigma_5 & \sigma_6' &= -\sigma_6 & \epsilon_5' &= -\epsilon_5 & \epsilon_6' &= -\epsilon_6 \end{aligned}$$

In the  $x_i'$  system the first of eq. (A.98) becomes

$$\sigma_1' = -\beta_1(T - T_0) + S_{11}\epsilon_1' + S_{12}\epsilon_2' + S_{13}\epsilon_3' + S_{16}\epsilon_6'.$$

Substitute the transformations for the stress and strain in the last equation to get

$$\sigma_1 = -\beta_1(T - T_0) + S_{11}\epsilon_1 + S_{12}\epsilon_2 + S_{13}\epsilon_3 + S_{16}\epsilon_6. \quad (\text{A.99})$$

In the  $x_i$  system the first of eq. (A.98) is

$$\sigma_1 = -\beta_1(T - T_0) + S_{11}\epsilon_1 + S_{12}\epsilon_2 + S_{13}\epsilon_3 + S_{16}\epsilon_6. \quad (\text{A.100})$$

Comparison of eq. (A.99) and eq. (A.100) leads to  $S_{16} = 0$ . Also, following the same procedure for the equation starting with  $\sigma_2'$  leads to  $S_{26} = 0$ , and starting with the equation for  $\sigma_3'$  leads to  $S_{36} = 0$ . Following this procedure for we find  $(\sigma_4' = S_{44}\epsilon_4' + S_{45}\epsilon_5') \rightarrow \sigma_4 = S_{44}\epsilon_4 - S_{45}\epsilon_5$ . Hence  $S_{45} = 0$ . Finally, consider  $(\sigma_6' = -\beta_6(T - T_0) + S_{66}\epsilon_6') \rightarrow -\sigma_6 = -\beta_6(T - T_0) - S_{66}\epsilon_6$ , Hence  $\beta_6 = 0$ . The material law for two orthogonal elastic planes of symmetry is

$$\begin{bmatrix} \sigma_1 \\ \sigma_2 \\ \sigma_3 \\ \sigma_4 \\ \sigma_5 \\ \sigma_6 \end{bmatrix} = - \begin{bmatrix} \beta_1 \\ \beta_2 \\ \beta_3 \\ 0 \\ 0 \\ 0 \end{bmatrix} (T - T_0) + \begin{bmatrix} S_{11} & S_{12} & S_{13} & 0 & 0 & 0 \\ S_{21} & S_{22} & S_{23} & 0 & 0 & 0 \\ S_{31} & S_{32} & S_{33} & 0 & 0 & 0 \\ 0 & 0 & 0 & S_{44} & 0 & 0 \\ 0 & 0 & 0 & 0 & S_{55} & 0 \\ 0 & 0 & 0 & 0 & 0 & S_{66} \end{bmatrix} \begin{bmatrix} \epsilon_1 \\ \epsilon_2 \\ \epsilon_3 \\ \epsilon_4 \\ \epsilon_5 \\ \epsilon_6 \end{bmatrix}. \quad (\text{A.101})$$

If we additionally impose the that the  $x_3x_1$  plane is a plane of elastic symmetry, this condition does not change the results given in eq. (A.101). An orthotropic material has three mutually orthogonal planes of elastic symmetry, nine independent elastic constants  $S_{ij}$ , and three independent thermal coefficients. Equation (A.101) is the material law for an **orthotropic** material; e.g wood.

The material properties are independent of direction for an **isotropic** material. Starting with the orthotropic material law (A.101) consider the following sequence of rotations from the  $(x_1, x_2, x_3)$  coordinates to the  $(x_1', x_2', x_3')$  coordinates.

1.  $90^\circ$  rotation about the  $x_1$ -axis. The direction cosine matrix  $[\lambda] = \begin{bmatrix} 1 & 0 & 0 \\ 0 & 0 & 1 \\ 0 & -1 & 0 \end{bmatrix}$ .
2.  $90^\circ$  rotation about the  $x_3$ -axis. The direction cosine matrix  $[\lambda] = \begin{bmatrix} 0 & 1 & 0 \\ -1 & 0 & 0 \\ 0 & 0 & 1 \end{bmatrix}$ .
3.  $45^\circ$  rotation about the  $x_3$ -axis. The direction cosine matrix  $[\lambda] = \begin{bmatrix} 1/\sqrt{2} & 1/\sqrt{2} & 0 \\ -1/\sqrt{2} & 1/\sqrt{2} & 0 \\ 0 & 0 & 1 \end{bmatrix}$ .

For the material law to be invariant from the first rotation we find

$$S_{12} = S_{13} \quad \beta_3 = \beta_2 \quad S_{33} = S_{22} \quad S_{55} = S_{66}.$$

For the material law to be invariant from the second rotation we find

$$\beta_2 = \beta_1 \quad S_{12} = S_{23} \quad S_{11} = S_{22} \quad S_{44} = S_{55}.$$

For the third rotation the material law for  $\sigma_1'$  in the  $(x_1', x_2', x_3')$  coordinates is

$$\sigma_1' = -\beta_1(T - T_0) + S_{11}\epsilon_1' + S_{12}\epsilon_2' + S_{12}\epsilon_3', \quad (\text{A.102})$$

since  $S_{13} = S_{12}$ . The stress transformation and the strain transformations relations are

$$(\sigma_1' = (\sigma_1 + \sigma_2)/2 + \sigma_6 \quad \epsilon_1' = (\epsilon_1 + \epsilon_2 + \epsilon_6)/2 \quad \epsilon_2' = (\epsilon_1 + \epsilon_2 - \epsilon_6)/2 \quad \epsilon_3' = \epsilon_3 \quad (\text{A.103})$$

Substitute the transformations in (A.103) into eq. (A.102) to get

$$(\sigma_1 + \sigma_2)/2 + \sigma_6 = -\beta_1(T - T_0) + \frac{1}{2}(S_{11} + S_{12})\epsilon_1 + \frac{1}{2}(S_{11} + S_{12})\epsilon_2 + S_{12}\epsilon_3 + \frac{1}{2}(S_{11} - S_{12})\epsilon_6 \quad (\text{A.104})$$

In the  $(x_1, x_2, x_3)$  coordinates the formulation of the quantity  $(\sigma_1 + \sigma_2)/2 + \sigma_6$  is

$$(\sigma_1 + \sigma_2)/2 + \sigma_6 = -\beta_1(T - T_0) + \frac{1}{2}(S_{11} + S_{12})\epsilon_1 + \frac{1}{2}(S_{12} + S_{11})\epsilon_2 + S_{12}\epsilon_3 + S_{44}\epsilon_6. \quad (\text{A.105})$$

For eqs. (A.104) and (A.105) to be identical we get that

$$\frac{1}{2}(S_{11} - S_{12}) = S_{44}. \quad (\text{A.106})$$

For an isotropic material there are two independent elastic constants and one thermal coefficient. Let  $S_{12} = \lambda$  and  $S_{44} = G$ , where  $\lambda$  and  $G$  are called Lamé's elastic constants. From eq. (A.106)  $S_{11} = \lambda + 2G$ . The isotropic material law is

$$\begin{bmatrix} \sigma_1 \\ \sigma_2 \\ \sigma_3 \\ \sigma_4 \\ \sigma_5 \\ \sigma_6 \end{bmatrix} = - \begin{bmatrix} \beta \\ \beta \\ \beta \\ 0 \\ 0 \\ 0 \end{bmatrix} (T - T_0) + \begin{bmatrix} \lambda + 2G & \lambda & \lambda & 0 & 0 & 0 \\ \lambda & \lambda + 2G & \lambda & 0 & 0 & 0 \\ \lambda & \lambda & \lambda + 2G & 0 & 0 & 0 \\ 0 & 0 & 0 & G & 0 & 0 \\ 0 & 0 & 0 & 0 & G & 0 \\ 0 & 0 & 0 & 0 & 0 & G \end{bmatrix} \begin{bmatrix} \varepsilon_1 \\ \varepsilon_2 \\ \varepsilon_3 \\ \varepsilon_4 \\ \varepsilon_5 \\ \varepsilon_6 \end{bmatrix}. \quad (\text{A.107})$$

The strain-stress form of eq. (A.107) is

$$\begin{bmatrix} \varepsilon_1 \\ \varepsilon_2 \\ \varepsilon_3 \\ \varepsilon_4 \\ \varepsilon_5 \\ \varepsilon_6 \end{bmatrix} = \begin{bmatrix} C_{11} & C_{12} & C_{12} & 0 & 0 & 0 \\ C_{12} & C_{11} & C_{12} & 0 & 0 & 0 \\ C_{12} & C_{12} & C_{11} & 0 & 0 & 0 \\ 0 & 0 & 0 & G^{-1} & 0 & 0 \\ 0 & 0 & 0 & 0 & G^{-1} & 0 \\ 0 & 0 & 0 & 0 & 0 & G^{-1} \end{bmatrix} \begin{bmatrix} \sigma_1 \\ \sigma_2 \\ \sigma_3 \\ \sigma_4 \\ \sigma_5 \\ \sigma_6 \end{bmatrix} + \begin{bmatrix} C_{11} + C_{12} + C_{12} \\ C_{12} + C_{11} + C_{12} \\ C_{12} + C_{12} + C_{11} \\ 0 \\ 0 \\ 0 \end{bmatrix} \beta (T - T_0), \quad (\text{A.108})$$

where

$$C_{11} = \frac{\lambda + G}{3\lambda G + 2G^2} \quad C_{12} = \frac{-\lambda}{2(3\lambda G + 2G^2)}. \quad (\text{A.109})$$

Consider a uniaxial tension test conducted on a circular cylindrical bar made of an isotropic, homogenous material at the reference state temperature. The test apparatus is configured such that the applied axial normal force divided by the cross-sectional area of the bar is equal to the normal stress  $\sigma_1$ , and the remaining stresses

$\sigma_2 = \sigma_3 = \sigma_4 = \sigma_5 = \sigma_6 = 0$ . The normal strains ( $\varepsilon_1, \varepsilon_2, \varepsilon_3$ ) are monitored and plotted with respect to the applied normal stress  $\sigma_1$ . In the linear elastic range of the test data the following relationships are established  $\varepsilon_1 = \sigma_1/E$ ,  $\varepsilon_2 = \varepsilon_3 = -\nu\varepsilon_1 = -\nu(\sigma_1/E)$ , where  $E$  denotes Young's modulus, or the modulus of elasticity, and  $\nu$  denotes Poisson's ratio. The tension test results correspond to the first column of the 6X6 compliance matrix (A.108). Hence,  $C_{11} = 1/E$  and  $C_{12} = -\nu/E$ . Substitute the values for  $C_{11}$  and  $C_{12}$  from the tensile test into eq. (A.109) to get

$$\frac{\lambda + G}{3\lambda G + 2G^2} = \frac{1}{E} \quad \frac{-\lambda}{2(3\lambda G + 2G^2)} = -\frac{\nu}{E}$$

From the previous equations we can write Young's modulus and Poisson's ratio in terms of  $\lambda$  and  $G$  as

$$E = \frac{3\lambda G + 2G^2}{\lambda + G} \quad \nu = \frac{\lambda}{2(\lambda + G)}. \quad (\text{A.110})$$

It can be shown from the two expressions in eq. (A.110) that the Lamé constants in terms of  $E$  and  $\nu$  are

$$G = \frac{E}{2(1 + \nu)} \quad \lambda = \frac{\nu E}{(1 - 2\nu)(1 + \nu)}. \quad (\text{A.111})$$

Also note that  $(C_{11} + C_{12} + C_{12})\beta = [(1 - 2\nu)/E]\beta = \alpha$ , where  $\alpha$  is the linear coefficient of thermal expansion. In shear tests of an isotropic, homogeneous material Lamé's elastic constant  $G$  is called the shear modulus

of the material. In terms of engineering constants the material law for a homogenous and isotropic material is

$$\begin{aligned}
 \varepsilon_{11} &= \frac{1}{E}[\sigma_{11} - \nu\sigma_{22} - \nu\sigma_{33}] + \alpha(T - T_0) & \gamma_{23} &= \sigma_{23}/G \\
 \varepsilon_{22} &= \frac{1}{E}[-\nu\sigma_{11} + \sigma_{22} - \nu\sigma_{33}] + \alpha(T - T_0), \text{ and } \gamma_{31} = \sigma_{31}/G. & & \\
 \varepsilon_{33} &= \frac{1}{E}[-\nu\sigma_{11} - \nu\sigma_{22} + \sigma_{33}] + \alpha(T - T_0) & \gamma_{12} &= \sigma_{12}/G
 \end{aligned} \tag{A.112}$$

#### A.4 Summary and the boundary value problems of elasticity

At a point  $P:(x_1, x_2, x_3)$  in the body the unknown functions are

- three displacements  $u_1(x_1, x_2, x_3)$ ,  $u_2(x_1, x_2, x_3)$ , and  $u_3(x_1, x_2, x_3)$
- six strains  $\varepsilon_{11}, \varepsilon_{22}, \varepsilon_{33}, \gamma_{23}, \gamma_{31}, \gamma_{12}$
- nine stresses  $\sigma_{11}, \sigma_{22}, \sigma_{33}, \sigma_{12}, \sigma_{13}, \sigma_{23}, \sigma_{21}, \sigma_{31}, \sigma_{32}$

The total number of unknown functions is eighteen.

The number of equations are

- six strain-displacement equations (A.32) and (A.33)
- three force equilibrium equations (A.68)
- three moment equilibrium equations (A.72)
- six equations for the material law from one of the following expressions: anisotropic (A.97), monoclinic (A.98), orthotropic (A.101), or isotropic (A.112).

The total number of equations is eighteen.

Let the boundary surface of region  $B_0$  be denoted by  $S$ . On the surface  $S$  we can prescribe the displacements and/or the tractions. In eq. (A.64) let  $\hat{n}$  be the unit outward normal to the surface  $S$ . We write eq. (A.64) in the form

$$\vec{T}^{(\hat{n})} = T_1^{(n)}\hat{i}_1 + T_2^{(n)}\hat{i}_2 + T_3^{(n)}\hat{i}_3 = \vec{T}_1 n_1 + \vec{T}_2 n_2 + \vec{T}_3 n_3,$$

where  $T_1^{(n)}$ ,  $T_2^{(n)}$ , and  $T_3^{(n)}$  are the cartesian components of the traction vector acting on the surface. We use eq. (A.59) to determine that these traction components are related to the stresses by

$$T_j^{(n)} = n_1\sigma_{1j} + n_2\sigma_{2j} + n_3\sigma_{3j}, j = 1, 2, 3.$$

On the portion of the surface where tractions are prescribed we have the boundary conditions

$$T_j^{(n)} = n_1\sigma_{1j} + n_2\sigma_{2j} + n_3\sigma_{3j} = \text{prescribed functions.} \tag{A.113}$$

1. Boundary value problem 1: Determine the distribution of stress and displacement in the interior of an elastic body in equilibrium when the body forces  $B_i(x_j)$  are prescribed and the distribution of the surface tractions  $T_j^{(n)}$  are prescribed.
2. Boundary value problem 2: Determine the distribution of stress and displacement in the interior of an elastic body in equilibrium when the body forces  $B_i(x_j)$  are prescribed and the displacements  $u_i$  of points on the surface of the body are prescribed functions.
3. Boundary value problem 3, or the mixed boundary value problem. Determine the distribution of the stress and displacement of an elastic body in equilibrium when body forces are prescribed, and the distribution of surface tractions are prescribed on surface  $S_\sigma$  and displacements are prescribed on surface  $S_u$ . That is, surface  $S$  is separated into parts  $S_\sigma$  and  $S_u$ .

In boundary value problem 1, the prescribed body forces and prescribed surface tractions must satisfy overall equilibrium of the body.

## A.5 *References*

Batra, R., C., 2006, **Elements of Continuum Mechanics**, American Institute of Aeronautics and Astronautics, Inc. 1801 Alexander Bell Drive, Reston, VA 2019-4344, p.37.